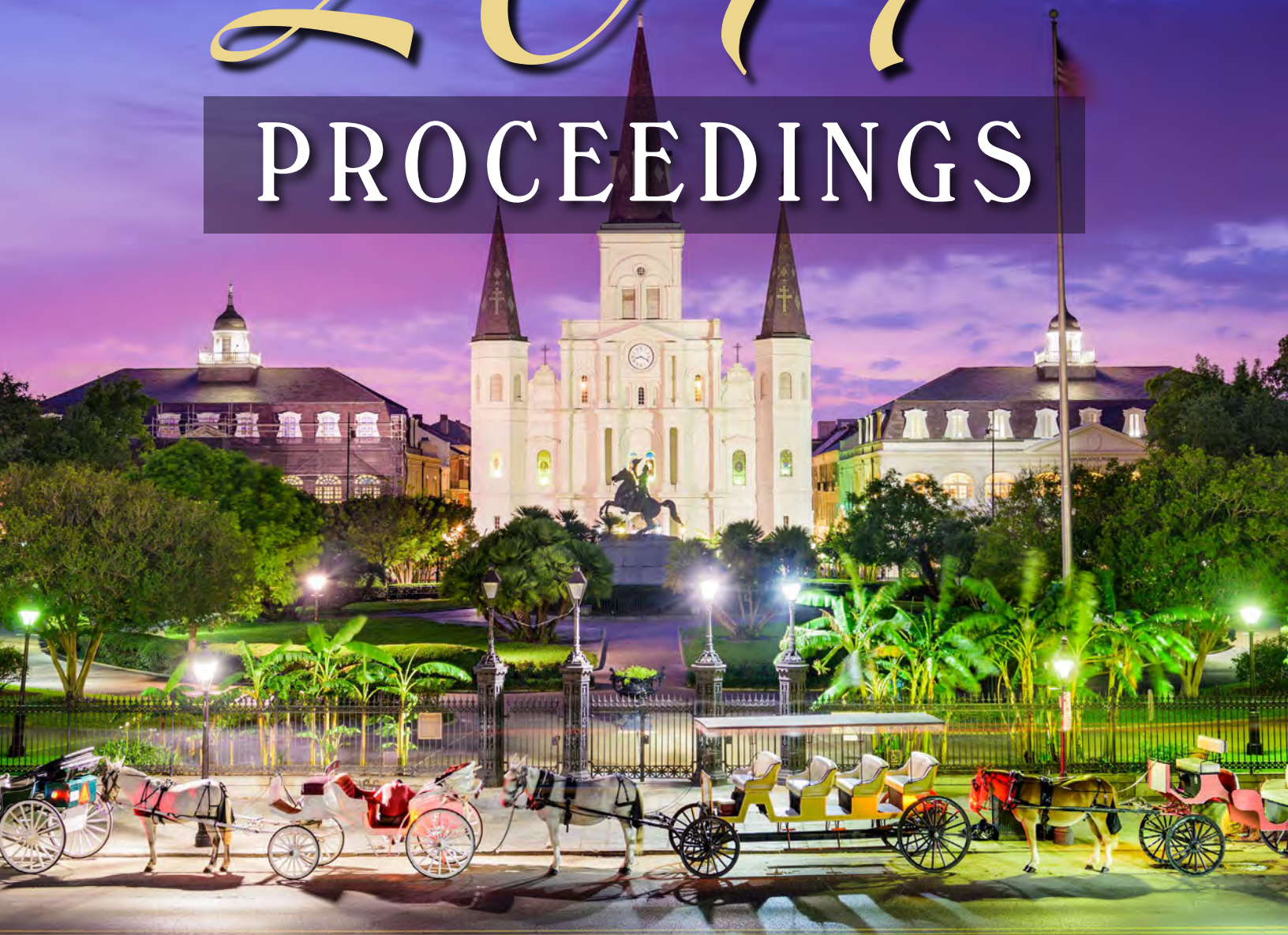
DEEP FOUNDATIONS INSTITUTE

42nd ANNUAL CONFERENCE

New Orleans Marriott | October 24-27, 2017

2017 PROCEEDINGS



Risk

Charleroi Locks: Repair Methods to Restore Structural Integrity of Large-Diameter Drilled Shafts

Alex J. Bredikhin, P.E., District Risk Manager for Mega-projects

Managing SOE Construction Risk through Design-Build Systems

Rob Jameson, VP Construction Engineering

PPP Contract Delivery System - Contractual Risks and Ethical Issues Regarding Deep Foundation Subcontractors

Alexander Filotti, M.B.A., P.E. and Richard Kalson, Esq. Partner

Prescriptive Specification Design: The Impact on Cost and Constructability - Case History

Shawna Munn, P.Eng, Allison Bennett, E.I.T. and Nadir Ansari, P.Eng, D.GE, M.ASCE

Challenges in Managing an Aging Infrastructure, Lessons Learned from a near Miss at the Lake Manatee Dam

Glen R. Andersen

Framework for Risk-Based Electric System Deep Foundation Design

Peter M. Kandaris, Steve Davidow and Ashley E. Evans

LRFD Resistance Factors for Design of Driven Piles Using the Texas Cone Penetration (TCP) Test

Hoyoung Seo, Ph.D., P.E., William D. Lawson, P.E., Ph.D, James G. Surles, Priyantha W. Jayawickrama, Ph.D. and Rozbeh Moghaddam, Ph.D., P.E.

Data Normalization and User Interface Design for the Nevada Department of Transportation Deep Foundation Load Test Database

Austin Metz, Kevin Stanton and Ramin Motamed

Mitigation of Environmental Impacts

Sustainability: A Role for Blended Cements and Industrial Byproducts in Soil Mixing, Grouting, and Slurry Walls

Charles M. Wilk and Lori Tiefenthaler

Noise Attenuation and Reduced Risk Associated with New Double-Walled Pile Technology

Per G. Reinhall and Julie H. N. Hampden

Energy Geostructures: Analysis from Research and Systems Installed around the World

Alice Di Donna, Marco Barla and Tony Amis

Ground Improvement for Reclaimed Landfills

William W. Haasz, Brandon T. Buschmeier, Steve E. Darnell and Frederic Masse

Recycling Jet Grout Backflow: Waste Mitigation and Cost Benefits

Craig T. Jones, E.I.T and Zachary Q. Maassen, E.I.T

Laterally Loaded Piles

Design and Construction of Driven H-Piles for Landslide Stabilization in Marlboro Clay Formation

Kofi B. Acheampong, Ph.D, P.E., ENV SP, M. DFI, Chief Geotechnical Engineer & Senior Associate, Charbel Khoury, Ph.D, P.E., M. DFI, Associate and Kwabena Ofori-Awuah, P.E., D.GE, ENV SP, M. DFI, Geotechnical Engineering Practice Leader

Large Diameter Helical Piles for Refinery Expansion

Eric Wey, Patrick Murray, Howard Perko, Paul Volpe, Chris Normand and Burt Ogilvie

Interpretation of Seismic Response Data from Full Scale Helical Piles Tests

M. K. ElSawy, M. H. El Naggar, M. Heidari, A. B. Cerato and A. Elgamal

Dulles Metrorail/Silver Line (Phase 2) Drilled Shaft Lateral Load Testing Program

William Billiet, P.E.

Instrumented Hybrid Shoring System for a Deep Temporary Excavation Incorporating Cutter Soil Mixing in Vancouver, BC, Canada

Marina S. W. Li, C.Eng., P.Eng., Nadir Ansari, P.Eng., D.GE. and Brian W. Wilson, C.Eng., P.Eng.

Design of Grillage and Helical Pile Foundation for Limited Access Transmission Line

Jason Herron and Benjamin Jennings

Analytical Expression for Plastic Hinge Length in Extended Pile-Shafts

Mehdi Heidari and M. Hesham El Naggar

Comparison of Static Lateral Behavior of Vertical and Battered Pile Groups of the I-10 Twin Span Bridge Using Finite Element Simulation

Ahmad F. Siouri and Murad Abu-Farsakh

Case Histories - Support of Excavation

Cutter Soil Mixing and Augered-Cast-in-Place Piling Close to the Gulf of Mexico

Justin Simmons, Michael Arnold and Bob Faulhaber

Design, Construction, and Performance of the Temporary Earth Retention System at No. 9 Walton

Joel B. Dellaria, S.E., P.E. and Justin R. Lewis, P.E.

Eglinton Crosstown, a New Step in Toronto's Subway System

Franz-Werner Gerressen and Lars Richter

A Tale of Two Dams: Performance of Deep Cutoff Walls

Wesley Schmutzler, James Sanders, Mark Harris and Donald Bruce

Evaluation of Crane Pad Performance on Partially Improved Ground Adjacent to a Seawall

Yazen A. Khasawneh and Paul J. Sabatini

Case Study: 1785 Massachusetts Avenue, NW, Washington, DC

SungJe Chi, P.E.

Case Histories - Deep Foundations

High-Capacity Driven-Pile Foundation for 33-Story High-Rise in Milwaukee, Wisconsin, USA

Van E. Komurka, P.E., D.GE, F.ASCE, William H. Walton, P.E., S.E., F.ASCE, Ryan C. Rusk, P.E., M.ASCE and Patrick J. Hannigan, P.E., M.ASCE

Deep and Shallow Soil Mixing for the SR-83/US-331 Choctawhatchee Bay Bridge Project in Santa Rosa Beach, Florida

Matteo Bertoni, Wesley Schmutzler, Alessandro Bertero and Dylan Pearson

Mitigating Embankment Settlement with Pile Supported Approach Slabs

Reda M. Bakeer

Overcoming the Challenges Endured by the Quality Assurance and Quality Control Teams during the Construction of a Deep Cutoff Wall in East Alton, Illinois

Matteo Bertoni, Raffaella Granata and Wesley Schmutzler

High Capacity Hollow Core Bar Piles

Lawrence F. Johnsen, Sr. Consultant, Felix Ferrer, President, Dino Tomasetti Jr., President and Owner and Cassandra A. Wetzel, Associate Principal

Case Study: MGM Casino National Harbor, Washington, DC - Displacement Cast-In-Place Piles in Coastal Plain Soils

James P. Racine, M.S.C.E., P.E., Senior Project Engineer and Karl A. Higgins III, M. Eng., P.E., D.GE, Chief Engineer

Foundations Settlement Estimation by Non-Linear Stress-Strain Approach Using CPT Records

Fatemeh Valikhah, Ph.D Candidate and Abolfazl Eslami, Professor

Structure Support on Laterally Swept Piles

Matthew R. Glisson, P.E. and Morgan L. Race, Ph.D., P.E.

Critical Infrastructure

Hydrocutter-Excavated Slurry Wall for Center Hill Dam Foundation Remediation

Michael Arnold, Bob Faulhaber and Joe Nichols

TTMJ - The New System for Slurry (Diaphragm) Wall Joints

Julian Crawley, Maurizio Siepi, Paul van Horn and John Coupland

Numerical Analysis of Pile-Supported T-Walls Subject to Large Settlements and Flood Loading

Alexander B. Reeb, George M. Filz, Jehu B. Johnson and Richard J. Varuso

Innovative Methods for Underground Parking in Central Cities

Guanglei Liu, Qi Wang, Zengzhu Kang and Jianguo Liu

Sheet Piling and Cofferdams

Challenges Associated with the Construction of Cofferdam - A Case Study

Khuram R. Mohib, Thomas J. Sabourin and Eric S. White

Assessment of Existing Bulkhead Walls for Dredging Impacts

Michael J. Byle, D.GE, F. ASCE, Rakam Lama Tamang, P.E. and Steve Ernst, E.I.T.

Permanent Canal Closures and Pumps Cofferdams - Support of Deep Excavation in Soft Ground Using the Open Cell Sheet Pile System

Matthew Anderson, King Chin, Mike Huggins, Ryan Higbie, Rian Johnson and Dave Sinsheimer

Advantages of Pressed-In Sheet Piles for New Orleans' Hurricane and Storm Damage Risk Reduction System Flood Control Project

Ian Vaz and Takefumi Takuma

RD Pile Wall - A Water Tight Retaining Wall Structure

Antti J. Perala and Teemu J. Yli-Kovero

Instrumentation/Soil-Pile Interaction

A Field Study to Analyze Pile Setup Behavior and Comparison of Pile Capacity Methods from CPT

Md. Nafiul Haque, Ph.D., Postdoctoral Researcher, Murad Y. Abu-Farsakh, Ph.D., P.E., Research Professor and Chris Nickel, P.E., Geotechnical Engineering Manager

Friction Fatigue and Drivability Analysis of Open Ended Pipe Piles Based on Cone Penetration Testing Results

Rozbeh B. Moghaddam, Frank Rausche and Scott D. Webster

Case History: Large Diameter Micropiles for the Highway 53 Relocation Project

David S. Graham, P.E., Paul J. Axtell, P.E., D.GE and Nathan W. Iverson, P.E.

Case Study: Large Diameter Helical Pile Foundation for High Voltage Transmission Towers in Soft Glacial Deposits

Kashiff Butt, John Dunn, Nicholas Gura and Matt Hawley

Residual Loads Measurements in Driven Steel H-Piles

Reda M. Bakeer

Innovative Techniques for Soft Soils

Ground Improvement for New Jersey Turnpike Interchange 14A Improvements: A Case Study

Shafiq I. Siddiqui, Daniel V. Cacciola, Sarah Ramp, Faisal Ahmed and Justin Labrozzi

Sloping Rubble Seawalls Founded on Soft Soil Improved by Stone Columns

Wilhelm S. Degen, Chengbin Miao, Eleonora Di Mario, Matthew G. Mills and Colin B. Turnbull

Staged Construction of an Interstate I69 Embankment: Coupled Hydro-Mechanical Numerical Simulation

Yazen A. Khasawneh and Malek Smadi

Smart Soil Improvement: The Use of Rigid Inclusion for the Soil Consolidation

Claudio Asioli, Federico Pagliacci and Marco Chiarabelli

Remedial Method for Collapsible Soil Foundation of Mosul Dam

Ali N. Ibrahim and Arash Khosravifar

Bearing Capacity of Semi-Deep Skirted Foundations

Samieh Rezazadeh and Abolfazl Eslami

Deep Foundations Technologies

Baum Station - A New Pile Drivng and Drilling Navigation System

Koji Mitani, Dzianis Proshchanka, Yoshi Izumi and Ayuna Kitaura

Capacity of Hydraulically Jacked Piles

Melinda J. Hummel and Howard A. Perko

Subsurface Exploration/Site Characterization

Quality Assessment of Seismic Data Sets and the Impact on Interval Velocity Estimates in DST

Erick Baziw and Gerald Verbeek

Probabilistic Subsurface Characterization for Transmission Line Foundation Design

Peter M. Kandaris, Jogi S. Gadok and Neil T. Russo

PREFACE

On behalf of Deep Foundations Institute (DFI) and the 2017 Conference Organizing Committee, we would like to extend our thanks and gratitude to all attendees, exhibitors, underwriters, and presenters who helped make the DFI 42nd Annual Conference on Deep Foundations a success. This year, the Annual Conference was held from October 24-27, 2017 in New Orleans, Louisiana. New Orleans was an ideal place to host the conference. The *Big Easy* may be know for its rich traditions of food, music and southern hospitality, but it has also been a prime location for DFI members to showcase their experience. Rebuilding efforts since Hurricane Katrina have incorporated all sorts of deep foundations and construction techniques and have highlighted design approaches that consider risk reduction and critical infrastructure needs.

The event continues to deliver a forum where a wide range of contractors, equipment manufacturers, material and service suppliers, design and consulting engineers, academicians, researchers, and owners gather to present, discuss, debate, and advance all aspects of the deep foundation industry. Prior to and during the conference, members of 18 technical committees and 4 working groups gathered to discuss, debate, and offer solutions to the various challenges affecting the deep foundations industry. During the conference, 46 technical presentations were delivered in 16 technical sessions, and 10 technical posters were presented. The student activities program included a paper competition, lecture and a tour of a major new pump station nearing completion of construction. A special session was held to gather engineers, contractors, and owners for a rational discussion about risk as related to deep foundations projects. The session emphasized the importance of clearly identifying and allocating risk during tender phase so that risks can be mitigated by parties best positioned to manage them and risks that become realities can be addressed fairly. DFI's Manufacturer, Supplier and Service Provider Committee presented 16 papers in 3 Expo sessions that highlighted products and services offered by DFI corporate members.

Archie Manning, the renowned football player, author and public relations consultant, was this year's Hal Hunt Lecturer, and his presentation was entitled "*The Manning Playbook for Communication and Leadership*." Also, notable industry experts were invited as Keynote Guest Lecturers. David B. Paul, P.E., Special Assistant for Dam Safety, U.S. Army Corps of Engineers, presented "*USACE Oversight of Remediation of the World's Highest Risk Dam – an Update on Mosul Dam."* Eric Halpin, P.E., Special Assistant for Dam and Levee Safety, U.S. Army Corps of Engineers, presented "*Being Approximately Right or Precisely Wrong: Risk Informed Lessons in a Standards Based Industry.*" Deborah D. Keller, P.E., D.D. Keller & Partners, presented "*Fostering Multi-Generational Work Teams.*" Ralph W. Junius, Jr., P.E., President, Linfield, Hunter & Junius, Inc., presented "*The Intersection of Engineering, Construction, Litigation and Ethics.*" Last but not least, Dale Biggers, P.E., Vice President, Boh Bros, was invited to give DFI members and conference attendees a brief overview presentation on the history of foundations in New Orleans.

This publication contains peer-reviewed technical papers pertaining to the session topics selected by the Conference Organizing Committee – Critical Infrastructure, Innovative Techniques for Soft Soils, Laterally Loaded Piles, Mitigation of Environmental Impacts, Sheet Piling and Cofferdams, Instrumentation and Monitoring, Application of Factors of Safety, Quality Assurance and Quality Control, Subsurface Exploration and Site Characterization, and Lessons Learned and Case Histories.

Without a doubt, this Annual Conference would not have been possible without the hard work and dedication of all those involved. We are especially grateful to the Conference Organizing Committee, Session Chairs and Moderators, authors, reviewers, underwriters, exhibitors, and volunteers. As always, the DFI Staff has done an amazing job organizing, preparing, guiding, supporting, corralling, and gently prodding to ensure the Conference is executed flawlessly. Nonetheless, we would be remiss if we did not specifically acknowledge the efforts of Theresa Engler, DFI Executive Director, Lauren Nance, DFI Senior Meetings and Events Specialist, and Mary Ellen Bruce Large, P.E., D.GE, DFI Director of Technical Activities.

Lastly, we appreciate the opportunity to be a part of the DFI 42nd Annual Conference on Deep Foundations.

Conference Chair, *Dale C. Biggers, P.E., Boh Bros. Construction Co., LLC*

Program Advisor, *Gwendolyn Sanders, P.E., Eustis Engineering LLC*

Program Co-Chairs, *Karishma Desai, P.E., Eustis Engineering LLC*
Nabil Mikhail, P.E., D.GE., Intertek-PSI, Inc.

CHARLEROI LOCKS: REPAIR METHODS TO RESTORE STRUCTURAL INTEGRITY OF LARGE-DIAMETER DRILLED SHAFTS

Alexandre (Alex) J. Bredikhin, PE, District Risk Manager for Mega-projects, Pittsburgh District, US Army Corps of Engineers

US Army Corps of Engineers
1000 Liberty Ave.,
Pittsburgh, PA 15222

DISCLAIMER: the statements presented herein are those of the author and do not necessarily represent the views of US DoD or its Components.

ABSTRACT

Progress on the $750M lock project on the Monongahela River was derailed by discovery of large anomalies in the 6.5-7-ft dia. drilled shafts of the new river wall foundation. The anomalies were located 45 to 50' below the top of the wall at the critical shaft-to-wall interface, and ranged in thickness from several inches to 2-plus feet. A Specialty team, comprised of representatives from the contractor, the Government, and structural design consultants, was formed to evaluate the extent of the problem and the impact on the new lock wall. With no standard method in place, the Government took the lead to develop acceptance criteria for the repairs while the contractor took the lead to identify the repair means and methods. The Government developed a detailed Quality Control plan to capture and document all of the repair data and to approve each shaft repair in a timely manner. This paper provides an overview of the anomalies encountered and the need for repairs; discusses the details of the repair plan; and provides details on the unique quality control measures employed to verify the repairs. By developing and adhering to a detailed quality control plan, the structural integrity of all of the shafts was successfully restored.

Keywords: drilled shafts, anomaly repairs, jet cleaning, pressure grouting

INTRODUCTION

The new Charleroi Locks Project is currently under construction by the U.S. Army Corps of Engineers (USACE) in Pittsburgh, Pennsylvania. In the region, the Corps of Engineers is modernizing the series of locks and dams on the Monongahela River. One facet of this modernization is replacement of the existing Locks #4 (aka Charleroi Locks) located upstream of Pittsburgh, Pennsylvania with new and larger capacity locks. The relative location of the project is shown on Fig. 1. The original construction of twin locks (56'x720' & 56'x360') and the fixed-crest dam was completed in 1932, with lock walls supported on timber pile foundations. The fixed crest dam was replaced with a gated dam in the 1960's. The existing lock is undersized and in poor condition and thus needs to be replaced. The project requires the construction of the new river chamber adjacent to the existing land chamber which must remain operational to navigation throughout the construction. In order to accomplish this, the lock walls need to be constructed in the wet. The river wall was constructed using two construction methods referred to on the project as "cofferbox" and "non-cofferbox" construction.

 © 2017 DFI Annual Conference, New Orleans, LA, USA

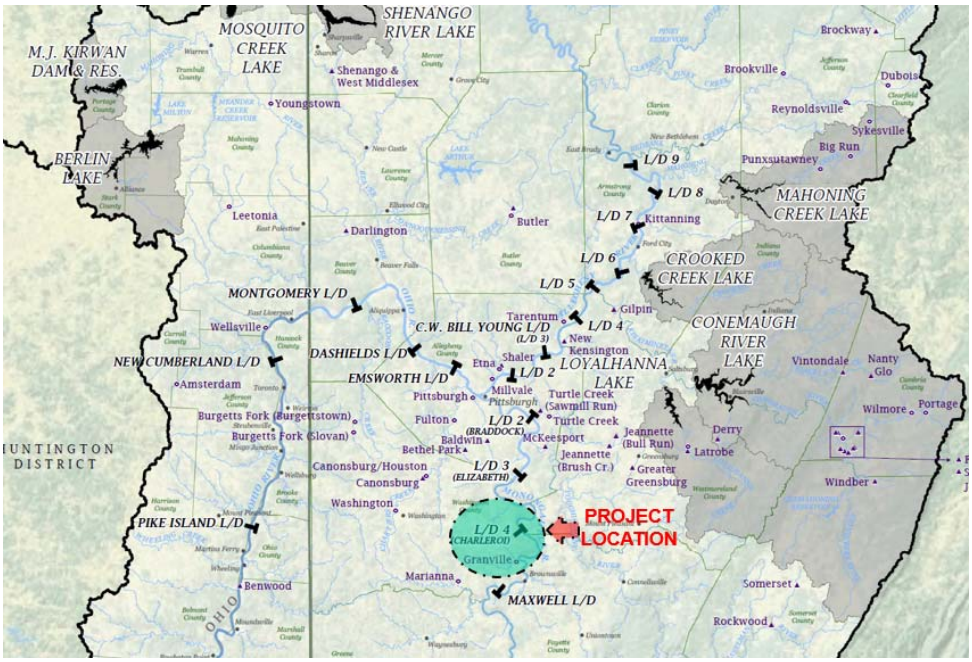


Fig. 1. Location map of the project site in northwest Westmoreland County, Pennsylvania

The new Charleroi locks has a through-the-sill filling and emptying system; therefore, the majority of the river wall does not contain any culvert or gallery and is essentially a rectangular wall section of solid concrete. The only complex monoliths (i.e. not a consistent rectangular shaped solid concrete section) were the gate monoliths and cross-culvert monolith which contains the emptying valves and operating gallery for the filling and emptying system; the culverts are inside the chamber and turn 90 degrees for depositing the emptying flow on the backside of the river wall. The miter gate and water culvert monoliths were constructed using the cofferbox method in which, in sequence, a small braced cofferdam is installed, a drilled shaft foundation and tremie slab installed, the cofferbox is dewatered, and the walls are constructed in-the-dry on top of the shafts and tremie slab. All of the other river wall monoliths used the non-cofferbox construction method in which the drilled shafts were installed (and their tops cleaned) in-the-wet, a full-height wall form work system was hung over the shaft foundation, tremie concrete was placed in the forms to bring the wall section out of the water, and conventional forming and concrete placement was used to bring the wall to its final elevation. The cofferboxes rely on and were structurally tied into the non-cofferbox wall sections; therefore, all of the non-cofferbox shafts and wall sections were completed prior to dewatering of the first cofferbox. See Figures 2, 3a, and 3b showing the cofferbox and non-cofferbox wall sections.

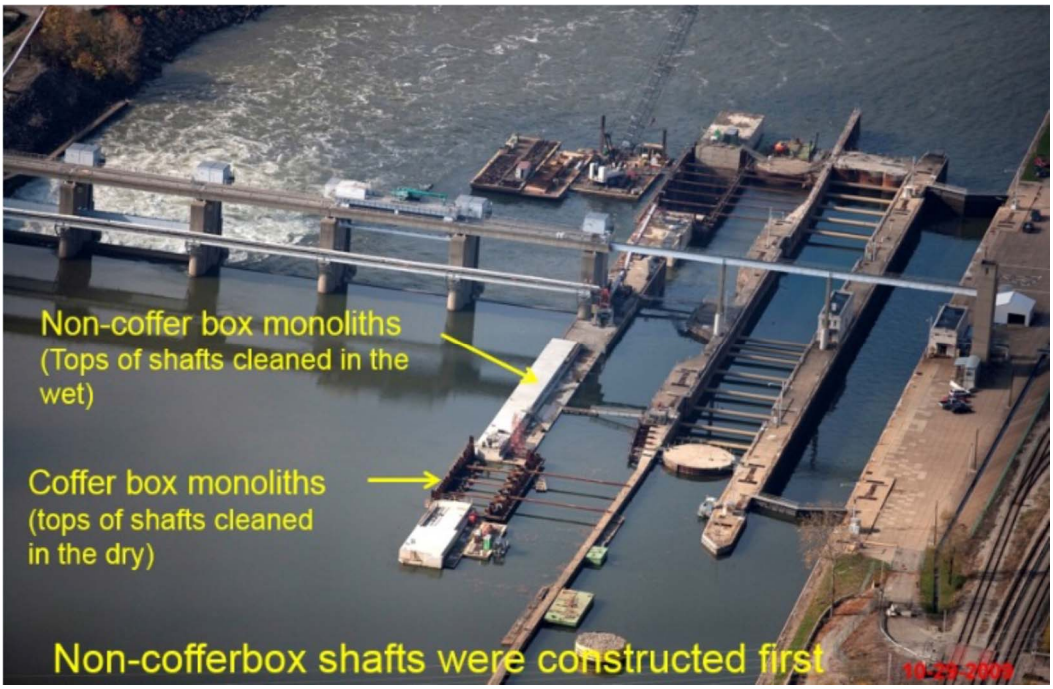


Figure 2. Cofferbox and non-cofferbox wall sections

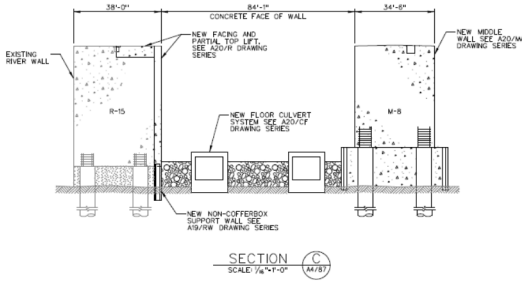


Figure 3a - Typical non-cofferbox monolith

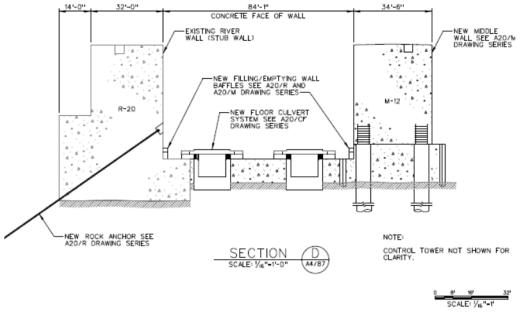


Figure 3b - Typical cofferbox monolith

DETAILS OF THE ANOMALIES AND THE REPAIR PLAN

The foundation for the non-cofferbox wall sections consisted of eighty-six (86) 78”-dia. shafts installed in-the-wet to support the new river wall and embedded 30-40 feet into limestone bedrock. The general construction sequence for the non-cofferbox wall sections consisted of the following steps performed in the wet: drill / core, clean out the hole, set the cage, place tremie in the shaft, verify shaft integrity via CSL testing (Figure 4), cut the casing, clean the tops of the shafts, install the non-cofferbox reinforcing cage over the shafts, place tremie concrete within the full-height forms, complete the walls using conventional concrete pour techniques once construction extends above the river elevation. From past experience, the project QC team ignored the CSL data at the top of the shafts showing somewhat slower strength gain in that region, due to its proximity to the water. The CSL sub-contractor did not provide comments on this area in their data report, since CSL testing was typically done when the concrete was still very “green” – usually, 6-7 days old. The results showed what, in the QC team’s opinion at the time, could have been misinterpreted as laitance or just weaker concrete due to water temperature, and thus disregarded.



Fig. 4 - CSL Tubes in completed shaft

The non-cofferbox wall sections were placed on top of the drilled shafts and the cofferboxes were installed to facilitate completing the wall sections (Figures 5a and 5b). The construction of the cofferbox wall also included drilling and placing the drilled shaft foundations "in-the-wet". The shafts sockets were hydraulically cleaned prior to placement of mass concrete. Divers were also utilized for additional quality control. They manually checked and cleaned (as necessary) the top of each shaft; however, cleaning inside the cage was difficult (due to low visibility and access) as the cage protruded +/-7' above the top of the shaft concrete and the river water was murky due to turbidity. The process was much more straight-forward for "in-the-dry" construction: once the tremie seal portion of the cofferbox was placed, the cofferboxes were dewatered; and the drilled shaft casing and the top of each shaft were cleaned in the dry.


Fig. 5a - In-the-wet shaft construction Part I



Fig. 5b - In-the-wet shaft construction Part II

When the first cofferbox was dewatered, a significant amount of latent material at the top of the cofferbox shafts (Fig. 6) was observed. This did not pose an issue for the cofferbox wall sections as the tops of the shafts could be cleaned in the dry prior to placing the first conventional lift of concrete; however, this did raise concern over anomalous material at the top of the non-cofferbox shafts. A review of the QC data did not provide a clear indication on whether anomalies were encountered and if they were, that they had been removed. Therefore, the Government directed the contractor to perform a selected exploratory drilling program on the non-cofferbox drilled shafts which revealed that there was an anomaly present at the top of the non-cofferbox drilled shafts at the interface of the top of the shaft and the bottom of the wall. The overall exploratory program took four months to complete, and revealed presence of the anomalous material (aka laitance) in all but one (1) shaft; the thickness of the anomalous material varied from a fraction of an inch to up to 24 inches.



Fig. 6 - Laitance on Top of the Cofferbox Drilled shafts

The anomaly was encountered at the top of the shaft/bottom of the wall connection, which is the critical load transition zone where the maximum moment and the maximum shear load is transferred from the monolith into the drilled shaft foundation. This cross sectional area experiences load reversal from compression to tensile depending on the pool elevations and dewatering scenarios. The typical non-guide pipe shaft has the following details; the top 11' 6" of the drilled is cased with a ½" thick steel casing and the rebar cage extends upward into the monolith another 13'6". The guide pipe drilled shafts also have a 24" diameter steel pipe at their center which was used to support the contractor's full height wall formwork system. Note that the drilled shaft steel casing was terminated beneath the monolith; therefore, it provides no moment carrying capacity at the top of the shaft. Fig. 7 shows the location of the anomaly at the top of the drilled shaft/ bottom of the wall interface.

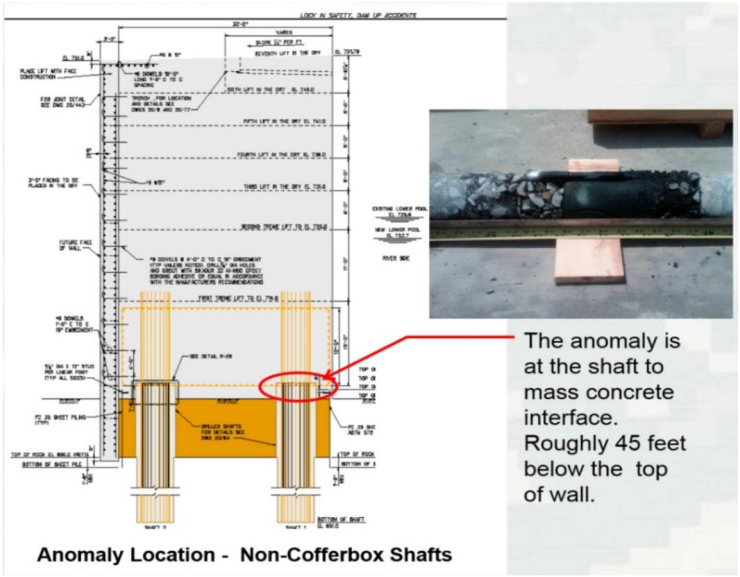


Fig. 7 –Typical anomaly location within the wall section

During the investigation phase, detailed analysis examining the biaxial strength and deformation was performed to determine the effect of the anomaly on the shaft capacity with the assumption that the anomaly existed over the entire cross section. It defined two critical compression zones for carrying the required load transfer and load reversal. The critical zones were quantified numerically through a detailed analysis

examining the biaxial strength and deformation (Fig. 8). The analysis revealed that deficiencies within the critical zone needed to be fully removed and restored (via pressure grouting) in order for the load-carrying capacity and performance requirements (deflection criteria of the wall) to be maintained for the design load cases.

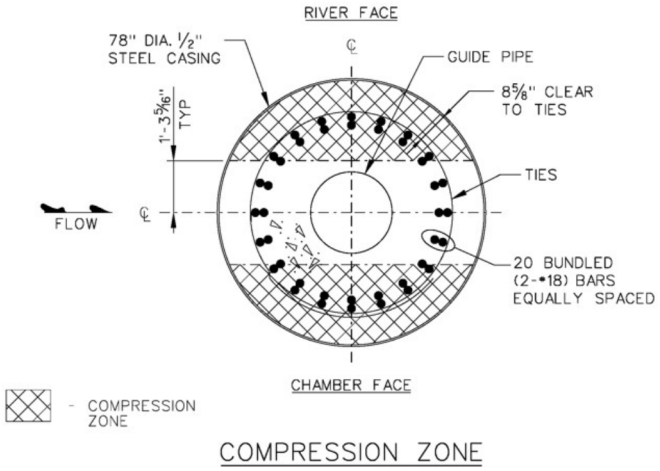


Fig. 8 – Cross section showing the critical compression zones for repair

Further, analysis on the guide pipe shafts concluded that the interior of the guide pipes did not need to be cleaned and repaired; the axial and bending moment capacities of the 24" diameter x 5/8" ASTM grade 50 steel pipe was greater than a 24" plain concrete column.

Acceptance Criteria and Repair Plan

The Acceptance criteria developed by the Government provided the details for each shaft to be repaired through the full removal of the anomalous material and filling the void with a designed grout as required to re-establish the joint and the load carrying capacity of the shaft. The Contractor was responsible to develop the repair plan and to identify the means and methods that would be used to clean and grout the shafts.

Cleaning Phase

The most critical and challenging aspect of the repairs was for the anomalous material to be fully removed over the critical compression zones. The Acceptance Criteria required the contractor to demonstrate their cleaning and grouting methods on two shafts prior to production. A shaft with a thick anomaly (i.e. greater than 7") and another one with a thin anomaly (i.e. less than ½") were selected to fully demonstrate the repair capabilities. Verification of the demonstration revealed that the method was not successful as there were voids at the top surface. The contractor then revised their repair plan and performed a new demonstration using two cleaning holes in the non-guide pipe shafts and four cleaning holes in the guide pipe shafts; the guide pipes were an obstruction and required additional cleaning holes to be placed. As the cleaning progressed, additional cleaning (aka flushing) holes were added as required to completely remove the anomalous material. The cleaning was performed using a specialized Hayward-Baker "super-jet" cleaning rig; triple super-jet technology was developed specifically for the project. It utilized high pressure water jet with three nozzle inclinations (straight and angled (20-degree from vertical, both up- and down-ward) – hence "triple jet") sheathed in air to clean the anomalies from laitance. The set-up was lowered into each hole in sequence, while an air lift was lowered into another (vacant) hole to evacuate water / eroded solids. With average jetting pressure of up to 4,500 psi, flow rate ranging from 40 gpm (high volume) to 125 gpm (high pressure), lift rate of 0.3 – 0.4 ft/min, and rotational speed of 1-3 rpm, vast majority of shafts were cleaned successfully.

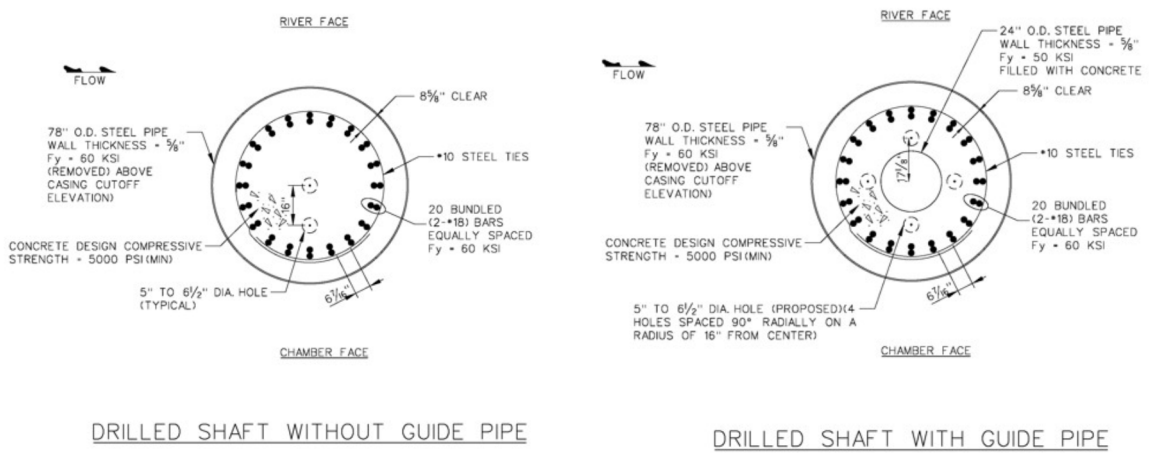


Fig. 9 – Showing the cleaning holes locations in the drilled shafts, as originally proposed

Cleaning Verification

Once the shaft was cleaned, a high-resolution GeoVision Dual Scan down-hole camera with high intensity LED lights, 360-degree vertical and horizontal tilt and pan was utilized in the field to provide a full record of the cleaning results in each hole (see Figure 10 for a screen shot example). A Government representative provided on-site quality control full-time.



Figure 10 – Video Camera shot of a Typical Cleaned Anomaly (44.9' below top of monolith)

The recorded videos were interpreted in the office later on by the Government quality assurance representative who developed sketches to depict the cleaning of the top and bottom surfaces (Figures 11 and 12).

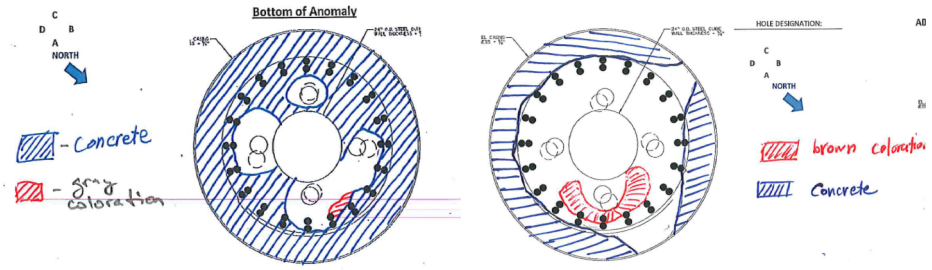


Fig. 11 – Examples of the cleaned (thin) anomaly zone shape as QA-sketched from the video

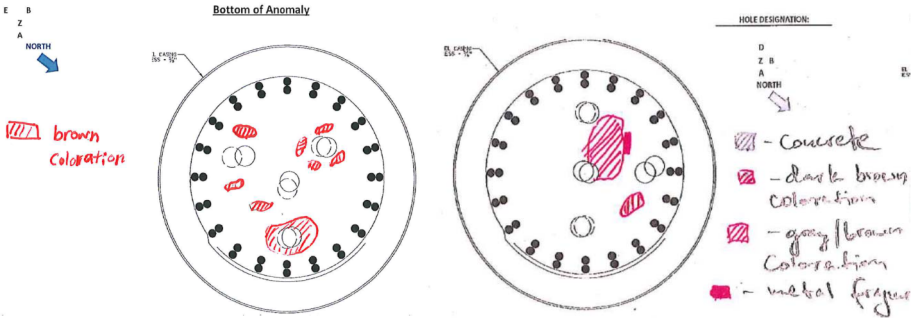


Fig. 12 - Examples of the cleaned (thick) anomaly zone shape as QA-sketched from the video

Repair Grout and Grout Placement

The critical aspects for the grout repairs were: for the shaft to be fully cleaned over the cross section (even though the analyses only required repairs in the critical compression zones); for the grout to fill the entire cleaned anomaly area; for the grout to achieve its full design strength; and for the joint (i.e. the top of the drilled shaft/bottom of wall joint) to be re-established, meaning full (no-void) contact between the grout and the concrete surface(s). The repair grout was the critical component for filling the entire void and to provide the full contact required. The grout had to have a combination of zero bleed, zero shrinkage, and considerable strength. Through a long process of trial batching, the contractor received approval to use "*Masterflow 1206"* grout (manufacturer: BASF). In addition, to assure the full contact, the grout was placed using packers. After the grout was placed, a packer was installed in each hole and the grout held under 50 psi pressure for five (5) minutes. This allowed the grout to fully fill the void area (of the removed anomaly) and provide the full contact required.

QUALITY CONTROL AND ASSURANCE OF THE GROUT REPAIRS

Three (3) verification core holes were drilled in each shaft after the grout fully cured (i.e. in 28 days). The verification holes were located in the critical compression zones. The core holes were also located based upon questionable features and imperfections as observed and documented in the cleaning phase video evaluation (see Figures 11 and 12 for examples). The verification cores were inspected by the Geotechnical lead to verify that there were no voids in the grout, at the grout / shaft (floor of the anomaly void), and/or grout / bottom of wall (roof of the anomaly void) interfaces. In addition, the GeoVision camera was lowered down all of the repair verification holes to inspect the grout in-situ. It was common for the extracted core to exhibit cracking throughout the repair grout – see Figure 13 for a typical set of pictures to document each verification core; however, the camera inspection revealed that the in-situ grout was intact and not cracked, thus indicating that the cracking occurred due to coring and extraction. A Government rep was present on-site full-time to provide quality control. The recorded videos were interpreted and documented in the office later on by the Government quality assurance representative. In addition, NX-sized cores taken through the grouted anomaly were logged and photographed in the field by the Government full-time geologist, and later on evaluated in the laboratory by the Government quality assurance representative (including strength testing, where applicable).



Fig. 13- Example cracked repair grout photos to document grout repair

Grout Strength Verification

In order to verify the in-situ strength of the repair grout, QC/QA grout cubes were produced for each shaft. The cubes were manufactured using return grout - that is the grout was injected into the repair location and exited through the relief port with the intent that the grout cubes had similar properties as the grout in the anomaly repair. Grout cubes were broken at 3, 7, and 28-day intervals to assure compliance with project design strength requirements. In addition, in instances that the extracted verification core had grout of adequate thickness to compression test (2 times the diameter of the core), the core was saw-cut and the in-situ repair grout was compression-tested. Both the QC/QA grout cubes and the compression tested core samples verified that the repair grout was achieving its required design strength.

Results of the Grout Repairs

Of the eighty-five (85) shafts repaired, seventy-four (74) were able to be cleaned and successfully repaired using the grout only. Of the eighty-five (85), there were eleven (11) instances in which the verification coring revealed a small void at the top of shaft/bottom of wall joint. For these shafts, the verification core holes were flushed (if needed) and a secondary grout was once again placed, with packers used to maintain 50 psi pressure for 5 minutes. Because of the minor nature of the voids encountered during the verification phase, a second round of verification coring was not required.

Structural Repair

Nine (9) shafts could not be fully cleaned over the critical compression areas despite numerous attempts. For the subject shafts, the camera inspection was used to develop a plot of the top and bottom surfaces to detail anomalous material remaining in the critical compression zones. From that data, a cross-sectional mesh was developed for the roof and floor surfaces of the deficiency zone (Fig. 14); the mesh allowed for a standard approach to quantify location and size of the zone for structural evaluation of the critical load transition. Step two was to perform a Finite Element sectional analysis (F.E.M.), using the BIAX computer software, of the upper and lower elevations of the drilled shafts under review. Of the nine shafts (9) evaluated, only four (4) were found to need a structural repair in addition to the grout repair. The structural repair consisted of placement of structural steel bars at locations determined by the analysis. Four (4) core locations for the structural bar placement were determined necessary for all four shafts. The locations required accurate positioning to maximize the effectiveness of the structural repair and were required to be within the allowable tolerance. Upon coring and cleaning the hole, the contractor was permitted no more than 24 hours to place and grout the structural repair bars after the holes were confirmed to be in proper

location and clean. As in all borehole verticality and location survey determination on this project, Boretrack™ Alignment surveys were performed in all holes. Two sets of *Masterflow1206* grout cubes (3 per set) were collected, for each repaired shaft. The cubes were compression strength-tested to ensure a compressive strength of 6,000 psi at 28 days was achieved in accordance with structural repair design plans and specifications.

Fig. 15 shows a typical structural repair bar installation detail; note that the structural repair bar spans between good material within the drilled shaft over the critical load transition zone and then into sound material within the monolith.

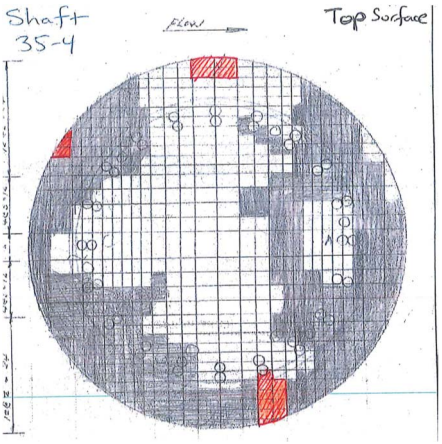


Fig. 14 – Example of FEM Structural Mesh Input

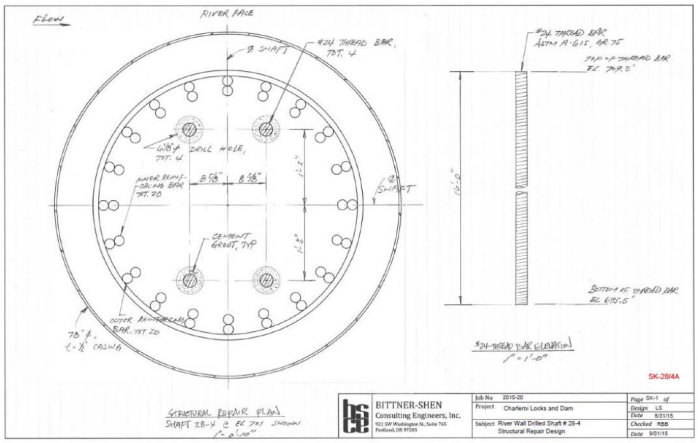


Fig 15 – Typical Structural Steel Installation Detail

Post –Repair Performance

Performance of the repaired shafts, as compared to the as-designed drilled shafts, was an area of concern and was evaluated. Displacement analysis was performed on a structurally repaired shaft which required the largest amount of structural steel needed to meet the shaft's load demand. The displacement analysis determined the difference of the displacement at the top of the drilled shaft between the as-designed and as-repaired section. The analysis utilized an equivalent elastic approach to further determine the lateral and vertical displacements. The analysis yielded a negligible increase of 0.0063" in lateral displacement at the top of the drilled shaft in comparison to the original design indicting that the repaired shafts will function as originally designed.

CONCLUSION AND LESSONS LEARNED

When anomalies were detected in the non-cofferbox drilled shafts, there was concern that the project could be jeopardized. Investigation revealed that, of the eighty-six (86) non-cofferbox drilled shafts, eighty-five (85) needed to be repaired. The Government and the contractor worked together as a team to successfully remove the anomalies and re-grout the anomaly voids. A unique triple-jet system was designed and utilized to remove the anomalous material. The majority of the shafts (74 of 85) were repaired with grout only. Shafts that were not able to be fully cleaned required structural evaluation; four (4) of these shafts required a structural repair which included the installation of steel bar to span the anomaly zone. Some of the repairs (11 of 85) required a secondary grout placement to fill a void at the top of repair/bottom of wall interface. By working together in gathering, tracking, and reviewing the various components of the repair data, the project team, consisting of the Government (the Owner), the Contractor (with various subs), and Engineering Consultants to both parties, ensured all of the shafts were successfully repaired.

Following are lessons learned from the Charleroi non-cofferbox drilled shaft repairs:

- From the owner's perspective, developing a detailed repair plan with clear acceptance criteria and strict adherence to the acceptance criteria is beneficial.
- Requiring the contractor to perform a demonstration repair to verify their proposed means and methods is an essential step in achieving successful repairs and allows for modification of the means and methods prior to production mode.
- There is a lot of data to be managed once the repairs are in production mode. The development and use of standardized forms for documenting the cleaning and repair verification phases was essential in allowing the Government team to review and provide direction to the contractor in a timely manner.
- Close coordination and communication between the Government and the contractor was required on the cleaning verification phase. The drilled shafts needed to be completely cleaned in the compression zones and the contractor was frequently required to re-clean shafts in order to meet the acceptance criteria. In several instances, the contractor had to decide if additional cleaning or structural evaluation and potential structural repair was a better option than spending excessive time cleaning any given shaft.

ACKNOWLEDGEMENTS

The author would like to acknowledge multiple field and office engineering and construction personnel of the USACE-Pittsburgh District, for spending countless hours on this project, including nights, weekends, and holidays (at multiple points in time, several overlapping operations, such as coring, cleaning, down-hole videoing, and grouting were taking place). Thanks also go to the Contractor and its jet-cleaning sub for designing and fine-tuning the innovative triple-jet cleaning system, keeping the project on-schedule, and effective field communication with the Owner.

MANAGING SOE CONSTRUCTION RISK THROUGH DESIGN-BUILD SYSTEMS

Rob Jameson, VP Construction Engineering, Malcolm Drilling Company, San Francisco, CA, USA
1.415.901.4400, rjameson@malcolmdrilling.com

ABSTRACT

The demand for commercial and residential construction has continued to evolve across the United States over the last decade. Our markets demand larger, deeper and inherently more complex structures, located within increasingly constrained urban locations and with challenging geotechnical conditions. As project demands incrementally escalate, specialty contractors are continuously challenged to extend their state of practice. Development in the size and capabilities of construction equipment, tooling, techniques, monitoring and verification systems over the last decade has consistently allowed contractors to build larger and deeper. For support of excavation (SOE), in addition to scale, selection of the most appropriate system has been a key to success in the most challenging ground conditions. This selection process is based on sound engineering and construction practice, and also prior experience, both positive and negative. Ultimately many Owners have chosen to manage their risk of SOE construction through design-build contracts, which allows specialty constructors to optimize the balance of cost, schedule, scope and associated risk based on their local expertise. Successful implementation of a design-build methodology begins long before a contractor is selected, with identification of key project requirements and risk factors during the feasibility studies and design development phases. In these early stages of the project development, advice and budgets are frequently solicited from Specialty Contractors. The Owner, Construction Manager and Consulting Team will filter this input from multiple sources to provide their specific recommendations, develop construction documents and select the appropriate form of contracting. Only in the final stages, after award of a Design-Build Subcontract, can the successful specialty contractor directly influence risk management approach on the project. A case study is presented from Block 9 in San Francisco's Transbay District. This project demonstrates the incremental identification, assignment and mitigation of construction risk through the planning and design build process for SOE on the deepest planned excavation in San Francisco.

INTRODUCTION

The mature urban development market in United States results in high demand for complex Support of Excavation (SOE) schemes on constrained sites. The Design-Build approach can be applied to increasingly difficult SOE challenges, combining regional specialty subcontractor knowledge and experience in order to optimize solutions for cost and schedule. The most successful applications will involve early engagement of shoring subcontractors within the project teams, during feasibility and design development stages, in order to identify key scope and risk issues, and their potential solutions. Throughout the project development, it is important to reasonably assign responsibility for construction risks amongst the project stakeholders who are best able to control them.

This paper presents a case history for San Francisco's Block 9, a well-planned and successfully executed design-build SOE project in San Francisco's Transbay Redevelopment area. Throughout the 4 year period from the Developers initial proposal to the Redevelopment agency, through completion of excavation down to subgrade, the project team developed a series of increasingly refined SOE schemes, with corresponding scope definition and cost and schedule estimates. This program relied on early identification of key challenges and risks for the project, and evolved through multiple phases of proposals as first the General Contractor (GC) and then Specialty Shoring Subcontractor were engaged for the project. The scheme, cost and schedule refinements continued throughout construction in order to accommodate unanticipated conditions and events as they unfolded.

 © 2017 DFI Annual Conference, New Orleans, LA, USA

The project is presented from the perspective of the Design-Build Shoring Subcontractor and highlights key issues and program features that identified and mitigated construction risk throughout the process.

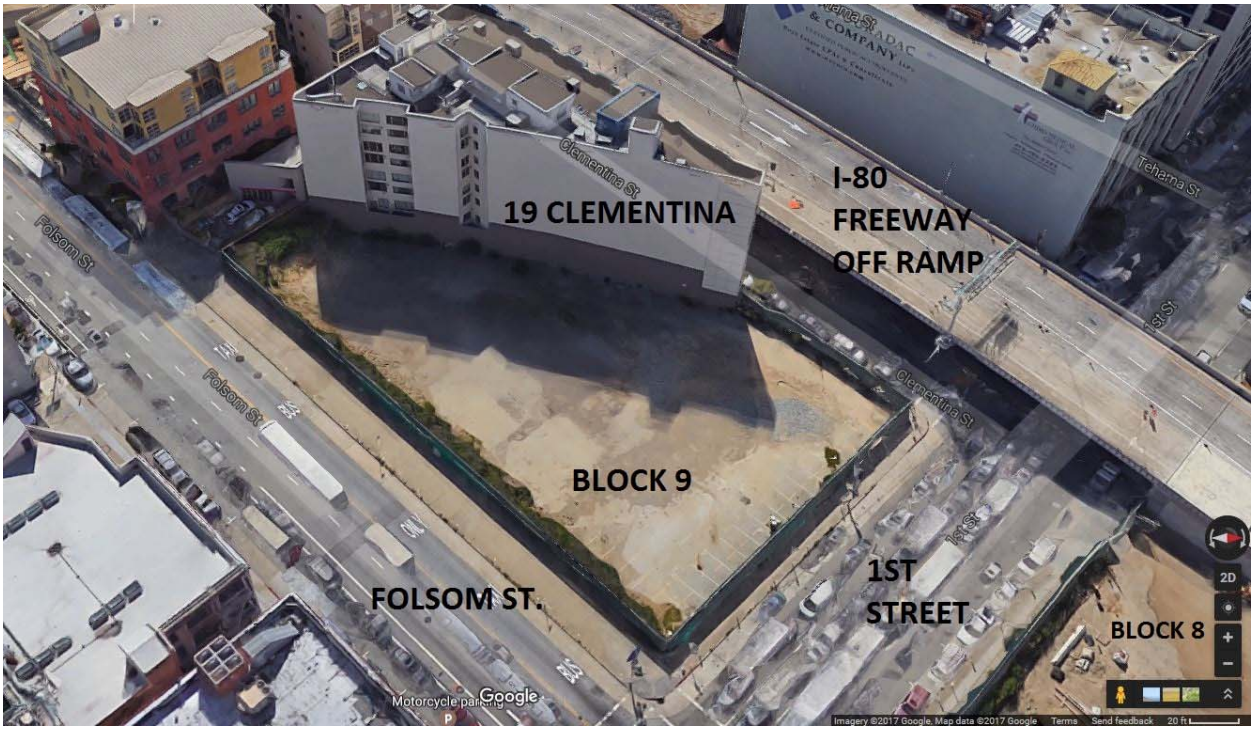


Figure 1: Aerial View of Site and Surrounding Conditions

PROJECT DETAILS

Block 9 is residential high rise development located at 1st & Folsom Street within San Francisco's Transbay Redevelopment Area. The irregular shaped lot is approximately 275 FT by 150 FT, constrained within the footprint of a now demolished freeway ramp structure. The northwest wall follows the curved property line of 19 Clementina Street, a mid-rise apartment building. The north wall abuts the State DOT right of way for an active freeway ramp which is supported on drilled shafts. Existing city streets, Folsom and 1st, run along the south and east perimeter respectively. The Transbay Block 8 redevelopment site is located across 1st street, to the east of the site. The complete Block 9 site will be excavated for a 6 level parking garage, extending from 63 to 77 FT below existing sidewalk grades. A 440 FT tower is proposed to rise on the center of the site, with podium structures extending to property lines on all sides.

The site is located on the north slope of San Francisco's Rincon Hill and the perimeter grades from Elev. 47 (SFCD) at southwest corner on Folsom street down to Elev. 36 (SFCD) in the northeast corner at 1st and Clementina Streets. A geotechnical section from southwest to northeast across this site is shown as Figure 2. The upper 10 to 15 FT of fill and dune sand are underlain by a thin layer of clayey and silty marsh deposits. The predominant ground within the excavation is the Colma Formation, a dense to very dense sandy soil with variable silt and clay components. In the southwest corner, base of the Colma is almost 30 FT above subgrade, and the interface between Colma Formation and the underlying interbedded sands and clays slopes down to the northeast at an average slope of 1 in 5. The bedrock, comprising sandstone and sheared shale of the Franciscan Melange Complex, is encountered 15 to 20 FT above subgrade in the southwest corner and will be excavated to reach subgrade over the western third of the site. The rock surface drops steeply and is over 80 FT below excavation grade on the 1st Street eastern perimeter. A layer of dense to hard interlayered sand and clay is observed in between the Colma and Bedrock. Design groundwater

table was set at Elev. +10, however after several years of drought, the groundwater elevation observed during investigation borings was at approximately Elev. 0.

The northern slope of Rincon Hill was developed with mixed residential and industrial use early in the Gold Rush era of San Francisco. After extensive damage in the 1906 Great Earthquake, this area was levelled and re-built. The Block 9 site was within the direct pathway into downtown from the Oakland-San Francisco Bay Bridge and was a key transportation corridor initially for rail and bus lines, and later an elevated freeway. Structural damage in the 1989 Loma Prieta earthquake, along with social pressure to remove the waterfront Embarcadero Freeway resulted in demolition of the elevated structure and the land area was assigned for redevelopment as the Transbay District. Eleven pile supported freeway footings were removed to grade, and then abandoned within the site footprint.

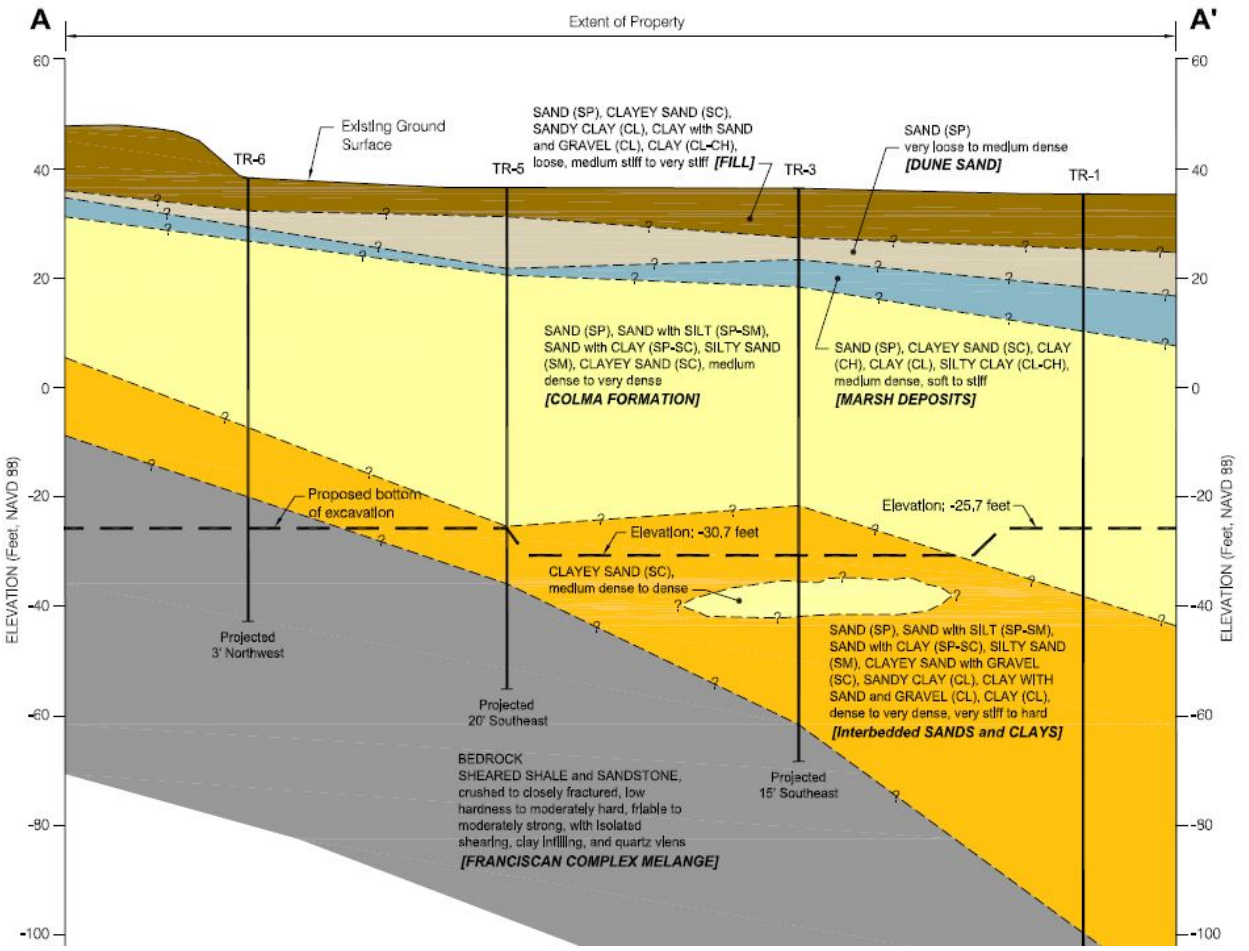


Figure 2: Geotechnical section from SW to NE across site (Langan Treadwell Rollo)

PROJECT TEAM AND DESIGN DEVELOPMENT

The Block 9 project falls within the Transbay Redevelopment area. The Transbay Authority issued a request for development proposals in Fall 2012. The successful development team, Essex Property Trust Inc. / TMG / Avant Housing were awarded the site in February 2013. Following 2 years of project development, the land purchase was finalized in February 2015. Essex Property Trust, Inc. began construction approximately 1 year later, after completion of design development and permitting.

Due to unusual depth of excavation and complexity of site, developers and their preferred general contractors solicited input for SOE feasibility and budgets from specialty contractors at the outset of the project. Initial contacts were made during Developer RFP period, and continued through GC selection in 2014 and final selection of specialty subcontractor in spring 2015. Malcolm was awarded the project in April 2015, based on a best value selection process from the GC. Groundbreaking was approximately 1 year later in spring 2016.

The SOE market in San Francisco is mature, with numerous deep excavations for high rise projects in the Transbay area having been constructed within the last 10 years. This local expertise results in both high quality initial evaluation and recommendations by the Owner's consultants, and similarly educated responses from the proposing SOE contractors. The majority of technical challenges encountered on the project were identified in the early RFP's for budget proposals, including:

- Abandoned footings and deep foundations from demolished freeway structures
- Encroachment limitations for tieback anchors below adjacent structures and freeway
- Groundwater table up to 40 FT above excavation subgrade
- Support and protection of adjacent structures, facilities and utilities, particularly the apartment building on shallow foundations along northwest wall alignment
- Sloping site topography with top of bedrock encountered 20 FT above subgrade in southwest corner and dipping 100 FT across the site footprint.

Throughout the conceptual development and budget phases, multiple specialty contractors provided cost and schedule estimates, but critically, also highlighted the available capabilities and limitations for cost effective state-of-practice construction. Input from these specialty contractors was employed to evaluate feasibility of many excavation configurations, enabling the Ownership group to select an optimal configuration. These budgeting exercises evaluated:

- Various depths, ranging from 4 to 7 levels with final design based on 6 sub-surface floors.
- Direct underpinning support to adjacent structures in comparison to stiff, impermeable SOE walls designed for surcharge loading along face of structure.
- Comparison between internal bracing and tieback anchors in response to potential to easement limitations from adjacent property owners around site perimeter.

Throughout the 30 month period of design development, the invited Specialty Contractors provided feasibility, budget and scope refinement recommendations to the Ownership Team, and on occasion directly to the Geotechnical Engineer. The Specialty Contractors highlighted areas of technical concern through both the narrative and qualifications presented in their proposals. These issues could then be scrutinized for cross-comparison and bid-levelling between the proposers. The risk management objectives for the Speciality Contractors were to establish realistic client expectations for scope, pricing and schedule which would address project challenges within their control and and allow them to offer a competitive proposal for final selection.

RFP REQUIREMENTS AND SELECTED SOLUTIONS

The final round of proposals for SOE Subcontractor selection were issued in the spring of 2015. Through the design development process, excavation geometry and constraints were refined including the notable adjustment to set-back permanent structure by 3 FT from Northwest property line. This allowed construction of a stiff shoring system along the face of the adjacent apartment building, instead of direct underpinning. Plans of the historic freeway structures over the site, with details on the abandoned in-situ

foundations were included in the SOE RFP. The final Geotechnical report advised that either soil mix retaining and cut-off walls could be employed, or soldier piles and lagging in combination with dewatering. However, the General Contractor scope requirements limited proposals to only the soil mix approach and precluded the use of tieback anchors below groundwater table. At the time of RFP, easement agreements were still under negotiation with the adjacent property owners and the State DOT, and a range of alternates were requested to accommodate the potential outcome scenarios. Critically for this project, the Geotechnical report included realistic estimates of ground deformation due to both shoring deformation and potential for dewatering induced settlement, compatible with the recommended SOE approaches.

The procurement program included initial proposals, followed by review interviews, then final updated best and final submittals. Subcontractors were permitted to note qualifications or exceptions to the RFP requirements, for consideration by the GC and Owner during their final selection of best overall value proposer. Malcolm's proposed SOE system, illustrated in Figure 3, addressed known project conditions and challenges as described in the follows paragraphs.

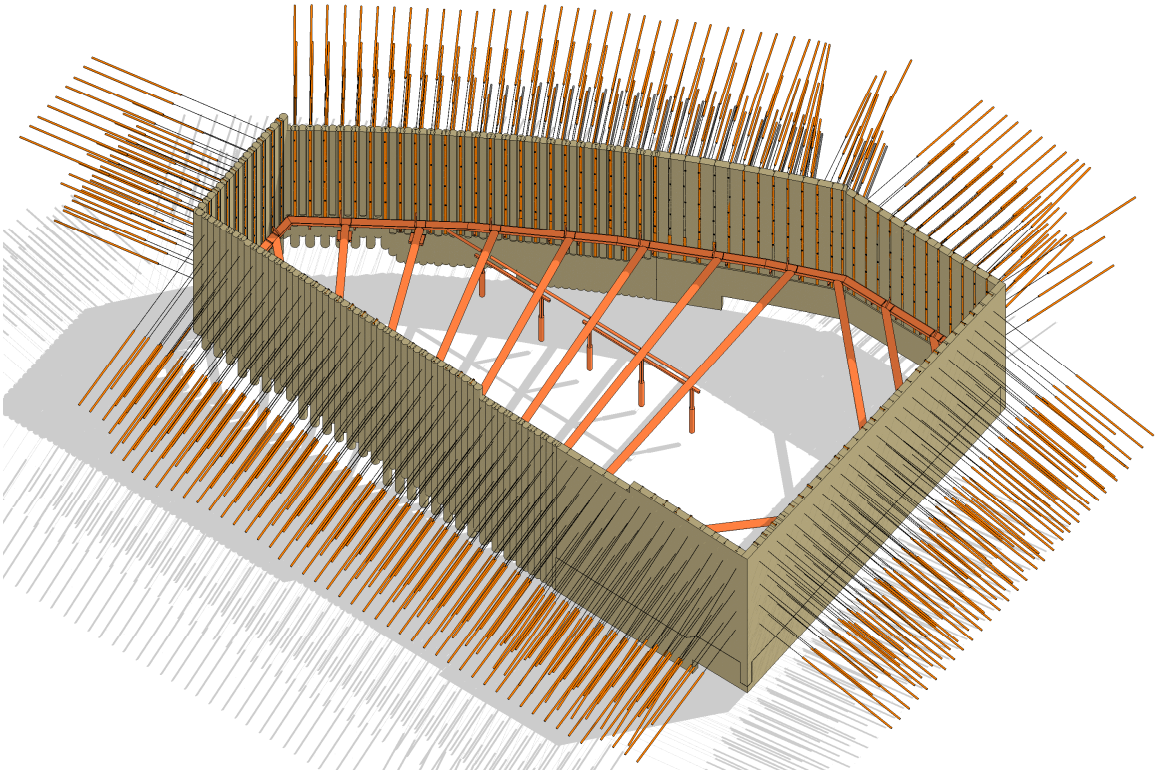


Figure 3: As-designed Support of Excavation Scheme

ABANDONED FOOTINGS FROM EXISTING FREEWAY: For footings and piles in direct conflict with the shoring wall alignment, a pile and lagging shoring shoring system would be used to expose and demolish the pile caps. The underlying piles would be drilled out using a high-powered rotary top drive rig. Pile caps and footings located within the site perimeter which did not conflict with the shoring system would be removed during mass excavation.

GROUNDWATER CONTROL: Construct low permeability site perimeter wall, with minimum toe length of 17 FT below soil subgrade, or keyed at least 3 FT into bedrock. Per RFP, no penetrations for tieback anchors were proposed below the observed groundwater elevation.

SLOPING BEDROCK INTERFACE: Cutter Soil Mix (CSM) walls were the preferred technical, cost and schedule solution for shoring construction. The CSM system employs two counter-rotating cutter wheels which advance into the ground and blend it with an injected cement slurry. This system creates rectangular panels of cemented soil which are overlapped to create a shoring wall. Due to concern over the ability of CSM to penetrate into the rock at western portion of the site, Malcolm's shoring scheme proposed a combination of CSM and secant drilled piling. In secant piling, a series of overlapped drilled shafts are constructed to form a continuous wall. The soldier pile spacing was selected to allow for either method of wall construction, and thereby optimized potential to use the faster and cheaper CSM method, subject to its ability to advance in the rock. Figure 4 presents layout employing both CSM and secant piling methods.

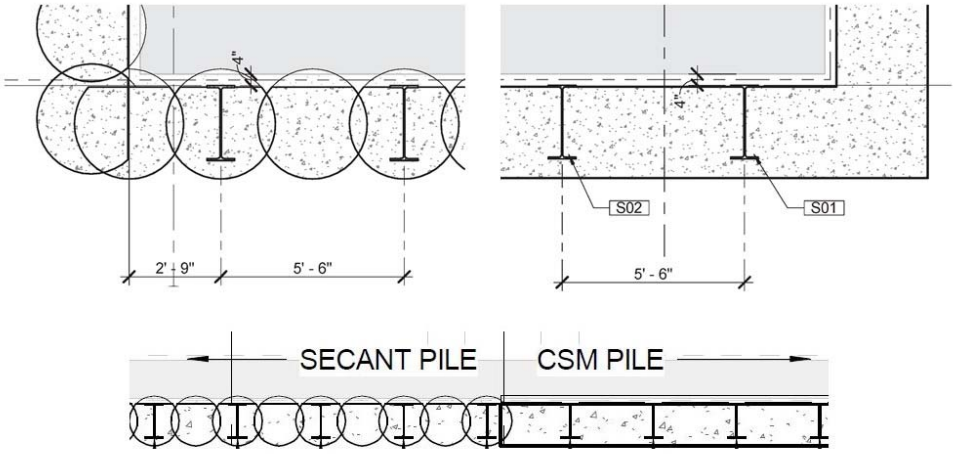


Figure 4: Secant Pile and CSM Wall Layouts with uniform soldier pile spacing

CONTROL GROUND DEFORMATION: The planned depth of excavation ranged from 63 to 77 FT below adjacent sidewalks. Based on standard empirical methods, lateral deformation and adjacent settlements were estimated for this exceptional height of retention system. In order to minimize ground deformation, the SOE walls were designed as stiff structural elements with very heavy steel beam reinforcement. W27 steel sections with weight of 84 to 117 LB/FT were to be installed along east, south and west walls. In order to accommodate the increased span below bracing at the deep central core, a steel heavier section was spliced into the wall. W24 steel sections were installed due to the limited clearance along the 19 Clementina structure. The lateral support was planned with up to 4 rows of post-tensioned anchors and two levels of internal pre-loaded bracing elements. Typically anchors were 4 to 6 strands in the upper rows, with 6 to 8 strands required on lowest level due to the added pressure from groundwater. Design accommodated at-rest active earth pressures adjacent to existing structures, resulting in tightly vertical spacing and an additional row of anchors on the part of northwest wall directly below the 19 Clementina structure, with wider vertical spans on the other walls to resist active design pressures.

EASEMENTS: The preferred SOE support schemes included tieback anchors. In order to employ tiebacks around the full perimeter, temporary easement agreements would be required with the adjacent property owners and agencies. A menu of different bracing configurations was developed to allow for the contingency that easements could not be obtained from any of these individual parties.

COST & SCHEDULE: The preferred solution for SOE was a reinforced CSM wall with tieback anchors. However in order to accommodate uncertainties and risk over rock penetration, easements and groundwater control, the selected scheme allowed for interchange with more robust drilled secant piling and internal

bracing elements along partial lengths of the shoring wall alignment, with corresponding schedule adjustments quantified in the proposal.

Key qualifications offered by the SOE Subcontractor were that the proposed scheme was anticipated to perform within the range of ground deformation identified in the geotechnical report based on sound construction practice. However the inherent risk that this magnitude of deformation may not be acceptable to, or could cause impacts to, adjacent properties and facilities remained with others. In addition, although the SOE contractor developed a work plan to address the known freeway footings, any impacts related to other unforeseen subsurface obstructions was excluded and would treated as a Contract Change. The Subcontractor proposal clearly identified any other technical exceptions or clarifications to RFP documents.

Through the negotiation period, the scheme was refined to optimize cost and schedule by installing 1 row of tieback anchors below groundwater level in place of the upper bracing level. This approach relied on center pockets on the soldier piles for ease of ground control during drilling, and for sealing after the anchor was installed and stressed. A full depth tieback solution was evaluated but rejected since the increased risk of installing anchors over 20 FT below groundwater table was consider by all parties to exceed the potential cost and schedule benefit of eliminating the lowest internal bracing level.

The overall SOE scheme was selected to manage known challenges and risks on the project. The SOE Subcontractor employed contractual mechanisms to limit their risk and exposure to factors within their direct control.

CONSTRUCTION

The shoring wall installation commenced in 2016, almost 4 years after the initial RFP to Developers was issued by the Redevelopment Agency. Overall, this time had allowed for careful evaluation of the project risks and requirements and development and contracting of an SOE scheme to meet the challenges. As always with Construction, several new challenges arose during the site operations, which were met and resolved to effectively complete the works.

Ultimately, the project owners executed temporary easement agreements with all the adjacent property owners, allowing the optimal tieback anchor solution to be employed around the full site perimeter. The most challenging was the State DOT where tiebacks were anticipated to advance and bond into ground in near proximity to drilled shaft foundations for the I-80 off-ramp along the north side of the project. In order to obtain the temporary easement into the State DOT right-of-way, design had to account a no-encroachment zone directly around each shaft. A full-scale test was required to demonstrate the ability to maintain direction and tolerance on anchor alignment during drilling in order to maintain the no-encroachment zone, and to show that stressing of the anchor would not disturb ground directly adjacent to the existing drilled shafts. MDCI performed these tests during site preparation period, including down-hole alignment surveys using gyroscopic tools, under observation of the project Geotechnical Engineer and State DOT representatives. After anchors were installed and surveyed, inclinometers were laid out at pre-determined offsets from the bond zone and continuously monitored during loading. This study satisfied the State DOT that anchor load transfer would not impact the adjacent shafts, and the easement was granted.

UNANTICIPATED OBSTRUCTIONS: The shoring scheme was developed to accommodate the known abandoned freeway footings and piles. However, during the planned site clearance activity, numerous other earlier foundation elements were identified, in many cases underlying the abandoned freeway footings. These remnants from earlier land-use dated from pre-1906 earthquake and from levelling and reconstruction in the early 20th Century before the freeway construction. In the most challenging cases, some concrete structures were identified which straddled property lines redrawn in the 1950's around freeway alignments and which were partially buried below adjacent occupied structures. A comprehensive program for

obstruction removal was developed and implemented, including trench shoring and sequential slot cutting, along with supplemental temporary pile and lagging shoring walls on the street perimeters.

INTERFACE WITH ADJACENT CONCURRENT DEVELOPMENT: When the project ultimately started in 2016, the excavation was advanced concurrent with a 40 FT deep soldier pile and lagging shoring system at Transbay Block 8, located on the opposite (east) side of 1st Street. Shoring schemes for both projects employed tieback anchors with maximum length of approximately 80 FT, which extending across the full street width from their respective property lines. Malcolm was the shoring subcontractor on both projects, and therefore was able to address and manage risk of damage to previously installed anchors on opposite sides of the street. A 3D BIM model was developed in order to identify potential conflicts. Minor layout adjustments allowed a nominal 30" minimum clearance between any interlaced anchors. For block 9, soldier piles had already been installed, adjustments were limited to 1 degree. For the adjacent Block 8 project, a total adjustment of up to 3 degrees was allowed for both beam installation and anchor alignment. Three walers were added to the interior face of Block 9 east wall in order to allow for load redistribution into adjacent piles in the event that existing pre-loaded anchors were hit and damaged during drilling on Block 8. In total, 100 interlaced anchors were constructed between the two projects, and by use of BIM to refine design, and careful field controls on layout and alignment, no anchors were compromised throughout this process.

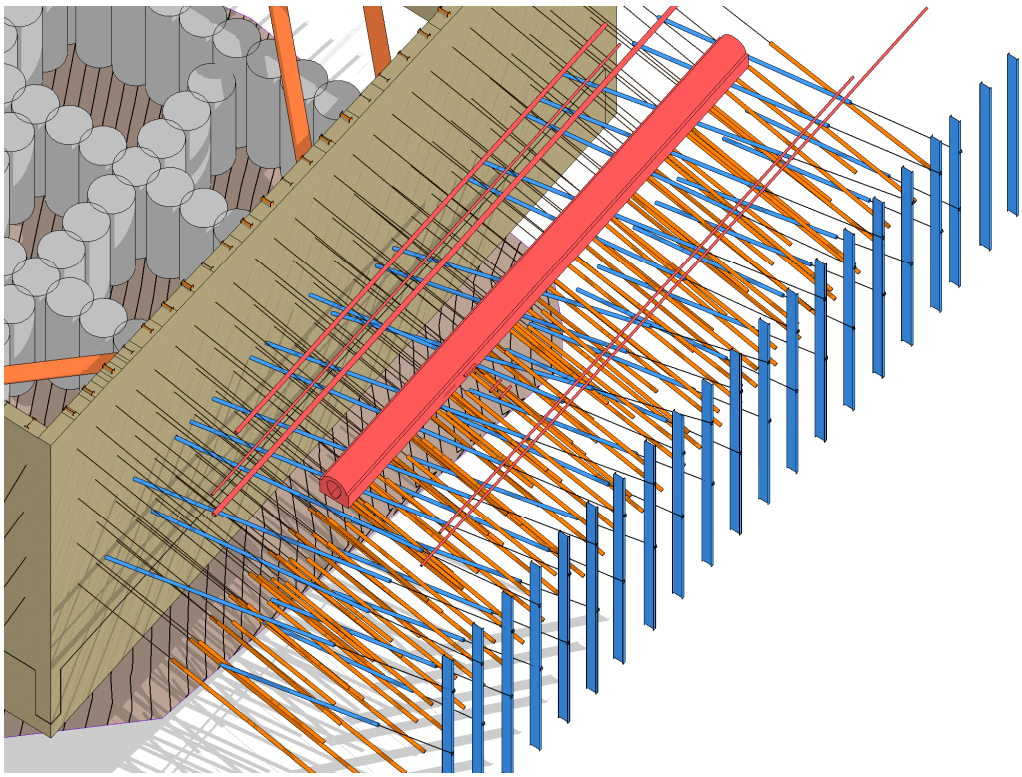


Figure 5: 3D view showing interlaced anchors and utilities below 1st Street

ROCK PENETRATION: The contractor work plan allowed for a combination of secant piling and CSM methods to construct the perimeter wall. CSM is the preferred solution since there are fewer joints, lower unit cost and faster production. Based on initial evaluations of the rock profile, MDCI anticipated approximately half of alignment would be constructed using each method. During construction, MDCI employed pre-drilling using an auger in order to break-up ground and facilitate CSM penetration into the Franciscan bedrock formation. Through this construction program, CSM was successfully employed along

over 90% of the site perimeter. The wall closure was completed with limited sections of secant piling in areas with the highest rock surface elevation and hardest rock conditions.



Figure 6: Excavation to Subgrade viewed from Northeast Corner

SYSTEM PERFORMANCE: The excavation for Block 9 was completed in early April 2017 and the system largely exceeded performance expectations. The geotechnical report had estimated deformation of 1 to 2", while in-wall inclinometers reported actual deformation of less than 0.75 inch, consistent with optical survey of targets on the shoring and adjacent structures. All walls experienced small movement (0.1 to 0.3 inch) back into the retained ground upon stressing of the upper tieback row. The 5 inclinometers around site perimeter all showed subsequent inward deformation during the remaining excavation. The maximum lateral movement at each location varied from 0.2 to 0.75 inches. The inclinometer in the west wall showed an order of magnitude variation in lateral deformation between the soil overburden (up to 0.2 inch movement) and the underlying bedrock (0.03 inch movement) which was present at lowest 20 FT of the exposed shoring wall. The perimeter cut-off walls were effective in isolating drawdown of groundwater within the excavation relative to adjacent areas. The drawdown within the excavation was recorded at 35 FT in the northeast corner. Groundwater outside the excavation at western end was observed to lower by 5 FT, however this is within range of seasonal variations. At the north east corner, a larger groundwater lowering outside the excavation was attributed to effects of a deep well system on the adjacent Block 8 site and a head differential of over 20 FT remained across the perimeter. The perimeter wall, bracing and anchor installation were performed within the timelines and budgets of the project. The main impact to schedule and cost was the removal of unforeseen obstructions which were encountered in addition known existing freeway footings.

SUMMARY AND CONCLUSIONS

Complex SOE can be successfully implemented by combining a well-informed client team and experienced contractors employing design-build to select appropriate shoring systems, optimized for cost and schedule. The groundwork for success is laid by identifying key risk and scope issues, and their potential solutions, early in design development. These construction risks should be assigned to the project stakeholder best able to control them. Although the specialty subcontractor is not formally engaged until late in the design development, their experience can have a large influence on the selected pathway for the project. The subcontractor's budgetary proposals can identify and highlight construction risks within their scope for review and evaluation by the Owner, GC and Design team. This allows critical risk issues to be mitigated by design modifications before permitting, or else clearly defined and assigned in the contract documents, and then managed by the selection of an appropriate temporary SOE plan. The subcontractors approach to critical risk concerns should be evaluated as part of the bid levelling and selection process. Shoring subcontractors should also retain the right to clarify risk assignment and limitations through the Subcontract language in the negotiation process. Once the SOE scheme is finalized, the Subcontractor is responsible to deliver their product in a cost effective and timely manner.

This case history of San Francisco's Block 9 presents the well planned and executed approach to SOE for an extremely challenging site. The project involved the deepest planned excavation in the Transbay District, addressed difficult soil, bedrock and groundwater conditions, known deep obstructions and provided tight deformation control for sensitive adjacent residential and freeway structures.

ACKNOWLEDGEMENTS

The author wishes to acknowledge the project team comprising of Essex Property Trust, Inc. and TMG Partners, the Ownership Group, Architects SOM and Fougeron, Structural Engineers SOM and Structus, and Langan Treadwell Rollo, the Geotechnical Engineer. The General Contractor was Balfour Beatty. Subgrade works executed by Malcolm Drilling included SOE, Dewatering and Subgrade Ground Improvement, with SOE Design performed by Brierley Associates, and excavation by EBi, as a second tier subcontractor to Malcolm. Special thanks to John Morgan of Malcolm Drilling, Eric Lindquist and Mike McTeer of Brierley Associates and Jeff Lambert of Essex Property Trust, Inc. for their assistance with preparation of this paper.

REFERENCES

Langan Treadwell Rollo, 2015. Updated Geotechnical Investigation Transbay Block 9.

PPP CONTRACT DELIVERY SYSTEM- CONTRACTUAL RISKS AND ETHICAL ISSUES REGARDING DEEP FOUNDATION SUBCONTRACTORS

Alexander Filotti, M.B.A., P.E., Underpinning and Foundation Skanska, Inc., Maspeth, NY, USA, 718-340-1021, alex.filotti@skanska.com
Richard Kalson, Esq. Partner- Benesch, Friedlander, Coplan & Aronoff LLP, Pittsburgh, PA, USA, 614.223.9380, RKalson@beneschlaw.com

1. INTRODUCTION- WHAT IS P3 OR PPP ?

The Public Private Partnership (PPP or 3P) is a project delivery scheme based on the government providing land and/or a concession agreement, and on a private entity providing the design, construction, financing, operation and maintenance of the project for an extensive duration of time (up to thirty years). At the end of the operation-maintenance period, the project is turned over to the public entity, which fully owns the project at all times. While there are many PPP delivery schemes used around the world, for the present paper, we are going to analyze the impact of the Design-Build-Finance-Operate-Maintain (DBFOM) scheme on the deep foundation specialty subcontractor. There are couple of reasons that the PPP delivery system started to be used and implemented not only by developed nations (e.g. United Kingdom, USA etc.), but also by the International Development Bank for delivering major infrastructure projects in developing nations. From the point of view of government agencies, some of the reasons to use PPP are the following:

- The primary use of private capital in an era where borrowing and/or supplemental taxation represents too much of a political risk. Budget deficits and taxation limits are extremely hot topics in every election (national or local) and the level of education of the electorate in this area is making it more and more difficult for politicians to use borrowed funds and additional taxation finance sources for public projects. At the same time, we see an increase in the social expenditures of the government in parallel with a needed increase in expenditures on infrastructure due to aging and neglect.
- Bundling the construction risks with the operational and maintenance risks naturally pushes the private entity to increase the level of innovation and communications in the primary phase (the construction phase) in order to develop future process based upon the innovation and communications utilized in the operation and maintenance phase of the project. This is true if contractual incentives are properly structured because "all revolves around incentives. In a world of 'incomplete' contracts, where it is difficult to foresee and contract about uncertain future events, it is important to get the incentive structure right" (Grimsey and Lewis, 2004).
- The transfer of very expensive risks such as differing site conditions, schedule, design, construction, maintenance and operation costs from the public authority to the private entity.
- The timespan of development and construction of a PPP project is usually shorter than the traditional procurement process (e.g. "… the I-595 P3 provided capacity improvements fifteen years sooner than a conventional plan would have offered. In Maryland, an innovative expansion of the Seagirt Marine Terminal in the Port of Baltimore was completed two years ahead of schedule due to the P3 model. As a result, the Port of Baltimore is only the second port on the US East Coast to have unrestricted access to both a fully functioning 50-foot channel and 50-foot berth.")

 © 2017 DFI Annual Conference, New Orleans, LA, USA

The study of the applicable literature shows that all of the aforementioned considerations are not positive and in the government's advantage on every type of project. Hart et al. (1997) concluded: "We have examined the conditions that determine the relative efficiency of in-house provision versus outside contracting of government services. Our theoretical arguments suggest that the case for in-house provision is generally stronger when non-contractible cost reductions have large deleterious effects on quality, when quality innovations are unimportant, and when corruption in government procurement is a severe problem. In contrast, the case for privatization is stronger when quality reducing cost reductions can be controlled through contract or competition, when quality innovations are important, and when patronage and powerful unions are a severe problem inside the government."

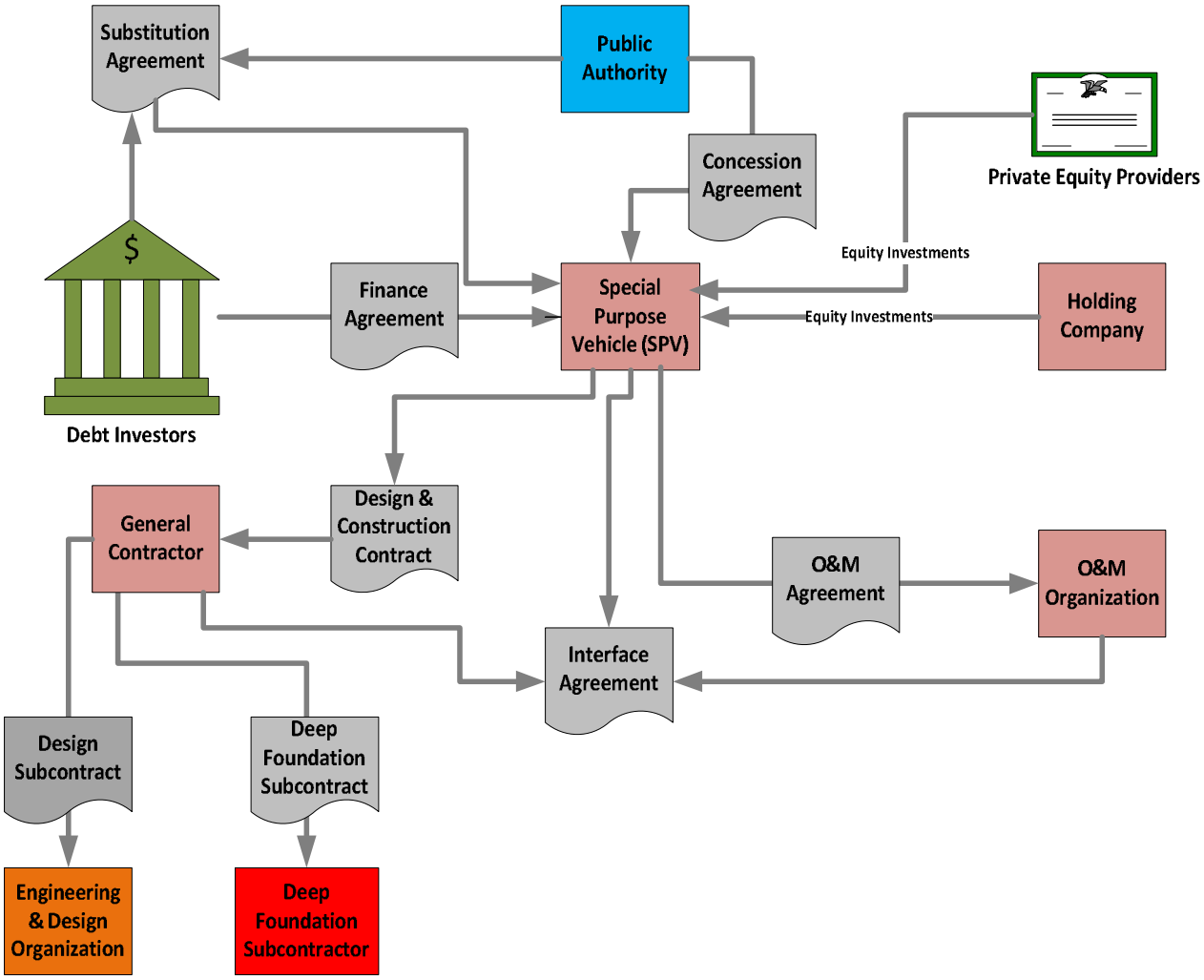


Figure No. 1
Contracting and financial relationship between the stakeholders of a DBFOM-PPP project

The figure shows the complexity of contracts and financial arrangements between the stakeholders, complexity accentuated also by the long duration of the relationship between the main players (up to 30 years). It is very clear from the theory of contracts, that for the public authority to gain the desired social function and public welfare from the project when all the design, construction and financial controls are in the hands of a private entity, the need for a faultless contract between the public authority and the special purpose vehicle is needed. Such contracts are put together by complex teams of legal, finance, and process specialists and requires an equally high level legal and management team to implement them. Hart (2003) states that ultimately the choice of government agency between PPP and conventional project delivery "…turns on whether it is easier to write contracts on service provision than on building provision."

2. THE IMPLICATION OF THE FINANCIAL STRUCTURE OF THE P3 ON THE RELATIONSHIPS BETWEEN THE STAKEHOLDERS

Looking on the organigram of the DBFOM in figure no. 1, a couple of things are worth noting:

- The General Contractor is a subcontractor to the special purpose vehicle (SPV) and the deep foundation subcontractor has a position of a second level subcontractor to the SPV being on the same line and position as the designer of the project.
- In order to separate the project from the private equity investors and the holding company(ies), and to limit their liability, a Special Propose Vehicle (SPV) company is created to hold the concession of the project. The shareholders of the SPV are the private equity investors and the holding company(ies). Most of the time, the holding company has as subsidiaries the company which manages the SPV or a part of it, the General Contractor and/or the Operation and Maintenance Company (O&M). In order to achieve all the function in the PPP project, the holding company must be a very large organization with vast capital resources and specialized divisions of infrastructure development, construction management, general construction and property management. The complexity and different role played by each division in the project lifetime creates divergent interests, contradictory goals, and personality conflicts, resulting in internal tensions that places the other stakeholders at risk having no leverage in resolving the internal conflicts of the holding companies. Our opinion is that these problems diminish as the project progresses due to the learning curve on each project and as these organizations perform more work on projects under the PPP delivery scheme.
- The shareholders and the financing institutions assert a tremendous amount of pressure on the SPV to deliver the project on time and at the quality parameters to guarantee a financially successful operation and maintenance phase of the project. All this pressure is channeled on the General Contractor and its subcontractors, deep foundation contractors included, to deliver the design and construction on a very fast paced schedule and with quality requirements surpassing the industry standards.
- The financial success of the project for the SPV shareholders is directly related to the success of the operation and maintenance of the project over its entire concession life. Naturally, this implies that all innovations and improvement of the design and construction that are geared to optimize the operation and maintenance phase will be pressed to be implemented, creating a highly dynamic design and construction

environment in which all the participants have to show flexibility and adaptability to change.

- Due to the fact that most of the financial risk is owned by the SPV, the public authority (owner) usually does not require that performance and payment bonds are provided for the project.

3. ROLE, RESPONSIBILITIES AND RISKS OF THE SPECIALTY DEEP FOUNDATION SUBCONTRACTOR ON A P3 PROJECT

The contractual and financial relationships between the principals of the DBFOM-PPP Project have profound implications on the deep foundation contractors operating on such projects.

a) Financial Implications
Only solid financial companies with the benefit of strong legal and management teams can execute subcontracts on a PPP project. The financial stability is also required to successfully implement all of the design and construction changes that are inevitable in a PPP project.

b) The deep foundation contractor has to be an innovative and flexible company to adjust to the dynamic environment of a PPP project. It must have a strong change management team to keep track of all cost implications of these changes. It has to be understood that rigid organizations which will not embrace change, endangering the project schedule, will be eliminated from the project team as a non-responsive organization. The pressure of the schedule is going to be incorporated from higher tier contracts in the form of substantial financial penalties (liquidated damages), therefore the need for good change management and cost management are paramount for the P3 project success of the deep foundation contractor.

c) In order to mitigate the internal tensions between different divisions of the holding company, as well as likely design changes, the deep foundation contractor should seek a collaborative relationship in order to gain a place as a design and construction partner at the general contractor's table. Our industry could bring a lot of value during the design and the construction of the foundation and should promote this created value in order to be recognized as a partner and not as a subcontractor. This collaboration and value can also mitigate another risk that the deep foundation contractor is subject to on PPP projects, the risk of not being paid.

d) The deep foundation contractor has to adjust to new standards of quality imposed by the obligation of the SPV to maintain and operate profitably the project over the concession period. The fast- passed schedule combined with complex QA/QC procedures could create tensions between subcontractor and designer and its QA/QC outfit. These tensions left unmanaged could be detrimental to the project's schedule with grave consequences for all stakeholders. A cooperative attitude and a profound understanding of the costs required by P3 project delivery system (i.e. speed, adaptability and quality) by the subcontractor could win the day.

4. THE LEGISLATIVE STATUS OF P3 AND ITS FUTURE AS A PROMINENT PROJECT DELIVERY METHOD IN THE UNITED STATES.

Thirty-four states along with the District of Columbia and Puerto Rico have passed legislation enabling P3 construction projects. While the continued growth of the number of states that utilize the P3 delivery method for public construction projects is expected to continue to grow in the next few years, Kentucky is the only state to pass P3 legislation for the first time during the last three years. However, given the urgent need to address the crumbling infrastructure that exists all too often in the United States coupled with the lack of available resources to address glaring and urgent infrastructure needs possessed by many state governments, logic would seem to dictate that more P3 construction projects will be taking place in more diverse locations. While P3 legislation has at times been vetoed, we expect that additional states, perhaps starting with Hawaii, will be compelled to pass P3 legislation in the not too distant future.

It is further anticipated that P3 will continue to grow beyond exclusively being a delivery method for transportation projects in many states. The District of Columbia, Florida, and Indiana are just a few of the states that allow P3 to serve as the construction method of choice for brick and mortar projects like schools and libraries with payments made through a fee in the public authority's revenue budget.

5. SUBCONTRACTOR RISK

The hallmark of a P3 project is the transfer of risk away from the government owner to a private contractor which is believed to be better situated to assume and address such risks. Different P3 delivery methods cover the entire spectrum of risk and responsibility allocation between the public and private sectors. The primary risks that the government seeks to shift to the private partnership are the financing of the project and then the long term maintenance costs of the project. In doing so, the public component of the public private partnership shifts the uncertainties and risks associated with ensuring that the asset remains available to the public for its useful lifetime by placing that responsibility in the hands of the private party which is believed to be more equipped to operate and maintain the asset. This framework allows the government to fix its costs associated with the asset over the course of the useful life of the constructed asset. As a result, the selected private bidder typically selects higher quality materials and construction methods than would typically be utilized on a hard bid project as the bidder's focus is on the best value of the constructed product over the lifetime of the project in order to reduce maintenance and replacement costs (which is a good development for the contractor members of the DFI in our opinion).

The tremendous risk that is being assumed by the private partnership will of course be attempted to be passed down to P3 project subcontractors who will not be on the receiving end of much of the tremendous rewards that come with such risks on P3 projects. Many of these subcontractors are not properly equipped to negotiate, manage or sustain the type of risk that they will be asked to assume on a P3 project. These risks begin with the very significant dangers of payment failure on a private financed project without income that in some instances cannot be remediated through the availability of a payment bond claim, as would always be the case on significant public projects.

6. KEY SUBCONTRACT CLAUSES

One of, if not the most, important clauses in any subcontract is the payment clause. After all, there is never a reason for a subcontractor to work for free due to the presence of a pay-if-paid clause or a lack of available remedies in the event of non-payment. The revenue stream for the private partnership does not begin until long after a foundation subcontractor completes its work and leaves the site. Without such a revenue stream, a contractor may not necessarily receive regular monthly payments as it would typically receive on a publicly owned project. Therefore, subcontractors, especially those who complete work early in the project, may potentially wait many months to receive payment. Should the project not be successful or sustain significant cost overruns, payment of progress payments and final payment can become quite questionable.

The primary weapon in a subcontractor's arsenal in the event of non-payment on a private project is to file a mechanic's lien. However, since the privately constructed project is still publicly owned, a subcontractor does not possess lien rights. Yet, the typical alternative to filing a mechanic's lien, the filing of a payment bond claim, is not necessarily available. States such as Ohio do not require that payment bonds be posted for the benefit of P3 project subcontractors. Other states such as Florida, Illinois, and Texas that have multiple statutes that regulate P3 projects, require that payment bonds or other security be provided on certain types of P3 construction projects that are governed by one specialized statute, but another specialized state statute that applies to a different type of P3 project may not require that a payment bond or other security be posted. Therefore, before even negotiating a P3 subcontract in a certain state, let alone before performing P3 work in that state, a subcontractor MUST be very knowledgeable about the precise state P3 statute that applies to its work.

Once the subcontractor (or its legal counsel) possess comprehensive knowledge of the applicable P3 statute), a subcontract can be negotiated with knowledge of whether the controlling state statute mandates the posting of a payment bond or other security measures such as a letter of credit, United States bond, parent company guaranty, or cash collateral. If such security is not mandated, a subcontractor should request that a payment bond, letter of credit or another comparable instrument be provided for its benefit.

Furthermore, a pay-if-paid clause should never be accepted by a subcontractor under the somewhat tenuous payment landscape of a P3 project, regardless of whether security is posted. Instead, a subcontractor should negotiate a payment provision that guarantees payment within thirty-five (35) or forty-five (45) days after submission of its payment application regardless of the status of any higher tier payments.

The clause seen by many contractors in the deep foundation industry to be the most important clause in any subcontract is the indemnification provision. As is true in any agreement, all DFI contractors should avoid indemnifying their clients for any damages beyond those related to personal injury and property damage claims that are covered by insurance. Furthermore, the subcontractor should not agree to indemnify any party for anything other than damages that are caused to the extent of the subcontractor's negligence. Finally, the subcontractor must be very careful not to agree to provide an insurance policy which provides greater coverage to additional insureds than has been agreed to in the contract itself.

7. ETHICAL ISSUES

In theory, a good contract allocates the risks based on the best ability of the parties to control, manage and mitigate the risks. This is a sound way to allocate the risks in contracts by being both ethically and economically efficient. The ethical issues occur when not only is the risk transferred to the party that cannot mitigate it, but it is also transferred with no possibility to be reasonably assessed at the time of transfer. In the case of 3-P projects, the risk, which is mostly unethically transferred, is the risk of differing site conditions. This risk, historically, belonged to the owner that is providing the land (in our case, the Public Authority). In a 3P delivery system, the owner transfers the risk to the special purpose vehicle (SPV) that is transferring it further down to the general contractor. At the time of transfer (effectively the time when the bid is put together), very little data, if any, are made available to the SPV and the deep foundation subcontractor. At this moment, the subcontractor has no good option in preparing a balanced bid:

- a high value contingency for this risk makes the bid uncompetitive;
- not bidding;
- bid with low contingency which makes the subcontractor competitive for the bid, but at the same time, risks the welfare of his business.
-taking exception to the risk in the subcontract that usually is not acceptable to the General Contractor, making the bid nonresponsive.

The question is what the subcontractor can do to get out of this situation, a situation that pins him between not having work or working and jeopardizing the welfare of his business. Unfortunately, working alone as a single entity, the subcontractor can do nothing. The only thing that can overcome this unethical situation is that a the subcontractor's professional associations to act throughout education and consensus building to provide the subcontractor with its best opportunity to reject this unethical risk by taking exception to it. In this way, the general contractor/ SPV will be forced to address the issue in an ethical manner.

The general contractor and the SPV have some proportion of common corporate ownership. Considering the SPV as the source of money for the project, the general contractor can find itself in a conflicted position when presented with a claim by the Deep Foundation Subcontractor. An ethical breach can occur when the general contractor is assessing the claim throughout the perspective of common ownership with the source of money instead to assess the claim on its merits. The unethical behavior of the general contractor in this case is increasing the financial risk of the Deep Foundation Subcontractor adding to the aforementioned risk of non-payment.

8. HOW TO SUCCEED AS A P3 SUBCONTRACTOR.

A late project completion can result in a P3 entity defaulting on its short-term loans. Therefore, due to the nature of private short-term financing and the necessity that the constructed asset be turned over in order to generate revenue, the subcontractor's timely completion of its work becomes even more imperative than on a typical public project. A P3 subcontractor must be prepared to negotiate the likely very aggressive schedule prior to the execution of a subcontract and should insist on attaching a mutually agreed upon schedule to its subcontract as an exhibit. A P3 subcontractor should specifically reserve its right to make a claim for additional compensation for unforeseen underground obstructions and include agreed upon unit prices for drilling through unforeseen underground obstructions in its subcontract. Furthermore, given the time and financial pressures that are especially inherent in a P3 project, all requests for change order involving a request for an extension of time and/or additional compensation must be timely submitted in strict accordance with the notice and claim provisions of the subcontract. As a result, it is critical that the notice provision provide the Subcontractor with at least three business days to make a claim, that all members of team know the time period in which notice must be provided and that this information is easily accessible to the project team in the field.

9. CONCLUSION

The P3 delivery system is bringing new challenges to the deep foundation industry such as contract complexity, allocation of differing site condition risks, design and schedule characterized by a dynamic environment, claims resolution process, and payment risks. If some of these challenges can be mitigated by the Deep Foundation Subcontractor (i.e. contract complexity, change management, etc.) they will have to be resolved at the level of the industry through the work of trade organizations by crafting common policies and guides to overcome the unethical transfer of risks (i.e. differing site conditions, payment and claims risks).

10. REFERENCES

Hart, O., Shleifer, A. and Vishny, R.W. (1997). 'The proper scope of government: theory and an application to prisons', Quarterly Journal of Economics, vol. 112 (4), pp. 1126–61.

Hart, O., (2003). Incomplete Contracts And Public Ownership: Remarks, And An Application To Public-Private Partnerships, The Economic Journal, 113 (March), C69–C76

Grimsey, D., & Lewis, M. K. (2004). Public Private Partnerships: The Worldwide Revolution in Infrastructure Provision and Project Finance. Cheltenham, UK: Edward Elgar Publishing.

USDOT Federal Highway Administration (2016).Guidebook for Financial Assessment of Public-Private Partnerships.
https://www.fhwa.dot.gov/ipd/p3/toolkit/publications/guidebooks/financing_of_highway_p3_projects/. Accessed April 2017.

PRESCRIPTIVE SPECIFICATION DESIGN: THE IMPACT ON COST AND CONSTRUCTABILITY – CASE HISTORY

Shawna Munn, P.Eng,
Isherwood Geostructural Engineers, Mississauga, Ontario, Canada; 905-820-3480;
Shawna@isherwood.to

Allison Bennett, E.I.T.
Isherwood Geostructural Engineers, Mississauga, Ontario, Canada; ABennett@isherwood.to

Nadir Ansari P.Eng, D.GE, M.ASCE
Isherwood Geostructural Engineers, Mississauga, Ontario, Canada; Nadir@isherwood.to

ABSTRACT

This paper outlines how specification driven design has made Toronto Area transit infrastructure projects more expensive than similar private projects, and provides a case study of the results of an excavation at Launch Shaft 1 (LS1) for the Eglinton Crosstown Light Rail Transit project in Toronto, Ontario. The paper will describe the impact specification driven design parameters can have on design economy, constructability, and schedule and will suggest an alternative approach utilizing the Observational Method. As a result of the initial specification based design, Isherwood was retained by both the General Contractor and the Specialty Excavation Shoring Contractor to provide value engineering leveraging the Observational Method to improve constructability and construction schedule. By using well known, accepted design methods coupled with local experience in lieu of the specified design pressures and parameters, the redesigned bracing scheme reduced construction cost and schedule. This excavation case history can be a lesson learned for future transit projects.

Keywords: specification, risk, constructability, schedule, Observational Method, shoring, excavation

The City of Toronto has been developing its transportation network since the mid 1800's. "Canada's First Subway" along Yonge Street opened in March 1954 (TTC 1954), with a few additions to the subway network through to the 1980's. The following two decades marked a long period of slow development due to recessions, budget cuts, and politics along with several cancelled projects. To fill the gap left by years of underfunding, several new transit projects are now under construction in the city as a part of Metrolinx's $50B, 25 year, "The Big Move" initiative (Metrolinx 2013). The work on these types of infrastructure projects is highlighting a different and developing challenge within the tendering and design specification structure we will call Prescriptive Specification Design (PSD).

PSD is a method used within contract specifications to control design risk on a project by applying conservative design methods, factors of safety, or other parameters to make a *"fool proof*" design. It is akin to requesting a colouring by numbers approach from a painter. There are inherent risks of using this method of tendering a project including increased project costs, longer construction schedules, and decrease of overall project economy. In PSD, the Owner "owns" all of the design risk on a project, including any additional costs due to changed site conditions. However, the Contractor commonly "owns" the risk of any deviations from the design specification they pursue, therefore making any improvements to the design, cost, or schedule less desirable from the Contractor's point of view. The impact of this type of strict specified approach to design has been seen in transit infrastructure projects in the Toronto area. Figure 1 outlines the range of specified AEPD design pressures as a function of excavation height (H) specified for use in Toronto underground transit projects since the 1970's to present day. A clear trend can be seen with respect to increased design pressures specified. The ranges shown for each project are intended to account for the potential differences in soil conditions for the highly overconsolidated

 © 2017 DFI Annual Conference, New Orleans, LA, USA

glaciated soils in the Toronto area. The graph also highlights the typical range, in blue, for the industry practice in Toronto for comparison.

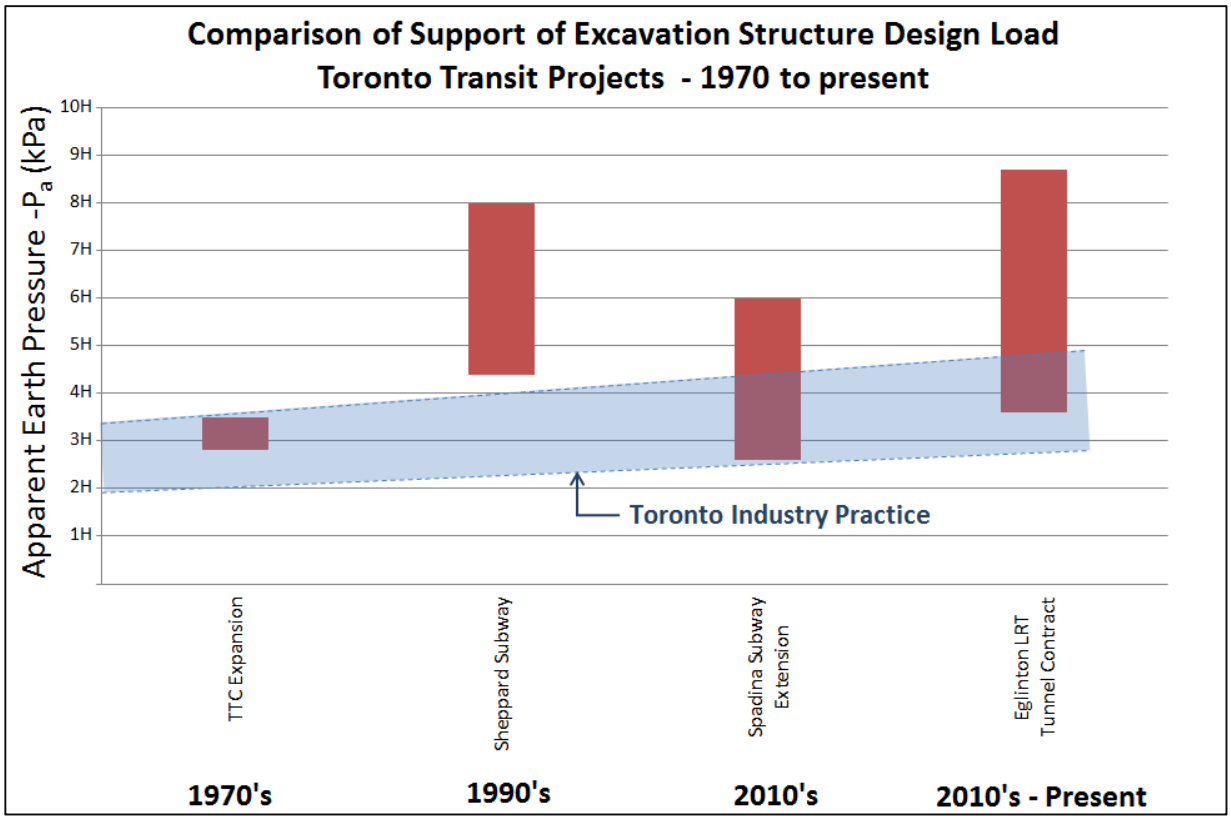


Fig. 1. Comparison of Design Loads of Transit Projects in Toronto from 1970 – Present

The subsurface work component of most projects represents the highest project risk with respect to time, cost, and liability. There is uncertainty with respect to the project geology, uncertainty in the geotechnical investigation, and uncertainty of the soil classification. It is important to note: uncertainty can also create opportunities within design.

RISKS WITH THE PSD APPROACH

There are a variety of risks with the PSD approach to projects, which increase in scale with the size of the project. Conservative or "heavier" design approaches lead to increases in material costs due to larger structural components, and manpower costs from increased installation time, material handling, and assembly. Large projects requiring large teams tend to involve international experts without the knowledge of the local construction environment and local soil conditions, understandably leading to more costly and conservative designs. In contrast, private projects with more flexible management systems leverage local knowledge to achieve lower project costs.

Another observed negative side effect of the PSD approach is the fixed mind-set of site personnel on projects viewed to be "conservatively designed" (Dweck 2007). On public infrastructure projects designed more conservatively than their equivalent private project counterparts, this conservatism is apparent to workers (comparing pile sizes, rows of anchors, etc.) and the "it's overdesigned" mentality can be pervasive. In our experience, this manifests in a variety of ways including: over excavation past support levels, use of shoring supports for secondary support purposes without proper review, construction activity damage to the shoring structure, less emphasis paid to timely or accurate monitoring of shoring and neighbouring structures, and less general respect paid to design restrictions. The increased

quality assurance and control programmes typically seen on infrastructure projects can somewhat balance the risk of this, however the presence of this mentality presents a risk as some components on a project are critical no matter how conservatively designed.

Using the PSD approach discourages creativity in choice of design and construction methods outside of those specified due to lack of an effective risk or cost-savings sharing mechanism for these alternatives. This leads to missed opportunities due to over commitment to the PSD approaches early in the projects leaving absent analyses of alternatives, and leading to increased commitment in later project stages (Flyvbjerg 2014**).** In these cases, the Owner is typically paying for the most conservative design rather than sharing in the risk and decision making opportunities and any subsequent economies.

While there are places for the PSD approach, it is not an ideal approach for every project and should not be used as a broad brush for public infrastructure projects. The PSD approach would be appropriate where reliable methods for measuring or observing performance of a structure are not available, for example on remote sites with intermittent site visits or projects with missing or unreliable monitoring data from which to make observations and design adjustment decisions.

CASE STUDY – LAUNCH SHAFT 1 (LS1)

The West Launch Area- Launch Shaft 1 (LS1), just east of Black Creek Drive along Eglinton Avenue West in Toronto, Ontario, is supported by a combination of internal bracing and tied-back anchor shoring systems. LS1 was awarded in advance of the main Eglinton Crosstown Light Rail Transit Project's tunnelling contract to expedite the overall construction schedule.

The site occupies the south half of Eglinton Avenue West bordered by the diverted road to the North, Keelesdale Park to the South and Black Creek to the West (Figure 2). The L-shaped excavation typically ranges from 12 to 15m deep and measures 44 m by 61 m. The shoring system constructed at LS1 was the result of contractor driven design changes to the original PSD driven shoring, transpiring after pile installation had begun in early 2012. Figure 3 and Figure 4 show contrasting schematics of the original prescriptive shoring design, and contractor-driven shoring alternative redesign, respectively.

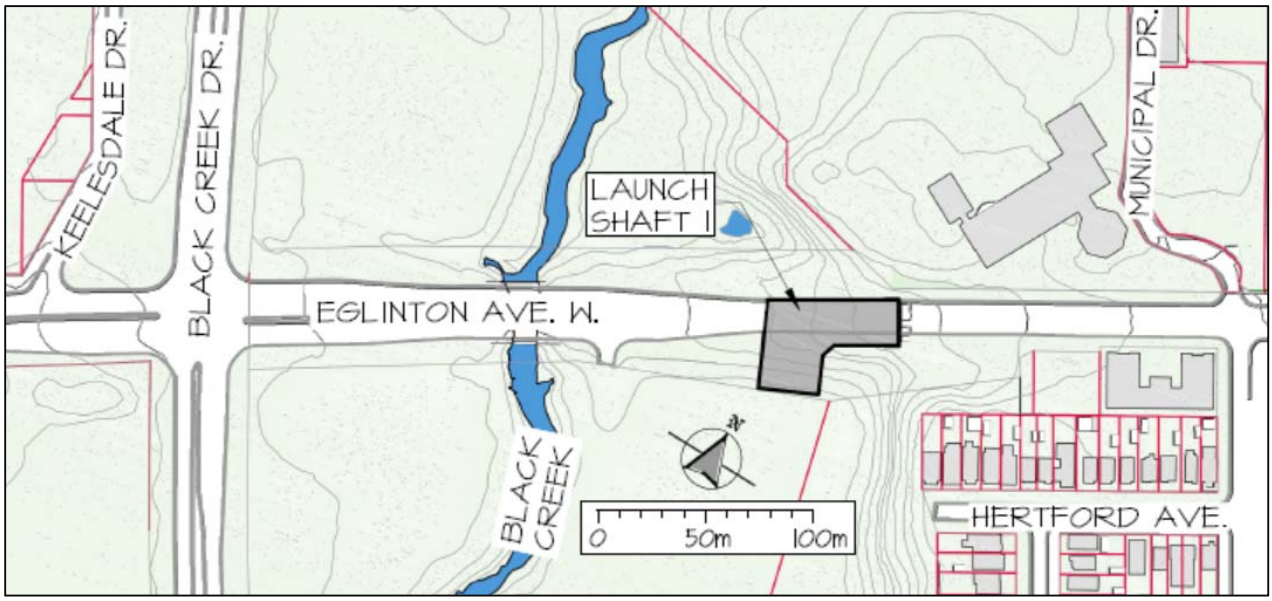


Fig.2. Launch Shaft 1 – Site Location Plan

Prior to construction, the Shoring Contractor considered retaining Isherwood to provide a Value Engineering design with hopes of realizing improved constructability and construction schedule while maintaining adequate shoring performance. Due to schedule and review process concerns the Shoring Contractor abandoned this approach. After pile installation was underway, the redesign initiative was restarted by the General Contractor and Shoring Contractor after the Owner realized the original scheme made it impossible to hand over the shaft to the next contract for tunnelling operations on schedule. The contractor-designer collaboration led to a shoring redesign by leveraging the Observational Method, the Contractors' strengths and resources, and local knowledge of Toronto's soils to realize significant improvements.

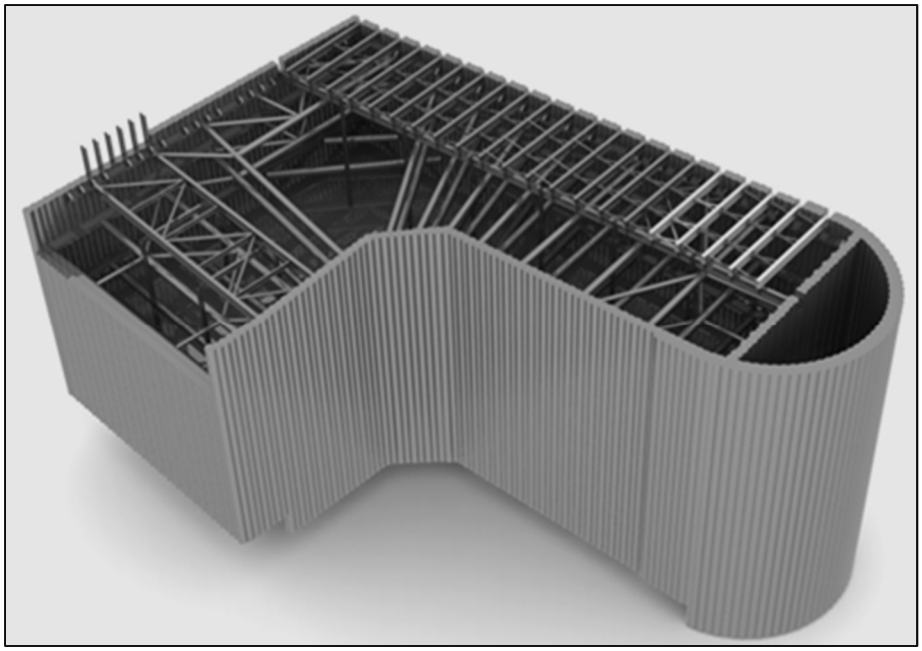


Fig. 3. Original PSD Design – Schematic (117 rock anchors not shown for clarity)

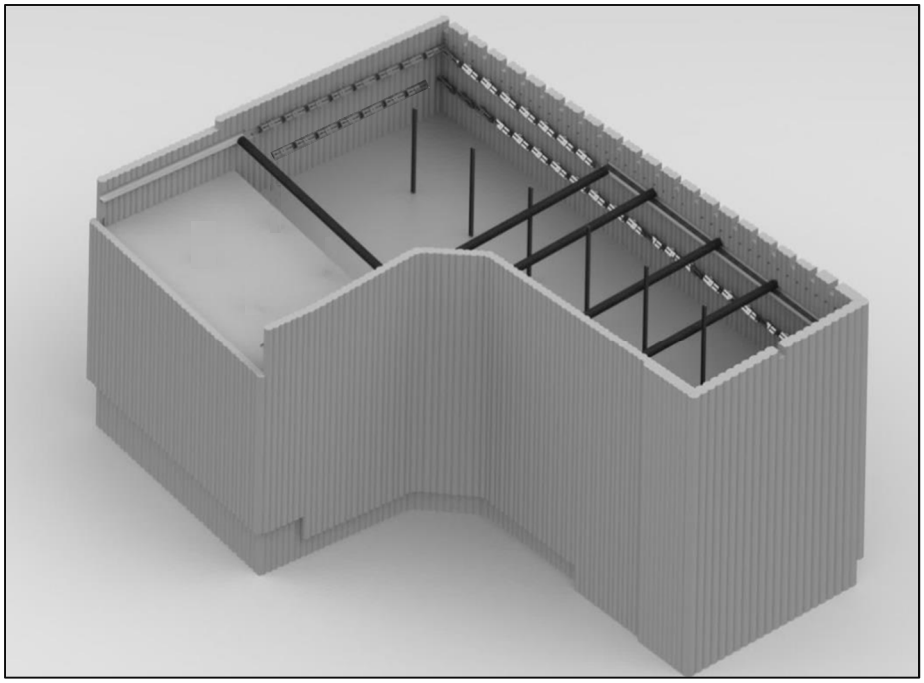


Fig. 4. Final Redesign – Schematic (16 contingency deflection control anchors not shown)

The redesigned shoring scheme was developed based on local excavation shoring design methods. Requests to the owner for deviation from the original PSD and the constraints which influenced its development, proved challenging. The owner's team was unmotivated to introduce "uncertainty" (or risk) into the original shoring design, already in hand: the result of an owner driven prescriptive specification intended to mitigate risk and generate "certainty" about the end product.

Original Shoring Design Inputs:

(a) Contract Geotechnical Design Parameters

(b) Uncertainty regarding the variability of the glaciated soil stratigraphy. Example of description provided for two of soil layers:

Material:	Silty clay to clayey silt	Silty sand to sandy silt
Elevation (m):	116.6 - 89	100.5-88.7
Relative Density (Typical):	Very soft to hard (stiff)	Loose to very dense (dense)

(c) Contract Loading Envelopes

(d) Contract Geometry Requirements:

   a. "Design vertical distance between horizontal restraints not to exceed 4 m."
   b. "Do not exceed 1 m for vertical distance from centre of line of lowest horizontal restraint to bottom of excavation."

The initial redesign initiative was focused on the headwall area where the original design included a caisson wall backed by an interlocking arched secant wall with jet grouting inside and outside the arch to create a solid block for the next contract tunnelling operations. The redesign of the headwall eliminated both the arch and jet grouting. Fibreglass reinforced cages in larger diameter holes were used to achieve the required design capacity. The design of the straight fibreglass wall significantly improved the schedule by allowing the elimination of forty 1.2 m (4 ft.) diameter drilled holes, but also eliminated the environmental risk of containing the jet grout spoils near Black Creek, various parks and conservation lands. The elimination of the arch and associated jet grouting also reduced the working area needed along Eglinton by 14 m (45 feet), improving the flow of traffic along Eglinton Ave. and reducing the impact to the public and local community. The redesign of the headwall saved over 3% of the total cost of construction.

The redesign significantly improved constructability and construction access in the shaft by using a combination of rock anchors, deflection control soil anchors, and internal bracing. The use of additional rock anchors allowed for improved construction access during excavation and subsequent tunnelling activities through elimination of struts and creation of a large strut free hoisting area to service both TBM operations. The initial project geotechnical report did not recommend use of soil anchors due to concerns with creep susceptible soils and shaft design life. Instead, design parameters for rock anchors were provided and installation challenges were discussed. In order to determine suitability of soil anchors instead of rock anchors, a sacrificial soil anchor test program was carried out in June 2012. Following review of the test results and findings, concerns still lingered within the Owner's consulting team and there was no desire within the Owner's team to share the risk of this change from the contract geotechnical recommendations. Despite proof of suitability per PTI testing and acceptance guidelines, the motivation for soil anchor use in the redesign disappeared, as the Contracting team would have to assume all performance risk. Instead, rock anchors were used as primary support members and secondary temporary soil anchors were added as a design contingency for deflection control for use until the base slab was installed.

In order to achieve agreement to proceed with the redesign from the owner, a clause in the contract design documents regarding use of a more complex soil-structure analysis in lieu of the specified pressure diagrams and constraints was utilized. A Finite Element Analysis using Plaxis 2D was submitted to the owner in November 2012 to confirm shoring redesign assumptions and establish a baseline for anticipated shoring performance. Permission was granted by the owner to proceed with the redesigned hybrid shoring

scheme in December 2012. Figure 5 shows the redesigned scheme for a section cut through the North and South Walls as illustrated in Figure 7. Struts were used as first row supports, rock anchors were used as second row bracing and deflection soil anchors were designed as a contingency to control potential shoring and toe movement to ensure shaft performance. Figure 6 shows FEA predicted final excavation total displacements for the section shown in Figure 5.

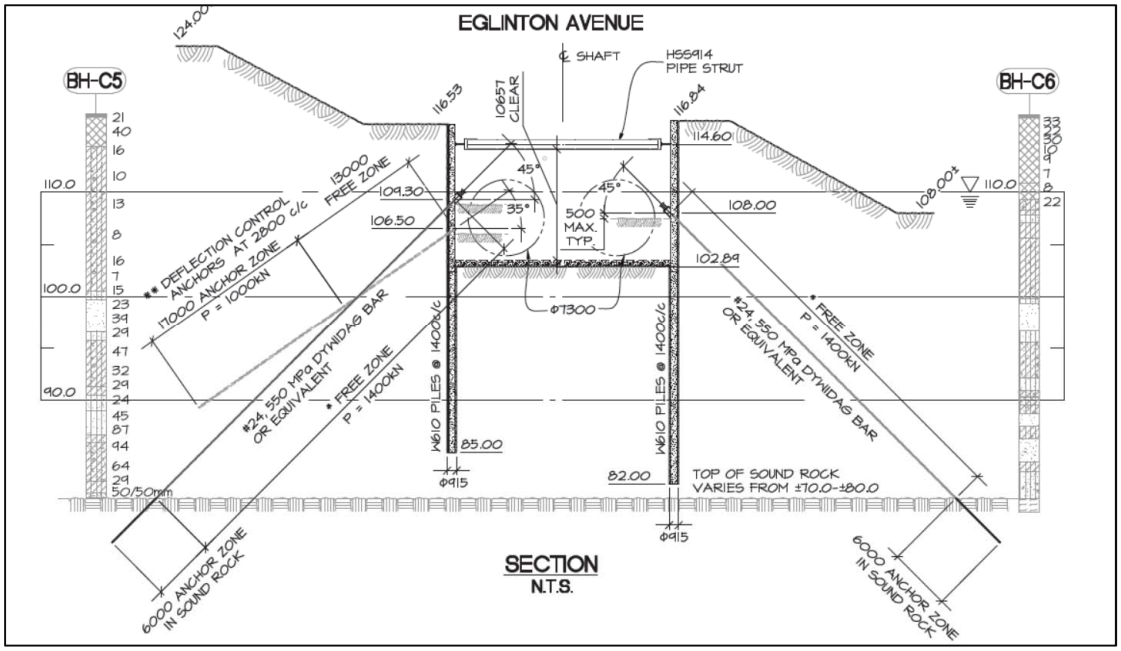


Fig. 5. Redesigned Shoring Section

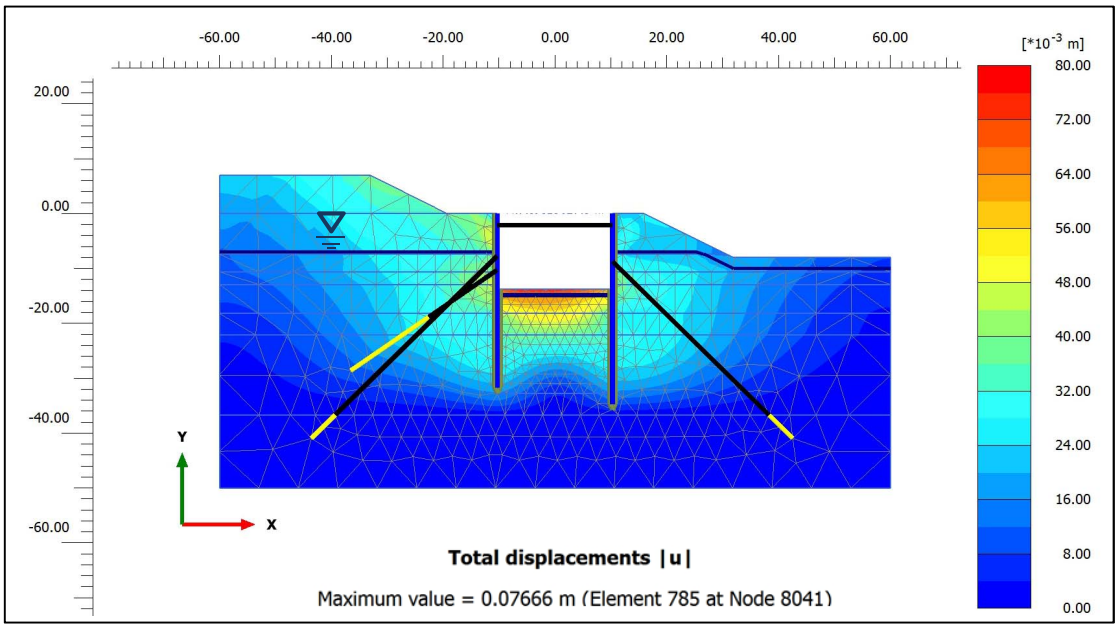


Fig. 6. FEA predicted final excavation total displacements

Shaft monitoring played a crucial role in the redesign and implementation of the observational method at LS1. Unfortunately, due to the original PSD approach, amending the monitoring plan to the new design proved contractually challenging. During construction, results of the monitoring program (inclinometers) were compared to the results predicted in the FEA Report to ensure the shoring system performed as anticipated and per agreed specification baselines.

Figure 7 highlights pile inclinometer locations. The inclinometer results for Pile SP110 on the North Wall and Pile SP84 on the West Wall are shown below in Figure 8 and 9 for various stages of the excavation.

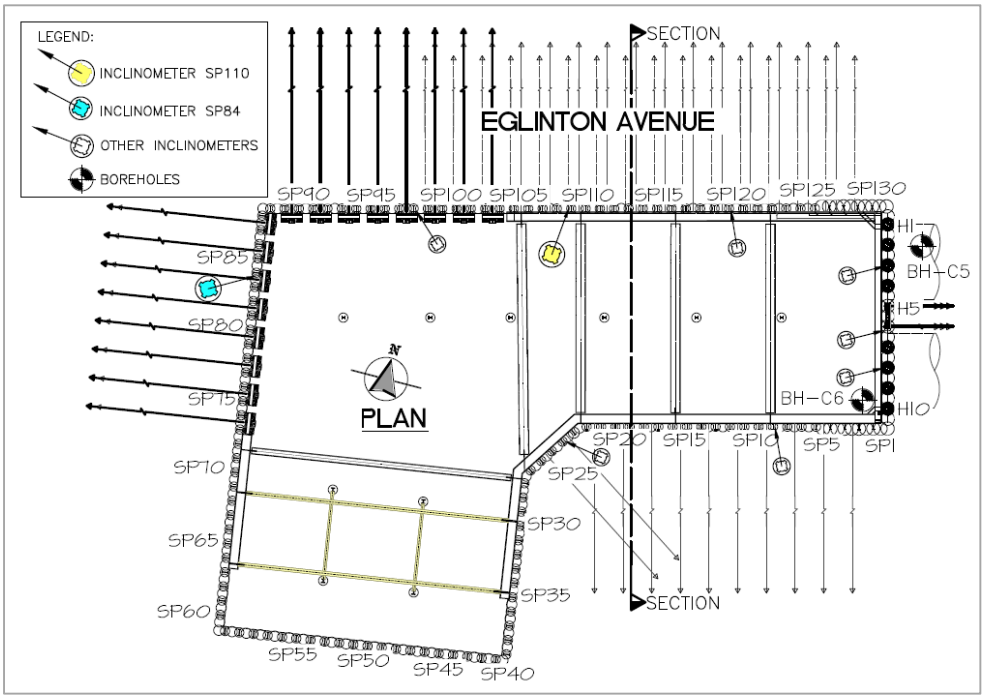


Fig.7. Inclinometer Monitoring Plan

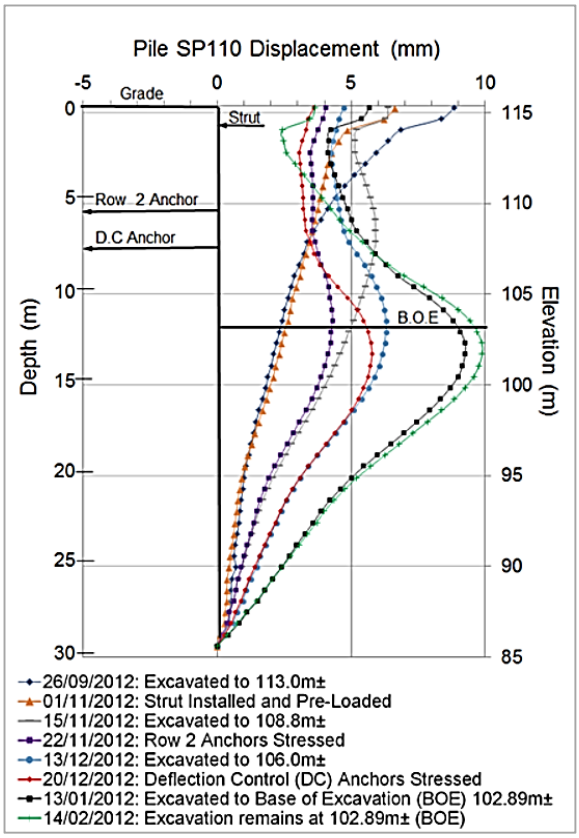


Fig. 8. Pile Inclinometer SP110 Results

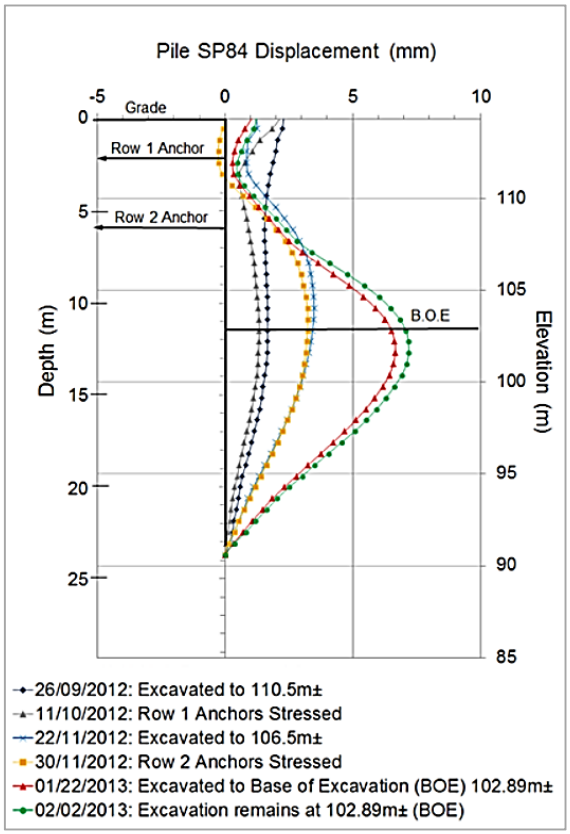


Fig. 9. Pile SP84 Inclinometer Results

The redesign saved at least 3 months on the shaft construction schedule, allowing it to be constructed in time for LS1 to successfully receive two tunnel boring machines, an impossibility with the original PSD. In addition, the redesign saved a significant amount of schedule for the following contract by providing a more efficient layout for removal and material handling for tunnelling of the next 3.5 km of the LRT line, and would have resulted in more cost competitive tenders. In addition to the schedule benefits to the Owner, the LS1 shoring redesign helped the Shoring Contractor save money as opposed to projecting a loss if the original PSD design had been built. A comparison of bill of materials for the internal bracing is presented in Table 1

Table 1: Comparison of Bill of Materials for PSD Design versus Redesign

	Original PSD Design	Final Redesign
Walers – Weight	160900 kg (354800 lbs)	75200 kg (165900 lbs)
Internal Bracing – Weight	293500 kg (647000 lbs)	88300 kg (194700 lbs)
Rock Anchors – Quantity	117	63
Deflection Control Soil Anchors – Quantity	N/A	16

Figure 10 shows a photo taken spring 2013 from the West Wall of LS1, looking towards the East Headwall during segmental assembly of TBM Dennis. The modest shoring movements of 10 mm were far less than the 35 mm review level and 50 mm alert level limits set in the contract. Thus, had a strictly performance based design been used from the inception of the project, with a harmonized shoring monitoring plan, there would have been a further opportunity for schedule and cost savings. A more efficient system could have been designed with use of shorter, lighter shoring piles and eliminating use of deflection control anchors, resulting in further improvements to schedule, constructability, carbon impact, and additional estimated project savings of $2M with no significant performance impact.



Fig. 10. Photo of LS1 taken Spring 2012, view looking East from the top of the West Wall

THE ALTERNATIVE APPROACH

Based on Isherwood's 45 years of experience with a variety of similar projects in the Toronto Area, the suggested alternative approach to the PSD method of tendering projects is to build opportunity for the use of the Observational Method into project contracts and specifications. The use of the Observational Method, as developed by Terzaghi and formalized by Peck (1969), allows for the design to be developed for maximum efficiency while guaranteeing safety and results in a performance based design specification rather than a prescriptive one. It is effective as a method of risk management to respond to geotechnical uncertainties with respect to soil parameters, soil structure analysis, and construction methodologies by using active feedback regarding the structure performance. This feedback is then used to confirm or modify the base design throughout construction **(**Powderham 2004).

Various researchers and authors (Peck 1969 and 2001, Le Masurier et al. 2006, Powderham 2004) discuss the Observational Method at length and show its proper use minimizes risk when dealing with uncertainty in the ground. Furthermore, the application of the method leads to increases in safety (Terzaghi et al. 1996) because as knowledge of the actual response to construction increases, uncertainties and risks reduce. If used from the beginning of a project the Observational Method may enable the best possible design with respect to safety, economy, and schedule by allowing time for the development of innovative and creative concepts to project constraints (Peck 1969). This approach also encourages engaging contractors and engineers who have local knowledge of the "dirt" required for effective use of the Observational Method.

While the concept of using the Observational Method is over half a century old, the authors are unaware of an effective method for its inclusion in major public subsurface infrastructure contracts that allows for its effective use, while sharing design change risk equitably between parties within a project. This is a significant hurdle on larger transit projects, where there are many parties reviewing and/or approving design methodology and there is no effective system set up to handle such changes with the speed required to make this approach reliable and effective. Without the risk sharing and management systems issues addressed properly within a contract and project organization, Contractors and Owners will not see the full benefit of its use, and the project team will be encouraged to try to shed risk rather than sharing opportunities resulting in inflated costs and construction schedules. This aversion to sharing risk will diminish the effectiveness of the method, and its ability to decrease costs, durations, and the environmental impact of a project.

Setting the framework for a successful project leveraging the Observational Method requires time for effective planning and innovation surrounding the design. This approach allows for a design based on the most probable conditions founded on experience, and modifications to the design based on performance. In these projects, a Geotechnical Baseline Report (GBR) is a solid foundation for contractually outlining the range of expected conditions for design of contingency plans. These designs would address for the range of conditions outside of those considered most probable, and conditions found outside those outlined in the GBR would still constitute changed conditions contractually. Further, the allowance for the contingencies would have to be built into projects in the beginning, so they are set up with adequate budgets and avoid potential cost overruns. Since this would be outlined during bidding of a project, Owners would have the time to evaluate the proposed alternatives and contingency plans in a competitive environment and choose the approach best suited to the project, geotechnical conditions, and risk assessment. Finally, after the established baseline is agreed by both the Owner and Contractor(s), the allowance for use of the contingency plans will have to be addressed in typical contract language, such as those surrounding liquidated damages.

THE SUGGESTED PROCEDURE – BASE COST PLUS CONTINGENCY

Based on Isherwood's experience with PSD and transit projects in the Toronto area like LS1, restructuring how these projects are tendered and bid will provide more opportunity to leverage local experience, promote design innovation, and encourage efficient designs reducing the financial, environmental, and societal costs to Owners and the public. This paper attempts to outline a suggested procedure to initiate a discussion on inclusion of performance based design using the Observational Method in similar projects:

(a) Owner's team to define project scope and develop a GBR including established geotechnical design parameter variability
(b) Bidding Contractors to establish:
    a. Base bid design founded on experience and judgement of most probable conditions
    b. Contingency design plans for GBR outlined geotechnical design parameter variability
(c) Bidding Contractors to submit tender price as "Base Cost plus Contingency"
    a. Summary of base bid design plus contingency plans with budgeted costs for contingency plan execution and associated schedule impacts.
(d) Project Agreement/Contract to include procedure for timely use of contingency designs and define the effect on the base contract
    a. Unit rates for contingency work, adjustment to liquidated damages clauses for additional contingency plan execution schedule, etc.
(e) Post contract award - Successful Contractor's team to outline method of observation to monitor design performance during construction. Applicable review and alert levels for engagement of contingency designs are to be agreed by project team prior to start of construction.

CONCLUSION

Contracts using a prescriptive specification design (PSD) approach can lead to unnecessarily conservative designs and less control over construction activity and structure performance. In addition, the PSD approach can foster an environment for development of an "it's overdesigned" mentality and this presents a risk to the industry as a whole. A performance-based approach to project contracts and specifications using the Observational Method can lead to more efficient projects with shorter construction durations, increased safety, and decreased project costs. This method relies on monitoring and therefore more emphasis on accurate, timely monitoring results within contract specifications. This approach allows for leveraging local experience from both Contractors and Consultants to the project benefit. Our hope is those entrusted with the responsibility of stewarding public money recognize there is a viable and valuable alternative approach.

ACKNOWLEDGEMENTS

Acknowledgement is given to John Goffredo and Dave Kirkland of Kenaidan Contracting Ltd., and Todd Barlow of Bermingham Foundation Solutions, for their assistance and support.

We thank Brian Isherwood, Bill Lardner, and Alan Macnab for comments that improved the paper.

REFERENCES

1. Flyvbjerg, B., 2014. What you should know about megaprojects and why. Project Management Journal 45(2).
2. Le Masurier, J.W., Blockley, D.I., Muir Wood, D., 2006. An observational model for managing risk. Civil Engineering 159(6) 35-40.

3. Metrolinx, 2013. The big move baseline monitoring report. http://www.metrolinx.com/en/regionalplanning/bigmove/The_Big_Move_Baseline_Monitoring_Full_Report_EN.pdf. 28 p. Accessed 17.04.19.
4. Powderham, A., 2004. The observational method: Learning from projects. International Conference on Case Histories in Geotechnical Engineering 8. 9 p.
5. Peck R.B., 1969. Advantages and limitations of the observational method in applied soil mechanics. Géotechnique 19 (2) 171-187
6. Peck R.B., 2001. The observational method can be simple. Geotechnical Engineering 149, 71-74
7. Dweck, C. 2007. Mindset: The New Psychology of Success. Ballantine Books, New York City, 302 p.
8. Terzaghi, K., Peck, R.B., Mesri, G.., 1996. Soil mechanics in engineering practice. John Wiley & Sons, Inc., 549 p.
9. Toronto Transit Commission (TTC), 1954. Canada's first subway, a cavalcade of progress, 1921-1954. 24 p.
10. Toronto Transit Commission (TTC), 1994. Contract No. SH-00-C1, Specification Section 02340, Excavation Support Systems, Rev.0, 12 p.
11. Toronto Transit Commission (TTC), 2010. Contract A35-35, Sheppard West Station, Specification Section 31-50-00, Excavation Support Systems, 12 p.
12. Toronto Transit Commission (TTC), 2011. Contract A27-1, Finch West Station, Specification Section 31-50-00, Excavation Support Systems, 10 p.
13. Toronto Transit Commission (TTC), 2011. Contract A31-1, Steeles West Station, Specification Section 31-50-00, Excavation Support Systems, 15 p.
14. Toronto Transit Commission (TTC), 2011. Contract A37-1, Vaughan Corporate Centre Station, Specification Section 31-50-00, Excavation Support Systems, 18 p.
15. Toronto Transit Commission (TTC), 2011. Contract ECLC1-1, Eglinton Crosstown LRT – West Launch Area, Specification Section 31-50-00, Excavation Support Systems, 10 p.

CHALLENGES IN MANAGING AN AGING INFRASTRUCTURE, LESSONS LEARNED FROM A NEAR MISS AT THE LAKE MANATEE DAM

Glen R. Andersen, Eustis Engineering, Metairie, LA, USA, 504-613-5804, gandersen@eustiseng.com

ABSTRACT

Two of the greatest challenges we face in managing our aging infrastructure are to perform accurate condition assessments and to realistically predict the risk of non-action. The aim of this paper is to discuss common pitfalls we face in performing accurate condition assessments of our aging infrastructure using the case history of a recent near miss at the Lake Manatee Dam in Central Florida. The dam was placed into service in 1967 and was inspected every couple of years by dam safety engineers beginning in 1978. Although there was substantial and repeated evidence of a serious piping and internal erosion problem in each of these inspections, the problem was overlooked by most of the inspection teams. In 2012, the inspection team concluded that: "the Lake Manatee Reservoir Dam is well maintained and is in very good overall condition." However, in 2013 a new team inspected the dam from an entirely different perspective, identified potentially serious conditions, performed an integration of the historical inspection data and concluded that: 1) the Lake Manatee Dam was in a severely distressed state; and, 2) without an immediate intervention there was a high risk of an uncontrolled release of the reservoir most likely following a large rainfall event and prolonged opening of the service spillway. This case history highlights human factors contributing to the near miss including group think and focusing on changes from prior inspections. The integration of historical inspection data is recommended for managing our aging infrastructure.

Keywords: case history, aging infrastructure, human factors, integration of historical inspection data

INTRODUCTION

The engineering analytical techniques most appropriate for assessing an aging infrastructure can be distinct from those used for the original design. To adequately manage our aging infrastructure it is necessary to change our perspective from anticipating failure mechanisms and designing to prevent them to assessing condition, detecting the presence of potential failure mechanisms, and assessing the potential risks. In many circumstances the failure mechanisms currently active may not have been anticipated by the original design team.

We have developed a substantial body of experience in the design of our infrastructure. Full scale and laboratory testing coupled with the application of scientific principles to model behavior has led to many powerful design tools. The continued serviceability of our infrastructure as its elements reach their design lives stands as a legacy to our profession. However, under the sustained effect of limited resources for maintenance and rehabilitation parts of our infrastructure are in a highly deteriorated state. Unfortunately, the condition of some of these has not been properly assessed. This paper focuses on the Lake Manatee Dam in Central Florida and the process used to clearly identify its highly deteriorated state. While there are many factors that contributed to the lack of a proper assessment of its condition, the focus herein will be on human factors and in particular how "Group Think", "Aversion to Bad News", and "Condition Assessments Based on Changes to Prior Condition" may have contributed to not properly identifying the development of a serious failure mechanism.

DESCRIPTION OF LAKE MANATEE DAM

The Lake Manatee Dam was constructed between 1965 and 1967 as an in-stream reservoir on the Manatee River approximately 20 miles upstream of its discharge point into Tampa Bay. It is a high hazard dam functioning as a drinking water supply. The U.S. Army Corps of Engineers, the Florida Department of

 © 2017 DFI Annual Conference, New Orleans, LA, USA

Environmental Protection, and the Southwest Florida Water Management District have regulatory authority over the dam. Land use in the flood zone is agricultural, light industrial, commercial and residential. The flood zone also includes sensitive ecological resources and state and federally protected species. A recent aerial view of the dam and its principal (service) spillway is presented in Figure 1.

The original dam consisted of an approximately 4,700-foot-long zoned-earth embankment with a clayey core, granular upstream and downstream shells, and a crest elevation of 52 ft (NGVD 29 Datum). After being placed into service, an emergency spillway was constructed in the north abutment. The present elevation of the crest ranges from approximately el 51 ft at the service spillway to el 55 in the embankment section, representing a 3 ft raise of the crest. The original upstream slope was designed at 4H to 1V from the toe to a horizontal bench, above which it was designed with a 3H to 1V slope to the crest with a soil-cement surface erosion layer on this upper portion. The upper portion of the downstream slope was originally designed on a 2.5H to 1V slope but was subsequently flattened to a 3H to 1V slope when the crest was raised. During this raising the upper portion of the embankment was slightly over-steepened on the upstream slope.

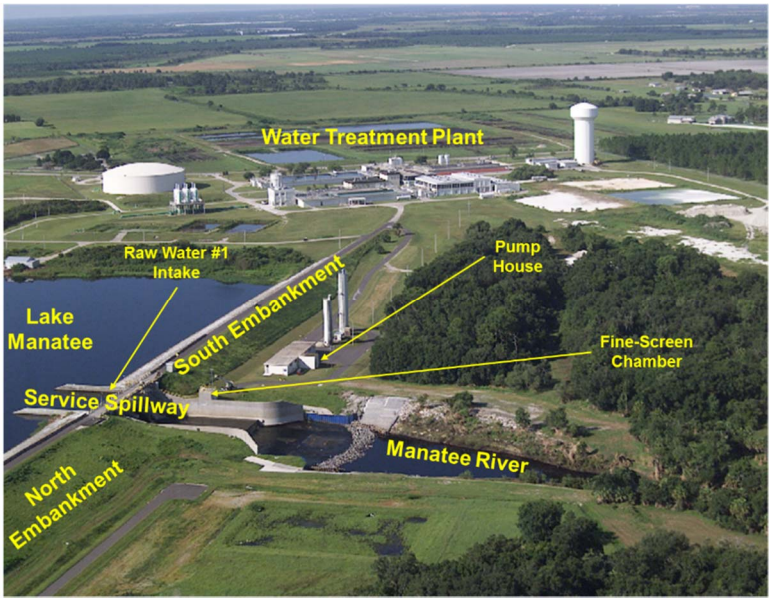


Fig. 1. Aerial view of Lake Manatee Dam and Principal Spillway Structure

The principal spillway, also called the service spillway, is located approximately 1,500 ft north of the southern abutment and just south of the original Manatee River channel and consists of three 15-foot radius tainter gates, each one spanning a 31.5-feet-wide bay. This spillway has upstream concrete approach walls, downstream concrete training walls, and a bare earth approach channel leading to a concrete approach apron immediately upstream of the Ogee-type spillway. It also has a concrete stilling basin with an end sill. The stilling basin floor slab is ground-founded and consists of individual reinforced concrete sections. The concrete approach walls and the downstream training walls each have an inverted T-shape and together with the Ogee section monoliths are founded on driven H-piles. The dam was designed without a low-level outlet. All water is removed from the reservoir through the two spillways, or by intake pipes to the water treatment plant.

The original clay core of the embankment was keyed into a geologic unit known as the Hawthorn Group that has alternating very low and very high permeability layers. An apparent low permeability layer at the bottom of the core was intended to function as a confining layer. However, just upstream of the embankment along the south shore of the reservoir, a very deep borrow pit was excavated during construction that

apparently extended completely through this confining layer. A toe drain was installed along the entire northern and southern embankments with discharge points in the service spillway downstream of the stilling basin.

The original underseepage cutoff system for the service spillway consisted of a series of driven sheet piles forming a box around the edges of the upstream approach slab and along the front edge of the Ogee spillway sections. These sheet piles pass underneath the base slabs of the two approach wall monoliths closest to the Ogee section and are connected to another sheet pile cutoff wall that extends north and south from the Ogee section, underneath the spillway bridge approach slabs and into the embankment's clayey core for a distance of approximately 30 ft. A second set of cutoff sheet piles also extend to the north and south away from the exterior monoliths and parallel to but downstream of the first set of sheet piles. A final sheet pile cutoff wall was placed under the end sill of the stilling basin running north to south between the two base slabs for the downstream training walls. No seepage cutoff was placed under the downstream training walls.

Further details on the design and construction of the dam, along with several original design drawings can be found in Andersen et al. (2015).

CASE HISTORY OF NEAR MISS AT LAKE MANATEE DAM

Figure 2 presents an aerial photo of the service spillway showing critical seepage paths and the locations of significant historical visual observations made during the multiple dam safety inspections. These locations are shown as a series of circles, ovals and boxes and are numbered and summarized in Table 1 along with the general types of observations and overall timeframe in which they were made. The northern and southern edges of the service spillway represent the shortest seepage paths from the lake to the river and are where the largest seepage gradients are expected occur. In these areas along the margins between the spillway and the embankment sections, loss of material should be expected if an internal erosion and piping failure mechanism is active. Figure 2 and Table 1 collectively represent an integration of the historical inspection data.

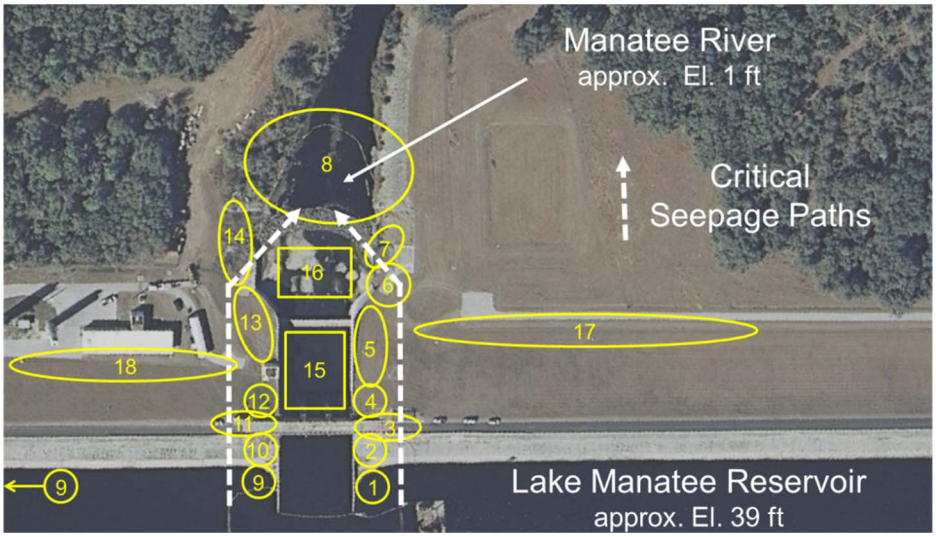


Fig. 2 Critical Seepage Paths and Locations of Significant Historical Observations

Since 1978 (eleven years after being placed into service) dam safety inspections have been performed by engineers from eight different engineering groups. One additional group was involved in a cofferdam design and issued a statement on the condition of the dam. In order to preserve the anonymity of these groups and focus on the lessons learned, references made to these groups are done by the designations A, B, C, D, etc.

Loss of embankment material on the surface of a dam and/or adjacent to a spillway structure can be interpreted in multiple ways. It could be due to surface erosion from runoff, movement of retaining walls causing settlement of the backfill soils, or internal erosion and subsequent settlement. Thus, in determining which visual observations were integrated into Fig.2 and Table 1, those identified by the engineers as either caused by surface erosion, or movement of the walls, or by internal erosion and settlement were included because the loss of embankment material on the surface could be due to one or more of these. In several of these inspections, photographs are included and/or statements are made about the presence of a sediment island in the downstream river channel. If internal erosion and piping is active, soil particles in the embankment and foundation would have been carried from their original positions and deposited downstream. Hence, the presence of a sediment island is a strong indicator of this potential failure mechanism.

Figure 3 presents a group-by-group visual integration of the inspection data. The following is a summary of the most significant observations made by each of the inspection teams. Refer to Fig. 3 for a visual representation of the approximate locations of these observations.

Group A Inspection. Specific observations made by Group A are indicated on Figure 3a and include: a) multiple vortices in the reservoir reported by the operators during low-pool conditions adjacent to the southern approach wall and along the southern embankment; b) an existing damp area on the downstream slope approximately 300 ft south of the service spillway; c) existing depressions in the service road approximately 700 ft south of the service spillway downstream of where one of the vortices occurred; d) a 3 ft diameter by 2 ft deep sinkhole immediately adjacent to the southern downstream training wall and directly above the existing toe drain outfall; e) loss of embankment material under the concrete stairway between the bridge deck and the southern downstream training wall; f) nearly continuous series of depressions in the toe road on the south embankment with wet spots and two conical depressions approximately 6 ft in diameter and 6 inches deep at 700 ft south of the service spillway; g) southern portion of the embankment has settled somewhat approximately 2 ft relative to the general embankment elevation; h) nearly continuous series of depressions along the toe of the northern embankment; and, i) extensive erosion downstream of the stilling basin and the subsequent placement of a concrete slab with sheet pile cutoffs (downstream apron) to decrease this erosion after construction.

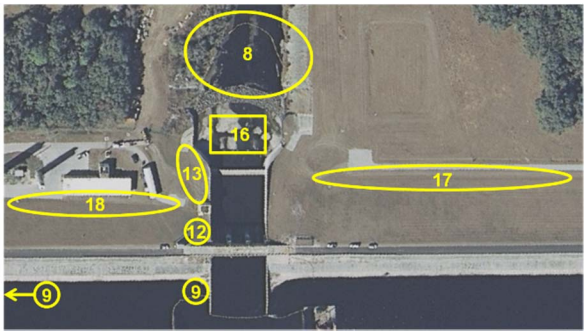
Group B Phase II Inspection, 1979. Specific observations by Group B are indicated on Figure 3b and include: a) loss of drilling fluid circulation and weight-of-hammer blow counts indicating very loose and soft soils at or near the bottom of the core at multiple locations; b) continuing erosion on the embankment slope just north of the service spillway downstream training wall; c) possible artesian pressure conditions at the embankment toe approximately 100 ft north of the service spillway; d) 2 ft diameter by 3 ft deep depression behind south downstream training wall; e) practically continuous series of depressions in the toe road on the southern embankment of the dam; and, f) toe drain collecting sediments and not functioning as designed, creating wet spots in the downstream toe areas on the south embankment.

Group C Inspection 1980 – 1981. Group C performed an annual inspection and made the following observations indicated on Fig. 3c: a) erosion and loss of embankment material along the upstream side of the sheet pile cutoff walls north and south of the spillway bridge; b) severe erosion and loss of material on the west end of the northern downstream training wall; c) erosion and undermining of the concrete stairway next to the southern downstream training wall; and, d) a previously wet area reported to inspectors between the downstream toe and the service road of the south embankment approximately 300 ft south of the service spillway.

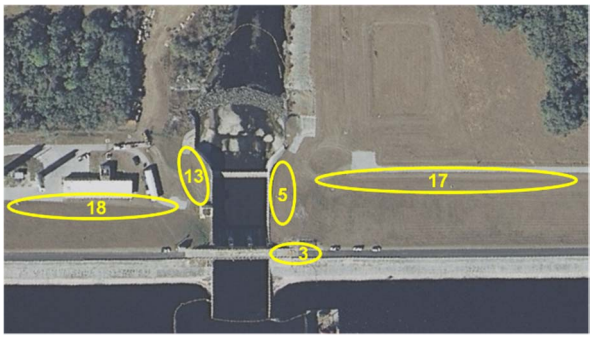
Table 1: Location and Types of Observations Consistent with Internal Erosion and Piping

Location Number	Location Description (Refer to Figure 3)	General Types of Observations	Range in Years Observed
1	Northern Approach Wall Below Water	Voids under wall foundations, voids with break in soil-cement slope and underlying embankment washout	2013
2	Northern Approach Wall Above Water	Depressions, surface erosion behind walls, outward movement/rotation of wall monoliths by as much as 2 inches, large void beneath soil-cement slope paving	1990 - 2013
3	Northern Bridge Approach Slab and Double Row Sheet Pile Cutoff	Weight-of-rod soil blow counts at bottom of clay core, persistent erosion adjacent to bridge, settlement along both sheet pile cutoff walls, subsidence of clay core between sheet piles, voids under secondary approach slab	1978 - 2014
4	Northern Downstream Training Wall Adjacent to Bridge Deck	Persistent erosion, depressions and soft zone in embankment slope, numerous surface irregularities, subsidence and voids under access ladder slab	1985 - 2013
5	Northern Downstream Training Wall Adjacent to Stilling Basin	Irregularities along embankment surface behind wall, outward movement/rotation of wall up to 2 inches, depressions, voids with the suspicion of a "chimney" drain against the wall, 20 cu. yd. sinkhole in 2009, very loose soils in backfill adjacent to the wall from the foundation level and upward	1978 - 2013
6	Western Corner of Northern Downstream Training Wall	Severe erosion, loss of backfill material, large voids under concrete slab behind toe drain outfall box	1981 - 2008
7	Northern Downstream Sheet Pile Wall	Severe erosion, seepage at west edge of sheet pile walls, multiple instances of depressions north of sheet pile wall and loss of backfill material, subsidence behind wall	1986 - 2004
8	Manatee River and Northern and Southern Riverbanks	Erosion, subsidence, large voids under surface protection materials on river banks, seepage daylighting on river banks, formation, dredging, and reformation of large sediment island in river channel	1973 - 2008
9	Southern Approach Wall and Embankment Below Water	Vortex in lake reported in 1975, large void with break in soil-cement slope and washout of embankment material	1975, 2013
10	Southern Approach Wall Above Water	Outward deflections of wall up to 2 inches, cracks, holes and voids in soil-cement slope with settlement and underlying soft soils	1987 - 2011
11	Southern Bridge Approach Slab and Double Row Sheet Pile Cutoff	Erosion, settlement and depressions along both sides of sheet pile walls and in roadway with a large void under the approach slab and under the secondary approach slab	1981 – 2013
12	Southern Downstream Training Wall Adjacent to Bridge Deck	Loss of soil, erosion and undermining of concrete steps, settlement of stairway and gate motor control slab with a large void under the slab	1978 - 2003
13	Southern Downstream Training Wall Adjacent to Stilling Basin	Voids, depressions and erosion in embankment behind the wall, wall movement towards the stilling basin, large void under concrete pads, soil in close proximity to the wall very loose beginning at the elevation of the bottom of the footing and extending upward, suspicion of "chimney" drain against wall	1978 - 2014
14	Southern Downstream Sheet Pile Wall	Erosion, displacement, and loss of material behind wall, void under concrete pad, flowing water behind wall	1989 - 2013
15	Stilling Basin	Void system underneath stilling basin discovered with dye study and confirmed with coring of floor slab	1997, 2013
16	Downstream Concrete Apron	Settling, cracking, undermining and deterioration of concrete, gap between sheet pile wall and concrete, voids detected underneath concrete	1978 - 2014
17	Downstream Slope and Northern Toe Drain	Artesian pressures in piezometers, sag in toe drain, settlement, depressions, and undulations along ground surface at toe, sedimentation in toe drain, depressions and undulations on downstream slope	1979 - 2013
18	Downstream Slope and Southern Toe Drain	Surficial seepage in toe area, nearly continuous depressions along service road near toe, large depressions downstream of where vortices were observed in the reservoir, settlement of toe drain	1978 - 2008

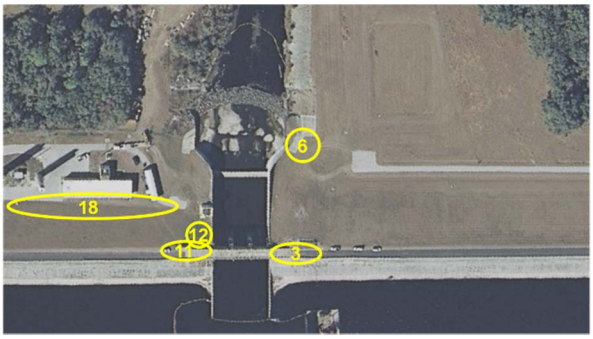
3a. Group A 1978



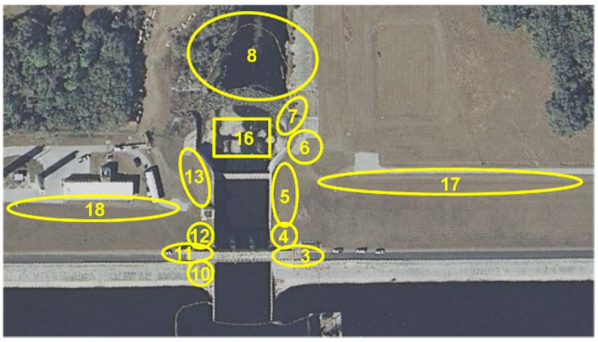
3b. Group B 1979



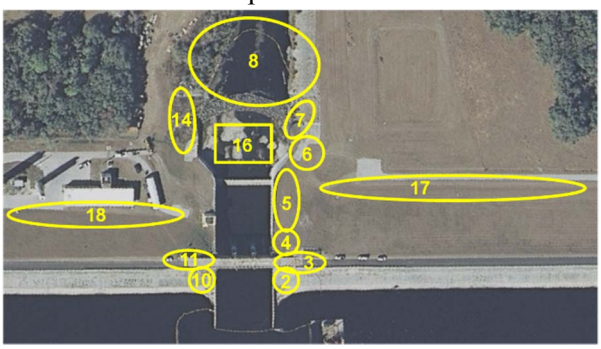
3c. Group C 1981



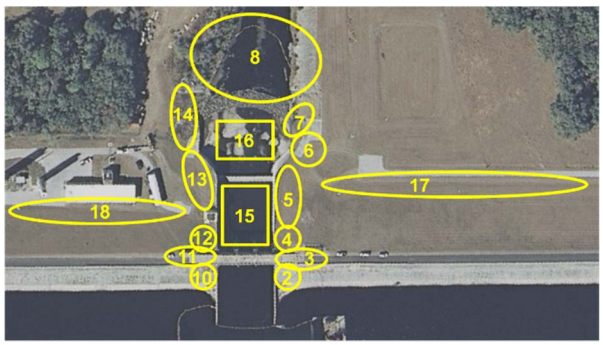
3d. Group D 1983 - 1988



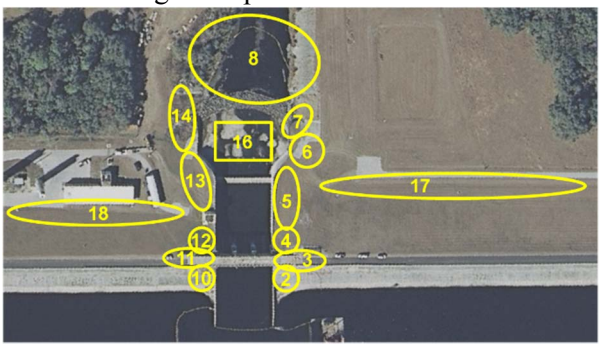
3e. Group E 1989 - 1992



3f. Group F 1993 - 1997



3g. Group G 1998 - 2011



3h. Group H 2012 - present

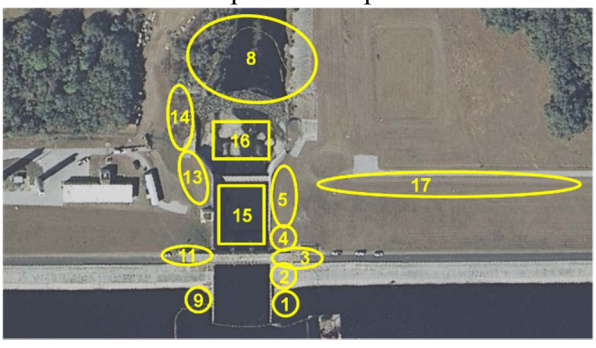


Fig. 3 Locations of Critical Visual and Physical Observations

Group D Inspections 1982 – 1988. Group D performed a series of inspections and commissioned a supplemental geotechnical subsurface investigation using a subconsultant engineering firm. Group D observations are shown on Fig. 3d and are as follows: a) lost the circulation of drilling fluid and very loose/soft soils in the clay core just north of the service spillway; b) piezometer levels approximately 900 ft south of the service spillway are above reservoir elevation, indicating groundwater flow from the southern abutment; c) artesian pressures coming from deeper soil layers in toe area and further downstream approximately 150 ft north of service spillway and in the location of the original river channel and a zone where piezometric water elevations increased moving downstream of the dam; d) erosion and loss of material along the sheet pile cutoff walls along both the northern and southern bridge approach slabs of the service spillway; e) ¾-inch outward displacement of southern approach wall monolith at the water intake structure for the water treatment plant (the first reported movement of one of the service spillway walls); f) undulations in the soil-cement surface cover on the upstream side of the dam near the northern and southern approach slabs to the bridge; g) severe erosion and loss of material immediately adjacent to the north downstream training wall and along the downstream riverbanks, resulting in undermining of the surface protection materials, and a photograph showing the edge of the apparent sediment island in the downstream river channel (but not identified specifically by the inspectors); h) erosion and undermining of the embankment materials under the stairway behind the southern downstream training wall; i) depression behind the south training wall; j) depressions in old baffle block locations in downstream concrete apron; and, k) settlement of the northern toe drain along with some unknown white substance being carried by the water in the drain.

Group E Inspections 1989 – 1992. Group E made the following observations as indicated on Fig. 3e: a) a depression and erosion in the soil-cement slope along the northern approach wall; b) outward deflections of up to 2 inches on both the northern and southern approach wall monoliths (this is the first reported movement of the northern approach wall in an inspection report); c) depressions and erosion adjacent to the northern bridge approach slab (both upstream and downstream) for the service spillway bridge; d) several locations where piezometric water elevations (PWE's) were either higher than the reservoir level or where they experienced fluctuations of a larger magnitude than corresponding fluctuations in the reservoir level; e) seepage between the northern downstream training wall and sheet piling; f) holes in the backfill behind the northern downstream training wall and sheet pile extension; g) depressions along the sheet pile cutoff wall and cracking of the bridge approach roadway adjacent to the south approach wall; h) separation of sheet pile wall sections and loss of backfill material downstream of south training wall; i) deterioration of the downstream concrete apron with sheet piling separating from downstream edge; j) seepage from downstream northern river bank with two slope instabilities adjacent to the sheet pile wall extension and further downstream, and a photograph of a sediment island in the downstream river channel; and, k) depressions and wet zones over the toe drains on both the northern and southern embankments, including a depression in the roadway below the dam near the service spillway on the southern embankment.

Group F Inspections 1993 – 1997. Group F suggested a potentially serious condition related to the observed movements of the approach and training walls. They also performed a dye study in the stilling basin underdrain and training walls backfill drain systems, as a result of reports from operators stating that running water could be heard through underdrain and backfill drain outflow pipes. The locations of the following observations are indicated on Fig. 3f: a) erosion, cracks and depressions in the soil-cement covering the slope adjacent to both the northern and southern approach walls; b) erosion and settlement of embankment materials immediately adjacent to cutoff sheet pile walls on the northern and southern bridge approaches and adjacent to the downstream training walls; c) outward displacements or rotations of both northern and southern approach walls and both northern and southern downstream training walls; d) evidence of vertical seepage from foundation soils into bottom of core at approximately 100 ft north of the service spillway (although there are irregularities in reported tip elevations of piezometers); e) voids and depressions behind both the northern and southern downstream training walls with possible drainage

"chimneys" into either joints between the retaining wall monoliths or into a void caused by the outward displacements of the walls; f) large erosion areas behind both downstream training walls near the junction of the sheet pile cutoff walls under the bridge approach slabs; g) erosion and loss of surface protection material on northern riverbank and a sediment island in the downstream river channel; h) a void system connecting the southern training wall base slab to the stilling basin end sill and extending underneath the downstream concrete apron; i) a depressed phreatic surface behind the northern downstream training wall at approximately 100 ft north of the service spillway indicating seepage from the downstream embankment shell towards the stilling basin; and, j) settlement, depressions, undulations, and bulging of the downstream slope near the locations of the northern and southern toe drains with no direct correlation between toe drain discharge and lake level.

Group G Inspections 1998 – 2011. Group G subcontracted with another engineering firm to perform geotechnical subsurface investigations focusing on the embankments behind the northern and southern downstream training walls. The two reports contain the following observations that are also indicated on Fig. 3g: a) large voids, settlement, and cracking on the upstream slopes behind both the northern and southern approach walls and voids under approach wall base slabs; b) subsidence of the clay core below the northern bridge deck approach slab, soft soils in the clay core, and settlement of the embankment along the sheet pile cutoff wall/embankment interface at the southern approach slab; c) settlement, erosion ruts, and depressions under concrete slabs behind both the northern and southern downstream training walls adjacent to the sheet pile cutoff walls; d) large voids, erosion ruts and loose to very loose soils in the embankments behind the northern and southern downstream training walls, including the formation of a 20-cubic-yard sinkhole behind the northern training wall in 2009 following a heavy rainfall event with a service spillway release and high tailwater; e) large voids, settlement, erosion and undermining of concrete mats and surfaces and loss of backfill material immediately downstream of the training walls, behind the sheet pile walls and along both the northern and southern riverbanks, accompanied with movement of the sheet piles; f) continued presence of a sediment island in the river channel downstream of the concrete apron until 2003 when it was removed by dredging; and, g) settlement of and sedimentation in the northern and southern toe drains.

Group H Inspections 2012 – 2014. Group H supplemented their inspections with diver inspections, ground penetrating radar, SPT borings, coring through the stilling basin floor slab, and video taping of the northern and southern toe drains. The following general observations were reported and are indicated on Fig. 3h: a) large voids and collapse of the soil-cement slope paving below the water surface adjacent to the northern and southern approach walls; b) large void under the soil-cement paving above the lake level and adjacent to the north approach wall; c) large voids under the primary and secondary bridge deck approach slabs and between the sheet pile cutoff walls on both the north and south sides of the service spillway; d) erosion, subsidence and loose to very loose embankment fill soils behind the north and south downstream training walls; e) undermining of slope erosion protection on the north riverbank; f) flowing water between the sheet pile wall and southern training wall; g) multiple voids under the stilling basin floor slab extending under the training wall base slabs; h) multiple voids under the downstream concrete apron; and, i) depressions in the downstream toe area of northern embankment just north of the service spillway. In 2012 Group H concluded that: "the Lake Manatee Reservoir Dam is well maintained and is in very good overall condition."

Group I Letter. In 2009, after an unsuccessful attempt to construct and dewater the cofferdam in 2011, Group I issued an unsolicited letter to Manatee County expressing significant concerns about the condition of the dam based upon observations made during the course of their work. The following is a list of conclusions about the condition of the dam from their letter:

a) there are voids beneath the pile supported upstream approach wall base slabs;
b) the dam's shell containment material upstream of and immediately adjacent to the clayey core material north of the north approach wall has been significantly loosened;

c) the soil-cement slope protection near the bottom of the upstream slope on the north side of the north approach wall has sloughed and failed;
d) there are potential voids/gaps beneath the downstream training wall base slabs;
e) there is concern about the condition of the corrugated and perforated piping that forms the underdrain system beneath the stilling basin floor slab;
f) there are voids and flowing water conditions beneath the concrete apron beyond the stilling basin end sill; and,
g) significant loss of material has occurred in the backfill zone behind the training walls at various times over the life of the structure and has been repeatedly backfilled by Manatee County.

SUMMARY AND CONCLUSIONS

When presented together using the data integration process depicted on Figure 3, these visual and physical observations provide a very strong indication that a serious internal erosion and piping failure mechanism was active at the Lake Manatee Dam shortly after construction and that it continued to evolve throughout the intervening years until it was finally addressed by the installation of a deep seepage cutoff wall in 2014. Some of the physical factors that contributed to this internal erosion and piping failure mechanism probably included: 1) a hydraulically connected backfill drain and stilling basin underdrain system with inadequate backflow prevention that aided in repeated saturation of the embankment during high tailwater releases; 2) a toe drain system with no backflow prevention that also aided in the saturation of the embankment; 3) an unlined discharge channel immediately adjacent to the end sill of the stilling basin and the downstream training wall foundations; 4) no seepage cutoff under the downstream training walls; 5) a deep borrow pit in the reservoir that cut through the designed confining layer for the embankment core cutoff trench; 6) regional artesian pressures in the aquifer immediately below the designed confining layer; and 7) pore soil compaction during initial construction of the dam. Each of these physical factors are significant and should have been addressed either during design or shortly after construction when observations indicated the presence of a potential internal erosion and piping failure mechanism, but they were not. Over the period of several decades this failure mechanism remained unidentified.

The most significant question about the near miss at the Lake Manatee Dam might be: “How could so many inspections be performed by so many engineers with such a large amount of physical evidence of the failure mechanism but without properly recognizing it?” The answer to this question goes to the heart of how we as a civil engineers evaluate aging infrastructure components and how human factors can affect our ability to recognize and respond to physical evidence. Perhaps the two most significant human factors that contributed to the near miss at the Lake Manatee Dam are: 1) Group Think and Aversion to Bearing Bad News; and, 2) Assessing Condition Based on Changes from Recent Condition. The following is a brief discussion of each of these human factors.

Group Think and Aversion to Bearing Bad News. As humans we tend to follow the combined thought of a group and are hesitant to go against the flow, especially when it requires us to deliver bad news to a client. If our conclusions are contradictory to those of prior engineers, there is the added pressure of not wanting to be wrong in our assessment. As with other aspects of our civil engineering practice, when we perform condition assessments of aging infrastructure components, we operate with high levels of uncertainty and there is rarely a definitive answer nor a perfect understanding of how a particular structure will perform. For this same reason we have historically used factors of safety or more recently load and resistance factors to rationally account for uncertainty in our design process. However, when evaluating the performance of an existing facility where we want to have as little uncertainty as possible about the actual condition and where there is the potential for making an incorrect assessment, we don’t have corresponding condition assessment procedures that rationally account for uncertainties. For this reason it is more difficult for us to recommend emergency actions when previous groups have seen the same condition but not recognized the emergency. In the case of the Lake Manatee Dam, the first few groups of inspectors found evidence of

serious internal erosion and piping occurring at the dam, but none of them clearly identified the problem nor recognized the emergency nature of the condition. In doing so, they set a "precedent" for future inspections by establishing a baseline of expected behavior. When the subsequent inspectors found evidence of a potentially serious internal erosion and piping failure mechanism did they default to the previous precedent and conclude that no emergency existed?

In order to avoid this human factor pitfall, the civil engineering profession needs to develop rational procedures to account for uncertainty in condition assessment techniques for our aging infrastructure. Additionally, as civil engineers we need to actively avoid falling into the group think mentality and approach the condition assessment of each aging facility from a different perspective, actively questioning the observations and conclusions of the prior inspectors. Unless we allow ourselves to consider that prior inspectors may have misinterpreted critical information or come to faulty conclusions, we may never recognize that such a situation is present at one of our facilities. This is not a recommendation to actively search for potential errors but to recognize that observations can be misinterpreted, thus triggering a reassessment of available information and the gathering of supplemental information.

Assessing Condition Based on Changes from Recent Condition. It is common practice for the condition assessment of aging infrastructure to look at changes from the most recent condition assessment. In particular, prior to the inspection, the dam safety engineers review the most inspection report, look at the descriptions of behavior (and photographs if available) and as a result "calibrate" themselves to the prior conclusions of the inspectors. As they perform the new inspection they look for evidence on how the previous conditions may have deteriorated. Such an approach is good for detecting rapidly deteriorating conditions. However, if the problem develops slowly and evolves over the years, inspectors may not be able to detect its severity by looking at changes from the most recent inspection. Of greater concern is that the baseline of acceptable behavior can shift under this approach. In other words, if a condition is serious for many years but it is observed on a year-to-year basis with little incremental change, inspectors can become complacent to its presence and actually conclude that: "The Lake Manatee Reservoir Dam is well maintained and is in very good overall condition", as was stated by Group H in 2012, even though it is in very serious condition.

In order to avoid this pitfall, inspectors of aging infrastructure components should perform an integration of the historical inspection data and map out signs of deterioration looking for trends, such has been illustrated herein.

ACKNOWLEDGEMENTS

The author gratefully acknowledges Mr. Mark Simpson and Mr. Bruce MacLeod of the Manatee County Utilities Department who worked tirelessly to implement the emergency measures necessary to protect the Lake Manatee Dam. The author also acknowledges the engineering staff of Amec Foster Wheeler in Central Florida who supported these inspection and emergency repair actions, including Mr. Nicholas Depin, Mr. Jeff Beriswill, and Dr. Les Bromwell.

REFERENCES

Andersen, G.R., Simpson, M. and MacLeod, B., 2015. The Importance of Integrating Historical Data in Preventing a Failure of the Lake Manatee Dam. Association of State Dam Safety Officials, The Journal of Dam Safety, Volume 13, Issue 1, pp. 19-38.

FRAMEWORK FOR RISK-BASED ELECTRIC SYSTEM DEEP FOUNDATION DESIGN

Peter M. Kandaris, DiGioia Gray, Inc., Tempe, AZ, USA, 480.666.9264, pkandaris@digioiagray.com
Steve Davidow, Quanta Subsurface, Spokane Valley, WA, USA, 509.789.7747, sdavidow@quantasubsurface.com
Ashely E. Evans, DiGioia Gray, Inc., Tempe, AZ, USA, 480.685.4952, aevans@digioiagray.com

ABSTRACT

Annually thousands of deep foundations are constructed across North America supporting high voltage transmission line structures. However, a recent state of the practice survey by the Deep Foundation Institutes' Electric Power Systems Foundation Working Group discovered that the electric power utility industry lacks consistent foundation design guidelines. The survey identified a wide variability in design assumptions, a minimal understanding of risk based analysis, and a need to standardize design methodologies. This paper summarizes the state of practice in electric system foundation design and proposes a framework for risk-based foundation design by accounting for uncertainty from both loads and resistances. Loads derived from electric system codes do not necessarily provide a compatible level of reliability for the design of foundations, as they are a mixture of probabilistic and deterministic values. Load uncertainty is derived from variability in weather conditions, structural models and material properties, typically accounted for by code derived overload factors. Resistance uncertainty arises from variability in natural soil properties, resistance models, subsurface construction techniques, material sampling methods, and limited observations. A consistent methodology is offered relating nominal resistance capacity (strength) to structure loads and service state criteria. Discussion also includes the need for risk-based assessments to account for non-structure load influences (fluvial loads, scour ground loss, liquefaction, etc.).

Keywords: transmission line foundations, risk based analysis, load, resistance, uncertainty, compatible reliability

INTRODUCTION

Nearly 40 years ago the Electric Power Research Institute (EPRI) embarked on a major research effort to optimize reliability and economics of transmission line foundation design. Strategies focused on improvements in design models, site characterization, exploration strategies and testing to reduce uncertainty and variance in analysis. Transmission line engineers realized that safety and reliability advancements in design based on probabilistic approaches, with a focus on the unique nature of transmission line, could better control risk and cost.

Some transmission line professionals took full advantage of these advancements, particularly where research led to improved software and models. Yet, even after two decades of extensive research, by 1995 the industry still had made little progress in changing design habits. The majority of designers were still characterizing sites via deterministic methods, using loads that may or may not relate to a consistent probability of occurrence, and applying a traditional global factor of safety approach (Phoon, et al. 1995). The following two decades have seen even greater developments in software and reliability-based analysis methods, but old habits seem to die hard as recent surveys show less than half of design professional quantitatively assess risk in their design process.

Unlike the commercial building and transportation industries, the power transmission industry does not have a unified code that explicitly covers the design and construction of the various foundation types currently utilized to support electrical structures. There is no overarching professional group that leads this effort. Guideline documents developed by other industries exist that describe different foundation types

 © 2017 DFI Annual Conference, New Orleans, LA, USA

used in the industry along with general design methodology, but practices vary from utility to utility. For this reason, the Deep Foundations Institute (DFI) established the Electric Power Systems Foundation Working Group to help address these issues.

BACKGROUND

State of the Practice

Recent industry surveys performed by EPRI (DiGioia 2010) and by DFI (Kandaris and Davidow 2015) attempt to quantify the state of the practice in terms of design methodology. These surveys examine the current design practices of electric power and overhead line design engineers working for U.S. engineering firms and utilities. Among the broader survey result, the EPRI study found two-thirds of responders were still using traditional deterministic (safety factor) approaches for design of transmission line foundations, with safety factors ranging upwards of 4.0 (depending on the structure type, foundation type and design model). The DFI survey a few years later showed about half of the electric system foundation professionals using traditional methods and just under 40% using probabilistic design approaches.

Probability-based design methods have enjoyed greater acceptance in foundation design for deep foundations in a number of industries such as buildings, bridges and similar public works where the load and resistance factor design approach (LRFD) is prescribed in federal, state and regional design specifications. Unfortunately, specifications and standards in the electric industry do not readily address foundation engineering for transmission line structures. Kulhawy and Hirany (2010) note that transmission lines are unique in that linearized systems that traverse great distances over potentially highly variable conditions. Adding to the fact that there is no single controlling authority on their loading conditions or design, there exists no universally accepted approach for determining transmission line loading, nor methods that should be used to evaluate these loads as they are transferred to foundations or foundation service performance requirements (CIGRE 2002).

Some professional societies have authored guide documents, attempting to present a more comprehensive approach to transmission line foundation design. Institute of Electrical and Electronics Engineers (IEEE) and American Society of Civil Engineers (ASCE) produced a guide for transmission structure foundation design and construction in 1985 (reaffirmed in 2007) (IEEE 2001). This general reference identifies sources of design loads and load combinations from transmission structures typically applied to design foundations. The guide notes that foundations should be designed to resist maximum designed loads relative to the structure it supports. But, the unique nature of both individual and combined steady-state and transient loads could cause foundation performance (deflection, settlement, uplift or rotation) to control foundation design. In addition, typical conservative practice is to envelope worst case foundation reactions components, shear, axial, and overturning moment, across all loading combinations into a worst case foundation loading condition. In practice, most utilities deterministically require loads applied to foundations be greater than the structure to prevent foundation failure prior to structure loss (IEEE 2001). Currently, there is not a consistent method to ensure uniform load increases for foundations as opposed to structure capacities.

As an example in evaluating industry inconsistency in design inputs, both surveys queried designers on the use and limits on laterally loaded foundation performance parameters (deflection and rotation) for reinforced concrete drilled shaft design. Both surveys found top of shaft allowable deflection as typically being deterministically selected with values ranging from 2 to 6 inches and pier allowable angular rotation ranging from 1.0 to 2.5 degrees. The DFI survey found about half of the respondents evaluated pier deflection and rotation using factored loads, another one-quarter evaluated these performance parameters at service loads and the remainder either did not know the load source or used other load criteria. When asked to describe the process for determining performance parameter limits, answers varied widely, with

designers using in-house standards, looking at past performance of foundation, obtaining values from published literature or asking local geotechnical consultants for recommendations.

Kalaga and Yenumula (2016) point out the importance of understanding the effects of angular rotation at ground level on transmission line structure performance. Even small angular rotations can induce large displacement at the top of these tall transmission line structures, leading to possible reductions in horizontal or vertical conductor clearances, poor aesthetic appearance and additional stresses on the pole structure. The authors note there are no universal standards for deflection or rotation limits on transmission pole foundations, leaving designers to use their best judgment. Complicating the analysis for the average practitioner, recent parametric studies on the effect of combined pole-foundation deflection found this type of analysis to be difficult, requiring the use of multiple software models (Bowland et al. 2015).

Foundation design standards and practices are generally left up to the judgment of design professional and utility organizations. The United States Department of Agriculture's Rural Development department provides guidance for the design and construction of rural utility services. Their specifications allow designers the option to specify foundation rotation either as a maximum for all load cases or as a certain value for each load case. Alternately, the engineer can opt to simply specify a fixed base with no allowable movement at any load value. The standard does recognize the need for varying performance parameters, matching types and probability of loads with foundation response and also requires the designer to include such effects in calculations as the final deflected pole stresses, but gives no guidance on how to approach the problem (USDA RDUP 2016).

With all the confusion, it is not surprising that many utilities and their consultants develop internal design manuals. The DFI survey indicates that nearly 60 percent do this in response to the lack of uniform guidance or to consolidate learned knowledge. Both the DFI and EPRI survey results show current practices for design of transmission line foundation vary widely and that these variations apply to all aspects of design including subsurface investigations, the foundation design process and the design of foundations for all types of transmission line structures. In response, EPRI produced in 2012 a transmission structure foundation design guide with suggested standard design processes for monopoles, H-Frame and lattice tower foundations within the framework of a Reliability Based Design (RBD) format (EPRI 2012).

It is clear that there is little consistency in the approach to transmission line foundation design among designers, consultants and utilities. Load factors (primarily safety factors) and performance factors used by designers vary greatly. Foundation design methodologies are not consistent. Methods to integrate structure load factors used for foundation design with reinforced concrete code factors differ or are not used at all (Kandaris and Davidow 2015). Foundation design loads are developed by enveloping worst case loading conditions that do not occur simultaneously, and strength and serviceability design checks are not consistently evaluated at separate loading levels. The consensus among transmission line design professionals is that there is a need to develop a guideline design document with recommendations for a uniform analysis and design approach for electrical system deep foundations.

Codes

Even though all transmission structure components are subject to the same laws of nature (gravity and weather – though intensity may vary) and obtain similar materials used worldwide from vendors who supply product internationally, there are no universal design codes for determining transmission line loading (CIGRE 2002). Regional, national, and local utility codes (mostly related to extreme weather conditions) typically govern transmission line structure design. Examples include the US National Electric Safety Code (NESC), the Canadian Electric Code (issued under CSA C22.3 No. 1-10), the International Electrotechnical Commission (IEC No. 60826), the joint Australian/New Zealand Standard (AS/NZS 4676), and General Order 95 (GO95) in the State of California. Most of these codes allow utilities to develop additional load

cases specific to their needs and conditions. These are broadly categorized to cover accidents, construction events and maintenance activities. Accompanying these load-related codes are recommended industry practice standards that are adopted by individual utilities or regional governing bodies as each sees fit, creating a unique agenda of loading cases for the design of their transmission line system (IEEE-691). These documents provide guidelines for transmission line structure and structure element design (ASCE MOP 74: Wong and Miller 2010; ASCE/SEI 7-10: ASCE 2010).

Maximum reactions used for transmission line foundation design are typically from weather-related events. Code and standard practices include some probabilistic evaluations of these conditions, but most often the loads are derived from successful local and regional experiences. Where there is a lack of experience or where structure loss becomes unacceptable, individual utilities may have special weather studies performed to more accurately define ice and wind events from a probabilistic approach.

These codes present weather-related loads in terms of wind pressure on lines and structures (for both mean and extreme conditions). For ice loading, ice thickness deposited on conductors during various storm events is given, with corresponding wind pressure that would occur with these events. As with most codes, loads are amplified with load or safety factors related to the given limit state. Table 1 presents common transmission line load factors for weather-related strength and extreme load cases from various utility codes. One or more of these load cases typically control foundation design. Other local weather related load cases, (as determined by utility owners) are usually variations on the extreme load cases with overload factors of 1.0 to 1.1.

Table 1. Common load cases for steel transmission line structures

Load Case	Load Type (Limit State)	Overload Factors		
		Vertical	Transverse	
		Dead	Wire Tension	Wind
CEC CSA C22.3 1-0	Strength	1.30	1.20 / 1.10	1.20
NESC Rule 250B	Strength	1.50	1.65	2.50
NESC Rule 250C	Extreme Wind	1.00	1.00	1.00
NESC Rule 250D	Extreme Ice	1.00	1.00	1.00
GO95 Rule 44.1	Strength	2.00	2.00	2.00

Loads used for foundation design are taken as maximum reactions, often enveloped, at the base of structures (e.g., base plates for steel monopoles/H-frames; top of concrete for lattice tower structures) and are governed by the structure manufacturer's design calculations. Foundation design loads are derived from all required code or owner-required overload factors and are typically considered "factored loads." For the purposes of foundation design, the term *design load* generally means the maximum top of foundation reactions obtained from structural analyses, to include all required factors.

Of interest, code loads relate only to those imposed by the above grade structure to the foundation at ground line. The effect of non-structure load conditions on the foundation by the surrounding environment can be present and include both sources of ground resistance loss and increased load. Load or resistance reduction sources generally related to foundations subject to flowing water including scour, fluid forces, and flowing/expanding ice forces. Sources related to ground motion include ground resistance loss due to liquefaction and loads due to liquefaction-induced subsidence or lateral spread. Landslides can both reduce resistance and increase foundation load. None of the identified codes directly address these conditions. Of particular interest are the climatic load levels the foundations should be evaluated at when considering non-structure additional loads and loss of geotechnical resistance.

Foundation Design Methodology

As a precursor to the future IEEE Guide for Transmission Structure Foundation Design and Testing, the co-chairs of that effort gave a detailed presentation in 1983 on the design of transmission line foundations (Tedesco and DiGioia, 1983). Their paper notes many alternative approaches can be used, but the steps involved remain the same:

- Perform subsurface investigation/obtain subsurface information
- Select subsurface foundation geotechnical design parameters
- Select appropriate foundation design model
- Determine required foundation performance criteria and apply loads to design model

Descriptions of each step described above are detailed in the most current version of IEEE-691 and are summarized in the following discussion.

Subsurface investigations are intended to accurately characterize the expected (nominal or characteristic) subsurface conditions at each structure site. Intrinsic in the process is the ability to access sites as needed to obtain information. Most often, though, structures are distributed across large distances and in variable geologic and geographic conditions where access may or may not be feasible at the time of the investigation. Additionally, most utilities do not have sufficient budget for sampling at all structure sites. Traditional investigations, therefore, focus on sampling at heavily loaded structures, at accessible points along the alignment, or at specified intervals (often one boring every one to two miles).

The recommended approach includes a preliminary investigation to collect existing data, assess subsurface conditions and make a geotechnical or geological field reconnaissance of the line route. This preliminary assessment is best performed by professionals skilled at geology or geologic engineering to optimize and apportion future investigation sites according to the geologic strata. If budget is available, preliminary sampling or field testing may be done to assist mapping and confirmation of expected subsurface conditions. A design investigation then follows this "desktop" assessment to provide the foundation engineer with sufficient information to select suitable foundation type(s), obtain samples for future testing and final foundation design, and evaluate potential problems during construction. Finally, it is recommended that the owner have representation in the field during construction to determine if actual conditions are similar to those used in foundation design. This is particularly important for transmission line foundation design since investigation information from single borings are typically extrapolated across multiple structure sites and site specific soil and rock resistance can often times be evaluated during the installation of the foundation element.

Geotechnical design parameter selection is generally recognized as the most critical step in implementation of the design process (DiGioia, 2010). The choice of design approach (deterministic or probabilistic), model and foundation type generally dictate the type of geotechnical design properties required for sizing the foundation. Most often, design properties for soil and rock layers are estimated from the site investigation and laboratory testing process. Subsurface and laboratory information for each boring are reviewed, including the field log and the final log which summarizes laboratory classifications and laboratory test data and the geotechnical design parameters assigned to each layer of soil and/or rock in the log.

At structures where borings have been tested, the foundations are designed with site specific geotechnical design parameters. For structures located between borings, foundations are designed with geotechnical design parameters derived from an evaluation of all of the borings drilled in each geologic zone. The geologic zone and specific borings are carefully examined and a representative subsurface profile is developed for each geologic zone or set of related foundations and structures.

IEEE-691 gives an extensive discussion on the range of models available for transmission line foundation design. Foundation dimensions are the result of calculating nominal foundation capacity where either strength or safety factors are used to reduce nominal strengths to design values. Of importance is understanding the required relative strength of the foundation to the strength of the structure it supports. Depending on utility practice or the needs of the specific project, foundations can be designed to be stronger than, equal to or less than the capacity of the structure. It is recommended that an analysis weighing all values and probabilities be made to determine the foundation criteria that meets requirements and provides economy.

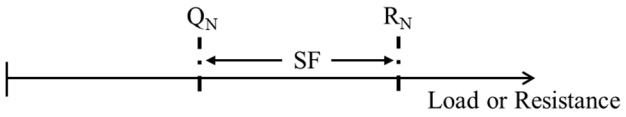
Most often, foundation design is controlled by steady-state and transient loads on structures (one or a combination of both). Construction and maintenance loads must be examined, but rarely influence foundation dimensions (Grigsby 2012). Present code-based loads provide maximum factored loads on foundations and are useful for evaluating the ultimate limit state. Foundation models are developed to estimate ultimate capacity in terms of nominal resistance values are reduced by various methods so that the foundation dimensions provide sufficient capacity when compared to factored applied loads. Reductions are made to account for material variability, construction techniques, and level of quality control provided during construction. Reduced nominal capacity is assumed so that normal operating loads are within the elastic range of the load-deformation relation, with the foundation functioning well below ultimate capacity.

Performance criteria are established for the design of safe and economical foundations. This requires a thorough understanding of failure, damage and service limits by the foundation and structure designers. Most often, foundation designers set performance criteria at the failure capacity of the foundation. But the survey of practice previously discussed strongly indicates that few designers really understand the difference between service and failure performance limits. Therefore, depending on the selection of performance parameters, top of pier settlement, deflection or rotation could dictate final foundation size.

RISK BASED DESIGN ELEMENTS

Foundation Design by Deterministic Approach

Traditional foundation design for transmission lines structures is based on deterministic methodologies (also referred to as Allowable Stress Design, or ASD). A global factor of safety (SF) accounts for total risk from both the load and resistance components (Fig. 1). Above grade structure component global safety factors are typically established by utility or state-specific design codes. For electric system foundations, the global safety factor value adopted by the designer is rarely from codes, but based on the background and experience of the designer. The State of California's General Order 95 (GO95) is an example of a deterministic approach that relates the material strength to design loads by upwards of a factor of 4.



$SF = R_N / Q_N$ Global Safety Factor Between Load and Resistance

Fig. 1. Deterministic Design Approach

With ASD, the working load (service load, Q_N) is the unfactored load, which must be obtained from the structure designer. Nominal resistance (R_N) is generally considered the foundation capacity based on nominal or characteristic material strength and deformation properties of the subsurface as needed by the component element design model being used by the designer.

Many have noted that global safety factors suffer from a major flaw in that they are not unique and can vary significantly over a wide range of conditions. Global factors of safety do not seek out and separate the more predictable variables from the highly unpredictable variables that shape foundation resistance. As these factors become institutionalized within organizations, they stagnate, making less efficient use of continued experiences, new learned knowledge and advances in state-of-the-art (Phoon et al. 1995; Phoon 2004). Changes in the design procedures used to determine structure loading are also difficult to capture with deterministic approaches, especially as load analysis becomes based more in probabilistic or semi-probabilistic limit state methods (CIGRE 2002).

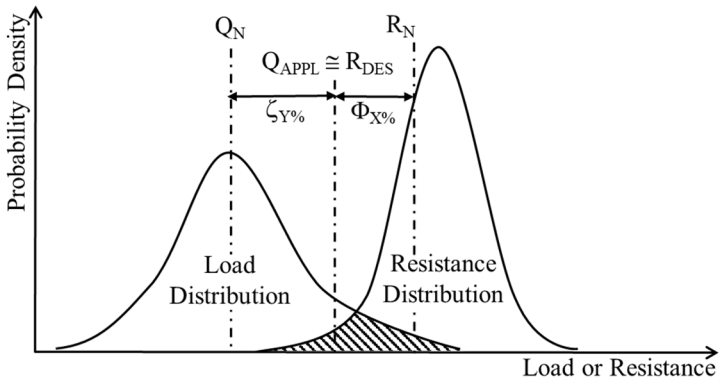
Foundation Design by Probabilistic Approach

Probabilistic methods are more commonly applied to structure load analysis with transmission line design work to account for variability in wind, ice and temperature conditions that change significantly with time. The approach (often referred to as RBD) is founded on the assumption that component applied loads (Q) are not unique but can vary significantly over the life of the component, from relatively low loads (such as everyday wind events) to very high loads (such as extreme wind and ice events). Likewise, the capacity of the structural foundation components and subsurface to resist load is not unique but varies due to the natural variation in structural and soil material properties, construction techniques, and foundation analysis models. Therefore, this risk-based approach accounts for uncertainty by using probability distributions rather than deterministic global safety factors. In a probabilistic approach, there is a point of compatibility for resistance and loads, each having their unique distribution. Conceptually, the point should occur as illustrated in Fig. 2, with a factored load and factored resistance. Note that the load factor increases nominal loading and the resistance factor decreases nominal resistance capacity. Factored load and resistance values need not occur at the intersection of the two probability distributions, but should be in close proximity.

The objective of RBD is to ensure that load and resistance factors will result in an acceptably low probability of failure (EPRI 2012). In terms of resistance (R), a lower exclusion limit is selected that is compatible with the reoccurrence interval used for determining the risk of maximum load effects. The combined probability of failure is determined by a convolution integral of the Q and R functions within the overlap area (hatched area in Fig. 2).

Level of Load and Resistance Reliability

The probability of failure can also be interpreted as the level of reliability needed for both structure and foundation design. This requires selecting load and strength factors based on a compatible level of reliability. The Canadian code previously discussed uses wind and ice reliability levels consistent with a 50-year recurrence interval. This recurrence interval is common among other electric industry codes. In many cases, a 50-year life is assumed for the line primarily to establish a defined level of reliability or probability of failure, and less to define the life of the line components. As an example, a 50-yr event return period (RP) results in a target reliability index (β) of 2.33 and would be compatible with a probability of failure of 1 in 100, where the probability of failure is approximately equal to 1/(2RP) (EPRI 2012).



$Q_{APPL} \cong R_{DES}$ Design Resistance Equivalent to Applied Load
$R_{DES} = \Phi_{X\%} R_N$ Factored Resistance from Subsurface
$Q_{APPL} = \zeta_{Y\%} Q_N$ Factored Load from Structure

Fig. 2. Probabilistic Design Approach

Industries select a level of (or target) reliability consistent with the risk associated in their design. Where there is a greater risk to life and property, higher target reliabilities are chosen. As an example, the U.S federal highway bridge design standards use a target reliability index of $\beta = 3.5$ for new designs, relating to a probability of failure at 1 in 10,000 (Ghosn et al. 2003). All load and resistance factors are then based on this level of reliability. Other public works such as dams and nuclear power plants would be expected to have even higher target reliability indices due to the greater consequence of failure with these facilities.

Resistance Factors

Establishing resistance factors involves taking available data (typically from full scale foundation testing) and statistically determining some acceptable lower limit of resistance that is calibrated to both the chosen reliability level and values seen in previous ASD. The major challenge in applying a fully probabilistic approach is the lack of sufficient and high quality full scale foundation test data to give designers confidence that their resulting designs provide an acceptable level of safety. Semi-probabilistic methods bridge this need (CIGRE 2002) and the methodology as used for the electric transmission industry is well documented in a number of publications (IEC 2017; Wong and Miller 2010).

Electric transmission system RBD methodology for determining soil resistance factors is based on defining a lower exclusion limit (LEL) using the estimated capacities of high-quality full scale foundation test results. ASCE 74 Task Committee adopted an LEL value of 5% (the probability that actual resistance will be less than the nominal value) for resistance of transmission line structure foundations (Wong and Miller 2010). Other industry groups have suggested using a higher value of 10% (Canadian Electric Code, Eurocode 7, for example.), but the ASCE task committee's opinion was that this LEL is consistent with a 50-year RP used for structure loading assessment. Of importance is that, although some research has been done to determine resistance factors for transmission line foundation design, the resistance factors developed to date have not been standardized and are not extensively used in practice. Foundation soil resistance values developed by the highway bridge design industry (AASHTO 2010), though, have gone through more vetting and may be applicable to transmission line foundation design (EPRI 2012).

One aspect left out of present utility RBD analysis is how to integrate these factors associated with ultimate capacity of the foundation system with performance criteria. The service limit state is rarely checked with transmission line foundation design since the industry has yet to develop performance service limits for settlement, rotation and deflection. Additionally, transmission structure designers and vendors do not, by

practice, provide unfactored loads to compare with service performance limits. More work is required to establish everyday service load levels and their associated performance criteria.

Outside Load Elements Effecting Risk

Traditional transmission line foundation design focuses on loads and load combinations applied to supporting structures. An entire chapter in the joint IEEE/ASCE guide for transmission line foundation design is devoted to structure loads imposed on foundations (IEEE 2001). Yet, the only mention of outside environmental conditions that could influence foundation performance is the evaluation of potential high groundwater and slope instability during field reconnaissance.

Non-structure load conditions that solely impact foundations can include environmental effects, causing both ground loss and increased load, and deep foundation construction techniques, which pose variable risk to foundation capacity when unchecked. Load sources generally related to foundations subject to flowing water including scour loss, fluid loads, and flowing/expanding ice loads. Sources related to ground motion include ground loss due to liquefaction and loads due to liquefaction-induced subsidence or lateral spread. Transmission line foundations within floodways and channels impede water flow and produce fluid flow pressure on foundations. These flows also result in increased flow velocities adjacent to foundations and the development of eddy currents that result in local scour. Foundations designed on slopes must recognize a reduced resistance due to uneven ground resistance or potential landslides.

Because of generally good performance during seismic events, the design of electric system transmission structures and foundations generally do not consider earthquake loading. The major influence of ground motion on foundations is the loss of support due to the liquefaction of susceptible subsurface layers and their possible lateral spread (CEATI 2015). Currently, no load combinations exist for the evaluation of structure loading in combination with seismically induced liquefaction. The use of ultimate climactic structure loading with earthquake induced loss of soil resistance is highly conservative.

Some utilities recognize the importance of accounting for non-structural loads and resistance losses, but at this time there are no codes to provide guidance within their documents to incorporate loads from the above grade structure with fluid loads on foundations or ground loss adjacent to foundations due to environmental conditions. The variability in foundation resistance, due to lack of site specific geotechnical data and variability inherent in subsurface construction, also necessitates the definition of a comprehensive foundation quality assurance and quality control program to ensure predictable reliability in foundation performance.

Load Factor Compatibility

Electric utility code organizations do not provide sufficient guidance within their documents to incorporate loads from the above grade structure with fluid or ground motion induced loads on foundations or ground loss adjacent to foundations due to these environmental conditions. It is important to match appropriate maximum probable transient events originating from the structure and those imposed on the foundation from the environment to provide a more reliable estimate of foundation reactions. Experiences from other fields may be useful in estimating appropriate load combination factors. For highway bridge design, nominal loads are usually associated with some long-term historical event that defines the loading (Ghosn et al. 2003). For example, the bridge design specifications require the design for a 50-year wind. But other events use different return periods for bridge design: earthquakes (2,500-year), traffic loads (75-year) and flood scour (100-year). The load factors used for extreme events are normally equal to or greater than 1.0 when each load is analyzed individually. When the load factor is greater than 1.0, it means that the true return period for the design event is greater than the specified nominal return period.

Even when two load types occur simultaneously, there is little chance that the intensities of both events will be close to their maximum lifetime values (Ghosn et al. 2003). For example, the probability of simultaneous occurrence of the maximum design earthquake and windstorm or flood event is minute. These load events are independent. It is reasonable to assert that maximum loads from infrequent events such as the earthquakes or floods should be evaluated in conjunction with more frequent (everyday) wind events. Fig. 3 diagrammatically presents an example this concept for structural wind loading, pier scour influence and soil resistance, where there is only a small overlap (as shown in the Venn diagram) of event occurrences within the joint probability region of each type of load and resistance (graphs).

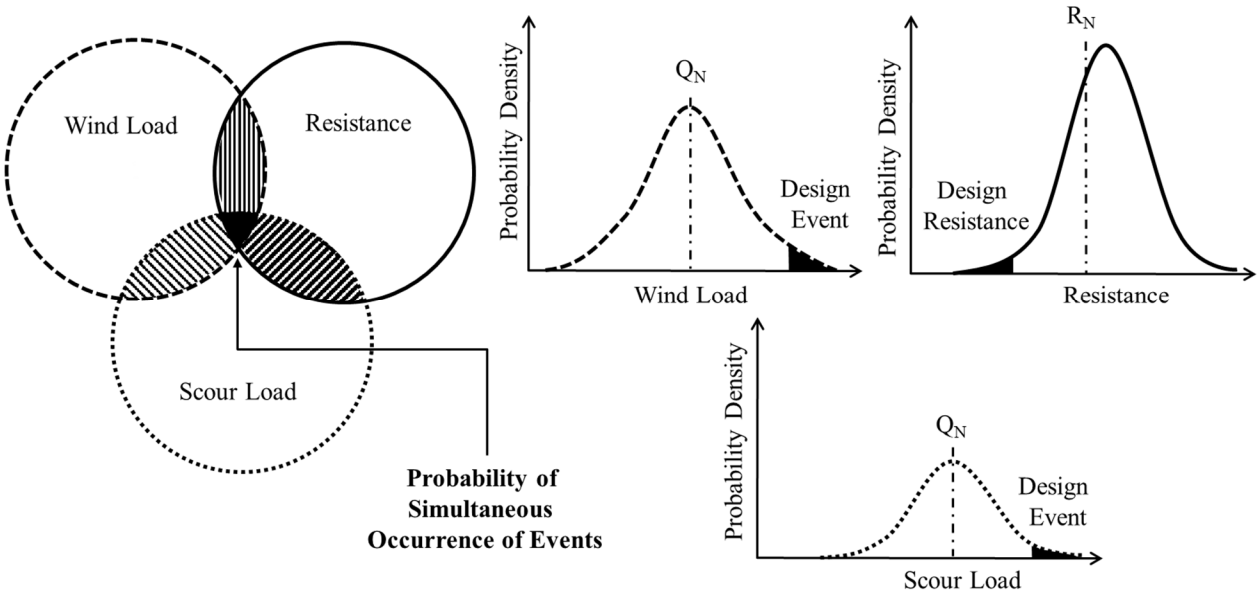


Fig. 3. Diagrammatic Representation of Probabilistic Combined Loads and Resistance

Present electric system foundation design practice typically evaluates maximum flood and ground motion induced loads or resistance losses as an additive effect on the standard structure load cases. Although regulatory and utility structure loading cases comprise steady-state, transient, construction and maintenance loads, more work is needed to provide compatible factors for evaluation with these other non-structural environmental events.

IMPROVING DESIGN METHODOLOGY

Load-Deformation Response

The goal of the engineer is to design a foundation that performs as expected under the anticipated range of applied loads. At a conceptual level, the mechanics of materials dictates a relationship between stress and strain as a function of soil-structure interaction. The non-linear nature of the load-deformation response for typical transmission line foundation types is well documented from full scale testing, laboratory scale tests and most foundation design models in both axial and lateral load modes (Davidson 1982; Kulhawy et al. 1983; DiGioia and Rojas-Gonzalez 1994). The relationship offers an opportunity to examine various load levels and performance at those levels in terms of settlement, deflection or rotation. Using either ASD or RBD approaches, foundation dimensions are typically sized to reach some ultimate limit of applied resistance capacity. This value is well above the factored applied load, accounts for variability in soils properties and results in large foundation movements as plastic motion has likely been achieved and foundation failure is imminent. Alternately, foundation movement at factored maximum applied loads tends

to be in the elastic-plastic transition range, while service (unfactored) applied loads are expected to be within the elastic range of foundation movement where normal deformation is mostly recoverable. Fig. 4 presents the concepts in general form.

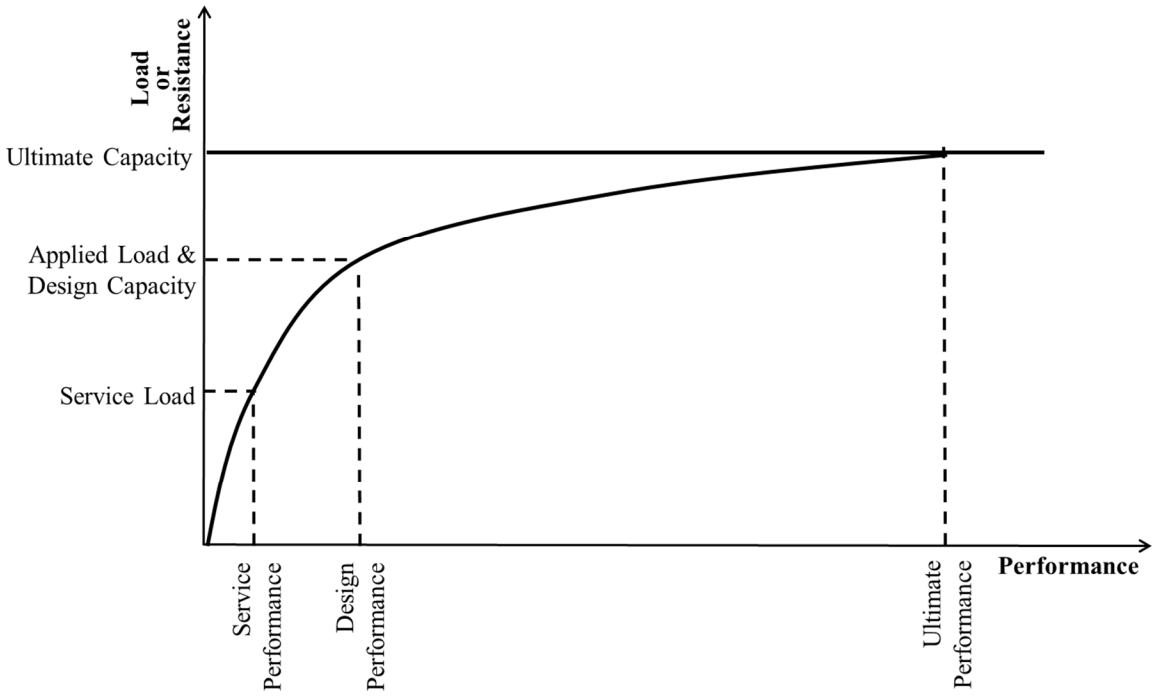


Fig. 4. Non-linear load (resistance)-performance relationship

As previously noted, the industry surveys indicate no consistency on how transmission line designers select performance parameters or the load level associated with those parameters. As Fig. 4 suggests, these parameters are not arbitrary, but should relate to performance at a specified load or resistance condition. It is easy to understand how improperly applied performance parameters could result in very conservative design if everyday service limits are assigned at maximum factored applied loads or (worse) at ultimate resistance capacity.

Most engineers have well developed concepts of deformation for service and design conditions, as these are in ranges of movement that would be expected. But, when asked to provided performance parameters for models at ultimate capacity, most still respond with limits they would desire at those lower load values. It is not intuitive to define deformations at failure.

Studies of laterally loaded, short, rigid drilled pier transmission line foundations tested by EPRI for development of their lateral load model explored theses load-deflection and load-rotation relationships (Davidson 1982; Kandaris et al. 2012). The earlier study determined that ultimate shaft resistance (capacity) is reasonably defined at the point where a pier rotates to an angle of about 2 degrees. The latter study found that for every one degree of pier rotation, the top of the pier laterally deflects from 3.5% to 4% of the pier diameter.

In other civil design sectors, service limit states are well defined and the associated working loads are based on either codes or experience. With transmission line foundation design, there is no controlling code to follow. Few design models present service load evaluations. Unfactored transmission line structure service

loads are rarely (if ever) calculated by structure designers or vendors. Fig. 5 is offered as a framework to better understand how various loads and resistances relate to foundation performance.

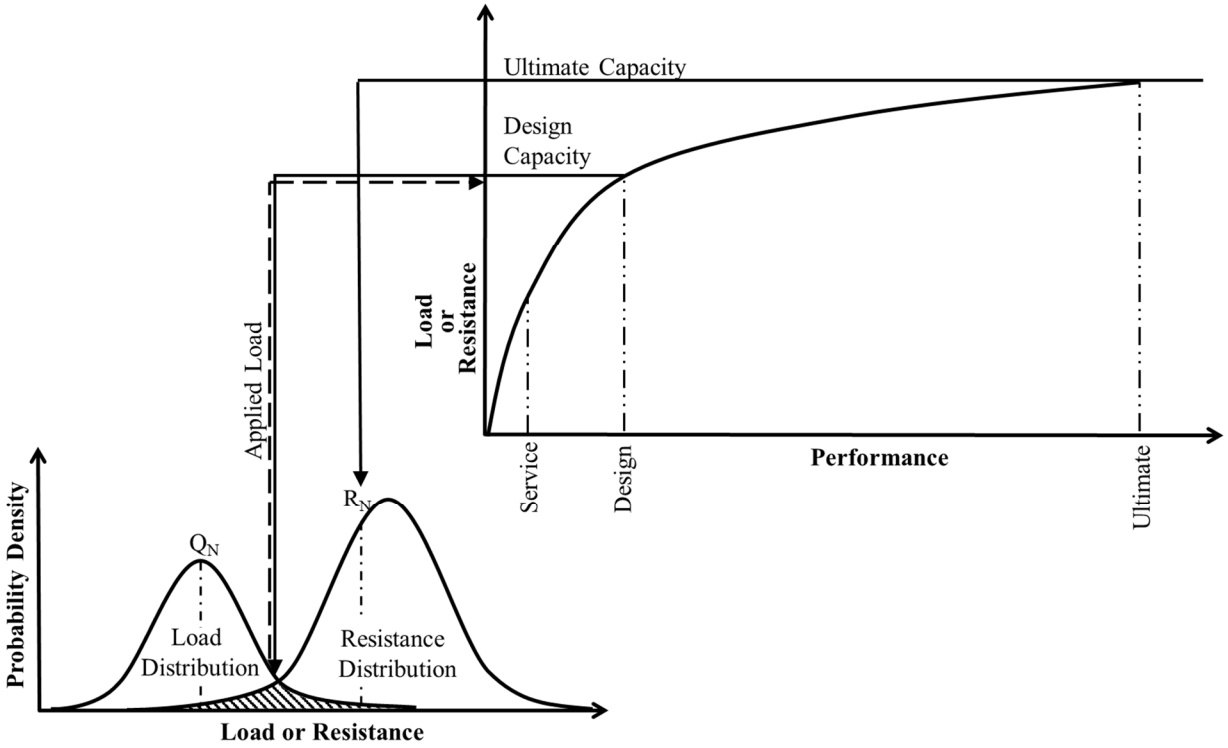


Fig. 5. Relationship of load and resistance probability to performance criteria

Compatible Load Factors

Although the utility industry has not directly addressed a probabilistic-based method to assess combined structure and environmental loads on foundations, guide documents developed other agencies and professional organization can be used to better understand how these can be incorporated with transmission line foundation design. These groups have developed load factors that vary depending on specified strength, extreme event and service load cases. These include:

- ASCE/SEI Standard 7-10 (ASCE 2010) – Probabilistic method of assessing variable load factors for combined dead, live, roof, wind and earthquake loads on structures.
- NCHRP 489 (Ghosn et al. 2003) - Probabilistic method of assessing variable load factors for combined dead, traffic, wind, collision and earthquake loads on bridge structures. Probabilistic foundation scour depth factors are also given for various extreme event load cases.
- AASHTO LRFD Highway Bridge Specifications (AASHTO 2012) - Probabilistic method of assessing variable load factors for combined loads from components/attachments, traffic and other live loads, wind on bridges, water on piers, ice on piers, collisions and earthquakes.

The NCHRP report presents analysis of target reliabilities for pier scour, combined maximum wind and scour, and combined maximum ground motion and scour.

SUMMARY AND CONCLUSIONS

There is a need to provide a unified approach or a comprehensive set of state of the practice guidelines that assess risk and account for variability in loads and soil resistances for the design of electric transmission line foundations. The electric power utility industry lacks consistent foundation design guidelines relating to design approach (allowable strength and reliability-based), compatible load and resistance factors, reliability level and performance parameters. This paper outlines a framework where given loads and resistances can be combined with the mechanistic model of foundation performance.

The continuing efforts of the DFI's Electric Power Systems Foundation Working Group intends to lay the groundwork for future guidelines and is presently preparing a state-of-the-practice white paper which summarizes current industry practices and evaluates existing foundation types, electric system codes and civil engineering standards. Future foundation design guidelines resulting from this effort will be prepared by this group to:

- Establish a consistent approach to Allowable Stress Design (ASD) and Reliability-Based Design (RBD) methods for all transmission line foundation types.
- Establish consistent reliability levels for load and resistance probability distributions.
- Incorporate resistance factors consistent with RBD methods using a target reliability index consistent with the risk associated with this type of facility.
- Emphasize the importance of following a consistent design process as detailed in IEEE-691, using probabilistic methods to better select geotechnical investigation sites and determine geotechnical design parameters.
- Address uniform ultimate and service limit states that are consistent with non-linear load-deformation responses observed with transmission line structure foundations.
- Provide recommendations for compatible probabilistic load factors and load cases for evaluation of transmission foundations subject to non-structural environmental events such as flowing water and ground motion. More research is needed to assess the probability of simultaneous occurrence of multiple extreme load events. Approaches used by the highway transportation industry provide a useful framework for establishing compatible load factors.
- Develop standards for foundation QA/QC programs consistent with various foundation construction techniques and field testing programs.

Dictating a single set of guidelines or methodologies is challenging due to the diversity of transmission line structure design approaches, load cases, environmental conditions and design philosophies utilized by various utilities. Recommendations of future guidelines must present best practices and sound reasoning that can be adapted to the variable nature of the transmission line foundation design.

ACKNOWLEDGEMENTS

The authors wish to thank the Deep Foundations Institute, and in particular Mary Ellen Large and Theresa Engler for their encouragement to establish the Electric Power Systems Foundation Working Group and their continued support in the group's efforts. We also thank the many group members who have helped and are continuing to provide time to write, review and edit the practice paper.

REFERENCES

American Associatgion of State Highway and Transpertation Officals (AASHTO), 2012. Sixth Edition, LRFD highway bridge specifications. American Associatgion of State Highway and Transpertation Officals. Washington, D.C.

American Society of Civil Engineeers (ASCE), 2010. Minimum design loads for buildings and other structures. American Society of Civil Engineeers. Standard ASCE/SEI 7-10. Reston, VA.

Bowland, A.G., Cass, P.G., and DiGioia Jr, A.M., 2015. Recommendations for steel pole and drilled shaft deflection criteria based on a parametric study of a 138kv double circuit transmission line. Electrical Transmission and Substation Structures 2015, 127 p.

Canadian Standards Association (CSA), 2010. Design criteria of overhead transmission lines. Mississauga, ON. Report Number CAN/CSA-C22.3 NO. 60826-10.

CEATI International, 2015. Best practices for design of transmission line structures located in water for protection against additional loads imposed during floods and foundation scour. Transmission Overhead Design & Extreme Event Interest Group. CEATI Report No. T133700-3390.

CIGRE Working Group 22-07, 2002. The design of transmission line support foundations – an overview. CIGRE Technical Brocdhure No. 206, 68 p.

Davidson, H.L., 1982. Laterally loaded drilled pier research. Report EL-2197 (2 volumes). Electric Power Research Institute, Palo Alto, CA.

DiGioia Jr., A.M., and Rojas-Gonzalez, L.F., 1994. Rock socket transmission line foundation performance, IEEE Transactions on Power Delivery, 9(3) 1570-1576.

DiGioia Jr., A.M., 2010. Guide for reliability-based design of transmission line structure foundation. 1019959. EPRI, Palo Alto, CA, 246 p.

Electric Power Research Institute (EPRI), 2012. Transmission structure foundation design guide, EPRI Technical Report 1024138, Palo Alto, CA.

Ghosn, M., Moses, F., and Wang, J., 2003. Highway bridge design for extreme events. National Cooperative Highway Research Program. NCHRP Report 489.

Grigsby, L. L., 2012. The electric power engineering handbook (3 ed.): CRC Press.

Institute of Electrical and Electronics Engineers (IEEE), 2001. IEEE guide for transmission structure foundation design and testing. New York, NY. Standard 691-2001.

Institute of Electrical and Electronics Engineers (IEEE), 2007. National electrical safety code (NESC). Piscataway, N.J.

International Electrotechnical Commission (IEC), 2017. IEC 60826 (2003) Design criteria of overhead transmission lines. Geneva, Switzerland.

Kalaga, S., and Yenumula, P., 2016. Design of electrical transmission lines: structures and foundations. CRC Press.

Kandaris. P.M., DiGioia, Jr. A.M. and Heim, Z.J., 2012. Evaluation of performance criteria for short laterally loaded drilled shafts. GeoCongress, pp. 165-174.

Kandaris, P. M., and Davidow, S., 2015. Study of electric transmission line deep foundation design. In Electrical Transmission and Substation Structures, pp. 577-587.

Kulhawy, F.H., O'Rourke, T.D, Stewart, J.P, and Beech, J.F., 1983. Transmission line structure foundations for uplift-compression loading: load test summaries, Rpt. El-3160, Electric Power Research Inst., Palo Alto, CA. 729 p.

Kulhawy, F.H. and Hirany, A., 2010. Foundation engineering for transmission line structures. Art of Foundation Engineering Practice, pp. 343-358.

Phoon, K. K., 2004. Towards reliability-based design for geotechnical engineering. Special Lecture for Korean Geotechnical Society, Seoul, Vol. 9, pp. 1-23.

Phoon, KK, Kulhawy, FH and Grigoriu, MD, 1995. Reliability-based design of foundations for transmission line structures, Rpt. TR-105000, Electric Power Research Inst., Palo Alto, CA., 380 p.

USDA Rural Development Utilities Program (USDA RDUP), 2016. Guide specifications for steel single pole and H-frame structures. Bulletin 1724E-204. Engineering Standards Branch; Office of Policy, Outreach and Standards.

Wong, C.J., and Miller, M.D., 2010. Guidelines for electrical transmission line structural loading: American Society of Civil Engineers Publications.

Tedesco, P.A. and DiGioia, Jr., A.M., 1983. IEEE/ASCE transmission structure foundation design guide. Proceedings of a Symposium, ASCE National Spring Convention, May 16-20, 1983, Philadelphia, PA. New York: ASCE.

LRFD RESISTANCE FACTORS FOR DESIGN OF DRIVEN PILES USING THE TEXAS CONE PENETRATION (TCP) TEST

Hoyoung Seo, Ph.D., P.E., Texas Tech University, Lubbock, Texas, hoyoung.seo@ttu.edu
William D. Lawson, P.E., Ph.D., Texas Tech University, Lubbock, Texas, william.d.lawson@ttu.edu
James G. Surles, Texas Tech University, Lubbock, Texas, james.surles@ttu.edu
Priyantha W. Jayawickrama, Ph.D., Texas Tech Univ., Lubbock, Texas, priyantha.jayawickram@ttu.edu
Rozbeh Moghaddam, Ph.D., P.E., GRL Engineers, Inc., 30725 Aurora Road, Solon, OH 44139

ABSTRACT

This study provides calibration of resistance factors (ϕ) for design of driven piles to implement Load and Resistance Factor Design (LRFD) for bridge foundations using Texas Cone Penetration (TCP) Test data. The basic research approach was to compile a database of published full-scale load tests including projects from the Texas Department of Transportation's (TxDOT) historical archive and projects from neighboring state DOTs. Load test results from neighboring states were leveraged by performing new geotechnical borings with TCP tests at the project sites. The final dataset consisted of 30 load tests performed on precast square concrete piles, with pile widths ranging from 356 to 508 mm and penetration depths ranging from 5.2 to 25.5 m, driven in soils. Ultimate capacities for each load test were interpreted based on Davisson, 5%, and 10% settlement criteria. These measured ultimate capacities were compared against predicted capacities estimated from TCP blow count values (N_{TCP}) and design charts following the procedures outlined in TxDOT's *Geotechnical Manual*. From the comparisons, statistical parameters of the biases (λ = measured capacity/predicted capacity) such as mean and coefficient of variation were obtained. Resistance factors (ϕ) for LRFD were then determined using Monte-Carlo simulations for each ultimate capacity criteria with the target reliability indices of 2.33 and 3.00.

Keywords: Texas Cone Penetration (TCP) test, Driven piles, LRFD, Resistance factor

INTRODUCTION

The Texas Department of Transportation (TxDOT) has used the Texas Cone Penetration (TCP) test since its development in the 1940s. The TCP test is an in-situ penetration test to characterize the materials encountered during geotechnical exploration. Texas currently maintains over 53,000 bridges in the National Bridge Inventory (FHWA 2016), and most of these bridges plus other transportation infrastructure in Texas are supported by foundations designed using the TCP test and its associated foundation design method. The Oklahoma DOT adopted the TCP test and foundation design approach in the 1970s, so the foundations for most of the 23,000 bridges in Oklahoma's inventory were also designed using the TCP method. With this significant body of experience, the TCP method has been viewed as a straightforward, relatively easy-to-use foundation design method that consistently yields safe, serviceable, economical, and maintainable foundations. TxDOT's deep foundation design method is documented in the TxDOT *Geotechnical Manual* (TxDOT 2012) and currently employs the allowable stress design (ASD) approach. However, the Federal Highway Administration (FHWA) has mandated that the states begin to implement the LRFD method in place of the older ASD approach (Densmore 2000). This paper presents resistance factors at ultimate limit state (ULS) for design of driven piles using the TCP test, resulting from efforts to be in compliance with the FHWA policy.

 © 2017 DFI Annual Conference, New Orleans, LA, USA

TCP TEST AND FOUNDATION DESIGN METHOD

Description of TCP Test. The TCP test is a dynamic field penetration test which assesses the consistency of the material encountered during geotechnical exploration. This test method is documented as TxDOT Designation Tex-132-E, "Test Procedure for Texas Cone Penetration" (TxDOT 1999). The TCP test uses a 77.0-kg hammer with 60-cm drop to force a 76-mm diameter steel cone into the soil or rock formation at the bottom of a borehole. Details of cone geometry are presented in Fig. 1. In current practice, the penetration is to be achieved in three separate increments. The first increment is completed to ensure proper seating, which consists of driving the cone 12 blows or approximately 15-cm (6-in), whichever happens first. The TCP blowcount is then determined as the sum of the number of blows required to achieve second and third 15-cm (6-in) increments of cone penetration. The total blowcount or N_{TCP} corresponding to 30-cm (12-in) penetration is used to obtain design parameters. The TCP test also accommodates penetration testing in very hard materials such as rock and intermediate geomaterials, but that aspect of the test does not apply for the driven pile data presented herein.

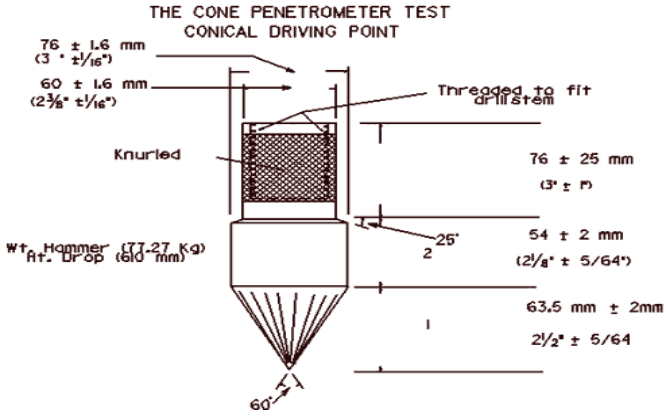


Fig. 1. TCP test conical driving point (TxDOT 1999)

Pile Design Method Using TCP. The TxDOT *Geotechnical Manual* (TxDOT 2012) provides two design charts for driven piles from which the allowable unit shaft and base capacities can be obtained for a given N_{TCP} value for various soil types. The design curves for determination of the allowable unit shaft resistance ($q_{s,all}$) are represented with the following equation for soils with N_{TCP} less than 100 blows per 30 cm:

$$q_{s,all}(kPa) = C_s N_{TCP} \leq 134\ kPa \quad [1]$$

where N_{TCP} = average measured TCP blowcount (≤ 100 blows/30 cm) for the stratum and C_s = constants based on soil classification (= 1.92 for CH, 1.60 for CL, 1.37 for SC, and 1.20 for other types of soils). Note that the allowable unit shaft capacity is capped to a value of 134 kPa as per the TxDOT *Geotechnical Manual*.

Similarly, the design curves for determination of the allowable unit base capacity ($q_{b,all}$) are represented with the following equation for soils with N_{TCP} less than 100 blows per 30 cm:

$$q_{b,all}(kPa) = C_b N_{TCP} \quad [2]$$

where N_{TCP} = average of measured TCP blowcounts (≤ 100 blows/30 cm) within two pile diameters below the base and C_b = constants based on soil classification (= 4.92 for CH, 5.78 for CL, 5.89 for SC, and 5.16 for other types of soils). According to TxDOT's *Geotechnical manual*, both $q_{s,all}$ and $q_{b,all}$ include a minimum factor of safety of two.

LOAD TEST DATABASE

Description. The load test data needed for this study were obtained from two separate sources. First, TxDOT possesses an archive of load tests which spans over several decades during which the TCP design method has been used for deep foundation design. The TxDOT data archive was supplemented with load test data available from Texas' neighboring states. In order to leverage these non-Texas load test data, new geotechnical borings were drilled and TCP tests conducted at those load test sites. The dataset compiled in this manner consisted of a total of 33 load tests on driven piles. All the 33 driven piles were precast square concrete piles with widths ranging from 0.356 to 0.508 m and penetration depths ranging from 4.6 to 25.5 m. Among the 33 load tests, 28 of them were conventional static top-down load tests and the remaining 5 tests were statnamic load tests. None of the 33 load tests were instrumented with strain gages and therefore resistance factors were determined only for total capacity in this study.

Among the 33 load tests, 22 of them were loaded beyond the ultimate capacity determined from Davisson's criterion (Davisson 1972). Among the 11 tests which did not reach the Davisson's offset line, eight of them reached at least an elastic line and were included in our dataset after extrapolation of the load-settlement curves. However, the remaining three tests which did not reach even the elastic line were deemed non-usable and therefore excluded from the dataset for the subsequent reliability analyses. Consequently, 30 tests on driven piles were included in the final load-test dataset. Fig. 2 shows an example of load-settlement curve and determination of the ultimate capacities for Case No. 15 from our dataset.

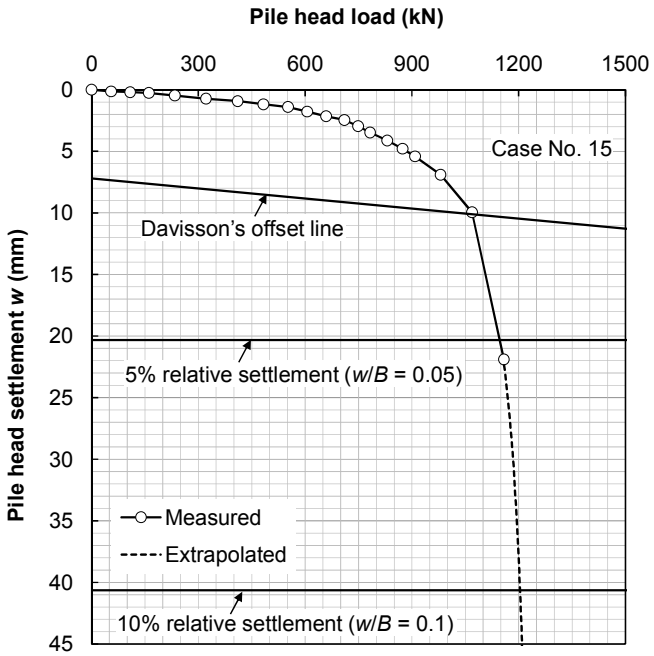


Fig. 2. Example of load-settlement curve and determination of ultimate capacities (Case No. 15)

Ultimate capacity of deep foundations is generally defined based on the load-settlement relationship obtained from a full-scale load test. In this study, Davisson, 5%, and 10% relative settlement criteria were used to determine the ultimate capacity (Q_{ult}) for driven piles. The prediction of the ultimate capacity of each test pile was accomplished using the procedure outlined in the TxDOT *Geotechnical Manual* (TxDOT 2012). It should be noted that the TCP design charts provide allowable unit shaft and base capacities rather than ultimate values. Therefore, allowable capacities were multiplied by factors of safety of two, as was provided in the *Geotechnical Manual*, to obtain ultimate shaft and base capacities. Table 1 presents a

summary of the measured and predicted ultimate capacities of the test piles used in this study, excluding the three tests disregarded in the subsequent analysis.

Table 1. Summary of load test database for driven piles in soils

Case No	Pile Dimensions		General Stratigraphy	Q_{ult} from Davisson's Criterion[a)]	Q_{ult} from 5% Criterion[a)]	Q_{ult} from 10% Criterion[a)]	Predicted Total Capacity (kN)	Composite Data Quality Score
	B (m)	L_p (m)		Total (kN)	Total (kN)	Total (kN)		
1	0.356	9.1	CL/SM	497	528	543	861	8.4
2	0.356	7.8	CL/SM/CL/SC	1654	1765	1882	769	8.4
3	0.356	6.7	CL/SM/CL	1161	1300	1380	874	8.4
4	0.356	10.5	CL/CL/SC/CL	866	909	940	1615	8.4
5	0.508	21.1	WATER/CL/SP/ CH/SM	2901	3261	3692	1497	6.4
6	0.381	10.7	CL/SC/SM	1574	1891	2214	1243	9.2
7	0.381	10.0	CL/SC/SM	1365	1487	1595	1354	9.2
9	0.406	13.0	CL/SW/CL/SP	1044	1162	1231	1969	7.8
10	0.406	13.4	MH/SP/SM/CL/ SP	1291	1452	1572	1046	8.4
11	0.406	14.2	CL/SP/CL/SP	1652	1873	2087	2482	6.4
12	0.406	5.0	CL/SC/CH	1047	1218	1305	626	8.4
13	0.406	4.6	SM/SP/CL	1598	1792	1906	472	8.4
14	0.406	14.2	SP/CL/SP/CL/ SP	1304	1443	1577	1820	8.4
15	0.406	9.1	CH	1049	1147	1205	1338	8.4
16	0.406	9.4	CH/SM/CL	1344	1409	1501	881	8.8
17	0.406	12.2	CH/SM/CH	579	1000	1464	933	8.2
18	0.381	9.4	CL/SM	1255	1507	1692	808	6.6
19	0.508	23.5	SM/CL/SM	1117	1177	1205	2690	7.2
20	0.356	8.1	CL	1570	1728	1779	3293	9
22	0.457	25.5	MH/SM	1222	1359	1466	1285	5.4
24	0.356	7.8	CL/SM	1122	1179	1214	1060	9
25	0.457	12.8	CH/SM/CH	1722	2011	2212	1222	8.6
26	0.457	12.8	CH/SM/CH	1712	1817	1887	1222	8.6
27	0.457	12.2	CH/SM/CH	1519	1739	1869	1132	8.6
28	0.457	12.8	CH/SM/CH	2668	3239	3827	1222	7.4
29	0.457	16.8	CH/SM/CH	3132	4832	9288	2026	8.6
30	0.508	21.9	CH/SC/CH/SP/ CH/SP	3031	2910	3728	3285	8.4
31	0.508	21.9	CH/SP/CH/SP/ CH	2173	2539	2614	2316	8
32	0.356	13.1	CH/SM/CH/SM	1096	1185	1216	970	8.8
33	0.356	24.4	SM/CH/SP/CH/ SP	3014	3962	3962	2653	5.4

Note: a) The ultimate capacity values in these columns represent measured capacities based on corresponding ultimate capacity criteria if those criteria were met. Otherwise, these values were obtained from extrapolation using weighted hyperbolic method.

Quality of Dataset. The quality and reliability of the load test data varied significantly from one project to another. As mentioned previously, some of the load tests records collected for this study were several decades old whereas others were very recent. Furthermore, although most of the load tests were loaded to the final loading step during the first loading cycle, some load tests were performed in multiple loading cycles. The level of capacity mobilization and extrapolation also varied widely. In order to capture and account for these differences in load test quality, we created and introduced an index called Measured Capacity Quality Rating for each load test project. As shown in Table 2, the factors considered were (a) settlement level at the end of the load test, (b) straightforwardness of load test procedures, and (c) completeness of documentation and records. A quality score assigned for each category was multiplied by a weight and summed up to give final quality rating, varying from 1 to 5, with larger numbers representing greater quality.

Table 2. Quality ratings for measured capacity

Settlement Level at the End of Load Test [60%]		**Straightforwardness of Load Test Procedures [20%]**		**Completeness of Documentation and Records [20%]**	
Reached or exceeded 100% of the Davisson offset line	5	Load test procedure is straightforward and unambiguous	5	Sufficient, high-quality data are available	5
Reached or exceeded 75% of but not 100% of the Davisson offset line	4	-	4	-	4
Reached or exceeded 50% but not 75% of the Davisson offset line	3	Load test procedure is somewhat unclear but overall straightforward	3	Some missing data; OR, average-quality data available	3
Reached or exceeded 25% but not 50% of the Davisson offset line	2	-	2	-	2
Reached or exceeded elastic line but not 25% of the Davisson offset line	1	Load test procedure is unclear and questionable	1	Significant gaps in available data; OR, low quality data	1

The reliability of the predicted load capacity estimated based on site characterization data also varied. In order to capture differences in site characterization data quality associated with load capacity prediction, we created and introduced an index which we termed the Load Capacity Prediction (LCP) Data Quality Rating. The LCP data quality rating was calculated based on an arguably-subjective-yet-systematic assessment of site characterization data quality for factors including (a) proximity of the geotechnical borings used to develop generalized soil profile to test shaft or pile, (b) site uniformity, (c) completeness of available data, (d) ease of interpretation of data, and (e) TCP and shear strength data, as shown in Table 3. The LCP data quality rating also varied from 1 to 5, with larger numbers representing greater quality.

Combining the quality ratings for measured and predicted capacities for a given load test yielded a composite quality index ranging from 2 to 10, and these values are presented in Table 1. Among the 30 driven pile load tests, 22 of them have a composite quality rating of 8 or higher. To facilitate the statistical analyses for this study, the composite quality index was converted into a weighting factor that ranged from 0 to 1. Weighting factors of 1 and 0.9 were assigned for composite quality indices of 10 and 7, respectively; a weighting factor of 0 was assigned for composite quality index less than or equal to 3. For other values of composite quality index, a linear interpolation was performed to obtain the weighting factor. Weighting factors were then used in the calculations of the effective sample size, mean, and coefficient of variation of the bias. More details of the quality-rating rubrics, composite quality index, and weighting factor are presented in research reports published by the authors (Seo et al. 2015a and 2015b).

Table 3. Quality ratings for predicted capacity

Proximity of Borings [20%]		**Site Uniformity [20%]**		**Completeness of GSP Data [20%]**		**Ease of GSP Data Interpretation [20%]**		**TCP and Shear Strength Data [20%]**	
Borings are in close (< 9 m) proximity to test pile/shaft	5	Multiple borings show uniform site conditions	5	Sufficient high-quality are available	5	Data interpretation is quite straightforward and unambiguous	5	Sufficient data that follow consistent trend; Data collected using current test protocol	5
Borings are at intermediate distance (9-46 m) from test pile/shaft	4	Site uniformity cannot be determined (i.e. single boring); single boring is in very close proximity	4		4		4	Sufficient data that follow consistent trend; Uncertainty re: test protocol used	4
Exact locations of borings relative to test shaft/pile not known; But relevant borings have been identified in original documentation	3	Multiple borings show somewhat uniform site conditions	3	Some missing data; Data of average quality	3	Some room for different interpretations of available data	3	Limited data or Data with significant scatter	3
Borings are at large distance (> 46 m)	2	Site uniformity cannot be determined (i.e. single boring); single boring at intermediate proximity	2		2		2	Data derived based on assumptions	2
Locations of borings relative to test shaft/pile cannot be determined; available borings were used	1	Multiple borings show variable site conditions; or single boring is at large distance	1	Significant gaps in available data or low quality data	1	Significant challenges with data interpretation	1	Data were obtained through indirect means (e.g. correlation)	1

DEVELOPMENT OF ULS RESISTANCE FACTORS

Bias Calculations. The measured ultimate capacities from the load tests were compared with the predicted capacities obtained using TCP blow counts (N_{TCP}), and biases (λ_R = measured capacity/predicted capacity) for each test were then computed for each ultimate capacity criterion. The form of the bias distribution was evaluated using histograms and probability plots to compare them to the normal and lognormal distributions. Examples of bias distributions using Davisson's criterion are given in Figs. 3(a) and 3(b). In Fig. 3(b), the "AD" value represents the value of the Anderson-Darling statistic to test whether data are represented by the hypothesized distribution, and the associated p-value is given beneath (Anderson and Darling 1954). As the p-value for the lognormal fit is 0.749, the lognormal cannot be rejected as the underlying distribution (i.e. the data are consistent with a lognormal). However, in the case of the normal distribution, the p-value was smaller than 0.05 indicating that the normal distribution can be rejected as the underlying distribution. Bias distributions using 5% and 10% relative settlement criteria also followed lognormal distributions.

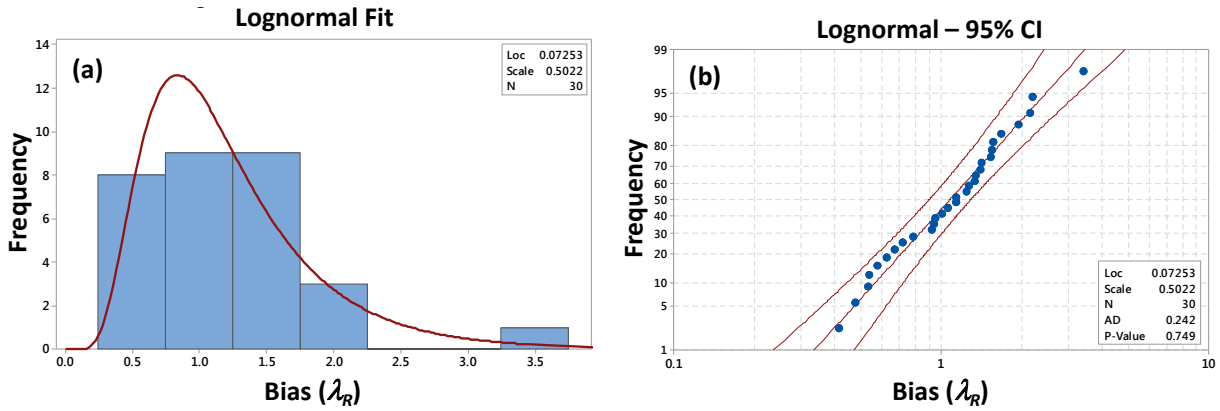


Fig. 3. (a) Histogram of biases and (b) Lognormal probability plot of biases using Davisson's criterion

Typically, Maximum Likelihood Estimators (MLE) are used to determine the mean and variance in LRFD study. However, in this study, the mean and variance for biases were estimated using the Uniformly Minimum Variance Unbiased Estimators (UMVUEs). Surles et al. (2017) explored the use of UMVUEs for lognormal distributions following the work presented by Finney (1941). An examination and comparison of MLE for the UMVUE method was presented with the conclusion that for a lognormal distribution, the UMVUE approach is more appropriate as it has higher precision and less data variability. Detailed procedures to obtain the weighted mean and coefficient of variation (COV) of the biases using UMVUEs are as follows:

a) Take the log transformation of the data (i.e. $x_i = \ln(\lambda_{Ri})$).
b) Compute the weighted mean ($\bar{x}$) and variance (s_x) of the log-transformed sample
c) Plug the weighted mean and variance of the log-transformed sample into the following equations to obtain weighted UMVUE for mean ($E[\lambda_R]$) and standard deviations ($SD[\lambda_R]$):

$$E[\lambda_R] = \exp(\bar{x})\, g(0.5 s_x^2), \text{ and} \quad [3]$$

$$SD[\lambda_R]^2 = \exp(2\bar{x})\{g(2s_x^2) - g\left(\frac{n-2}{n-1} s_x^2\right)\}, \text{ where} \quad [4]$$

$$g(t) = 1 + \frac{n-1}{n}t + \frac{(n-1)^3}{n^2 2!}\frac{t^2}{n+1} + \frac{(n-1)^5}{n^3 3!}\frac{t^3}{(n+1)(n+3)} + \cdots \quad [5]$$

d) Compute COV by dividing $SD[\lambda]$ by $E[\lambda_R]$ obtained from Eqs. (3) and (4), respectively.

The weighted UMVUE summary statistics for the 30 load tests on driven piles in soils are given in Table 4 (note that a weighting factor that ranged from 0 to 1 was used for calculations of mean and COV to consider the uncertainties associated with the data quality). As expected, the mean biases for 5% and 10% criteria are greater than that for Davisson's criterion. It was observed that the COVs for 5% and 10% criteria were also greater than that for Davisson's criterion.

Table 4. Summary statistics for biases of resistances for driven piles in soils

Ultimate Capacity Criteria	Total number of load tests considered (Total sample size)	Effective sample size	Mean of Bias	COV of Bias
Davisson	30	26.8	1.224	0.532
5%	30	26.8	1.397	0.559
10%	30	26.8	1.600	0.620

Calibrations of Resistance Factor. Resistance factors were obtained following the first order second moment (FOSM) method and the Monte Carlo simulation using the bias statistics presented in Table 4. In the FOSM method, resistance factor (ϕ) is obtained from the following equation:

$$\phi = \frac{\lambda_R\left(\gamma_{DL}\frac{Q_{DL}}{Q_{LL}} + \gamma_{LL}\right)\sqrt{\frac{1 + COV_{Q_{DL}}^2 + COV_{Q_{LL}}^2}{1 + COV_R^2}}}{\left(\lambda_{DL}\frac{Q_{DL}}{Q_{LL}} + \lambda_{LL}\right)exp\left\{\beta\sqrt{\ln\left[(1 + COV_R^2)\left(1 + COV_{Q_{DL}}^2 + COV_{Q_{LL}}^2\right)\right]}\right\}} \quad [6]$$

where λ_R = mean bias of the resistance, λ_{DL} = bias of the dead load, λ_{LL} = bias of the live load, COV_R = coefficient of variation of the resistance, COV_{QDL} = coefficient of variation of the dead load, COV_{QLL} = coefficient of variation of the live load, γ_{DL} = load factor for dead load, γ_{LL} = load factor for live load, Q_{DL}= dead load, Q_{LL} = live load, and β = target reliability index.

In Monte Carlo simulation, resistance factors were obtained by trying different values of resistance factors (ϕ_{trial}) until the target probabilities of failure of 0.01 (corresponding to $\beta \approx 2.33$) and 0.001 (corresponding to $\beta \approx 3.00$) were achieved. In this study, total simulation size was chosen to be 1,000,000. Since none of the 30 load tests was an instrumented test, resistance factor was calibrated for total capacity only.

For both FOSM method and Monte Carlo simulation (MCS), $Q_{DL}/Q_{LL} = 2$, $\lambda_{LL}= 1.15$, $COV_{LL} = 0.2$, $\lambda_{DL}= 1.05$, and $COV_{DL}= 0.1$ were used for statistics for biases of loads following suggestions by NCHRP (Paikowsky 2004). Tables 5 and 6 present LRFD resistance factors obtained both from FOSM method and MCS for target reliability indices of 2.33 and 3.00, respectively. Surles et al. (2017) advocated that confidence intervals should accompany the resistance factors when presenting the results from a calibration study because the resistance factor is subjected to sampling error as with any other statistic. The 95% confidence intervals presented in Tables 5 and 6 were obtained using a bootstrap method and based on the FOSM resistance factors.

Table 5. Resistance factors for total capacity of driven piles in soils (β = 2.33)

Ultimate Capacity Criteria	Effective Sample Size	Mean of Bias	COV of Bias	ϕ (Monte Carlo Simulation)	ϕ (FOSM)	Lower 95% CI	Upper 95% CI
Davisson	26.8	1.224	0.532	0.44	0.41	0.30	0.53
5%	26.8	1.397	0.559	0.47	0.44	0.31	0.58
10%	26.8	1.600	0.620	0.47	0.44	0.30	0.59

Table 6. Resistance factors for total Capacity of driven piles in soils (β = 3.00)

Ultimate Capacity Criteria	Effective Sample Size	Mean of Bias	COV of Bias	ϕ (Monte Carlo Simulation)	ϕ (FOSM)	Lower 95% CI	Upper 95% CI
Davisson	26.8	1.224	0.532	0.30	0.28	0.19	0.39
5%	26.8	1.397	0.559	0.32	0.30	0.20	0.42
10%	26.8	1.600	0.620	0.31	0.29	0.19	0.42

According to our analyses, resistance factors for β of 2.33 obtained from Monte Carlo simulations are 0.44, 0.47, and 0.47 for Davisson, 5%, and 10% criteria respectively. Similarly, resistance factors for β of 3.00 are 0.30, 0.32, and 0.31 for Davisson, 5%, and 10% criteria respectively. Although the mean bias is the greatest for 10% criterion, it does not necessarily yield the greatest resistance factors because the COV is also the largest for 10% criterion.

SUMMARY AND CONCLUSIONS

This research study has developed resistance factors for total capacity of driven piles in soils using Davisson, 5% and 10% relative settlement criteria as ultimate capacity criteria. A database containing 30 load tests performed for driven piles in soils was developed for this study. With consideration to data quality, the effective sample size was 26.8. Davisson's criterion yielded the resistance factors of 0.44 and 0.30 corresponding to target reliability indices of 2.33 and 3.00, respectively. Although the mean bias was the greatest for 10% criterion, it did not necessarily yield the greatest resistance factors because the COV is also the largest for 10% criterion. Considering the wide spread use of Davisson's criterion for driven piles in United States and the small increase in ϕ values when other criteria were used, resistance factors from Davisson's capacity are recommended for driven piles in soils for LRFD using TCP method.

ACKNOWLEDGMENTS

The authors express their gratitude to the Texas Department of Transportation for sponsoring the TCP Reliability research study.

REFERENCES

Anderson, T.W. and Darling, D.A. (1954). "A Test for Goodness-of-Fit." *Journal of the American Statistical Association*, 49: 765-769.

Davisson, M.T. (1972). "High Capacity Piles." Proceedings, Lecture Series on Innovations in Foundation Construction, ASCE, Illinois Section, Chicago, March 22, pp.81-112

Densmore, D. H. (2000, May 30). Load and Resistance Factor Design (LRFD) Memo. Retrieved March 19, 2012, from http://www.fhwa.dot.gov/bridge/062800.htm

FHWA (2016). "National Bridge Inventory." Bridges and Structures, Safety, Bridge Inspection. U.S. Department of Transportation, Federal Highway Administration: Washington, DC.

Finney, D. J. (1941). "On the Distribution of a Variate whose Logarithm is Normally Distributed." *Journal of the Royal Statistical Society, Series B*, 7: 155-161.

Paikowsky, S. G. (2004). *NCHRP Report 507 Load and Resistance Factor Design (LRFD) for Deep Foundations*. Washington, DC: Transportation Research Board.

Seo, H., Moghaddam, R. B., Surles, J. G., Jayawickrama, P. W., Wood, T. A. and Lawson, W. D. (2015). *Reliability Based Deep Foundation Design Using Texas Cone Penetrometer (TCP) Test: VOLUME 1, Development of Load Test Dataset.* DRAFT Report. FHWA/TX-14-0-6788-1-Vol. 1. Texas Tech University Center for Multidisciplinary Research in Transportation: Lubbock, TX.

Seo, H., Moghaddam, R. B., Surles, J. G., Jayawickrama, P. W., Wood, T. A. and Lawson, W. D. (2015). *Reliability Based Deep Foundation Design Using Texas Cone Penetrometer (TCP) Test: VOLUME 2, Resistance Factors for Driven Pile Foundations.* DRAFT Report FHWA/TX-14-0-6788-1 Vol. 2. Texas Tech University Center for Multidisciplinary Research in Transportation: Lubbock, TX.

Surles, J.G., Seo, H., Doerzbacher, J., Lawson, W.D., Jayawickrama, P.W. (2017). "Confidence Intervals for Resistance Factors in Geotechnical LRFD Applications." *Acta Geotechnica* (Submitted).

Texas Department of Transportation. (2012) *Geotechnical Manual*. Texas Department of Transportation, Austin, TX

Texas Department of Transportation. (1999). *TxDOT Designation: Tex-132-E, Test Procedure for Texas Cone Penetration*, Texas Department of Transportation, Austin, TX

DATA NORMALIZATION AND USER INTERFACE DESIGN FOR THE NEVADA DEPARTMENT OF TRANSPORTATION DEEP FOUNDATION LOAD TEST DATABASE

Austin Metz, University of Nevada, Reno, NV, USA, ametz@nevada.unr.edu,
Kevin Stanton, Arup, San Francisco, CA, USA, kevin.stanton@arup.com
Ramin Motamed, University of Nevada, Reno, NV, USA, motamed@nevada.unr.edu

ABSTRACT

A recent study calibrated Load and Resistance Factor Design (LRFD) resistance factors for local soil conditions in the Las Vegas Valley. As a part of this calibration, an extensive database of drilled shaft load tests and associated subsurface soil information were collected and compiled. This database, deemed the Nevada Department of Transportation Deep Foundation Load Test Database or NDFLTD, was designed with the presentation of load test data, the subsurface soil conditions, and the spatial distribution of the data in mind. In addition, the NDFLTD was developed in a way that allows additional data to be added as it becomes available. As such, the rules of database normalization were followed to allow for additional and different types of data to be added to the database and reports. Microsoft Access was chosen to present the data because it is easily accessible to anyone with Microsoft office software, it has a quick learning curve, and it has the ability to present a relational database. The largest obstacle faced when creating the NDFLTD was normalizing the data used in the LRFD calibration, with the goal of reaching the 5th normal form.

Keywords: deep foundations, database, data normalization

INTRODUCTION

LRFD is based on statistical performance of engineering components, as opposed to the more traditional Allowable Strength Design (ASD), which divides the strength of a component by a safety factor. Calibration of resistance factors for LRFD requires a robust statistical analysis of past performance. For drilled shafts this requires a database of full scale load tests (Abu-Hejleh et al. 2014). The FHWA developed the largest US based deep foundation load test database, deemed the DFLTD, collecting data from 1985 to 2003 when funds ran out (Abu-Hejleh et al. 2014). Recently, the DFLTD has been updated to modern standards (Petek et al. 2016). In October of 2007, the FHWA mandated state department of transportations (DOTs) to follow AAHSTO LRFD guidelines for their highway foundation designs (Abu-Hejleh et al. 2014). Since then multiple state DOTs have developed their own, region specific deep foundation load test databases. Florida has a long history of developing databases for deep foundation LRFD resistance factor calibration, with the two main databases being the FL database, and The Deep Foundations Database (Abu-Hejleh et al. 2014). Iowa developed a Microsoft Access based database in 2014 (Garder et al. 2014). Oregon developed a database compiling pertinent data from the DFLTD, Florida DOT's Deep Foundation Database, as well as from other databases (Smith et al. 2011). Illinois developed the "International Database" for static and dynamic reliability based calibration (Long et al. 2009). Louisiana developed a database for LRFD Calibration of driven piles in 2009 (Abu-Farsakh et al. 2009). The California Department of Transportation has its own internal foundation database, which is housed within the Foundation Testing Branch archive (Smith et al. 2011). In 2016, the Nevada Department of Transportation (NDOT) presented its own LRFD calibration for the Las Vegas Valley (Stanton et al. 2017), and the NDFLTD was developed as a part of that project (Motamed et al. 2016).

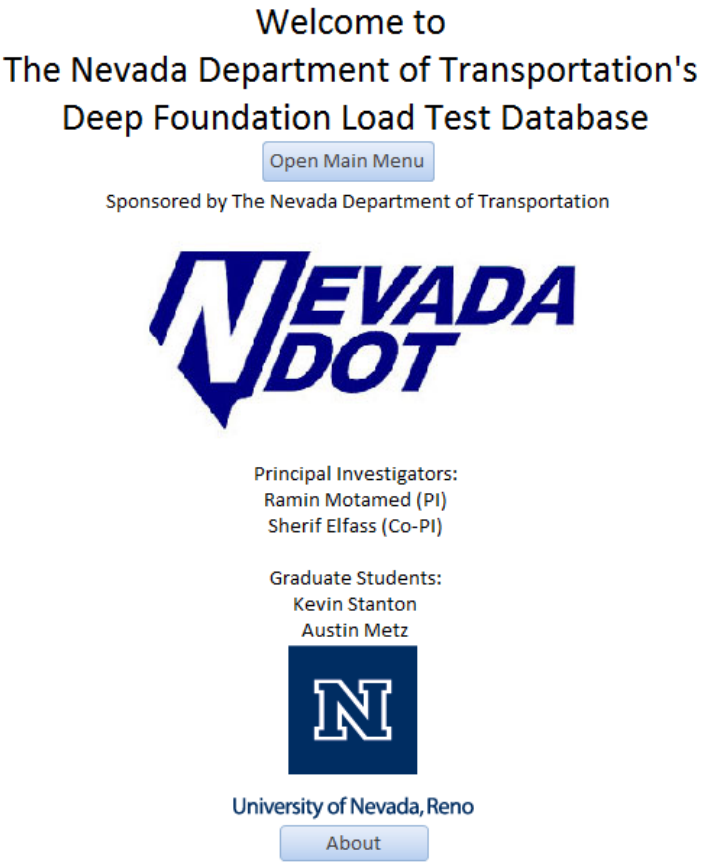
The primary goal of the NDFLTD is to present the data used for LRFD calibration in a simple, user-friendly way. The user is expected to be an NDOT or private geotechnical engineer familiar with drilled shaft design. The database has two major components: the "front end" and the "back end". The "front end" is the user interface, which the engineer will use most often. The "back end" contains the raw data and relationships

 © 2017 DFI Annual Conference, New Orleans, LA, USA

housed and presented by the database. If an engineer is interested in something not presented by the predesigned reports (front end), they must familiarize themselves with Microsoft Access, and design a query (and optionally a report) to retrieve the information they are interested in. This paper presents an overview of NDFLTD from a database developer perspective and provides details on the user interface and the developer interface. In addition, details are provided about the data housed within the database and how it was used to enable the LRFD calibration for the Las Vegas Valley.

NDFLTD USER INTERFACE

The NDFLTD has a simple navigation scheme. Opening the database brings the user to a welcome screen (Fig. 1). The welcome screen shows the persons involved in the database development, as well as references and acknowledgments. Additionally the welcome screen has two navigation buttons, the user can "Open Main Menu" or click "About". The About section gives a quick summary of how to use the database, and how to show hidden objects. The main menu shows a list of projects, filtering options, and report types.



Reference:
Motamed, R., Stanton, K., Elfass, S., and Kluzniak, B. (2016) "Development of the Nevada Deep Foundation Load Test Database: Drilled Shaft Component" TRB 95th Annual Meeting, January 10-14 2016, Washington DC, Presentation No. 16-3925.

Figure 1: NDFLTD Welcome Page.

NAVIGATING THE NDFLTD

Within the NDFLTD main menu (Fig. 2.) there is a list of projects, filtering options, and report types. The projects are listed with the Project Description, Boring Log ID, and Foundation Name. Within the database there are 44 projects (5 names and locations are removed per requests by the data providers) with 1-4 test

shafts each. The user can filter projects by foundation type (as of now there are only drilled shafts), diameter (less than or greater than), and by foundation depth or soil layer thickness. Once the user has selected the interested projects, they can select a report to generate, or show the projects on a map. The user can generate a report with the foundation boring logs (click "Show Boring Logs"), or with the load test data (click "Show Foundation Data").

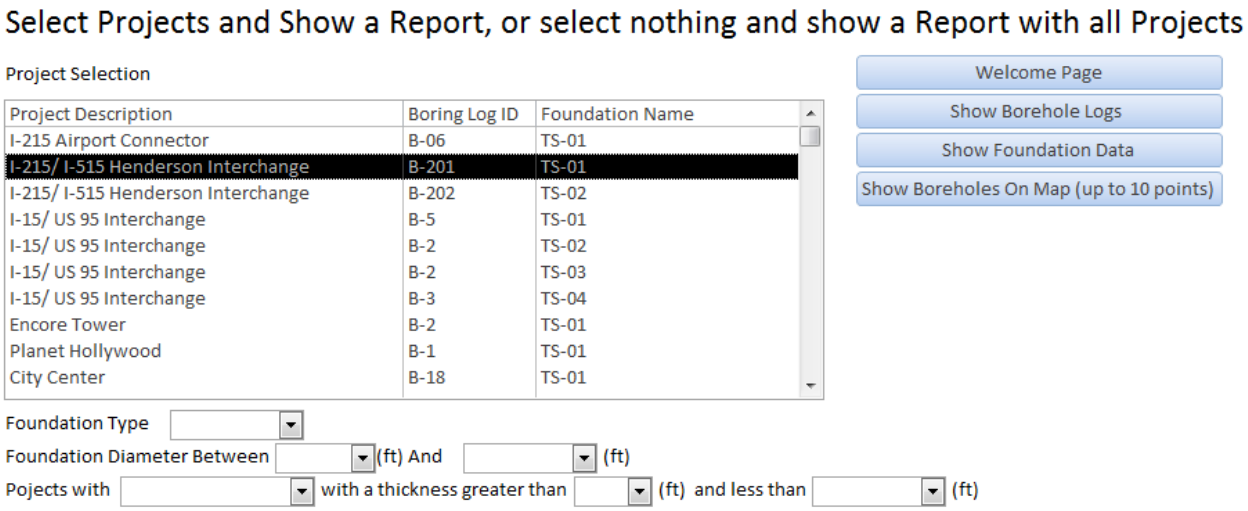


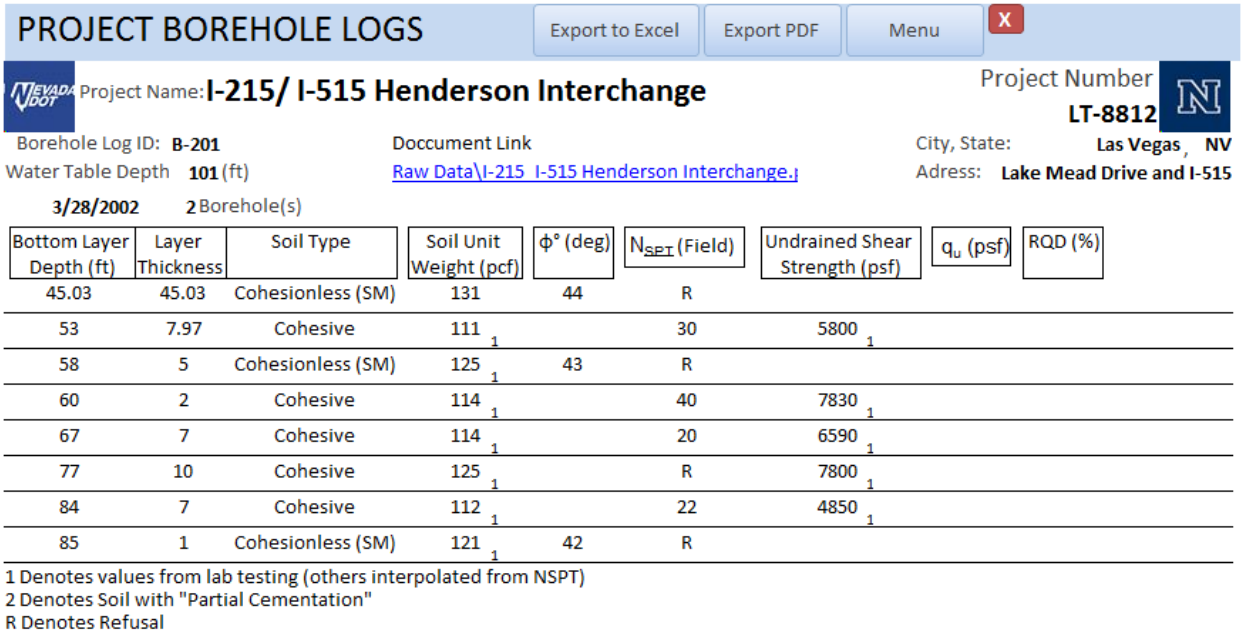
Figure 2: NDFLTD Boring Logs page. (Example showing the I-215/I-515 Henderson Interchange Project)

The Boring Log (Fig. 3) shows the data from boring, and lab tests, as well as general information such as location, water table depth, date, project information, and a link to the raw boring log. The "Foundation Data" report (Fig. 4) shows the general information associated with the raw load test data. The report shows information on the location of the foundation/borehole (if known), and foundation diameter with depth. An equivalent "top down" curve is presented for each load test with measured displacements, displacements with adjustments for elastic compression, and extrapolated values. A list of contractors and their role in the project is then presented, along with the website for each, and whether or not they are currently in business. Finally for both reports the user can select to export the data to a PDF file, or export to Excel.

In conjunction with the previously described reports within the main menu, the user can select to show the selected projects on a map. The map tool utilizes Bing Maps, placing a star on the location of each selected project. Currently the map tool is limited to only mapping 10 projects at a time. In order to view all projects on the same map, the user must save the locations and add them to a list through the Bing Maps user interface.

DATABASE NORMALIZATION

Understanding the "back end" of the NDFLTD requires the user to be familiar with the process of database normalization. Database normalization is the practice of organizing the contents and relationships of tables within a relational database in order to improve efficiency, reduce redundancy, and improve integrity. Database normalization was first proposed by Codd (1971; 1972). Codd described the requirements for the first three Normal Forms (NF). The first normal form (1NF) states that there will be no repeating groups in individual tables, that each set of related data must be contained in its own table, and each record (or row) within a table must be identified by a primary key.



PROJECT BOREHOLE LOGS

Export to Excel | Export PDF | Menu

Project Name: I-215/ I-515 Henderson Interchange

Project Number LT-8812

Borehole Log ID: B-201

Water Table Depth 101 (ft)

3/28/2002

Doccument Link: Raw Data\I-215_I-515 Henderson Interchange.

2 Borehole(s)

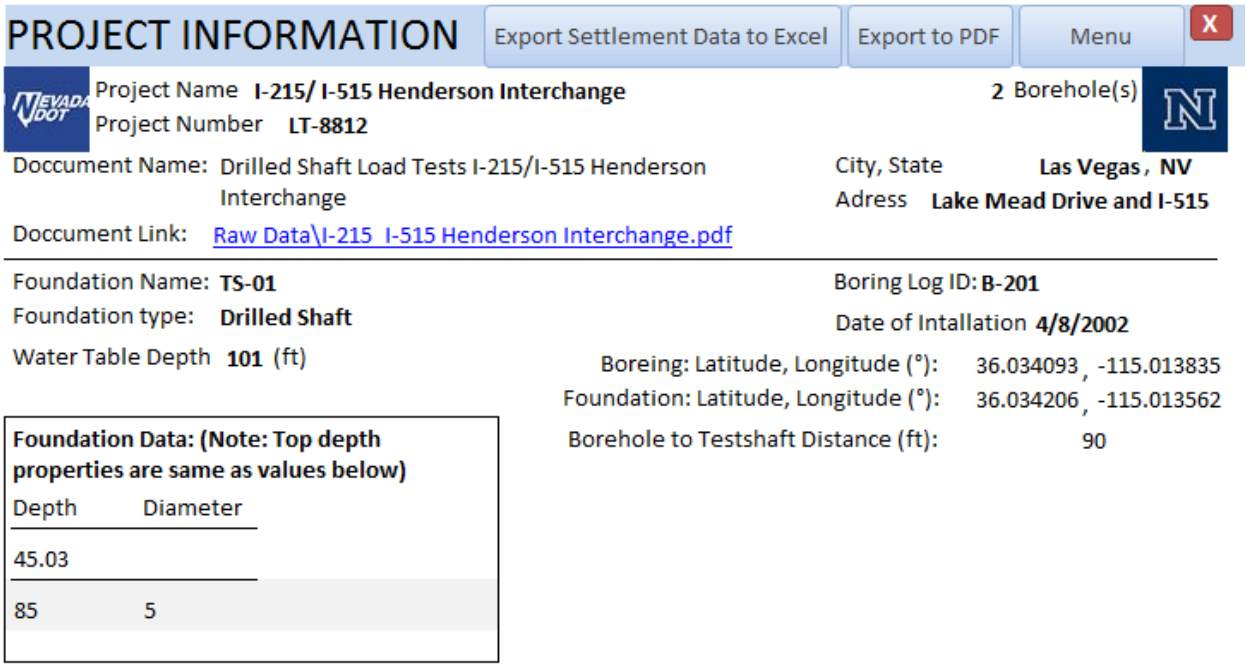
City, State: Las Vegas, NV

Adress: Lake Mead Drive and I-515

Bottom Layer Depth (ft)	Layer Thickness	Soil Type	Soil Unit Weight (pcf)	ϕ° (deg)	N_{SPT} (Field)	Undrained Shear Strength (psf)	q_u (psf)	RQD (%)
45.03	45.03	Cohesionless (SM)	131	44	R			
53	7.97	Cohesive	111 [1]		30	5800 [1]		
58	5	Cohesionless (SM)	125 [1]	43	R			
60	2	Cohesive	114 [1]		40	7830 [1]		
67	7	Cohesive	114 [1]		20	6590 [1]		
77	10	Cohesive	125 [1]		R	7800 [1]		
84	7	Cohesive	112 [1]		22	4850 [1]		
85	1	Cohesionless (SM)	121 [1]	42	R			

1 Denotes values from lab testing (others interpolated from NSPT)
2 Denotes Soil with "Partial Cementation"
R Denotes Refusal

Figure 3: NDFLTD Boring Logs page (Example showing the I-215/I-515 Henderson Interchange Project)



PROJECT INFORMATION

Export Settlement Data to Excel | Export to PDF | Menu

Project Name I-215/ I-515 Henderson Interchange

Project Number LT-8812

2 Borehole(s)

Doccument Name: Drilled Shaft Load Tests I-215/I-515 Henderson Interchange

Doccument Link: Raw Data\I-215_I-515 Henderson Interchange.pdf

City, State Las Vegas, NV

Adress Lake Mead Drive and I-515

Foundation Name: TS-01

Foundation type: Drilled Shaft

Water Table Depth 101 (ft)

Boring Log ID: B-201

Date of Intallation 4/8/2002

Boreing: Latitude, Longitude (°): 36.034093, -115.013835

Foundation: Latitude, Longitude (°): 36.034206, -115.013562

Borehole to Testshaft Distance (ft): 90

Foundation Data: (Note: Top depth properties are same as values below)

Depth	Diameter
45.03	
85	5

Figure 4a: NDFLTD Foundation Data page (example showing first load test from the I-215/I-515 Henderson Interchange)

Within a relational database, a number of tables are related to each other by the use of "Keys": either unique (primary keys), or non-unique. Each record in a table must be identified by a primary key. Non-unique keys allow rows in one table to be related to a record, or records in another table. For example the first table in our database is the "Project Information" table the primary key (identified with a small key icon) is a unique

number for each project called the “Project ID”. This table is related the “Project Boreholes” table with the “Project ID” key. Each borehole within “Project Boreholes” has its own unique identifier, “Borehole ID”.

The second normal form (2NF) requires that the table in question follows 1NF, and that each attribute within the table is dependent on the whole of all non-primary keys. For a database to be in 2NF, each attribute within a table must be dependent on the record in the parent table. Codd (1972) defined a table (R) passing the third normal form (3NF) as passing 2NF, and requiring that every non-prime attribute of the table is non-transitively dependent on every key of R. A transitive dependency, or functional dependency is one in which X→Z(X determines Z) indirectly, or X→Y and Y→Z and Y does not determine X.

Load Test Information

Type of Loading	Failure Criteria	Assumed Failure Mode	Axial Capacity (kip)	Displacement at Capacity (in)	Load Test Data Score	Ceep Limit (kips) -Load Test INC-
O-Cell	Nominal O-Cell capacity	2	3423.183	1.83119	4	1906

Assumed Failure Mode: 1 Denotes Shaft Head Settlement = 5% of Shaft Diameter.
2 Denotes Plunging Failure.

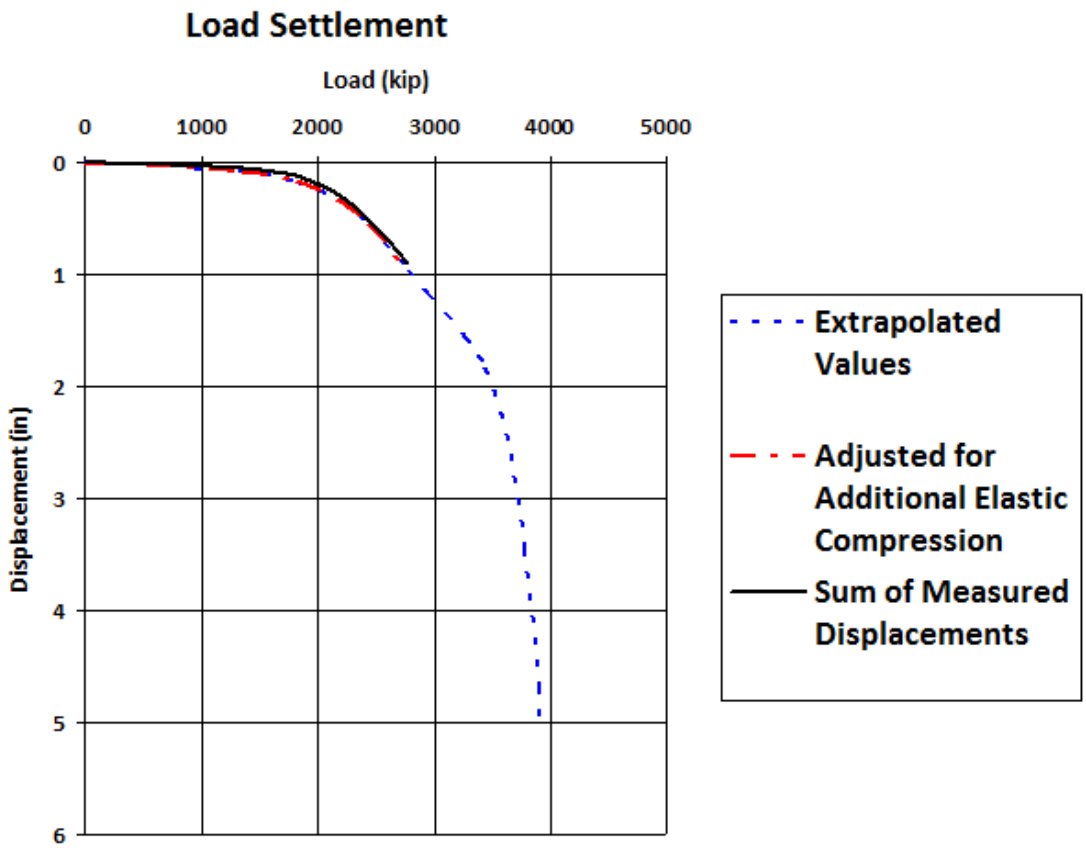


Figure 4b: NDFLTD Foundation Data page (Example showing first load test from the I-215/I-515 Henderson Interchange)

The fourth and fifth normal forms (4NF and 5NF), were defined by Fagin (1977; 1979) . Fagin defines a table to be 4NF if and only if it follows 3NF and it does not contain multiple dependent values. This NF

causes tables to reduce redundancy, a table following 4NF will not have repeating information. For example a company may have the ability to work on many different aspects of deep foundation installation and testing but may have only fulfill limited (and different) roles for different projects. Following 4NF two tables should be used to represent this knowledge, allowing there to be no blanks, nor repeating information. A table is defined to be in 5NF if and only if each "join" dependency (or how the tables are related to each other) is implied by the candidate keys (or that there are no unused candidate keys) (Fagin, 1979). Put simply by Domokos (2012), a table is in 5NF if it is in 4NF and it cannot be recreated by several tables containing fewer attributes. Information on data normalization is widely accessible online, the authors suggest Wikipedia, and the data normalization "puppy poster" (Rettig, 1989) to start.

NDFLTD Data Normalization and Organization

The NDFLTD attempts to pass the 5NF in all applicable cases. The data contained in the NDFLTD is broken down into two main groups: the Boring Information group, and the Foundation Information group. Figure 5 shows the relationships for the Boring log information. Within this group there are many tables related to each other with 1-∞ (one to many), or 1-1 relationships. Figure 6 shows the relationships for the Foundation data with similar relationship types.

One major hurdle in the design of this database was accounting for the fact that some projects had multiple test shafts which used one borehole for design, while others had multiple borings for a single project, and some had no boring information provided with the foundation/load test information. Deep foundation design requires some information on subsurface condition, therefore the authors elected to require a project borehole before a Pile/Shaft could be included within the database. Projects without boreholes had their "Boring Log ID" reported as "No Boring Log". Many of the tables presented in Figures 5 and 6 such as those branching from the "Soil Profile Data" table exist in order to remove blank spaces in a large table (pass 4NF), such as what would be present in an excel spreadsheet used to present the same data (i.e. A "Sand" soil type will not have a value for cohesion). Tables such as "P/S Lat Long" are present because this information was not available for every Pile/Shaft.

The "Borehole to TestShaft Distance" table is present for querying convenience, as calculating the difference between two Latitude/Longitude coordinates proved rather complicated to do within the Microsoft Access Query design user interface. The "Soil Data Source" table is an example of where this database failed to normalize to the correct degree, ideally each of the tables linked to "Soil Profile Data" with the "Layer Id" key should have a soil data source field with a 1 or a 2 denoting lab or field data. But as a matter of convenience in updating and presenting this data, the authors elected to use the existing "Soil Data Source" table so that only a note at the base of the report was needed to denote the data source.

NDFLTD Data and LRFD Calibration

The data housed within the database is described extensively within Motamed et al. (2015). The database houses 44 deep foundation projects, with load tests and boring logs included. The projects are distributed across the Las Vegas valley, with many in the "Strip" area, and some as far as Henderson (Fig. 7). The distribution of the data is further summarized in Figure 8.

Stanton et al. (2017) calibrated resistance factors for LRFD of axially loaded drilled shafts in the Las Vegas Valley, using the data housed within the NDFLTD. They proposed a new design approach and presented an area-specific resistance factor for cemented sandy soils colloquially known as "caliche". Additionally, calibrated resistance factors were presented for three other possible design approaches as a part of the study. In order to calibrate the resistance factors, Stanton et al. first used the traditional Monte Carlo (MC) simulation technique, then developed and proposed a more robust method. This new method takes into account the uncertainty associated with the interpretation of material properties from in situ data and relies on nested MC simulation to capture the uncertainty of individual design inputs.

SUMMARY

The NDFLTD presents the user with the basic information needed to assess various foundation designs and conduct foundation-related research. Location, subsurface information, foundation properties, and foundation performance are presented in a user friendly way. Additional information can be queried and brought up on an as needed basis. If NDOT or any group using the database wishes to save their custom query and or report, they are free to do so.

The NDFLTD is organized as a relational database. The majority of the database reaches the 4th or 5th normal form, while some tables are left only reaching the 3rd normal form as a matter of convenience. Although the database has some missing or incomplete data, the design of the tables and relationships is meant to ignore such inconsistencies, while encouraging data entered in the future to include it.

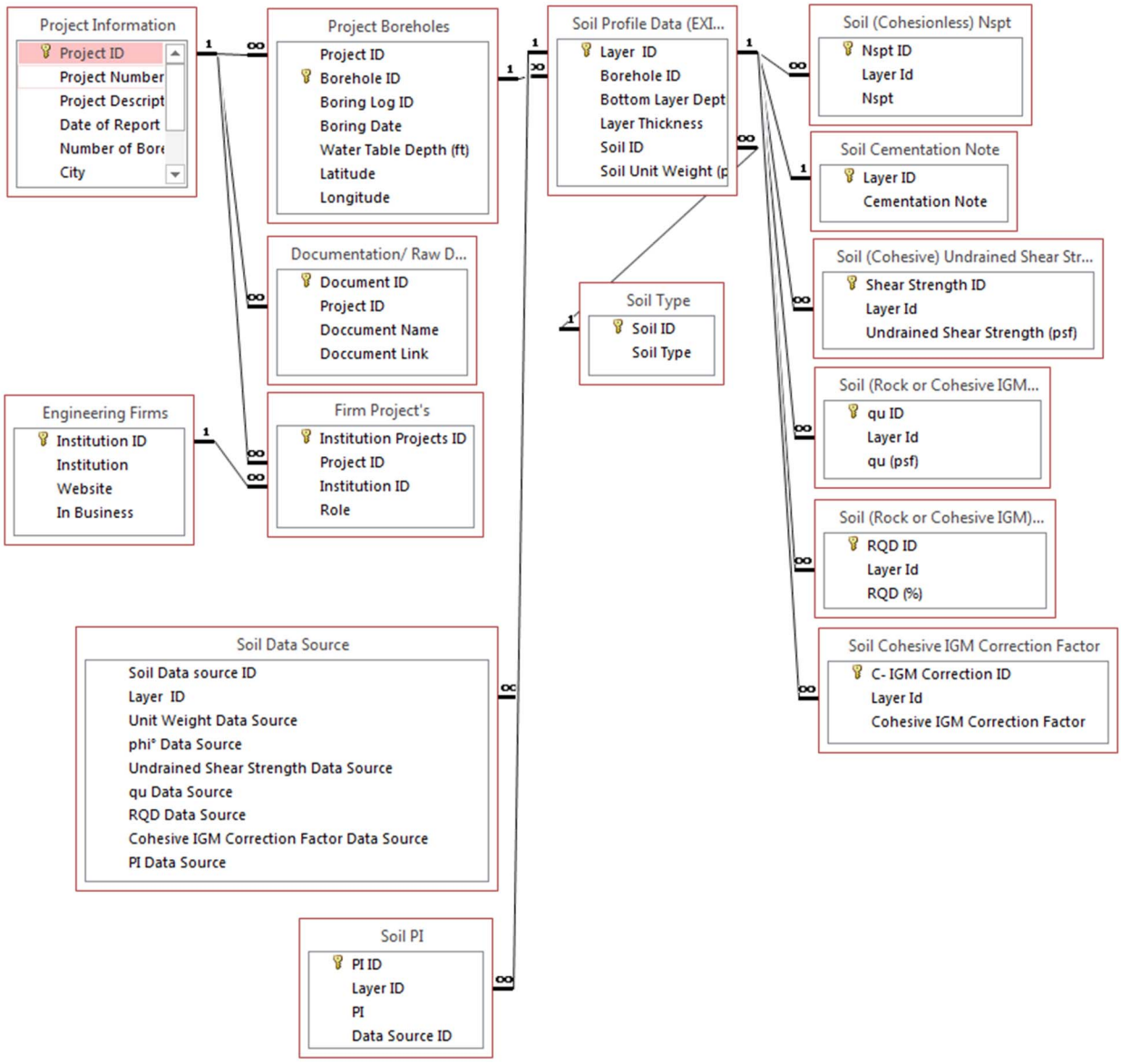


Figure 5. Boring Log tables/relationships

ACKNOWLEDGEMENTS

The authors would like to thank Load Test Inc., Terracon, Western Technologies, and Dr. M. Karakousian of UNLV for providing the data housed within this database, as well as Klinefelder and Arup for providing subsurface soil information. The authors would also like to thank NDOT for funding the development of this database, and specifically Abbas Bafghi for providing direction in the user interface design process. Finally we would like to thank Dr. Elfass for his help in development of the database.

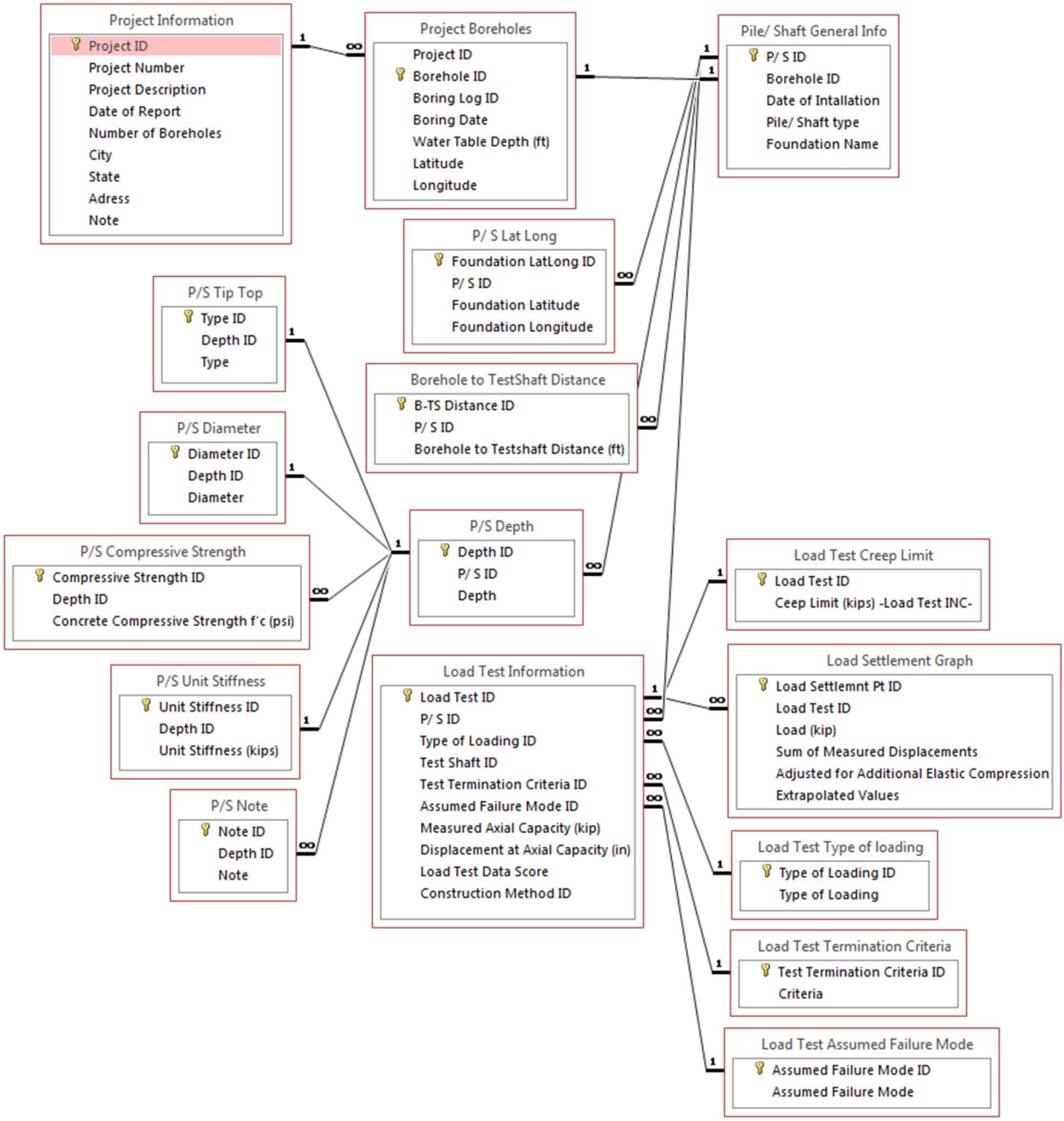


Figure 6. Foundation Information Tables/Relationships

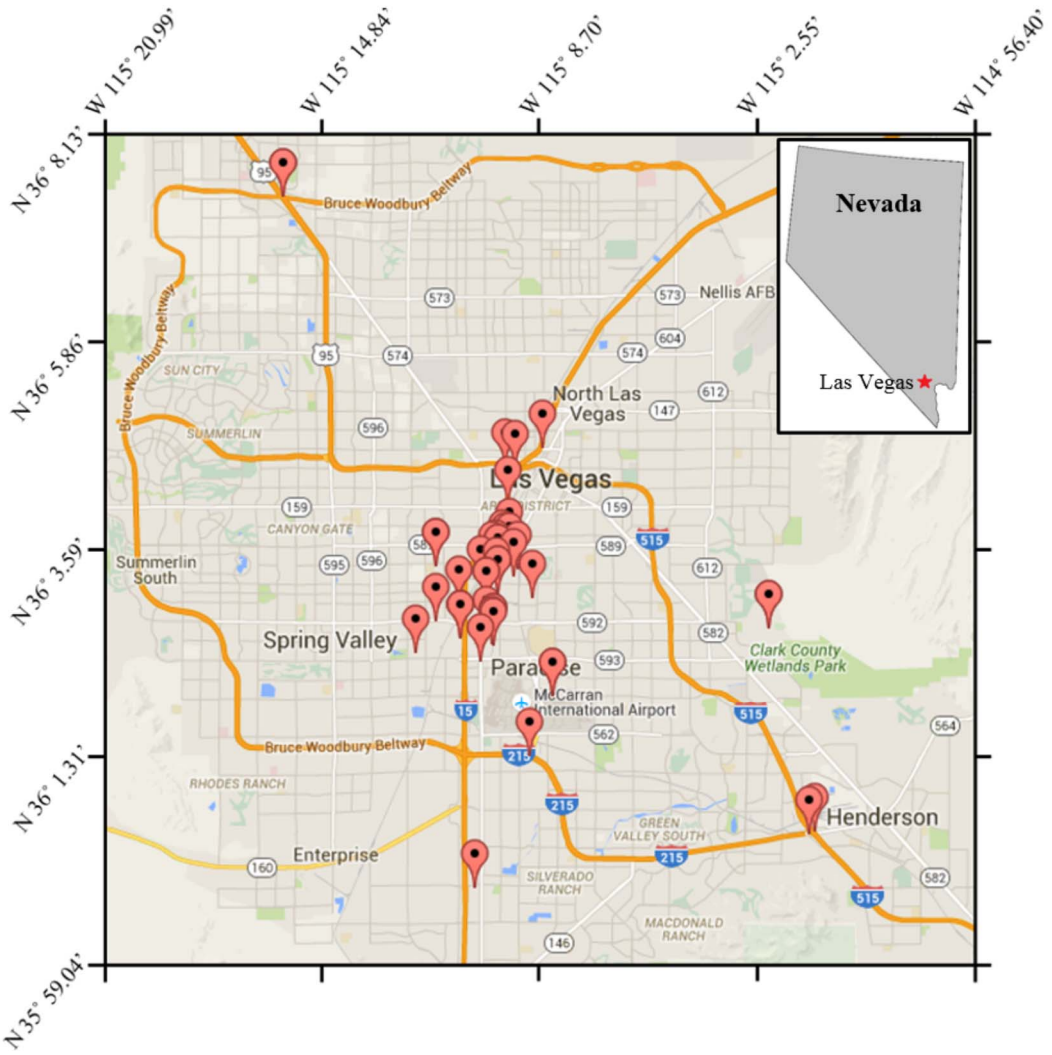


Figure 7: Spatial Distribution of Data housed within the NDFLTF (From Motamed et al. 2016)

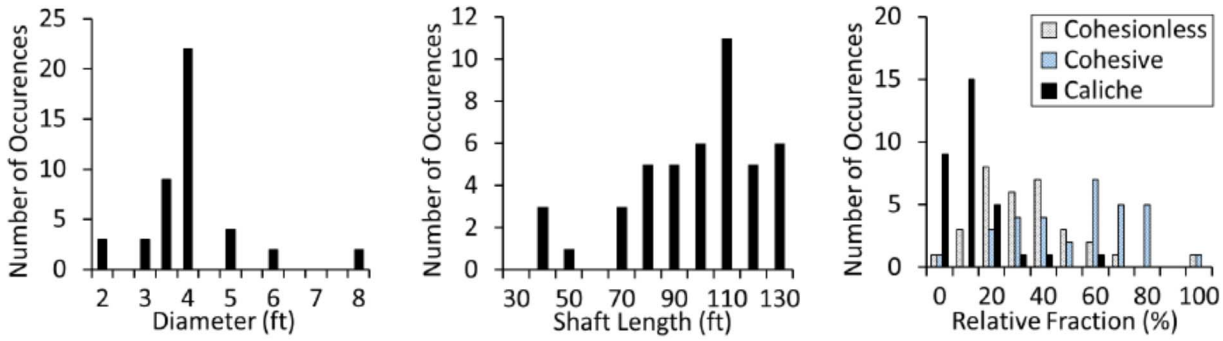


Figure 8: Statistical Distribution of Data housed within the NDFLTF (From Motamed et al. 2016)

REFERENCES

Abu-Farsakh, M.Y., Yoon, S., Tsai, C., 2009. Calibration of Resistance Factors Needed in the LRFD Design of Driven Piles. Federal Highway Administration Report No. FHWA/L.A.09/449, Louisiana Transportation Research Center.

Abu-Hejleh, N.M., Abu-Farsakh, M., Suleiman, M.T., Tsai, C., 2014. Foundation Load Test Databases: Applications, Contents, and Development. 92nd Transportation Research Board Annual Meeting.

Codd EF. 1972. Relational completeness of data base sublanguages. In: R. Rustin (ed.). Data Base Systems, Proceedings of 6th Courant Computer Science Symposium (May 24-25, 1971: New York, N.Y.), pp. 65-98.

Domokos, D.A., Pamfil, D., Grebenisan, M., 2012. Database Optimization Techniques Applied to a Database Contain Soy and Corn Based Products to Ensure a Quick Search in this Database. Bulletin UASVM Horticulture, 69(2)/2012, pp.422-426.

Fagin, R., 1977. Multivalued Dependencies and a New Normal Form for Relation Databases. Association for Computing Machinery Transactions on Database Systems, Vol 2, No. 3, September 1977, Pages 262-278.

Fagin, R. 1979. Normal Forms and Relational Database Operators. Association for Computing Machinery SIGMOD International Conference on Management of Data, Boston, Mass. (May 30 – June 1), pp. 153-160.

Gardner, J.A., Ng, K.W., Sritharan, S., Roling, M.J., 2012. Development of a Database for Drilled SHAft Foundation Testing (DSHAFT). Iowa Department of Transportation Report No. InTrans Project 10-366, Bridge Engineering Center, Iowa State University.

Long, J.H., Hendrix, J., Baratta, A., 2009. Evaluation/Modification of IDOT Foundation Piling Design and Construction Policy. Illinois Center for Transportation Report No. FHWA-ICT-09-037., Illinois Center for Transportation.

Motamed, M., Stanton, K., Elfass, S., Kluzniak, B., 2015. Development of the Nevada Deep Foundation Load Test Database: Drilled Shaft Component. Transportation Research Board 95th Annual Meeting

Motamed, R., Elfass, S., Stanton, K. 2016. LRFD Resistance Factor Calibration for Axially Loaded Drilled Shafts in the Las Vegas Valley. Nevada Department of Transportation Report No. 515-13-803. University of Nevada Reno.

Petek, K., Mitchell, R., Ellis, H., 2016. FHWA Deep Foundation Load Test Database Version 2.0 Uerse Manual. Federal Highway Administration Report No. FHWA-HRT-17-034.U.S. Department of Transportation.

Rettig, M. 1989. 5 Rules of Data Normalization. http://www.informationqualitysolutions.com/FreeStuff/rettigNormalizationPoster.pdf. 1 p. Accessed 4-3-22.

Smith, T., Banas, A., Gummer, M., Jin, J.,2011. Recalibration of The GRLWEAP LRFD Resistance Factor for Oregon Dot. Oregon Department of Transportation Report No. FHWA-OR-RD-11-08, Portland State University.

Stanton, K., Motamed, R., Elfass, S., 2017. Robust LRFD Resistance Factor Calibration for Axially Loaded Drilled Shafts in Las Vegas. Journal of Geotechnical and Geoenvironmental Engineering, 06017004.

SUSTAINABILITY: A ROLE FOR BLENDED CEMENTS AND INDUSTRIAL BYPRODUCTS IN SOIL MIXING, GROUTING, AND SLURRY WALLS

Charles M. Wilk, SolidStable Remediation Consulting Inc, Arlington Heights, IL USA, 224-443-7466, charlesmwilk@gmail.com

Lori Tiefenthaler, Lehigh Hanson, Inc. Irving, TX, USA, 972-653-6130, lori.tiefenthaler@lehighhanson.com

ABSTRACT

Information presented in this paper can be used to support deep soil mixing, subsurface grouting and slurry wall technology as sustainable construction technologies.

Ordinary Portland Cement (OPC) is the default cementitious material used by Deep Foundation Institute (DFI) Members for geotechnical work. Owners, engineers and contractors can contribute to the sustainability of a geotechnical project by increasing the use blended hydraulic cements and industrial byproducts to replace some of the OPC in mix designs.

Sustainability is defined as the quality of not being harmful to the environment or depleting natural resources. Production of cementitious materials consumes natural raw materials and energy while also generating air emissions and waste. Life Cycle Assessments can be used to compare the relative environmental impacts of one cementitious material to another.

Blended hydraulic cements (BHCs) are interground (or blended) mixtures of Supplementary Cementitious Materials (SCMs) with OPC. Commonly used SCMs include fly ash, ground granulated blast furnace slag (GGBFS) and limestone. Examples of industrial byproducts commonly used in geotechnical work include coal combustion residuals (CCR) (aka fly ash), and ground granulated blast furnace slag (GGBFS). Much of life cycle impact of these SCMs and industrial byproducts have already been borne by the industries that generated them. There is increasing awareness to LCA and sustainability of different materials used on projects. This is evident in the application of the Leadership in Energy and Environmental Design (LEED) program. The savings in environmental impact with the use of SCMs and industrial byproducts can make proposed use of these materials in a geotechnical project more attractive in terms of sustainability.

This paper presents (a) information that compares published life cycle assessment data of OPC, BHCs, and slag cement (SC) to illustrate the potential benefits to sustainability and (b) general strategies for positioning a geotechnical application, use, project design or cementitious material mix as a more sustainable alternative.

Keywords: sustainability, deep soil mixing, subsurface grouting, slurry wall, life cycle assessment, LCA, environmental product declaration, EPD, portland cement, slag cement, blended hydraulic cement, fly ash, coal combustion residuals, ground granulated blast furnace slag, CCR, leadership in energy and environmental design, LEED

 © 2017 DFI Annual Conference, New Orleans, LA, USA

INTRODUCTION

This paper describes the positive contribution to a project's sustainability when blended hydraulic cements or industrial byproducts are used in deep soil mixing, subsurface grouting, and slurry walls. These contributions can be used to position a proposed geotechnical application or cementitious material mix design as accomplishing a more sustainable project.

Ordinary Portland Cement (OPC) has historically been a "default" cementitious material used in deep soil mixing, subsurface grouting, and slurry walls. OPC use as part of mix designs can be expected to continue given the proven track record and engineering acceptance in these applications.

Sustainability is defined as the quality of not being harmful to the environment or depleting natural resources. Production of OPC at cement plants uses natural resources (e.g., fossil fuels, limestone, shale, clay). OPC production also results in environmental impacts such as emission of carbon dioxide (CO_2) into the atmosphere.

Owners, design engineers and contractors can contribute to the sustainability of a project by increasing the use of BHCs and industrial byproducts. These lower-impact materials displace some of the OPC in a mix design. BHCs are interground (or blended) mixtures of Supplementary Cementitious Materials (SCMs) with OPC. Commonly used SCMs include fly ash, ground granulated blast furnace slag (GGBFS) and limestone. Examples of industrial byproducts commonly used in deep soil mixing, grouting, and slurry walls include coal combustion residuals (CCR) (aka fly ash), and ground granulated blast furnace slag (GGBFS). Much of life cycle impact of these SCMs and industrial byproducts have already been borne by the industries that generated these materials.

Life Cycle Assessment and Environmental Product Declaration

Production of materials usually consumes natural resources and energy and produces waste. Life Cycle Assessment (LCA) is a standardized system to quantify the environmental impacts of subject materials across the full life cycle: from raw materials acquisition through manufacturing, use and final disposition. Information developed from an LCA on a subject material is presented on an Environmental Product Declaration (EPD). The EPD provides data on environmental impacts, consumption of material resources and energy, and waste generated caused by the subject material. LCA when carefully considered, can provide a means to compare impacts between subject materials. Most product LCA's tend to be cradle-to-gate as a subject material's use cannot always be defined beyond the product's manufacturing plant gate. The methods used in LCAs and reporting on EPDs have been somewhat standardized to allow some simple comparisons. This is true of some of the cements used in geotechnical work including deep soil mixing, subsurface grouting, and slurry walls. We researched for existing Type III EPD for materials that could be used in these geotechnical applications and found that portland cement, blended hydraulic cement and slag cement each had an industry-wide EPD. A Type III EPD means the document has third party verification and certification by an EPD program operator (in these cases by ASTM).

Comparison of Cement's Life Cycle Assessments

Owners, design engineers and contractors involved in deep soil mixing, subsurface grouting, slurry wall have an opportunity to increase the sustainability of a project by selecting cements that have lower environmental life cycle impacts.

Comparisons can be made between cements using data reported on the latest industry wide EPDs that are now publicly available. The cements compared on Table 1 below include:

- Ordinary Portland Cement
- Blended Hydraulic Cement
- Slag Cement

Table 1 illustrates that the environmental impacts decrease with the use of SCMs and industrial byproducts. Greater use of SCMs and/or industrial byproducts in cements increases the sustainability of a project.

Table 1. Sample Comparison of Life Cycle Assessment Results of Cements

Category Indicator	Unit	Ordinary Portland Cement 1 Metric Ton	Blended Hydraulic Cement 1 Metric Ton	Slag Cement 1 Metric Ton
Global warming potential	kg CO_2 eq.	1040	892	147
Acidification potential	kg SO_2 eq.	2.54	2.26	2.1
Eutrophication potential	kg N eq.	1.22	1.11	0.27
Smog creation potential	kg O_3 eq.	48.8	42.3	26.5
Ozone depletion potential	kg CFC 11 eq.	2.61E-05	2.48E-05	1.69E-05
Total primary energy				
Non-renewable (incl. fossil and nuclear)	MJ	5595	5071	2434
Renewable (incl. solar, wind, biomass, hydroelectric & geothermal)	MJ	292	172	76
Material resources consumption				
Non-renewable materials	kg	1420	1240	11
Renewable materials (incl. recovered materials)	kg	7.64	3.42	1105
Net fresh water	l	9700	9240	32
Total waste generated				
Non-hazardous	kg	8.99	10.5	0.3
Hazardous	kg	0.0518	0.0511	0.02

MT-Metric Ton

Data Sources:
OPC and BHC: Portland Cement Association www.cement.org/structures/manufacturing/environmental-impact-reporting

SC: Slag Cement Association
http://www.slagcement.org/pdf/197.EPD_for_Slag_Cement_Association_Industry_Average_EPD_for_Slag_Cement.pdf

Note about cements described in Table 1:
Cementitious materials are produced by a great number of facilities. Available published EPDs were developed by industry-wide direct participation by many companies in the sector, but not all. Therefore, to use the data recorded on an EPD, your supplier's company would need to be listed as participating in the industry-wide developed EPD. This is to ensure that the EPD is relevant to your project. OPC is described as common general use (GU) portland cement. BHCs vary based on producers. The BHC data on Table 1 is for an "industry average" BHC. These blended cements meet the ASTM C595 which include Type IP (fly ash or pozzolan), IS (slag), IT(ternary) and IL (portland limestone cement) being produced in the USA. The SC is ground granulated blast furnace slag (GGBFS).

Caution note: Care must be taken when deciding to compare the results of material's EPDs that are made according to different Product Category Rules (PCR) to ensure the boundaries are somewhat similar as to what is included or is not included in the LCA for the product you are reviewing.

Sustainability Strategies

Comparing Life Cycle Impacts

Owners, design engineers and contractors involved in deep soil mixing, subsurface grouting, slurry walls may use the LCA data to position a proposed geotechnical application and/or mix design as a more sustainable alternative.

It is necessary to know the proportion of materials used in mix designs to quantify the contributions to sustainability of an alternate mix design. Supplemental cementitious materials or industrial byproducts are rarely used to completely replace OPC in a mix design. Typically, SCMs and industrial byproducts replace a portion of OPC in a design. Cement producers make this "replacement" when they produce BHCs. An EPD from a cement producer or industry association can be useful when a BHC is sole cementitious material of the mix design. A geotechnical contractor can make this "replacement" by combining materials from separate silos at project site. Example storing and blending OPC and SC at a project site. Two or more EPDs could be used when a geotechnical contractor combines material at the project site. The percent proportions of the material and reported EPD data would be used in a calculation for project site-combined mixes.

The most sustainable mix design could be generally determined by comparing the LCA of the different cementitious material components and their proportions in one complete mix to another complete mix. Obviously, the most sustainable mix design would still be required to meet the project's performance specifications. Enhanced sustainability may also be accomplished by performance optimization with the use of GGBFS or SC leading to a reduction of the total cementitious materials needed to meet project specifications. The cementitious combination or performance optimization along with costs and material availability would continue to be considerations in developing the final mix design.

As described in Table 2 below, environmental life cycle impacts of BHC and SC are significantly lower than OPC. Industrial byproducts are "raw materials" in the production of BHC and SC. This recovery or reuse of industrial byproducts generates significantly less environmental impacts and consumes significantly less energy and non-renewable materials compared to production of OPC. For example, production of BHC generates 86% and SC generates 14%, of the amount of CO_2 generated by a like amount of OPC. Since the production of SC is principally the processing of the industrial byproduct GGBFC, the production of SC recovers 145 times more renewable material compared to OPC.

Table 2. Sample Environmental Impacts of BHC and SC Compared to OPC

Category Indicator	Ordinary Portland Cement	Blended Hydraulic Cement	Slag Cement
Global warming potential	1	0.86	0.14
Acidification potential	1	0.89	0.83
Eutrophication potential	1	0.91	0.22
Smog creation potential	1	0.87	0.54
Ozone depletion potential	1	0.95	0.65
Total primary energy			
Non-renewable and renewable energy	1	0.89	0.43
Material resources consumption			
Non-renewable materials	1	0.87	0.008
Renewable materials (incl. recovered materials)	1	3.42	145
Net fresh water	1	0.95	0.003
Total waste generated			
Non-hazardous	1	1.17	0.03
Hazardous	1	0.99	0.38

Relationship to LEED

There is increasing awareness to LCA and sustainability of different materials used on projects. This is evident in the application of the Leadership in Energy and Environmental Design (LEED) program devised by the U.S. Green Building Council. For projects enrolled in the LEED program, points toward a higher-level LEED certification are awarded when more transparency on sustainable materials and technologies are used. For example, a LEED point is awarded when an enrolled project building is constructed on a former contaminated industrial property or brownfield (High Priority Sites). Use of deep soil mixing to solidify and stabilize the hazardous contaminants in soil or use of a slurry wall to prevent groundwater contamination may facilitate the use of the brownfield. The High Priority Sites in the Location and Transportation (LT) credit category is worth up to 2 points. A design engineer or contractor proposing these geotechnical applications with materials that have an industry-wide EPD can also help the project obtain points in the new Materials and Resources (MR) credit category within LEEDv4. Before proposing this advantage to the project be sure to read if your suppliers were involved with the slag or cement industry work on the EPD published. Another way that DFI Members can help contribute to a project's LEED rating, may be in the Sustainable Sites (SS) credit. Using soil mixing, grouting, or slurry walls to improve ground conditions and assist a chosen building site development to be able to accommodate greater density (below ground parking, etc.) and preserve more natural land area.

EXAMPLE PROJECTS

Jade Signature Building, Sunny Isles Beach, Florida, Deep Soil Mixing

The Jade Signature luxury condominium is located on Atlantic beachfront property in Sunny Isles, Florida. Plans for the building included a 3-level deep underground parking garage. The groundwater table was located almost immediately below ground surface. Bearing capacity of existing site soils was inadequate for support of the planned condominium tower. Deep soil mixing was the geotechnical technique used to allow excavation, construction and support. The DSM used a mixture of slag cement and OPC, saving significant environmental impact from use of the materials.

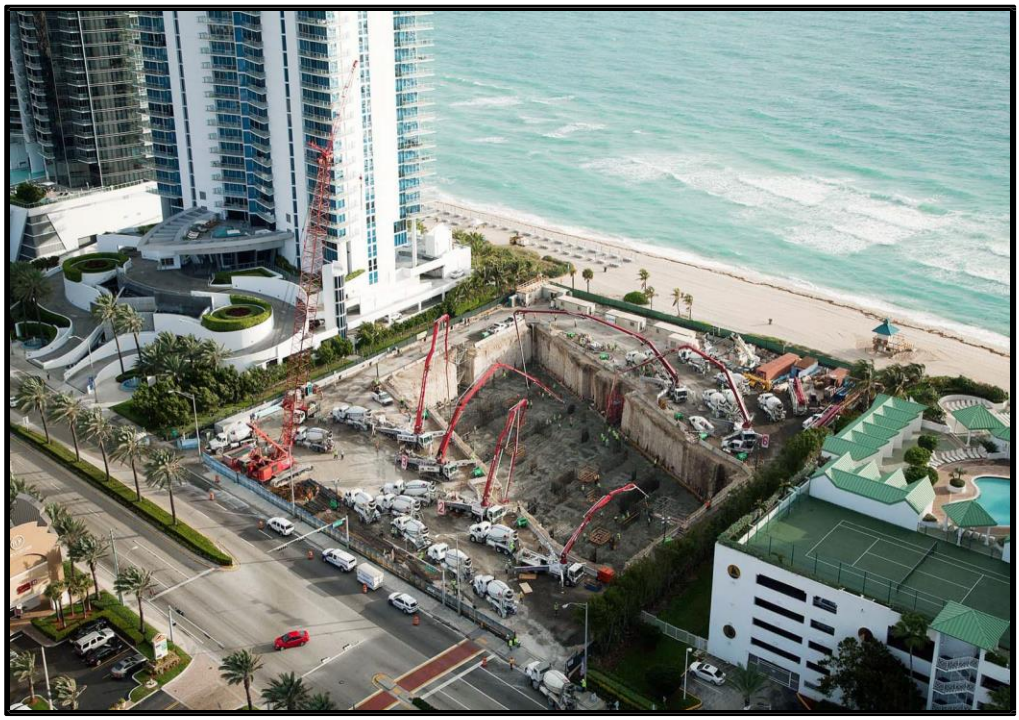


Fig. 1 Foundation Construction at Jade Signature Condominium
Photo: Central Concrete Supermix, Inc. Miami, FL

At the Jade Signature site, 27,000 cubic meters (35,000 cubic yards) of soil was treated by DSM. The mix design ranges were 80-90% SC and 20-10% OPC. The approximate amount of SC used was 11,800 metric tons. Assuming a mix design of 85% SC and 15% OPC, approximately 2100 metric tons of OPC was used. The approximate total of cementitious material used in DSM was 13,900 metric tons. Using the LCA data in Table 1 above approximate life cycle impacts can be calculated:

Table 3. Sample Approximate Life Cycle Impacts, 13,900 metric tons of 85/15 SC/OPC compared to 13,900 metric tons of OPC

Category Indicator	LCA Savings/Benefits Use of 85/15 SC over 1/1 OPC
Global warming potential	Generated 10,500 metric tons less CO_2
Total primary energy	Consumed 40 million megajoules less energy
Non-renewal materials	Consumed 17000 metric tons less non-renewable materials
Renewable material use incl. recovered materials	Reused/recovered 13,000 metric tons more material
Fresh water	Consumed 20 million liters less fresh water

Herbert Hoover Dike Rehabilitation Projects

Lake Okeechobee is a 1900 square kilometer (730 square mile) freshwater lake in central Florida. The lake is surrounded by 228 km (143 mile) of levee. Work is underway to improve the safety of the levee system. Over 32 km (20 mile) of levee were improved with a cut-off wall during 2007-2013 and another 11 km (7 mile) of improvement planned during 2017-2020.



Fig 2. Map of Lake Okeechobee Graphic: U.S. Army Corps of Engineers

The completed phases of cut-off wall installation used over 36,000 metric tons of slag cement. Using the LCA data in Table 1 above approximate life cycle impacts can be calculated: for a typical mix design used 70-80% slag cement as a replacement for OPC as the most cost effective method of meeting the U.S. Army Corps of Engineers' Engineering permeability specifications.

Table 4. Sample Approximate Life Cycle Impacts, 36,000 metric tons SC compared to 36,000 metric tons of OPC

Category Indicator	LCA Savings/Benefits Use of 36,000 metric tons SC over OPC
Global warming potential	Generated 32,000 metric tons less CO_2
Total primary energy	Consumed 90 million megajoules less energy
Non-renewal materials	Consumed 51,000 metric tons less non-renewable materials
Renewable material use incl. recovered materials	Reused/recovered 40,000 metric tons of material
Fresh water	Consumed 348 million liters less fresh water

SUMMARY

DFI Members involved in geotechnical work can contribute to a sustainable built environment by selecting cements with the lowest environmental impacts documented in life cycle assessments that still meet the performance standards of a project. Some portion of OPC in mix designs may be replaced by SCMs and/or industrial byproducts. Much of life cycle impacts of these SCMs and industrial byproducts have already been borne by the industries that generated these materials. Enhanced sustainability may also be accomplished by performance optimization with the use of SC leading to a reduction of the total cementitious materials needed to meet project specifications.

Results of an LCA for cements are reported on an EPD. The relative environmental impact or sustainability of a cementitious material may be compared by using the EPDs of the materials.

There is increasing awareness to LCA and sustainability of different materials used on projects. The life cycle impacts as depicted by estimates from completed projects can be dramatic. Project design engineers and contractors may be able to use their more sustainable solution to position their geotechnical application and/or mix design against competing proposals.

ACKNOWLEDGMENTS

Authors wish to thank Lehigh Hanson Incorporated, Irving, Texas, USA for support in writing this paper and Mr. Gordon McLellan, Lehigh Cement Company, Cape Canaveral, Florida for SC use data.

REFERENCES

Kosmatka, S.H. and Wilson M.L. 2016. Design and Control of Concrete Mixtures. EB01, 16th Edition, Portland Cement Association, Skokie, Illinois, USA, 632 p.

Concrete's Contribution to LEED v4, Concrete Sustainability Report, July 2014. National Ready Mixed Concrete Association, Silver Spring, Maryland, USA. 8 p.

Portland Cement-Environmental Product Declaration. 2016. Portland Cement Association, Skokie, Illinois, USA, 11 p.

Blended Cements -Environmental Product Declaration. 2016. Portland Cement Association, Skokie, Illinois, USA, 11 p.

Slag Cement-Environmental Product Declaration. 2015, ASTM International, West Conshohocken, Pennsylvania, USA, 16p.

"Brownfield Remediation" (n.d.) U.S. Green Building Council Retrieved 12 May 2017 from http://www.usgbc.org/credits/neighborhood-development-plan-neighborhood-development/v4-draft/sllc2?view=resources

NOISE ATTENUATION AND REDUCED RISK ASSOCIATED WITH NEW DOUBLE-WALLED PILE TECHNOLOGY

Per G. Reinhall, University of Washington, Department of Mechanical Engineering. (206) 375-6295. reinall@uw.edu.
Julie HN Hampden, Marine Construction Technologies, PBC. julie@marinecontech.com. (206) 755-8397

Executive summary:

Impact pile driving of steel piles is a common construction practice in freshwater and marine environments for the building of structures and foundations. This practice produces extremely high sound levels underwater that have proven injurious to aquatic fish and wildlife. To limit impacts to sensitive species, resource management agencies employ a variety of different strategies including timing restrictions to limit in-water construction windows to those months when there are low flow conditions in lakes or rivers, to those hours when tides are low, or to periods of the year when species of concern are least likely to be present in the project vicinity. In addition, permitting agencies have identified noise thresholds above which sensitive species could be injured, resulting in additional project conditions to curtail the extent of project noise impacts including: limiting the number of piles or pile strikes per day, requiring biological monitoring, and mandating the use of noise attenuation techniques, such as bubble curtains and cofferdams. Numerous studies have shown current noise attenuation techniques are costly and provide limited or variable noise reduction [1-3]. This is because the noise from pile driving is not only transmitted through the water column, it is also transmitted through the sediment back into the water column [1, 4-8]. Though these protective measures may help to reduce project impacts, they also result in additional complexity, expense, and potential risk for project delivery.

Marine Construction Technologies, a Public Benefit Corporation, in collaboration with University of Washington and Washington State Department of Transportation, has developed a pile that can be installed with standard pile driving technologies (vibratory or impact hammers) and consistently decreases the total noise transmitted into the water. The double-walled pile is relatively quiet in comparison to unattenuated piles or existing noise attenuation techniques. This technology not only reduces the risk to sensitive species by minimizing the extent of potential impacts, it also reduces potential risks to project delivery by limiting the size of monitoring areas, minimizing the need to cap daily production rates, and eliminating the need for deployment of additional noise attenuation devices.

Results from finite element modeling of the pile, scaled prototype testing, and full scale field testing in Commencement Bay (October 2014) and Vashon Island (October 2015) in Puget Sound, Washington indicate a reduction the peak sound pressure between 14 and 20 dB relative to single walled piles at a range of approximately 10 meters. These tests also confirm that the double-walled piles provide drivability similar to standard steel piles. In addition, preliminary calculations for capacity and structural characteristics demonstrate that double-walled piles provide equivalent or better performance than same-sized standard piles.

 © 2017 DFI Annual Conference, New Orleans, LA, USA

Background:

The primary source of underwater sound from an impact driven pile originates from radial expansion of the pile as a compression wave propagates down the pile after each strike. This supersonic (with respect to the water) radial expansion wave produces an acoustic field in the shape of an axisymmetric cone [1], or Mach cone (Figure 1).

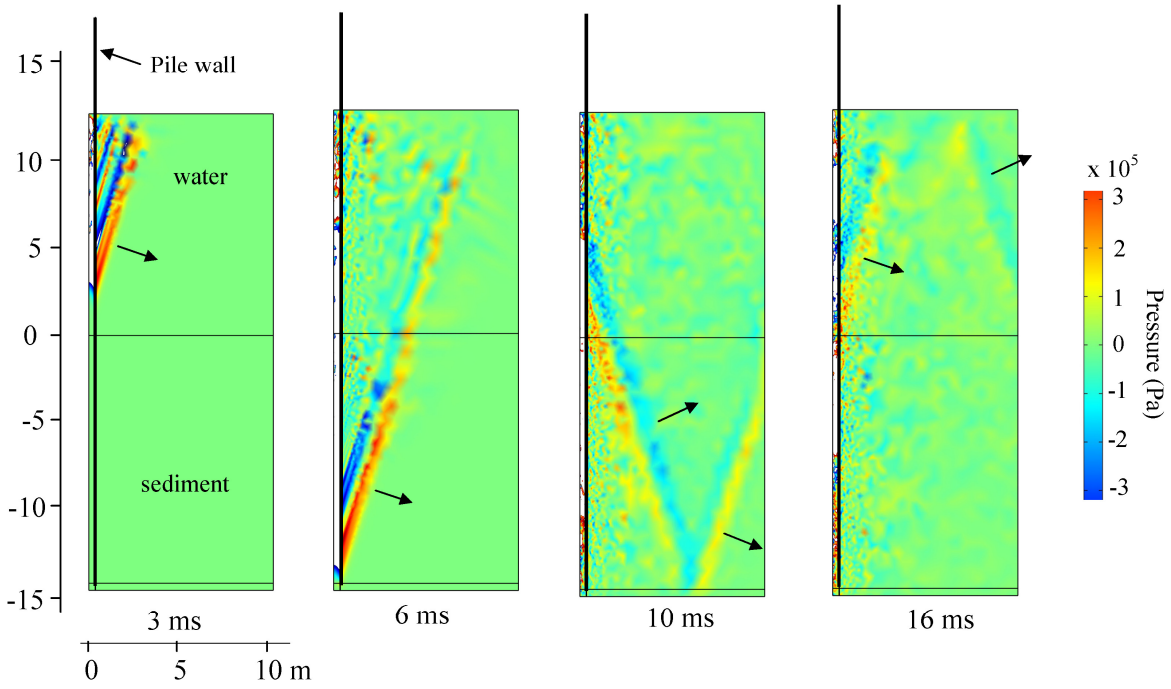


Figure 1: Acoustic pressure surface plots showing the acoustic radiation from the pile at 3, 6, 10, and 16 ms after impact by pile hammer. The propagation direction of the wave front associated with the Mach cones produced in the water and the sediment is indicated by the arrows.

After this downward moving mach sound wave reaches the sediment, a portion of the wave energy is reflected back into the water column from the sediment. The amount of noise reflected back into the water depends upon the characteristics of the substrate; soft substrates tend to absorb more sound than hard sediments. This upward moving reflected Mach sound wave is the reason why many commonly used sound attenuation devices demonstrate variable effectiveness; they do not address noise reintroduced into the water from sediment. Figure 2 illustrates how sound from the seabed leaks out from the sediment, circumventing a bubble curtain.

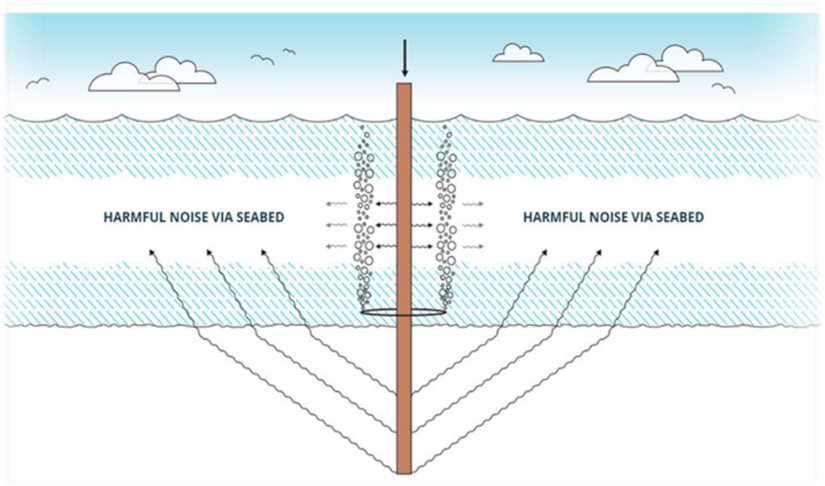


Figure 2: Illustration of how sound from the seabed is transmitted unhindered by a sound shield surrounding the pile in the water, e.g., a bubble curtain.

Sound is a pressure wave. In air, we hear sound because this pressure wave expands then contracts the membranes and coclear hair structures of our ears as it passes. Quieter sounds vibrate our hearing structures more subtly; louder sounds vibrate our hearing structures more violently. Barotrauma occurs when noise pressure is so extreme that it bursts or collapses hearing membranes or other gas filled organs as the pressure wave passes through them. In water, which is far denser than air, sound travels five times faster, at 5,000 meters per second. Like it does in air, noise moves through water as a pressure wave that expands and contracts any gas filled organ or membrane it passes. As a result, for aquatic fish and wildlife (i.e. marine mammals and diving birds) underwater noise can range from an unwanted annoyance to a fatal blow, depending upon its intensity.

To protect economically and ecologically valuable resources, resource management agencies have been striving to minimize underwater noise via a range of different strategies and mechanisms. Though each of these approaches reduces risk to aquatic species, in many cases they can serve to increase risk for project delivery by affecting project scopes and timelines.

For example, by requiring biological monitoring during pile driving, the resource agencies necessitate that a detailed monitoring plan be developed by the project proponent and qualified staff hired to implement it, safety plans be revised to accommodate monitoring activities, communication plans and protocols be updated to include monitoring activities and staff, construction be limited to the time and weather conditions specified in the monitoring plan, and that project schedules accommodate frequent or prolonged work stoppages if species are present or when site specific conditions inhibit effective monitoring.

Another common impact minimization requirement is deployment of a noise attenuation device to reduce underwater noise during pile driving. This requirement necessitates that project proponents acquire or rent such a device, that the project is adequately staffed by people qualified

and experienced with deploying the device during pile driving, the appropriate additional equipment is acquired and staged (i.e. generators, air compressors, barge), and that the timeline for the project accommodate consistent deployment of the device during pile driving activities.

While noise from pile driving poses a significant risk to important aquatic resources, so too does underwater noise and effectively managing it pose potentially significant risks to project delivery. Reinhall Piles limit risk to aquatic species as well as to project delivery.

A New Approach:

The Reinhall Pile design uses two conventional steel piles, one smaller pile sleeved inside of a larger pile, which is attached by a special shoe to encapsulate noise along the entire length of the double-walled pile. The inner pile can be fixed or a reusable mandrel inserted for driving purposes. With this design, only a minimal amount of noise escapes at the pile toe.

In October 2014, a full-scale test of the double-walled pile was performed at a site within the Port of Tacoma in Puget Sound near Tacoma, Washington to test the noise attenuation effectiveness of the new technology. During the test, three 80 ft (24.4 m) long piles were driven: (1) a 30 in. (760 mm) diameter control pile, which was a conventional steel pile driven using standard impact methods, with and without a bubble curtain, (2) a 30 in. (760 mm) diameter double-wall pile, and (3) a 30 in. (760 mm) diameter mandrel-driven double-wall pile.

Underwater noise levels were measured with underwater microphones (hydrophones), which converted noise pressure to voltage and were calibrated to express the pressure in Pascals (Pa). The pressure, using a logarithmic scale, was expressed as decibels (dB). Several metrics are used to describe underwater noise. Three common metrics are the instantaneous peak sound pressure level (dB peak), the Root Mean Square pressure level (dB RMS), and the sound exposure level (dB SEL) referred to as the peak, RMS, and SEL levels.

At a distance of 33 ft (10 m), the double-wall and mandrel piles showed a reduction in peak noise levels (the maximum peak over- and under-pressures) greater than 20 dB in underwater noise compared to a 6 dB reduction for the bubble curtain.

A second full-scale test of the double-walled pile occurred on December 7-8, 2015, at the Vashon Island Ferry Terminal in Puget Sound near West Seattle, Wash. At this test site, three 76.5 ft (23.3 m) long piles were driven within a steel driving template in a manner similar to the first test: (1) a 30 in. (760 mm) diameter control pile, which was a conventional steel pile driven using standard impact methods (no bubble curtain was used for this test because it did not fit within or around the template used to drive the piles), (2) a 30 in. (760 mm) diameter double-wall pile; and (3) a 30 in. (760 mm) diameter mandrel-driven double wall pile. This test primarily evaluated drivability of the Reinhall piles, and to a lesser degree the noise attenuation effectiveness. The Reinhall Pile showed statistically equivalent drivability to conventional piles over the last three feet (0.9 m) of driving. At a distance of 33 ft (10 m), the double wall and mandrel piles showed a reduction in the peak noise levels in excess of 13 dB.

How Reduced Environmental Risk Results in Reduced Project Risk:

By reducing noise levels at the source, the area affected by elevated noise levels during pile driving shrinks dramatically. A hypothetical representation of this change is provided in Figure 3 below, for a project that will drive three steel piles per day, and requires striking each pile up to 1,000 times. For this example, we assume the single strike SEL for effective quiet is 150 dB, or indiscernible from existing conditions. We juxtapose the distances (in meters) noise will travel before attenuating to quiet conditions for standard piles with no attenuation, piles surrounded by bubble curtains, and double-walled piles. The estimated noise levels generated by each of the technologies is as follows:

- Piles with no attenuation - 215 dB peak, 205 db SEL, and 190 dB RMS
- Piles with a bubble curtain (3 dB reduction) - 212 dB peak, 202 db SEL, and 187 dB RMS,
- Double-walled piles (15 dB reduction) - 196 dB peak, 191 db SEL, and 175 dB RMS.

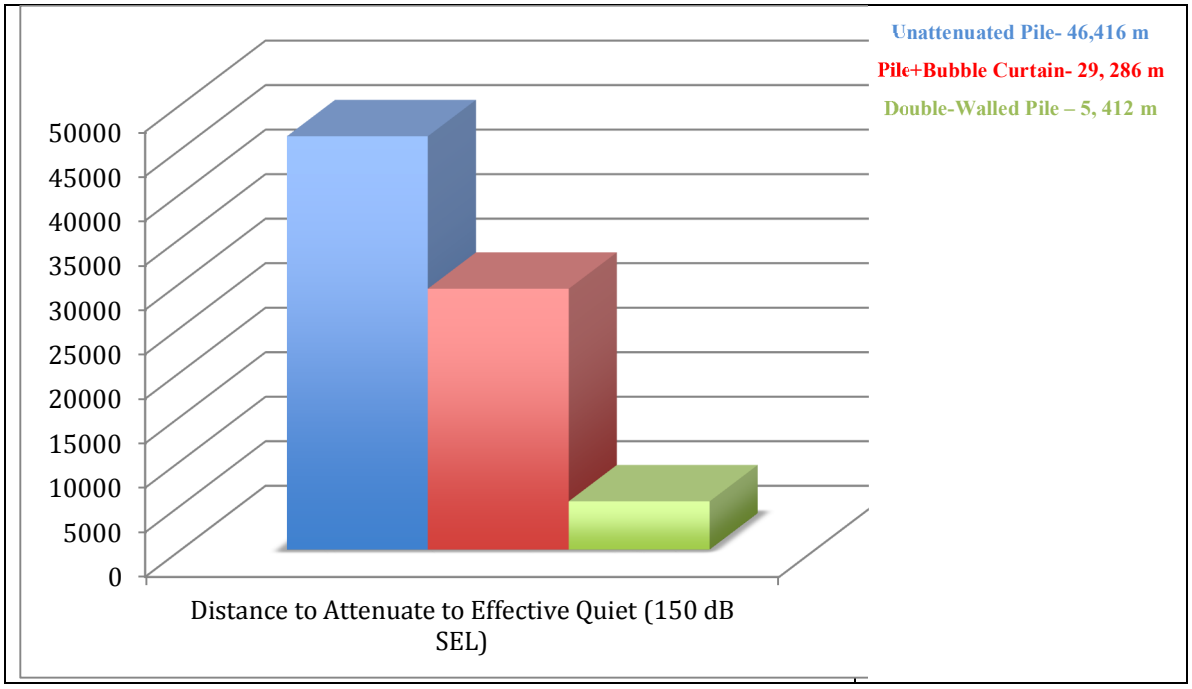


Figure 3: Comparison of distances (meters) to effective quiet associated with use of different noise attenuation technologies during pile driving.

This reduction in the geographically affected area directly translates to a reduced risk of exposure for aquatic species, a smaller biological monitoring area, and a concomitant reduction in monitoring effort.

Table 1 juxtaposes the isopleths or impact distances associated with the three technologies described above. The table provides several established biological thresholds that have been defined by regulatory agencies to represent sound levels above which potential injury to sensitive species can occur. The distances (in meters) represent how far from the pile noise levels that exceed these thresholds and potentially injure sensitive species will extend.

Table 1: Comparison of distances (meters) to regulatory thresholds associated with use of different noise attenuation technologies during pile driving.

Regulatory Thresholds	Unattenuated Pile	Pile with Bubble Curtain	Double-Walled Pile
206 dB peak (fish barotrauma)	40	25	2
183 dB SEL (fish <2g)	46,416	29,286	5,412
187 dB SEL (fish >2g)	32,967	20,801	3,844
202 dB SEL (murrelet auditory injury)	3,297	2,080	384
208 dB SEL (murrelet barotrauma)	1,312	828	153
230 dB peak (PTS marine mammals – mid-frequency hearing group)	NA	NA	NA
185 dB SEL (PTS marine mammals – mid-frequency hearing group)	2,163	1,365	252

Changes of this magnitude (~10 times) represent a significant reduction in the potential risk to sensitive species. There is far less potential for a marine mammal or marbled murrelet to enter the much smaller impact area associated with the double-walled pile during construction than the large area resulting from the conventional pile. Reduced risk to resources, in a regulatory context, generally results in a streamlined permitting process that results in fewer constraints to project delivery.

Figure 4 roughly depicts the difference in areas that would be required for monitoring to minimize potential injury to marbled murrelets (~3,297 meters/ 2.04 miles versus ~384 meters/ 0.23 miles) or marine mammals (~2,163 meters/ 1.34 miles versus ~252 meters/ 0.15 miles) for



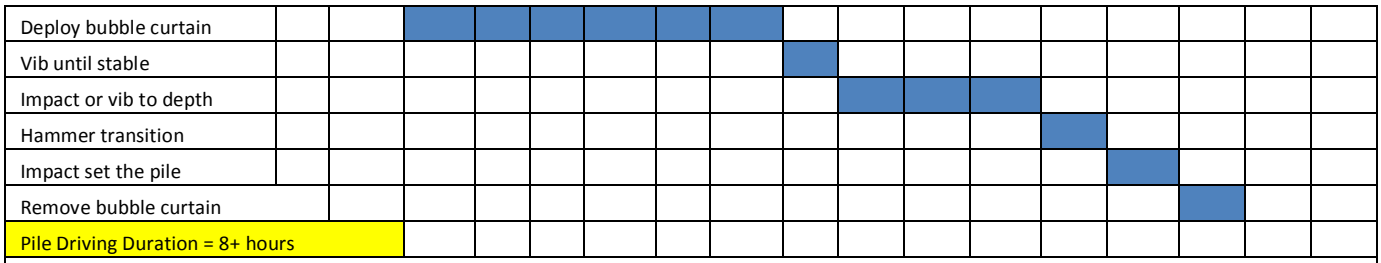
Figure 4. Graphic representation of potential monitoring zones for biological resources.

our hypothetical project, comparing conventional piles with no attenuation versus double-walled piles. A reduction in the monitoring area from the blue polygon to the orange circle would reduce the number of boats and biologists required to effectively monitor the area for target species. For the conventional pile with no attenuation, the impact area could necessitate the use of 20 or more boats, each staffed with one to two biologists and a boat operator, totaling 40 or more project staff. The monitoring area for the double-walled pile would require 1-2 boats at most, totaling up to 6 project personnel.

Reinhall Piles allow contractors to use existing pile driving technologies to drive piles (impact or vibratory hammers) while achieving consistent noise attenuation, without needing to switch hammer types or deploy additional technologies to acoustically isolate the piles during installation. A hypothetical representation of the potential time savings for the implementation phase of a project is provided by Table 2 below. The table shows the estimated installation times for three standard piles with bubble curtains (8+ hours) versus three double-walled piles (3+ hours).

Table 2: Comparison of pile installation duration with use of different noise attenuation technologies during pile driving.

Pile Installation - Standard with Bubble Curtain																	
	Minutes																
Activity	10	20	30	40	50	60	70	80	90	100	110	120	130	140	150	160	170
PILE 1- 7 AM start						8am						9am					
Loft																	
Place																	
Deploy bubble curtain																	
Vib until stable																	
Impact or vib to depth																	
Hammer transition																	
Impact set the pile																	
Remove bubble curtain																	
Transition to pile 2																	
PILE 2 - 9:50 AM start	10am						11am						12pm				
Loft																	
Place																	
Deploy bubble curtain																	
Vib until stable																	
Impact or vib to depth																	
Hammer transition																	
Impact set the pile																	
Remove bubble curtain																	
Transition to pile 3																	
Lunch 12:40-1:40 PM																	
PILE 3 - 1:40 PM start		2pm						3pm						4pm			
Loft																	
Place																	



Pile Installation - Double-Walled Pile

Activity	Minutes 10	20	30	40	50	60	70	80	90	100	110	120	130	140	150	160	170
PILE 1- 7 AM start						8am											
Loft																	
Place																	
Vib until stable																	
Hammer transition																	
Impact to depth																	
Transition to pile 2																	
PILE 2 - 8:30 start			9am						10am								
Loft																	
Place																	
Vib until stable																	
Hammer transition																	
Impact to depth																	
Transition to pile 3																	
PILE 3 - 10am start						11am											
Loft																	
Place																	
Vib until stable																	
Hammer transition																	
Impact to depth																	
Transition to pile 2																	
Lunch 11:30-12:30																	
Pile Driving Duration = 3+ hours																	

This > 50% time savings would result in a higher production rate for pile installation per day, increasing project efficiency and reducing the overall project implementation timeline.

In conclusion, the double-walled pile technology is not only effective in minimizing underwater noise to benefit the environment, it also potentially reduces project risk by expediting project implementation by reducing potential project effects and facilitating installation of piles without requiring any additional technology to drive piles or attenuate noise.

References:

1. Reinhall, P. G. and P.H. Dahl. 2011. Underwater Mach wave radiation and pile driving: theory and observation. Journal of the Acoustical Society of America. February, 2011. 25 pp.

2. Koschinski, S. and K. Luedemann. 2013. Development of Noise Mitigation for Offshore Wind Farm Construction. Prepared for the Federal Agency for Nature Conservation (Bundesamt für Naturschutz, BfN). Original report published July 2011, English translation published February 2013. 102 pp.

3. Petrie, F.S. 2005. Washington State Ferries' Experience with Bubble Curtains: Purpose, Hardware, and Use. Presentation for 2005 Summer Meeting/Conference of the Transportation Research Board ADC40 (A1F04) Noise & Vibration Committee.

4. CALTRANS (California Department of Transportation). 2009. Technical Guidance for Assessment and Mitigation of the Hydroacoustic Effects of Pile Driving on Fish_Prepared by ICF Jones & Stokes and Illingworth and Rodkin. Sacramento, CA. February 2009. 298 pp.

5. Kim, .H. 2011. Prediction of Structure Borne Noise Radiation and Propagation from Offshore Impact Pile Driving. Open Access Dissertations. Paper 201. 152 pp.

6. Dardis JT and Reinhall PG. New Offshore Pile for Reduced Acoustic Emissions – Results from Full Scale Testing, Proceedings from the 22nd Int. Congress on Sound and Vibration, July 2015

7. Reinhall PG, Dardis T, Dahl PH, Underwater Noise Reduction of Marine Pile Driving Using a Double Pile, WSDOT Report WA-RD 849.1, December 2015

8. Applied Physical Sciences. 2010. Mitigation of Underwater Pile Driving Noise During Offshore Construction: Final Report. Prepared for Department of the Interior, Minerals Management Service Engineering & Research Branch. Herndon, VA. 104 pp.

ENERGY GEOSTRUCTURES: ANALYSIS FROM RESEARCH AND SYSTEMS INSTALLED AROUND THE WORLD

Alice Di Donna[a]*, Marco Barla[a] and Tony Amis[b]

[a] *Politecnico di Torino, Department of Structural, building and geotechnical engineering, Italy*
[b] *GI Energy*

* alice.didonna@polito.it

Abstract

Energy geostructures are becoming an increasingly popular solution around the world for Developers looking to reduce CO_2 and system running costs. Energy geostructures are geotechnical structures that provide both the important role of structural stability while also acting as a heat exchanger with the ground, enabling the supported buildings and or infrastructure to be heated and cooled using the principle of low enthalpy geothermal systems. The main advantage of this innovative technology with respect to standard geothermal plant is the reduction of the initial installation costs and construction schedule benefits, compared to installing conventional geothermal solutions, largely due to the additional use of structures which would be constructed in any case. However, it is important with respect to energy geostructures that additional aspects need careful consideration. For this very reason, several research studies have been carried out over the last decade on this subject and a number of real case studies have been monitored and analysed. The key difference with respect to conventional shallow geothermal systems are mainly related to the geometry, which is imposed by the geotechnical project, and the need to ensure that the primary structural role is always guaranteed. Special boundary conditions, the reduced depth, the influence of atmospheric external temperature can also play an important role for energy geostructures. They can affect, both energy efficiency and, the geotechnical behaviour because of the possible thermal induced mechanical effects. This paper presents a picture of the current situation regarding energy geostructures and their peculiar features, and collects available data to provide a reference framework. Data has been collected from literature and personal communications and then processed to provide easy-to-read charts useful for practical consultation at a glance. This paper provides, an indication of the distribution of such systems worldwide, their spread in time, and a global view of their actual efficiency from the structural, energy, economic and environmental point of view.

Keywords: Energy Piles, Energy Walls, Energy Tunnels, Database

1. Introduction

Energy geostructures are becoming an increasingly popular consideration around the world. Energy geostructures are geotechnical structures with a dual role of providing structural stability and the ability to exchange heat with the ground, to provide low carbon heat and coolth to supporting and or adjacent buildings and infrastructure, using the principle of low enthalpy geothermal systems (Barla and Di Donna, 2016; Laloui and Di Donna, 2013). A closed circuit of high density polyethylene (HDPE) pipes is embedded in the concrete, and a heat carrier fluid circulates through them exchanging heat with the ground. The HDPE pipework circuit inside the geostructure is linked to one of the above buildings or infrastructure through a heat pump, which adapts the temperature of the circulating fluid to the heating (winter mode) and cooling (summer mode) needs. In this way, heat can be injected into the ground during summer and extracted from it during winter. In principle, all structures in contact with the ground can be used as energy geostructures. The first examples of energy geostructures date back to the eighties in Austria and were mainly piles and shallow foundations. A decade later, Henderson et al. (1999) reported on what would appear to be the first successful use of geothermal energy piles in the US, with loops incorporated into the foundation for a hotel in Geneva, New York. As was their use in this New York case history, the typical geothermal energy pile

 © 2017 DFI Annual Conference, New Orleans, LA, USA

application is used in conjunction with additional closed loop boreholes to provide the required energy capacity for a structure. Interestingly the report concludes that the geothermal energy piles had a better heat transfer performance than the borehole field. The first energy walls appeared slightly later, while still today only a few experimental cases of energy tunnels exist (Brandl, 2006; Franzius and Pralle, 2011; Riederer et al., 2007; SIA DO 190, 2005). However, with respect to conventional geothermal systems additional aspects need to be considered to make a proper use of this technology. Amongst these, there are those related to energy efficiency and, also, those related to the geotechnical design and structural integrity, which must be guaranteed, even in the presence of the temperature variations that will be induced by the geothermal activation. Examples are the effects of underground conditions on the heat exchange potential, the effect of temperature on the response of soils and soil-structure interaction and the possible additional thermal-induced displacements and stresses inside the structures.

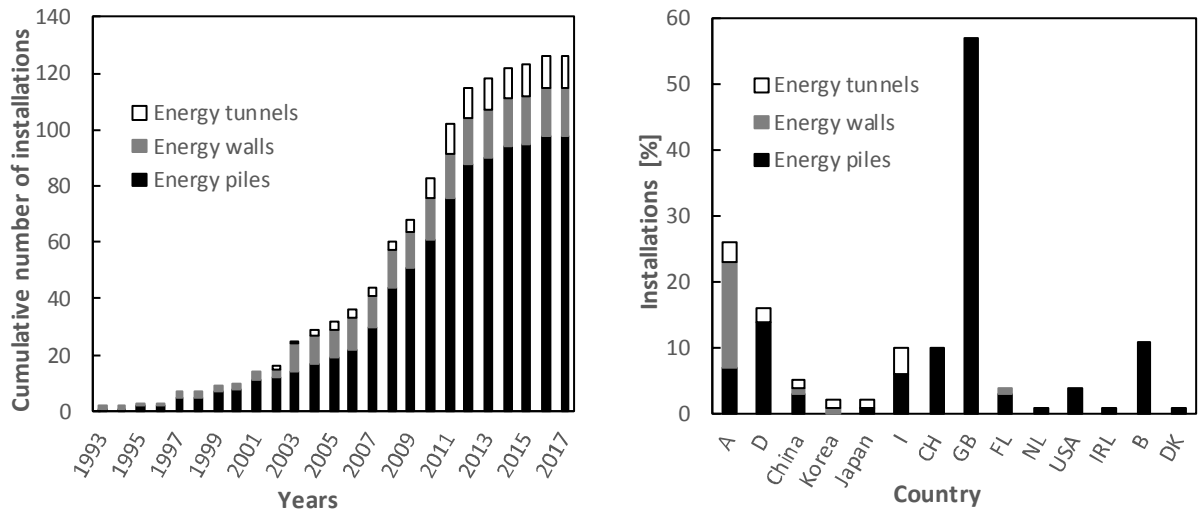
Data on operational and trial energy geostructures have been collected into a database by the Authors over the last decade, with the intent of providing an overview of the current state of diffusion, advancement, and efficiency of this technology. In the following, after an update on the current status of geoenergy structures around the world, the paper provides an introduction on the structure of the database, the observations from the analysis of the collected data are discussed in terms of (i) diffusion of the technology in time and space, (ii) energy efficiency, (iii) geotechnical aspects and (iv) economic and environmental considerations.

2. Current status of geoenergy structures around the world

The cumulative number of energy geostructures installed since 1993 is presented in Figure 1a. The graph shows a steep increase in using this type of geoenergy technology between 2005 and 2011; this is largely as a result of the UK market being driven by tighter planning requirements and also incentives associated with installing renewable technologies. In more recent years, uptake of energy geostructures has eased somewhat but known opportunities exist in France and the USA that are likely to show a revitalised trend in the coming years. As mentioned earlier, most installations are energy piles, while energy walls and tunnels have started to play a role more recently and can be considered an interesting and exciting future application of this technology. The use of tunnels as ground heat exchangers has clearly the advantage of involving much larger volumes of ground, but also some additional challenges exist associated with the identification of the owner of heat and the distribution of the resource. It is felt by the authors that this is possibly the reason why the evolution of energy tunnels has been somewhat slower with respect to other energy geostructures, however trials currently underway in Turin (Italy) are hoping to identify the best means of loop installation and heat dissemination (Barla et al., 2017). Figure 1b shows the percentage of installations per country (A=Austria, D=Germany, I=Italy, CH=Switzerland, GB=Great Britain, FL=Liechtenstein, NL=Netherlands, USA=United States of America, IRL=Ireland, B=Belgium, DK=Denmark), with respect to the total. Austria, where the technology was born, together with the United Kingdom and Germany, are the countries where most of energy geostructures have been constructed. However, data might be missing for certain countries such as France, Switzerland and others outside Europe. Known USA projects include:

- 1997 Hotel Geneva -New York 198 Piles
- 2004 Art Stable –Seattle 150 piles
- 2014 Trevor Day School New York 360 energy piles

And the USA looks like it will eclipse Europe over the next few years as more large companies look to reduce their CO_2 footprint. For example, Google's San Francisco headquarters is currently under construction with over 3000 energy piles (not included in graph below)



(a) (b)

Figure 1. Evolution of energy geostructures installations (a) over time and (b) in different countries.

3. Structure of the data base

The database is divided into two sections, the first one is devoted to energy efficiency, costs and environmental issues, while the second to geotechnical aspects. For the first section, information on existing energy geostructures was collected from papers (Amis et al., 2010; Brandl, 2006; Franzius and Pralle, 2011; Frodl et al., 2010; Islam et al., 2006; Lee et al., 2012; Markiewicz and Adam, 2009; Schneider and Moormann, 2010; Unterberger et al., 2004; Xia et al., 2012; Zhang et al., 2013), published documents (Riederer et al., 2007), recommendations (SIA DO 190, 2005), companies or contractors web sites and personal communications. They include operational plants and trial installations. Data collected includes:

- Name of the installation;
- Country;
- Year of installation;
- Geometry (number of piles, surface of walls, length of tunnel etc.);
- Normalised extracted/injected heat in W/m of pile length and W/m2 of wall or tunnel surface;
- Heat power provided in winter and summer (in kW);
- Annual energy provided in winter and summer (in MWh/y);
- Soil-structure temperature;
- Pipes dimension and configuration;
- Inlet – outlet temperature;
- Heat carrier fluid flow rate;
- CO_2 reduction;
- Ground conditions;
- Costs and payback period;
- Contractor;
- Reference;

The second section (geotechnical aspects) includes only data related to experimental real scale energy piles, as no information on monitored energy walls and tunnels are available to date, to the author's best knowledge. The data was collected from published papers (Akrouch et al., 2014; Amatya et al., 2012; Di Donna et al., 2016; Laloui et al., 2003; McCartney and Murphy, 2012; Murphy et al., 2015; Rotta Loria and Laloui, 2017; Sutman et al., 2014; Wang et al., 2014; You et al., 2016) and include:

- Pile typology;
- Ground;
- Mechanical load applied;
- Geometry;
- Temperature range;
- Thermal induced stresses;
- Thermal induced head displacements;
- Degree of freedom;
- Reference.

For both sections, the available data is not uniform and neither complete, but provides a preliminary global view on this exciting technology. In the first section, a total of 151 records were collected: 119 energy piles, 20 energy walls and 12 energy tunnels. In the second section, data from a total of 8 energy piles was collected.

4. Energy efficiency

Compared to the conventional method of constructing closed loop geothermal systems, using purpose drilled boreholes, energy geostructures have a dual role and the structural and geotechnical design imposes the geometry and dimension of the ground heat exchanger. In this sense, the number and length of energy piles, the depth of energy walls, the diameter of an energy tunnel is not designed to satisfy the heat demand but depends on the structural constraints. Consequently, a designer will need to evaluate, how much heat such structures can effectively and sustainably exchange with the ground and, also the factors most affecting the energy efficiency. Among these are some site-specific parameters, e.g. soil thermal properties, underground temperature, degree of saturation. Other factors can be engineered, such as the number of geothermal pipes, fluid flow rate, and the concrete thermal properties. A number of research studies have been recently carried out on these aspects (Cecinato and Loveridge, 2015; Di Donna et al., 2017; Di Donna and Barla, 2016). Data collected in the database in terms of heat exchange in kW for real case studies was, when possible, normalised over the piles length or walls and tunnels surface in contact with the ground, to provide a more generalised figure. The output is presented in the following.

4.1. Energy piles

Exchanged heat in the case of energy pile installations are presented in Figure 2, in terms of W/m exploited in winter and summer. It can be seen that, for the data available, the heat exchange is generally in the range between 40 to 100 W/m, with some exceptions. The differences might depend on the pile depth and diameter, soil thermal and hydraulic properties and underground conditions, and especially where there is the presence of groundwater flow. Longer piles involve a volume of surrounding soil which is less influenced by the external atmospheric temperature changes, being consequently more efficient in terms of heat exchange. On the other hand, the bigger their diameter, the wider is the soil-structure contact surface, the higher is the heat exchange. In addition, the thermal conductivity of the ground can dramatically affect the heat exchange, which improves considerably in the case of saturated soil. The presence of groundwater flow allows for heat transfer between the soil and the pile to occur not only through conduction, but also through convection, being more favourable if the system is used for heat exchange only, while less convenient for underground heat storage.

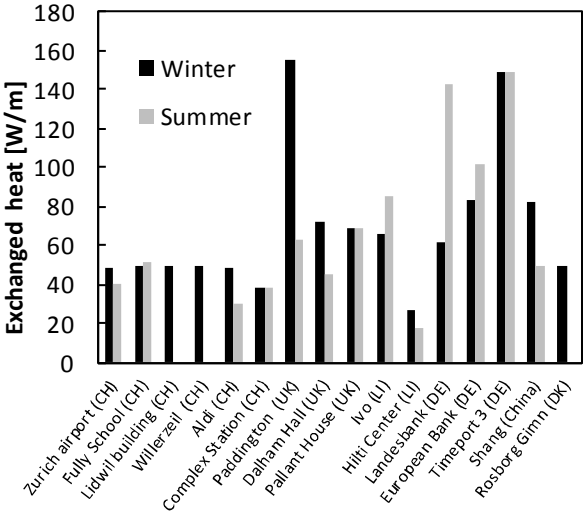
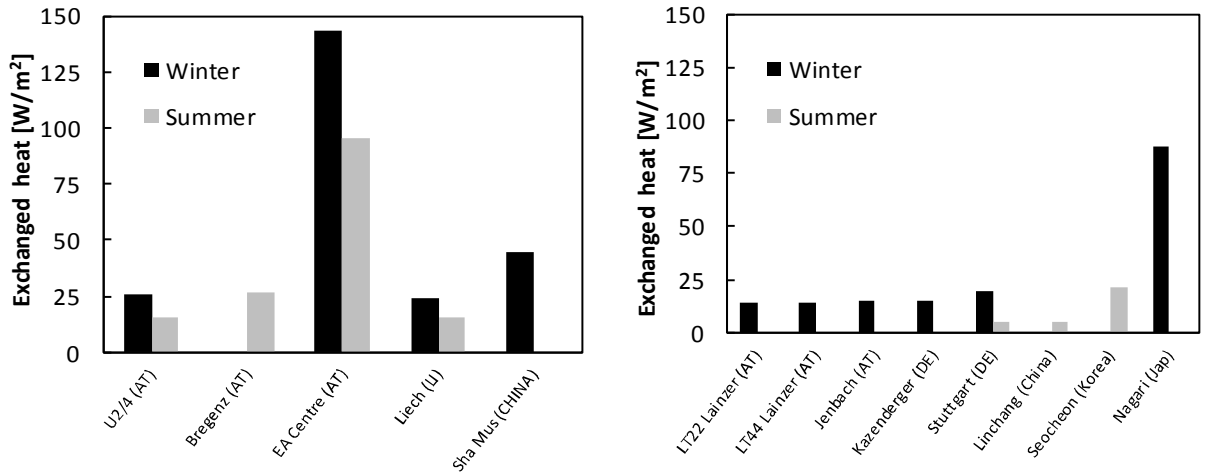


Figure 2. Heat exchange in real energy piles per meter of pile.

4.2. Energy diaphragm walls and tunnels

Figure 3a and b show respectively, the heat exchanged in winter and summer in terms of W/m^2 for the existing cases of energy walls and tunnel installations. It can be seen that the heat exchange is generally in the range between 10 to 50 W/m^2, with some exceptions. It is anticipated that the differences might depend on the depth of the installation and, as for the case of energy piles, on soil thermal and hydraulic properties and underground conditions, especially the presence of groundwater flow.

With respect to cut-and-cover tunnels, and underground tunnels in urban areas, these tunnels are more likely to be constructed in saturated soils and will be less influenced by the external air temperature variation as a result of their higher cover, this should at the same time improve their heat exchange potential. An additional aspect which must be considered specifically for energy walls and tunnels, that is not necessary with energy piles, is the effect of temperature and speed of the air inside the tunnel or underground space (Nicholson et al., 2014). These energy geostructures will exchange heat not only with the ground, but also with the air inside the underground space. In the case of hot tunnels this might represent an additional source of heat during winter, but a drawback during summer. Trials currently being undertaken in Turin will provide more detailed results which will be available in 2018.



(a) (b)

Figure 3. Heat exchange per square meter of wall in real (a) energy walls and (b) energy tunnels.

5. Geotechnical aspects

It is important that the use of geostructures as ground heat exchangers must consider that they have a primary structural role which must be preserved even in the presence of the temperature variations induced by the geothermal activation (Di Donna et al., 2013). This is considered to be one of the reasons why engineers and practitioners have not been fully confident with the technology and its diffusion has been slower in some countries. For current applications, the temperature changes are usually limited in the range of ±20°C, but they might increase in cases where geostructures are used for underground heat storage.

Generally speaking, when a structural element (concrete, steel...) is heated/cooled without any constraints, it dilates/contracts according to the material thermal elastic expansion coefficient. However, geostructures are not free to deform, as their deformation is partially prevented by the soil around and over-structures. Hence, heating/cooling will induce additional thermal stresses, which will correspond to the portion of thermal deformation which is not allowed, according to the theory of thermo-elasticity. Accordingly, Laloui et al., (2003) defined the degree of freedom of energy piles as the ratio between the observed and the free thermal deformation (i.e. the deformation that would occur if the pile was completely free to deform). The ratio is equal to zero when the pile is completely restrained (no observed deformation) and to one when it is completely free to deform under temperature changes (observed and free deformation are equal).

The same conceptual framework would apply also for tunnels and walls. Depending on the degree of freedom, thermally induced stresses and displacement might be more or less significant: the higher the restraints, the higher the thermal stresses and the lower the thermal displacements, and vice versa (Amatya et al., 2012; Laloui et al., 2003).

These aspects have been largely studied for energy piles, and are on the way to being studied in detail for tunnels and walls. However, to the author's best knowledge, monitoring data for thermal induced stresses and strains is only available for energy piles. These are also easier to assess from a theoretical point of view, considering a pile as a 1D element for the sake of simplicity.

To have an order of magnitude, considering a L=15 m long concrete pile having a linear thermal expansion coefficient β of 10^{-5} °C^{-1}, the maximum head displacement d (assuming the pile completely free to dilate and fixed at the toe) for a temperature variation of ΔT=30°C would be:

$$d = \beta \cdot \Delta T \cdot L = 10^{-5} \cdot 30 \cdot 15 \cdot 10^{3} = 4.5\, mm \quad (1)$$

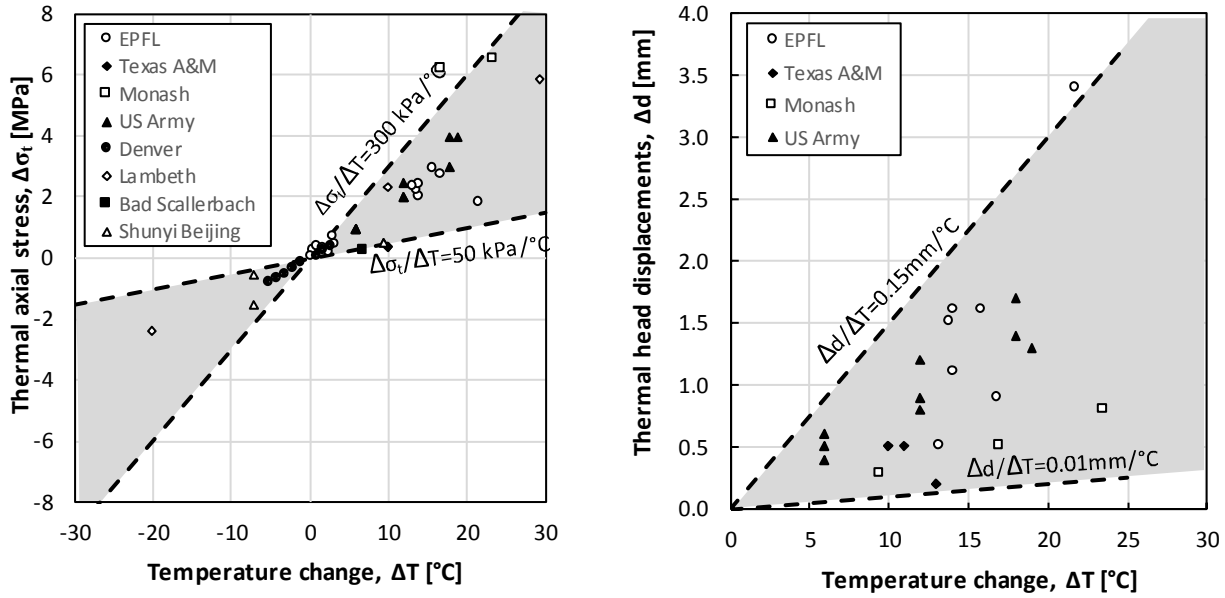
i.e. 0.15 mm/°C. Considering the same thermal loading, the same geometry and a Young's modulus for the pile equal to E=30 GPa, the maximum thermal stress (assuming the pile completely blocked) would be:

$$\Delta\sigma_t = E \cdot \beta \cdot \Delta T = 30 \cdot 10^3 \cdot 10^{-5} \cdot 30 = 9\ MPa \quad (2)$$

i.e. 300 kPa/°C. These are clearly the theoretical upper and lower bounds; real conditions are between these two extreme cases.

Available monitoring data from experimental sites includes a single pile and a group of piles at EPFL (Switzerland) (Di Donna et al., 2016; Laloui et al., 2003; Rotta Loria and Laloui, 2017), a single pile in a piled foundation in Texas (USA) (Akrouch et al., 2014), a single pile in Monash (Australia) (Wang et al., 2014), a piled foundation for the US Army (Murphy et al., 2015), a single pile in Denver (USA) (McCartney and Murphy, 2012), a single pile at Lambeth College (UK), another in Bad Scallerbach (Austria) (Amatya et al., 2012) and a group of six piles in Shunyi in Beijing (China) (You et al., 2016).

Data was analysed and is presented below in terms of the thermally-induced axial stress in Figure 4a and thermally-induced displacement at the pile head in Figure 4b, as function of the temperature variation imposed to the pile. The results indicate that the thermally-induced axial stress is in the range between 50 to 300 kPa/°C and the thermally-induced displacement in the range of 0.01 to 0.15 mm/°C. These values are generally acceptable with respect to concrete strength and buildings requirements in terms of serviceability performance.



(a) (b)

Figure 4. Geotechnical aspects of energy piles: (a) thermally-induced axial stress and (b) thermally-induced head displacement as a function of the imposed temperature variations in real-scale tests.

6. Environmental and cost benefits

One of the main advantages and interests of using geothermal systems is that they represent local resources, which are renewable and environment-friendly, in accordance with the current energy politics. In the interest of environmental protection, the reduction of CO_2 emissions and other pollutants is increasingly becoming an important issue and a relevant cost factor. Data regarding the reduction of CO_2 emissions due to energy geostructures was collected or computed, when not directly available, assuming 320 kg of CO_2 saving for every kW of energy produced using ground sourced heat pump technology, according to the British, Building Services Research and Information Association. The result, presented in

Figure 5 in terms of ton of CO_2 saved cumulated per year since 1993, shows that the contribution of energy geostructures to the pollution reduction is significant.

From an economic point of view, available data is limited. Payback periods of operative energy geostructures are set between 4 to 8 years (Riederer et al., 2007; SIA DO 190, 2005). In the case of energy tunnels, the initial investment is usually estimated around 2% of the total cost (Barla et al., 2016; Schneider and Moormann, 2010).

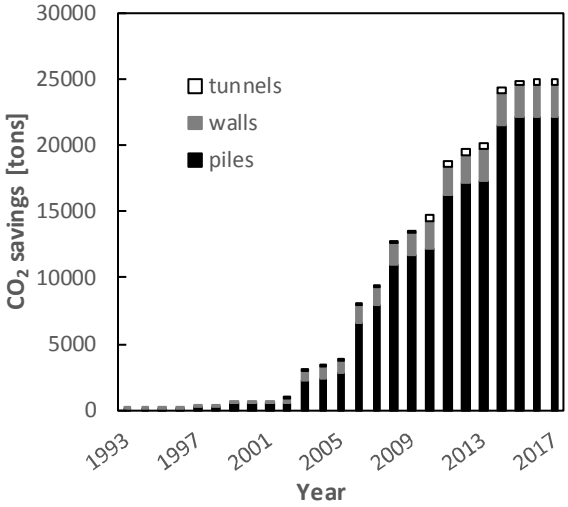


Figure 5. CO_2 savings in Europe thanks to energy geostructures.

On city center sites, economic pressures to maximise building footprint space will require a geothermal installation to be installed under the footprint of the new structure as generally there is no adjacent site to install them. This leads the geothermal designer to consider three possible solutions:

- Option 1 Open loop wells;
- Option 2 150-200 m deep purpose drilled geothermal boreholes;
- Option 3 Energy piles.

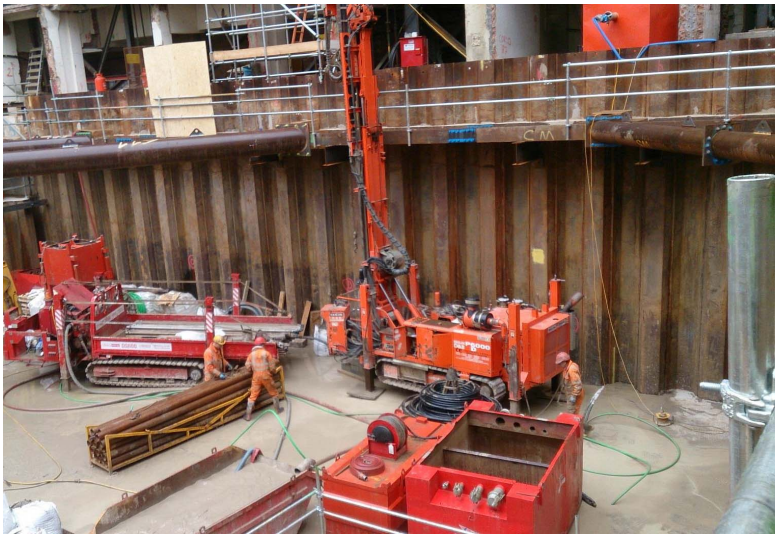
While Option 1 and 2 are likely to provide a greater heating and cooling output than option 3, there are significant additional costs associated with doing so. Both option 1 and 2 requires the supplementary use of large drilling equipment and associated plant to construct the boreholes and will generate significant additional volumes of spoil to be removed from site. On a limited city center site this will significantly impact upon a construction schedule (Fig 6), restricting other activities from commencing, resulting in geothermal work falling onto the critical path, thereby extending the overall construction period of a project.

An additional delay on a city center project can run into significant amounts of money/week. In addition to this additional time required, are the costs associated with:

- Mobilizing drilling equipment and associated plant;
- Providing suitable working platforms to ensure rig stability;
- Spoil and slurry removal, which is highly likely to be contaminated.

These are the fundamental reasons why utilizing the very foundations that are required to provide structural support to the building to also provide heating and cooling make such sense. Indeed, a recent proposed building located on a highly contaminated site in San Francisco, made using energy piles, rather than installing supplementary boreholes an easy “no brainer” of a decision.

Table 1 demonstrates the cost benefits of utilizing energy piles versus boreholes.



(a)



(b)

Fig 6. (a) Constructing 25 200 m deep boreholes in basement in Central London, added 8 weeks to construction schedule, (b) Installation of Geothermal Loops into 260 25 m deep 900 mm Rotary Bored Piles at Westminster Academy, incurred no impact on construction schedule.

Table 1. Comparison between cost benefits of boreholes and energy piles.

Item	Option 2 borehole loop	Option 3 thermal pile
Diameter Heat transfer Number of loops Length	0.2 m 35 W/m One 100 m (3500 W)	0.6 m 35 W/m Two 27 m x 2 No (1750 W)
Boring/installation cost	$50/m x 100 = $5000	Pile included anyway Allow 2 hours' attach loops $270/crew time
Thermal grout Pipe – 25 mm ID Spoil removal	$7/m x 100 m = $700 $7/m – 1 loop = $700 $1000	N/A $7 x 2 x (27 m x 2) = $756 Nil
Total installation	**$7400**	**$1026**
Header pipes	$1500/borehole +trenching	$1100 per pile
Grand total for 3500 W	**$8900 + trenching**	**$4,252 (2 piles)**
Construction work	Additional construction time required if under footprint of building	On critical path. Addition of loops in piles adds no additional construction period.

7. Conclusions

Energy geostructures are a very cost effective and convenient technology which couples the structural aspects to the energy needs, providing a renewable source for heating and cooling, with respect to conventional shallow geothermal systems. Data available, shows that energy piles can exchange between 40 and 120 W/m, while energy walls and tunnels between 10 to 50 W/m^2. The thermally-induced mechanical aspects are present but usually acceptable. Data is available only for energy piles, from which results show that thermally induced stresses are in the range between 50 to 300 kPa/°C and the thermally-induced displacements are in the range of 0.01 to 0.15 mm/°C. Ultimately an energy geostructure that is designed using standard engineering procedures, ensuring design concrete stresses are not exceeded, and conventional factors of safety for skin friction and end bearing are maintained, will adequately deal with the additional stresses that will be imposed on them as a result of heating and cooling. What is also noted as being important is that the geothermal designer/installer provides a control strategy that enables the long-term management and system optimisation of the ground loop to ensure that the installed system operates within its design parameters for the life of the building.

Acknowledgements

The Authors would like to thank the members of the Cost Action GABI TU1405 "European network for shallow geothermal energy applications in buildings and infrastructures" for the help in collecting data.

References

Akrouch, G.A., Sánchez, M., Briaud, J.L., 2014. Thermo-mechanical behavior of energy piles in high plasticity clays. Acta Geotech. 9, 399–412.

Amatya, B.L., Soga, K., Bourne-Webb, P.J., Amis, T., Laloui, L., 2012. Thermo-mechanical behaviour of energy piles. Géotechnique 62, 503–519.

Amis, T., Robinson, C.A.W., Wong, S., 2010. Integrating Geothermal Loops into the Diaphragm Walls of the Knightsbridge Palace Hotel Project. Proceeding 11th DFI / EFFC Int. Conf. London 10.

Barla, M., Di Donna, A., 2016. Editorial Themed issue on energy geostructures. Environ. Geotech. 3, 188–189.

Barla, M., Di Donna, A., Insana, A., 2017. Energy Tunnel Experimental Site in Turin Metro, in: 15th IACMAG. Whan, China.

Barla, M., Di Donna, A., Perino, A., 2016. Application of energy tunnels to an urban environment. Geothermics 61, 104–113.

Brandl, H., 2006. Energy foundations and other thermo-active ground structures. Géotechnique 56, 81–122.

Cecinato, F., Loveridge, F., 2015. Influences on the thermal efficiency of energy piles. Energy 82, 1021–1033.

Di Donna, A., Barla, M., 2016. The role of ground conditions and properties on the efficiency of energy tunnels. Environ. Geotech. 3.

Di Donna, A., Cecinato, F., Loveridge, F., Barla, M., 2017. Energy performance of diaphragm walls used as heat exchangers. Proc. Inst. Civ. Eng. - Geotech. Eng. 170, 232–245.

Di Donna, A., Dupray, F., Laloui, L., 2013. Numerical study of the heating-cooling effects on the geotechnical behaviour of energy piles, in: International Symposium on Coupled Phenomena in Environmental Geotechnics, Torino, Italy.

Di Donna, A., Rotta Loria, A., Laloui, L., 2016. Numerical study of the response of a group of energy piles under different combinations of thermo-mechanical loads. Comput. Geotech. 72, 126–142.

Franzius, J.N., Pralle, N., 2011. Turning segmental tunnels into sources of renewable energy. Proc. ICE - Civ. Eng. 164, 35–40.

Frodl, S., Franzius, J.N., Bartl, T., 2010. Design and construction of the tunnel geothermal system in Jenbach / . Planung und Bau der Tunnel-Geothermieanlage in Jenbach. Geomech. Tunn. 3, 658–668.

Henderson, H., Carlson, S., Walburger, A., 1999. North American Monitoring of a Hotel with Room Sized GSHPs.

Islam, S., Fukuhara, T., Watanabe, H., Nakamura, A., 2006. Horizontal U-Tube road heating system using

tunnel ground heat. J. Snow Eng. Japan 22, 229–234.
Laloui, L., Di Donna, A., 2013. Energy geostructures: innovation in underground engineering. ISTE Ltd and John Wiley & Sons Inc.
Laloui, L., Moreni, M., Vulliet, L., 2003. Comportement d'un pieu bi-fonction, fondation et échangeur de chaleur. Can. Geotech. J. 40, 388–402.
Lee, C., Park, S., Won, J., Jeoung, J., Sohn, B., Choi, H., 2012. Evaluation of thermal performance of energy textile installed in Tunnel. Renew. Energy 42, 11–22.
Markiewicz, R., Adam, D., 2009. Energy from earth-coupled structures, foundations, tunnels and sewers. Géotechnique 59, 229–236.
McCartney, J.S., Murphy, K.D., 2012. Strain Distributions in Centrifuge Model Energy Foundations, in: DFI Journal - The Journal of the Deep Foundations Institute. pp. 26–38.
Murphy, K.D., McCartney, J.S., Henry, K.S., 2015. Evaluation of thermo-mechanical and thermal behavior of full-scale energy foundations. Acta Geotech. 10, 179–195.
Nicholson, D.P., Chen, Q., de Silva, M., Winter, A., Winterling, R., 2014. The design of thermal tunnel energy segments for Crossrail, UK. Eng. Sustain. 167, 118–134.
Riederer, P., Evers, G., Gourmez, D., Jaudin, F., Monnot, P., Pertenay, V., Pincemin, S., Wurtz, E., 2007. COnception de FOndations GEothermiques 170.
Rotta Loria, A.F., Laloui, L., 2017. Thermally induced group effects among energy piles. Géotechnique 67, 374–393.
Schneider, M., Moormann, C., 2010. GeoTU6 – a geothermal Research Project for Tunnels. Tunnel 2, 14–21.
SIA DO 190, 2005. Utilisation de la chaleur du sol par des ouvrages de fondation et de soutènement en béton. Guide pour la conception, la realization et la maintenance. Société Suisse des ingénieurs et des architects, Switzerland.
Sutman, M., Brettmann, T., Olgun, C.G., 2014. Thermo-mechanical behaviour of energy piles: full-scale field test verification, in: DFI Conference.
Unterberger, W., Hofinger, H., Dietmar Adam, Roman Markiewics, 2004. Utilization of Tunnels as Sources of Ground Heat and Cooling–Practical Applications in Austria. Proc. ISRM Int. Symp. 3rd ARMS 421–426.
Wang, B., Bouazza, A., Singh, R.M., Haberfield, C., Barry-macaulay, D., Baycan, S., 2014. Posttemperature Effects on Shaft Capacity of a Full-Scale Geothermal Energy Pile. J. Geotechnol. Geoenvironmental Eng. 141, 4014125.
Xia, C., Sun, M., Zhang, G., Xiao, S., Zou, Y., 2012. Experimental study on geothermal heat exchangers buried in diaphragm walls. Energy Build. 52, 50–55.
You, S., Cheng, X., Guo, H., Yao, Z., 2016. Experimental study on structural response of CFG energy piles. Appl. Therm. Eng. 96, 640–651.
Zhang, G., Xia, C., Sun, M., Zou, Y., Xiao, S., 2013. A new model and analytical solution for the heat conduction of tunnel lining ground heat exchangers. Cold Reg. Sci. Technol. 88, 59–66.

GROUND IMPROVEMENT FOR RECLAIMED LANDFILLS

William W. Haasz, Menard, Philadelphia, PA, USA, 215-971-2654, whaasz@menardusa.com

Brandon T. Buschmeier, Menard, Philadelphia, PA, USA, 215-971-2648, bbuschmeier@menardusa.com

Steven E. Darnell, Menard, Spokane, WA, USA, 412-518-1284, sdarnell@menardusa.com

Frederic Masse, Menard, Carnegie, PA, USA, 412-620-6000, fmasse@menardusa.com

ABSTRACT

Landfills often cover expansive areas in locations where large building facilities or infrastructure is in high in demand after the land has been reclaimed. Most landfills have soil or fill properties that vary widely over small distances; combined with the strict guidelines and restrictions for the removal and treatment of soil or material that is on site, these projects can be a major challenge for any prospective developer. In order to make landfills suitable for the construction of any project it is necessary to conduct a detailed evaluation of the subsurface conditions. Ground improvement techniques are among the most typical methods for making reclaimed landfills suitable for the construction of any major project. The paper will discuss the approach that was taken to support a proposed warehouse in Elizabeth, New Jersey using Controlled Modulus Columns Rigid Inclusions (CMC Rigid Inclusions), which are grouted, auger-displacement elements. Additionally, we will discuss the use of Dynamic Compaction (DC) that was performed in areas outside the proposed warehouse footprint. Through the combination of CMC rigid inclusions and DC, the general contractor's project schedule was expedited, the costs to support the warehouse were economized, and the anticipated settlement of the parking lot areas was drastically reduced. Furthermore, the paper will outline the benefits of using CMC rigid inclusions and DC methods in order to minimize the impact of working with contaminated soils from a landfill.

OVERVIEW OF THE ELIZABETH WAREHOUSE PROJECT

Over the past several decades the foundations industry has seen an increase in demand for the support of developments on reclaimed landfills; particularly, on the east coast where many landfills were capped before the 1980's and steady population growth and city expansion have caused high demand for this now highly desired real estate. Unfortunately, these landfills, often as large as twenty (20) or more acres present tough geotechnical and environmental challenges for Owners planning to develop or build structures of any size on the reclaimed land. Consequently, the options for building on reclaimed landfills can quickly become cost prohibitive.

Site Specific

Selected by a developer for the location of a future warehouse, the 29 acres (114,424 sq-meters) project site is located in Elizabeth, New Jersey and demonstrates the complexities of designing over a once reclaimed landfill. The landfill was used for municipal solid waste (MSW) consisting of trash, wood, metal, glass, plastic, brick, concrete fragments, and other types of debris. This landfill was capped in the 1960's, and developed in the 1970's for a warehouse. The new project included the demolition of the existing warehouse and the development of the site to be repurposed for a new 481,650 sq-ft single-story warehouse, surrounded by paved parking and truck loading areas. Figure 1 below, shows an overview of the project site layout.

 © 2017 DFI Annual Conference, New Orleans, LA, USA

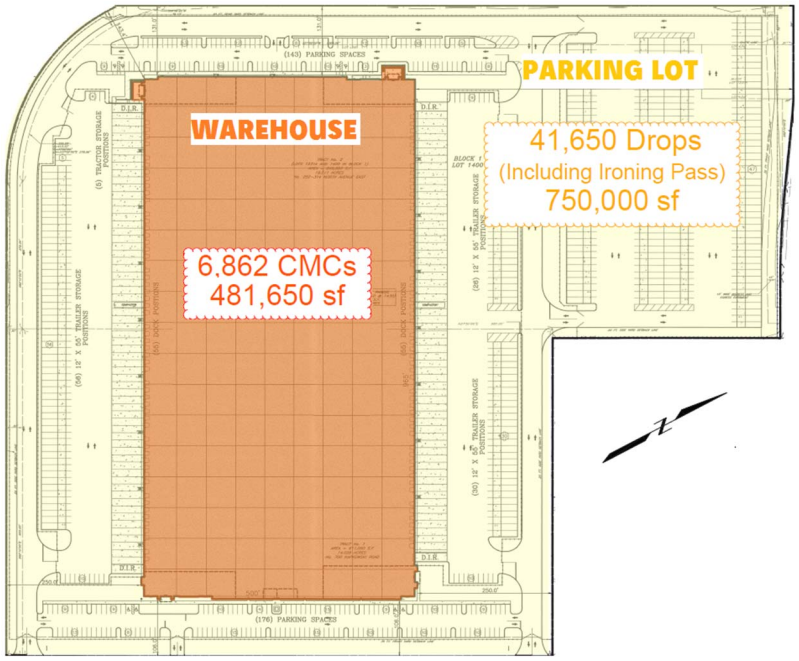


Figure 1: Project Site Overview

The warehouse constructed in the 1970's was approximately 490,000 sq-ft (150,000 sq-m) and was supported on timber piles. The parking lot areas for the previous warehouse were capped with a 1.5 to 3 ft (.45 to .91 m) layer of granular fill and paved. When the building was demolished it was found that several feet of settlement had occurred below the slab and around the timber piles. Figure 2 below, shows the extents of the existing timber piles in the project area.

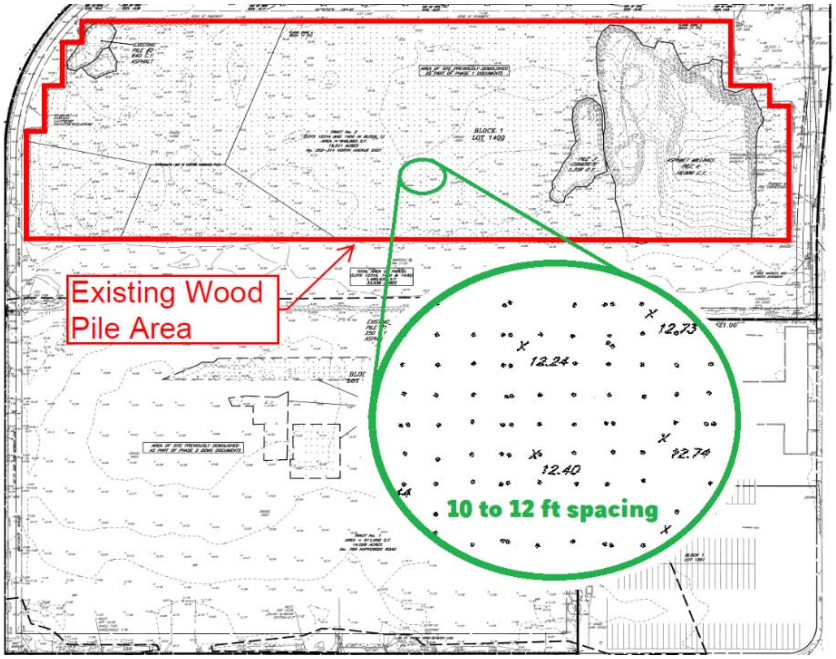


Figure 2: Existing Timber Pile Area

Subsurface Conditions

The upper subsurface portion of this site is relatively consistent across the entire area, with variations in the stiffness and composition of the MSW. The generalized soil profile consists of approximately 4 to 8 inches of existing pavement with a stone subbase that varies between 6 and 12 inches in thickness. Below the subbase is between 9 and 18 feet of fill that is relatively granular in the upper 4 feet, the remaining fill is comprised mainly of MSW. Beneath the fill is an organic silt and peat layer that varies in thickness from about 1 to 6 feet (averaging 4 feet). Below the organic stratum a medium dense to dense sand extends to approximately 15 to 30 feet in thickness, and is underlain by approximately 10 to 20 feet of stiff to very stiff silts and clayey silts. Decomposed shale bedrock could be found approximately 50 to 70 feet below the sites working platform (WP) elevation at the time of construction, (elevation +15.5 feet for the building footprint). A generalized cross-section of the subsurface can be found below in Figure 3. The cross-section shows the approximate width of the warehouse and the finished floor elevation at +19 feet. The groundwater table (GWT) is at approximate elevation +6 feet across the site and is assumed to change with tidal fluctuations.

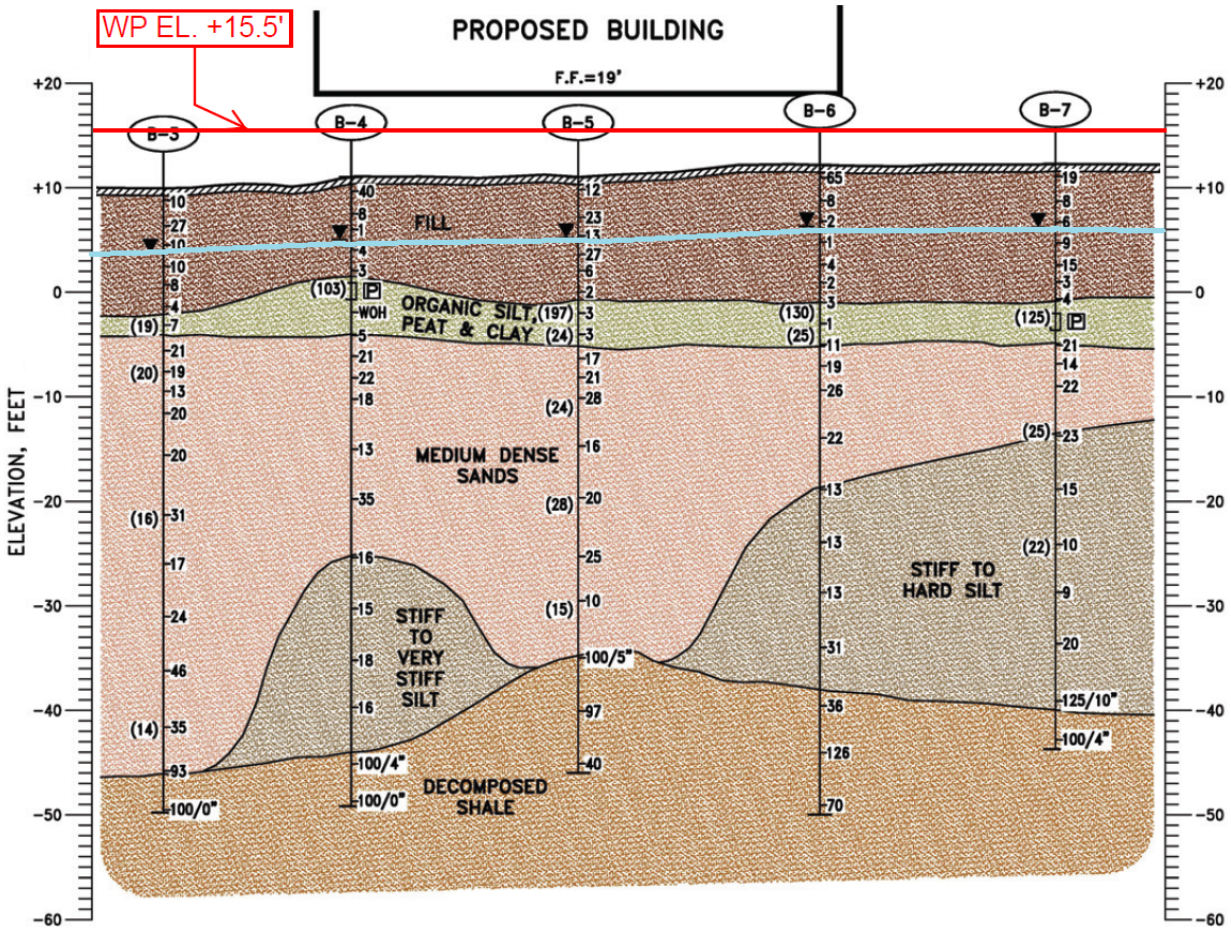


Figure 3: Typical Subsurface Cross-Section

Geotechnical Recommendations

The geotechnical investigations led to several conclusions and recommendations for the proposed warehouse and its surrounding parking lot truck loading areas. The first conclusion was that the existing fill and organic soils would not be suitable support for the warehouse using spread footings without ground improvement. It was also concluded that dynamic compaction and surcharging alone would not be cost effective in limiting the post construction settlement of the building within an acceptable tolerance. The geotechnical Engineer recommended that Controlled Modulus Column (CMC) Rigid Inclusions (ASIRI, 2012) be used to support the warehouse wall footings, column footings and the slab. CMC Rigid Inclusions are grouted, auger-displacement elements which are well suited for this type of large warehouse support (Buschmeier et al, 2015). In addition to being much more economical than piles, CMC Rigid Inclusions generate virtually no spoils and offer a high level of settlement control.

For the surrounding parking lot and truck loading areas, the final geotechnical report recommended that Dynamic Compaction (DC) ground improvement be implemented in an effort to limit post construction settlements to within an acceptable tolerance for maintenance and repaving schedules determined by the Owner.

What Happens in a Land Fill, Stays in a Landfill

The geotechnical report, as well as the Phase I & II environmental assessments, outlined in detail the procedures, rules, and guidelines that were to be strictly followed when dealing with materials and groundwater exposed and brought to the surface during construction. Since most of the material excavated on-site for utility installation would consist of MSW, or contaminated fill, it was assumed that these materials would likely not be suitable for use as backfill for the utility excavations. Moreover, it was expected that some overexcavation would be required in order to create an acceptable stone bedding layer for new utilities. Therefore, it was estimated that an approximate 5,000 cubic yards (3,800 m^3) of contaminated landfill materials would need to be reused and placed somewhere on the site and capped with 1 foot (.3 m) of clean dirt or stone. If that was not possible, the material would be required to be removed from the site to another landfill at an extremely high cost.

The working platform for the warehouse and installation of CMC Rigid Inclusions was set at EL. +15.5 feet; whereas, the working grade for the proposed DC was between EL. +10.5 and +12 feet. Considering that the groundwater table ranged from EL. +5 to +8 feet in some borings, increasing the pore water pressure (PWP) during high energy impacts was of primary concern when determining a plan for DC across the site. If the pore water pressure increased to a point that caused groundwater to rise to the surface, the potentially contaminated water would have to be pumped to another location on-site, or stored in tanks and hauled off-site for treatment.

CMC RIGID INCLUSIONS FOR GROUND IMPROVEMENT

General Description of a CMC System

Ground improvement techniques enable developers to consider building on sites where traditionally a deep foundation system may have been the only option. One of the more technical ground improvement methods that is offered and discussed in this paper is Controlled Modulus Columns (CMC) Rigid Inclusions. CMC Rigid Inclusion systems are a cost-effective alternative to deeper pile foundations. The system allows for the load of a structure to be bypassed through highly compressible, problematic soil strata to virtually eliminate concerns for post-construction and long-term settlement.

In the case of a warehouse, CMC Rigid Inclusions are used to support shallow spread footings for columns and walls, and a slab-on-grade. In order to transmit the load from the structure to a stiffer bearing stratum a CMC Rigid Inclusions system utilizes an engineered layer of compacted granular material known as a Load Transfer Platform (LTP) that is placed in compacted lifts beneath footings, and the slab above installed CMC Rigid Inclusions. The LTP is typically two to five feet thick and replaces the traditional structural slab system. The LTP's purpose is to allow for the load from the structure to 'arch' into the CMC Rigid Inclusions (Okyay et al, 2012). The entire CMC Rigid Inclusion system is designed to 'share' the load based on the stiffness of the existing soil matrix and the strength of the targeted embedment stratum where the CMC Rigid Inclusions are terminated. Figure 4 below, shows the fundamental differences between a CMC Rigid Inclusion System and a typical reinforced pile system for the support of structures similar to warehouses.

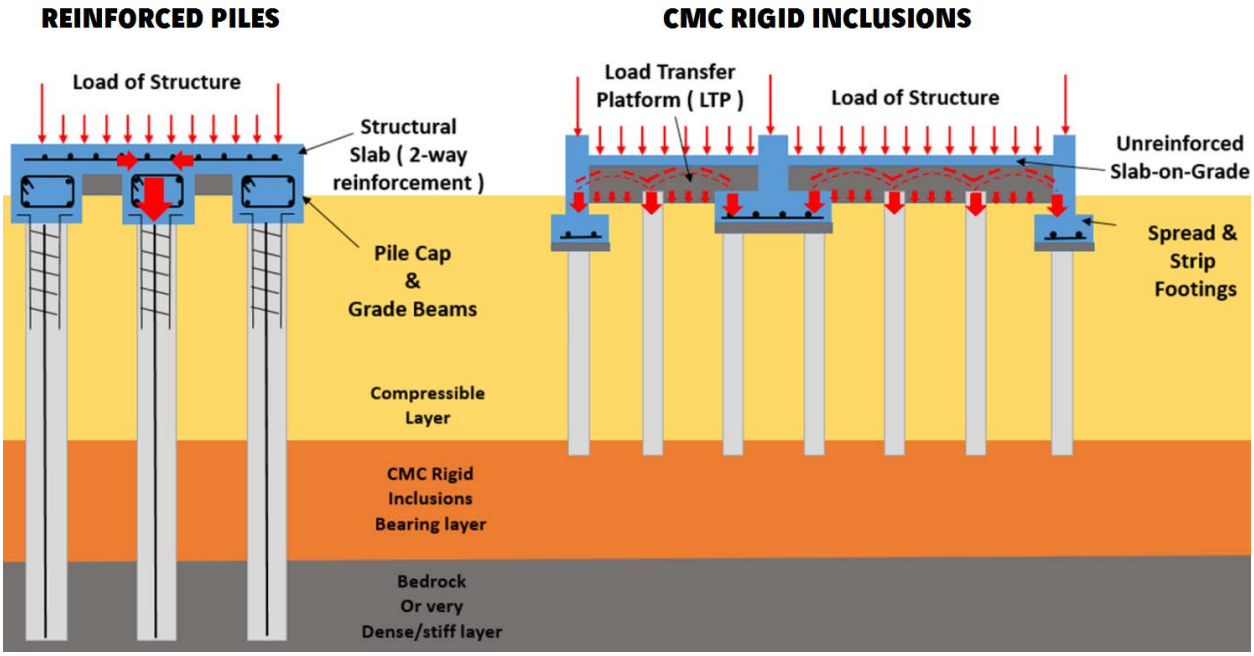


Figure 4: Reinforced Pile Systems vs. CMC Systems for Warehouses

CMC Design Approach for Reclaimed Landfills

For this project, the CMC Rigid Inclusions system was designed to meet the project settlement criteria of 2 inches long-term settlement and 0.5 inches differential settlement (50.8 and 12.7 mm, respectively) between building columns. The design loads for this warehouse include a slab load of 800 psf and spread footing loads that vary from 128 to 142 kips per footing. Since the existing site grades vary greatly across the length of the warehouse, the building was divided into six (6) separate regions that were analyzed individually, since the amount of new, net fill impacts the total and differential settlement estimations. The portion of the proposed warehouse located within the old warehouse limits was identified as Region 1 and required a separate analysis due to the presence of the existing timber piles that were to remain in place. These timber piles were exposed, surveyed, and cut to a consistent elevation below the working platform. Once the piles were documented, they were covered with approximately one foot of crushed concrete. In summary, the six (6) regions of the site were delineated based on the following existing grades and regions as shown in Figure 5.

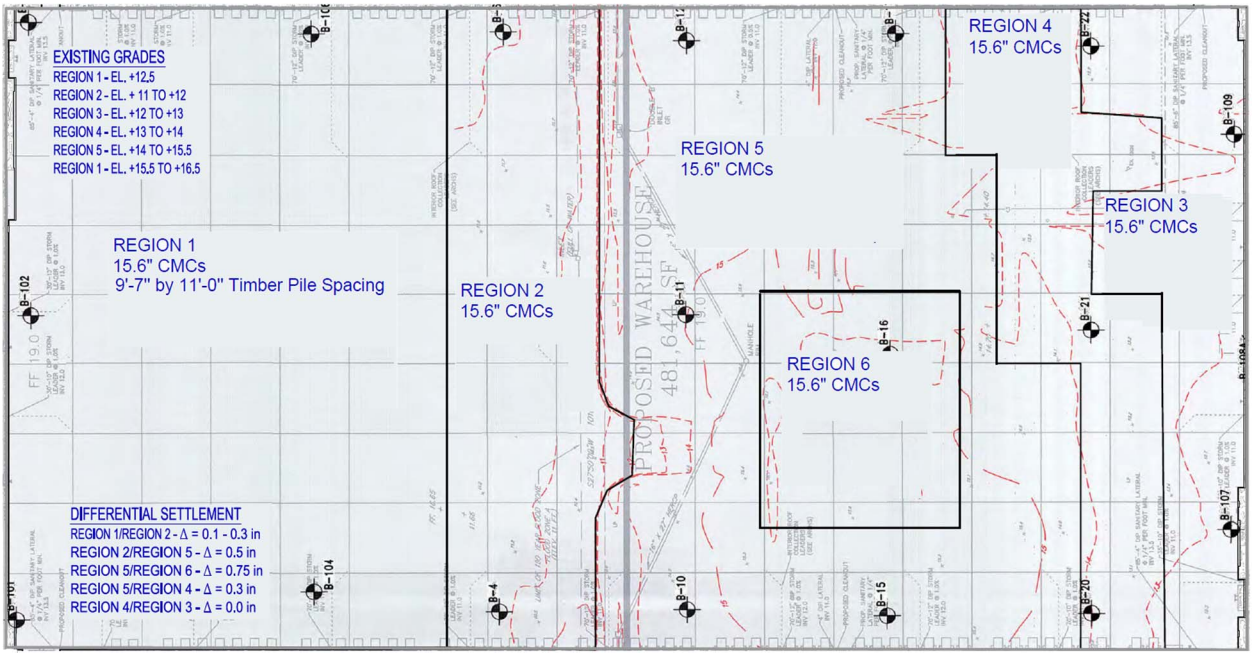


Figure 5: Six Regions for CMC Design Supporting the Warehouse

In each of the six (6) regions a 2D axisymmetric finite element model was created using Plaxis software to model one-dimensional, volumetric compression with the various changes in spacing of the CMC Rigid Inclusions per the changes in EGS of the site. The 2D axisymmetric models represent a single element and do not include the effects of adjacent rigid inclusions, but are appropriate for the conditions in the center of a grid, where the conditions are symmetrical on all sides. Each model was used to confirm that the proposed spacing and diameter of CMC Rigid Inclusions would meet the project settlement criteria. An example of the 2D axisymmetric typical profile and model results for Region 1 is shown below in Figure 6.

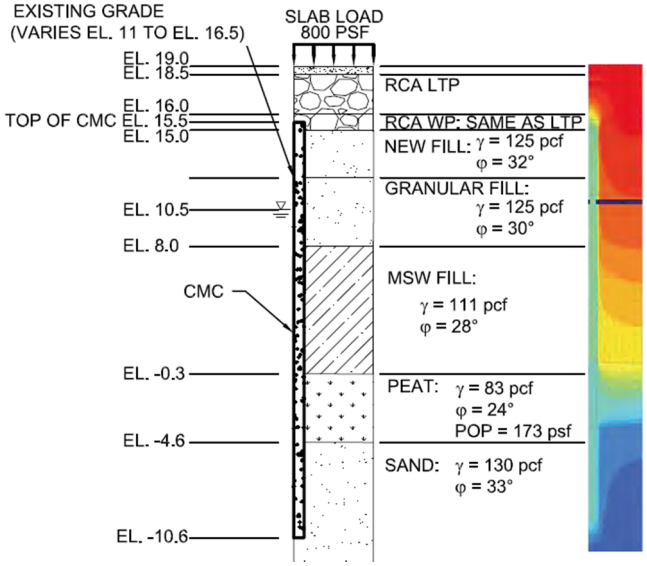


Figure 6: Region 1 - 2D Typical Profile & Total Vertical Displacement Results

In order to further refine the design and understand the impact of the timber piles in Region 1, a 3D Model was performed to better understand the performance and interaction between the timber piles and CMC

Rigid Inclusions under the footings and slab. The 3D model represents approximately one quarter of a footing bay. Typical timber pile spacing was determined from the survey to be approximately 9 foot - 7 inches x 11 feet. Figure 1 below, shows an example of the 3D model results adjacent to the typical profile used to construct the modeled layers. Based on the results of the analysis, each area was designed with a specific CMC spacing and diameter, with grid spacing's ranging between 7 and 10 feet.

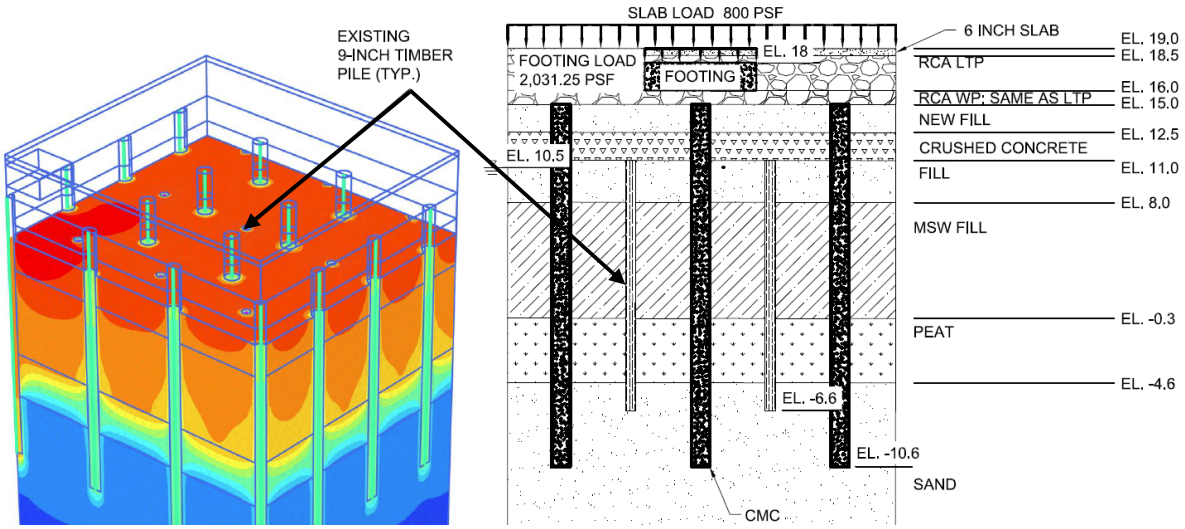


Figure 7: 3D Model Results and Typical Profile

Table 1: Summary of Finite Element Models

Region	Model Type	Total Long-term Settlement (inches)	CMC Load (kips)
1	Axisymmetric	1.41	63
1	Axisymmetric	1.94	61
2	Axisymmetric	1.42	57
3	Axisymmetric	1.63	99
4	Axisymmetric	1.61	101
5	Axisymmetric	1.94	113
6	Axisymmetric	1.19	96
1	3D (under footing)	1.29	96
1	3D (under slab)	1.09	71

DYNAMIC COMPACTION APPROACH

General Description of DC

Dynamic Compaction involves dropping a weight of ten tons or more from a predetermined height using a large crane. The weight is repeatedly dropped on points known as 'prints'. For this project, a required 'energy' was used to determine a baseline for estimating the DC to be completed. Energy is calculated by multiplying the drop weight in pounds by the height of the drop. For example, a 10 ton weight dropped from a height of 50 feet represents 20,000lbs x 50ft=1,000,000 lbs-ft of energy, or 1,000 kip-ft applied per drop.

The weight is dropped on print locations in a predetermined grid pattern, which is typically 8 to 15 feet (2.4 to 4.6 m). If the soils are loose and prone to heave or the GWT is high, multiple passes may be required to deliver the specified number of drops per location. A 'pass' is defined as dropping the weight the required number of times on a print, then backfilling the crater with material so the weight can be dropped on the same location again to ensure that all of the design energy is being delivered to the ground. Additionally, depending on the final grid spacing, the compaction effort is split into different phases from a wider spacing to a tighter spacing. Without proper phasing of the work, the risk is, by applying too much energy in each area too quickly, to locally "liquefy" the soils and laterally displace them instead of compacting them causing heave at the surface. Phasing DC prints therefore mitigates the negative effects of platform heave and increases in PWP. Figure 8 below, shows an example of the four-phase DC layout and testing area that was developed for this site. As shown, the phase 1 prints are located furthest apart, followed by the phase 2 prints, and so forth.

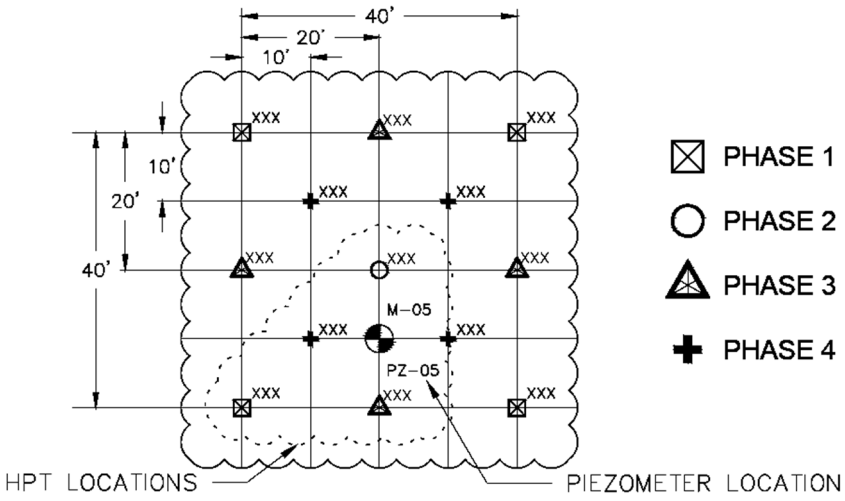


Figure 8: Example of Four Phase DC Layout & Testing Area

Initially, the design approach for the DC that was completed in the parking lot and truck loading areas of the site was based strictly on planning the number of drops, passes, and phases to prevent a spike in the pore water pressure, while also achieving the project requirements for energy delivered. If the PWP increased too quickly, the project team was concerned that it could cause groundwater to come to the surface; or worse, liquefy the upper fill and compromise the integrity of the working surface. Prior to arriving on-site, an extensive testing program was developed to ensure that an optimal DC plan was prescribed for the specific site conditions.

In total, six testing areas were chosen based on the thickness and stiffness of the MSW fill indicated by the borings performed across the site. For each of the testing areas piezometers were installed to a depth corresponding to just above the expected GWT, and/or just above the organics layer in the MSW fill. Piezometer readings were taken between successive drops and prints to track changes in PWP as the testing area was completed. Additionally, heave penetration tests (HPT) were performed in the test areas to identify the effectiveness of the DC program by measuring the heave and penetration of the weight between successive drops. Figure 9 below shows an overview for one of the heave penetration tests that was conducted. Approximately five (5) drops were performed on each print in the test areas. In this particular testing area, the total reduction in surface elevation based on the volume of the craters that were created was approximately 0.9 feet.

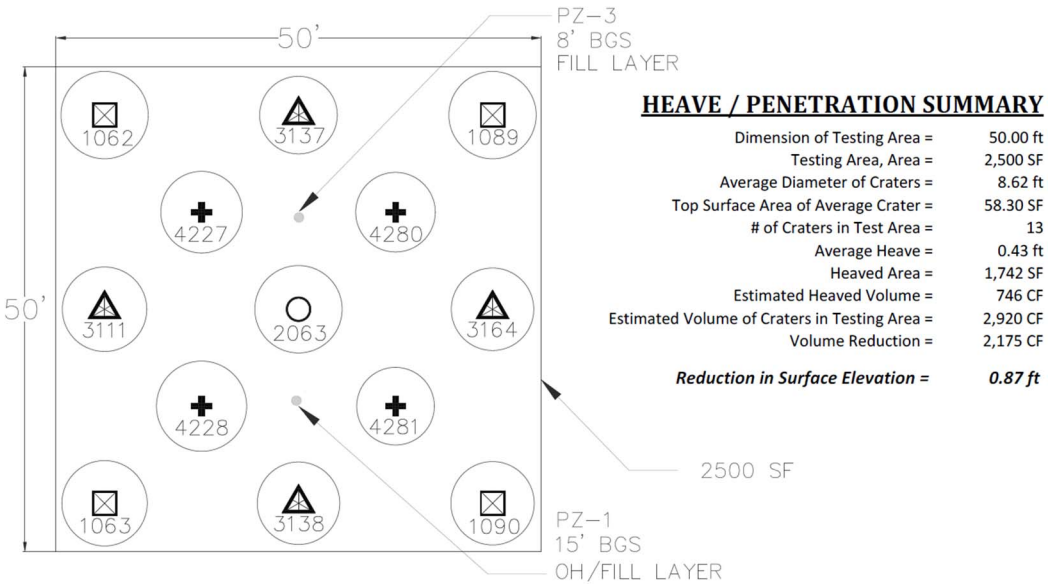


Figure 9: Heave Penetration Test Summary

For this particular testing area two (2) piezometers were used, one at 8 feet (2.4 m) below the ground surface in the MSW/fill layer, and another at 15 feet (4.6 m) below the ground surface in the top of organics or bottom of MSW layer. Figure 10 below, shows the pore pressure vs. time as the testing program was performed. Moving along the curves the print IDs are listed on the data points, these IDs correspond to the print IDs in Figure 9. As each print received drops the PWP increased in steps until the entire area was completed. Several hours after the test area was complete, the PWP dropped to a resting pore pressure that was 7% higher than the baseline in the organics/lower MSW layer, and 11% higher in the upper MSW fill layer. Over the next several days the PWP stabilized at 5% and 9% higher than the original baselines.

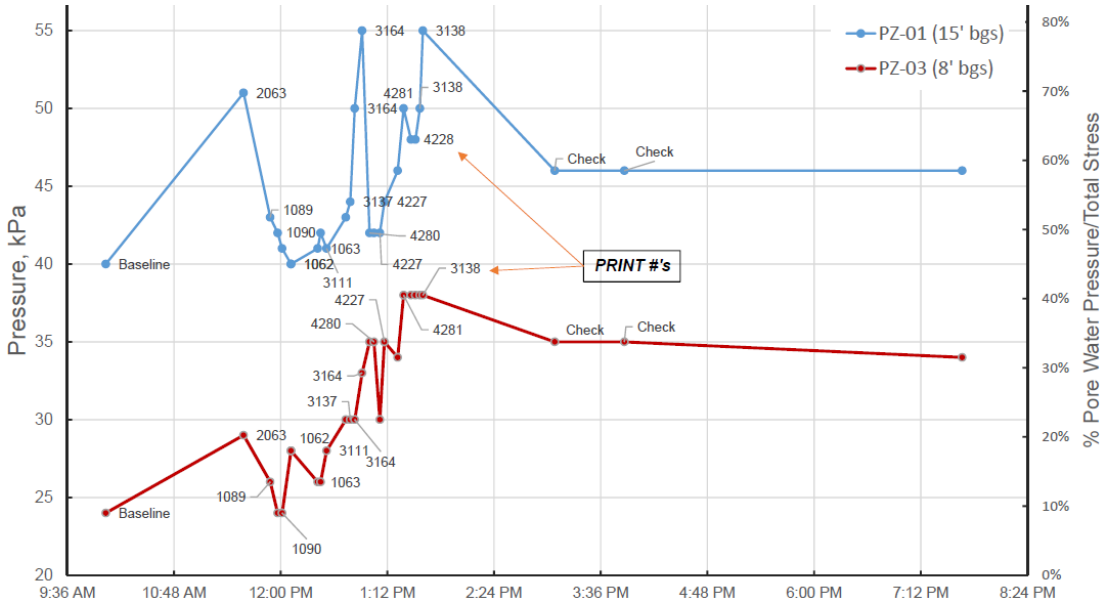


Figure 10: Testing Area Piezometer Data

Results of the HPTs concluded that the entire DC area could be split into two (2) halves: The first half in the area of the existing warehouse supported by piles, and the other half in the existing paved parking lot.

On the first half of the site, five (5) successive drops in one pass was not possible because the weight would penetrate excessively (up to 7 feet (2.1 m)) into the ground after approximately three (3) drops. This meant that the energy from the weight would not be properly transmitted to the ground on the last three (3) drops. Conversely, the portion of the site that was previously a paved parking lot responded well to DC, as all five (5) drops could be completed in one pass with craters only reaching 2 to 5 feet (0.6 to 1.5 m) in depth. In all of the testing areas little heave was observed, ensuring that the tamping energy was properly compacting the loose heterogeneous landfill material. Furthermore, an estimated ground lowering of approximately one (1) foot across the site enabled the client to predict the quantity of imported fill that would be required to backfill craters and bring the site to proposed grades.

Furthermore, the testing program revealed that by properly controlling the way the DC energy was applied, the pore water pressure would not become an issue while performing DC across the site. This could also be contributed to the void space that was inherent to the MSW, because rises in pore water pressure were presumed to be mitigated by large voids in the first 15 feet (4.6 m) of the subsurface. In conclusion, the testing program showed that half of the site could be completed in one pass of five (5) drops, while the other half of the site needed to be completed with a minimum of two (2) passes.

CONCLUSIONS

CMC Rigid Inclusions were the most economical solution for support of the warehouse based on costs associated with traditional deep foundation as well as savings in the structure by replacing pile caps, grade beams and structural slabs with spread footings and slabs-on-grade. Furthermore, CMC Rigid inclusions reduced costs and setbacks that were associated with the development of a reclaimed landfill by avoiding excavation and replacement of poor quality soils and also by reducing the amount of contaminated spoils. Additionally, the CMC Rigid Inclusion system improves the performance and reduces the cost of the vapor barrier system by eliminating complex detailing around pile caps.

Moreover, a pile supported foundations would have been installed to underlying rock formations, whereas CMC Rigid inclusion systems typically targeted shallower embedment layers. The shallower CMC Rigid Inclusion systems can greatly reduce the risk of compromising groundwater quality with contaminates from a landfill.

DC provided this specific project with a means to eliminate the costs to truck the approximate 5,000 cubic yards (3,800 m^3) of contaminated spoils that were generated from the excavation to install the sites utilities. Large crater volumes after a single pass and ground lowering estimated to be up to 2 feet in some areas enabled the client to confidently make the decision to spread the potentially contaminated excavated materials over a large area in a capped layer so that it could be compacted with the typical DC program eliminating the expensive need to transport spoils to an outside facility.

ACKNOWLEDGMENTS

Jean-François Morel, ing, M.Sc.A – Vice President, Geopac (Menard Canada)
Christian Marcotte – Operations Manager, Geopac (Menard Canada)
Tom Beafore – Senior Construction Manager, Menard Group USA
Luc Sauvageau – Construction Manager, Menard Group USA
James Ramp, Project Manager, Menard Group USA
Mary Nodine, P.E. – Project Manager, GEI Consultants
Jessica Debellis, P.E. – Project Engineer, GEI Consultants

REFERENCES

ASIRI, Multiple Authors, 2012. ASIRI 2012, Amélioration des sols par inclusions rigides Presses des Ponts et Chaussées, ISBN 978-2-85978-462-1

Buschmeier, B., Masse, F., Swift, S. & Walker, M., 2015. The use of Controlled Modulus Column (CMC) ground improvement for support of large warehouses. DFI Annual Conference 2015, Oakland, California

Cuira F. & Simon B., 2009. Two simple tools for evaluation the complex interactions in a soil reinforced by rigid inclusions. 17th ICSMGE, Alexandria, pp. 1163-1166

Dias D. & Simon B., 2012. Spread Foundations on rigid inclusions subjected to complex loading: Comparison of 3D numerical and simplified analytical modeling. ISSMGE – TC 211 International Symposium on Ground Improvement, Brussels

Okyay U.S., Dias D., Thorel L. & Rault G., 2012. Centrifuge modeling of a pile-supported granular earth-platform over soft soils. Journal of Geotechnical and Geoenvironmental Engineering, ASCE

Plomteux, C. & al., 2003. Controlled Modulus Columns (CMC): Foundation system for Embankment support: a case history. Geosupport 2004, Orlando, USA, pp. 980 - 992

Simon B., 2012. General Report – Session 5 – Rigid Inclusions and Stone Columns. ISSMGE – TC 211 International Symposium on Ground Improvement, Brussels

RECYCLING JET GROUT BACKFLOW: WASTE MITIGATION AND COST BENEFITS

Craig T. Jones, E.I.T, BOS Solutions, Calgary, Alberta, Canada, # 403-234-2137, Craig.Jones@bos-solutions.com

Zachary Q. Maassen, E.I.T, BOS Solutions, Houston, Texas, United States, #281-477-5313, Zachary.Maassen@bos-solutions.com

ABSTRACT

Jet grouting is a method of ground improvement that relies on the erosive capacity of high-speed jets to cut and mix the ground in place with a cementitious grout. A continuous return flow of cuttings, called jet grout backflow or spoils, is expelled to the surface during the grouting process. Data from projects completed in Toronto and Ottawa is presented where BOS Solutions' services provided significant savings compared to the traditional spoils treatment utilizing vacuum trucks for spoils disposal. These traditional treatment methods are cumbersome and expensive by nature. BOS Solutions provided an alternative solution that is environmentally friendly and capable of handling full flow to process these jet grout spoils utilizing a tank system paired with centrifuges and flocculation additives to remove the ground soils and grout product from the spoils slurry. BOS' process produced a clean water for reuse in the project while reducing the overall waste volume by producing a dry, stackable solid that could be hauled to a landfill. Benefits observed by using the BOS process were disposal waste volumes decreased over 30% and at least a 19% reduction on disposal costs.

SCOPE OF WORK

Jet grouting is a method of ground improvement that relies on the erosive capacity of high-speed jets to cut and mix the ground in place with a cementitious grout. A continuous return flow of cuttings, called jet grout backflow or spoils, is expelled to the surface during the grouting process. The backflow, or spoils, is a mixture of grout, water and soils. Traditionally, the spoil would be collected in in-ground pits and allowed to solidify for a few days prior to hauling to a final disposal site. For the projects completed in Toronto and Ottawa, the jet grouting work was performed at street level, in high traffic congested areas, presenting the challenge of insufficient space for the contractors to process the jet grout spoils in the traditional way. At first, attempts were made of using vacuum trucks to collect and haul the wet spoils to an off-site location where the spoils would be allowed to solidify. However, this method proved cumbersome and expensive due to the high volumes of spoils generated daily and the high number of vacuum trucks required to support the jet grouting operations, respectively.

 © 2017 DFI Annual Conference, New Orleans, LA, USA

BOS Solutions was contracted to offer a different alternative method to manage the jet grout spoils. BOS utilized a tank system, centrifuges and flocculation additives to remove the ground soils and grout product from the slurry producing clean water for reuse. This is an environmentally friendly process and reduces several steps of the conventional handling and disposal methods.

OBJECTIVES

1. Process jet grouting waste to:
    - Reduce overall waste volume and cost
        - Eliminate vacuum truck hauling
        - Reduced environmental impact of waste hauling
2. Provide a clean fluid for reuse and/or economical disposal methods
    - Control pH in recovered water as needed to pass for reuse or disposal
3. Operate at full capacity of operations to eliminate downtime associated with disposal or waste treatment

EQUIPMENT & PERSONEL REQUIRED

- PreMix Tank – 79.5 m^3 (500 bbl)
    - 2 Derrick Drying Shakers mounted on top
- BOS Tank – 34 m^3 capacity (246 bbl)
    - 2 BOS 40 Centrifuges on hydraulically lifted stand
- Shale Bin
- Track Hoe
- Ancillary Equipment (Pumps, Hoses, Pipe Fittings, Tools)
- 1 BOS Field Technician

PROCEDURE

The following bullet points explain the typical flow pattern in treating the jet grout waste. Refer to Figure 1 for an onsite diagram of the equipment.

- Jet grouting spoils slurry is discharged into PreMix tank.
- The slurry is pumped over the Drying Shakers to remove large solids and floating debris.
- The Drying Shaker underflow is contained in the PreMix tank and is pumped to the BOS Tank system to remove the remaining ground soils, colloidal solids and grout.
- The BOS Tank is primed with fresh water such as lake, river or storm water. These are ideal fresh water sources as chlorines and other chemicals in typical city water can contribute to micro toxins in the clear treated fluid to be pumped off.

- The fresh water is circulated through the BOS 40 centrifuge establishing the BOS Clear Water Loop.
- Polymer is mixed to a specific and predetermined concentration.
- Screened slurry from the PreMix is injected into the BOS Clear Water Loop.
- The polymer mixture is injected with the slurry before the centrifuge.
- This process is continuous until the waste is treated. This results in an increased volume of clean water in the BOS Tank. This additional water that was removed from the slurry is called recovered fluid.
- The recovered fluid can be used to mix new polymer batches, flush equipment and reused on next project or pumped down a sanitary sewer.
- Solids that are removed will be collected on ground or in supplied bin for removal.
- Once processing is complete, equipment will be drained, serviced and prepared to be on standby for next batch to be processed.

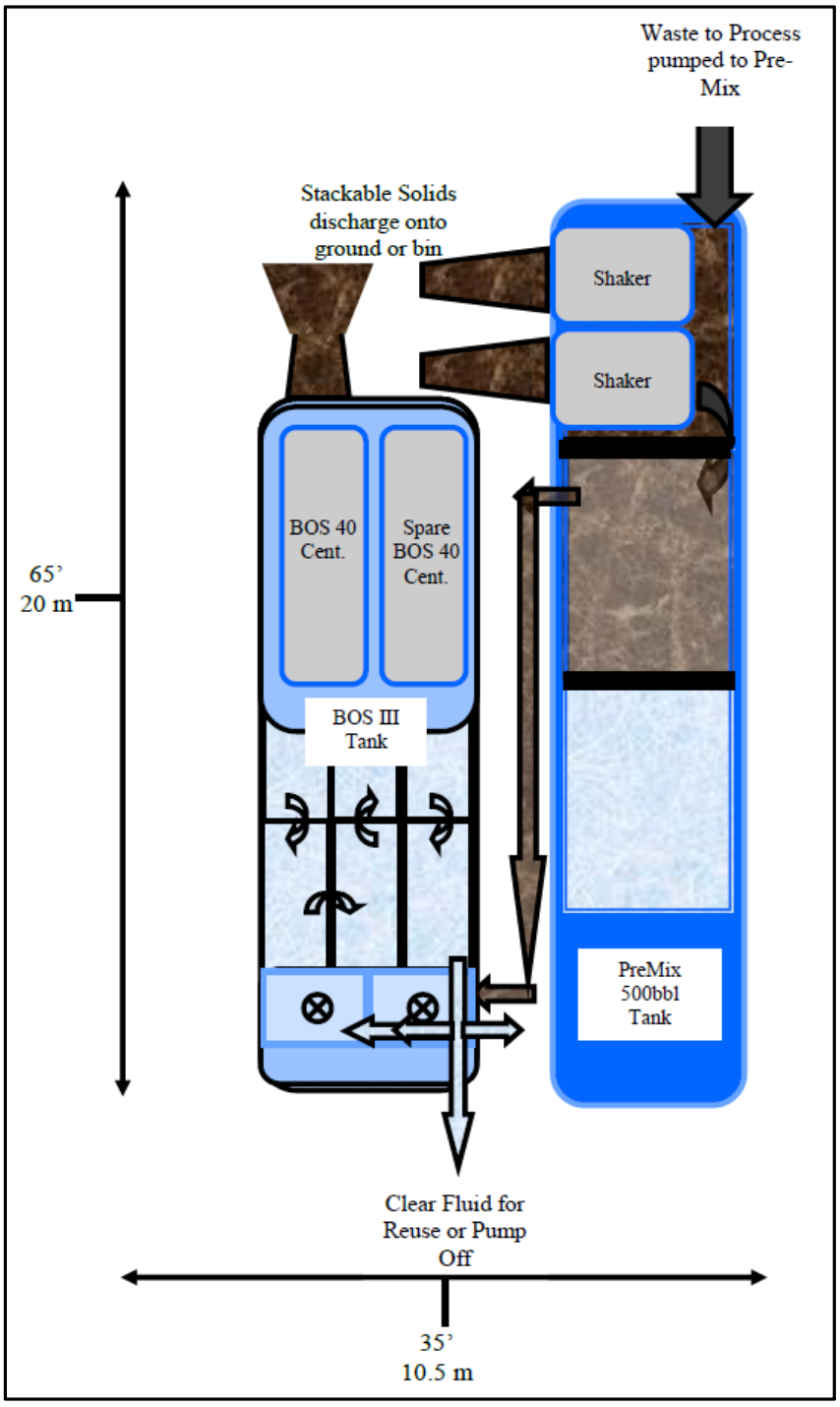


Fig 1. Site Layout with Flow Pattern

TECHNICAL DATA

Project 1: Eglington Crosstown East Tunnels

Job Details

- Location: Toronto, Ontario, Canada
- Number of columns: 28
- Column Diameter (m): 2.4 (7.87 ft)
- Column Depth (m): 30 (98.43ft)
- Volume of Jet Grout Spoils per Column (m^3): 90 (3,178 ft^3)
- Daily Volume of Jet Grout Spoils Generated (m^3): 180 (6,357 ft^3)
- Peak Flow of Jet Grout Spoils: 800 L/min (211 gal/min)
- Specific Gravity of Jet Grout Spoils: 1.3-1.8

Performance Results

By processing the jet grout spoils, BOS successfully reduced the overall waste volume and created a dry, stackable waste product. The dry stackable waste product eliminated the need for vacuum trucks and resulted in fewer standard end dump trucks to haul off spoils to the final disposal site. BOS recover 40 m^3 of clean reusable water per column (totaling 1120 m^3). The reuse of this recovered water was not needed so it was disposed of into the sewer system; no additional equipment or chemicals were needed to pass sewer acceptance criteria outlined by City of Toronto. By processing the jet grout spoils at an average of 0.6 m^3/min there was no operational downtime associated with the treatment or disposal of the waste product.

At the conclusion of this project, a total project savings analysis was done as provided below in Table 1.

Table 1. Toronto Total Project Savings

Total Project Savings					
Vacuum Trucks			*BOS System*		
Parameters	Value	Units	Parameters	Value	Units
Waste for Disposal (Grout, Soil, and Water Mix)	3,024 (3,333)	tonnes (tons)	Waste for Disposal (Dried Grout and Soil)	1,960 (2,160)	tonnes (tons)
Vacuum Truck Cost ($.30 cents/L) *projected	$756,000.00	Canadian Dollars	End Dump Truck Cost ($97.65 per tonne)	$191,394.00	Canadian Dollars
			BOS Equipment and Labor Costs	$419,423.03	Canadian Dollars
TOTAL COST	$756,000.00		$610,817.03		
TOTAL COST SAVINGS			**$145,182.97 (19% reduction)**		
TOTAL WASTE SAVINGS			**1,064 tonnes (1,172 tons) (35% reduction)**		

*NOTE: The traditional disposal method of utilizing vacuum trucks is an estimated cost. It was calculated using an industry stand of 30 cents per litre. This estimate covers both the trucking and disposal of the liquid waste.

Project 2: Lite Rail Transit Expansion

Job Details

- Location: Ottawa, Ontario, Canada
- Number of columns: 60
- Column Diameter (m): 1.8 (5.9 ft)
- Column Depth (m): 24 – 31 (78.74 – 101-71 ft)
- Volume of Jet Grout Spoils per Column (m^3): 29 (1,024 ft^3)
- Daily Volume of Jet Grout Spoils Generated (m^3): 58 (2,048 ft^3)
- Jet Column Length Range: 5 – 23m (16.4 – 75.46 ft)
    - Average: 11.1 m (36.42 ft)
- Specific Gravity of Jet Grout Spoils: 1.2 – 1.8

Performance Results

Consistent with the Toronto project, BOS successfully reduced the overall waste volume and created a dry, stackable waste product, resulting in fewer truck loads needed to haul off spoils to disposal. Additional water was added to the spoils. This water addition was required to reduce the density and viscosity of the spoils for them to be pumped over to the BOS System. The addition of water would have been used in either disposal method whether it was by traditional vacuum truck transportation or an onsite treatment option such as the BOS System. These water additions did increase the volume of recovered water. Due to the

chemical properties of the grout and hole conditions, citric acid was added to the spoils to lower the pH within the City of Ottawa's disposal criteria. The addition of citric acid to reduce the pH would have been needed regardless of the method of onsite treatment. BOS Technicians used 88 bags of citric acid for the entirety of the project. No downtime to the jet grout operation was ever caused by the BOS System. The cleaned fluid met the Ottawa City Sewer disposal criteria and the disposed solids complied with all the solid waste landfill requirements.

At the conclusion of this project, a total project savings analysis was done which can be seen in Table 2.

Table 2. Ottawa Total Project Savings

Total Project Savings					
Vacuum Trucks			*BOS System*		
Parameters	Value	Units	Parameters	Value	Units
Waste for Disposal (Grout, Soil, and Water Mix)	2,177 (2,399)	tonnes (tons)	Waste for Disposal (Dried Grout and Soil)	1,161 (1,279)	tonnes (tons)
Vacuum Truck Cost ($.30 cents/L) *projected	$525,000.00	Canadian Dollars	End Dump Truck Cost ($133.19 per tonne)	$154,637.00	Canadian Dollars
			BOS Equipment and Labor Costs	$247,947.00	Canadian Dollars
TOTAL COST	$525,000.00		$402,584.00		
TOTAL COST SAVINGS			**$122,416.00 (23% reduction)**		
TOTAL WASTE SAVINGS			**1,016 tonnes (1,119 tons) (47% reduction)**		

*NOTE: The traditional disposal method of utilizing vacuum trucks is an estimated cost. It was calculated using an industry stand of 30 cents per litre. This estimate covers both the trucking and disposal of the liquid waste.

Additional Project Savings

In addition to the spoils treatment and disposal savings, numerous environmental savings can be contributed as a direct result from utilizing the BOS System. Through creating a dry, stackable, solid material BOS significantly reduce the amount of waste hauling trucks that would have been required using traditional methods. Thus, resulting in less traffic, decreased carbon footprint and increasing public safety by reducing potential vehicular accidents or spills that could have occurred.

A summary of estimated environmental savings can be seen in Table 3.

Table 3. Estimated Environmental Savings

Environmental Impact Reductions	
Waste Trucking Loads Saved	**240**
Fuel Cost Savings	**$15,396**
Fuel Saved, L (gal)	**14,453 (3,818)**
Mileage Saved, km (miles)	**18,867 (11,723)**
Greenhouse Gas Emissions Reduced, kg CO_2 (lbs)	**38,814 (85,570)**

SUMMARY

BOS Solutions is an established environmental solutions company that has had great success applying its technologies across many industries. One of these industries has been jet grouting, where the improvement of subsurface soils is made through the erosive capacity of high-speed jets to cut and mix the ground in place with a cementitious grout. BOS Solutions was tasked with reducing the amount of spoils, a byproduct of the jet grouting process, trucked off location to a disposal facility while complying with each city's environmental regulations. Results presented from two jet grout projects completed by BOS in Toronto and Ottawa, Ontario, Canada, show that BOS was successful in reducing the amount of volume trucked off location to disposal by 35% and 47% these projects respectively. These reductions in disposal volume contributed directly to overall waste treatment costs for the customers by 19% and 23% respectively, totaling over $267,598.00 in savings between both projects. BOS' clients were not only able to substantially reduce their spoils treatment costs, but were also able to vastly reduce their environmental footprint by utilizing less trucking services which reduced the consumption of over 14,000 L (3,800 gal) of diesel fuel resulting in a decreased greenhouse gas, CO_2, Methane, and Nitrous Oxide, emissions by over 38,000 kg (85,000 lbs). Increasing public safety through lowering the potential accidents, vehicular or spills, that could have occurred.

See Figures 2 and 3 for a visual representation of project savings related to the projects completed in Toronto and Ottawa respectively.

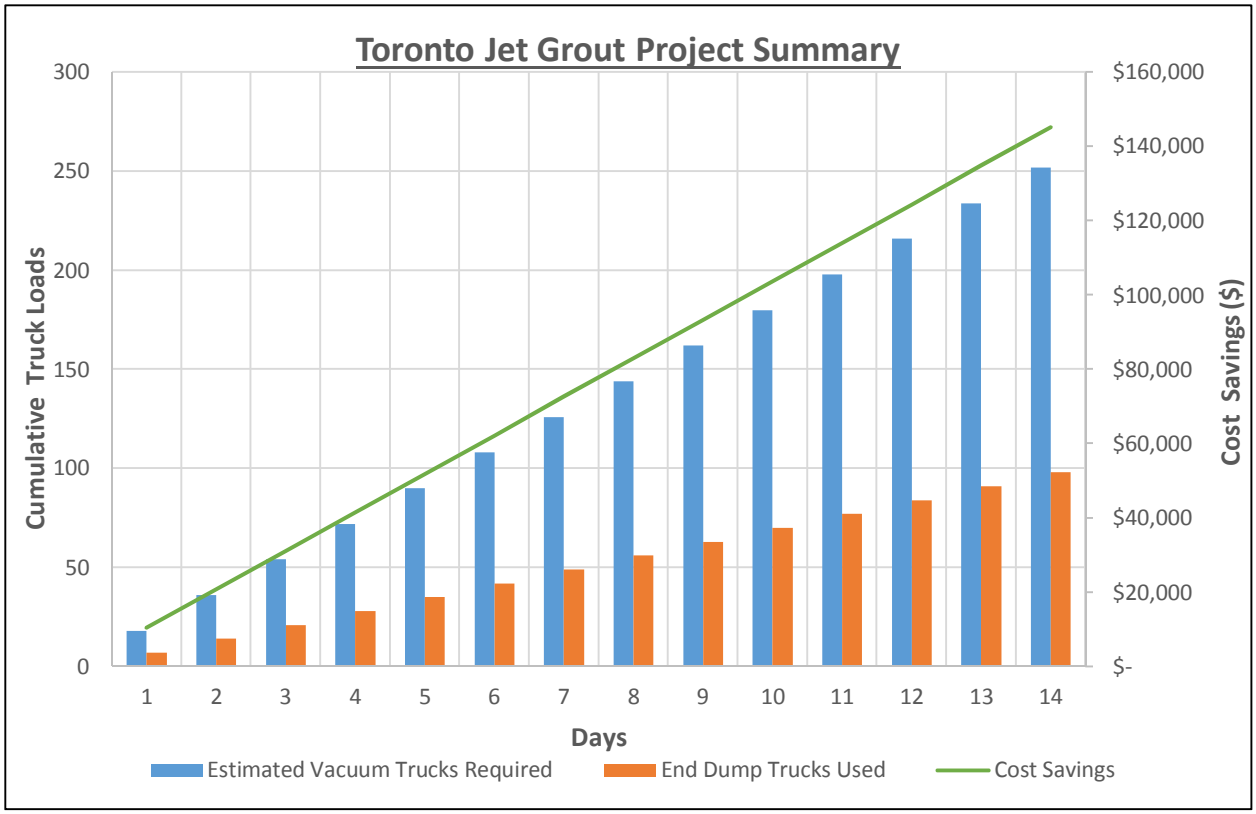


Fig 2. Toronto Truck Load Reductions and Cost Savings

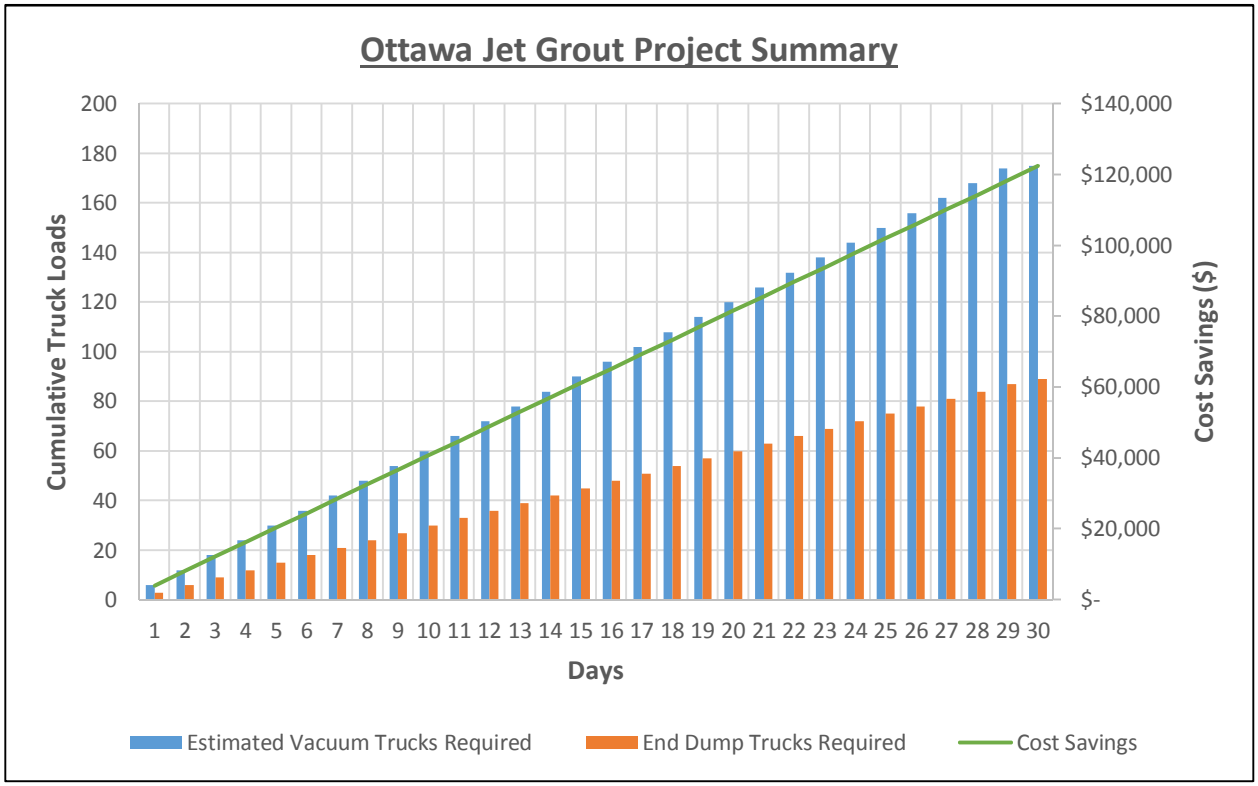


Fig 3. Ottawa Truck Load Reductions and Cost Savings

CONCLUSIONS

Traditional methods for handling and treating spoils can create logistical, environmental and economic challenges. Through the data collected on these projects and the analysis presented in this paper, BOS Solutions' alternative to handling jet grout spoils addresses these challenges with proven technology. Replacing a traditional method with new technology yielded increased saving for the customer with reduced environmental and public exposure.

ACKNOWLEDGMENTS

Andrew Pow, Director of Integrated Services, BOS Solutions, Leduc, Alberta, Canada, #780-809-8723, Andrew.Pow@bos-solutions.com

Michael Dykalski, Director of Engineering, BOS Solutions, Houston, Texas, United States, #281-477-5305, Michael.Dykalski@bos-solutions.com

REFERENCES

GasBuddy Website. Gas Prices: Historical Price Charts. http://www.torontogasprices.com/retail_price_chart.aspx . Accessed 3-16-2017.

United States Energy Information Administration Website. Frequently Asked Questions. https://www.eia.gov/tools/faqs/faq.php?id=307&t=11 . Last Updated May 6, 2016. Accessed 3-16-2017.

United State Environmental Protection Agency Website. Green Vehicle Guide: Greenhouse Gas Emissions from a Typical Passenger Vehicle. https://www.epa.gov/greenvehicles/greenhouse-gas-emissions-typical-passenger-vehicle-0 . Last Updated November 21, 2016. Accessed 3-16-2017.

DESIGN AND CONSTRUCTION OF DRIVEN H-PILES FOR LANDSLIDE STABILIZATION IN MARLBORO CLAY

Kofi B. Acheampong, PhD, PE, ENV SP, M. DFI, Chief Geotechnical Engineer & Senior Associate, KCI Technologies, Inc., 936 Ridgebrook Rd, MD 21152; E-mail: Kofi.Acheampong@kci.com

Charbel Khoury, PhD, PE, M. DFI, Associate, KCI Technologies, Inc., 936 Ridgebrook Rd, MD 21152; E-mail: Charbel.Khoury@kci.com

Kwabena Ofori-Awuah, PE, D.GE, ENV SP, M. DFI, Geotechnical Engineering Practice Leader, KCI Technologies, Inc., 936 Ridgebrook Rd, MD 21152; E-mail: Kwabena.Ofori-Awuah@kci.com

ABSTRACT

Following heavy rains in spring of 2014, Prince George's County officials issued a mandatory evacuation for homes in the Piscataway Hills subdivision of Fort Washington, Maryland where a landslide along a 1700-foot hillside destabilized homes, collapsed the single access road, and resulted in water and sewer mains break. Forensic investigations, including geologic assessments, test borings and in-situ Cone Penetrometer and Dilatometer soundings, were performed to evaluate subsurface conditions and provide stabilization options for the roadway and slopes. Post-failure ground movements were monitored using inclinometers. Critical failure planes were identified within the underlying 30-foot thick Marlboro Clay formation, a known geologic hazard with historic occurrences of landslides and slope failures.

This paper discusses the remedial design for stabilizing the landslide and 60-foot hillside slope failure, and protecting the roadway. Amongst several feasible options, driven piles were selected in consultation with the County and retained contractor based on cost, environmental impacts and site constraints. Constraints included private ownership of hillside slope, upslope buildings safety; deep-seated failure, relocation of underground water and sewer mains, and accelerated construction schedule.

Pile design included global slope stability analyses and lateral pile analyses using several loading configurations to optimize pile geometry and spacing, and determine a value-engineered design satisfying both serviceability and strength limit states to achieve long-term stability with factor of safety of 1.3. Soils within the active landslide plane were assumed to provide no resistance, while soils below the failure plane provided lateral resistance. This stabilization scheme, which extended along the 1700-foot roadway section and toe of hillside slope area, consisted of 410 steel HP16x141 piles in two to three rows driven to depths between 60 and 70 feet below the Marlboro Clay stratum at 5 to 7-foot spacing.

KEYWORDS

Coastal Marlboro Clay, Landslide, Slope Failure, Slope Stabilization, Driven Piles, Lateral Pile Analyses.

INTRODUCTION

The project site is located along Piscataway Drive north of the Piscataway Creek and includes steep hill side slopes with residential homes above and along the roadway. Historically, the slopes above and below Piscataway Drive have experienced surficial movements. However, following heavy rainfalls, cracks appeared in the pavement and adjacent slopes on May 2, 2014 and escalated into a landslide on May 4, 2014. Ground fractures and movements occurred over a 450-foot section of the roadway. Upslope soil movements averaged about 3 feet towards the roadway, and settled approximately eight feet. The pavement also settled up to a maximum of about four feet deep. Earth and trees tumbled down the 60-foot high ridge, leaving six homes sitting precariously at the crest of slope. The damage that occurred to the roadway and adjacent slopes, along with broken water and sewer mains, fractured power lines and the unsafe hillside, led to an immediate road closure and subsequent evacuation of 28 homes. There were

 © 2017 DFI Annual Conference, New Orleans, LA, USA

evidence of ground fissures and lateral movements, foundation wall settlements and cracks at a nearby abandoned and unsafe two-story structure south of the slope and roadway. In addition, there has been repeated incidents of underground water and sewer pipe breaks along the roadway.

The site is within the Coastal Plain geologic formation and underlain by unconsolidated deposits of Marlboro Clay (TM) sandwiched between a lower Aquia (Ta) and upper Nanjemoy (Tn) Formations (Geologic Map of Prince George's County, 2003). The Marlboro Clay is a continuous stratum throughout Southern Maryland. Marlboro Clay is a thin but highly distinctive soil composed of dense, brittle, pale-red to silvery-gray clay, ranging from thickly-bedded to finely laminated, containing thin lenses of micaceous and lignitic laminated, gray silt. The Aquia and Nanjemoy are mainly composed of gray to dark greenish gray, fine to coarse sand with a varying amounts of silt and clay, and shelly sandstone.

Historic information (Pomeroy, 1988) suggests that Marlboro Clay is highly susceptible to slope failures. Localized and mass ground movements associated with slumps and earthflows are known to be associated with Marlboro Clay with numerous slope failures having occurred in south-western and east-central Prince George's County. The presence of Marlboro Clay rendered the site vulnerable to slope failures and hazardous ground movements. However, the heavy and sustained rains resulted into rapid infiltration through the relatively permeable surficial sandy soils into the Marlboro Clay layer creating weak and unstable conditions at the sand-clay interface. This resulted in ground movements and slope failures along Piscataway Drive. Within the same period, a similar ground fracturing and slope failure occurred off Pine Road about ¼-mile north of Piscataway Drive landslide. Slope movements were consistent with the presence of Marlboro Clay in the area.

This paper discusses the design and construction of the landslide stabilization using driven H-Pile foundations based on the subsurface investigations, instrumentation data, slope stability and pile analyses.

FORENSIC INVESTIGATIONS

Site and Subsurface Explorations

An emergency site reconnaissance was performed part of the forensic investigation to assess existing site conditions. The site slopes appeared steep and ranged from slightly steeper than 1H:1V to 3H:1V. There was no evidence of surficial or ponded water although the area had experienced heavy rainfall over a short period of time. Temporary measures were implemented to minimize water infiltration into the soil by installing berm and pipe system to divert water away from the unstable slope. Forensic investigations (KCI 2014a and 2014b) included subsurface explorations consisting of Standard Penetration Test (SPT) borings to depths of 100 feet, in-situ cone penetration tests (CPT) and flat-plate dilatometer tests (DMT) to identify major soils strata. A geotechnical instrumentation and monitoring program with inclinometers was implemented to measure post-failure and secondary ground movements during investigation, design and construction phases. Figure 1 depicts borings, CPT, DMT, and inclinometer locations plan.

Figure 2 shows typical soil profile at the site. The subsurface profile indicated 20 to 30 feet thick Marlboro Clay stratum between the upper Nanjemoy and lower Aquia formations. Based on visual classifications and laboratory data, Marlboro Clay consisted of moist to wet, soft to stiff, Lean Clay and Fat Clay with occasional thin lenses of micaceous Silt. The Nangemoy formation extended up to a depth of about 15 feet below grade, and consisted of moist, very loose to medium dense Silty Sand, Clayey Sand, Sand with Gravels interbedded with Sandy Silt and Clay layers. The Aquia formation consisted of medium dense to dense, moist to wet, Silty Sand and Sandy Silt with mica and calcareous shell fragments. Note, however that loose zones appeared to occur at the interface with the below Marlboro Clay layer.

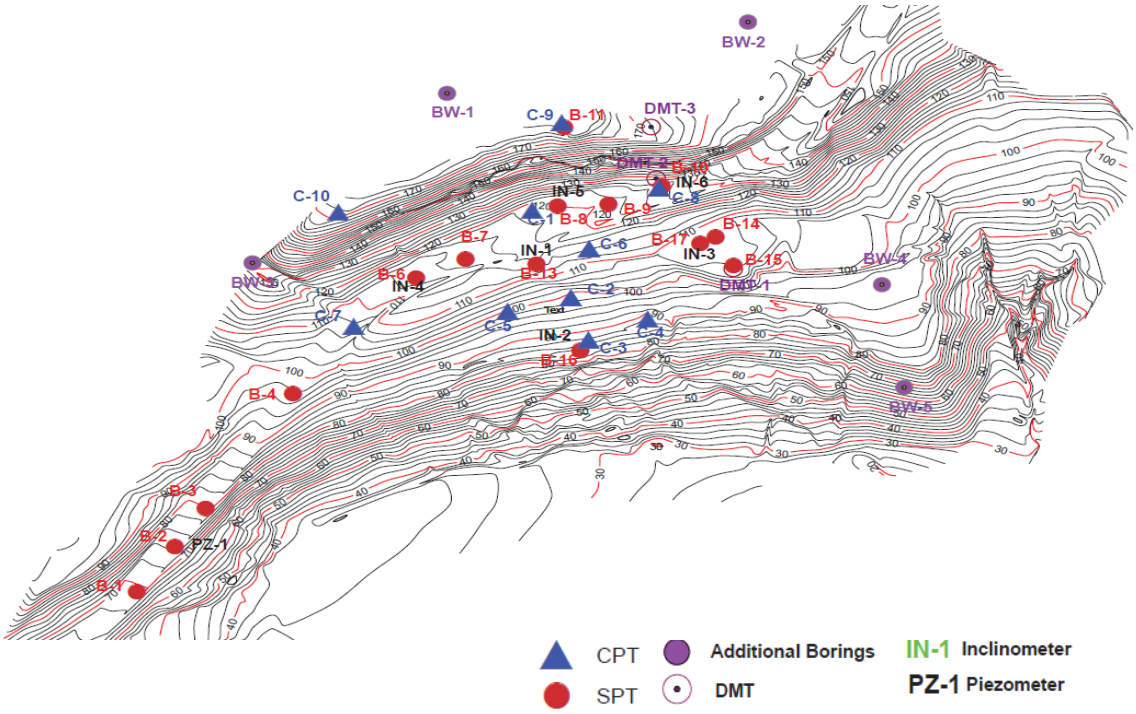


Fig. 1 – Exploration and Instrumentation Location Plan

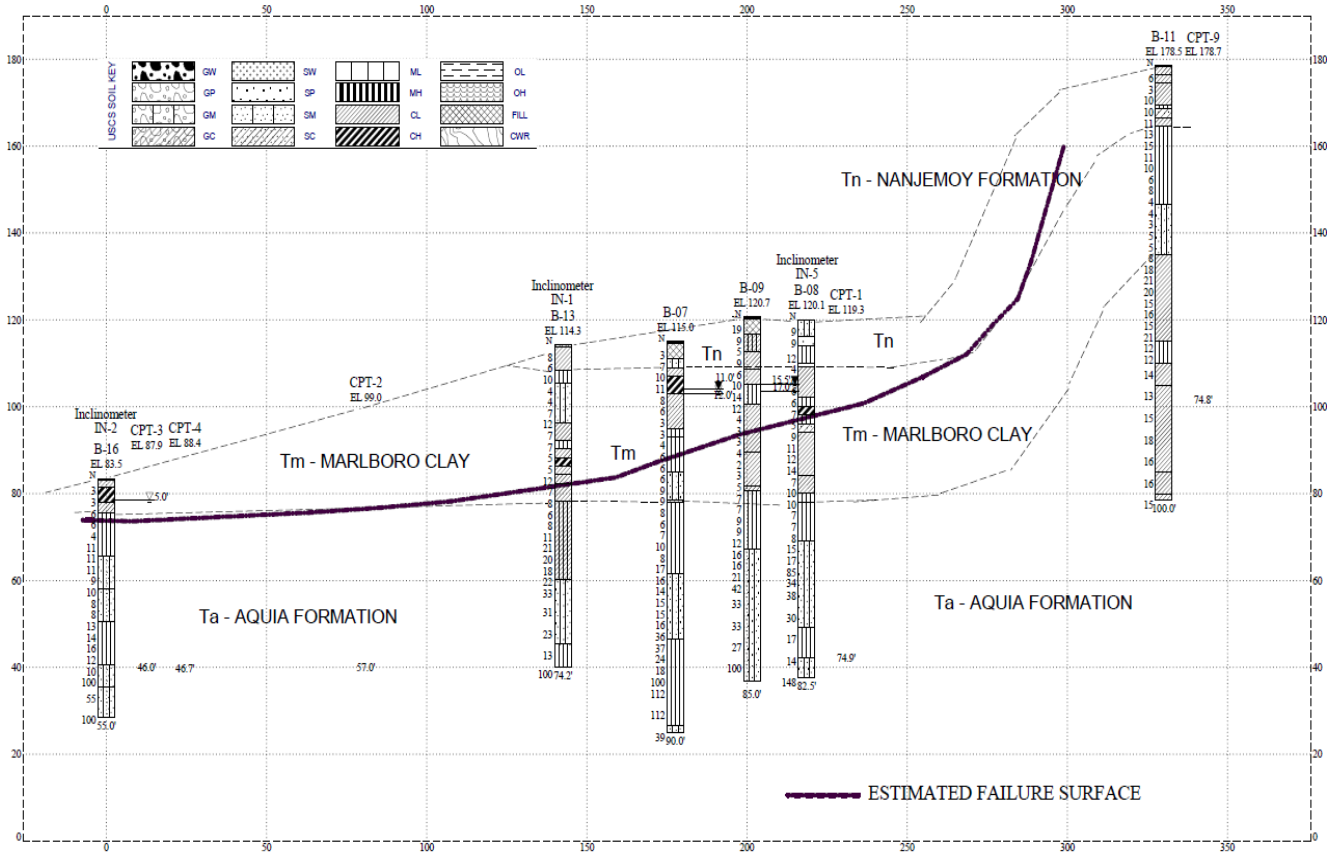


Fig. 2 – Typical Subsurface Profile with Major Soil Strata

Ground Monitoring Data

Six inclinometers (designated as IN-1 through IN-6) were initially, installed between May 9 and May 13, 2014 to monitor post-failure ground movements at the project site. Baseline readings were obtained between May 13, 2014 and May 19, 2014. However, additional inclinometers and piezometers were later installed during the design and construction phases, and post-construction. Typical plots of recorded ground movements with depth are presented in Fig. 2 at selected periods. Table 2 provides a summary of the ground movements and estimated depths of critical failure planes used in design.

Table 2: Summary of Post-failure Inclinometer Data

Incl. #	EX. GS Elev. (ft)	Observed Max Lateral Movements* (in)				Est. Depth of Failure Plane (ft)	Est. Elev. Failure Plane (ft)
		5/13/14 –5/19/14	6/18/14	9/19/14	3/18/15		
IN-1	114.3	0.27	0.29	0.30	0.30	36	79
IN-2	83.5	0.98	0.98	0.98	2.0	9	75
IN-3	110.0	0.48	0.61	0.61	0.61	31	79
IN-4	112.9	0.07	0.16	0.17	0.17	34	79
IN-5	120.0	0.20	0.27	0.29	0.29	32	88
IN-6	125.0	0.09	0.18	0.25	0.25	30	95
IN-1	*Insignificant Post-Construction movements of 0.01"+/- (From 2/18/2016 to 6/20/2017)*						

*The accuracy of the inclinometer measurements is within +/-0.01-inch per reading.

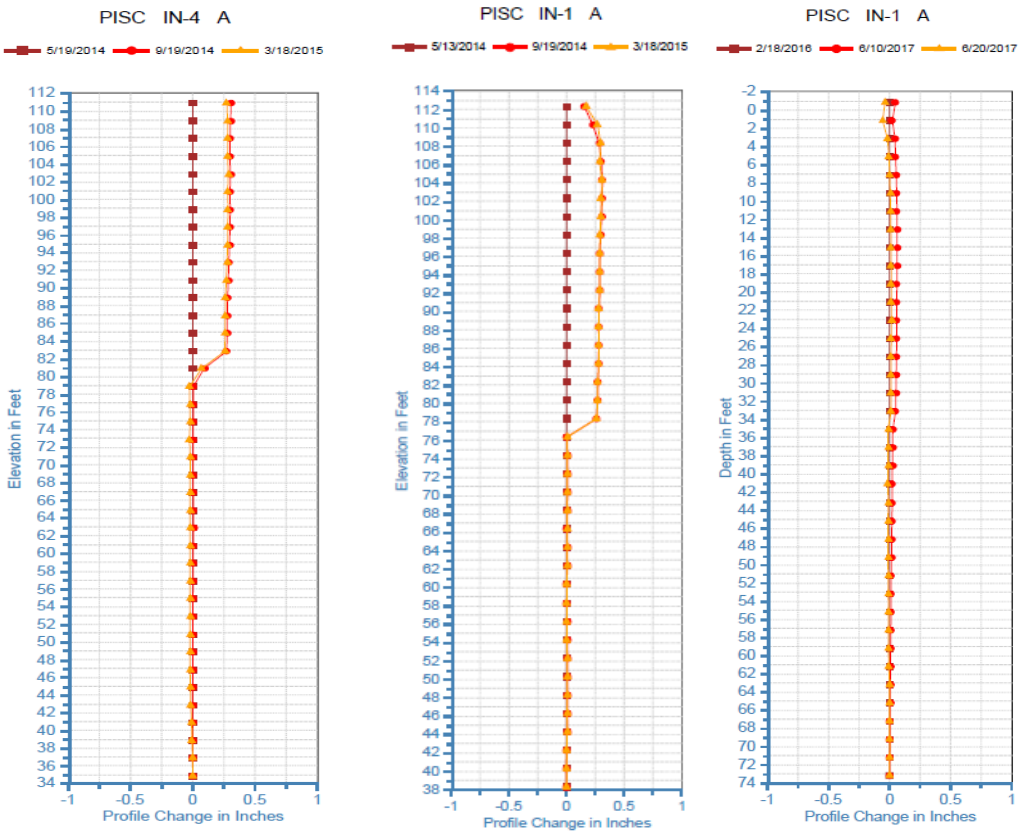


Fig. 3- Typical Post-Failure and Post-Construction Ground Movement Data

Landslide Mechanism

Based on subsurface profiles and inclinometer data there is evidence of failure planes at the Marlboro Clay-sand interface and within the clay. Typical failure planes occurred between 20 and 36 feet indicating a deep-seated failure within the Marlboro Clay; however, along the hill side slopes relatively shallow failure (less than 15 feet) occurred at the interface between the Nanjemoy and Marlboro Clay.

The landslide was triggered by heavy rains with rapid infiltration through the relatively permeable surficial soils to the Marlboro Clay. During wet periods as rainfall percolates through the overlying permeable sandy soils, it encounters the relatively impermeable Marlboro Clay. Infiltrated water will thus move primarily along the surface of the clay layer. Over time, infiltrated water gradually dissipates with easing of pore pressures and causing little or no slope movements. However, during the intense and rapid rainfall, infiltrated water is not able to quickly dissipate in the Marlboro Clay and generates high pore pressures within the saturated sediments. Seepage pore pressures resulted in shear strength degradation, creating weak layers and zones with significant reduction in the interfacial frictional resistances along the contacts between the overlying soils and Marlboro Clay. This condition produced new slide surfaces, and potentially regenerated existing failure planes leading to landslide and slope failures.

SLOPE FAILURE ANALYSES

Based on the results of the subsurface investigation, critical cross section profiles were developed for slope stability analyses using the Slide (Version 6.029, by RocScience, Inc.) software. Slide is a commercially available software, which supports various analyses methods (e.g., *Simplified Bishop*, *Simplified Janbu, Spencer, Morgenstern-Price, etc.).* Conventional two-dimensional limit equilibrium methods were used in order to find critical slip surface and the minimum slope safety factor (FS). Both circular slip and block slip search were utilized with several scenarios part of the analyses.

Estimated depths of the landslide and failure planes were based on subsurface profiles, in-situ testing, and inclinometer data. Back calculation stability analyses were performed for the pre-existing failure conditions of the slopes (under marginal stability with FS=1.0) to determine the design residual shear strength parameters of the Marlboro Clay. Laboratory testing was performed to classify the in-situ soils and mainly determine the shear strength parameters for the encountered Marlboro Clay stratum for modeling and analyses. CPT and SPT data were used to determine undrained shear strengths. Table 1 summarizes the shear strength results from both laboratory and in-situ testing.

Table 2: Summary of Lab and In-situ Shear Strength Results for Marlboro Clay

		Laboratory Results				In-Situ Testing (CPT, SPT)	
Boring No.	**Sample Depth**	**Test Type**	**USCS**	**Cohesion c' (psf)**	**Friction Angle (deg)**	**Undrained Shear Strength (ksf) – CPT**	**Undrained Shear Strength (ksf) – SPT**
B-13	22'-24'	DS	ML	997	29	1 to 2	0.5 to 1
B-13	28'-30'	DS	CL	473	22	1 to 2	0.5 to 1
B-14	26.5'-28.5'	DS	CL	650	14	-	1
B-15	22'-24'	DS	CL	11.3	31	-	0.5 to 1
B-15	22'-24'	CIUC	CL	130	18	-	0.5 to 1
B-17	22'-24'	DSR	CL	759	30	-	0.5 to 1
Notes: DS=Direct shear without residual cycles; DSR = Direct shear with residual cycles							

The design parameters, summarized in Table 3, and used in geotechnical modeling for the landslide were developed based on in-situ testing (SPT, CPT, DMT), laboratory data and back-calculation analyses.

Table 3 - Summary of In-Situ Soil Strata and Design Soil Parameters				
Natural Soil Stratum	**Nanjemoy Formation**	**Marlboro Clay**	**Aquia Formation**	
Soil Properties	**Stratum I**	**Stratum II**	**Stratum III-a**	**Stratum III-b**
Moist Unit Weight (pcf)	115	115	115	120
Saturated Unit Weight (pcf)	120	120	120	125
Effective Cohesion, C' (psf)	0	50	0	0
Effective Friction Angle ϕ ' (deg.)	30	18	30 to 32 *	35
* Used appropriate friction angle based on the in-situ density conditions of the natural SAND.				

SLOPE STABILIZATION CONCEPT AND DESIGN APPROACH

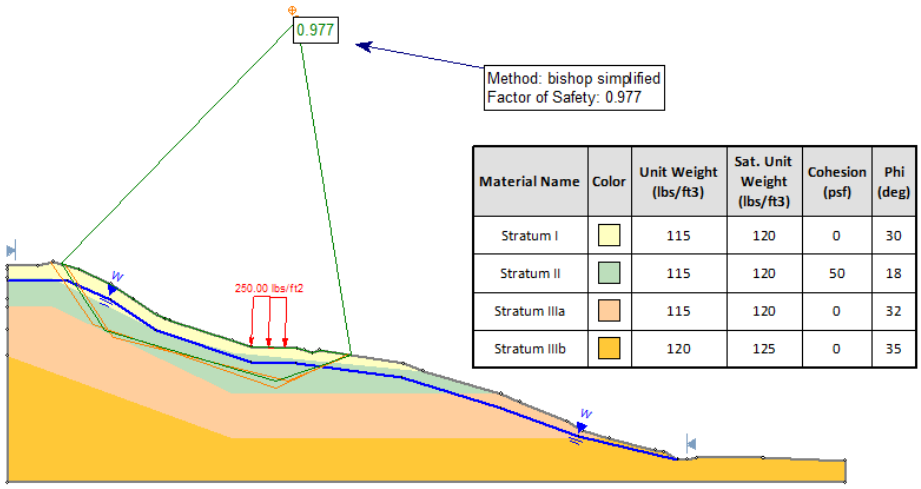
Several stabilization options were considered including: H-Pile foundation; micropile slope stabilization; hybrid slope stabilization with soil nails, micropiles and ground anchors; and a retaining wall with slope flattening. Due to site and legal constraints including right-of-way limitations, utility relocations and environment requirements and constructability considerations, the selected cost effective stabilization was a deep foundation option consisting of steel H-Piles and geogrid reinforced slopes (Fig. 6).

Slope Stability Analyses and Pile Design

Slope stability analyses of 24 representative cross-sections (GT-1 to GT-11; GT-20 to GT-32; Fig. 9) across the 1400-foot long landslide area were performed part of this study (KCI, 2015). Analyses were based on the design soil parameters presented in Table 4, assuming phreatic water surface at depths between 5 feet and 10 feet below grade. Minimum safety factors for slope failure surfaces were determined using simplified Bishop (or Janbu). For the proposed slope stabilization, a minimum FS of 1.3 under static loading conditions is required for long term stable conditions with no upslope properties and structures. The existing buildings on top of the slopes were acquired by the County and demolished.

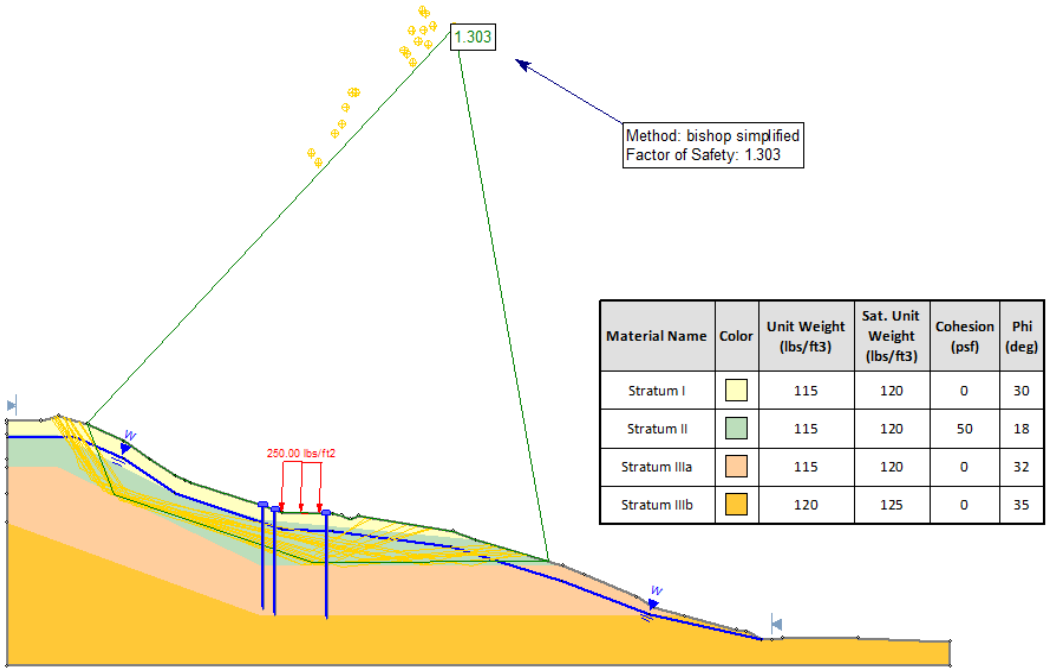
Slope stability analyses were performed for both post-failure slope conditions (Fig. 4), and proposed slope stabilization option (Fig. 5) for the typical steel H-Piles and geogrid reinforced slope (Fig.6). The Slide software was used in conjunction with the LPILE V7 2013 (ENSOFT, Inc.). LPILE uses the p-y method (based on soil type and parameters) to compute the soil response pressures acting on the pile, the moment, and shear and deflection. Table 4 summarizes the soil parameters use for Lateral Analyses.

Table 4 - Summary of Lateral Analyses Soil Parameters							
Soil Stratum	Depth to Bottom of Layer (fT)	Average SPT "N"	Effective Unit weight, γ (pcf)	Friction Angle, Φ (deg)	Undrained Shear Strength, Su (ksf)	Lateral Subgrade Modulus, kh (pci)	Strain Modulus e_{50}
Nanjemoy	8	17	115	30	-	90	-
Marlboro	35	6	52.6	-	0.5 to 1.0	100 to 500	0.01
Aquia (a)	73	19	52.6	32		20 to 60	-
Aquia (b)	100	52	57.6	35	-	125	-



Material Name	Color	Unit Weight (lbs/ft3)	Sat. Unit Weight (lbs/ft3)	Cohesion (psf)	Phi (deg)
Stratum I		115	120	0	30
Stratum II		115	120	50	18
Stratum IIIa		115	120	0	32
Stratum IIIb		120	125	0	35

Fig. 4- Post Failure Analysis



Material Name	Color	Unit Weight (lbs/ft3)	Sat. Unit Weight (lbs/ft3)	Cohesion (psf)	Phi (deg)
Stratum I		115	120	0	30
Stratum II		115	120	50	18
Stratum IIIa		115	120	0	32
Stratum IIIb		120	125	0	35

Fig. 5- Pile Stabilization Analysis

Unbalanced Lateral forces anticipated on the piles to obtain a stable slope with a desired Safety Factor of 1.3 were determined based on the slope stability analyses and the recommended stabilization measures. The obtained unbalanced forces were input as lateral forces in LPILE (Bateman and Walberg, 1998) to determine the structural capacity (moment, shear and deflection) of the pile. Several trials were necessary to determine the pile location, size, depth of embedment, and the required pile spacing. Driving forces are either input as triangular or uniform active load distribution (Bateman and Walberg, 1998) on the pile. Bateman and Walberg (1998) reported that uniform load distribution load resulted in maximum deflection at top of pile, whereas triangular load distribution results in maximum moment and shear loads in the pile. We used a triangular load distribution linearly increasing with depth as is illustrated in Fig. 7, which is

slightly different approach from Bateman and Walberg (1998). For this study, the triangular load distribution extends from the pile head to a depth of 1.5 times the critical surface depth, and represents the resultant driving force at the critical surface. Above the failure surface passive soil shear strength is not considered, therefore the pile is modeled with an exposed length above the critical failure surface depths.

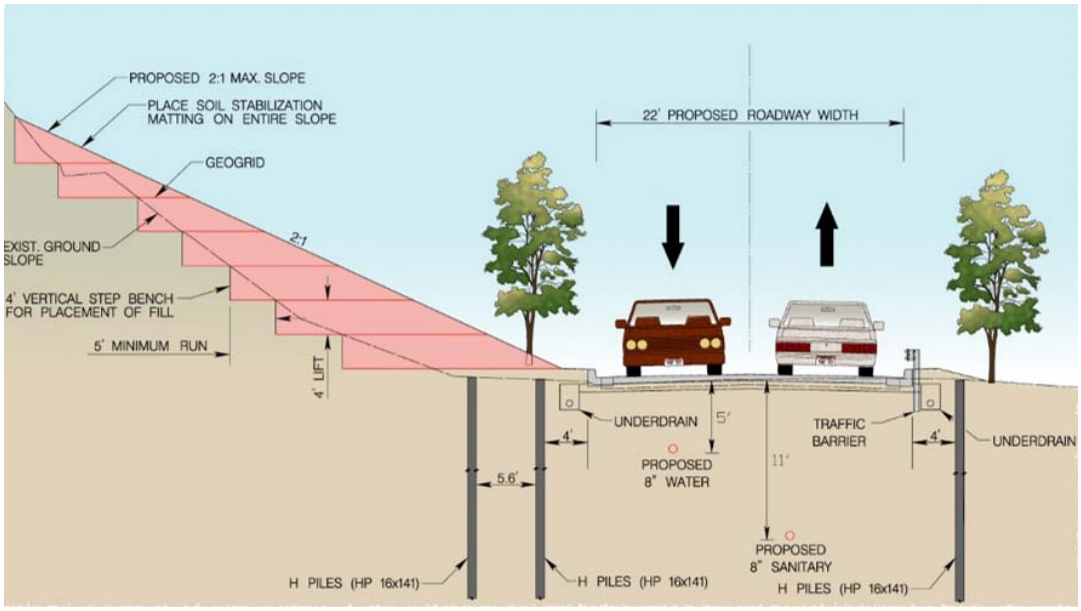


Fig. 6 – Typical Stabilization Section

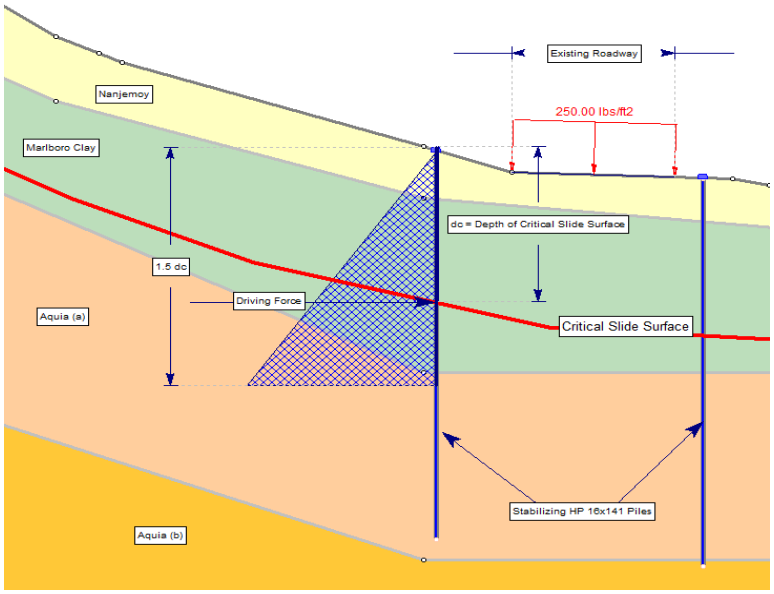


Figure 7 – Triangular Load Distribution on Piles

Summary results of the stabilization analyses are presented in Tables 5 and 6. Results indicate that Steel HP16x141 piles installed to minimum depths between 60 and 70 feet and spaced between 5 to 7 feet center-to-center will achieve the desired factor of safety of the slopes. Analyses indicated maximum pile deflections of less than 2 inches with typical deflections between 0.75-in and 1.0-in. Typical results are shown in Fig. 8. The design required single and two pile rows (at 5 to 7 feet apart) installed along the toe of the slope and along Piscataway Drive (Fig. 9).

Table 5 - Summary of Slope Stabilization Analyses					
Baseline Station		**Cross Section**	**Factor of Safety (FS)**	**Proposed HP 16x141 Stabilization**	**Factor of Safety (FS)**
from	**to**	**#**	**Post-Failure**	**Description**	**Remediation**
102+50	103+25	GT-20/GT-21	1.05- 1.13	1 Row South of Roadway	1.30-1.31
103+25	105+00	GT-22 - GT-25	0.78 – 1.16	2 Rows South of Roadway	1.30 – 1.31
105+00	107+00	GT-26 - GT-29	0.94 – 1.20	1 Row South of Roadway	1.31 – 1.33
107+00	108+00	GT-30/GT-31	0.98 – 1.14	2 Rows South of Roadway	1.30 – 1.31
108+00	113+25	GT-1 - GT-9	0.67 – 1.02	2 Rows North of Roadway; 1 Row South of Roadway;	1.30 – 1.31
113+25	114+00	GT-10	0.81	2 Rows North of Roadway; 2 Rows South of Roadway	1.31
114+00	114+50	GT-11 GT-32	1.01 0.95	2 Rows South of Roadway 2 Rows South of Roadway	1.30 1.30

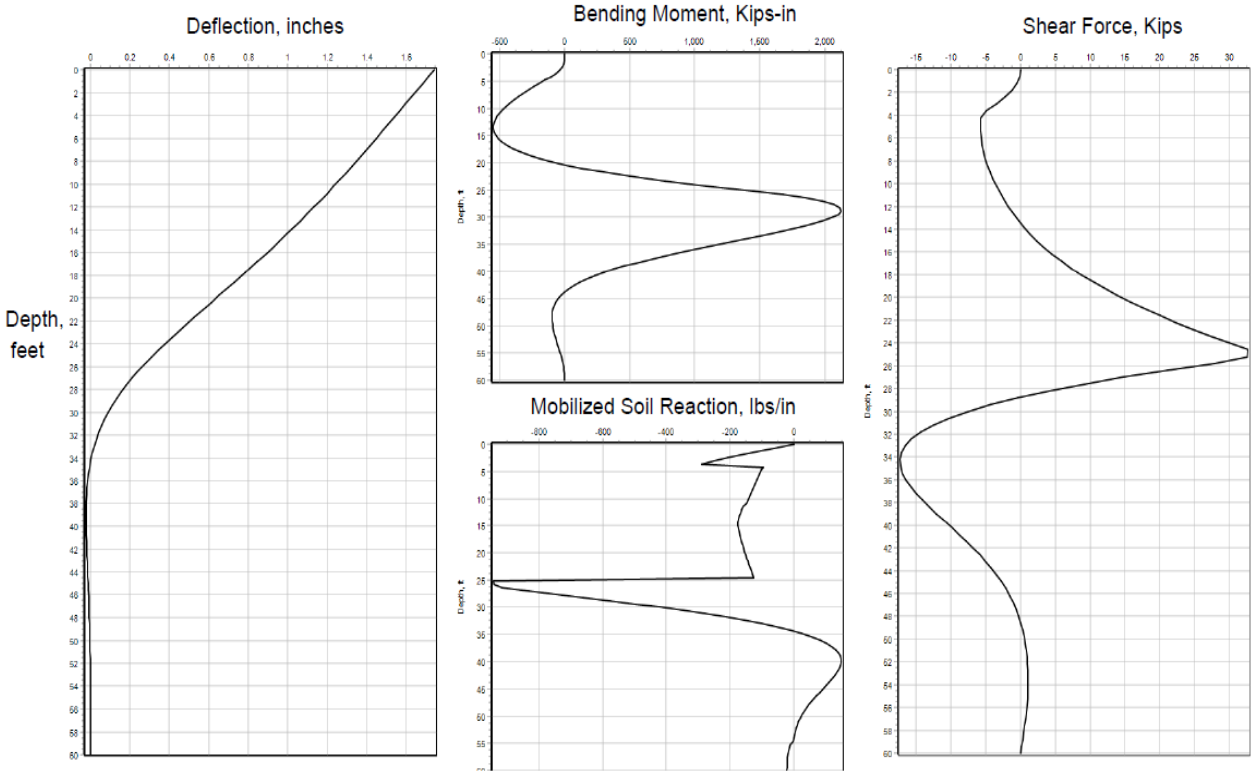


Fig. 8 – Typical Lateral Pile Analyses Results

Table 6 - Summary of Lateral Pile Analyses				
Cross Section	**Pile Length (ft)**	**Critical Surface Depths (ft)**	**Triangular Load (lbs/in)**	**Max.Pile Lateral Deflection (in)**
GT-1 thru GT-11;	70	17 to 36	470 to 760	0.3 to 1.9
GT-20 & GT-21	60	15 to 24	536 - 569	1.8 to 1.9
GT-22 thru GT-30	60	22	160 - 510	0.02 – 0.6
GT-31	60	22	370	0.8
GT-32	70	22	415	0.4

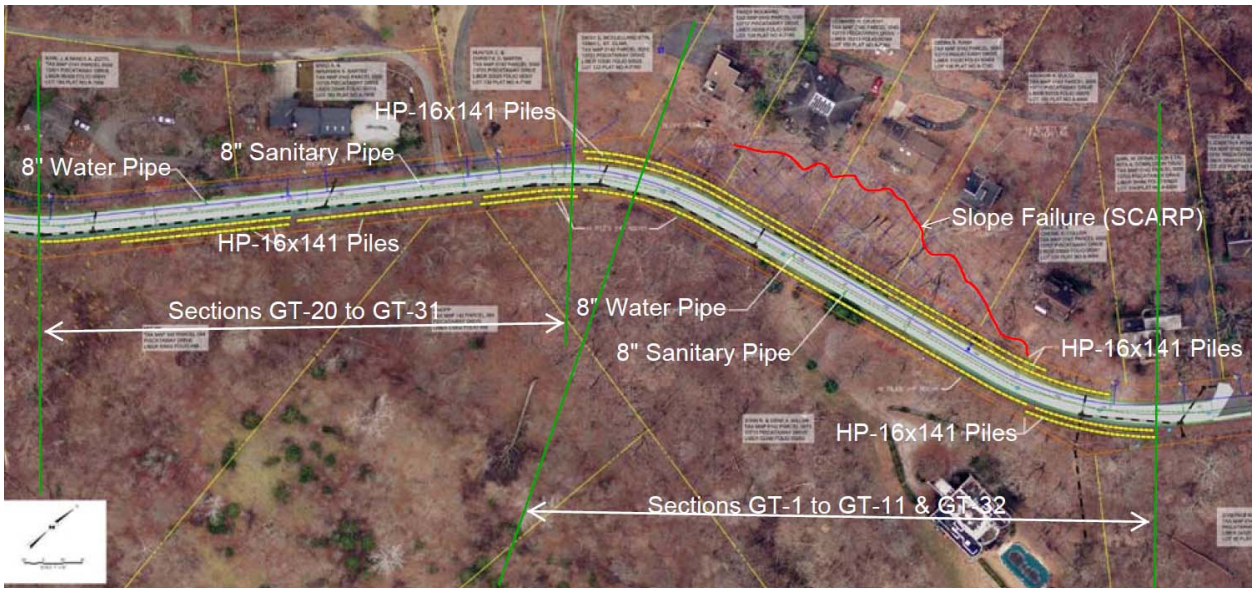


Fig. 9 – Final Pile Layout Plan

CONCLUSIONS

This study utilized a practical slope stabilization approach for deep seated landslide and slope failure using a combination of limited equilibrium slope stability and p-y lateral analyses to determine optimal design of driven H-piles. The piles were driven to the required depths with 35 to 50 feet embedment depths below the anticipated slip surfaces. Continuing ground and slope movements were monitored during and after installation; however, no significant movements have been recorded within the stabilized and adjacent areas.

ACKNOWLEDGEMENT

The authors would like to thank Prince George's County for giving us this opportunity to provide engineering services for this challenging project and KCI Team for working towards a successful project.

REFERENCES

Bateman R. L., and Walberg, F.C, 1998. Pile Design Procedure for Stabilizing Channel Slopes. Proceedings fourth International Conference on Case Histories in Geotechnical Engineering, Saint Louis, Missouri, March 9 to 12, 484-490.

Pomeroy, J.S., 1988. Map Showing Landslide Susceptibility in Maryland, USGS Miscellaneous Field Studies Map MF-2048.

KCI (2014a). Draft Preliminary Geotechnical Engineering Report - Piscataway Drive Slope Failure. Prince George's County Government, Maryland. May 19, 2014.

KCI (2014b). Addendum to Draft Preliminary Geotechnical Engineering Report - Piscataway Drive Slope Failure. Prince George's County Government, Maryland. June 25, 2014.

KCI (2015). Geotechnical Design Report- Piscataway Drive Slope Stabilization. Prince George's County Government, Maryland. February 26, 2015.

LARGE DIAMETER HELICAL PILES FOR REFINERY EXPANSION

Eric Wey, Fluor Corp, One Fluor Daniel Drive, Sugar Land, TX, USA, (281) 263-4060
eric.wey@fluor.com

Patrick Murray, Marathon Petroleum Company, Marathon Avenue, Garyville, LA, USA, (985) 535-7973
pemurray@marathonpetroleum.com

Howard Perko, Magnum Piering Inc., 138 East 4th Street, Loveland, CO, USA, (970) 635-1851
hperko@magnumpiering.com

Paul Volpe, Marathon Petroleum Company, Marathon Avenue, Garyville, LA, USA, (985) 535-7471
psvolpe@marathonpetroleum.com

Chris Normand, Cajun Deep Foundations, LLC, Baton Rouge, LA, USA, (225) 753-5857
chris@cajunusa.com

Burt Ogilvie, Cajun Industries, LLC, Baton Rouge, LA, USA, (225) 753-5857
burt.ogilvie@cajunusa.com

ABSTRACT

A refinery expansion project for Marathon Petroleum Company in Southern Louisiana required existing medium to large pipe racks to be expanded for additional capacity. Foundation modifications were necessary in order to add levels to the existing pipe racks. New piles were added and existing pile cap foundations were expanded. Several different pile types were considered. Custom designed large diameter helical piles were chosen, because they can be installed quickly with low overhead restrictions, produce minimal soil spoils, and are cost effective. The load capacity required for piles was higher than typical, off-the-shelf helical piles. In particular, the lateral load capacity demand was high due to wind loads of a hurricane prone region. Methods used to design and size helical piles are summarized including capacity to torque ratio estimation for composite helical piles. Pile load testing was performed in order to confirm design capacities of the helical piles under axial and lateral loading. Measured axial and lateral deflections compared well with predicted values. This case history evaluates the effectiveness of modern helical pile design methods within the context of a real and practical example.

Keywords: helical piles, lateral load, pile testing, foundations, headroom, pipe racks, non-building structures

INTRODUCTION

As the capacity of modern installation equipment increases, large-diameter helical piles are being used to support higher loads in more diverse applications. Currently, large-diameter high-capacity helical piles are used for electrical power transmission, power generation, high-rise buildings, bridges, and industrial applications. This case study regards a 2.5-mile pipe rack modification project within an existing refinery. One of the many challenges for engineering and construction of refinery revamp projects is determining how to effectively expand the capacity of existing foundations for additional equipment, piping, and other facilities. Custom designed large-diameter helical piles provided an effective solution to the challenges faced when expanding the capacity of existing pipe racks.

In previous paper by Wey, et al. (2017), the overall project was briefly described along with the need for a safe, reliable, low-headroom solution involving helical piles that does not produce drill spoil. A description

 © 2017 DFI Annual Conference, New Orleans, LA, USA

of the helical pile design and load testing program was provided with particular emphasis on vertical and lateral pile head movements, prediction, and tolerance for refinery equipment. Results of load tests were shown to compare well with design predictions. Test loads were held for an extended period showing minimal pile movement, which supported that helical piles are not prone to creep under sustained static loads. Also discussed in the previous paper was the importance of early clarification with regard to governing building codes and pile performance expectations.

This paper differs from the previous document by focusing less on design and more on installation obstacles and how they were overcome by the contractor. Also discussed are field quality control and the development of final pile termination criteria. Helical piles selected for the project consisted of a 5.5-inch diameter shaft with four 24-inch diameter helical bearing elements transitioning to a 13.4-inch diameter casing for the upper 16 feet. Composite helical piles, which are those with varying shaft size, have been used for several decades (Perko, 2009). However, little has been published regarding the installation torque produced by composite helical piles. Torque is often used as a final termination criterion for helical pile installation. Estimation of torque is valuable for sizing equipment and pile design.

In the past, one or two static load tests have been used to establish a project site specific capacity to torque ratio, K_t, for a particular helical pile design. The authors argue that one or two tests do not represent a statistically significant measure of pile performance that properly captures variability of a given site. For this reason, the authors advocate establishing capacity to torque ratios using well-known and published average values for a particular pile shaft lead section, evaluating the effect of the upper section, combining the required torque for both lead and upper section, and then conducting static load tests to verify the ratio K_t. This paper describes steps used to establish the termination torque for the composite helical piles used on this project. Three static load tests were performed as a final step in the process to verify the final K_t values.

SITE CONDITIONS

The project site is located within an existing developed refinery operated by Marathon Petroleum Company in Garyville, Louisiana. The approximately 2.5 miles of pipe rack, depicted by the yellow lines in Fig. 1, weave between existing tanks and processing units. A snapshot showing the existing pipe rack is provided in Fig. 2. The congested nature of existing well-developed industrial facilities is represented in the photograph. Refinery revamp work presents many challenges including low overhead restrictions, limited access, noise and vibration concerns. In many refineries, drill spoils often need to be hauled away and require special disposal. Perhaps the most important criteria for refinery revamp work are that interruptions to processing must be minimized, and safety of workers and existing equipment is paramount.

The generalized soil profile in this area of Louisiana consists of recent deposits of medium stiff clays and sands with an average unconfined compressive strength of 0.5 tsf overlying a Pleistocene age stiff clay at a depth of about 40 feet below the ground surface. The Pleistocene clay has a lower bound unconfined compressive strength on the order of 1.2 tsf. Groundwater is present only a few feet below ground surface.

Table 1 shows pile design loads. Design lateral and overturning loads are primarily from hurricane winds due to the proximity to the Gulf coast. A robust lateral load capacity was required for the piles because the additional height of pipe racks would significantly increase the wind profile. Allowable deflection under lateral loads was determined from an analysis of the equipment to be supported and its tolerance for movement. Allowable deflection will vary depending on type, height, and configuration of petro-chemical processing equipment and piping.

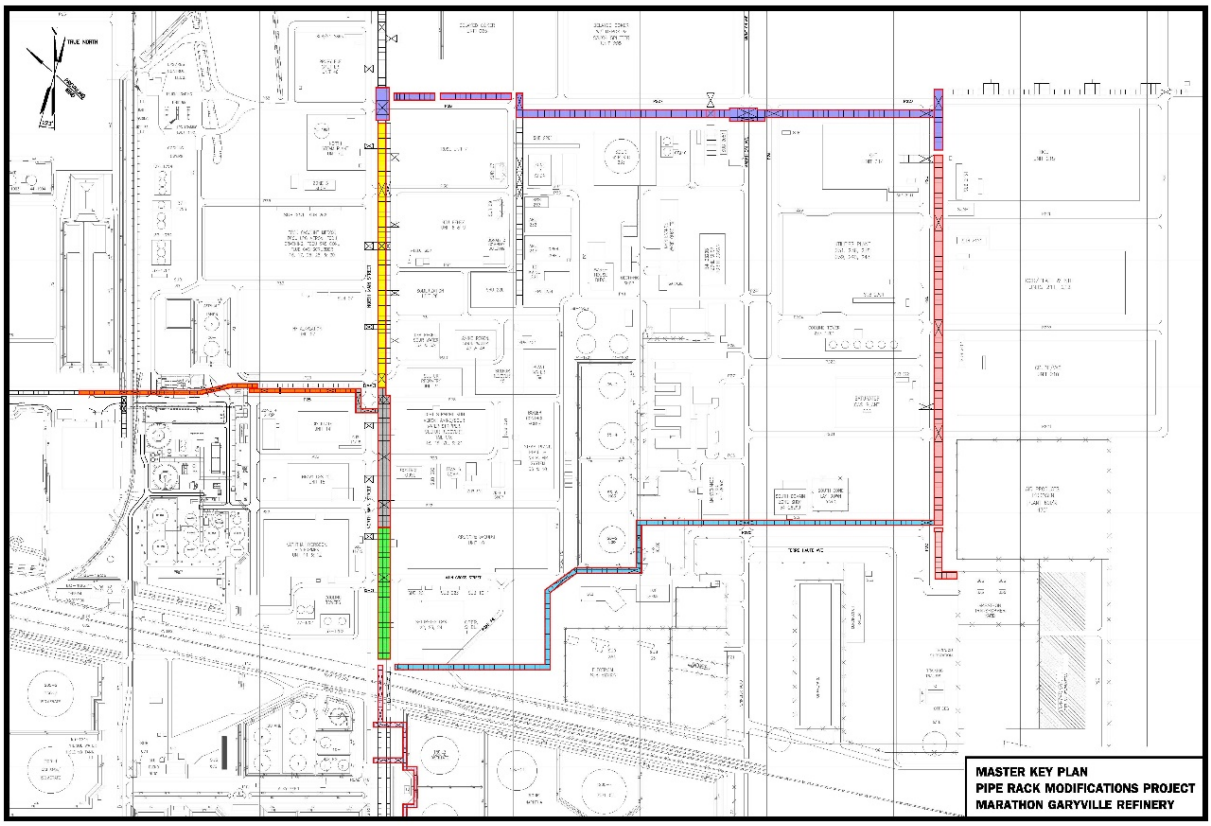


Fig. 1. Location of Pipe Rack Augmentation Work

PILE SELECTION

There were three different pile types initially considered in the project; 16-inch diameter auger-cast piles, 16-inch square pre-stressed concrete driven piles, and helical piles. Each of these piles was required to support the loads shown in Table 1. Low-overhead auger-cast piles are very labor intensive and produce a large quantity of spoils for disposal. A photograph of a typical low-overhead auger-cast pile drilling machine is shown in Fig. 3. Driven piles require high headroom for installation with additional risk of disturbing or damaging existing pipes, duct banks, or foundations.

Table 1. Expansion Pile Design Loads

Type of Loading	Axial Compression	Axial Tension	Lateral (horizontal) load (based on free-head) [5/8-in deflection]
Sustained (dead and Live)	60 kips	45 kips	9 kips
Transient (wind or seismic)	80 kips	60 kips	12 kips

The selected pile type was base upon constructability and cost effectiveness. The modification to the existing pipe racks required the pile to be installed in locations with low overhead obstructions and limited access. Overhead obstructions were typically about 15 feet above grade; however, some obstructions were as low as 10 feet above grade. Minimizing the number of new pile rows in order to mitigate the group pile shear reduction factor was a challenge for the engineers because of the existing conditions including existing battered precast piles. Underground obstructions were carefully avoided by studying existing underground drawings, exploratory trenching, and hydro-excavation pilot holes at the location of piles.

Helical piles were chosen for the speed of installation in low-overhead conditions which played a role in being the most economical solution. Helical piles minimized spoils while providing the optimum pile layout with the aid of high torque, low RPM motors, which allow advancement with minimal soil disturbance. A photograph of a typical low-headroom helical pile installation is shown in Fig. 4.

In order to provide best economy and efficient use of materials, a composite helical pile was chosen consisting of an upper 16 feet long, 13-3/8" diameter by 3/8" wall steel casing coupled to a lower section consisting of 5.5" diameter by 0.47" wall high-strength steel shaft with four 24" diameter helical bearing elements. Each helix has a 6" pitch. A schematic diagram of the selected pile is shown in Fig. 5. Helical pile properties and installation criteria are summarized in Table 2. Determination of helix size and quantity was discussed in Wey, et al. (2017). How the design team arrived at the final installation torque used for pile termination is described in the next section.



Fig. 2. Photograph Showing a Portion of Existing Exaggerated 3-Story Tall Pipe Racks Subject to Expansion (Courtesy of Fluor Corporation)



Fig. 3. Low Overhead Auger Cast Pile Installation (Courtesy of Fluor Corporation)

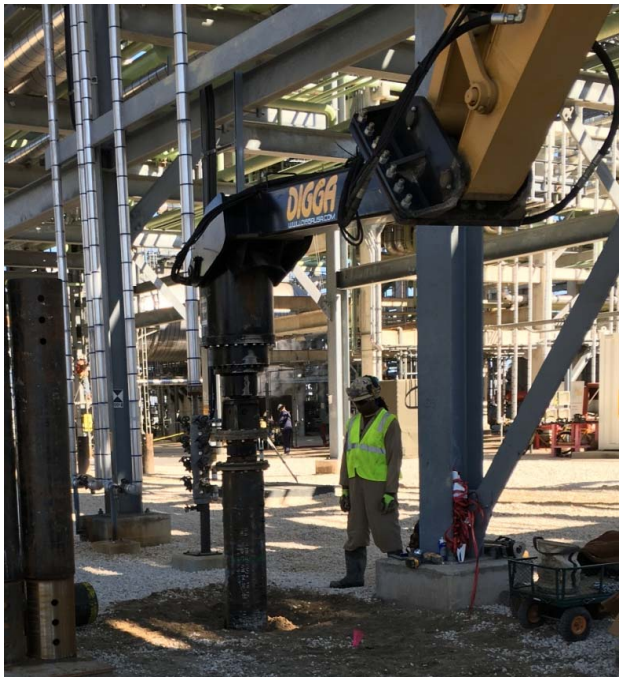


Fig. 4. Low Overhead Helical Pile Installation (Courtesy of Cajun Deep Foundations, LLC)

Table 2. Helical Pile Installation Criteria

Shaft size	Helix	Pitch	Installation Torque	Anticipated Length	Minimum Casing Length	Batter Angle
13.38” x 3/8 5.5” x 0.47”	4qty 24”dia.	6”	41,560 ft-lbs	46-ft to 54-ft	16-ft	0

TERMINATION CRITERIA

Installation torque is commonly used as a termination criterion for helical piles. It has been known since the 1970's that installation torque indicates average soil strength at the depth of the helical bearing elements and, therefore, pile capacity (Cherry and Perko, 2013). Capacity to torque ratios, K_t, are a function of shaft diameter. A common formula for estimating K_t values for different diameter helical piles is as follows (ICC-ES, 2016 and Perko, 2009),

$$K_t = 22.285\ (d_{eff})^{-0.9195}$$

where d_{eff} is the effective shaft diameter in inches. The units of K_t are ft^{-1}.

Based on the above formula, the lead section of the helical piles for this project has a capacity to torque ratio of 4.7 ft^{-1}. In order to achieve the project required capacity of 80 kips with a factor of safety of 2.0, final installation torque is found by taking ultimate capacity divided by the capacity to torque ratio,

$$80 \text{ kips} \times 2.0 = 160 \text{ kips}$$

$$160{,}000 \text{ lbs}/4.7 \text{ ft}^{-1} = 34{,}000 \text{ ft-lbs}$$

However, the upper larger-diameter casing section will affect the installation torque. The effect of the casing on installation torque was accounted for in two ways:

First, the theoretical torque produced by the casing was determined by multiplying the adhesion of the upper soils by the surface area of the casing times the radius of the casing. Adhesion was taken as the undrained shear strength times 2/3 to account for soil-to-steel friction. For an undrained shear strength of the upper soils of 0.5 tsf, one arrives at 9,800 ft-lbs of additional torque due to the casing.

Second, six field installation tests were conducted. In the first four tests, a 5.5" diameter shaft with helical bearing elements was installed to a depth of 21 feet while recording torque at 3-foot intervals. The next two tests consisted of a 15-foot long lead section with 5.5" diameter shaft and a 16-foot long section of casing with 13.38" diameter. As can be seen from the results shown in Fig. 6, the average increase in installation torque at 21 feet was 7,560 ft-bs, or roughly 77% of theoretical. Pore pressures generated during installation likely resulted in the observed difference.

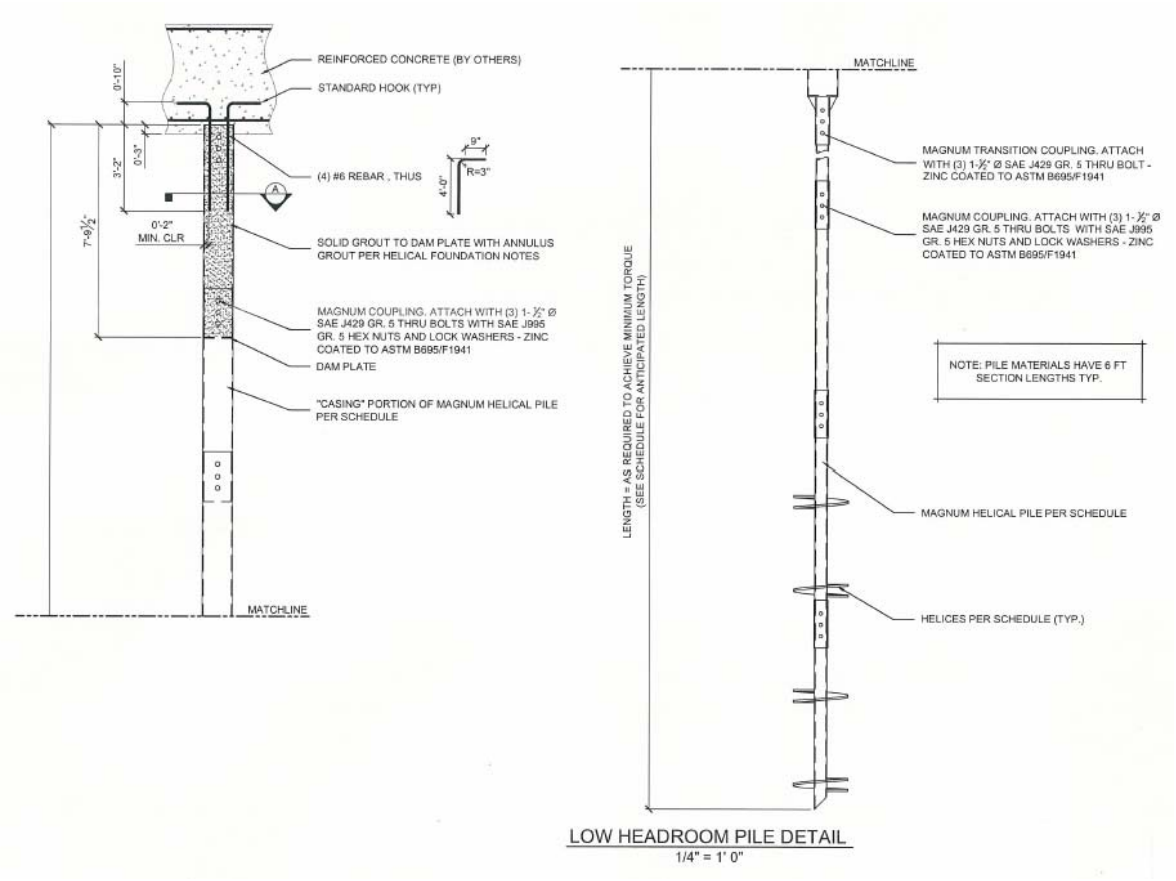


Fig. 5. Pile Schematic Details (Courtesy of Magnum Geo-Solutions, LLC)

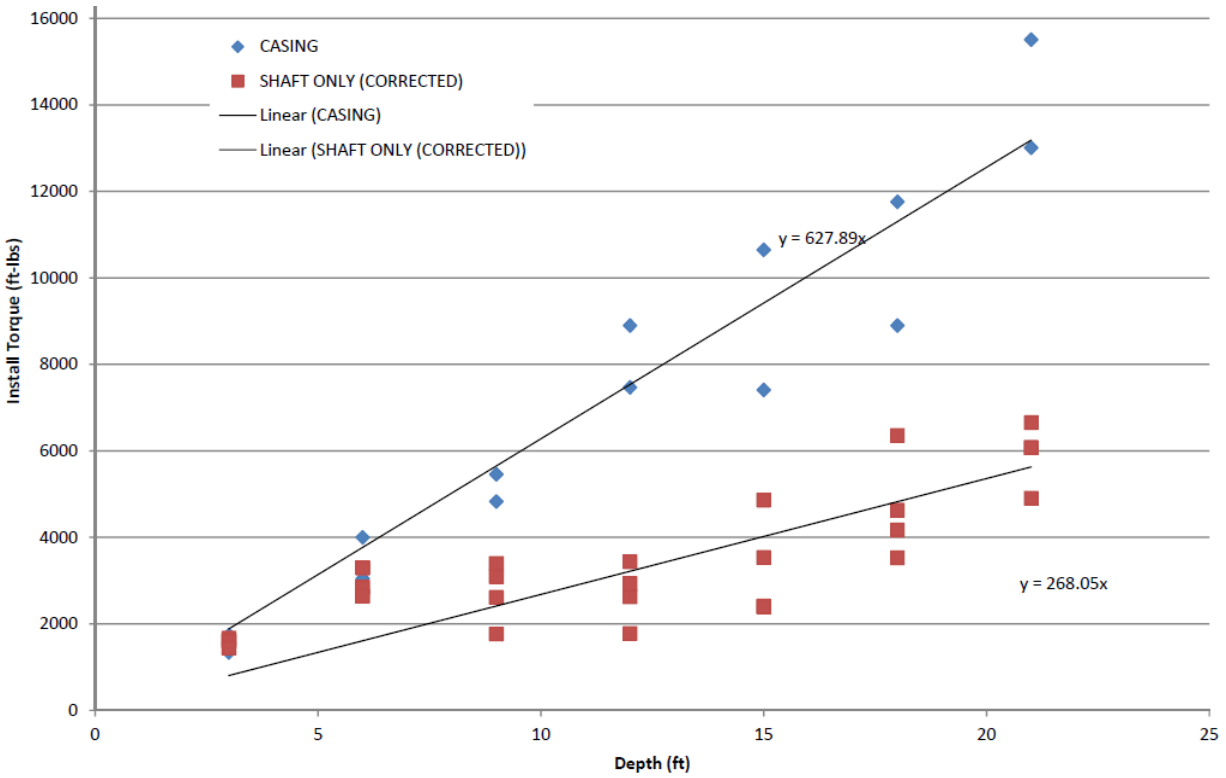


Fig. 6. Casing Installation Torque Field Tests

Final installation torque required for the helical piles on this project was computed by adding the required torque from the empirical K_t value for the lead section (34,000 ft-lbs) and the torque anticipated form the upper casing (7,560 ft-lbs) for a total of 41,560 ft-lbs as shown in Table 2.

Three axial compression, three axial tension, and two lateral load tests were performed per ASTM Standards on the helical piles to verify design. The "maintained" load procedure was followed so each increment was held for an extended time period. A photograph of one of the compression load tests is shown in Fig. 7. The load tests and results were described in Wey, et al. (2017). Pile load tests were conducted on site with the sacrificial helical piles matching the size and configuration used for the final design on the project. After load testing, the reaction piles and helical test piles were removed by unscrewing the piles and backing them out of the ground. Remaining holes were backfilled from the surface. In general, the installation depth and final torque matched design predictions very well. Load tests confirmed pile capacity and the capacity to torque ratio.

INSTALLATION

Helical piles were installed by Cajun Deep Foundations, LLC of Baton Rouge, Louisiana with a CAT 323F excavator equipped with a two speed, 110,000 ft-lb Digga torque motor and a Digga jib attachment for added reach. Despite challenging conditions, overhead constraints, and access restrictions, the contractor was able to install an average of 15 piles per work day. Helical pile sections ranged from 15 feet with no overhead restrictions to as short as 4 feet where low overhead conditions prevailed. Helical pile sections were bolted together. All piling materials were manufactured by Magnum Piering, Inc. of Cincinnati, Ohio and trucked to the site in weekly recurring shipments. Approximately 1,200 piles were installed.



Fig. 7. Compression Load Test (Courtesy of Magnum Piering, Inc.)

Photos showing examples of the challenging installation conditions are contained in Figures 8 through 10. The image in Fig. 8 shows the installation machine set outside of the pipe rack area with jib arm reaching between existing braces to the pile location below. The image in Fig. 9 shows the same installation machine reaching over an existing low pipe rack and alongside the existing taller pipe rack. The image in Figure 10 shows the hydraulic machine parked under the existing pipe rack and installing a pile within inches of an array of vertical pipes.

Installation torque was measured using a redundant system consisting of a wireless in-line torque sensor and differential hydraulic pressure. Torque and depth readings were obtained every 3 feet during installation. On occasions where the installation torque was close to the required final torque at the anticipated depth, the piles were rested for 3 days or more and then re-torqued. Most conventional helical piles with slender shaft do not exhibit pile freeze except in sensitive clays (Perko, 2009). Pile freeze is defined as an increase in capacity with time caused by changing effective stress. Pile freeze is predominantly due to soil displacement and pore pressure generation during installation. Slender shaft helical piles are a low-displacement pile. On this project, the helical piles did exhibit significant pile freeze most likely caused by the large diameter upper casing and moderately long shaft. Anecdotal evidence from field inspectors suggests pile freeze was generally on the order of 25 to 50% and sometimes as large as 100% of the final installation torque.



Fig. 8. Limited Access Helical Pile Installation (Courtesy of Cajun Deep Foundations, LLC)



Fig. 9. Cross Equipment Helical Pile Installation (Courtesy of Cajun Deep Foundations, LLC)



Fig. 10. Confined Area Helical Pile Installation (Courtesy of Cajun Deep Foundations, LLC)

CONCLUSIONS

This paper regards a case study of a recently completed onshore pipe rack revamp project in the United States in a hurricane prone region. A number of conclusions were presented in Wey, et al. (2017) including factors that make helical piles beneficial in existing refineries namely low overhead restrictions, contaminated soils, construction schedule, and restrictions with importing materials. That paper explained how the design team accurately predicted pile head deflections under axial and lateral loads. The importance of maintained load tests also was discussed.

In this paper, steps were taken by the design team to develop pile termination criteria. Specifically, capacity to torque ratio was derived for a composite shaft helical pile by adding the anticipated torque of the upper casing to the empirical torque required for the lead section. Load tests confirmed pile capacity and the capacity to torque ratio. The piles on this project exhibited significant pile freeze. Helical piles that did not reach required torque during initial installation at the design depth were successfully re-torqued.

Use of helical piles to support large refinery equipment has been slow to acceptance due to the lack of history and experience. Case studies are needed to support use of large helical piles for refinery work. A greater understanding of the expected settlements under operating loads and long-term resistance to corrosion will help decision makers feel more comfortable with the choice of helical piles for refinery work.

REFERENCES

Cherry, J.A. and Perko, H.A. (2013) "Helical Pile Deflection and Reliability", DFI Magazine, Jan/Feb Edition, New Jersey

ICC Evaluation Services, Inc. (2016) "AC358 Acceptance Criteria for Helical Foundation Systems and Devices", International Code Council, Wittier, CA

Perko, H.A. (2009) *Helical Piles: A Practical Guide to Design and Installation*, Wiley & Sons, New York

Wey, E., Murray, P., Perko, H., Mondoy, M. and Volpe, P. (2017) "Custom Helical Pile Use for Refinery Revamp: A Case Study", Proceedings of the SEI Structures Congress, Denver, CO, Structural Engineering Institute, ASCE Press, Reston, VA

INTERPRETATION OF SEISMIC RESPONSE DATA FROM FULL SCALE HELICAL PILE TESTS

ElSawy[1], M.K., El Naggar[2*], M.H., Heidari[3], M., Cerato[4], A.B., Elgamal[5], A.

[1] Dept. of Civil and Environmental Engineering, Western University, London, ON, Canada.
Email: melsawy@uwo.ca
[2] Dept. of Civil and Environmental Engineering, Western University, London, ON, Canada.
Email: naggar@uwo.ca
[3] Dept. of Civil and Environmental Engineering, Western University, London, ON, Canada.
Email: msarvest@uwo.ca
[4] School of Civil Engineering and Environmental Science, University of Oklahoma, Norman, OK, United States. Email: acerato@ou.edu
[5] Dept. of Structural Engineering, University of California – San Diego, CA, United States.
Email: aelgamal@ucsd.edu
*Corresponding author

ABSTRACT

Helical piles are gaining popularity as foundations for new construction as well as retrofitting option for deficient foundations. More recently, large diameter helical piles are used to support structures in regions characterized with high seismic hazard. Even though they have proven to be viable in seismic areas such as New Zealand, where they experienced little damage during the Christchurch earthquake, the knowledge about their seismic analysis and performance is largely lacking. Therefore, there is a need for comprehensive study to evaluate their performance under seismic loading. The current objective of this study is to investigate the performance of helical piles through a full-scale testing program that was performed at the NEES/UCSD Large High Performance Outdoor Shake Table (LLHPOST). The experimental setup involved ten steel piles of different configurations installed in dry sand. The piles were loaded with different masses and were subjected to different earthquake signals to simulate different dynamic behavior. This paper compares the performance of different moment curve fitting methods used to interpret the test data. Furthermore, the effects of different frequency content of loading on the pile response is illustrated in terms of deflection along the shafts of tested piles with different configurations.

Keywords: full-scale, seismic, helical pile

 © 2017 DFI Annual Conference, New Orleans, LA, USA

INTRODUCTION

Earthquakes are a major hazard for structures situated in seismic regions, and dynamic loading must be a design consideration. Successful design of a foundation system entails providing a safe and economic foundation solution to resist earthquake loading. Different foundation options have been used to support buildings in high seismic regions. Helical piles represent a viable foundation option that offers several advantages in terms of ease of installation, lower cost and environmental impact, ability to approximate the axial capacity directly from torque readings and more (Perko 2009). However, they are not typically considered as an option in many seismic regions. Meanwhile, several buildings supported on helical piles in New Zealand have survived the Christchurch earthquake with negligible damage, which encourages performing further research to understand the behaviour of these piles under seismic loading.

A helical pile consists of a steel shaft fitted with a steel helix/helices. The helical pile is installed by applying torque to its head via mechanical torque. Nowadays, helical piles are used in a wide range of applications such as foundations for light posts and residential houses. The static behaviour of helical piles has been studied extensively and is relatively well understood (Tsuha and Aoki 2010; Mittal et al. 2010; Sakr 2011; Elsherbiny and El Naggar 2013; El Sharnouby and El Naggar 2012; Elkasabgy and El Naggar 2015; Weidong et al. 2015 and Bagheri and Naggar 2015) However, the dynamic and seismic behaviours of helical piles is seldom investigated (Elkasabgy and El Naggar 2013). This underscores the knowledge gap currently present regarding the seismic behaviour of helical piles.

Different experimental techniques have been used to investigate the dynamic and/or seismic behaviour of piles. El-Marsafawi et al. (1992), Burr et al. (1997) and Fleming et al. (2015) have applied dynamic loading at the pile head using an oscillator in their studies of small scale model piles installed in the field. However, these tests may not represent realistic earthquake loading conditions. Scott et al. (1982), Prevost and Scanlan (1983) and Ting and Scott (1984) tested model piles installed in a small laminar box mounted on a geotechnical centrifuge and subjected them to dynamic loading. Certain assumptions taken while performing scaled-down testing may lead to difficulties in the interpretation of the results (Kagawa et al. 2004). Yasuda et al. (2000), Abe et al. (2004), Cubrinovski et al. (2006) and Sato et al. (2010) used full-scale shaking table tests to study the behavior of piles under seismic loading. Full-scale testing using a shake table provides the closest representation of piles' behaviour during an earthquake event.

OBJECTIVES

A total of ten steel piles were subjected to two real ground motions with different frequency content and loading intensity at the Large High Performance Outdoor Shake Table (LHPOST). The main objectives of the current study are to assess the suitability of different moment curve fitting techniques available in the literature; determine the dynamic characteristics of the soil-pile systems tested using a white noise signal; and to investigate the effect of loading frequency on different pile configurations.

TEST SETUP

The LHPOST was used to perform the seismic tests. The soil was placed within a laminar shear box with a length, width and height of 6.7m, 3.0m and 4.7m, respectively. The sand used was well-graded (SW) and was compacted to approximately 100% relative density. Several blocks of concrete were attached to the pile heads to simulate the weight of a structure and produce different dynamic behaviours for the same physical property of the pile. Each pile was instrumented with a minimum of six pairs of strain gauges at

different elevations as shown in Fig. 1. The piles were installed with a minimum spacing centre-to-centre of 1.05 m along the direction of shaking and 1.0 m in the perpendicular direction. Ten steel piles were used in the test, but due to size limitations only six piles are considered here and their details are shown in Table 1.

Table 1. Details of different pile physical characteristics

Pile	Type	Length (m)	Helix level (m)	Helix diam. (m)	Outer diam. / Wall thickness (mm)	Mass (kg)
P1	Circular single helical	3.96	-3.40	0.254	88 / 5	770
P2	Circular single helical	3.66	-3.15	0.254	88 / 5	750
P3	Circular single helical	3.66	-3.15	0.254	88 / 5	780
P4	Circular double helical	3.66	-2.55 -3.15	0.203 0.254	88 / 5	750
P5	Driven	3.66	---	---	88 / 5	370
P6	Square single helical	3.66	-3.15	0.254	76 / 5	435

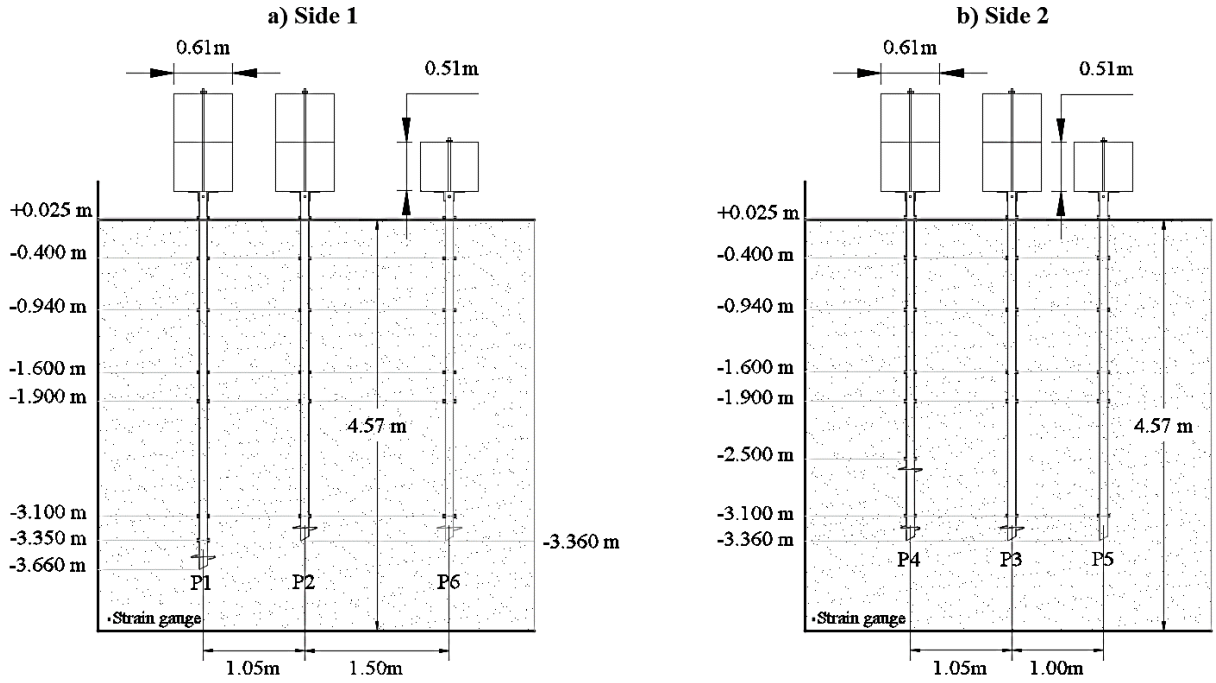


Fig. 1. Details of strain gauge and pile locations

TEST SCHEME

Two different loading schemes were adopted in this test: white noise and real ground motion records. The white noise is used to determine the dynamic characteristics of a system and should not cause any large deformations that may lead to non-linear behaviour. Two real ground motions records were used: The 1994 Northridge recorded in California and the 1995 Kobe earthquake recorded at Takatori. These two ground motions were also scaled to 75% and 50% to facilitate the comparison. Table 2 shows the peak acceleration in all ground motion records. Figure 2 shows the 5% damped response spectrum of the records used in the experiment. As can be noted from Fig. 2 a & b Northridge's spectral acceleration peaks at a period of 0.25s, while Takatori's spectral acceleration peaks at a period of roughly 1.3s.

Table 2. Peak acceleration for scaled ground motion records

Earthquake	Peak acceleration (g)		
	100% intensity	75% intensity	50% intensity
Northridge	0.50	0.37	0.25
Takatori	0.67	0.50	0.33

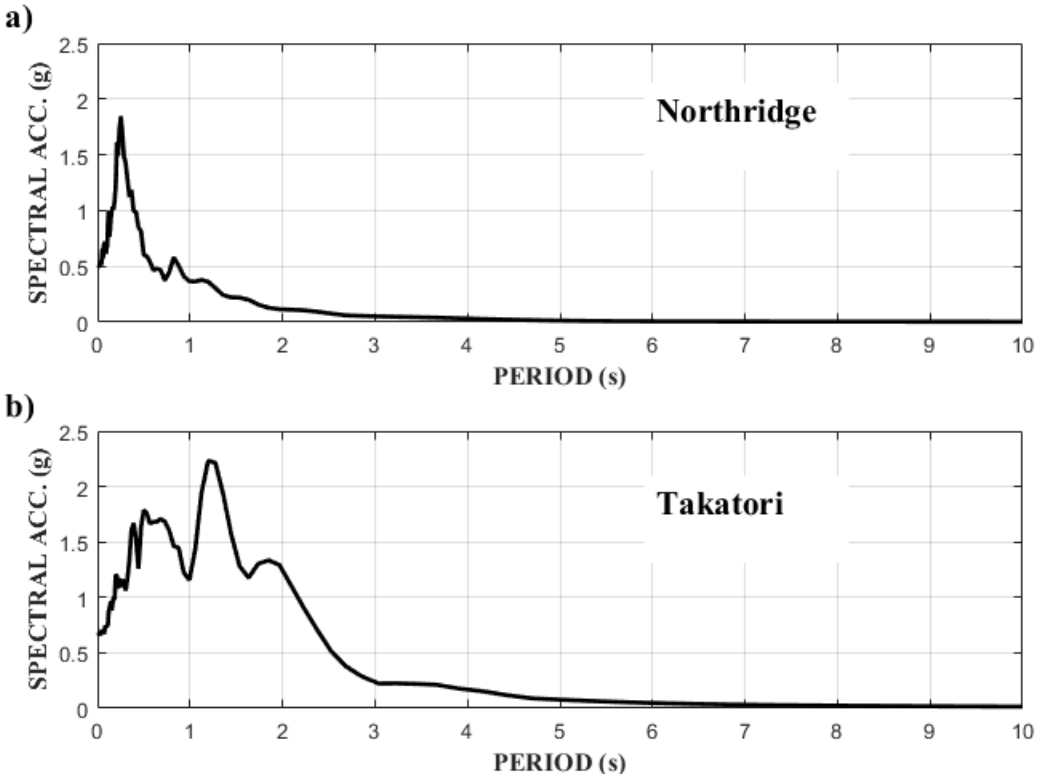


Fig. 2. 5% Damped Response spectrum a) Northridge b) Takatori

Interpretation of Strain gauge data

Strain gauges are an economic method of capturing pile response under earthquake loading. The moment at each pair of strain gauges at a given time step is as follows:

$$M(z)=\frac{E_p I_p(\varepsilon_1-\varepsilon_2)}{d_{out}} \quad [1]$$

Where E_p = elastic modulus of pile's material, I_p = second moment of inertia of pile's cross-section, $\varepsilon_1, \varepsilon_2$ = strain gauge readings at opposite sides of the pile cross-section, and d_{out} = distance between strain gauges. The pile lateral deflection can be obtained by double integration of the bending moment function as follows:

$$y_{pile}(z)=\iint \frac{M(z)}{E_p I_p} dz \quad [2]$$

Where z = depth along pile and $M(z)$ = moment curve fitted equation.

Before processing the raw data captured by the strain gauges, the data was filtered using a Butterworth filter to remove any unnecessary high frequency noise that might affect the results. Since strain gauge readings are available at discrete depths only, a curve fitting method was adopted to provide a mathematical formulation that can be integrated. Several curve fitting methods have been used in the literature for this purpose.

Moment curve fitting

Two main methods are available in the literature to curve fit the moment data points: Global polynomials and piece-wise polynomials (also known as splines). Several studies indicated that the curve fitting method should be selected with due consideration of the test and instrumentation setup used (Ting 1987; King 1994; Mezazigh and Levacher 1998; and Bouafia and Bouguerra 2006). To determine the method suitable for the current setup, lateral response analysis of a test pile was conducted using the computer code LPILE (Ensoft 2011). A pile with the same physical properties as the test pile was used and a lateral load was applied at the point corresponding to the center of the masses attached to the pile head. Moment readings were extracted at the elevations corresponding to the elevations of the strain gauges used; these readings serve as the "data points". These "data points" were used to produce the curve fitted moment profiles, which were then compared with the full moment profile calculated by LPILE. Also, the deflection profiles resulting from the integration of the curve fitted moment profiles were compared with the full deflection profile calculated by LPILE.

The performance of global polynomials and splines was evaluated. The global polynomials included all degrees starting from the 4th degree up to the 9th degree. The implemented splines were interpolation splines with two interior knots with degrees ranging from the 3rd degree up to the 5th degree. Due to the nature of splines that allows several formulations over the length of the pile, they showed superior performance when compared with global polynomials for all piles. Also the high degree global polynomials tend to suffer from Runge's oscillating phenomenon as the formulation approaches the tip of the pile where the readings are almost zero. Figure 3 shows the performance of the 9th degree global polynomial compared to the quintic (5th degree) interpolation spline for Pile 2. Runge's phenomenon is manifested in the big bump in the 9th

degree global polynomial curve that causes the deflection to contain large errors due to the numerical integration process. As can be noted from Fig. 3. quintic interpolation splines provide a good fit for both the moment and the deflection; thus the quintic interpolation splines method was used for all piles in this test.

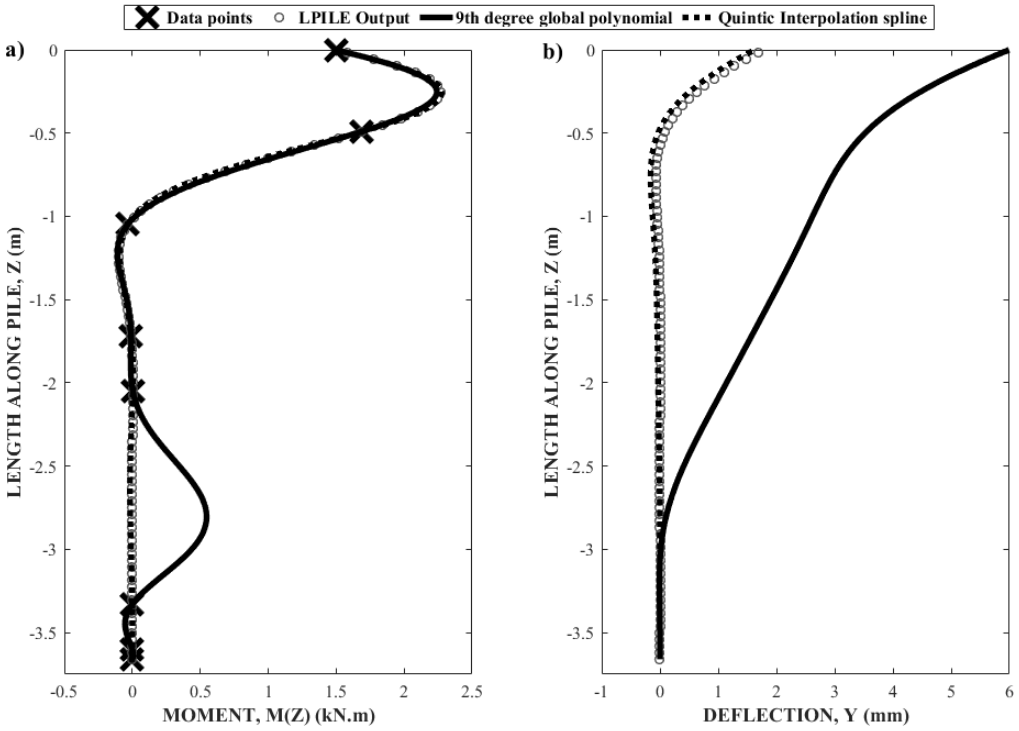


Fig. 3. 9th degree global polynomial versus Quintic (5th degree) interpolation spline for Pile 2. a) Moment b) Deflection

RESULTS AND DISCUSSION

Dynamic characteristics of soil-pile system

The strain gauges were used to determine the response of the soil-pile system due to the white noise signal. By analysing this response in the frequency domain using Fourier transform, the natural frequency of the pile-soil system could be attained. The results obtained from the Fourier transform were used to investigate the behaviour of each pile under the certain seismic events. Figure 4 shows an example of the Fourier transform output for Pile 3 due to white noise. All results in the frequency domain are presented in terms of period (as opposed to frequency) to be consistent with the ground motion signals. Table 3 presents the natural frequencies and periods of piles considered in this study.

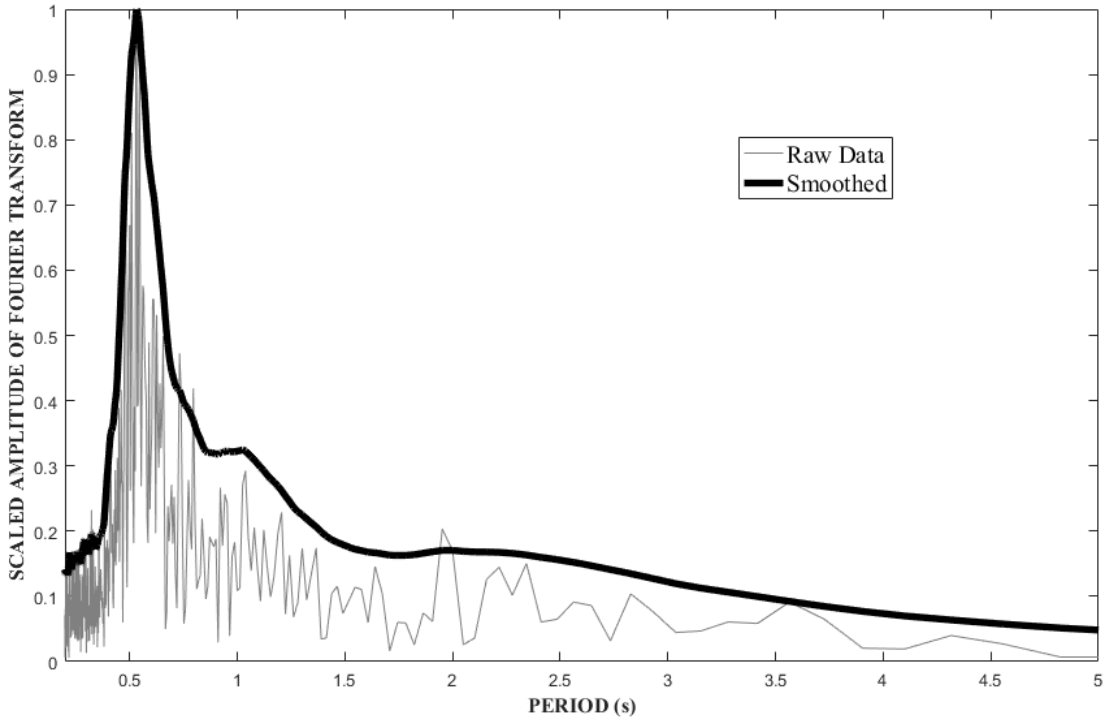


Fig. 4. Fourier transform of top strain gauge reading for Pile 3 due to white noise signal

Table 3. Dynamic characteristics of the pile-soil systems

Pile	Frequency (Hz)	Period (s)
1	2.12	0.47
2	2.34	0.43
3	1.87	0.53
4	2.05	0.48
5	4.09	0.24
6	3.42	0.29

Seismic response of the piles

The response of the pile is highly affected by the closeness of the loading period to the natural period of the soil-pile system. Inspecting the response spectra presented in Fig. 2, which indicates the response of a given system with a certain period to the ground motion, could aid in understanding the varying response of soil pile system to ground motions with different pre-dominant periods.

It is noted from Table 3 that the additional helix in Pile 4 has resulted in a higher period when compared with Pile 2. This indicates slightly more disturbance due to the second helix (Lutenegger et al. 2014). For all circular helical piles (Piles 1-4), the natural period ranged between 0.43s - 0.53s. According to Fig. 2, the period range (0.47s – 0.53s) is close to the predominant period of Takatori earthquake; therefore, all circular helical piles had a higher response compared to the driven and square shaft piles during Takatori. On the other hand, the driven and the square helical piles have a period of 0.24s and 0.29s respectively. This happens to coincide with the peak of Northridge; therefore, they had higher response during Northridge

earthquake. Figure 5 shows the response of Piles 2, 5 and 6 to two ground motions with equal peak ground acceleration but different frequency content; 100% Northridge and 75% Takatori.

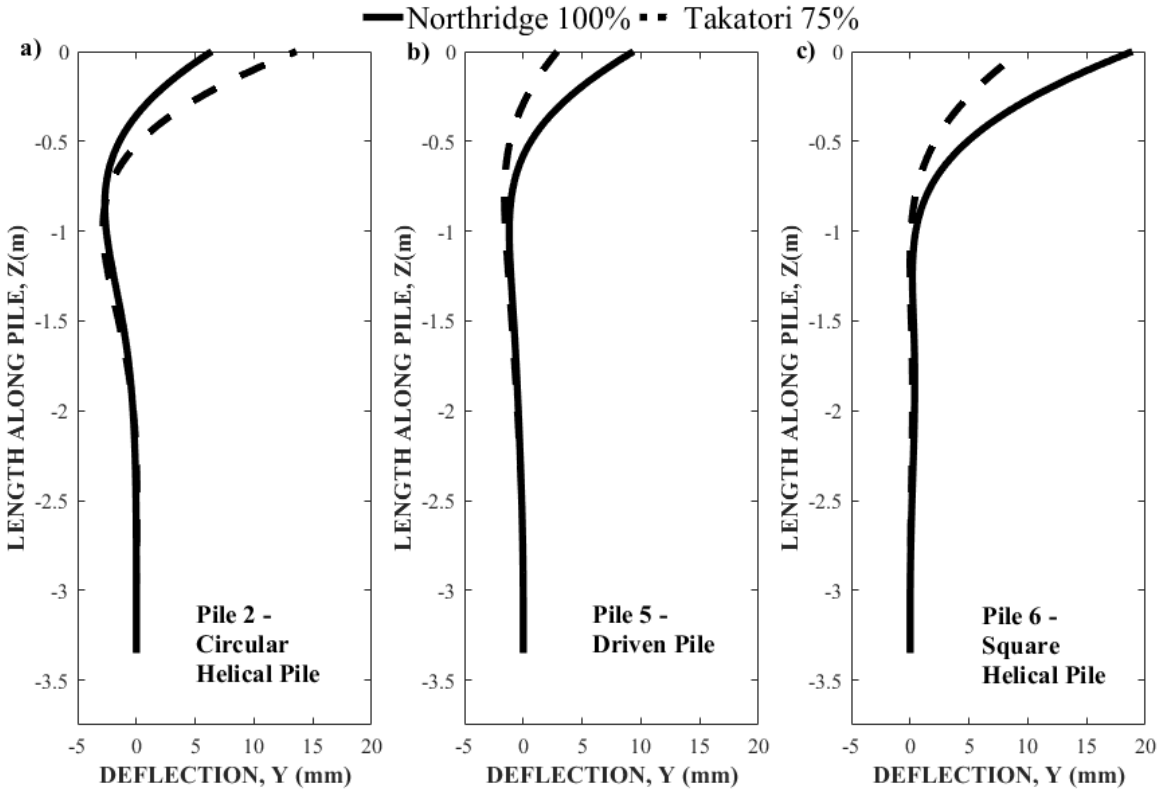


Fig. 5. Response to 100% Northridge and 75% Takatori a) Pile 2 b) Pile 5 c) Pile 6

CONCLUSIONS

A full-scale shaking table test has been conducted on ten steel piles with different configurations. The testing scheme included white noise signal and two real ground motions with different intensities and frequency content. The findings can be summarized as follows:

1. A simple moment curve fitting study was performed utilizing the response of the test piles evaluated from LPILE analysis. Although this method deals with theoretical "data points" containing no experimental errors, it provides an idea about what curve fitting technique suits the experimental setup used (number of strain gauges and locations). Splines outperformed global polynomials and were used to curve fit the tests moment data points for all piles.
2. The dynamic characteristics of the test piles were evaluated from their response to a white noise signal. The Fourier spectra results show that all circular helical piles had the same range of periods (0.47s – 0.53s) while the driven and square helical piles had lower periods of 0.24s and 0.29s, respectively. Depending on the closeness of the period of the soil-pile system to the predominant frequency of the ground motions, the response of the piles could be predicted.

ACKNOWLEDGEMENTS

The authors would like to express their great appreciation and gratitude to Helical Pile and Tiebacks Committee members through the Deep Foundation Institute's (DFI) Special Projects Fund, as well as the grant by the National Science Foundation (NSF) (Grant No. 1624153). The authors would also like to thank Ram jack Foundation, Torcsill Foundations LLC, Magnum Piering, Hubbell-Chance, and AMSquared Construction for transporting, donating and installing the piles and masses. Finally, the authors would like to recognise the huge efforts of all NEES/UCSD shaking table facility staff.

REFERENCES

Abe, A., Meneses, J., Sato, M., and Mohajeri, M. 2004. Near-full scale testing and analysis of saturated sand-pile interaction under earthquake condition. *In* Proc. 13th World Conference on Earthquake Engineering, Paper. pp. 1–6.

Burr, J.P., Pender, M.J., and Larkin, T.J. 1997. Dynamic response of laterally excited pile groups. Journal of geotechnical and geoenvironmental engineering, 123(1): 1–8. American Society of Civil Engineers.

Cubrinovski, M., Kokusho, T., and Ishihara, K. 2006. Interpretation from large-scale shake table tests on piles undergoing lateral spreading in liquefied soils. Soil Dynamics and Earthquake Engineering, 26(2–4 SPEC. ISS.): 275–286. doi:10.1016/j.soildyn.2005.02.018.

El-Marsafawi, H., Han, Y.C., and Novák, M. 1992. Dynamic experiments on two pile groups. Journal of geotechnical engineering, 118(4): 576–592. American Society of Civil Engineers.

Fleming, B.J., Sritharan, S., Miller, G.A., and Muraleetharan, K.K. 2015. Full-Scale Seismic Testing of Piles in Improved and Unimproved Soft Clay. Earthquake Spectra, 32(1): 239–265. Earthquake Engineering Research Institute. doi:10.1193/012714EQS018M.

Prevost, J.H., and Scanlan, R.H. 1983. Dynamic soil-structure interaction: centrifugal modeling. International Journal of Soil Dynamics and Earthquake Engineering, 2(4): 212–221. Elsevier.

Sato, M., Tabata, K., and Abe, A. 2010. Large-Scale Shake Table Test On Lateral Spreading Of A Sheet-Pile Wall Model And Its Centrifuge Simulation. International Conferences on Recent Advances in Geotechnical Earthquake Engineering and Soil Dynamics,. doi:10.2208/jscejc.65.834.

Scott, R.F., Tsai, C.F., Steussy, D., and Ting, J.M. 1982. Full-scale dynamic lateral pile tests. *In* 14th Annual Offshore Technology Conference. pp. 435–450.

Ting, J.M., and Scott, R.F. 1984. Static and Dynamic Lateral Pile Group Action'. *In* 8th World Conference on Earthquake Engineering. pp. 641–648.

Yasuda, S., Ishihara, K., Morimoto, I., Orense, R., Ikeda, M., and Tamura, S. 2000. Large-scale shaking table tests on pile foundations in liquefied ground. *In* Proc., 12th World Conf. on Earthquake Engineering.

DULLES METRORAIL/SILVER LINE (PHASE 2) DRILLED SHAFT LATERAL LOAD TESTING PROGRAM

William Billiet, PE, Schnabel Engineering, Rockville, Maryland, USA, 301-417-2400, wbilliet@schnabel-eng.com

ABSTRACT

The Dulles Silver Line Phase II is an 11.4 mile extension of the Washington Area Metro Transit Authority's Silver line in northern Virginia. There are three miles of elevated guideway, which are supported on 188 large diameter mono-shafts founded within the Triassic Geologic Aged Culpeper Fault Basin. Three lateral load tests were performed on fully instrumented test shafts. The challenge in developing the load testing program was how to reproduce the effects of the extremely high design loads along the test shafts, considering the limitations of the load test equipment. Development, execution, and analysis of the lateral load test program is discussed.

INTRODUCTION

Plans for Dulles Silver Line Phase II include two Aerial Guideway sections on elevated track, the Main Line and Yard Leads. The Aerial Guideways are supported on mono-shafts (single, large-diameter drilled shafts) socketed into rock. Lateral loads are resisted primarily through the stiffness of the shaft and the geotechnical resistance of the rock socket. The monoshafts were designed in accordance with AASHTO LRFD 2014. Based on our preliminary analyses, the production mono shafts were expected to consist of 6.5, 7.5, and 8.5 foot diameter drilled shafts with rock socket lengths varying between 8 and 34 feet (averaging 14 feet). Table 1 summarizes the maximum service load combinations for each size production shaft along the aerial guideway alignment.

Table 1: Summary of Monoshaft Maximum Production Loads

Load Condition	Shaft Diameter (feet)	Axial Load (kips)	Shear Load (kips)	Moment (ft-kips)
1	8.5	3,750	300	15,000
2	7.5	3,600	165	8,500
3	6.5	3,200	110	5,000

GEOLOGY

The project is located within the Piedmont Province, a major physiographic province on the east coast of the USA extending from Alabama to Pennsylvania. Within the Piedmont, a number of Mesozoic basins formed in rift valleys. Dulles Airport is located in the Culpeper Basin, characterized by a relatively shallow siltstone rock surface compared to the adjacent areas underlain by Piedmont crystalline rocks. The geologic stratigraphy at the load test sites generally consist of residual soils and intermediate geo-material (IGM) overlying siltstone rock. IGM is a term used by Virginia Department of Transportation (VDOT) to describe residual material as it transitions between soil and rock. For the purposes of the load test, the siltstone rock is classified as fractured rock (RQD<50), and competent rock (RQD≥50). Table 2 summarizes the stratigraphy encountered at each test site.

 © 2017 DFI Annual Conference, New Orleans, LA, USA

Table 2: Stratigraphy at Load Test Sites

Test Site	Depth to IGM* (feet)	Depth to Fractured Rock* *(RQD<50)* (feet)	Depth to Competent Rock* *(RQD≥50)* (feet)	Comment
1	17	25	65.3	Deep Rock Site
2	8	--	10	Typical Site
3	4	--	7.5	Shallow Rock Site

**Depth below ground surface*

GEOTECHNICAL DESIGN PARAMETERS

RQD values for the siltstone rock cored at the load test borings range from 13 to 100 percent, generally increasing with depth. Uniaxial compressive strength (UCS) testing of rock samples from the load test borings indicates compressive strengths between 2,139 and 6,473 psi. Pressuremeter testing performed in each load test boring indicates pressuremeter moduli between 11,430 psi to 1,057,607 psi. Pressuremeter and UCS test results generally indicated higher values with depth and increased rock quality. Tables 3A and 3B provide the LPile parameters for soil and rock, respectively, that we used for preliminary design of the aerial guideway drilled shafts.

Table 3A: Soil and IGM LPile Parameters for Lateral Analysis of Drilled Shafts

Soil Type	LPile Material Model	Unit Weight (pcf)	Friction Angle	k value (psi)
Residual Soil	Sand (Reese)	130	32	60
IGM *(above GW table)*	Sand (Reese)	140	38	260
IGM *(below GW table)*	Sand (Reese)	140	38	150

Table 3B: Rock LPile Parameters for Lateral Analysis of Drilled Shafts

Rock Type	LPile Material Model	Unit Weight (pcf)	Uniaxial Compressive Strength (psi)	Initial Modulus of Rock Mass (psi)	RQD	Strain Factor k
Fractured Rock *(RQD < 50)*	Weak Rock	145	2,000	87,500	0	0.0005
Competent Rock *(RQD ≥ 50)*	Weak Rock	145	4,000	375,000	50	0.0005

LATERAL LOAD TEST

Conventional static lateral load testing was performed in accordance with ASTM D3966 on three test shafts to evaluate the lateral resistance properties of the rock sockets and to verify the P-Y curves of the rock and overburden used for preliminary design of the production monoshafts. P-

Y curves describe the deflection (Y) of the surrounding soil and rock in response to the lateral pressure (P) imposed on it by the shaft.

Program Development

The lateral load test program was developed so the mobilized rock socket responses within the test shafts would be similar to the maximum mobilized rock socket responses in the heaviest loaded production monoshaft. The LPile computer program was used to evaluate the maximum mobilized rock socket response expected from an aerial guideway monoshaft under combined production loading conditions (axial, shear and moment). The LPile models estimate the bending moments, shear forces, and deflections along the length of the lateral test shafts under the combined loading, as well as the stiffness of the composite shaft model and the response of the surrounding soil and rock socket.

The LPile models were created with the same properties of the concrete, reinforcing steel, and permanent steel casing expected to be used in the production shaft construction, and considered the actual stratigraphy at each test site as well as the preliminary soil and rock design values provided in Tables 2, 3A and 3B.

Table 4 presents the depth and magnitude of the maximum mobilized response expected from the heaviest loaded production monoshaft at each of the three load test sites. The mobilized response is normalized for the shaft diameter and is described in terms of lbs/in to represent the total force in pounds imposed by a 1-inch long segment of shaft onto the rock socket.

Table 4: Predicted Lateral Response of Monoshafts to Maximum Production Loads

Test Site	Shaft Diameter (feet)	Load Condition (from Table 1)	Maximum Mobilized Response (lbs/in)	Depth to Maximum Response* (feet)	Depth to Top of Rock Socket* (feet)
1	8.5	1	73,600	25.0	25.0
2	8.5	1	110,100	10.5	10.0
3	8.5	1	92,000	10.5	7.5

**Depth below ground surface*

Replicating the production monoshaft response in the test shafts presents a significant challenge. Because the load cell only applies a shear (lateral) force to the test shafts, a larger test load is required to obtain a similar response in the test shaft rock sockets as a monoshaft rock socket acting under combined shear and moment production loading conditions. As the test shaft diameter becomes larger, increasing test loads are necessary to replicate the response within the rock socket, which can present challenges in designing a safe jacking system. Smaller shaft diameters can require excessive amounts of reinforcing steel to be stiff enough to transmit the lateral loads to the rock socket without yielding. Through an iterative evaluation process, 6 foot diameter test shafts were selected with a maximum test load of 1,100 to 1,200 kips.

We estimated the maximum rock socket response during the load test by creating LPile models of each test shaft considering the maximum test loads. The LPile models were created with the

properties of the concrete, reinforcing steel, and steel casing used to construct the test shafts, and considered the stratigraphy and preliminary soil and rock design parameters described above. Table 5 summarizes the results of the LPile analysis on each test shaft.

Table 5: Predicted Lateral Response of Test Shaft to Maximum Test Loads

Test Site / Test Shaft	Maximum Lateral Test Load* (kips)	Top of Shaft Deflection (inches)	Maximum Moment (in-kips)	Depth to Maximum Moment** (feet)	Maximum Mobilized Response (lbs/in)	Depth to Maximum Response** (feet)
1	1,101	1.9	172,400	20.0	83,200	26.0
2	1,117	0.6	135,800	10.8	109,800	11.2
3	1,126	0.4	104,700	8.5	93,500	10.5

** Adjusted to reflect actual test load*
*** Depth from ground surface*

Comparing the mobilized responses provided in Tables 4 and 5, the maximum responses of the test shaft rock sockets under the test loads are similar to the maximum response of the larger diameter monoshaft rock sockets under the maximum production loading condition, indicating the test loads are appropriate for the size of the test shafts. The actual pressures in the test shaft rock sockets will be higher than in the monoshafts for a similar mobilized response, since the mobilized response in the monoshafts are distributed across a larger diameter.

Test Shaft Construction

At each test site, two 6 foot diameter drilled shafts were installed to depths of 27.0 to 49.9 feet below the ground surface. One shaft at was fully instrumented and served as the test shaft, while the other shaft was used as the reaction shaft and was not instrumented. The section of the shafts above the rock sockets were fully cased with 5/8-inch thick 72-inch inside-diameter Grade 36 permanent steel casing. The casing was screwed into place after excavating to the top of rock and was left ungrouted. The top of the shafts and their casing extended about four feet above surrounding grade. The rock socket lengths were chosen so the base of the test shafts would be fixed with respect to lateral movement under the ultimate test load. Table 6 provides key as-built dimensions and properties of each test shaft.

Table 6: As-built Lateral Load Test Shaft Dimensions

Test Shaft	Depth to Top of Rock Socket* (feet)	Depth to Bottom of Shaft* (feet)	Total Rock Socket Length (feet)	Total Test Shaft Length** (feet)	% Reinf. Steel	Est. Test Shaft Concrete Strength on Test Day (psi)
1	25.0	49.9	24.9	53.9	3.7%	5,500
2	10.0	30.0	20.0	34.0	3.2%	3,700
3	7.5	27.0	19.5	31.0	2.1%	6,700

** From the ground surface*
*** From top of shaft (4-ft above the ground) to bottom of shaft*

The strains and deflections along the length of each test shaft were measured with a pair of strain gauge arrays and an array of inclinometer sensors placed during installation of the shaft. The strain gauges were distributed at two to four foot intervals in each array along the length of the test shafts. The strain gauge arrays were placed symmetrically along the far and near side of the test shaft reinforcement, respectively, in the direction of lateral loading, to allow measurement of strain along the extreme compression and tension members. The inclinometer arrays consisted of in-place inclinometers running the full length of the shafts along their neutral axis, and were spaced at approximately 2 feet intervals.

Load Test Execution

The lateral load tests were performed by pushing the test shafts away from their adjacent reaction shafts using a hydraulic load cell. The test loads were gradually increased in increments until reaching the ultimate test load (1,101 to 1,126 kips) in accordance with ASTM D3966. After maintaining the ultimate test loads for 60 minutes, the test loads were removed in four increments.

The load cells applied the lateral test loads to the sides of the test shafts at the ground surface elevation, about 4 feet below the top of the test shafts. The loads were measured by load cells positioned adjacent to the jacks. In addition to the inclinometer arrays, top of the shaft movement were independently measured using displacement transducers mounted to reference beams. All instruments were measured and recorded digitally during both the loading and unloading sequence.

LATERAL LOAD TEST RESULTS AND ANALYSIS

At the conclusion of the load tests, the instrument data was reduced and validated for analysis. Inclinometer data readings were compared to readings from the displacement transducers and adjusted for bias and error. The inclinometer data indicated the base of the test shafts remained fixed under the ultimate test loads. Strain gauge readings were reviewed and outliers were eliminated from the analysis. Because the diameter of the test shafts are similar to the monoshafts (6.5-ft, 7.5-ft, & 8.5-ft), no scaling factors were not used when applying these values to the aerial guideway drilled shafts.

Shaft Deflections

The deflections within all the rock sockets measured by the inclinometer arrays are the same or slightly less than those predicted by the LPile models, at all test loads. Top of test shaft deflections varied from 0.6 inches to 1.8 inches under the maximum test loads. Figure 1 below shows the shaft deflections vs. depth.

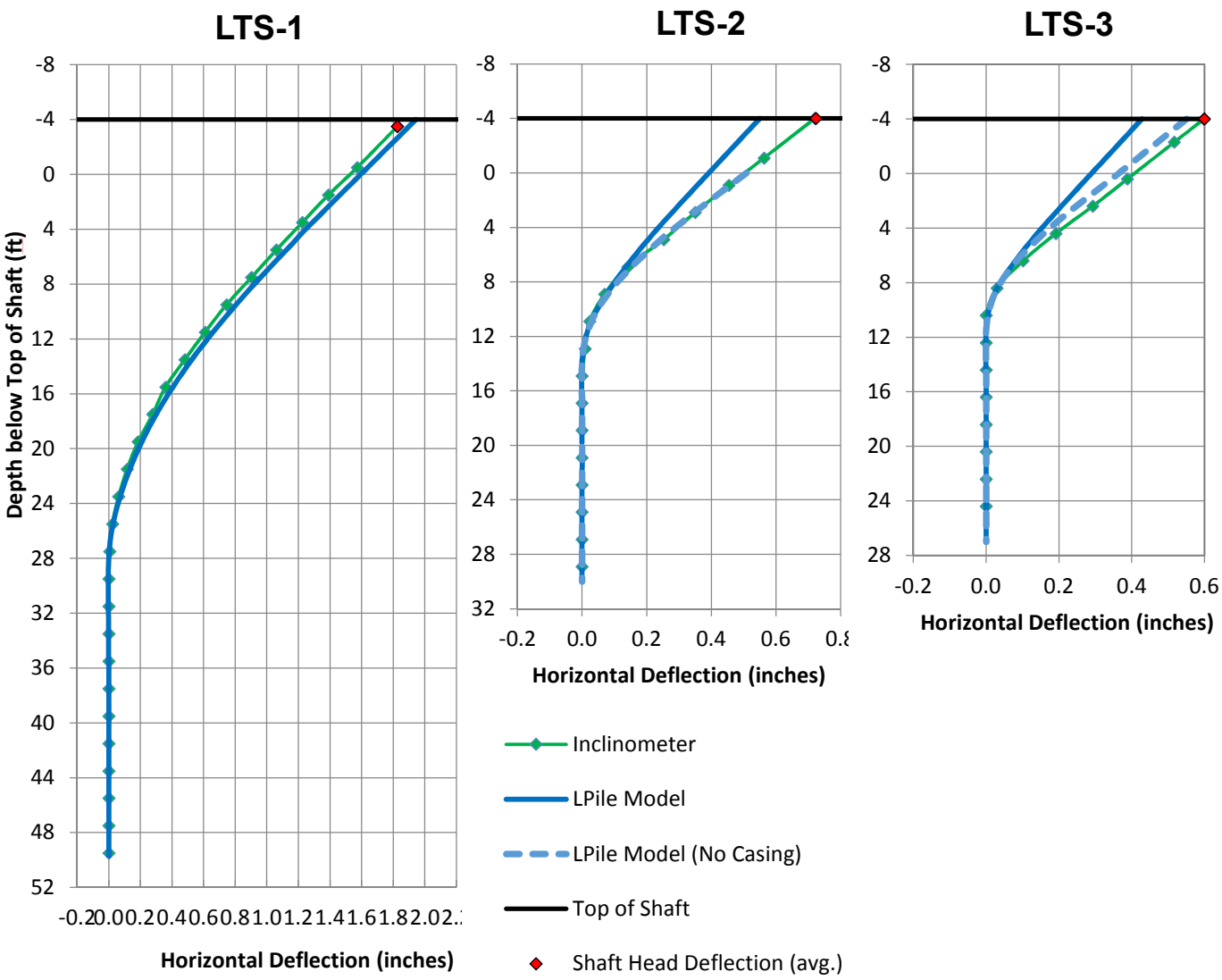


Figure 1: Horizontal Shaft Deflection vs. Depth for Test Shafts

Table 7 provides the top of shaft deflection data for each test and reaction shaft under its ultimate testing load. These measurements were recorded at the top of shaft, four feet above the ground surface.

Table 7: Lateral Test Shaft Top-of-Shaft Deflection Comparison

Test Site	Test Shaft ID	Maximum Lateral Test Load (kips)	Depth to Top of Rock Socket* (feet)	Top of Shaft Deflection At Maximum Test Load**		
				LPile Model (inches)	Test Shaft (inches)	Reaction Shaft (inches)
1	LTS – 1	1,101	25.0	1.9	1.8	2.2
2	LTS – 2	1,117	10.0	0.6	0.7	0.6
3	LTS – 3	1,126	7.5	0.4	0.6	0.6

** Depth from ground surface, ** At top of shaft, 4-ft above the ground surface*

The test shaft deflections predicted by the LPile models are generally in good agreement with the actual deflections measured during the load tests. The top of test shaft LTS-1 deflected about 0.1 inches less than the LPile model predicted, while test shafts LTS-2 and LTS-3 deflected about 0.1 and 0.2 inches more, respectively, than predicted.

Differences in deflections between associated test and reaction shafts were attributed to slight variations in shaft stiffness, load application, casing length, and depth to the top of rock between the test and reaction shafts. The differences in deflection were not caused by the overburden or IGM stiffness, which had little effect on the deflection of the shaft since the material is so much weaker than the shaft and rock socket, particularly at LTS-3 and LTS-3 where rock was relatively shallow. The analyses indicate the soil and IGM above the rock socket do not significantly affect the shaft deflections until the top of the rock socket is greater than 15 feet deep.

The additional deflections measured in LTS-2 and LTS-3 appears to have occurred at the bottom of the cased portion of the test shafts, just above the rock socket. Closer analysis reveals these shafts may have yielded near the bottom of the casing at higher test loads. This is supported by the high strain gauge readings recorded near the bottom of casing. Plastic yielding of the extreme tension reinforcement would cause a localized increase in curvature in the shaft at those elevations and would explain the higher than expected deflection at the top of shaft.

LTS-2 and LTS-3 had greater than expected deflection at the top of shaft even at lower test loads where the shafts had not yielded. The cased portion of these shorter shafts may not have behaved compositely as LPile predicted. The casings for LTS-2 and LTS-3 are installed to depths of 7.8 and 10 feet, extending only 1.3 and 1.7 times the shaft diameter, respectively, below the load application. If the casing did not to act compositely (i.e. if the casing slipped along the edges of the shaft as bending occurred), the actual stiffness of the shaft would be less than predicted and the cased portion of the shaft would exhibit greater curvature and deflections than predicted by the LPile model.

Shaft Bending Moments

The bending moments in the test shafts were estimated by fitting a cubic polynomial to the deflection data recorded by the inclinometer arrays and twice differentiating it with respect to depth using the beam equation:

$$M = EI\frac{d^2y}{dx^2} \qquad [1]$$

Where M = moment, EI = composite staff stiffness (from LPile model), x = depth, and y is the horizontal deflection of the shaft.

The measured bending moments were compared to the bending moments predicted by the LPile models. Table 8 compares the magnitude and depth of the maximum bending moments predicted by our LPile models to our estimates of the actual moments in the test shafts. In general there is good agreement with the general shape and maximum depth of the bending moments between the test shafts and LPile models.

Table 8: Lateral Test Shaft Maximum Bending Moment Comparison

Test Site	Test Shaft ID	Maximum Lateral Test Load (kips)	LPile Model		Test Shaft	
			Maximum Moment (in-kips)	Depth (ft)	Maximum Moment (in-kips)	Depth (ft)
1	LTS – 1	1,101	172,400	20.0	152,100	24.0
2	LTS – 2	1,117	135,800	10.8	128,000	11.5
3	LTS – 3	1,126	104,700	8.5	118,500	7.5

The bending moment was also evaluated with the strain gauge data by determining the position of the neutral axis and the resulting forces on the rebar in the tension zone and concrete in the compression zone for the following equation:

$$M = \sum Fx(R - Yx) \quad [2]$$

Where Fx = forces on the rebar or concrete, R = distance from the centroid to the end of the shaft, and Yx = the distance of the section of the edge of the shaft.

In general, the bending moments observed in the test shafts were in good agreement with those predicted by the LPile model, except at the depth of maximum moment, where we expect there may be significant error in the readings.

The bending moments calculated from the strain gauge data generally agreed with the bending moment calculated from the inclinometer data and LPile model, albeit with significant variability, particularly at the top of the rock socket in LTS-2 and LTS-3 where rock is most shallow. This variability is caused by several factors. The strain gauges are very sensitive to their depth, relative position of the (variable) neutral axis, and the actual distribution of cracking along the tension portion of the shaft. Slight variations in any of the above could significantly affect the localized strain readings and exaggerate the measured level of strain and derived bending moment. Under ideal conditions, the strain gauges will provide a measurement of the strain across a very small area at the center of the gauge. However, the strain gauges are mounted to 3 foot long sister bars. In the vicinity of the bottom of the casing, near the maximum bending moment, the bending moment changes sharply with depth. Slight differences in the engagement length or effective engagement depth of the sister bars could result in significant variations in the calculated bending moment. Furthermore, as the bending of the test shaft increases, the concrete within the tension zone begins to crack. Where a strain gauge spans a crack, the resulting strain reading could record a much larger strain. Therefore we expect the calculated bending moments from the strain gauge data to show greater variance in the vicinity of the maximum moment (near the bottom of casing). The bending moments within the test shafts are also highly dependent on the stiffness of the shafts. Small differences in the stiffness of the shaft significantly affects the calculated bending moment. If the casing did not act compositely in test shafts LTS-2 and LTS-3, the actual bending moment for any strain level could therefore vary greatly.

Mobilized Rock Socket Resistance

The mobilized responses in the test shafts were estimated by differentiating the shaft deflection data in the inclinometer array four times with respect to depth using the beam equation:

$$p = EI\frac{d^4y}{dx^4} \quad [3]$$

Where p = pressure, EI = composite staff stiffness (from LPile model), x = depth, and y is the horizontal deflection of the shaft.

The maximum mobilized rock socket responses expected from the heaviest loaded production monoshafts were compared to the expected mobilized rock responses of the test shafts under the maximum test loads. We used our LPile models to estimate the mobilized resistance along the length of the test shafts. Because the measured test shaft deflection and bending moment distribution generally match our LPile models, we expect the LPile models provide a reasonable estimate of the mobilized rock response. Table 9 compares the maximum mobilized rock responses of our test shafts under their maximum test loads to an 8.5 foot diameter aerial guideway monoshaft under the heaviest production loading. Both conditions were modeled with the same stratigraphy for comparison purposes. The results indicate the test shaft rock sockets were mobilized to about the same level of resistance expected in the actual aerial guideway monoshafts.

Table 9: Lateral Test Shaft Maximum Mobilized Soil/Rock Response Comparison

Test Site	Test Shaft ID	Maximum Lateral Test Load (kips)	Maximum Mobilized Soil/Rock Response	
			Load Test Shaft (lbs/in)	Aerial Guideway Monoshaft (lbs/in)
1	LTS – 1	1,101	83,200	73,600
2	LTS – 2	1,117	109,800	110,100
3	LTS – 3	1,126	93,500	92,000

The precision of the back-calculated mobilized response is limited by the fact we are using the assumed LPile shaft stiffness model, and interpolating shaft curvature from an inclinometer array spaced at 2 foot intervals.

CONCLUSIONS

Shaft deflections, bending moment distribution and depth of maximum moment were in fairly good agreement with those predicted by our LPile models, demonstrating that the LPile model parameters for the bed rock are valid across the loading conditions expected from the aerial guideway monoshafts.

The top of the two shorter test shafts (LTS-2 and LTS-3) deflected more than predicted by the LPile model, particularly at larger test loads, however we expect this may have been caused by a combination of structural yielding of the shaft at the top of the rock sockets and the casing acting

non-compositely at higher test loads. We could not replicate the deflection curve of LTS-2 and LTS-3 at higher test loads, even when varying the properties of the bed rock or soil between their extreme values, unless we assumed the shaft structurally yielded. While the top of the shorter test shafts deflected more than predicted, deflections of the shaft within the rock sockets were less than predicted by our LPile models, even at the maximum test loads. Comparison of deflections and bending moments at test loads less than the maximum show even better agreement with the LPile models. This suggests the increased deflections observed in LTS-2 and LTS-3 were not caused by the rock socket performance, but rather the structural behavior of the shaft above the rock socket.

At the higher test loads, the LPile models predict the test shafts were loaded beyond their ultimate moment capacity. The strain gauge readings indicate that yielding of the tension steel occurred. Beyond the ultimate moment capacity, we expect the ability of LPile to accurately predict the top of the test shaft deflections would decrease. The portion of the test shaft above the rock was only used to transfer the test load into the rock socket. In addition, the 6 foot diameter test shafts were loaded similar to 8.5 feet diameter production shafts and lower factors of safety were used to design the reinforcing steel in the test shafts than will be used in the production shafts. Therefore structural yielding is not expected to occur in the aerial guideway monoshafts.

In general, the results of the load tests and our analysis indicate the depth to rock (top of socket) has the greatest effect on the performance of the shaft. Differences of less than 1-ft to the depth of rock will affect the deflection at the top of shaft more than varying the LPile design values for the rock between their extreme values. The load test results indicate the effect of the overburden soils and IGM on short shafts (10-feet or less to rock) are negligible and the response of the shafts are primarily controlled by the structural behavior of the shaft.

Because the tips of the test shafts are fixed in rock, the top of shaft deflections are very sensitive to the stiffness of the shaft. The load test results indicate when the base of the shaft is fixed in rock, the structural properties of the shaft appear to have a greater influence over their deflection than the elastic properties of the rock socket. This is demonstrated by the differences in top of shaft deflections between adjacent test and reaction shafts. The shafts have the same reinforcing steel cage and are installed in nearly identical geological conditions. Analyses show the difference in deflection between the test and reaction shafts is primarily due to slight differences in the depth to rock and depth of casing.

REFERENCES

Brown, Dan A., Turner, John P., and Castellie, J. Raymond. Drilled Shafts: Construction Procedures and LRFD Design Methods NHI Course No. 132014. Washington, D.C.: National Highway Institute, 2010.

Isenhower, William M., and Shin-Tower Wang. Technical Manual for LPile, Version 6. Ensoft, Inc., 2011.

Ooi, P. and Ramsey, T. (2003). "Curvature and Bending Moments from Inclinometer Data." *Int. J. Geomech.*, 10.1061/(ASCE)1532-3641(2003)3:1(64), 64-74.

Turner, John P. NCHRP Synthesis 360 Rock-Socketed Shafts for Highway Structure Foundations. Washington, D.C.: Transportation Research Board, 2006.

INSTRUMENTED HYBRID SHORING SYSTEM FOR A DEEP TEMPORARY EXCAVATION INCORPORATING CUTTER SOIL MIXING IN VANCOUVER, BC, CANADA

Marina S.W. Li, C.Eng., P.Eng., Isherwood Associates, Burnaby, BC, Canada, +1-604-428-7080, marina@iserwood.to
Nadir Ansari, P.Eng., D.GE., Isherwood Associates, Mississauga, ON, Canada, +1-905-820-3480, nadir@isherwood.to
Brian W. Wilson, C.Eng., P.Eng., Pacific Ground Engineering, Burnaby, BC, Canada, +1-604-205-6866, brian.wilson@norlandlimited.com

ABSTRACT

A hybrid shoring system consisting of cast-in-place soldier piles with Cutter Soil Mixing (CSM) infill panels was constructed for temporary support of a 19.8 m (65 ft) deep excavation in Vancouver, British Columbia, Canada. Deep Mixing (DM) was completed up to 9.7 m (32 ft) in fill, peat, wood waste and clayey silt with embedment in dense till, and soldier piles constructed through the dense till extending to below final excavation level. Two trial CSM panels were installed ahead of production to assist with developing the termination criteria of the CSM panels in the dense till. The constructed depth of the CSM panels was based on interpretation of real-time monitoring data obtained through the Bauer B-tronic system. Inclinometer monitoring data from two CSM panels and two soldier piles, as well as soldier pile survey target data was used to assess and monitor the performance of the hybrid shoring system throughout bulk excavation. The objectives of this paper are to provide an overview of the design and construction aspects of the hybrid DM shoring system and to present inclinometer and pile target data to demonstrate the lateral performance of the CSM infill panels and soldier piles. This paper also discusses the merits of using real-time monitoring data as part of the engineering decision-making process for validating CSM panel construction.

Keywords: hybrid shoring, deep mixing, cutter soil mixing, inclinometer monitoring, real-time monitoring.

BACKGROUND

A hybrid DM shoring design was recently completed for a high-rise development in downtown Vancouver, British Columbia for temporary support of a five level basement excavation. Deep mixing was proposed by the excavation and shoring design-build team as the preferred method to construct infill panels between soldier piles because of the speed at which the shoring system could be constructed in variable fill, peat, wood waste and overburden compared with traditional secant piling methods.

The development site is generally a truncated triangle in plan, with the longest side of the triangle being approximately 115.7 m (380 ft) long and the two shorter sides being approximately 71.6 m (235 ft) (Hybrid Shoring Wall 1) to 75.0 m (246 ft) (Hybrid Shoring Wall 2) long. The site is bounded by an existing bridge off-ramp structure along its longest side, and by city streets on the other two sides, as shown in Figure 1. The truncated section is approximately 16.8 m (55 ft) (Hybrid Shoring Wall 3) long. Due to project constraints, the hybrid DM and soldier pile shoring system was only proposed for the two shorter sides of the triangle and the truncated section. Traditional secant piles were installed for the longest side. This paper focusses on the hybrid shoring system. A typical detail showing the CSM infill panel with the soldier piles is presented in Figure 2.

A total of 57 No. CSM panels (2.8 m (9.2 ft) long by 1.0 m (3.3 ft) wide) were installed as part of the hybrid shoring system with depths ranging from 6.1 m (20 ft) to 9.7 m (32 ft) with an average depth of

 © 2017 DFI Annual Conference, New Orleans, LA, USA

approximately 9.0 m (29.5 ft). The CSM panels were generally installed to achieve a 0.5 m (1.6 ft) to 1.0 m (3.3 ft) embedment in dense till with a target design strength of 2.0 MPa (290 psi) at 56 days. A number of panels terminated on obstructions, typically consisting of nested cobbles and boulders and/or buried wood logs. The zone between the top of the obstruction and the top of the till was remediated by drilling a sequence of small diameter (178 mm (7 in)) holes down behind the CSM panel and grouting up the zone to the top of the till to limit groundwater ingress.

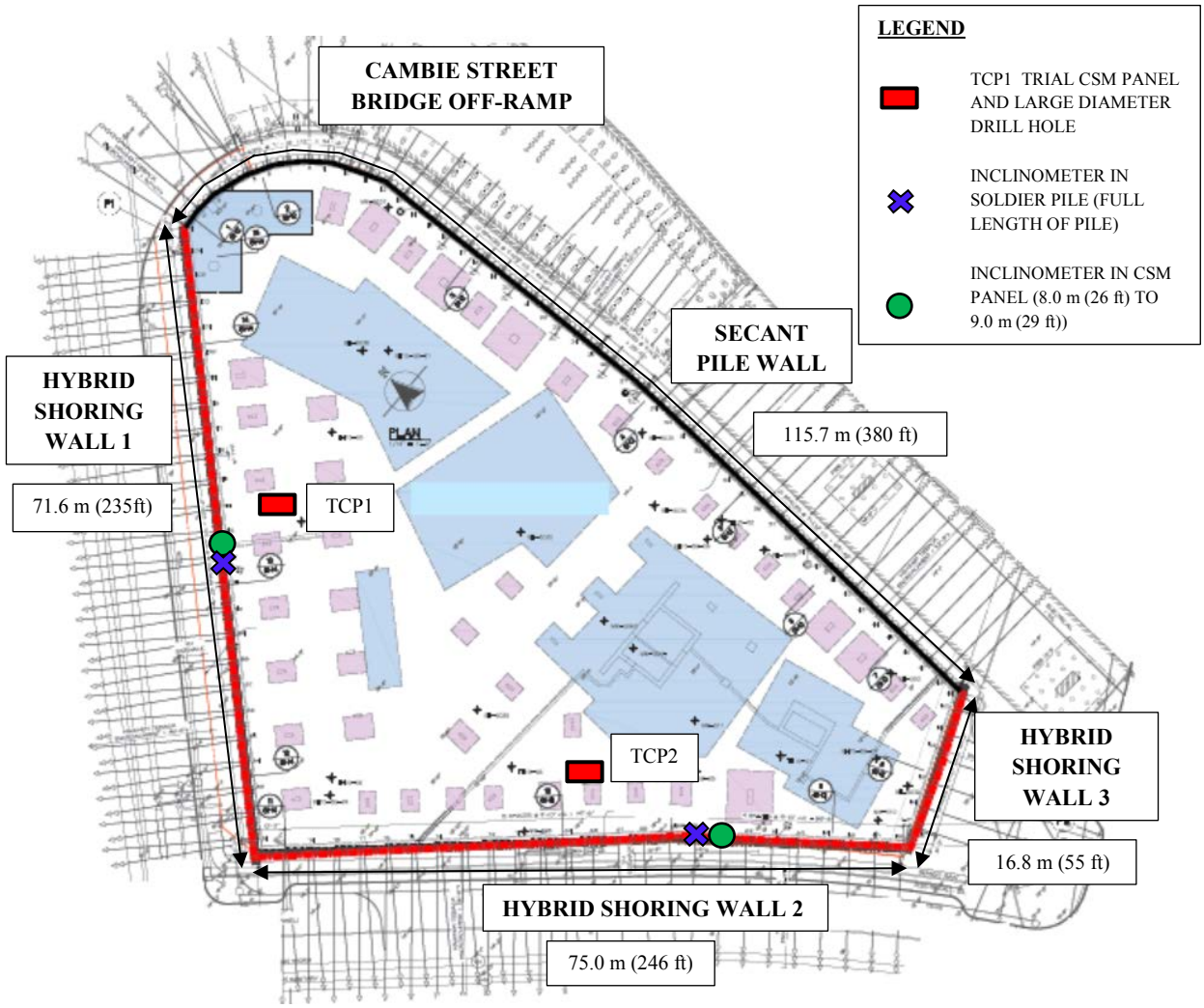


Fig. 1 General layout of proposed development showing location of hybrid shoring walls, trial CSM panels and inclinometers

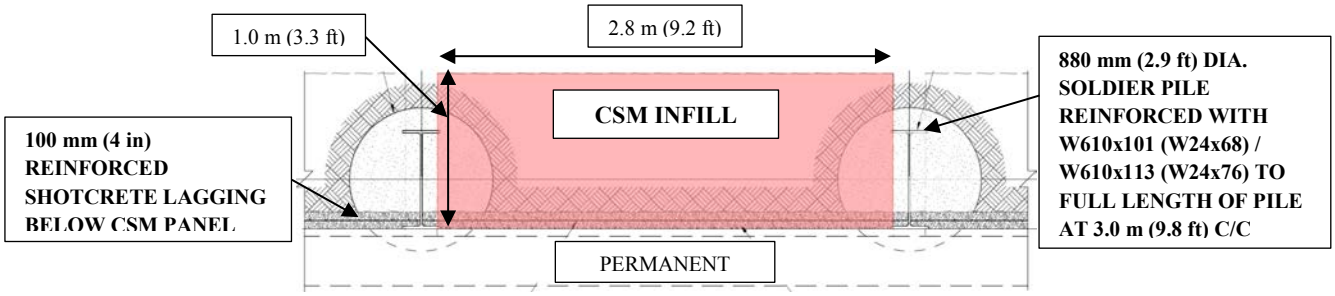


Fig. 2 Typical detail of CSM infill panel with soldier piles

The soldier piles supporting the CSM infill panels were 880 mm (2.9 ft) diameter piles situated at 3.0 m (10 ft) centres reinforced with W610X101 (W24X68) to W610X113 (W24X76) steel beams. The soldier piles extended through the till to between 3.5 m (11.5 ft) and 4.0 m (13.0 ft) below the ultimate base of excavation with reinforced shotcrete serving as lagging between piles below the base of the CSM panels.

HYBRID SHORING DESIGN SUMMARY

The temporary shoring design for this development was based on meeting project-specific performance requirement of achieving less than 20 mm (0.8 in) of lateral displacements to minimize impacts on buried utilities along the perimeter of the proposed shoring. Factors taken into consideration for shoring design included the lateral earth pressures from the fill and native soils; groundwater pressures; temporary construction loads (e.g. due to crane or heavy plant/equipment placed within the zone of influence of the shoring system); and permanent structural requirements, i.e., final footing elevations and slab elevations of the basement structure. The subsurface conditions at this site typically consisted of fill (cohesive and granular), overlying peat and/or wood waste, overlying clayey silt to sandy silt (thickness of fill and overburden ranging from 7.0 m (23 ft) to 8.5 m (28 ft) thick), overlying weathered to dense to very dense clayey silt till to sandy silt till with silt layers. Localized, perched groundwater was observed within the fill, peat, wood waste and sandy silt layers above the dense till.

The CSM panels were designed based on compressive "arching" of 1.0 m (3.3 ft) wide panels in between the reinforced soldier piles spaced at approximately 3.0 m (9.8 ft) apart (Huybrechts and Denies, 2016), to provide lateral support for the upper 7.0 m to 8.5 m of weak fill and overburden soils. The target design strength of the CSM lagging panels was estimated to be approximately 2.0 MPa (290 psi), consistent with previous shoring experience using interlocking caisson walls in similar subsurface conditions. The target strength of 2.0 MPa (290 psi) was achieved based on an average cement factor of 350 kg/m^3 (590 lb/yd^3), target water-cement ratio of 0.6 and an average injection rate of 900 l/min (238 US gal/min). The actual strength of the CSM infill panels is dependent on the in situ moisture content of the fill, overburden and till layers.

Based on local experience of the dense to very dense till, it was anticipated that there would be sufficient arching between soldier piles, consequently a 100 mm (4 in) layer of 35 MPa (5,075 psi) shotcrete reinforced with a single layer of welded wire mesh was proposed between the soldier piles in the dense till. The soldier piles were designed based on the bending moments due to lateral loading considering three levels of tie-back anchor supports, and a "composite reinforced concrete section" with 880 mm (2.9 ft) diameter concrete pile with target strength of 8.0 MPa (1,160 psi) reinforced with W610X101 (W24X68) or W610X113 (W24X76) steel beams. The three levels of tie-back anchor supports were designed considering design loads of 845 kN (190 kips) to 1,045 kN (235 kips) per anchor with bond length of 10.7 m (35 ft) to 13.4 m (44 ft) in dense to very dense till, as shown in Figure 3.

HYBRID SHORING CONSTRUCTION SUMMARY

The construction sequence of the hybrid DM shoring system comprised installing CSM panels at approximately 3.0 m (9.8 ft) centre-to-centre spacing, followed by installing the 880 mm (2.9 ft) diameter soldier piles. This would ensure intimate contact between the CSM panels and the soldier piles. Ahead of the production work, a trial CSM program consisting of two trial CSM panels installed adjacent to two large diameter holes was implemented. The large diameter holes were used to initially verify subsurface conditions indicated from the available existing geotechnical data, and to establish termination criteria of the CSM panels in dense till. The location of the trial CSM panels and supporting large diameter drill holes are shown in Figure 1. Real-time monitoring using the Bauer B-tronic system (Bauer) was carried out during installation of the trial CSM panels. Following installation, in-situ wet grab samples were

taken generally from the centre and mid-point of the trial CSM panels for Unconfined Compression Strength (UCS) testing of the soil-cement samples. UCS testing was carried out at 4, 7 and 28 days to confirm strength and strength gain rates that would meet project performance requirements relative to the construction schedule.

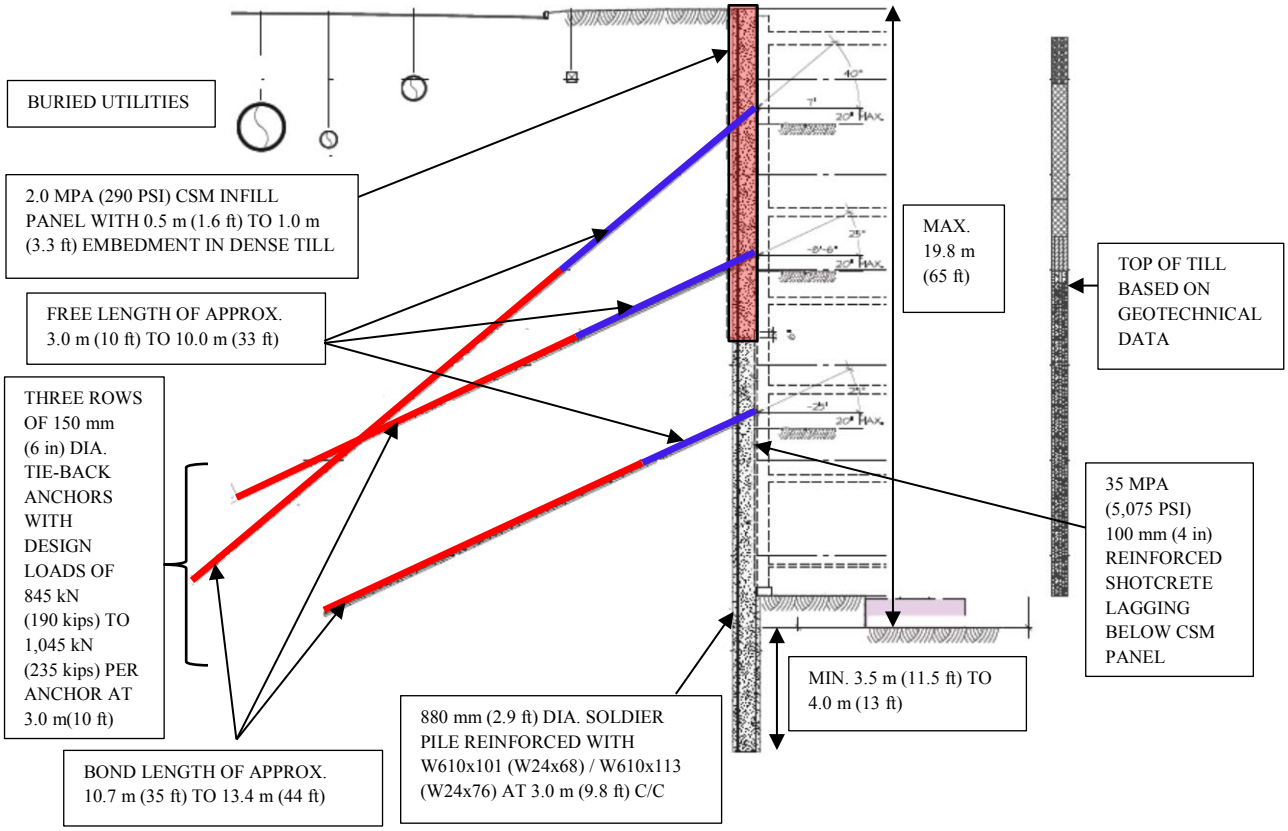


Fig. 3 Typical hybrid shoring section

During production works, pre-trenching was generally carried out within the upper 2.0 m (7 ft) to 3.0 m (10 ft) to verify the proximity of adjacent buried utilities and/or permit the removal of shallow obstructions (concrete waste, boulder, wood logs, etc.). CSM panels were typically constructed with water or cement-slurry as the cutting agent with cement-slurry injected on mixing out of the panels. At least one complete restroke of the cutter head was carried out for the full depth of the panel to promote homogeneous mixing throughout the peat and wood waste layers. A total of 5 No. CSM panels terminated on buried wood logs and/or boulders in the sandy silt, between approx. 6.1 m (20 ft) and 7.5 m (24.6 ft) below ground. Two rows of 178 mm (7 in) diameter 30 MPa (4,350 psi) grout columns at 300 mm (1 ft) centre-to centre spacing were installed behind the CSM panels, terminating at approximately 0.5 m (1.6 ft) in the dense till to provide seepage control and prevent significant material flow during bulk excavation below the CSM panels. During excavation, material flow was successfully prevented and minor seepage was observed at one CSM panel location. At these locations shotcrete and mesh was installed from the base of the CSM panels down to provide a planar surface to the wall.

Following deep mixing, wet grab samples were taken from representative CSM panels, typically at two depths (i.e., at mid-point and towards the bottom 1.5 m (5 ft) of a CSM panel) for UCS testing of the soil-cement samples. Wet grab samples were taken from a total of 23% of production CSM panels, consistent

with published guidelines (Bruce et al., 2015) and these samples were cured on site for a minimum of 7 days prior to transportation to an off-site facility for continued curing and/or testing.

Real-time monitoring was carried out during installation of all CSM panels and inclinometer casings were installed in three CSM panels as well as two soldier piles for shoring performance assessment (Dunnicliff, 1988). The inclinometer casings were vibrated into the centre of the CSM panel to within approximately 1 m (3.3 ft) of the bottom of the panel. For the soldier piles, inclinometer casings were attached to the full length of the steel reinforcements and lowered into the drill holes, prior to concreting.

Following completion of the CSM panel installation and secant piling, bulk excavation was carried out in stages to install the three levels of tie-back anchors. A total of seven performance tests were carried out on selected tie-back anchors ahead of production work, where the design adhesion value of 80 kN/m (5.5 kips/ft) to 90 kN/m (6.2 kips/ft) in the dense to very dense till was confirmed with factors of safety of between 1.5 and 2.2. All remaining production anchors were tested to approximately 133% of the design load (i.e., between 860 kN (193 kips) and 1,390 kN (313 kips)) prior to being locked off.

Throughout the bulk excavation and anchor installation process, inclinometer monitoring combined with pile target monitoring was carried out to assess performance of the hybrid shoring walls. Reflective pile targets were installed within 0.3 m (1 ft) of the top of all soldier piles and baseline readings were taken prior to the start of the bulk excavation. To assess performance of the overall design, pile target monitoring was also undertaken on the reinforced piles

REAL TIME MONITORING OF CSM PANELS

As previously discussed, two trial CSM panels were installed adjacent to two large diameter drill holes to initially verify subsurface conditions, and to establish termination criteria of the CSM panels in dense till. The constructed depths of the trial CSM panels were based on interpretation of real-time monitoring data and the knowledge of the actual depth to till identified by the large diameter drill holes. The parameters considered for assessment included Rate of Penetration (ROP), pressures at the cutter wheels (pressure), and rotational speed of the cutter wheels (rotational speed), which were compared with available Standard Penetration Tests (SPT) N values from existing geotechnical investigations carried out prior to construction. Consistent trends were observed when comparing all three parameters i.e., ROP, pressures and rotational speed with SPT N values. Consistently, where dense to very dense till was encountered between approximately 8.0 m (26 ft) and 9.5 m (31 ft) below ground, the ROP reduced significantly, while pressures were markedly increased. Changes in the rotational speed were generally less noticeable when passing through variable soils, compared with ROP and pressures.

Based on the trial CSM real-time monitoring data and geotechnical data, the following termination criteria were established to meet project-specific performance requirements of 0.5 m (1.6 ft) to 1.0 m (3.3 ft) embedment into dense to very dense till:

- Rate of Penetration $\leq$ 20 cm/min;
- Pressures at cutter wheels $\geq$ 200 bar; and
- Rotational speed of cutter wheels $\leq$ 20 to 25 rotations/min.

Modifications were made to the above termination criteria on a “case-by-case: basis to take into consideration areas where significant obstructions were encountered at depth. These included buried concrete structures/wood logs in the fill below approximately 4.0 m (13 ft) below ground and boulders in the till below approximately 7.5 m (25 ft) below ground, which were beyond the reach of a typical excavator for removal. Figures 4A and 4B present simplified plots of selected CSM output real-time monitoring data for representative CSM panels constructed.

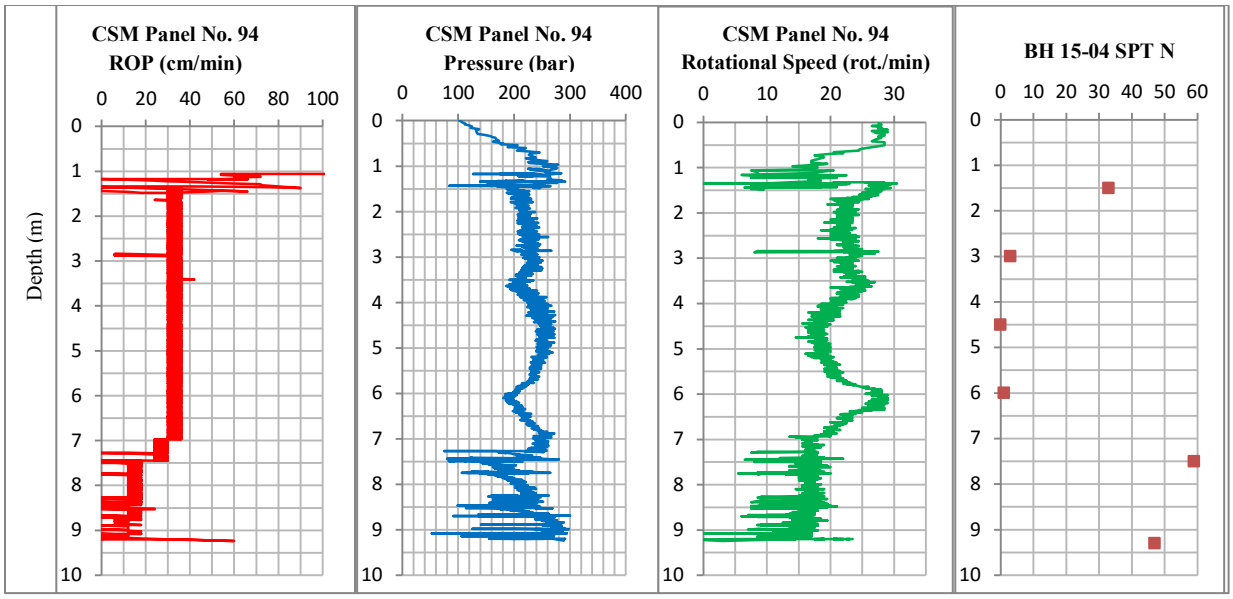


Fig. 4A Hybrid Shoring Wall 1 typical CSM output parameters compared with SPT N values

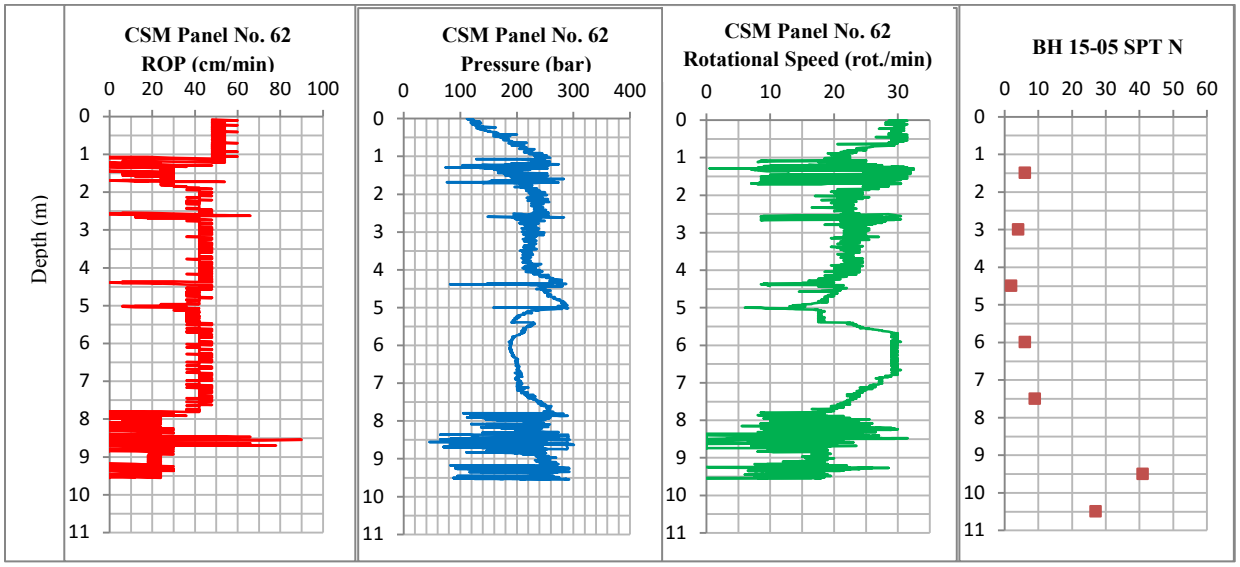


Fig. 4B Hybrid Shoring Wall 2 typical CSM output parameters compared with SPT N values

Five CSM panels out of a total of 57 No. production CSM panels terminated at depths shorter than expected based on our interpretation of expected subsurface conditions. Typical output results of a CSM panel terminated shorter compared with an adjacent CSM panel constructed with approximately 0.5 m (1.6 ft) to 1.0 m (3.3 ft) embedment in dense till are presented for comparison in Figures 5A and 5B.

As part of the Quality Assurance/Quality Control (QA/QC) program, wet grab samples were taken, typically at mid-point and towards the bottom 1.5 m (5 ft) of a CSM panel, from a total of 13 No. panels for verification of the strength of representative CSM panels. A total of 28 No. sets of samples were taken for UCS testing with strain gauge measurement at generally 14, 28 and 56 days to confirm that the target strength of 2.0 MPa (290 psi) at 56 days (and greater) had been achieved prior to bulk excavation adjacent to the hybrid shoring system. Selected additional UCS testing was carried beyond 56 days to demonstrate the long-term strength gain. The representative UCS data are presented in Figure 6.

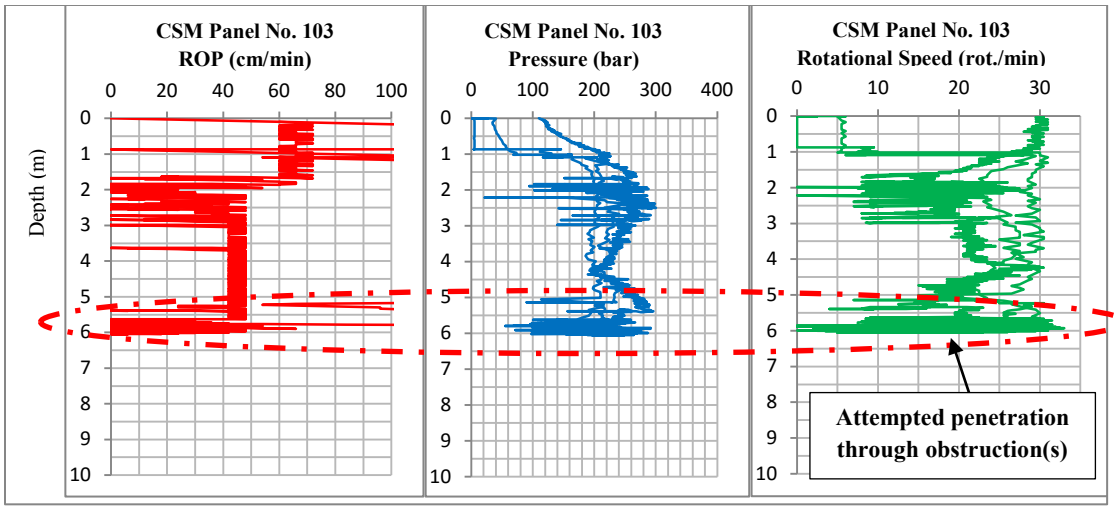


Fig. 5A Typical CSM output parameters for CSM panel terminated on obstruction(s)

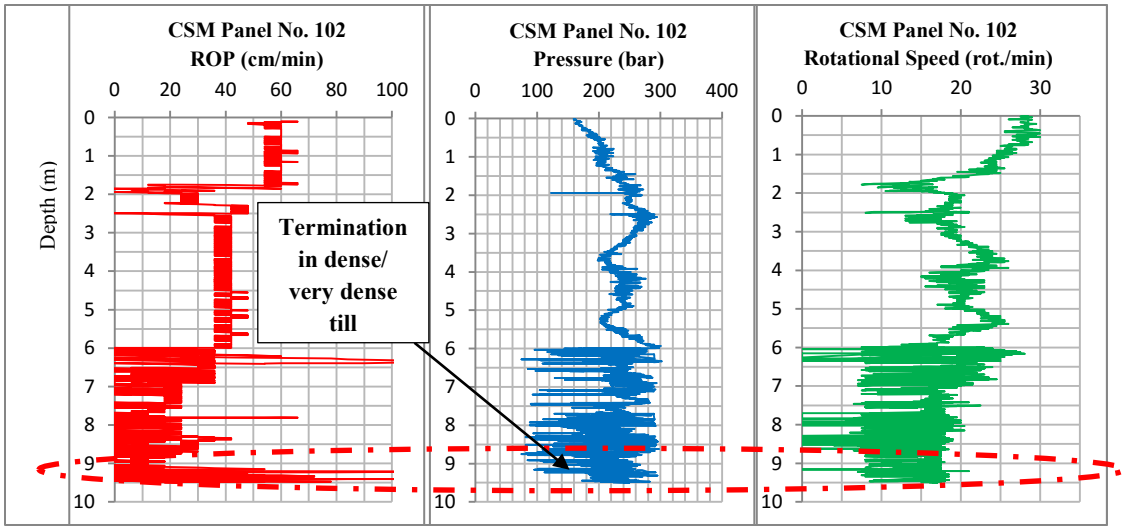


Fig. 5B Typical CSM output parameters for CSM panel terminated as per design requirements

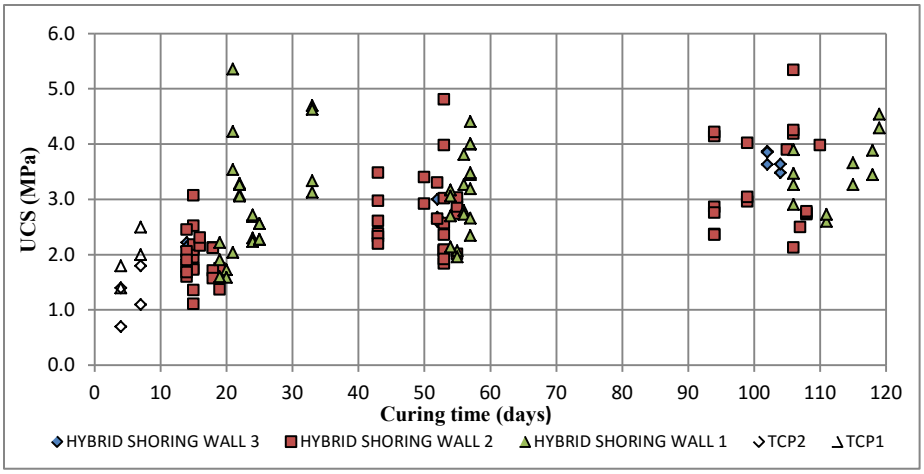


Fig. 6 UCS versus Cure Time plot

CSM infill panels were exposed during bulk excavation. Upon inspection, CSM panels were generally found to be terminated with 0.5 m (1.6 ft) to 1.0 m (3.3 ft) embedment in dense till, as per design requirements. Figure 7 presents a portion of Hybrid Shoring Wall 1 exposed to approx. 9.5 m (31 ft) below ground with CSM panels exposed.



Fig. 7 Hybrid Shoring Wall 1 exposed during bulk excavation showing CSM panels exposed

INCLINOMETER MONITORING DATA FOR PERFORMANCE VERIFICATION

Inclinometer monitoring data from two CSM panels and two soldier piles, as well as soldier pile survey target data was used to assess and monitor the performance of the hybrid shoring system throughout bulk excavation. The inclinometers were generally located at the mid-point or at the deepest excavation zone in order to assess the maximum expected movements without "corner effects". Inclinometer readings were taken at intervals of 0.6 m (2 ft) along the length of the CSM panels and along the entire length of the soldier piles. Pile target readings were taken along the top of the hybrid shoring walls at a typical spacing of 3.0 m (10 ft) between targets. Baseline readings of the inclinometers and pile targets were recorded prior to the start of bulk excavation and the frequency at which readings were taken is summarized as follows:

1. Following excavation to the underside of Row 1 tie-back anchors at approximately 3.5 m (11 ft) below ground;
2. After installation and stressing of Row 1 tie-back anchors;
3. Following excavation to the underside of Row 2 tie-back anchors at approximately 6.7 m (22 ft) to 8.9 m (29 ft) below ground;
4. After installation and stressing of Row 2 tie-back anchors;
5. Following excavation to the underside of Row 3 tie-back anchors at approximately 11.3 m (37 ft) to 13.1 m (43 ft) below ground;
6. After installation and stressing of Row 3 tie-back anchors; and
7. Following completion of excavation to final depth at approximately 14.3 m (47 ft) to 19.8 m (65 ft) below ground.

The inclinometer readings and pile target data were compared with expected design performance to assess whether modifications were required to the shoring design and construction to meet project performance requirements of less than 20 mm (0.8 in) of lateral displacement of the temporary shoring walls. The monitoring data indicated an average time-delay response of approximately one week for the hybrid shoring walls in the fill and overburden i.e., additional lateral displacements without further excavation, which would be an expected behaviour of the shoring walls given the presence of the weak layers of fill, peat, wood waste and clayey silt to sandy silt located within the upper 7.5 m (24.6 ft) to 9.0 m (29.5 ft). Overall, the monitoring data confirmed performance of the shoring walls to meet project performance requirements throughout bulk excavation.

Along Hybrid Shoring Wall 1, the total lateral displacements following excavation to approximately 19.8 m (65 ft) below ground was approximately 19 mm (0.75 in) and the total lateral displacements following excavation to approximately 16.5 m (54 ft) along Hybrid Shoring Wall 2 was approximately 16 mm (0.6 in), as shown in Figure 7. Over excavation to 21.0 m (69 ft) below ground in the localized area of the inclinometer at Hybrid Shoring Wall 1 for installation of permanent sumps combined with saturated silt layers encountered within the stiff clayey silt till led to increased lateral displacement of up to 27 mm (1.1 in), as shown in Figure 7. The inclinometer monitoring data was used to monitor the lateral displacements of the shoring wall as excavation progressed and the data assisted the design-build team in determining whether additional anchor supports were required. As the increased lateral displacements were localized i.e. central portion of Hybrid Shoring Wall 1 and did not affect build-out of the permanent structure, no additional supports were required.

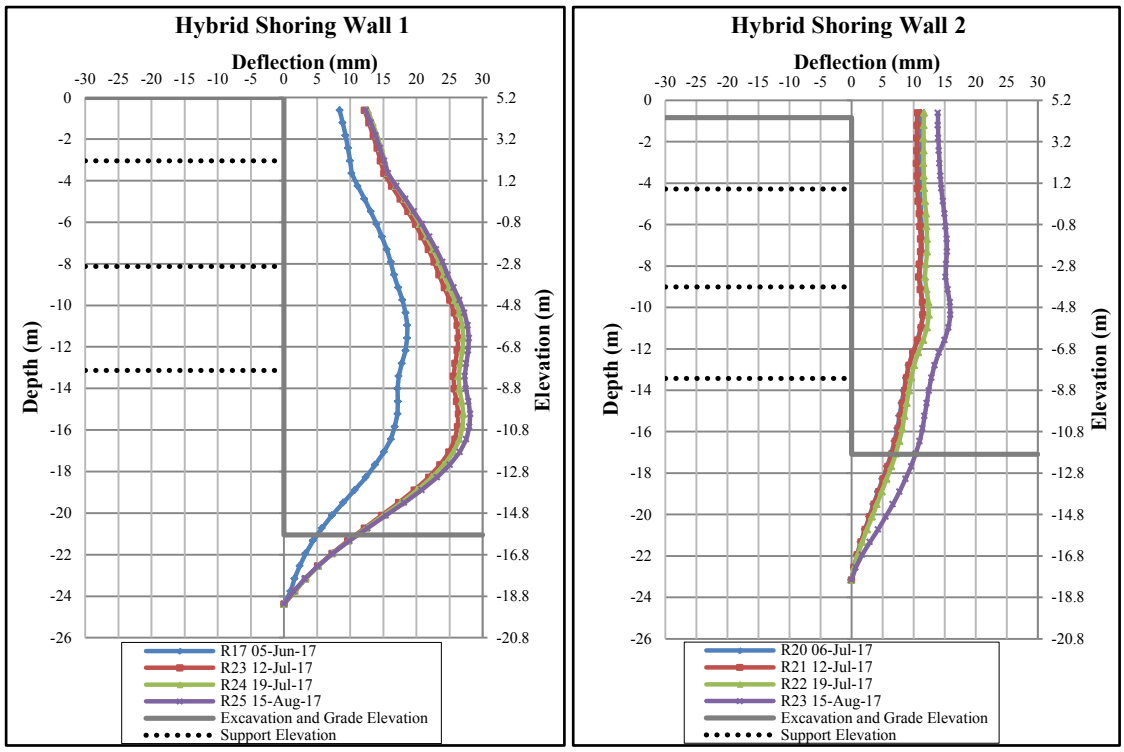


Fig. 7 Inclinometer readings at Hybrid Shoring Walls 1 and 2 – Soldier Piles

The results of the inclinometer monitoring for the CSM infill panels are presented in Figure 8. Lateral displacements were initially relative to the bottom of the CSM panel until excavation progressed to below the bottom of the CSM panels. The inclinometer data generally suggests that the lateral displacements of

the CSM infill panels were consistently less (between 2 mm (0.08 in) and 4 mm (0.16 in) compared with the adjacent soldier piles as excavation progressed to final depth.

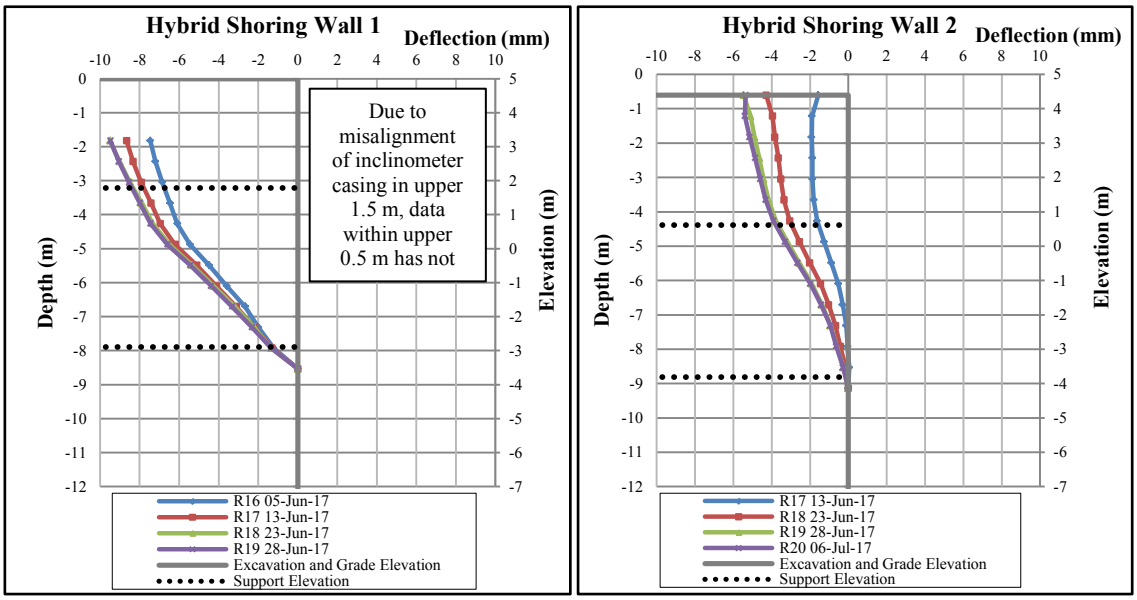


Fig. 8 Inclinometer readings at Hybrid Shoring Walls 1 and 2 – CSM infill panels

A comparison of the inclinometer monitoring data (Figure 7) with the pile target data is presented in Table 1 for Hybrid Shoring Walls 1 and 2, which indicated maximum lateral displacements of 9 mm (0.35 in) to 11 mm (0.43 in) into the excavation area, following excavation to final depth.

Table 1: Summary of inclinometer readings at Hybrid Shoring Wall 1

Excavation stage	Max. lateral displacements at approx. 0.3 m (1 ft) of the top of wall			
	Hybrid Shoring Wall 1		Hybrid Shoring Wall 2	
	Soldier Pile	Pile Target	Soldier Pile	Pile Target
Excavation to underside of Row 1 tie-back anchors	3 mm (0.12 in) into site	6 mm (0.24 in) into site	5 mm (0.20 in) into site	8 mm (0.31 in) into site
Stressing of Row 1 tie-back anchors	1 mm (0.04 in) into site	2 mm (0.12 in) out of site	6 mm (0.24 in) into site	5 mm (0.20 in) into site
Excavation to underside of Row 2 tie-back anchors	1 mm (0.04 in) out of site	2 mm (0.12 in) out of site	6 mm (0.24 in) into site	6 mm (0.24 in) into site
Stressing of Row 2 tie-back anchors	2 mm (0.08 in) out of site	2 mm (0.08 in) out of site	7 mm (0.28 in) into site	No reading taken
Excavation to underside of Row 3 tie-back anchors	0 mm (0 in)	No reading taken	7 mm (0.28 in) into site	No reading taken
Stressing of Row 3 tie-back anchors	3 mm (0.12 in) into site	4 mm (0.16 in) into site	11 mm (0.43 in) into site	10 mm (0.39 in) into site
Final excavation depth	9 mm (0.35 in) into site	7 mm (0.28 in) into site	11 mm (0.43 in) into site	11 mm (0.43 in) into site

The inclinometer monitoring data provided a "continuous" profile of the lateral displacements for the full depth of the soldier pile with excavation, which was advantageous in the monitoring of the shoring wall performance, as well as the assessment of whether design/construction modifications were required to meet project performance requirements e.g., adjust elevation of tie-back anchors, increase design load of tie-back anchors, adjust number of tie-back anchors, etc. The pile target data offered complementary information to supplement areas where increased lateral displacements could be expected e.g., localized, unexpected over-excavation, which was also considered as part of the hybrid shoring wall performance assessment.

REAL-TIME MONITORING FOR CONSTRUCTION MODIFICATIONS AND QA/QC

Using the real-time monitoring data from CSM panel construction, the "inferred" subsurface conditions were determined for the variable soil conditions such that modifications could be made to support production CSM panel installation, and allow panels to be terminated based on "inferred" conditions rather than a target elevation.

Based on the trial CSM real-time monitoring data and comparing this to the available geotechnical data, associated "signature" ROPs, pressures at the cutter wheels, and rotational speeds for these specific subsurface conditions were recorded. These were then used to guide installation of production CSM panels in similar subsurface conditions. Areas where modifications were made included re-stroking of the cutter head through specific layers such as wood waste or organic soils to promote homogeneous mixing, as well as increased pressures and reduced amount of slurry delivery on encountering obstructions. Cement-slurry was generally used as a cutting agent during mixing in peat, clayey silt and till, whilst water was the preferred cutting agent when mixing through fill, wood waste and obstructions. The real-time monitoring data was also used to identify areas where increased wet grab sampling would be beneficial for QA/QC e.g., areas where significant low pressures combined with high ROP and high rotational speed were observed.

CONCLUSION

For performance-based design of temporary shoring structures, inclinometer monitoring combined with pile target monitoring enabled the design and construction team to continually monitor and assess shoring wall performance, as well as making timely decisions for modifications to the design and/or construction to meet project performance requirements. The hybrid DM shoring wall constructed in variable subsurface conditions proved to be successful in terms of shoring wall performance, as well as construction scheduling because of the speed at which the shoring system could be constructed in variable fill, peat, wood waste and overburden compared with traditional secant piling methods.

The B-tronic data provided by the CSM equipment can be used to interpret subsurface conditions in real time particularly when variable subsurface conditions such as fill containing obstructions and soft and loose overburden is encountered overlying dense to very dense soils. Further work is recommended such that interpretation of the real-time monitoring data could be simplified. Currently, the interpretation of the data is not straightforward and relies heavily on the experience of the Engineer to establish the parameters and present them in a meaningful format for the CSM operator and field crew to interpret and implement. The development of a graphical portrayal of resistance to penetration of the cutter head such as an "inferred torque" parameter would provide a valuable tool to both the Engineer and Contractor, particularly when dealing with subsurface conditions where termination is based on in-situ relative density and not a target elevation. Data from additional sites in variable geotechnical environments are required to better establish such a relationship.

REFERENCES

BAUER Maschinen GmbH. 2016. CSM Cutter Soil Mixing Process and equipment, Document No. 905.656.2.

Bruce, M.E.C., Berg, R.R., Collin, J.G., Filz, G.M., Terashi, M. and Yang D.S. 2013. Federal Highway Administration Design Manual: Deep Mixing for Embankment and Foundation Support. Report No. FHWA-HRT-13-046. Contract/Grant No. DTFH61-06-C-00039.

Dunnicliff, J. 1988. Geotechnical Instrumentation For Monitoring Field Performance. A Wiley-Interscience Publication, John Wiley and Sons Inc., New York, 577 p.

Huybrechts, N. and Denies, N. 2016. Handboek Soilmix-Wanden Ontwerp en Uitvoering. www.sbrcurnet.nl, WTCB.be, Printsupport4U, Delft, 282 p.

DESIGN OF GRILLAGE AND HELICAL PILE FOUNDATION FOR LIMITED ACCESS TRANSMISSION LINE

Jason Herron, Hubbell Power System, Inc, Centralia, MO, USA, (573) 682-8630, jwherron@hubbell.com
Benjamin Jennings, Hubbell Power Systems, Inc, Centralia, MO, USA, bjennings@hubbell.com

ABSTRACT

In the summer of 2016 Xcel Energy experienced a storm event that resulted in the collapse of approximately 8.5 miles of a 345 KV transmission line near Rogers, Minnesota. In design of the new transmission line, Xcel Energy determined that ten tower locations would be replaced with steel H-frame structures supported by helical piles instead of wood H-frame structures supported by driven wooden piles. A steel foundation was proposed for the towers due to time constraints and site conditions unfavorable to large pile driving equipment. Xcel Energy contacted the helical pile manufacturer Hubbell Power Systems, Inc. (HPS) for aid in the design of a complete steel foundation for the structure legs. With the shear, moment, and axial loads provided, the manufacturer used pile group modeling and axial capacity software to design a four helical pile group; and used 3D modeling and finite element software to design a moment resistant grillage to connect to the tower base. The steel grillage utilizes a new moment resistant connection and clamp system to transfer loads from the piles to the grillage. This connection provides a true fixed head condition and reduces lateral deflection issues typical to smaller diameter piles in pinned head connections. The clamp is designed to deform the helical pipe pile shaft and transfer the full axial load of the structure through the mechanical and friction connection. The helical piles and the moment resistant grillage were manufactured with shorter than average lead times and a helical pile installation contractor performed the installation. An expedient plan of install was developed by the contractor that resulted in an average installation rate of one complete set of tower foundations per day. The design of the moment resistant grillage, clamping system, and excellent foundation construction by the contractor provided an expedient and efficient foundation system to be discussed in this paper.

INTRODUCTION:

On July 5, 2016 , during a storm event, existing H-frame structures failed and cause the collapse of 8.5 miles of parallel 345 KV transmission lines. During the design of the replacement towers and foundations, representatives of manufacturer, Hubbell Power Systems contacted Xcel Energy (Xcel) to offer the use of a new steel grillage system being developed through the manufacturer's research and development team. Xcel contacted the manufacturer's engineering team and worked in conjunction to create a foundation solution. 10 locations were selected based upon the special existing soil conditions. The soil profile in these locations was a soft cohesive material with high water table, making standard foundation systems extremely difficult to install. The foundation solution would consist of a fixed-head, moment-resistant grillage and four 3 in. schedule 80 helical pipe piles (RS3500.300) connected by a new clamp and grout system to the new H-frame steel structures. Xcel required the foundation system to be a turnkey solution with the installation of the foundations being required as part of the foundation package. A helical pile contactor, Atlas Foundation Systems Co. in Rodgers, MN, partnered with the manufacturer to fulfill Xcel's requirements. Manufacturing of the first set of piles and grillages finished and shipped on

 © 2017 DFI Annual Conference, New Orleans, LA, USA

September 22, 2016 and the installation of the foundations began on October 3, 2016. This paper will discuss the design, manufacture, and installation of these foundations.

The locations for installation of the grillages were predominantly unseasonably wet. Due to these wet conditions some of the locations for the towers were saturated and others were submerged by up to 5 feet of water. Access was only attained by floating swamp matting. This resulted in making access for larger equipment extremely difficult due to the low allowable ground pressures on the matting.

Borings provided by Xcel showed 10 to 15 feet of soft clay with cohesion less than 500 psf overlaying sandy stiff clay with cohesion greater than 1200 psf. The depth of the water table was reported at approximately 2 feet below the surface. Actual conditions as stated above were slightly different. The stiff clay at approximate depths of 15 to 20 feet was assumed as the bearing stratum for the helical piles. Figure 1 is typical a representation of the soil profile.

DEPTH (FT)	DESCRIPTION OF MATERIAL	N
0	MUCK, black, soft (PT)	1.5
	CLAYEY SILT, brown and gray	3
	CLAYEY SILT, gray and a little brown, soft (ML)	
5		
	SILTY CLAY, gray, soft to rather stiff, some lenses of clayey silt (CL)	3
		5
10		4
		11
15		9
17	End of Boring	
	Water Table = 2.5 feet	

Fig 1. Typical Soil Profile

FOUNDATION OPTIONS

There were several different options available for the foundations of these towers as well as the piles. Both a concrete cap and grillage were considered for pile caps and Helical Pulldown Micropiles, Round Shaft piles, and Combination piles were considered for the piles. This section will discuss the pros and cons of the options as well as what was chosen for this project.

PILE CAP OPTIONS

CONCRETE CAP

Piles are installed in the required layout and then encased in concrete and tied together with rebar to ensure fixity of the piles and for load transfer. Generally a new construction cap is utilized to ensure that the concrete can transfer the axial loads of the piles. This is a cost effective option when forming and pouring a concrete pile cap is a viable solution based on existing conditions and location. There are situations when this is not a good option. For example, where water tables are high, reveal is required, or where concrete is not easily accessible. It is typical that if a contractor can form and pour a concrete cap; a drilled shaft then could also be constructed to support the structure.

STEEL GRILLAGE

A steel grillage is a predesigned system to transfer the loads from the structure to the piles through the moment and shear capacity of steel members. It is generally a welded assembly of plates, beams, tubes, etc. that is a good option where concrete caps are not feasible. One main benefit to steel grillages are the ease/speed of installation and the ability to provide reveal heights for the structure carried by the piles instead of an additional member. Steel grillages may be installed with above or below grade connections. For this application it was preferred that the steel grillage be used above grade and the piles be extended as much as five feet above grade to accommodate for the fluctuating water levels around the structures.

HELICAL PILE OPTIONS

HELICAL PULLDOWN® MICROPILE

A Helical PULLDOWN® Micropile is a helical pile that utilizes lead and extension displacement plates to create a column of grout around a central steel shaft. This creates a pile that has both bearing and friction capacity and can be cased to add bending capacity (generally used if lateral loads are applied), or uncased if bending moments are not being applied.

ROUND SHAFT (RS) HELICAL PILE

Type RS helical piles are structural tubing with welded helixes and upset or welded coupling with bolted connections. RS helical piles are used to resist buckling in weaker soils and to carry shear and moment loads imparted by a structure. The large benefit to RS helical piles is that they have the same moment, shear, and torque capacity through the entire length of the shaft.

COMBINATION PILE**:**

A Combination Pile is a pile that utilizes the penetration and installation efficiency of a square shaft and transitions to a round shaft (pipe pile) for buckling and lateral capacity. The torque to capacity ratio (K_t) of the combo pile is greater than its corresponding pipe pile, but lower than square shaft. Generally the K_t is somewhere between 8 and 9.5 depending upon depth, pipe diameter, and soil type for a 1-3/4 in. round corner square helical lead to RS3500.300 extensions that comprise the combination pile. The standard K_t for standard RS3500.300 Helical Round Shaft piles is 7. This means that for the same torque, the combo pile can get higher capacities than a pipe pile.

FOUNDATIONS SYSTEM SELECTION

The options that were chosen for this project were a steel grillage connected to 4-RS3500.300 helical piles.

The grillage option was chosen because of the high water table of the site as well as the soft soil conditions at the surface. Some of the advantages of the grillage for these sites included: The ability to use small machines to install the piles instead of large pile driving equipment required for driving timber piles or heavy concrete trucks required for cast-in-place drilled shafts and pile cap. Another advantage is the installation rate in the field. The standard installation rate was 1 tower (2 grillages) per day. This is something neither of the other two options could accomplish. These installation rates were able to be accomplished in part because of the clamp and grout system discussed later in this paper.

RS3500.300 piles were chosen to keep the torque capacity and section properties of the piles the same throughout. For a combo pile, the torque capacity of the lead is slightly lower than the torque capacity of the pipe. The original design reveal height for the grillages was 2 feet from grade to the bottom of the grillage, but existing conditions and unseasonably wet conditions meant that for installation the reveal height needed to be as high as 5 feet. A 4 in. schedule 80 sleeve was applied to the RS3500.300 shaft for reveal heights greater than 2 feet to in to increase the buckling and bending moment resistance of the shaft.

GRILLAGE DESIGN

The grillage designed for this project had to be able to transfer the axial, moment, and shear loads of the H-frame structure used by Xcel. The maximum allowable reactions for each structure provided by Xcel were as follows in TABLE 1.

TABLE 1. Design Groundline Reactions

STRUCTURE	LONG. SHEAR (KIPS)	TRANS SHEAR (KIPS)	LONG MOMENT (FT-KIPS)	TRANS MOMNET (FT-KIPS)	COMPRESSION LOAD (KIPS)	TENSION LOAD (KIPS)
80F	0.77	7.7	58.45	108.42	40.15	18.0
85F	0.74	7.69	63.11	130.15	38.38	17.7
90F	0.8	8.88	73.17	174.36	45.14	21.06
95F	0.75	10.19	76.87	225.95	52.82	24.99

The piles for this project were designed using a mixture of software products including: Ensoft's GROUP® and HeliCAP®v2.0 Helical Capacity Design Software. The manufacturer developed load vs axial deflection plots (T-Z Curves) to allow GROUP to estimate the axial deflection of the pile with a given load and better estimate the passive resistance of the soil. This resulted in a better analysis of the moment, axial, shear, and overall displacement results of the piles. A typical lateral deflection plot from GROUP is shown in Fig. 2. This design required the use of four RS3500.300 piles with a helical configuration of 10 in., 12 in., 14 in., and 14 in. helix bearing plates with larger structures requiring a fifth 14 in. helix plate. This pile group was on a 5 ft. pile circle with piles battered at 15 degrees from vertical. With these results, a grillage could be designed to transfer the loads from the structure to the piles.

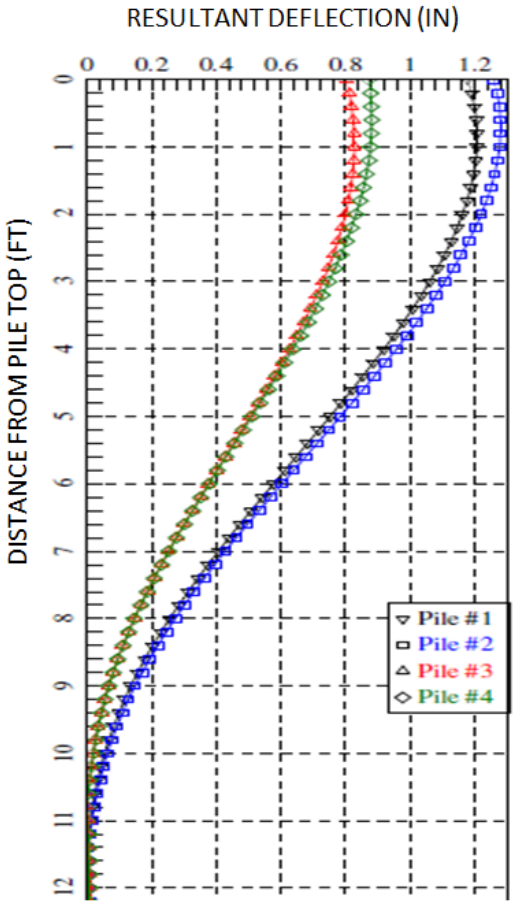


Fig. 2. Typical Lateral Deflection Plot from GROUP Software

The general connection between a steel grillage and helical piles is a pinned head connection. This is mainly because it is generally the easiest and most cost effective means of assembly in the field. A typical grillage connection will look similar to Fig. 3. As can be seen, the pinned head allows for some installation tolerances through slots for bolts. The most common method of having a fixed head condition for a grillage is by welding. This is expensive in the field, so most people prefer to go with the bolted/pinned connection. However, for this grillage, a fixed head condition was required to transfer some of the moment of the structure to the piles and also reduce the lateral deflection of the pile cap to within Xcel requirements.

There are some pros and cons to having a fixed head condition. The positives are that it greatly reduces the lateral deflection of the piles by making the foundation more rigid. However, this does increase the moments in the piles which could be a negative (especially in smaller diameter piles). Another benefit of a fixed connection is that a battered pile design is more efficient and effective than a similar design with a pinned head condition. With the battered piles being fixed in place, there is less vertical deflection from the axial load of the tower because the pile and grillage are working more like a frame rather than two pinned pipes.

The manufacturer had been working to develop a new clamping system for RS3500.300 pipe piles to transfer both compression and tension loads. With the addition of a tube and grout, the connection could be considered fixed. This connection allows for installation tolerances similar to a bolted connection with the fixity of a welded connection. The basic idea behind this clamp and can connection is that a tube can be welded to the grillage and battered at the angle the pile is to be installed at. These tubes can be round

or square and are generally between 6 and 10 in. diameter/side length. This generally will result in about 2-4 inches of installation tolerance on the pile location depending upon the size of the tube. The pile is cut off within an inch of the top of the tube and the tube is filled with grout. This grout is what provides the fixity of the connection. Plates are used on both sides of the grillage to hold the grout in place as well as transfer the axial load to the clamps. The clamp is placed under these plates and tightened under the grillage to resist the compressive load. Before the clamp is tightened, a small round puck that is slightly smaller than the inner diameter of the pipe and connected to a threaded bar is pushed below the area of the pipe to be crimped by the clamp. After the clamp is tightened, this puck is then pulled up tight again the area of pipe crimped by the clamp and tightened on the plates on top of the tube providing the tension capacity. Once the grout has hardened, this connection has the ultimate capacity of the RS3500.300 in tension and compression as well as the ability to transfer the full moment capacity without welding or drilling holes.

With this connection, pile locations, and pile loadings determined. The grillage itself could be designed. The basic design for the grillage included an 18-in-diameter tube in the middle with thick enough wall to carry the loads from the baseplate of the grillage to the spreading beams. It was determined that four beams would be required to transfer the load from this central tube to the clamp and can connection. The resulting design of the grillage can be seen in Fig. 3 and Fig. 4. These beams were originally sized using allowable stress calculations and then were checked using the finite element analysis (FEA) software ANSYS seen in Fig. 5. To aid the load transference amount the four beams, two circular washer plates were sleeved over the central tubing and welded to the top and bottom of the beams. This reduced the moment load on the central shaft and removed the need for a coped beam that fit the radius of the central shaft improving manufacturability.

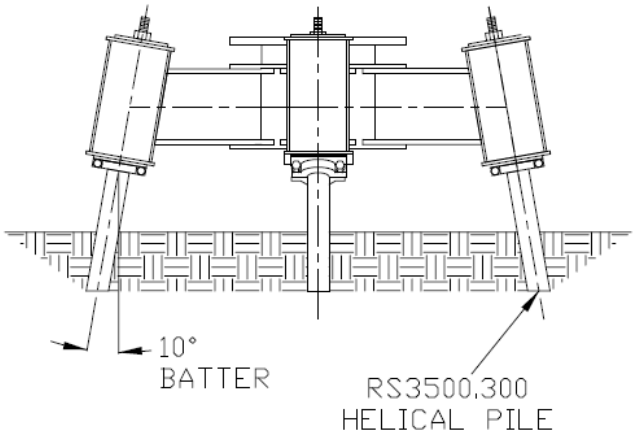


Fig. 3. Elevation View of Grillage

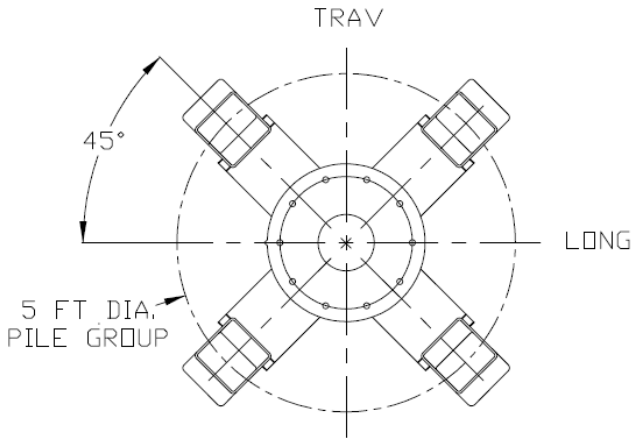


Fig. 4. Profile View of Grillage

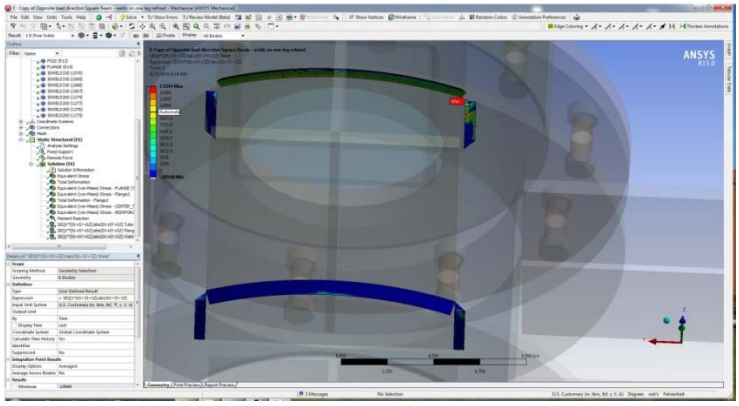


Fig. 5. Weld Analysis using Finite Element Software ANSYS

INSTALLATION

Installation began on October 3, 2016. The helical pile contractor was contracted to install the piles and the grillages. Prior to installation, the helical pile contractor designed a system to install the grillages that would hold the grillage temporarily above the saturated (swampy) soils while using the grillage itself as a template to locate the piles. The center of the tower legs were marked by survey crews provided by Xcel and an RS3500.300 helical pile was installed at the center of the tower leg. A 48 in. square cap was placed over the central helical pile and the grillages of both legs were lowered into place on top of the cap to set elevation and location. A steel square tube was connected between the two grillages to set the lateral spacing between the structures legs. Wooden boxes were inserted into the square tubing grout reservoirs on the ends of the grillage. These wooden boxes were sized such that they would fit the I.D. of the square tubing and had cap boards on the top and bottom of the box with a centered hole large enough to stick a wooden dowel through. The wooden dowel was placed through the box and driven into the soil. After the wooden boxes and the grillages were removed, the four wooden dowels marked the location and angle for installation of each pile. During installation, the alignment and angle of batter of the piles was

checked regularly. The piles were installed to the minimum torque requirements for each structure. The torque and allowable axial pile loads requirements for each structure were as follows in TABLE-2 based on GROUP software analysis:

Table 2. Torque and Axial Capacity Required

STRUCTURE	EFFECTIVE TORQUE (FT-LBS)	ALLOWABLE AXIAL PILE LOADS (KIPS)
80F	7,900	55.3
85F	7,900	55.3
90F	11,600	81.2
95F	11,600	81.2

The grillage was lowered back onto the piles and the required cut elevation was marked on the piles. The cut-off height is 1 to 3 inches below the top of the grillage. The grillage was removed and piles were cut with a portable band saw. The lower pipe clamps were installed with the bolts tightened to finger tight. Void fill material was placed in the pipe a minimum 6 inches below the clamp. This is to insure that the threadbar and grout within the pipe can be installed properly without material falling down the shaft of the pile. A foam sponge was used as void fill material and expanding foam was placed on top of the sponge to seal the void. Once the material was expanded the threadbar with the puck was lowered into the shaft with the puck below the clamp. The large washers were placed over the piles and then the grillage was placed on top of the washers. When the grillage was positioned in the correct location and level in all directions, the bolts below the grillage were tightened to 450 ft-lb. The majority of the tightening was done with an impact wrench with the final torque completed with at torque wrench.

Tape was wrapped around the pile washer to seal the connection between the large washers and the grillage pipe so that grout was contained. A non-shrink grout with a minimum 4,000 psi rating was then used to fill the void around the piles and the square tubing. The pipe is also filled with grout from the void fill material to the point of cut off. This provides a fixed end condition for the helical pile. With the voids and rectangular tubing filled with grout, the top washers and nuts were installed. The nut was tightened until all slack is taken out of the connection. When all components came to bear the nut was tightened a minimum ¼ turn past snug. No structural connections were allowed for the first 7 days so that the grout had time to setup within the square tubing and voids.



Fig. 6. Connection Prior to Grout

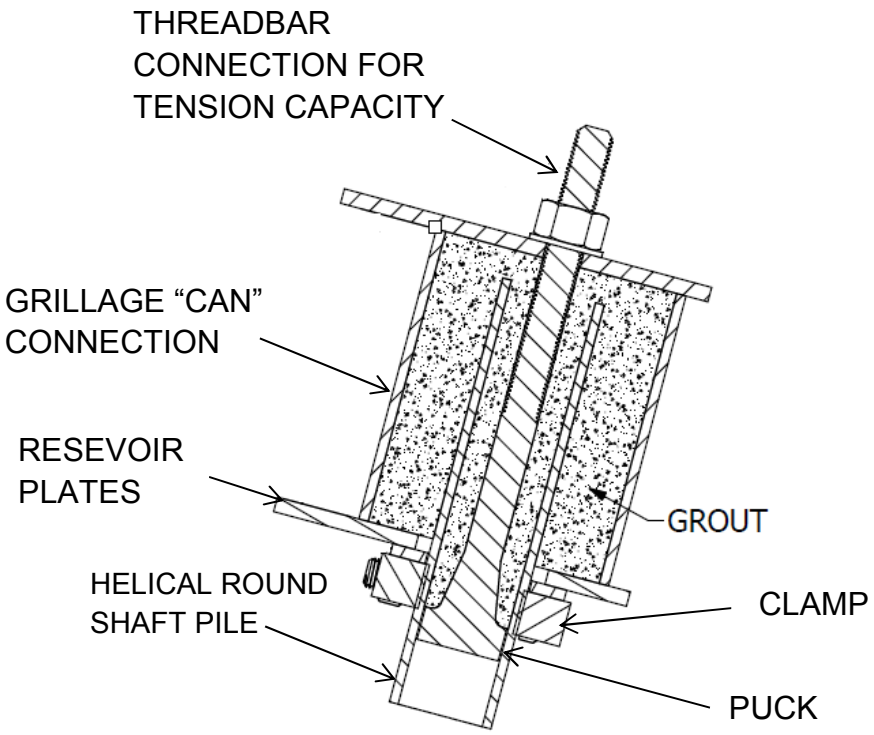


Fig.7. Section of Pile Connection



Fig. 8. Complete Grillage

Conclusion:

This paper discussed the reconstruction of a 345 KV H-Frame transmission line in Rodgers, MN for Xcel Energy. The lines required reconstruction after a storm toppled 10 miles of parallel H-frame structures. The site in question had limited access because of the seasonably wet conditions. Since some of the locations were underwater five feet, floating mats and small equipment were required for the installation of the piles. The piles were designed using both GROUP and Helicap software to model the behavior of the piles in the soils. The boring showed about 10-15 feet of soft clay underlain by a layer of stiff clay that

the helices were to bear in. With the results from HeliCAP (axial loading software for helical piles), a model of how the piles work together in the soil can be created using GROUP (an Ensoft product). This GROUP model assisted in the design of both the piles and the grillage.

Because of the requirements of the site: high water table, small equipment access, and requirement for substantial reveal, a fixed-head condition grillage was designed that utilized four RS3500.300 helical piles. These RS3500.300 piles were sleeved with a 4 in. schedule 80 sleeve on some piles to increase the acceptable bending moment and thus allow for greater reveal than was originally planned. These piles were connected to the structure by a new clamp and grout system designed by Hubbell Power Systems that removes the necessity of a welded connection to get a fixed-head condition on a grillage. The clamp crimps the pipe creating a mechanical and friction connection to transfer both tension and compression loads to the pile. The grouted tube fixes the top of the pile in place and transfers both the moment and the shear into the pile. This system also allows for 2-3 inches of installation tolerance on the piles.

The installation began on October 3, 2016. The helical pile contractor designed a system that was very effective in ensuring the grillages and piles were in the correct location and oriented correctly. The grillages were installed at the rate of 2 grillages (one structure) per day. That includes installing the piles, tightening the clamps, placing the grillages, and grouting both grillages.

Bibliography:

"Group v2016." ENSOFT, INC., < http://www.ensoftinc.com/> (Jan. 2016)

Herron, J., and Kosir, T. (Fall 2016). "Xcel Project." Personal.

Herron, J., and Moore, T. (Fall 2016). "Xcel Grillage." Personal

Seider, G. (2014). *Technical Design Manual*, 3rd Edition.

"ANSYS" ANYSYS, INC., http://www.ansys.com/ (Jan. 2016)

ANALYTICAL EXPRESSION FOR PLASTIC HINGE LENGTH IN EXTENDED PILE-SHAFTS

Heidari, Mehdi and El Naggar, M. Hesham
Department of Civil and Environmental Engineering, Western University
Ontario, London, Ontario, Canada, N6A 3L9

ABSTRACT

Equivalent fixed-base cantilever model is a common approach for performance base seismic design of bridge structures supported by extended pile-shaft. In this method, global displacement ductility factor is related to local curvature ductility demand by assuming a concentrated plastic hinge at location of maximum bending moment. Equivalent plastic hinge length is one of the key parameters that should be assumed accurately in kinematic expression of the cantilever model. Although, some expressions have proposed to estimate the length of the in-ground plastic hinge; however, these relations yield differing results. In this paper, a general expression is derived based on the concept of distributed plasticity to predict the plastic region of yielded piles in clay and sand. A length modification factor is defined to relate the equivalent length of plastic hinge to the real plastic zone. Then, results from nonlinear pushover analyses are used to propose an equation for the modification factor as a function of displacement ductility factor.

Keyword: pile-column, performance, plastic hinge length.

Introduction

During severe earthquake events, development of the plastic hinge in pile foundation below ground level is inevitable for bridge structures supported on extended pile-shafts. A common approach for seismic design of the yielding pile-shafts is to replace the pile-soil system by an equivalent fixed-base cantilever assuming the equivalent system has the same global response as that of the pile-shaft (Budek et al. 2000; Chai 2002). In this method, plastic curvature is concentrated at the center of the equivalent plastic hinge below ground surface. Prior knowledge of plastic-hinge length is essential for proper assessment of assess plastic displacement at the top of the pile-shaft. Unfortunately, existing recommendations for estimating plastic-hinge length are largely incomplete and/or inadequate.

During the last two decades, several relationships have proposed for evaluating the equivalent plastic hinge length, L_p, based on experimental and numerical studies. Budek et al. (2000) conducted numerical modeling to calculate the plastic-hinge length of piles embedded in cohesionless soil. They found that the plastic-hinge length varies linearly with both soil stiffness and aboveground height, e. Chai and Hutchinson (2002) conducted full-scale experimental tests on reinforced concrete piles in sand. They reported that L_p depends primarily on the aboveground height of the pile, neither sensitive to the soil stiffness nor to the value of displacement ductility factor. They stated that the equivalent plastic hinge length is relatively independent of the displacement ductility factor and is not very sensitive to the change in soil density. On the contrary, Goel (2014) and Liu et al. (2016) conducted nonlinear numerical analyses which revealed that L_p changes with the displacement ductility factor and even suggested that using different values of L_p for different seismic design levels is essential for a reliable estimation of the ductility capacity.

 © 2017 DFI Annual Conference, New Orleans, LA, USA

The paper aims is to derive analytical expressions for the in-ground plastic region of extended reinforced concrete (RC) shafts embedded in clay and sand. The proposed expressions could account for several key parameters such as the pile cross-section properties (diameter, longitudinal and transverse reinforcement ratio, etc.), axial force ratio, height of loading aboveground, and soil properties. A modification factor is then defined to relate the equivalent length of plastic hinge to the real plastic zone. Using a newly developed *Geo-Structural Nonlinear Analysis Program* (named ***GSNAP***) (Heidari and El Naggar, 2017), nonlinear static pushover analyses are conducted to analyze lateral performance of RC piles in cohesive and cohesionless soils. In GSNAP, fiber-based beam-column elements have employed to simulate the structural members and surrounding soil is replaced by a series of nonlinear springs distributed along the pile length. Results obtained from the numerical modeling are validated against full-scale experimental tests. Then, an extensive parametric study is performed to propose a relationship for the modification factor needed in the evaluation of equivalent length of plastic hinge.

Analytical model

In the equivalent cantilever model, the pile-column is replaced by an equivalent fixed-base cantilever as shown in Fig. 1, where the both system should have same inelastic load-displacement response under lateral loading. The ultimate displacement at top of the pile, Δ_u, is equal to the summation of equivalent elastoplastic yield displacement, Δ_y, and plastic displacement, Δ_p and can be represented by:

$$\Delta_u = \Delta_y + \Delta_p \; ; \qquad \Delta_p = (e + h_p)(\phi_u - \phi_y)L_p \qquad [1]$$

Moment curvature, $M - \phi$, analysis provides curvatures associated with a range of moments for the cross-section of a structural based on the principles of strain compatibility and force equilibrium. The $M - \phi$ curve can be approximated by an elastic-perfectly-plastic response as shown in Fig. 2a. For reinforced concrete element, the elastic portion of the idealized bilinear curve should pass through first-yield point, (ψ_{fy}, M_y), (yielding of first longitudinal reinforcement bar) and the plastic moment is determined by equating areas beneath the actual $M - \phi$ curves and the bilinear curve from the first-yield curvature point to the point of ultimate curvature (Caltrans 2006).

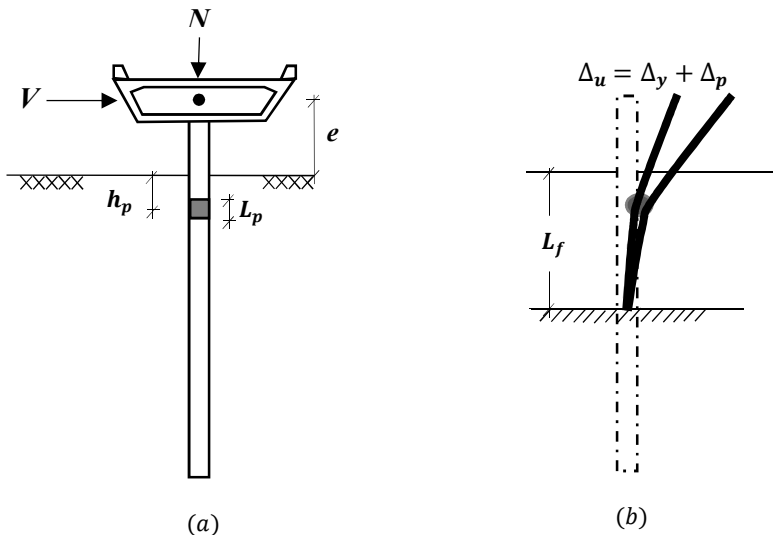


Fig. 1. a) Extended pile-shaft, b) Equivalent fixed-based cantilever model

In performance-based design of bridge structures, local curvature ductility, $\mu_\psi = \frac{\phi_u}{\phi_y}$, of the structural member at a presumed limit-state strain is related to displacement ductility factor, $\mu_\Delta = \frac{\Delta_u}{\Delta_y}$. Kowalsky (2000) recommended strain limits for "serviceability" and "damage control" limit states applicable to concrete compression and steel tension. These strain limits are implemented herein to attain the ultimate curvature. As shown in Fig. 2b, Δ_{fy} and V_y are first-yield displacement and lateral load corresponding to the yielding of first longitudinal rebar in the pile.

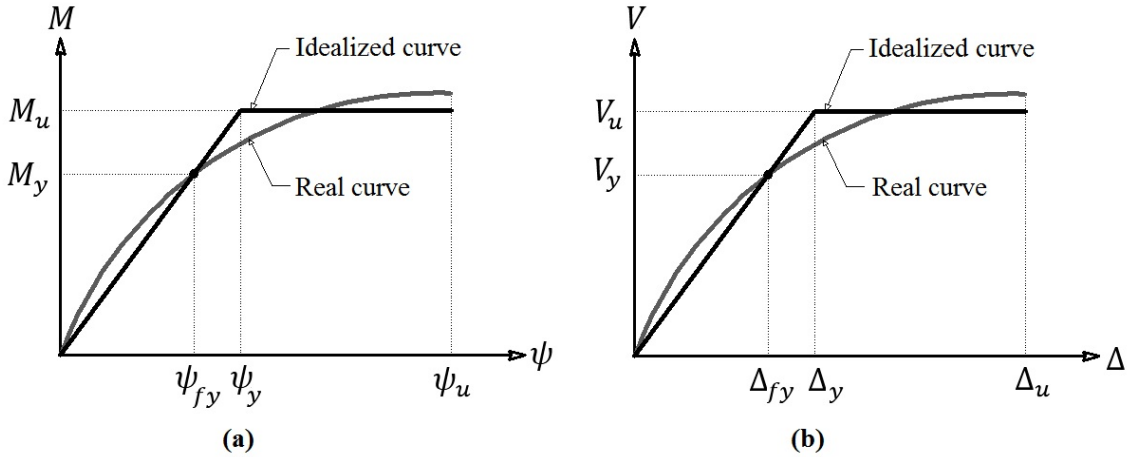


Fig. 2. a) Actual and idealized Moment-curvature curve, b) Actual and idealized lateral load-displacement curve.

The actual size of plastic zone along the pile can be established by separating the elastic and plastic regions of curvature profile. Chiou et al. (2009) traced propagation of the plastic zone in pile from numerical pushover analyses using a series of plastic hinges distributed along the pile. The plastic-hinge length was evaluated as a fraction of the actual range to capture the gradual spreading of the yielded region. In the

present study, the same concept of distributed plasticity is adopted to propose analytical expressions for the equivalent length of plastic hinge of piles embedded in cohesive and cohesionless soil.

The extended pile-shaft under lateral loading begins to yield at any location when bending moment exceeds the first-yield moment. M_y. By increasing the applied load, the inelastic region progressively spreads over a definite length both above and below the critical section. As shown in Fig. 3, the values of bending moment at both extreme ends of the plastic zone should be equal to M_y, and the ultimate moment, M_u, is assumed to occur at the midpoint of the yielded region due to approximate symmetry of plastic curvature profile about the critical section. Satisfying the equilibrium equation for a free-body of the pile, a general expression can be derived for the actual length of plastic-hinge:

$$L'_p = \sqrt{\frac{8(M_u - M_y)}{p'D}} \qquad [2]$$

where the soil reaction on the pile, p', is assumed to be uniform over half-length of the yielded region. Using adequate moment-curvature-thrust curve to obtain the values of M_y and M_u, the proposed expression could implicitly account for the effects of transverse and longitudinal reinforcement ratios, concrete strength, applied axial load on the lateral performance of extended pile-shafts.

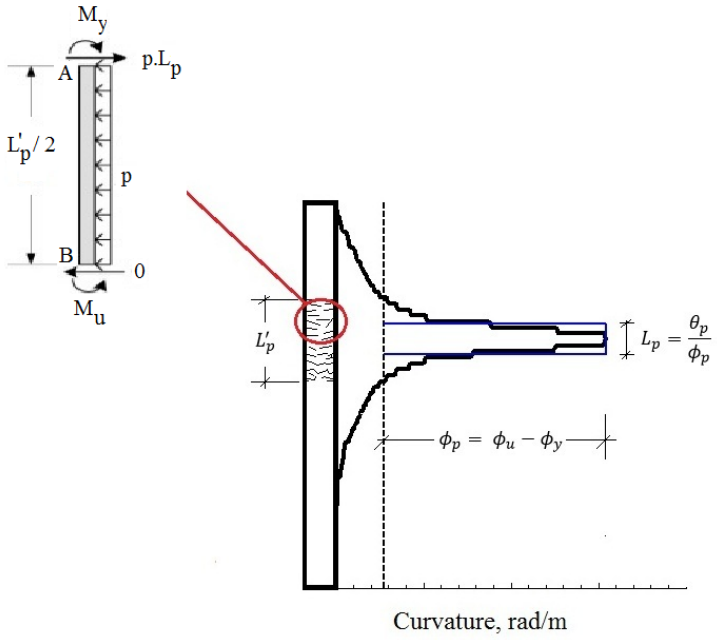


Fig. 3. Methodology to determine equivalent plastic-hinge length

As mentioned previously, the actual plastic curvature profile of the structural member should be replaced with the equivalent rectangular block. The main requirement for the equivalent curvature distribution is that the area of this individual block should represent be equal to the real plastic rotation, thus, the equivalent length of plastic hinge can be calculated by:

$$L_p = \frac{\theta_p}{\phi_p} \quad [3]$$

Where ϕ_p is plastic curvature and θ_p is plastic rotation obtained by integrating the calculated plastic curvature at all integration points along the pile shaft as shown in Fig. 3.
In this paper, the equivalent length of plastic-hinge length, L_p is related to the actual length of plastic-hinge, L'_p, by a modification factor, i.e.

$$\alpha = \frac{L_p}{L'_p} \quad [4]$$

For piles embedded in clay, limiting soil pressure acting on the pile is assumed to be constant, i.e., $p = N_c S_u$, where N_c is bearing capacity parameter and S_u is soil undrained shear strength within the length of plastic-hinge. Substituting this relation into Eq. (2) yields:

$$\frac{L_p}{D} = \alpha \left[\frac{8\left(M_u - M_y\right)}{N_c S_u D^{\,3}}\right]^{0.5} \quad [5]$$

A limiting value of strength parameter is suggested to be 2 at the ground level, 9 and 11.3 at depths of 3D and 6D, respectively, and a constant value of 11.3 for a depth greater than 6D (Chai 2002).
For piles embedded in sand, the soil resistance is assumed to vary linearly with depth with an average value at the depth of plastic-hinge, $p = N_s \gamma' h_p$ where N_s is soil strength parameter within the plastic-hinge length. Substituting this expression into Eq. (2) yields:

$$\frac{L_p}{D} = \alpha \left[\frac{8\left(M_u - M_y\right)}{N_s \gamma' h_p D^{\,4}}\right]^{0.5} \quad [6]$$

Where γ' is soil effective unit weight. Pan (2012) suggested an ultimate value of N_s = 3 for a full-strength interface and $N_s = K_p = \frac{1+sin\phi}{1-sin\phi}$ for zero-strength pile–soil interface. In the following, results of numerical study will be used to propose practical expressions for the modification factor as a function of global ductility factor.

Non-linear Model for Pile-Soil System

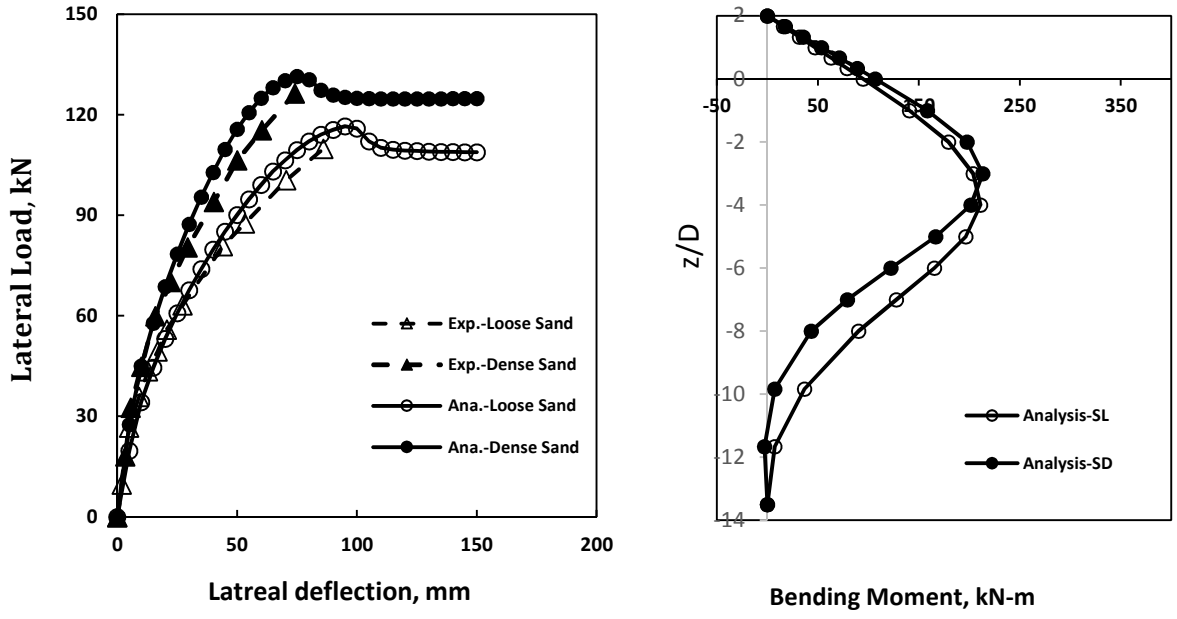
A Geo-Structural Nonlinear Analysis Program (named GSNAP) has been developed recently by Heidari and El Naggar (2017) for the analyses of pile under various types of loading including static, cyclic, dynamic/seismic and soil movement capable of accounting for soil and pile nonlinearities. The inelastic behavior of pile material is modelled using fiber technique by subdividing the element cross-section into longitudinal fibers (Filippou et al. 1983). For each fiber along the axis of element, the response is calculated at some controlling sections using appropriate material constitutive models representing the local behavior. For steel, constitutive relationship proposed by Filippou et al. (1983) (which is an enhanced version of Menegotto-Pinto model, 1973) is used accounting for material nonlinearity and isotropic strain hardening. For reinforced concrete, monotonic envelope curve is based on the model proposed by Kent and Park (1973)

extended by Scott et al. (1982). Tensile strength of concrete is neglected due to its negligible effect on the behavior of RC section after cracking occurred.

Nonlinear disconnected springs are attached at both sides along the pile length to simulate different features of pile-soil interaction and gap formation (Heidari and El Naggar 2016). Although, there are different approaches available to develop load-transfer curves of nonlinear springs in the analysis of laterally loaded pile (Heidari et al. 2014), however, formulations suggested by API (1993) for piles in clay and sand are used in this research.

Validity of GSNAP for the nonlinear response analysis of pile is verified using the results of full-scale load tests conducted by Chai and Hutchinson (1999) on reinforced concrete (RC) piles in sand. The piles had a diameter of $D = 406\ mm$ and were embedded in loose and dense sand beds to a depth of $5.5\ m$. The piles were subjected to a combination of axial compression and lateral loading at an aboveground height of 2D. The pile longitudinal reinforcement comprised 7 $No.22$ bars (Grade A706) and its transverse reinforcement comprised continuous spiral of $MW25$ or $MW45$ smooth wire at a $50\ mm$ pitch. The concrete compressive strength f_c' was approximately $41\ MPa$. The sand unit weight was $17\ \mathrm{kN/m^3}$and the effective friction angle of loose and dense sand beds were reported to be 37° and 44°, respectively.

Figure 4a compares the computed and measured pile-head load versus deflection of the extended pile-shafts in loose and dense sand beds. Figure 4a shows that the numerical responses obtained from GSNAP are in good agreement with experimental data over a wide range of loading. Figure 4b indicates that the ultimate moment occurs at depth of 3d and 4d below ground surface for piles embedded in loose and dense sand, respectively, which means the location of plastic hinge is almost 25% shallower for the pile in dense sand compared to that of loose sand.



(a) (b)

Fig. 4. Lateral load-deflection curves and maximum bending moment profiles for the test piles.

Numerical modeling

Practical configurations are assumed in the parametric study of lateral performance of extended pile-shafts. The pile-shafts used in the analyses have a diameter of D = 1.83 m, an embedded length of L = 26 m and various aboveground heights of e = 2D, 4D and 6D m. An expected compressive strength of concrete, f'_{ce}, is assumed to be 45 MPa and an expected steel yield strength, f_{ye}, of 455 MPa is taken for longitudinal and transverse steel rebars. The longitudinal reinforcement ratio of $\rho_l = 0.02$ and the confinement reinforcement ratio of $\rho_s = 0.0089$ are used for the RC cross-section. Combined lateral and axial loads are applied at the top of the pile-shaft, where the axial load remains constant during the pushover analyses with two different values of 5% and 15%$(f'_c A_g)$. Figure 5 shows the moment-curvature curves for the two axial load ratios obtained from GSNAP based on the structural properties of the pile's cross-section. The idealized elastoplastic M − ϕ curve is also determined based on the method explained previously.

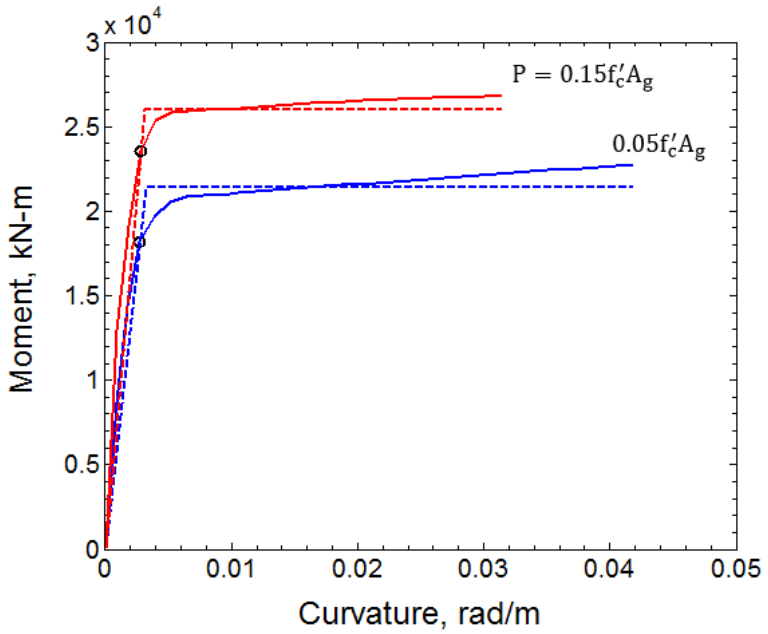


Fig. 5. Moment curvature of cross-section at different axial loads used in numerical analyses.

The effect of pile-soil relative stiffness is investigated by changing the main characteristic of surrounding soil. An average effective unit weight of 18 kN/m^3 and a range of effective friction angles of 30°and 42° are used for loose and dense sand, respectively. For pile in clay, different values of C_u = 36 and 72 kN/m^2 are assumed representing medium stiff and stiff clay.

Figure 6 presents the variation of deflection, bending moment, soil reaction and curvature with depth for a typical response of pile-shaft in sand. It is evident that the soil reaction varies linearly with depth and reaches its ultimate strength within the half-length of plastic zone as assumed in the derivation of analytical expressions for piles in sand. As depicted, the elastic and plastic curvature is separated to evaluate the equivalent length of plastic hinge by calculating the area beneath the profile of plastic curvature over the yielded region.

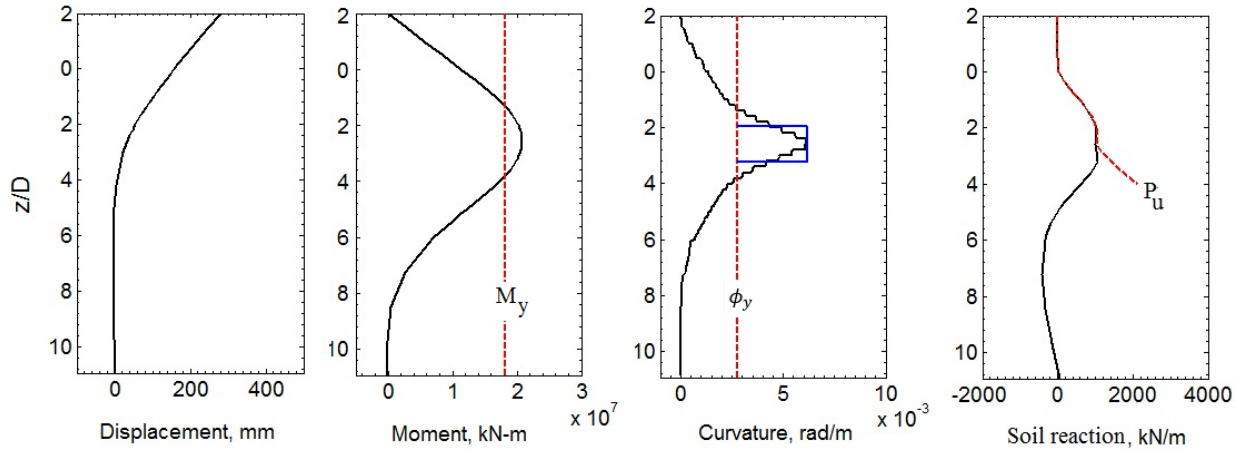


Fig. 6. Variation of several parameter with depth including: a) pile deflection, b) bending moment, c) actual and equivalent curvature distribution and d) soil reaction compared with its limiting value

Using the results from numerical modeling for all cases, variation of the modification factor, α, with displacement ductility factor, μ_Δ of the extended pile-shafts embedded in clay and sand are presented in Fig. 7. As illustrated in Fig. 7, α decreases from 0.6 to 0.3 gradually with the increase of μ_Δ from 1 to 1.5, reaching a constant value of almost 0.30 for higher values of displacement ductility factor.

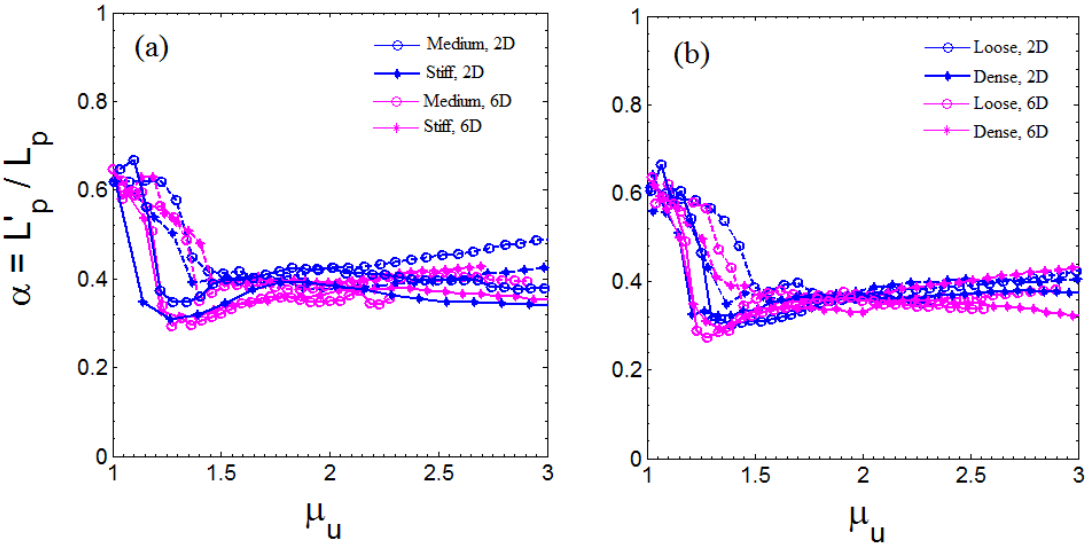


Fig. 7. Variation of length modification factor with displacement ductility factor for pile-shafts in: a) Clay, b) Sand (Dashed line and solid line represents 5% and 15% axial load ratio, respectively).

Conclusion

In seismic performance-based design of bridge structures supported by extended pile-shafts employing the equivalent fixed-based model, prior knowledge of equivalent length of hinge length is essential. Therefore,

a general expression is derived herein based on the distributed plasticity concept to evaluate the yielded region of the pile below the ground level. The expression accounts for the effects of pile diameter, longitudinal and transverse reinforcement ratios, applied axial load, and material properties of pile and surrounding soil. A modification factor is defined to relate the length of concentrated hinge to the actual length of yielded zone by equating the plastic rotation obtained from the equivalent block and the real plastic curvature distribution. Using a newly developed software program for nonlinear analysis of piles under general loading condition (GSNAP), extensive static pushover analyses were performed for a range of pile-shafts embedded in clay and sand to propose useful equations for the variation of modification factor with displacement ductility factor. It is noted that unlike the depth of plastic hinge which is insensitive to the displacement level, the equivalent length of plastic hinge decreases up to a specific value and then remains constant with the increase of displacement ductility factor.

References

American Petroleum Institute (API). (1993). Recommended practice for planning, designing and constructing fixed offshore platforms-working stress design. API Recommended Practice 2A-WSD (RP 2A-WSD), 21st edn.

Budek, A. M., Priestley, M. J. N., and Benzoni, G. (2000) "Inelastic seismic response of bridge drilled-shaft RC pile/columns." Journal of Structural Engineering. 126(4), 510–517.

Caltrans (2006). ''Seismic design criteria Version 1.3.'' Calif. Dept. of Trans., Sacramento, Calif.

Chai, Y. H. (2002), "Flexural Strength and Ductility of Extended Pile-Shafts. I: Analytical Model", ASCE Journal of Structural Engineering, Vol. 128, No. 5, pp. 586-594.

Chai, Y. H. and Hutchison T. C. (2002) "Flexural strength and ductility of extended pile-shafts II: experimental study," Journal of Structural Engineering, 128(5), 595–602.

Chiou, J., Yang, H., & Chen, C. (2009). Use of Plastic Hinge Model in Nonlinear Pushover Analysis of a Pile. J. Geotech. Geoenviron. Eng., 135(9), 1341-1346.

Filippou, F., Popov, E., & Bertero, V. (1983). Effect of Bond Deterioration on Hysteretic Behavior of Reinforced Concrete Joints. Rep. No. UCB/EERC-83/19, Earthquake Engrg. Res. Ctr.: University of California, Berkeley, Calif.

Goel, R.K., (2014) "Analytical evaluation of plastic hinge length and depth for piles in marine oil terminals" 10th National Conference on Earthquake Engineering (NCEE), Anchorage, Alaska, July 21-25.

Heidari, M. and el Naggar, M.H. 2017. Geo-Structural Nonlinear Analysis of Piles. Reprot No?, Gotechnical Research Centre, Western University

Heidari, M. and El Naggar, H. (2016). Effect of Pile Nonlinearity on Its Cyclic Lateral Response. 69th Annual Canadian Geotechnical Conference – GeoVancouver, 2 – 5 October.

Heidari, M., El Naggar, H., Jahanandish, M., & Ghahramani, A. (2014). Generalized cyclic p-y curve modeling for analysis of laterally loaded piles. Soil Dynamics and Earthquake Engineering, 63, 138-149.

Kent, D., & Park, R. (1971). Flexural Members with Confined Concrete. Journal of the Structural Division, ASCE, 97(ST7), 1969–1990.

Kowalsky, M. J. (2000) "Deformation limit states for circular reinforced concrete bridge columns," Journal of Structural Engineering, ASCE, 126 (8), 869–878.

Liu, T., Ye, A. and Wang, X., (2016). "Equivalent Plastic Hinge Length of Extended Pile-Shafts embedded in sand." IABSE Symposium Report, Guangzhou, China.

Menegotto, M., & Pinto, P. (1973). Method of Analysis for Cyclically Loaded Reinforced Concrete Plane Frames Including Changes in Geometry and Non-Elastic Behavior of Elements. Proc.: IABSE Symp. on Resistance and Ultimate Deformability of Struct. Acted on by Well-Defined Repeated Loads, Lisbon.

Pan, D., Smethurst, J. A., & Powrie, W. (2012). Limiting pressure on a laterally loaded pile in a frictional soil. Geotechnique Letters, 2(2), 55–60.
Scott, B., Park, R., & Priestley, M. (1982). Stress-Strain Behavior of Concrete Confined by Overlapping Hoops at Low and High Strain Rates. ACI Journal, Vol. 79, No. 1, pp. 13-27.

COMPARISON OF STATIC LATERAL BEHAVIOR OF VERTICAL AND BATTERED PILE GROUPS OF THE I-10 TWIN SPAN BRIDGE USING FINITE ELEMENT SIMULATION

Ahmad F. Souri, Louisiana State University, Baton Rouge, LA, asouri2@lsu.edu
Murad Abu-Farsakh, Louisiana Transportation Research Center, Louisiana State University, Baton Rouge, LA, cefars@lsu.edu

ABSTRACT

In this study, the static lateral resistance of vertical and battered pile groups was analyzed using 3D finite element analysis. The battered pile group finite element model was verified using the results from a case study performed on the M19 pier foundation of the I-10 twin span bridge in Louisiana. The vertical pile group model was created by adjusting pile inclinations of the verified battered pile group model. The finite element models utilized nonlinear constitutive models for materials behavior and a soil-pile interface model. The results showed that the battered pile group had greater lateral resistance than the vertical pile group with 60-70% lower pile cap displacement. The largest lateral load share was found in the middle rows in the battered pile group, while it was in the leading row for the vertical. The soil resistance profiles showed that the vertical pile group mobilized greater soil resistance compared to the battered pile group.

Keywords: lateral behavior, pile group, vertical pile, battered pile, soil resistance, finite element analysis.

INTRODUCTION

The lateral resistance of a pile-soil system depends on both pile stiffness and soil reaction. The soil reaction is a nonlinear function of deflection, depth, pile stiffness, and soil stiffness and strength. The lateral capacity of single piles is evaluated at the maximum deflection limit, and can be predicted using established methods such as the *p-y* curve method (e.g., Matlock 1970, Reese *et al.* 1974), elastic solution by Poulos and Davis (1980), the strain wedge model (Ashour *et al.* 2004), and the finite element method (e.g., Yang and Jeremić 2002, Comodromos and Pitilakis 2005, Isenhower *et al.* 2014). For pile groups, the lateral capacity of a pile-in-group is less than the isolated single pile case because the soil in front of the pile-in-group is weakened by the overlap of stress zones from surrounding piles. The latter is referred to as the shadowing or group effect (Fig. 1). Prediction of the lateral capacity for pile groups is based on the *p-y* curve method for single piles with the use of empirical factors called "*p*-multipliers". The *p*-multipliers accounts for the shadowing effect, and are a function of pile-pile spacing and soil type (e.g., Brown *et al.* 1987, 1988, McVay *et al.* 1995). Moreover, the lateral capacity of pile groups is also influenced by vertical load, piles arrangement, and slenderness ratio (e.g., Rao *et al.* 1998, Patra and Pise 2001, Ilyas *et al.* 2004, Hussien *et al.* 2012).

Battered piles refer to piles installed at an angle with respect to the vertical to increase their lateral capacity. The greater lateral resistance is achieved by the additional axial reaction in the pile. Battered piles are called "negative battered" when inclined in the load direction, and "positive battered" when inclined opposite to the load direction (Fig. 1). Previous studies concluded that the lateral resistance is highest in positive battered piles followed by negative battered and vertical piles, respectively (Murthy 1964, Meyerhof and Yalcin 1993, Zhang *et al.* 1999).

Our examination of literature found a limited number of experimental studies for battered pile groups (Ranjan *et al.* 1980, Chow 1987, McVay *et al.* 1996, Zhang *et al.* 2002, Abu-Farsakh *et al.* 2011). Ranjan et al. (1980) showed that mixed pile groups of both vertical and battered piles have greater lateral resistance than groups of only vertical piles. McVay *et al.* (1996) evaluated the lateral performance of battered pile groups in-centrifuge and showed that the pile head fixity condition significantly affects their lateral

 © 2017 DFI Annual Conference, New Orleans, LA, USA

capacity. Zhang *et al.* (2002) concluded that the lateral resistance of battered pile groups improves with larger vertical loads. Abu-Farsakh *et al.* (2011) conducted a full-scale field study to evaluate the lateral resistance of a 24-piles battered group of the I-10 twin span bridge in Louisiana.

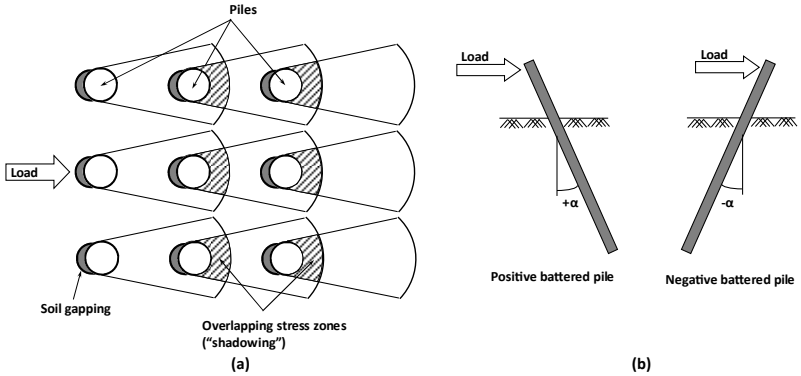


Fig. 1. (a) Illustration of the "shadowing effect" in pile groups, (b) types of battered piles

Battered piles were also studied using numerical methods such as the finite element and finite difference methods. Rajashree and Sitharam (2001) performed analysis of single battered piles under static and cyclic lateral load using hyperbolic soil model. Mroueh and Shahrour (2009) investigated the influence of load inclination with respect to pile's major axis on the lateral capacity of single battered piles, and found that increasing the load inclination angle decreases the lateral capacity. Chow (1987) evaluated the lateral capacity of mixed vertical and battered pile groups with various arrangements using the stiffness method. Isenhower *et al.* (2014) analyzed battered pile group for flood barrier using 3-D finite element modeling, and evaluated the long-term lateral loads and bending moments in the piles due to settlement and storm surge. Souri *et al.* (2015) used 3-D finite element modeling to study the lateral resistance of the M19 battered pile group foundation at the I-10 twin span bridge, and back-calculated the *p-y* curves and the *p*-multipliers per pile.

In this paper, the lateral resistance of vertical and battered pile groups is investigated using 3D finite modeling. The study motivation is to examine some of the differences between vertical and battered pile groups subjected to lateral loads. The 3D finite element method provides a more practical and convenient alternative to field investigations, which are costly and laborious. Moreover, in finite element modeling, the nonlinear behavior of pile groups can be accounted for using nonlinear constitutive models and interface models. The case study of M19 pier foundation of the I-10 twin span bridge (Abu-Farsakh *et al.* 2011) is used as a benchmark to develop and validate the battered pile group finite element model. Then, the results for the vertical and battered pile groups were compared in terms of load-displacement, axial load, and soil resistance.

STATIC LATERAL LOAD TEST ON M19 PIER FOUNDATION

The M19 pier foundation composed of 24-battered piles arranged in 4x6 configuration (Fig. 2). The prestressed concrete piles had 0.3 m wide square section and were 33 m in length with 1H:6V batter angle. The static load test was conducted by pulling the eastbound and westbound piers toward each other using two high capacity strand jacks and steel tendons (Abu-Farsakh *et al.* 2011). The maximum lateral load achieved was H_{exp} = 8.48 MN, and was applied in increments of 0.9 MN. Selected piles were instrumented with series of six inclinometers for piles' slope and deflection measurements, and two pairs of strain gages for bending moment estimation (Fig. 2d).

The subsurface soil investigation showed a stiff to medium stiff clay profile with a medium dense sand layer at 11.6-14.9 m from the mudline, and a dense sand bearing strata at 30.5 m from the mudline. Fig. 2c shows the adopted soil stratigraphy in the FE models, which was assumed based on the CPT sounding. Pile rows and columns numbering are shown in Fig. 2d, in which numbers are used for pile columns, and letters L/ML/MT/T for pile rows. A pile column refers to the piles located on the line parallel to load direction, and a pile row refers to the piles on the line transverse to the load direction.

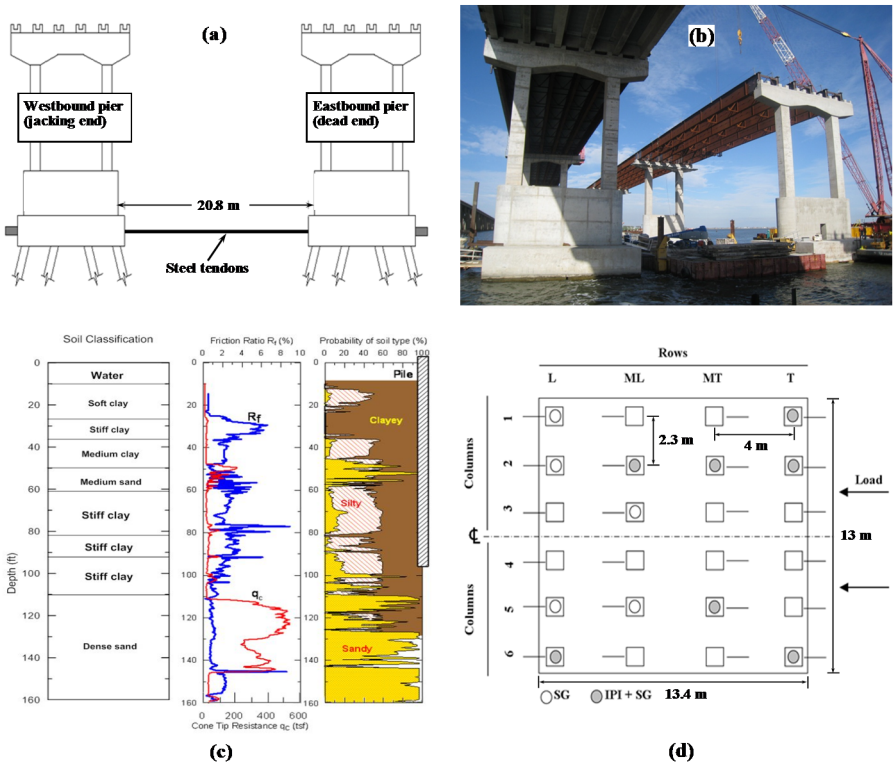


Fig. 2. (a) Illustration of lateral load test of M19 pier foundation, (b) test site, (c) soil layering and CPT profile, and (d) pile cap plan and piles labeling

FINITE ELEMENT MODEL DESCRIPTION

Two finite element (FE) models for the vertical and battered pile groups were developed in Abaqus finite element software package (v6.12). Each pile group model composed of pile group mesh and soil body mesh, and the two meshes interact at the pile-soil interface thru the interface model. To reduce the FE solution cost, the FE model geometry resembled half of the physical pile group geometry assuming the mirror plane passing along the load direction (Fig. 2d, Fig. 3). The pile group and soil meshes were created using the linear continuum brick elements with eight nodes (C3D8R). The number of elements for the pile group mesh was ~10500, and ~72000 for the soil mesh. The piles were placed in pre-bored holes created in the soil mesh (i.e. wish-in-place). The connection between the piles and the cap was assumed as a fixed-head connection. The prestress force in the piles was introduced using the embedded shell elements technique, which simulates the behavior of reinforcement bars (Abaqus 2011).

Load and boundary conditions

The loads applied in the FE models were: gravity, weight of superstructure, and lateral load. The geostatic stress equilibrium was initially achieved by applying the gravity load. The superstructure weight was applied as uniform distributed load on top of the pile cap in the global vertical direction. The lateral load was incrementally applied as uniform distributed load on the side of the pile cap in the global horizontal

direction. The maximum lateral load in the FE models was increased to a value higher than the experiment (H_{max} = 24.94 vs H_{exp} = 8.48 MN) to fully mobilize the soil resistance (Souri *et al.* 2015). For the boundary conditions, a pin-type constrained displacement was assumed on the far sides and bottom boundaries of the soil mesh, and a roller-type displacement condition was applied on the symmetry plane (Fig. 3).

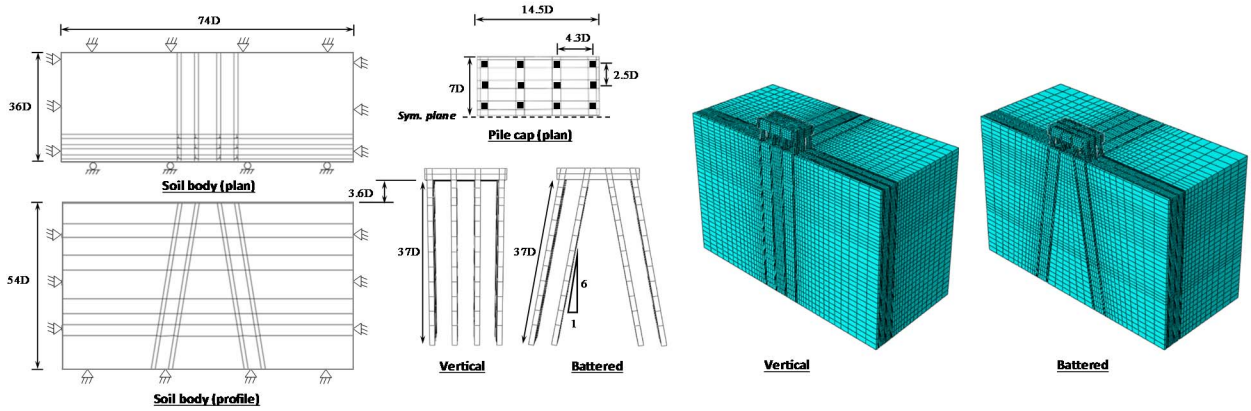


Fig. 3. Geometry and dimensions of the finite element models

Material constitutive models

The nonlinear material behavior is incorporated using elastoplastic constitutive models for pile concrete and soil materials. For piles, the concrete damaged plasticity (CDP) was adopted for its features such as the distinct stress-strain behavior in tension and compression regions and the material stiffness degradation (Abaqus 2011). The material stiffness degradation is introduced by the scalar damage parameter "*d*" as

$$D^{el} = (1 - d)D_0^{el}$$

where D^{el}, D_0^{el} are the damaged and undamaged elasticity matrices, respectively.

The modulus of elasticity used was $E_c = 35$ GPa corresponding to the concrete compressive strength $f'_c = 55$ MPa. The plastic behavior is controlled by the yield surface function and a non-associated flow rule with Mohr-Coulomb plastic potential function for the plastic strain rate. The scalar damage parameter '*d*' is a function of plastic strain and was back-calculated using analytical concrete models and data from the literature (Mander *et al.* 1988, Gupta and Maestrini 1990, Cicekli *et al.* 2007).

The Anisotropic Modified Cam-clay (AMCC) model was used to simulate the clay soil behavior (Dafalias *et al.* 2006). This model has the additional feature to capture the anisotropy of clays on top of the capabilities original of Modified Cam-clay model (Roscoe and Burland 1968). The elastic stiffness of the soil in the AMCC model is given by the bulk modulus $\left(K = \frac{1+e}{\kappa}\,\sigma'_m\right)$, which is a function of the effective mean-stress (σ'_m), void ratio (e), and the Cam-clay model parameter (κ). The plastic behavior is controlled by the yield surface and the associative flow rule for the evolution of plastic strains. The anisotropic soil behavior is numerically introduced by the variable 'α', which controls the rotation of the yield surface. More details for the AMCC model formulation and features can be found in Dafalias *et al.* (2006). The AMCC model was incorporated in Abaqus using the UMAT subroutine (Abaqus 2011), and the model parameters are summarized in Table 1.

For sands, the Drucker-Prager (DP) model was used. It is an elastoplastic model which is well known for modeling granular materials (Chen and Han 2007). Similar to AMCC model, the elastic stiffness is mean-stress dependent, and the plastic behavior is triggered by the DP yield surface with non-associative flow rule to control dilation. The DP model parameters are summarized in Table 1.

Pile-soil interface model

Gap formation at the pile-soil interface was achieved using the contact interaction feature. In the normal (to the surface) direction, a hard contact rule was adopted, which prevented pile-soil interpenetration and allowed separation (i.e. no transfer of tensile stresses). In the tangential direction, a friction contact rule was adopted, which controlled the sticking-slipping behavior. The slipping behavior at the interface is triggered when the interface shear stress limit ($\tau_{\lim}$) is exceeded. $\tau_{\lim}$ is selected as the smaller of stress values from the Coulomb friction criteria ($\tau = \sigma \tan\delta$) and the user-defined maximum stress limit ($\tau_{\max}$). The reason for using $\tau_{\max}$ is to cap the shear stress limit values for the cases of very large normal stress (σ). $\tau_{\max}$ is assumed as the average undrained shear strength for the soil profile. The interface model properties assumed were $\tan\delta = 0.5$, and $\tau_{\max} = 100$ kPa.

Table 1. Parameters for AMCC and DP models

Soil layer	Depth from G.L. (m)	Unit weight (γ) (kN/m^3)	Poisson's ratio (ν)	AMCC parameters						DP parameters			K_0
				κ	λ	M	α_{ini}	x	C	κ	β	d' (kPa)	
Soft clay	0-4.5	19.3	0.25	0.03	0.14	0.9	0.034	1.33	4	-	-	-	0.95
Stiff clay	4.5-7.6	18.7	0.20	0.01	0.12	1.1	0.111	1.33	4	-	-	-	0.85
Medium stiff clay	7.6-11.6	17.0	0.25	0.02	0.13	1.0	0.219	1.33	4	-	-	-	0.73
Medium sand	11.6-14.9	18.8	0.38	-	-	-	-	-	-	0.003	53	0.5	0.70
Stiff clay	14.9-21.3	17.7	0.20	0.01	0.12	1.2	0.271	1.33	4	-	-	-	0.65
Stiff clay	21.3-24.5	19.1	0.20	0.01	0.12	1.2	0.271	1.33	4	-	-	-	0.65
Stiff clay	24.5-30.1	20.1	0.20	0.01	0.12	1.2	0.363	1.33	4	-	-	-	0.60
Dense sand	> 30.1	19.4	0.40	-	-	-	-	-	-	0.003	58	0.5	0.60

* κ is slope of reload line in e-log p' plot; λ is slope of virgin consolidation line in e-log p' plot; M is slope of critical state line; α_{ini} is initial anisotropy ($\alpha_{ini} = \frac{1+3K_o}{1-2K_o}$); x and C are model constants; β is the friction angle in DP model; d' is soil cohesion in DP model; K_o is the coefficient of lateral earth pressure (σ_h/σ_v)

VALIDATION OF THE FE BATTERED PILE GROUP MODEL

The results from the FE model for the M19 battered pile group was compared to the static load test results for validation. The field test results utilized here are the displacement profiles obtained from the inclinometers, and the bending moment results at two depths from the strain gages. Fig. 4 compares the displacement profiles from the field test and FE battered pile group model. Good agreement between the field and FE model results is observed at the field lateral load H_{exp} = 8.48 MN. The profile with the dashed line represents the displacement profile from the FE model at the fictitious lateral load level H_{max} = 24.94 MN. It is noticed that the displacement in the piles diminished at depths greater than 18 m, which indicates that the depth of influence zone was about 15D (D is pile width) from the mudline.

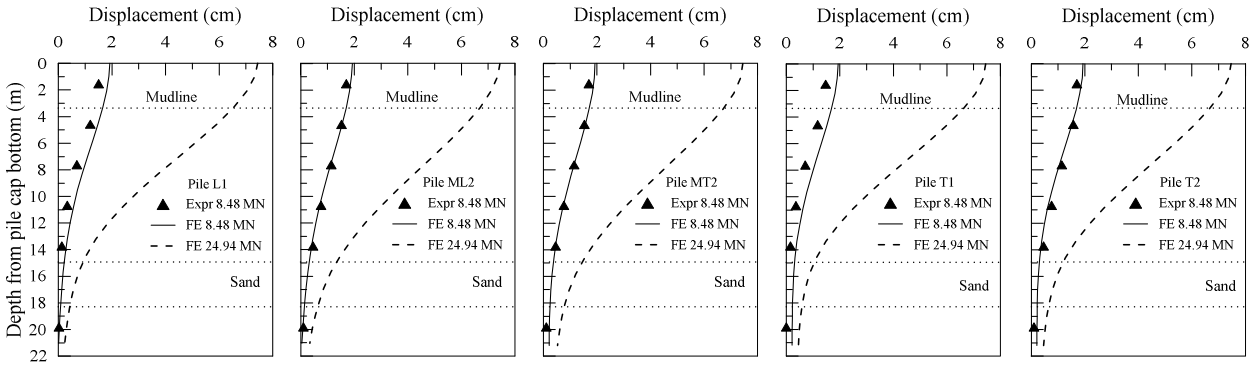


Fig. 4. Displacement profiles for instrumented piles for the battered pile group (Souri et al. 2015)

The bending moment results from the field test were obtained for the strain gages at depths 3.0 and 4.5 m from the pile cap bottom. The experimental and FE model results at lateral loads H = 2.58 and 7.91 MN are shown in Fig. 5. The load levels were selected following the strain gage data collected at the time of the experiment (Abu-Farsakh *et al.* 2011). A fairly good agreement between the field and FE model results can be seen.

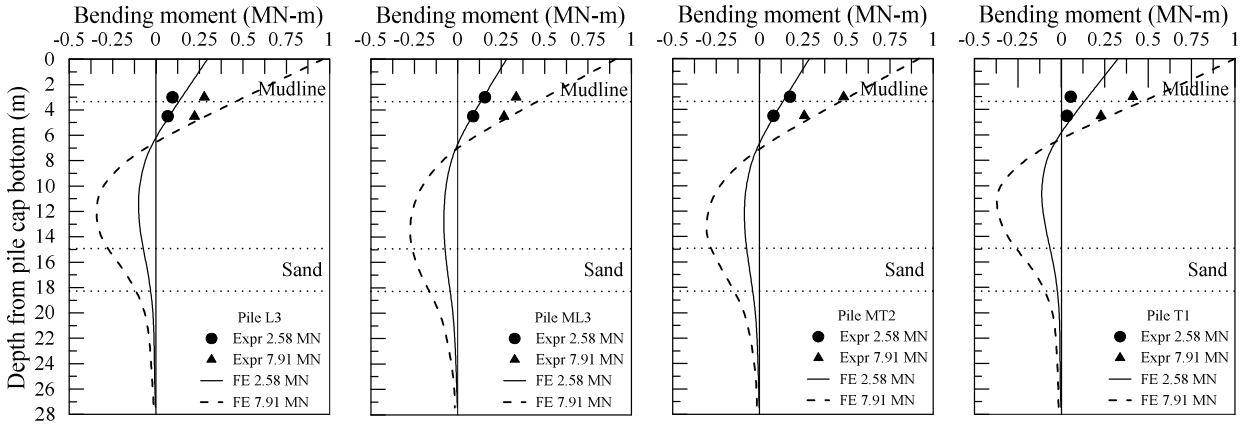


Fig. 5. Bending moment results for instrumented piles for the battered pile group (Souri et al. 2015)

RESULTS

After validating the FE battered pile group model, the FE model for the vertical pile group was developed by adjusting the inclination of piles. The results from both FE models are compared in the following sections.

Load-displacement curves

Comparison of the load-displacement curves is shown in Fig. 6. The vertical axis in the figure was normalized using the maximum lateral load applied in the FE model (H_{max}), and the horizontal axis was normalized using the pile width (D). The vertical pile group (PG) exhibited significantly lower lateral resistance compared to the battered PG at similar pile cap displacement. The maximum cap displacement in the vertical PG was ~70% higher than the battered PG, which is attributed to the greater lateral resistance of battered piles. The figure also shows the average lateral load carried by each pile row, which was determined from piles' shear at the pile cap level. It is noticeable that the load distribution is affected by the presence of battered piles. In the vertical PG, the largest load share was carried by the leading row L (31% at H_{max}) followed by rows ML (24%), MT (23%), and T (22%). Whereas in the battered PG, the middle rows (ML, MT) carried larger load share at 31% and 28%, whereas rows L and T carried 22% and 19%, respectively. The larger load share in the middle rows in the battered PG is attributed to the greater axial load in the middle row piles, which is presented in the next section.

Axial load

The variation of average axial load (F_{axial}) per row versus the lateral load (H) is shown in Fig. 7. Note that the sign convention used is positive for the compressive load (i.e. push in) and negative for the tensile load (i.e. pull out). First, it is noticed that the axial load in a row and its mirror was similar in magnitude and opposite in sign, assuming that the mirror axis passes between the middle rows (ML, MT) and perpendicular to the load direction. For example, the axial load in rows L and T was similar in magnitude and different in load sign. Second, the rows carrying the largest axial load were switched between the vertical and battered PGs. In the vertical PG, the axial load was largest in the leading and trailing rows (L and T) with an average of 8%. In the battered PG, the axial load was largest in the middle rows (ML and MT) and increased linearly with the lateral load from 10% to 12.5%.

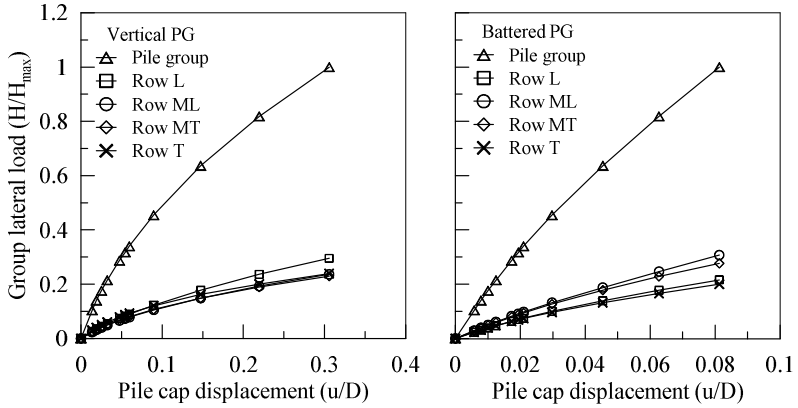


Fig. 6. Load-displacement curves for the pile cap and pile rows

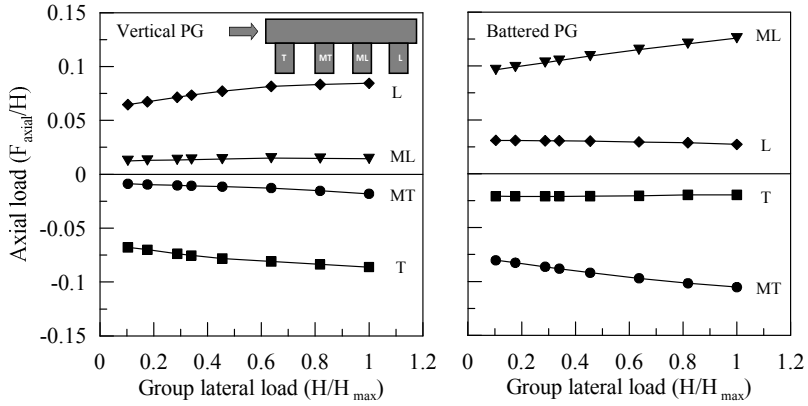


Fig. 7. Average axial load per row at the pile cap level

Soil resistance

The soil resistance to lateral pile movement is given by the sum of the net pressure on the front face of the pile and the side friction (Fig. 8). The soil resistance profiles from the FE models were obtained using the double differentiation of bending moment curve technique (e.g., Ilyas *et al.* 2004, Nip and Ng 2005, Abu-Farsakh *et al.* 2011). Fig. 9 presents the calculated soil resistance profiles for pile columns 1 and 2 in the PGs, with the zero-depth referring to the mudline. A positive soil resistance indicates that the resistance direction was opposite to the pile movement direction, and vice versa. It can be noticed that the shape of the profiles is similar in the same PG and is not affected by the pile position within the column (i.e. presence of other piles ahead and/or behind). Comparing the profiles in columns 1 and 2, there was a slight reduction in the soil resistance for column 2 piles, which was due to the influence of the shadowing effect. The depth at which the soil resistance changed sign was greater in the vertical PG at 18-20D compared to 15D in the battered PG, which indicates a greater influence depth for the vertical PGs. The negative soil resistance diminished at a shallower depth in the battered PG at 20D compared to 28D in the vertical PG. Finally, the mobilized soil resistance on the front face of piles was 58% higher in the vertical PG based on the average positive area under the soil resistance curves.

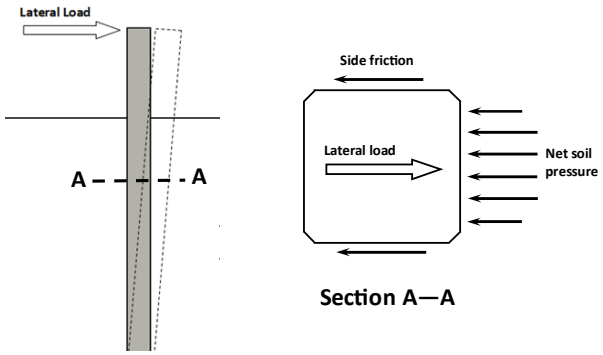


Fig. 8. Definition of the soil resistance for laterally loaded piles

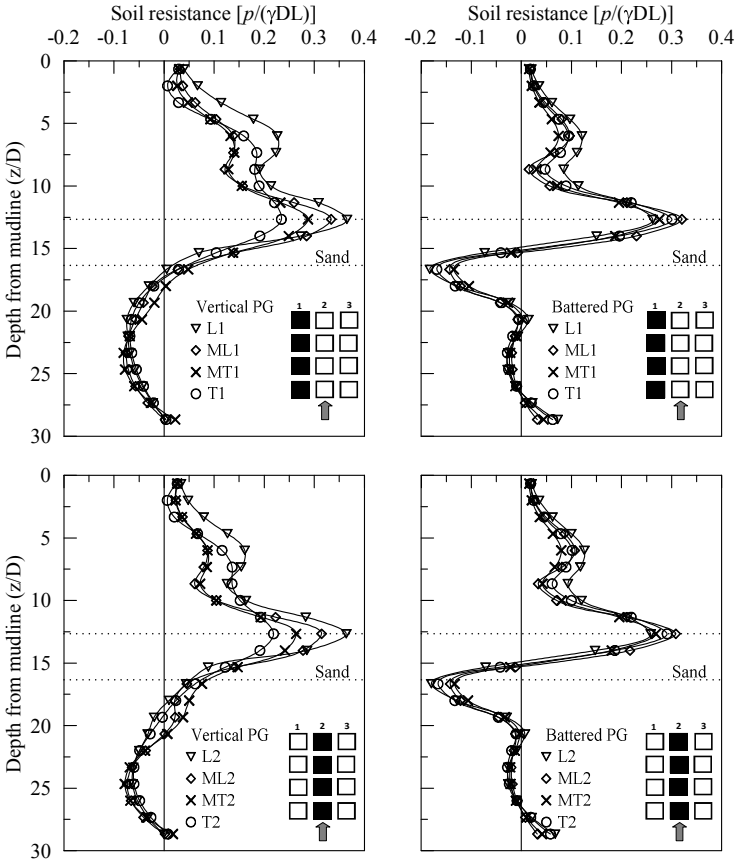


Fig. 9. Soil resistance profiles for columns 1 and 2 at load level H = H_{max}

SUMMARY AND CONCLUSIONS

The static lateral resistance of the vertical and battered pile groups was studied using 3D finite element modeling. The battered pile group model was developed and verified by the case study of M19 pier foundation of the I-10 twin span bridge in Louisiana, and the vertical pile group model was created by adjusting the inclination of piles from the battered pile group model. The lateral resistance of the pile groups was compared in terms of load-displacement curves, axial load in the piles, and soil resistance. The results showed that:

- The battered pile group had notably higher lateral resistance than the vertical pile group, in which the battered group had 60-70% lesser pile cap displacement at similar lateral loads.
- The distribution of lateral load within the rows was different between the pile groups. In the vertical pile group, the lateral load share in the first row was 31%, while it was closely distributed in the remaining rows at 24-22%. In the battered pile group, the percentage was 31-28% in the second and third rows, and 22-19% in the first and fourth rows, respectively.
- Only two rows in both pile groups generated a significant percentage of axial load. In the vertical pile group, the largest axial load percentage was in the first and fourth rows, while it was in the second and third rows in the battered pile group.
- The soil resistance profiles were similarly shaped for all piles within the same pile group. The mobilized soil resistance and the influence depth were notably less in the battered pile group, which highlights the influence of battered piles in improving the lateral resistance.

REFERENCES

Abaqus, 2011. *Abaqus Documentation*. Providence, RI: Dassault Systèmes.

Abu-Farsakh, M., Yu, X., Pathak, B., Alshibli, K., and Zhang, Z., 2011. Field testing and analyses of a batter pile group foundation under lateral loading. *Transportation Research Record: Journal of the Transportation Research Board*, 2212, 42–55.

Ashour, M., Pilling, P., and Norris, G., 2004. Lateral behavior of pile groups in layered soils. *Journal of Geotechnical and Geoenvironmental Engineering*, 130 (6), 580–592.

Brown, D., Reese, L., and O'Neill, M., 1987. Cyclic lateral loading of a large-scale pile group. *Journal of Geotechnical Engineering*, 113 (11), 1326–1343.

Brown, D., Reese, L., and O'Neill, M., 1988. Lateral load behavior of pile group in sand. *Journal of Geotechnical Engineering*, 114 (11), 1261–1276.

Chen, W. and Han, D., 2007. *Plasticity for Structural Engineers*. J. Ross Publishing.

Chow, Y.K., 1987. Three-dimensional analysis of pile groups. *Journal of Geotechnical Engineering*, 113 (6), 637–651.

Cicekli, U., Voyiadjis, G., and Abu Al-Rub, R., 2007. A plasticity and anisotropic damage model for plain concrete. *International Journal of Plasticity*, 23 (10–11), 1874–1900.

Comodromos, E.M. and Pitilakis, K.D., 2005. Response evaluation for horizontally loaded fixed-head pile groups using 3-D non-linear analysis. *International Journal for Numerical and Analytical Methods in Geomechanics*, 29 (6), 597–625.

Dafalias, Y., Manzari, M., and Papadimitriou, A., 2006. SANICLAY: simple anisotropic clay plasticity model. *International Journal for Numerical and Analytical Methods in Geomechanics*, 30 (12), 1231–1257.

Gupta, A. and Maestrini, S., 1990. Tension-stiffness model for reinforced concrete bars. *Journal of Structural Engineering*, 116 (3), 769–790.

Hussien, M.N., Tobita, T., Iai, S., and Rollins, K.M., 2012. Vertical loads effect on the lateral pile group resistance in sand. *Geomechanics and Geoengineering*, 7 (4), 263–282.

Ilyas, T., Leung, C., Chow, Y., and Budi, S., 2004. Centrifuge model study of laterally loaded pile groups in clay. *Journal of Geotechnical and Geoenvironmental Engineering*, 130 (3), 274–283.

Isenhower, W.M., Vasquez, L.G., and Wang, S.-T., 2014. Analysis of Settlement-Induced Bending Moments in Battered Piles. *In*: *From Soil Behavior Fundamentals to Innovations in Geotechnical Engineering*. Presented at the IFCEE 2015, San Antonio, TX: American Society of Civil Engineers, 497–511.

Mander, J., Priestley, M., and Park, R., 1988. Theoretical stress-strain model for confined concrete. *Journal of Structural Engineering*, 114 (8), 1804–1826.

Matlock, H., 1970. Correlation for Design of Laterally Loaded Piles in Soft Clay. Presented at the Offshore Technology Conference, Offshore Technology Conference.

McVay, M., Casper, R., and Shang, T., 1995. Lateral response of three-row groups in loose to dense sands at 3D and 5D pile spacing. *Journal of Geotechnical Engineering*, 121 (5), 436–441.
McVay, M., Shang, T., and Casper, R., 1996. Centrifuge testing of fixed-head laterally loaded battered and plumb pile groups in sand. *Geotechnical Testing Journal*, 19 (1), 41–50.
Meyerhof, G. and Yalcin, A., 1993. Behaviour of flexible batter piles under inclined loads in layered soil. *Canadian Geotechnical Journal*, 30 (2), 247–256.
Mroueh, H., and Shahrour, I. 2009. "Numerical analysis of the response of battered piles to inclined pullout loads." *International Journal for Numerical and Analytical Methods in Geomechanics*, 33(10), 1277–1288.
Murthy, V., 1964. Behavior of batter piles subjected to lateral loads. Ph.D dissertation. Indian Institute of Technology, Kharagpur, India.
Nip, D. and Ng, C., 2005. Back-analysis of laterally loaded bored piles. *Proceedings of the Institution of Civil Engineers - Geotechnical engineering*, 158 (2), 63–73.
Patra, N.R. and Pise, P.J., 2001. Ultimate Lateral Resistance of Pile Groups in Sand. *Journal of Geotechnical and Geoenvironmental Engineering*, 127 (6), 481–487.
Poulos, H. and Davis, E., 1980. *Pile foundation analysis and design*. New York: Wiley.
Rajashree, S., and Sitharam, T. 2001. "Nonlinear finite-element modeling of batter piles under lateral load." *Journal of Geotechnical and Geoenvironmental Engineering*, 127(7), 604–612.
Ranjan, G., Ramasamy, G., and Tyagi, R., 1980. Lateral response of batter piles and pile bents in clay. *Indian Geotechnical Journal*, 10 (2), 135–142.
Rao, S.N., Ramakrishna, V.G.S.T., and Rao, M.B., 1998. Influence of Rigidity on Laterally Loaded Pile Groups in Marine Clay. *Journal of Geotechnical and Geoenvironmental Engineering*, 124 (6), 542–549.
Reese, L., Cox, W., and Koop, F., 1974. Analysis of laterally loaded piles in sand. *In*: *Offshore Technology Conference*. Presented at the Offshore Technology Conference, Houston, TX.
Roscoe, K. and Burland, J., 1968. On the generalized stress-strain behaviour of 'wet' clay. *Engineering plasticity*, 535–609.
Souri, A., Abu-Farsakh, M., and Voyiadjis, G., 2015. Study of static lateral behavior of battered pile group foundation at I-10 Twin Span Bridge using three-dimensional finite element modeling. *Canadian Geotechnical Journal*, 53 (6), 962–973.
Yang, Z. and Jeremić, B., 2002. Numerical analysis of pile behaviour under lateral loads in layered elastic–plastic soils. *International Journal for Numerical and Analytical Methods in Geomechanics*, 26 (14), 1385–1406.
Zhang, L., McVay, M., Han, S., Lai, P., and Gardner, R., 2002. Effects of dead loads on the lateral response of battered pile groups. *Canadian Geotechnical Journal*, 39 (3), 561–575.
Zhang, L., McVay, M., and Lai, P., 1999. Centrifuge modelling of laterally loaded single battered piles in sands. *Canadian Geotechnical Journal*, 36 (6), 1074–1084.

CUTTER SOIL MIXING AND AUGERED-CAST-IN-PLACE PILING CLOSE TO THE GULF OF MEXICO

Justin Simmons, BAUER Foundation Corp., Odessa, Florida, USA, (727) 531-2577,
justin.simmons@bauerfoundations.com
Michael Arnold, BAUER Foundation Corp., Odessa, Florida, USA, (727) 531-2577,
michael.arnold@bauerfoundations.com
Bob Faulhaber, BAUER Foundation Corp., Odessa, Florida, USA, (727) 531-2577,
bob.faulhaber@bauerfoundations.com

ABSTRACT

In order to remodel an existing beach resort on the Gulf of Mexico, an existing three story structure, founded on stepped tapered piles, was to be replaced by a ten-story building with service rooms on a daylight basement level, conference rooms on the next levels and up-scale hotel rooms on the upper levels. The new building was founded on augered-cast-in-place (ACIP) piles. The pile caps and the basement required excavations between nine and fifteen feet (three to five meters) below ground surface.

BAUER Foundations Corp. (BFC) successfully used Cutter Soil Mixing (CSM) to install the support of excavation walls. This technique allowed for the adjustment of the wall alignment during execution in order to avoid existing and new piles and other underground obstructions. Nearly 1600 – 16-inch (400 mm diameter) ACIP piles were installed to an average depth of 71.5 feet (22m) below ground surface (BGS) by BFC to support the new hotel structure. Initial grout overages in piles were excessively high and ground stability issues were encountered in some pile locations. By identifying specific areas of concern BFC was able to modify the approach to ACIP installation, effectively mitigating the ongoing risks and successfully completed the project.

Keywords: cutter soil mixing (CSM), augered-cast-in-place (ACIP) piles

PROJECT

Marriott Hotels began the $300 million renovation and upgrade of their Marco Island Marriott Beach Club Hotel in Marco Island, FL to JW Marriott status in May 2015. The renovation included the demolition of a portion of their existing hotel tower, and the construction of a new 10-story hotel tower consisting of 94 new guest rooms and a 10,000 SF (900 m2) ballroom, among other amenities. As is typical with hotel construction, time was of the essence. The schedule was the driving factor of this project as the owner had already booked events in their new ballroom starting in January of 2017.

BFC provided the client with a deep foundation package that included the installation of 1562 Augered Cast-In-Place (ACIP) piles supporting the new tower, and the design and construction of approximately 36,500 SF (3,400 m2) of soil-mixed retaining wall for support of excavation (SoE).

 © 2017 DFI Annual Conference, New Orleans, LA, USA

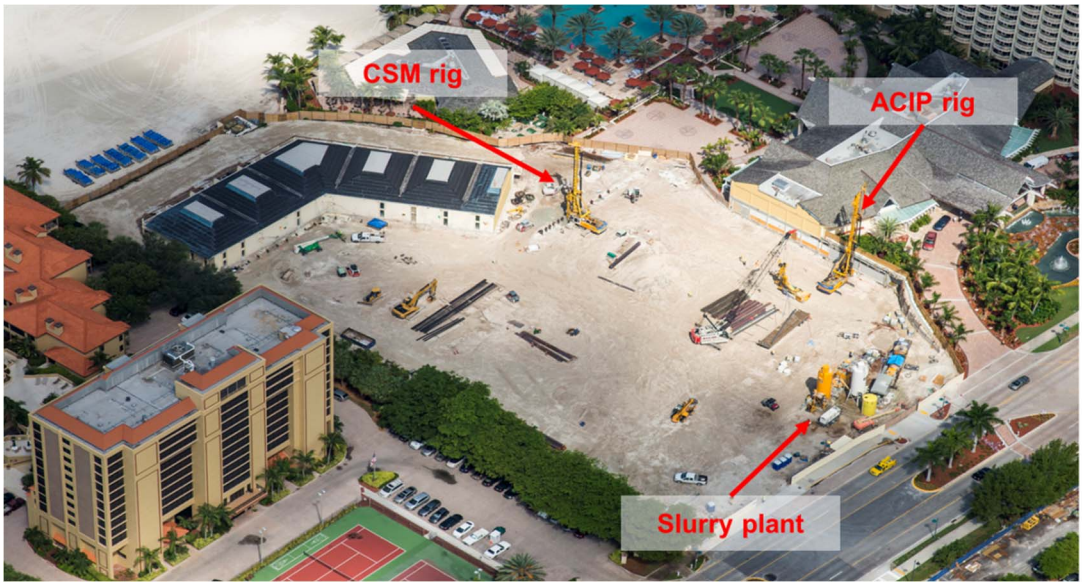


Figure 1: Site Aerial. Source: Austin/Gilbane Joint Venture

GROUND CONDITIONS

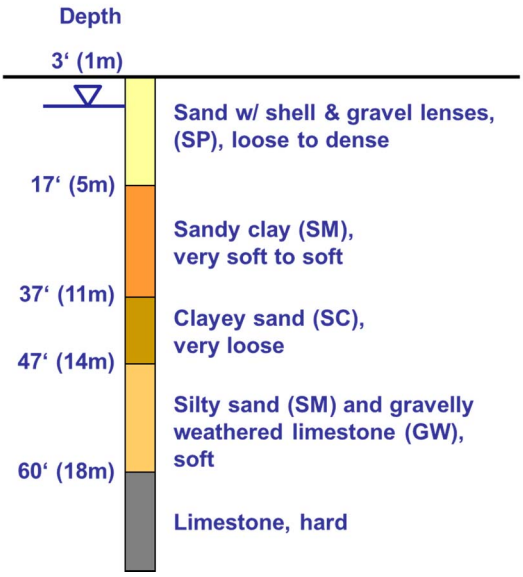


Fig. 2 : Idealized Soil Profiles

The site was generally flat with a working grade elevation of +6 to +9 feet NGVD, depending on the location. The groundwater table was generally encountered at an elevation of +3 to +5 feet NGVD. However, thin lenses of shell and gravel in the upper 17’ (5 m) of the soil across the site allows rapid lateral water movement. These lenses allow nearly free flow of water in the lateral direction and soil transport with it. As a result, the groundwater level fluctuates with the Gulf of Mexico tide levels and also with rainfall.

Based on the site soil borings, the generalized soil profile consists of loose to dense sand extending from grade to a depth of approximately 17’ (5 m), underlain by a very soft to soft sandy clay from 17’ to 37’ (5 to 11 m) deep, followed by a very loose clayey sand from 37’ to 47’ (11 to 14 m), and then a soft weathered limestone to a depth of 60’ (18 m), atop a hard limestone layer extending to 90’ (27 m) below grade. Figure 2 shows an idealized soil profile of the site.

CUTTER SOIL MIXED SUPPORT OF EXCAVATION WALLS

BFC proposed Cutter Soil Mixing (CSM) to install the support of excavation (SoE) walls. The CSM method provided two significant benefits for the project, little to no vibrations during installation and higher stiffness than traditional sheet piles. The reduction in potential vibration and deformations were both of critical importance to this project because of the proximity to existing, occupied buildings.

Design

To design the SoE system, BFC worked with Gordon Geotechnical Engineering of Salt Lake City, Utah. The following description is based on DeBernardi (2015)

The general contractor decided to install a dewatering system inside the excavation. The SoE terminated in the silty sands and cut off the lateral groundwater inflow. The different finished floor elevations within the footprint of the building and the different pile cap geometries resulted in exposed wall heights of 9.5 to 15 feet (2.9 to 4.6 m), c.f. Fig. 3. Walls up to 10 feet (3.0 m) exposed height were designed as cantilever walls, while most of the deeper excavations received one layer of tiebacks approximately 3 feet (0.9 m) below ground surface. The total wall depths varied from 26 to 35 feet (7.9 to 10.6 m).

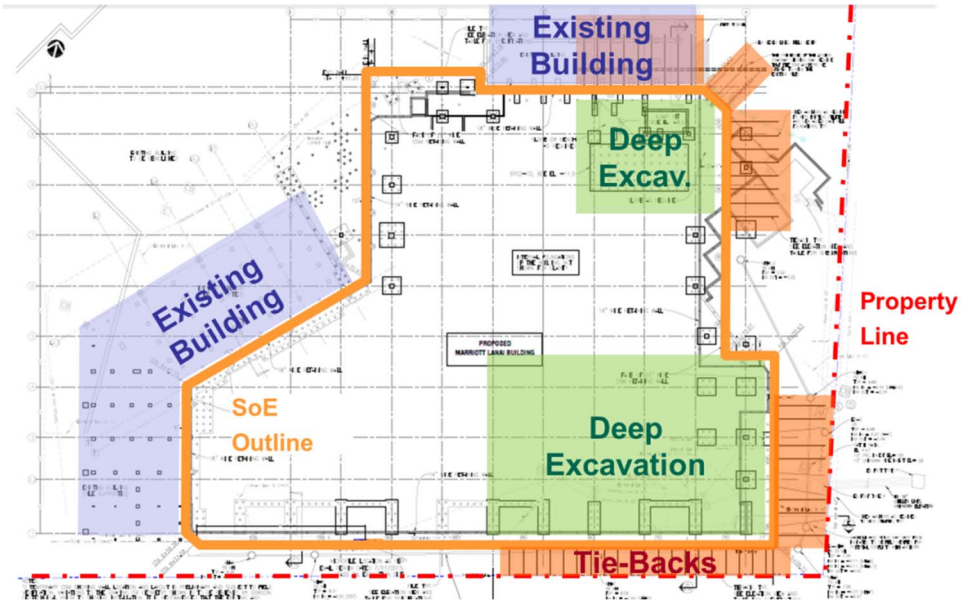


Figure 3: Plan View SoE.

BFC selected a wall width of 25 inches (640 mm). A minimum 28-day unconfined compressive strength (UCS) of 350 psi (2.5 MPa) was used in the design for the soil mix material, which acts as lagging in this soldier pile wall system. Different weights of 18-inch (460 mm) deep wide flange beams were used as soldier piles. Where tie-backs were installed, the single wide flange beams were replaced by two lighter wide flange beams with a 8-inch (200 mm) clear spacing. The spacing of the soldier piles was typically 8 feet (2.4 m), but was reduced to 4 feet (1.2 m) at the north west section of the SoE where a forest of piles at a slightly deeper excavation prevented the use of tie-backs.

The two-strand tie-backs carried typical design loads of 62 to 70 kips (275 to 310 kN). The proximity of the property line at the south side and the owner's decision not to seek easements, neither temporary nor permanent, restrained the available tie-back and bond lengths considerably. Due to the limited tie-back capacity of 31 kips (140 kN) in this section the loads on the CSM SoE wall had to be reduced, which was achieved via additional dewatering on the outside of the wall.

Installation

The cementitious slurry was mixed with a MAT SCC40 colloidal batch mixer. The CSM SoE wall was installed with a BCM10 CSM tool mounted on a BG28 drill rig (Fig. 4). Following completion of the CSM scope the tooling on the BG28 was changed and the rig was able to continue with ACIP installation. This versatility saved both cost and time by eliminating a mobilization.



Figure 4: BG28 with CSM tool installing a CSM panel

The CSM SoE system consisted of panel elements 110 x 25 inches (2.8 m x 0.64 m) in dimension installed sequentially with steel soldier pile members. The steel soldier piles were installed as soon as a panel was completed, by lowering the members in the fresh soil mix with a crane. (Fig. 5)



Figure 5: Freshly installed wall with soldier piles

Obstructions

The client provided an as-built drawing of the existing site conditions, but unfortunately, several conditions were not accurately reflected. This included three existing piles that were found in the alignment of the CSM wall. While it was possible to extract the first one encountered, the trials to remove the other two piles failed. In one of the cases it was possible to shift one panel 6 inches (0.15 m) towards the excavation in order to bypass the pile. In another case, four panels were realigned creating a V-shaped section of the wall. Other obstructions not included in the plans during the design of the wall included a short soldier pile and lagging wall at the northeast corner of the excavation and electrical lines on the southeast corner. In both cases it was possible to redesign the wall alignment including soldier pile position and tie-back orientation in order to avoid the obstructions. Because of the flexibility of the CSM SoE system obstructions were accommodated with alignment changes in the field.

Quality Control and Results

The cementitious slurry was checked at the batch plant by taking at least one sample per panel. The slurry sample was tested for specific gravity, Marsh time and temperature. Furthermore, 3 inch x 6 inch (75 mm x 150 mm) cylinder samples were produced twice daily and tested after 28 days for unconfined compressive strength (UCS). Wet grab samples were taken daily from the fresh CSM panels at arbitrary 5-foot (1.5 m) intervals. Pairs of these samples were tested for UCS after 7, 14 and 28 days. The average strength after 28 days was 470 psi. Several samples at a depth of 30 feet (9 m) throughout the project did

not achieve the minimum design strength. The Quality Control testing of the grout/slurry did not reveal any issues. The samples consistently developed strength. Samples taken from the same CSM panels but at different depth also achieved the design strength. For these reasons it was concluded that the reason for the low strength at this depth was related to a higher water content than anticipated in this layer. Based on the strength gain beyond 28 days and the load conditions at this depth the Engineer accepted the wall.

Performance

The excavation took place without reported issues after BFC had demobilized from site. The client expressed later that they were very happy with the CSM SoE wall as it was installed without vibrations and it performed well while being excavated (Fig.6).



Figure 6: Excavated wall at south side with internal and external dewatering

AUGERED-CAST-IN-PLACE PILING

Design

Augered Cast-In-Place (ACIP) piles were selected by the design engineer as the primary foundation system for the new hotel structure. The ACIP deep foundation system consisted of 1,572 16-inch (400 mm) diameter piles, with compression loads of 150T (1,330 kN) and tension loads of 65T (580 kN). The piles were designed with a tip elevation of – 64.0’ NGVD/71.5’ (21.8 m) BGS, and were configured in a system of pile caps as well as individual piles that provided both uplift resistance and vertical support for the structural slab.

Due to the local ground conditions, and based on previous experiences with ACIP pile construction in the area, initial estimates of grout overages were in the range of 170% of neat line volume. Despite the

anticipated large grout overages, ACIP piles were considered the best system based on both schedule and costs.

Installation

Prior to the start of production piles, a load test program including both static compression and tension tests was conducted to confirm the pile design assumptions. The ACIP piles were installed in parallel to CSM production. Due to the zones of loose sands and soft silts, along with tidal influences, initial grout overages in piles were excessively high, in the range of 300% of neat line volume. During the installation of the final compression test reaction pile, a complete grout return was never achieved. As the auger was extracted, a loss of grout head occurred resulting in a collapse of the pile. Rather than abandoning the test pile location and the seven previously installed piles, BFC recommended and installed two micropiles on either side of the abandoned reaction pile location to allow for a uniform reaction on all piles. The micropiles were installed using the Klemm 806 rig (Fig. 7), which was onsite for tieback installation.



Figure 7: Klemm 806 installing micropiles for load test reaction

Following the successful load test program, production was scheduled for an immediate start. Due to the aggressive schedule of the project two (2) BG-28 rigs were utilized for the pile production.

Installation of initial piles proved difficult in areas of the site, particularly at the west side of the site, nearest the Gulf of Mexico. During installation of these piles, initial attempts to maintain a positive head of grout resulted in grout overages exceeding 400% of the pile volume. This was mostly attributed to grout losses into the lenses of shell and gravel in the upper soils which provided a nearly direct connection to the Gulf of Mexico. Grout return was never achieved and surface collapses were experienced on multiple piles during auger extraction (Fig. 8). It is suspected, that some of those soils had developed an overcritically loose grain skeleton or even some voids due to internal erosion caused by tidal groundwater flow. When subjected to auger-induced mechanical action, the grain skeleton or the voids collapse.



Fig. 8: Ground collapse at pile locations

Collapses at ground surface present a major safety issue when drilling with a BG rig, as the tracks sit within a few feet of the pile being installed. Following initial attempts on multiple piles in the area of concern, and multiple pile and ground surface collapses, a different approach to grouting was considered in an effort to reduce safety risks, time, and costs related to the grouting of piles. Following discussions with the client and geotechnical engineer, it was agreed that the best approach to mitigating the time and cost risk to the project was to establish a 10-foot (3 m) theoretical minimum head of grout above the auger tip at the beginning of grouting, and extract the auger at a continuous rate such that a minimum volume of 110% of theoretical volume was achieved per lineal foot of pile. While this approach did not reduce the risk of ground collapse, BFC felt that there was no additional risk to the crew of equipment. In order to try and mitigate the large grout takes, BFC focused on installing the piles along the perimeter of the site nearest the Gulf of Mexico, subsequently improving the ground around the entire site, and creating a barrier which would help reduce excessive grout overages.

Following the completion of the line of piles closest to the Gulf of Mexico, it was immediately observed that the grout takes were significantly reduced and were in the average range of 150% of theoretical volume. At this stage, no further ground collapse issues were encountered for the duration of the project.

In total, 1,562 piles were installed following design changes during production. Pile production took place during the months of July – October, much of which was during the peak rainy season. The jobsite experienced afternoon thunderstorms nearly every day for the months of July and August. The GC initially graded and prepared the working platform without the addition of a stone working surface. This condition, coupled with the excessive rain during the months of July and August, resulted in significant delays to production because the condition of the work platform (Fig. 9) prevented work from being performed in a safe and efficient manner. These delays prompted the GC to dewater and re-grade the

work area and install a 4 inch thick stone working surface. After the installation of this platform, work recommenced and no further delays were experienced.



Fig. 9 – Poor platform conditions due to rain and lack of platform maintenance

Quality Control and Results

Installing rebar cages from a working grade above the top of rebar elevation requires care to insure that the cage is installed to the proper elevation. This is even more difficult with cages which do not extend to the bottom of the pile, as they need to be tied off at the proper elevation. Multiple slab design elevations presented additional difficulties with placing rebar cages at the proper elevation. In total there were 50 different cage elevations utilizing two different cage designs, with some top of rebar cage elevations being as deep as 14' (4.3 m) below working grade.

The first quarter of the project was constructed by trying to install the rebar cages to the exact elevation. This proved to be difficult, time consuming, and led to confusion for both the field personnel and engineers. To reduce confusion and speed installation of the rebar cages, BFC provided a design that reduced the type and lengths of cages to three (3) different options. In order to accomplish this, BFC agreed with the Contractor to install a single cage design and extend the reinforcement cages in certain piles to allow a more efficient means of tracking and installing cages. This solution required additional expense for BFC, because of the additional steel required, but the time saved and the assurance of installing the reinforcement to the proper elevation more than made up for the additional costs. As the Contractor was already providing pile cutoffs, there was little to no impact to their costs, and the majority of the upper portion of the pile was cutoff, as opposed to chipped down to expose the rebar.

BAUER's B-Tronic on-board computer system provided the necessary information to confirm the piles were installed to the proper depth, and that the required grout volumes per unit of pile were introduced into the pile. Fig. 10

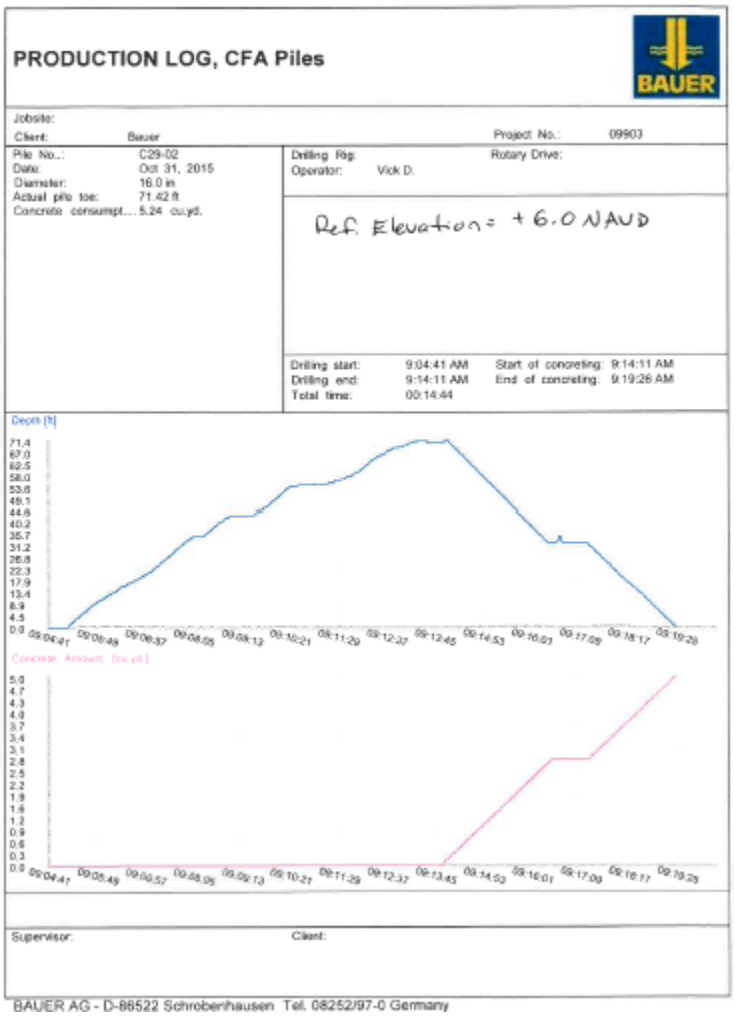


Fig. 10: B-Tronics Record from ACIP Pile Installation

CONCLUSION

A combination of in service facilities, unforeseen existing foundations, proximity to the Gulf of Mexico, and challenging geotechnical conditions resulted in a complex foundation and support of excavation project. Many of these challenges had to be addressed "on the fly" while the project was under construction in a schedule critical environment. BFC was able to address these challenges by applying the versatility of the CSM system and creative thinking to complete the foundation and SoE system within the project schedule.

REFERENCES

DeBernardi, B., 2015. Project plans and design memorandum: Temporary Cutter Soil Mix (CSM) wall Marriott Lanai Building.

DESIGN, CONSTRUCTION, AND PERFORMANCE OF THE TEMPORARY EARTH RETENTION SYSTEM AT NO. 9 WALTON

Joel B. Dellaria, SE, PE, Hayward Baker Inc., Roselle, Illinois, United States, 630-339-4300, jbdellaria@haywardbaker.com
Justin R. Lewis, PE, Hayward Baker Inc., Roselle, Illinois, United States, 630-339-4300, jrlewis@haywardbaker.com

ABSTRACT

No. 9 Walton is a new high-rise condominium building located in the Gold Coast area of Chicago. The adjacent building, *Walton on the Park*, featured 4 levels of below grade parking and utilized a secant pile wall with integral drilled shafts to support the exterior columns. The earth retention system (ERS) for *No. 9 Walton* also employed a secant pile wall in combination with drilled shafts. The excavation into the soft Chicago clays varied in depth from 9.75 m to 12.5 m (32 feet to 41 feet) below grade. The temporary excavation support used internal braces from the new secant piles to the existing foundation system of *Walton on the Park* to provide earth retention. Engineering teams for both projects worked together to design the bracing scheme and connections to ensure that the new excavation and internal bracing would not overstress any elements of the existing structure. Further complicating the project, immediately to the west of the project was a historic church founded on shallow spread footings which required underpinning to minimize movements.

The project involved three different building owners, small values for acceptable wall movement, an extensive monitoring program and the challenges of merging two earth retention systems. The subsurface conditions at the site, the adjacent structures, the excavation, and the performance are described. A summary of the design methods and the expected movements of the ERS are discussed, and the performance monitoring system is described. Overall, the ERS performed better than expected with less than 1 inch of measured lateral wall movement during and after the excavation was completed. Measured performance of the ERS is compared to the predicted performance and to the performance requirements for the project.

INTRODUCTION

No. 9 Walton is a new high-rise condominium building in Chicago located in the Gold Coast. The building has 3 levels of below grade parking and 36 levels of living space above grade. Developers originally slated the project to be Phase 2 of the *Walton on the Park* development built in the mid 2000's, using portions of the existing foundation system for development of the new structure. However, the housing market crash in 2007 prompted cancellation of Phase 2 of the *Walton on the Park* development. The property sat undeveloped until 2015 when design and construction for *No. 9 Walton* began under a new development and design team. The project team completed foundation excavation and below grade structures in 2016 with the first units of the building turned over to new homeowners in 2017.

The structural design for *No. 9 Walton* consisted of reinforced concrete columns and slabs, supported laterally by a heavily reinforced concrete central core. Drilled shafts to rock supported the interior columns and core with the exterior columns and foundations integrally included in the earth retention system. The structure had a below-grade footprint of approximately 1,490 m^2 (16,000 ft^2). The general excavation extended 9.75 m to 12.5 m (32 feet to 41 feet) below street level with the deepest portions at the central building core mat foundation.

 © 2017 DFI Annual Conference, New Orleans, LA, USA

SITE CONDITIONS

Soft to medium clays that extended a substantial distance below grade dominated the subsurface stratigraphy of the site and influenced the ERS design. Approximately 4.3 m (14 feet) of loose to medium dense urban fill, sands, and silts with N-values ranging from 1 to 36 and averaging 7, characterized the top of the site soil profile (Figure 1). In some borings, a thin crust layer of stiff to very stiff clay existed, but designers did not consider it to be consistent or thick enough to affect the design. Approximately 6.7 m (22 feet) of soft to medium clay, with pocket penetrometer test results between 24 kPa (0.25 tsf) and 72 kPa (0.75 tsf), and moisture contents ranging from approximately 20 to 31 percent underlaid the fill and silt. Beneath the soft to medium clay was stiff to very stiff clay with pocket penetrometer results generally between 96 kPa (1.0 tsf) and 335 kPa (3.5 tsf), and moisture contents ranging generally from 12 to 18 percent.

In situ vane shear tests, conducted to evaluate the strength of the soft to medium clay, revealed shear strengths ranging from as low as 14 kPa (300 psf) to as high as 53 kPa (1,100 psf). The stiff to very stiff clays below -11 m (-36 ft) had shear strengths generally above 48 kPa (1,000 psf), and increasing with depth (Figure 2). The presence of the soft clay immediately below the cut provided a challenge for the ERS design.

Existing buildings located west and south of the proposed site of the new building further complicated the design (Figure 3). The building to the west of the site was a 3-story historic church with one level of basement and founded on shallow foundations consisting of unreinforced limestone blocks. The building to the south was the previously referenced, *Walton on the Park*, which was a 39-story residential tower with 4 levels of below grade parking and founded on drilled shafts.

City streets bordered the east and north sides of the site with many utilities located below the streets and sidewalks. On the north side, the nearest utility, located approximately 4.0 m (13.0 feet) north of the property line, was an electrical duct bank. Other utilities included additional electrical duct banks and a water main. On the east side, the nearest utility, located approximately 4.3 m (14.0 feet) east of the property line, was a water main. Other utilities on the east side included an electrical duct bank, a gas line, and a communication line. Additionally, the Chicago Transit Authority Red Line tunnels

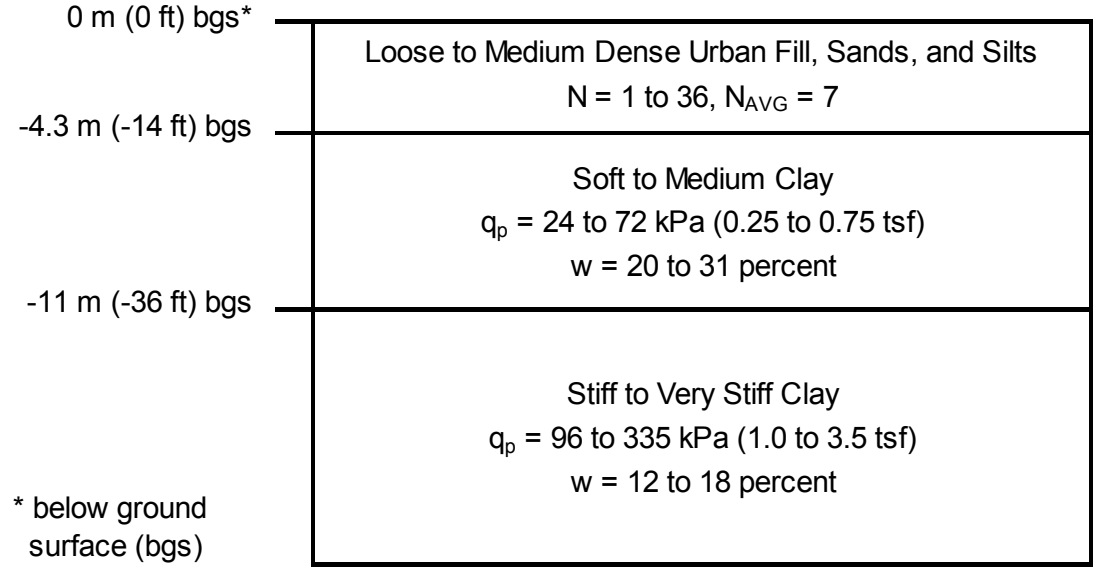


FIG. 1: Generalized Soil Profile

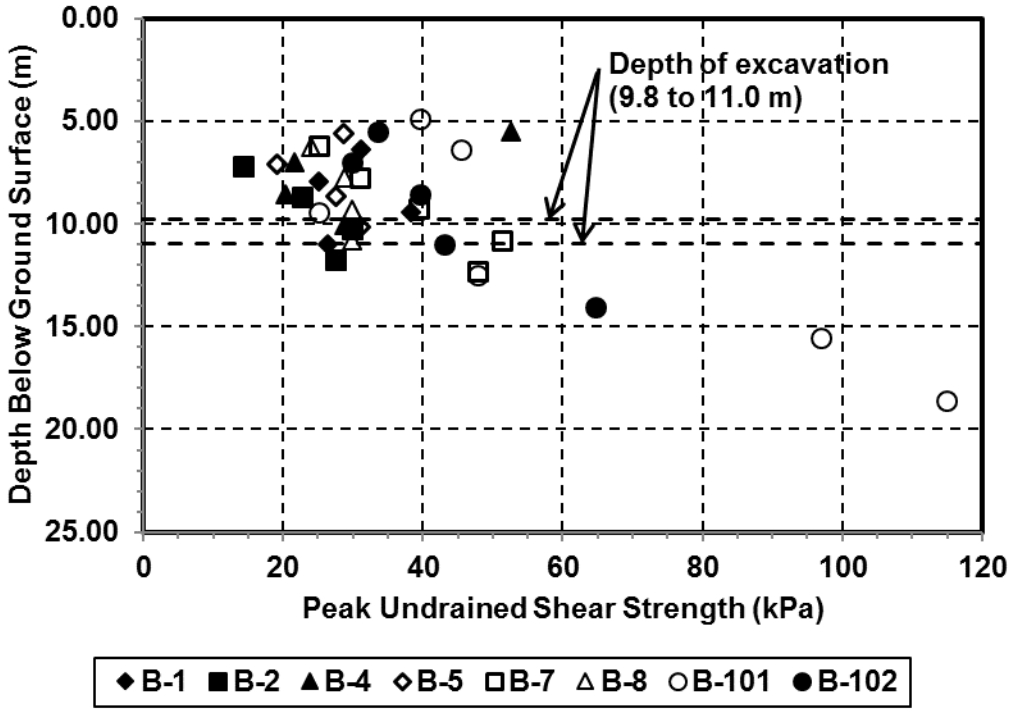


FIG. 2. Peak Shear Strength Results from Vane Shear Tests

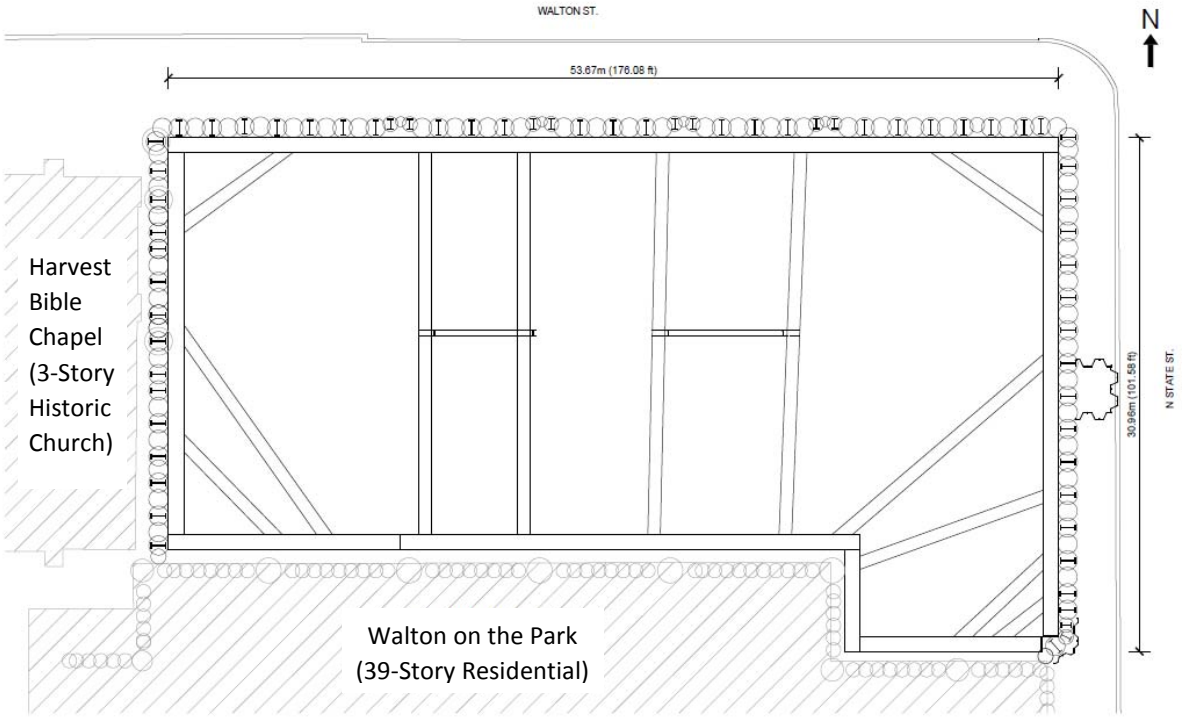


FIG. 3. Plan View of Proposed ERS (Not to Scale).

(subway) existed approximately 3.4 m (11.0 feet) east of the property line, below State Street. The excavation did not affect the tunnels due to the depth of the tunnels relative to the excavation depth.

SELECTION AND DESIGN OF EARTH RETENTION SYSTEM

In 2007 and 2008, Hayward Baker Inc. (HBI), in partnership with Case Foundation Company (CFC), designed and constructed the internally-braced earth retention system for *Walton on the Park*, adjacent to the site of *No. 9 Walton*. The system consisted of a secant pile wall with integrated drilled shafts to rock supporting the exterior columns of the building. Due to the success of *Walton on the Park* a decade earlier, the proposed depth of excavation, and the subsurface characteristics, the owner wanted to utilize a similar system at *No. 9 Walton*.

Project plans located the earth retention system tight to the property line on all four sides of the project to maximize building space. The secant piles served as the temporary earth retention, as well as the long-term foundation and exterior wall for the below grade parking area. Designers considered two diameters of secant piles, 880 mm (34.6 in) and 1180 mm (46.5 in). There were two advantages to the 880 mm piles. First, the 880 mm piles required a smaller total volume of concrete and second, they allowed for additional space in the below grade parking area due to their smaller size. Alternately, the 1180 mm piles were stiffer leading to smaller deflections of the wall. Also, there were fewer 1180 mm piles required to complete the perimeter of the excavation than the smaller 880 mm piles.

Ultimately, the advantages of stiffness and efficiency of the 1180 mm piles prevailed over the slight increase of building space provided by the 880 mm piles for most of the wall sections. Exceptions included four locations of columns that were offset from the north perimeter of the excavation so the drilled shafts supporting those columns could be belled without crossing the property line. These four locations required the use of two (2) 880 mm and one (1) 610 mm (24 in) piles to fit between the offset building column and the property line limits. A W36x160 beam placed in every second column reinforced the 1180 mm secant piles, and a W24x146 beam reinforced each of the 880 mm columns.

Two (2) levels of internal wales and pipe braces supported the secant pile walls during excavation and the garage floor slabs supported the secant pile walls in the permanent condition. Designers considered tiebacks as a means of support but these were ultimately rejected due to municipal right-of-way issues and conflicts with existing utilities and the subway. The internal bracing consisted of wide-flange wales, ranging in size from W36x262 to W36x361, with steel pipe struts (76.2 cm x 1.27 cm [30 inches x ½ inch] and 76.2 cm x 1.59 cm [30 inches x 5/8 inch]). The longest struts utilized mid-span supports to minimize the unbraced length of the strut. The mid-span supports consisted of vertical H-piles with horizontal support beams welded to the vertical piles.

Existing grade was approximately elevation +4.3 m (+14.25 feet) Chicago City Datum (CCD) with a 9.8 m (32 foot) excavation to elevation -5.4 m (-17.75 feet) CCD at the west and east sides of the site and an 11.0 m (36 foot) cut to elevation -6.6 m (-21.75 feet) CCD at the middle portion of the north side of the site. The tops of the secant piles were at elevation +3.0 m (+9.75 feet) CCD with the top of cap beam approximately at existing grade (Figure 4).

The design of the ERS considered four (4) temporary support conditions:

1. First Intermediate Stage Condition (Cantilever)
2. Second Intermediate Stage Condition (1-Level Brace)
3. 9.8 m (32 foot) cut
4. 11.0 m (36 foot) cut

The designers used the following assumptions to prepare the design calculations:

- Moist and Saturated Unit Weight of soil = 1920 kg/m^3 (120 pcf)
- Uniform Surcharge Loading (for Construction Equipment/Material) = 12 kPa (250 psf)
- Internal Angle of Friction for Fill Layer = 30°

For simplicity of design, the designers assigned constant shear strength values to six clay layers consistent with the stratigraphy reported from the soils exploration. Table 1 lists the strength values.

Rankine earth pressure theory determined the lateral soil pressure coefficients for the active and passive earth pressure calculations of all cross sections and construction stages. For design stages with multiple brace levels, the design used apparent earth pressures above the excavation line. The soil friction of the active block above the cut also reduced active pressures below the bottom of the excavation.

For predicting the deflections of the ERS, the design utilized the methods presented in Clough (1985). This empirical method predicts deflections based on the factor of safety against basal heave and the stiffness of the ERS. For this project, the stiffness of the system was relatively high. Therefore, the predicted deflection was much more dependent on the factor of safety against basal heave. With the calculated factors of safety less than 2.0, small changes in the shear strength values used in the calculation of the basal heave factor of safety had a large impact on the predicted deflections.

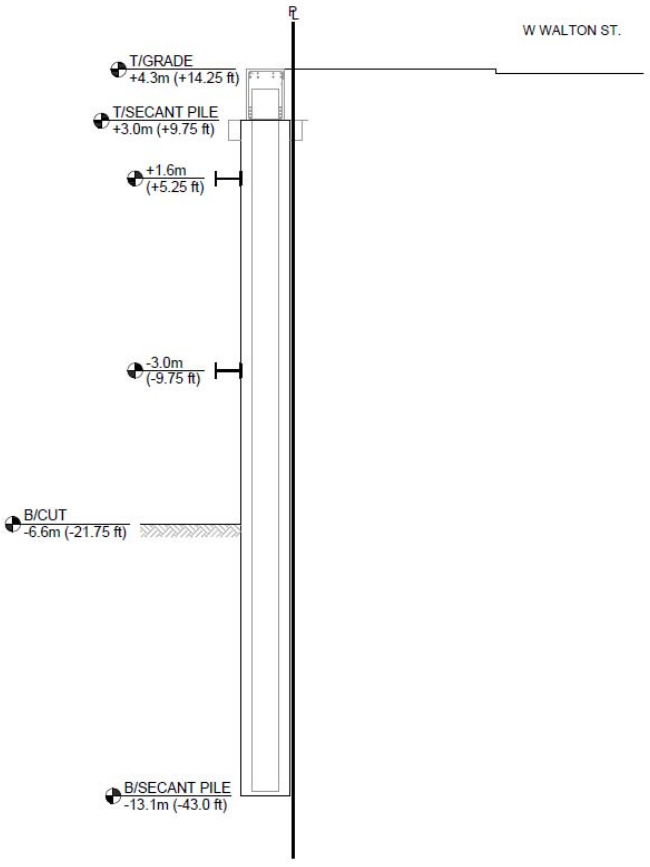


FIG. 4. Typical Section for the 11.0 m (36 ft) Excavation Depth

Table 1. Shear strength values for the very soft to medium clays based on the available geotechnical information.

Depth to		Shear Strength used in Design		Range of Vane Shear Test Results	
Top of Layer	Bottom of Layer	(kPa)	(psf)	(kPa)	(psf)
4.3 m (14 ft)	5.5 m (18 ft)	38.3	800	33.5 - 52.7	700 - 1,100
5.5 m (18 ft)	9.1 m (30 ft)	23.9	500	14.4 - 45.5	300 - 950
9.1 m (30 ft)	12.2 m (40 ft)	31.1	650	25.1 - 51.5	525 - 1,075
12.2 m (40 ft)	15.2 m (50 ft)	47.9	1,000	47.9 - 64.9	1,000 - 1,350
15.2 m (50 ft)	16.5 m (54 ft)	71.8	1,500	97.0	2,025
16.5 m (54 ft)	19.5 m (64 ft)	95.8	2,000	114.9 - 193.9	2,400 - 4,050

INTERNAL BRACING – WORKING WITH ADJACENT BUILDING DESIGNER

The results of the ERS design indicated that the maximum load in the wales (level 1 and 2 were approximately the same) was 394 kN per meter (27.0 kips per foot). The maximum estimated deflection was 4.32 cm (1.70 inches) using Clough (1985).

As noted previously, the internal bracing of the secant piles consisted of wide flange beams for wale members and pipes for struts. The longest struts (north-to-south) in the middle of the site used mid-span supports to reduce the unbraced length of the strut, and therefore, reduce the required pipe section. Additionally, to further reduce the movement of the ERS due to elastic shortening of the longest struts, installers added pre-stress to the struts to lock in the load.

Due to the area, shape, and depth of the excavation, the bracing design balanced forces between walls to provide stability. While balancing forces were readily available due to the soil loading on the west, north, and east sides, the existing *Walton on the Park* building structure with a multi-level basement on the south side complicated the equilibrium of the system. Balancing the forces north-to-south consequently required bracing to the existing structure and introducing point loads to the existing foundation wall which consisted of secant piles and integral caissons.

The design team approached the *Walton on the Park* building owner to request permission for bracing to the outside of the existing foundation wall. Through collaborative efforts, the design teams agreed on the following conditions to allow for the proposed bracing scheme:

(1) The relatively high stiffness of the caissons causes the caissons to attract significantly more load than the secant piles. Compressible material placed between the wales and caissons limited the load transfer into the caissons.
(2) Locating the brace elevations at mid-points between existing floor slabs creates excessive moment and movement in the existing wall. The design located bracing elevations near the existing floor slab elevations to minimize such effects.

UNDERPINNING

As mentioned previously, shallow spread footings, comprised of unreinforced limestone block, supported the historic masonry church building immediately adjacent to the west property line of the *No. 9 Walton* site. The age and structure of the church made it susceptible to even the smallest of movements resulting from the adjacent excavation. The previous project for *Walton on the Park* partially underpinned the church

where that earth retention influenced the structure. The *No. 9 Walton* project extended the underpinning to further protect the church from the influence of the new ERS.

The underpinning consisted of individual piers of hydraulically pushed steel pipe (10.2 cm x 0.56 cm [4 in x 0.220 in]). A reinforced concrete grade beam, doweled into the existing limestone foundation, connected the piers to the existing structure. Installers hydraulically pushed the piers into the ground using the existing load of the structure as a reaction. Installation procedures required each pier to be installed to 1.5 times the design capacity of the pier while monitoring the structure for any movement during installation, then lock off each pier at its design load. This procedure verified the capacity of every pier during construction.

CONSTRUCTION

After completion of the underpinning, installation of the ERS began with construction of a guide wall, followed immediately by installation of the secant piles. The excavation and bracing then proceeded sequentially to final grade. The excavator cut each stage to an elevation generally level with the bottom of the wale flange. Proper connection of the lookouts and wale to the secant piles then required exposing the reinforcing beams of each secant pile. Installers added studs to the back of the wale and to the face of the secant pile reinforcing beam, set the wide flange beam in place, and grouted the area between the back of the wale and secant pile wall to provide a uniform transfer of load across the wall. Crews then set the bracing, pre-stressed the longer struts, and repeated the process for Level 2. Figure 5 shows the completed excavation and earth retention system.

MONITORING AND RESULTS

The movement of the ERS and any associated settlement of the surrounding ground, the existing structures, utilities, and public rights-of-way needed careful monitoring. Any unanticipated movement or settlement required additional analysis and possible remediation.

Monitoring the performance of the ERS used two quantitative weekly observation methods:

1. **Slope Inclinometers –** Five (5) inclinometers behind the ERS around the perimeter (Figure 6)
2. **Optical Survey –** Sixty-seven (67) points, including six (6) points directly attached to the adjacent buildings

The results of the monitoring indicated the system performed better than predicted. Settlement points on grade surrounding the site revealed movements in the general range of 1.27 cm to 1.91 cm (0.5 to 0.75 inches), with some localized areas as much as 4.57 cm (1.80 inches). Generally, the largest movements occurred at the midpoints of the north and east walls, approximately 6.1 m (20 ft) behind the ERS.

Building survey points showed even better ERS performance with three (3) of the six (6) points showing no movement at all. The maximum recorded settlement of an adjacent building at the completion of excavation was 0.61 cm (0.24 inches). Observations and visual surveys revealed no damage to existing facilities.

The authors considered inclinometers to be the best indicator of performance of the system. Data from the 6 inclinometers indicated very good ERS performance. Maximum lateral movements ranged from 0.94 cm to 1.70 cm (0.37 inches to 0.67 inches). The data indicated that the actual movements were significantly less than predicted. Table 2 reports a comparison of the predicted movements to the actual maximum movements recorded by the inclinometers.



FIG 5: No. 9 Walton Excavation and Earth Retention System at Completion of Excavation

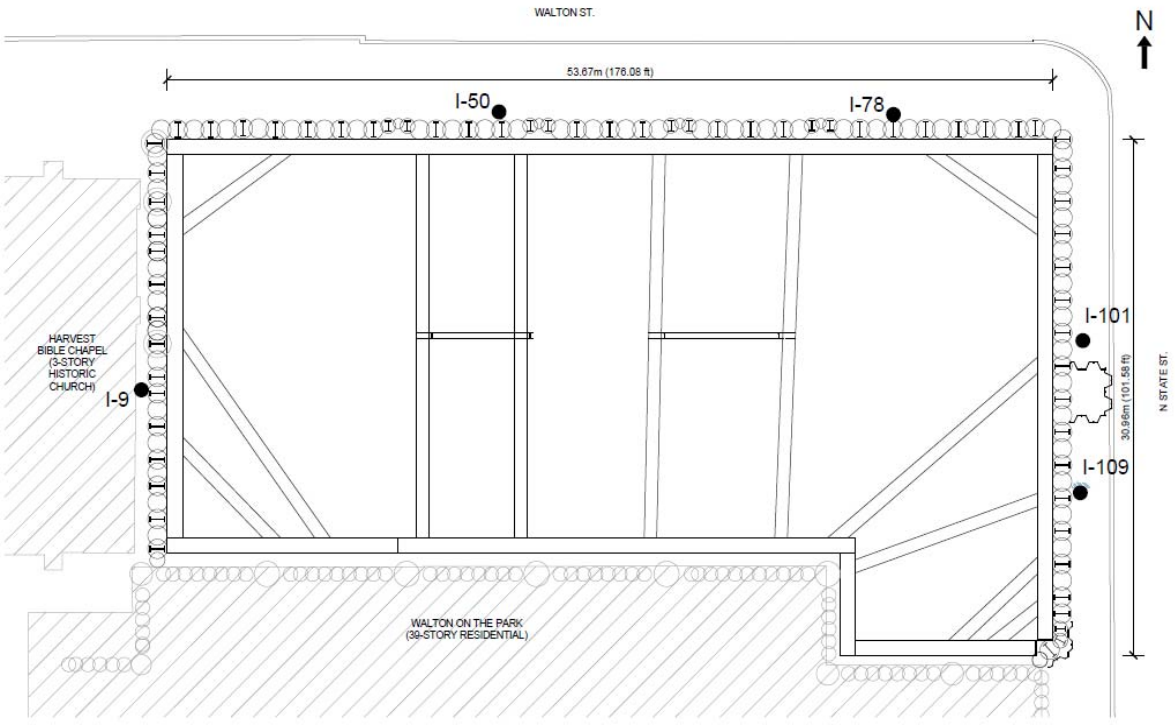


FIG 6. Locations of Slope Inclinometers

Table 2. Predicted versus actual maximum movement

Inclinometer No.	Maximum Movement	
	Predicted cm (in)	Actual cm (in)
I9	3.05 (1.20)	1.46 (0.57)
I50	4.32 (1.70)	1.15 (0.45)
I78	3.05 (1.20)	1.61 (0.63)
I101	3.05 (1.20)	1.71 (0.67)
I109	3.05 (1.20)	0.95 (0.37)

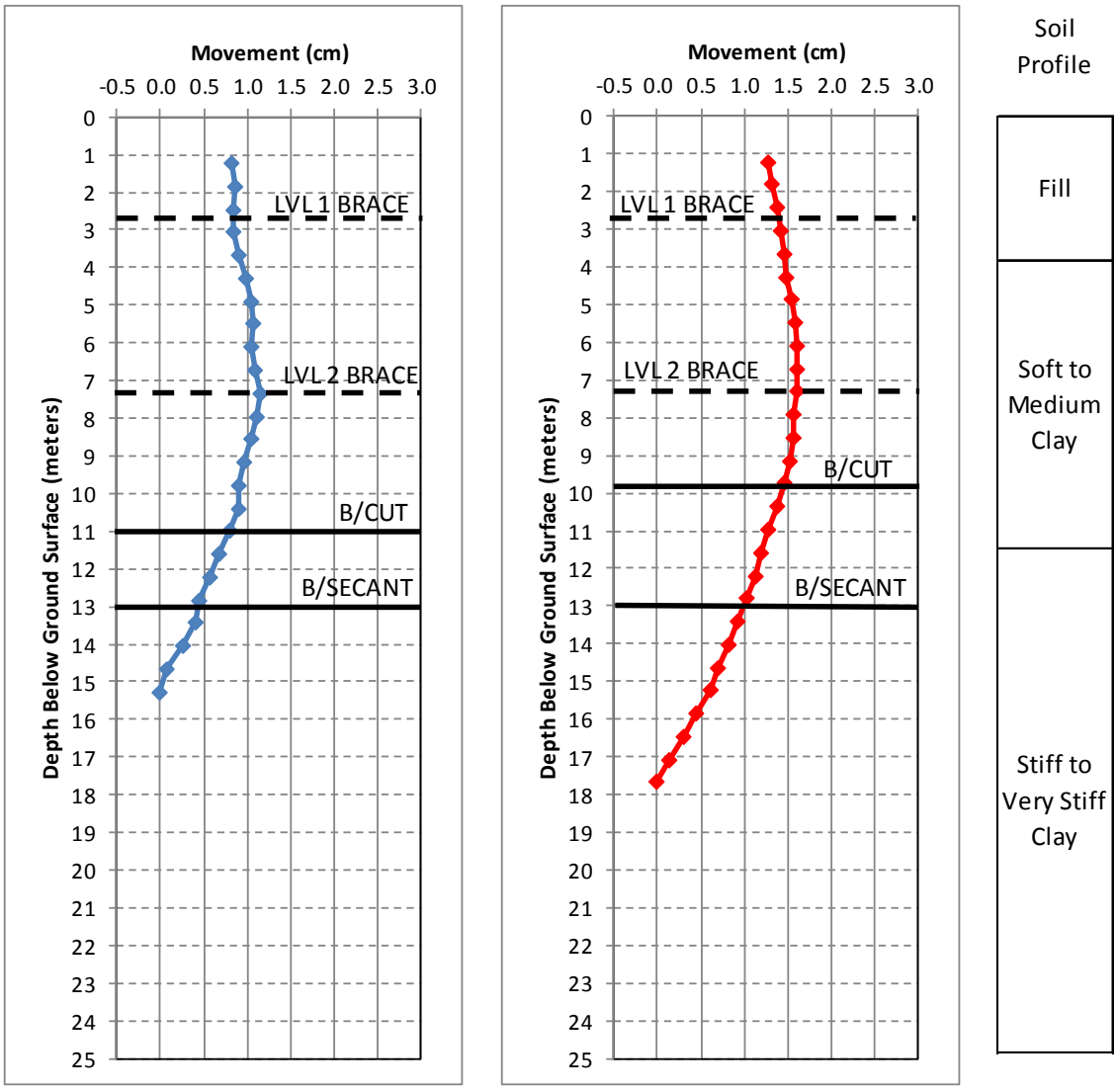


FIG 7. Final Inclinometer Results (I50 on Left, I78 on Right)

CONCLUSIONS

Use of ERS in urban environments requires designers and builders to overcome challenges beyond the soil conditions. Existing buildings, utilities, and public areas must be protected, and in the case of *No. 9 Walton*, used in concert with the ERS to achieve the desired results for the owner, adjacent owners, engineers, and municipalities. Collaboration with other stakeholders can lead to positive results for all parties involved.

At *No. 9 Walton*, designers collaborated to produce an ERS that exceeded performance requirements and predictions and protected surrounding facilities. The blend of several technologies produced a successful project for all involved.

ACKNOWLEDGMENTS

The authors appreciate the support of their fellow colleagues at Hayward Baker and Case Foundation Company who helped make this project a success. The authors also thanks those at JDL Development, Lend Lease (US) Construction, Lindahl Brothers Excavating, Hartshorne Plunkard Architecture, Magnusson Klemencic Associates, Samartano and Company, and GEI Consultants who contributed to the success of the project.

REFERENCES

Clough, G.W., "Effects of Excavation Induced Movements in Clays on Adjacent Structures", Contributions on the Influence of Earthwork Construction on Structures, Eds. D. Resendiz and M. P. Romo, XI ICSMFE, San Francisco, 1985.

EGLINTON CROSSTOWN, A NEW STEP IN TORONTO'S SUBWAY SYSTEM

Franz-Werner Gerressen, BAUER Maschinen GmbH, Germany
Lars Richter, Aecon Group Inc, Canada

ABSTRACT

The Eglinton Crosstown Line was conceived as the Eglinton Crosstown LRT, a partially underground light rail line, announced in 2007 as part of the Transit City plan, which included the implementation of six other light rail lines across Toronto.
There were 43 stops planned for the Eglinton Crosstown LRT, 13 of which would be underground .
For those underground stations a lot of specialty foundation works needed to be carried out. King piles, soldier piles with lagging and secant piles were mainly required fulfilling the tasks of installing the retaining wall system.
The paper will focus on the original design and alternative solutions, discussing the benefits and limits of these. It will also explain the installation process in general as well as some specific features related to specific site conditions, e.g. limits in installation depth, soil characteristics etc.
The required equipment will be explained showing the benefits and limits.

Keywords: Retaining Wall, Secant Pile Wall

INTRODUCTION

The Eglinton Crosstown project is a 19-kilometre LRT line that will bring much needed relief to the transit woes of Torontonians. Traversing the city in an east-west slice across the midtown artery of Eglinton Avenue, the Crosstown rail line involves a combination of 15 underground stations and 10 at-grade surface stops. It is one of the largest transit infrastructure projects under way in North America today. Aecon has joined partners ACS Infrastructure Canada, Ellis Don, and SNC-Lavalin to form Crosslinx Transit Solutions (Crosslinx).
As with many of today's mega public transportation projects, the Crosstown LRT follows the Public-Private Partnership (P3) model. Aecon is an equal partner in the $5.3-billion Crosslinx consortium to develop the Eglinton Crosstown LRT project in Toronto. Upon the LRT's completion in 2021, Metrolinx, the region's transit authority and also the project client/owner, will turn to the Toronto Transit Commission (TTC) to operate it.
The impact of this highly anticipated LRT line on commuters in the Greater Toronto Area (GTA) is expected to be dramatic and immediate once the first train leaves the station five years from now. In fact, Metrolinx is estimating that within its first 10 years of service, the Crosstown line will be carrying 5,500 passengers per hour (in peak direction) and making 100 million passenger trips annually.

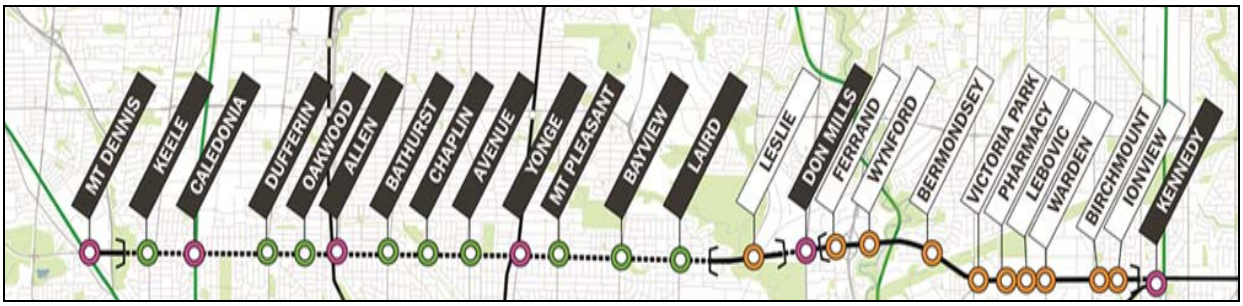


Figure 1: Station layout Eglinton Crosstown project

 © 2017 DFI Annual Conference, New Orleans, LA, USA

Because of the enormous size of the project, the construction of the project is divided into 5 different segments. The value of each segment is between $600million and $1.1 Billion CAD. Every segment almost acts as an own entity.

Aecon Foundations were awarded four stations of segment No. 2 which are

- Dufferin/ Fairbanks
- Bathurst/ Forest Hill
- Chaplin
- Mt. Pleasant

The scope of work included:

- Secant pile wall
- Soldier pile and wooden lagging
- Ground Anchors
- Utility support structures
- Micro piles for underpinning
- Working platform
- Guide wall
- Struts/ Steel bracing

DESIGN AND DESIGN MANAGEMENT

Aecon Foundations has subcontracted the design to Pedelta Engineering. Because of numerous stakeholders involved, the design management is one of the most challenging parts for this kind of project. Especially the utilities required a lot of attention as were not diverted in our design concept. Another challenge to consider was the tunnels for the LRT which were already installed under a separate contract prior to the installation of the shoring. The right of way didn't allow enlarging the station. In several areas, the piles of the shoring wall were as close as 12 centimetres or 5 inches away from the tunnel segments. When drilling the secant pile walls it was required to build around the tunnel with at tolerance of less than .5% accuracy.

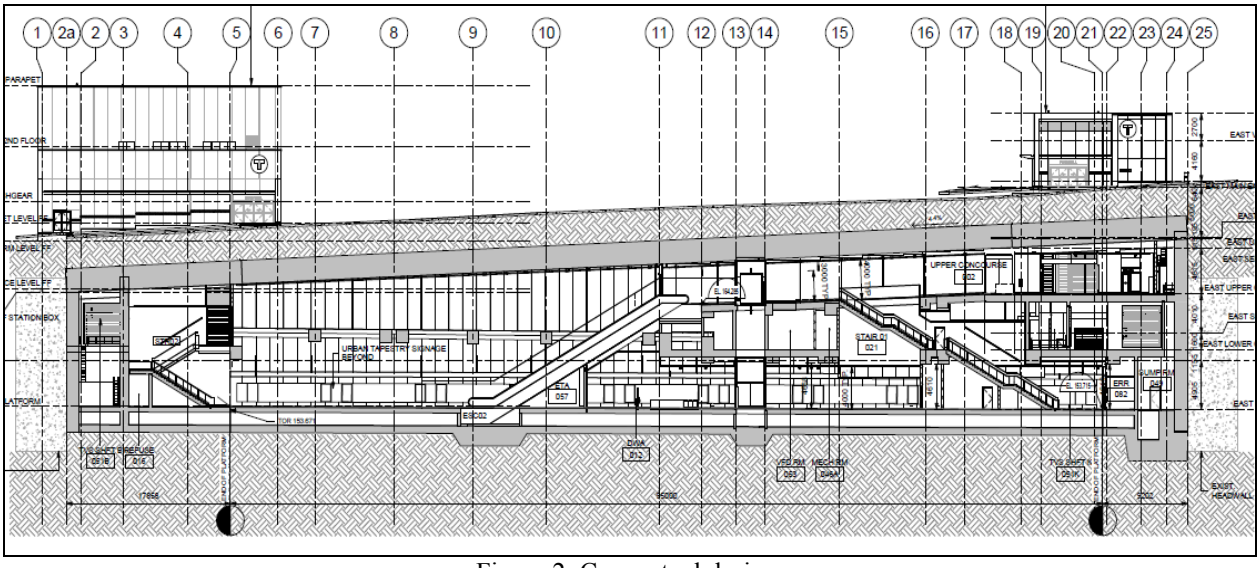


Figure 2: Conceptual design

The level of accuracy could be achieved with the support of the equipment suppliers and the Jean Lutz system. On our way down the verticality was measured at 3 different levels. And only if the required tolerance was achieved at a depth of 15m drilling could be continued.

SEQUENCE OF WORK/ STAGING

Forest Hill station

The layout of every station is very similar. The station box itself is around 120m long to accommodate the 4 wagon trains and usually there is an entrance on either side. At Forest Hill it is a little different; both entrances are on one side. The grade of 4% in this area required not only to implement staging related to the traffic and utilities but also to the drilling rigs steep slope of the area. We ended up with 5 different elevations on each side for this 120m long stretch. In the very narrow areas we had no space for a service crane. The drilling rig BG 39 needed to drill, offload rebar cages from the trucks, splice the cages, assemble and disassemble the tremie pipes. The piles in that area were in a range of 35m to 40m length. Due to the circumstances, a performance of max. one pile per day could be achieved.

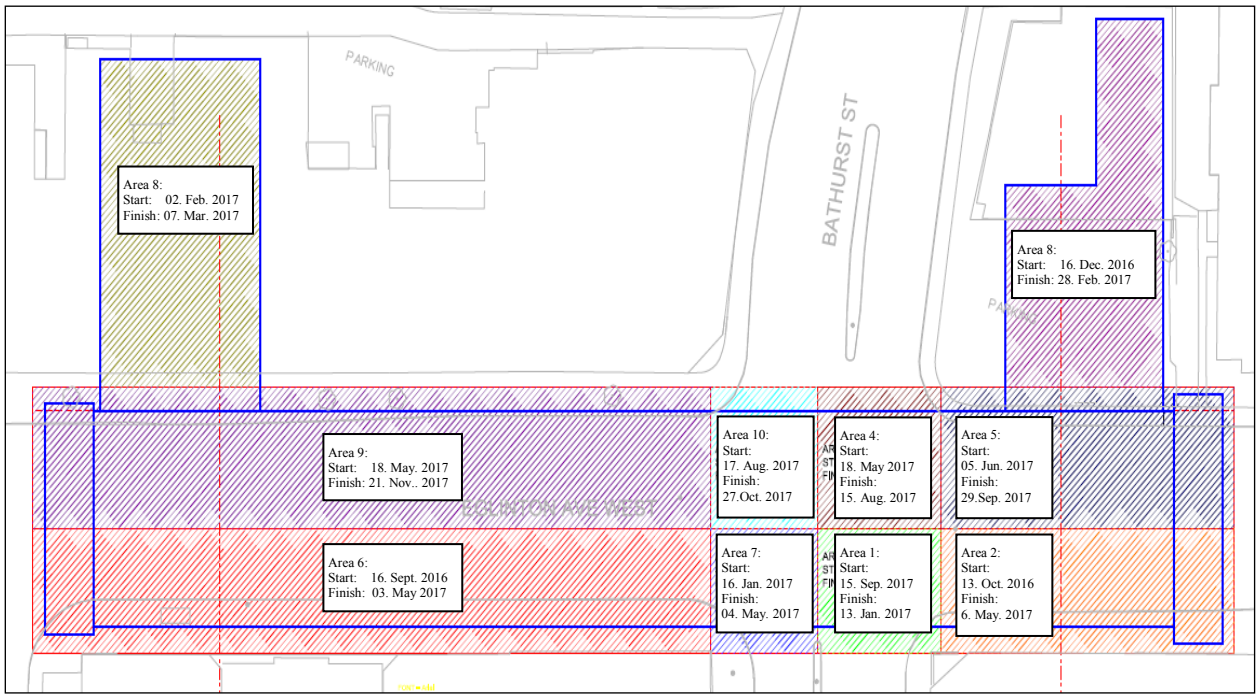


Figure 3: Layout of Forest Hill station

Sequencing

The client CTS had to pay a considerable rent for the usage of the roads and the diverting of the traffic. The goal was for our stations, to develop a concept to reduce the disruption of the traffic at Eglington Avenue to a minimum. Therefore, the top down method seemed to be the best approach. Unfortunately, we couldn't convince together with our client the authorities to work with a true top down method where the secant pile walls would be the permanent outside walls of the stations. Finally we ended up with a hybrid solution where the secant pile walls were rated as a temporary structure and the structural piles of the secant pile wall have a permanent function to carry the roof slab of the station box.

Sequencing:

Step 1
Installation of secant pile walls and King piles with plunged H-beams. The H-beams were installed in the filler piles at a distance of 2.2m to 3m. Rebar cages of the structural piles ended 7m below ground level.

Step 2
Shallow excavation and installation of whalers and struts and the hanging of the utilities onto the steel structure

Step 3
Excavation up to 6m below ground level for the construction of the roof slab

Step 4
Construction of the concrete roof slab (permanent structure). The roof slab is in its middle a 3m high concrete beam.

Step 5
Backfilling on top of the roof slab and reinstalling the road

Step 6
Flipping the traffic to the other side of the road and starting with step 1 or where the walls are already in place with step no 2 again.

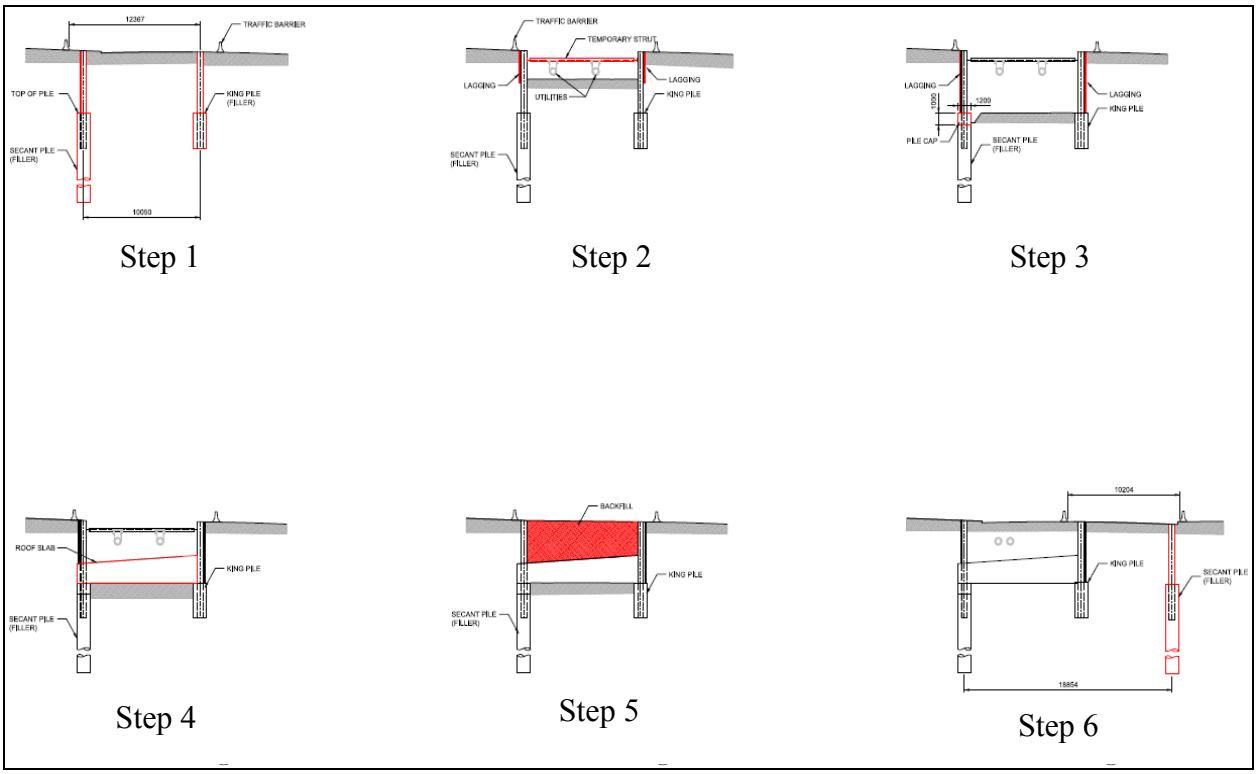


Figure 4: Sequencing

Secant pile wall installation

As the secant pile wall installation was the main scope, the system will be explained in more detail. A secant pile wall may be defined as a series of piles that are constructed in a configuration such that they intersect one another.

They are constructed at centre-to-centre distances that are smaller than the sum of the radii of the two adjacent piles. In this configuration adjacent piles intersect and therefore interlock.

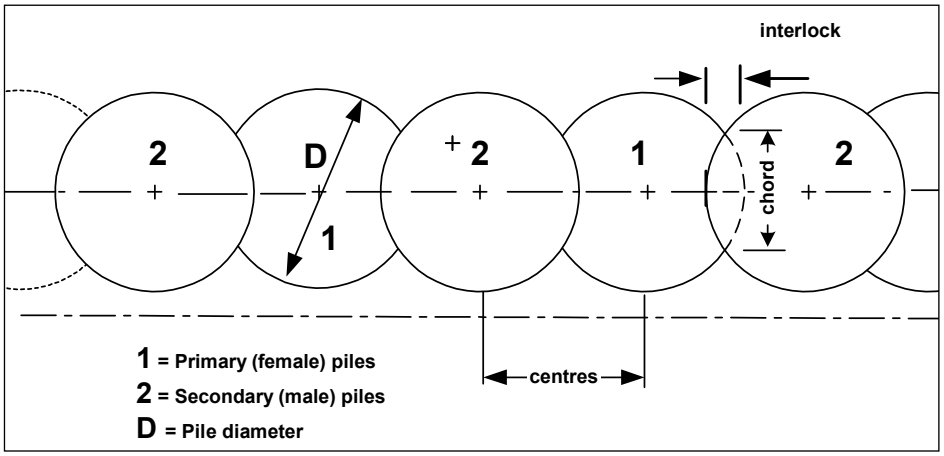


Figure 5: Secant pile wall definition

This method is applied to form reinforced concrete earth retaining structures, otherwise known as secant pile walls, in many different subsoil conditions to replace the more conventional sheet piles or diaphragm walls.

Secant pile walls have a number of advantages which became also relevant for this particular project:

- Secant pile walls can be constructed effectively in all soils; their use becomes particularly attractive when soils are difficult to drill and where boreholes are difficult to support. For example in loose or poor quality fills or where soils contain obstructions such as boulders or where the formations are very hard.
- Secant pile walls are constructed by excavating alternate, primary piles first. These are allowed to gain some strength before the intersecting secondary piles are drilled. This method of operating together with the use of temporary casings to support the boreholes reduces significantly the deformation of soils surrounding the wall, thereby reducing settlements and their adverse effects on nearby structures and services.
- In built up areas and on confined sites where retaining walls need to be constructed close to adjacent structures it is possible because of the use of a mechanically supported borehole to chisel or to drill through an obstruction with minimum risk of damage or disturbance to the structure nearby. Whereas with sheet piling or diaphragm walling these conditions can present a much more difficult problem particularly where there is a risk of loss of drilling mud, a serious event inherent with the diaphragm wall method.
- Secant piles are load-bearing structures and can be incorporated to form an integral part of the main structure.
- There is great flexibility in the choice of pile diameter and different combinations of hard and soft piles can be used to produce a wall apt for the purpose for which it was designed.

- Secant piles are built using rigid casings. The stiffness of these casings makes it easy to produce well aligned columns. Mechanical borehole support allows the use of the most suitable drilling methods excavate the specific formations at the site.

When constructing secant piles, three important criteria must be satisfied in order to guarantee the designed amount of intersection throughout their length:

- Alignment
- Location
- Verticality

In order to satisfy these, it is good practice to build proper guide walls along the wall alignment before commencing any excavation.

The guide walls serve four main purposes:

- They guarantee the correct location of every pile, particularly the secondary intersecting piles, and thereby ensure the required amount of interlock.
- They facilitate setting up of the rig, particularly the alignment and verticality of the mast.
- They support the reinforcing cage or steel section and assist in its correct vertical location.
- They provide support for the casing oscillator or extractor when these are used to extract the casings.



Figure 6: Guide wall

A series of primary piles are constructed first using any of the conventional drilling methods such as the Kelly bar driven auger or bucket. The allowable tolerance for the inclination of the casing is as per Specification. After installing the first section of casing, drilling with an auger or bucket is performed until the excavation inside the casing reaches 0.5 m above the lower end of the casing. The casing is then driven further. Whenever driving of the casing with the rotary drive alone becomes difficult, a casing oscillator may be used. Once the borehole has been drilled and properly cleaned out, reinforcement, if required by the design, is inserted and properly located. The borehole is then concreted using the accepted practice for cast-in-situ bored piles by placing the concrete preferable using the tremie method. Immediately after concreting, the temporary casing, when this is used, is extracted using the drilling equipment, a casing oscillator or casing extractors. Care must be taken during this operation, to ensure that withdrawal or oscillation of the casing commences before the concrete starts to set. This is particularly important in deep boreholes or those of large diameter or when there is a delay in pouring successive batches of concrete due to breakdown of machinery. Generally, special attention must be given in all those instances where there is a risk that the first concrete poured will start to set before the concreting operation is completed.

The secondary piles are drilled in between two adjacent primaries so as to intersect these and to cut into their shafts. For this operation to be successful timing becomes of critical importance as the strength gain of the primary pile concrete, which is to be cut to form the interlock, is related to time, temperature and the mix design. Ideally, before drilling the secondary piles, the strength of the primary pile concrete should be high enough to prevent it from slumping or cracking, but it should be low enough to offer minimum resistance to the action of the cutting crown.
Drilling the secondary piles proceeds with care; special attention being paid to maintaining verticality in order to ensure that the minimum designed amount of intersection is obtained throughout the length of the shaft, particularly at depth.

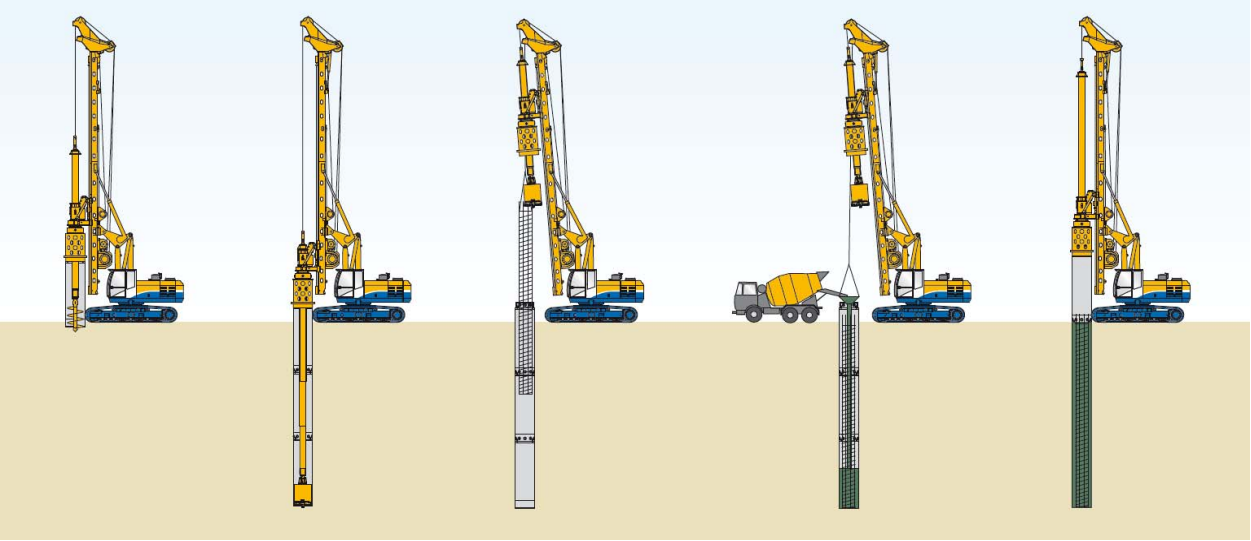


Figure 7: General construction sequence

Equipment strategy

The project was not rated as a production job. The pile length, the constraints for the supply of concrete wouldn't allow more than one pile per 10h shift. Aecon Foundations initial approach was to work with machines which are smaller and more agile in the very small areas available to work in. The machines classes planned for this job was in the area of 28-36 ton meter of torque.
Once the design was close of being finished it became clear that those machines could only do a part of the works. The ground conditions and the forces coming from the roof slab extended the structural piles up to a depth 44m with a 1.2m diameter.
Equipment strategy was changed together with the equipment suppliers to rig size in a range of 36-44 ton meter of torque to accommodate the new demands of the project.
Later in the project we introduced as a speed up measure oscillators for the casing extraction during the concreting process. Using this technique, one additional pile was installed every other day.

Generally speaking, job site requirements create an increasing demand for the development of technical support systems. For example, systems like the so called "drilling" assistant should enable a more constant and quality ensured installation of the piles. As part of the quality control, real time installation control of the production process, data transfer and reporting systems become more and more important. The system enables you to efficiently operate, maintain, and administer individual machines as well as entire fleets. It helps you to securely monitor and precisely evaluate your projects and work processes. The system is an integrated system for controlling all operations and visualizing actual operating parameters in real-time on a large interactive touch-screen monitor.

In addition to these basic operational data, general machine operating parameters (e.g. engine data) are also acquired and monitored. The display of current machine operating states and error messages is a valuable aid for targeted and effective fault finding by service personnel on site, but also by specialists based at the offices, as data can be transferred real time via internet connection. This does not only allow the control of equipment and installation process including relevant reporting, it also allows comparing "virtual reality" and "reality", hence planned and actual execution, which enables the project manager to control not only the schedule, but also the use of budget.
A special focus was given in the past to the development of so called assistance systems (see Gerressen, March 2017). These systems relieve the operator by automating or repetitive operations. They help to prevent faulty operation of the machine and therefore protect both man and machine. Automatic, fast control processes increase the drilling performance and reduce wear of both, equipment and tools. Assistance systems thereby ensure a consistently high production quality.



Figure 8: BG 39

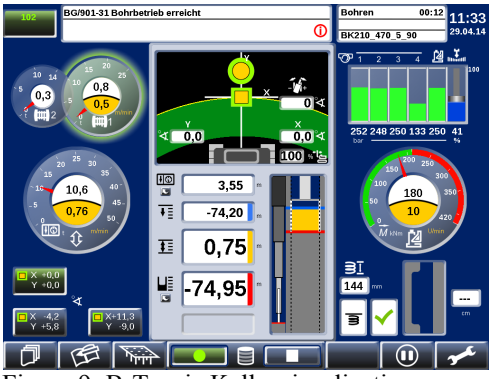


Figure 9: B-Tronic Kelly-visualization

CONCLUSION

It is always preferable to work with the client together on the most effective solution for the project. Unfortunately, this is rarely possible. Time constraints, willingness to revisit the initial design and reservation against different approaches make it often difficult to convince or even to discuss with the client changes in the initial solutions. For this particular project the client took a broader approach and factored in the follow-on works, schedule savings and the resulting cost savings but also reduced amount of construction impact for the effected community.

REFERENCES

F.-W. Gerressen, March 2017, Newest developments in quality Control and soil mixing for actual and future demands, PFSF 2017, Melbourne

A TALE OF TWO DAMS: PERFORMANCE OF DEEP CUTOFF WALLS

Wesley Schmutzler, TREVIICOS, Charlestown, MA, wschmutzler@treviicos.com
James Sanders, USACE Mobile District, James.H.Sanders.Jr@usace.army.mil
Mark Harris, USACE Little Rock District, Mark.C.Harris@usace.army.mil
Donald Bruce, Geosystems L.P., dabruce@geosystemsbruce.com

ABSTRACT

This paper evaluates the history, construction and most importantly the performance of two remedial seepage cutoff walls installed in two major dams in the United States. Beaver Dam, on the White River in northwest Arkansas, was completed in 1966 and seepage through the karstic limestone under the embankment was apparent almost immediately upon filling of the reservoir. Several attempts to stop the seepage by grouting were unsuccessful. In 1994 a cutoff wall consisting of secant piles drilled with 32" diameter down-the-hole hammers to a maximum depth of 185′ was completed and the seepage was reduced to a negligible amount. It has been over 20 years since the completion of the cutoff wall, and all indications are that the cutoff wall is performing as expected. Walter F. George Lock and Dam on the Chattahoochee River near Fort Gaines, Georgia, was completed in 1963 and suffered the same problem as Beaver Dam due to the limestone on which the dam was founded. Cutoff walls were installed in both embankments (1980s) and solved the problem in these areas, but under-seepage at the concrete lock, dam and spillway structures increased to the point that remediation was essential. The cutoff wall had to be installed through 110′ of water and another 100′ into rock upstream of an active dam that continued to generate electricity during the construction of the cutoff wall. A secant pile wall, in combination with a diaphragm wall, was completed in front of these structures in 2004. It has been over 10 years since the completion this cutoff wall and, again, the cutoff wall is performing as expected. The paper describes the construction of these cutoffs, but focuses on the long-term performance in terms of controlling seepage and piezometric levels.

Key Words: cutoff, seepage, diaphragm wall

BEAVER DAM

Beaver Dam is located on the White River, 609 miles above its mouth, in Carroll County, Northwest Arkansas. The construction of the dam and Beaver Reservoir was authorized on September 1954 by the Congressional Flood Control Act for purposes of water supply, flood control and hydroelectric power generation. The dam site was selected in 1957: construction began in November 1960 and was completed in June 1966. (FIG. 1)

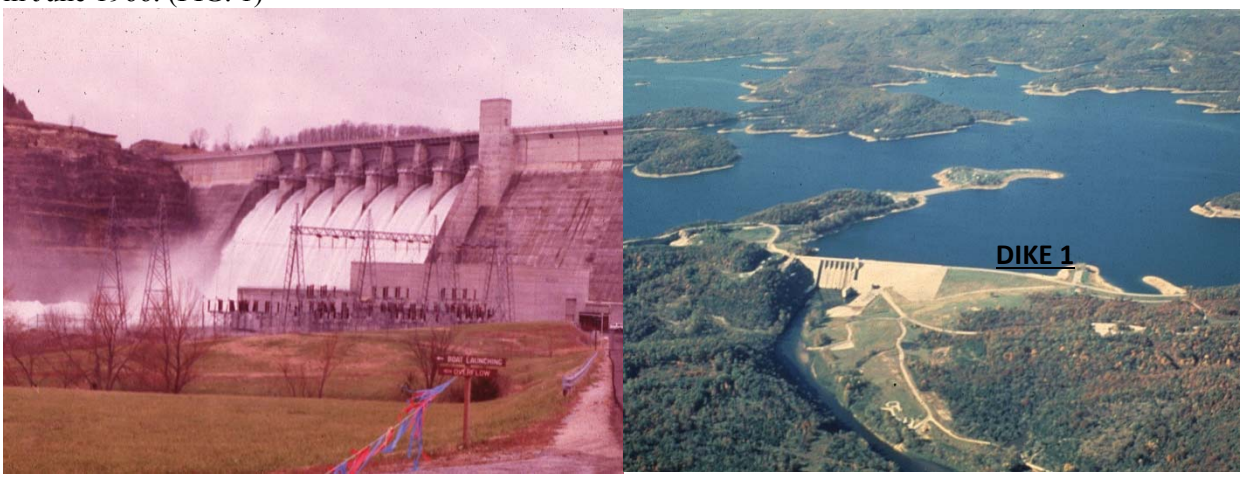


FIG. 1 Beaver Dam

 © 2017 DFI Annual Conference, New Orleans, LA, USA

The Problem

Soon after the initial filling of the reservoir, in April 1966, seepage was observed at several exits on the downstream side of Dike 1 and seepage flows were estimated totaling 800 gallons per minute. To monitor the seepage through Dike 1, a network of flow measuring devices such as Parshall Flumes, weirs, and piezometers was installed downstream of the dike. A remedial grouting campaign, performed in 1968-1971, reduced the seepage flow to about 300 gallons per minute, but failed to stop the seepage below the dike. The reasons are attributable to the presence in the foundation of many open and clay filled cavities, channels, porous (sponge like) rock, with deep intensively weathered, pervious zones. (FIG. 2) A muddy seepage was discovered in December 1984, after a long period of unseasonably heavy rains. Fearing the possible failure of Dike 1 due to material loss, the United States Army Corps of Engineers (USACE) decided in early 1985 to lower the level of the pool from el. 1,130 feet to el. 1,128 feet.

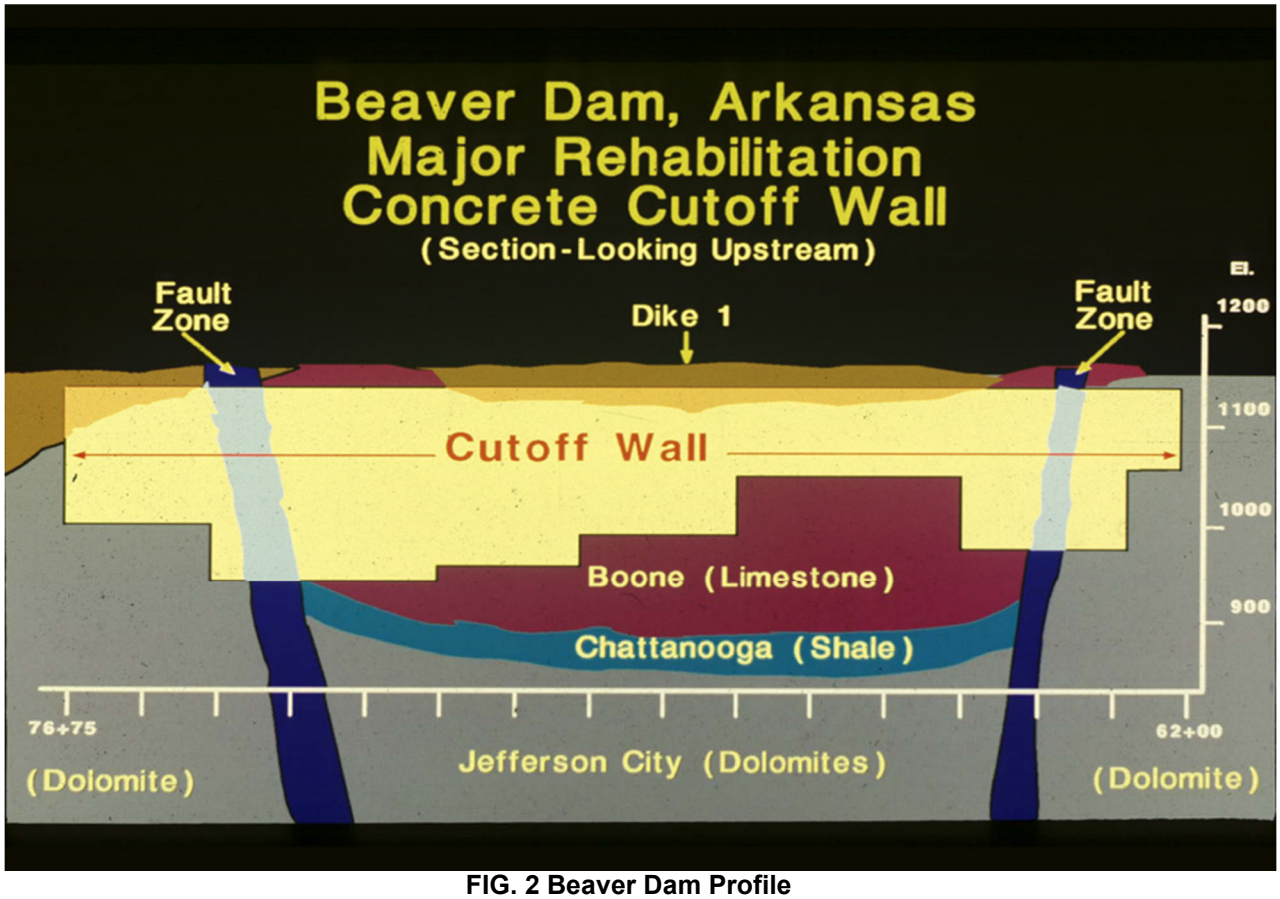


FIG. 2 Beaver Dam Profile

These operative restraints, and the increase of unplanned flows through Dike 1, prompted the USACE to design, in February 1988, a positive cutoff wall in the bedrock, upstream of the dike, with a depth varying from 80 to 185 feet. The first attempt to construct a slurry trench type cutoff wall using a hydromill, failed. Apparently, the un-weathered rock at the site, having an in-situ compressive strength as high as 27,000 psi, could not be excavated economically. After the end, in August 1990, of the original contract, the Rodio/Nicholson Joint Venture (RNJV), responding to the USACE's re-solicitation of Request for Proposals, submitted a Technical Proposal for the construction of an equivalent cutoff wall formed by secant piles. The proposed technology was the one perfected during construction of a similar cutoff wall at Khao Laem Dam, on the Quae Noi River, in Thailand.

The Solution

The RNJV's proposal was based on the use of direct circulation large down-the-hole hammers, with bits of 34-inch diameter, for drilling a continuous cutoff wall formed by overlapping piles (FIG. 3). The RNJV's Technical Proposal, revised according to the USACE's observations, was approved for execution. The "Notice to Proceed" was issued by the COE on May 19, 1992. The construction of the cutoff wall began on October 14, 1992 and it was completed on August 26, 1994. The restoration plan ended in early December 1994, within the planned terms of the construction schedule.
Due to the position of the cutoff wall, it was necessary to construct a work platform. It was benched in the upstream slope of Dike 1 and had crest at el. 1,130 feet and width of 65 to 75 feet. The cutoff wall depth generally ranged from 80 feet to 185 feet. Pile No. 572 reached the depth of 215 feet to investigate bedrock conditions.

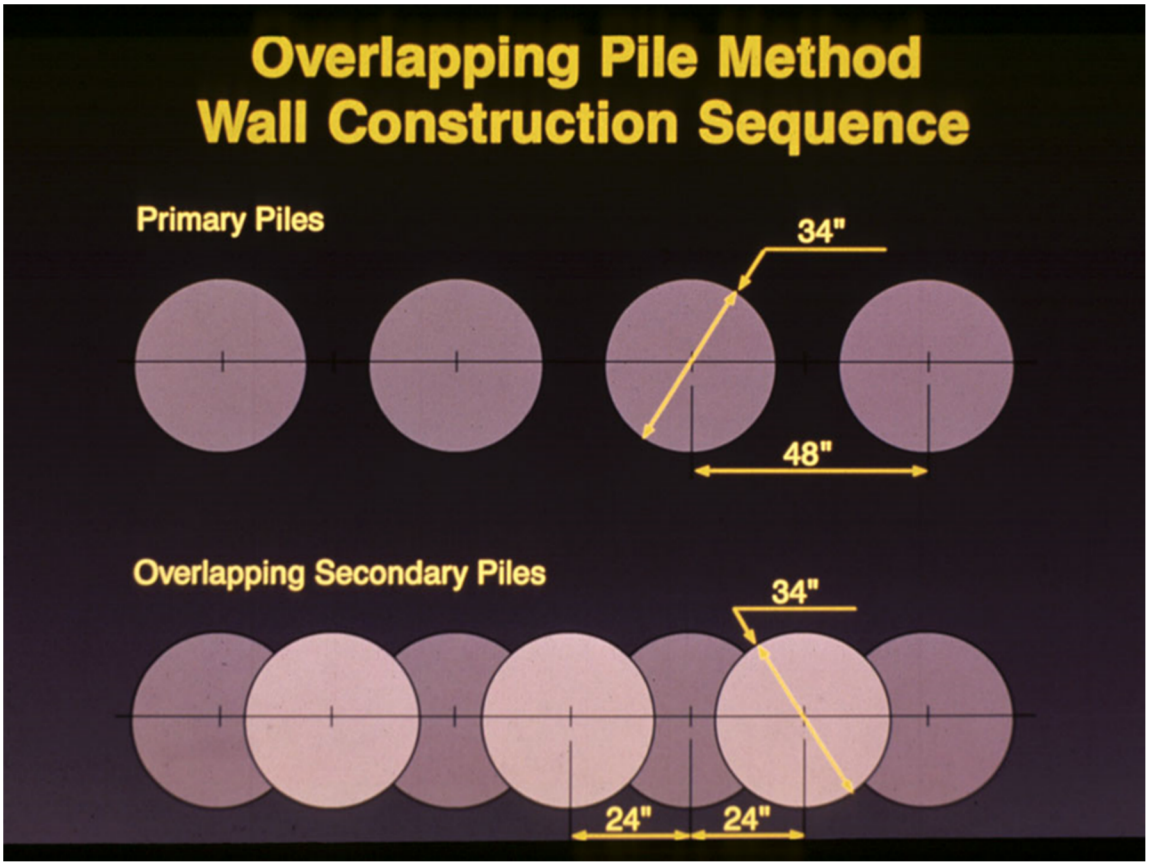


FIG. 3 Secant Pile Layout

The down-the-hole hammers were pneumatically driven, and mechanically rotated by the rotary head mounted atop the mast of the drill rig (FIG 4). During drilling, the piston was the only moving part of the hammer. The two stroke movement of the piston was controlled by the flow of compressed air through passages in the piston case. The piston force was transmitted directly to the bit, which in turn impacted and crushed the rock beneath it. The compressed air used to move the piston up and down was then vented through the bit. The air transported the drilling cuttings to the surface of the pile, traveling upwards in the annular space between the outside surface of the hammer and the pile walls. In order to operate the two drill



FIG. 4 Drill Rigs in Operation

rigs a bank of nine air compressors that each developed 300 psi and 960 cubic feet per minute was set up. Over 40,000 cubic yards of concrete was used for the Cutoff Wall.

Since the completion of this project the USACE has published guidelines in ER 1110-1-1807 that prohibit the use of compressed air in embankments. The entire team was cognizant of the problems that could occur using this amount of air and daily monitoring of the downstream side of the embankment was performed to ensure that no air was traveling through the core of the embankment. Some air did travel upstream and was evidenced by bubbling in the lake.

The verticality of the pile was measured by a device called a "Submersible Reverse Plumb Bob" (FIG. 5). It consisted of a weighted barrel, having a diameter of 30 inches, lowered to the bottom of the pile. Rigid cables around the outside surface of the barrel, giving it an outside diameter of 34 inches, ensured that it was centered in the pile. A target attached to a cable, independent of the barrel, was then suspended from the center of the cylinder, just below the surface of the water in the pile. This was achieved by tensioning a cable running through a pulley located on the center of the barrel. Because the hole was filled with water, the target floated toward the surface and sought the center of the cylinder. The process was completed by lowering a plumb bob, with a fixed end measured against a set axis on the top of the pile, from the top of the pile to the center of the target. The verticality test could be repeated at several depths, progressively withdrawing the barrel toward the collar of the pile. The use of this measuring device required the presence of water in the hole. Therefore, a dry hole had to be first filled with water up to the uppermost level at which the verticality control was to be carried out. While this method for checking verticality would be considered rudimentary in today's world, the results are undisputable given the performance of the Cutoff Wall.

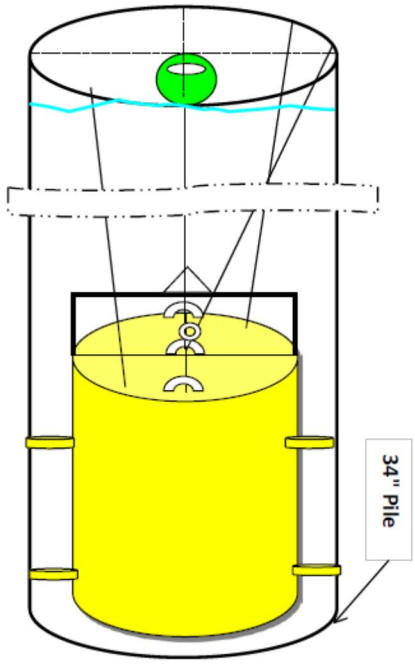


FIG. 5 Verticality Device

Results

In general, prior to construction of the wall, the seepage was several hundred gallons per minute, varying with lake levels. In mid-March 1994, when area D was completed and grout stabilization in Area B was commenced, all devices showed a sharp decrease as can be seen in Fig. 6 (Bruce and Dugnani 1995). This trend continued until the completion of the whole wall in August 1994, when all five seepage areas had dried up and the total under seepage was less than 4 GPM. (Bruce 2012) In 1995, less than one year after completion of the cutoff wall, the pool reached 9.5 feet above conservation pool for six weeks (approximately 1 foot lower than pool of record, elevation 1130.4 feet, in 1984). No seepage was evident in the old seepage areas and the piezometers downstream of the Dike 1 and the cutoff wall did not rise with the pool. These observations demonstrated the integrity of the cutoff wall. This was the first time in 29 years that no visible seepage existed below Dike 1. Beaver Lake had a record pool in 2008 of elevation 1132.2 feet and in 2015 the pool rose to elevation 1132.0 feet with no evidence of seepage downstream of the cutoff wall at Dike 1. The cutoff wall project by the secant pile method, utilizing downhole hammer drilling techniques, proved to be an excellent method of excavating the very hard and fractured Boone Limestone.

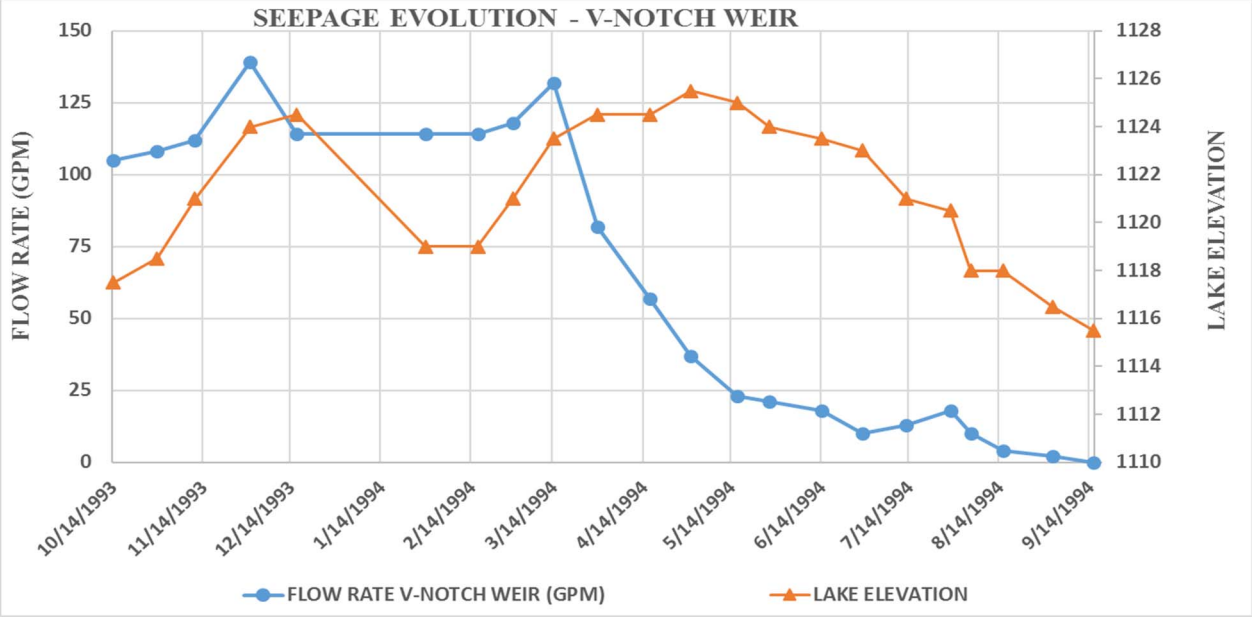


FIG. 6 Seepage Evolution

Walter F. George (WFG) Lock and Dam

The Walter F. George Lock, Dam and Powerhouse structures are located within the Apalachicola, Chattahoochee, and Flint River (ACF) System on the Chattahoochee River near Fort Gaines, Georgia straddling the Georgia and Alabama border. The powerhouse was completed in June 1963, essentially completing the project. The lock was opened to navigational traffic in June 1963, and the powerhouse went into full operation in November 1963. The total cost of the project, including $1.3 million for recreation development, was $87.1 million.

The Problem

The WFG project had experienced serious seepage problems that became progressively severe from beginning the impoundment of the reservoir in 1963. The concern for safety of the embankments was so great that a concrete cutoff wall was installed through the earth embankments on the Alabama and Georgia ends between 1981 and 1985 that was considered successful. In the early 1980s, a flow of about 30,000 gallons per minute (gpm) developed beneath the powerhouse, and in 1991 a flow of about 3,000 gpm (and climbing) developed beneath the spillway. During the 1990s, up to 1¼-inch-diameter limestone fragments piped from the foundation were collected from the powerhouse drainage system discharge. Seepage became evident in the Shell Limestone foundation beneath the powerhouse and spillway. Seepage through the Shell Limestone is more complicated than that under the embankments. Construction features and natural features (joints in the Earthy Limestone overlying joints in the Shell Limestone) combined to provide seepage paths to lower portions of the Shell Limestone (FIG. 7). These lower portions contain some strata in which the shell fragments are very poorly cemented. High hydraulic gradients, which developed in these strata, caused piping which ultimately developed direct connections with the lower pool.

After an exhaustive analysis by the USACE, the final plan recommended was a positive concrete cutoff wall that extended down into the impervious black clay of the Providence Sand formation at Elevation –5.0 feet and tied into the cutoff walls previously installed . The project was approved, plans and specifications were drawn up, requests for proposals were made, and the TREVIICOS-Rodio/JV won the contract and received the notice to proceed on October 5, 2001.

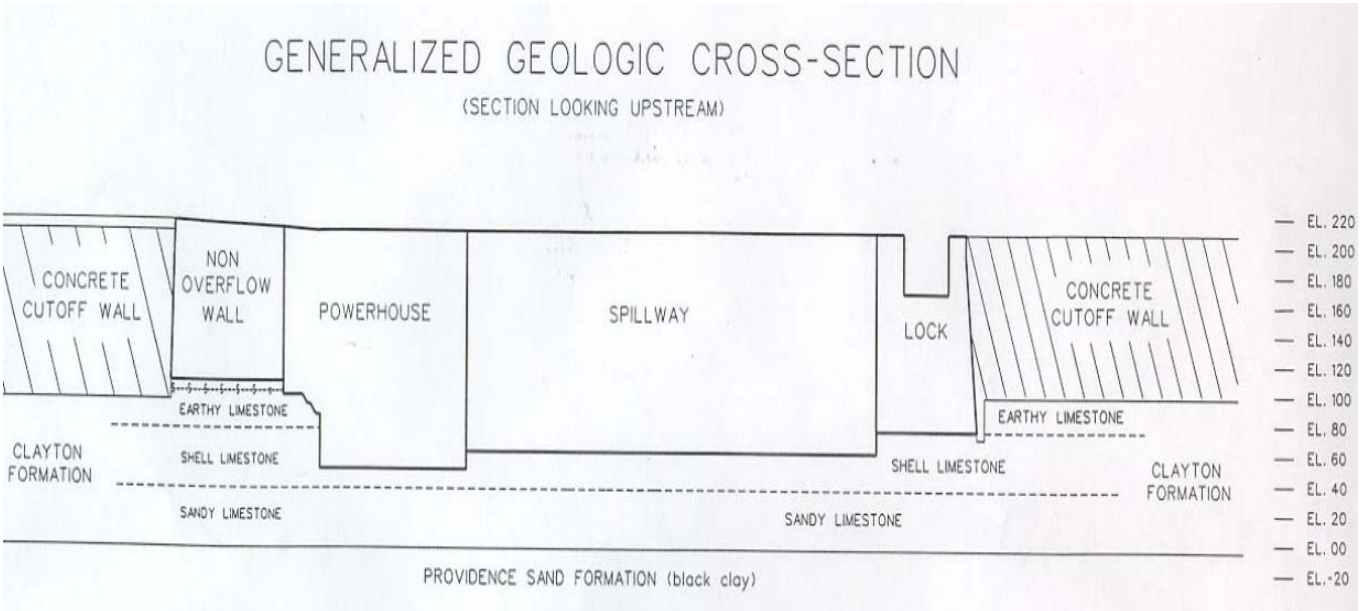


FIG. 7 Geological Profile

The Solution

The JV's proposal for installation of the Cut-off Wall consisted of a combination of two reverse circulation methods, Secant Piles using a casing mounted drill rig in the areas in front of and through the concrete structures (FIG. 8), and Slurry Walls done by a Hydromill on the two embankments. Over 65,000 cubic yards of concrete were used for the cut-off walls. The under-water cutoff wall was comprised of a series of



FIG. 8 Pile Installation

overlapping 50-inch-diameter secant piles. A flowable fill concrete apron was installed on the bottom of the lake to facilitate casing installation. Once the work apron was in place, specially designed templates were installed on the dam buttresses. The steel templates attached to the concrete structures were used as guides to install and drive the temporary casings into the apron. Whenever possible, the guide beams and templates were installed and secured to the existing concrete structures of the powerhouse and spillway. Out of a total of 492 secant piles that were installed over 225' feet deep from the top of the casing, 24 piles (approximately 5 percent of the total) were re-drilled for failure to meet the minimum wall thickness criterion of 24". When drilling of a shaft was completed, the shaft was checked for verticality by using one of a combination of the following: a biaxial inclinometer, caliper or Koden. Then the results were plotted against adjacent piles to ensure that a minimum cutoff thickness of 24 inches was achieved. Concrete was then placed using a tremie pipe installed to within 1 foot of the bottom of the shaft up to a level corresponding to the bottom of the lake. When placement of the concrete was completed, the casing was removed with a vibratory hammer and reset, and the operation was repeated. An aerial photograph showing the entire site is provided in Fig. 9 below.

A combination of a hydromill and a clamshell was used to construct the cutoff wall through the Georgia and Alabama embankments on either side of the concrete structures to a depth of 215'. The hydromill was also used in a very unique capacity. The lock walls needed to be cut in order for the Secant Piles to be continuous. The hydromill was used to cut into the two concrete lock walls. These walls were 110' deep and up to 88' thick at their base with concrete strengths of over 5,000 PSI. The slot in the lock wall needed to be 63" in order to allow the installation of the 54" diameter secant pile casings. The hydromill was connected to a series of full depth pipes that were held in place by hydraulic jacks that were controlled from the surface. Another unique use of the hydromill on this project was the need to cut a slot in an underwater

retaining wall on the Alabama side of the project. In order to accomplish this the area behind the retaining wall was first stabilized by jet



FIG. 9 WFG Site

grouting. The jet grouting behind the underwater retaining wall needed to be done in order prevent the material behind the retaining wall from collapsing when the slot was created for the secant pile wall.



Then **FIG. 10 Barge Mounted Hydromill**

the hydromill was mounted on a barge (Fig.10) and was utilized to cut the concrete underwater retaining wall to allow the installation of the secant pile wall.

Results

As can be seen in FIG. 11 some of the piezometers fell over 60 feet once the cutoff wall was complete and have remained at that level for over 15 years. Also an evaluation of the project by the USACE in 2016 states "With the completion of both the left and right embankment cutoff walls, and the secant cutoff wall along the toe of the concrete structures (with a combined length of approximat1y 10,200 feet), seepage from the reservoir at the Walter F. George Project is thought to not be a problem. Therefore, it is considered that the Walter F. George Project is in generally **excellent** condition".

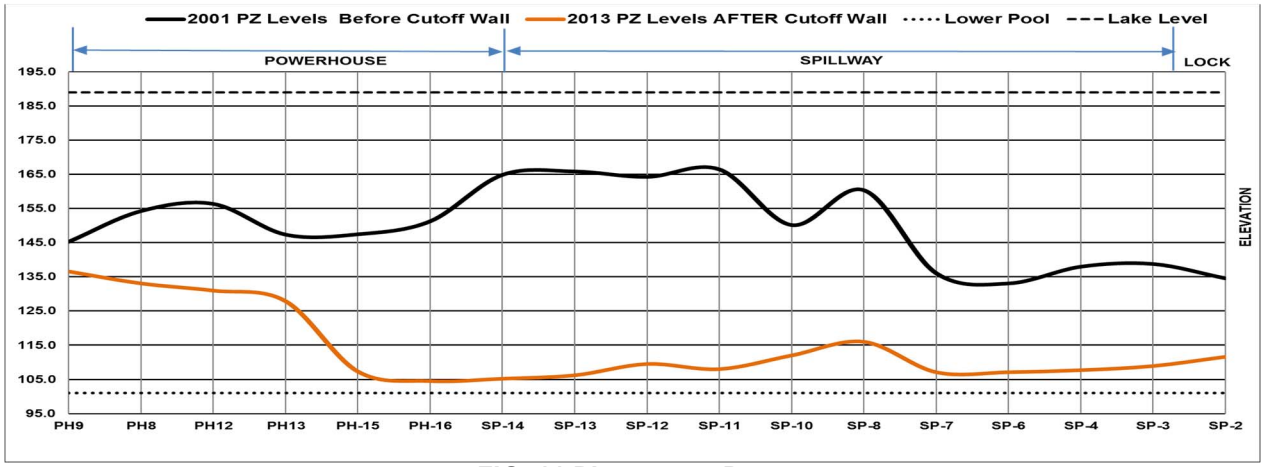


FIG. 11 Piezometer Data

Conclusions

Beaver Dam and W.F. George Lock and Dam were remediated over 20 years and 10 years ago respectively. At the time of the remediation the technology utilized was cutting edge. Both projects were bid as an RFP and the contractors chose the technical approach suitable for each application and developed a quality control program to "fit" the technology. As can be seen by the data concerning the performance of the remedial efforts, both projects were and still are a technical success.

By today's standards, the quality control implemented during construction of these projects is nowhere near as complicated and redundant as is required for a similar project in today's world. The advent of new procedures and processes in Quality Control has made today's remediation efforts much more time consuming and complicated adding a considerable cost to the final product.

REFERENCES

Bruce, Donald A., 2012. Specialty Construction Techniques for Dam and Levee Remediation

Bruce, Donald A. and Dugnani, G. 1995. The Rehabilitation of Beaver Dam: A Major Seepage Cut-off Wall

EVALUATION OF CRANE PAD PERFORMANCE ON PARTIALLY IMPROVED GROUND ADJACENT TO A SEAWALL

Yazen A. Khasawneh, NTH Consultants, Northville, Michigan, khasawneh10@gmail.com
Paul J. Sabatini, Geosyntec Consultants, Oak Brook, Illinois, PSabatini@Geosyntec.com

ABSTRACT

A Demag CC1800 crawler crane was partially erected on crane mats adjacent to a seawall when settlements near a corner of the crane mat area were observed to be slightly larger than previously assessed. A ground improvement program including installation of dry soil cement mix (DSM) piers was implemented to improve soil bearing capacity. Due to near-surface obstructions, only 75 percent of the DSM piers were installed to the design depth. Because of the partial installation of the DSM piers, an evaluation of the crane pad stability and the effect of the crane loading on the stability of an adjacent 10-ft high concrete seawall, which was believed to have limited (if any) reserve capacity, was required. A two-dimensional finite element model was developed to evaluate the responses of the partially improved ground and the sea wall to the loads imposed by the crane. Geotechnical site investigation and laboratory testing programs were performed to better define the subsurface conditions near the area where settlements occurred and to provide the required mechanical parameters for the soil constitutive model. Analysis results indicate that total and differential settlements of the crane pad and the increase in load on the seawall were tolerable provided limited excavation and replacement of weak dredged soils outside the DSM area would be implemented.

Keywords: ground improvement, soil cement piers, crane foundation, finite element, constitutive model

INTRODUCTION & BACKGROUND

A Demag CC1800 was erected on 8 ft × 16 ft crane lattice mats at about 12 ft from an existing seawall. Approximately 3.5 in. of subsidence was observed at one corner of the crane mats, while the crane was partially erected and stationary. The approximate location of the crane mats with respect to the existing seawall when the subsidence occurred is shown on Fig. 1.

The seawall consists of a reinforced concrete wall connected by reinforced concrete bents to a composite section of sheet pile wall; the total depth of the seawall is about 29 ft. The bents are spaced at about 20'4" and supported by five piles at each bent location. The composite sheet pile consists of concrete and a sheet pile section with a reinforced concrete wale section. The retaining wall is about 10 ft in height and is supported at three levels. The first support level comprises a 2-½" diameter steel rod near the top of the wall spaced at 40'8" the second and third level supports comprise 1-½" diameter steel rods spaced at about 5'6". The second level support is inclined at about 10 degrees below horizontal and the third level support is oriented horizontally through the wall footing. A schematic of the seawall section is shown on Fig. 2.

A geotechnical site investigation was implemented soon after the subsidence was observed. The program included advancing four borings to a depth ranging from 16 ft below ground surface (bgs) to about 30 ft bgs. In general, the investigation showed sandy material (likely fill that was used behind the retaining wall) from the ground surface in two borings located immediately behind the retaining wall. The other two borings furthest from the retaining wall showed very soft to soft clay (possibly dredged material) from the ground surface to a depth of about 10 ft bgs. Based on this information, the ultimate bearing capacity of the subsoils was estimated to range from 1,200 to 2,000 pounds per square feet (psf). From the anticipated crane loading (weight of the crane and loading lifts), a minimum allowable bearing capacity of about 1,500 psf would be required for safe operation. To achieve the required bearing capacity a ground improvement program was selected and implemented.

 © 2017 DFI Annual Conference, New Orleans, LA, USA

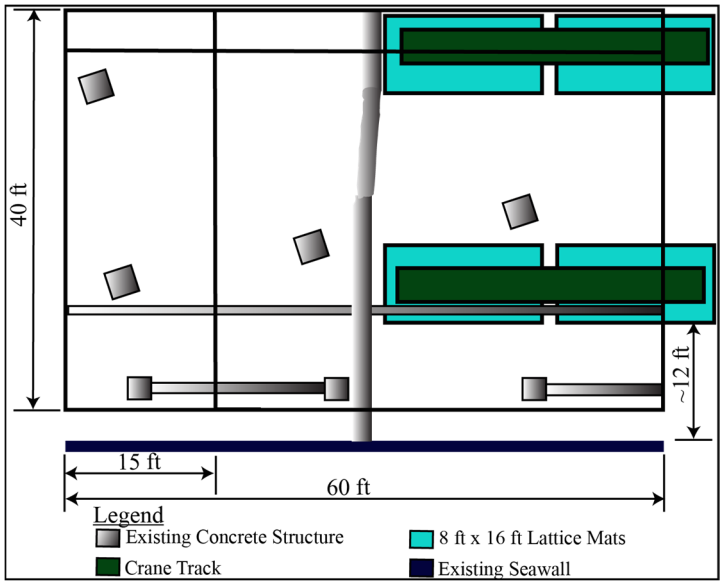


Fig. 1. Location of crane mats.

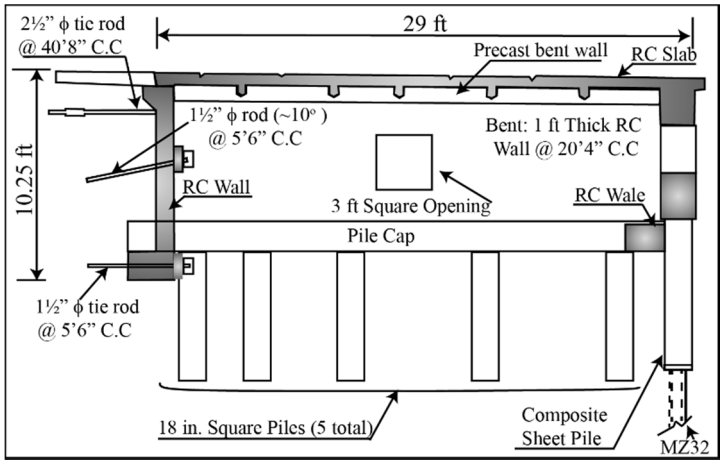


Fig. 2. Schematic of seawall section.

A specialty geotechnical contractor was subsequently hired to design and install dry soil cement mix piers (DSM piers) to achieve the required bearing capacity of the 40 ft × 60 ft crane pad area (see Fig. 1). The design comprised 3.28 ft diameter DSM piers at about 5 ft spacing for a total of 94 DSM piers. The design depth and minimum compressive strength of the DSM piers were about 25 ft bgs, and 50 pounds per square inch (psi), respectively. Because of encountered near surface obstructions, 20 of the DSM piers reached early refusal and were terminated at approximately 5 ft bgs.

An assessment of the as-built conditions was required to ensure that sufficient bearing capacity could be mobilized with tolerable total and differential settlements, to assure that the capacity of existing retaining wall will not be exceeded because of crane operation, and to evaluate the global stability of the retaining wall under imposed crane loads. The evaluation of the anticipated settlements and the demand on the retaining wall were performed using two-dimensional finite element analyses with relatively simplified nonlinear (hyperbolic) constitutive model for the foundation soils. A supplemental (and targeted) geotechnical site investigation and laboratory testing programs were necessary to better identify the extent of the very soft to soft clay encountered in the previous investigation and to provide the necessary mechanical parameters for the soil constitutive model.

SUBSURFACE CONDITIONS, DSM PIERS, AND CRANE MAT CONFIGURATION

Based on the two geotechnical investigations performed at the site and historical geotechnical information provided in the construction drawings of the original pier and seawall, five different soil units, designated as Units I through V, were identified (see Table 1).

Table 1 – Soil units designation and definition

Unit	Designation	Notes
I	Very Loose to Loose Sand	clean sand material with SPT N values less than 10 bpf
II	Very Loose to Loose Silty Sand	more silty than Unit I
III	Soft Clay	moderate to high plasticity
IV	Medium Dense to Dense Silty Sand	alluvial deposits with SPT N values from 15 to 30 bpf
V	Medium to Very Stiff Clay	mostly encountered in the historical borings

The ground water table was encountered at various depths ranging from the ground surface (0 ft) to about 7.5 ft bgs. The generalized east-west (i.e., orthogonal to the retaining wall) subsurface stratigraphy model for the project is presented in Fig. 3a.

The DSM piers were installed from the ground surface (approximately 1 ft below the top of the existing concrete apron) to improve the bearing capacity of the foundation soils. The depth of the "successful" piers (74 of the 94 designed piers) is about 25 ft. The location of the as built DSM piers is shown on Fig. 3b. Laboratory QA/QC testing results on collected soil-cement samples from four piers indicate that the minimum required unconfined compressive strength of 50 psi was achieved.

The proposed crane pad configuration to support the crawler crane comprised 20 sets of 4 ft × 20 ft × 12-inch timber crane mat and two sets of steel load spreaders with each set comprising 9 W 10 × 49 steel sections with a 1-inch thick steel cover plate. The crane pad configuration is shown on Fig. 3c. The pressure from the load spreaders on the crane mates was estimated by the crane engineer for different anticipated lifts and different boom locations. For the investigation of the as-built condition, two load configurations were considered: (i) the heaviest lift with maximum pressure closest to the retaining wall, and (ii) the case of zero lift load, which reflects the sustained loading and includes the dead load of the crane at a stationary position. The estimated pressures from the two cases are presented in Table 2.

Table 2 – Estimated pressure for the two load configurations

Configuration	Position of Boom	East Pad (Nearest to Wall)	West Pad	Notes
Heaviest Lift (Case 1)	Over Toe	1,283 psf	1,087 psf	Maximum force effect for transient load
Lift Load = 0 (Case 2)	Over Front	1,010 psf	1,010 psf	Maximum force effect for sustained load

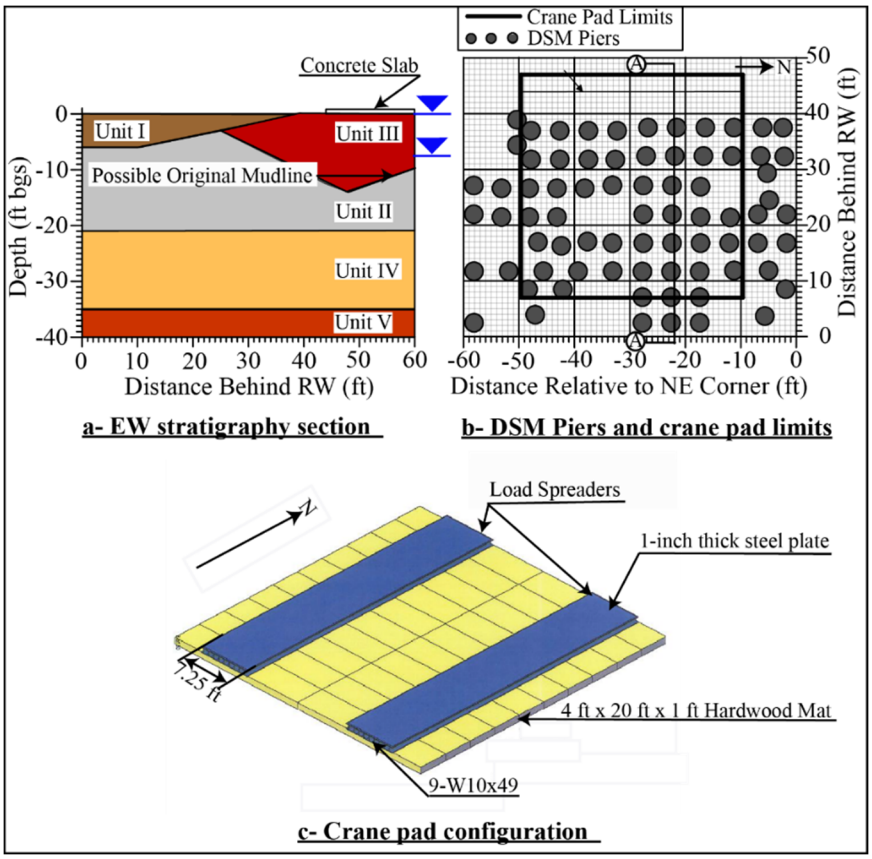


Fig. 3. Generalized subsurface profile, DSM piers and crane pad limits, and crane mat configuration.

NUMERICAL SIMULATIONS

A two-dimensional (2D) finite element model was developed to assess the stability of the proposed crane pad and to estimate the additional load demand on the adjacent seawall. The assessment was performed for the provided loading and the as-built configuration of the DSM piers. It should be noted, however, that relatively large settlement would be anticipated west of the DSM piers in the soft clay layer (i.e., Unit III shown in Fig. 3a). Therefore, the scenario considered for the numerical models includes partial excavation and replacement of the clayey soils with crushed stone at the western limits of the crane pad area just to the west of DSM Piers.

Method of Analysis

The computer program PLAXIS 2D Version 8 (2012) was used to conduct the 2D finite element analyses of the proposed crane pad area. The baseline analysis model comprises an east-west cross section. The finite element mesh for the selected east-west cross section is shown on Fig. 4.

Constitutive Models and Associated Parameters

The elements of the numerical model include foundation soils, DSM piers, crane mats, and the retaining wall. The hardening soil constitutive model (Schanz et al., 1999) was used to model the response of the foundation soils. The DSM piers and the crushed stone (which is used to replace the soft clay west of the DSM piers) were modeled as an elastic perfectly plastic material. The structural elements of the model (e.g., crane mates and the retaining wall) were modeled with plate elements and as isotropic elastic material.

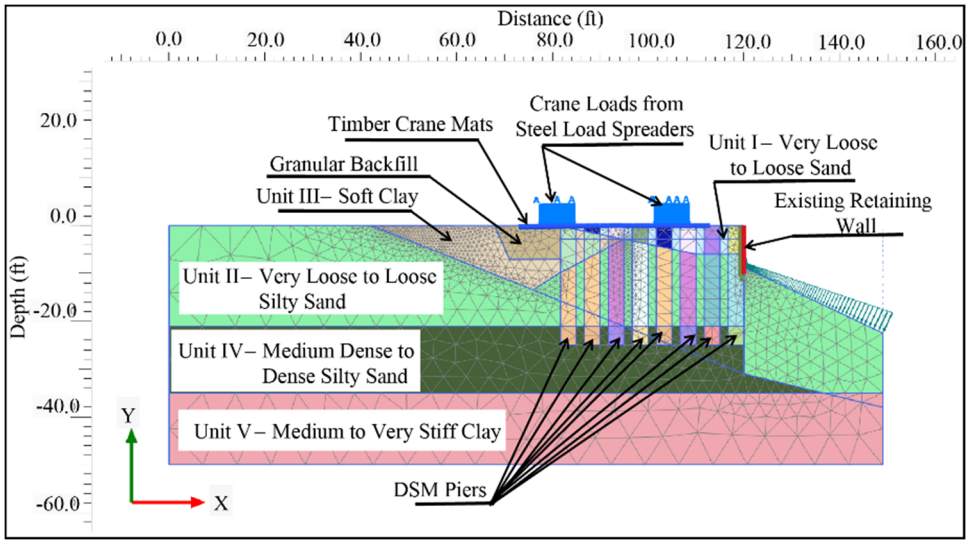


Fig. 4. Finite Element mesh.

The hardening soil model is a nonlinear soil model formulated within a plasticity framework with a hyperbolic stress strain relation and associative flow rule that requires three moduli values at a reference pressure to identify loading (E_{50}^{ref}), unloading/ reloading (E_{ur}^{ref}), and hydrostatic loading (E_{oed}^{ref}). The hardening soil model is strain hardening (requiring the definition of the hardening exponent "m") and it obeys the Mohr-Coulomb yield criteria (i.e., c and ϕ are required).

The elastic perfectly plastic constitutive model used for the DSM piers and the crushed stone assumes a linear elastic relationship and it obeys the Mohr-Coulomb yield criteria. The required parameters are the elastic modulus, Poisson ratio, c, and ϕ.

The isotropic elastic model used for the structural elements requires the elastic modulus as an input parameter.

Soil Model Parameters for Granular Soil Units

For granular soils the hardening soil model parameters were estimated based on empirical correlations. Three soil units are considered as granular soils (i.e., Units I, II, and IV) with relative densities ranging from very loose to dense.

The initial effective tangent modulus for granular soils is calculated based on Kulhawy and Mayne (1990) as follows:

$$E_i' = \kappa p_a \left(\frac{\sigma_{vo}'}{p_a}\right)^{0.5} \quad [1]$$

$$\kappa = 300 + \left(\frac{\phi - 25}{20}\right) 900 \quad [2]$$

For a hyperbolic stress-strain relation

$$E_{50}' = \frac{E_i'}{2} \quad [3]$$

Where E_i' = the initial effective tangent modulus, κ = constant defined in Eq. 2, p_a = atmospheric pressure (= 2,100 psf), σ'_{vo} = effective vertical stress, ϕ = friction angle for the granular deposit, and E'_{50} = secant modulus.

Based on information and recommendations in the PLAXIS material manual for granular soils, the various moduli at the reference pressure can be estimated as follows:

$$E_{50}^{ref} = E'_{50}\left(\frac{c\cos\phi+\sigma'_3\sin\phi}{c\cos\phi+p^{ref}\sin\phi}\right)^{-m} \quad [4]$$

$$E_{oed}^{ref} = E_{50}^{ref} = \frac{1}{3}E_{ur}^{ref} \quad [5]$$

Where E_{50}^{ref} = reference secant modulus, c = cohesion, ϕ = friction angle, p^{ref} = reference pressure, m = hardening exponent constant, E_{oed}^{ref} = one-dimensional modulus, and E_{ur}^{ref} = modulus for unloading/ reloading.

The hardening soil model parameters for the granular soil units are provided in Table 3.

Table 3 - Hardening soil model parameters for granular units

Parameter	Unit I - Very Loose to Loose Sand	Unit II – Very Loose to Loose Silty Sand	Unit IV – Medium Dense to Dense Sand
ϕ (°)	25	30	38
σ'_{vo} (psf)	285	942	1,507
κ	300	525	885
E'_i (psf)	2.33 E5	7.41 E5	1.34 E6
E'_{50} (psf)	1.16 E5	3.70 E5	6.70 E5
p^{ref} (psf)	2,100	2,100	2,100
E_{50}^{ref} (psf)	4.16 E5	7.83 E5	1.50 E6
E_{oed}^{ref} (psf)	4.16 E5	7.83 E5	1.50 E6
E_{ur}^{ref} (psf)	1.25 E6	2.35 E6	4.51 E6
m	1.0	0.5	0.5

Soil Model Parameters for Fine Grained Soil Units

For the fine-grained soils encountered (i.e., Units III and V), the compressibility parameters from constant rate of strain (CRS) consolidation tests were used to derive the hardening soil model parameters. In addition, the "Soil Test Module" in PLAXIS was used to check the hardening soil model prediction with the selected parameters based on the CRS tests against CIU triaxial test results on clayey soil specimens from Unit V.

The required elastic moduli for the hardening soil model can be calculated from the compressibility parameters as follows:

$$E_{oed}^{ref} = \frac{2.3p^{ref}}{c_c^*} \quad [6]$$

$$E_{50}^{ref} = \begin{cases} 2E_{oed}^{ref} & soft\ clay \\ 1.25E_{oed}^{ref} & stiff\ clay \end{cases} \quad [7]$$

$$E_{ur}^{ref} = 6E_{oed}^{ref} \sim 10E_{oed}^{ref} \quad [8]$$

Where c_c^* = modified compression index (= $c_c/(1+e_o)$)

The hardening soil model parameters for the fine-grained soil units are provided in Table 4.

Table 4 - Hardening Soil Model Parameters for Fine Grained Units

Parameter	Unit III (Soft Clay)	Unit V (Medium to Very Stiff Clay)
e_o	0.944	0.829
E_{50}^{ref} (psf)	7.79 E4	5.02E4
E_{oed}^{ref} (psf)	3.90 E4	4.02E4
E_{ur}^{ref} (psf)	3.12 E5	3.21 E5
m	1.0	0.0

Model Parameters for DSM Piers, Retaining wall, and Crane Mats

The parameters for the DSM piers, retaining wall, and crane mats are presented in Table 5.

Table 5 – Parameters for DSM piers, retaining wall, and crane mats

Model Element	Material Model	E (psi)	I (ft^4/ft)	C (psf)	ϕ (°)
DSM Piers	Elastic-Perfectly Plastic	7,500 (=$150q_u$)[1]	Not required	3,600 (= $0.5q_u$)	0
Retaining Wall	Linear Elastic	$3.12*10^6$ ($57{,}000\sqrt{f_c'}$)	0.0833	Not required	Not required
Crane Timber Mats	Linear Elastic	$1.19*10^6$	0.0833	Not required	Not required

[1] based on FHWA-HRT-13-046 (2013)

To account for using the 2D analysis, an equivalent elastic modulus that recognizes the percentage of DSM pier material and soil material along a row of DSM piers was calculated as follows:

$$E_{eq} = \frac{E_{DSM} \times A_{DSM} + E_{soil} \times A_{soil}}{A_{total}} \quad [9]$$

Where E_{soil} = modulus for the soil, E_{DSM} = modulus for the DSM material, A_{DSM} = total area of DSM pier along a DSM row, A_{soil} is the total area of soil along a DSM row, and A_{total} = total area.

Restraint to lateral translation of the retaining wall was applied at the location of the concrete apron and the 2-½" diameter tie rod near the top of the wall. It was assumed that the pile cap (spaced at approximately 20 ft) in front of the retaining wall (and at approximately 8.5 ft below the top of the wall) provides some restraint on lateral wall movement, which was modeled as a spring with a stiffness reduced to account for the 20 ft spacing along the wall.

ANALYSIS RESULTS

The finite element analyses were performed as a series of construction stages. These stages comprise:

- defining the initial stresses in the ground,
- placing the sloped dredged material,
- constructing the retaining wall and backfilling behind it,
- installing the DSM piers,
- partial replacement of the soft clay west of the piers by crushed stone,
- constructing the aggregate pad and the leveling sand,
- installing the crane mats and applying the crane loads, and
- a consolidation stage for an assumed duration of one year for crane operation.

The analysis was conducted with the nearest edge of the crane mat located 7 ft behind the retaining wall. An analysis was conducted for each of the two loading cases presented in Table 2.

Total Pressures on Retaining Wall due to Crane Loading

To estimate the total pressure acting on the backside of the retaining wall, loading case 1 (see Table 2) was used with the maximum pressure acting on the east crane pad (closest to the wall). The analysis results are shown on Fig. 5. For this analysis, it is noted that a portion of the total pressure acting on the wall results from the assumption of 5 ft of water pressure acting on the back of the wall.

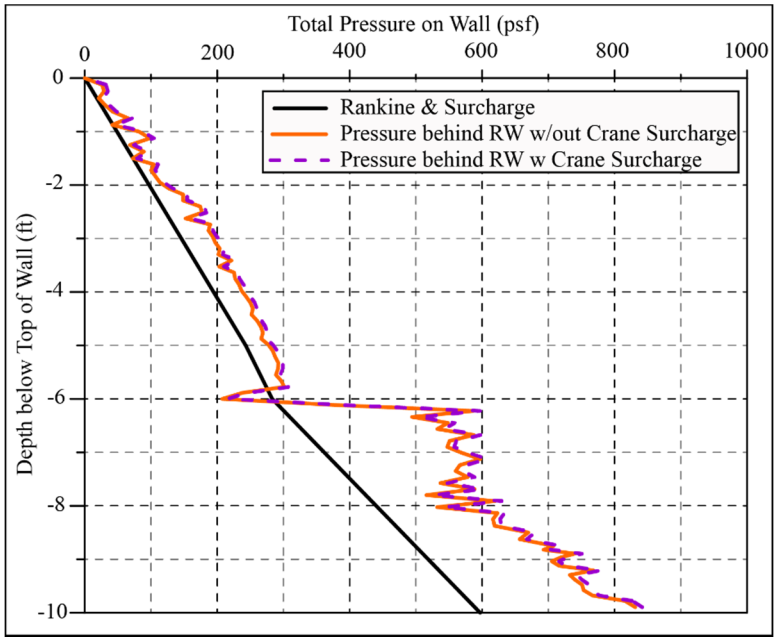


Fig. 5. Total pressure behind retaining wall.

Information in Fig. 5 indicates that there is a small difference between the analysis result that considers the crane loading as compared to the total pressure on the existing retaining wall that is computed to exist prior to crane loading. The position of the crane pad behind the existing retaining wall (i.e., at least 7 ft, outside the theoretical active wedge) and the beneficial effect of the DSM piers result in the small incremental load applied to the existing retaining wall from the crane pad surcharge, which indicates that the crane surcharge would not impose additional structural demand on the retaining wall. Given some of the uncertainties in the serviceability of the existing retaining wall, this condition of negligible load increase was considered beneficial by the project stakeholders. It can be also observed from Fig. 5 that the Rankine active earth pressure is lower than the pressure resulting from the finite element analysis at depths deeper than about 6 ft. This suggests that an active state of stress was not reached at the bottom of the wall possibly due to the

tendency of the deeper soils to displace towards the wall while the retaining wall displacement is restricted by the pile cap (modeled as spring) and the anchors.

Settlements of Crane Pad

Settlements of the crane pads were estimated for the "sustained load" case which reflects the dead load of the crane with a zero-lift load (i.e., Case 2 loading from Table 2). Settlement estimates were developed for the case of immediate compression (i.e., immediate settlements associated with the crane pad loading) and for consolidation settlements associated with time dependent settlements of clayey soils in the subsurface profile. The analysis was performed for two scenarios involving different soft clay thicknesses west of the crane pad area. For both scenarios, 7 ft of the soft clay layer (i.e., Unit III) would be excavated and replaced with crushed stone. However, one of the scenarios assumes the clay is about 14-ft thick at the edge of the western crane pad and for the second scenario, the left-in-place clay thickness is assumed to be about 10 ft (which is based on the maximum thickness of Unit III encountered during the geotechnical investigation). The 14-ft thickness was estimated in consideration of the presumed geometry of the original mudline behind the wall prior to filling. Calculated settlements under the crane mat for the two scenarios are presented in Figs. 6a and 6b.

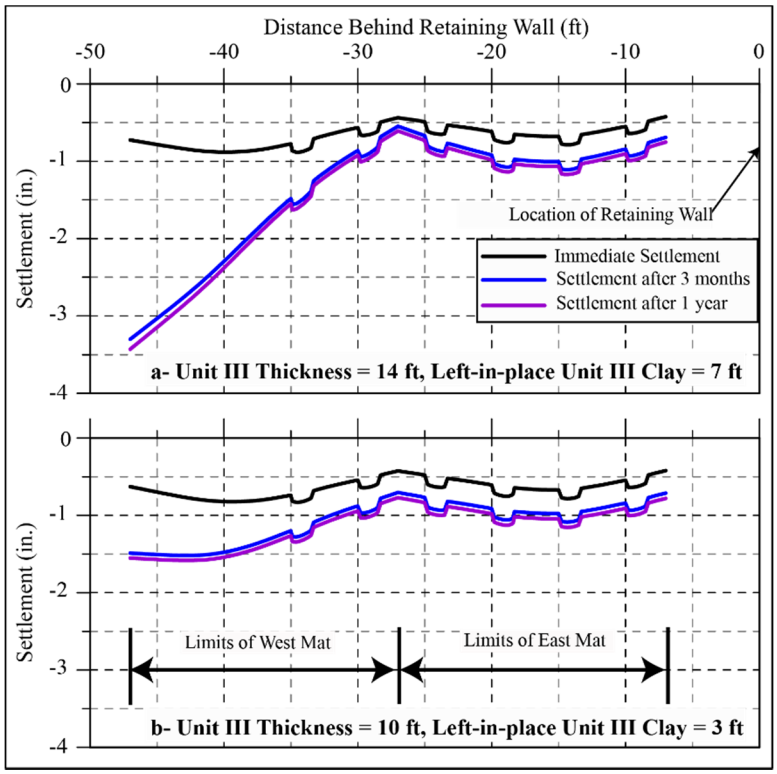


Fig. 6. Settlement under the crane mat.

For the analyses shown in Fig. 6a and 6b, it was assumed that no gap would form between the two sets of crane pads (at about -27 ft behind the retaining wall). This was considered reasonable since the crane mats would be "butted together" in the field prior to imposing the large crane weight. An additional analysis, however, was conducted wherein a gap could form. For that analysis, the computed settlement profile was more uniform than that shown in Fig. 6a and 6b. It should be noted that settlement monitoring of the crane pad showed a more uniform settlement across the crane pad on the order of 3-in (after 6-months).

Information in Figs. 6a and 6b indicates that there is a significant contribution from the time dependent settlement (corresponding to consolidation of the remaining Unit III and Unit V) to the total settlement. It can be observed that the effect of the left-in-place Unit III clay on the immediate settlement is not as significant as its effect on the consolidation settlement. The maximum immediate settlement under the crane mat was about 0.7 in. and 0.9 in. for the east and west crane pad, respectively for the first scenario (14 ft maximum thickness of Unit III), as shown on Fig. 6a.

It can be seen from Figs. 6a and 6b that most of the time dependent settlement occurs within three months after applying the crane load. The west mat is subjected to a larger differential settlement than the east mat. For a maximum Unit III thickness of 14 ft, the calculated differential settlement is about 1.2 in. (assuming consolidation under the full crane pad load) over a distance of 23'10" (i.e., the distance between the centerline of the two crawlers located at -15 and -39 ft). This corresponds to a cross-track differential settlement of about 0.4 percent (which is considered acceptable).

Because of the potential for continued consolidations settlements, it was recommended to the contractor excavate and replace as much as practically possible in the area west of the DSM piers.

SUMMARY AND CONCLUSIONS

Finite element analyses were used to assess settlements below a crane pad and loads on a retaining wall for a case where a complete ground improvement program comprising DSM piers could not be completed due to near-surface obstructions. Analysis results indicate that total and differential settlements of the crane pad and retaining wall loadings were tolerable for multiple crane loading cases provided weak dredged material (just outside the limit of the DSM piers) was removed and replaced with compacted crushed stone fill.

We worked closely with the EPC contractor over only a 4-week period to complete the work described herein and to construct the excavation and replacement of the weak dredged material along the western edge of the crane pad area. The design was constructed and the crane has operated without incident of excessive settlements or distress in the retaining wall.

ACKNOWLEDGEMENT

The authors of this paper wish to acknowledge the significant effort and diligence provided by the EPC's engineering, construction, and project management team throughout the course of the project.

REFERENCES

FHWA-HRT-13-046 (2013). Federal Highway Administration Design Manual: Deep Mixing for Embankment and Foundation Support.

Kulhawy, F.H. and Mayne, P.W. (1990). "Manual on Estimating Soil Properties for Foundation Design", EPRI EL-6800, Project 1493-6.

PLAXIS (2012). "Material Models Manual", Plaxis bv, Delft Netherland.

Schanz, T., Vermeer, P.A., and Bonnier, P.G. (1999). "The Hardening-Soil Model: Formulation and Verification." R.B.J. Brinkgreve, Beyond 2000 in Computational Geotechnics, Balkema, Rotterdam, pp. 281-290.

CASE STUDY: 1785 MASSACHUSETTS AVENUE NW, WASHINGTON, DC

SungJe Chi P.E., Berkel and Company Contractors Inc., Stewartstown, Pennsylvania, USA,
+1 (717) 993-8512, schi@berkelapg.com

ABSTRACT

This project involved the renovation and restoration of a National Historic Landmark constructed in 1917 at 1785 Massachusetts Avenue, NW, Washington, DC. The renovated structure would serve as the new headquarters building for the American Enterprise Institute (Fig. 1). The existing structure consisted of five levels above grade and one level below grade. The scope of new construction involved extensive renovations and structural upgrades to the superstructure along with construction of an additional basement level. A new deep foundation system and perimeter shoring system was required to allow excavation beneath the existing spread footing foundations. To accomplish this, existing interior steel columns were supported by one hundred thirty-eight micropiles that provided temporary support during excavation to new subgrade and later served as the permanent foundation system for the renovated structure. Load transfer from interior columns to micropiles was accomplished using transfer beams and a trussed-tower system consisting of the micropiles and lacing (Figs. 2 and 3). To support the perimeter walls and columns, sixty-seven battered micropiles were installed first along the perimeter followed by hand dug concrete pit underpinning. The piles were strategically positioned to provide support for the completed underpinning. During excavation to new subgrade, the underpinning was laterally supported by two levels of temporary tiebacks drilled through the pits. Once excavation reached subgrade, new pile caps were constructed that were supported by the interior micropiles. Concrete columns were then constructed connecting the caps to the base of the steel columns. A load transfer program was performed as the final step in transferring the building loads to the new foundation system. The project required a total of two hundred and thirty-six micropiles installed in low headroom conditions.

Keywords: micropile, shoring of excavation, underpinning, tieback, pile cap



Fig. 1. 1785 Massachusetts Avenue Building (Photo Courtesy of Grunley Construction Co.)

 © 2017 DFI Annual Conference, New Orleans, LA, USA



Fig. 2. Micropile truss tower for interior column support.



Fig. 3. Micropile truss tower to support two columns.

INTRODUCTION

The preservation of a historic building is an environmentally sound practice and is essential to understanding our national heritage. The site is located at 1785 Massachusetts Avenue, NW, in Washington, D.C. The project involves renovation and rehabilitation of a National Historic Landmark to preserve its historic elements both interior and exterior. The American Enterprise Institute, owner of the property since 2013, planned to expand the 99-year-old, five-story, Beaux Arts building to provide additional space for their needs.

The existing building was supported on perimeter column spread and wall footings and the interior columns were supported on forty-two spread footings. The new construction would increase the service area of the building from 72,000 sq. ft. to 100,000 sq. ft. and result in additional load to be carried by the deep foundation system.

SUBSURFACE SOIL CONDITION AND FOUNDATION SELECTION

Subsurface conditions as summarized from the Geotechnical report are as follows:

- Stratum A: The ground surface elevation is at El. 82.0 ft, and below the ground surface to the depth up to 23.5 ft (El. 58.5 ft), the boring encountered FILL consisting of sandy silt, poorly-graded sand with gravel with blow counts mainly varying in N-value from 3 to 9.
- Stratum B: Below the fill of Stratum A to a depth to 33.5 ft (El. 48.5 ft), the boring encountered well graded GRAVEL (GW) and clayey sand (SC) and N-value varied between 36 and 54.
- Stratum C: Below Stratum B to a depth of 61.3 ft (El. 20.7 ft), the boring encountered disintegrated rock and N-value varied between 66 and 100.

Existing basement finished floor elevations were 76.0 and 73.0 feet. Bottom elevations for existing spread footings were a few feet below finished floor. New basement finished floor elevations were set at elevations 62.0 and 58.0 feet requiring excavation depths up to 15.0 feet. The new basement and modifications to the structure resulted in a 10 percent (+/-) increase in foundation load compared to the original structure.

A new deep foundation system was required prior to the excavation for the new subgrade. The major challenge was to stabilize and support the existing structural steel building and preserve the limestone façade and plaster interiors during the construction process. A trussed-tower system utilizing micropiles was selected to serve as both the temporary load transfer system for the existing building and the permanent foundation system as shown in Fig. 2. Both 7-in and 9-5/8-in micropile casing were selected for use on the project based on availability. As the maximum design load for all the piles was established at 200 kips, Berkel decided to load test the 7-in pile as a conservative test.

The static compression load test was performed in general accordance with ASTM D1143 Quick Load Test Procedures and Load Testing Setup requirements. The pile design load was 200 kips and the pile was loaded to a maximum load of 500 kips. The test pile was installed from the existing slab-on-grade level at El. 76 feet by advancing a 7 inch. diameter (0.408 in. thickness, API N80) casing to El. 37 feet (39 feet length of casing) and then a 12 feet long rock socket was drilled using a down-hole-hammer with mechanical wings that create a 7.75 in. nominal diameter. Casing was filled with 5000 psi site batched neat cement grout. As shown in the Load-Settlement curve (Fig. 4), the total settlement at the pile design load of 200 kips was 0.286 in., which was slightly larger than the specified 0.25 in. limit. However, a larger elastic shortening was anticipated because the test pile was 14 feet longer than the production pile length. The permanent pile settlement was 0.122 inch which was within the specified maximum settlement of 0.125 inch; and the slope of maximum load versus settlement curve was 0.222 inch/kips for load between 480 kips and 500 kips, which was within the maximum specified rate of 0.04 inch/kips. Per the load test results, it was confirmed that the installed test pile was capable of sustaining the design load with a factor of safety of 2.5.

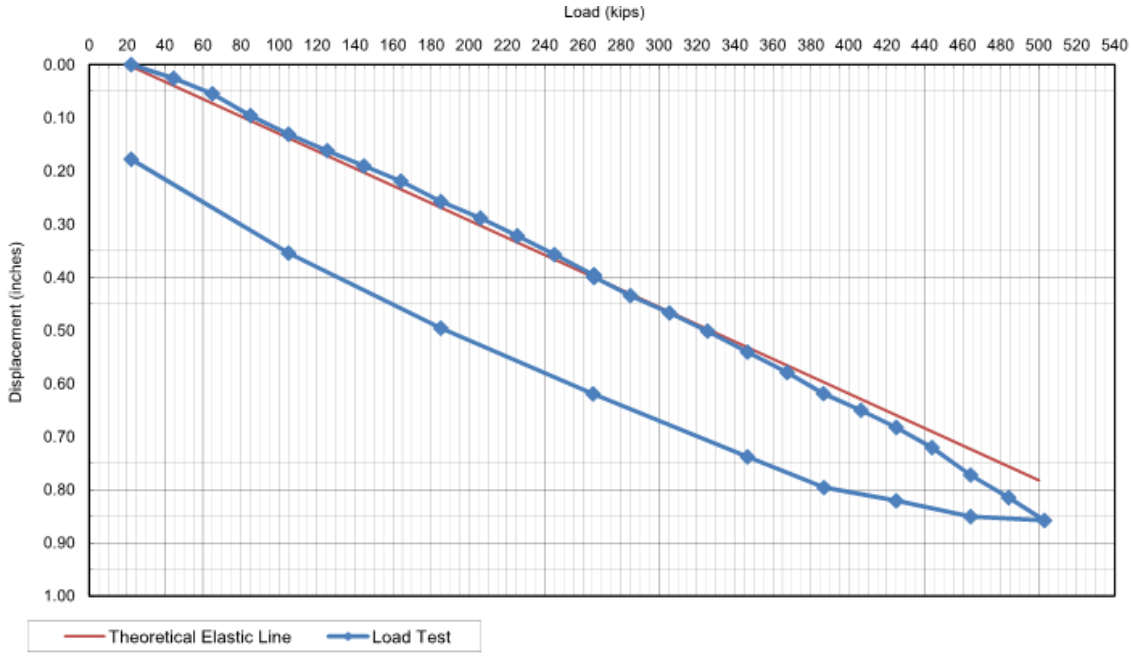


Fig. 4. Load settlement curve referenced with load test report by Schnabel Engineering.

SUPPORT OF INTERIOR COLUMNS

To support the interior columns and the final increased foundation loads, 9-5/8 inch O.D. micropiles were selected to carry a maximum 200 kip design compressive load. After basement slab removal (elevations 73.0 and 76.0), mass excavation (by Grunley subcontractor) to top of existing footing elevations, and pre-coring holes in the existing footings (by Grunley subcontractor), 126 vertical micropiles were installed in approximately 10 feet of headroom using low headroom drills. Four to eight micropiles per column (Fig. 5) were required to support the 25 existing interior steel columns and 5 new interior columns. Steel brackets and transfer beams were erected on the top of the micropiles and welded to the existing columns.



Fig. 5. Micropile truss tower construction during excavation in progress.

The existing column service loads were estimated to determine jacking loads during the construction. Two hydraulic jacks per column were utilized to lift up each column. The jacking process was monitored to limit the upward movement to less than $5/100^{th}$ of an inch to ensure that the existing column service load had been transferred from the columns to the micropile trussed-towers as shown in Fig. 5. After the completion of the load transfer sequence, shims were installed and welded, and the jacks were removed. Footing demolition and excavation to new sub-grade then proceeded along with perimeter wall support.
Once subgrade was reached (elevation 61.77 and 57.77), new pile caps and columns (by Grunley subcontractor) were constructed. Prior to pouring the pile caps, shear connectors were welded to the micropiles to transfer column loads to the piles. Up to sixteen headed studs (3/4 in. diameter and 4 in. long) were welded to the micropile casing as the load transfer connection to the new pile caps as shown in the Fig. 6.



Fig. 6. New concrete column on new subgrade elevation and shear connectors in new pile caps.

SUPPORT OF EXTERIOR COLUMNS

For 25 exterior columns along the perimeter of the building, 55 concrete underpinning pits (4 ft. x 3.5 ft. x 9 to 15 ft. deep) with micropile support were installed to control possible differential settlement. As shown in Fig. 7, 69 micropiles were installed using 7.0 in. O.D. casing prior to the underpinning construction to provide the load transfer mechanism to prevent differential settlement between the interior and exterior columns. The differential settlement limit of 0.25 in. was specified to prevent cracking of the existing limestone façade and plaster interiors. Each column was monitored during the entire sequence of the construction to ensure that the differential settlement was less than the 0.25 in. limit.

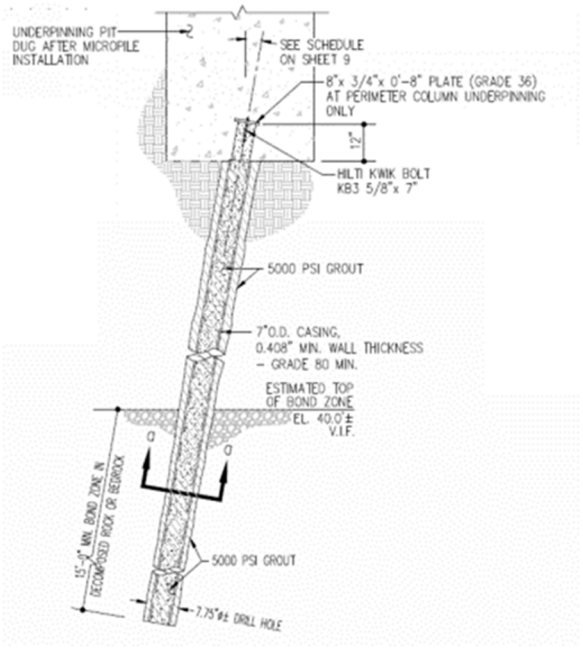


Fig. 7. Perimeter underpinning with micropiles.

After consultation with the construction team, it was agreed that as a precaution, jacking blockouts would be installed in the underpinning directly beneath the column footings. Column footings could then be raised if excessive settlement occurred. Fig. 8 shows the typical jacking detail which consists of three jacking pockets (13 in. x 8 in x 48 in. each). In the event of jacking, four 150 ton, low profile hydraulic jacks would be inserted in the blockouts with steel bearing plates. The plan was to lift the entire footing and limit the upward movement to less than $5/100^{th}$ of an inch. Support plates would then be installed, jacks removed, and the pockets grouted with high strength non-shrink grout. Jacking was not required during construction.

After completion of the perimeter micropiles and underpinning pits, excavation to new subgrade commenced. Two levels of temporary tiebacks provided lateral support for the pits until new floor slabs provided permanent support. Tiebacks extended approximately 45 feet outside the building perimeter as shown in Figs. 9 and 10.

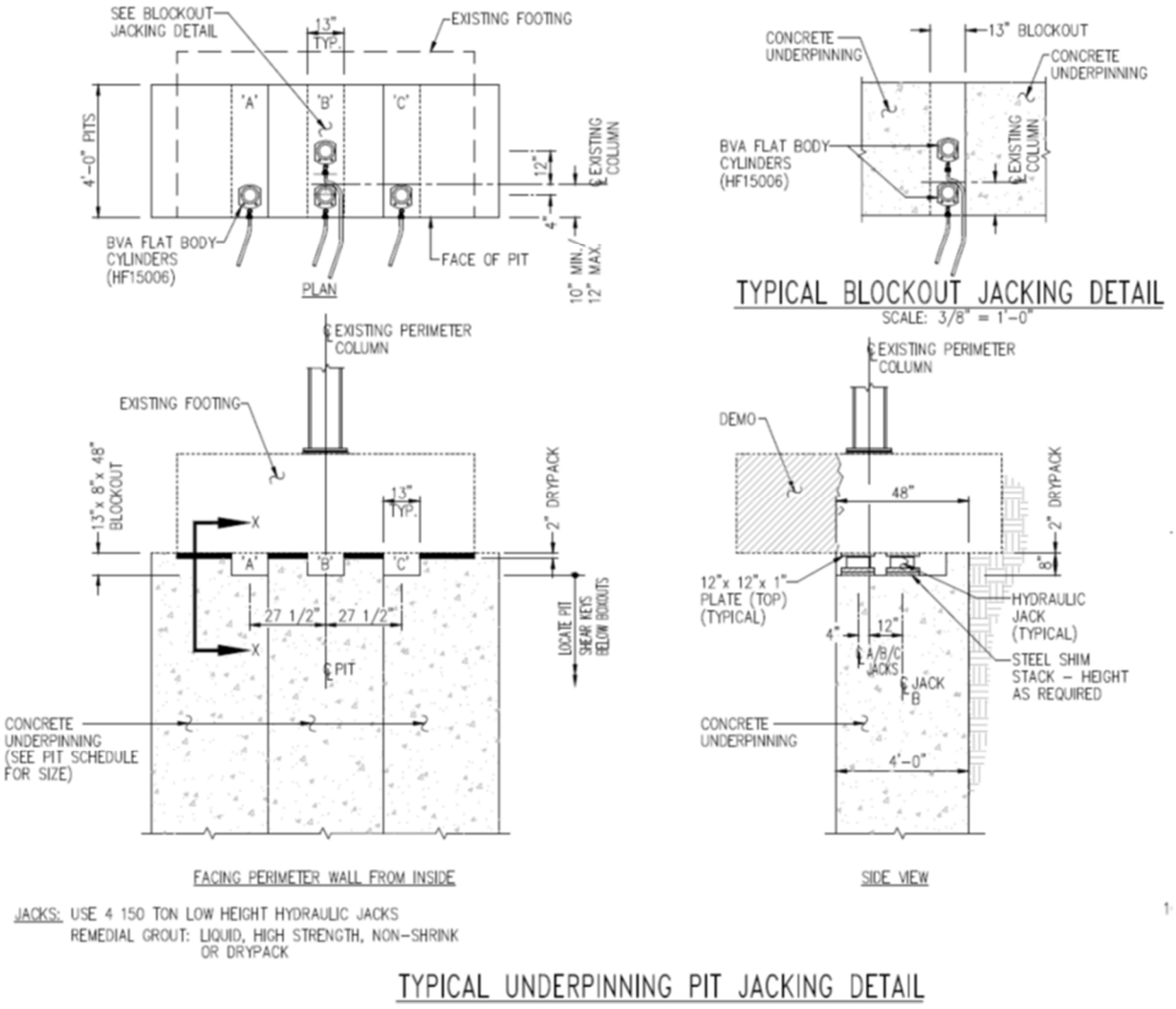


Fig. 8. Typical underpinning pit jacking detail.



Fig. 9. Concrete underpinning pit with tiebacks.

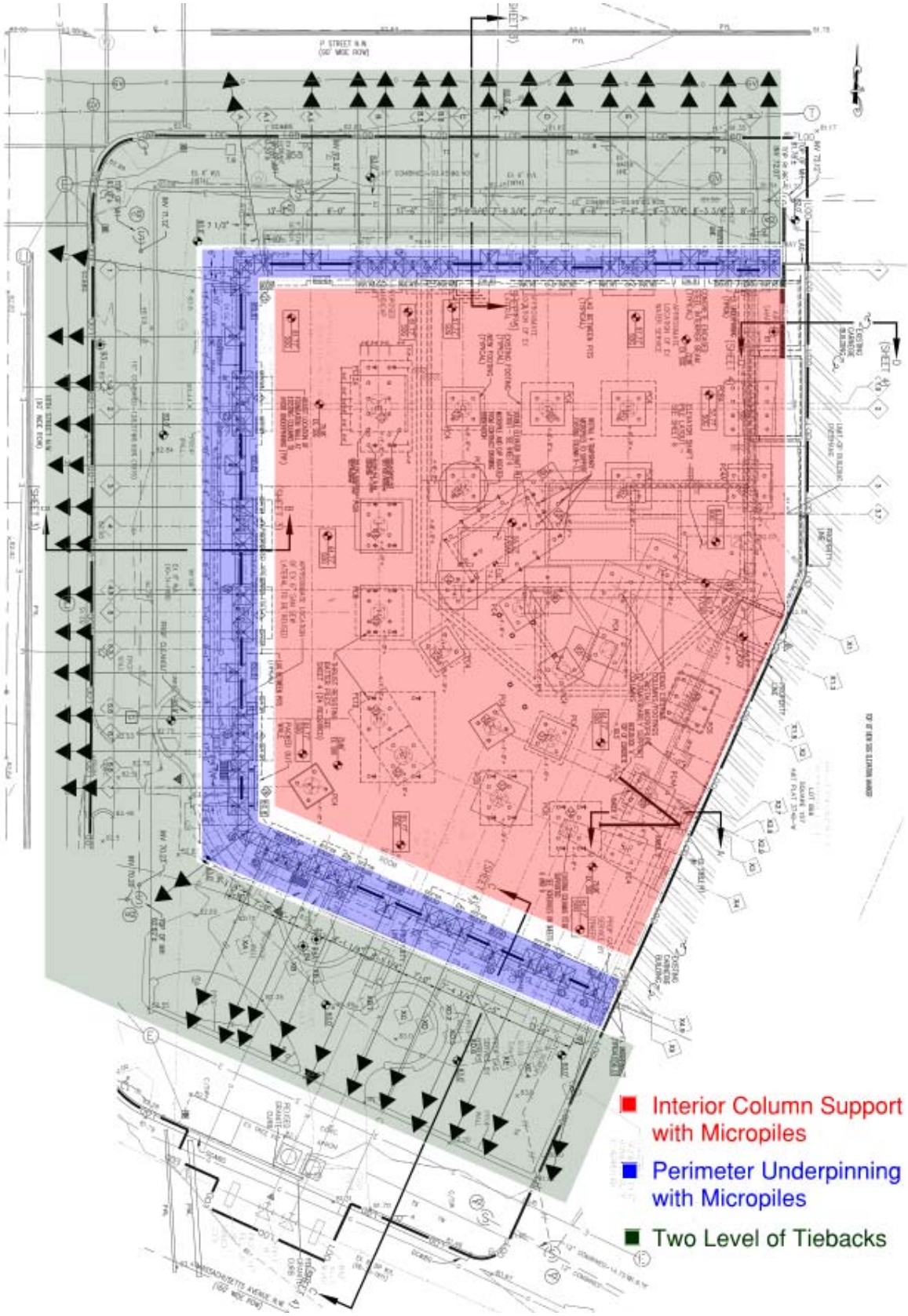


Fig. 10. Foundation plan; major construction of project.

LOAD TRANSFER TO NEW COLUMNS AND PILE CAPS

Following the installation of micropiles, underpinning pits, tiebacks, and micropile lacing, mass excavation proceeded to new subgrade elevations. New pile caps were then constructed around the interior micropiles followed by new concrete columns extending up to the base of the supported steel columns. The concrete columns were constructed within the micropile truss towers (Fig. 11). As the construction proceeded, building loads increased due to the renovations of the upper structure. Another jacking procedure was required to transfer the new building loads to the new concrete columns and pile caps.

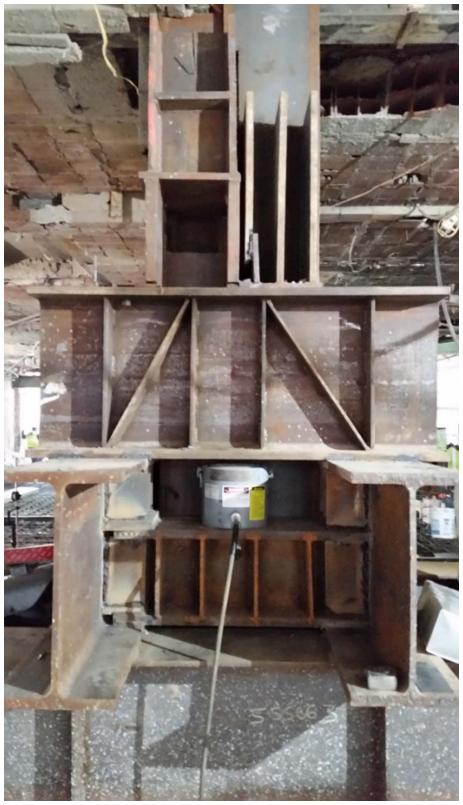


Fig. 11. Load transfer from existing column to new footings.

The column loads in the final service condition of the building were estimated during construction and varied from 37 kips to 788 kips at 100% completion. Jacking was performed at each interior column using two hydraulic jacks, one on each side of the column web as shown in Fig. 12. During jacking, column movement was closely monitored and the upward movement was limited to less than $5/100^{th}$ of an inch before the jacks were locked off. The gap between the bottom of the column base plate and the top of the new cast-in-place column was then filled with high strength, non-shrink grout to provide precise and level bearing for the existing column. The jacks remained in place until the grout achieved adequate strength.



Fig. 12. New column construction under existing column.

SUMMARY AND CONCLUSION

The 1785 Massachusetts Avenue site is located in a busy section of Washington, DC and surrounded by pedestrians and traffic on three sides.

Storage areas outside the building were severely limited and most materials had to be stored at a remote location and trucked to the site as needed. Access into the structure was initially limited to a handical ramp and doorway and a small wall opening in a narrow alley.

Berkel was tasked with installing over 200 micropiles in low headroom conditions, connecting many of the the micropiles to the existing columns through a steel transfer system, and jacking each interior column twice to finalize the load transfer to the temporary and permanent support systems. In addition, extensive pile supported underpinning was required to support the perimeter columns and walls.

The major challenge for this project was to transfer the entire load of the building from existing spread footings to a new deep foundation system while preserving the limestone façade and plaster interiors. Differential settlements exceeding ¼" could not be tolerated by the historic structure.

Despite the logistical hardships and congested working conditions, Berkel was able to successfully design and install a deep foundation support system that achieved the project objectives.

ACKNOWLEDGEMENTS

The author would like to acknowledge the excellent cooperation, support and contribution throughout the project from the general contractor, Grunley Construction Company; the structural engineer, Robert Silman Associates; the architect, Hartman Cox; and the geotechnical engineer, Schnabel Engineering.

Daniel S. Stevenson, P.E., is the Chief Structural Engineer at Berkel and Company Contractors. He has more than 30 years of experience with deep foundation engineering and is an active member of DFI, ACI and IBC.

Robert W. Bergwall, P.E., is a Senior Foundation Manager at Berkel and Company Contractors. He is a licensed engineer in District of Columbia, Maryland, Virginia and Massachusetts. He has more than 30 years of experience with the design and management of excavation support system projects.

Ray Rhodes-General Superintendent for Berkel and Company

Steve Harris – Site Superintendent for Berkel and Company

REFERENCE LIST

Post-Tensioning Institute, (2004). "Recommendations for Prestressed Rock and Soil Anchors."

Federal Highway Administration, (2005) "Micropile Design and Construction Reference Manual" FHWA-NHI-05-039.

HIGH-CAPACITY DRIVEN-PILE FOUNDATION FOR A 33-STORY HIGH-RISE IN MILWAUKEE, WISCONSIN, USA

Van E. Komurka, P.E., D.GE, F.ASCE, GRL Engineers, Inc., Cleveland, OH, USA, (216) 831-6131, vkomurka@grlengineers.com
William H. Walton, P.E., S.E., F.ASCE, GEI Consultants, Inc., Vernon Hills, IL, USA, (847) 984-3494, bwalton@geiconsultants.com
Ryan C. Rusk, P.E., M.ASCE, GEI Consultants, Inc., Vernon Hills, IL, USA, (847) 984-3494, rrusk@geiconsultants.com
Patrick J. Hannigan, P.E., M.ASCE, GRL Engineers, Inc., Cleveland, OH, USA, (216) 831-6131, phannigan@grlengineers.com

Keywords: depth-variable criteria, driven piles, dynamic testing, instrumentation, load testing, restrike testing, set-up, static testing

ABSTRACT

The project consists of a 33-story building with two levels of below-grade parking across the entire building footprint. Timely and cooperative teamwork among the owner/developer, geotechnical engineer, testing agency, structural engineer, construction manager, and pile-driving contractor resulted in an efficient, cost-effective, high-capacity driven-pile foundation on a constrained urban site with significantly variable subsurface conditions. Design objectives included utilizing the highest allowable pile loads reasonably installed from a drivability perspective, using readily available equipment. A pre-production test program was performed on 16-inch-diameter (406-mm-diameter) steel pipe piles, driven closed-ended and subsequently filled with concrete. The test program included dynamic monitoring of 10 piles during installation, and of select piles during long-term restrike testing with a drop hammer, with one instrumented static load test. CAPWAP® analyses were performed on both end-of-initial-drive and beginning-of-restrike dynamic test records. The site exhibited significant soil set-up, even after relatively short wait times. Test-program objectives included characterizing set-up profiles. A design set-up profile was used to develop depth-variable driving criteria for both 500- and 600-kip (2,224- and 2,669-kN) allowable load piles. Test program results permitted more-accurate reduced capacities to be assigned to damaged piles, and to piles which experienced practical refusal. These more-accurate assigned reduced capacities decreased the number of replacement piles required by 50 percent, saving both time and cost.

PROJECT DESCRIPTION

The project, located in Milwaukee, Wisconsin, USA consists of a 33-story mixed-use residential building with two levels of below-grade parking across the entire site footprint. Column service loads range from 1,400 to 4,200 kips (6,228 to 18,683 kN). The project is located immediately adjacent to an existing two-story masonry retail building with a partial basement, supported on shallow spread-footing foundations.

Subsurface Conditions – The generalized soil conditions are presented in Fig. 1. Site grades were relatively level, with a ground-surface elevation of approximately +53 feet (16 m), Milwaukee City Datum ("MCD"). Fill material from previous construction was encountered to approximate Elev. +33 feet (10 m). Below the fill, medium dense silty sand, to silt with sand, was encountered to approximate Elev. +23 feet (7 m). Underlying deposits consisted of lean clay, with undrained shear strengths ranging from approximately 1,000 to 3,000 pounds per square foot (psf) (48 to 144 kPa). Silty sand, to silt with sand, exhibiting increasing relative density with depth, was found below the lean clay to approximate Elev. -92 feet (-28 m), where hard lean clay (glacial till) with undrained shear strengths in excess of 5,000 psf (239 kPa) was encountered. Borings did not extend below Elev. -103 feet (-31 m).

 © 2017 DFI Annual Conference, New Orleans, LA, USA

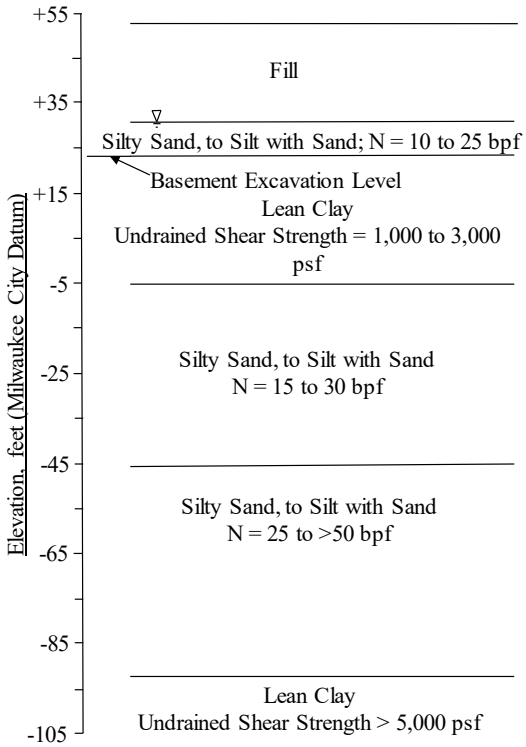


Fig. 1. Generalized soil profile

Foundation Selection – The project owner had previously completed foundation work for a similar building a short distance away that was founded on a mat, which had encountered significant difficulties during subgrade preparation. As a result of this experience, the design team was tasked with identifying alternate foundation systems.

In the Milwaukee area, closed-end pipe piles with diameters ranging from 10.75 to 16 inches (273 to 406 mm) are readily available, and multiple contractors are experienced with their installation. Drilled shafts and augered cast-in-place piles were evaluated, but were considered to have higher installation risks due to the many sand and silt layers throughout the soil profile. This, in combination with area contractors being less-experienced with installing these types of deep foundations than with installing driven piles, eliminated these options from consideration.

Based on a review of the project service loads, it was determined that the project would benefit from a program to maximize pipe-pile allowable loads while maintaining reasonable installation methods, including readily available pile sections, and hammer types and sizes. The project design team reviewed the option of 16-inch-diameter closed-end pipe piles, and estimated that piles with an allowable load on the order of 500 to 600 kips (2,224 to 2,669 kN) could reasonably be obtained utilizing a carefully planned and executed test program which included both dynamic and static load testing.

Test Program Objectives – A pre-production test program was performed. The drivability of 16-inch piles was assessed, including the ability of the closed-end section to penetrate dense upper soil layers prior to reaching desirable toe elevations (which ranged approximately from Elev. -40 to -74 feet (-12 to -23 m)), using readily available equipment. A major objective of the test program was to establish the highest long-term axial compression capacity to which the 16-inch piles could reasonably be installed, from which the maximum allowable load that could be used for design would be established. To evaluate tension resistance, it was desired to determine long-term capacity resistance distribution (relative shaft and toe capacity

contribution, and capacity distribution along the shaft). Toe resistance relaxation of piles terminating in dense fine-grained granular deposits was also evaluated.

To aid in demonstrating high capacities, soil set-up (time-dependent capacity increase) was characterized. Set-up characterization included determining both total set-up magnitude and distribution along the shaft, allowing set-up to be incorporated into production-pile driving criteria. Test pile locations were selected to provide good general site coverage, to evidence variability in subsurface conditions, helping to estimate production-pile lengths. An axial compression static load test was performed, the purpose of which was to provide a full-scale proof-test demonstrating ultimate pile capacity, including load-transfer behavior. This information was then compared to the static load test pile's dynamic monitoring results and analysis, and used to correlate the dynamic model on which final production pile driving penetration resistance criteria were based.

TEST PROGRAM SCOPE

Installation

Test pile locations are presented in Fig. 2. Because site constraints precluded pile driving in the southern portion of the site, pre-production testing was performed on the northern half of the site. Test pile locations on the northern half of the site were selected based on providing general site coverage, accessibility, impact to existing site operations, reuse of test piles as production piles (to save cost), building loads distribution, and proximity to boring locations. All tested piles were steel pipe, having a nominal outside diameter of 16 inches (406 mm) and a nominal wall thickness of 0.50 inches (13 mm), and filled after driving with concrete having a minimum 28-day strength of 6 ksi (41 MPa). The piles were fabricated to ASTM A252 Grade 3 requirements, which specify a minimum yield strength of 45 ksi (310 MPa). The piles were fitted and driven with a 1-inch-thick (25 mm), 16.5-inch-diameter (419 mm), oversized toe plate.

A total of 10 test piles were installed: 5 indicator piles, 1 static load test pile, and 4 reaction piles. Each pile installation consisted of a bottom section with a flat toe plate, and varying numbers of upper sections, which were spliced to the bottom section (and sometimes to each other) during a pause in driving using full-penetration butt welds against backup rings. The piles were driven using a Delmag D46-32 single-acting diesel hammer. According to the manufacture's literature, the Delmag D46-32 has a 10.14-kip (45.10-kN) ram, a rated maximum stroke of 12.05 feet (3.673 m), and a maximum rated energy of 122.2 foot-kips (165.7 kJ). The hammer was equipped with a four-step fuel pump, allowing it to be operated over a range of rated energies. Fuel setting selection during installation was intended to result in terminal equivalent blow counts in the range of 30 to 120 blows per foot ("bpf"; blows per foot are roughly equivalent to blows per 0.3 meter).

Dynamic testing using a Pile Driving Analyzer® ("PDA") was performed on each test pile for its full depth of driving to monitor hammer and driving-system performance, calculate pile driving stresses, assess pile structural integrity, and evaluate pile bearing capacity. To satisfy the test program objective of establishing the highest long-term capacity to which production piles could reasonably be installed, test pile driving tended to approach the upper limits of reasonable blow counts and driving stresses. Test-pile driving termination was a field decision which considered subsurface conditions apparent from borings, anticipated shaft set-up, desired ultimate capacity, blow count, potential to mobilize capacity during restrike testing, driving stresses, pile purpose, pile material available, and dynamic monitoring results available in the field during initial driving. A CAPWAP analysis was subsequently performed on a representative end-of-initial-drive ("EOID") dynamic test record from each test pile to further evaluate ultimate pile capacity, including the relative soil resistance distribution along the pile shaft, and at the pile toe. Details of the test pile installations are summarized in Table 1.

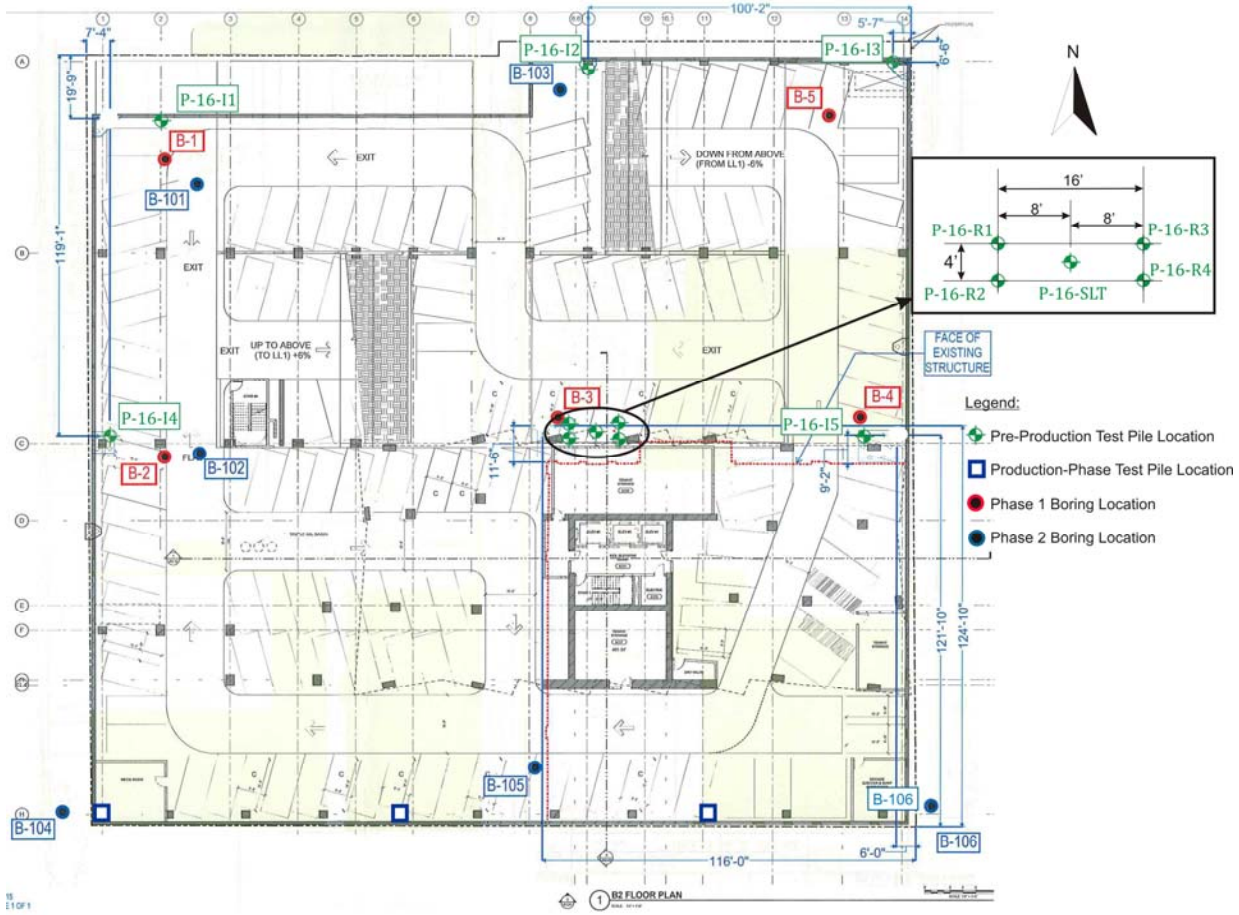


Fig. 2. Test Pile Location Diagram

Axial Compression Static Load Test

The static load test's purpose was to provide a full-scale proof-test demonstrating ultimate pile capacity, including load-transfer behavior. This information was then compared to the static load test pile's dynamic monitoring results and analysis, and used to refine the dynamic model on which production pile driving penetration resistance criteria were based.

Prior to filling the static load test pile with concrete, vibrating-wire strain gages ("VWSGs") were installed at various elevations within the pile. The VWSGs were located in the pile by attaching rebar strain meters ("sister bars") to a 1-inch-diameter (25-mm-diameter) steel water pipe which was installed in the pile with centering devices attached to it. The VWSG elevations were selected to have the uppermost gage coincident with the ground surface, and gages below coincident with major stratigraphy changes indicated by the most-proximate boring. The purpose of the internal strain gages was to determine the load in the pile section at discrete elevations, and by doing so, allow for load-transfer determinations.

Four surface-mounted VWSGs were attached to the static load test pile's exterior, equidistant around its perimeter, just above ground surface. These strain gages served two purposes: 1) to aid in assessing composite-section action, and 2) to aid in determining the composite-section modulus of elasticity (required to determine both the pile's theoretical elastic shortening, and the embedded strain gages' data reduction and load-transfer determinations).

Table 1. Test Pile Summary

Pile	Driving Status	Hammer	Toe Elevation, feet (MCD)	Penetration Resistance		Elapsed Time Since EOID, days	Average Hammer Stroke, feet[1]	Average Transferred Energy, ft-kips	Average Maximum Pile Head Compression Stress, ksi	Maximum Pile Compression Stress, ksi[2]	Average Case Method Capacity (RX9), kips	Mobilized CAPWAP Capacity, kips		
				Reported	Equivalent bpf							Shaft	Toe	Total
P-16-I1	EOID	D46-32	-43.4	22 / 3 in.	88	---	10.0	83	37.2	37.4	873	359	435	794
	BOR1	D46-32	-43.4	13 / 1 in.	156	3.913	11.0	94	43.9	46.2	1,158	834	415	1,249
	BOR2	APPLE	-43.4	1 / 0.15 in.	80	52.967	3.0	75	---	7.4	---	940	400	1,340
P-16-I2	EOID	D46-32	-70.2	38 / 3 in.	152	---	9.8	82	36.8	37.8	765	432	260	692
	BOR1	D46-32	-70.2	13 / 1 in.	156	0.808	11.8	96	42.4	43.6	965	722	255	977
	BOR2	APPLE	-70.7	1 / 0.25 in.	48	44.019	4.0	149	---	9.5	---	1,401	260	1,661
P-16-I3	EOID	D46-32	-63.3	20 / 3 in.	80	---	10.6	82	37.9	40.1	905	734	125	859
	BOR1	D46-32	-63.3	20 / 1 in.	240	1.821	12.2	100	44.1	47.0	1,112	1,040	145	1,185
	BOR2	APPLE	-63.3	1 / 0.2 in.	60	45.150	2.5	77	---	7.4	---	1,416	125	1,541
P-16-I4	EOID	D46-32	-63.0	21 / 3 in.	84	---	10.7	84	38.6	38.1	871	344	565	909
	BOR1	D46-32	-63.0	16 / 1 in.	192	1.847	11.3	96	39.6	42.7	1,038	541	495	1,036
	BOR2	APPLE	-63.0	1 / 0.05 in.	240	54.006	3.5	80	---	7.3	---	1,012	350	1,362
P-16-I5	EOID	D46-32	-52.0	25 / 3 in.	100	---	10.5	89	39.4	38.4	879	184	695	879
	BOR1	APPLE	-52.0	1 / 0.15 in.	80	36.249	3.6	94	---	7.3	---	604	700	1,304
P-16-R1	EOID	D46-32	-46.5	21 / 3 in.	84	---	10.5	82	36.0	36.3	786	202	595	797
P-16-R2	EOID	D46-32	-52.3	34 / 3 in.	136	---	10.7	82	36.8	40.0	880	208	645	853
P-16-R3	EOID	D46-32	-39.8	24 / 3 in.	96	---	10.0	82	38.1	37.1	765	107	710	817
P-16-R4	EOID	D46-32	-40.5	20 / 3 in.	80	---	10.5	90	37.6	37.8	781	106	708	814
	BOR1	APPLE	-40.5	1 / 0.2 in.	60	38.865	3.5	112	---	7.5	---	624	655	1,279
P-16-SLT	EOID	D46-32	-49.0	5 / 3 in.	20	---	9.1	65	33.6	32.6	456	178	295	473
	SLT	---	-49.0	---	---		---	---	---	---	---	977	368	1,345
	BOR1	APPLE	-49.0	1 / 0.05 in.	240	37.118	3.0	62	---	6.4	---	1,096	290	1,386

1. With the exception of the APPLE restrike on P-16-I5 which used a 40-kip (178-kN) ram, all the APPLE restrikes used a 48-kip (214-kN) ram.
2. For restrikes performed with the APPLE, the maximum pile compression stress acts on the composite (steel and concrete) section.

The static load test pile was loaded in axial compression by jacking against an overhead steel frame assembly. Reaction to overhead frame uplift was provided by four reaction piles. The assembly was designed by the pile-driving contractor to provide a maximum reaction of 1,530 kips (6,806 kN).

Restrike Testing

Short-Term – Displacement piles (such as closed-end pipe used for this project) terminating on dense fine-grained granular deposits (fine sands, and silts) can exhibit decreased toe capacity after driving, referred to as relaxation [Morgano and White 2004]. Capacity loss due to relaxation is unconservative with respect to long-term compression capacity, allowable load, safety factor, and settlement. Since the conditions encountered in the borings indicated that piles for this project might terminate on dense fine-grained deposits, the test program evaluated potential relaxation by performing short-term restrike testing on 4 unfilled test piles. Restrike testing consisted of redriving the pile a limited number of blows with the Delmag D46-32 hammer on Fuel Setting 4. Dynamic monitoring was performed during short-term restrike testing, and a CAPWAP analysis was performed on a representative beginning-of-restrike ("BOR") dynamic test record for each test pile. The elapsed times after EOID at which the short-term restrikes were performed are reported in Table 1.

Long-Term – It is recognized that piles which have been in place for some time typically develop greater capacity than their EOID capacity [Komurka et al. 2003a; 2003b]. This capacity increase with time

phenomenon is referred to as soil set-up, which is defined as the difference between the capacity at the time initial driving terminates and the capacity at some later time. Set-up can refer to total pile (both shaft and toe) capacity increase, shaft capacity increase, or toe capacity increase. Generally, set-up is considered to be predominately related to shaft capacity increase. Unit shaft set-up determination is typically appropriate for discrete pile sections, such as the sections between strain-gage elevations for static load test data, or some fraction of the total pile length for CAPWAP analyses. Unit shaft set-up for a particular pile segment is defined as the shaft resistance increase on the segment, divided by the pile segment surface area. Accounting for both end-of-drive capacity and set-up results in more-accurate capacity estimates, and therefore more-economical pile installations [Komurka 2004; Komurka and Arndorfer 2009].

To aid in determining shaft set-up magnitude and distribution, 8 test piles received long-term restrike testing (2 reaction piles were inaccessible for restrike testing). The elapsed times after EOID at which the long-term restrikes were performed ranged from 36.25 to 54.01 days, and are reported in Table 1. Generally, since set-up has occurred by the time the piles are restruck, a hammer capable of delivering more impact force than used for initial driving may be required to mobilize soil resistance [Likins and Rausche 2008]. Concreting closed-end pipe piles increases their impedance, which increases the applied impact force and also aids in mobilizing their capacity during restrike testing [Likins 2017].

Long-term restrikes were performed on the concrete-filled test piles using an APPLE drop-weight system. The APPLE system consisted of a support/guide frame, and a 40- to 48-kip (178- to 214-kN) ram. Ram weights and drop heights, and transferred energies, are reported in Table 1. A subsequent CAPWAP analysis was performed on a representative BOR dynamic test record for each restruck test pile.

TEST PROGRAM RESULTS

Driving Behavior

Blow Count – The test piles' equivalent blow count (measurements of blows per driving distance converted to units of bpf) profiles are presented in Fig. 3. A review of Fig. 3 indicates that none of the test piles experienced significant equivalent blow counts above approximate Elev. -30 feet (-9.1 m), final toe elevations ranged from -39.8 to -70.2 feet (-12.1 to -21.4 m), and final equivalent blow counts ranged from 20 to 152 bpf. P-16-SLT's final toe elevation of –48.0 feet (14.6 m) (and its associated relatively low terminal equivalent blow count of 20 bpf) was limited by the length of available pile material. Final penetration depths and blow counts are summarized in Table 1.

Case Method Capacities – The test piles were installed using a variable-stroke (and therefore variable-energy) hammer, and the piles' equivalent blow counts presented in Fig. 3 do not account for variations in stroke and transferred energy. For this reason, the equivalent blow counts of individual piles are not directly comparable. A more-direct comparison of driving behavior can be made using initial-drive Case Method geotechnical compression capacities estimated by the PDA based on dynamic monitoring results [Rausche et al. 1985]. PDA-estimated capacities for each blow were averaged for each foot of penetration. The test piles' Case Method estimated geotechnical compression capacity profiles as determined from PDA monitoring data are presented in Fig. 4. A review of Fig. 4 indicates that Case method EOID capacities ranged from 456 to 905 kips (2,028 to 4,026 kN). EOID Case method capacities are summarized in Table 1.

EOID CAPWAP Capacities – EOID CAPWAP-estimated capacities are reported in Table 1. A review of Table 1 indicates that EOID CAPWAP-estimated total capacities ranged from 473 to 909 kips (2,104 to 4,043 kN). CAPWAP estimation of total capacity can potentially be affected by the pile set for the CAPWAPed blow. For pile sets which are too low (blow counts that are too high), CAPWAP may underpredict capacity [Likins and Rausche 2008]. For pile sets which are too high (blow counts that are too low), CAPWAP may overpredict capacity [Rausche 1991]. For this reason, it is generally desired to have

equivalent penetration resistances to between 30 and 120 bpf, for both end-of-initial-drive and

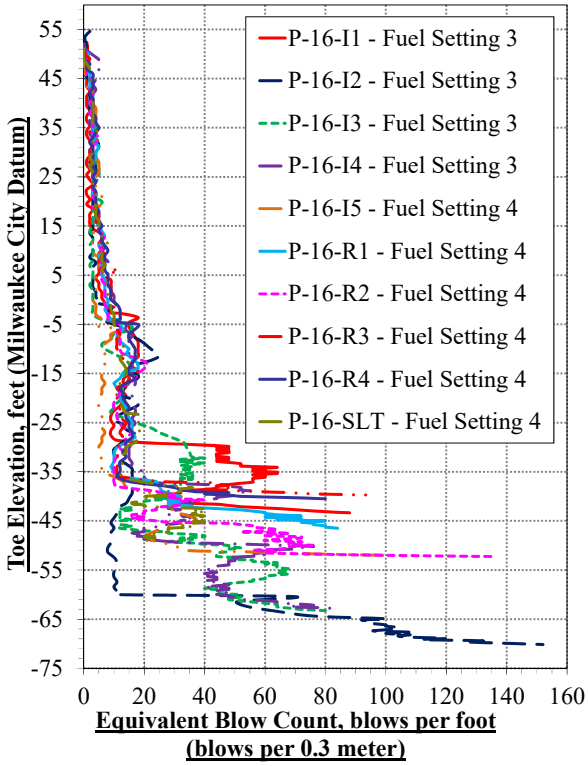


Fig. 3. Equivalent Blow Count Profiles

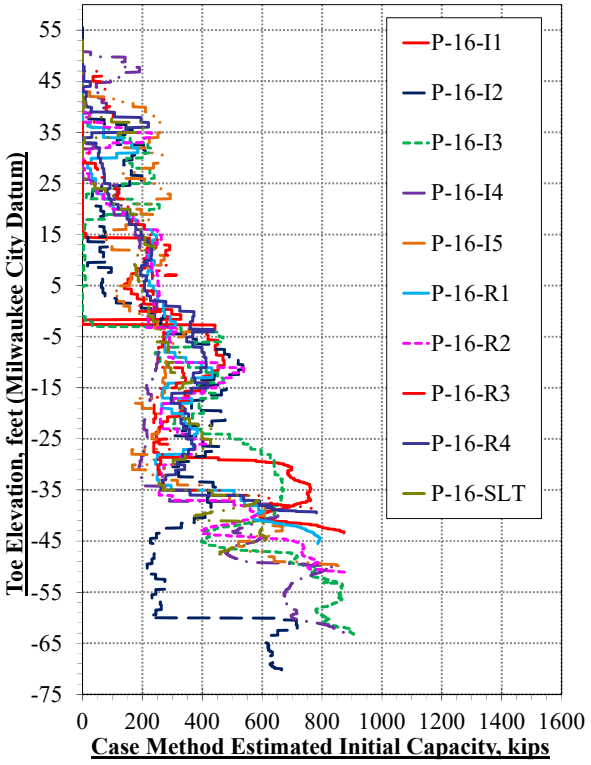


Fig. 4. Case Method Estimated Initial Capacity Profiles

restrike testing [Hannigan 2016]. To aid interpretation of CAPWAP-estimated capacity in this respect, the reported equivalent blow count or pile set associated with CAPWAPed blows is also presented in Table 1.

EOID CAPWAP Unit Shaft Resistance Distributions – The test piles' CAPWAP-determined EOID unit shaft resistance distributions are presented in Fig. 5. Occasionally, CAPWAP analyses may have difficulty distinguishing large toe resistance from large shaft resistance on the pile segment immediately above the toe. This difficulty tends to become more-pronounced at higher blow counts, and can potentially lead to over- or under-prediction of unit shaft resistance values for the pile segment(s) above the toe. This potential phenomenon associated with CAPWAP analyses can affect EOID data, as well as BOR data, and therefore can potentially affect calculated unit set-up values for the pile segment(s) above the toe. To aid interpretation of Fig. 5 in this respect, the reported equivalent blow count associated with each CAPWAP-determined unit shaft resistance distribution is also presented in Fig. 5.

Short-Term Restrikes

One of the test program objectives, and the reason short-term restrikes were performed, was to evaluate the potential for toe relaxation of piles terminating in dense, fine-grained deposits. A comparison of EOID CAPWAP toe capacities to restrike toe capacities in Table 1 indicates no significant toe relaxation. The pile which evidenced the maximum apparent toe relaxation was P-16-I4. However, the apparent relaxation can likely be attributed to both the short- and long-term restrikes' high equivalent blow counts (192 and 240 bpf, respectively) not fully mobilizing all available toe capacity, not to real toe relaxation.

Static Load Test

Capacity – During the static load test, a discrepancy between applied loads indicated by the load cell and jack pressure became apparent. Using strain-gage data, and elastic modulus values from previous similar static load tests, it was determined in the field that the jack pressure was likely the more-accurate of the two readings. Subsequent office analysis agreed with this field assessment. Accordingly, reported load test applied loads are based on jack pressure readings.

The load-movement behavior of the static load test pile is presented in Fig. 6. Several methods exist for data interpretation, and ultimate capacity definition, from load-movement results [Fellenius 1990]. For this project, the criterion selected to define capacity was that developed by Davisson (1972). Using this criterion, the static load test pile was assigned a geotechnical axial compression capacity at the time of the static load test of 1,346 kips (5,987 kN).

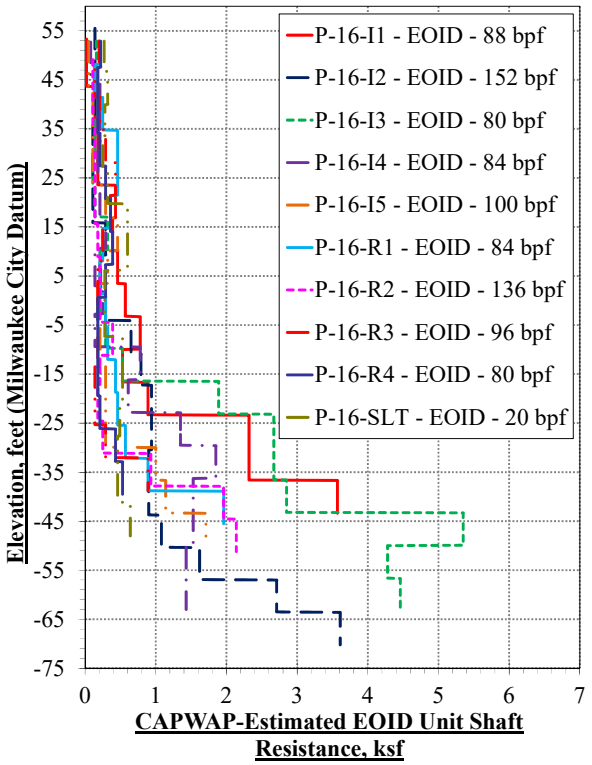


Fig. 5. CAPWAP-Estimated EOID Unit Shaft Resistance Profiles

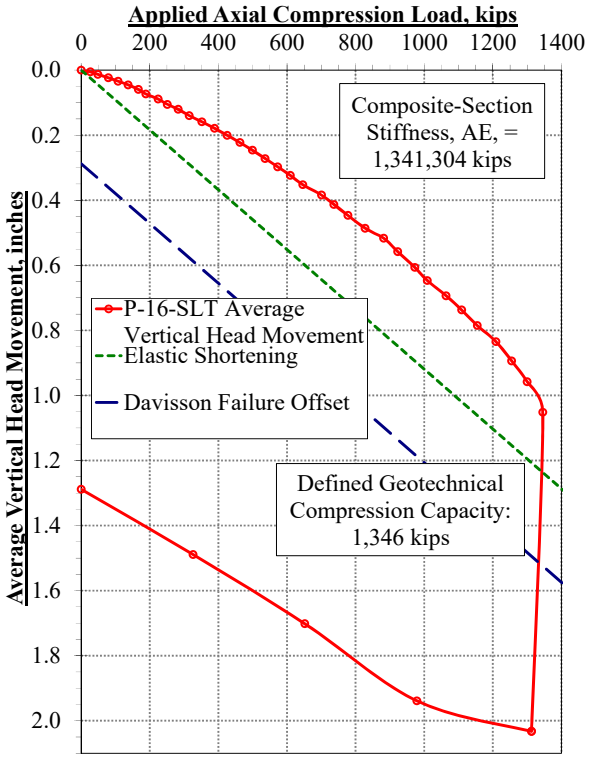


Fig. 6. Compression Static Load Test Load-Movement

Load Transfer – In our experience, concrete at different elevations within a pile may attain differing elastic moduli values during curing. Accordingly, the internal strain gage data at each strain-gage location were evaluated individually using the tangent modulus method presented by Fellenius (2001). This location-specific evaluation yielded a range of back-calculated composite-section elastic moduli, which were used to reduce the below-grade internal strain gage data and determine load-transfer behavior. The static load test pile's EOID CAPWAP analysis estimated residual loads. This estimated residual load distribution was used to correct the strain-gage-determined load transfer at the static load test's maximum applied load.

The static load test pile was restruck 0.88 days after static load test completion. A comparison between the static load test pile's mobilized shaft, toe, and total capacities determined by strain-gage data, and CAPWAP analysis of BOR dynamic results, is presented in Table 2.

Table 2. Static Load Test and Beginning-Of-Restrike CAPWAP Capacities

Capacity Component	Static Load Test Capacity, kips (kN)	BOR Dynamic Load Test Capacity, kips (kN)
Shaft	977 (4,346)[A]	1,096 (4,875)
Toe	368 (1,637)	290 (1,290)
Total	1,346 (5,987)	1,386 (6,165)

A. The static load test pile's shaft resistance was estimated by subtracting the strain-gage-determined load at the toe (incorporating residual loads) at the maximum sustained load from the maximum sustained load (1,346 kips (5,987 kN)).

Long-Term Restrikes

Rather than trying to determine only set-up magnitude, it is more-useful to characterize set-up distribution along the pile shaft. This allows for the development of depth-variable driving criteria [Komurka 2004]. EOID and long-term restrike shaft resistance profiles determined from CAPWAP were used to determine unit, and cumulative, shaft set-up profiles.

Long-Term Restrike Unit Shaft Resistance Profiles – The test piles' CAPWAP-determined long-term unit shaft resistance distributions are presented in Fig. 7. For piles P-16-I1, P-16-I2, P-16-I3, and P-16-I5, the long-term resistance over the lower portion of the pile was not fully mobilized. This resulted in long-term unit shaft resistance profiles that decrease in magnitude over the last two or three CAPWAP soil segments.

Long-Term Unit Shaft Set-Up Profiles – A pile's unit shaft set-up profile can be determined by subtracting its EOID unit shaft resistance profile from its long-term restrike unit shaft resistance profile (i.e., subtracting the profiles in Fig. 5 from the profiles in Fig. 7). This was done for each test pile on which a long-term restrike was performed. The resulting unit shaft set-up profiles are presented in Fig. 8.

Long-Term Cumulative Shaft Set-Up Profiles – Using the relationship between a piles' toe elevation and its embedded shaft area, the unit shaft set-up profiles presented in Fig. 8 can be used to calculate estimated cumulative shaft set-up profiles presented in Fig. 9. These cumulative set-up profiles present the estimated set-up each pile would have experienced had its driving been terminated at any toe elevation above its final toe elevation.

Set-Up Accuracy Scenarios – Since set-up is determined from the difference between two capacity determinations (EOID and some later time), its accuracy depends upon the accuracy of both capacity determinations. In the case of capacity estimates obtained from dynamic load testing data and subsequent CAPWAP analysis, potential over- or under-prediction of capacity must be assessed, and taken into account when evaluating apparent set-up results. For this project, such assessment was discussed previously. Potential set-up accuracy determination scenarios are presented in Table 3.

Design Cumulative Shaft Set-Up Profile – Based on a review of the test piles' cumulative shaft set-up profiles presented in Fig. 9, a lower-bound set-up profile was selected for design. As indicated in Fig. 9, the design cumulative set-up profile selected was that determined for Test Pile P-16-I4. The lower portion P-16-I5's profile was discounted for the reasons discussed previously.

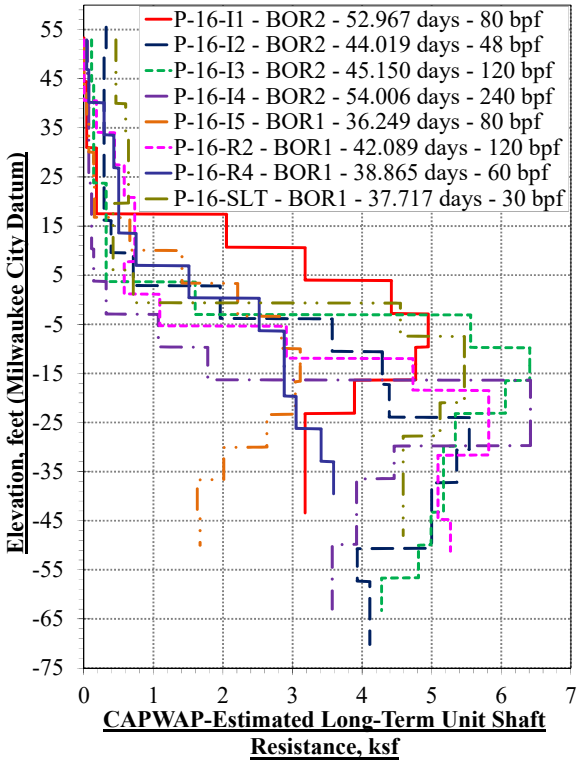


Fig. 7. CAPWAP-Estimated Beginning of Long-Term Restrike Unit Shaft Resistance Profiles

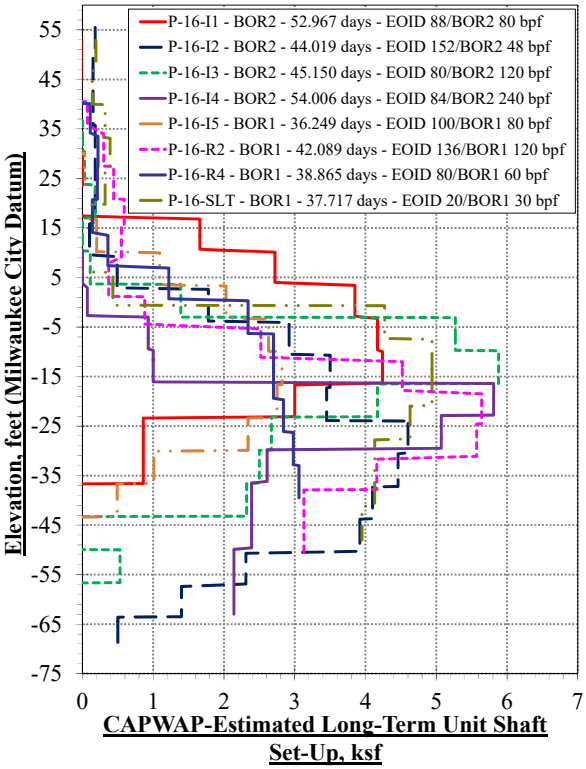


Fig. 8. CAPWAP-Estimated Long-Term Unit Shaft Set-Up Profiles

Set-Up Rate

Multiple restrikes to determine set-up time rate were not included in the test program. However, set-up which occurred during a pause in driving to splice one of the test piles provides insight into set-up time rate.

The bottom section of Test Pile P-16-I2 was driven to an embedded depth of 56.2 feet (17.1 m), when driving was paused to splice on a second section. Following splice completion, the pile was driven to an embedded depth of 115.6 feet (35.2 m) (toe Elev. -60.0 feet (-18.3 m)), when driving was paused for 97 minutes to splice on a third section. Immediately prior to pausing to splice, the equivalent blow count was 10 bpf with a hammer stroke of 7.5 feet (2.3 m), and a CAPWAP-estimated shaft resistance of 143 kips (636 kN). When driving resumed, the equivalent blow count was 70 bpf with a hammer stroke of 9.5 feet (2.9 m), and a CAPWAP-estimated shaft resistance of 535 kips (2,380 kN).

Allowable Geotechnical Load Selection

Compression – This project's foundation piles were designed using allowable stress design ("ASD"). In ASD, allowable geotechnical load is equal to geotechnical capacity divided by a safety factor. Based in part on the type, amount, and quality of the testing performed and results obtained, a safety factor of 2.0 was selected for the project piles. To select the highest practical allowable load for the project, the highest practical capacity to which piles could be installed was established first.

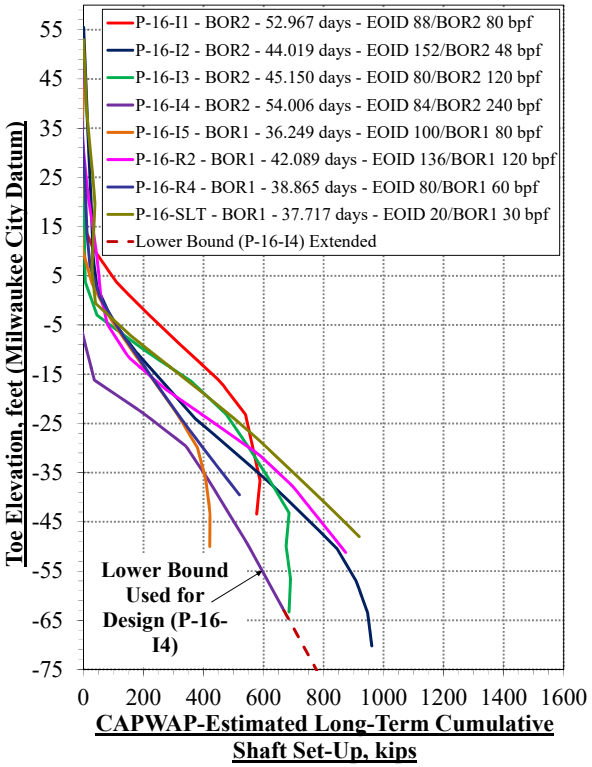


Fig. 9. CAPWAP-Estimated Long-Term Cumulative Shaft Set-Up Profiles, Including Design Profile

Table 3. Potential Set-Up Accuracy Scenarios

	Long-Term Capacity		
	Potentially Underestimated	Reasonably Estimated	Potentially Overestimated
Potentially Over-Estimated	Set-Up Potentially Underestimated	Set-Up Potentially Underestimated	Set-Up Potentially Indeterminate
Reasonably Estimated	Set-Up Potentially Underestimated	Set-Up Reasonably Estimated	Set-Up Potentially Overestimated
Potentially Under-Estimated	Set-Up Potentially Indeterminate	Set-Up Potentially Overestimated	Set-Up Potentially Overestimated

Long-term capacity profiles can be estimated for each test pile by adding each pile's Case method initial capacity, and cumulative set-up, profiles together [Komurka 2004]. A benefit of this is approach is that it provides an estimate of long-term capacity not only for a test pile's terminal toe elevation, but also for any shallower terminal toe elevation. Estimated lengths can be estimated for lesser capacities, which improves length estimates and economic evaluations.

It follows that to use test program results to select the highest practical capacity to which piles can be installed, the design cumulative set-up profile should be added to each test pile's Case method initial capacity profile. These profiles are presented in Fig. 10.

Based on the results presented in Fig. 10, 1,200 kips (5,338 kN) was considered the highest practical capacity to which production piles could be installed, and a maximum allowable load of 600 kips (2,669 kN) per pile was selected for the project. Test Pile P-16-SLT was excluded from this evaluation, because its depth (and therefore its end-of-drive and long-term capacity) was limited by the length of available pile material.

Tension – Resistance to tension loads is considered to be provided by only the pile shaft. Long-term shaft capacity profiles based on BOR CAPWAP analyses are presented in Fig. 11. When dynamic test results are used to assess tension capacity, GRL recommends that the shaft resistance be reduced to 80% of the CAPWAP-determined value to account for the difference in loading direction. GRL also recommends that safety factor of 2.5 be applied to this reduced shaft resistance value to account for analysis sensitivity in separating shaft and toe resistances. The resulting safety factor with respect to CAPWAP-estimated ultimate shaft capacity is 3.125. The profile resulting from applying a safety factor of 3.125 to a lower-bound beginning-of-restrike cumulative shaft capacity profile is also presented in Fig. 11.

A review of Fig. 11 indicates that the allowable tension resistance following the above procedure is a function of pile toe elevation. Accordingly, tension resistance requirements must be incorporated into production-pile driving criteria by requiring both a minimum embedment depth, and a minimum blow count below the minimum embedment depth. Minimum embedment depths may govern installed lengths.

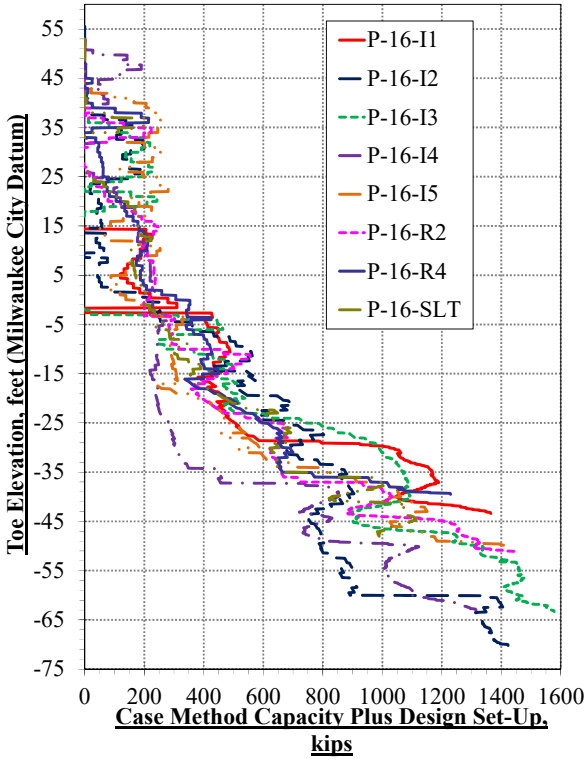


Fig. 10. Design Set-Up Profile Added to Individual Case Method Initial Capacity Profiles

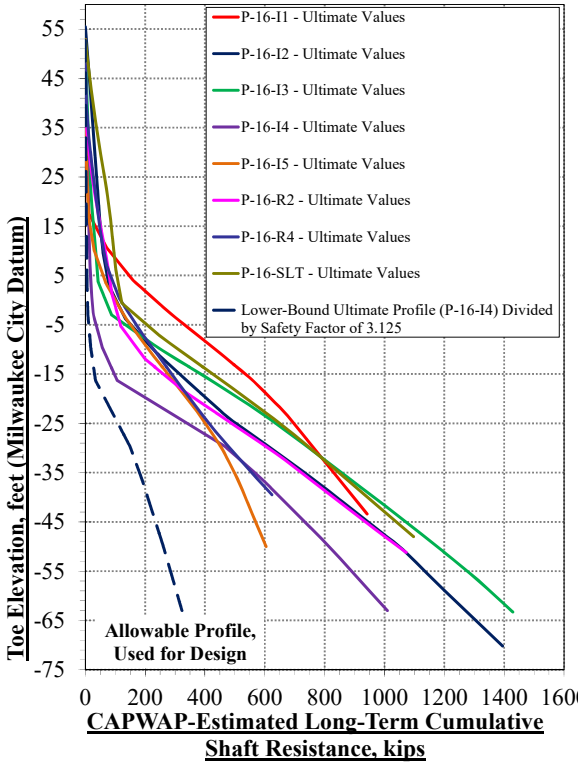


Fig. 11. CAPWAP-Estimated Beginning of Long-Term Restrike Cumulative Shaft Resistance Profiles, Including Design Profile Used for Allowable Tension Resistance

Driving Criteria

Depth-Variable Driving Criteria – Production pile driving criteria were developed using the wave-equation software GRLWEAP. A number of wave equation input parameters were refined by matching EOID dynamic results determined from CAPWAP with wave equation results [Hannigan et al. 2016]. Since set-up begins virtually immediately after driving termination, driving operations were required to be as continuous as possible; driving multiple bottoms prior to completing each pile's installation was precluded.

Long-term capacity is the sum of two components: EOID capacity, and set-up. The pile test program characterized both these components individually as functions of pile toe elevation. This provides the flexibility to provide driving criteria for driving from grades which differ from test-pile driving grades. And if desired, separate safety factors could be applied to initial capacity and to set-up when developing production–pile penetration resistance installation criteria [Komurka et.al. 2006].

Cumulative shaft set-up is a function of pile embedded shaft area. The greater a pile's embedment length, the more set-up occurs, and therefore the less EOID capacity is required. Since required initial ultimate capacity decreases with increasing embedment depth, so does required penetration resistance. Therefore,

the lower-bound cumulative shaft set-up profile presented in Fig. 8 can be used to develop depth-variable production-pile driving criteria which reflect decreasing required initial capacity with increasing embedment depth. This concept is illustrated in Fig. 12. Resulting production pile installations will be driven only as deep as necessary to achieve (after set-up) their required long-term ultimate capacities, reducing unnecessary driven length.

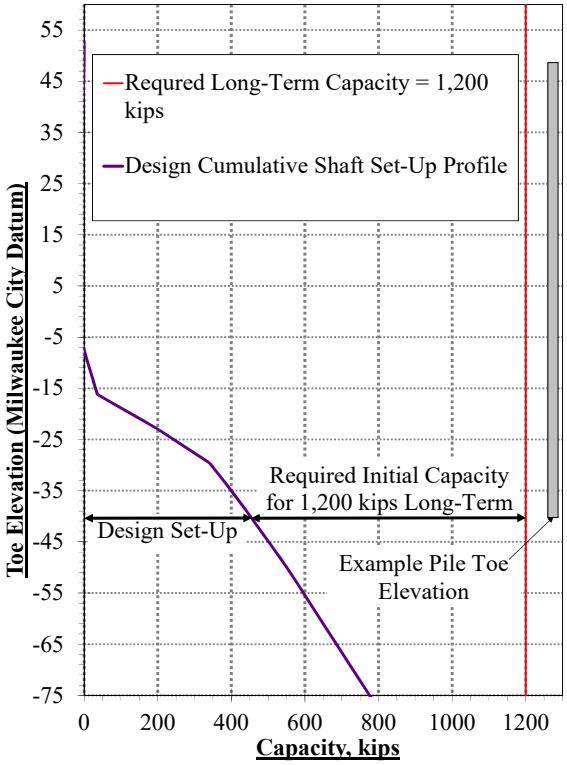


Fig. 12a. Determination of EOID Capacity Profile for 1,200-Kip Long-Term Capacity

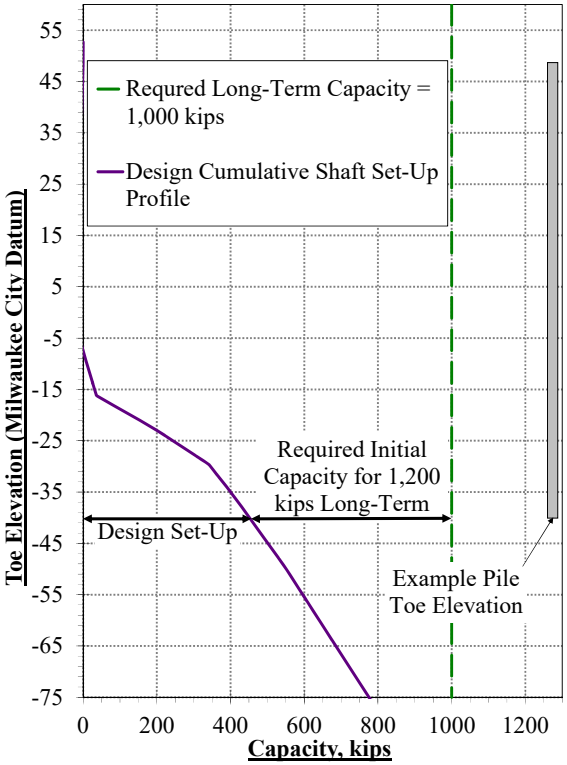


Fig. 12b. Determination of EOID Capacity Profile for 1,000-Kip Long-Term Capacity

Production-pile driving criteria are a function of the energy the hammer transfers to the pile during driving (transferred energy). Transferred energy is a function (among other things) of hammer stroke. For diesel hammers, the stroke (and hence transferred energy) is variable and indirectly only somewhat controllable. Therefore, since a variable-energy hammer was used for production-pile driving, stroke-dependent driving criteria were developed. An example of depth-variable stroke-dependent driving criteria is presented in Table 4. Table 4 presents depth-variable driving criteria with 3-foot (0.9-m) depth intervals. The depth intervals for criteria development can be selected based on the rate of set-up increase with increasing depth.

Multiple Allowable Loads – The approach presented above can be used to develop depth-variable driving criteria for multiple allowable loads using the results from a given test program. For this project, to further optimize the foundation design, the structural engineer identified a number of locations where 500-kip (2,224-kN) allowable load piles would more-efficiently support structure loads. Depth-variable driving criteria for 500-kip (2,224-kN) allowable load piles were readily developed using the approach illustrated in Fig. 12. To accomplish this, a different required EOID capacity profile was determined by subtracting the design set-up profile from a depth-constant required long-term capacity of 1,000 kips (4,448 kN).

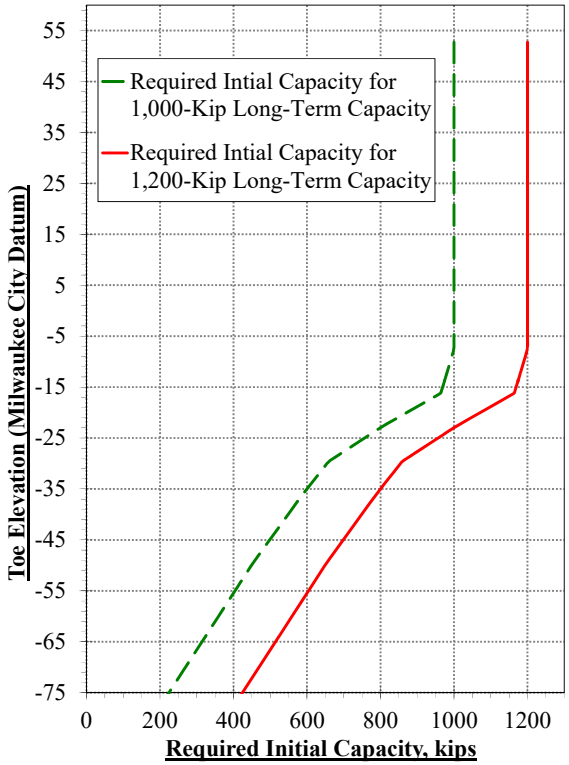


Fig. 12c. Required EOID Capacity Profiles for Multiple Long-Term Capacities

Multiple Driving Elevations – Production piles were driven from several different pile-cap subgrade elevations. Design set-up, and therefore required EOID capacity, are elevation-specific, not embedment-length-specific. Accordingly, several driving criteria tables were developed for both allowable loads. Each driving criteria table was applicable for driving from a small range of pile-cap subgrade elevations (on the order of 3 to 4 feet (0.9 to 1.2 m)).

PRODUCTION DRIVING/CONSTRUCTION MONITORING

As mentioned previously, site constraints precluded pre-production testing in the southern portion of the site. To confirm hammer performance, pile drivability, and driving behavior, full-depth dynamic monitoring was performed during the driving of three test piles on the southern portion of the site at production-driving startup.

During production-pile installation, hammer stroke and blow count were measured and documented with a Saximeter. The piles were installed to requisite blow counts based on depth-variable criteria, taking into account the hammer stroke and pile toe elevation. Internal pile inspection was performed by viewing the completed piles from the surface by dropping a weighted tape and light into the pile. Select piles were also internally observed using a downhole camera. Where pile damage was noted (i.e., partial collapse, gouging, bulging, rupture, etc.), piles were assigned reduced capacities based on shaft resistance (determined from the test program) above the damage. Other piles in the same group as the damaged pile(s) were assigned individual capacities base on depth and EOID blow count, and the need for additional piles was determined by the structural engineer.

The number of production piles damaged during driving was approximately 3 percent. Test program results were used to assist in both assigning reduced capacities to the damaged piles, and in assigning individual

Table 4. Depth-Variable Driving Criteria Table Example

Delmag D46-32 - I.D. No. 890
16"x0.50" Closed-End Pipe Piles
300-Ton Allowable Load - Driving Elevations +14.0 thru +17.9 feet

Penetration Depth, feet		Minimum Required Equivalent Blow Count, blows per foot Hammer Ram Stroke, feet									
From	To	6.5	7.0	7.5	8.0	8.5	9.0	9.5	10.0	10.5	11.0
55.1	58.0							---	---	---	94
58.1	61.0						---	116	93	77	66
61.1	64.0				---	---	96	77	65	55	49
64.1	67.0		---	---	98	76	65	54	47	43	39
67.1	70.0	---	103	80	65	54	47	42	37	34	31
70.1	73.0	90	70	58	49	42	38	34	31	28	26
73.1	76.0	62	52	44	39	34	31	28	26	24	23
76.1	79.0	47	40	36	32	29	26	24	223	21	20
79.1	82.0	37	32	29	26	24	23	21	20	19	18
82.1	85.0	30	27	24	22	21	20	18	17	16	16
85.1	88.0	25	23	21	19	18	17	16	15	15	14

capacities to the undamaged piles in the group. This was done in close coordination with the structural engineer who evaluated the actual required load for each group, and for each pile within the group, where damaged piles occurred. These combined efforts reduced the number of replacement piles which would have otherwise been required by 50 percent.

Pile Support Cost – Pile support cost based on available support is defined as pile installation cost divided by allowable pile load [Komurka 2015]. For this project, dividing the total cost of all concrete-filled production piles by the sum of their allowable loads results in a pile support cost based on available support of $9.26 per available kip. Dividing the total cost of all concrete-filled production piles by the total of all the building's service loads results in a pile support cost based on utilized support of $12.45 per structure design kip.

SUMMARY AND CONCLUSIONS

The project consists of a 33-story mixed-use residential building with two levels of below-grade parking across the entire building footprint. A pre-production driven-pile test pile program included dynamic monitoring, an instrumented static load test, and long-term restrike testing on ten 16-inch-diameter closed-end pipe piles. A major objective of the test program was to establish the highest long-term axial compression capacity to which the 16-inch piles could reasonably be installed, from which the maximum allowable load that could be used for design would be established.

The site soils exhibited significant soil set-up, even after relatively short wait times, such as during a pause in driving to splice. From dynamic testing results, long-term cumulate shaft set-up profiles (set-up as a function of pile toe elevation) were developed. Estimated long-term capacity profiles which included both initial capacity and set-up were developed, from which a maximum allowable load for the project was selected. Long-term restrike cumulative shaft resistance profiles were used to determine a design tension resistance profile, from which minimum pile embedment lengths were established.

A design set-up profile was established for the project, and was used to develop depth-variable driving criteria for both 500- and 600-kip (2,224- and 2,669-kN) allowable load piles. The depth-variable criteria provided for increasing cumulative set-up with increasing embedment length, and so required decreasing terminal blow counts with deeper pile penetrations, thus saving production pile lengths and driving time. Test program results were used to assign reduce capacities to short or damaged piles, reducing the required number of replacement piles by 50 percent, saving additional cost and time.

ACKNOWLEDGEMENTS

The authors wish to acknowledge and gratefully thank members of the ownership, development, design, and construction team for their contributions to the project: Northwestern Mutual Life, Hines, Magnusson Klemencic Associates, Zenith Tech, Inc., and C.D. Smith Construction, Inc.

REFERENCES

Davisson, M.T. (1972). "High Capacity Piles," *Proceedings*, ASCE Lecture Series, Innovations in Foundation Construction, Illinois Section.

Fellenius, B.H. (2001). "From Strain Measurements to Load in an Instrumented Pile," *Geotechnical News Magazine*, Vol. 19, No. 1, pp. 35-38.

Fellenius, B.H. (1990). "Guidelines for the Interpretation and Analysis of the Static Load Test," *Short Course Text Notes*, Deep Foundations Institute, Hawthorne New Jersey.

Hannigan, P.J., Rausche, F., Likins, G.E., Robinson, B.R., and Becker, M.L. (2016). "Design and Construction of Driven Pile Foundations" Geotechnical Engineering Circular No. 12, Vol. I and II, National Highway Institute, U.S. Department of Transportation, Federal Highway Administration, Publication No. FHWA-NHI-16-010.

Komurka, V.E., Wagner, A.B., and Edil, T.B. (2003a). "A Review of Pile Set-Up," *Proceedings of the 51st Annual Geotechnical Engineering Conference*, University of Minnesota, St. Paul, Minnesota, pp. 105-130.

Komurka, V.E., Wagner, A.B., and Edil, T.B. (2003b). "Estimating Soil/Pile Set-Up," Wisconsin Highway Research Program Contract No. 0092-00-14, Report No. 03-05.

Komurka, V.E. (2004). "Incorporating Set-Up and Support Cost Distributions into Driven Pile Design," *Current Practices and Future Trends in Deep Foundations*, ASCE/Geo-Institute, Geotechnical Special Publication No. 125, 0-7844-0743-6, pp. 16-49.

Komurka, V.E., Winter, C.J., and Maxwell, S.G. (2006). "Applying Separate Safety Factors to End-of-Drive and Set-Up Components of Driven Pile Capacity," *Geotechnical Applications for Transportation Infrastructure – Featuring the Marquette Interchange Project in Milwaukee, Wisconsin*, ASCE/Geo-Institute, Geotechnical Practice Publication No. 3, 0-7844-0821-1, pp. 65-80.

Komurka, V.E., and Arndorfer, R.P. (2009). "Driven Pile Cost Comparison for Two Large Wisconsin DOT Bridge Projects," *Proceedings of the Deep Foundations Institute 34th Annual Conference on Deep Foundations*, (CD Rom).

Komurka, V.E. (2015). "Foundation Support Cost – Applications to Driven-Pile Design," *Proceedings of the International Foundations Congress and Equipment Expo 2015*, ASCE/Geo-Institute, Geotechnical Special Publication No. 256, 978-0-7844-7908-7, pp. 990-1005.

Likins, G.E., and Rausche, F. (2008). "What Constitutes a Good PDA Test?" *Proceedings of the Eighth International Conference on the Application of Stress-Wave Theory to Piles 2008*, Lisbon, Portugal, pp. 403-407.

Likins, G.E. (2017). "Dynamic Testing: Proper Practice," *Presentation for PDCA Dynamic Testing and Analysis Workshop*, Orlando, Florida.

Morgano, C.M., and White, B. (2004). "Identifying Soil Relaxation from Dynamic Testing," *Proceedings of the Seventh International Conference on the Application of Stress-Wave Theory to Piles 2004*, Petaling Jaya, Selangor, Malaysia, pp. 415-421.

Rausche, F., Goble, G.G., and Likins, G.E. (1985). "Dynamic Determination of Pile Capacity," *ASCE Journal of Geotechnical Engineering*, Vol. 111, No. 3, Reston, VA, pp. 367-383.

Rausche, F. (1991). "Recommended CAPWAP Matching Procedure, Remedies Against Faulty Capacity Predictions," *Notes from PDA Users Day in Cleveland*, *OH*, Pile Dynamics, Inc., Cleveland, OH, pp. 1-15.

DEEP AND SHALLOW SOIL MIXING FOR THE SR-83/US-331 CHOCTAWHATCHEE BAY BRIDGE PROJECT IN SANTA ROSA BEACH, FLORIDA

Matteo Bertoni, Treviicos, Charlestown, MA, USA, 617-241-4800, mbertoni@treviicos.com
Wesley Schmutzler, Treviicos, Charlestown, MA, USA, 617-241-4800, wschmutzler@treviicos.com
Alessandro Bertero, Trevi Group, Design, Research & Development Dpt., Cesena, Italy, +39 340-106-1059, abertero@trevispa.com
Dylan Pearson, Treviicos, Charlestown, MA, USA, 617-241-4800, dpearson@treviicos.com

ABSTRACT

The SR 83/US 331 highway is located in the Florida panhandle, where it connects the Walton County beaches to the I-10 corridor. The roadway is of vital importance to the economy of the area as well as its safety since it represents the primary hurricane evacuation route from southern Walton County. The Florida Department of Transportation (FDOT) decided to increase the number of traffic lanes from two to four and improve the geotechnical properties of the moderately deep, very loose foundation soils, that had affected the highway rideability for years. The soil mixing was selected as the method to meet the unique deep ground improvement challenges of the project. The design required that Shallow Mixing Method (SMM) be used to build a 10-foot thick platform that transferred axial load to the bottom soil layers through a series of Deep Mixing Method (DMM) columns. Upon completion over 8,300 SMM columns and 1,500 DMM columns had been installed, with no remedial work required. Also, only 1% of the almost 1,500 specimens tested did not meet the specification requirements. This paper will describe the challenges encountered and provide valuable information that may be useful for other future projects, including details not previously published.

Keywords: soil mixing, challenges, quality control.

INTRODUCTION

The counties of Walton and Okaloosa have been a very popular vacation destination for many ears. The 50-mile long coastline boasts beautiful, sugar-white beaches and waters the color of emeralds. The popularity of the area has been growing even further, over the last few years. A consequence of this phenomenon is a fast-paced increase of the traffic flow on the SR83/US331 highway, especially at the bridge that connects the Walton County beaches across Choctawhatchee Bay (Fig. 1) to the heavily traveled I-10 corridor. The highway plays a very important role for the area also as a commercial link and as the primary hurricane evacuation route from southern Walton County. The increase in traffic has produced higher travel time, when not a complete traffic paralysis, and exacerbated the issue of ground settlement where accelerated wearing of road foundation occurred due to the presence of very loose, moderately deep, soils, that had afflicted the highway for several years. The Florida Department of Transportation (FDOT) decided to put an end to these issues by increasing the number of traffic lanes from two to four and improving the geotechnical properties of the foundation soils. The Design-Build Maximum Price Request for Proposal (RFP) issued for the expansion of the Choctawhatchee Bay Bridge saw the participation of numerous D/B teams which produced various technical solutions. Among them, the FDOT selected the Skanska/Parsons Brinckerhoff (General Contractor) proposal which provided for the use of soil mixing as the ground improvement technology. The design/build team assigned Foundation & Geotechnical Engineering (Designer of Record) the ground improvement design which Treviicos South (Specialty Contractor) would execute.

 © 2017 DFI Annual Conference, New Orleans, LA, USA



Figure 1: Project Location

SITE GEOTECHNICAL SETTING

The entire coastal portion of the Florida panhandle consists of Quaternary strata of the eastern Gulf of Mexico Coastal Plain and the Florida Platform, and lies within the Gulf Coastal Lowlands of the Southern Pine Hills Geomorphic District, and the Lower Delta Plain of the Apalachicola Delta Geomorphic District (see Scott, 2005; Brooks, 1981).

The soil boring data indicated the presence in the project area of fill material atop varying lenses of soft clays, and very loose to moderate dense silty and clayey sands (Fig. 2). Isolated pockets of organics were identified in the northern area of the project. The existing roadway laid directly on a layer of fill material placed in the late 1930's on top of the bay bottom, presumably by a combination of dredge, fill, and push processes.

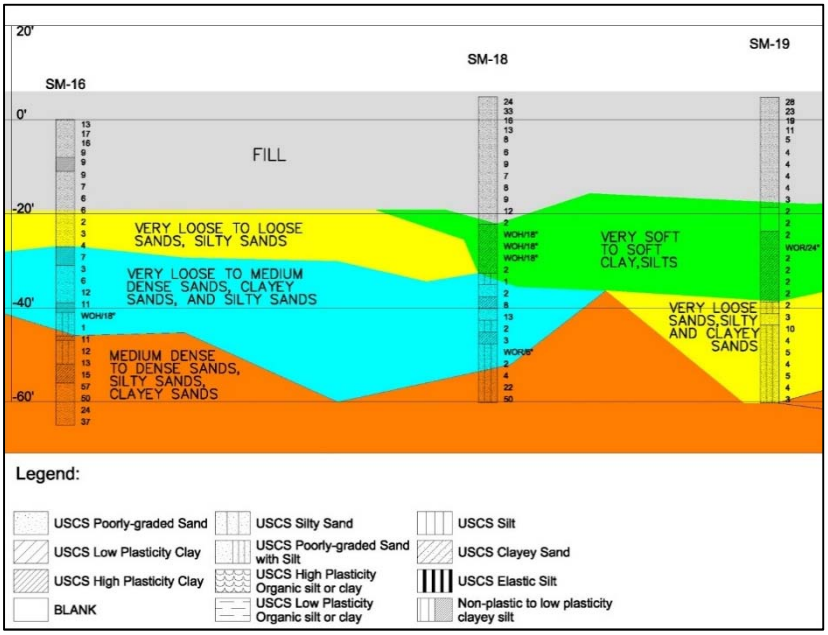


Figure 2: Portion of the project's extensive soil profile

GROUND IMPROVEMENT DESIGN AND TECHNICAL PROVISIONS

The RFP required that the design/build team "either bridge, or utilize a deep ground improvement method to stabilize, the three segments of the existing earthen causeway" and stated that "one possible method of deep ground improvement which is considered viable is deep soil mixing". If the stabilization method were selected, the design had to guarantee, among other things, a maximum differential settlement of less than 2" over any 1000 ft stretch.

The Designer of Record, to meet the RFP requirements, developed a design that included a 10-foot thick rigid platform of SMM elements supported by DMM columns that extended to the deep bearing layers (Fig. 3). The project was divided into three sections, one per each causeway of the SR83/US331 Highway: South, Center, and North. South and North causeways were, in turns, divided into two subsections: South and North bound.

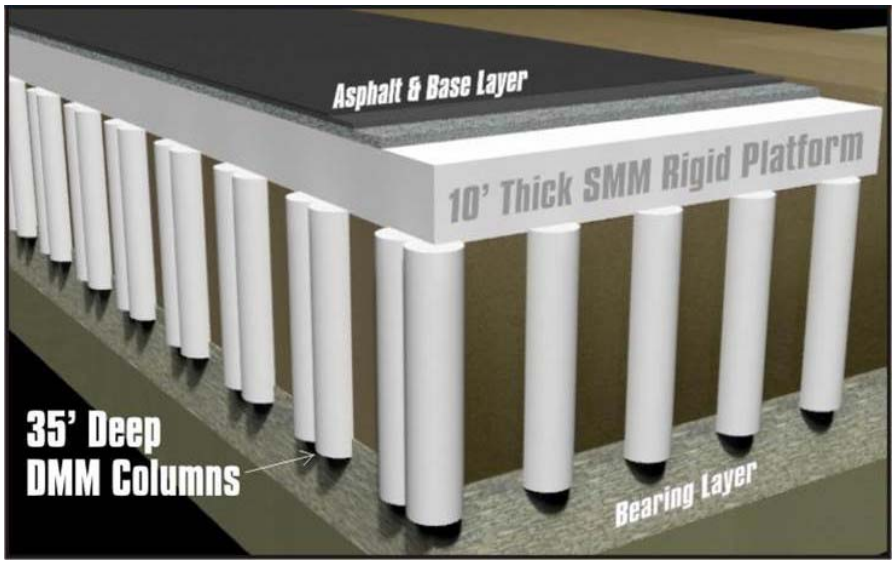


Figure 3: Ground improvement system.

The elements were composed by two overlapping columns, each one having a diameter of 5.75 ft. A total of over 1,500 DMM elements and over 8,400 SMM elements were to be installed.

The double column elements had an alignment either transversal or longitudinal to the axis of the road (Fig. 4), and DMM and SMM elements were positioned based on five typical patterns.

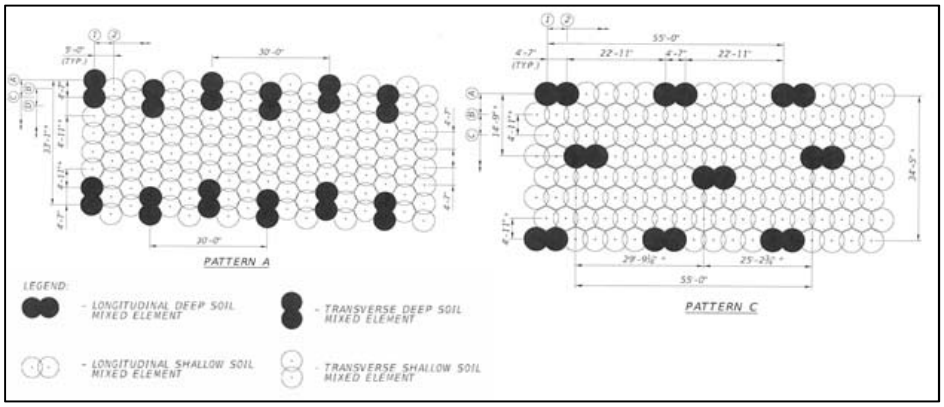


Figure 4: Soil mixing typical layout for transverse and longitudinal alignment

The Designer of Record produced a Technical Special Provision (TSP), which intent was to supplement the provisions provided by the FDOT Soils and Foundations Handbook. The TSP contained guidelines and requirements for the execution of the ground improvement and the Quality Control/Quality Assurance (QC/QA) program.

The QC team was required to collect Wet Grab (WG) samples at depths of 3' and 8' from the top of SMM elements. Samples were to be taken in 4% of the first 200 SMM elements installed in each causeway and 2% of the remaining SMM elements in each causeway. The same sampling frequency was set for the DMM elements but the samples were to be obtained by coring the treated soil.

CONSTRUCTION METHOD

The ground improvement by soil mixing requires that many factors be taken into account. In addition to the mix design, typical of every ground improvement technology, the two primary parameters of concern when regarding the effectiveness of deep and shallow mixing methods are the cement factor and blade rotation number (see Bertero et Al., 2012), detailed as follows:

$$CF = \frac{W}{V} \quad [1]$$

Where CF = cement factor, W = weight of cement injected, and V = volume treated.

$$BRN = \frac{N \times R_1}{d} + \frac{N \times R_2}{w} \quad [2]$$

Where BRN = blade rotation number, N = number of tool blades, R_1 = rotation speed during drilling, d = drilling speed, R_2 = rotation speed during withdrawal, and w = withdrawal speed.

The Specialty Contractor, to carry out the installation of the elements, chose to use a drill rig equipped with the Trevi Turbo Mix technology in a double axis configuration (TTM2) (Fig. 5). The TTM2 technology had previously been used by the Specialty Contractor, with excellent results, on several projects (see Schmutzler et Al., 2012, Bertoni et Al., 2015, and Leoni et Al., 2015).

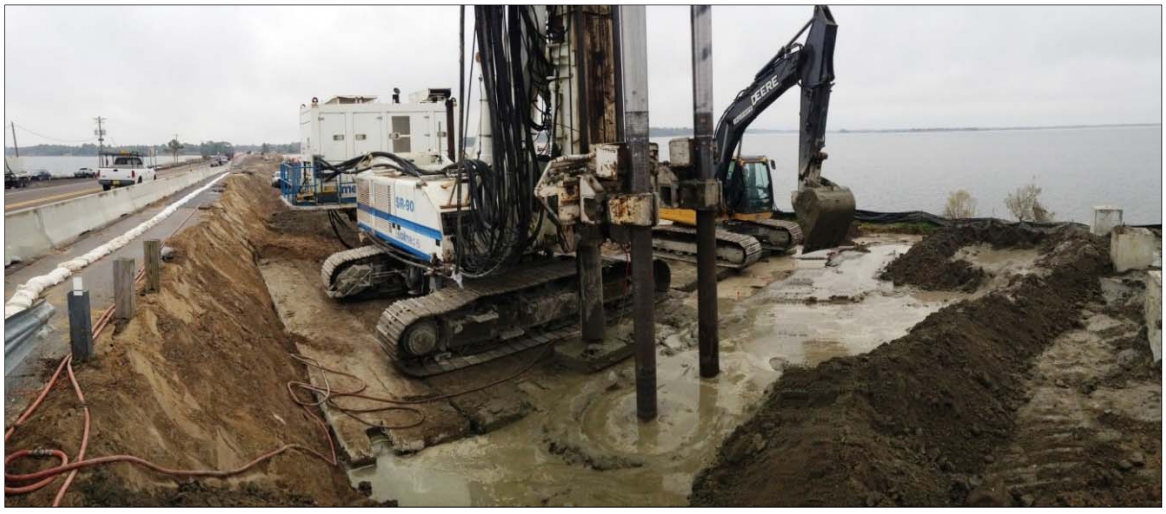


Figure 5: SR90 Rig at North Causeway

The Drilling Mate System, an automated monitoring system installed on the rig, recorded in real-time the installation parameters and controlled some of the drilling operations. The system also automatically set the verticality of the mast, at the beginning of each element, to be less than 0.2 degrees as required by the TSP.

The sequence of installation depended on the alignment of the elements. Transversal elements required that a row be completed before the rig could move to the next one, while a total of 15 to 18 longitudinal elements were installed per row at once.

BENCH SCALE TEST AND FIELD TRIAL/VALIDATION PROGRAMS

The Specialty Contractor, as required by the TSP, designed and carried-out a Bench Scale Test program to determine ranges of mix designs that would likely produce field-mixed elements that met the acceptance criteria. Several soil samples were mixed with grout mixes of different composition and numerous specimens were cast and tested for Unconfined Compressive Strength (UCS). Per the TSP, for each sample tested in an SMM element, a 28 day UCS of 75 psi was to be met or exceeded, while for each sample tested in a DMM element, a 28 day UCS of 150 psi was to be met or exceeded.

The test results indicated the use of water/binder (W/B) ratios 0.80 and 1.00 would likely produce elements in compliance with the specifications requirements. A third mix, with a W/B ratio of 1.25, was to be considered as a viable alternative option. Two were the binders that could be used: 1. A 50% Slag/50% Ordinary Portland Cement; 2. 100% Ordinary Portland Cement.

The TSP provided that the Bench Scale Test indications be used during the Field Trial/Validation program to determine the field mixing parameters.

The location selected for the execution of the Field Trial/Validation Program was the South Causeway/North Bound of the project. Delays in approval of some of the General Contractor's permits postponed the beginning of the test section by about a month. The program started on January 23, 2014 when 6 SMM elements were installed, to depths ranging from 10 to 12 feet, using a unique set of installation parameters per each element. Another 6 sets of parameters were used between January 27 and February 6, 2014, to install 6 DMM elements to an average depth of 45.5 feet.

Upon withdrawal of the mixing tools, two WG samples were obtained from each SMM element, one at 3' and one at 8' from the top of the treatment. Three cylinders from each sample were cast for 28-day UCS testing.

Every one of the twelve installed elements were cored 28 days after completion. In general, at least five specimens were selected from each core for UCS testing, as required by the specifications. In some circumstances, the limited length of the SMM columns, in conjunction with mechanical fractures induced on the samples by the coring procedure, made so that less than five specimens could be tested.

The test results showed that all the SMM and DMM elements were in compliance with the respective TSP requirements (Fig. 6). Also, the testing of both core and WG specimens taken from SMM elements provided results that confirmed how the coring procedure generally induces significant disturbance on the samples (more information on the issue can be found in Bruce and Mauro, 2016).

The Specialty Contractor selected to use, for both SMM and DMM production elements, a grout mix with a W/B ratio of 1.00 where the binder was 100% Ordinary Portland Cement binder.

Further details on the Field Trial/Validation Program can be found in Bertero et al. (2015) and Schmutzler et al. (2017).

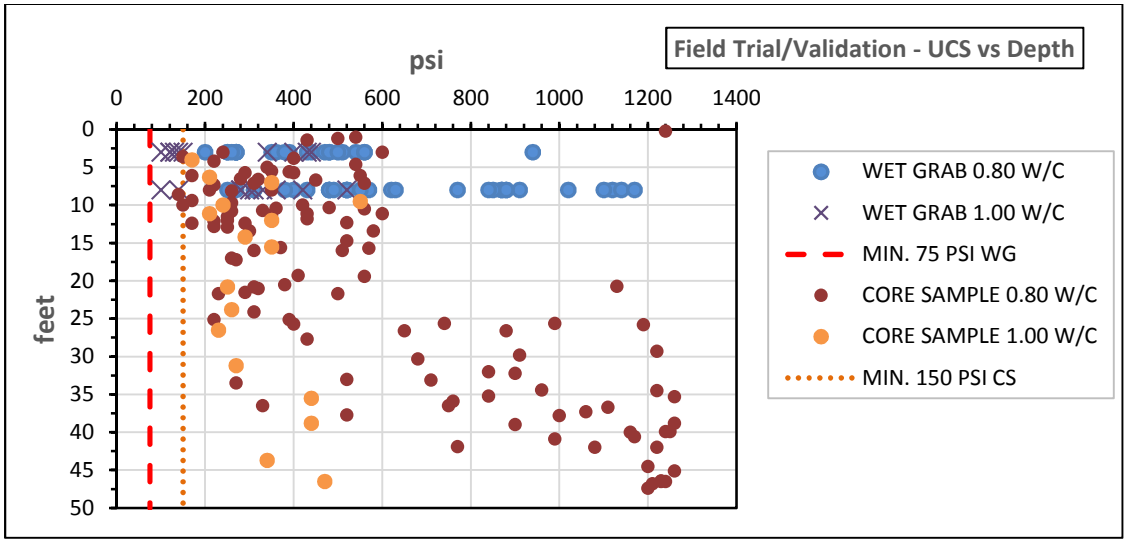


Figure 6: Field Trial/Validation Program UCS test result

PRODUCTION PHASE

The production phase of the project started on March 27th, 2014, at the south end of the South Causeway/North Bound area. This portion of the project included an area to be constructed using the pattern that would eventually support the greatest load on the project which was the approach to the bridge beneath the Mechanical Stabilized Earth Wall (Fig. 7).

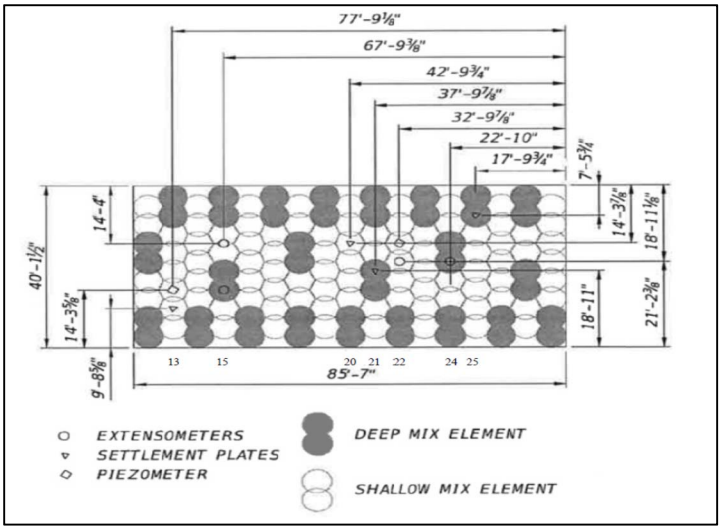


Figure 7: Plan view of surcharge area

The area was part of a surcharge and plate load test program designed to evaluate the performance of the global system and was to be completely independent from the rest of the causeway ground treatment to avoid bridging and load distribution. Therefore, one row of elements at each end of the test area was left uninstalled. The instrumentation included settlement plates, piezometers, and extensometers to monitor various parameters during the required tests. The results proved that the treatment method would easily

satisfy the RFP required 2-inch maximum differential settlement criterion (Schmutzler et al., 2017). The area was then connected to the rest of the system by installing the two missing rows of elements.

The delays experienced prior to start of test section installation had a severe impact on the original schedule for the soil mixing production phase. Initial start of production was delayed, consequent delays to preparatory work before treatment prevented access to phases as scheduled, and additional standby periods of greater length were introduced. The Specialty Contractor proposed several revisions to the schedule to mitigate such delays. The revisions would further increase the challenges associated with the execution of the ground treatment, particularly from a logistical standpoint, but shorten the time needed for completion of the whole project. The sequence of installation by causeway and bound can be found in Table 1.

Table 1

Dates Worked			Section (Causeway/Bound)				
From	To	Days	SC/NB	SC/SB	CC/SB	NC/NB	NC/SB
3/27/14	7/18/14	113	X				
8/6/14	2/10/15	188			X		
2/23/15	5/27/15	93				X	
6/8/15	6/26/15	18	X				
8/13/15	10/5/15	53		X			
10/22/15	11/25/15	34					X
5/31/16	7/1/16	31					X
7/8/16	8/25/16	48			X		
9/6/16	9/23/16	17		X			

Several challenges were faced by the Specialty Contractor during the execution of the project.

The limited space available for the day-to-day operations (Fig. 5) resulted in a very congested work area that required a great effort by the team to guarantee the usual high safety standards and a satisfactory production rate.

The presence of sands with actual n-values higher than those provided in the pre-bid phase of the project (Fig. 8) impacted both productivity and profitability. While drilling speeds had to be reduced, field attempts proved that grout injection couldn't be proportionally adjusted due to increased strain on the equipment, , resulting in higher than expected installation time and cement consumption for each element.

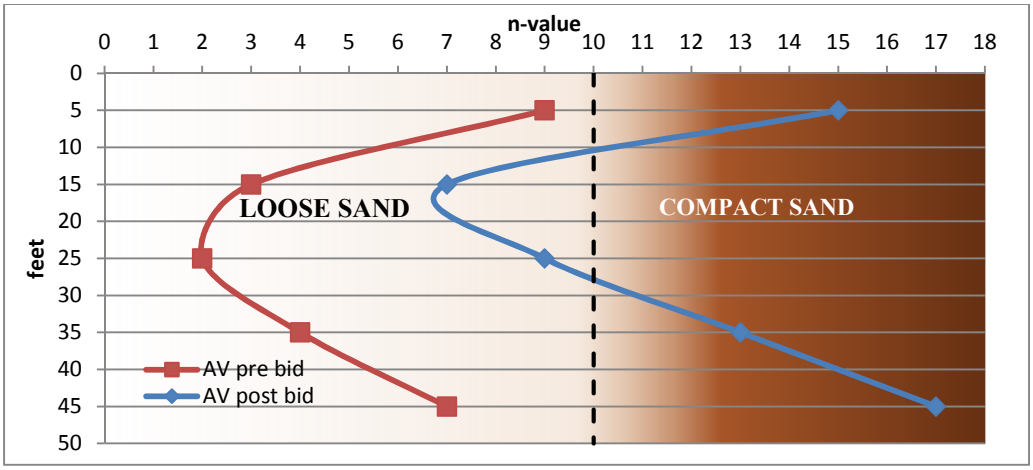


Figure 8: Pre- and Post-Bid average SPT n-value comparison at South Causeway

Along the alignment of each causeway section, the ground conditions changed greatly and, at times, suddenly, throughout the whole project. DMM element installations within close proximity demonstrated completely different behaviors; an uncomplicated element installation could be followed by a lengthy, challenging one. The extra effort to accomplish ground treatment within these elements led to much higher than anticipated QC results in several instances; however, a significant reduction in parameters used could not follow due to risk of under-treating areas of lesser resistance.

The phenomenon of extreme variability was most apparent at the Center Causeway. Difficulty in treating DMM elements varied excessively within few feet of alignment, with speed and effort of drilling and withdrawal phases within the same element further displaying a divide. In a few instances, the drilling phase was followed by an over 2 hour retrieval to withdraw the tools (Fig. 9). Due to the impacts to work of the Specialty Contractor, a second Field Test/Validation Program was performed. With the approval of the Designer of Record, several new columns were installed using a W/C ratio of 1.25. The increase in water content allowed a reduction of the drilling speed without producing an increase of the cement consumption, while significantly lowering the wear on mixing tools and rig. The new ratio produced results in compliance with the TSP requirements and was approved for use at the Center Causeway.

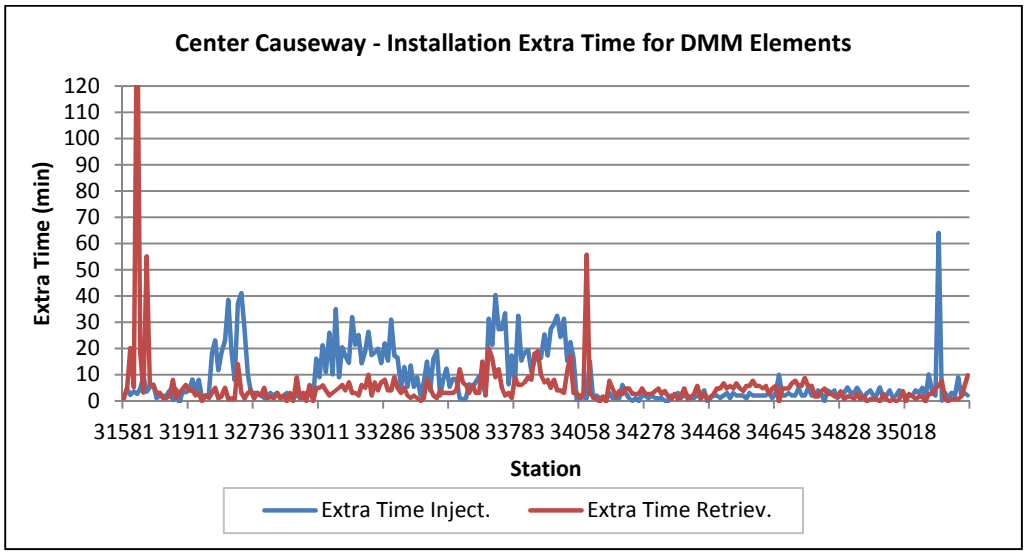


Figure 9: DMM elements installation extra time

Despite the many issues faced, the soil mixing treatment was completed on time, with the final installation of all 9,845 columns completed on 9/23/2016 (Table 2).

Table 2

Causeway	Bound	Column Type	Quantity Installed #	Net Treated Volume (CYD)
South	North	DMM	274	21721
		SMM	1191	19555
	South	DMM	245	19589
		SMM	1224	20178
Center	South	DMM	454	36253
		SMM	3173	51931
North	North	DMM	289	21860
		SMM	1376	22571
	South	DMM	221	17260
		SMM	1398	22881

Overall, the quality of the product proved excellent due to the extensive quality control involved in every phase of the project (for additional information on the QC/QA Program of the project see Schumtzler et al., 2017).

Throughout the entire project 43 DMM elements were cored and WG samples were collected from 179 SMM elements. Every one of the DMM elements reached the minimum strength required by the specifications. Although 3 of the 179 wet grabbed SMM elements failed their 28 day UCS test minimum psi specification, verification coring confirmed the minimum strength (UCS test results can be found in figure 10).

At project completion, none of the SMM and DMM elements had required remedial work.

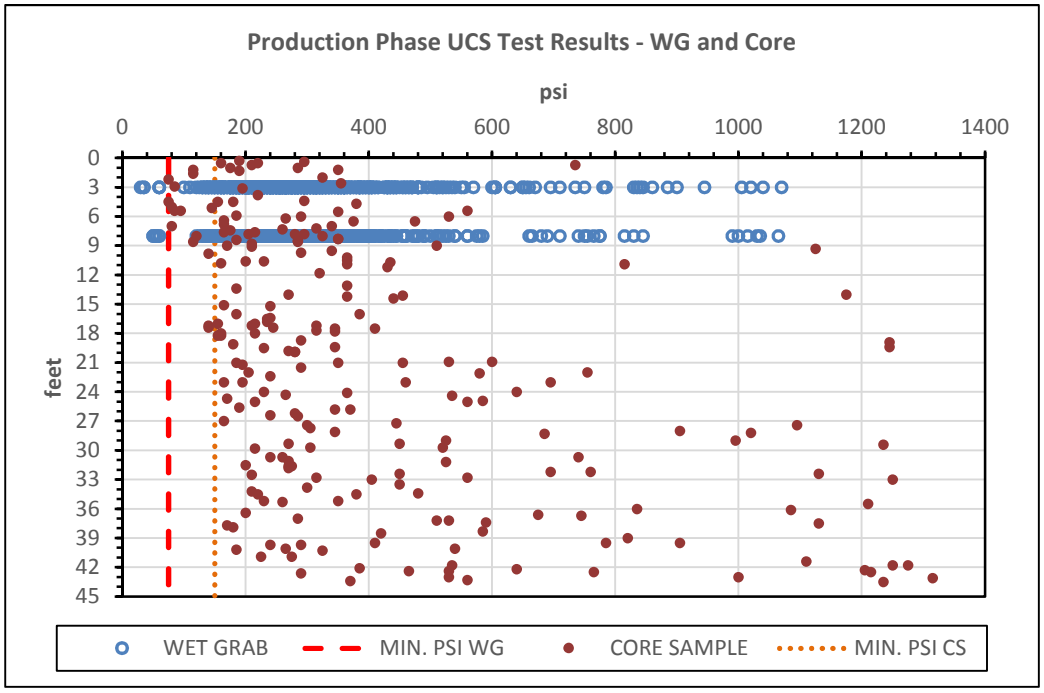


Figure 10: Production UCS test results

CONCLUSIONS

The construction method produced a stabilization system that guarantees a maximum differential settlement of less than 2" over any 1,000 ft stretch.

The soil mixing technology proved as a viable option for future ground improvement works for roadways. The ground treatment produced a large scale, homogenous soil-concrete mass of consistent strength, utilizing a reduced in-situ replacement ratio over traditional excavation methods, with increased coverage to a comparable drive pile foundation.

A more robust soil investigation, with increased knowledge of soil properties and distribution, is fundamental to avoiding major issues, especially in design-build contracts. However, soil mixing method demonstrated a capability to treat multi-variable soil conditions.

Team work, constructive criticism and a proactive attitude are fundamental components for the successful completion of a project.

ACKNOWLEDGMENTS

The authors would like to thank all the many people who contributed to the success of the project.

Special thanks go to: Mario Mauro for his invaluable technical contributions. Raul Horta for his dedication, expertise, and leadership in the field. Giuseppe De Pra for the hard work and the innovative ideas he had. Manuel Toniolo for his patience, availability, and constant support.

REFERENCES

Bertero, A., Leoni F.M., Filz, G., Nozu, M., and Druss, D., 2012. Bench-Scale Testing and QC/QA Testing for Deep Mixing at Levee LPV111. Proceedings of the 4th International Conference on Grouting and Deep Mixing, New Orleans, LA, L. Johnsen, D. Bruce and M. Byle Editors, American Society of Civil Engineers Publishers, Vol. 1, pp. 694-705.

Bertero, A., Morales, C., Leoni, F. M., and Filz, G., 2015, Three Deep Mixing Projects: Comparison Between Laboratory and Field Test Results.

Bertoni M., Leoni, F.M., Schmutzler, W., and Filz, G., 2015, Soil Mixing for the LPV111 Levee Improvements, New Orleans: A Case History, Deep Foundations Institute 2015 Deep Mixing Conference, June 2015, San Francisco, CA, USA.

Brooks, 1981, Physiographic Divisions of Florida (map and guide), Florida Cooperative Extension Service, Gainesville.

Bruce, D.A. and Mauro, M., (2010). "Quality Control & Assurance & Performance Verification for Cutoff Walls," Proceeding of Association of State Dam Safety (ASDSO), Officials Annual Conference 2010, September 2010, Seattle, Washington.

Florida Department of Transportation, Soils and Foundations Handbook, FDOT, Available on-line: http://www.fdot.gov/structures/Manuals/SFH.pdf.

Leoni, F.M., Bertoni, M., Schmutzler, W., Soil Mixing for the Rio Puerto Nuevo Project in San Juan, PR: A Case History, Deep Foundations Institute 2015 Deep Mixing Conference, June 2015, San Francisco, CA, USA.

Schmutzler, W., Leoni, F.M., Bertero, A., Leoni, F., Nicholson, P., Druss, D., and Beckerle, J., 2012, Construction Operations and Quality Control of Deep Mixing at Levee LPV 111 in New Orleans. Proceedings of the 4th International Conference on Grouting and Deep Mixing, New Orleans, LA, L. Johnsen, D. Bruce and M. Byle Editors, American Society of Civil Engineers Publishers, Vol. 1, pp. 682-693.

Schmutzler, W., Mullins, G., and Bertoni, M., 2017, Soil Mixing for the SR-83 Project in Florida, American Society of Civil Engineers (ASCE) Grouting 2017 International Conference, July 2017, Honolulu, Hawaii.

Scott, 2005, Revisions to the geomorphology of Florida focusing on the eastern panhandle and north-central Florida. In: Southeastern Geological Society Field Trip Guidebook 44, pp. 18-36.

MITIGATING SETTLEMENT WITH PILE-SUPPORTED APPROACH SLABS

Reda M. Bakeer, Intertek PSI, Jefferson, LA, USA, (504) 733-9411, reda.bakeer@psiusa.com

ABSTRACT

An approach slab is the roadway segment that immediately follows a bridge intended to provide a smooth transition between the two elements. Some approach slabs have developed rough rideability with time due to differential settlement between the roadway embankment and the bridge. Soils in south Louisiana are generally poor and highly compressible and, therefore, pile-supported approach slabs were occasionally used. Timber piles of variable lengths are driven into the soft soils where no appreciable toe support exists. This resulted in the soils both supporting loads through shaft resistance and yet experiencing long-term consolidation settlement. Field testing and review of the records of over 120 approach slabs constructed in south Louisiana yielded the conclusion that their performance is primarily governed by negative skin friction (downdrag) imposed on the relatively short timber piles. A software (TU-DRAG) was developed to evaluate the deflection profile of a pile-supported approach slab based on its geometry and conditions of the underlying soils. It evaluates the effect of dragload considering the number and spacing of the piles at each transverse row and their variable lengths along the approach slab. TU-DRAG was utilized in the design of two transportation related projects which have been in service for more than 10 years.

Keywords: Bridge, approach slab, abutment, embankment, settlement, downdrag, negative skin friction

INTRODUCTION

The problem of differential settlement at bridge approaches or "the bump at the bridge" has been recognized for many years. Research studies (1986, 1989, 1997, 2009 and 2013) by the Transportation Research Board (TRB) and the Federal Highway Administration (FHWA) provided comprehensive evaluations of the performance of bridge approach slabs by assessing their field conditions and construction and maintenance records. Various states have also performed their own studies to investigate the performance of bridge approach slabs. The studies considered various types of structures including soil- and pile-supported approach slabs, integral bridge abutments and open-end abutments. Recommendations were provided for the design of new structures and for maintaining and repairing existing structures. Guidelines were offered regarding tolerable movements of bridges and their foundations based on measurements of vertical and horizontal movements of 580 bridges Moulton (1986). Vertical and horizontal movements greater than 102 mm (4 inches) and 51 mm (2 inches), respectively, were considered intolerable. Tolerable limits for angular distortion (differential settlement to span length) were suggested to be 1/250 and 1/200 for continuous and simple spans, respectively. It was reported that a differential settlement greater than 13 mm (0.5 inch) at the bridge interface would be sufficient to constitute a "bump" requiring mitigation.

PILE-SUPPORTED APPROACH SLABS

Holmberg (1978) described the design, construction, and performance of pile-supported bridge approaches at eleven sites in Thailand and concluded that supporting the bridge approach on piles would mitigate differential settlement due to consolidation of the underlying soft soils. The Louisiana Department of Transportation and Development (DOTD) used timber piles of variable lengths to support approach slabs Whals (1990). As shown in Figure 1. Piles installed along the approach slab starting from near the bridge end bent and shortened progressively towards the roadway edge are designed to carry the anticipated dead load and live load. The long-term deflection profile of the approach slab due to the underlying embankment settlement is targeted to be either a reversed parabola (lazy-S curve) or a single parabola, as shown in Fig. 2. Either profile will result in a gradual transition from the pile-supported bridge abutment to the soil-

 © 2017 DFI Annual Conference, New Orleans, LA, USA

supported roadway. The timber pile lengths vary from 4.6 m (15 ft) at the roadway edge to 18.2 m (60 ft) near the bridge abutment. The typical length of an approach slab varies from 15 to 30 m (50 to 150 ft) depending on the grade difference and anticipated settlement along the span. This empirical DOTD design assumes that the approach slab is intended to yield a smooth lazy-S transition as settlement of the long piles near the bridge abutment will be less than those of the shorter piles that follow. The approach slab is structurally designed to resist the additional moment caused by the anticipated theoretical deflection. Allen (1985) described a DOTD pile-supported approach slab designed to transition a differential settlement of about 0.31 m (1 ft) between a soil-supported roadway embankment and a pile-supported bridge abutment.

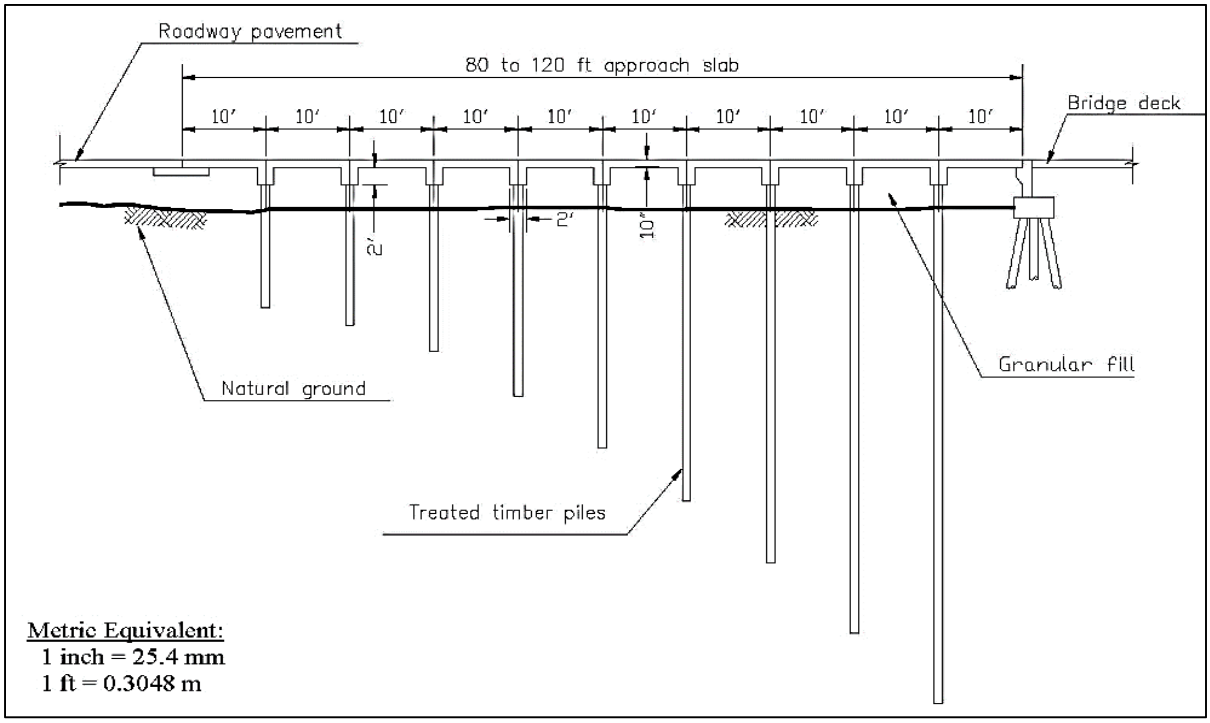


Fig. 1. A typical DOTD pile-supported approach slab

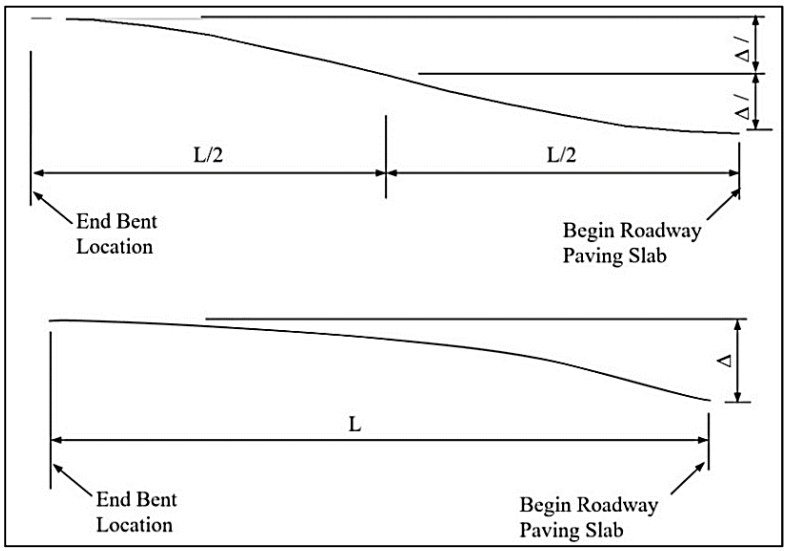


Fig. 2. Long-term deflection of a pile-supported approach slab (Allen 1985)

Field inspections indicated that some DOTD pile-supported approach slabs have performed well, while others have settled differentially creating bumps at the interface or undesirable deflection profile. The inconsistent performance was attributed to the specific subsoil conditions and approach slab configuration at each site which were not accounted for in the empirical design. In most cases, the undesirable deflection profile resulted from negative dragload imposed by the self-weight of the roadway embankment and any sustained surface loads on the relatively short timber piles of variable lengths.

The Louisiana Transportation Center (LTRC) sponsored a study to investigate the performance of pile-supported approach slabs to identify the factors that affected their long-term performance. The study examined over 120 bridge approach slabs (Das et al. 2000) where the as-built drawing, subsoil conditions and traffic and maintenance records were reviewed. They included both soil and pile supported approach slabs for comparison. Seven representative test sites were selected for thorough in-situ evaluation of their pile-supported approach slabs. Sites 1 through 4 were concrete bridges constructed in the 1990's within a cypress swamp along interstate I-310. Site 5 was the concrete approach of a cable-stayed bridge on the Mississippi River constructed in 1979. The approach slabs at Sites 6 and 7 were on LA 3139 in New Orleans constructed in 1982. Field testing included walking profiler, falling weight deflectometer (FWD), laser profiler, geodetic survey, soil borings and Cone Penetrometer Test (CPT) soundings. Measurements made with the walking profiler agreed well with the results of the geodetic surveys. The FWD and non-destructive testing were used to detect any voids present under the approach slabs. The study (Bakeer et al. 2005) concluded that the empirical DOTD design methodology yielded inconsistent performance primarily due to the differences in roadway embankment and subsoil conditions, which, in turn, affect dragload on the piles. The impact of other variables such as ramp type, speed limit, traffic volume, etc. was found to be insignificant. Results of the study were used to develop a new rating system for approach slabs (IRIS) based on the IRI measurements obtained with a laser profiler. As per the IRIS rating system, the pile-supported approach slabs in the study were classified as: 4 percent in very good condition, 22 percent in good condition, 33 percent in fair condition, 22 percent in poor condition and 19 percent in very poor condition. Guidelines were developed based on the outcome of the study for the design of pile-supported approach slabs. This paper presents a numerical model and software developed as part of the LTRC study which calculates the long-term deflection profile of a pile-supported approach slab considering its specific configuration and subsoil conditions and the effect of dragload.

THEORETICAL BACKGROUND AND NUMERICAL MODEL

Pile load carrying capacity is the summation of the mobilized shaft resistance (R_s) and toe resistance (R_t). Positive shaft resistance is mobilized during compression loading and negative shaft resistance develops under tension or uplift loads (Fig. 3). When a surcharge load or fill is placed, the underlying compressible cohesive and organic soils consolidate resulting in subsidence. Theoretically, this would extend to some depth depending on fill thickness and size of the loaded area. Therefore, additional stresses will develop along the pile shaft as the surrounding soils displace relative to the pile shaft due to consolidation. Negative skin friction or "downdrag" will develop when the consolidating soils and the pile settle differentially adding compressive dragload on the pile. Therefore, a single vertical pile will be subjected to dead loads and sustained live loads applied at the pile head (Q_d) and possibly additional dragload (Q_n) acting along its shaft. The impact of downdrag is influenced by the fill thickness, sustained surface loads, time-rate and consolidation characteristics of the foundation soils and embedded pile length.

The location along the pile shaft where equilibrium of vertical forces occurs (Fig. 3) is termed the "neutral plane" or "neutral point." It is defined as the depth at which the shear stress along the pile shaft changes from negative to positive skin friction or the location where no relative displacement exists between the pile and the surrounding soils. In south Louisiana, consolidation is greatest within the upper Holocene Age deposits consisting primarily of soft and highly compressible organic and normally consolidated clays. Long piles installed into a dense sand stratum or stiff Pleistocene Age clays are typically used to support

bridge bents and end abutments to achieve good toe support and essentially negligible settlement of about 12 mm (0.5 inch). Meanwhile, the variable length timber piles supporting an approach slab and embedded in more compressible soils experience higher settlements which vary depending on the pile length, embankment height and subsoil conditions. To mitigate differential settlement along a pile-supported approach slab, it is necessary to quantitatively predict its long-term deflection profile. An optimum design could then be achieved by performing a parametric study considering various configurations for the approach slab. A spreadsheet type software "TU-DRAG" containing Visual Basic Application (VBA) macros was developed as part of the LTRC study (Zhong, 2004). Its numerical model uses the downdrag criterion proposed by Fellenius (1989) and adopted in FHWA (1997) which defines the neutral plane at the depth where settlement is equal to 12 mm (0.5 inch). TU-DRAG is available from LTRC/DOTD.

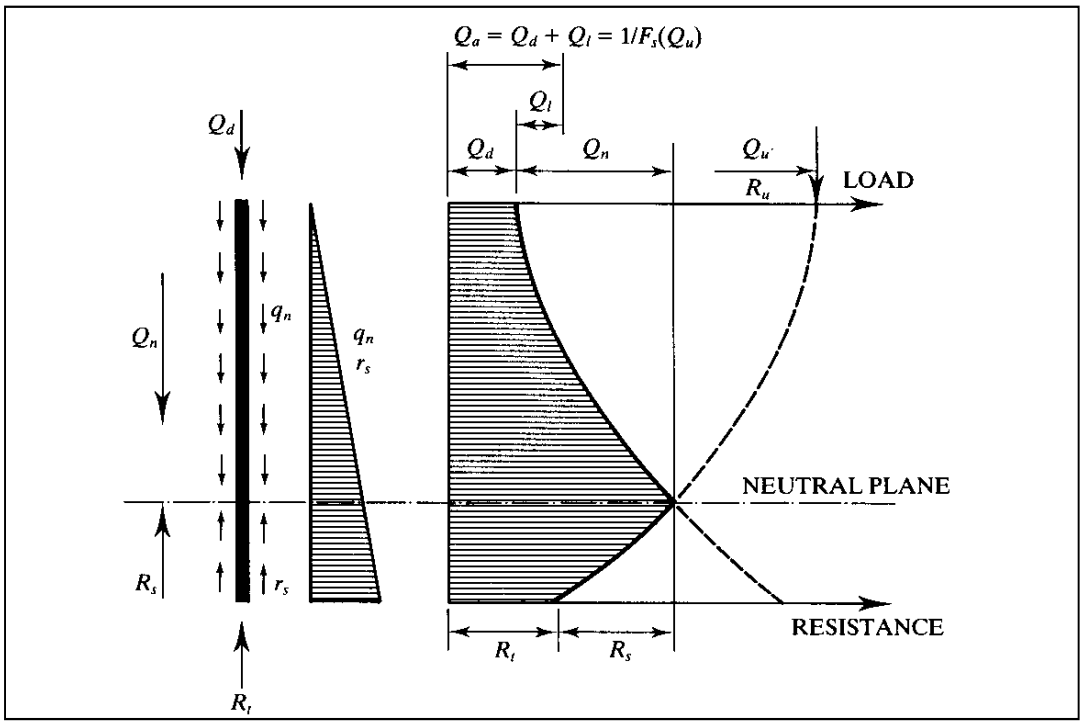


Fig. 3. Downdrag model used in TU-DRAG (Fellenius 1989)

The sequence of a typical TU-DRAG session consists of the following steps:

1. Identify the properties and stratification of the foundation soil and embankment/fill material.
2. Determine the design load on the pile head.
3. Calculate and enter the anticipated consolidation settlement profile with depth.
4. Calculate and enter the distribution of shaft resistance and toe support of a single vertical pile.
5. Enter a trial configuration for the approach slab and its pile arrangement.
6. TU-DRAG calculates pile stiffness and deflection profile for the selected trial approach slab.
7. Compare the screen displayed calculated longitudinal deflection profile for the trial approach slab with the desired lazy-S deflection profile.
8. Enter a new trial configuration (repeat Step 5) until an optimized deflection profile is achieved.

The main parameter affecting the deflection of the approach slab modeled in the present TU-DRAG model in Step 6 is the calculated equivalent pile/soil spring stiffness due to pile/soil interaction which represents the force-displacement along each transvers row of piles of equal lengths. Using a longer pile increases the pile/soil spring stiffness, and consequently, have the most influence on the calculated longitudinal

deflection profile of the approach slab. The approach slab stiffness, which is not presently coded in TU-DRAG, provides a secondary effect in mitigating differential deflection between any two consecutive transverse rows of different pile lengths. Therefore, it also affects the longitudinal deflection profile of the approach slab. Using TU-DRAG without considering the approach slab stiffness yields acceptable conservative designs (i.e., the slab stiffness improves deflection prediction). The effect of pile lengths along the transverse rows within the first half of the approach slab away from the bridge abutment has more impact on the calculated deflection profile. The magnitude of the pile head load has more effect on the transverse rows of piles within the middle-third of the approach slab, which is critical for achieving smooth long-term performance. Varying pile spacing or the approach slab span does not significantly affect the anticipated deflection profile, but it could spread the deflection over a shorter or longer distance. Variations of the settlement profile with depth, due to different embankment height, embankment material unit weight, surcharge period, etc. does not significantly affect the calculated approach slab deflection profile, instead it simply magnifies or reduces the approach slab deflection.

TU-DRAG CALIBRATION

TU-DRAG was calibrated using the information gleaned from the seven test sites which were extensively investigated during the LTRC study. However, only the analysis of Site 1 is discussed herein in detail due to space limitations. Site 1 is the south approach to a concrete bridge on I-310 located about 1.6 km (1 mile) north of the Hale Boggs (Luling) Mississippi River bridge. The study examined the southbound (S/B) and northbound (N/B) approaches of the concrete bridge constructed in 1992. The roadway embankments were surcharged for a period of six months to induce some long-term consolidation settlement in advance of construction. The surcharge consisted of about 0.92 m (3 ft) of additional fill above the design embankment grade. The embankment was 2.75 m (9 ft) high, 13.1 m (42.8 ft) wide and had side slopes of 1 vertical on 4.8 horizontal (1V on 4.8 H). One soil boring and one CPT sounding were performed within the median separating the roadways during the LTRC study. The soil profile (TU-DRAG Step 1) consisted of about 1.8 m (6 ft) of sand fill placed during the embankment construction (thicker fill was present within the roadway embankment than at the median where the exploration was made). The fill was underlain by about 16. 8 m (55 ft) of mainly very soft to soft clays. The clays had an undrained shear strength (C_u) of about 10 to 29 kPa (200 to 595 psf) and a compression index (C_c) is 0.48 to 0.82. A highly compressible organic stratum extended between the 3.1 m (10 ft) and 7.6 m (25 ft) depths. The stiffer and less compressible Pleistocene Age soils were encountered at about the 19.8 m (65 ft) depth. This soil profile is typical of a cypress swamp region. Therefore, the timber piles supporting the approach slabs were installed within the Holocene soils while the long prestressed, precast concrete (PPC) piles supporting the abutments extended into the Pleistocene. Table 1 shows the pile lengths used along each transverse row of the approach slabs (Step 5). The head load (Step 2) on a single vertical pile was 126.5 kN (28.43 kips). The calculated consolidation settlement profile under self-weight of the embankment and fill is shown in Fig. 4 (Step 3).

Table 1. Details of the N/B and S/B approach slabs at Site 1

Element	Distance m, (ft)	Pile Length m, (ft)
Bridge Abutment	0	N/A
Transverse Row 1	3.1(10)	18.3 (60)
Transverse Row 2	6.1 (20)	15.9 (52)
Transverse Row 3	9.1 (30)	13.4 (44)
Transverse Row 4	12.2 (40)	11.3 (37)
Transverse Row 5	15.2 (50)	9. 5 (31)
Transverse Row 6	18.3 (60)	7.6 (25)
Transverse Row 7	21.3 (70)	6.1 (20)
Transverse Row 8	24.4 (80)	5.2 (17)
Transverse Row 9	27.4 (90)	4.6 (15)
Roadway Edge	30.5 (100)	N/A

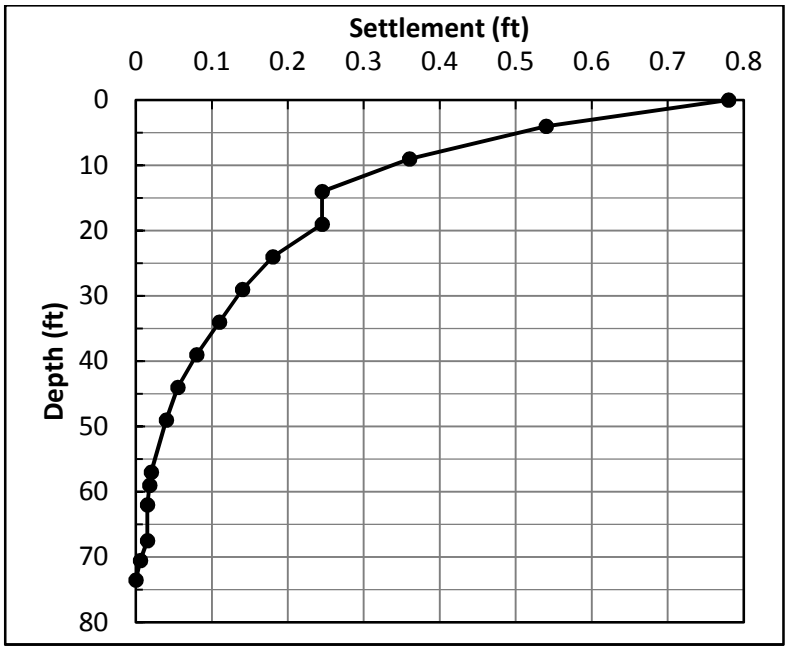


Fig. 4. Long-term settlement profile at Site 1 (1 ft = 0.305 m)

Visual inspection and field measurements made during the study indicated that both approach slabs at Site 1 have performed poorly despite of the preload/surcharge program. Both slabs experienced significant differential settlement of up to 0.2 m (0.7 ft) including noticeable bumps at the bridge interface. The N/B and S/B slabs exhibited an abrupt change in slope about 1.5 and 3.1 m (5 and 10 ft) away from the bridge abutments, respectively. The surface profiles of the 30.5 m (100 ft) long approach slabs obtained from the geodetic surveys and the calculated deflection profile by TU-DRAG (Step 6) for the as-built configuration indicated good agreement, as shown in Fig. 5 (Step 7). The analysis and actual field measurements showed that the empirical design of both approach slabs did not yield the desired lazy-S deflection profile.

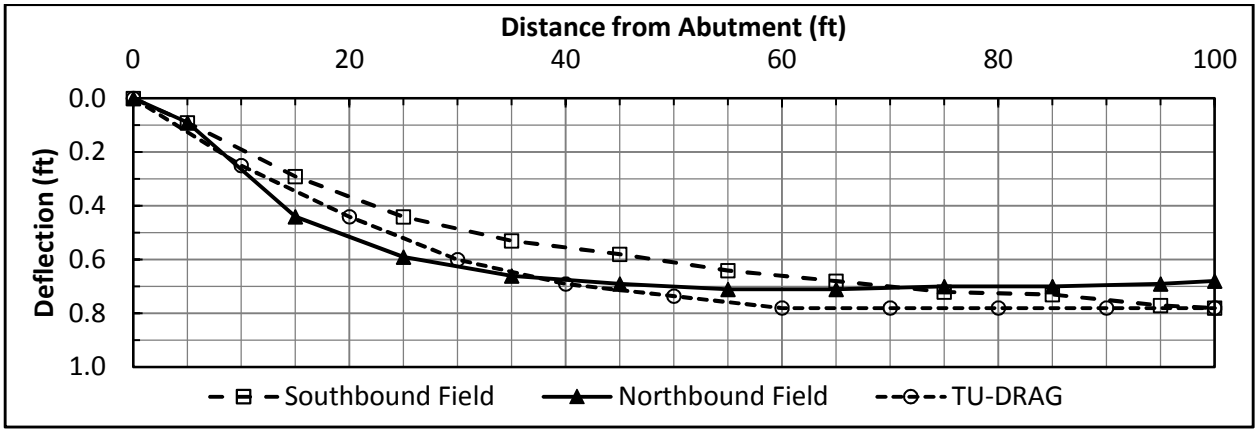


Fig. 5. Measured and calculated deflection profiles for Site 1 (1 ft = 0.305 m)

The optimized deflection profile shown in Fig. 6 and Table 2 was obtained by varying the timber pile lengths along the approach slab in a trial-and-error process (Steps 5 to 8). Table 2 indicates that an increase of 35 to 115 percent is needed beyond the as-built pile lengths to offer a smooth transition. The optimized deflection profile shown in Fig. 6 is close to the ideal lazy-S profile shown in Fig. 2 except at the first transverse pile row on the approach slab (Row 1) which immediately follows the bridge end abutment

supported on relatively long PPC piles. Longer piles are needed along Row 1 of the approach slab to mitigate settlement due to dragload which is impractical for timer piles but other pile types could be used. The deflection profile could also be mitigated by increasing the structural stiffness of the initial segment of the approach slab following the bridge. As previously discussed, contribution of the approach slab stiffness and its connection to the bridge abutment were not incorporated in the present version of TU-DRAG.

Table 2. Optimized approach slab design at Site 1

Transvers Rows		Distance m, (ft)	Pile Length m, (ft)		
No.	Piles		Used	Optimized	Required Increase
1	9	3.1 (10)	18.3 (60)	24.7 (81)	35%
2	9	6.1 (20)	15.9 (52)	24.4 (80)	54%
3	9	9.1 (30)	13.4 (44)	22.9 (75)	71%
4	9	12.2 (40)	11.3 (37)	12.0 (59)	60%
5	9	15.2 (50)	9. 5 (31)	16.8 (55)	77%
6	9	18.3 (60)	7.6 (25)	15.2 (50)	100%
7	9	21.3 (70)	6.1 (20)	13.1 (43)	115%
8	9	24.4 (80)	5.2 (17)	10.7 (35)	106%
9	9	27.4 (90)	4.6 (15)	8.5 (28)	87%

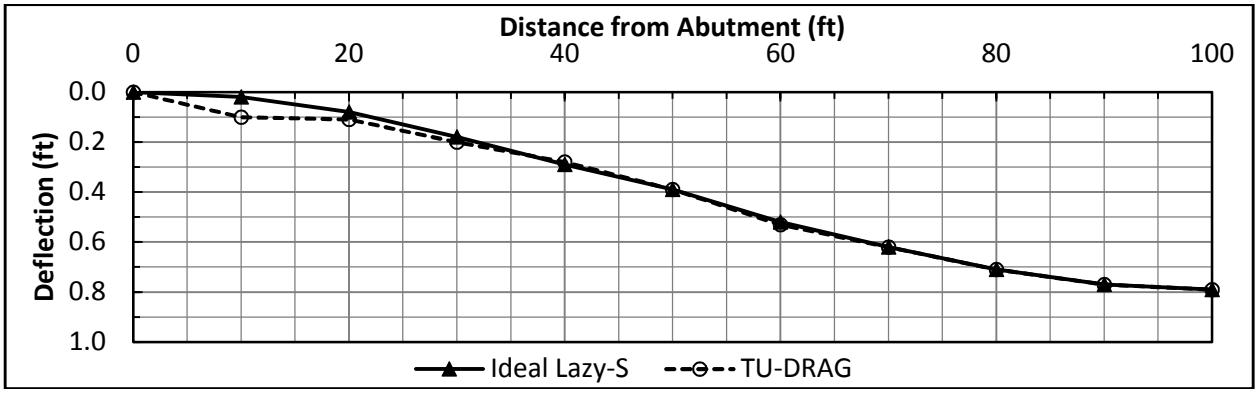


Fig. 6. Optimized versus idealized deflection profiles at Site 1 (1 ft = 0.305 m)

The 30.5 m (100 ft) long bridge approach slabs at Sites 1 through 4 were constructed in the 1990's within the same cypress swamp along interstate I-310. Therefore, they essentially yielded comparable deflection profiles, but Sites 2 through 4 did not experience abrupt slope changes. The minor deviations in the measured deflection profiles at Sites 1 through 4 are attributed to variations in subsoil conditions (thicker and/or shallower organic stratum, character and stratification of the foundation soil, presence of intermittent granular strata, etc.), embankment height and use of a preload/surcharge program.

Site 5 included the southbound and northbound approach slabs constructed in 1979 as part of the I-310 elevated south concrete approach to the Hale Boggs Mississippi River cable-stayed bridge. In comparison with Sites 1 through 4, Site 5 was located on the opposite bank of the Mississippi River and within mostly sugarcane fields. The much older 36.6 m (120 ft) long concrete approach slabs at Site 5 have performed poorly and experienced significant differential settlement of about 0.3 m (1 ft) including a relatively steep incline over a 16.8 m (55 ft) distance away from the abutments of the elevated concrete approach.

Sites 6 and 7 are the eastbound (E/B) and westbound (W/B) approach slabs of the Earhart Expressway bridge near the Orleans Parish line. The 24.4 m (80 ft) long approach slabs at Sites 6 and 7 were constructed in 1982 and their conditions worsened with time. Consolidation settlement of the underlying highly organic soils resulted in about 0.6 m (2 ft) gap beneath the underside of the W/B approach slab at the bridge

abutment. Both approach slabs developed noticeable bumps at the bridge interface. The W/B approach slab experienced severe and abrupt deflection of about 0.4 m (1.2 ft) about 1.5 m (5 ft) away from the bridge abutment where a transverse crack developed. Both approach slabs were subsequently repaired including the placement of asphaltic overlay of variable thickness to smoothen rideability.

TU-DRAG was used to determine the required increase in pile lengths needed to achieve a lazy-S deflection profile at each of the seven test sites. The calculated optimized deflection profiles by TU-DRAG using longer piles yielded better agreement with the desired lazy-S deflection profile. Figure 7 shows the mathematical average of the required percent change in pile lengths along the approach slabs beyond the as-built designs for all seven test sites. Also shown on Fig. 7 are the most extreme cases of Sites 1, 5 and 7 for comparison. The length deficiency decreased with distance away from the bridge abutment with the smallest change needed near the roadway edge. Figure 7 indicates that the required percent increase in pile length is significant near mid-span regardless of the approach slab span. The average curve for the seven test sites indicated that the empirically selected pile lengths were deficient by about 64 percent on average. Site 7 was the most deficient and it exhibited the worst performance where the required percent increase in pile length was over 160 percent at transverse Row 5. Results of the study showed that increasing the pile lengths along the transverse rows near mid-span of the approach slab is extremely critical to achieve the desired lazy-S deflection profile. Deviations between the measured deflection profiles at all seven sites from the theoretical lazy-S curve varied between -0.01 and 0.62 m (-0.03 and 0.62 ft).

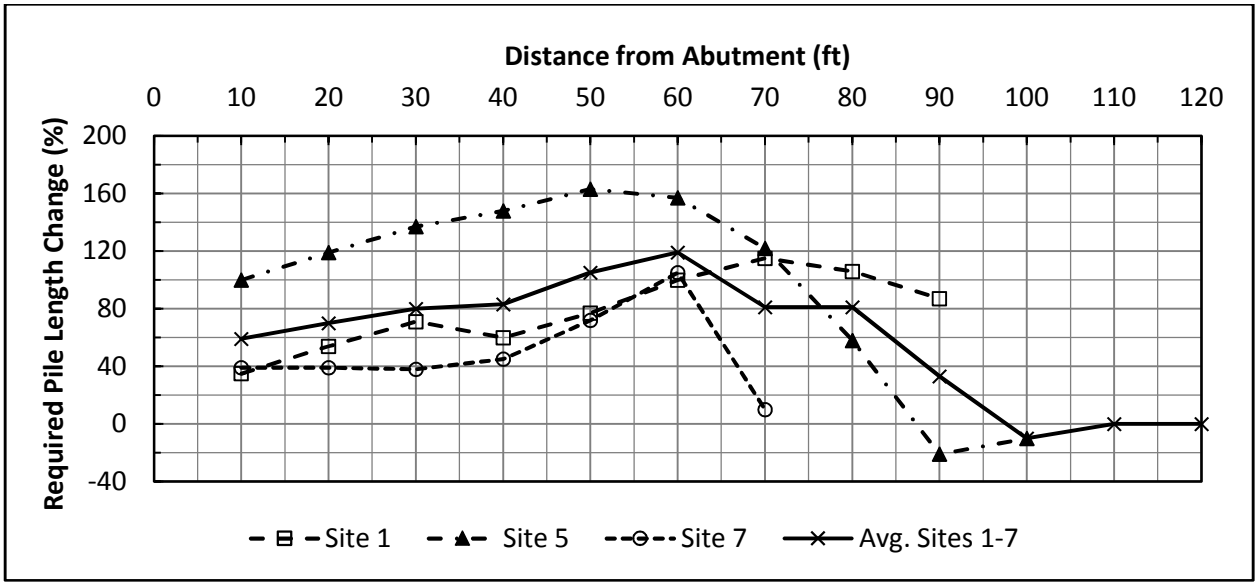


Fig. 7. Deviation in pile lengths needed to achieve the idealized lazy-S profile (1 ft = 0.305 m)

APPROACH SLAB STIFFNESS

The effect of the approach slab stiffness and the pile/soil equivalent spring stiffness used in the TU-DRAG model (Step 6) on the calculated approach slab deflection profile was investigated (Zhong 2004) using the finite element method (FEM). The calculated approach slab deflection profiles using the FEM while considering the contribution of the approach slab stiffness agreed reasonably well with the measured profiles at the seven test sites. The error in the calculated deflection along the first transverse row of piles near the bridge abutment was significantly reduced. Results of the FEM analysis indicated that contribution of the approach slab stiffness is more significant on the settlement of the transverse pile rows within the first half of the slab starting from the bridge abutment. Strength of the approach slab material within the range of typical concrete mixes had little effect on the deflection profile. While some increase in slab

stiffness could be achieved if the pile head beam orientation is changed from a transverse to a longitudinal direction, the effect of the added stiffness on the overall slab deflection was found to be minimal.

TU-DRAG DESIGN APPLICATIONS

TU-DRAG was used to design a relatively large approach slab leading to a streetcar maintenance barn in New Orleans supported on timber piles. The streetcar barn was constructed around 1900 and was converted in the 1960's to become a bus barn. It was renovated again in 2002/03 and converted back to become a streetcar barn as part of the new Canal Street Streetcar Line project. The area surrounding the barn settled substantially more than the pile-supported floor of the barn creating a bump that would not be negotiated by streetcars. The new streetcar tracks leading to the barn were soil-supported. Therefore, the multitrack approach slab leading to the barn was supported on 13 transverse rows of treated timber piles of variable lengths. The first 5 rows of piles have essentially the same length of 15.2 m (50 ft) as those used to support the barn to minimize differential settlement along the interface joint along the entrance. The remaining piles along the approach slab were tapered down gradually with the shortest pile being 3.1 m (10 ft) near the edge of the soil-supported tracks to yield a long-term lazy-S deflection profile.

Piles of variable lengths were used to support two 36.9 m (121 ft) long approach slabs constructed along the east/west runway at the New Orleans Louis Armstrong International Airport. The purpose of the approach slabs was to create to a "bridge" over a 24.4 m (80 ft) wide underground tunnel supported on 18.3 m (60 ft) long timber piles that crosses under the runway. The tunnel was built in the 1980's and two diagonal bumps developed in the runway with time along the exterior vertical walls of the tunnel which required frequent maintenance to safeguard aircraft landing and takeoff. Reconstruction of the runway in 2005 included supporting this runway segment on the vertical walls of the tunnel and on two new end bents located 9.1 (30 ft) away from the edges of the tunnel on both sides. The end bents and approach slabs that followed were supported on 0.4 m (14 inch) square PPC piles of variable lengths starting with 30.5 (100 ft) long piles at the end bents and ending with 10.1 m (33 ft) long piles at the approach slab edge.

CONCLUSIONS

The comprehensive LTRC study identified and evaluated 120 pile-supported and soil-supported approach slabs associated with ninety bridge sites across south Louisiana. Seven representative sites with pile-supported approach slabs were selected for extensive in-situ evaluation. Performance of the approach slabs was assessed based on visual inspection, geodetic surveys, and road surface conditions. Field instruments included a walking profiler, FWD, laser profiler and digital total station. Soil borings and cone penetrometer tests were also performed at three of the seven test sites. A rating system, IRIS, based on the laser profiler readings was developed and used to assess the conditions of the 120 approach slabs.

Based on examination of the approach slab records and field testing at the representative test sites, it was concluded that the inconsistent performance of pile-supported approach slabs is primarily due to dragload and differences in subsoil conditions. Dragload could be accounted for by increasing surcharge height and/or period, soil improvement, or by using longer piles along the approach slabs. Downdrag due to consolidation settlement and pile/soil interaction is an extremely complex phenomenon. Therefore, accurate calculations of the anticipated settlement and pile capacity are crucial to properly design a pile-supported approach slab. A long-term deflection profile that is close to the ideal lazy-S curve could be achieved by selecting the appropriate variable pile lengths along the span of the approach slab.

Results of the study indicated that the empirical design of pile-supported approach slabs used by DOTD does not always yield acceptable field performance. The empirical design methodology yielded pile lengths about 64 percent shorter on average than those required to achieve a lazy-S deflection profile. The calculated deflection profiles of the approach slabs using TU-DRAG based on as-built conditions were in

general agreement with the field measurements. However, TU-DRAG generally overestimates deflection since it does not account for the approach slab stiffness. The error in all predictions by TU-DRAG when compared with the field measurements was highest at the location of the first transverse row of piles that follows the bridge end abutment (Row 1). The difference between the calculated and measured deflections became smaller with distance away from the bridge abutment. TU-DRAG was successfully used to design approach slabs for two major projects in Louisiana which have been in service for more than 10 years.

ACKNOWLEDGEMENTS

This research was conducted at the Department of Civil and Environmental Engineering at Tulane University under Grant No. 97-4GT from the Louisiana Transportation Research Center (LTRC) in cooperation with the Louisiana Department of Transportation and Development (DOTD). Intertek PSI provided the author with the time and support needed to prepare the manuscript and presentation.

REFERENCES

Allen, D.L., 1985. A survey of the states on problems related to bridge approaches. Kentucky Transportation Research Program, Report No. UKTRP-85-25, Lexington, October, 188 p

Bakeer, R.M., Shutt, M.A., Zhong, J., Das, S.C. and Morvant, M., 2005. Performance of pile-supported bridge approach slabs," ASCE J. Bridge Eng., 10(2), pp. 228-237

Das, S.K., Bakeer, R.M., Zhong, J. and Schutt, M., 2000. Assessment of mitigating embankment settlement with pile supported approach slabs. Report to LA Transportation Research Center, Baton Rouge, LA.

Fellenius, B.H., 1989. Unified design of piles and pile groups. Transportation Research Board, National Research Council, TRB Record, 1169, pp. 75-82

Holmberg, S., 1978. Bridge Approach on soft clay supported by embankment piles, Geotechnical Engineering, 10, pp. 77-89

Moulton, L.K., 1986. Tolerable movement criteria for highway bridges. Final Report No. FHWA-TS-85-228, Federal Highway Administration, Washington D.C.

Puppala, A.J., Saride, S., Archeewa, E., Hoyos, L.R. and Nazarian, S., 2009. Recommendations for design, construction, and maintenance of bridge approach slabs. Final Report FHWA/TX-09/0-6022-1, Texas Dept. of Transportation, Austin, TX, 186 p

Thiagarajan, G., Myers, J. and Halmen, C., 2013. Field evaluation of alternative and cost-efficient bridge approach slabs. Final Report NUTC R272/R273, U.S. Dept. of Transportation, Washington, D.C., 159 p

TRB 1989. NCHRP synthesis of highway practice 147: Treatment of problem foundations for highway embankments. Transportation Research Board, National Research Council, Washington D.C., 72 p

TRB 1997. NCHRP Synthesis of highway practice 234: Settlement of bridge approaches (The bump at the end of the bridge). Transportation Research Board, National Research Council, Washington D.C., 75 p

Whals, H.E., 1990. "NCHRP Synthesis of highway practice 159: Design and construction of bridge approaches. Transportation Research Board, National Research Council, Washington D.C. 45 p

Zhong, J., 2004. A numerical model for the analyses of downdrag on piles. Ph.D. Dissertation, Tulane University, New Orleans, Louisiana.

OVERCOMING THE CHALLENGES ENDURED BY THE QUALITY ASSURANCE AND QUALITY CONTROL TEAMS DURING THE CONSTRUCTION OF A DEEP CUTOFF WALL IN EAST ALTON, ILLINOIS

Matteo Bertoni, Treviicos, Charlestown, MA, USA, 617-241-4800, mbertoni@treviicos.com
Raffaella Granata, Trevi Group, Design, Research & Development Dpt., Cesena, Italy, (+39) 347-972-7588, rgranata@trevispa.com
Wesley Schmutzler, Treviicos, Charlestown, MA, USA, 617-241-4800, wschmutzler@treviicos.com

ABSTRACT

The Lower Wood River Levee system, at the confluence of the Wood River Creek and the Mississippi River, in East Alton, Illinois, has been plagued with underground seepage and, in 2010, remediation was deemed necessary by the Southwestern Illinois Flood Prevention District Council and the United States Army Corp of Engineers (USACE). The experts enlisted by the council produced a design that provided for constructing a cutoff wall approximately 2,000 feet long and up to 140 feet deep, through alluvial and outwash soils, and embedded in bedrock. This paper will describe the challenges faced by the Quality Control (QC) and Quality Assurance (QA) teams due to the complex nature of the project in conjunction with an extremely thorough QC/QA program.

Keywords: deep cutoff wall, QC/QA program, challenges.

INTRODUCTION

The "American Bottom" is an area of 453 km^2 (175 square miles) in Southwestern Illinois, extending from Alton south to the Kaskaskia River, which is home to 156,000 people. In the 1940s and 1950s the U.S. Army Corp of Engineers (USACE) designed and built a 120 kilometer (74 mile) long levee system to protect the area from a 500-year flood event on the Mississippi River, which flows through it. The levee system has been plagued by under-seepage for several years. The phenomenon has worsened to varying degrees, depending on location, to the point that remediation was needed.

The Southwestern Illinois Flood Prevention District Council (SIFPDC), to obtain Federal Emergency Management accreditation, in June 2010 commissioned a team lead by Amec Foster Wheeler for the design and management of the required levee improvements. The team presented in 2011 the project's first set of drawings showing proposed design features throughout the levee system. The project was subdivided in four areas, based on the controlling levee districts, one of which, the Wood River Drainage and Levee District, was split into three subdivisions: Upper Wood River, East-West Forks of Wood River, and Lower Wood River.

The project included the installation of a cutoff wall at the confluence of the Wood River and the Mississippi River in East Alton, IL (Fig. 1). The Engineer of Record (Amec Foster Wheeler) considered the cutoff wall as the only viable solution to stop the severe under-seepage that was undermining the integrity of the Lower Wood River Levee. The Lower Cutoff Wall (LCW) project is the subject of this paper.

 © 2017 DFI Annual Conference, New Orleans, LA, USA

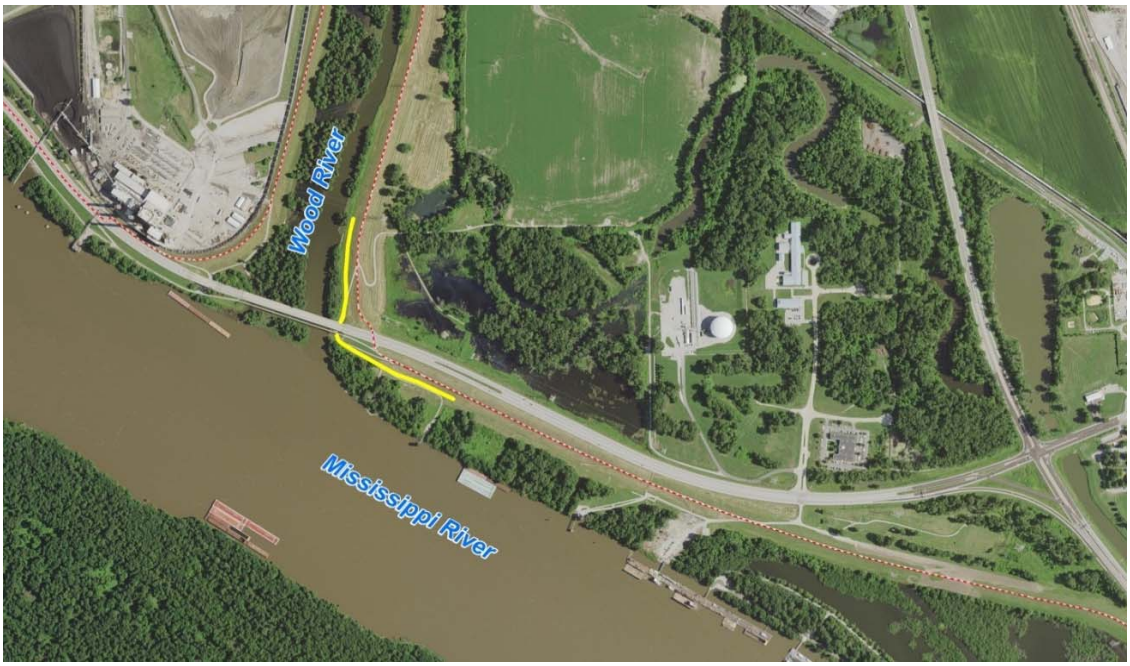


Figure 1: Location of the Lower Cutoff Wall Project (yellow line represents the cutoff wall)

GEOLOGY

The LCW project is located in the Wood River Quadrangle, which is mostly contained within the alluvial valley of the Mississippi River known as the American Bottom. The ground level elevation of the area ranges from 130 to 135 m (420 to 440 ft) above sea level and is the result of processes of excavation and filling of the valley that likely occurred several times during the Quaternary Period.

The deposits of the Mississippi River valley consist of mixtures of water-laid clay, silt, sand, and gravel, up to 38 metre (125 feet) thick above bedrock. These deposits are highly variable in the upper 50 feet due to former channels of the Mississippi River and its tributaries. There is a general coarsening trend with depth, with outwash (sand with gravel) typically comprising the lower one-third to one-half of the sediment volume. The underlying bedrock consists mainly of limestone or shale; locally the bedrock is covered by glacial till, preserved underneath thick alluvial sediments (Grimley and Lepley, 2005).

There is a direct correlation between the alluvial deposits and the under-seepage occurrences of the area, as explained in the Technical Memorandum prepared in 1956 for the St. Louis District, Corps of Engineers by Waterways Experiment Station (WES TM 3-430, 1956).

SCOPE OF WORK, CONSTRUCTION METHOD, AND CONSTRUCTION PHASES

The project design provided that a cutoff wall be installed adjacent to the river side toe of the levee. The wall total length was approximately 600 m (2000 feet), of which, 275 m (900 ft) located along the Wood River and 335 m (1100 ft) along the Mississippi River.

The technical specifications required that the COW be homogeneous, a minimum 60-cm-wide (2-ft), and with a maximum hydraulic conductivity of 1 x 10^{-6} cm/s. The Unconfined Compressive Strength (UCS) at 28 days was to be between 350 and 1240 kPa (50-180 psi) with no individual specimen strength being lower than 207 kPa (30 psi) or greater than 1380 kPa (200 psi).

The cutoff wall was to be excavated through layers of granular soils, including dense sands, gravels, and cobbles, to depths of up to 43 m (140 ft), to be keyed a minimum of 1.5 m (5 ft) into till or, a minimum of 0.3 m (2 ft) into competent rock in those areas where the till was not present. The "panel method" (i.e.: overlapping primary and secondary panels) was to be used, and a minimum overlap between primary and secondary panels of 0.5 m (20 in) was required.

The geotechnical properties of the foundation soils constituted a reason of concern for the design firm and the contractor. Fifteen inclinometers were to be installed and continuously monitored for differential movements, a potential sign of an undergoing deformation of the trench walls.

The Contractor (Treviicos South) selected for the project a construction method consisting of using a combination of clamshell and hydromill, under a self-hardening slurry (SHS). The method had been successfully used few years before for the rehabilitation of over 11,850 linear meters (38,000 linear feet) of the Herbert Hoover Dike in Florida (Granata el Al., 2016), a project with similar geotechnical properties.

The LCW project presented the Contractor with an additional and major challenge as never before it had installed a cutoff wall using a hydromill under SHS to such depths. The Herbert Hoover Dike project required a maximum depth of 84 feet, while the maximum depth of the cutoff wall at the LCW project was 140 feet.

The Contractor decided to limit the maximum length of the primary panels to 7.0 m (23 ft) and 2.8 m (9.2 ft) for the secondary panels. The width of the panels was set to 0.9 m (3 ft), to account for vertical deviations and guarantee the minimum required width.

A mixing plant was positioned at the toe of the land side of the levee for the preparation of the SHS. The equipment present included two high shear colloidal mixers supplied by vertical silos for cement and bentonite, one agitator, and baker tanks for bentonite slurry hydration and water storage.

The project specifications required that the installation of the full length of the cutoff wall be preceded by the construction of a test section located on the Mississippi River side of the project.

The test section included one 2.8-metre-long (9.2-ft) single-bite primary panel, two 7-metre-long (23-ft) primary panels, and two 2.8-metre-long (9.2-ft) secondary panels. Construction started on September 22, 2015, and was completed October 8, 2015. The construction method selected by the Contractor proved to be efficient and safe, and produced a wall in compliance with the specification requirements. Therefore, on December 8, 2015 the operations were resumed to complete the installation of the COW. The production phase consisted of installing 66 primary panels and 65 secondary panels and was completed 4.5 months later, on April 22, 2016. Completion was delayed by over a month due to the rising of the Mississippi River to historic levels for the season, which resulted in the flooding of the work platform.

Further details on the scope of work, construction method, and construction phases of the project can be found in the paper Construction of a Deep Cutoff Wall Along the Mississippi River at East Alton, IL (Granata et Al., 2017), which also discusses the SHS design phase.

QC/QA PROGRAM: DESIGN AND IMPLEMENTATION

The Engineer of Record, under the supervision of the USACE, designed a thorough QC/QA program to monitor the execution of the work and verify the compliance of the COW with the specification requirements. The program underwent some revisions and implementations, deemed necessary by both the QC and QA teams to better address the needs and challenges of such a challenging project.

The QC team, at the beginning of the production shift, was responsible for preparing and distributing the panels installation sequence to supervisors and operators, controlling that all the paperwork necessary to the operators to correctly perform and record operations were present in the rigs cabin, verifying the proper functioning of the rig instrumentation, and assuring the correct composition of the SHS. Also, SHS and bentonite slurry, were tested for viscosity, density, and bleeding, at a minimum three times per shift.

Every step of the installation of a panel was closely followed by both QC and QA teams. When setup operations were performed in preparation for the beginning of excavation, a representative of the QC team would verify the correct positioning of the rig with respect to the installation sequence and the limits of the panel to be installed. During installation, verticality and depth of the excavation were monitored in real-time by means of the Drilling Mate System, the onboard automated monitoring system. The system provided also the pressure of the cutting wheel motors. This information, in association with the observation of the cuttings at the hydromill de-sanding unit, was fundamental to the QA personnel to determine when the top of the key material had been reached. Once a pressure spike had been observed, normally a sign of the presence of rock, a thorough analysis of the cuttings was carried out to confirm the assumption. The process would then be completed by interpolating the data collected with the available soil boring information. The procedure proved more challenging in those areas where till was the key material. As the pressure spikes were less pronounced, priority had to be given to the analysis of the cuttings. Samples of the key material were collected in sealed bags, and stored on site.

Once the final depth was reached, the hydromill stayed in place, with the high capacity reverse circulation pump running, to clean up the bottom of the excavation until not greater than 3-inch loose particles remained, as dictated by the specifications.

The completion of the panel installation was followed by several QC operations. The specifications required that two methods be used to verify verticality, depth, and cleanliness of the bottom of a panel. The first method to verify verticality and depth was the monitoring system installed on the hydromill, while the cleanliness of the bottom of a panel was confirmed by the observation of the size of the cuttings at the de-sander. The determination of viable second methods required the collaboration of QC and QA team representatives.

Typical procedures to check the depth and cleanliness of a panel, such as probing the bottom of the excavation with a weighted tape measure or a graduated steel pipe, were not feasible. The density of the mix in the trench would cause the weight to float, while the depths reached by the COW made the use of a pipe cumbersome and lengthy. The Contractor used a system composed of a steel graduated cable and a heavy weight capable to overcome the buoyancy effect of the slurry, which was utilized to check the depth and cleanliness of the excavation every 3 meters (10 ft), as required.

Finding a second method to verify the verticality of a panel proved even more challenging. As the SHS was the excavation fluid, the use of ultrasonic drilling monitors, the most common method to verify verticality, was excluded. The QC and QA teams concluded that the “plumb bob method” was the only viable method. The distance of the hydromill cable from the closest edge of the panel, and from one side of the guide-walls was measured every 3 m (10 ft). Trigonometric calculations would then provide the vertical deviation. As there were concerns regarding the consistency of the results, due to the dense fluid inside the trench, the

Engineer of Record and the Contractor agreed that priority be given to the data recorded by the hydromill monitoring system. Only if the two sets of data differed by more than 76 mm (3 in) new measurements had to be taken. It was also agreed that the frequency at which the hydromill triaxial sensors were calibrated be increased to two weeks.

Upon retrieval of the hydromill from the trench, three bulk samples (wet grab, WG) of SHS were collected at three depth intervals: between 0 and 12 m (0 and 40 ft), 12 and 24 m (40 and 80 ft), and within 3 m (10 ft) from the bottom of the excavation.

The QC team gathered the data collected in the field and recorded by the DMS during the installation of a panel to prepare the required as-built drawings, Panel Construction Report, and Detailed Verticality Analysis (DVA).

The Panel Construction Report was a thorough description of how the installation of a panel had been carried out. All the relevant aspects of the process were presented in a multi-page report. This was intended to provide a permanent record of the work done, which would be clear to anyone not involved with the project. The QC team developed the report, under the supervision and approval of the QA team and USACE, before the beginning of the test section of the project. The experience of the test section provided valuable insights to fine-tune the report to its final format.

The Detailed Verticality Analysis was composed of discrete transverse cuts, shown at 3 m (10 ft) intervals, along the full depth of a closure, defined as one primary panel and the two adjacent secondary panels. Any dimension that described the closure had to be reported, at each interval, to verify the compliance with the requirement of a COW having an effective width of at least 0.60 m (2 ft) along its entire depth. The data to perform the task was provided by the automated monitoring system installed on the hydromill. Originally the specifications called for the DVA to be provided as a series of drawings, each one representing one interval. Upon completion of the test section, the Contractor proposed that the analysis be performed by an internally designed Excel spreadsheet. The spreadsheet was submitted to the Engineer of Record and the QA personnel, along with the required drawings for comparison. After a brief review, the specifications were revised, with the requirement that the indications provided to produce the DVA be followed for the preparation of the final as-built drawings.

Sampling and testing program

The COW was required to have a maximum hydraulic conductivity of 1×10^{-6} cm/s, and an Unconfined Compressive Strength (UCS) at 28 days between 350 and 1240 kPa (50-180 psi) with no individual specimen strength being lower than 207 kPa (30 psi) or greater than 1380 kPA (200 psi). To verify that such requirements were met, a comprehensive sampling and testing program was developed.

Three bulk samples (wet grab, WG) of SHS were collected, right after a panel was completed, at three depth intervals: between 0 and 12 m (0 and 40 ft), 12 and 24 m (40 and 80 ft), and within 3 m (10 ft) from the bottom of the excavation. Normally, twenty-four cylinders were cast out of each bulk sample. The number went up to 32 in the panels randomly picked for QA testing. Two specimens from a primary panel were tested for UCS to demonstrate that the panel had reached the minimum strength of 20 psi required to proceed with the excavation of the adjacent secondary panels.

Verification core holes were drilled into two test section panels and 5% of the production panels, down to 0.60 m (2 ft) below the bottom of the cutoff wall. Each core had to demonstrate the homogeneity of the backfill material, and the quality of the contact between the bottom of the panel and the key layer. The minimum core recovery was fixed at 95%, and the Contractor was required to select 10 or 12 specimens, depending on the location of the panel. One half of the specimens was tested for UCS while the other half

underwent permeability testing (ASTM D5084). In situ permeability tests were not required by the specifications.

The test results showed a noticeable discrepancy between WG and core samples. The former produced always higher UCS and lower permeability values than the latter, some of which exceeded the 1 x 10^{-6} cm/s threshold during the test section (see Fig. 2).

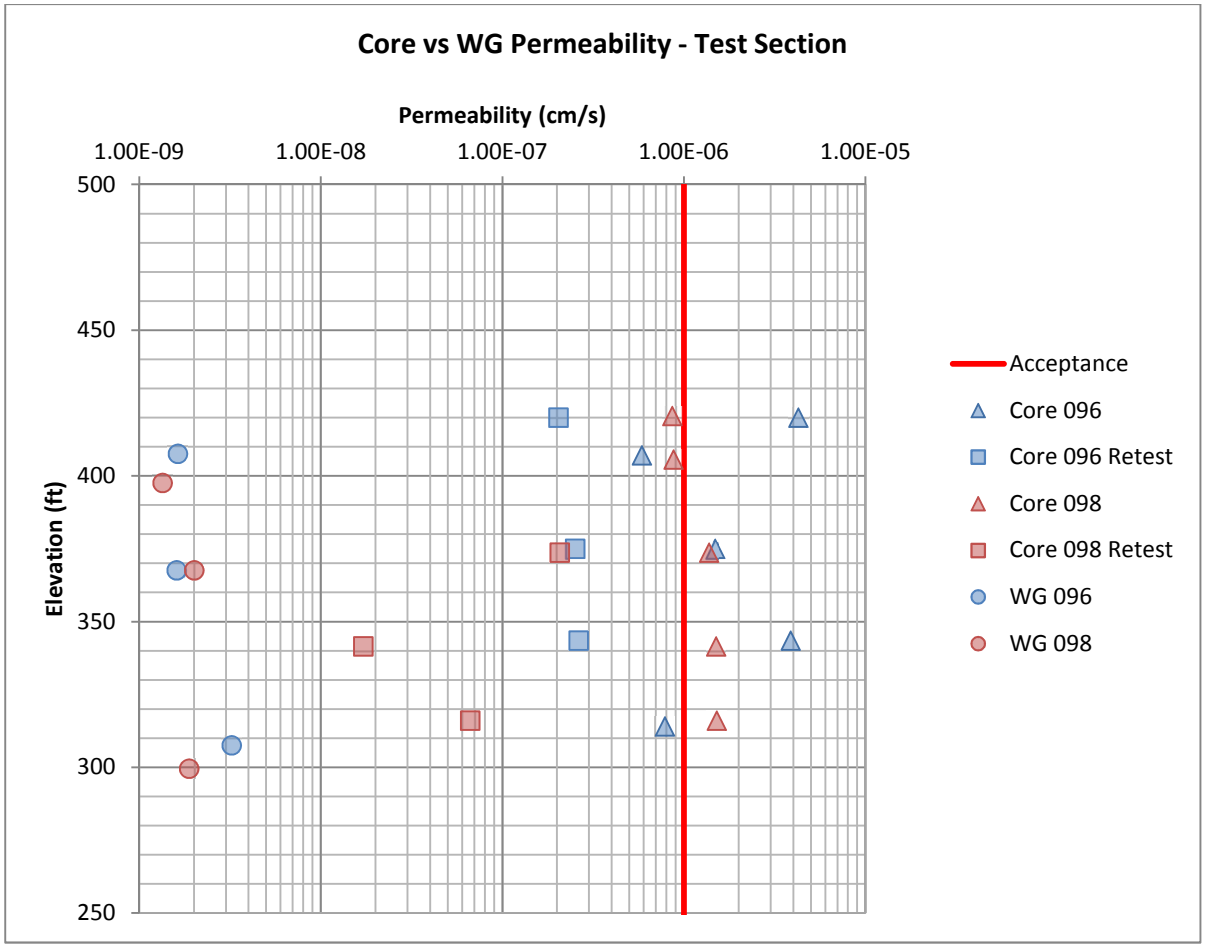


Figure 2: Test Section Permeability vs Depth

These results did not come as a surprise to the QC/QA teams. Publihed literature, as well as personal experience, indicate that even careful coring operations generally induce significant disturbance on the samples, and the borehole itself, that tend to produce lower UCS and permeability values than those existing in situ (Bruce and Mauro, 2010). This is particularly true for the permeability test, which can be greatly affected by even one very small fissure, caused by the tension forces commonly applied during sample recovery.

All the parties involved with the project acknowledge the issue and worked on finding a solution compliant with the ASTM test standard, before the beginning of production. On December 1st, 2015, the Engineer of Record held a meeting with representatives of both QC and QA teams, and the USACE. The participants agreed upon an addition to the testing procedure, proposed by USACE. A thin layer of membrane-compatible high vacuum grease was to be applied on the membrane, taking care not to transfer any grease

to the top or bottom ends of the specimen. Even though the procedure did not fully solve the problem, as shown in Fig. 3, the test results seemed to improve enough to generally comply with the specifications.

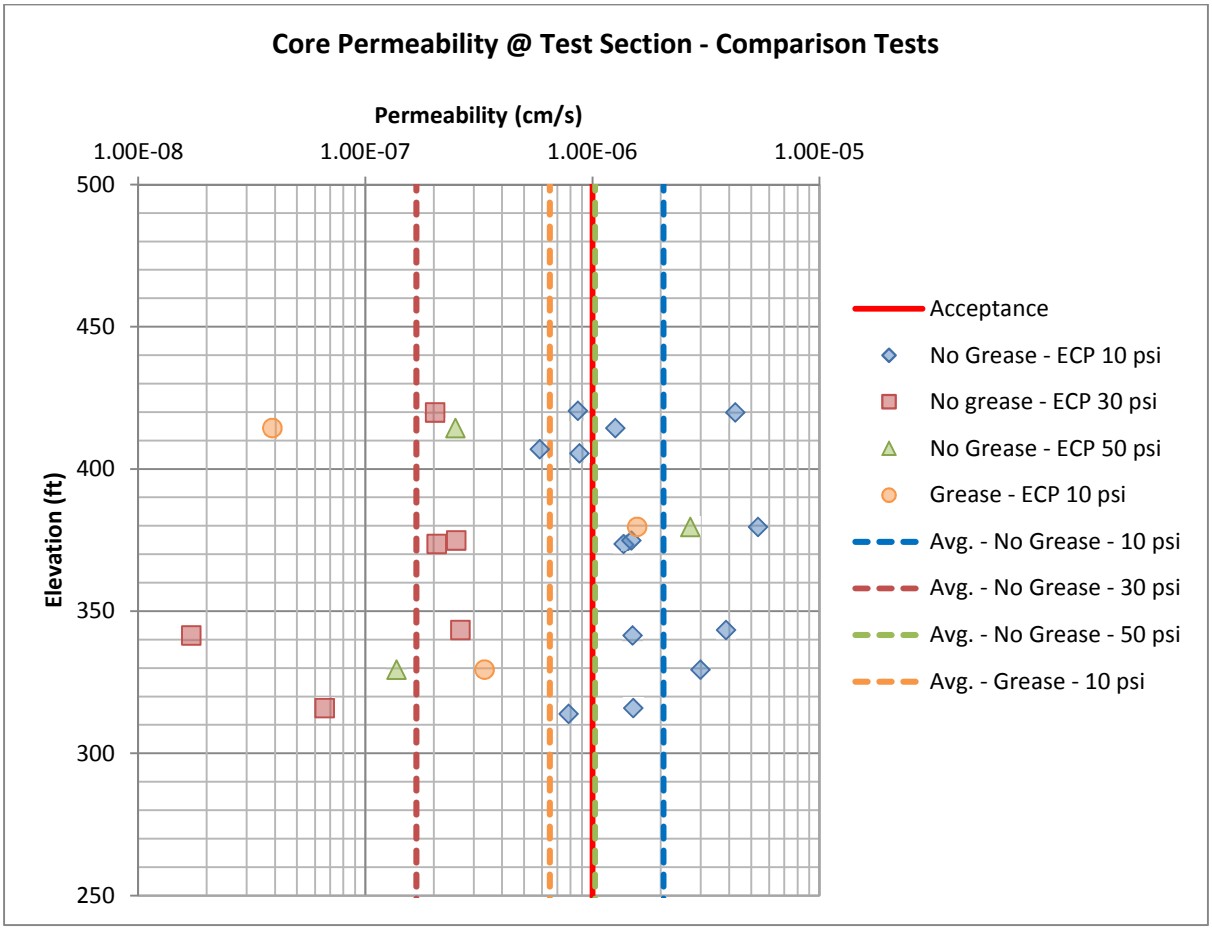


Figure 3: Test results produced by different testing procedures.

The WG samples, to the contrary, generated consistent and very low permeability test results, generally in the range of 10^{-9} cm/s. The low permeability of the specimens, in conjunction with the low prescribed hydraulic gradient (i.e.: 15), caused the tests to run for a very long time, up to several weeks, before results could be obtained. This, in turn, produced severe delays in the testing program and a shortage of available storage space.

A case by case analysis of the tests represented a first step toward a permanent solution. The Contractor would submit a Request for Information (RFI) with a package of all the tests which it was requesting an early termination for, and would wait for a written approval by the Engineer of Record to proceed.

After a couple of weeks, on February 11, 2015, the Engineer of Record issued a memorandum on the issue which included a Standard Operation Procedure for reporting permeability test results. Per the procedure a test could be terminated when it had been running for at least 5 days and all measurable intervals had values lower than $1x10^{-7}$ cm/s. Test results were to be reported as lower than $1x10^{-6}$.

The extensive test program requirements resulted in almost 450 WG samples collected, over 10,000 specimens cast, and 1,600 UCS tests and 400 permeability tests performed throughout the whole project. The six production panels and two test panels cored along the COW produced a total length of retrieved

samples that exceeded 300 m (1,000 ft). Sixty core samples were collected and tested during the production phase (30 for UCS, 30 for permeability).

The test results (at 28 days of age for WG samples and minimum 28 days of age for core samples) were overall in compliance with the specification requirements, with few exceptions (test results are summarized in Fig. 4).

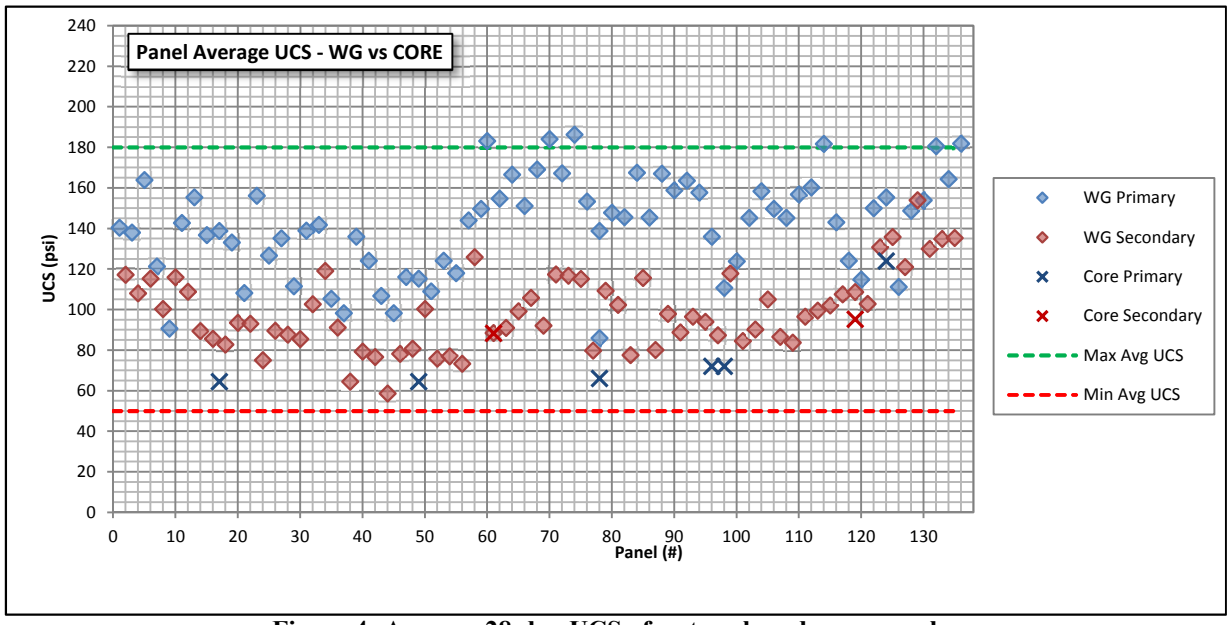


Figure 4: Average 28-day UCS of wet grab and core samples

CONCLUSIONS

The construction method produced a homogeneous and continuous cutoff wall meeting the required performance criteria.

The hydromill under SHS excavation method was successfully used for the installation of a cutoff wall, through layers of loose soils, to depths of up to 140 feet.

The thoroughness of the QC/QA program was considered necessary due to the complexity of the project. However, its implementation presented both the QC and the QA teams with great challenges.

The involvement of multiple parties (Owner, Engineer, Contractor, and USACE) with the decision making process was at times challenging, yet constructive criticism and a proactive attitude led to the successful completion of the project.

The involvement of the contractor during the design phase of a project (i.e.: the Early Contractor Involvement process used by the USACE for the LPV111 project, see Schmutzler et Al. 2012 and Bertoni et Al. 2015) could lead to a reduction of the costs and to a QA/QC program that is less challenging for both the contractor and the owner of the project.

ACKNOWLEDGMENTS

The authors would like to thank all the many people who contributed to the success of the project. Special thanks go to: Jo Tucker, Amr Ragy, Raul Horta, Dylan Pearson, and all the Barr Engineering personnel who in a way or another was part of the team.

REFERENCES

Bertoni M., Leoni, F.M., Schmutzler, W., and Filz, G., 2015, Soil Mixing for the LPV111 Levee Improvements, New Orleans: A Case History, Deep Foundations Institute 2015 Deep Mixing Conference, San Francisco, CA, USA.

Bruce, D.A. and Mauro, M., (2010). "*Quality Control & Assurance & Performance Verification for Cutoff Walls,*" Proceeding of Association of State Dam Safety (ASDSO), Officials Annual Conference 2010, September 2010, Seattle, Washington.

Granata, R., Mauro M., Santillan F., (2016). "*Diaphragm Walls for Seepage Control and Remediation: Three Case Histories,"* DFI International Conference on Deep Foundations, Seepage Control and Remediation," October 2016, New York, NY.

Granata, R., Tucker, J., Bertoni, M., Schmutzler, W., (2017), *"Construction of a Deep Cutoff Wall Along the Mississippi River at East Alton, IL"*, American Society of Civil Engineers (ASCE) Grouting 2017 International Conference, July 2017, Honolulu, Hawaii.

Grimley D.A and Lepley S.W., (2005). *Surficial Geology of Wood River Quadrangle Madison County, Illinois*; Illinois Preliminary Geologic Map IPGM Wood River-SG; Department of Natural Resources Illinois State Geological Survey.

Schmutzler W., Leoni, F.M., Bertero A., Leoni F., Nicholson P., Druss D. and Beckerle J., 2012, Construction Operations and Quality Control of Deep Mixing at Levee LPV 111 in New Orleans, 4th International Conference on Grouting and Deep Mixing, New Orleans, LA.

WES TM 3-430, (1956). *Investigation of Underseepage Mississippi River Levees, Alton to Gale, IL - technical memorandum* - Publisher: Waterways Experiment Station - Available Online: http://acwc.sdp.sirsi.net/client/en_US/search/asset/1004940.

HIGH CAPACITY HOLLOW CORE BAR PILES

Lawrence F. Johnsen, Sr. Consultant, GZA GeoEnvironmental, Inc., Trumbull, CT
Felix Ferrer, President, FNA Associates, Inc., Ridgefield, NJ and President, Stressbar Systems International, LLC, Ridgefield, NJ
Dino Tomasetti, Jr., President and Owner, The Laquila Group, Brooklyn, NY
Cassandra A. Wetzel, Associate Principal, GZA GeoEnvironmental, Inc., Manhattan, NY

ABSTRACT

A 17 story building was constructed at the Brooklyn Navy Yard on a site with a long history of development. Most recently the site supported a dewatering well and craneway to service two adjacent drydocks. The subsurface conditions generally consist of the following strata and approximate depths: miscellaneous fill and debris to 20 ft., organic soils to 35 ft., liquefiable sand to 45 ft., varved clay to 65 ft., glacial till to 95 ft. and gneiss bedrock.

Hollow core bar piles replaced 18 in. diameter caissons on a 1.67:1 basis. The resulting service loads on the hollow bar piles were 600 kips compression, 21 kips lateral, 180 kips tension and 450 inch-kips moment. The top 30 feet of the hollow bar was cased with a 16 in. x 0.375 in. Grade 50 steel pipe. The piles were socketed 6 feet into bedrock. An extensive load testing program confirmed the axial and lateral load capacities. The paper will also discuss some adjustments to the installation procedure based on the load test program.

PROJECT

The hollow bar piles were installed to support a 95,000 sf footprint, 17-story office building at the Brooklyn Navy Yard. The Brooklyn Navy Yard was first developed in the late 1700's to build merchant vessels. The federal government purchased the old docks and adjoining 40 acres in 1801. The site was an active U. S. Naval Shipyard from 1806 to its decommissioning in 1966. At its peak in World War II it employed 70,000 people, 24 hours a day. Since 1966 the property has been converted to private manufacturing and commercial activity.

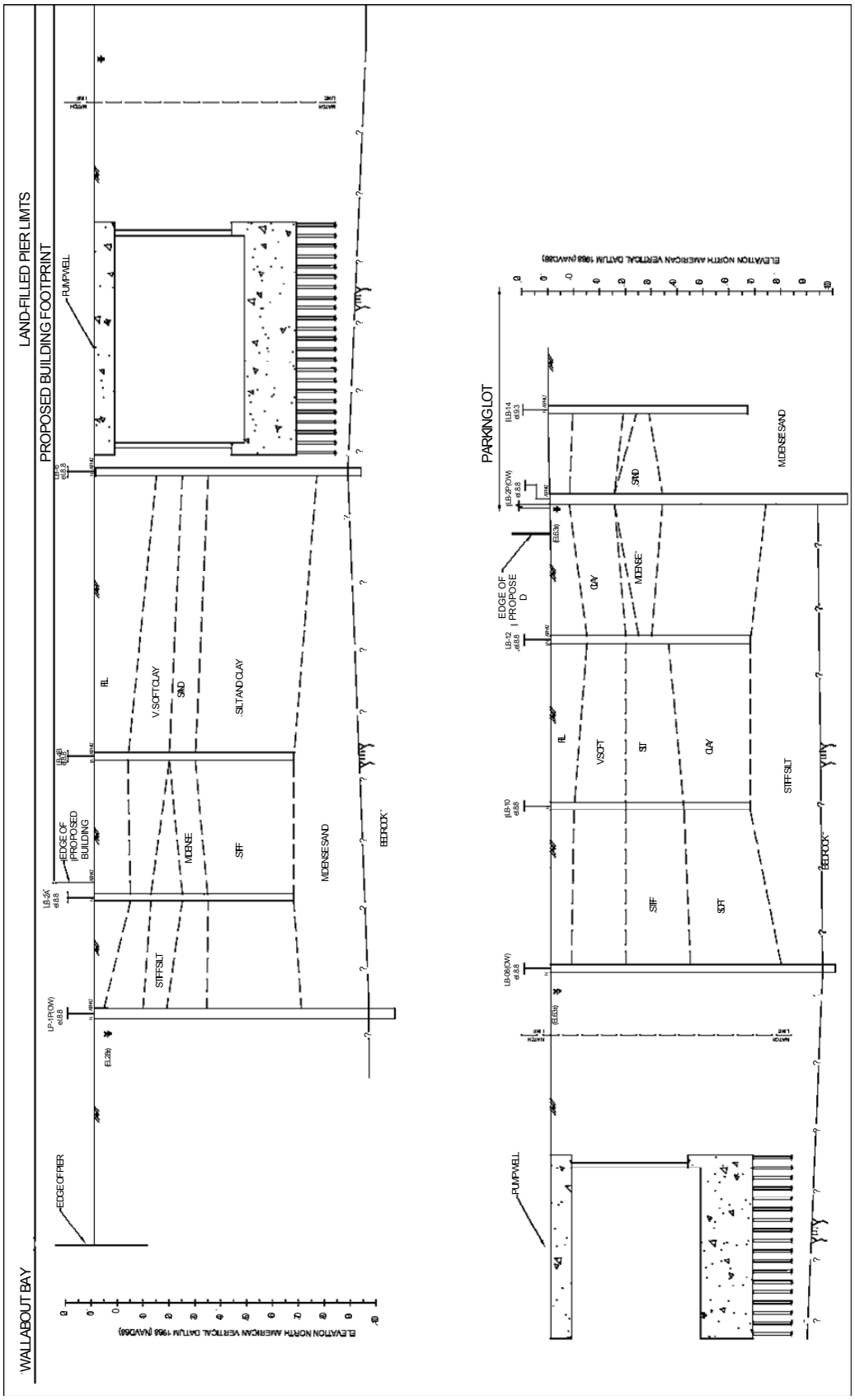
The site is located between Dry Docks 2 and 3. The adjacent drydocks extend 40 to 43 feet below grade. The drydock walls are restrained by tierods extending back to deadman anchors. The site is also underlain by piles that were installed to support rail lines and a craneway. The building footprint also covered an 85 ft. wide, 70 ft. deep dewatering well which had a thick slab. The structural engineer for the project, ARUP, designed the building to span over the dewatering well.

SUBSURFACE CONDITIONS

In September 2014, Langan Engineering conducted a geotechnical engineering study for the project. Figure 1 provides a subsurface profile through the long axis of the site.

The general soil profile was very erratic but generally consisted of miscellaneous fill and debris to 20 ft., organic soils to 35 ft., liquefiable sand to 45 ft., varved clay to 65 ft., glacial till to 95 ft. and gneiss bedrock. The fill contained numerous obstructions from the over 200 years of site development. The organic soils were mostly very weak and compressible organic silt. The depths and thicknesses of the varved clay, and sand varied

 © 2017 DFI Annual Conference, New Orleans, LA, USA



SUBSURFACE PROFILE

considerably across the site. A layer of dense glacial till covered bedrock. The bedrock was encountered at depths of approximately 100 feet.

Bedrock consisted of hard to very hard, white-gray-pink silimanite-garnet, micro plagioclase-biotite-muscovite-quartz with fresh to slightly weathered fractures. Core recoveries varied from 62 to 97 %, and averaged 83%. RQD's varied from 53 to 93% and averaged 66%.

The NYC Building Code defines bedrock as Hard sound rock (Class 1a), Medium hard rock (Class 1b), Intermediate rock (Class 1c) and Soft rock (Class 1d). Section 1810.7.3 of the 2014 NYCBC allows rock sockets in Class 1c or better bedrock to be designed with an allowable bond of 200 psi. The NYCBC requires Class 1c rock that is cored with a double tube, NX size diamond core barrel to have RQD's of 35percent or more. Weathered zones up to one inch thick are permitted as close as 1 foot apart.

PILE DESIGN

The structure was originally designed to be supported on 242 caissons with four sets of loads:

Caisson Type	Compression Load, kips	Tension Load, kips	Lateral Load, kips	OD, in.	Socket Length, ft.
A	1000	300	35	18	15
B	1000	0	35	18	15
C	1000	0	5	18	15
D	225	0	1	10	5

Hollow bar piles replaced Type A, B and C caissons on a 5:3 basis, and Type D caissons on a 1:1 basis.

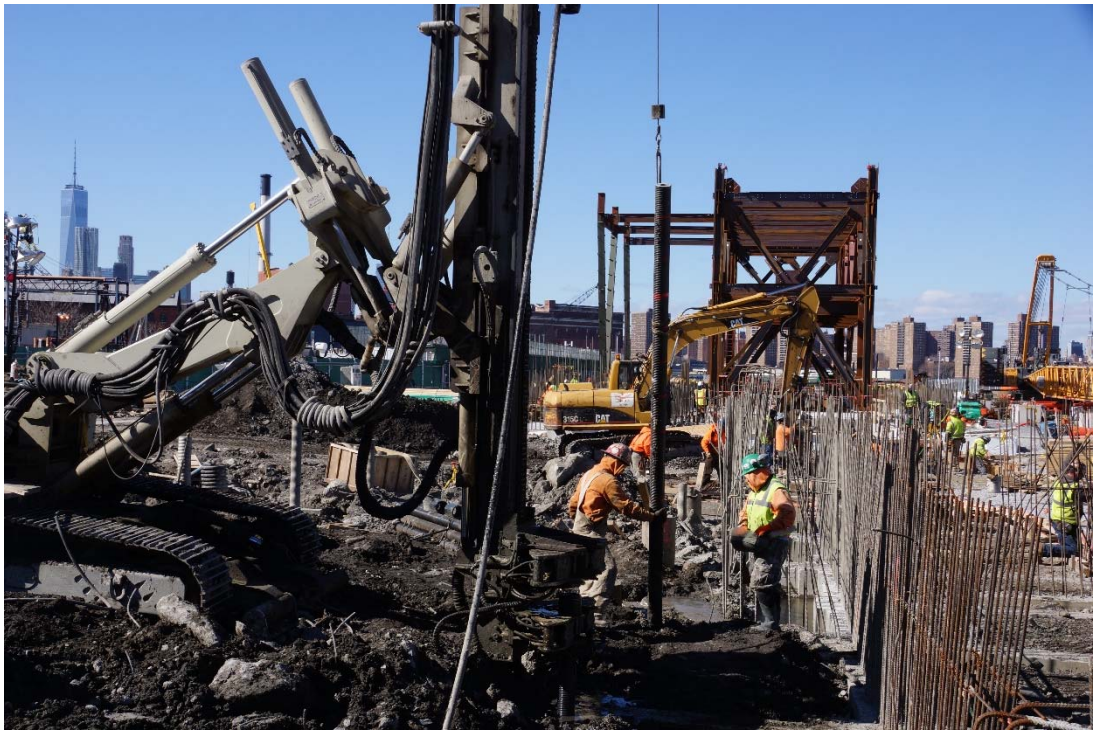
The 2014 New York City Building Code (NYCBC) does not specifically address hollow core bar piles, but its micropile section does refer to holes drilled with grout. The design was based on the micropile provisions of the code, which allow 0.33 f'c for grout and 0.4 Fy, not exceeding 32 ksi, for steel.

As an aid to the value engineering effort by GZA GeoEnvironmental and FNA Associates, ARUP provided a breakdown of lateral loads and identified pile caps that would resist the lateral loads in each orthogonal direction. The primary lateral loads on the building are wind, which has a force of 3000 kips in the north-south direction and seismic which has a force of 1000 kips in any direction. The structure transfers the north-south lateral load to the building core and 12 pile caps, and the east-west lateral load to the building core and 18 pile caps. This resulted in 224 hollow core bar piles resisting the wind force of 3000 kips and 254 hollow core bar piles resisting the seismic force of 1000 kips. Langan Engineering conducted a liquefaction effective-stress ground response analysis to estimate pore water pressure ratios that could develop for three of the soil layers. Those values were incorporated into the lateral load analyses.

PILE MATERIALS

The TB 130/60 hollow core bar by Stressbar Systems International, LLC has a nominal diameter of 5.11 inches, area of 14.81 in^2, ultimate strength of 1785 kips and tensile yield point of 1180 kips (80 ksi). The hollow core bar was fitted with a T-130 drill bit with J teeth to core into the gneiss bedrock. The hollow core bar was provided in 13.2 foot (4 meter) lengths and connected with couplers. Photograph 1 shows the TB 130/60 hollow core bar being added to the pile.

The grout consisted of a neat cement grout with a water:cement ratio of 0.49. The grout was mixed on site with a Scheltzke mix pump unit. Grout strengths typically varied from 5500 to 7500 psi at 28 days. The design compressive strength was 4500 psi. Grout pressures varied from 750 to 1500 psi.



Adding Hollow Core Bar Section
Figure 2

The 16 in. x 0.375 in. steel casing was 30 feet in length with no welded or threaded joints and a yield stress of 50 ksi. For Type B, C and D piles the casing was shortened to 15 feet.

INSTALLATION PROCEDURE

Pile installation began with a Comacchio MC22 drill rig drilling the hollow core bar to its full depth. Grout was mixed and pumped from a Scheltzke mix pump unit during the drilling of the hollow core bar. After the hollow core bar was fully installed and grouted, the 30 foot long casing was picked up by a Cat 349E excavator and set into the grout surrounding the hollow core bar. The bucket of the excavator was used to push the casing when required. The hollow bar bit formed a grouted hole of approximately 15 in. diameter in soil and 10 in. diameter in bedrock.

The initial static load testing did not meet the NYCBC criteria. An evaluation of the load test results showed the pile to have been socketed into a boulder, and the pile to have a lower composite modulus than what the 15 inch diameter of grout and bar was calculated to provide. The contractor then modified his installation procedure by lengthening the rock socket to six feet and slowing the drilling rate to create a more consistent installed grout volume. A grout factor of 140 per cent of theoretical grout placement was adopted for quality control. Socket lengths varied from 6 to 16.5 feet based on rock quality as judged by penetration rate.

STATIC LOAD TESTING

Six static compressive load tests were performed in accordance with ASTM D1143 on Type A and B piles to maximum test loads of 1200 kips. Two static compressive load tests were performed on Type C piles to maximum test loads of 450 kips. Pertinent data for the six Type A and B are tabulated below. Load settlement plots are provided in Figures 3a-3f.

Test Pile Summary Table

Pile No.	Pile Length	Casing Length	Type	Grout Factor	Rock Socket Length
46	96.4 ft.	30 ft.	A	1.75	6 ft.
51	93.7 ft.	15 ft.	B	1.83	8 ft.
76	80.1 ft.	30 ft.	A	1.23	6 ft.
158	98.1 ft.	30 ft.	A	1.01	6.9 ft.
219	105.5 ft	30 ft.	A	1.95	6 ft.
309	84.7 ft.	30 ft.	A	1.95	3.25 ft.

Sister bar strain gages were installed in the initial test piles after the pile reached its final depth. The bars were placed in the annular space between the bar and soil. Installation of the strain gages below the 30 ft. cased length was difficult, with several refusing before their desired depth. The inside bar diameter of 2.36 inches did not provide sufficient space to insert a telltale.

Section 1808.4.1.5 of the 2014 NYCBC limits the allowable load to the lesser of: (1) 50% of applied load causing a net settlement of not more than 0.01" per ton of applied load, where net settlement is the recorded pile top settlement after rebound; and (2) 50% of applied load causing a net settlement of 0.75", where net settlement is gross settlement minus calculated elastic shortening although net settlement can be measured with a telltale. As mentioned above, telltales could not be installed and the pile exhibited a lower than theoretical elastic modulus. However, the pile top settlement after rebound was less than 0.75 in. Since the test was run in compression, the settlement of the pile tip settlement cannot be greater than the pile top.

Based on the results of the static load test program, the allowable compression load was reduced to 520 kips.

LATERAL LOAD TESTING

Two lateral load tests were performed in accordance with ASTM D3966. Since the pile to pile cap connection was designed for partial fixity, and the test piles were not embedded, the lateral load tests were used to verify the soil parameters in the lateral load analyses. The analyses indicated that 0.5 in. deflection would occur at 15 kips, and 1 in. deflection at 25 kips.

Both lateral load tests met the deflection criteria and were taken to larger loads to better understand the actual factor of safety.

SUMMARY

The 1200 kip successful compression load test is the largest ever supported by a hollow core bar. The design load was reduced from 600 kips to 520 kips due to differential settlement concerns. The extensive load testing program resulted in modifications to the initial design and installation procedures.

The load test results on Pile #309 indicated that the pile was set in a boulder. Subsequently, the initial socket length of 3 feet was increased to 6 feet.

The initial load test curves were steeper than expected. This was due to either the piles not achieving their full diameter or the grout/soil mixture having a lower elastic modulus. Subsequently, a minimum grout factor of 1.40 was established and the contractor reduced the penetration rate.

Installation of strain gages was very difficult beyond the 30 foot cased section. Consequently, the effects of residual stresses on net settlement after rebound could not be quantified.

ACKNOWLEDGMENTS

FNA Associates initially proposed the value engineering approach to Laquila Construction. FNA designed the piles for axial loads. GZA GeoEnvironmental, Inc. performed lateral load analyses to determine the number of piles required to resist the lateral loads. The construction services division of GZA instrumented the test piles.

ARUP Engineers designed the building and foundations. Langan Engineering conducted the geotechnical investigation and provided field services during construction.

The success of the project was due to all parties working together to provide the most economical foundation solution for the owner.

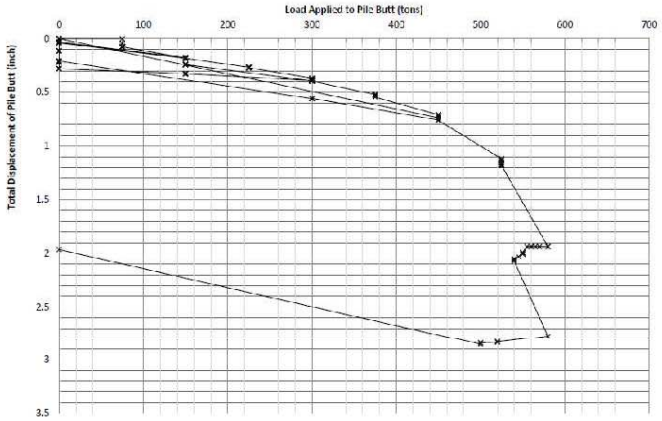


Figure 3a: Static load test on Test Pile #309 - First Test

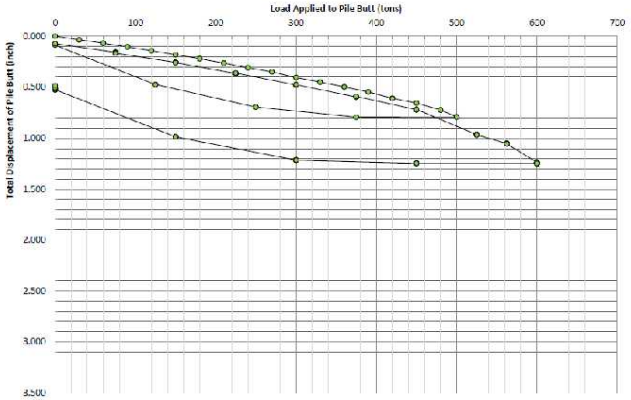


Figure 3b: Static load test on Test Pile #309 - Second Test

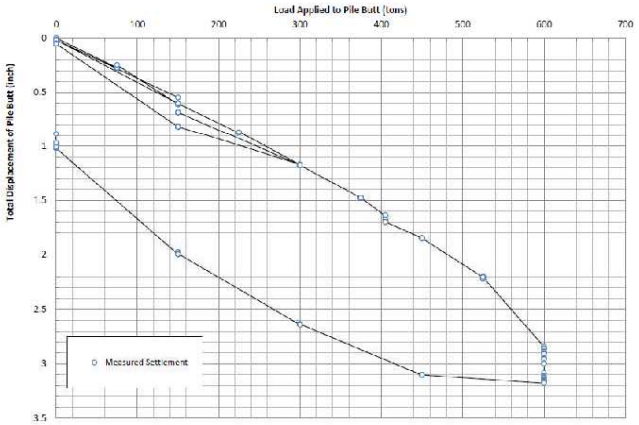


Figure 3c: Static load test on Test Pile #76

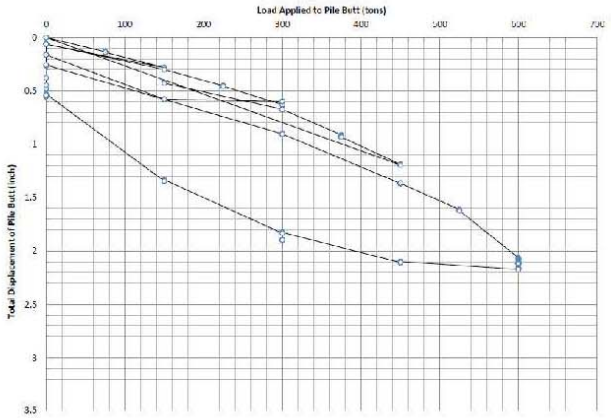


Figure 3d: Static load test on Test Pile #51



Figure 3e: Static load test of Pile #46

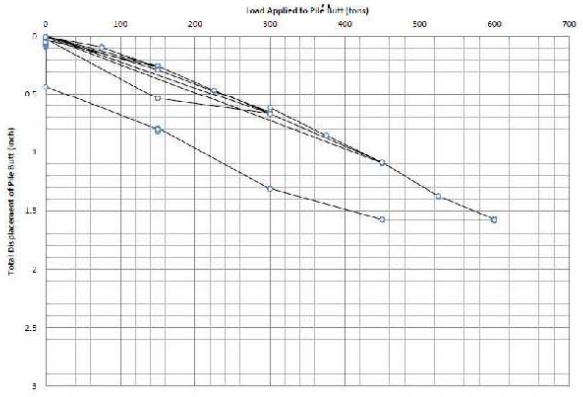


Figure 3f: Static load test of Pile #219

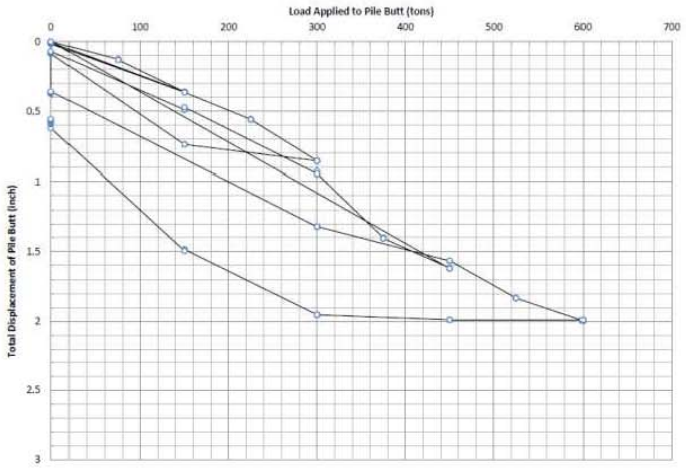


Figure 3g: Static load test of Pile #158

CASE STUDY: MGM CASINONATIONAL HARBOR, WASHINGTON, DC

DISPLACEMENT CAST-IN-PLACE PILES IN COASTAL PLAIN SOILS

James P. Racine, M.S.C.E., P.E., Senior Project Engineer, ECS Mid-Atlantic, LLC, 14026 Thunderbolt Place, Suite 100, Chantilly, Virginia, USA, Tel: 703-471-8400: jracine@ecslimited.com

Karl A. Higgins, III, M. Eng., P.E., D. GE, Chief Engineer, ECS Mid-Atlantic, LLC, 14026 Thunderbolt Place, Suite 100, Chantilly, Virginia, USA, Tel: 703-471-8400: khiggins@ecslimited.com

ABSTRACT

Displacement Cast-in-Place (DCIP) piles are not a common deep foundation type in the Washington, DC Metro Area market. As a result, less regional data is available for these foundations compared to other alternate deep foundation types. Displacement cast-in-place piles (DCIP) differ from traditional Auger Cast-In-Place (ACIP) piles in that the pile annulus is formed by pushing a partially-flighted, auger bit to depth via a large mandrel. The auger bit includes a displacing body near the bottom of the tooling. Therefore, little to no spoils are generated during installation and the soil around the annulus is largely densified in-place due to the displacing body being slightly larger than the mandrel it is attached to.

Due to this densification, one would expect that the theoretical DCIP capacities (compression or tension) would be greater than an ACIP pile (assuming a pile of similar length and diameter). After 20 static load tests and the installation of over 6,000+ piles on the MGM National Harbor Casino Project, the differences in pile support characteristics between DCIP and ACIP piles of same size and depth was small. The performance of both pile types depended on the density and type of soil within the bearing stratum. In some early cases of DCIP use, the performance exceeded expectations and appeared to be more in line (or better) than typical capacities obtained from driven displacement piles. Other times, the tip elevations could not be achieved or were so difficult to achieve that installation delays occurred and/or significant additional engineering effort was required to address piles short of their requirement embedment.

This paper will discuss the limitations of DCIP pile installation in dense Coastal Plain soils and will present the lessons learned during this project. The paper will also compare the DCIP pile type to both conventional ACIP and driven displacement piles utilizing regional and site-specific load test and installation data.

 © 2017 DFI Annual Conference, New Orleans, LA, USA

INTRODUCTION

The 1.3 Billion dollar MGM National Harbor Casino project opened in the winter of 2016. The flagship casino features 125,000 square feet of casino floor space, a 24-story hotel, and over 35,000 square feet of combined retail, restaurant, and meeting space. All this is located over an impressive 850,000 square foot (19.5 acre) footprint. The building is notched into the hillside, with several lowest floor elevations ranging between EL. 70 to 120 ft.

While the building footprint ranks with some of the largest ever in the DC-Metro area, the geotechnical challenges were quite common to the urban and Coastal Plain geology. Had the project been constructed with foundations common to Washington, DC such as drilled shafts, ACIP piles, or driven piles, this paper may not have been written. Fortunately, the project was initially (but not completely) constructed on Displacement Cast-In-Place (DCIP) piles, which are a drilled/pushed, cast-in-place deep foundation-type and are not commonly seen in the DC area at this time. This paper will discuss the limitations of DCIP pile installation in dense/hard Coastal Plain soils by using the lessons learned on the MGM National Harbor Casino project. Additionally, the DCIP foundations will be compared to both conventional auger cast-in-place (ACIP) and driven displacement piles (pre-cast, pre-stressed concrete (PPC)) utilizing regional and site-specific load test results.

DISPLACEMENT CAST-IN-PLACE PILES

According to Basu and Prezzi (2009), the DCIP (synonymous with Drilled Displacement, DD) pile type is considered between a partial- and large-displacement pile. That is, it provides more lateral densification than a drilled or bored pile, but less densification than a driven, full-displacement pile. While several pile types occupy the "partial-displacement" category, the DCIP pile has evolved into a sub-category of its own thanks to continued advancements in rig power and crowd pressure. Fig. 1 depicts the categories of non- to large-displacement piles as described by Basu and Prezzi (2009).

The DCIP pile, similar to other deep foundations, gets its capacity primarily through skin-friction and end bearing components. However, instead of a continuously-flighted auger, the tooling includes a simple displacement body followed by a few cutting flights and a smooth steel mandrel/casing. The tooling is depicted in Fig. 2.

As the displacement body (which is slightly larger than the rest of the tooling) is advanced, the adjacent soils are compressed into the borehole sidewalls and densified in place. The pile therefore generates little to no spoils and also has the added benefit of densifying the load bearing layers, which in general, increases the overall axial capacity of the pile.

PROJECT EXPLORATION AND GEOLOGY

A robust subsurface exploration consisting of 57 Soil Borings with SPT samples(75 to 100 feet), 20 Cone Penetrometer Test (CPT) soundings (20 to 100 feet), 6 Test Pits (up to 15 feet), and several Geophysical Surveys was conducted. Based on this exploration, 30 to 50 feet of clayey fill material was observed across the entire site due to filling operations some 30+ years ago. In the eastern two-thirds portion of the site, dense/hard Potomac soils of Cretaceous age were encountered immediately below the fill layers. In the western one-third portion of the site, a 20 to 50 foot thick loose to dense alluvial sand layer of Quaternary age was observed before the Potomac soils were encountered. A representative cross section

through the middle of the site can be seen in Fig. 3. The finished floor elevations (red line) and soil groups have been overlaid on this data as well.

INITIAL RECOMMENDATIONS

The casino is a unique structure with a plinth base of 2 to 5 levels of below-grade parking supporting a large gaming and entertainment level that spans the entire site. A relatively small (in footprint), 24-story hotel (purple trapezoid seen on Fig. 4) is located interior of the P5 and P6 level plinth areas. ECS provided several foundation options for the plinth and hotel structure. Due to the thick undocumented fill layers below the finished floor elevations, shallow foundations were not feasible. Instead, deep foundations consisting of 150 ton, driven, pre-stressed, pre-cast concrete (PPC) driven piles were primarily recommended. Driven PPC piles were used successfully and extensively for the neighboring National Harbor development built between 2005 to 2008. Approximately 100 dynamic test piles were performed for these projects in similar soil conditions.

An alternate deep foundation-type consisting of auger cast-in-place piles (ACIP) was also provided. Deep foundation recommendations were provided for both the plinth and hotel areas. Table 1 below summarizes the various deep foundation recommendations provided in our geotechnical report.

Table 1: Summary of Foundation Options

Location	Foundation Type	Range of Lengths (feet)	Dimensions (inches)	Capacity (tons)
Hotel Tower	Driven PPC	54 to 64	14 Square	150
Hotel Tower	ACIP	64 to 74	16 Diameter	150
Plinth	Driven PPC	54 to 70	14 Square	150
Plinth	ACIP	64 to 80	16 Diameter	150

FOUNDATION CHOICE

After our report was submitted, we awaited the start of the project. A couple months before the start of the project, we were informed that a DCIP pile alternative was being considered by the client. At the client's request, we evaluated the proposed alternative. We noted several key concerns with using a DCIP pile in this geology including: 1) ability to reach the design tip elevation and bearing stratum embedment due to the presence of dense/hard soils, 2) ability of achieving a uniform tip elevation due to the varying density of on-site soils, and 3) more costly and slower methods of load testing than driven piles. Each of these concerns would ultimately be realized. Despite our concerns, the project moved forward with the

alternative foundation type, DCIP piles. The owner made the foundation type decision independent of our involvement.

PROJECT STARTS OFF WELL - WESTERN PORTION (P1) OF THE SITE

Despite the foundation changes, the project started off smoothly. Two initial load tests were conducted at the western portion of the building at the P1 plinth area. The test piles were installed at EL. +68 and had lengths between 45 and 55 feet (nominal 14-inch diameter, displacement cast-in-place). Based on the nearby boring (ECS-2), the test piles were installed through the upper fill materials and had an embedment into the natural, loose to medium dense, alluvial soils of 13 and 23 feet for TP-1 and TP-2, respectively.

In the western portion of the plinth and at this lower elevation of the site, alluvial soils were present below the fill overburden material. Sands (SP and SM) with SPT N-Values ranging from predominately 10 to 26 blows per foot, indicating loose to medium dense relatively densities, were observed within the pile bearing stratum. A representative cross section (Section A-A) can be observed in Fig. 5.

The load tests results were relatively similar as geotechnical failure was not reached; the maximum load frame capacity of 400 tons was reached on both piles with less than 0.2 inches of downward deflection measured at the design load of 150 tons (300 kips). Because the piles did not fail geotechnically, we did not learn much about this pile type's ultimate pile capacities (shaft friction and end bearing). The load tests for TP-1 and TP-2 can be seen in Fig. 6. Please note that strain gauges were not used for any of the load tests for this project.

Based on this information, the required lengths for 150 ton piles in the P1 area were determined; tip elevations for this area ranged from EL. +16 to EL. +29 feet or embedment into natural soils (below the fill) on the order of 15 to 18 feet. We back-calculated shaft friction and end bearing values from the load test results using our judgment from nearby driven-pile projects. While we would have preferred to have instrumented load tests, these requirements were not part of the contract between the owner and contractor. These production embedment lengths were then compared to the embedment lengths estimated within the geotechnical report in Table 2 below.

Table 2: Comparison of P1 level pile lengths

Location	Foundation Type	Diameter (inches)	Length Range (feet)	Bearing Stratum Embedment (feet)	Method of Analysis
P1 Level	DCIP	14	35 to 48	15 to 18	Based on Load Tests
P1 Level	Driven PPC	14	64 to 69	40 to 45	Based on Calculation
P1 Level	ACIP	16	74 to 79	50 to 55	Based on Calculation

Based on this summary, it is clear that the DCIP piles outperformed preliminary estimates for both the PPC and ACIP piles by a reduction in pile length of 30 to 40 feet. It is possible that PPC dynamic or ACIP static load testing may have resulted in shorter lengths than initially estimated from local correlations. The fact remains DCIP piles performed well in this portion of the structure. Pile installation rates in the plinth P1 area (western portion of the building) were generally very good with start-to-finish times varying between 5 to 10 minutes per pile. Production in the P1 area was generally 25, 40-feet long piles per day with some days reaching counts of 40 piles in a single days' work. This pile installation rate was perhaps 1.5 to 2 times faster than similar length PPC or ACIP piles installed in this geographic area.

Based on the shorter piles and the relatively fast production times, it is clear that DCIP piles perform very well in loose to medium dense sandy alluvial soils. This success is likely due to the densification action of the displacing body in loose to medium dense granular soils.

HARD DRILLING SETBACK

As the project moved eastwards from the plinth P1 level to the P3 level, the bearing stratum began to transition from loose to medium dense predominately sandy alluvial materials to medium dense to very dense/ very stiff to hard Potomac Formation soils. Looking back at the Figure 2 cross section above, one can see a transition generally occurring between the P1 and P3 finished floor elevations. The graphic (Fig. 7) depicts the transition zone in better detail. ECS-25 is emblematic of a typical urban Potomac Formation soil boring; after the fill soils, medium dense to very dense SILTS (ML) with N-Value blowcounts of 19 to 65 blows per foot are encountered.

The Potomac Formation materials are associated with Cretaceous Age estuarine/deltaic deposits which are 70 to 150 million years old. The materials are overconsolidated (10-15 OCR), generally dense to very dense or very stiff to hard, and contain sands, clays, and gravels. Potomac soils are encountered below the surficial fill material on-site shortly after entering the P3 level to the far eastern end of the project.

It was within these denser/harder Potomac materials where the first drilling issue was encountered; the issue consisted of very hard drilling conditions that took a significantly longer time to drill through to obtain the target tip elevation. Drilling times slowed by fourfold; install times of 20 to 30 minutes for a 50 foot long pile were recorded with some piles taking up to an hour to complete. The displacing tool bits were wearing down at a high rate requiring frequent welding rehabilitation/buildup. The contractor tried to improve the speed by proposing a predrilling program and establishing a shallower termination criterion. Predrilling would require a separate rig.

A production pile that was short of required bearing stratum embedment was load tested to determine if a reduction in embedment based on hard drilling was feasible. This resulted in a successful load test and a supplemental installation criteria of: piles tips can be terminated with a minimum rotary crowd pressure of 200 bars, advancement rate of 2 minutes per foot (or slower) and a defined tip embedment of 5 ft into these dense soils. A shallow termination criterion was helpful at some locations, but required significant additional engineering oversight to approve piles short of the design tip elevation and bearing stratum embedment that was previously established by load testing.

Our concerns regarding the ability to achieve the required embedment into the dense to very dense sands and very stiff to hard clays were realized. It was clear that DCIP piles have trouble reaching design tip

elevations (and presumed bearing stratum embedments) within dense to very dense granular soils as well as very stiff to hard cohesive clays. The required pile type embedments were established by prior load testing and piles that were able to achieve these embedments. In other words, not all P3 areas exhibited hard drilling. In the next section, we will compare the DCIP production lengths to the proposed driven PPC and ACIP pile designs in the Potomac Formation.

DCIP INSTALLATION IN THE POTOMAC FORMATION

Several load tests were conducted in the P3 area of the site, which was the largest area of the casino. Five axial compression tests were conducted in the P3 area with embedments into the Potomac Formation ranging from 15 to 27.5 feet. Ultimate pile capacities ranged from 323 to 389 tons, which were noticeably lower when compared to the load tests of piles embedded in the sandy alluvial materials of the P1 area. The required ultimate load was 300 tons. The load tests results are summarized in the Table 3 below. Please note that all of the piles, with the exception of TP-16, were tested to geotechnical failure.

Table 3: Summary of P3 area DCIP load tests

Test Pile Number	Pile Length (feet)	Recorded Deflection at Design Load of 150 tons (inches)	Penetration into the Potomac Formation (Feet)	Pile Tip Elevation (feet)	Ultimate Pile Capacity (tons)
TP-6	50	0.26	19.0	+47.6	345
TP-7	60	0.26	29.0	+38.6	327
TP-16	65	0.19	15.0	+37.0	323
TP-17	77.7	0.22	27.5	+24.5	389

Based on these load test results, design lengths ranging from 46 to 58 feet (bearing stratum embedment of 23 to 28 feet) were selected for the P3 area. Table 4 below compared the final design lengths for the DCIP piles versus the estimated lengths for PPC and ACIP piles.

Table 4: Comparison of Foundation Designs in the P3 area

Location	Foundation Type	Diameter (inches)	Length Range (feet)	Method of Analysis
P3 Level	DCIP	14	46 to 58	Based on Load Tests
P3 Level	Driven PPC	14	54	Based on Calculation
P3 Level	ACIP	16	64	Based on Calculation

Based on the data in Table 4, it is clear that the DCIP piles match up well with the assumed driven PPC and ACIP pile lengths in dense and hard Potomac Sands and Clays. We believe this is due to the fact that the Potomac Formation soils are by their nature, already dense and therefore little to no additional

densification is occurring due to the displacing body. These results, coupled with the hard drilling issues noted within this Formation, may make one reconsider recommending DCIP piles bearing in the Potomac soils.

SWITCH TO ACIP PILES

The contractor continued with the difficult drilling conditions for the remainder of the P3 areas. As the contractor was preparing to mobilize to the Hotel footprint and the P5/P6 area, an alternative pile type was proposed to increase production. The contractor recommended that full-auger flight ACIP piles be substituted for DCIP piles. ACIP piles were advantageous for this project in that they could more easily be installed through dense/hard layers to achieve both the target tip elevation and also a uniform bearing stratum embedment. The switch was also desirable as the contractor could also utilize the same rig with only a change to the tooling; no additional mobilizations were required. We requested additional load testing to confirm the capacities utilizing the alternative installation technique, which as one recalls is considered a non-displacement to partial-displacement pile. A total of six static load tests (three DCIP and three ACIP) were conducted in the P5/P6 area. These results are summarized in Table 5 below.

Table 5: Load Tests in the P5/P6 Area

Pile Type	Test Pile (TP) Number	Embedment into Bearing Stratum (feet)	Ultimate Failure Capacity (tons)
ACIP	TP-35	27	360
	TP-42	23	375
	TP-43	27	375
DCIP	TP-30	37	400
	TP-31	27	300
	TP-32	16	285

Based on this summary, one can see that with approximately 20 to 25 feet of embedment into the Potomac Formation soils, the design ultimate capacity of 300 tons is achievable for either the ACIP or the DCIP pile type. In fact, the differences in pile support characteristics between each pile type appear negligible, and consistent with our earlier conclusion that the Potomac soils don't improve in strength (i.e., shaft friction and end bearing) by densification. Based on these load test results, the final design lengths were established. The design lengths were then compared to the estimated length in the geotechnical report.

Table 6: Comparison of Foundation Designs in the P5/P6 area

Location	Foundation Type	Diameter (inches)	Length Range (feet)	Method of Analysis
P5 Level	DCIP	14	51 to 61	Based on Load Tests
P6 Level	DCIP	14	43 to 55	Based on Load Tests
P5 Level	ACIP	14	60	Based on Load Tests

Location	Foundation Type	Diameter (inches)	Length Range (feet)	Method of Analysis
P6 Level	ACIP	14	62	Based on Load Tests
P5 Level	Driven PPC	14	54 to 64	Based on Calculation
P6 Level	Driven PPC	14	54	Based on Calculation
P5 Level	ACIP	16	64 to 74	Based on Calculation
P6 Level	ACIP	16	69	Based on Calculation

In a similar fashion as the P3 level results, one can see that in the Potomac Formation soils, the production lengths compared very well between ACIP, driven PPC, and DCIP piles. The lengths also compared very well with the initial static capacity estimates.

RESIDUAL SOIL STRENGTHS

Another theory for similarities in pile shaft friction and end bearing for both pile types (DCIP and ACIP) is that the DCIP piles, based on their method of installation, may have densified the bearing soils yet also resulted in residual shear strengths vs. peak strengths. For example, the penetration rate for DCIP piles dropped as low as 2-3 ft/minute with a rotation of 9-15 RPM in the Potomac Bearing soils, while ACIP piles in the same stratum were 5-12 ft/min and 18-20 RPM. DCIP penetration rates in the bearing stratum for the Alluvial soils was 10-18 ft/min with a rotation of 10-20 RPM by way of contrast. Please recall also the excessive bit wear on the DCIP tooling in the Potomac formation and the fact that DCIP tools displace vs. remove soil – both items that result in repeated soil disturbance at the concrete to soil interface. It is surmised that the slower penetration rate (and same RPM) values exhibited by the DCIP piles in the Potomac formation resulted in residual vs. peak strengths due to excessive rotation in the bearing stratum. The analogy of a ring shear (RST) or repeated direct shear (DST) test used to measure peak followed by residual shear strengths could apply (see Fig. 8).

CONSTRUCTABILITY ISSUES

In addition to the hard-drilling and excessive tool wear with DCIP piles, there are two other constructability issues worth considering when evaluating DCIPs for a project: 1) size/weight of rig and 2) installing piles to cut-off elevation. The rigs used to install DCIPs for this project were large, tracked machines weighing some 80 tons. Large vertical masts are needed to push the deep mandrels. These machines require a firm base while installing piles to avoid concerns about rig instability/tipping. As such, for this project, a 4-ft thick, reinforced aggregate mat had to be installed anywhere the rig worked. This required a large import of aggregate material that was ultimately contaminated with soil and not easily reusable after the piles were installed. Further, there was a desire to install piles flush with the top-of-slab subgrade versus to the bottom of pile cap some several feet deeper. This resulted in a need to dispose of the upper portion of the hardened concrete piles upon pile cap excavation (not an easy task multiplied by 6,000). From our observations, piles that were completed above the traditional “cut-off”

elevations risk the potential of the reinforcing cage not being installed at the right elevation, particularly when it's difficult to see the final position of the cage when it's covered with 5-6 feet of concrete.

SUMMARY AND CONCLUSIONS

Based on the significant amount of subsurface testing and static load testing information, DCIP piles perform very well in loose to medium dense sandy soils associated with Alluvial Coastal Plain deposits of Quaternary age. As the project transitioned into the dense, Cretaceous-aged Potomac soils, the DCIP piles had difficulties reaching the target tip elevation without significant changes to the installation procedures and criteria. Delays in pile installation ensued due to slower installation time and pre-drilling needs. In the Potomac Formation, where the soils are already dense and over-consolidated, the displacing nature of DCIP piles does not result in improvement in pile capacity as is generally implied. It is also surmised that residual shear strengths were developed due to excessive rotation in the bearing stratum. This fact was proven when both ACIP and DCIP piles were load tested in same P5/P6 area with essentially the same results. When you factor in the drilling difficulties and potential for delays, either ACIP or driven PPC piles may be better options.

REFERENCES

1. Basu, P. and M. Prezzi, Design and Applications of Drilled Displacement (Screw) Piles. Publication FHWA/IN/JTRP-2009/28. Joint Transportation Research Program, Indiana Department of Transportation and Purdue University, West Lafayette, Indiana, 2009.

2. Prasenjit Basu, Monica Prezzi, and Dipanjan Basu, Drilled Displacement Piles – Current Practice and Design, DFI Journal - The Journal of the Deep Foundations Institute, Vol. 4, Iss. 1, 2010

3. Duncan, J. M., & Wright, S. G. (2005). Soil Strength and Slope Stability. Hoboken, New Jersey: Wiley.

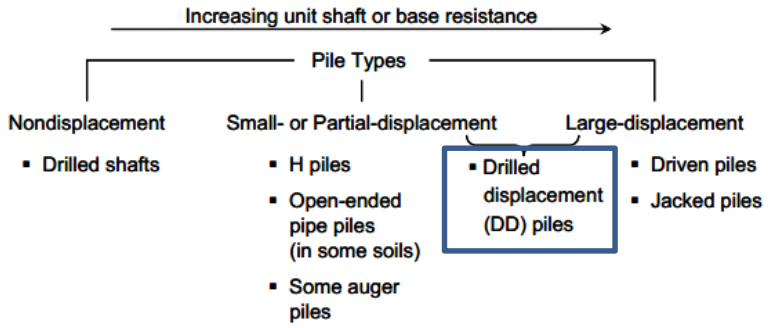


Fig. 1 Various Categories of Deep Foundation Types, Basu and Prezzi (2009)

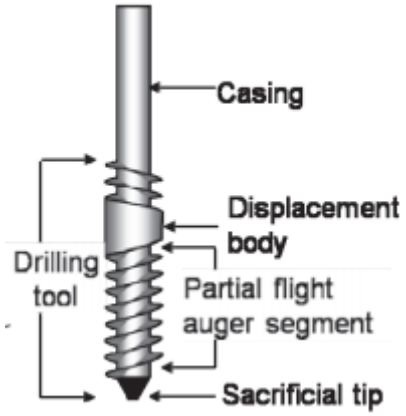


Fig. 2 Diagram of Typical DCIP Tooling, Basu and Prezzi et al. (2010)

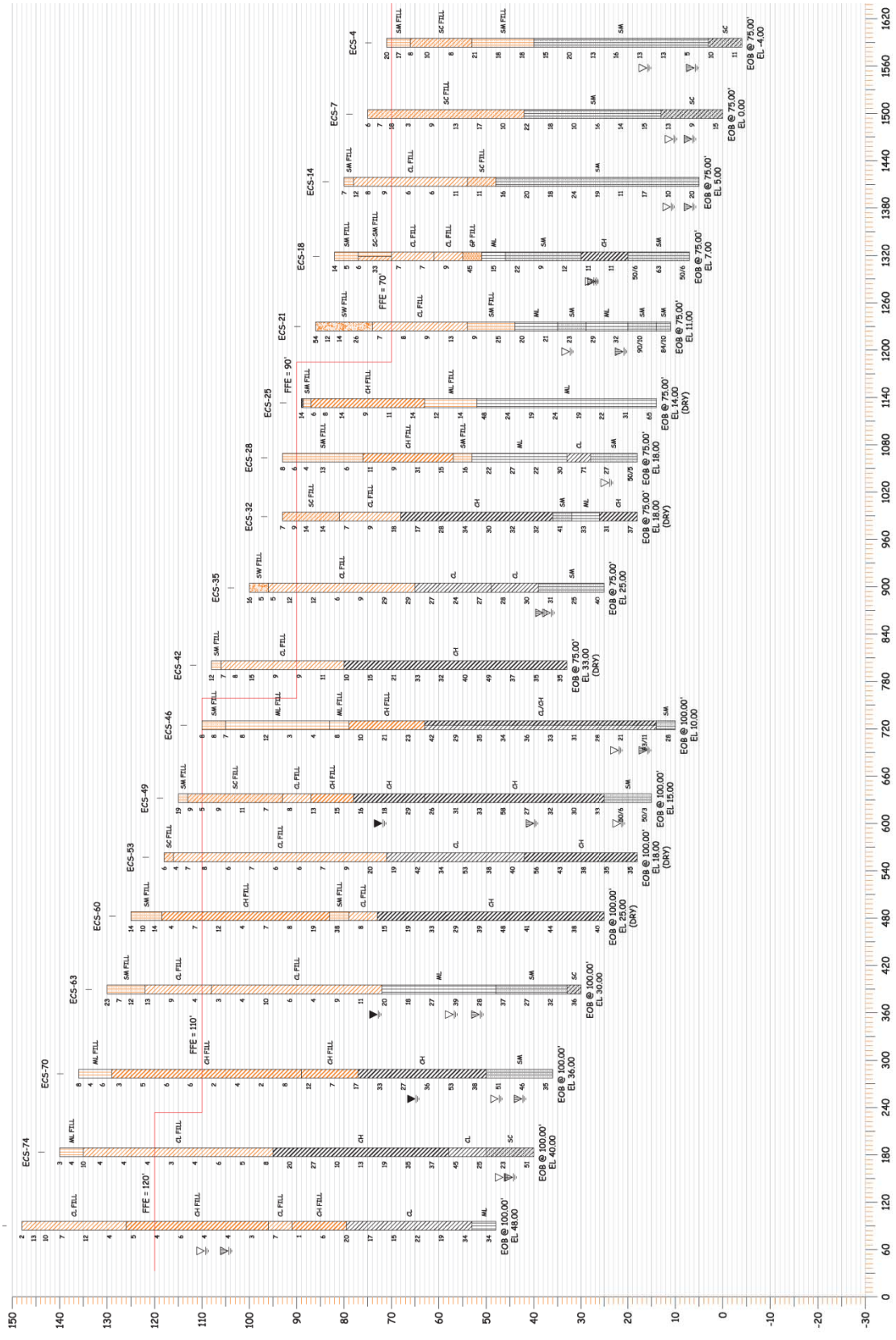


Figure 3: Typical Subsurface Cross Section along the Long Axis of Site (East to West)



Figure 4: Building Layout and Finished Floors – Note changes in FFE Elevation

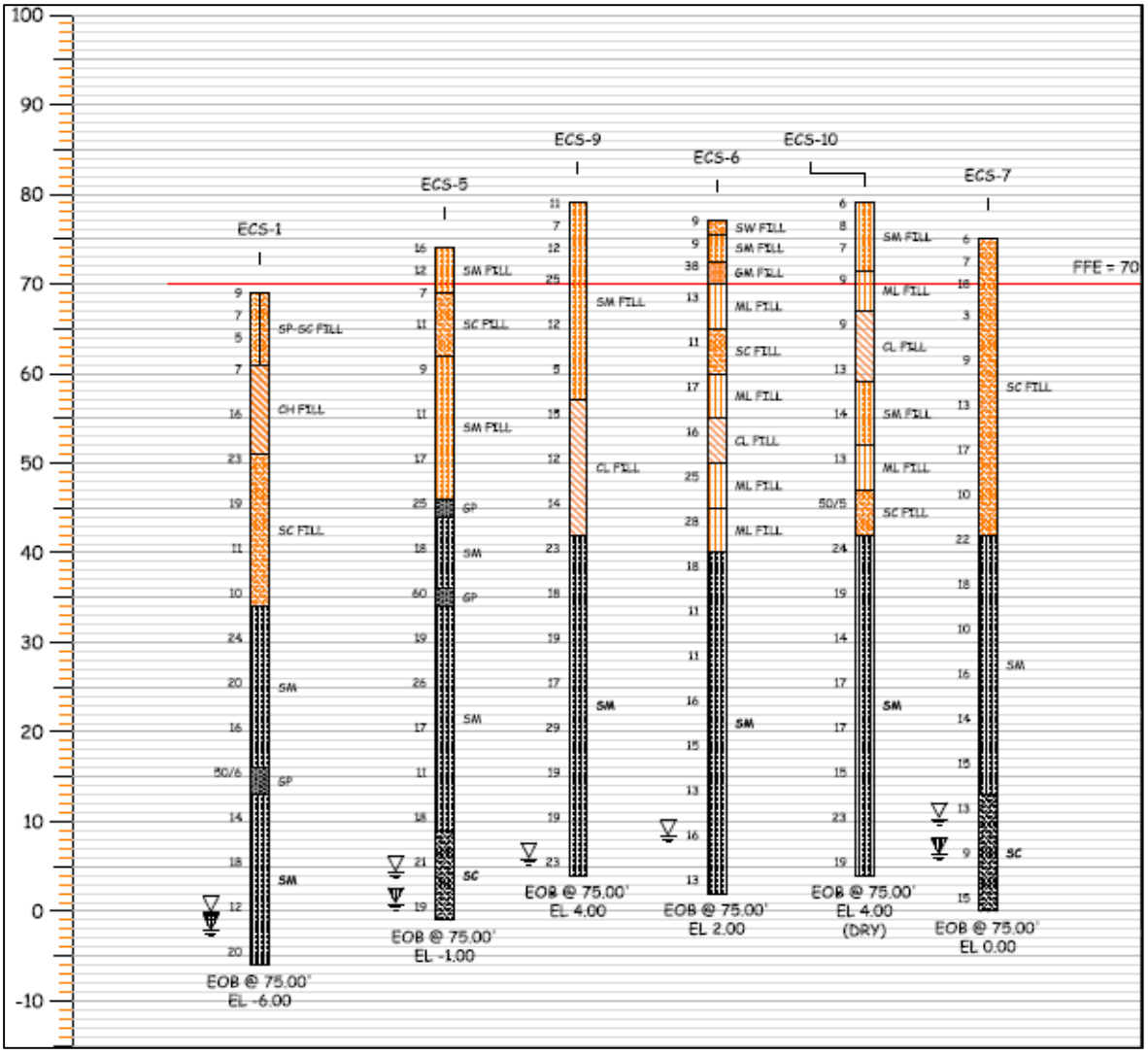


Figure 5: Westernmost Subsurface Cross Section A-A

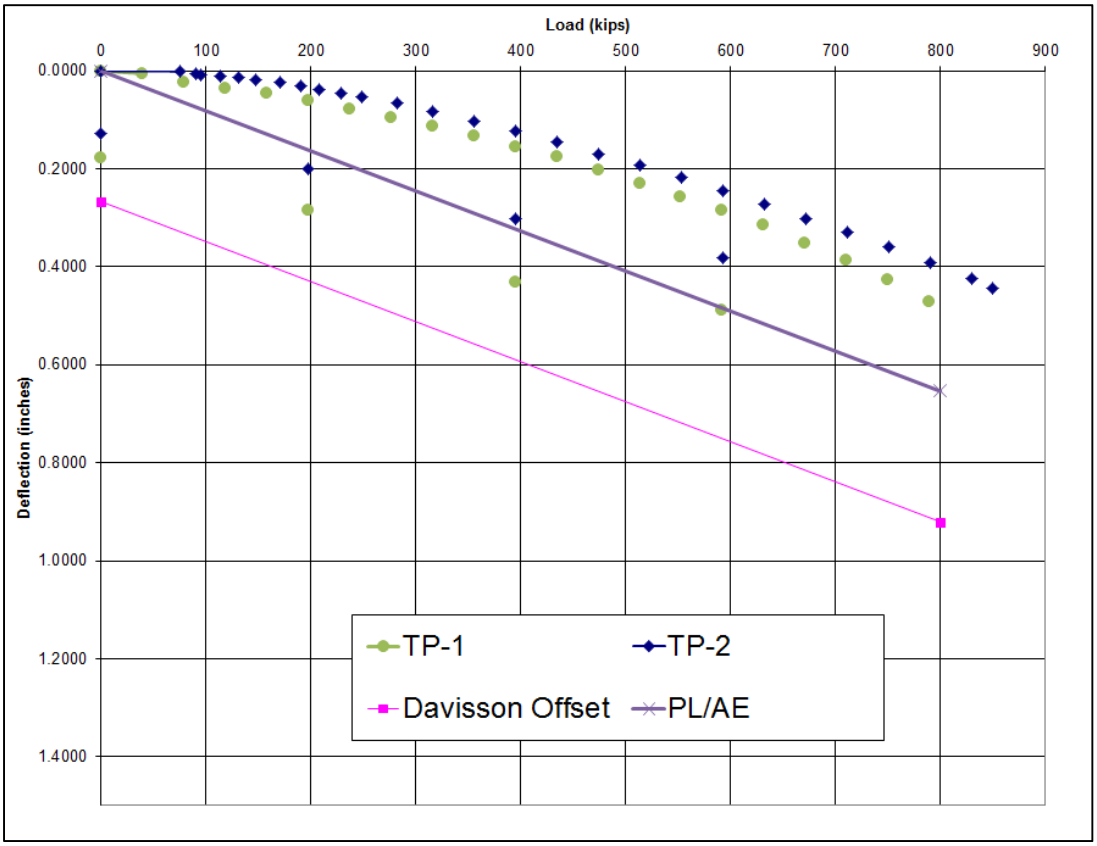


Figure 6: Load Test Comparison of TP-1 and TP-2

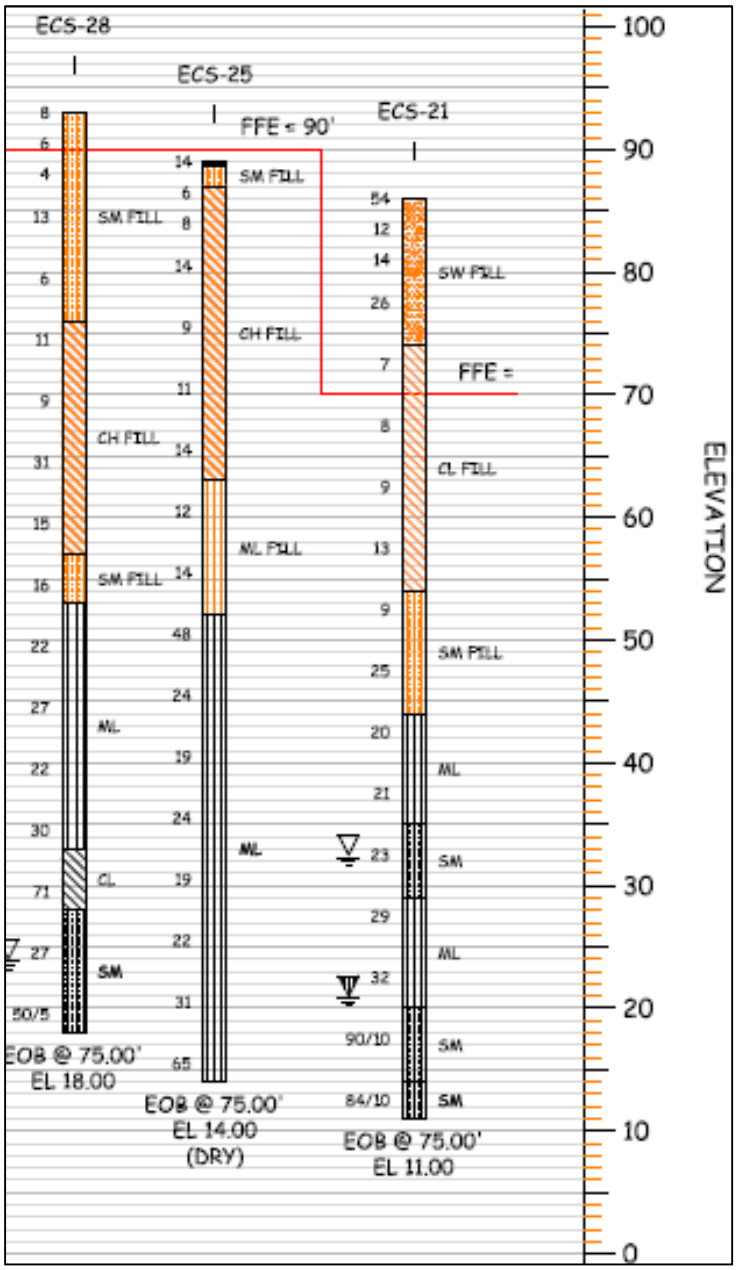


Fig. 7 Enlarged Transition from Alluvial to Potomac

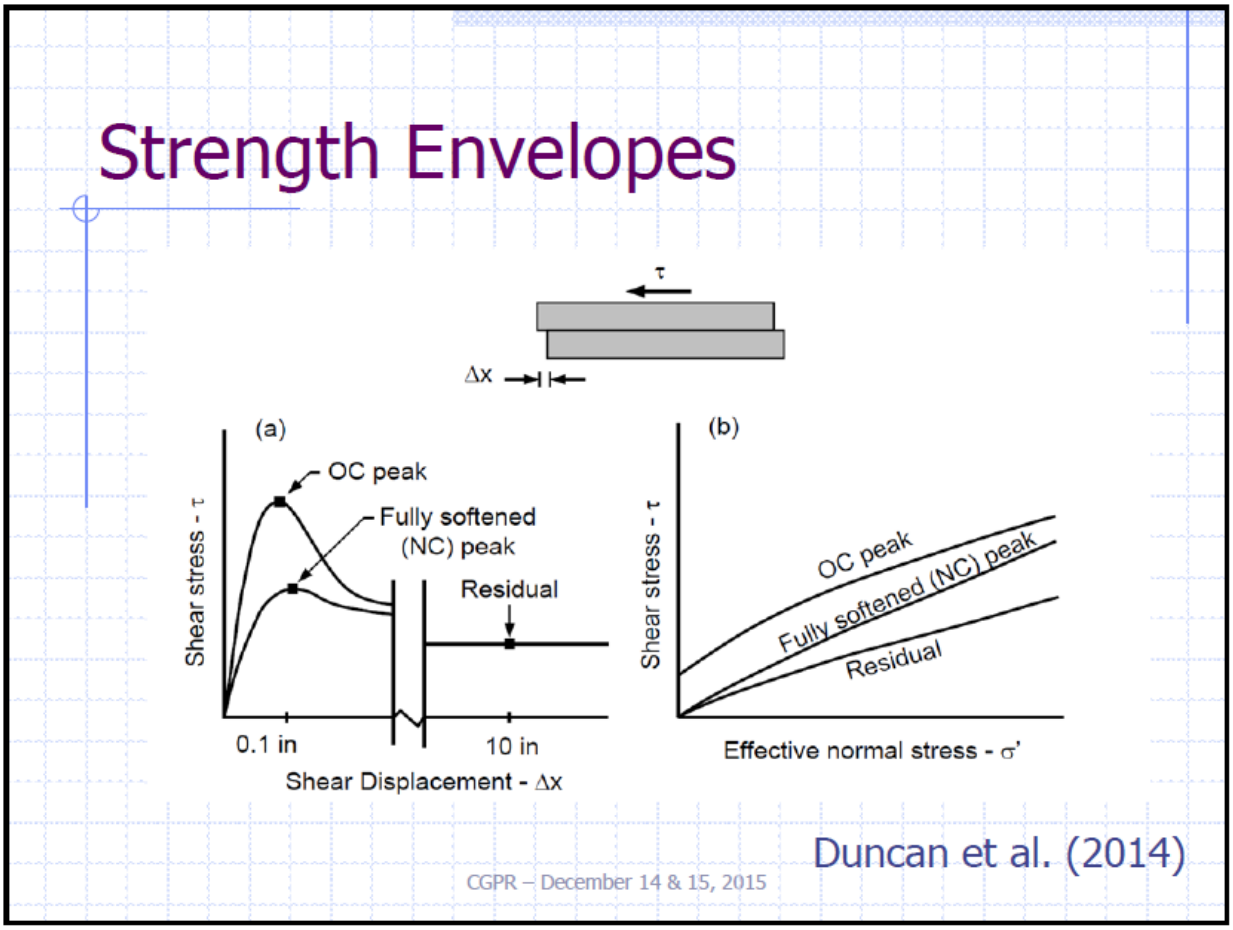


Fig. 8 Comparison of Peak to Residual Shear Strengths

FOUNDATIONS SETTLEMENT ESTIMATION BY NON-LINEAR STRESS-STRAIN APPROACH USING CPT RECORDS

Fatemeh Valikhah, Ph.D Candidate, Amirkabir University of Technology, Tehran, Iran. +98-9123268854, fvalikhah@aut.ac.ir
Abolfazl Eslami, Professor, Amirkabir University of Technology, Tehran, Iran, +98-2164543057, afeslami@aut.ac.ir

ABSTRACT
Complexity in soil-foundation interaction and subsoil nonlinear behavior cause difficulties and uncertainties in evaluating the actual values of foundation design factors such as settlement. The acquired continuous records of Cone Penetration Test (CPT) can be used to determine the soil profile and characteristics those are applicable in the geotechnical design. In this paper, it has been attempted to present a new non-linear stress-strain approach to estimate the foundations settlement by using CPT data in the form of soil behavior classification charts. This new approach is based on Janbu method (1960s and also 1998). Instead of using fixed and constant values for stress exponent (j) and modulus number (m), continuous coefficient variations can be used. The proposed approach also can be used as a new method to predict pile group settlement. A data bank has been compiled containing twenty-two practical case histories to investigate the accuracy of the predictions made by the proposed and available common methods. The comparisons indicate that the proposed approach is relatively able to predict the settlement close to their real values. Therefore, it can be considered as an alternative method based on valuable CPT data and non-linear stress-strain approach for foundations and pile groups settlement estimation.
Keywords: Settlement, Non-linear Stress-strain, CPT Records, Soil Behavior Classification, Case Histories

INTRODUCTION

Complexity in soil behaviour for settlement analysis is the result of non-linear and time dependent stress-strain behaviour of soils, their elasto-plastic performance under loading and unloading situation and also effects of stress history (Holtz et al., 2011; Fellenius, 2015). Hence, many relations and equations have been proposed to predict foundation settlement, where most of them are based on typical different parameters such as soil stiffness (E), foundation width (B), contact pressure (q) and pressure developing in depth (Janbu, 1967 also 1998; Briaud and Gibbens, 1999; Uzielli and Mayne, 2012).

The Janbu approach for settlement estimation, proposed by Janbu in the early 1960s, combines the basic principles of linear and non-linear stress-strain behaviour of material. The method is applied to all types of soils. The relation between stress and strain is a function of two non-dimensional parameters which are unique for any soil: a stress exponent, "j", and a modulus number, "m". The Janbu relations are derived from the definition of tangent modulus by the following expression:

$$M_t = \frac{\partial \sigma}{\partial \varepsilon} = m\sigma_r \left(\frac{\sigma'}{\sigma'_r}\right)^{1-j} \quad (1)$$

where ε, σ', j and m are strain induced by increase of effective stress, effective stress, a stress exponent and a modulus number respectively, and σ'_r is a constant stress which is equal to 100 kPa. The Janbu expressions for strain in different soils types are presented in Table 1.

 © 2017 DFI Annual Conference, New Orleans, LA, USA

Table 1. Janbu expressions for strain (Janbu, 1967)

Soil Type	The stress exponent (j)	ε	Description
Cohesionless Soil	>0	$\varepsilon = \frac{1}{mj}\left[(\frac{\sigma'_1}{\sigma'_r})^j - (\frac{\sigma'_0}{\sigma'_r})^j\right]$	σ'_0 = original effective stress σ'_1 = final effective stress
Dense Coarse-Grained Soil	=1 (The stress-strain behaviour can be assumed to be elastic.)	$\varepsilon = \frac{1}{100m}(\sigma'_1 - \sigma'_0) = \frac{1}{100m}\Delta\sigma'$	Units should be in kPa (The equation is not independent of units.)
Sandy or Silty Soil	0.5	$\varepsilon = \frac{1}{5m}(\sqrt{\sigma'_1} - \sqrt{\sigma'_0})$	Units should be in kPa (The equation is not independent of units.)
Cohesive Soil	0	$\varepsilon = \frac{1}{m}\ln\frac{\sigma'_1}{\sigma'_0}$	The cohesive soil is normally consolidated. The formula is independent of the stress units.
		$\varepsilon = \frac{1}{m_r} ln\frac{\sigma'_p}{\sigma'_0} + \frac{1}{m} ln\frac{\sigma'_1}{\sigma'_p}$	The cohesive soil is overconsolidated. The formula is independent of the stress units.

The modulus numbers to use in a particular case can be determined from conventional laboratory testing as well as in-situ tests. As a reference, Table 2 shows a range of normally conservative modulus numbers, "m", which are typical of various soil types. The modulus numbers presented in Table 2 are approximate and cover wide ranges of values for mixed soils.

Table 2. Range of Modulus number (m) and Stress exponent (j) for different soils in Janbu (1967) approach

Soil Type		Modulus Number (m)	Stress Exponent (j)
Till, Very dense to dense		300-1000	1
Gravel		40-400	1
Sand	Dense	250-400	0.5
	Compact	150-250	0.5
	Loose	100-150	0.5
Silt	Dense	80-200	0.5
	Compact	60-80	0.5
	Loose	40-60	0.5
Silty Clay and Clayey Silt	Hard, Stiff	20-60	0
	Stiff, Firm	10-20	0
	Soft	5-10	0
Soft Marine Clays and Organic Clays		5-20	0
Peat		1-5	0

The most important step for the settlement estimation is finding precisely the soil stiffness values. The more exact soil stiffness measuring would result in the more accurate prediction of settlement. Obviously, to estimate the settlement in soil profile, which the layers change frequently, the stiffness of each layer must be measured and used just for that specific layer. For this purpose, to determine the stress-strain modulus, the in-situ testing records such as Standard Penetration Test (SPT), Cone Penetration Test (CPT), Pressuremeter Test (PMT) and Dilatometer Test (DMT) can be realized, representing the actual soil performance in the field under loading. It has been well recognized in geotechnical practice that soil stiffness modulus is proportional to q_c (cone tip resistance in CPT records) ($E_s \approx (2\text{-}7)\times q_c$).

While CPT can be definitely useful due to repeatability and accuracy of results specially in sensitive and fine soils including better description of thin layers (Schmertmann, 1978a; Mayne, 2002; Eslami and Gholami, 2006; Mayne and Illingworth, 2010).

In this study, a new approach is proposed to estimate the foundations settlement which is based on non-linear stress-strain Janbu approach. Instead of using fixed values for stress exponent and modulus number in coarse-grained and fine-grained soils, a continuous coefficient variation is used based on CPT records. The procedure is described and verified among compiled data bank.

CASE STUDY RECORDS

A data bank, including twenty two cases with width more than 1m (relatively wide foundations), has been collected from different reliable references, including eleven square, five circular and six rectangular footings of variable embedded depth between 0 to 2.35 m. In these cases, the values of q_t, f_s, loads on the foundation, footing dimensions, embedded depth and finally the amount of settlement have been calculated. These cases had been used to calibrate the new formulation for settlement estimation and also for evaluation of the new proposed method. The summary of cases for calibration is presented in Table 3 and for comparison in Table 4.

CPT Records and pressure versus settlement over width for five actual footings have been shown in "Fig. 1" (Briaud and Gibbens, 1999).

Table 3. Summary of case history records for calibration

Case No.	Reference	Main Reference	Location	Soil Type	Footing Shape	B (m)	D_f (m)	GWT (m)	q ($\frac{kg}{cm^2}$)	$\frac{q_t}{(\frac{kg}{cm^2})}$	R_f	S_m (mm)
1	Eslami and Gholami (2006)	Amar (1979)	France	Silt	Square	1	0	-	3	25	0.5	98
2						1	0	-	3.25	28	0.5	97
3	Mayne and Illingworth (2010)	Bergdahl et al. (1984)	Sweden	Glaciofluvial Sand	Rectangular	1.2	0.6	8	17.4	107.2	0.51	119
4						1.7	0.8	8	17.4	107.2	0.51	170
5						2.4	1.1	8	17.4	107.2	0.51	245.8

B= Foundation width
D_f= Embedment depth
GWT= Ground Water Table
q= pressure developing in depth
q_t= Corrected cone resistance for pore water pressure in CPT records
R_f= Friction ratio
S_m= Foundation settlement

Table 4. Summary of case history records for comparison

Case No.	Reference	Main Reference	Location	Soil Type	Footing Shape	B (m)	D_f (m)	GWT (m)	q ($\frac{kg}{cm^2}$)	$\frac{q_t}{(\frac{kg}{cm^2})}$	R_f	S_m (mm)
6	Briaud and Gibbens (1999)	Briaud and Gibbens (1999)	USA	Sand, Silty Sand	Square	1	0.76	4.9	15.4	75.2	0.65	100
7						1.5	0.76	4.9	15.4	75.2	0.65	154
8	Eslami and Gholami (2006)	Amar (1979)	France	Silt	Square	1	0	-	3.75	17	0.5	115
9						1	0	-	3.7	20	0.5	100
10	Mayne and Illingworth (2010)	Bergdahl et al. (1985)	Sweden	Glaciofluvial Sand	Rectangular	1	0	3	8.4	40.1	0.63	102.4
11						1	0	3	8.4	40.1	0.63	102.4
12						2.4	1.1	1.5	6.4	32	0.63	260
13		Tand et al. (1994)	USA	Alluvial Sand	Circular	2.2	2.2	1.9	12.8	67.2	0.6	250
14						2.2	2.2	1.9	12.8	67.2	0.6	250
15						2.35	2.35	1.9	17.3	104.6	0.52	245
16						2.35	2.35	1.9	17.3	104.6	0.52	245

Case No.	Reference	Main Reference	Location	Soil Type	Footing Shape	B (m)	D_f (m)	GWT (m)	q ($\frac{kg}{cm^2}$)	$\frac{q_t}{(\frac{kg}{cm^2})}$	R_f	S_m (mm)
17		Amar et al. (1998)	France	Dune Sand	Square	1	0	3	8.4	40.1	0.66	102.4
18						1	0	3	8.4	40.1	0.66	102.4
19						1	0	3	8.4	40.1	0.66	102.4
20		Anderson et al. (2006)	Florida	Brown Silty Sand	Circular	1.82	0.6	3	17.1	97.8	0.55	186
21		Lehane (2008)	Australia	Siliceous Dune Sand	Square	1	1	5.5	4.8	34.4	0.44	102
22						1	1	5.5	4.8	34.4	0.44	102

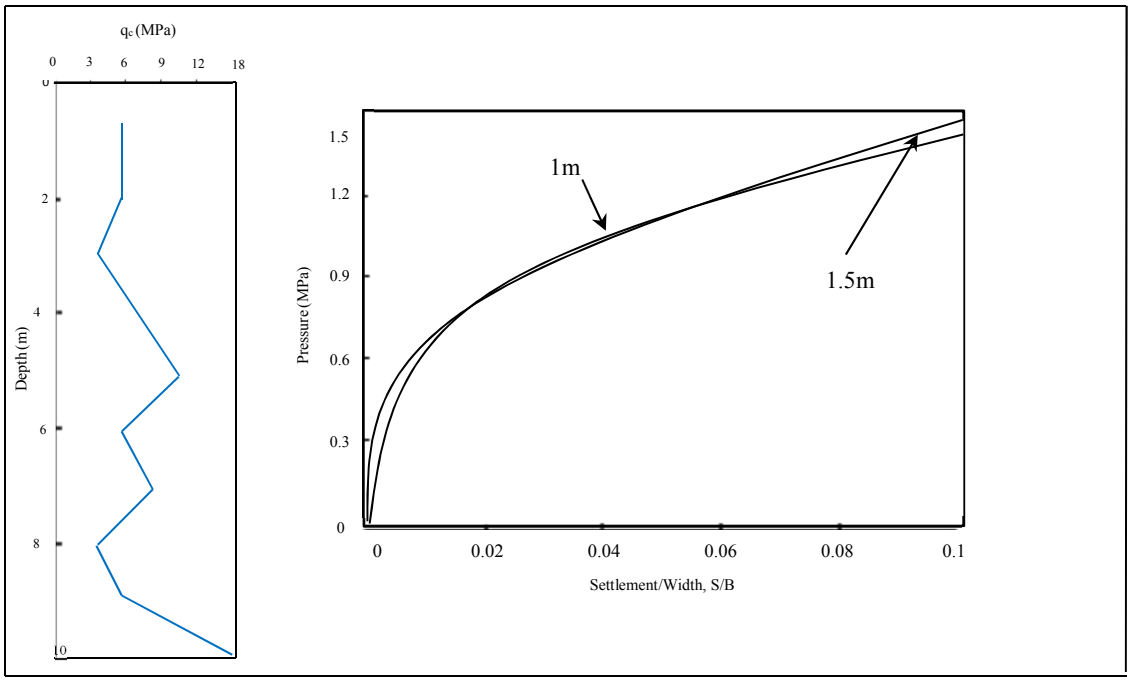


Fig. 1 CPT Records and pressure versus settlement over width for cases 6 and 7 (Briaud and Gibbens, 1999)

PROPOSED APPROACH

As it is expressed in Janbu approach for determination of strain, the stress exponent (j) is considered 0.5 for sand and silt in three states of dense, compact and loose. This parameter is zero for hard, firm and soft clay. Furthermore, the proposed ranges for modulus number (m) are very wide depending on the soil type as shown in Table 2. This wide range of the values of "j" and "m" can cause great error and vast predicted values in the calculated strains for different soils. Therefore, the choice of a suitable value for "m" among these wide ranges is one of Janbu method difficulties in settlement estimation.

The new approach has been proposed, in which instead of using two different equations for granular and cohesive soils, the unique equation is used for settlement estimation of all types of soils.

To modify Janbu equation so that only the results of CPTu will be used for calculations, the appropriate values of "j" for soils must be considered. The new equation for estimation of "j" value, resulted from studies on actual cases for calibration presented in Table 3, is proposed as follows:

$$j = \frac{q_t\left[1 + (0.05\ logq_t) \times R_f^2\right]}{5^{logq_t}(11\sqrt{R_f} + R_f^2)} \quad (2)$$

In which, q_t is corrected cone resistance for pore water pressure ($\frac{kg}{cm^2}$ or bar) and $R_f = \frac{f_s}{q_t}$ is friction ratio.

Also, with careful study on the range of "m" in Janbu approach, as a matter of fact the values of "m" are in the high ranges for dense and hard soils and in the low ranges for the loose and soft soils like the values of q_t from CPT records.

The value of modulus number, "m", can be replaced by applying a coefficient to q_t as follows:

$$m = \alpha q_t \quad (3)$$

Studies show that the value of "m" in settlement calculation, in addition to relating to the soil type and compaction is a function of foundation width (B).

As it is known in "Fig. 2", CPT records result in large strains and do not report the other values of soil stress corresponding to small strains. While, all deformations of soil beneath the foundation from small ranges of strains to large ones are known as the settlement of foundations. Therefore, in using CPT records to estimate the foundations settlement values, which may be in small strains, a modification factor is needed.

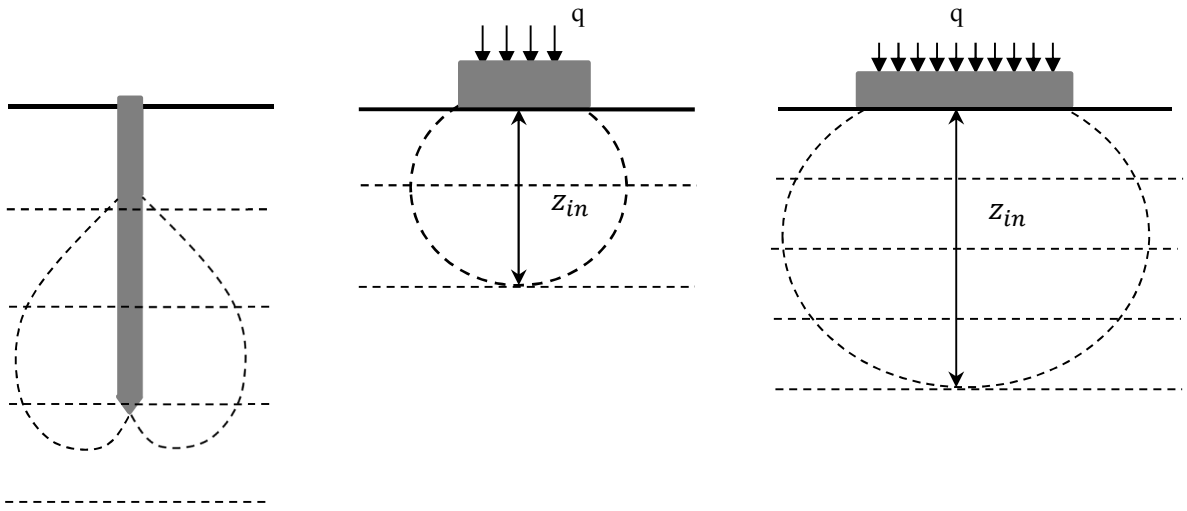


Fig. 2 Influenced zone beneath CPT and foundations with different widths

Hence, this scale effect has been considered in proposed approach to estimate more realistic settlement value. The calibration studies show that the best value of α to reach the maximum accuracy is as follows:

$$\alpha = (\frac{2B+1}{3B})^3 \quad (4)$$

Subsequently, the strain could be obtained from the Eq. 5 as follows:

$$\varepsilon = \frac{1}{mj}\left[\left(\frac{\sigma'_0 + \Delta\sigma'}{100}\right)^j - \left(\frac{\sigma'_0}{100}\right)^j\right] \quad (5)$$

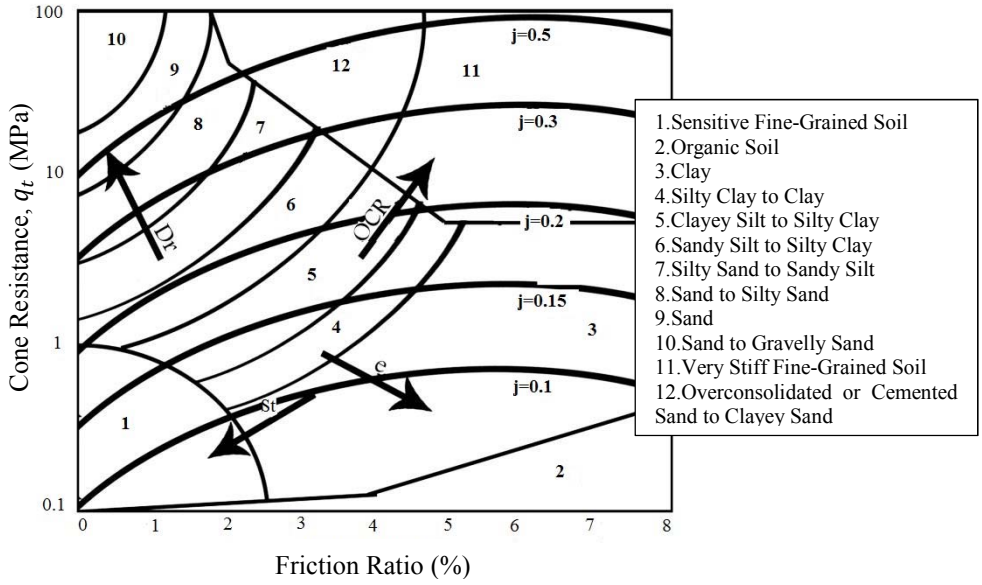
where, σ'_0 is initial effective stress in the middle of investigated layer under in-situ pressure. $\Delta\sigma'$ indicates the increase of effective stress in the middle of studied layer under the loads of surcharges or applied stress. The stress influenced depth is considered as (2-3)× B beneath the single foundations.

The value of settlement in the soil can simply be calculated from the Eq. 6:

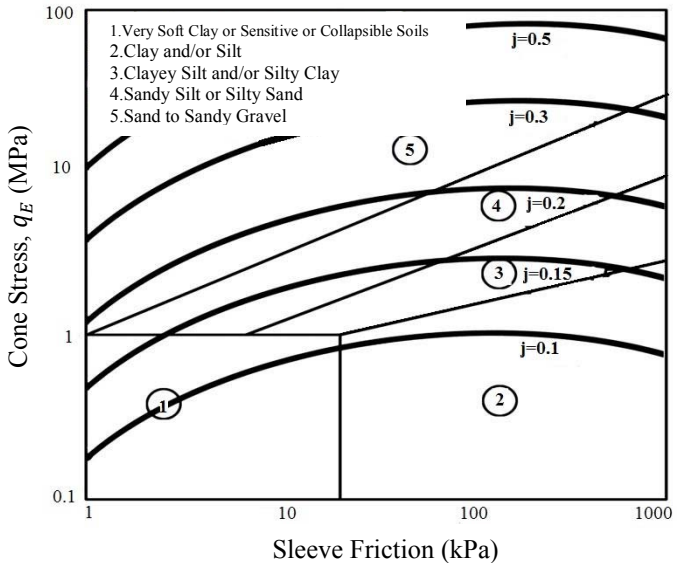
$$\varepsilon = \frac{\Delta H}{H} \qquad (6)$$

In this equation ΔH is the settlement and H is the thickness of the subject layer. The investigating zone can be divided to several thin layers in order to increase the accuracy of the calculations.

The values of proposed "j" in different zones of Robertson *et al.* (1986) chart and Eslami-Fellenius (1997) chart have been demonstrated in "Fig. 3".



(a)



(b)

Fig. 3 Soil behaviour classification chart with proposed "j" values, (a) Robertson *et al.* (1986) and (b) Eslami and Fellenius (1997)

Implementation of this new approach is shown by an example calculation. The case 7 is a square footing with B=1.5 m and D_f=0.76 m. The GWT is in 4.9 m and q=15.4 $\frac{kg}{cm^2}$. The foundation settlement is estimated as presented in Table 5. As it is shown the difference between the estimated and measured settlement is about 10%, which is acceptable.

Table 5. Implementation of the proposed procedure

Case No.	$\sigma'_0(\frac{kg}{cm^2})$	$\Delta\sigma'(\frac{kg}{cm^2})$	$q_c(\frac{kg}{cm^2})$	R_f	α (from the Eq. 4)	m ($\frac{kg}{cm^2}$) (from the Eq. 3)	j ($\frac{kg}{cm^2}$) (from the Eq. 2)	ε	S (mm)	S_m (mm)
7	0.19	3.85	75.2	0.65	0.7	52.64	0.36	0.059	177	154

σ'_0= The initial stress in the middle of target layer
$\Delta\sigma'$ = The increase of effective stress under applied pressure
q_c = The average of CPT data in the influenced zone
R_f= Friction Ratio
ε = The strain
S= Estimated settlement
S_m= Measured settlement

SETTLEMENT ESTIMATION OF PILE GROUP USING PROPOSED APPROACH

This new proposed approach can be used to estimate pile group settlement based on equivalent foundation concept which had been presented by Terzaghi and Peck (1967) and also "Unified method" presented by Fellenius (1988). The loads in the pile increase due to negative skin friction to a maximum drag load value at the neural plane (NP) and reduce from there to positive shaft resistance (Fellenius, 1988). This concept is shown in "Fig. 4-a".

Based on this approach presented by Fellenius (1988), above the neural plane, the soil settlement is more than pile settlement and below this level, it is vice versa. Hence, it can be assumed that the settlement of

pile group is equal to the settlement of imaginary equivalent foundation located on neural plane level (Terzaghi and Peck, 1967; Fellenius, 1988). The procedure is shown in "Fig. 4-b".

In this study, based on presented concepts, the equivalent foundation can be assumed and by using proposed approach, "j" parameter can be calculated by Eq. (2) and "m" parameter from Eq. (3). Finally, the pile group settlement can be estimated. In fact, it is proposed that to estimate the pile group settlement, the equivalent foundation, as the concept was presented, will be assumed similar to shallow footing, just located on the neural plane. Then, the new proposed approach can be used for its settlement calculation.

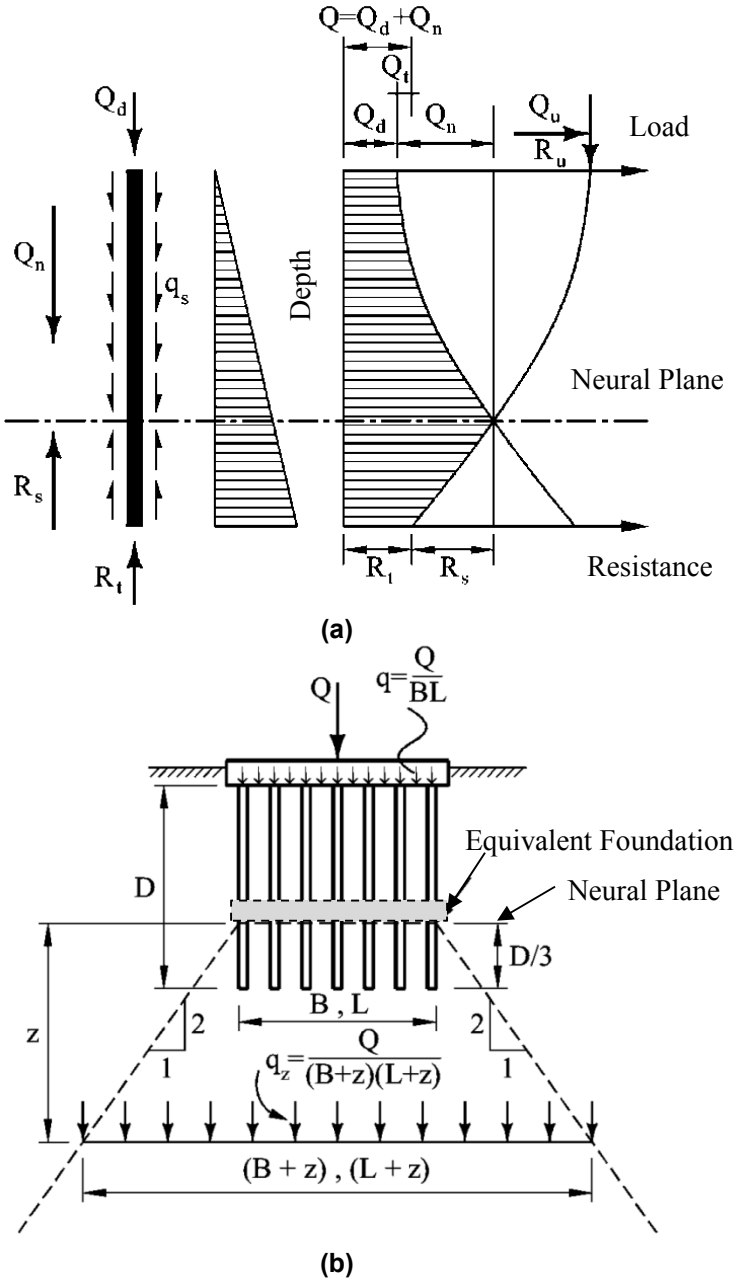


Fig. 4 (a) Neural plane concept to calculate deep foundation settlement (Fellenius, 1988) and (b) Equivalent foundation concept to estimate the pile group foundation settlement (Terzaghi and Peck, 1967)

COMPARISONS AND DISCUSSIONS

Twenty two foundations have been studied in this research. By statistical and probability approaches, the accuracy of equations can be better calibrated. The most important magnitude of tendency to sample centre is “average of sample” and dispersion or sample data expansion is indicated with standard deviation. The greater the standard deviation of a sample, the greater dispersion or data expansion. The summary of determinable characteristics through these curves is presented in Table 6.

Table 6. Summary of normal distribution coefficients for predictive methods

	Schmertmann Equation	Janbu Equation	Proposed Equation
Average	60	107	18
Standard Deviation	39	66	9

Measured and predicted values by suggested equation and other approaches are illustrated in "Fig. 5". It can be seen that the prediction accuracy of the proposed equation is higher than other equations. Other approaches especially Janbu (1967) and Schmertmann (1978) equations, underestimated the settlement value and are highly conservative. While, the predicted settlement by new approach is close to measured values.

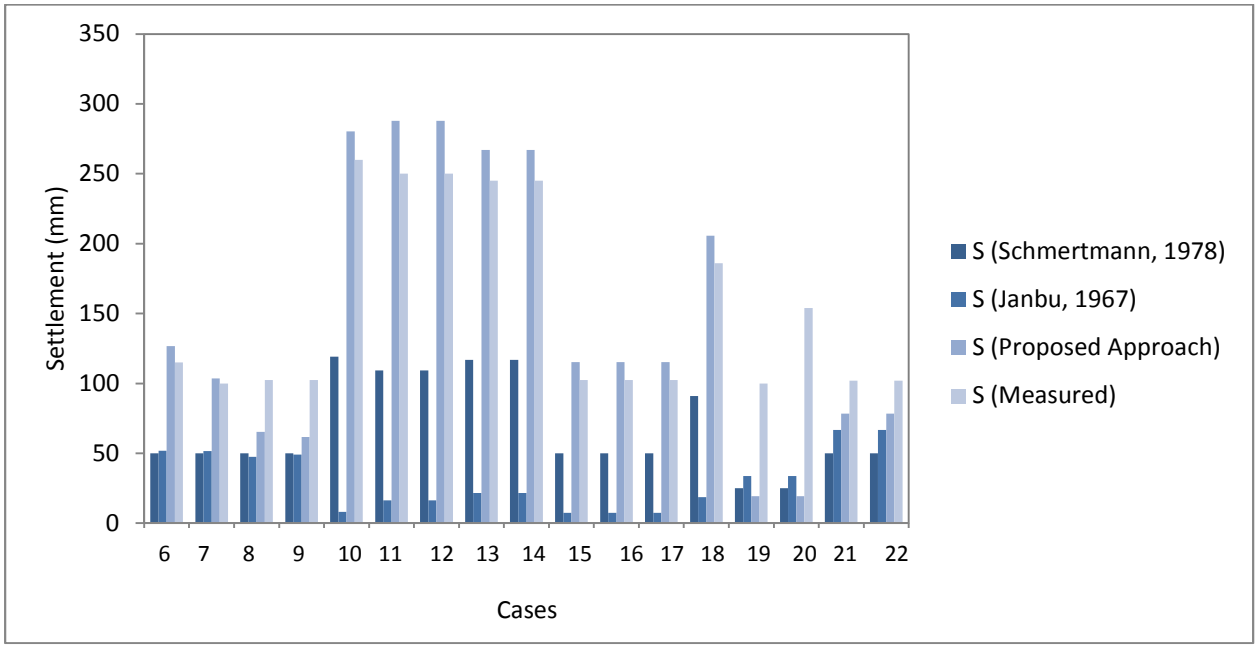


Fig. 5 Comparison of measured and predicted settlement by proposed approach and other equations

CONCLUSIONS

In stress-strain approach proposed by Janbu (1967 and 1998), the parameter “m”, modulus number, is represented for soil stiffness and “j”, stress exponent, for type of geomaterial. Wide ranges of “m” magnitude are specified to each of the different soil conditions cause errors in settlement estimation.

In this study, a new correlation has been defined to estimate the foundations settlement based on Janbu basic equations. Instead of using constant values for stress exponent (j) and modulus number (m) in coarse-grained and fine-grained soils, continuous coefficients are used based on CPT records.

To examine suggested equation in settlement estimation, twenty two practical cases (five cases for calibration and seventeen cases for comparison) compiled from valid sources around the world. Average settlements for these cases have been measured in the range of 97 to 260 mm, about 10% of foundation width (S/B). The recorded profiles of q_t in these sites are between 1.7 and 10.72 MPa and the soil type beneath the foundations include sand and in some parts, a combination of silt, clay and sand.

Assessment of probability and statistical analysis to compare the proposed method and other current methods for settlement estimation such as Janbu (1967) and Schmertmann (1978) equations, indicates that the suggested relations has been able to predict the closest value to measured settlement.

Furthermore, based on equivalent foundation concept which had been presented by Terzaghi and Peck (1967) and unified method presented by Fellenius (1988), the new proposed approach can be used to estimate the pile group settlement.

REFERENCES

Anderson, B.J., Townsend, F.C. and Rahelison, L. 2007. Load testing and settlement prediction of shallow foundation, Journal of Geotechnical and Geoenvironmental Engineering (ASCE), 133(12), 1494-1502.

Briaud, J.L. and Gibbens, R.M. 1999. Behavior of five large spread footing on sand, Journal of Geotechnical and Geoenvironmental Engineering (ASCE), 125(9), 787-796.

Eslami, A. and Fellenius, B., 1997. Pile capacity by direct CPT and CPTu methods applied to 102 case histories, Canadian Geotechnical Journal, 34, 886-904.

Eslami, A. and Gholami, M. 2006. Analytical model for the ultimate bearing capacity of foundations from cone resistance, International Journal of Science and Technology, Scientica IRANICA, 13(3), 223-233.

Fellenius, B.H., 1988. Unified Design of Piles and Pile Groups, Transportation Research Board, Washington, TRB Record 1169, 75-82.

Fellenius, B.H., 2015. Basics of Foundation Design, Electronic Edition, April, 2015.

Holtz, R.D., Kovacs, W.D., and Sheahan, T.E., 2011. An introduction to geotechnical engineering, 2nd Edited, Prentice Hall.

Janbu, N., 1998. Sediment deformations. University of Trondheim, Norwegian University of Science and Technology, Geotechnical Institution, Bulletin 35, 86 p.

Malekdoost, M. and Eslami, A. 2011. Application of CPT Data for estimating foundations settlement, Sharif Civil Engineering Journal, 27(2), No. 1, 75-85. (in Persian)

Mayne, P.W., 2002. Equivalent CPT method for calculating shallow foundations settlements in the piedmont residual soils based on the DMT constrained modulus approach, Georgia Institute of Technology Atlanta, GA, 1-5.

Mayne, P.W. and Illingworth, F. 2010. Direct CPT method for footing response in sands using a database approach, Proceedings, 2nd International Symposium on Cone Penetration Testing (CPT'10), Vol. 3, Huntington Beach, California, 315-322.

Robertson, P.K., Campanella, R.G., Gillespie, D. and Grieg, J. 1986. Use of piezometer cone data, Proceedings of American Society of Civil Engineering, ASCE, In-Situ 86 Specialty Conference, 1263-1280, Publication GSP No. 6.

Schmertmann, J.H., 1978a. Guidelines for Cone Test, Performance and Design, Federal Highway Administration, ReportFHWA-TS-78209, Washington, 145 p.

Terzaghi, K., and Peck, R.B., 1967. Soil Mechanics in Engineering Practice, Second Edition: John Wiley & Sons, New York, 729 p.

Uzielli, M. and Mayne, P.W., 2012. Load-displacement uncertainty of vertically-loaded shallow footings on sands and effects on probabilistic settlement estimation, Georisk: Assessment and Management of Risk for Engineered Systems and GeoHazards. Vol. 6 (1): Taylor & Francis: 50-69.

STRUCTURE SUPPORT ON LATERALLY SWEPT PILES

Matthew R. Glisson, PE, Braun Intertec Corporation, St. Louis, MO, US, 314.569.9883, mglisson@braunintertec.com
Morgan L. Race, Ph.D., PE Braun Intertec Corporation, Lenexa, KS, US, 612.708.6791, mrace@braunintertec.com

ABSTRACT

Most driven pile projects have plumbness limits from 0.25 in/ft (21 mm/m) to 0.5 in/ft (42 mm/m) to control bending stresses. For two projects, the project teams performed static load testing to evaluate performance of piles with sweep. One project, located in Grand Forks, North Dakota, used 9.625-inch (244-mm) diameter piles with a wall thickness of 0.395 inch (10 mm) and lengths ranging from about 130 to 160 feet (40 to 49 m). Measured pile sweep (lateral offset distance of the pile toe from the pile top) was between 12 and 17 inches (305 to 432 mm). Static load testing indicated that the piles could support the design load with axial deflection of less than 1 inch (25 mm) but only provided about 80 to 90 percent of the ultimate resistance at axial deflections of about 1.9 to 1.7 inches (49 to 43 mm), respectively. The other project, located in Shakopee, Minnesota, used 9.625-inch (244-mm) diameter pile but with a wall thickness of 0.352 inch (9 mm) and lengths around 50 to 90 feet (15 to 27 m). The measured sweep varied between about 20 and 63 inches (508 and 1,600 mm) for 9 of 214 piles driven at the site. Load testing indicated that these piles could provide the required design resistance with less than 0.3 inch (8 mm) of axial deflection and support the required ultimate resistance with about 0.5 to 0.6 inch (13 to 15 mm) to of axial deflection.

Keywords: Driven Pile; Axial Capacity; Construction Problems

INTRODUCTION

Anyone who has observed a significant number of piles has seen that, inevitably, the pile is not perfectly straight after driving. In spite of the best efforts of contractors, there are a whole host of reasons for piles to end up out-of-plumb or to have a curve, sometimes referred to as pile sweep. Most project specifications set limits for plumbness typically between 0.25 in/ft (21mm/m) and 0.5 in/ft (42mm/m) (USACE, 1991; PDCA, 2007; MnDOT, 2016; MoDOT, 2016). Closed-end pipe piles, including monotube or tapertube, are the only pile type that allow actual measurement of the final alignment of the pile.

As Nadeem, et al. (2015) note, buckling failure of long, slender piles is the predominant mode of pile failure in soft soils. Pile sweep is just one source of buckling failure in long, slender piles. The nonlinear buckling analysis showed that increasing slenderness ratio and/or increasing degree of curvature decreases the load-carrying capacity of a driven pile. Nadeem, et al. (2015) considered solid, steel pile with lengths from 24 to 66 feet (7.5 to 20 m), diameters from 9.75 to 26 inches (244 to 660 mm), initial bends from 2 to 6 inches (50 to 150 mm), and half- and quarter-sine shapes.

The authors' internet search resulted in a limited number of research papers investigating the effect of bent piles in soft clay, and even fewer that incorporated full-scale testing in the field. Dunlop, et al. (1993) performed an instrumented, static load test on a tapered-pile tip (TPT), composite pile driven through fly ash and soft silt and silty clay. The over-sized, concrete tip was attached to a 16-inch (406-mm), outside-diameter, corrugated steel shell, creating an annular space that was partially filled by dumping sand at the ground surface. As installed, the pile length below grade was about 45 feet (14 m) and the measured sweep resulted in a toe offset of about 20 inches (508 mm). At the maximum test load of 600 kips (2,669 kN), the pile top plunged to a maximum displacement of about 1.5 inches (38 mm) and after unloading, the permanent pile top displacement was 0.789 inches (20 mm). Dunlop, et al. (1993) concluded that the Johnson method and the STRUDL computer program reasonably predicted the horizontal displacement

 © 2017 DFI Annual Conference, New Orleans, LA, USA

along the pile. They also note that the test pile was capable of supporting the 300-kip (1,334 kN) design load but not the 600-kip (2,669 kN) ultimate load.

For two recent projects with numerous swept pile, the available research was determined to be limited in application given the investigated pile sizes, lengths and measured sweep. As a result, the project team chose to perform static load testing to evaluate the ultimate resistance of the swept piles.

UND SCHOOL OF MEDICINE AND HEALTH SCIENCES

UND SMHS Subsurface Conditions

The University of North Dakota (UND) was building a new, four-story, steel and post-tensioned concrete structure for the School of Medicine and Health Sciences (SMHS). Located in Grand Forks, North Dakota, the project site is in the Red River Valley. The general soil profile in the Red River Valley consists of relatively weak, unconsolidated, glacial lake deposits overlying glacial till.

Based on the subsurface exploration undertaken at the site, the stratigraphy consisted of 7 to 9 feet (2 to 3 m) of topsoil and uncontrolled fill, underlain by Glacial Lake Agassiz fat clay to a depth of about 128 to 138 feet (39 to 42 m). These deposits typically have standard penetration test (SPT) N-values of 2 to 10, moisture contents of 30 to 70 percent and total unit weights between 105 and 110 pounds per cubic foot, pcf (16.5 to 17.3 kN/m^3). Undrained shear strengths vary within the specific deposits but are generally between 500 and 1,000 pounds per square foot, psf (24 to 48 kPa).

Below the Glacial Lake Agassiz deposits are glacial till soils classifying as lean clay and fat clay with varying amounts of sand and gravel. The glacial till soils in the Red River Valley typically have N-values of 30 to over 100, moisture contents between 15 and 30 percent, and total unit weights of 125 to 135 pcf (19.6 to 21.2 kN/m^3). Undrained shear strengths are at least 2,000 psf (96 kPa) and generally greater than 4,000 psf (192 kPa).

UND SMHS Pile Design

In the Red River Valley, driven pile foundations consisting of closed-end pipe pile or H-pile are the most common deep foundation types. For this project, closed-end pipes were identified as the most cost-effective solution. The project team conducted a pre-construction test pile program to evaluate the most-effective pile-load combination, which consisted of driving four test piles with high-strain dynamic testing. The test piles consisted of 9.625-inch (244-mm), outside-diameter pipe with a wall thickness of 0.395 inches (10 mm) driven to depths of between 156 and 176 feet (48 and 54 m). Test Piles 1 and 4 were tested during initial drive, and all four piles were tested during restrike. Test Pile 2 was filled with concrete prior to restrike. The restrikes occurred five days after initial driving.

The wave matching evaluation for Test Pile 2 had a calculated ultimate resistance of 699 kips (3,109 kN) at a length of 156 feet (48 m). Using superposition, combining the resistances from the initial drive and the restrike drive, for Test Piles 1 and 4, the calculated ultimate resistances were 700 and 614 kips (3,113 and 2,731 kN), respectively, with lengths of about 176 feet (54 m) for each pile. Based on these results, the project team selected a design using an ultimate resistance of 600 kips (2,669 kN). This resulted in an allowable load of 300 kips (1,334 kN) with a safety factor of 2.0. The safety factor was chosen based on a quality-control program including independent, full-time pile installation observations and high-strain dynamic testing on at least 2 percent of the production piles. In addition to the four design-phase piles, seven production piles were subjected to high-strain dynamic testing out of 371 production piles. Wave matching evaluations of high-strain dynamic testing results during installation of production piles calculated ultimate resistances between about 600 and 750 kips (2,669 and 3,336 kN) at lengths of about 140 to 160 feet (43 to 49 m).

UND SMHS Swept Pile

Observations of the installed production pile revealed that 313 out of 371 piles had noticeable sweep. For more than half of the piles, the amount of sweep was large enough that the toe was not visible. The project specifications did not list a tolerable amount of horizontal deviation for the pile. However, at lengths of 140 to 160 feet (43 to 40 m), a toe sweep of 40 inches (1,016 mm) would be within the typical tolerance 0.25 in/ft (21 mm/m). Based on the test results of the static load test on Pile F13.05, the project team chose to perform testing on a second pile and selected Pile G10.05.

Prior to filling the piles with concrete for the static load test, an inclinometer test was performed to measure the actual pile sweep. The 2.75-inch (70-mm), outside-diameter, inclinometer casing was installed in the pile using centralizers spaced about 10 feet (3 m) on-center. As Fig. 1 shows, the toe of Piles F13.05 and G10.05 were offset 11.6 and 17.4 inches (295 and 442 mm), respectively, from the pile top.

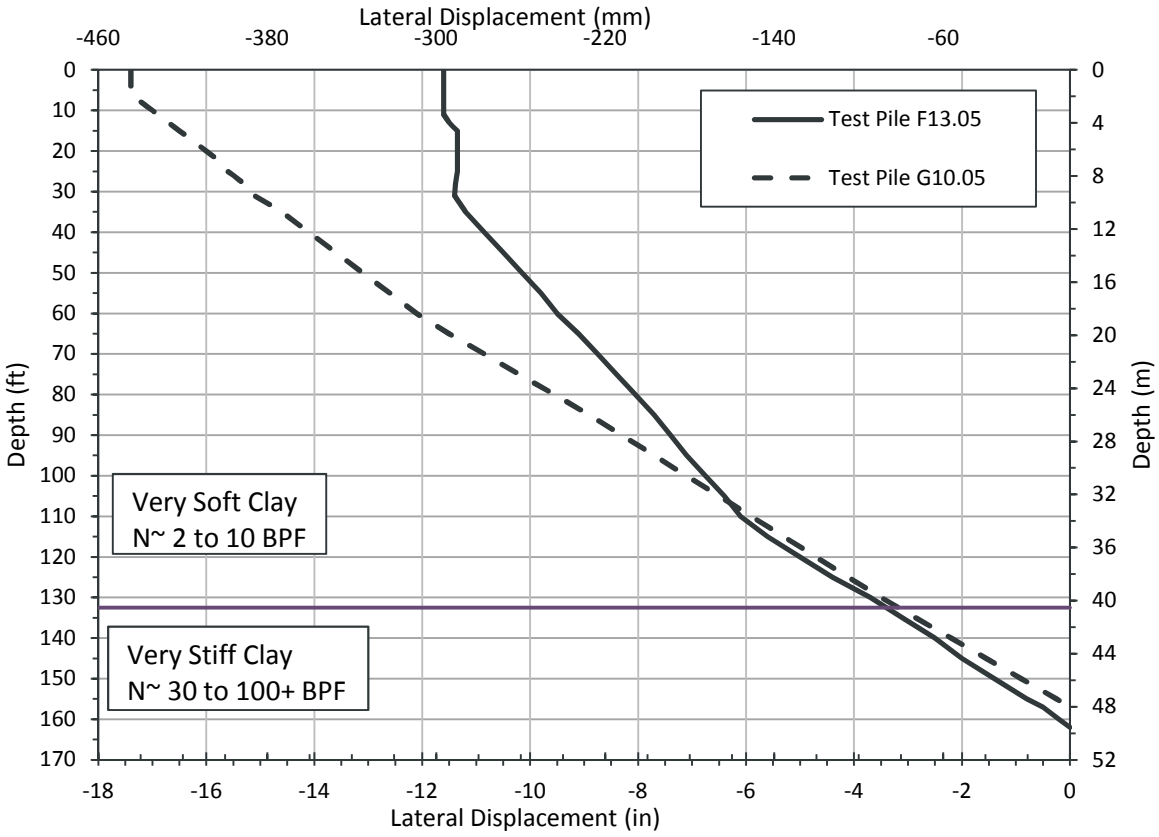


Fig. 1. UND SMHS Inclinometer Results

The piles were then instrumented with a strain gage at depths of 70, 90 and 110 feet (21, 27 and 34 m) in Pile F13.05, and at depths of 60, 80 and 150 feet (18, 24 and 46 m) in Pile G10.05. The strain gages were attached to a single piece of rebar located in the center of the pile. High-strain dynamic testing was performed on Pile G10.05 two days before performing the static load test, five days after being filled with concrete (high-strain dynamic testing was not performed on Pile F13.05). The high-strain dynamic test was performed using an SPI D30-32, open-ended, diesel, pile hammer. The measured, equivalent penetration resistance was 120 blows per foot (120 blows per 0.3 m) at a hammer stroke of about 10.6 feet (3.23 m). Based on the high-strain dynamic test data, the energy transfer ratio was about 82 percent. Based on a wave

matching evaluation, the results indicated that Pile G10.05 had an ultimate resistance of about 732 kips (3,256 kN), 38 days after the pile was installed. The evaluation indicated 405 kips (1,801 kN) was side shear resistance and 327 kips (1,455 kN) of toe resistance. Table 1 summarizes the details of the tested piles.

Table 1. UND SMHS Swept Pile Information

Pile	Date Installed	Date Tested	Pile Length (feet)	Toe Offset (inches)	Slenderness Ratio
F13.05	April 24, 2014	Static: May 14, 2014	164.5	12	211
G10.05	April 22, 2014	Dynamic: May 27, 2014 Static: May 29, 2014	153.5	17	196

Static, top-down load tests were performed on the two test piles generally following the requirements of ASTM D1143 (2013) and using Loading Procedure A: Quick Test. Figure 2 shows the load-deflection curves for the two test pile. While attempting to go from the 500-kip (2,224-kN) load increment to the 540-kip (2,402-kN) load increment, Pile F13.05 exhibited plunging behavior at a load of 525 kips (2,335 kN). Similarly, Pile G10.05 plunged at a load of 504 kips (2,242 kN).

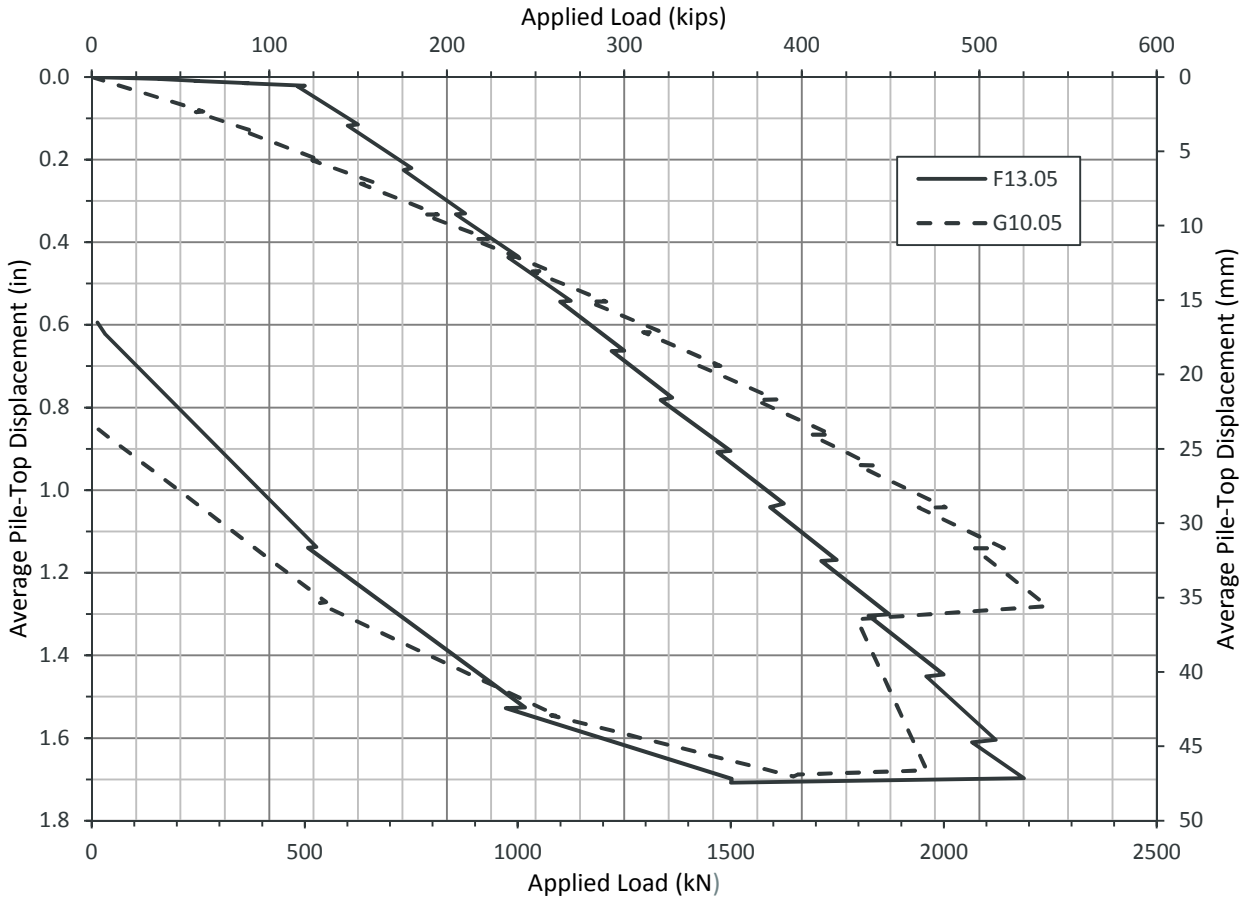


Fig. 2. UND SMHS Static Load Test Results

MYSTIC HOTEL AND CONVENTION CENTER ADDITION

Mystic HCCA Subsurface Conditions

The SMSC Gaming Enterprise was expanding the existing hotel and convention center located at the Mystic Lake Casino in Prior Lake, Minnesota, about 20 miles (32 km) southwest of Minneapolis. Referred to as the Mystic Hotel and Convention Center Addition (HCCA), the construction included a 12-story hotel tower and a two-story convention center. Only the hotel area is supported on deep foundations. The remaining structure utilized ground improvement for support.

Historically, this site was agricultural land until development of Mystic Lake in the 1990s. The project site has undergone multiple grading processes associated with construction of other existing structures. As a result, the general subsurface profile is fill over glacial till with areas of buried organic deposits in between the fill and glacial soils. The fill deposits are about 6- to 32-feet (2- to 10-m) thick and predominately classify as sandy lean clay with intermittent layers of lean clay and silty sand. The majority of the fill placed at the project site was only intended for pavement support. As such, the consistency varies as indicated by SPT N-values ranging from 4 to 67; generally, they are between 6 and 10. Cone penetrometer (CPT) tip resistances ranged from 0 to 40 tons per square foot, tsf, (0 to 3,830 kPa).

Three of the five borings performed in the hotel area encountered buried organic layers below the existing fill. The organic layers were approximately 5- to 10-feet (2- to 3-m) thick and consisted of peat or organic clay with N-values from 4 to 7. The organic deposits are not readily apparent on the CPT soundings. Most of the fill has been in place for more than 20 years. However, the soil is continuing to consolidate and is relatively weak.

The glacial till classifies as lean clay, sandy lean clay, silty clay or silty sand. Extending to the termination depth of the borings and soundings, the glacial till had N-values from 6 to 51 and CPT tip resistances from about 40 to 100 tsf (3,830 to 9,576 kPa). In general, the consistency of the till increased with depth. Typical, total unit weights in the glacial till are between 130 and 135 pcf (20.4 to 21.2 kN/m^3), although some layers are as low as 115 pcf (18.1 kN/m^3).

Mystic HCCA Pile Design

In Minnesota, closed-end pipe piles are the most common, driven pile type due to the presence of bedrock or hard/dense glacial till/outwash that is typically within 130 feet (40 m) of the ground surface. Similar to the UND SMHS project, the chosen pile was a 9.625-inch (244-mm), outside-diameter, closed-end pipe pile with wall thickness of 0.375 inches (10 mm). The driven depths ranged from about 54 to 96 feet (16 to 29 m) below the planned pile cap elevation.

The Mystic HCCA project had a required allowable pile resistance of 200 kips (890 kN) with a safety factor of 2.0. Therefore, the required ultimate pile resistance was 400 kips (1,779 kN). Similar to the UND SMHS project, the safety factor was selected based on full-time pile installation observation and high-strain dynamic testing on at least two of 214 production piles. Three piles were eventually tested with high-strain dynamic testing when one of the test piles was damaged during installation.

Using data obtained from restrike tests on Piles 10 and 145 six days after their installation, wave-matching resulted in ultimate resistances of 550 and 415 kips (2,447 and 1,846 kN), respectively. Pile 145 was determined to be damaged during observations of the pile shell after restrike testing. The high-strain dynamic test indicated damage during driving to a depth of about 80 feet (24 m) below grade. However, the measured length below grade after installation was only about 60 feet (18 m). Restrike testing was performed on Pile 100 to supplement the damaged test pile. The wave-matching evaluation of Pile 100 indicated an ultimate resistance of 436 kips (1,939 kN).

Mystic HCCA Swept Pile

Observations of the pile after installation for the Mystic HCCA project also indicated that many of the pile were swept such that the pile toe could not be observed. The project documents provided to the authors did not indicate a required tolerance for plumbness of driven piles. Assuming a tolerance of 0.25 in/ft (21 mm/m), the allowable sweep would be from 13 to 24 inches (330 to 610 mm), based on installed lengths.

The project team chose to evaluate the actual sweep using inclinometer testing on multiple piles, at various dates near the end of pile installation. For this project, centralizers for the inclinometer casing were not able to be obtained quickly enough to satisfy the project schedule. In all, nine piles were tested with measured toe offsets from about 20 to 63 inches (508 to 1,600 mm). Figure 3 shows the results of inclinometer testing.

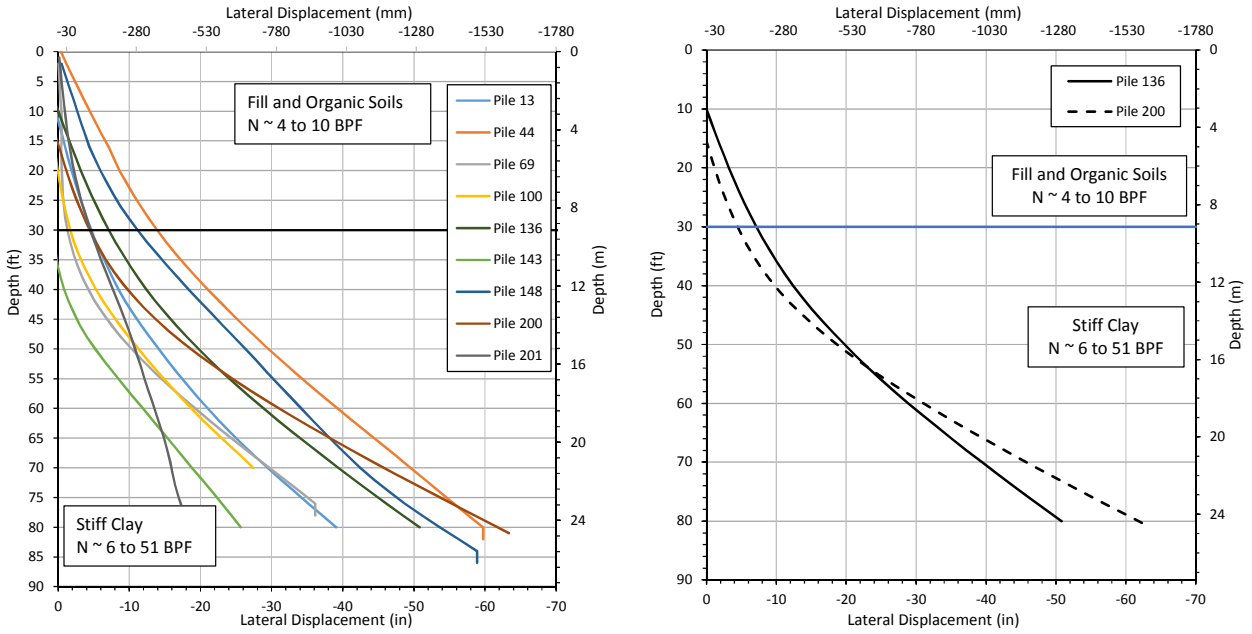


Fig. 3. Mystic HCCA Test Pile Inclinometer Results for a) all the inclinometer tested piles and b) static load test piles

Based on inclinometer test results, Piles 136 and 200 were selected for static load testing because they had relatively moderate to severe sweep and larger toe offsets compared to other piles tested initially. Strain gages were not installed in either pile for static load testing due to schedule constraints for the project. Both piles were tested 31 days after installation following ASTM D1143 using Loading Procedure A: Quick Test. Table 2 summarizes the installation and test dates, as well as the pile lengths and measured toe offsets while Fig. 4 graphically presents the measured pile top displacement and applied load.

Table 2. Mystic HCCA Swept Pile Information

Pile	Date Installed	Date Tested	Pile Length (feet)	Toe Offset (inches)	Slenderness Ratio
136	May 16, 2016	June 16, 2016	79.7	52	101
200	May 24, 2016	June 24, 2016	82.5	66	105

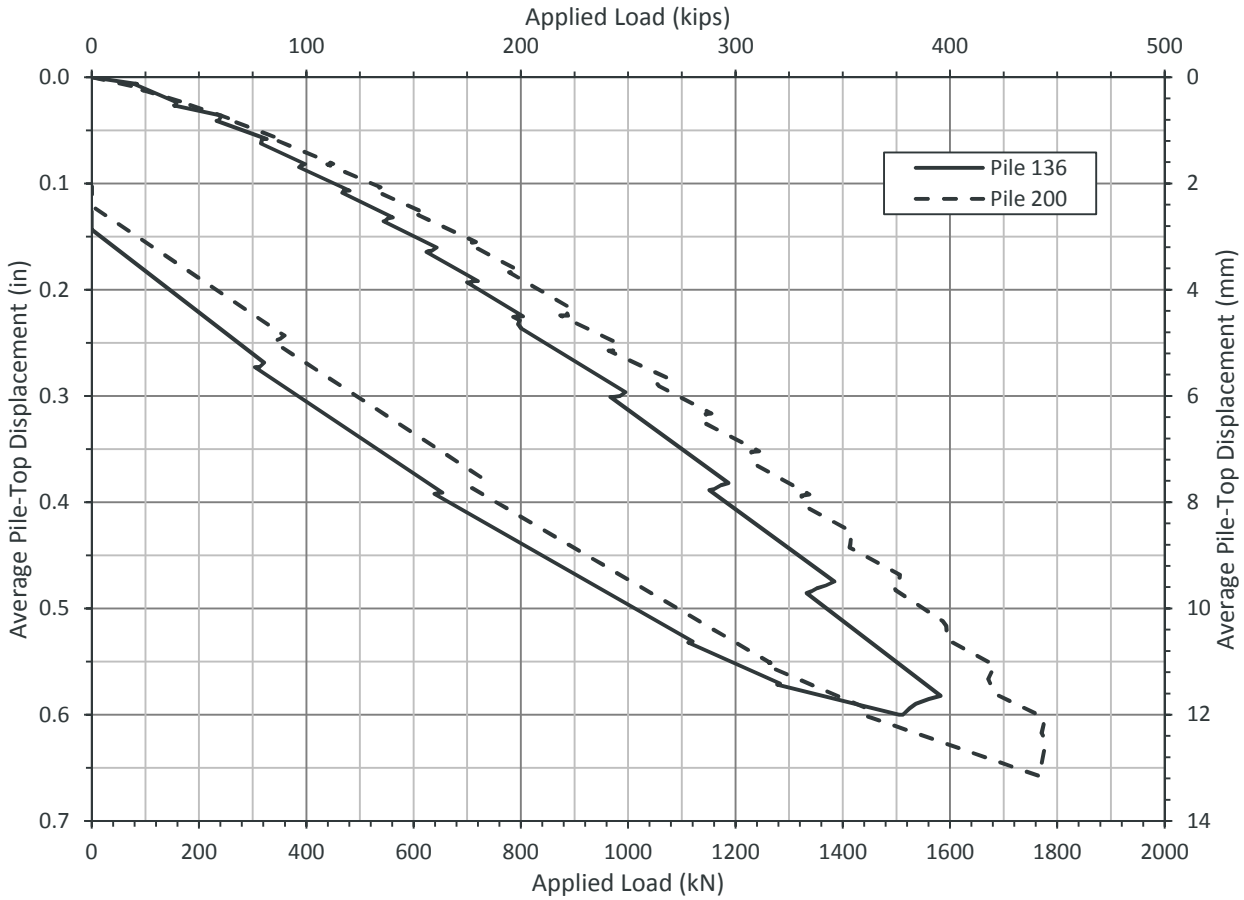


Fig. 4. Mystic HCCA Static Load Test Results

RESULTS

Tables 3 and 4 summarizes the results of the static load testing for the two projects. However, not reflected in the table, Piles 136 and 200 have a slightly thinner wall than Piles F13.05 and G10.05, 0.375 to 0.395 inches (9.5 to 10 mm), respectively.

Table 3. Summary of Static Test Pile Data and Results

Pile	Pile Length (feet)	Toe Offset (inches)	Allowable Resistance (kips)	Maximum Test Load (kips)	Average Pile Top Displacement (inches)			Slenderness Ratio
					At Design Load	At Maximum Test Load	After Unload	
F13.05	164.5	11.6	300	525	0.78	1.70	0.59	211
G10.05	153.5	17.4	300	504	0.68	1.85	0.93	196
136	79.7	50.8	200	400	0.24	0.60	0.13	101
200	82.5	63.4	200	400	0.18	0.52	0.08	105

Table 4. Pile Top Movement for Given Applied Load

Pile	Average Pile Top Displacement (inches) At Applied Load of	
	200 kips	400 kips
F13.05	0.30	1.10
G10.05	0.41	1.00
136	0.24	0.6
200	0.18	0.52

The slenderness ratio values, calculated in the manner presented by Nadeem et al. (2015), for the UND SMHS piles are higher than for the Mystic HCCA piles. On the other hand, the UND SMHS pile have less horizontal displacement per foot, or curvature, of pile than the Mystic HCCA piles. Furthermore, the UND SMHS piles exhibited more pile-top deflection than the Mystic HCCA piles by a factor of approximately two at a pile-top load of 400 kips (1,779 kN).

CONCLUSIONS

The results of load testing indicate that typical, construction tolerances of 0.25 to 0.50 inches per foot (21 to 42 mm/m) for bending may not be suitable for all projects. The UND SMHS piles had an average curvature of 0.07 to 0.11 inches per foot (6 to 9 mm/m) while the Mystic HCCA piles had an average curvature of 0.65 to 0.80 inches per foot (54 to 67 mm/m). The UND SMHS piles are well below typical tolerances but were unable to provide the required ultimate resistance. On the other hand, the Mystic HCCA piles were above typical construction tolerances and did provide the required ultimate resistance.

Nadeem, et al. (2013) concluded that piles with a higher slenderness ratio will have a lower, load-carrying capacity, and that piles with a greater "initial bend" or curvature will also have a lower, load-carrying capacity. With the small number of load tests and the Mystic HCCA piles not being tested to failure, the results of these two projects presented here cannot directly validate the conclusions of Nadeem, et al. However, the UND SMHS piles have a higher slenderness ratio and less curvature than the Mystic HCCA piles. The UND SMHS piles also exhibited significantly more pile-top deflection than the Mystic HCCA piles at the same pile-top load while being designed for a higher allowable load. Thus, the slenderness ratio may have greater effect on pile-top deformation, and possibly even on a pile's load-carrying capacity, than the degree of curvature.

Neither of these projects were initially approached with the intent of investigating the factors that affect the performance of swept piles. However, the similarities and differences in results identify potential shortcomings in current construction tolerances and identify opportunities for further research on this topic.

ACKNOWLEDGEMENTS

The authors gratefully acknowledge the contributions of our partners for their support and assistance during these projects and with this paper. For the UND SMHS project, we thank the University of North Dakota, PCL Construction Services, Inc. and Swingen Construction Company. On the Mystic HCCA project, we thank the SMSC Gaming Enterprise, PCL Construction Services, Inc. and L.H. Bolduc Company, Inc.

REFERENCES

ASTM Standard D1143, 2007 (2013). Standard Test Methods for Deep Foundations Under Static Axial Compressive Load. ASTM International, West Conshohocken, PA, DOI: 10.1520/D1143_D1143M, www.astm.org.

Dunlop, P., Sandiford, R.E., and Erali, D.R., 1993. Instrumented Load Test on a Bent Pile. Proceedings of the Third International Conference on Case Histories in Geotechnical Engineering, St. Louis, MO, June 1-6, S. Prakash, Editor, University of Missouri – Rolla, Publisher, pp. 25-30.

Minnesota Department of Transportation (MnDOT), 2016. Standard Specifications for Construction Section 2452. Minnesota Department of Transportation, St. Paul, MN, 695 p.

Missouri Department of Transportation (MoDOT), 2016. Missouri Standard Specifications for Highway Construction, Section 702. Missouri Highways and Transportation Commission, Jefferson City, MO, 673 p.

Nadeem, M., Chakraborty, T. and Matsagar, V., 2015. Nonlinear Buckling Analysis of Slender Piles with Geometric Imperfections. American Society of Civil Engineers, ASCE J. of Geotechnical and Geoenvironmental Engineering 141(1), DOI: 10.1061/(ASCE)GT.1943-5606.0001189, www.ascelibrary.org.

Pile Driving Contractors Association (PDCA), 2007. Installation Specification for Driven Piles, Section 4.3: Accuracy of Piles. Pile Driving Contractors Association, Orange Park, FL, 35 p.

U.S. Army Corps of Engineers (USACE) 1991. Design of Pile Foundations, Chapter 5: Engineering Considerations Pertaining to Construction. Department of the Army Engineer Manual 1110-2-2906, 186 p.

HYDROCUTTER-EXCAVATED SLURRY WALL FOR CENTER HILL DAM FOUNDATION REMEDIATION

Michael Arnold, BAUER Foundation Corp., Odessa, Florida, USA, (727) 531-2577,
michael.arnold@bauerfoundations.com
Bob Faulhaber, BAUER Foundation Corp., Odessa, Florida, USA, (727) 531-2577,
bob.faulhaber@bauerfoundations.com
Joe Nichols, BAUER Foundation Corp., Odessa, Florida, USA, (727) 531-2577,
joe.nichols@bauerfoundations.com

ABSTRACT

Center Hill Dam is a critical part of the infrastructure controlling floods at the Caney Fork River and reducing flood levels at the Cumberland, lower Ohio and Mississippi Rivers. The Center Hill Dam Foundation Remediation Project was necessary to address Karst features in the foundation rocks and observed signs of distress of the dam. From 2011 to 2014 BAUER Foundation Corp. (BFC) performed deep foundation works for this project. The executed features of work include the installation of two walls. The first wall extends throughout the clay embankment into the underlying rock to provide encasement during the construction of the second wall. Its width of 7.4 feet makes it the widest diaphragm wall ever installed. The second wall is the actual seepage barrier and provides a continuous 2-feet wide wall. It extends through the first wall into the underlying rock and is up to 300 feet deep. The paper introduces the project, the requirements specified by United States Army Corps of Engineers (USACE) for encasement and barrier wall and the approaches taken by BFC. It discusses the ground conditions and describes the excavation equipment as well as the excavation methods used. A special focus is put on the steering capabilities of the hydrocutter equipment and the verticality performance.

Keywords: slurry wall, hydrocutter, dam rehabilitation,

PROJECT

Beginning in 2011, BFC was tasked by the USACE with the installation of a seepage barrier/cutoff wall at the Center Hill Dam Foundation Remediation project under a partially performance based specification. The remediation was necessary due to karst features in the foundation rocks and observed signs of distress, which led USACE to rate the dam with the most critical dam safety action classification (DSAC I). The executed features of work include the installation of two walls. The first wall, an encasement wall, extends vertically through the clay embankment and is embedded minimally into the underlying bedrock to provide embankment stability during the construction of the second wall, the barrier wall. The encasement wall is constructed of overlapping panels 7.4 feet (2.25 m) wide, which is the widest diaphragm wall ever installed, and up to 210 feet (64 m) deep. The second wall is the seepage barrier and provides a continuous 2 feet (0.6 m) wide wall consisting of overlapping panels. It extends through the encasement wall into the underlying bedrock and is up to 307 feet (93 m) deep. BAUER BC40 and BC50 hydrocutters mounted on MC96 and MC128 foundation cranes were used to perform the majority of the works (Figure 1). Excavations were performed under bentonite slurry (encasement wall) and water (barrier wall) and concrete was poured with the tremie method. Adding to the challenges, the project had

 © 2017 DFI Annual Conference, New Orleans, LA, USA

to be executed in an environmentally sensitive area. Based on the high risk, a special focus was put on monitoring, quality control and geometric accuracy. The WallTracker information management system was used to share all relevant data between BFC and USACE (Roff et al. 2014).



Figure 1. BAUER MC 128 (left) and MC 96 (right), both equipped with hydrocutters, working during barrier wall installation

GROUND CONDITION GROUND CONDITIONS AND PRIOR REMEDIATIONS

The following description is based on the Geotechnical Baseline Report (USACE 2011). The right rim of the Caney Fork River is characterized by a steep rock slope, while the left rim rises more gently about 240 feet (70 m) from the riverbed to the crest of the earthen embankment. The earthen embankment section of the dam wraps around the left end of the concrete monolith and extents about 850 feet (260 m) at the crest to its end at the intersection with the left rim. The earthen embankment consists of compacted fill made of impervious silty clay and clayey silts.

The embankment was constructed directly on the existing overburden after topsoil was stripped. A cutoff trench was excavated in the centerline of the embankment removing the alluvium and the weathered surface rock. The alluvium is underlain by the flat lying Catheys, Cannon and Hermitage formations, with the Hermitage being underlain by the non-daylighting Carters and Lebanon formations (Figure 2). The Catheys, Cannon, Carters and Lebanon formations consist of limestone with bands of shale, while the Hermitage is composed of two limestone and two shale members. The Carters formation is divided into an upper and lower layer by 1.5 to 2 feet (0.45 to 0.6 m) thick bentonite layer. The Cannon formation is massive bedded, all other formations are thin bedded or medium to thin bedded. The limestone contains

two well-defined vertical joint sets. The unconfined compressive strength of the rock was up to 32,000 psi (220 MPa) in the Cannons with formation averages ranging from 7,000 to 27,000 psi (50 to 190 MPa).

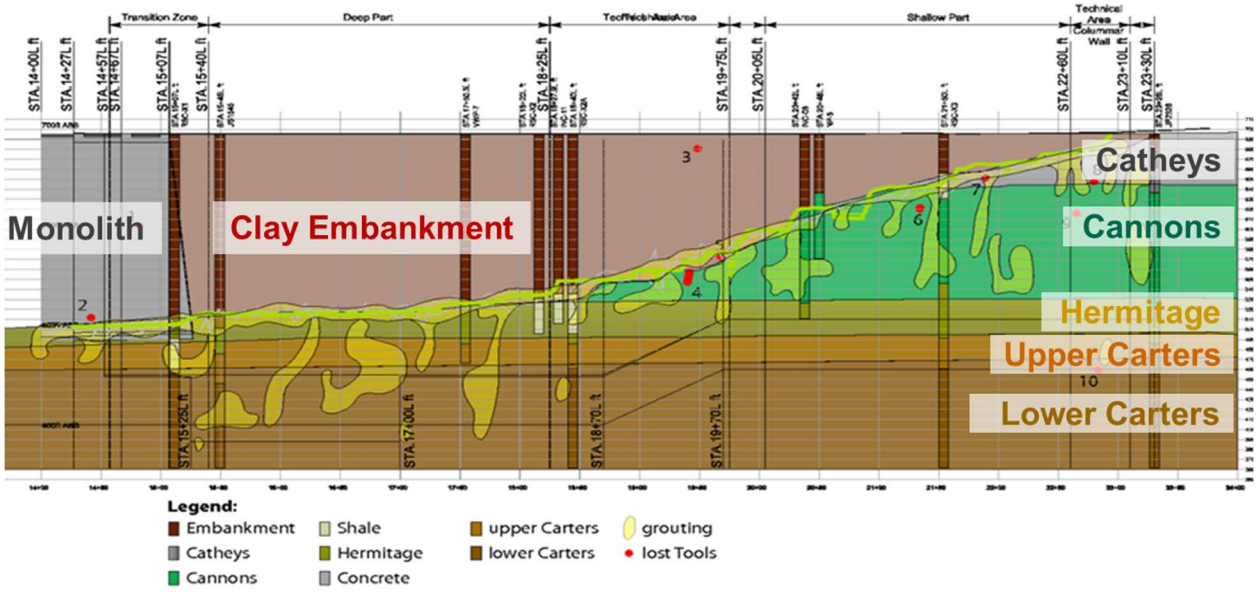


Figure 2. Geological profile in the wall alignment including areas of high grout takes (looking upstream)

Physical evidence of karst is visible throughout the site including disappearing streams, sinkholes, caves and extensive solution features. Limestone bedding planes and the contact zones between Catheys, Cannon and Hermitage show localized karst development. The vertical joints also promote solution processes and have created vertical soil-filled or open fractures. Bedding planes and vertical fractures have the potential to form interconnected systems of open features. These systems are especially threatening if they reach the embankment, creating piping features in the soil rock interface and potentially causing an erosion failure of the embankment.

A grout curtain was installed from and below the cutoff trench during original construction of the dam. Later, after several potential conditions were detected in the late 1970's, a grout curtain was installed about 10 feet (3 m) downstream of the embankment center line through the embankment into the bedrock from 1982-1984. Finally, in order to reduce seepage through the bedrock and in order to allow for a safe Barrier Wall construction, grout curtains were installed 12 feet (3.6 m) upstream and downstream of the wall alignment from 2009 to 2010.

HYDROCUTTER AND SUPPORT TECHNOLOGY

The encasement wall and barrier wall were excavated using BAUER trench cutters mounted on BAUER foundation cranes. The encasement wall, which included panel elements 7.4 by 10.5 feet (2.25 by 3.2 m), was executed with a BC50 trench cutter mounted on a MC128 foundation crane. The barrier wall, which included panel elements 2.7 by 10.5 feet (0.83 by 3.2 m), was executed utilizing the BC50/MC128 setup with different cutter wheels and a BC40 trench cutter mounted on a MC96 duty cycle crane. All cutters

were equipped with inclinometers as well as with a gyroscope providing the operator with real-time information on inclination, deviation and rotation on the B-Tronic screen (Figure 3). Based on this information the operator controls the steering plates (flaps) via the B-Tronic touchscreen (Figure 4) to steer the cutter into the desired direction.

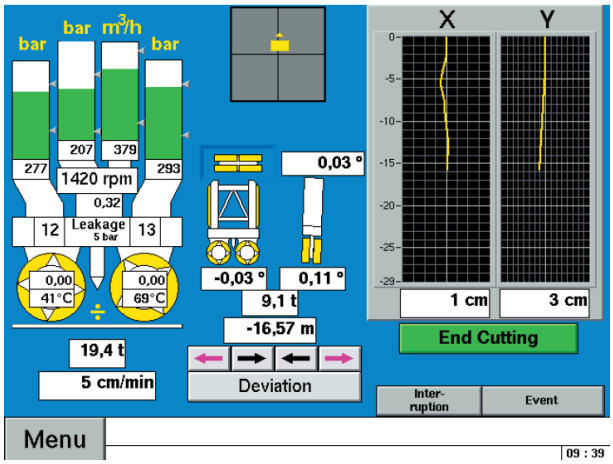


Figure 3. B-Tronics screen with deviations profile (BAUER 2016)

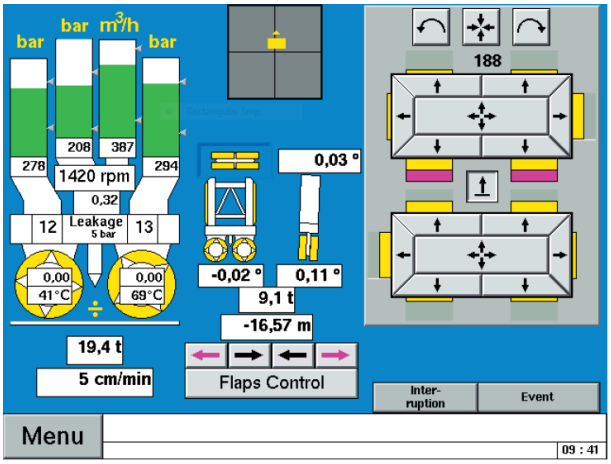


Figure 4. B-Tronics screen with control window. (BAUER 2016)

During encasement wall construction, which included excavation through embankment clay and in-situ rock, bentonite slurry was used to stabilize the excavation and transport cuttings from the excavation. Bentonite slurry was chosen over polymer slurry due to environmental concerns in case of a slurry loss into the tailwater, namely overloading the Caney Fork river with nutrients and endangering the trout population in it. During barrier wall construction, which included excavation through the encasement wall concrete and in-situ rock, water was used to transport cuttings from the excavation as no stabilization was required in the Encasement Wall and underlying rock. Under both scenarios, a substantial de-sanding plant was used to clean and recycle the fluid to the trench.

The de-sanding plant was capable of supporting two trench cutters operating simultaneously around the clock. The plant was assembled utilizing a series of machines to progressively remove cuttings of increasingly smaller sizes until the fluid was clean enough to return to the trench. These machines included scalpers, shakers, de-sanders, de-silters and a centrifuge. During encasement wall construction, the bentonite slurry was recycled approximately three times before its properties exceeded specification requirements and needed to be replaced with fresh slurry. During barrier wall construction, where the excavation was through concrete and rock, the water had to be replaced more often, typically after each panel excavation.

One of the most significant achievements of the project was the level of precision in which the verticality and orientation of the panels were excavated. This accuracy was achieved through a system that allows the trench cutter's verticality and orientation to be monitored and controlled in real time during the excavation process. The BC40 and BC50 trench cutters are equipped with an inclinometer that measures the inclination of the cutter frame continuously in both the x-axis and y-axis. A gyroscope was also fitted to the frame to measure the rotation of the trench cutter on the vertical (z) axis. All of this information is transmitted to the BAUER B-Tronic control system in the cab of the machine. Using this information

(and considerable knowledge and skill) the operator is able to steer the cutter using steering flaps and by independently controlling the rotational speed of the cutter wheels. For controlling verticality and orientation, the cutter frame is fitted with 12 individually controlled hydraulic plates that can adjust the position of the cutter frame in the trench in both the longitudinal and transverse direction. The rotational speed of the wheels can also be adjusted individually to correct measured deviations in the longitudinal direction.

ENCASEMENT WALL

Trenches excavated during barrier wall construction had the potential to intersect open solution features and connect the slurry-filled trench with the tailwater and in this way cause a sudden and substantial loss of fluid. This fluid loss could destabilize the excavation (trench) and therefore put the dam embankment at risk. To address this risk an encasement wall was built that extends from the crest of the dam down to a minimum of 2 feet (0.6 m) into the foundation bedrock. In this configuration, the encasement wall would support the embankment by bearing earth and water pressure in the event of trench fluid loss, protecting both the embankment and the excavation equipment. Based on the design strength of the encasement wall concrete of 3,000 psi, the required barrier wall cover was 12 to 17 inches (305 to 430 mm), depending on depth. The encasement wall was installed using three different approaches (see Figure 5).

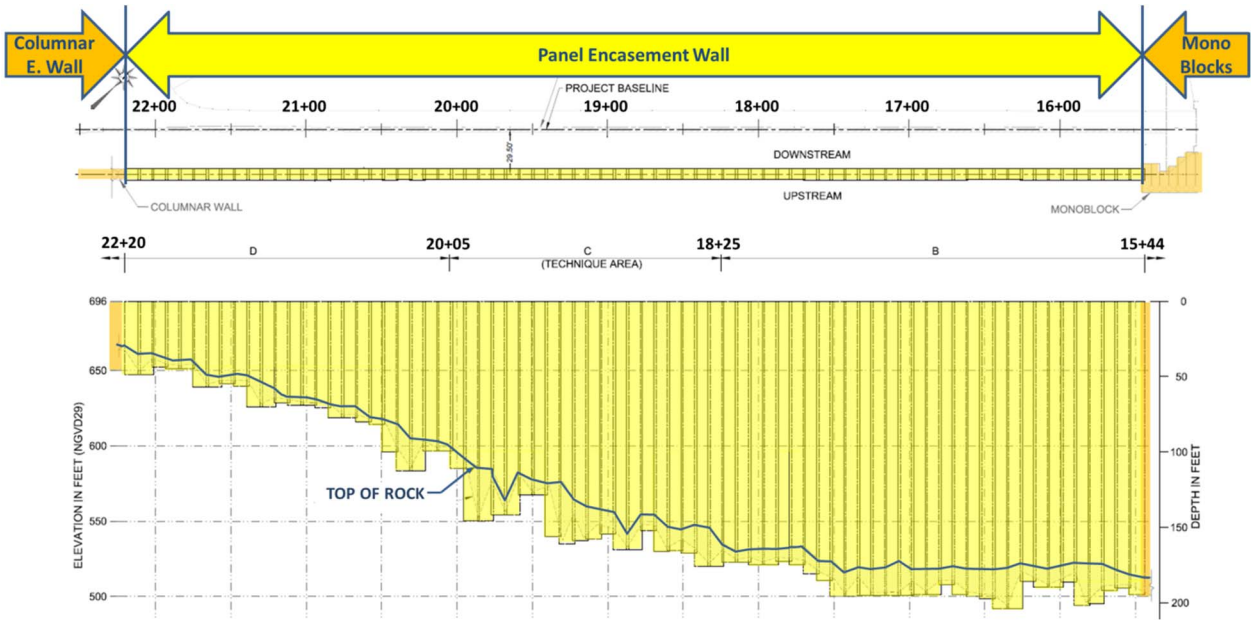


Figure 5. Panel encasement wall plan and profile (looking downstream, USACE 2011)

Columnar Encasement Wall and Mono Blocks

In the shallow section at the left rim, about 120 feet (36 m) long, the encasement wall was designed as a secant wall consisting of up to 35 feet (11 m) deep unreinforced concrete columns. The columns were excavated under dry conditions using fully cased Kelly drilling by a BAUER BG 50, the most powerful drilling rig currently made by BAUER.

In the area at the right end of the encasement wall where the barrier wall ties into the upstream face of the existing dam monolith, BFC decided to fully replace all soil with unreinforced concrete. This was achieved by a series of grab-excavated multi-bite panels (mono blocks) approximately 200 feet (60 m) deep, which touch each other along the long side. To seal the joints between the mono blocks and to allow for arching across the joints, concrete columns (mono block closing piles) were installed close to the ends of the joints by uncased Kelly drilling methods with the BG 50. The mono blocks were excavated under bentonite slurry, while the closing piles were excavated with minimal water.

Panel Encasement Wall

The 700 feet (210 m) long main section of the encasement wall was excavated in 10.5 feet (3.2 m) long panels reaching depths of over 200 feet (60 m) (Figure 5). Each primary panel was pre-excavated using a hydraulic grab mounted on the MC 96 (Figure 6). Due to the overlap of the panels, the length of the secondary panel pre-excavation was considerably shorter and therefore was performed by the BG 50 using uncased Kelly drilling. After pre-excavation, the panel was fully excavated using a BC 50 hydrocutter mounted on a BAUER MC 128 foundation crane (Figure 7). All excavations were performed in bentonite slurry-supported trenches and boreholes. Concrete was placed via two tremie pipes per panel.



Figure 6. MC96 with hydraulic grab



Figure 7. MC128 with BC50 cutter

The technical specifications (USACE 2011) called for tolerances of 0.25% maximum panel verticality deviation, maximum six degrees panel rotation (twist) and a minimum 6-inch (150 mm) overlap between primary and secondary panels throughout the full width and depth of the wall. To achieve these goals the cutter needs to be steered, which requires both precise in-formation about the actual position of the tool with respect to design and steering capabilities.

BFC used BAUER's proprietary Cutter Inclination System (CIS) in conjunction with advanced instrumentation to determine the position of the cutter in the trench. This information, in combination with the steering capabilities as discussed above, allowed the operators to excavate all elements well below the contractual tolerances despite locally adverse conditions of a steeply angled soil-rock interface at the slopes of the cutoff trench. As-built surveys were initially performed using the CIS, Koden and SoniCaliper methods as well as by performing free-fall passes with the tool. Analyses comparing the results of the different methods indicated the Koden method produced the most accurate as-built information. The Koden data were ultimately used to determine the as-built data set, which showed a maximum recorded deviation out of plumb of 0.43 feet (130 mm) and a maximum panel rotation of 4.3 degrees with averages being only a fraction thereof. The minimum overlap achieved was 0.58 feet (180 mm), providing more than the required overlap of 0.5 feet (150 mm).

BARRIER WALL

For barrier wall construction two wall types were specified: a 50 feet (15 m) long columnar section with depths up to 186 feet (56 m) and two sections totaling about 850 feet (260 m) of hybrid panel/column wall with depths up to 306 feet (93 m) deep (Figure 8). A 150 feet (45 m) long extension of the hybrid wall was later added to the contract scope. The objective was to create a continuous, minimum 2 feet (0.6 m) wide wall with elements overlapping by a minimum of 0.5 feet (152 mm) and a permeability of less than $1x10^{-6}$ cm/sec. Additional element verticality and panel rotation tolerances of 0.25% and 6 degrees, respectively, were imposed. The specifications (USACE 2011) also called for steerable exploratory pilot holes for all columns.

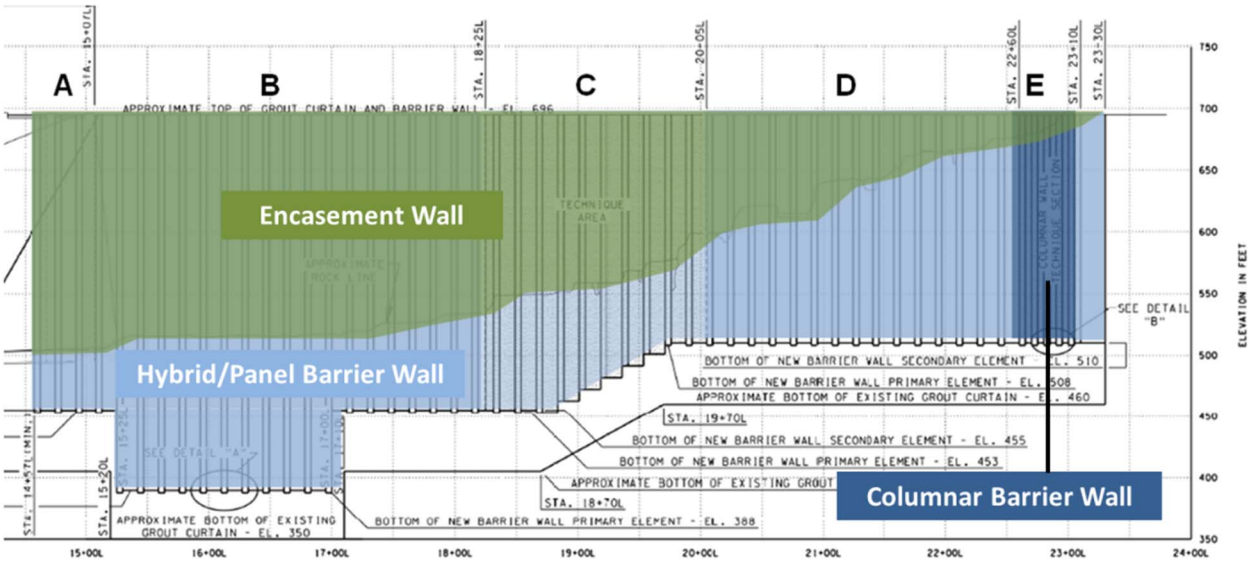


Figure 8. Barrier wall profile (looking upstream)

Columnar Barrier Wall

BFC's design consisted of twelve 4-foot (1.2 m) diameter primary columns up to 188 feet (45 and 57 m) deep, and eleven 4.5-foot (1.4 m) diameter secondary columns up to 186 feet deep. Pilot holes were used

to guide the excavations. Downhole water hammers, Wassara W150 and W200, in conjunction with a Klemm KR 806-4 drilling rig were used to drill the pilot holes. Rock augers and drilling buckets, both equipped with stingers (extended pilot bits) to follow the pilot hole, were used to excavate the columns. Drilling was per-formed dry at the top and under water at depth with the BG 50.

Panel Barrier Wall

In their proposal, BFC followed specifications and proposed a hybrid wall configuration (Figure 9). The columns in the USACE plan were designed to provide additional wall thickness at the panel overlaps because of USACE concerns that the required vertical and rotational accuracies would be difficult to achieve at 300+ feet (90+ m) deep. However, based on the ability of the BAUER hydrocutter to excavate the hard rock and maintain excellent verticality as demonstrated at the panel encasement wall, BFC made a value engineering cost proposal (VECP) to eliminate the columns (red circles in Figure 9) including the required pilot holes without increasing the nominal overlap between the barrier wall panels. The government accepted the VECP, which saved approximately 100 columns, at a cost savings of over $13 million.

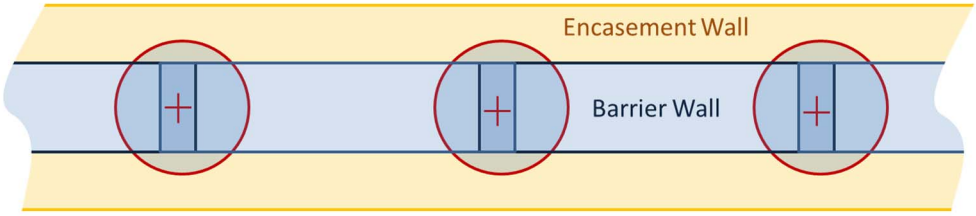


Figure 9. Schematic plan view hybrid barrier wall

The barrier wall was excavated through the encasement wall concrete into the foundation rock to depths between 146 feet (44 m) and 306 feet (93 m). A MC 128 and a MC 96 foundation crane (Figure 1) were used simultaneously; both equipped with BC 40 cutter units cutting panels with 10.5 x 2.7 feet (3.2 x 0.83 m) footprint. Water was used as trench support and transport fluid. No excessive water loss, defined in the specifications as a loss of three feet of water or more, occurred during the barrier wall works, demonstrating the effectiveness of the 2009/2010 grouting program. Concrete was again placed using two tremie pipes. The concrete of the secondary panels was dyed red to differentiate between different panels during the verification coring program. Cores and borehole images showed that the use of water as fluid in conjunction with a rigorous joint cleaning procedure with panel brushes (Figure 10) allowed for an excellent bond without any film between the primary and secondary panels.

To achieve the stringent geometric requirements resulting from the VECP, the operators focused on panel verticality and panel rotation and made use of the CIS to obtain the most accurate position of the cutter. Panel rotations of less than 2 degrees were targeted. As-built surveys were performed using the CIS, Koden and free-fall pass methods. The as-built Koden data set indicated a maximum recorded deviation out of plumb of 0.56 feet and a maximum panel rotation of 3.3 degrees. This means that both the verticality specification of maximum 0.25% as well as the rotational specification limit of maximum 6 degrees were met by all elements. The rotational target of 2 degrees was only exceeded in isolated cases.

Due to these excellent results the wall continuity was also achieved at all overlaps. Based on 6 inches (0.15 m) of minimum overlap along the wall axis the wall thickness at the overlap was at almost all overlaps 2.5 feet (0.75 m) or more with a recorded minimum of 2.33 feet (0.71 m). This represents a benefit of almost 25% in wall thickness over the specified wall thickness of 2.0 feet (0.6 m). The largest deviations and rotations were recorded at random depths typically above the bottom of the wall. This is a direct effect of the active steering of the hydrocutter during excavation.



Figure 10. Panel brush

CONCLUSION

The hydrocutter technology was used by BFC with great technical success at the Center Hill Dam Foundation Remediation project. The geometric accuracy of both the barrier and the encasement wall well exceeded the stringent specification requirements. This is even more remarkable as almost half of the originally planned number of elements were eliminated with a value engineering approach that also resulted in significant cost savings to the government. BFC was able to achieve this through the use of innovative techniques and hydrocutter equipment that allows for extremely accurate excavations in complex geotechnical conditions such as steeply inclined soil-rock interfaces and hard, massive bedded rocks.

REFERENCES

BAUER Maschinen GmbH, 2016. BAUER Trench Cutter Systems.

Roff et al., 2014. Geographic Information Systems Technology Use in Tracking Quality Control in In Situ Barrier Wall Construction. Proceedings of the 39th Annual Conference on Deep Foundations, 2014, Atlanta, GA, USA

United States Army Corps of Engineers, 2011. Center Hill Foundation Remediation, Solicitation, Amendments, and Technical Specifications

TTMJ – THE NEW SYSTEM FOR SLURRY (DIAPHRAGM) WALL JOINTS

Julian Crawley, CCMJ Systems, Basingstoke, Hampshire, UK. julian.crawley@ccmjsystems.com
Maurizio Siepi, Trevi SpA., Cesena, Italy. msiepi@trevispa.com
Paul van Horn, Arup, Amsterdam, Netherlands. paul.van-horn@arup.com
John Coupland, CCMJ Systems, Strathpeffer, Highlands, UK. john.coupland@ccmjsystems.com

ABSTRACT
TTMJ is the acronym for the Slurry (Diaphragm) Wall Tension Track Milled Joint currently in development as part of the European Union's innovative and far-reaching Horizon 2020 initiative (FTI Pilot-2015-1 720579). The TTMJ Project has been specifically set up to deliver this versatile new step-forward in Slurry Wall technology. The TTMJ System is protected by patent in Europe and the USA, and is currently under development by a consortium comprising Trevi SpA (Italy), Arup (Netherlands) and CCMJ Systems (UK). The principles of the TTMJ System together with the installation process are herein described in general terms. The system is still under development with field trials scheduled for early 2018, so some of the detail will not be disclosed at this stage. It is the intention of the Authors that the results of these field trials and a more complete description of the System will be presented in a paper we intend to submit for the DFI/EFFC International Conference on Deep Foundations and Ground Improvement to be held in Rome, Italy in June 2018. The final section of this paper explains how the TTMJ system can be applied to a common application of slurry wall construction; deep circular or multi-cell shafts. The system can be used to construct shafts more easily and at less cost than current methods. It also allows shafts with smaller internal dimensions to be constructed than is currently practical.

Keywords: slurry walls, diaphragm walls, milled joints, trimmer, guide track

INTRODUCTION
CCMJ Systems (UK) realised that an innovative new approach to forming joints in both Slurry (Diaphragm) Walls and Secant Pile Walls would provide greatly improved joint integrity to greater depths, to the overall benefit of retaining wall quality, across the world-wide foundations industry.

In particular this new system is designed to:

- Increase the effective depth range of Slurry Walls (especially walls excavated by grab) and Secant Walls
- Remove the requirement for Stop-ends or Joint Formers
- Allow for a Shear Key at the joint
- Allow for a Water Stop to be installed at the joint
- Permit Continuous Reinforcement across the joint
- Optimise Reinforcement Density and hence Concrete Flow
- Facilitate joints in corner panels eliminating the need for “L” shaped cages and reducing large single-pour concrete volumes and slurry storage capacity requirements.
- Enable the construction of smaller-dimensioned square and circular deep shafts (especially useful for city-centre sites) than is possible with current methods.

CCMJ Systems approached other industry specialists with a view to forming a development team to explore the possibilities for this new technique.

TTMJ is the acronym for the Diaphragm Wall Tension Trimmed Milled Joint, currently in development as part of the European Union's innovative and far-reaching Horizon 2020 initiative. The TTMJ Project has been specifically set up to deliver this versatile new step-forward in Slurry Wall technology. The TTMJ

 © 2017 DFI Annual Conference, New Orleans, LA, USA

Joint is protected by patent in Europe and the USA, and is currently under development by a consortium comprising Trevi SpA (Italy), Arup (Netherlands) and CCMJ Systems (UK).

BACKGROUND

The average depth of Slurry or Diaphragm Walls has increased steadily over the last 50 or so years. When the technique was first developed in the 1950s, the grabs had rounded clam shells and the joints were formed by installing steel tubes at the end of the panel and extracting them immediately after the concrete had achieved an initial set. When square ended clamshell grabs came into use, the steel stop-end / joint-former became rectangular with a protrusion to form a shear key or a row of smaller diameter pipes welded together (organ pipes). These joint formers still needed to be extracted at the right time. In the United States the preferred method was to use cast-in steel wide flange beams (W beams). The soil side of the beam was filled with a void forming material which could be removed during excavation of the adjacent panel.

In the 1990s the "peel off" continuous water stop (CWS) Steel Joint Former (*Fig.1*) came into use, particularly in Europe. This became a highly successful and efficient method for forming the joint between adjacent Slurry Wall panels. The joint could incorporate a water bar and it was no longer necessary to pull out steel joint-formers in the middle of the night!

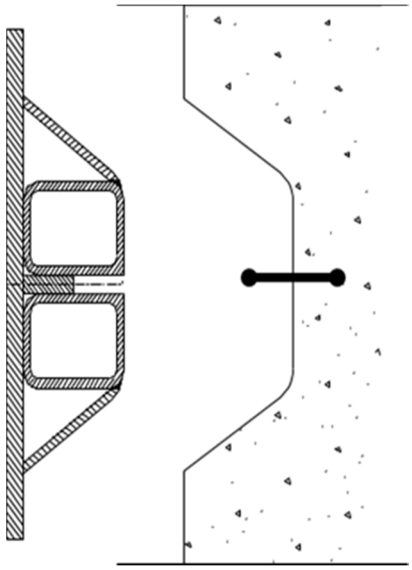


Fig.1 CWS Stop-end

As slurry wall depths have increased, problems have arisen with the removal of the CWS joint formers. It was found that beyond 30m (100ft) it was sometimes difficult and time consuming to install, and peel them away from the concrete of the previously constructed panel. The trend to change from rope operated grabs to the more cumbersome but more efficient hydraulic grabs seemed to exacerbate the problem. As the depths increased, contractors began fixing plywood and other materials to the steel surface, to try and reduce the bond between the CWS former and the concrete (*Fig.2).* Using such methods, the CWS system has been used to depths in excess of 50m (165ft) but only by the most experienced specialist foundation companies and even then the risk of problems with removal is high.



Fig. 2 Wood and plastic covered CWS Stop-end

The other option, particularly used for the construction of circular shafts and dam cut off walls is to employ reverse-circulation 'hydro-mills' to form joints by cutting into the concrete of the adjacent panels. Hydro-mills are now routinely being used to install slurry walls to depths of over 50m, and 100m deep is not uncommon. In 2012, Trevi installed a test panel to a depth of 250m (820ft) (Pagliacci, 2013). However, a joint formed by over-cutting the concrete with the "hydro-mill" cannot accommodate a water stop and shear connection between the panels is likely to be limited. When used in the construction of circular shafts the joints are all in compression - wall movement tends to be inwards due to the external radial pressures. Water leakage through the wall is often minimal (although seepage may still result from the presence of joint defects or voids in the wall) but this may not be the case if the structure is a propped or cantilever linear wall, where there is a greater potential for differential movement between panels.

To summarize; the existing joint forming methods have 'lagged behind' to the extent that they no longer adequately fulfil the role for which they were originally designed. The result is that the integrity of the completed joint may be compromised as a result of unrealistic expectations for verticality and other tolerances.

THE BASIC PROCESS / OBJECTIVES

The reader is invited to imagine a road planer removing the surface of a road. The TTMJ Trimmer works in a similar manner, but on the vertical concrete end surface of the slurry wall panel, to form a profiled (vertical) joint. Guides attached to the body of the trimmer run in Guide Tracks fitted to and installed with the reinforcement cage in the previous panel. These Guide Tracks maintain the vertical alignment and plan position of the trimmer cutting wheel relative to the guide track, and ensure that the trimmer cannot move away from the concrete (joint) surface.

The fundamental basis for the TTMJ process is to allow Slurry Wall excavation to increased depths, without compromising the quality of the joint between adjacent Slurry Wall panels. Crucially, the trimming of the secondary panel is controlled by the profile of the primary panel. With suitable care and attention (standard procedure for the competent Slurry Wall specialist contractor!) the joint can be formed to considerable (ie. increased) depth without risk to vertical or plan tolerances. This process automatically compensates for all reasonable verticality tolerance issues to any depth that can be (sensibly) excavated by hydraulic grab. If the TTMJ system is used with a hydro-mill there is theoretically no limit to the depth that can be achieved.

If we consider a Slurry Wall of alternating primary and secondary panels:

- The circular guide tracks (2 per joint) are attached to the primary panel reinforcement cages.
- The guide tracks are allowed to fill with bentonite (or polymer) fluid as the reinforcement cage is placed in the excavated trench, but 'closed' sufficiently to ensure that high-slump concrete is unable to penetrate into the tracks during concreting of the primary panel.
- Secondary panels can be excavated when the concrete in the adjacent primary panels has attained sufficient strength.
- When excavation of the secondary panel has been completed, the Trimmer is used to prepare the TTMJ Joint. The guides are introduced into the guide tracks and the Trimmer is run down the joint to the required depth, removing concrete cover and the sacrificial wall of the guide tracks
- When the concrete and track debris has been removed and other Slurry Wall cleaning processes completed, the water-bar positioned (if specified) and any other operations completed, the secondary panel can be concreted.

TTMJ TRIMMER & GUIDE TRACK

TTMJ Trimmer

The Trimmer *(Fig.3)*, which is being designed and built by Trevi with the assistance of sister company Soilmec, is required to work under considerable hydrostatic pressure, resulting from the trench support fluid (bentonite or polymer), constraints that mirror Slurry Wall operating conditions. For most applications, the Guide Track will have a typical concrete cover of ±50mm (2ins) so the anticipated output of the Trimmer is expected to be similar to the road planer ie. ~ 50 to 60m (165 to 200ft) of joint per hour.

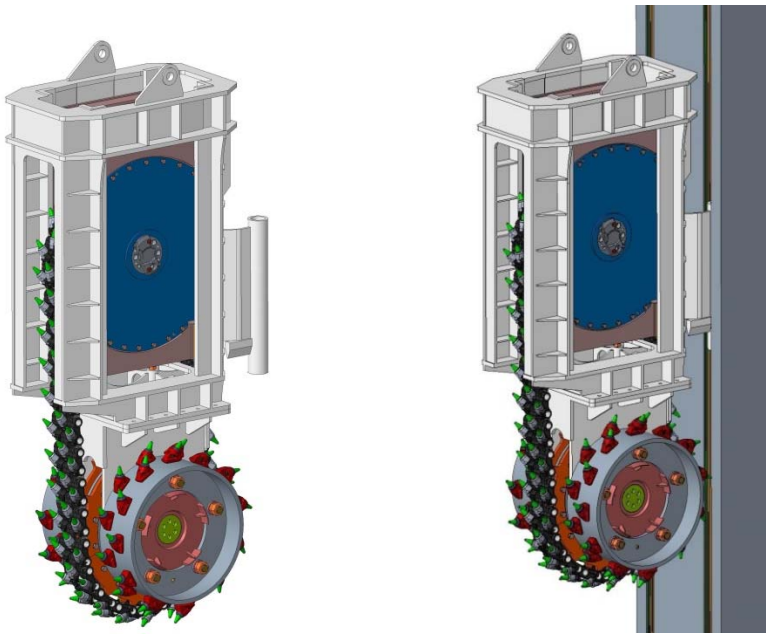


Fig.3 The TTMJ Trimmer

The trimmer design is based on a combination of Slurry Wall mill and road planer technology. (One of the key considerations is the ability to work under a considerable head of bentonite or polymer). The trimmer is being designed to remove a variable thickness of concrete as well as the sacrificial portion of the Guide Track. It incorporates an hydraulic motor powering a cutter drum via a chain drive. The chain drive can be used to form a profiled joint ie. to deliver a shear key between adjacent Slurry Wall panels.

At this stage there is no plan to incorporate a pump or other system to remove the cuttings. They will fall to the bottom of the trench and will need to be removed periodically by a grab or possibly by a separate air lift or pump.

TTMJ Guide Track

The TTMJ Guide Track is being developed by CCMJ Systems. A simplified illustration of how it might look is shown below (*Figs 4 & 5).* The track will be installed with the reinforcement cage in the adjacent completed panel. The trimmer removes a sacrificial portion of the track as it passes to allow the guides to descend.

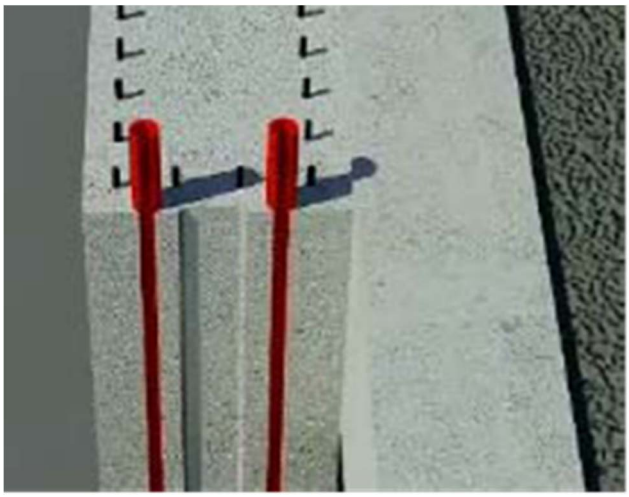


Fig. 4 Guide Tracks fixed in the primary panel



Fig.5 End of Primary Panel showing trimmed face of concrete & shear key

TTMJ SYSTEM – ADDITIONAL BENEFITS

The Trimmer has to follow the Guide Track set in the concrete of the adjacent constructed panel; consequently concrete-to-concrete contact is assured. It should be noted that the prototype machine is intended to form joints in 1.2m (4ft) thick slurry walls. It will have a 1m (3.3ft) wide cutter wheel so that soil from the side walls will only be removed if the excavation of the second panel has deviated vertically relative to the adjacent concreted panel by more than 100mm (4ins).

The Trimmer cutter wheel can have a raised centre section to form a shear key, as required.

When the design demands, the TTMJ System will allow the installation of an effective water stop in the panel joints. Details are currently confidential.

The Guide Tracks used for the TTMJ System can also be used to provide a tension connection across the panel joint. A simplified illustration is shown below. (*Fig.6)*

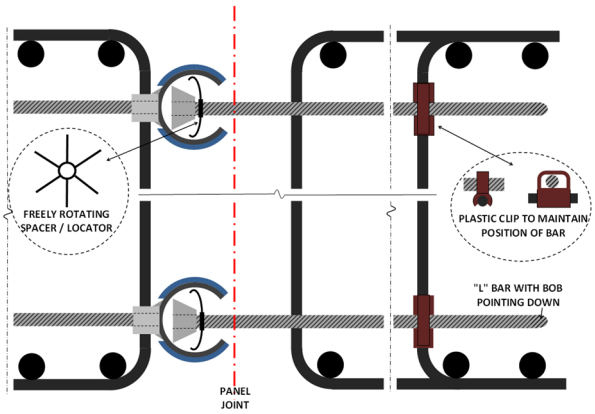


Fig.6 Simplified sketch of the tension joint arrangement

In early 2015, ARUP carried out research into the TTMJ tension joint based on Finite Element modelling. Their preliminary study focused on the capacity of a diaphragm wall panel joint to carry shear and tension across the interface of adjacent panels, important as it allows diaphragm walls to spread concentrated loads from the building structure over a wide area of the foundation. On the completion of their desk study ARUP concluded that the TTMJ system *"promises to offer designers an opportunity to deliver foundation solutions that are more efficient, effective, robust and buildable…."*. (Internal Arup Report).

The TTMJ Development Project will bring innovation to the market for the benefit of the foundations industry worldwide, and at the same time will bring substantial added value at different levels:

- Construction Sector: the achievements of the action will improve the technical procedures for constructing slurry walls. TTMJ is a better way to construct slurry wall joints; the benefits for companies using the system will include the ability to generate cost savings whilst delivering a superior quality product. This represents a clear commercial advantage and an equally clear improved risk profile.

- Clients: for Clients and Owners, the commercial advantage can be translated into project-cost savings, a higher-quality product and a better profile in terms of risk reduction, quality and durability of walls. The risk of conflict with residents in the area will be diminished, due to the reduced impact of construction.

- Economy and Society: the improvement in slurry wall technique will be sustainable and have a lesser impact on the environment, by reducing the effect on the integrity of surrounding buildings in highly urbanized areas. This innovation has global appeal and potential to achieve a substantial market share. Alongside the commercial advantages, it delivers a step□change improvement in Health and Safety, and Environmental and Quality considerations.

The TTMJ system fills a current void in the market and provides a fundamental step forward in slurry walling, leading to technical, environmental and economic advantages:

- An effective jointing system for deeper hydraulic grab excavation.
- An improved jointing system for slurry wall excavation.
- Shear/tension capacity across slurry wall joints.
- Ability to construct 'tighter' slurry wall shafts (reduced land-take)

TTMJ DEVELOPMENT

The TTMJ System development, funded by the EU, started from the work already completed by CCMJ Systems (which confirmed the viability of the system) and will finish with its commercial use on an actual project. Development proceeds through the following stages:

- Develop, design and construct a full scale Joint Trimmer.
- Develop and test the guide track system, the tension joint and water stop.
- Laboratory trials of the guide track and tension joint,
- Full scale field trials of the Joint Trimmer and guide track.
- Specify, validate and issue industry accreditation for the TTMJ System.
- Enter the final stage of the project, by creating the right conditions to introduce the new product into the worldwide market place.

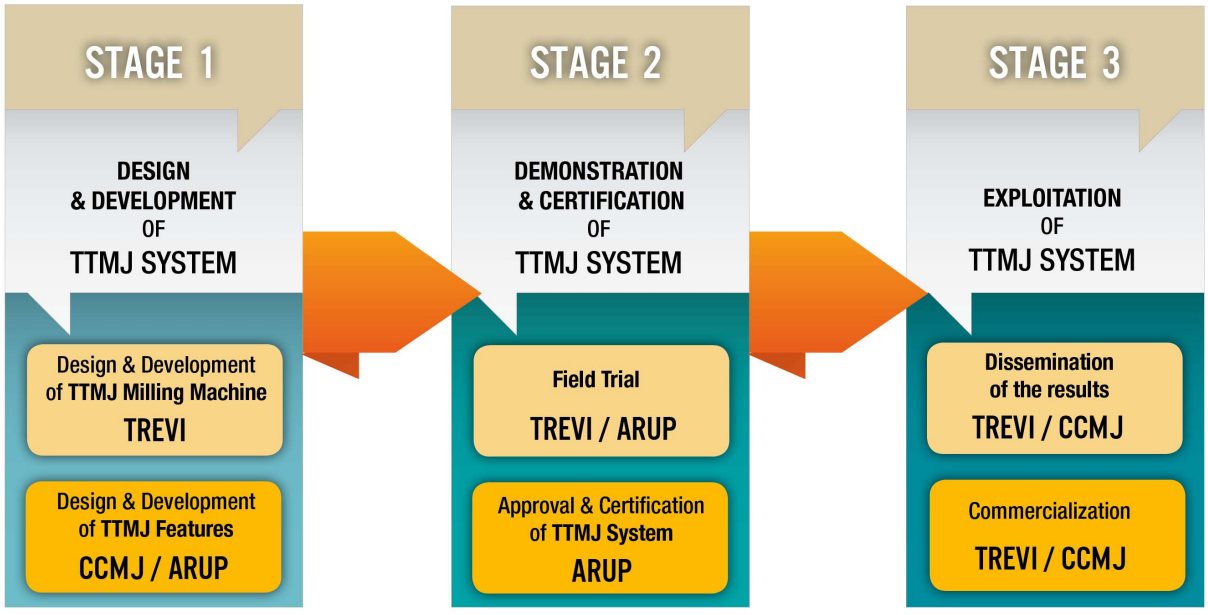


Fig.7 Principal Roles of Consortium Members

VALIDATION

Arup is responsible for formal validation of the system. The first consideration is that the TTMJ System must work within current Slurry Wall specifications – the second that is provides the next step forward in Slurry Wall technology. The Project will clearly benefit from the scrutiny of the world's leading geotechnical consultancy!

Materials Testing

Testing of the guide track components and the way they will interact with the Slurry Wall reinforcement cage / concrete will be carried out by CCMJ. Testing falls into two basic areas:

- Fundamental definition of system strengths and the efficiency of introducing new materials.
- Optimisation of design parameters, including developing the most cost-efficient product.

FIELD TRIAL

Full scale field trials are typically extremely difficult to specify, organise, deliver and analyse. The TTMJ Project has the all-important advantage of access to the 20m (65ft) deep test facility in the Trevi / Soilmec works at Cesena, Northern Italy. This will allow the team to build a mock-up of the panel joint for test trimming – with detailed observation - and recourse to a repeat trial if deemed necessary. In terms of industry confidence, this will provide clear confirmation of the effectiveness of the complete system *in situ*.

There will undoubtedly be some modifications and improvements carried out during the trials to optimise performance. Concurrent with the manufacturing stage, laboratory testing on guide and tracks will be undertaken. Throughout the process, the work will be monitored to ensure compliance with recognised standards and allow a specification to be compiled such that at the end of the Field Trials a fully accredited system will be ready to enter the market. The TTMJ Project Management Team will ensure the results of all the tests and trials are recorded and disseminated.

TTMJ SYSTEM – SHAFT CONSTRUCTION

During the development process to date it has become apparent that where slurry walls are used for shaft construction there could be considerable benefits from the introduction of the TTMJ System. In 2014 Trevi tendered for five deep slurry wall shafts in London. For one of these shafts, the slurry wall had an internal diameter of 28m (90ft), and the panels were more than 70m (230ft) deep. Due to the close proximity of apartment blocks, houses and a school, there were noise limits and restricted hours of working. In order to meet these constraints, the work was tendered on the basis of single 'bite' panels (essentially one grab in plan-length) because longer multiple-bite panels (typically 6-7m (20-23ft) in plan length) could not have been concreted within the available working hours. The panel arrangement consisted of 17 x 2.8m (9ft) long primary panels and 17 x 2.8m (9ft) long secondary panels which overcut the primary panels. Excavation of the primary panels was to be carried out by both hydraulic grab and hydro-mill working concurrently. As it was necessary to overcut the concrete of the primary panels, the secondary panels could only be excavated with the hydro-mill.

If the TTMJ System had been available, the panel arrangement would have been 14 x 2.8m (9ft) long primary panels and 14 x 3.2m (10.5ft) long secondary panels. Both primary and secondary panels would have been excavated by both the grab and the hydro-mill - with the grab crane also used with the TTMJ trimmer to form the joints.

Using exactly the same excavation rates for the grab and the hydro-mill, the revised scheduled construction duration was reduced by 40%, and the cost reduced by 20%.

Possible shaft panel layouts using the TTMJ System are shown below:

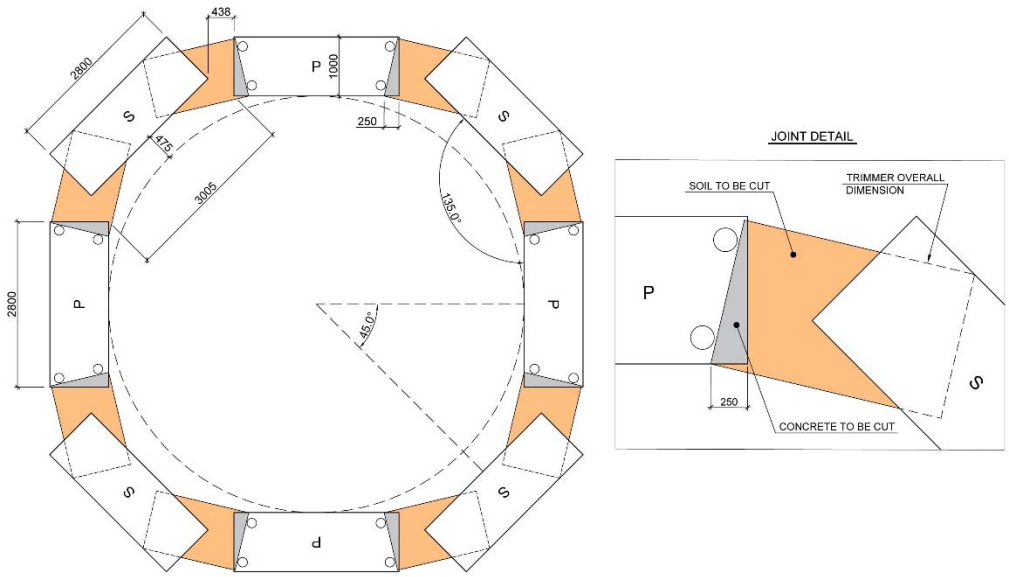


Fig. 8 7m (23ft) Internal Diameter Shaft using 8 panels

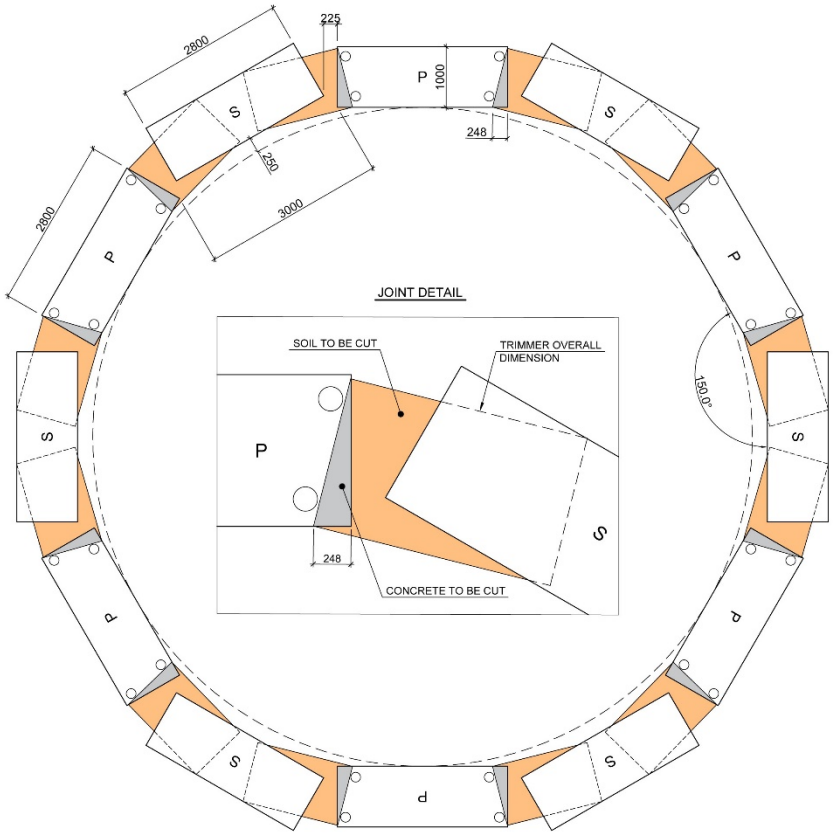


Fig. 9 11m (36ft) Internal Diameter Shaft using 12 panels

Small diameter shafts such as those shown above are not easy to construct solely using just grab excavation - unless either very large panels are used, or joints are formed with either steel or precast concrete elements cast permanently into the wall. Hydro-mills can be used to construct such shafts but we believe the TTMJ System will provide a better technical solution at lower cost.

CONCLUSION

Since the development of the hydro-mill, improvements in slurry wall technology have only been incremental advances. In particular, real-time verticality monitoring during excavation and steerable excavation equipment are two important developments. Hydraulic grabs have improved excavation rates. Depths have increased. Polymer use, instead of bentonite, has become more common. Filter presses and centrifuges for treating waste slurry are now more and more popular on sites.

The one thing that has not really moved forward in the last 25 years is the method of forming panel joints. We believe that the TTMJ System will be the catalyst and step change needed to push the Foundation Industry to the next level in constructing better Slurry (Diaphragm) and Secant (Pile) Walls.

REFERENCES

2013, Pagliacci, F. – Paper on 250m (800ft) deep Gualdo Test Diaphragm Wall.

NUMERICAL ANALYSIS OF PILE-SUPPORTED T-WALLS SUBJECT TO LARGE SETTLEMENTS AND FLOOD LOADING

Alexander B. Reeb, Burns Cooley Dennis, Inc., Ridgeland, MS, USA, (601) 856-9911, alexreeb@bcdgeo.com
George M. Filz, Virginia Tech, Blacksburg, VA, USA, (540) 231-7151, filz@vt.edu
Jehu B. Johnson, U.S. Army Corps of Engineers, Baltimore, MD, USA, (410) 962-5632, Jehu.B.Johnson@usace.army.mil
Richard J. Varuso, U.S. Army Corps of Engineers, New Orleans, MD, USA, (504) 862-2984, Richard.J.Varuso@usace.army.mil

ABSTRACT

T-walls, which are concrete floodwalls in an inverted "T" shape, are an integral component of the Greater New Orleans Hurricane and Storm Damage Risk Reduction System (HSDRRS). In order to resist large lateral flood loads, T-walls are typically supported on long batter piles that extend through the weak and compressible clays and peats commonly encountered in southern Louisiana. Since the piles are battered, settlement of the compressible foundation soils can result in loads acting normal to the piles and induce pile bending moments. Therefore, the design of pile-supported T-walls is a complex soil-structure interaction problem that requires detailed and careful numerical analysis to accurately estimate the stresses and bending moments in the piles. For this paper, numerical analyses were performed for three cross sections that each included a two-pile T wall system that was installed within a 15-ft tall new levee embankment. The cross sections were identical except that the elevation of the T-wall base was varied. This paper discusses the analyses, and it compares the influence of settlements and flood loading on the pile stresses and bending moments. In addition, this paper includes general recommendations for the analysis and design of pile-supported T-walls in practice.

Keywords: settlement, moment, batter pile, T-wall, floodwall, levee, New Orleans

INTRODUCTION AND BACKGROUND

The recently completed Greater New Orleans Hurricane and Storm Damage Risk Reduction System (HSDRRS) includes 350 miles of levees and floodwalls and is designed to defend against a 100-year storm surge event. The floodwalls predominantly consist of I-walls and T-walls. I-walls are comprised of a sheet pile wall curtain capped with a monolithic concrete wall above grade. T-walls are similar to I-walls, but they include a wide concrete base at grade, which forms an inverted "T" shape, and they are generally supported by long batter piles that provide additional lateral and rotational stability for resisting flood loads.

During Hurricane Katrina, several I-walls failed, resulting in large breaches and devastating flooding (Duncan et al. 2008, IPET 2009). T-walls on the other hand performed quite well, including T-walls that were overtopped and eroded on the protected side, yet still did not collapse. As part of the HSDRSS, more conservative designs and height restrictions were required for I-walls (USACE 2011), and a number of I-wall sections were replaced with T-walls. However, the design of pile-supported T-walls is complex and requires careful consideration of both flood loading and settlements.

The soils in the New Orleans area can include thick deposits of clays and peats that are relatively weak and compressible. When pile-supported T-walls are constructed, some new fill is typically placed adjacent to and on top of the T-wall base as part of the slope regrading and armoring/scour protection. At transitions between levee and floodwall sections, large amounts of fill (e.g., in excess of 15 ft) may be placed adjacent to and on top of the T-wall base. Since the T-wall piles are battered, the resulting settlement of the compressible foundation soils produces loads acting normal to the piles and induces pile

 © 2017 DFI Annual Conference, New Orleans, LA, USA

bending moments. Understanding the magnitude and distribution of settlement-induced bending moments is an important component of pile-supported T-wall design and can possibly result in significant modifications to the overall design.

For this paper, two-dimensional plane-strain numerical analyses were performed using the finite difference computer program FLAC (Itasca 2011) to calculate the axial loads and bending moments that would develop in T-wall batter piles for cross sections subject to long-term consolidation settlements and subsequent flood loading. This research was part of a much larger program designed to account for many different configurations and soil conditions as detailed in Reeb (2015). Three cross sections were analyzed, and each included a two-pile T-wall system that was installed within a 15-ft tall new levee embankment. The cross sections were identical except that the elevation of the T-wall base was varied. For the first cross section, the bottom of the T-wall base was even with the base of the new levee embankment as shown in Fig. 1. For the second cross section, the bottom of the T-wall base was 10 ft above the base of the new levee embankment. For the third cross section, the T-wall was installed on top of the new levee embankment. This paper describes the modeling approach and presents and compares the resulting pile axial loads and bending moments for the three T-wall cross sections.

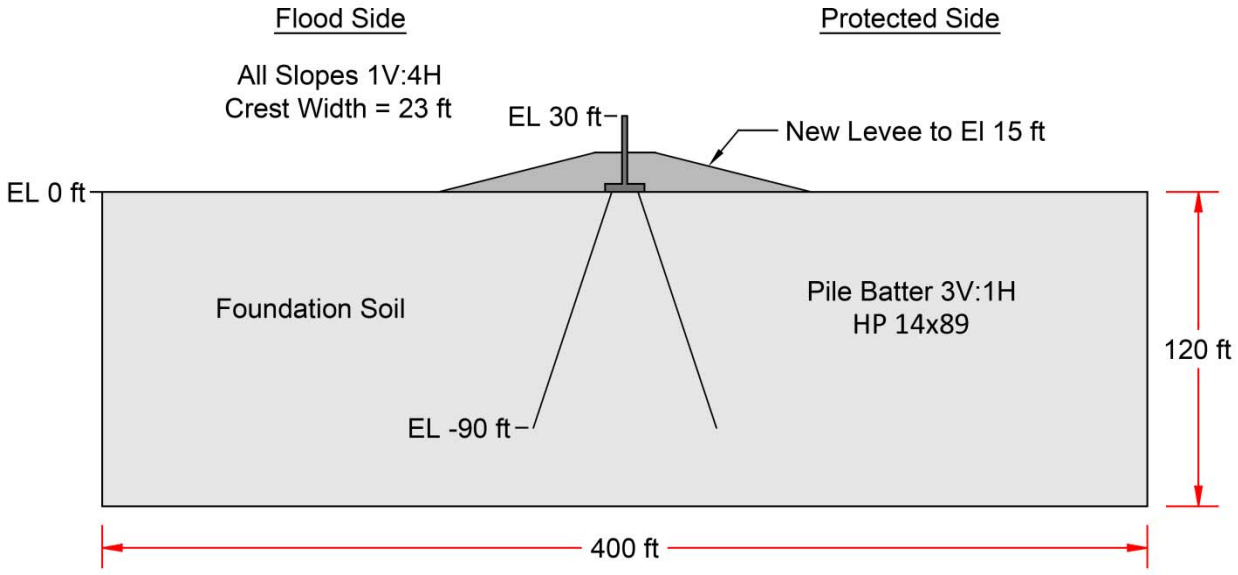


Fig. 1. Cross section with T-wall base at EL 0 ft

PROBLEM STATEMENT

The foundation soil and new levee geometry shown in Fig. 1 was used for all three cross sections. The elevation of the bottom of the T-wall base was varied and was set at either EL 0 ft, 10 ft, or 15 ft. For all three cross sections, the pile tips were at El -90 ft, and the top of the T-wall was at El 30 ft. The width of the T-wall base was 13 ft. The piles were symmetrical and intersected with the T-wall base at a distance of 1.5 ft from the edges. The connections between the piles and T-wall were assumed to be fixed (i.e., zero displacement and rotation relative to the T-wall base). The foundation soil properties, levee fill properties, and T-wall and pile properties are provided in Tables 1 to 3, respectively.

Table 1. Foundation soil properties

Layer	Top El (ft)	Bot El (ft)	Soil Type	G_s	γ_{sat} (pcf)	ϕ' (deg)	$s_{u,top}$ (psf)	$s_{u,bot}$ (psf)	$C_{c\varepsilon}$	$C_{r\varepsilon}$	USR
1	0	-24.2	CH	2.65	100	23	200	200	0.20	0.040	0.22
2	-24.2	-70	CH	2.65	105	23	200	629	0.30	0.060	0.22
3	-70	-120	CH	2.65	110	23	1200	1724	0.10	0.020	0.22

Table 2. Levee fill properties

Soil Type	G_s	γ_{sat} (pcf)	ϕ' (deg)	c' (psf)	ϕ (deg)	s_u (psf)	Young's Modulus, E (psf)	Poisson's Ratio, ν
CH	2.65	115	23	50	0	600	$2x10^5$	0.45

Legend: G_s - specific gravity, γ_{sat} - saturated unit weight; ϕ' - drained friction angled; c' - drained cohesion; s_u - undrained cohesion

Note: Assumed $E=2x10^5$ psf based on Figures 32 through 34 of Duncan and Bursey (2007). Assumed ν=0.45 based on unnumbered table on page 123 of Bowles (1996). These values are applied because the soils are compacted clays with relatively high water contents and sustained negative pore pressures. These values apply for both short-term and long-term conditions unless the clay settles below the water table, in which case the clay is treated on an effective stress basis due to the long-term consolidation behavior.

Table 3. T-wall and pile properties

Structure	Spacing (ft)	Depth x Width (in. x in.)	Area (in^2)	Moment of Inertia (in^4)	Unit Weight (pcf)	Young's Modulus (psi)[1]	Poisson's Ratio[2], ν
Concrete T-wall	-	-	-	-	150	$3.6x10^6$	0.2
HP 14x89	5.0	13.8 x 14.7	26.1	904	490	$29x10^6$	-

Notes:

[1]For the concrete, the assumed concrete strength is 4,000 psi and $E=57,000(4,000)^{0.5}=3.6x10^6$ psi.

[2]Poisson's ratio is not needed for one-dimensional pile elements in FLAC because a plane-stress formulation is used, but it would be needed for continuous pile elements, e.g., plates oriented perpendicular to the plane of the analyses.

In the analysis, the water table was assumed to be at El 0 ft, and the foundation soil preconsolidation pressures were equal to the undrained shear strength, s_u, divided by the Undrained Strength Ratio, USR. Based on this relationship, the preconsolidation pressure was 909 psf for Layer 1, and it varied linearly from 909 psf to 2861 psf for Layer 2 and from 5455 psf to 7836 psf for Layer 3. Layer 2 was normally consolidated, and Layers 1 and 3 were lightly overconsolidated. Poisson's ratio, ν, was calculated based on Equation [1], which applies to sands and clays according to Duncan and Bursey (2007).

$$\nu = (1 - \sin\phi')/(2 - \sin\phi') \quad [1]$$

Where ϕ' = effective stress friction angle.

When analyzing the combined settlement and flood loading cases, s_u values were determined based on the major principal effective stresses after settlement under all of the fill loading had occurred and based on the specified USR values. These values were compared with the initial s_u values, and whichever value was larger was used as the s_u value for the flood loading portion of the analysis.

MODELING APPROACH

The foundation soil, levee fill, and T-wall were represented by continua discretized into grid zones. The T-wall zones and the levee fill sitting on top of the T-wall base were generated as a separate grid from the rest of the model to allow separation during the large-strain analysis. The grid zones were about 2 by 2 ft near the top middle and 5 by 5 ft at the bottom corners of the model. The FLAC grid extended 200 feet laterally on either side away from the T-wall and model centerline and 120 feet below the foundation soil

surface as shown in Fig. 1. The models were fixed in the x-direction along the sides and in the x- and y-directions along the base.

The piles were represented by pile elements, which have the same formulation as structural beam elements but can be connected to the soil grid with coupling springs. The coupling springs connect the piles to the soil while allowing the soil to "flow around" the piles such that the average effects of three-dimensional pile-soil interaction can be simulated in a two-dimensional analysis. The normal pile-soil coupling spring responses were based on the non-linear p-y curves developed by Matlock (1970) for clays. The axial shear pile-soil coupling spring responses were based on the recommendations in USACE (1991) and the analyses performed by Amec (2014).

The analyses were performed in two sequential stages. In the first stage of the analysis, settlements and the response of the T-wall system was calculated after consolidation of the foundation soils under the new levee loads. In the second stage, 25 ft of flood loading was applied to the model, and the response of the T-wall system due to combined settlement and flood loading was calculated. A brief description of the analysis steps is provided below:

Settlement Analysis

1. Set the initial material property values and conditions. Linear elastic, perfectly plastic constitutive models with a Mohr-Coulomb failure criterion are used for all soils. Effective stress property values are used for the clay foundation soils below the ground water table, and total stress property values are used for the clay levee fill above the ground water table. Non-linearity is addressed by updating tangent modulus values for clays below the ground water table based on the compressibility parameters.
2. The model is solved, and stresses and displacements are checked. If initial pore pressures and stresses are correctly specified in the Step 1 and the system is stable, then the model converges in very few timesteps with only negligible changes in stresses and displacements.
3. Place the levee fill and install the T-wall and piles. The initial density of the levee fill and T-wall are set to very small values in this step. Pore pressures are maintained at hydrostatic values during the analysis.
4. Slowly increase the density of the levee fill and T-wall to the actual value as the model is solved. This approach minimizes inertial effects and reasonably simulates the slow consolidation of the clay foundation soils. In contrast, it would be incorrect to both place all of the levee fill and immediately set the density to the actual value, and then solve the model. Following this latter approach would shock the model and result in locked-in dynamic stresses and displacements. The maximum rate of loading which still produces acceptable results can be estimated by performing a convergence study with progressively smaller load increments or based on FLAC modeling experience.
5. Record bending moments and stresses in the piles, and other parameters of interest. This step provides results for the end of the settlement analysis.

Flood Loading Analysis

6. Change the properties for clays below the ground water table to total stress property values. This change is done using a technique that minimizes any induced incremental deformations in the model.
7. Incrementally apply the flood loading to the flood-side ground surface and T-wall to the desired elevation. After each additional increment of flood loading is applied, the model is solved.

Similar to Step 3, the flood loads are applied slowly to avoid shocking the model and to minimize inertial effects.

8. After full flood loading to El 25 ft is applied, record final bending moments and loads in the piles, and other parameters of interest. These results incorporate the combined effects of settlements and flood loading.

A more complete description of the T-wall modeling approach, as well as a discussion of the validation of the approach based on centrifuge physical model tests, is included in Reeb (2015).

ANALYSIS RESULTS

Pile bending moments and axial loads for the settlement analyses are shown in Fig. 2. Only the results for the flood side piles are shown because the cross sections are symmetrical. The bending moment distributions for the protected-side piles are equal and opposite compared with the flood-side piles. The axial load distributions for the flood-side and protected-side piles are identical.

The pile bending moments and axial loads for the settlement analyses are compared with the results from the combined settlement and flood loading analyses in Fig. 3 and 5. The maximum values are shown in Table 4. These figures show the responses of both the flood-side and protected-side piles after flood loading is applied. In Fig. 3, the signs of the moments for the protected side pile for the combined settlement and flood loading case have been reversed to allow for easier comparison with the bending moment distribution due to settlement only. As noted earlier, the flood-side and protected-side piles bending moments and axial loads were identical after settlement loading and one can see how each pile either increased or decreased in bending moment or axial load after flood loading was applied.

Table 4. Results

T-wall Elev.	Max. Bending Moment Settlement Loading Only (in-kips)	Max. Bending Moment Combined Flood Loading Flood-Side (in-kips)	Max. Bending Moment Combined Flood Loading Protected-Side (in-kips)	Max. Axial Load Settlement Only (kips)	Max. Axial Load Combined Flood Loading Flood-Side (kips)	Max. Axial Load Combined Flood Loading Protected-Side (kips)
0	3242	-4335	2960	181	-90	204
10	3971	-5467	7296	190	-30	141
15	4465	-5841	7014	195	-24	95

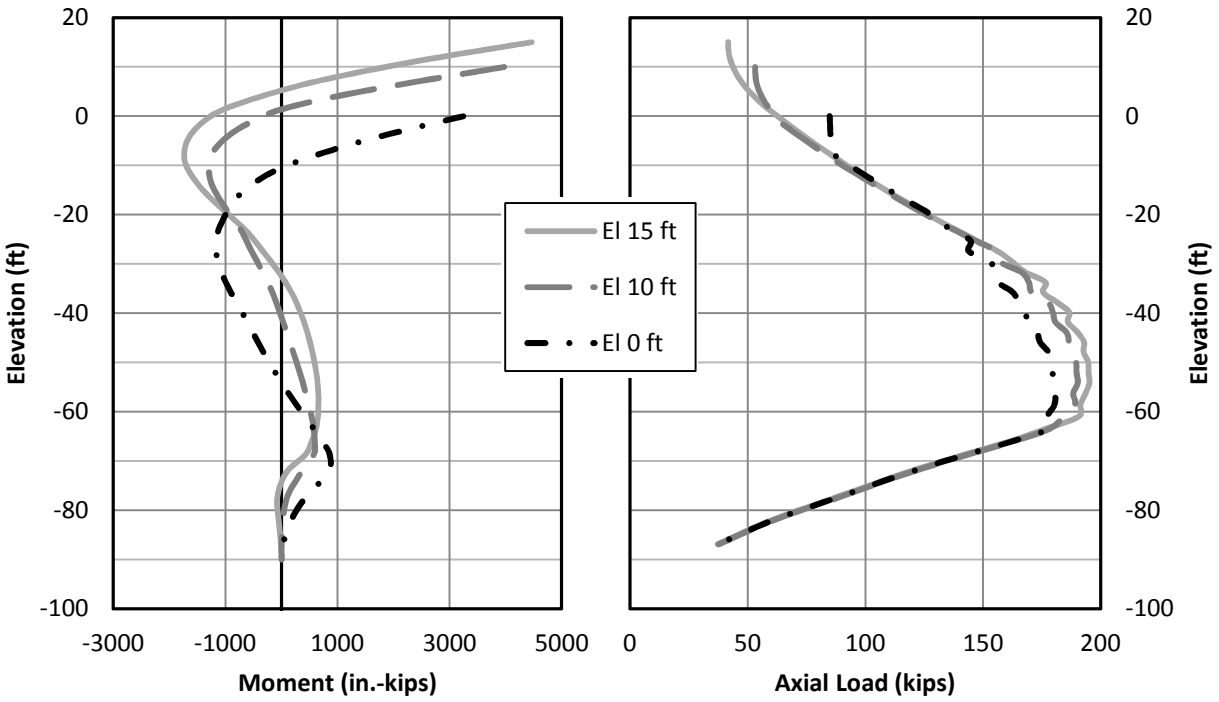


Fig. 2. Flood-side pile (a) bending moments and (b) axial loads due to settlement only

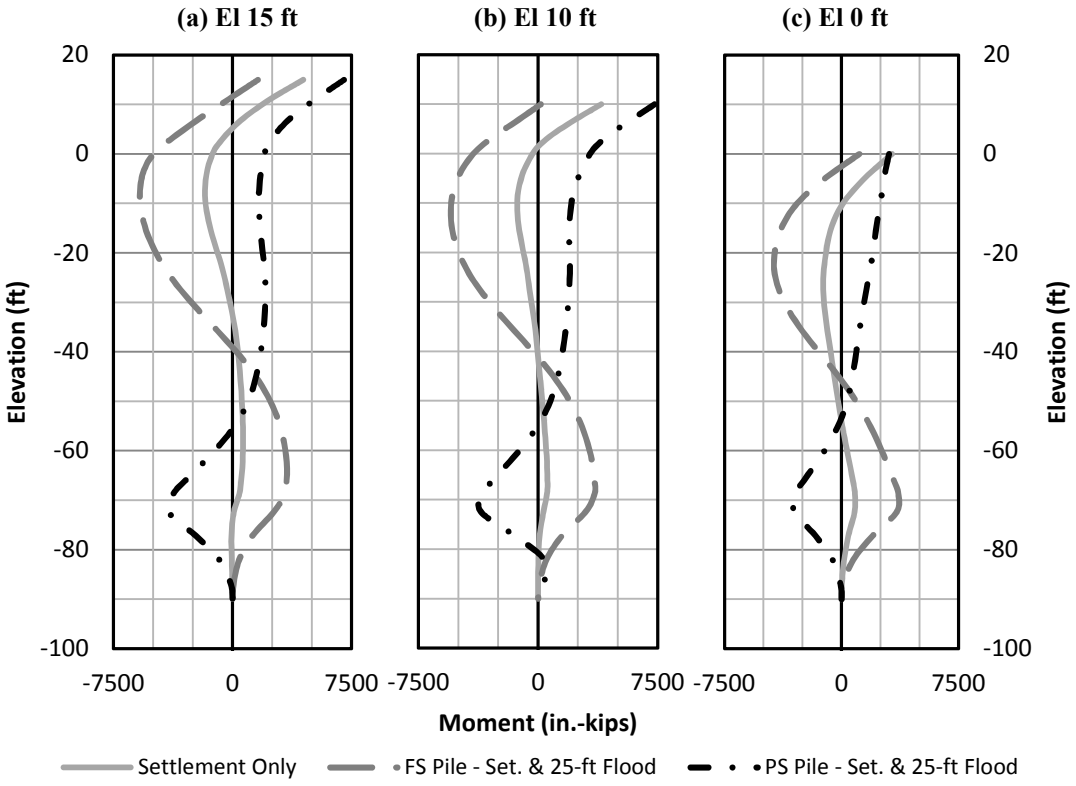


Fig. 3. Comparison of pile moments before and after 25-ft flood loading

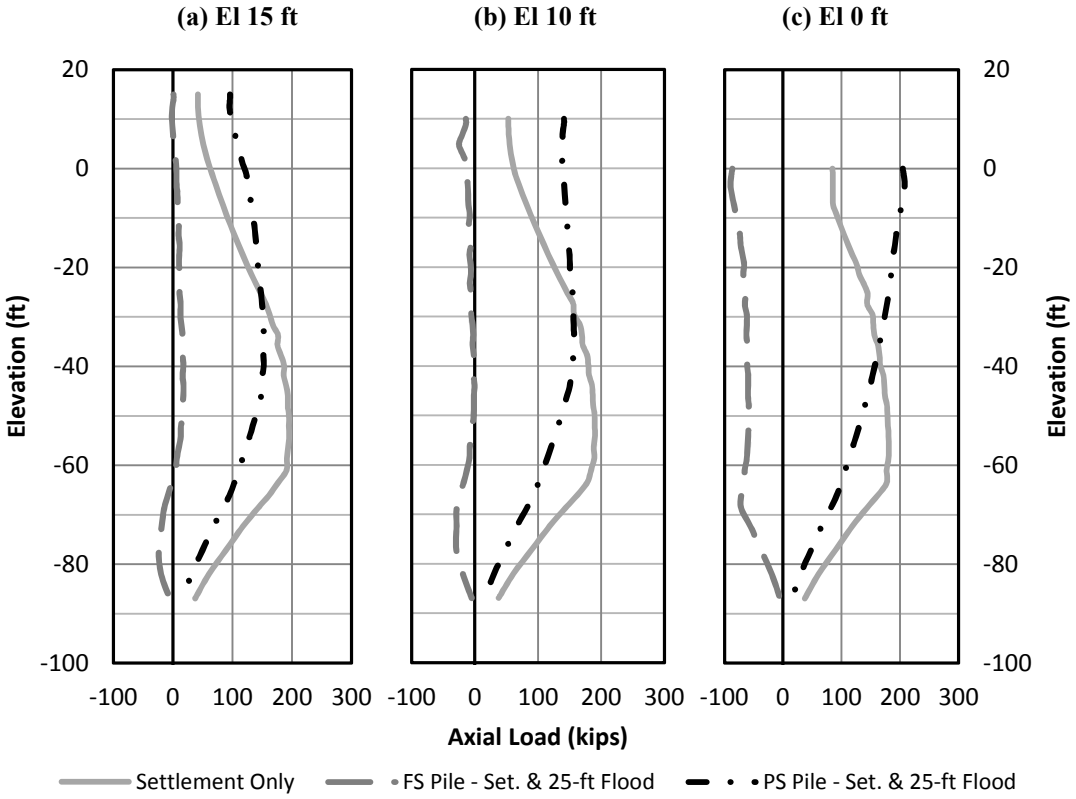


Fig. 4. Comparison of pile axial loads before and after 25-ft flood loading

DISCUSSION OF RESULTS

Influence of Settlements

In all three cases, the piles tend to bend inwards due to the large settlements. The maximum bending moments occur at the piles tops due to the fixed connections. The maximum axial loads occur in the middle of Layer 2 (~El 50 ft), which was normally consolidated, due to the downdrag loads on the piles.

The T-wall installed at El 15 ft developed larger axial loads and significantly larger bending moments compared to the T-walls installed at lower elevations. The maximum bending moments for the El 15 ft wall are 12.4% greater than the El 10 ft wall and 37.7% greater than the bending moments of the El 0 ft wall. The axial loads for the El 15 ft wall are 2.6% greater than the El 10 ft wall and 7.7% greater than the bending moment of the El 0 ft wall. There are several factors that could be influencing this behavior such as the greater strength of the levee embankment compared to the foundation soils, the location of the settlement on the various parts of the pile, and the greater length of the pile installed above the compressible layers.

Influence of Combined Settlements and Flood Loading

As shown in Fig. 4 and 5, the addition of flood loading significantly changes the calculated axial loads and bending moments compared with the settlement only results. This can be explained by the rotation and lateral displacement of the T-wall and lateral movement of foundation soils due to the flood loading.

In all cases, the moment at the top of the flood-side pile decreased in magnitude, but the moment around 22 ft below the pile top greatly increased in magnitude. The flood loading caused the maximum moment (absolute value) in the flood-side pile due to combined settlement and flood loading to exceed the

maximum moment due to settlement only and also changed the location where the maximum moment occured. The maximum pile load increased by 33.7%, 37.7%, and 30.8% for El 0, El 10, and El 15, respectively. There was significant reduction in axial load in the flood-side pile due to the applied flood loading. The resulting axial load in the flood-side pile is close to zero for the T-walls at El 10 and El 15 ft, and for the T-wall at El 0 ft, the flood-side pile is in tension. For typical T-wall cross sections not subject to settlement and downdrag loads, the flood-side pile will be in tension during flood loading.

For the protected-side pile, the bending moment at the pile top increased for T-walls at 10 and 15 ft, and stayed approximately the same for the T-wall at El 0 ft. The maximum moments (absolute values) in the protected-side piles due to combined settlement and flood loading was greater than the maximum moment due to settlement only for T-walls at 10 and 15 ft, and stayed approximately the same for T-walls at El 0 ft. The combined settlement and flood loading resulted in the T-wall at El 10 ft having the greatest moment of all three configurations. The axial loads at the pile tops increased, but the downdrag loads near El. 50 correspondingly decreased for the piles. For the T-wall at El 0 ft, the axial load at the top of the protected-side pile for the combined settlement and flood analysis was greater than for the settlement only analysis. Based on these results, the influence of the loading on the protected-side piles seems to be very complex and there does not seem to be a consistent trend between the three different T-walls.

There are several things to note when comparing the flood-side and protected-side pile response. For the T-walls at El 10 and 15 ft, the overall maximum moments occurred in the protected-side piles at the pile tops. For all the T-walls, the maximum moments in the flood-side piles occurred approximately 22 ft below the pile tops. Due to the application of flood loading, there was generally an increase in the protected-side pile axial loads at the pile tops and a corresponding decrease in the flood-side pile axial loads.

RECOMMENDATIONS FOR PRACTICE

As shown in the results, settlement-induced bending moments and axial loads can be significant and may reduce the available capacity of a pile to resist flood loading. It is important to consider the influence of settlement-induced bending moments and to minimize these bending moments as much as practical as part of the T-wall design. Pile bending moments should be calculated considering the combined effects of settlements and flood loading. The combined loading should be developed jointly and not by just combining the maximum moments from either analysis separately. To reduce pile bending moments, T-walls should be installed directly on the foundations soils rather than within or on top of new fill.

SUMMARY AND CONCLUSIONS

Settlement-induced bending moments can occur in batter pile foundations installed in settling soils. The results of numerical modeling of T-wall/levee cross-sections with the T-wall placed at three varying elevations within the levee show that large bending moments and axial loads can develop in the piles. The T-walls installed completely beneath the new levee fill loads at El 0 ft developed the smallest settlement-induced bending moments (37.7% less than for a T-wall at El 15 ft) and axial loads (7.7% less than for a T-wall at El 15 ft). The addition of flood loading significantly altered the bending moment distributions within the flood-side piles, increasing the maximum bending moment magnitudes (average of 34% increase) and also changing the locations of the maximum moments. The combined influence of settlement and flood loading is very complex and requires careful consideration in T-wall design.

ACKNOWLEDGEMENTS

This work was sponsored by the United States Army Corps of Engineers (USACE), New Orleans District. In addition, support was received from the Virginia Tech Via Foundation and the U.S. National Science Foundation (NSF) under grant No. DGE-0504196. The opinions and conclusions expressed or implied in this report are those of the authors. They are not necessarily those of the research sponsors.

REFERENCES

Amec Foster Wheeler Environment & Infrastructure, Inc. (2014), "Final Report – Numerical Modeling and Evaluation of a Pile-Supported T-Wall in St. Bernard Parish, LPV 145, Repair Area 2." (Prepared for Department of the Army, St. Paul, MN – Project No. OD13164560). Oakland, California, Vol. 1, p. 190.

Bowles, J. E. (1996). *Foundation Analysis and Design, Fifth Edition*, McGraw-Hill, New York.

Duncan, J. M., Brandon, T. L., Wrights, S. G., and Vroman, N. (2008). " Stability of I-Walls in New Orleans during Hurricane Katrina." *J. Geotech. Geoenviron. Eng.*, 134(5), 681–691.

Duncan, J. M. and Bursey, A. (2007). "Soil and Rock Modulus Correlations for Geotechnical Engineering." Center for Geotechnical Practice and Research, Virginia Tech, Blacksburg, VA, p. 88.

Interagency Performance Evaluation Task Force (IPET) (2009). "Performance evaluation of the New Orleans and southeast Louisiana hurricane protection system." Final Rep. of the Interagency Performance Evaluation Task Force, U.S. Army Corps of Engineers <http://biotech.law.lsu.edu/katrina/ipet/ipet.html>.

Itasca (2011). *FLAC – Fast Lagrangian Analysis of Continua, Version 7.0*, Itasca Consulting Group, Inc., Minneapolis, MN.

Matlock, H. (1970). "Correlation for design of laterally loaded piles in soft clays." *Proc. 2nd Offshore Technology Conference*, Houston, TX, Vol. 1: 557-559.

Reeb, A.B. (2015). "Response of Pile-Supported T-Walls to Fill Loading and Flood Loading Based on Physical Model Studies and Numerical Analyses." Ph.D. thesis, Virginia Polytechnic Institute and State University, Blacksburg, VA.

USACE (2012). "Hurricane and Storm Damage Risk Reduction System Design Guidelines, Interim with revisions through June 2012." USACE, New Orleans, <http://www2.mvn.usace.army.mil/ENG/PageA.asp>.

USACE (1991). "Design of Pile Foundations." *USACE Rep. No. EM 1110-2-2906,* USACE, Washington, DC.

INNOVATIVE METHODS FOR UNDERGROUND PARKING IN CENTRAL CITIES

Guanglei Liu, Zhongyan Technology Co., Ltd., Beijing, China, +86-10-57712508, liuguanglei@zydd.com
Qi Wang, Zhongyan Technology Co., Ltd., Beijing, China, +86-10-57712508, wangqi12240205@163.com
Zengzhu Kang, Zhongyan Technology Co., Ltd., Beijing, China, +86-10-57712508, kangzengzhu@zydd.com
Jianguo Liu, Zhongyan Technology Co., Ltd., Beijing, China, +86-10-57712508, liujianguo@zydd.com

ABSTRACT

Due to the increase of automotive vehicles, available parking spaces become a new type of limited resource in central cities of China, especially in those old districts without visionary urban planning. Additional mechanical parking in underground space is an efficient solution to provide parking spaces under the situation where the urban space is constrained. Shichahai district is an old protected zone in Beijing which is close to the Forbidden City and there are many Hutong (alleyway) and Quadrangles (courtyard house). No spaces are available for car parking on the ground and all vehicles are parking in Hutong without order currently. The local government plan to do renovation work for this district and improve the residential environment. Several innovative solutions are studied including parking in deep shafts, parking under existing buildings by under-pinned method, parking under buildings by covered excavation method, parking under roads built together with utility tunnel etc. 5000 difference types underground parking spaces are planned to be constructed in the following three years. Project examples are also introduced in this paper.

Keywords: underground parking facilities, deep excavation, sinking caisson

 © 2017 DFI Annual Conference, New Orleans, LA, USA

INTRODUCTION

Car parking resources are very limited in central cities, especially in old districts without planning for increasing automotive vehicle volume. Traffic get worse when cars park on the side of the roads or move slowly to find parking spaces. Investigation shows the normal (parking space/ automotive vehicle volume) ratio is about 1.2 in most big cities such as New York, Tokyo and Hong Kong, while this ratio is only 0.5 in Beijing. One solution is to move cars out of central cities. But there are still huge parking requirements for the citizens living in central cities. Shichahai district is an historic protected zone in Beijing which is close to the Forbidden City and there are many Hutong and Quadrangles (refer to Figure 1 for project location). No spaces are available for car parking on ground and all vehicles are parked in Hutong without order currently. The local government had a plan to do renovation work of this district and improve the residence environment. 5000 different types of underground parking spaces are planned to be constructed in the following three years. One project designed and to be constructed by Zhongyan Technology will be introduced in this paper. Other innovative solutions will be introduced briefly as well.



Figure 1. Project location

PROJECT DESCRIPTION

One example presented in this paper is about the design and construction consideration of one underground parking facility to be built in a quadrangle. The basement is 8.9m x 18.8m in plan and 23.2m deep. An 8-storey mechanical parking equipment will be installed in the basement and provide 44 parking spaces. Refer to Figure 2 for the section and 3D model of this structure. The challenge of this project is the limitation of the construction site, adjacent old buildings and narrow traffic path. Innovative methods are proposed for this special site and the construction work is expected to start from June 2017.

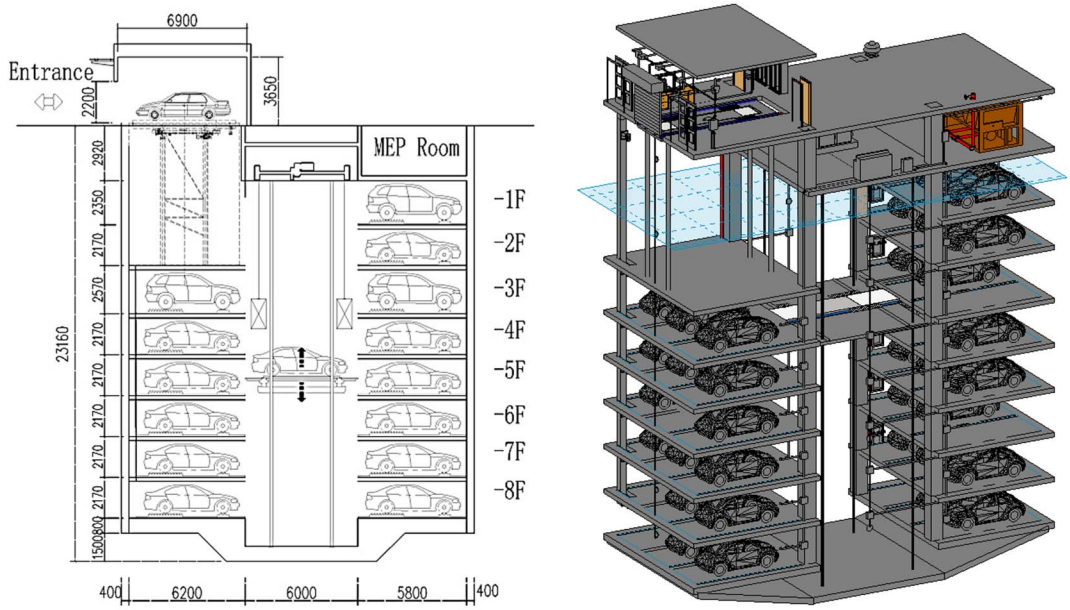


Figure 2. Proposed underground parking facility in a quadrangle

SITE CONDITIONS

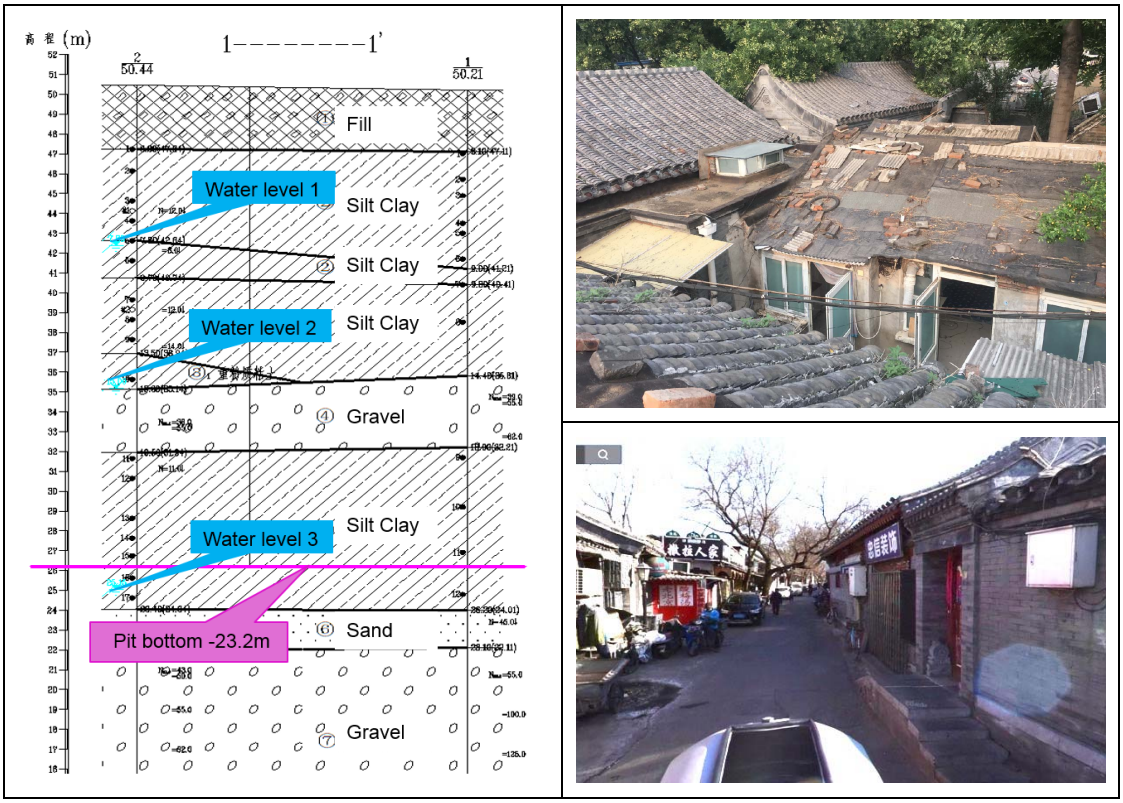


Figure 3. Soil profile and site photos

The site is close to Shichahai Lake and there are three layers of ground water observed in the construction zone, including one layer of confined water. The basement pit bottom is designed above water level 3 to avoid high water pressure under construction. The closest adjacent building is 1.5m away from the proposed new basement wall. So the protection of the surrounding builds is a major challenge to this project. Figure 3 shows the soil profile and the site photos of this project.

DESIGN AND CONSTRUCTION CONSIDERATIONS

Structural and foundation scheme

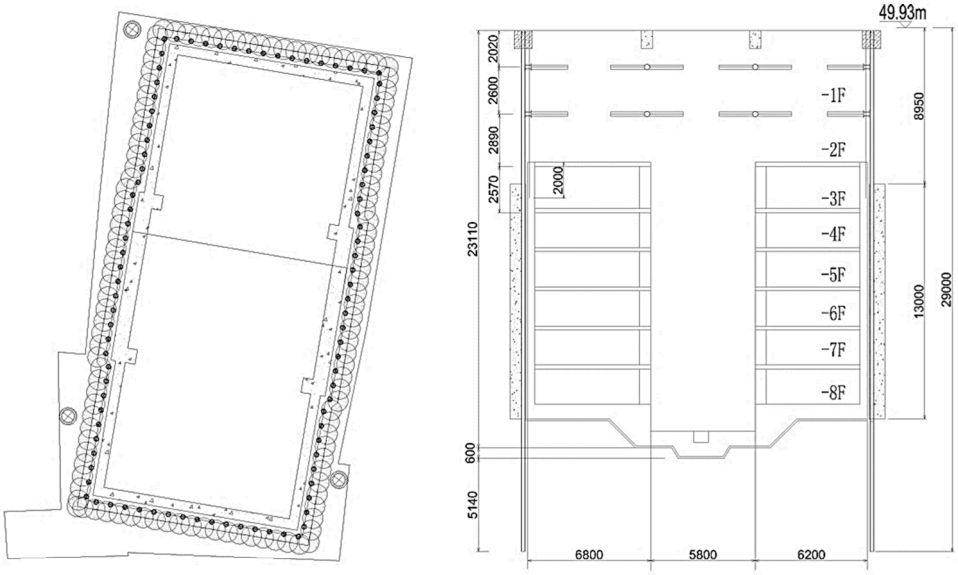


Figure 4. Structural and foundation scheme

Figure 4 shows the structural and foundation scheme of this project. The major challenges are:

1) Close to old residence buildings (1-2 storey brick buildings)
2) Protected trees in the yard
3) Deep excavation with abundant ground water
4) Limited construction space and narrow traffic path
5) High requirement on noise and dust control

Considering the conditions above, covered excavation and Top-down method was chosen to control the settlement during the construction. The retaining structure is 203x10mm steel pipe pile supported by concrete structure which will be built story by story from top to bottom. The concrete structure will provide strong support to the retaining pile. 850mm@500mm high-pressure jet grouting piles will be used to resist the ground water. This scheme was proved successfully in other similar projects according to previous experience.

Construction plan

Small piling equipment (refer to figure 5) is required because of the site limitation. The steel pipe piles are divided to 2m long parts and connected by screw threads. The double casing piling equipment can ensure

the verticality error less than 5‰. One cover slab will be constructed after piling work and a 6m x 6m opening will be kept for vertical transportation. Other parts of the cover slab can be used as construction platform. Soil will be lifted to the truck directly and shipped away.

The piling work is expected to start in June 2017 and the whole construction period is about 8 months.



Figure 5. Construction plan and equipment

OTHER INNOVATIVE METHODS AND EXAMPLES

Sinking Caisson Method

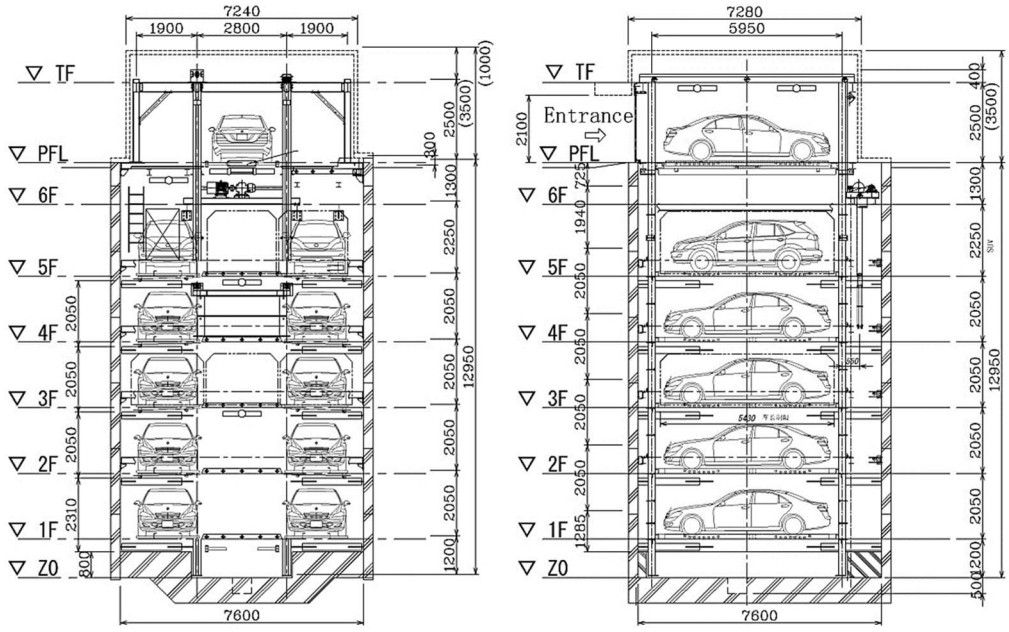


Figure 6. Underground parking facility constructed by sinking caisson method

One underground parking project in Chaoyang (Thanks) district, Beijing by sinking caisson method was achieved by Zhongyan Technology in April 2016. This basement parking was built in an existing ground parking area to provide more spaces. Distinguish from common sinking caisson method, the caisson walls in this project were prefabricated and assembled on site. There was no concrete work except the base slab concrete pouring. It took us five days for one standard story construction including caisson wall assembling, steel brace installation, excavation and caisson sinking. The steel structure and parking equipment was installed after the basement construction. The parking facility is now open to public and in a good condition.

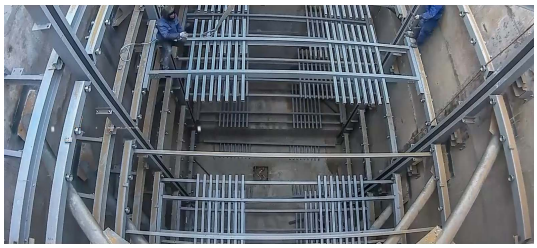
1. Caisson wall assembling	2. Excavation
	
3. Caisson sinking	4. Basement finish
	
5. Parking equipment installation	6. Entrance structure construction
	

Figure 7. Sinking caisson construction procedure

Additional Basement by Under-Pinned Method

This underground parking project is in Shijiazhuang city and achieved by Zhongyan Technology in May 2016. The existing sales center is close to the entrance of this logistic park and it is a 2-storey steel structure building without basement. No garages were planned for the building. After scheme study, the client decided to build an extra basement with mechanical parking equipment in September 2015. The new basement was 8m x 10m in plan and 7.65m deep. Automatic mechanical car parking equipment with four parking spaces were proposed. The demolishing work of partition structure was conducted in December 2015. The under-pinning work started from the beginning of 2016 and the main structure was accomplished in March 2016. All jobs are finished in May 2016 including the installation and testing of the parking equipment. Before the excavation, each column was under-pinned by four SAP (Screw Anchor Pile) piles and the pile lengths were 24m and 25m. The sales center was kept open to public and the rooms at level two above the construction zone were also kept operational during the construction.

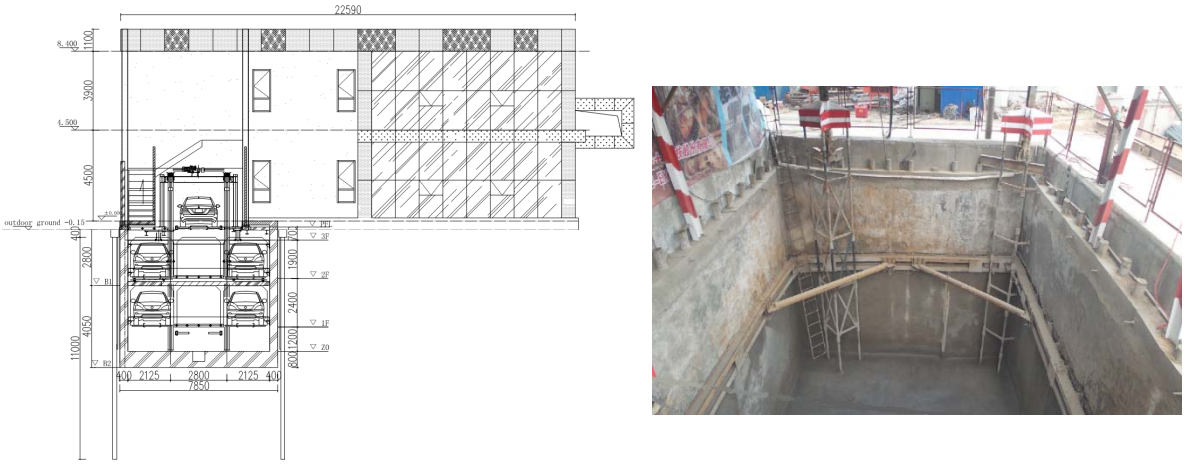


Figure 8. New basement parking by under-pinned method

Undermining Method

One underground parking project is proposed in Hutong area, central Beijing and is planned to be constructed starting from late 2017. The highlight of this project is that the undermining method will be used to expand the basement to the space under the road. The road is the only access to the residence buildings in this Hutong area and cannot be blocked during the construction. Undermining method is considered accordingly. The equipment for piling work in the pilot tunnel has been developed to suit the tunnel size, which is 3m wide and 4m high. The steel pipe piles and the rotary churning piles will be constructed in the pilot tunnel. A strong cover slab under the road area will be constructed after the piling work and the following work will be similar to the normal covered excavation method.

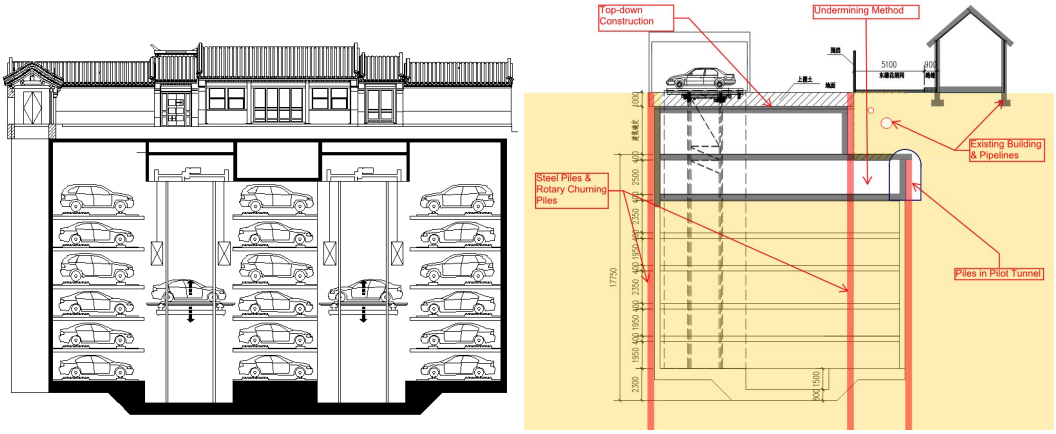


Figure 9. New basement parking by undermining method

CONCLUSIONS

There are huge shortage on car parking spaces in central cities considering the limited available ground spaces. We provide some examples to use underground space development to improve the district environment and provide functional spaces, which is also an efficient way for city renovation. Compared to the cities' new construction work, renovation is more difficult because of the site constraint, existing buildings and residences around, noise and dust control requirement, transportation difficulty etc. Innovative methods and suitable small equipment are required. Some methods introduced in this paper are proved to be effective based on project experiences. More studies will be implemented towards design, analysis methods, monitoring, equipment development and risk management.

ACKNOWLEDGEMENTS

We are grateful to Mr. Siyu Wu, Mr. Wubao Li, Mr. Jianping Li, Mr. Xiaoqing Luo, Ms. Shunnv Fang from Zhongyan Technology Co., Ltd. for their support during this project and in preparation of this paper.

REFERENCES

FHWA(2005), Micropile Design and Construction: Reference Manual, Sabatini P., Tanyu B., Amour T., Groneck P., and Keeley J., FHWA-NHI-05-039, Federal Highway Administration, December

NAFAC(1983), Department of the Naval Facilities Engineering Command, Naval Facilities Engineering Command, Soil Mechanics Design Manual 7.1

Cadden A. and Gómez J.(2002), "Buckling of Micropiles-A Review of Historic Research Experiences", ADSC-IAF Micropile Committee

DIN 4128 (1983). "Small Diameter Injection Piles (Cast-in-place Concrete Piles and Composite Piles).

DS Choi，GJ Hasenfus，PS Carter (1997), “A case study of undermining impoundment embankments by the longwall mining method”, International Journal of Rock Mechanics & Mining Sciences.

Z Dong，S Wang (1998), “Optimization study of undermine method and undermine parameters”, Explosion & Shock Waves.

CHALLENGES ASSOCIATED WITH THE CONSTRUCTION OF A COFFERDAM – A CASE STUDY

Khuram R. Mohib, Peter Kiewit Sons ULC, Oakville, Ontario, CAN; (905)337-4049; Khuram.Mohib@Kiewit.com

Thomas J. Sabourin, Peter Kiewit Sons ULC, Oakville, Ontario, CAN, Tom.Sabourin@Kiewit.com

Eric S. White, Kiewit Engineering Group Inc., Omaha, Nebraska, USA, Eric.White@Kiewit.com

ABSTRACT

This paper presents the challenges associated with the design and construction of a steel sheet pile cofferdam supported with one level of grouted anchors in clean to silty sand with gravel. The initial assessment of the subsurface conditions indicated loose to medium dense soil with intermittent dense to very dense layers with no occurrence of cobbles and boulders. Sheet piles were proposed to be installed to a depth of 24 m below the ground surface to limit dewatering requirements for the cofferdam. During sheet pile installation, refusal of piles occurred at multiple locations forming passages for increased flow into the cofferdam. Modifications were made in the design of the dewatering system as a result of the increased flow. Finite element modeling was used to select the necessary modifications to the dewatering system within the cofferdam. Wells were installed based on the findings of the numerical model. Model simulations showed good comparison with monitoring of the field installed dewatering system.

Keywords: Cofferdam, Steel sheet piles, Grouted anchors, Finite element modelling, Dewatering

INTRODUCTION

It is necessary to consider the impact of the ground water, subsurface stratigraphy, strength, and drainage behavior of the soil for the design and construction of cofferdams. This paper presents a case history of the construction of a cofferdam in Northern Ontario, Canada. The project consists of the construction of a powerhouse, intake, and tailrace which will generate around 28 MW of renewable clean energy by diverting water from New Post Creek through a power house and discharge into the Abitibi River. The focus of this paper is the dewatering and excavation support required to permit construction of the powerhouse. The layout of the cofferdam is shown in Fig. 1. The cofferdam for the powerhouse is rectangular in shape with sheet piles on all four sides intended to be driven to the design toe El. 101 m. The east and west walls have a length of 46.3 m. North and south sides are 47.6 m long; and in addition, two cantilever sheet pile walls bound the tailrace on the west side and two cantilever walls were installed on the east for construction of the penstock inlet. The ground surface in the powerhouse cofferdam area, before commencement of sheet pile driving, was brought to El. 125; the ground then slopes up to the East, toward New Post Creek, and the site is bounded on the West by the Abitibi River. 186 pairs of sheet piles were used to create the cofferdam and cantilever walls. The deepest excavation is to elevation 114.4 m. Within the west half of the cofferdam footprint, the base of excavation slopes upward at 3H: 1V to facilitate the tailrace discharge into Abitibi River.

SOIL STRATIGRAPHY

The cofferdam design was based on the geotechnical investigation conducted by AECOM (2014) which included two relevant boreholes near the powerhouse footprint. The ground elevation at the time of investigation varied between 131 to 129 m. The material observed to the full depth of investigation was comprised generally of coarse to fine sand and gravelly sand or a sand matrix with gravelly inclusions. Some intermittent layers of clay and silt intrusions were also observed. Generally the soils grade finer away from the river. SPT N_{60} values were recorded in two borings during the field investigation with values reported from 3 to 92. The in-situ conditions ranged from compact to dense with some loose and some very dense zones. Figure 2 shows the variation in SPT N_{60} values with elevation.

 © 2017 DFI Annual Conference, New Orleans, LA, USA

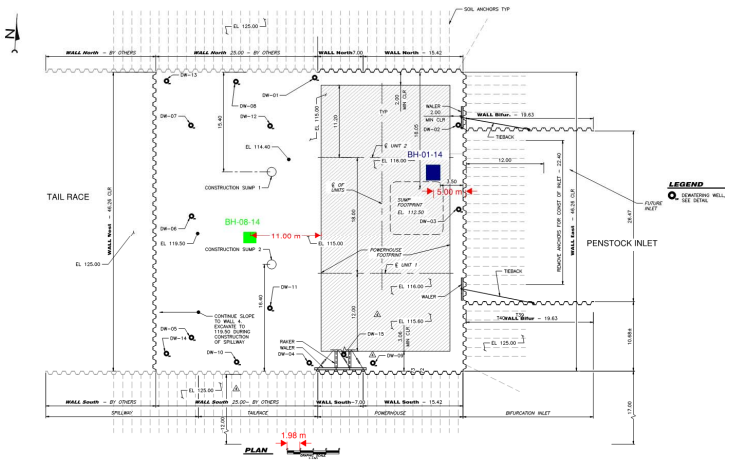


Fig. 1. Sheet pile wall layout for powerhouse cofferdam

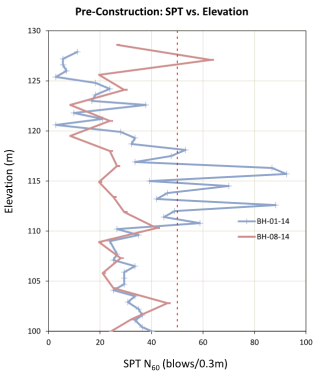


Fig. 2. SPT N_{60} Profile

The two boreholes, both within the footprint of the excavation, were only about 30m apart, but indicated significant differences in SPT values between El. +120m and +110m. The high blow counts in BH 01-14 indicated the presence of a till soil with cobbles and boulders that was observed during excavation, as discussed later. Particle size distribution (PSD) curves for the samples collected from 2.5 m to 48 m depth from the ground surface are shown in Fig. 3.

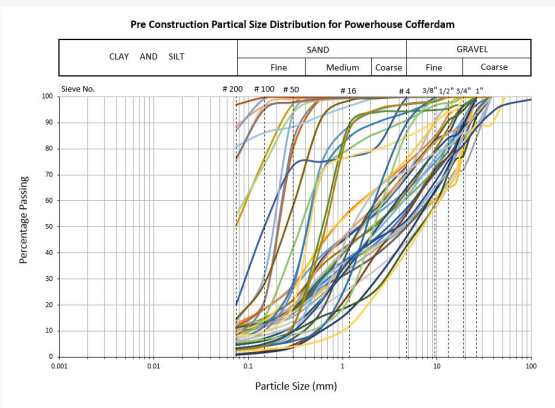


Fig. 3. Preconstruction Particle Size Distribution Curves

DESIGN OF EXCAVATION SUPPORT SYSTEM

Design of the cofferdam required the design of both excavation support and dewatering systems. Brief details of the design of these components are provided below;

Design of Steel Sheet Piles

The permanent sheet pile walls along the tailrace, which have to remain functional throughout the design life of the powerhouse, were designed by the powerhouse design engineer. Temporary excavation support was designed by the contractor; permanent walls were also reviewed by the contractor relative to temporary loading and surcharge conditions. For design of the temporary sheet piles, soil was divided into two stratigraphic units based on the field investigation results. The properties of these two layers are summarized below:

Layer 1 (El. 125 m - 115 m): Poorly graded Sand (SP), loose to medium dense, total unit weight of 18 kN/m^3, effective unit weight of 8 kN/m^3 and friction angle of 33 degrees.

Layer 2 (El. 115 m to design toe and below): Poorly graded Sand (SP), medium dense to dense, total unit weight of 20 kN/m^3, effective unit weight of 10 kN/m^3 and friction angle of 37 degrees.

Based on the material type, in-situ compactness and a WEAP analysis, steel sheet piling, as installed using a vibratory hammer, was considered a suitable option. A sheet pile wall design was performed using the computer program Support IT (GT Soft, Ltd, 2007). Calculation methods used by Support IT are based on the British Steel Piling Handbook and US Steel Sheet Piling Design Manual. A summary of the sheet pile wall design is presented in Table 1. The following considerations were applied to the design of the sheet piles:

- Ground elevation on the active side at El. 125 m and on passive side varying between El. 116 to 114.4 m depending on depth of excavation necessary to facilitate the powerhouse construction. The maximum depth of excavation was 10.6 m.
- Active water elevation of 123.75 m, and passive water elevation was assumed at base of excavation.
- Transient surcharge loads (construction equipment with bearing pressure of 29 kPa, 4m wide strip load at 2m offset from the wall).
- The design penetration for all the sheet piles was 24 m (toe elevation of 101 m) to provide an increased seepage path for groundwater fed by the Abitibi River.
- Design of anchored sheet pile walls was done using fixed earth method using Coulomb's earth pressures theory.

Table 1. Summary of temporary and permanent sheet pile walls

Sheet Piles	Walls	Maximum Supported Height (m)	Supports	Support Type
AZ24 700	East	9.0	Tied Back	Pressure Grouted Anchors
	South	10.6		
	North	10.0		
AZ40 700N	West	4	Cantilever	None

Design of Temporary Anchors

The design of the sheet pile walls required one level of anchors 1 m below the ground surface at (El. 124 m) to control deformations and bending stresses in sheet piles. The elevation of the anchors was selected to keep the head of the anchor above the water table to simplify installation. A piling subcontractor was hired to install the sheet piles and design and install helical anchors. The design length of the anchors was 17.1 m. The angle of installation was 25 degrees below horizontal. The anchors consisted of six 305 mm diameter helixes spaced at 550 mm with a 50 mm square shaft. The anchor working load was 443 kN and required ultimate load of 665 kN with an intended safety factor of 1.5. Pullout testing of the temporary helical anchors failed to meet the design load requirements, likely because of the close helix spacing, and consequently, the helical anchors were replaced by cement grouted anchors. The anchors were designed to have 10 m of un-bonded length and up to 12 m of bonded length and were installed at an angle of 15 degrees below horizontal. A single 36 mm (#11) diameter Dywidag thread bar was used with minimum yield strength of 517 MPa. The maximum anchor design load was 411 kN and anchors were tested to 1.75 times the design load and performed satisfactorily as per the recommendations of the Post Tensioning Institute (PTI 2014).

Design of Dewatering System

The initial dewatering design of the cofferdam, as based on the preconstruction geotechnical information, was developed using the finite element software Plaxis 2D as well as hand calculations to validate the modeling. For hand calculations, homogeneous soil was considered and hydraulic conductivity of 0.01 cm/sec was adopted. The capacity of a single well was calculated using the simple well formula as follows.

$$Qwell = \frac{\pi k(H^2 - h^2)}{\ln(R_o/r_w)} \qquad [1]$$

Where k = permeability, H = aquifer thickness below ground water, $h = H$ – drawdown, R_o = radius of influence and r_w = well radius. Single well inflow was calculated to be 1,680 m^3/day. Hand calculations also included a simple flow net analysis, assuming isotropic homogeneous flow conditions and water head outside the sheet piles at El. 123.75 m and inside the cofferdam at El. 114m. Four flow paths were used with eleven head drops resulting in a total inflow of 5,765 m^3/day. Four wells were estimated for dewatering the cofferdam. The preconstruction geotechnical investigation for the site included the installation of a pumping well in the powerhouse area with three piezometers installed nearby to monitor drawdown at various distances. Based on the results of the test (AECOM 2014) a horizontal to vertical permeability ratio of 5 was considered to simulate deposition characteristics of the soil. For the Plaxis 2D model, this anisotropic behavior and modeling of the sheet piles as no flow boundaries was included. The following hydraulic conductivity values were used for estimating the dewatering requirements of the powerhouse cofferdam: Sand and Gravel 0.01 cm/sec, Fine sand 0.005 cm/sec, and silt: 0.001 cm/sec.

Figure 4 shows the 2D Plaxis model considering three rows of dewatering wells spread across the length of the cofferdam. The Plaxis model was run with the following conditions a) considering sand and gravel extending well beyond the toe of the sheet piles b) fine sand extending to grade to limit recharge on the east (up slope) side. Considering these scenarios the total discharge required to lower the ground water table 0.5 m below the base of excavation was calculated to be 3,240 m^3/day. Considering a single 406 mm diameter well, and calculating its capacity after reducing it to half to take into account the inefficiencies and close proximity to the sheet pile walls, the individual capacity of each well was calculated to be 840 m^3/day. Thus four wells were required as per the model simulations, however, six wells were proposed for dewatering to provide redundancy and cover potential variation in the subsurface conditions.

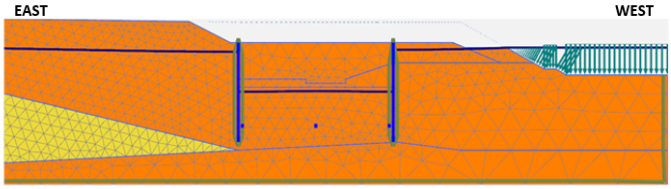


Fig. 4. Layout of 2D Plaxis model with 3 rows of wells

CHALLENGES ASSOCIATED WITH SHEET PILE DRIVING

Pile driving activity started in the field in August 2015. The in-situ state of compactness and stratigraphy were used to perform pile driveability analysis. Analyses were performed using the computer program GRL WEAP 2010 to assess hammer performance. The method of analysis was based on recommendations from the American Petroleum Institute (API) as outlined in their Recommended Practice 2A-WSD (API 2014). The APE 300 vibratory hammer was considered suitable for driving the piles to the full depth. Pile driving was started in the northeast corner moving south in a clockwise direction, however initial driving was faced with difficulty. Along half the length of the east wall early refusal occurred. In order to expedite driving to the full toe depth, an APE 400 vibratory hammer was mobilized to site. Pile driving was continued with both hammers around the perimeter of the cofferdam. However, refusal occurred at selected locations. Continued driving, or extraction and re-driving did not help to install sheet piles to full depth. Water was flooded around the perimeter of the cofferdam at sheet pile locations to reduce the effective stress and improve driveability. The cofferdam was closed and each pair of sheet piles was driven sequentially, maintaining not more than 1 m of difference at the top between adjacent sheet pile pairs. All these execution techniques helped to some extent, however, refusal was attributed to the possible presence of cobbles or boulders not detected in the geotechnical investigation. Figure 5 shows a photo of a sheet pile extracted after refusal. The damage to the toe indicates the possible presence of a cobble or boulder. It may be noted that final inspection of the cofferdam showed the walls to be true and straight with no misalignment issues.



Figure 5. Extracted sheet pile after early refusal; damage indicates possible obstruction

The final layout of the installed sheet piles and toe elevations along the perimeter walls of the cofferdam is shown in Fig. 6. This layout shows the open windows that were created at the northeast corner of the cofferdam and two additional openings on the south wall. The close proximity of the cofferdam to the Abitibi River on the west side, the high water table, and the presence of these openings combined to pose a major challenge to dewatering. Flows significantly higher than initially calculated were expected. This required a reassessment of the dewatering to facilitate construction of the powerhouse.

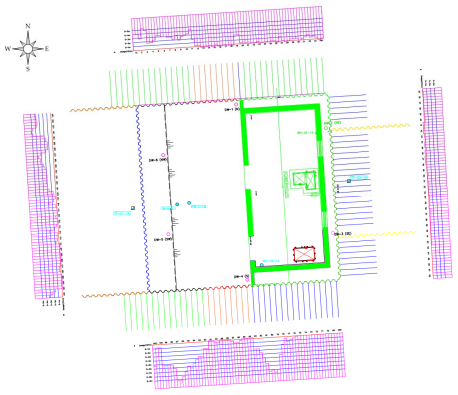


Figure 6: Final layout of driven sheet pile toe elevations, showing windows

An additional geotechnical borehole investigation was conducted in the powerhouse cofferdam area to assess the reason for the early sheet refusal. The results did not specifically identify the cause; yielding results very similar to the original investigation, leading to the same conclusions and supporting the original design.

During excavation of the cofferdam the presence of local gravelly pockets along with cobbles and boulders was confirmed. Figure 7 shows some photos taken during excavation of the powerhouse cofferdam.



Figure 7. Local gravelly pockets and boulders observed during excavation

Powerhouse Cofferdam Dewatering

Initially, the proposed wells were installed at the site and monitored for flowrates and piezometer levels, to assess the response to dewatering. Additional pumping wells were then installed based on numerical simulations as discussed in the next section

3D FINITE ELEMENT MODEL

A 3D geotechnical finite element model, using Midas GTS NX 2015, was developed to simulate the drawdown of ground water inside the powerhouse cofferdam. The model includes the final configuration of all fourteen installed wells and nine piezometers used to monitor the water levels while pumping. Figure 8 shows the layout of the dewatering wells and piezometers within the footprint of the cofferdam. In order to best approximate the model boundary conditions and material properties, specifically the

permeability, the model was calibrated to match the recorded piezometric head elevations corresponding to the measured well flow rates for different combinations of active wells at different times. The initial ground water table was measured to be 121.5 m and was used as one of the model boundary conditions. The Abitibi River was also set as a boundary condition for groundwater, to the West. The number of wells were incrementally increased and model simulations were run in parallel to arrive at the desired number and placement of wells to achieve drawdown. Only results of the final model simulations are presented below.

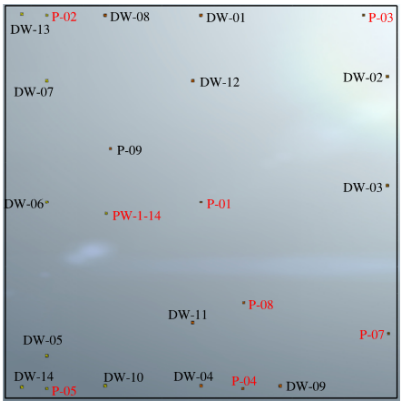


Figure 8. Layout of final well and piezometer configuration

The overall configuration of the model with 3D mesh elements and assigned material types is shown in Figure 9. The sheet piles and anchor layout used in the FE model is also shown in Figure 9. The as-built sheet profile which created windows along the perimeter was included in the model to allow for increased inflow and to facilitate assessment of appropriate dewatering needs. A cross-section of the cofferdam is shown through the center of the excavation, facing north, in Figure 10.

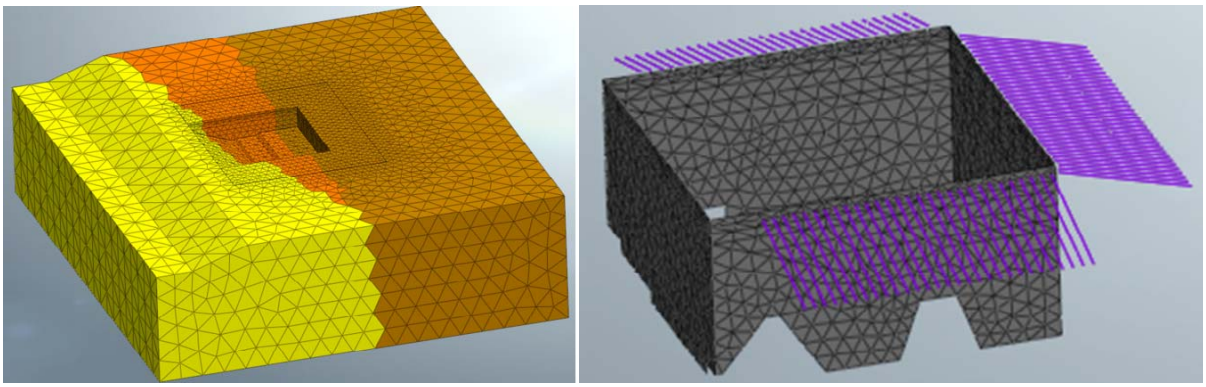


Figure 9: 3D Model geometry and Mesh

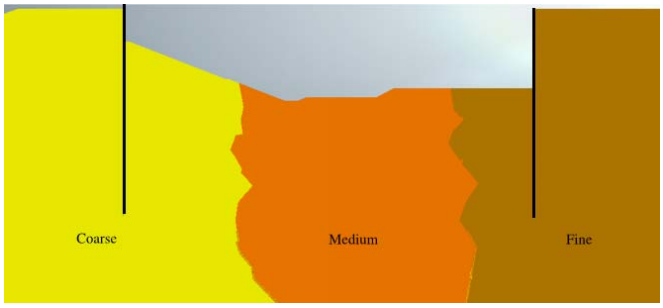


Figure 10: Typical cross section through the middle of the cofferdam

The model calibration was based on three soil types with low permeability to the east progressively increasing to the west (adjacent to the Abitibi River). The permeability values used for the final model for the coarse, medium and fine soils were 0.12, 0.015 and 0.0058 cm/sec respectively with an anisotropy ratio of 1.0. Modelling was initially performed using a transient flow analysis with sheet piles (no flow boundary) installed and no excavation. Various runs were performed in GTS NX to determine the most appropriate combination of soil permeability and soil boundaries to match the real time measured ground water drawdown results. Subsequently, the model was ran as a tool to assess the required number, capacity, and placement of wells. Additionally the construction sequence was modeled including excavation, potential rise in ground water to elevation 123.75 m, and the effects of a complete power outage. The summary of the well performance recorded readings and matching model results are presented below in Table 2

Table 2: Summary of Well piezometer data used in 3D finite element model

Well / Piezometer ID	Screen El.		Well Size		Model Comparison	Modelled El.	Diff.
	Bottom (m)	Top (m)	Pump Size hp	Flow Rate gpm	Measured El. m	m	m
P-01	111.0	114.0	-	-	114.1	114.6	-0.5
P-02	111.0	114.0	-	-	115.8	114.1	1.7
P-03	111.0	114.0	-	-	113.7	111.6	2.1
P-04	111.0	114.0	-	-	-	111.9	-
P-05	111.0	114.0	-	-	116.6	115.0	1.6
P-07	111.0	114.0	-	-	-	113.3	-
P-08	111.0	114.0	-	-	-	113.8	-
P-09	111.0	114.0	-	-	-	115.4	-
PW-1-14	99.0	102.0	-	-	118.4	117.1	1.3
DW-1	107.3	113.5	7.5	328	112.5	105.8	6.7
DW-2	102.7	109.1	7.5	227	114.5	100.9	13.6
DW-3	103.8	110.1	5.0	83	108.6	109.1	-0.5
DW-4	107.2	113.6	7.5	124	108.9	112.1	-3.2
DW-5	106.8	112.8	10.0	436	115.4	114.9	0.5
DW-6	106.7	112.5	10.0	503	115.5	115.2	0.3
DW-7	106.3	113.1	10.0	480	114.4	114.5	-0.1
DW-8	106.9	113.0	7.5	234	110.9	109.9	1.0
DW-9	106.8	113.0	10.0	434	112.2	106.1	6.1
DW-10	106.8	113.0	10.0	474	115.9	114.7	1.2
DW-11	107.0	113.0	5.0	180	112.1	112.6	-0.5
DW-12	107.0	113.0	7.5	275	109.4	109.0	0.4
DW-13	107.0	113.0	10.0	590	115.0	113.1	1.9
DW-14	107.0	113.0	10.0	495	109.9	114.1	-4.2

RESULTS

The final results of the flow model were performed with a “fully coupled stress seepage” analysis with construction stages. This analysis method allows the effects of construction to impact pore pressures and ground water flow. The construction stages modelled are as follows:

1. Initialize the model with original in-situ conditions
2. Install sheet piles including the “windows”
3. Install wells and piezometers, then activate with discharge rates matching field measurements

4. Excavate inside the cofferdam in 5 stages
5. Raise the ground water elevation from 121.5m to 123.75m (high flood water)
6. Deactivate all wells to simulate power outage

The result of stages 1 to 4 are presented here. Stages 5 and 6 were simulated to plan for contingency measures in the event of a flood or power outage at the site, however these events did not happen and the results are not included. Figure 11 presents the initial pore water pressure condition in the soil prior to dewatering and shows uniform hydrostatic conditions across the site.

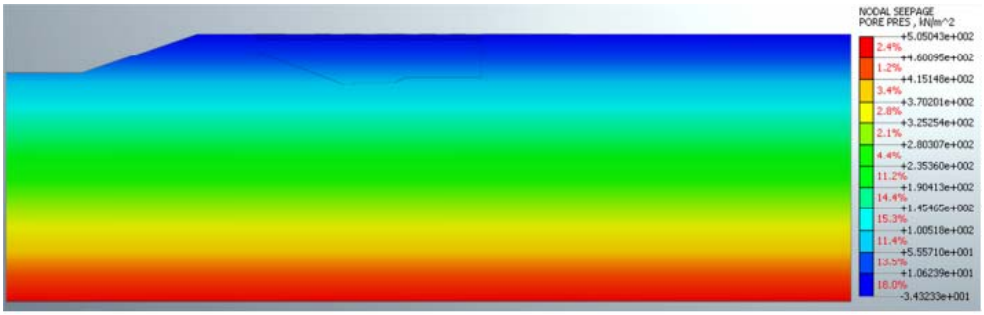


Figure 11: Pore pressure initial stage

Figure 12 presents the total head condition at the completion of drawdown within the cofferdam and indicates a water elevation ranging from about 112 to 115 m across the footprint of the powerhouse.

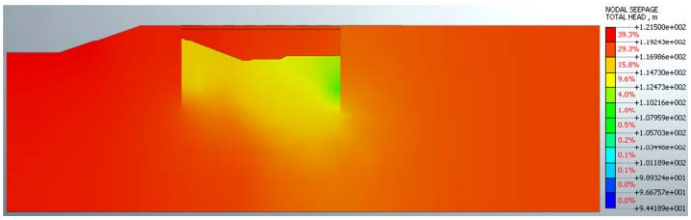


Figure 12: Total head after dewatering and final excavation

Pictures taken at the end of excavation show the effectiveness of the final dewatering system configuration as shown in Fig. 13. Subsequently the powerhouse was constructed in the dry without any further challenges associated with the dewatering system.

SUMMARY AND CONCLUSIONS

The construction of a cofferdam in unpredictable and difficult field conditions may lead to changes in final construction execution that may not be as per the preconstruction design. These changes may lead to significant adjustments and additional design effort in order to meet the construction schedules without compromising the safety, quality and intent of design. The case history presented in this paper is one such example where early refusal of sheet piles led to an increase in groundwater flow into an excavation.



Figure 13: Dry excavation before pouring the mud slab for the Powerhouse foundation

The additional resources required to satisfy the changed condition were provided based on field measurements and numerical simulations. The field observations and close monitoring during the construction of the cofferdam led to the following conclusions;

1. Field measurements provide a reliable source to input boundary conditions in a numerical model.
2. Numerical modeling is a reliable tool and can be successfully used to simulate construction conditions provided the model is calibrated and checked with field observations.
3. Proper application of numerical modeling can be used to plan and optimize construction resources.
4. Construction is an evolutional process and actual conditions may vary from anticipated conditions. The observational approach is a necessary method to validate the need for design changes and adjustment to construction resources. It is crucial that the design engineer be involved in construction activities, as they can have a significant impact on the design.

ACKNOWLEDGEMENTS

The authors are thankful to Peter Kiewit Sons' for providing resources and data for this paper. We are also thankful to our client Ontario Power Generation.

REFERENCES

AECOM 2014. New Post Creek hydroelectric development project –Peter Sutherland Sr. G. S, 2014 geotechnical investigation report.

American Petroleum Institute, 2014. API Recommended Practice 2A-WSD, Planning, Designing, and Constructing Fixed Offshore Platforms – Working Stress Design, Twenty-Second Edition.

GTS NX 2015. V.1.1 64 bit, Copy right (C) Since 1989 MIDAS Information Technology Co., Ltd.

Plaxis 2D 2015. Version 2015.01, Build 5460, Copyright 2006-2015 Plaxis bv

PTI 2014. Recommendations for prestressed rock and soil anchors, PTIDC-35 Prestressed rock and soil Anchor committee.

Support IT 2007. Version 2.36, GT Soft Ltd.

ASSESSMENT OF EXISTING BULKHEAD WALLS FOR DREDGING IMPACTS

Michael J. Byle, D.GE, F. ASCE, Tetra Tech, Inc., Langhorne, PA (215) 702-4113 michael.byle@tetratech.com
Rakam Lama Tamang, P.E., Tetra Tech, Inc., Langhorne, PA (215) 702-4076 rakam.lamatamang@tetratech.com
Stephen Ernst, E.I.T., Tetra Tech, Inc., Langhorne, PA (215) 702-4049 steve.ernst@tetratech.com

Abstract

For various reasons, dredging may become necessary in front of existing bulkhead walls, either for channel deepening or for environmental remediation of contaminated sediments. The removal of sediments at the base of bulkhead walls removes support for the toe of the wall that must be assessed. Evaluation of this impact can be problematic for aging bulkheads for which no design or construction records exist. This paper will address the steps that should be taken in investigation and analysis to assure proper assessment and means to address uncertainties and gaps in information. The steps include pre-investigation data review, field inspection, geotechnical and geophysical investigation tools, parametric analysis and design tools. Examples from several bulkhead assessment projects will be provided that include a variety of conditions and tools for application. The focus of the paper will be on the integration of technologies to assess bulkhead geometry, geotechnical properties and stability, structural safety and constructability issues with removal of support, and means of temporary and permanent stabilization for environmental applications.

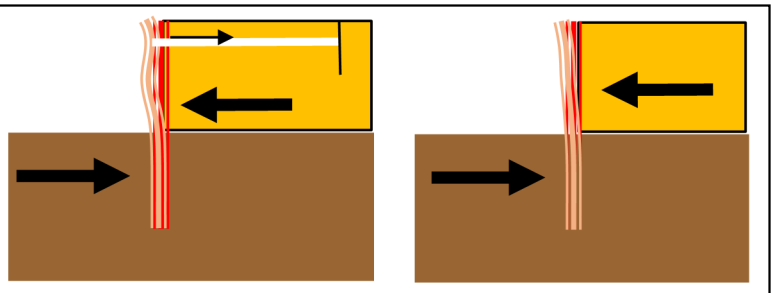
Keywords: Bulkheads, Analysis, Dredging

Introduction

Bulkheads and quays have existed as long as there have been waterfront activities. Some of the earliest date back to 1200 B.C.E.(Raban, 1987), however in the United States few predate the eighteenth century. Most extant bulkhead structures, and all steel sheet pile bulkhead walls date from the early 20th century or later. These structures function to protect the shore from erosion, support landside activities, and serve as place to moor and offload vessels. Regardless of the age or usage of existing bulkheads, it is essential to assess and protect them if needed where removal of soils on the water side of the bulkheads is planned to dredging.

Waterfront Bulkheads

Existing bulkhead structures can be classified into two types: Cantilevered, and anchored. Cantilevered walls are completely supported by the soil on the water side, while anchored bulkheads are supported both by the soil on the water side and anchorage on the land side (Figure 1). Walls may be constructed of timber, steel, or concrete. Timber walls may be lagging with soldier piles, cribbing with soldier piles, or timber sheeted such as Wakefield walls (Figure 2). Steel bulkheads are most commonly constructed using sheet piling comprised of interlocking A or Z shapes, though some historic walls were constructed with flat sheets. Precast concrete sheet piling has also been used in construction of bulkhead walls. Anchorage may be provided by steel bars or tendons attached to deadmen, sheet piling, driven piles, or earth anchors.



(a) Anchored Bulkhead (b) Cantilevered Bulkhead

Figure 1: Bulkhead Anchorage

Dredging Concerns

Typically, dredging involves excavation of the bottom sediments from a barge (Figure 3). The primary concern for structures adjacent to any dredging activity is the removal of soil support. The soil on the waterside of the bulkhead

 © 2017 DFI Annual Conference, New Orleans, LA, USA

provides support through passive earth pressure. Even where the soils are soft and loose, they provide an important component of support, since any lowering of the soil surface increases the moments in the wall as the passive force resultant is depressed. Also, many old bulkheads, were not designed to current standards, and previous dredging to permit access for larger vessels may have already reduced the wall stability. These conditions are largely unknown and the impact of new dredging cannot easily be evaluated without some in depth study.

Other impacts of dredging might include damage to the wall structure through contact with dredging equipment. Loss of support could also ensue due to subaqueous slope failure or dredging induced global instability.

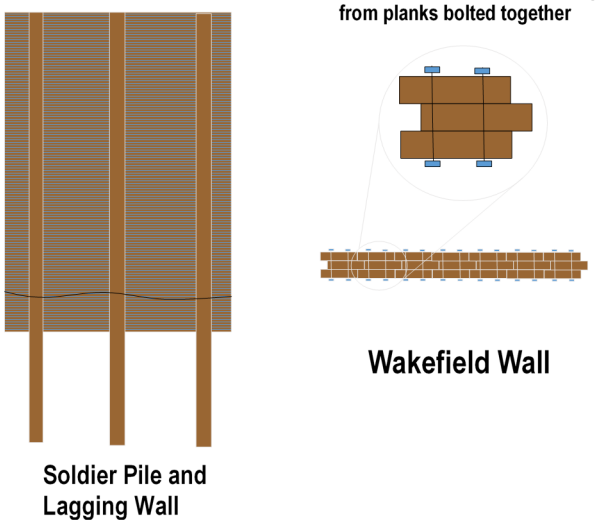


Figure 2: Timber Walls

Uncertainties for Assessment and Evaluation

Evaluation of existing bulkheads is an exercise in managing uncertainty. For some walls, often the more recently constructed ones, as-built drawings and specifications may be available, greatly resolving many uncertainties. However, for most older walls, plans may not be available, or may have too little information to be of much use. Fundamental structural dimensions may be unknown. Condition of submerged or buried portions of the wall may not be easily evaluated, as well as the condition of anchors and anchorage. Likewise geotechnical parameters and soil profiles may be unknown. Because bulkhead walls are often backfilled with whatever may have been available at the time of construction, the nature of the backfill can vary along a wall or from place to place behind the wall depending upon the source of material, how it was placed, and surcharge loadings that have been placed on it.

Bulkhead Data

In order to evaluate any bulkhead structure for the impacts of dredging, one must assess fundamental characteristics and properties for use in the evaluation. It is essential to understand the existing conditions in order to understand the impact of any modification. The basic parameters necessary are described in Table 1.


Figure 3: Typical Dredging operation

Desktop Data Collection

Collection of supplemental data from outside sources including state and local regulatory agencies, NJDOT, public records, on-line resources, U.S. Army Corps of Engineers, U.S. EPA, and riparian owners can be valuable for information on existing bulkheads. This data typically includes previous geotechnical

studies, design drawings, structural assessments, topographic maps, relevant historical data concerning shoreline development and construction.

Table 1. Parameters for Bulkhead Evaluation

Geometric Parameters
• Exposed Wall Height above the mudline
• Slopes (waterside and landside)
• Embedment of the wall below the mudline
• Height of anchors above mudline
• Spacing of anchors
• Location of structures supported on or behind the bulkhead
• Thickness of wall
• Wall cap type and size
• Anchorage configuration
	Structural Parameters
	• Structural sections
	  o Timber size
	  o Sheet pile size
	  o Wale size
	  o Anchor bar or strand size
	  o Anchor pile size
	  o Connection details
	• Structural properties
	  o Modulus
	  o Yield Point
	  o Section Properties

Geotechnical Properties • Soil profiles • Shear strength (drained and undrained) • Classification • Unit weight (moist, saturated, and submerged) • Groundwater level(s)	**Condition** • Presence and degree of corrosion • Physical damage to the wall **Loads** • Surcharges • Earthquake • Seiche • Mooring Forces

Online map software and aerial programs (Google™ Earth Pro, Bing Maps, GIS Aerial Databases, etc.) can provide high definition images, some with 3D terrain depending on the location that can allow you to gather information on bulkhead plan dimensions and site layout. In addition, historic aerials can provide data on the site layout in the past.

Construction records: Construction records, if available, are an excellent source of information. They will typically contain the material specifications, the construction sequence, plan layout, and bulkhead cross sections showing wall types, anchors, wall depth, and backfill specifications. Obtaining construction record can be difficult depending on the riparian owner. If the bulkhead is owned by a public entity (Dept. of Transportation, City, or State/Federal Entity), depending on the age of the bulkhead documents should be available and can be requested through the appropriate office. Private corporations and owners will depend on what the owner has retained. When performing a bulkhead evaluation every attempt should be made to obtain construction records. In addition, construction records should be obtained for adjacent structures critical to the bulkhead evaluation.

Design and as-built drawings of the bulkheads, structures, and foundations obtained from riparian owners can be used to determine the dimensions, geotechnical and structural properties of the bulkheads and foundations. The evaluation design basis including dredge line, and surcharge loadings can then be examined to assess whether the bulkhead structure design would accommodate the proposed dredging. Where the proposed dredge depth extends below the original design mudline, and analysis of the structure is needed to assess the impact for dredging, available geotechnical and structural data for the bulkheads from design or as-built drawings can be used to evaluate the stability of the bulkhead. Where data indicates a potential impact, or where data is insufficient, the needs for additional information should be assessed and should be used to refine the plan for the field investigations.

Survey Data: Available topographic mapping of the existing shoreline, areas adjacent to the shoreline, and behind existing bulkheads should be reviewed to assess conditions. Available topography will typically include USGS topographic maps and survey drawings made available through requests from riparian owners. Additional survey data can be obtained from review tax maps and property deeds in the local government office or databases. If construction drawings are obtained survey data may be presented on the drawings with respect to control points, site topography, and locations of surrounding features and structures. This data in combination with field measurements and additional survey during the evaluation will help define the limits of the wall and any critical evaluation analysis considerations, such as surcharges for adjacent structures and other surrounding conditions.

Bulkhead Structural Properties: When assessing existing bulkheads, one of the more difficult tasks can be determining the steel section properties of the wall. Depending on the time period of construction, the sheet pile shape, section modulus, moment of inertia, and type of steel can be difficult to determine. If the approximate shape dimensions can be measured in the field, then the section can be compared to historical sections from various publications to obtain published properties such as section modulus and the yield point (fy) for evaluation analysis. Some example of historical references would include the Lackawanna Steel Company Hand Book, Bethlehem Steel Sheet Piling Specifications, USS Steel Sheet Piling Design Manual, and other current manufacturer specifications. Other approximate methods based on field dimensions can be used to estimate the section properties using the properties of the geometric section to calculate the approximate section modulus and moment of inertia.

The strength of the steel for structural evaluation will vary depending on the time period of construction. When evaluating the structural capacity of the wall, the specified yield point (fy) of the steel when it was constructed needs to be determined for analysis. Assuming steel strengths based on modern steels used today, even A36 (fy = 36 ksi), may not be a conservative assumption. Industry use of A36 carbon steel first began for structural steel beginning in 1962. Prior to 1962, most steel for structural shapes had a yield point less than 36 ksi. For a comprehensive timeline of ASTM specified structural steel from 1900 to present, refer to the AISC Design Guide 15: Rehabilitation and Retrofit Guide: Historic Shapes and Specifications (2002), Table 1.1a. For historical bulkhead evaluation, Table 2 contains conservative yield point strengths that are recommended for structural evaluation based on review of AISC Design Guide 15, Lackawanna Steel Company Hand Book, Bethlehem Steel Sheet Piling Specifications, and USS Steel Sheet Piling Design Manual. If the steel strength is limiting the result of the structural analysis, and depending on the critical nature of the bulkhead, it may make sense to obtain coupons of steels from the existing structure and have them tested in laboratory for the structural properties if it is believed the actual values may be higher (or lower) than assumed.

Table 2: Recommended Conservative Yield Points for Structural Evaluation

Period of Construction	Recommended Yield Point (f_y), ksi
1900-1931	30
1932-1961	33
1962-1968	36
1968-2000	36*
2000-Present	42**

* A572 steel was first specified by ASTM in 1968 with varying grades (f_y = 42ksi – 65ksi), if confirmed by existing design documents or specifications for the steel is available for the actual wall under evaluation then higher yield points are appropriate.

** For bulkhead walls constructed from 2000-2017, typically A572 steel, Grade 50 (f_y =50 ksi) is commonly specified. The lowest grade available for A572 is Grade 42 (f_y =42 ksi). This assumption may be easier to confirm through design documents and available specifications due to the more recent construction. However, it should be noted that there is a possibility A36 steel may have been used.

Field measurements

The bulkhead structure should be evaluated to determine the elevation of the river bed and top of the bulkhead should be collected to determine the wall height and supported slope. The data collected then can be used for the planning of geotechnical investigation and form the basis for stability evaluation of the bulkheads and shoreline. Critical slopes

should be identified for additional assessment in the field and that may require global stability analysis during engineering design for the impact of dredging. Simple field measurements can be used to determine section properties (Figure 4). While collecting measurements in the field, this time should also be used to identify data gaps and the need for additional topographic surveys that may be needed if the existing data is not sufficient to complete evaluations at specific bulkhead. In addition, the existing condition of the bulkheads and natural shoreline should be visually assessed. This assessment should include the top of the wall, wall condition, wall anchorage, land use behind wall, accessibility for drilling equipment and geophysical survey. Where corrosion is observed, the depth of pitting should be measured and amount of section loss estimated as a thickness reduction.

Other evaluations to map the existing bulkhead above and below water include bathymetric and Aerial LIDAR and Photogrammetry survey. The results of that survey can be evaluated together with other topographic data to identify shoreline slopes and wall heights. The types of the bulkhead along the shoreline such as sheet pile wall, soldier pile wall, rip rapped area or natural shoreline can be identified from the bathymetric and LIDAR images.



Figure 4: Measuring to determine existing steel section for analysis.

Geotechnical Investigation

The soil parameters needed for the evaluation of the bulkhead can be collected through geotechnical investigation. The required minimum geotechnical investigation includes soil borings along with Standard Penetration Test (SPT) and piston tube sampling. The data obtained from the geotechnical investigation are utilized in sub surface characterization in the vicinity of the bulkhead.

Borings: The soil data required for the subsurface characterization of the soil in the vicinity of the bulkhead can be collected from geotechnical borings. As significant variation is soil properties on land and riverside of the bulkhead may exist, the geotechnical borings are required on both land and riverside of the bulkhead. The availability of the soil data reduces the risk on evaluating the bulkhead. Geotechnical borings can be drilled using traditional boring methods. However, waterside borings require the use of barge and special safety precautions needs to be followed in environmentally contaminated site.

SPT: In order to estimate the soil parameters needed for the evaluation of the bulkhead, Standard Penetration Tests (SPT) are performed. The SPT N-values are used to estimate the soil parameters required for the bulkhead stability evaluation using available correlation. The soil samples collected from the SPT are used for the laboratory testing of the samples.

Piston Tube Sampling: The likelihood of the getting soft sediment is higher on the coastal area. In order to properly characterize the soft soil, undisturbed samples are required to be collected during geotechnical borings. The piston tube samples can be collected using the available standards. The undisturbed samples collected can be tested in a lab to determine drained and undrained shear strength parameters required for the evaluation of the bulkhead.

Soil Property Testing

Uncertainty in soil properties is a critical challenge in the assessment of existing structures. The use of conservative parameters can lead to calculated safety factors less than 1.0 for walls that have been standing stable for many decades. Unconservative values can produce failures. In evaluating existing structures it is essential to accurately assess conditions, and this means more and higher quality data is required. Both laboratory and in situ tests are needed to assess soil properties and in sufficient quantity to assess variability.

Laboratory Testing: Critical parameters for soils in bulkhead assessment requires high quality undisturbed samples to obtain:

- In Situ Unit Weight
  - Moist
  - Saturated
- Drained shear strength (c', Φ')
- Undrained shear strength (c, Φ)
  - Consolidated – For cohesive soils consolidated drained and undrained parameters are most representative for dredging projects where no new loadings are created.
  - Unconsolidated – This is not typically a factor for dredging evaluations, since all soils are typically consolidated under the existing loads, but may be a factor for specific cases.
- Consolidation properties (if filling or capping is proposed)

For granular soils, gradation, and direct shear testing may be most appropriate.

In Situ Testing: In situ tests can provide inexpensive measures of soil strength not possible in the laboratory, particularly for granular soils and soft sediments that cannot be easily sampled without disturbance. In situ testing to determine undrained strength should include:

- Vane shear test
- Cone penetrometer test
- Flat dilatometer test

Geophysical Investigation

In addition to the geotechnical investigation, the geophysical investigations are required to determine the geometrical properties of the bulkhead components such as length of the bulkhead, depth of anchor etc. The parallel seismic and ground penetration radar (GPR) are pertinent geophysical tests that can be used to collect the bulkhead data.

Parallel Seismic: Where the design drawings of existing bulkheads are not available, the parallel seismic method can be used to determine the unknown length of the bulkhead. The method is based on generating an acoustic impulse at the top of the pile (created by striking the top of the pile with a sledgehammer). The resulting travel times of the impulse are measured in a borehole parallel to the foundation. This method of testing is applicable to many different foundation types including wood piles, concrete piles, pile walls, and sheet piles.

GPR: Ground Penetrating Radar (GPR) survey can be conducted to identify the buried structures such as anchors, deadmen, utility pipes etc. GPR survey is performed in accordance with ASTM D 6432 in the area behind the bulkheads. GPR survey can be performed in a parallel grid pattern so that length, spacing, and depth of anchors can be determined.

Analytical Approach

Generally, if a bulkhead structure appears unsound, either due to corrosion, deformation or failure, analysis of the bulkhead is of little but academic value, since dredging cannot be safely permitted near these structures. Therefore only those bulkheads which appear stable during visual assessments are subjected to analytical evaluation. The

precursor to the analytical evaluation would include definition of the wall geometry and structure, including the estimation of material properties for soils and structural components. The next step is the definition of loadings to which the bulkhead will be subjected and defining the analyses required to assess them. In some new construction, where consolidation will occur after construction, the undrained conditions will control the overall performance. In an unloading condition, such as dredging, the determination of whether drained or undrained conditions will govern is not always so obvious. It is essential to evaluate both drained and undrained conditions for some load cases unless the drainage conditions are well defined. Typically, undrained soil properties are used for the evaluation of the short term conditions such as rapid drawdown and new construction conditions, while drained soil properties for the long term conditions. Cohesion has a profound effect on the active earth pressures and calculated stability of the bulkhead. It is therefore essential to assess the potential for tension cracks, drainage pathways, and consider drained behavior for these analyses.
Bulkhead can be evaluated using limit equilibrium method, finite difference method and finite element method using commercially available software such as Shoring Suite, LPile, PY Wall , SPW, DeepEx, AMRetain, FLAC, Plaxis, etc.

Limit Equilibrium Analysis

The adequacy of the wall to facilitate dredging is commonly evaluated using limit equilibrium method. The limit equilibrium evaluation includes the local and global stability analysis of the bulkhead. The local stability evaluation considers the geotechnical stability including overturning failure and structural stability. The geotechnical stability evaluation is based on the equilibrium of active and passive earth pressure acting on the wall. The earth pressures acting on the bulkhead are calculated using either Rankine or Coulomb earth pressure theory depending upon the wall type and slope of backfill. Depending upon the level of anchor supports either triangular or trapezoidal earth pressure distribution are assumed. Generally, triangular earth pressure distribution is used for the bulkhead supported with single row of anchor, whereas trapezoidal earth pressure distribution is considered for the bulkhead with multiple levels of anchors. The structural assessments of the bulkhead components are performed using the force obtained from limit equilibrium methods.

Global stability evaluation of the bulkhead and surrounding soils is also commonly performed using limit equilibrium methods. Methods such as Bishop, Janbu, Spencer and Morgenstern-Price can be used with depending upon conditions. Unless there is a condition or stratification that would indicate non-circular failure modes would be likely, Bishop provides sufficiently accurate analysis with minimal assumptions. Those walls which meets local as well as global stability criteria are considered to be stable.

Nonlinear Analysis

In those areas where sensitive structures are present adjacent to the bulkhead, to better analyze stress-strain behavior and deformation analysis, the bulkhead can be evaluated using methods that include non-linear soil response such as the finite difference method (FDM) or nonlinear finite element method (FEM). The commercially available finite difference method based retaining wall design computer programs are generally simpler than FEM analysis and incorporating the soil-structure interaction effect based on p-y curves for nonlinear soil response together with linear elastic bulkhead elements. P-y curves can be estimated from soil properties or derived from stress strain behavior from laboratory or field tests. Nonlinear FEM relies on nonlinear soil elements, some of which involve parameters that can be difficult to estimate. Both FDM and FEM can provide improved estimates of load distributions and deflections over limit equilibrium methods. The results of these methods together with limit equilibrium method can be used to assess the soil structure interaction related to dredging adjacent to the bulkhead and impact to facilities supported behind or on the wall.

Load Cases

The stability of the bulkhead should be ensured for all load cases to which it may be subjected during its service life. The loads on the bulkhead will vary during its service life including construction conditions, surcharges, traffic loads, loads related to buildings and structures within the limit of the active earth pressure, earth pressure, and unbalanced hydrostatic load due to seiche events (rapid drawdown). For the purposes of a dredging assessment, the load cases for

the bulkhead can be categorized into: existing condition, dredging condition, post dredging condition and seiche event. At a minimum following load cases should be considered in the evaluation of the bulkhead.

Existing condition: The loads associated with this condition should include live loads due to land use behind the wall, structure loadings due to buildings and equipment, surcharge due to material stockpiles, rail and traffic loads, and earth pressures. The load case should include temporary and permanent surcharge within the active zone of the bulkhead and earth pressure. These loads should consider the existing configuration of the wall including mudline and water levels.

Dredging condition: The loads associated with the construction condition depends upon the means and methods of dredging and may include consideration of staged, or phased, approaches. These loads should consider a relevant subset of loads outlined above for the existing condition that will be present during the dredging activities. Loads due to construction equipment and other temporary surcharges should be considered, or may be eliminated where they can be restricted during the dredging, the load case should include earth pressure and permanent surcharge within the active zone of the bulkhead. If there is no control over the temporary loadings, such as the loadings due to construction equipment and the loads due to land use and operations in the retained area, these loadings should be considered as part of the dredging conditions.

Post dredging condition: The loads associated with this condition are long term in nature and would include all of existing condition loads for analysis under the post dredging configuration, including final mudline elevation.

Seiche event: Seiche events are those that produce rapid changes in water levels and can produce unbalanced water levels across bulkhead walls. Seiche events may be produced by storm surges, extreme tides, and landslides into lakes or reservoirs. The loads associated with seiche event are short term in nature. The load case should include unbalanced hydrostatic pressure based on the mean low water table and mean high water table, earth pressure. Historic level data can provide the basis for the levels to be used.

Case Analysis

In order to assure the stability of the bulkhead throughout the service life, analyses of multiple cases is necessary. The cases should include all load cases of the bulkhead as discussed above. Additional cases may be added where staged dredging is proposed.

Existing condition analysis: Analysis of the existing condition of the bulkhead is intended to provide an assessment of the wall stability prior to dredging. This analysis enables evaluation of the current stability of the bulkhead as a basis for assessing the potential impacts of dredging. The condition of the bulkhead, such as deterioration and deformation should be considered in this analysis. If the wall is severely deteriorated and significantly deformed, there may be little need for further analysis, since the wall may be marginally stable and the risk of dredging adjacent the structure may be too great to proceed safely. However, where the wall appears sound and straight based on a visual assessment, the wall should be analyzed. Where possible, the degree of section loss due to corrosion should be assessed and wall structural properties adjusted accordingly. The evaluation shall include local, global as well as structural stability.

The analysis should include the current mudline, top of wall, depth of embedment, backfill slope and loadings as described above in 3.3.1. Where the wall cross section and loadings vary along its length, it will be necessary to analyze multiple sections to determine the critical conditions. Analytical results may indicate different critical conditions at different sections. For example, one may find that stresses in steel sheeting may be the limiting factor at one section, but anchor capacity, or embedment limitations may control at other sections depending on mudline elevation, backfill grading, surcharge loads, etc. that may vary along the wall. These conditions must be evaluated so that the effect of dredging may be evaluated.

Dredging condition analysis: If the wall is stable in the existing condition, evaluation of the dredging operation can be performed. The stability of the wall should be checked during dredging, and for each phase/stage if the dredging is phased. Typically undrained soil parameters are be used for the dredging condition evaluation of the bulkhead. However, since the dredging unloads the toe of the wall, total stress analysis must consider that pore pressures may

be negative. If temporary surcharge loading can be restricted, evaluation may be performed with reduced surcharge loading.

Post dredging condition analysis: The wall shall be evaluated for the post dredging condition in its final configuration (i.e. with the revised post-dredging mudline) to ensure the stability after dredging. The post dredging evaluation should generally be performed using the drained soil parameters depending upon the soil type.

Seiche condition analysis: Where appropriate, seiche effects should be analyzed to assess bulkhead stability. The seiche event shall be analyzed using undrained soil parameters and load cases as discussed above in Existing Condition Analysis. Sieche events may be considered for any condition; existing conditions, dredging case, post dredging case. It may be reasonable to neglect the seiche event for the dredging case depending upon the nature of the events and likelihood of the event occuring during the dredging operation.

Alternative Development

In the situation where the dredging operation would result in unacceptable performance such as excessive deflection, settlement, unacceptable factors of safety or failure of the bulkhead, the existing bulkhead can often be reinforced with a variety of measures. This section describes some of the potential alternatives that may be considered and implemented to facilitate the dredging operations. These alternatives include staged construction, bracing/anchoring, replacement of the bulkhead and installing additional structure considering the combined interactions of existing and additional structure.

Staged Construction

The primary objective of the staged construction is to maintain the stresses and safety factors of the wall within acceptable limits throughout the dredging operation. Staging is often used to limit the affected portions of the bulkhead so that it can be stabilized prior to additional dredging. One of the best examples of staged construction could be to excavate the backfill side of the bulkhead, dredge, and place a buttress fill on the water side, then replace the excavated backfill. In this approach, the soil backfill is removed to reduce the stress on the bulkhead so that the area can be safely dredged. The depth of the excavation is usually limited by the presence of existing underground utilities, deadmen, and anchors. The safe depth of the dredging may be limited due to limitations of the soil that can be removed behind the bulkhead. In such cases, over-dredging may be done so that the dredged area may be backfilled with a material of higher strength and unit weight to safely achieve a target elevation. After the completion of dredging, the dredged area and area behind the bulkhead can be backfilled with suitable granular or lightweight material to the pre-dredged level to restore the pre-existing grade with suitable factors of safety.

Bracing/anchoring

Anchoring is a method to increase the permanent structural support to the bulkhead. The stiffness of the bulkhead system can be increased by installing the anchor system where existing anchors may be overstressed. For cantilever walls, adding anchors will relieve bending stresses and reduce the required embedment for passive lateral support. It may be necessary to add wales to distribute loads from sheeting to anchors. Anchor systems may include conventional steel anchor rods and deadmen, drilled and grouted soil anchors, helical anchors, etc. Alternately the wall can be braced through the addition of soldier piles, where vessel mooring is not an issue, or embedded toe-piles to brace the toe of the wall and increase embedment (Figure 5).

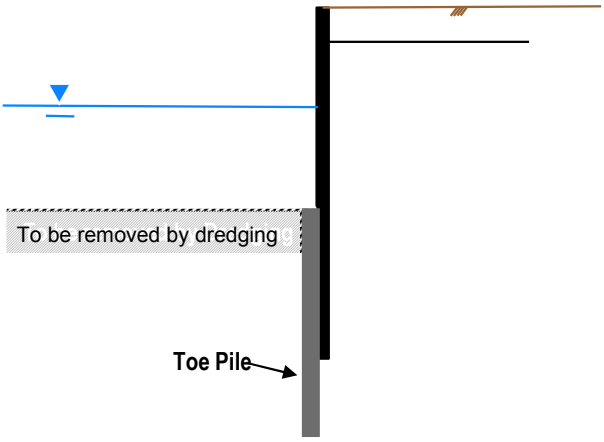


Figure 5: Toe Supports

Replacement

In some cases, it may not be practical to modify the existing bulkhead to accommodate the post-dredging conditions. In such instances, the most practical solution may be to replace the bulkhead. The replacement alternatives are many and will depend upon site conditions, access restrictions, utilities, and land use. Replacement structures often consist of sheet pile walls constructed within 1 m of the exposed face of the existing wall (Figure 6). Wall may be cantilevered or anchored, sheet pile, combi-wall (H or Pipe shapes alternating with sheet piling), or soldier pile walls or cellular walls. Anchorage may be by drilled and grouted anchors; anchor rods or tendons tied to deadmen, sheet piling, or driven piles; helical anchors, duckbill or manta-ray anchors.



Figure 6: Replacement wall being constructed in front of existing wall.

Compound interactions

One of the alternatives could be the installation of toe supports in front of the existing bulkhead. Where the condition of the bulkhead is good, but the wall has insufficient embedment to accommodate dredging, adding support at the toe of the wall is sometimes an option. This may be accomplished using sheet piling, or drilled or driven soldier piles. The analysis and design of such an arrangement can be performed considering the combined performance using the strength of the new and existing bulkhead element, however details must be designed to assure interactions required are attained. This approach can reduce the construction cost over a full replacement option.

Conclusions

Evaluation of existing bulkheads to evaluate impacts of dredging is a complicated process. Walls are affected through reduction in passive support and increased bending moments that may also increase anchor stresses. Evaluation of these conditions requires specific knowledge of bulkhead construction, special investigative methods to determine wall geometries and soil parameters. Generally consolidated drained and undrained shear strengths are critical to evaluating performance. Viable alternatives to stabilize walls influenced by dredging processes will depend on the site conditions, wall configurations, geotechnical stability, structural conditions, access, and constructability issues. Tools exist to complete these evaluations, but require attention to detail.

References

Avner Raban, 1987: *The Biblical Archaeologist*, Vol. 50, No. 2. (Jun., 1987), pp. 118-126.

United States Steel (USS) Sheet Piling Design Manual, Updated and reprinted by FHWA July 1984.

U.S. Army Corps of Engineers. 1994. Design of Sheet Pile Walls. EM 1110-2-2504.

U.S. Army Corps of Engineers. 1989. Design of Retaining and Flood Walls. EM 1110-2-2502.

PERMANENT CANAL CLOSURES AND PUMPS COFFERDAMS – SUPPORT OF DEEP EXCAVATION IN SOFT GROUND USING THE OPEN CELL SHEET PILE SYSTEM

Matthew Anderson, PND Engineers, Inc., Seattle, WA, (206) 624-1387, manderson@pndengineers.com
King Chin, GeoEngineers, Inc., Redmond, WA, (425) 861-6098, kchin@geoengineers.com
Mike Huggins, PND Engineers, Inc., Seattle, WA, (206) 624-1387, mhuggins@pndengineers.com
Ryan Higbie, Traylor Bros., Inc., Evansville, IN, (502) 807-6923, rhigbie@traylor.com
Rian Johnson, PND Engineers, Inc., Seattle, WA, (206) 624-1387, rjohnson@pndengineers.com
Dave Sinsheimer, Kiewit Infrastructure South Co., Fort Worth, TX, (817) 337-7000, dave.sinsheimer@kiewit.com

ABSTRACT
The Permanent Canal Closures and Pumps (PCCP) project is the capstone piece of New Orleans' extensive hurricane risk-reduction system constructed following Hurricane Katrina. The project consists of three discrete pump stations and flood gates on the shore of Lake Pontchartrain which provide a storm surge barrier and pump rainwater from the City of New Orleans' primary drainage canals. The depth of the pump station structures ranged between 39 and 45 feet below sea-level. USACE developed the PCCP project for design-build delivery; granting the project team latitude to develop innovative, cost effective solutions for the project. The use of OPEN CELL™ cofferdams to construct the pump station structures was one such innovation. OPEN CELL structures utilize the strength of the retained soil to anchor cellular sheet pile face arcs; allowing a free-field of construction within the cofferdam. This cofferdam design did not require ground improvement or dewatering around the perimeter of the cofferdam. The free-field cofferdams streamlined construction and large equipment installation within the structures with no encumbrance from internal bracing. Meticulous force-based design, soil-structure numerical modeling, and physical testing were all techniques used to present and gain USACE acceptance of the design on this vital element of the work.

Keywords: Soft ground, soil retention, Hurricane Katrina, pump station, cofferdam, geotechnical, OPEN CELL, USACE, PCCP, heavy shoring.

PROJECT DESCRIPTION
The Permanent Canal Closures and Pumps (PCCP) project is the capstone piece of the City of New Orleans' extensive hurricane risk-reductions system constructed following Hurricane Katrina in 2005. The project encompasses three separate pump stations and floodgate structures located at the mouths of three outfall canals (17th Street, Orleans, and London) on the south shore of Lake Pontchartrain. These three canals, running from the south to north, act as the primary conduits for discharging water from the New Orleans area. Prior to Hurricane Katrina, these canals were operated with pump stations two to three miles upstream of the mouths at Lake Pontchartrain. This left long stretches of levee on each side of the canals exposed to storm surges entering from the lake. Three levee failures occurred along these canals during Katrina; two at London Canal and one at 17th Street Canal. The failures resulted in major flooding of the surrounding neighborhoods, significant damages, and loss of life.

Following initial canal levee repairs after Hurricane Katrina, USACE, in partnership with the Louisiana Coastal Protection and Restoration Authority (CPRA), took action to move the line of flood protection to the mouths of these three canals at the edge of the lake. By cutting off the storm surges from Lake Pontchartrain at the entrance to the canal, over ten miles of canal levee would no longer be exposed to storm surge water elevations, significantly decreasing the risk of failure.

Initially, temporary pump station and gate systems were installed, the Interim Closure Structures, at each canal to provide this increased protection. The goal of the PCCP project was to replace these temporary steel structures with permanent concrete pump stations designed to protect against 100-year storm-surge

 © 2017 DFI Annual Conference, New Orleans, LA, USA

and evacuate the rain water from the associated event. This system would also allow non-storm canal conditions to bypass the pump station and flow directly to Lake Pontchartrain. During specified storm conditions, this bypass canal is to be closed off by gates to complete the floodwall protection at the mouth of each canal. Storm waters in the canals, collected from the New Orleans area will then be pumped over this floodwall and into the lake.

The project was awarded to the Design-Builder, PCCP Constructors JV (Kiewit Louisiana South Co., Traylor Bros. Inc., and the M.R. Pittman Group, LLC with Stantec as the lead designer, PND Engineers as the cofferdam designer, and GeoEngineers as the cofferdam numerical modeler) on April 17, 2013 and design began immediately. Each of the three pump stations and corresponding gate structures were designed to meet specified criteria including maximum flows, minimum and maximum water surface elevations, and site layout limitations. This also included criteria to accommodate a possible future state where the canal pool elevations would be significantly lowered and the water would gravity flow to the pump stations at the lakeshore. Pumping capacity requirements vary at each site with the largest site (17th Street) at 12,600 CFS. Figure 1 shows the 17th Street pump station site during early construction and a 2017 photo showing the pump station nearing completion.

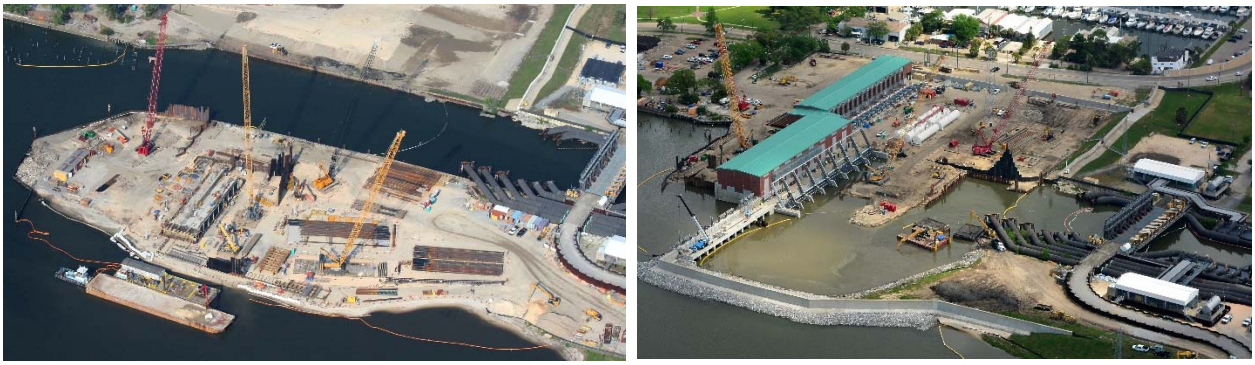


Fig 1. 17th Street Pump Station Site. Early Construction (Left); Nearing Completion (Right). (Aerial photos provided by PCCP Constructors JV.)

The project horizontal footprint was limited at each site and required continuous flows through the existing canals running through the sites including hurricane event conditions throughout all phases of construction. This required detailed planning in the site layouts and sequencing of construction. The largest pump station, at 17th Street, required a footprint of approximately 250 feet by 130 feet which was to be constructed within a cofferdam. To accommodate the large pump sizes and associated discharge and intake requirements, as well as the possible future state criteria, the floor of the pump station was established at EL -39. Adding in the thickness of the pump station footing and the thickness of the pump station tremie concrete resulted in an excavation to EL -53. PCCP is one of the deepest excavations ever accomplished in this region and required a significant and innovative cofferdam design solution.

THE NOVEL DESIGN CONCEPT FOR THE COFFERDAM

The New Orleans area presents unique challenges to a deep cofferdam. Common to most of the southern Louisiana region is a high water table. Underlying soil deposits are primarily composed of unconsolidated clays with occasional sand layers to a significant depth below the surface. These features prompted several construction considerations in the selection of the cofferdam system: available and necessary equipment to install the cofferdam; equipment access adjacent to the cofferdam; pile driving operations in and around the cofferdam; bracing interferences; concrete forming and construction joints; and large equipment installation within the cofferdam.

The Design-Builder had past experience in all of the considerations described above, and therefore was able to draw on past costs, production rates, and knowledge of the advantages and disadvantages to each system. Primary considerations were: 1) the significant retained soil loads applicable to the cofferdam 2) the need to support construction activities with heavy equipment immediately adjacent to the cofferdam walls and 3) the hydrostatic forces and seepage control required for deep cofferdams. The Design-Builder focused on selecting a system that would provide the least amount of interference to the work in the cofferdam. Conventional braced cofferdams tend to require detailed, staged installation; and present difficulty in all aspects of the construction of the structure within the cofferdam. Another project limitation was that the canals had to be fully functional during construction. When considering the option of combi-walls supported by batter piles, it was noted that batter piles would have created a large impediment to construction. Batter piles would either extend into the cofferdam, hampering construction, or would extend into the canal and behind the cofferdams, and effect canal flow. Regardless of batter pile orientation, site soils required the length of these batter piles to be extremely long to develop the required resistance.

The Design-Builder had utilized OPEN CELL cofferdams and bulkheads on many past projects, and therefore had experience with the system. After evaluating preliminary designs and overall costs of the different systems, the Design-Builder selected the OPEN CELL system for this high profile project.

One component of the cofferdam that was common to all systems was the tremie seal. The cofferdam was designed for a maximum water elevation in the canal of +6.0. The bottom of the footing is at -45.0. This 51.0 foot of water head would have required a conventional gravity-weight, tremie seal thickness of over 30 feet alone. Accounting for frictional tension capacity in the piles could reduce this, but without additional measures would have still require a significant tremie seal.

An OPEN CELL cofferdam with a pile-supported tremie is a relatively novel and unique design application. The design for the system is not incorporated in the USACE Engineering Manuals or reference documents. Therefore, many of the critical failure modes needed to be demonstrated theoretically using first principles. As a secondary method of verification, the Design-Builder needed to demonstrate the suitability of the cofferdam for this application through soil-structure interaction analysis testing and monitoring.

FUNDAMENTAL CHALLENGES WITH COFFERDAM DESIGN

The backdrop of the PCCP project included the notorious geotechnical failures near the site, the difficult ground conditions, the large magnitude of loading, and the uniqueness of the system. These cofferdams are considered high risk support-of-excavation structures. Failure of the cofferdam to perform as expected would have potential of life threatening hazards to the workers within the cofferdam. In addition, there is risk exposure to the work itself, the equipment and materials. In this context, the unique cofferdam design drew considerable attention from the project sponsor and technical reviewers.

The OPEN CELL cofferdam is a soil retention system which functions in a different manner than conventional earth retaining structures. Unlike conventional earth retention systems the OPEN CELL cofferdam is designed to resist lateral soil force by mobilizing horizontal tension forces in circular face arc across the sheet pile interlocks. The face arcs transfer lateral load to tailwalls behind the cofferdam face. The tailwall deliver tension forces into the soil via friction and/or cohesion along the entire area of the tailwall. Continuous interlocking sheet piles also provide uniform restraint over the height of each tailwall. The tailwall uniformly distributes the applied load minimizing stress concentrations in the anchoring soil mass and allows for the efficient anchorage of the system using the inherent strength of the soil mass. The utilization of horizontal hoop tension makes the system more structurally efficient than traditional steel flexure-based systems.

The hurdles facing the design of an OPEN CELL cofferdam are in principle the same as those experienced by other traditional cofferdam systems. Cofferdam designers seek to ensure that a design adequately

stabilizes the surrounding ground, structural elements are not overstressed (yet economized as much as possible), and that deflections will not impede the construction process.

Design was complicated by the project criteria and site conditions. The cofferdams for PCCP needed to be fully un-watered without ground improvement. The three project sites contained uniquely difficult ground conditions. Site clay layers exhibited properties of low shear strengths, shear softening, and low shear moduli. Given the low strength and stiffness of the soils it was understood early in the design phase that the OPEN CELL would sustain large deflections, greater than 12 inches; much larger typical for a conventional retained earth system. Such deflections are necessary to mobilize the shear capacity of the large volume of soil into which each tailwall is embedded. During the design phase these cofferdam deflections were predicted to be large enough to induce strain softening in the upper retained soil layers. Another consequence of these deflections was that plastic flexural bending of the steel was anticipated to occur in the OPEN CELL face sheets. Coupled with plastic flexure of the sheet pile was consolidation layers of native clays. This consolidation would apply axial down-drag loads to the face arc sheet pile. Anticipated plastic strain of the sheets combined with down-drag forces could, in principle, lead to a structural instability if not properly evaluated and addressed. This potential mechanism triggered additional evaluation by the design team and scrutiny by project's technical reviewers regarding the stability of the bulkhead face.

Resolution of the technical challenges centered on geotechnical analysis to verify that the anticipated movements would not trigger progressive failure via the movement of strain softening clays. Structural analysis and testing performed by the Design Team and Design Builder was performed to demonstrate that plastic deformation of the sheet piles would not degrade the capacity of the interlocks and that the estimated displacements of the cofferdam face would not result in instability under soil downdrag load.

The design program included a first principles analysis of the system, demonstrating the adequate size of design components such as tailwalls and face arcs. Supplemental geotechnical testing was implemented to quantify the strength of soils under high strains. Additionally, destructive structural testing was performed as part of the program to validate the performance of the sheet pile once loading beyond the elastic range. The design demonstrated that the OPEN CELL cofferdam was adequate to support applied loads while meeting industry standard levels of care. Figure 2 illustrates OPEN CELL function.

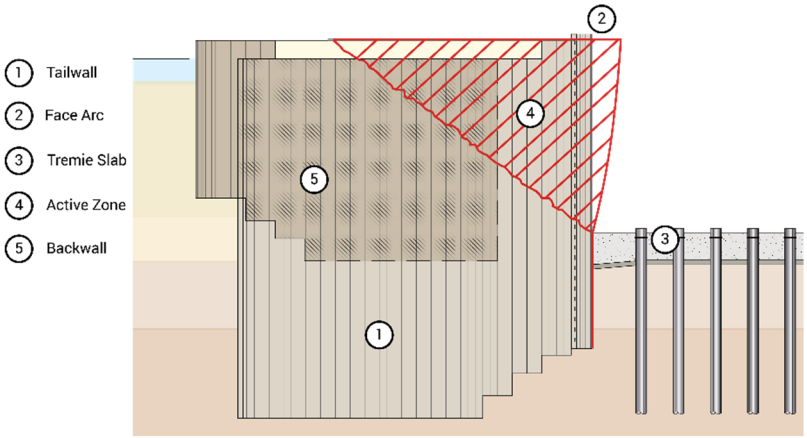


Fig 2. OPEN CELL Function

Integral to the success of the design was solid theoretical prediction of ground displacement. Deflection data was a crucial metric with which to gage the performance of the system. Deflections of the soft soils into which the OPEN CELL was embedded is challenging. The Design Team utilized numerical model to generate estimates for the displacement of the retained soil mass. The numerical model would include all

known characteristics of the site soils, included strain softening. Inclusion of strain softening in particular required careful consideration. Development of these numerical models is described below.

NUMERICAL SOIL MODELING

It was essential to produce a thorough geotechnical and structural analysis for the cofferdam design. In particular this meant producing the theoretical predictions to compare with to real-life field measurements. A three dimensional numerical model was developed using a typical OPEN CELL cofferdam section to evaluate the response of the system for the excavation and dewatered conditions using the computer program PLAXIS 3D Foundation. The 3D model includes two half-cells with six soil units: Fill, Marsh deposit, Lacustrine deposit, Pine Island Beach Sand, Bay Sound Clay deposit, and Pleistocene soils (clay and sand), as illustrated in Fig. 3. The soil layers were a simplified and judicial interpretation of the extensive subsurface exploration performed at the sites.

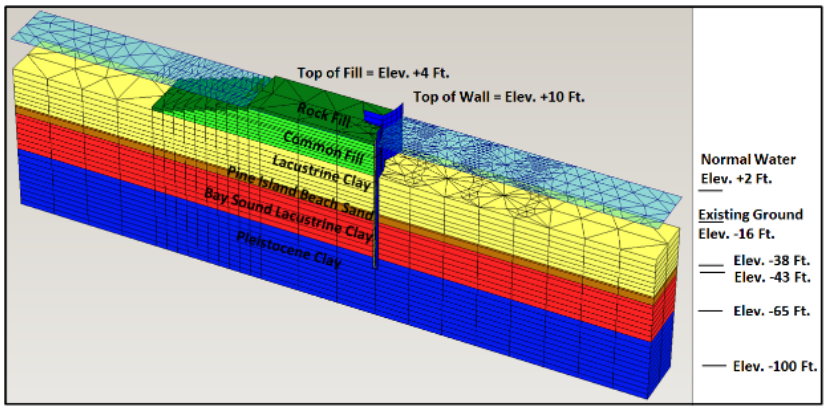


Fig 3. Modeled Soil Stratigraphy (Credit: GeoEngineers)

Soils were modeled using the nonlinear Hardening Soil model, developed and calibrated using laboratory testing program which included consolidation tests, undrained unconsolidated triaxial tests, consolidated with at-rest stress conditions, undrained (CKoU) triaxial tests and the direct simple shear (DSS) tests. The testing provided data on the soils peak shear strength and the degraded soil strength under high strains.

Based on past project experience, the Design Team expected that the OPEN CELL cofferdam would deform a considerable amount under the full excavation and dewatering conditions. Laboratory shear strength test results indicated that the shear strength of the clay decreases with deformation (i.e. strain softening effect). Published literature (Seed et al, 2008) provided a ratio of the peak strength and reduced strength ranging from 0.75 to 0.80 for similar soils in the Lakeshore site vicinity. After extensive evaluation of the shear strength test results, the Design Team concluded that an average reduction factor of about 0.70 was appropriate to account for the strength reduction at large strains. The reduction factor was applied to the entire Marsh and Lacustrine Clay soil layers. This was considered to be an upper bound on the soil displacements as only a portion of the soils behind the temporary cofferdam would experience large strain under the temporary excavation and dewatering conditions. Applying the reduction factor to the entire soil layer also eliminate the need to update the softening soil zones during the various simulation stages in the model. Another set of PLAXIS analysis was completed using the peak soil shear strength (i.e. unreduced) to establish the lower bound soil displacements.

The sheet piles of the OPEN CELL cofferdam were modeled as “wall” elements that require input of structural thickness, unit weight and stiffness. The stiffness of the sheet pile was modeled as anisotropic with the horizontal stiffness taken as three percent of the vertical stiffness. The vertical stiffness was taken as the stiffness of steel. The small ratio between horizontal and vertical stiffness accounts for the horizontal slack associated with the sheet pile interlock take up as well as the more flexible response of the interlock under tension. This modeling approach is consistent with the recommendations per USACE EM-1110-2-2503 “Design of Sheet Pile Cellular Cofferdams and Retaining Structures”. Figure 4 presents the results of the numerical modeling of the cofferdam wall face and wye pile under the various temporary excavation

conditions computed using the peak and reduced soil strength models. Figure 5 presents the deformation map of the tailwall within the soil mass using peak strength and reduced strength soil models.

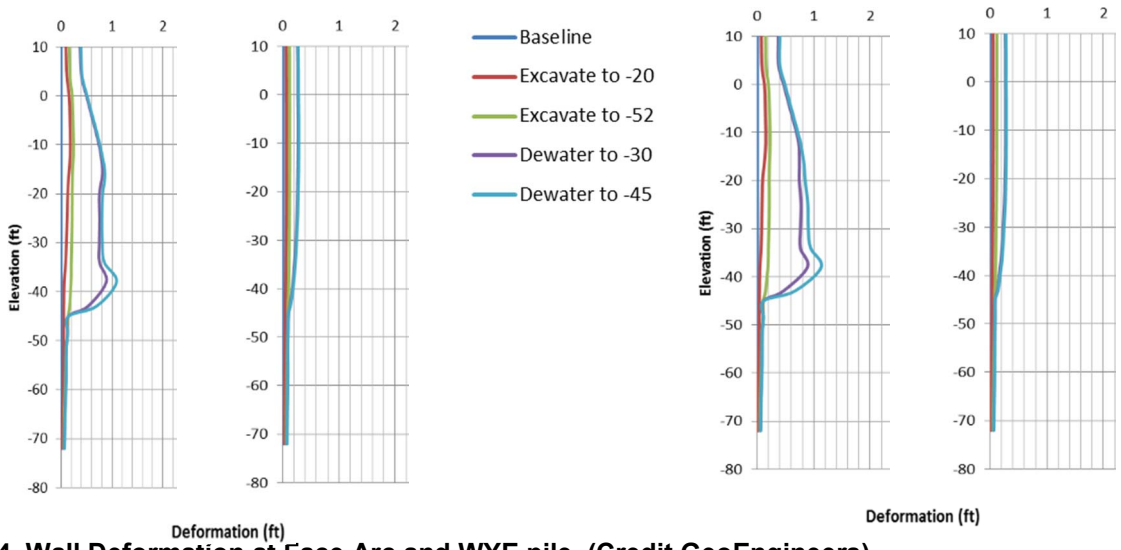


Fig 4. Wall Deformation at Face Arc and WYE pile. (Credit GeoEngineers)

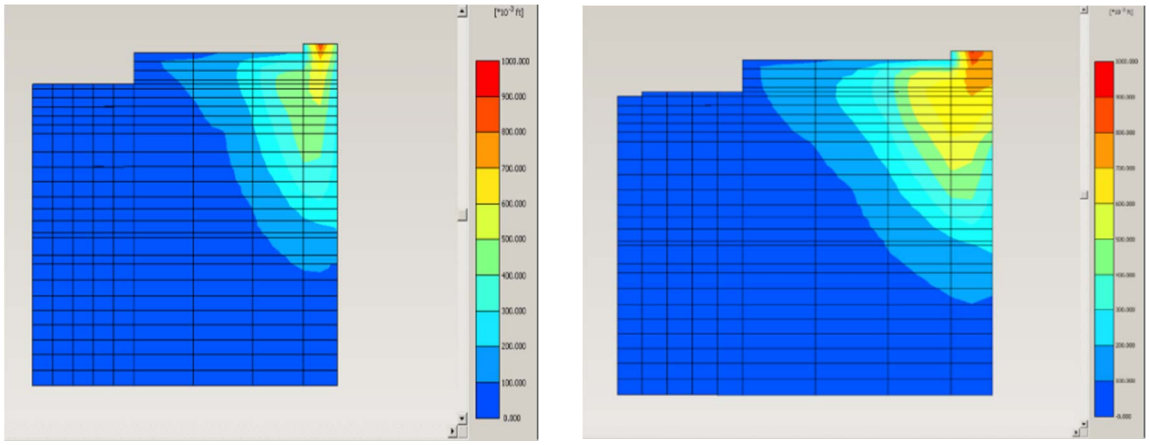


Figure 5. Tailwall Deformation Contours with Peak (Left) and Reduced Strength Models (Right). (Credit: GeoEngineers)

Once the numerical modeling was complete and deflections estimated, the Design-Build team needed to develop field techniques to measure and verify the performance cofferdam as referenced to the design to satisfy the Engineer and Owner and to ensure the safety of the crews working deep below sea level.

MEASUREMENT/QUALITY ASSURANCE TECHNIQUES

Due to the high risk nature of the cofferdams a thorough operation, maintenance and surveillance plan was developed. A normal cofferdam monitoring system primarily consists of survey points located at strategic locations on the sheet piles. For the PCCP project, a detailed plan was prepared which required extensive instrumentation in addition to survey points

During the design process, the Design Team performed detailed analyses to demonstrate that the overall load path was coherent and that factors of safety, deflection and stability met or exceeded the performance required by industry-accepted standards.

Notwithstanding past project experience and advanced analytical methods; the design team recognized that the field performance of geotechnical structures is difficult to quantify in exact terms. Indeed the difficulty of predicting displacement of a soil mass is acknowledged in documents such as Eurocode EN 1997-1 (2004) Section 11.6, which states:

> "Since the analytical and numerical methods available at present do not usually provide reliable prediction of the deformation of a natural slope, the occurrence of serviceability limits states should be avoided by one of the following: limiting the mobilized shear strength or observing the movements and specifying action to reduce or stop them if necessary."

Field performance consistent with analytical results and empirical evidence was key goal of the cofferdam phase of the project. Given the unknowns associated with the soil conditions and the magnitude of loading: monitoring (as described by Eurocode EN 1997) provided an avenue for evaluation of cofferdam performance. Demonstration of satisfactory field performance would assure stakeholders such as USACE or CPRA that the cofferdam was performing to the satisfaction of the Design Team. The Design Team developed a series of "thresholds" that triggered notifications to all parties involved. The Design Team, in conjunction with the Design-Builder, established predetermined actions to be taken at each of the following three threshold levels. These ranged from automatic notifications sent to all parties to higher thresholds which required evacuation and flooding the cofferdam in the extreme condition.

Monitoring would generally fall into three separate categories: Deflection Monitoring, Stress Level Monitoring and Curvature Monitoring.

Deflection Monitoring: Observed deflections were considered an index of the state of stress in the soil mass. The Designer utilized numerical models to capture deflections anticipated during the various stages of construction. Deflection monitoring techniques included observation of strategic survey points and use of inclinometers. Continuous monitoring throughout the construction of the cofferdam was deployed. In this manner a large sampling of deflection data was collected during the early stages of construction. The body of data could be used to analyze and understand the progressively larger deflections experienced during later stages of cofferdam construction.

Deflection monitoring was provided to anticipate a progressive failure of the cofferdam. In the event anomalous deflections were observed, the measurements could be compared with adjacent monitor points and inclinometers. Excessive deflections would be indicative of unanticipated cofferdam behavior and remedial action could be implemented in a before jeopardizing the safety of the workers inside.

Stress Level Monitoring: The design was based on predicted stresses in the structural sheet pile controlled by the face arcs. Overstress of the sheet pile would obviously be undesirable and would require remedial action. Stresses in the sheet piles were gauged by the field measurements. The Designer develop two methodologies for the measurement of stress in the system. These were face arc length measurements and strain gauges. Neither of these two techniques directly measured the stress in the sheet pile steel: both infer the stress on the basis of measured strains. Strain is directly measured in the base metal as a discrete location by strain gauges. These strains are converted into stresses by multiplying the measured strain by the elastic modulus. Face arc measurements consider the accumulated deflection resulting from interlock tension. Interlock tension is evaluated as function of the face arc length and magnitude of arc length change measured versus the theoretical un-deflected arc length.

Curvature Monitoring: During the design phase the Design Team noted that the sheet pile would displace sufficiently to induce plastic strains in the face arc sheet pile due to impingement on the rigid cofferdam tremie slab. To resolve concerns about the structural stability of this system, the Design-Build team performed a series of physical tests to ensure that interlock tension capacity would not be degraded as a

result of these plastic strains. Curvatures were monitored to ensure that the face arc curvature would remain within the limits considered by the testing program. Curvature is physically a measurement of the rate change angle as a function of distance. Constant curvature is simply a circular arc. The curvature was imposed and measured by placing a calibrated template (see: Fig. 6a), with the peak tested curvature radius against the face sheets. Twelve samples were tested to interlock failure (see Fig. 6b) and the result indicated on appreciable loss of interlock strength under vertical curvature.



Fig. 6a. Curvature Test Specimen

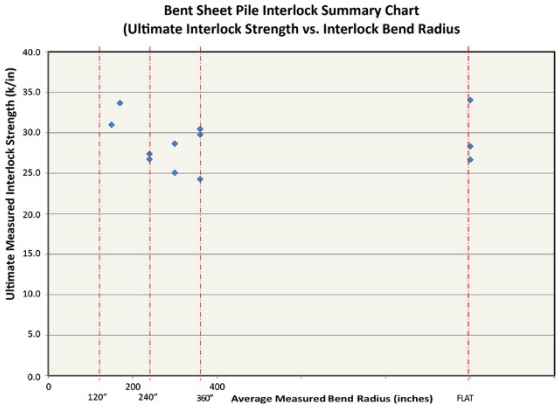


Fig. 6b. Bent Sheet Pile Interlock Summary Chart

For each stage of construction, the Design Team predicted a range of values which was anticipated to be observed in the field. Maximal values of field observables were also estimated. These values represent the maximum value a field measurement could have before the risk of instability required consideration. Maximal values were useful for identifying when heightened monitoring or repair would be required. The staged nature of the construction also allowed the Designer to make predictions on the basis of previously measured data. This was particularly useful for the cofferdams, as most of the load would be applied rapidly during un-watering. Extrapolation of previously observed data (during the actual construction of the cofferdam) allowed the Designer to give realistic bounds anticipated bounds of behavior, after unwatering.

After the monitoring instrumentation was installed on the cofferdams, the data was baselined to the pre-excavation condition of the pump station cofferdams. The Design-Build team began receiving valuable information on the performance of the cofferdams immediately upon commencement of excavation for the cofferdams. This information was used to verify the design and update the theoretical predictions.

NOTED OBSERVATIONS

Construction of the three OPEN CELL cofferdams began in 2014. The first cofferdam, at Orleans Avenue Canal was un-watered in February of 2015 followed shortly thereafter by the cofferdams at London Avenue and 17th Street Canals. Continuous monitoring of the cofferdams during construction, particularly prior to un-watering was key to interpreting the implication of observed movements. This is highlighted by movement effects brought about by changes in the construction sequence.

The original analysis was predicated on the assumption of that water surface elevations would remain constant at EL. 0 inside the cofferdam during excavation, pile driving and tremie placement. However, post-design the construction team requested a modification of to the sequence, wherein the cofferdam would be partially excavated “in-the-dry”. The Design Team evaluated this request using classic limit equilibrium methods and determined that the wall would remain stable and approved the request.

During the dry excavation monitoring data indicated that the wall was moving significantly more than anticipated in the original design predictions. Since the magnitude of movement was larger than predicted, the Design Team updated the numerical model to re-assess movements based on the revised construction

sequence. These updated numerical models validated the observed movements and confirmed that the OPEN CELL was performing normally. The difference in wall performance was attributed to the dry excavation loading the OPEN CELL system more heavily during an earlier stage of construction as a result of performing the excavation in-the-dry. Although the design limits were not exceeded, the dry excavation sequence effectively loaded the system to 70% of maximum predicted design load (Fig. 7).



Fig. 7. Initial Excavation of Orleans Pump Station Cofferdam with water drawdown.

Observation of the unanticipated movements proved advantageous in predicting the future performance of the system post un-watering. The numerical model is limited in its power to make predictions because of the discrete nature of soil sampling. Variations in soil properties and stratigraphy cannot be known with sufficient accuracy to produce a complete assessment of soil movement. However, during dry excavation a suite of measurements were made on cofferdams. These measurement were scaled based on the relative intensity of the dry excavation loading (as compared to the fully un-water load case) to produce another creditable estimate of cofferdam displacements. Further, the observed variability of field measurement provided and index to the variability of measurements post un-watering.

The change in load sequence meant that the OPEN CELL system was loaded in an entirely different manner than previously analyzed. This variation in load path, would result in different deflection estimates. In light of this sequence change, the Design Team re-assessed the established threshold limits based on the new construction sequence. However, the Design-Build team was better equipped to assess future displacements, since field data was available for comparison. Revised thresholds better suited the observed performance of the OPEN CELL cofferdam post un-watering as shown in Table I.

Table I. Revised Thresholds (For Post Un-Watered Condition), Post Dry Excavation and Observed Cofferdam Deflections (Average)

Project Site	Predicted Displacement Thresholds			Observed Deflections at Various Stages		
	Alert	Heightened Alert	Emergency	Partial (Dry) Excavation Deflection	Excavation Complete (Watered-Up)	Un-Watered
17th Street	9 Inches	14 Inches	20 Inches	2.8 inches	5.7 Inches	10.5 Inches
London	9 Inches	14 Inches	20 Inches	2.8 inches	4.2 Inches	7.9 Inches
Orleans	12 Inches	14 Inches	20 Inches	4.3 Inches	5.3 Inches	9.8 Inches

Validity of the revised threshold would have been questionable, in the absence of other corroborating observations. The best relationship between stresses and displacement is via a non-linear numerical model, which is sensitive to variations in soil properties, stratigraphy and load sequence. However, monitoring of observable indices, provided assurance that the un-watered cofferdam would not be over-stressed.

CONCLUSIONS

The pump stations' OPEN CELL cofferdams were successfully completed, flooded, and removed in the first quarter of 2017. Today, the completed PCCP structures at the mouth of the 17th Street, London Avenue, and Orleans Avenue Canals are impressive even to the casual observer. However, a significant chapter in the story of this project lies hidden beneath the canals' muddy water surface. Deep below that surface, these

unique structures provide a physical testament to the extraordinary effort put forth on the part of the Designers and Constructors to safely and efficiently build New Orleans' capstone flood protection project. The effort of the team to employ innovative construction methods along with the data extracted during construction has helped to advance industry techniques for support of excavation in soft soils.



Fig. 8. Initial Excavation of 17th Street Pump Station Cofferdam with water drawdown

An integral component to the success of this novel design was the ability of the designer to communicate the theoretical attributes of the system, produce robust estimates of the system performance and effectively monitor system performance indicators. These three components of design deployment ensured that the project remained safe under unprecedented circumstances.

Innovation into the field of geotechnical engineering and deep foundation construction will provide new cost efficiencies into the infrastructure marketplace. While difficult to develop, novel structures can be monitored for verification of initial design assumptions. Through field verification of the design, project safety can be maintained without significantly hampering design creativity. In this regarding, key critical lessons learned on this project are:

1. Solutions should be assessable and expressed clearly. It is essential that all stakeholder have an accurate understanding of any innovation. Overly complex analyses inhibit clear communication of legitimate design concerns.

2. Insure that all stakeholders are aware of the limitations of the analytical techniques deployed. Regardless of the how extensive an analytical and monitoring program are used, all techniques have error. Engineering judgement is always important in assessment of real performance.

3. Field monitoring precision is the yard-stick to measure numerical model performance. In a physical environment which experiences settlement, pile driving, and dramatic changes in water elevation monitoring to a predetermined baseline is challenging. The sensitivities of numerical modeling make it difficult to choose a quantity to field measure. However, selection of the most field tolerant measurement will provide the best insight into structural performances.

4. Engagement of the Design Team throughout construction provides assurance that monitoring data is properly interpreted and provides a feedback loop to improve cofferdam design for the future.

REFERENCES

Design of Sheet Pile Cellular Structures, 1989. Engineering Manual EM 1110-2-2503. U.S. Army Corps of Engineers, Washington, D.C.

Seed, R.B., et al., 2008. New Orleans and Hurricane Katrina. III: The 17th Street Drainage Canal. Journal of Geotechnical and Geoenvironmental Engineering. ASCE 1090-0241(2008) 134:5 (740)

Eurocode EN 1997-1 (2004): Eurocode 7: Geotechnical Design – Part 1 General Rules, Section 11.6

ADVANTAGES OF PRESSED-IN SHEET PILES FOR NEW ORLEANS' HURRICANE AND STORM DAMAGE RISK REDUCTION SYSTEM FLOOD CONTROL PROJECT

Ian Vaz, Giken America Corp.; Orlando, Florida; (407) 380-3232 ivaz@gikenamerica.com
Takefumi Takuma, Giken America Corp.; Orlando, Florida; (407) 380-3232 ttakuma@gikenamerica.com

ABSTRACT

The New Orleans area has been repeatedly flooded by major storms and hurricanes since its French colonial era. After severe flooding in May 1995, the U.S. Congress authorized a massive flood protection project called the Southeast Louisiana Urban Flood Control Program (SELA) in 1996 to improve interior drainage in Orleans, Jefferson, and St. Tammany parishes. However, the project was not fully funded before the landing of Hurricane Katrina in 2005 and Hurricane Rita, which breached many of the area's levees and flooded 80 percent of the city. Finally, the project was fully funded in 2008 and has been worked on towards its 2017 completion. Another large project simultaneously worked on in the area is the Hurricane and Storm Damage Risk Reduction System (HSDRRS). This system was designed for a 100-year level of flood risk reduction. One particular project within the HSDRRS rendered successful due to an unconventional method of pile driving that was utilized to install sheet piles to reinforce an existing concrete I-wall. This paper will discuss how and why this non-vibratory method of sheet pile installation allowed the project to be successfully completed ahead of schedule.

Keywords: press-in, sheet pile, seawall

INTRODUCTION

Steel sheet piles were utilized on many of the SELA and HSDRRS projects for permanent cutoff walls under concrete I-walls or T-walls or for temporary earth retaining walls of drainage structures. Although the SELA Project was established in 1996 after severe flooding the year before, hardly any work was done on it until the two catastrophic storms Hurricanes known as Katrina and Rita triggered its revival. These two hurricanes also triggered the HSDRRS soon after the storms' devastation. The SELA project authorized to improve interior drainage systems while the HSDRRS project was authorized to raise or restore levees and floodwalls mainly along Lake Pontchartrain, the Mississippi River, and Lake Borgne in addition to other areas. Figure 1 shows the SELA Projects that have been completed, are still under construction, or approved for construction. The projects fully highlighted in yellow within the map specified the press-in piling method. These improvements included drainage systems, pump stations, surge walls, and outfall canals as enhanced protection for future storms similar to Hurricane Katrina that caused so much damage by inundating the New Orleans area in August and September 2005 respectively (Facts and Figures, 2012). The completion of these projects were the responsibility of the U.S. Army Corps of Engineers, New Orleans District.

Due to the fact that many of the projects were in densely populated areas, the Army Corps of Engineers specified a non-impact, non-vibratory press-in piling method for driving and extracting sheet piles for many of the projects to mitigate noise and vibration impacts. The soft soil conditions in the New Orleans area was also a contributing factor in the Army Corps of Engineers' decision to specify this piling method due to the risk of settlement for existing historical as well as modern structures. In addition, there were other projects that elected to use the press-in method without any contractual requirements. One of these projects was the Inner Harbor Navigational Canal Reach II Emergency Interim Repair which was part of the HSDRRS project that has been under construction since its authorization in 2005 (Facts and Figures, 2012).

 © 2017 DFI Annual Conference, New Orleans, LA, USA

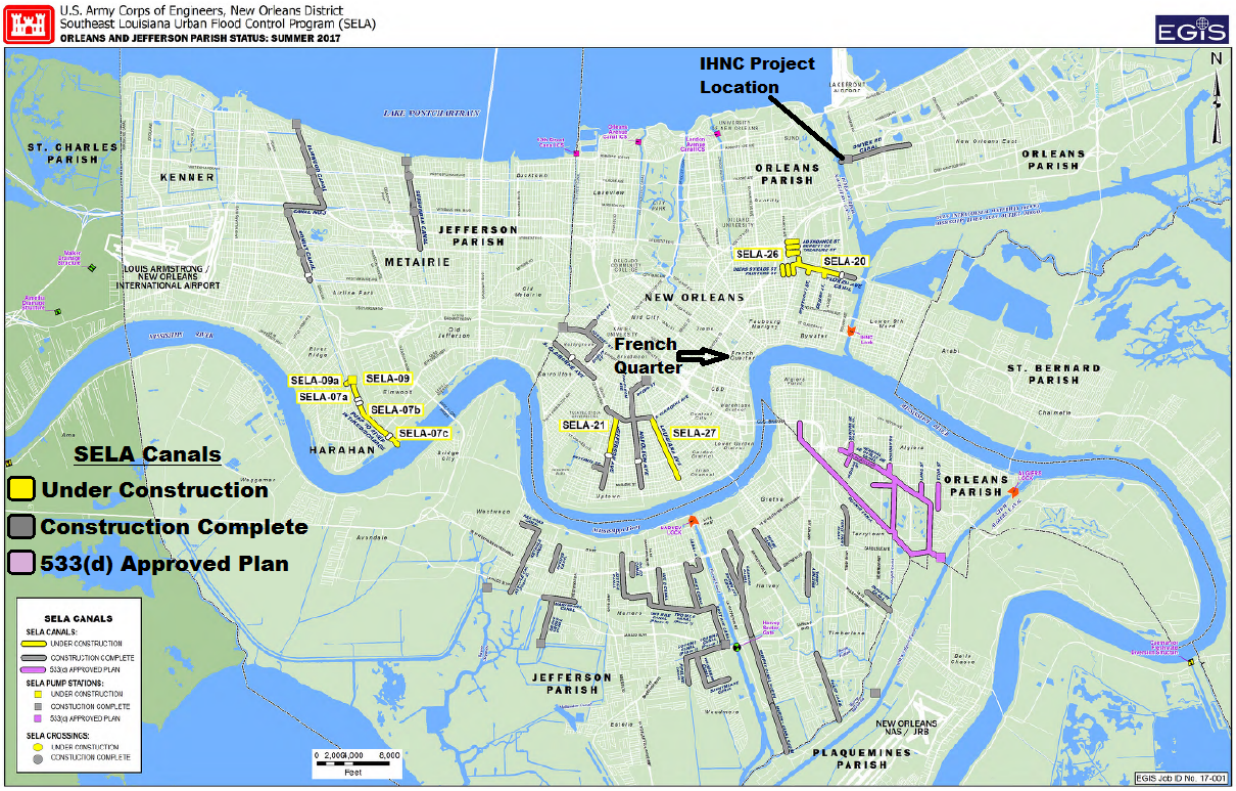


Fig. 1 Map of SELA Projects Summer 2017 Map via Link Below (http://www.mvn.usace.army.mil/Portals/56/siteimages/SELA/Jefferson_Orleans_Eastbank_Westbank.pdf)

Projects that were completed or are currently under construction for HSDRRS are a combination of the Lake Pontchartrain & Vicinity (LPV) and West Bank & Vicinity (WBV) projects which are shown in Fig. 2. (Facts and Figures, 2012). Since SELA projects were drainage improvements within the city, most of them specified the press-in piling method. However, of all the numerous SELA and HSDRRS projects in the area that had specified the press-in piling method due to noise, vibration, and/or space constraints, the Inner Harbor Navigational Canal Reach II Emergency Interim Repair Project was the one project in the New Orleans area that did not specify the press-in method but can be considered the most successful of all the other specified press-in piling projects given the circumstances of the project. Refer to Fig. 2 for the location of the project in relation to the other HSDRRS projects in the area. 55 ft. long sheet piles were pressed into a dense sand layer to form a cutoff wall. The contractor struggled with three vibratory hammers in different sizes and one diesel hammer to drive them before they switched to a press-in piling machine to successfully complete the project which lasted from February until June 2010 (Bergeron, 2010).



Fig. 2 HSDRRS Projects June 2013 Map via Link Below (http://www.mvn.usace.army.mil/Portals/56/docs/HSDRRS/Staus-Map-2013.pdf)

THE PRESS-IN PILING METHOD

The press-in piling method typically utilizes a reaction force derived from a few previously installed piles to hydraulically press in the next pile. The press-in piling equipment of this type works on top of already installed piles and moves forward on its own as shown in Fig. 3. Due to the fact that this method does not use vibratory or percussive force to install the pile, it is regarded as an environmentally friendly piling method. Its advantages are:

1. Low noise and practically vibration free. It enables pile driving projects close to houses, schools, hospitals, and other sensitive structures as well as in the areas where sensitive fish and/or animals are around.
2. The equipment size is relatively small and its clamping point is much lower than those of other pile driving methods. This fact enables the equipment to work in physically tight working conditions, both horizontally and vertically. It worked out well for the construction within close proximity of the barrier wall. (Takuma, 2015)
3. It can achieve much more accurate and safer pile installation due to a combination of better control of the piles and lower clamping points compared with other pile driving methods. Installing the 55 ft. long relatively flexible PZC 19 sheet piles into dense sand was successful on this project.

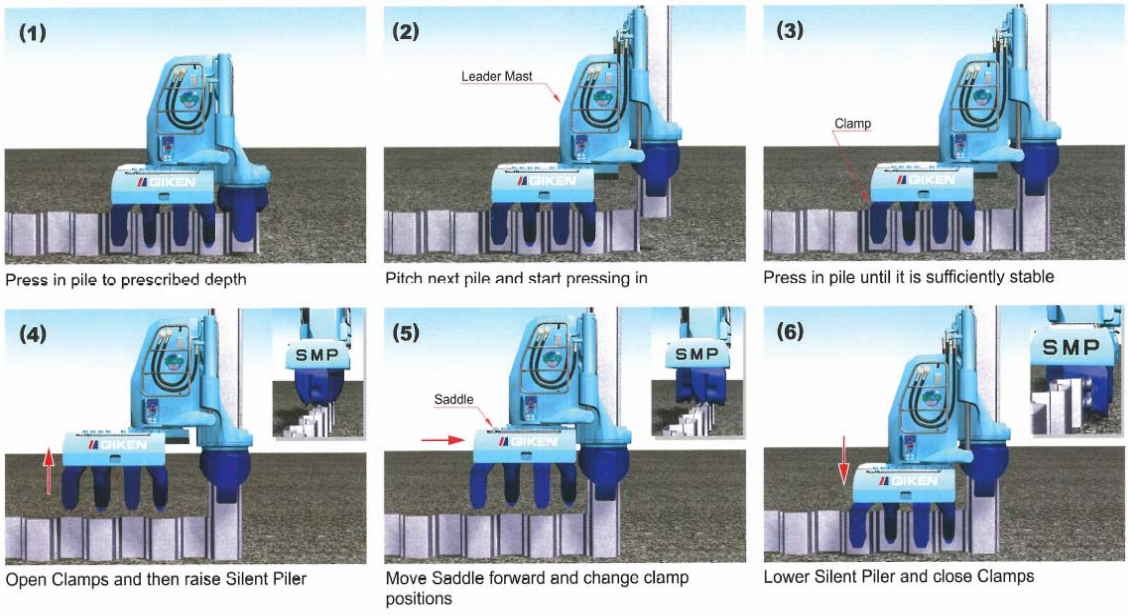


Fig. 3 "Self-walking" Sequence with the Press-in Piling Machine

For a typical press-in piling machine to get started off, it uses what is called a Reaction Stand. The Reaction Stand is a steel component that is used for the assembly of the press-in machine. It has outriggers that can extend laterally, forward, and backward and is designed to hold counterweight (Fig. 4) to keep the machine grounded so that the first sheet piles can be installed. With the press-in machine model used for this IHNC project, the first 2 pairs of sheet piles needed to be installed before the press-in machine could walk off of the Reaction Stand and continue advancing on its own on top of the sheet piles.



Fig. 4 Initial Press-in Piling Sequence

For the IHNC Emergency Interim Repair Reach II project, a 10 ft. x 30 ft. compacted level pad two feet below top of pile elevation was required at the starting point for the Reaction Stand.

DESIGN AND SOIL CONDITIONS

This IHNC project in Orleans Parish called for the installation of approximately 885 linear wall feet (48,670 ft^2) of steel sheet piles along a stretch of concrete I-wall (Fig. 5) to prevent seepage through a sand strata. The steel sheet piles installed were 55 ft. PZC 19 sheets as a cutoff wall that was to be constructed at an elevation of -50 to intercept seepage (Fig. 6). See Fig. 7 to get an idea of the difference between the existing I-wall and the new sheet pile wall from an elevation vantage point.
Originally, the Army Corps of Engineers was planning to install relief wells at this location. However, the installation of relief wells would have led to increased costs, time, and coordination since there would have been issues with underground collection lines such as those under railroad tracks nearby.

What can be considered rather unusual for the New Orleans area is the soil conditions that were encountered on this IHNC project. Figure 8 illustrates the type of soils that were dealt with throughout the project. The soil conditions along the road at this site location (Fig. 9) had proven to be the biggest challenge with the utilization of vibratory and impact hammers. Although the first 10 ft. below the ground surface was soft soil, it became rather dense at 13.5 ft. The general contractor for this IHNC project tried to use large vibratory hammers to drive the sheet piles into a dense fine sand layer where the SPT N-value was between 40-60 blows per foot for much of the distance between the ground surface and sheet pile tip elevation.



Fig. 5 General Plan for IHNC Emergency Interim Repair Reach II

SHEET PILE DRIVING AND UNFORESEEN DIFFICULTIES

With the inability to drive the sheet piles into the dense sand with 3 different hammers starting with 1,100 inch-pounds then attempting with 2,800 lb-in. and finally with a 4,400 lb-in. vibratory hammer. An impact hammer that was able to deliver 43,000 lb-ft. of energy was also brought in to try and finish the work. However, not only was the impact hammer not able to drive the sheet piles through the dense sand, the tops of the sheet piles were starting to bend due to the excessive force that the hammer needed to use as an attempt to try and finish the sheet piling work (Bergeron, 2010). The general contractor finally decided to employ the press-in piling method as the last resort. What helped the press-in piling machine install the sheet piles easier than the conventional methods used previously is the fact that the point of contact between the sheet pile pair and the machine was at ground elevation, allowing for more accuracy with all the energy to press in the piles at ground elevation instead of the point of contact being suspended 10 to 15 ft. above the ground surface and as high as 50 ft. in the air where energy can be lost. According to Captain Nicholas Cali, Army Corps of Engineers project manager for the IHNC, energy is not lost through deflection with press-in piling machines since they grip the sheet piles at the bottom (Bergeron, 2010).

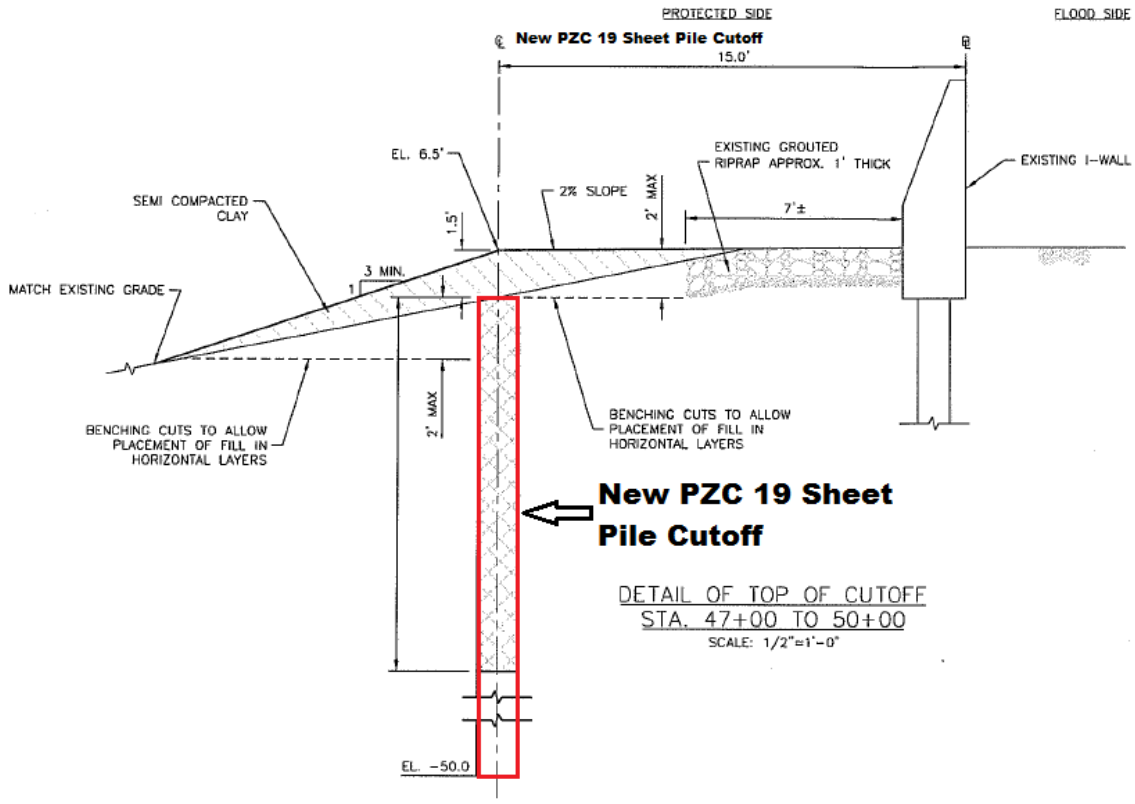


Fig. 6 Cross Section View

The PZC 19 sheet piles are considered a lighter and less rigid than other heavier sheet pile sections that the vibratory and impact hammers were not able to drive in with the hard soil conditions. The press-in method and its associated press-in machine allowed the same PZC 19 sheet piles to be installed efficiently without damage to the sheet piles since it handled the piles at the ground surface with the aid of a high pressure water jet attachment; thus, allowing for less expense on steel without upgrading to a stronger and more costly sheet pile section while completing the project in a timely manner.

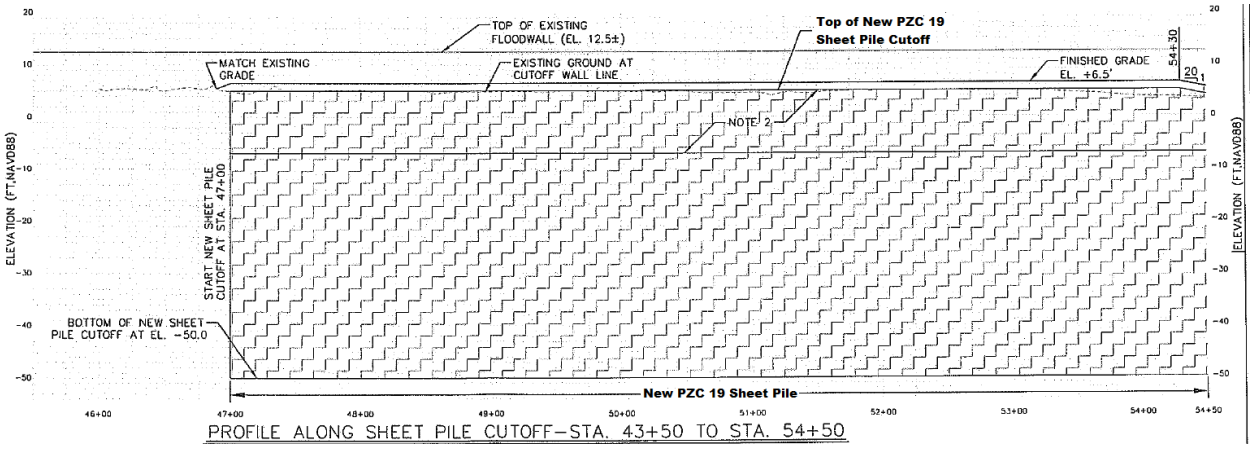


Fig. 7 Elevation View

SAMPLE Depth in Feet From	To	STRATUM Depth in Feet	VISUAL CLASSIFICATION	*Blows per Foot	Symbol Log	Scale (feet)
		.0				0
		.3	LIMESTONE & SAND (FILL) [GW]			
1.0	2.5			6		
2.5	4.0		LOOSE GRAY SILTY FINE SAND [SM]	7		5
			(W/ 3" ORGANIC CLAY LAYER @ 3')			
8.5	10.0			2		10
			(W/ CLAY LAYER @ 9.0'-9.5')			
		13.5				
13.5	15.0		DENSE GRAY FINE SAND [SP]	30 = .7'		15
		18.5				
18.5	20.0			30 = .5'		20
23.5	25.0			30 = .5'		25
			VERY DENSE			
28.5	30.0		GRAY FINE SAND [SP]	30 = .5'		30
33.5	35.0			30 = .5'		35
		38.5				
38.5	40.0		DENSE GRAY FINE SAND [SP]	30 = .7'		40
		43.5				
43.5	45.0		MEDIUM DENSE GRAY FINE SAND [SP]	17		45
		48.5				
48.5	50.0		SOFT GRAY CLAY W/ SAND POCKETS & LENSES [CH]	4		50
		53.5				
53.5	55.0		MEDIUM DENSE GRAY CLAYEY FINE SAND W/ CLAY LAYERS [SC]	29		55

PZC 19 Sheet Piles

Fig. 8 Soil Conditions



Fig. 9 Inner Harbor Canal beyond Starting Point

Figure 10 illustrates how a press-in piling machine typically operates with a water jetting system compatible with the equipment. A water source was required for the jetting operations to allow the water jetting system for the press-in piling machine to temporarily loosen up granular soils and soften cohesive soils. Typically, a water jetting system is used for silty or clayey sands that have an N-value between 25-50. Depending on the soil type, composition, and relative density, the utilization of various pressures with a high pressure water jet pump can be adjusted accordingly to achieve a smoother sheet pile installation.

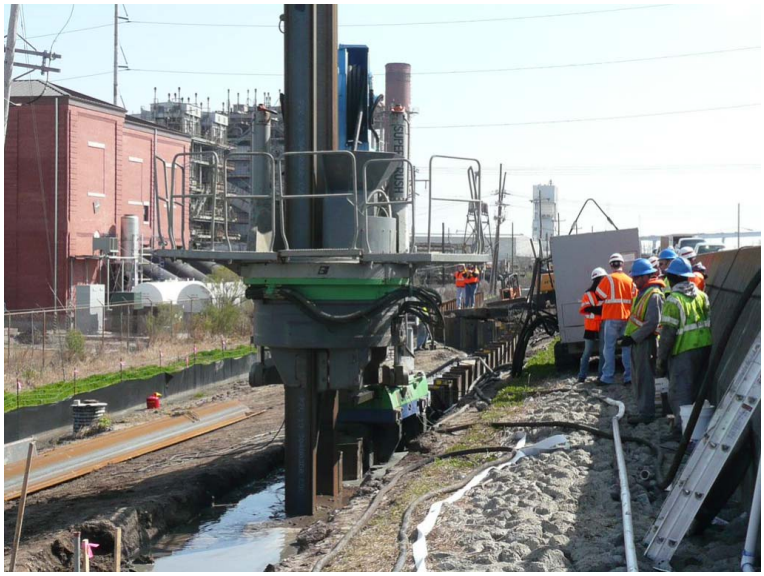


Fig. 10 Press-in Piling Machine with Water Jet

As much as 2,000 psi was used by the water jet system to break up the compacted soil on site with as many as 10,000 gallons of water was used per day for this project (Bergeron, 2010). Although water jetting was used with the aforementioned vibratory and impact hammers, that combination started to show shifting of the soil and some cracking near the railroad bed; which resulted in the Army Corps of Engineers suspending the construction until a better solution was found. Eventually the combination of the press-in piling method and water jetting would prove to be successful. According to Deborah Boyle, senior Army Corps of Engineers construction project manager, the press-in piling machine on this project had proven to be much faster than the other methods. Boyle added that sheet pile pairs for this project were being pressed in with the press-in machine every 8 to 11 minutes. Figure 11 shows an example of how a leveled top elevation and verticality of installed sheet piles are typically achieved with a press-in piling machine, even with a production of 8 to 11 minutes for every 55 ft. long sheet pile pair. At one point of the IHNC project the project was 17% ahead of schedule and was able to be completed by June 2010; thanks in part to the press-in method (Bergeron, 2010).

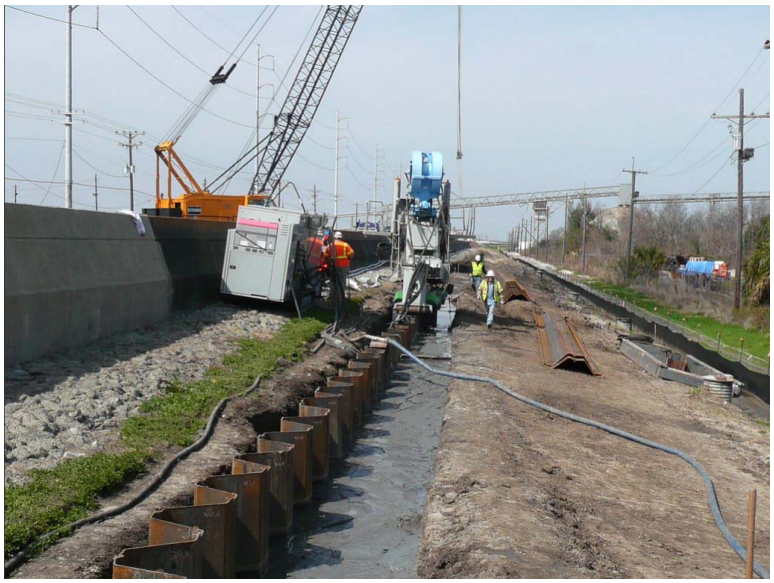


Fig. 11 Symmetrical Pile Line Achieved with a Press-in Machine

CONCLUSION

The success of this project was entirely dependent on executing the construction within somewhat limited space without damage from construction surcharge or unnecessary disruption to the existing concrete I-wall. The press-in piling system in combination with water jetting was the most feasible way this work could have been accomplished. This non-vibratory yet very effective system succeeded in pressing in long piles as was demonstrated in such difficult soil conditions. For the Inner Harbor Navigation Canal Emergency Interim Repair Reach II project, the press-in system was able to work with quicker production than the conventional methods previously used on and required little in preparation work and disruption outside its footprint next to an existing wall and nearby existing railways. Other SELA and HSDRRS projects in the New Orleans area also successfully adopted the press-in method through specification and even in several cases by a contractor's choice.

ACKNOWLEDGEMENTS

The authors acknowledge Shigeru Kambe of Blue Iron Foundations and Shoring, LLC and Jerry Whittle of Shavers-Whittle Construction, LLC for providing their insight as well as informative documents & images for this paper.

REFERENCES

Bergeron, Angelle, 2010. Banging and shaking get beat by 98 tons of quiet persuasion. ENR Magazine, March 22, pp. 14.

Takuma, Takefumi, 2015. Low noise and low vibration press-in piling method in soft soil in congested urban areas. Proceedings of the 3rd International Symposium of Deep Foundations, Mexico City, November 11-12, 2015

US Army Corps of Engineers Mississippi Valley Division, 2012. Facts and figures. January 11.

White, D., Finlay, T., Bolton, M., and Bearss, G. (2002), Press-in piling: ground vibration and noise during piling installation, ASCE Special Publication 116.

RD PILE WALL – A WATER TIGHT RETAINING WALL STRUCTURE

Antti J. Perala, SSAB Europe Oy, Hameenlinna, Finland, antti.perala@ssab.com
Teemu J. Yli-Kovero, SSAB Europe Oy, Hameenlinna, Finland, teemu.yli-kovero@ssab.com

ABSTRACT

Efficient use of land is constantly requiring more underground construction. Minimized execution time and disturbance to surroundings and nearby structures are essential benefits for all construction techniques. To meet the demands of a modern construction project, suppliers have to be able to provide high-quality and tailor-made products just on time. RD pile wall is a retaining wall based on drilled steel pipe piles which are connected to each other with special interlocking profiles. RD pile wall is a solution which enables penetration of overburden soil, dense fill layers including stones and boulders, and embedding into the bedrock in one single operation. Several test installations and laboratory tests have been made to develop the system and to test and improve the water tightness of the wall. Beside these tests, RD pile wall has also proven its reliability in almost 70 projects. Largest project so far has been Pasila Tripla project in Helsinki, Finland. A permanent retaining wall with surface area of 18,000 m^2 (193,750 ft^2), excavation depth of 21 m (68 ft) and over 17 m (56 ft) of water pressure was made with 711 mm (28") and 406.4 mm (16") pile sizes. Piles were delivered to site in one piece with lengths up to 33.5 m (110 ft).

INTRODUCTION

Excavations in cramped city centers and in between of existing buildings and other structures are facing more and more challenges. Installation of sheet pile walls is often problematic or even impossible due to obstacles in ground from old structures and due to demand to extend the excavations to even deeper and harder soil layers. Also installations of secant pile walls are facing difficulties due to cramped construction sites and constantly tightening execution times.

On the other hand, an efficient and reliable piling technique suitable for the demanding soil conditions described above, percussion drilling, has been developed since the 1960's, and especially from the mid-1990's, when the concentric drilling method with the ring bit and pilot was introduced. A new retaining wall application, the RD pile wall, was developed by combining that drilling method with the widely used retaining wall solution based on steel pipe piles and welded interlocks (a pipe pile wall normally installed with vibratory or impact hammers).

PRINCIPLE AND MAIN BENEFITS OF THE METHOD

RD pile walls can be used in all soil conditions. Most beneficial the system is in extremely demanding soil conditions where the installation of traditional retaining walls is challenging or even impossible. The RD pile wall is a combination of drilled steel pipe piles and interlocking sections as shown in Fig. 1.

Individual RD piles are connected to each other with interlocks welded to the piles on the automated welding line at the workshop. The matching dimensions of the drilling system and interlocking sections allow the installation of RD piles through stones and boulders and even into the bedrock, if necessary, in a single operation. Installation is done by a down-the-hole (DTH) hammer using the centric drilling system and oversized ring bits or a drilling system consisting of a pilot bit and reamer wings shown in Fig. 2.

 © 2017 DFI Annual Conference, New Orleans, LA, USA

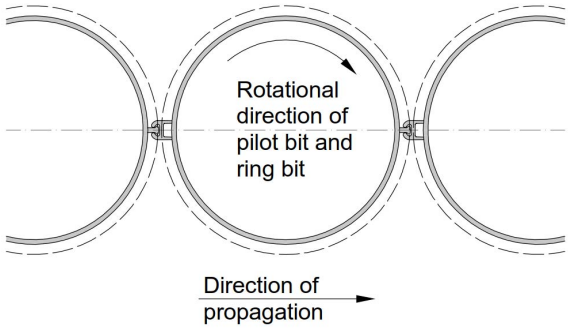


Fig. 1 Principle of pipe piles and interlocks (Uotinen and Jokiniemi 2012)



Fig. 2 Pilot bit with reamer wings

The RD pile wall can be implemented as a watertight construction using interlock sealants. Watertightness of the joint between the lower end of the wall and the underlying bedrock can be ensured by grouting through the injection channels located in the wider interlock section.

INTERLOCK PROFILES, WATERTIGHTNESS AND STIFFNESS OF PILE TOE

Interlock profiles used

Due to strict demands for watertightness in most of the projects, it was noticed that RD pile wall needs its own specially designed and shaped interlock profiles. The development led to introduction of RM/RF interlock profiles. RM is a narrow male profile and RF is a wide female profile. During installation the pile with RM profile is always installed first and RF profile is connected to RM profile during the installation of next pile. RM/RF interlock profiles are shown in Fig. 3.

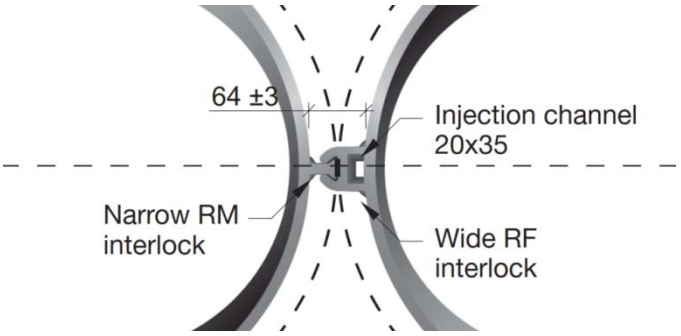


Fig. 3 RM/RF interlock profiles (SSAB 2016)

E21 interlocks can also be used in RD pile wall. Those are used only in special projects where RD pile wall is connected to a sheet pile wall. Typical connections between RD pile walls and sheet pile walls are shown in Fig. 4.

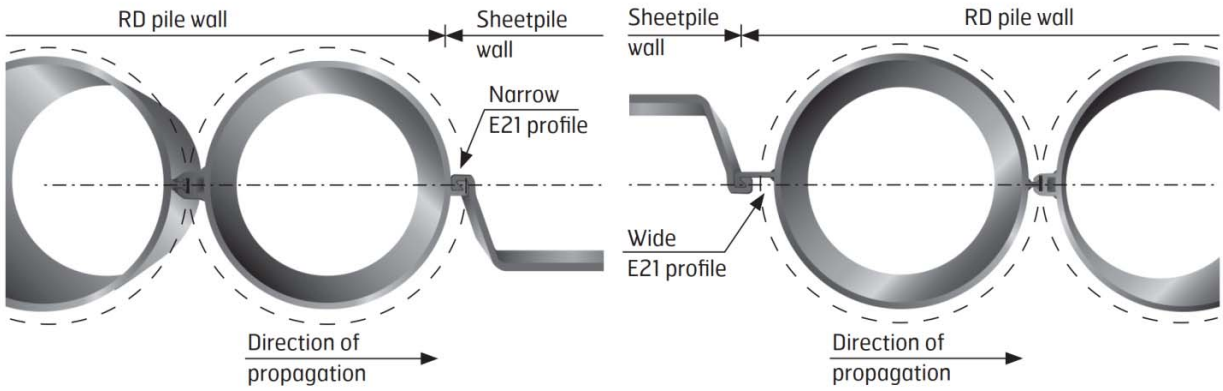


Fig. 4 Typical connections between RD pile walls and sheet pile walls (SSAB 2016)

RF profile has two "legs". Two legged profile forms an injection channel inside the interlock profile. This injection channel can be used to improve watertightness and stiffness of pile toe.

Mechanical resistance of interlocks

The load resistance of RM/RF interlocks has been tested in SSAB's Raahe Steel Works Testing Laboratory. To compare the results to "standard" interlock profiles, also E21 interlock profiles were tested. Automatic servo-hydraulic tensile test equipment shown in Fig. 5 was used. Data acquisition was done by using calibrated load cell and displacement sensor of the tensile test equipment. The ARAMIS optical measuring solution and the corresponding program was applied to measure and record the relative 2D strains of the interlock cross-section surface during tests. (Rantala 2014.)



Fig. 5 Automatic testing machine (MTS1200 kN) applied in interlock tests (Rantala 2014)

Test results show the resistances of the interlock profiles during installation (without corrosion). The resistance during service life depends on the amount of corrosion the interlocks are facing. The resistances of the interlock profiles during installation are given in Table 1.

Table 1. Structural resistances of E21 and RM/RF interlocks during installation

Interlock	Axial tensile resistance T_d (kN/m)	Axial compression resistance C_d (kN/m)	Shear resistance perpendicular to interlock cross-section $V_{y,d}$ (kN/m)
E21	1202	-	374
RM/RF	1702	4260	790

The effect of the corrosion on the tensile resistance of the RM/RF interlock was examined using 3D FEM model. First the interlock profile without corrosion was modeled and the model was verified against actual tensile test results. 3D model, corresponding mesh and Mises stress distribution of the interlock cross-section at the failure load are shown in Fig. 6.

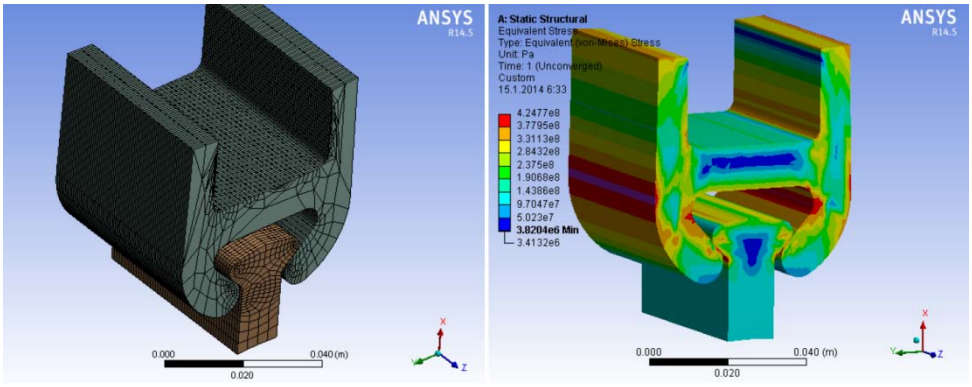


Fig. 6 3D model of RM/RF interlock, corresponding mesh and Mises stress distribution at the failure load (Rantala 2014)

Three different corrosion reduction cases were calculated: 1 mm (3/64") and 2 mm (5/64") reduction from the outer surfaces of the male and female interlock profiles (named as 1 mm and 2 mm in Fig. 7) and 2 mm (5/64") reduction from the outer surface with simultaneous 1 mm (3/64") reduction from the inner surfaces (cavities including the injection channel) of the RF profile (named as 2 mm + 1 mm in Fig. 7). Here the gap corrosion was not taken into account, i.e. the corrosion reduction was not made from the initial contact surfaces between the male and female interlock profiles. Figure 7 illustrates the load-displacement curves of the performed analysis and reference curve of the tensile test *t1* (named as Test (0 mm) in Fig. 7) and the reference analysis with no corrosion (0 mm in Fig. 7). (Rantala 2014)

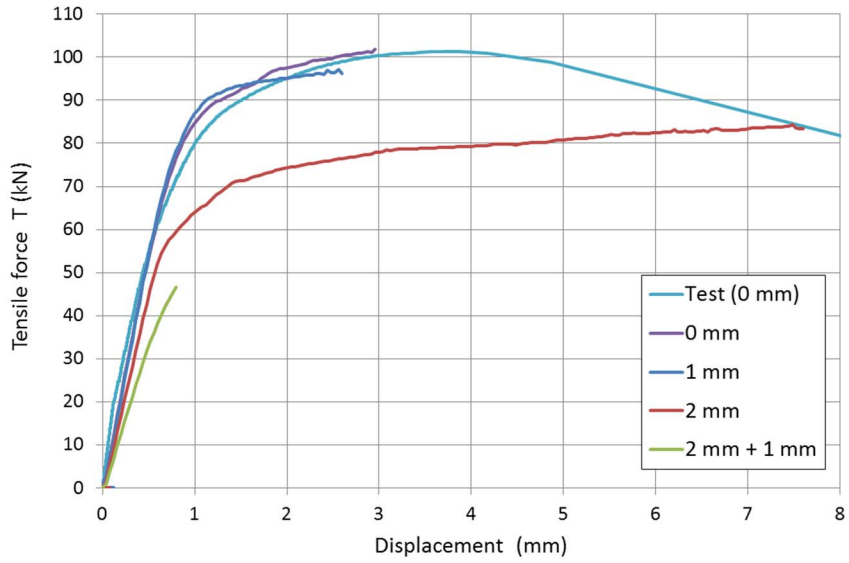


Fig. 7 Load-displacement curves of the tensile analysis performed for the RM/RF interlock with various corrosion reductions (Rantala 2014)

Based on these analyzes a table was made to show the reduction in resistances due to most often used corrosion reductions in interlocks. Table 2 shows the relative reductions in percent.

Table 2. Relative resistance reductions of RM/RF interlock due to corrosion (SSAB 2016)

Corrosion reduction on the outer surface of the interlock	Reduction in axial tensile resistance (%)	Reduction in axial compression resistance (%)
1.2 mm (3/64”)	5	20
2.0 mm (5/64”)	20	30

Watertightness of RM/RF interlock with different sealant materials

Watertightness of RM/RF interlocks has been tested in several test sessions at Tampere University of Technology. Tests have included water flow tests for empty (no sealant) interlocks, watertightness tests with different sealant materials and tests to find out the amount of sealant needed for sufficient watertightness.

Watertightness tests were done for 148 mm (3 1/32”) long RM/RF interlock sections which were welded to steel plates. Sealant material was applied between interlock sections and steel plates were connected to a compression chamber shown in Fig. 8. All seams of compression chamber without weld were sealed carefully using neoprene rubber. (Haavisto 2014b)

The watertightness tests were performed in steps increasing the hydrostatic pressure after each step. The amount of water leaking during each pressure step was recorded. (Haavisto 2014b.) Table 3 shows the water flow through an empty RM/RF interlock at different water pressures.

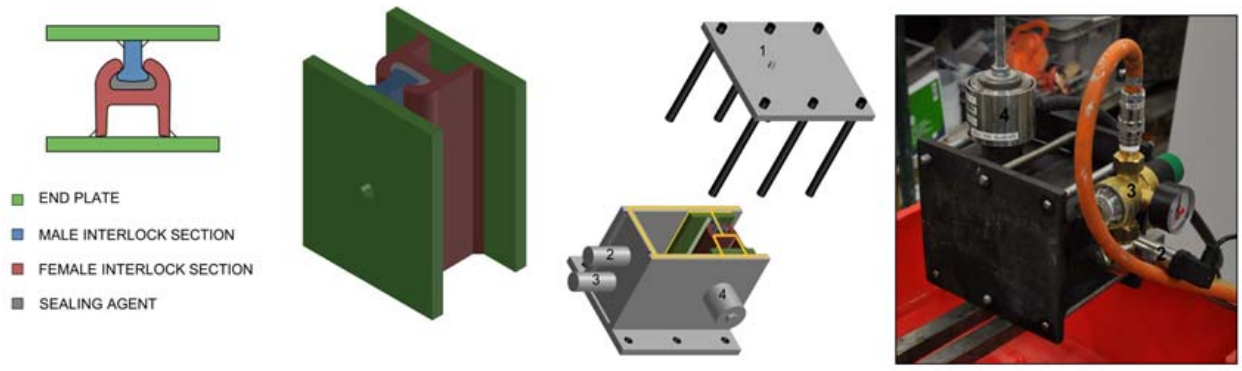


Fig. 8 Test arrangement of watertightness tests and test chamber (Haavisto 2014b)

Table 3. Water flow through an empty RM/RF interlock at different water pressures (SSAB 2016)

	Water flow through interlock [l/min] Water pressure [m]								
	1	2	3	4	5	6	7	8	9
Empty RM/RF interlock	50	100	150	200	250	300	350	400	450

The equipment used in first watertightness test could measure only pressures up to 150 kPa (21.8 psi), which equals to 15 m (49.2 ft) of water pressure. Some of the samples showed no leaking with this pressure. Therefore new testing equipment was acquired and some of the tests were made again with higher water pressure values. Table 4 shows the watertightness levels for interlocks with different sealant materials.

Table 4. Watertightness estimate of RM/RF interlock with different sealant materials (SSAB 2016)

Sealant material	Water pressure achieved in test [m]		
	Immediately after installation	1 day after installation	1 month after installation
Empty RM/RF interlock	0	0	0
Bitumen based sealant	60*	60*	60*
PU based sealant	0	15*	15*
Tar – Grease mix	0	0	0

*) The value is the maximum possible water pressure reached with the particular test equipment.

Amount of sealant material needed for watertightness

Watertightness of interlocks depends on the amount of sealant material in RF profile. The amount of sealant material needed to acquire required watertightness was also tested. Tests were made by verifying the thickness of sealant material at the bottom of the RF profile. Sealant thicknesses used in tests were 4 mm (5/32”), 7 mm (17/64”) and 10 mm (13/32”). Different sealant thicknesses and naming of the test

samples are shown in Fig. 9. These tests were made only for bitumen based sealant material. (Haavisto 2015.)

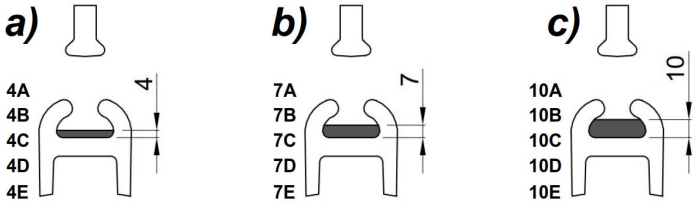


Fig. 9 Three different sealant thicknesses tested (Haavisto 2015)

Based on these tests the required amount of bitumen based sealant in the RF profile is 10 mm (13/32”). With smaller sealant thicknesses the water flow varied from significant to extremely high. Volumetric flow rate through the interlock with different sealant thicknesses is shown in Fig. 10.

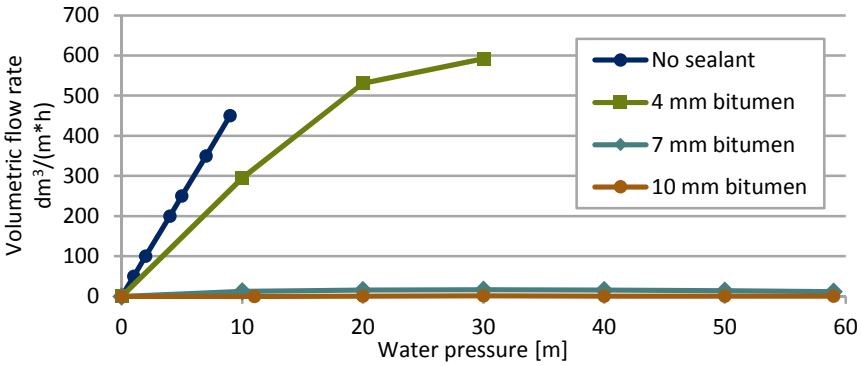


Fig. 10 Volumetric flow rate through RM/RF interlock on different water pressures and different sealant thicknesses

When fabricating the piles at the mill, the thickness of sealant cannot be controlled very accurately. Therefore RF profile is always almost full of sealant to ensure that amount of sealant is always adequate. An RF interlock filled with bitumen based sealant at the mill is presented in Fig. 11.

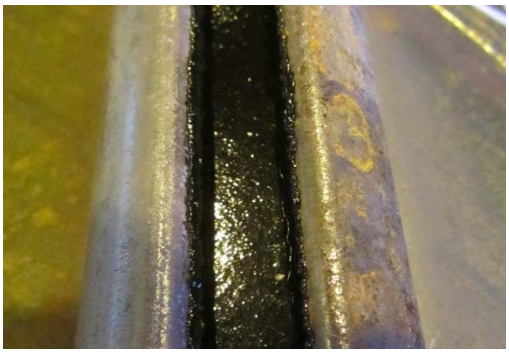


Fig. 11 RF profile filled with bitumen based sealant at the mill

Stiffness of RD pile wall in bedrock contact

The bending moment distribution in a retaining wall depends on the stiffness of the lower end of the wall. When connection between bedrock and wall at the lower end of the retaining wall is rigid, the moment

distribution in the wall is more economical and also the amount of support levels can be minimized. A series of installation, grouting and load tests were made by Miettinen (2013) to study the effect of drill depth and grouting to the stiffness.

In field tests drill depth into the bedrock and the grouting methods were varied. Piles were loaded laterally to see the stiffness of the connection between pile and the bedrock. Loading arrangement of a test pile is shown in Fig. 12.



Fig. 12 Loading arrangement of a test pile (Miettinen 2013)

Equal arrangement was also modeled with ANSYS 3D FEM program. 3D model and real load test results showed rather small differences (Miettinen 2013). 3D FEM was used to widen the test results for other pile sizes than the ones used in field tests. Based on these load tests and simulations, easy to use graphs were made for designers. Graphs can be used to evaluate the stiffness of pile toe in bedrock contact. The graphs are shown in Fig. 13. Graph on the left shows stiffness of non-grouted RD pile wall with drill depth of three times the diameter of the pile. Graph on the right shows stiffness of grouted RD pile wall with drill depths of three and four times the diameter of the pile.

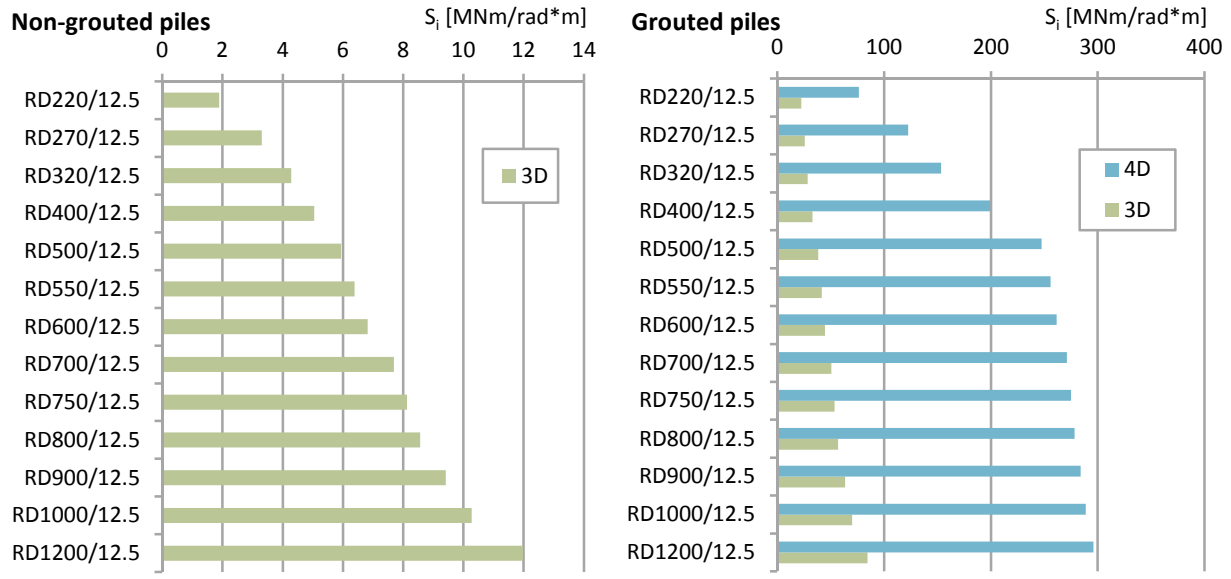


Fig. 13 Stiffness of RD pile wall. Non-grouted and grouted piles, drill depths 3D and 4D. Nominal strength of concrete grouting C20/25 (SSAB 2016)

CASE STUDIES

RD pile wall has been used in almost 100 projects so far. Most of the projects have been in Nordic countries, but RD pile walls have also been done in United Kingdom and in New Zealand.

Largest single project so far has been Pasila Tripla in Helsinki, Finland. The RD pile wall in Pasila Tripla consisted of totally 820 piles of which 760 pcs were RD700/14.2 (d = 28”, t = 9/16”) pile size and 60 pcs were RD400/12.5 (d = 16”, t = 1/2”) pile size. Total amount includes 4795 tons of steel and 35 km (21.7 mi) of interlocks. The steel grade of all the piles was S440J2H (Mara 2017). Northern RD pile wall of Pasila Tripla is shown in Fig. 15.

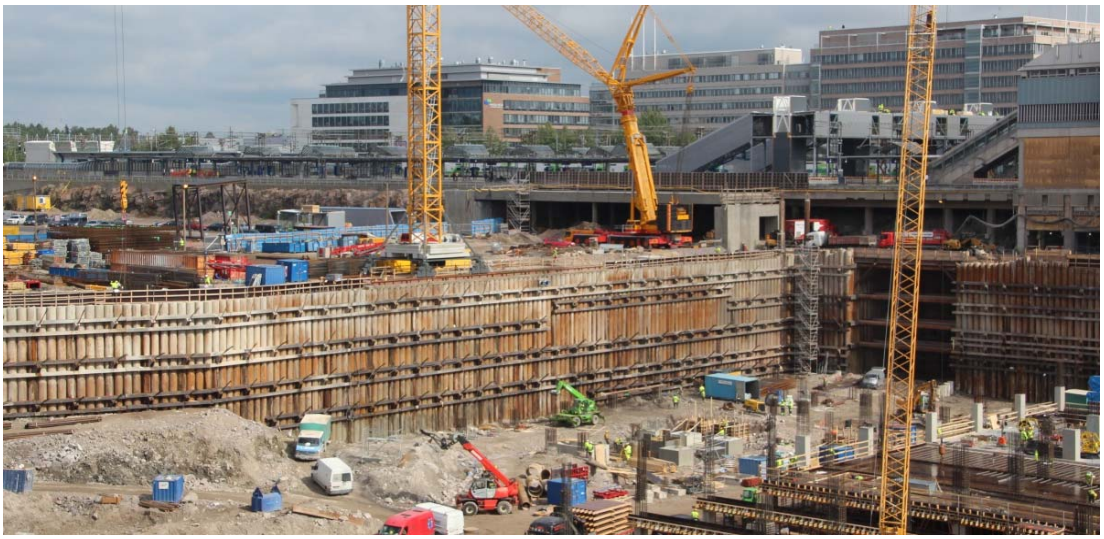


Fig. 15 Northern RD pile wall of Pasila Tripla (Mara 2017)

All RD700/14.2 piles were delivered to site in desired lengths without need for splice welding on site. The lengths of the piles were up to 33.5 m (110 ft). Up to 26 m (85 ft) long RD400/12.5 piles were drilled at limited space under an old railway bridge and those were delivered as 4 m (13 ft) long elements. Splicing was done by welding on site.

Bottom area of the Pasila Tripla excavation was about 23,000 m^2 (247,500 ft^2). Excavation depth was 21 m (69 ft) and the groundwater pressure behind RD pile wall was 17 m (55.8 ft). Water permeability requirement for the whole excavation was only 60 l/min (15.9 gal/min) (Tyynelä 2016). This requirement set high standards for the watertightness of the interlocks and for the pile toe. All the interlocks were filled with bitumen based sealant at the mill. Final watertightness was achieved with a steel plate welded in front of the interlocks (Tyynelä 2016). This was needed because of the service life of all structures in Pasila Tripla was set to 200 years. During excavation the interlocks showed no problems with watertightness. The watertightness of the bottom of the wall was more difficult to achieve, even though also curtain injection of the bedrock was used. The bedrock had some fracture zones and those needed extra care for grouting and injection.

CONCLUSIONS

Experiences from several projects and from tests have showed RD pile wall is a reliable solution for retaining wall in difficult soil conditions. Wide co-operation and sharing of information between the pipe pile manufacturer, manufacturers of the drilling system components, piling contractors and designers has

made successful development of the retaining wall solution possible. Drilling as an installation method enables penetration through hard and thick fill layers and also through possible obstacles in ground. Also the ability to install a retaining wall in to the bedrock and thus provide good lateral support for the lower end of the wall is a huge advantage of the system.

Installation of the RD pile wall is more expensive than that of ordinary sheet pile wall. In situations where embedding of a sheet pile wall is very difficult or even impossible, RD pile wall is at its best. This can also be seen from the projects where RD pile wall has been used. The installation speed is almost independent of soil conditions, which means that the installation time can be estimated quite accurately. The installation speed is many times that of a secant pile wall.

REFERENCES

Haavisto, J. 2014. Friction tests on Ruukki building products (infra) RM/RF interlock sections of RD pile wall. Research report No. TRT/2321/2014, August 13th 2014. Tampere University of Technology, Faculty of Business and Built Environment, Department of Civil Engineering, 25 p.

Haavisto, J. 2014. Water-tightness tests on RM/RF interlock of RD pile wall. Research report No. TRT/2327/2014, September 24th 2014. Tampere University of Technology, Faculty of Business and Built Environment, Department of Civil Engineering, 22 p.

Haavisto, J. 2015. Water-tightness tests on RM/RF interlocks of RD pile wall with different sealant thicknesses. Research report No. TRT/2373/2015, October 26th 2015. Tampere University of Technology, Faculty of Business and Built Environment, Department of Civil Engineering, 20 p.

Mara, J. 2017. Pasila Tripla, paalutoimittajan näkökulma. Presentation at Finnish Steel Pile Day, January 19th 2017, Helsinki. http://www.ssab.fi/tuotteet/terasluokat/infrastruktuuri/events/fi-steelpile-day-2017. 13 p. (in Finnish) Accessed 17-04-06.

Miettinen, L-V. 2013. The rotational stiffness and watertightness of RD pile walls in the bedrock and pile interface. Master of Science Thesis. Tampere University of Technology, Faculty of Business and Built Environment, Department of Civil Engineering, 104 p.

Rantala, J. 2014. Load resistance of the RM-RF and E21 -interlocks. Test report and analysis, March 13th 2014. Ruukki Construction Oy, Building Products, Infra, 25 p.

RD pile wall, Design and Installation Manual, 2016. https://www.ssab.com/products/steel-categories/infrastructure/infrastructure-downloads. SSAB, 36 p. Accessed 17-04-06.

Tyynelä, P. 2016. Case Tripla suunnittelijan näkökulmasta. Presentation at Finnish Steel Pile Day, January 21st 2016, Helsinki. http://www.ssab.fi/tuotteet/terasluokat/infrastruktuuri/events/fi-steelpile-day-2016. 8 p. (in Finnish) Accessed 17-04-06.

Uotinen, V-M. and Jokiniemi, H. 2012. RD pile wall – A new way to build micropile retaining wall structures. Proceedings of the 11th International Workshop on Micropiles, Milan October 3-6, International Society for Micropiles, 13 p.

A FIELD STUDY TO ANALYZE PILE SETUP BEHAVIOR AND COMPARISON OF PILE CAPACITY METHODS FROM CPT

Md. Nafiul Haque, Ph.D., Murad Y. Abu-Farsakh, Ph.D., P.E., and Chris Nickel, P.E.

[1]Postdoctoral Researcher, Louisiana Transportation Research Center, Baton Rouge, LA 70808.

[2]Research Professor, Louisiana Transportation Research Center, Louisiana State University, Baton Rouge, LA 70808. (Corresponding Author; Email: cefars@lsu.edu and Phone: 225-767-9147)

[3]Geotechnical Engineering Manager, Department of Transportation and Development, Baton Rouge, LA. 70804.

ABSTRACT

This paper presents the results from a pile load testing program for a bridge construction project in Louisiana. The testing includes two 54-inch open-ended spun cast concrete cylinder piles (OECP), one 30-inch open-ended steel pile (OESP), and two (30-inch and 16-inch) square prestressed concrete (PSC) piles driven at two locations with very similar soil conditions. All the test piles were instrumented with vibrating wire strain gauges to measure the load distribution along the length of the test piles and the skin friction and the end bearing were derived from strain gauge measurements. High strain dynamic load tests (HSDLT) were performed on all test piles at different times after pile installations to quantify the amount of setup with time. Static load tests were also performed on the PSC and open-ended steel piles. Due to expected large pile capacities, the statnamic test method was used on the two open-ended cylinder piles. The pile capacities of these piles were evaluated using various CPT methods (such as Schmertmann, De Ruiter and Beringen, LCPC, COFS methods). The result showed that all the methods can estimate the skin friction with good accuracy; but not the end-bearing capacity. Setup was observed for all the piles, which was mainly attributed to increase in skin frictions. The setup rate parameters "A" [The "A" parameter is defined as the rate of increase of pile capacity ratio (R_t/R_{to}) per log cycle of elapsed time] were back-calculated for all the test piles and the values were between 0.31 and 0.41.

KEYWORDS: Large diameter cylinder pile, PSC pile, Pipe pile, open ended pile, Statnamic load test, High strain dynamic load test, CAPWAP, Pile setup.

INTRODUCTION

Due to greater efficiency (capacity to weight ratio) of the pipe piles, open-ended piles are a viable option to solid piles. However, the behavior of open-ended piles is more complicated compared to the close-ended piles owing to possible formation of "soil plug" inside the open-ended pile. Many researchers have analyzed the behavior of both types of piles for different purposes; however, very few studies in the literature offer the side-by-side comparison of the close-ended and open-ended piles.

It is well-known that the behavior of open-ended pile is different than that of close-ended pile. The field studies showed that the blow count necessary for driving an open-ended pile to certain depth

 © 2017 DFI Annual Conference, New Orleans, LA, USA

is generally lower than the close-ended pile for same size of pile and under similar driving condition (i.e., similar hammer type). Thus, it is normally acknowledge that an open-ended pile requires less installation effort than a close-ended pile under the same soil properties. However, this might be different under plugging condition. Open-ended piles usually exhibit more settlement compared to the close-ended piles under a specific load during performing the static load test. The inference is that the capacity of open-ended piles is typically lower than that of close-ended piles based on load settlement criterions. Of cause, the difference in load capacities varies depending on the degree of soil plugging during driving and post driving and also on the relationship between shaft friction and end bearing. If the shaft friction contributes much more than the end bearing the picture is completely different.

CPT-Based Design Methods

The cone penetrometer is an in-situ testing device that has been used since the 1930s for site characterization and the evaluation of different soil properties. Due to similarity between the cone and pile, the cone can be considered as a simple model pile. Several methods have been proposed to estimate the axial pile capacity utilizing the Cone Penetration Test (CPT) and Piezocone Penetration Test (PCPT) data (e.g., Schmertmann, 1978; De Ruiter and Beringen, 1979; Bustamante and Gianselli, 1982; Lehane et al. 2013). A number of investigators (e.g., Abu-Farsakh and Titi, 2004) have studied and compared the predicted pile capacities from the different CPT methods with the measured pile capacities using static or high strain dynamic load tests.

Pile Setup

It is well-known that the axial capacity of piles usually increases with time after driving in cohesive soils. This increase in pile capacity with time is known as "setup" or "freeze" (Bullock et al. 2005; Fellenius, 2008). It has been well recognized that the magnitude of setup is dependent upon pile size, pile lengths, pile material, soil type, soil strength and consolidation properties, and stress history of the soils, among other factors.

Several empirical models (e. g, Skov and Denver, 1988) have been proposed to estimate the pile capacity change with time. Of these, the model developed by Skov and Denver (1988) is considered the most popular one due to its simplicity and reliability. They proposed the following model:

$$\frac{R_t}{R_o} - 1 = A \log_{10} \frac{t}{t_o} \quad \ldots (1)$$

where: R_t = Total pile capacity at time, t, R_o = Total pile capacity at initial time, t_o, t = Time elapsed since end of initial pile driving, t_o = A reference time before which the capacity cannot be reliably predicted, and A = Setup rate parameter.

OBJECTIVE AND SCOPE

This case study in this paper includes analyzing the behavior (during driving and following load tests) of two 54-inch open-ended cylinder piles (OECP), one 30-inch steel pipe (OESP) pile and two PSC piles that were installed side by side in the same soil condition. High strain dynamic load tests were performed in accordance with ASTM 4945 in order to evaluate the amount of "setup". Either static (SLT) or statnamic load test (SNLT) were performed on the test piles. The load distribution was evaluated with the aid of strain gauges. Finally, the load distribution was compared with the skin friction predicted using different pile capacity design methods based on

CPT data. It is important to note that the purpose of this paper is to present the valuable results and observations that were gleaned during performing this full scale load testing program on different types of piles.

TEST SITE AND SUBSURFACE GEOTECHNICAL CONDITION

Project Description

The Louisiana Department of Transportation and Development (LADOTD) constructed an elevated highway between Golden Meadow and Port Fourchon to replace the previously existing LA-1 highway. A pre-design pile load testing program consisting of testing various sizes and types of piles along the project alignment was performed. Nine test piles were driven at four different locations in this project. These test piles consisted of six different sizes of PSC piles, two 1.37-m (54-in) open-ended spun cast cylinder piles and one 0.76-m (30-in) open-ended steel pipe pile. The open-ended steel and cylinder piles were located at the TP-2 and TP-3 locations along the LA-1. This study focuses on the comparison of open-ended piles to that of PSC piles. Table 1 presents the details of these test piles (i.e., length, width of the test piles, casing information and hammer information).

Table 1: Test pile information

Pile ID	Pile Type	Width	Length			No of Strain Gauges Pairs	Hammer Type
			Total	Embedment	Above G.L.		
		m (inch)	m (feet)	m (feet)	m (feet)		
TP-2a	PSC	0.41 (16)	39.6 (130)	36.6 (120)	3.0 (10)	7	Vulcan 010
TP-2b	OECP	1.37 (54)	48.8 (160)	44.5 (146)	4.3 (14)	5	Vulcan 040
TP-3a	PSC	0.76 (30)	57.9 (190)	54.9 (180)	3.0 (10)	8	Vulcan 020
TP-3b	OESP	0.76 (30)	59.4 (195)	56.4 (185)	3.0 (10)	9	Vulcan 020
TP-3c	OECP	1.37 (54)	48.8 (160)	44.5 (146)	4.3 (14)	4	Vulcan 040
G.L. Ground level							

Subsurface Geotechnical Condition

Extensive laboratory and in-situ testing programs were performed to characterize the subsurface soil conditions at the test pile locations. Shelby tube samples (7.6-cm, 3-in. diameter) were taken in cohesive soils and standard penetration tests were performed in the sandy soils. In addition to the borehole data, one piezocone penetration test (PCPT) was conducted close to the pile at each test locations. The soil stratification from soil boring, results of laboratory tests and profiles of cone tip resistance (q_c) from CPT tests is depicted in Figure 1 for TP-2 location.

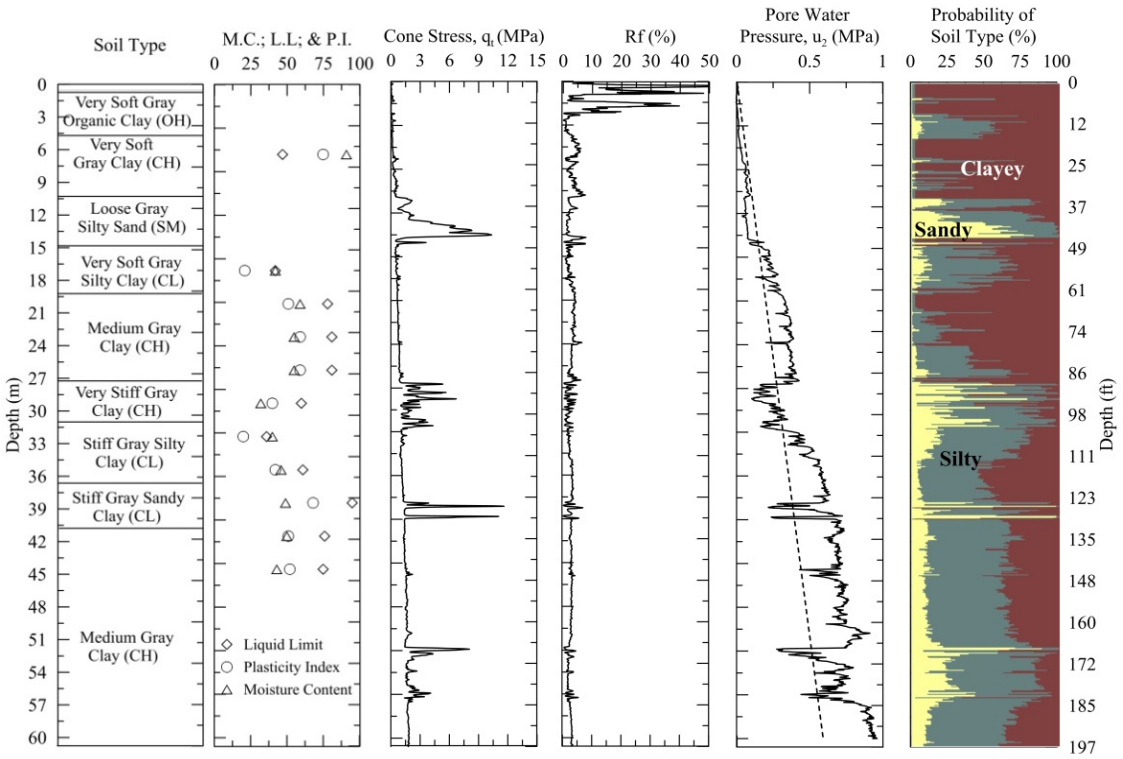


Figure 1: Soil profile and CPT soil classification at TP-2 location

LOAD TESTING PROGRAM

The purposes of pile load tests were to confirm the pile capacity, study the pile setup behavior, and assess drivability. Using multiple SLTs or SNLTs to measure the capacities was determined to be too costly. It was decided that multiple restrikes and one SLT or SNLT would be used to study the setup behavior. The test schedules for conducting SLT, SNLT and HSDLTs for TPs at TP-2 location are presented in Table 2. The other load test results can be found at Abu-Farsakh et al (2016). HSDLTS at different time intervals were performed in order to evaluate the setup behavior. Research has shown that blow counts during HSDLT in excess of 120 blows/0.3m may not cause enough displacement to fully mobilize the pile capacity for PSC pile (Rausche et al. 1985; Fellenius et al. 1989). In this study, all the pile capacity for PSC pile has been mobilized during the load tests which assisted to perform the study (Table 2a). Moreover, there should be sufficient time lag in between the load test to fully regain the pile capacity in order to measure the true pile setup; otherwise, there is a high potential some skin friction might be lost due to performing repeated load testing on same pile. Hence, sufficient time lags had been left during performing the load tests in this study or the clock was restarted during performing each load test (Tables 2a and 2b). HSDLTs calculate the total capacity of pile and distribute the skin friction along the length of the pile during the testing. End-bearing capacity is usually calculated by subtracting the skin friction from the total capacity. The literature shows that the end-bearing capacity usually doesn't change over the time and remains constant during the testing period. However, during the testing period, small amount of discrepancy were observed in end-bearing capacity within the allowable limit. Moreover, the SLT over-estimated the end-bearing capacity by a small amount. In order to analyze the setup accurately, the average value of end-bearing capacity during the initial HSDLT

and SLT was calculated and was used as a constant value during all the HSDLTs. This aided the authors to analyze the skin-friction setup accurately.

Table 2a: Load test results for 16 inch PSC pile at TP-2 location

Events	Time	Skin Friction, R_s		End-bearing Capacity, R_{tip}			Total Capacity, R_t		Set Per Blow
				Meas.	Aver.*				
	Hours	kN (kips)	Ratio (R_s/R_{so})	kN (kips)	kN (kips)	Ratio (R_{tip}/R_{tipo})	kN (kips)	Ratio (R_t/R_{to})	cm (inch)
EOD	-	253 (57)	1.0	153 (34)	137 (31)	1.0	390 (87)	1.0	-
1st HSDLT	2.2	695 (156)	2.7	219 (49)	137 (31)	1.0	832 (187)	2.1	1.3 (0.5)
2nd HSDLT	3.9	921 (207)	3.6	144 (32)	137 (31)	1.0	1058 (237)	2.7	0.6 (0.2)
3rd HSDLT	6.0	1101 (247)	4.4	161 (36)	137 (31)	1.0	1238 (278)	3.2	0.3 (0.1)
4th HSDLT	21.6	1302 (293)	5.1	186 (42)	137 (31)	1.0	1439 (324)	3.7	0.3 (0.1)
5th HSDLT	56.0	1366 (307)	5.4	186 (42)	137 (31)	1.0	1503 (338)	3.9	0.3 (0.1)
6th HSDLT	76.9	1573 (353)	6.2	167 (37)	137 (31)	1.0	1710 (384)	4.4	0.3 (0.1)
7th HSDLT	96.9	1659 (373)	6.6	181 (41)	137 (31)	1.0	1796 (404)	4.6	0.0
Static Test	168.0	1762 (396)	7.0	120 (27)	137 (31)	1.0	1899 (427)	4.9	-

*Aver. = Average of EOD and Static Test

Table 2b: Load test results for 54 inch open-ended cylinder piles at TP-2 location

Events	Time	Skin Friction, R_s		End-bearing Capacity, R_{tip}			Total Capacity, R_t		Set Per Blow
				Meas.	Aver.*				
	Hours	kN (kips)	Ratio (R_s/R_{so})	kN (kips	kN (kips)	Ratio (R_{tip}/R_{tipo})	kN (kips)	Ratio (R_t/R_{to})	cm (inch)
EOD	-	1078 (242)	1.0	566 (127)	497 (112)	1.0	1575 (354)	1.0	-
1st HSDLT	2.0	2294 (515)	2.1	695 (156)	497 (112)	1.0	2791 (627)	1.8	0.2 (0.1)
2nd HSDLT	5.0	3330 (749)	3.1	617 (139)	497 (112)	1.0	3827 (861)	2.4	0.05 (0.02)
3rd HSDLT	23.0	4033 (906)	3.7	651 (146)	497 (112)	1.0	4530 (1018)	2.9	0.03 (0.01)
4th HSDLT	46.0	4784 (1075)	4.4	632 (142)	497 (112)	1.0	5281 (1187)	3.4	0.04 (0.01)
5th HSDLT	70.0	4993 (1122)	4.6	659 (148)	497 (112)	1.0	5490 (1234)	3.5	0.0
6th HSDLT	93.0	5194 (1167)	4.8	534 (120)	497 (112)	1.0	5691 (1279)	3.6	0.04 (0.01)
SNLT	168.0	5263 (1183)	4.9	427 (96)	497 (112)	1.0	5760 (1295)	3.7	

*Aver. = Average of EOD and SNLT

RESULTS

Pile Capacity from CPT Data

Several methods are available in the literature to predict the axial pile capacity utilizing the CPT data. Four direct CPT methods for estimating the pile capacity are considered here in this study. These methods are: Schmertmann method (1978), De Ruiter and Beringen method (1979) and LCPC method (1982), Lehane et al. (2013) method. The method developed by Lehane et al. (2013) is well suited to predict the pile capacity for open-ended pile and it is used in this study to predict the skin friction of open-ended pile only.

Table 3 compares measured versus predicted capacities of skin friction, end-bearing and total capacity for all the test piles. Three different methods [i.e., Schmertmann (1978), De Ruiter and

Beringen (1979) and LCPC (1982)] are used here to predict the capacity using the CPT data for all test piles. Lehane et al. (2013) method is used to predict the only skin friction of open-ended pile. The authors used the previously developed LPD-CPT software to predict the pile capacity for all types of piles for Schmertmann method (1978), De Ruiter and Beringen method (1979) and LCPC method (1982). The static, statnamaic and high strain dynamic load tests were used to measure the capacities. However, the tests were not conducted at the same time, which affected the comparison with the predicted capacities. The HSDLT results presented here are performed before conducting the SLT or SNLT (i.e., the last restrike). The distributions of the skin frictions along the length of the piles for both the predicted and measured capacities are depicted in Figure 2. Figures 2a, 2b, 2c, 2d and 2e present the comparison of skin frictions for predicted and measured capacities of TP-2a, 2b, 3a, 3b and 3c, respectively.

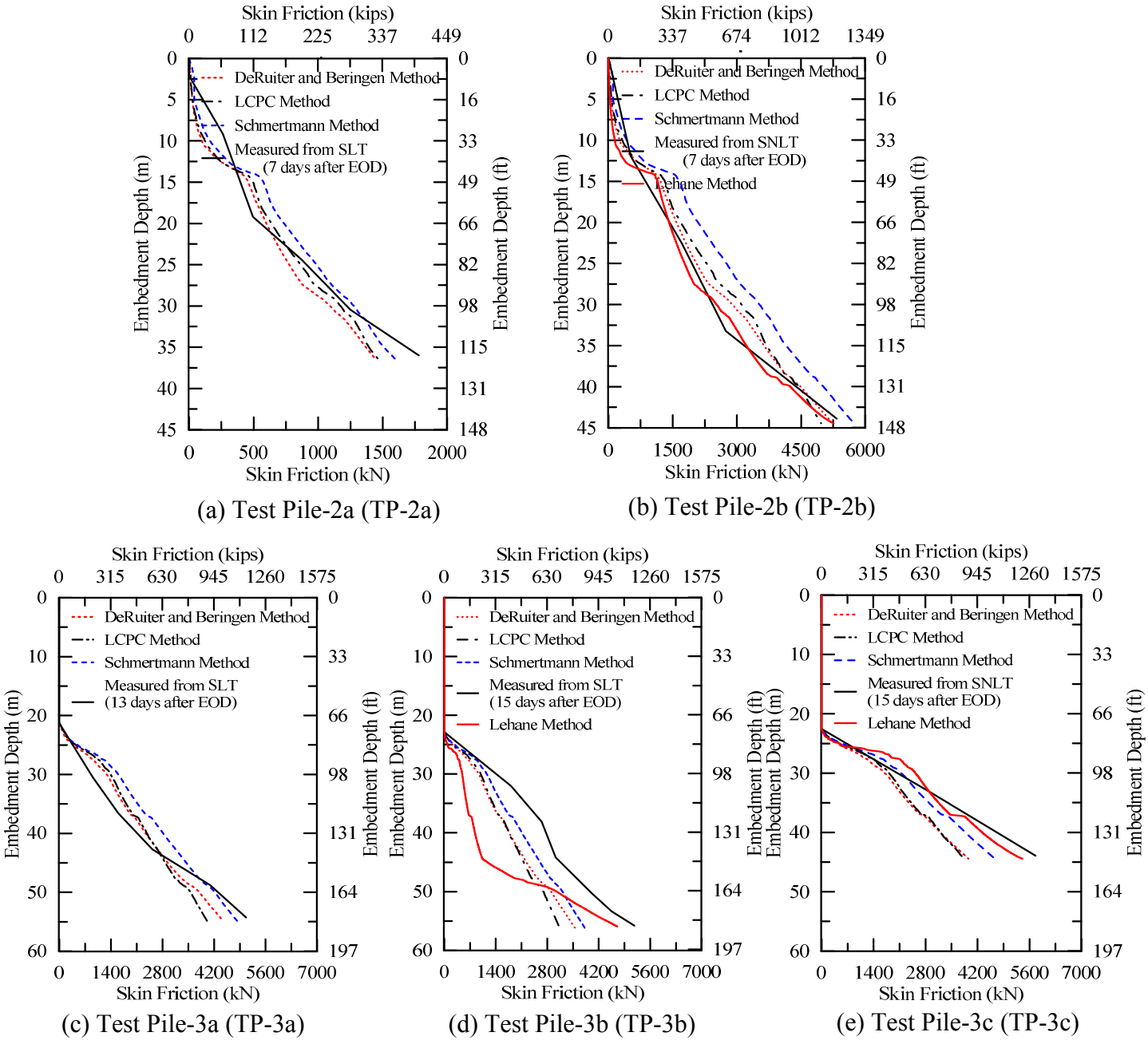
Table 3: Comparison of measured versus predicted results using different CPT methods

Pile No/Type	Res. kN (kips)	Predicted Capacity by Available Methods, kN (kips)				Measured Capacity, kN (kips)	
		Schmertmann (1978)	De Ruiter and Beringen (1979)	Bustamante and Gianeselli, LCPC Method (1982)	Lehane et al. (2013)	Dynamic Load Tests**	Static/ Statnamic Load Tests
TP-2a/ PSC	Skin friction	1603 (360)	1450 (326)	1471 (331)	-	1615 (363)	1779 (400)
	End-bearing	208 (47)	93 (21)	131 (29)	-	181 (41)	120 (27)
	Total	1811 (407)	1543 (347)	1602 (360)	-	1796 (404)	1899 (427)
TP-2b/ OECP*	Skin friction	5731 (1288)	5313 (1194)	4965 (1116)	5258 (1182)	5157	5333 (1199)
	End-bearing	2316 (521)	1618 (363)	1494 (336)	-	534 (120)	427 (96)
	Total	8050 (1809)	6931 (1557)	6459 (1452)	-	5691	5760 (1295)
TP-3a/ PSC	Skin friction	4826 (1085)	4448 (1000)	4010 (901)	-	3673 (826)	5067 (1139)
	End-bearing	962 (216)	540 (121)	622 (140)	-	1469 (330)	2318 (521)
	Total	5788 (1301)	4988 (1121)	4632 (1041)	-	5142	7385 (1660)
TP-3b /OESP	Skin friction	3838 (863)	3572 (803)	3149 (708)	4705 (1058)	3988 (896)	5173 (1163)
	End-bearing	764 (171)	430 (97)	477 (107)	-	534 (120)	1931 (434)
	Total	4602 (1034)	4002 (900)	3626 (815)	-	4522	7104 (1597)
TP-3c /OECP*	Skin friction	4665 (1049)	3956 (889)	3847 (865)	5412 (1217)	4800	5760 (1295)
	End-bearing	2121 (477)	954 (214)	1452 (326)	-	900 (202)	445 (100)
	Total	6786 (1525)	4910 (1103)	5299 (1191)	-	5700	6205 (1395)

It is observed that all the Pile-CPT predicted methods of all the test piles can estimate the capacity with good accuracy. Schmertmann (1978) method is the best suited among all the three different predicted methods to predict the total and skin friction capacity for the PSC piles in this study. The result showed that for the PSC piles (i.e., TP-2a and TP-3a), all the predicted methods underestimated the capacity measured by the SLT. The total predicted capacity by Schmertmann (1978) method for TP-2a and TP-3a underestimated the total capacity of SLT by 5% and 27%, respectively. The authors believe the large difference between the predicted and measured capacity for TP-3a is due to the setup factor. The SLT conducted at TP-2a location 7 days after EOD, whereas the SLT conducted for TP-3a at 13 days after EOD. This time difference at TP-3a location assisted to increase in capacity.

The results show that for the open-ended cylinder pile at TP-2 location (i.e., TP-2b), the skin friction predicted by pile-CPT methods is much closer to the skin friction measured by the SNLT.

For TP-2b, the Schmertmann (1978) method overpredicted the skin friction by 7% and the LCPC method underestimated the skin friction by 8%. However, at TP-3 location, the Schmertmann (1978), De Ruiter and Beringen (1979) and LCPC (1982) methods largely underestimated the measured skin friction for both open-ended piles. The skin friction for TP-3b during the SLT was underestimated by 34%, 45% and 64% using the Schmertmann (1978), De Ruiter and Beringen (1979) and LCPC (1982) methods, respectively. Similar to the pile TP-3b, the skin friction was underestimated by 24%, 46% and 50% using the Schmertmann (1978), De Ruiter and Beringen (1979) and LCPC (1982) methods, respectively for the pile TP-3c during the SNLT. As mentioned earlier, the methods proposed by Lehane et al. (2013) is the best suited for open-ended pile to predict the skin friction. The method developed by Lehane et al (2013) under predicted the capacity for pipe pile which may be due to the material for pipe pile (Figure 2d); however, it predicted the capacity for spun cast cylinder pile with good accuracy (Figures 2b and 2e). The predicted skin friction was underestimated by only 1%, 9%, and 6% using the Lehane et al. (2013) method for TP-2b, TP-3b and TP-3c, respectively.



(a) Test Pile-2a (TP-2a)

(b) Test Pile-2b (TP-2b)

(c) Test Pile-3a (TP-3a)

(d) Test Pile-3b (TP-3b)

(e) Test Pile-3c (TP-3c)

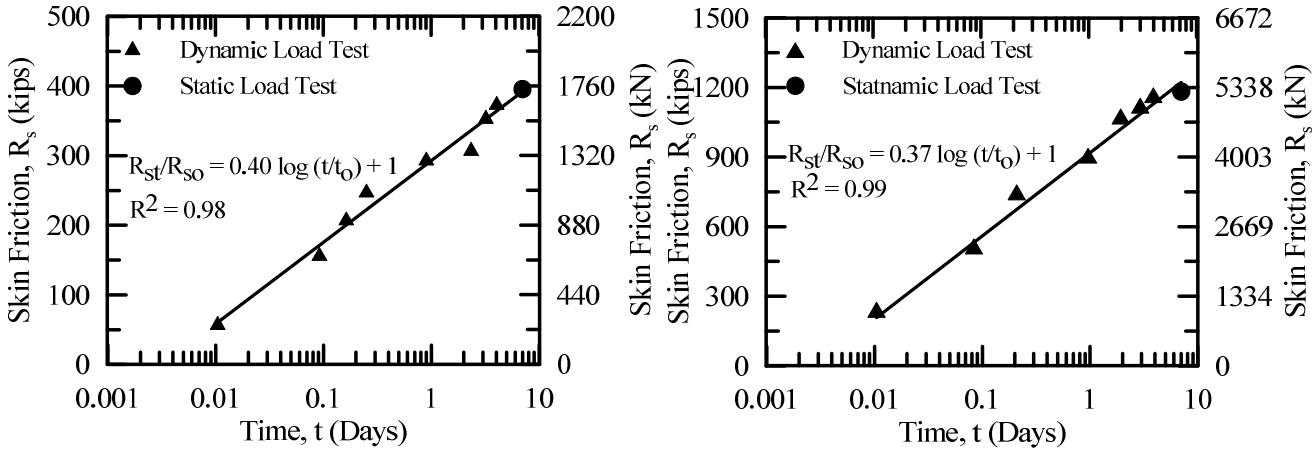
Figure 2: Comparison of skin friction obtained from different CPT methods

Setup Behavior

The skin frictions (R_s) recorded during the final load test were 7.5, 5.3, 3.0, 5.7 and 7.1 times higher compared to the EOD skin frictions for TP-2a, TP-2b, TP-3a, TP-3b and TP-3c, respectively (Table 2). However, with the exception of TP-3b during SLT (i.e., open-ended steel pile), the end-bearing capacity for all piles was almost constant during the whole testing program. As stated earlier, the formation of "soil plug" during the SLT for this open-ended steel pile may contribute to the increase in end-bearing capacity. The test results demonstrated that the setup behavior is mainly attributed to increase in skin friction. Figures 3a, 3b, 3c, 3d and 3e present the measured

skin friction versus elapsed time for TP-2a, TP-2b, TP-3a, TP-3b and TP-3c, respectively. As shown in the figures, the pile skin friction was best fitted to a linear logarithmic time scale with a coefficient of correlation (R^2) of 0.98, 0.90, 0.86, 0.83 and 0.97 for TP-2a, TP-2b, TP-3a, TP-3b and TP-3c, respectively. It has to be mentioned here that the skin friction presented here were adjusted after modifying the end-bearing capacity which was assumed constant throughout the testing period. This suggests a linear logarithmic time relationship do exist for setup of all test piles, as suggested by other researchers (e.g., Skov and Denver, 1988; Bullock et al. 2005; Ng et al. 2013).

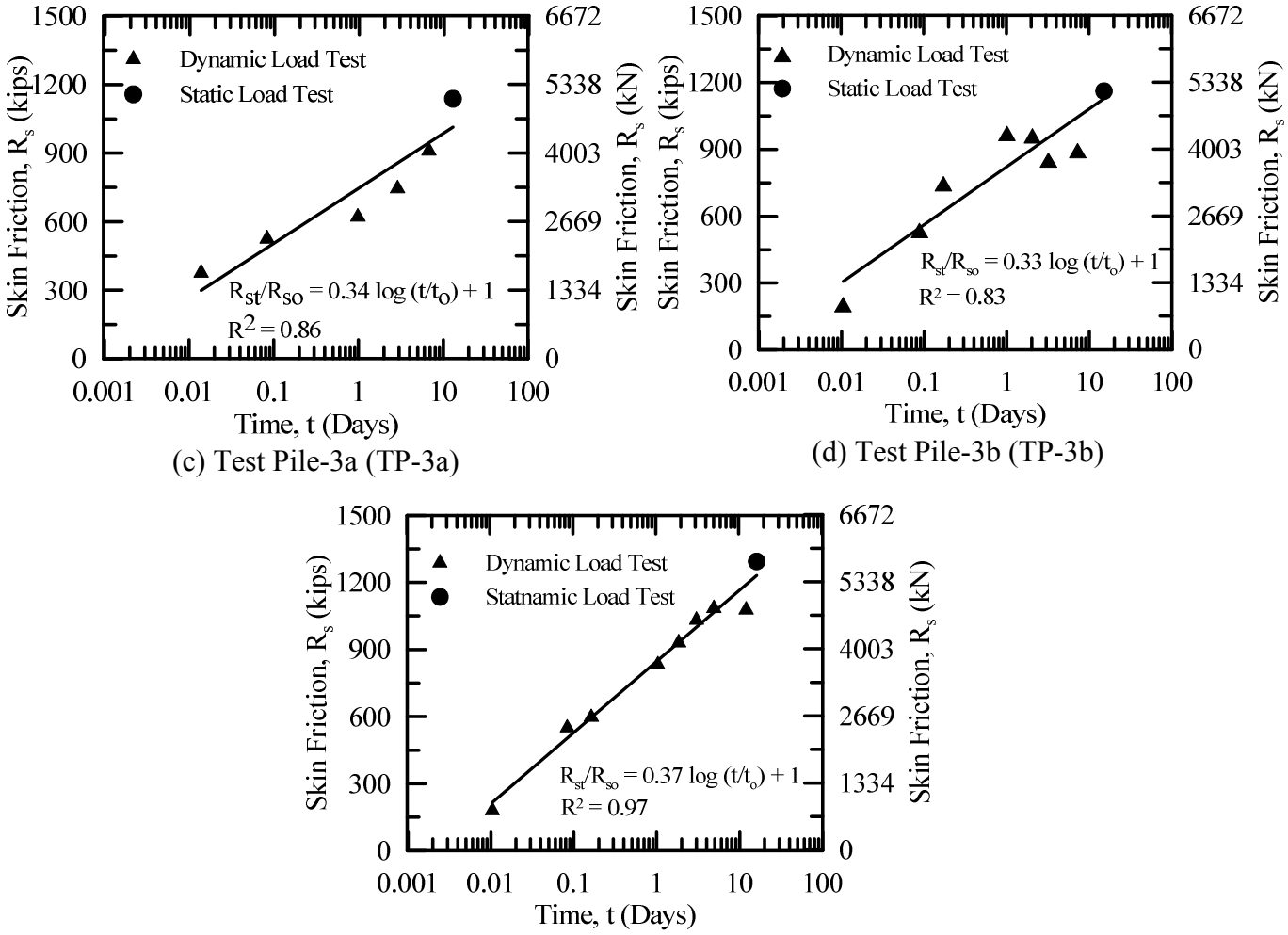
It can be observed from Figure 3 that the setup rate parameters "A" are very close for the test piles at TP-2 location (0.41 and 0.39 for TP-2a and TP-2b, respectively). The results of HSDLTs and the SLT for TP-3a as a function of time were best fitted to a logarithmic time scale suggesting a linear logarithmic trend exists like the results of other test piles as shown in Figure 3c. The "A" factor for TP-3a is 0.33 which is also very close to the observed "A" values of TP-3b (0.31) and TP-3c (0.36). Since the setup of the PSC piles (TP-2a and TP-3a) are mainly due to outside friction and the setup rate "A" of the PSC piles and open-ended pipe and cylinder piles (TP-2b, TP-3b and TP-3c) are close, the reader can postulate that no significant amount of setup was observed due to inside friction for the open-ended pipe and cylinder piles. Therefore, we can conclude that setup was mainly due to the outside friction between the pile surface and surrounding soil.



(a) Test Pile-2a (TP-2a)

(b) Test Pile-2b (TP-2b)

Figure 3: Skin friction setup for type of piles (continued)



(c) Test Pile-3a (TP-3a)

(d) Test Pile-3b (TP-3b)

(e) Test Pile-3b (TP-3b)

Figure 3: Skin friction setup for type of piles.

SUMMARY AND CONCLUSIONS

Based on the observations from this study, the following conclusions can be drawn:

- Pile capacities were predicted using different CPT methods. The predicted capacities using CPT methods were underestimated compared to the EOD pile capacities. However, the results showed that all the methods can estimate the skin friction of piles with good accuracy while the end-bearing capacity cannot be predicted well. Schmertmann (1978) method is well suited to estimate the capacity for the SLT of the PSC piles, while Lehane et al. (2013) method is the best method to predict the capacity for the open-ended pile.
- All the test piles (i.e., both open and close-ended pile) exhibited significant amount of setup which is mainly due to increase in skin friction. The end-bearing capacity was almost constant for all test piles except for open-ended steel pile during the SLT. The end-bearing capacity for the open-ended steel pile during the SLT was 6.9 times higher compared to the end-bearing capacity during EOD.

- Significant amount of end-bearing capacity is observed for the open-ended steel pile during the axial compression SLT, which is mainly due to possible formation of "soil-plug" inside the pile. This behavior was not observed for the open-ended cylinder pile during the quick loading test such as the SNLT.
- The logarithmic setup rate parameter "A" for all test piles were back-calculated and the results revealed that for the large diameter open-ended cylinder piles, the "A' parameter was about 0.38 and that for PSC pile "A" was about 0.37. The "A" parameter for open-ended steel pile was 0.31, slightly lower than the concrete piles.
- No significant amount of setup was experienced inside the open-ended pile between the inner pile surface and plugged soil as the setup rate "A" for the PSC piles and open-ended piles were very close in magnitude.

ACKNOWLEDGEMENTS

This research is funded by the Louisiana Transportation Research Center (LTRC Project No. 11-2GT) and Louisiana Department of Transportation and Development (State Project No. 736-99-1732). The help and support from the LADOTD geotechnical design section personnel are also highly appreciated.

REFERENCES

Abu-Farsakh, M. Y. and Titi, H. H., 2004. Assessment of direct cone penetration test methods for predicting the ultimate capacity of friction driven piles. *Journal of Geotechnical and Geoenvironmental Engineering,* Vol. 130(9), 2004, pp. 935-944.

Abu-Farsakh, M., Haque, Md. N., and Chen, Q., 2016. Field instrumentation and testing to study set-up phenomenon of piles driven into Louisiana clayey soils. *Report No. FHWA/LA.15/562*, Louisiana Transportation Research Center, Baton Rouge, LA.

Briaud, J. L. and Tucker, L. M., 1988. Measured and predicted axial response of 98 piles, *Journal of Geotechnical Engineering*, Vol. 114(8), pp. 984–1001.

Bullock, P. J., Schmertmann, J. H., McVay, M. C., and Townsend, F. C., 2005. Side shear setup I: Test piles driven in Florida. *Journal of Geotechnical and Geoenvironmental Engineering*, Vol. 131(3), pp. 292-300.

Bustamante, M. and Gianeselli, L., 1982. Pile bearing capacity predictions by means of static penetrometer CPT. *Proceedings to 2nd European Symposium on Penetration Testing*, ESOPTII, Amsterdam, pp. 493–500.

De Ruiter, J. and Beringen, F. L., 1979. Pile foundations for large North Sea structures. *Marine Geotechnology*, Vol. 3(3), pp. 267–314.

Lehane, B. M., Li, Y. and Williams, R., 2013. Shaft capacity of displacement piles in clay using the cone penetration test. *Journal of Geotechnical and Geo-environmental Engineering*, Vol. 139(2), pp. 1-13.

Schmertmann, J. H., 1978. Guidelines for cone penetration test. Performance and Design. U.S.Department of Transportation, *Report No. FHWA-TS-78-209*, Washington, DC, p. 145.

Skov, R. and Denver, H., 1988. Time dependence of bearing capacity of piles. *Proc. of the 3rd Int. Conference on the Application of Stress-Wave Theory to Piles*, Canada, pp. 879-888.

FRICTION FATIGUE AND DRIVABILITY ANALYSIS OF OPEN ENDED PIPE PILES BASED ON CONE PENETRATION TESTING RESULTS

Rozbeh B. Moghaddam, GRL Engineers, Inc., Cleveland, OH, USA, 216-831-6131,
rmoghaddam@grlengineers.com

Frank Rausche, GRL Engineers, Inc., Cleveland, OH, USA, 216-831-6131,
frausche@grlengineers.com

Scott D. Webster, GRL Engineers, Inc., Charlotte, NC, USA, 216-831-6131
swebster@grlengineers.com

ABSTRACT

Pile foundation driveability is a function of several variables such as subsurface characteristics, hammer type, hammer efficiency, pile type, and plugging conditions. One important phenomenon occurring during pile driving, and yet not well documented and published, is the *friction fatigue*, where a reduction of shaft resistance is observed as the pile is driven to greater embedment. This paper introduces current soil models developed for the assessment of friction fatigue, and further presents a comparison between predicted driveability obtained from Wave Equation Analysis Program (GRLWEAP) and field driving records. From a literature survey, and review of technical articles, a widely-used soil model known as AH-01 has been selected to analyze the friction fatigue concept. Using a WEAP software, two driveability analysis were completed using the standard approach with setup factors, and adapting the AH-01 model into the WEAP input file. Driveability predictions were compared to the driving records corresponding to a 1676-mm x 44-mm open-ended pipe pile with a total and embedment lengths of 180-m and 119-m, respectively. Results from analyses and the comparison presented in this paper provide further information regarding existing methods for the incorporation of the friction fatigue concept to the driveability analyses, and contributes to a better prediction of driveability of open-ended pipe piles.

Keywords: Friction fatigue, Driveability, Open-ended pipe piles, Wave Equation Analysis, Static Resistance to Driving, SRD

 © 2017 DFI Annual Conference, New Orleans, LA, USA

Introduction

Dynamic measurements during pile installation provide more dependable information as compared to results obtained from predictive models used for design. Despite uncertainties associated with a specific project site and foundation type, measured data provides a reliable understanding of the soil resistance and its distribution throughout the length of the pile. Back-calculations or back-analyses based on a series of measured data from a pile driving process could help to obtain reliable models to better predict events related to pile installation process in spite of all variability related to fitted models. One of the widely-used analysis regarding pile driving during the design phase is the "driveability analysis" where capacity, blowcounts, maximum stresses in the pile element, and transferred energy from the hammer to the pile element are predicted using mathematical models along with a software. Such analysis requires relevant information regarding soil, pile, and hammer properties combined with a deep understanding of the level of impact each one of these properties could have on the analysis.

One of the properties that could significantly impact the driveability prediction is the effect of the embedded pile length on the soil resistance distribution along the pile. This effect has been commonly studies under the *friction fatigue* phenomenon where the soil resistance is decreased along the pile shaft as the pile is driven deeper into the soil layers. Traditionally, instead of using the friction fatigue approach, driveability analyses were performed assuming an empirical soil setup factor for each layer. It was then assumed that during driving, regardless of the number of load cycles (i.e., hammer blows), the soil resistance would be the long term static resistance divided by the soil setup factor. For example, if the soil setup factor was 2 then the resistance during driving was assumed to be 50% of the long-term resistance. This approach has been satisfactory for land piles with moderate pile penetrations. Unfortunately, the setup factor was not well defined for marine clays, and varied between 2 and 10. Experience in a certain geology was needed to select the correct value.

Appropriate mathematical approaches and formulations have been proposed and implemented to assess the friction fatigue. Throughout several studies, it has been proposed and assumed that the friction fatigue is more noted in granular soils (i.e. sandy soils) compared to fine grained soils (i.e. clay material), and the effect is further observed in dense to very dense sands compared to those results reported for loose sands, Schneider et al. (2010).

Throughout this paper, a brief background and review of existing studies related to friction fatigue is presented, the driveability analysis and its associated parameters are discussed in detail, a mathematical model proposed by Alm and Hamre (2001) (A&H) to assess the friction fatigue during pile driving is introduced, and the wave equation analysis program used for related analyses is described. Furthermore, a case study is presented where the driveability analysis was completed with and without considering the friction fatigue effect, and the results are compared to driving logs representing measured blowcounts obtained from the pile driving monitoring.

Friction Fatigue

Hypothetically, the unit skin friction for a pile installed in a uniform material increases as the depth is increased, and consequently more resistance is encountered at higher depths which results in higher driving resistance (i.e. high blowcounts as the depth increases). However, throughout a series of observations Heerema (1979) concluded that the unit shaft resistance decreased during the driving process as the piles were driven to greater depths, Figure 1. The reduction of skin friction was primarily attributed to the cyclic shearing process that the soil surrounding the pile suffers during the driving process, and it was further introduced as the friction fatigue theory.

In addition to documenting observations made at a pile driving project, Heerema (1980) developed a laboratory device to further study the friction fatigue phenomenon, and simulate the interaction between the steel wall of the pipe pile and the soil material. For the laboratory test, a thin wall tube was recovered containing an undisturbed sample, and it was cut to a length of approximately 19-cm with vertical stresses applied to the soil sample from above and below using bearing plates. Using a relatively small opening in the upper plate, a 1.5-mm thick and 12-mm wide steel blade was pushed into the soil sample, and through an actuator cyclic, displacements were generated in the sample, Figure 2a. During this process, strain gages and accelerometers were connected to the steel blade to continuously record force and velocity measurements. Results from the laboratory tests showed that the initial shear strength of the soil was decreasing as the number of oscillations were increasing which further confirmed the observations reported by Heerema (1979), Figure 2b. It is interesting to note that in the traditional setup approach, the results of Figure 2b would have been interpreted to suggesting a soil setup factor of approximately 300/40 = 7.5.

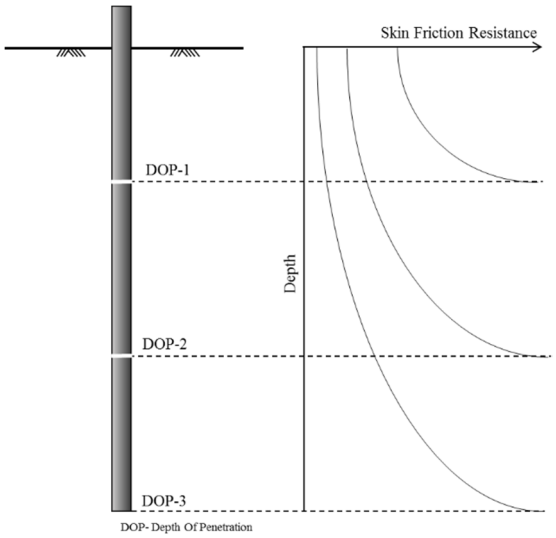
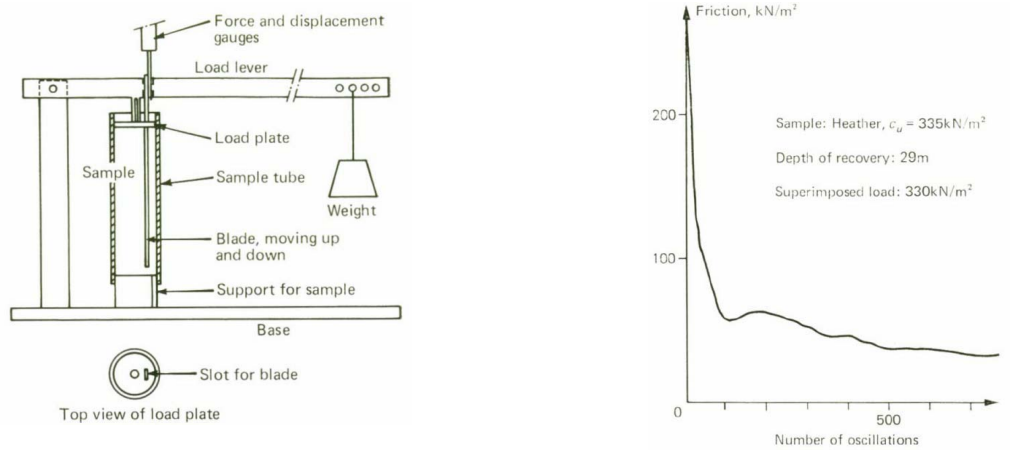


Figure 1. Schematics of skin friction resistance at different depths of penetration (after Heerema 1980)



a) Laboratory Apparatus b) Laboratory Results

Figure 2. Evaluation of friction fatigue concept through laboratory testing (after Heerema, 1979)

After results presented by Heerema (1979 and 1980), other studies have evaluated the relationship between the friction fatigue and hammer blows (White et al. 2004, and White 2005), the ratio of the soil height above the pile tip and the pile diameter (Randolph et al. 1991), and the height of the soil above the pile tip (Alm and Hamre, 2001).

The research study presented by White et al. (2004) evaluated the effect of friction fatigue on displacement piles in sands using a centrifuge model instrumented with lateral stress sensors. The results from the experiment were combined with laboratory tests as well as field observations, and it was concluded that for a given installation method the lateral stress acting on the pile-soil interface at any depth can be expressed as a function of the cone penetrometer tip resistance (q_t) and the number of cycles that the soil element is exposed to shearing. In the context of the research, White et al. (2004) associated the number of cycles with the hammer blowcounts during pile installation. In a subsequent work, White (2005) evaluated the combined effect of friction fatigue and the geological stress history of the soil surrounding the pile element to develop predictions of unit skin friction for displacement piles.

Open-ended pipe piles present additional challenges as far as end bearing and internal friction is concerned. For example, under plugged conditions the soil mass moves downward with the pile and end bearing develops over the fully plugged area. In an unplugged condition (i.e. where coring condition is presented), end bearing only occurs against the steel annulus, but friction resistance may occur inside of the pipe and partially considered for a driveability analysis. The plugged behavior is mainly observed under static loading conditions (Randolph at al. 1991) which differs from conditions where the pile is exposed to higher loading rates, particularly in the case of open-ended pipe piles installed for offshore projects. Under fast loading rate conditions, the increase in the effective stress acting on the soil plug is limited while the plug inertia is very high, which causes a significant reduction of resistance at the bottom of the pile. A one-dimensional analysis of the plugging conditions was presented by Randolph et al. (1991) and design charts were developed as a function of soil plug parameters and loading rate.

An important concept to consider before driving a pile is the prediction of the driveability which consequently impacts installation method, construction equipment selection, and hammer selection. Important parameters such as soil conditions, pile material properties, pile dimensions, the friction fatigue concept, and in the case of open-ended pipe piles the plugging conditions have notable impact on the pile driveability predictions. A&H presented a fitted model based on driveability studies of large diameter pipe piles installed in the North Sea. In order to reduce uncertainties associated with the selection of soil parameters, the strength parameters used for the determination of pile predicted capacities were determined using cone penetration results, and both unit skin friction (f_s) and unit base resistance (q_b) were correlated to the cone penetration test tip resistance (q_t). From field logs and driving records, A&H concluded that the skin friction of a pile driven into soil layers will decrease exponentially from an initial skin friction ($f_{s\text{-}i}$) to a residual value of ($f_{s\text{-}res}$). The model fitted to the measured, and correlated data is presented by equation (1). A&H proposed the values and expressions presented in Table 1 to determine unit skin friction during driving ($f_{s\text{-}res}$) and long-term unit skin friction ($f_{s\text{-}i}$), classified based on soil type, and related to CPT data and effective vertical stress.

$$f_s = f_{s\text{-}res} + (f_{s\text{-}i} - f_{s\text{-}res})\, e^{-kh} \quad (1a)$$

$$k = \frac{1}{80}\sqrt{\frac{q_t}{\sigma'_0}} \quad (1b)$$

In Eq. 1a and 1b, f_s is the unit skin friction resistance during driving (also called Static Resistance to Driving, SRD) at a distance h above the pile tip, $f_{s\text{-}res}$ is the residual unit skin friction resistance during driving which

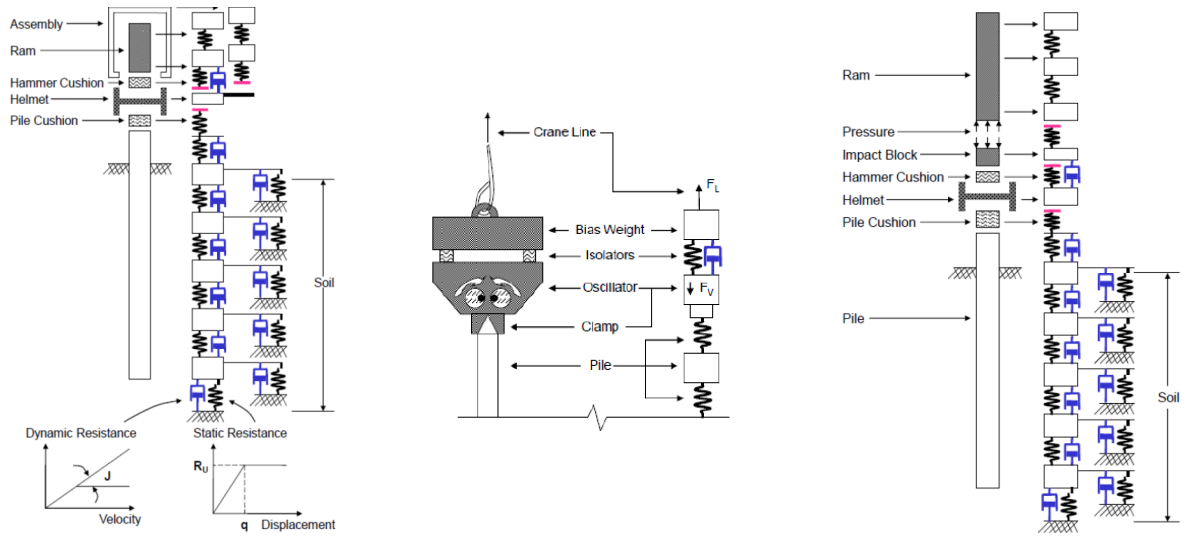
is reached after an infinite number of hammer blows, and $f_{s\text{-}i}$ is the initial long-term unit skin friction resistance computed from the CPT cone resistance, q_t. The parameter k is the exponential function's shape factor determined from equation 1b, and σ'_0 is the effective vertical stress at the CPT depth.

Table 1. Expressions derived for $f_{s\text{-}i}$ and $f_{s\text{-}res}$ (Alm & Hamre 2001)

Soil Type	$f_{s\text{-}i}$	$f_{s\text{-}res}$
CLAY	Recorded CPT Sleeve Friction (q_{sf})	$0.004q_t(1-0.0025\frac{q_t}{\sigma'_0})$
SAND	$0.0132q_t(\frac{\sigma'_0}{P_a})^{0.13}\tan(\delta)$	$0.20f_{s\text{-}i}$

Wave Equation Analysis Program

The original, non-proprietary Wave Equation Analysis Program, WEAP, simulates the conditions in the hammer, pile, and soil element during and immediately after the ram impact. The analysis is completed based on modeling the components of the system (i.e. hammer, pile, and soil) with masses, springs and dashpots. Displacement and velocities of the masses, and the forces in the springs are calculated. Pile movement and stresses along the pile elements are determined from an exact solution of the wave analysis differential equation. Figure 3 illustrates the modelling and components of the system used in WEAP. Considering the wide use of the WEAP program and its offshore feature which allows to model offshore pile driving process, all analyses and modeling presented in this paper has been performed using the WEAP-based, proprietary Offshore Wave version of GRLWEAP-2010. It is important to mention that to the knowledge of the authors the A&H model have not been used yet for driveability analyses completed for a vibratory hammer.



a) ECH* Hammer b) Vibratory Hammer c) Open Ended Diesel Hammer

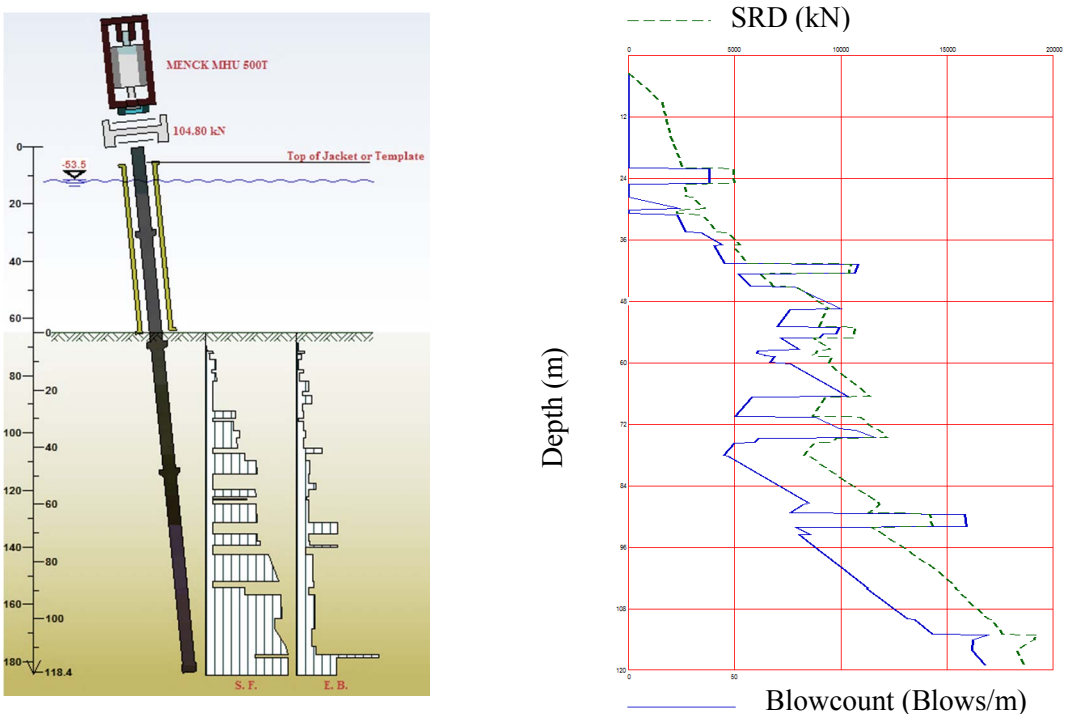
Figure 3. Model Components and schematics for three typical hammers (GRLWEAP, 2010)
**External Combustion Hammer*

Driveability Analysis

To evaluate the expected Static Resistance to Driving (SRD), and to further predict blowcounts associated with the pile driving process, driveability analyses are performed using the above-mentioned computer program. Driving hammers used in the pile driving operations have variable energies which makes the selection of appropriate hammer energy setting the primary concern of the driveability analysis.

To perform a driveability analyses, input data representing the soil and pile properties as well as hammer and driving system are required. These parameters include pile length, final depth, location of splices, pile profile and inclination, driving system parameters, hammer stroke (energy level) and hammer efficiency. The following input requirements for each soil layer are important in the context of this paper: unit shaft resistance, $f_{s\text{-}i}$, shape factor, k, the ratio $f_{s\text{-}res}/f_{si}$ (called setup factor), unit base resistance, the toe resistance area, quake and damping values. In addition, this program version allows for the input of data considering stabbing guides, add-on sections, jacket or template details for the consideration of static pile bending stresses. Once all input data has been entered, the resistance distribution, including shaft resistance and end bearing, along with the schematics of the modeled pile, are displayed as shown in Figure 4a.

A graph showing the SRD, based on the initial shaft resistance, $f_{s\text{-}i}$, toe area and unit toe resistance, and blowcount vs. depth is one of the important output plots obtained from a driveability analysis, Figure 4b. The primary objective of such plot is to illustrate the blowcounts required to drive the pile through the various soil layers with corresponding ultimate resistance. This type of plot aids to properly select a hammer to be used for the driving process. Other important parameters such as compressive stress, and combined compressive and tensile stresses are also obtained from a driveability analysis.



a) GRLWEAP input schematics
S.F. Skin Friction- E.B. End Bearing

b) Static Resistance to Driving, SRD, and Blowcount vs. Depth

Figure 4. Schematic input and output data for driveability analysis using GRLWEAP

Case Study

The following section presents details of a pile driving project where a driveability analysis has been completed with and without consideration of the friction fatigue concept. Calculated blowcount vs. depth obtained from the traditional setup-factor approach and the friction fatigue approach are compared with the driving records obtained during pile driving monitoring. Note that GRLWEAP's friction fatigue algorithms allow for the A&H resistance distribution calculation as discussed earlier and further presented below.

The project selected is an oil platform which is supported by a series of open-ended pipe piles installed in rows. A representative pipe pile (i.e. the foundation with largest diameter and longest length) has been selected for the analysis. The platform foundation system also included piles with other dimensions as well as skirt piles. However, for purposes of the analyses presented in this paper, only the foundation described above has been analyzed and discussed. It is also important to mention that due to client confidentiality, the authors have abstained from providing further details regarding project location and properties of the superstructure.

Pile Properties

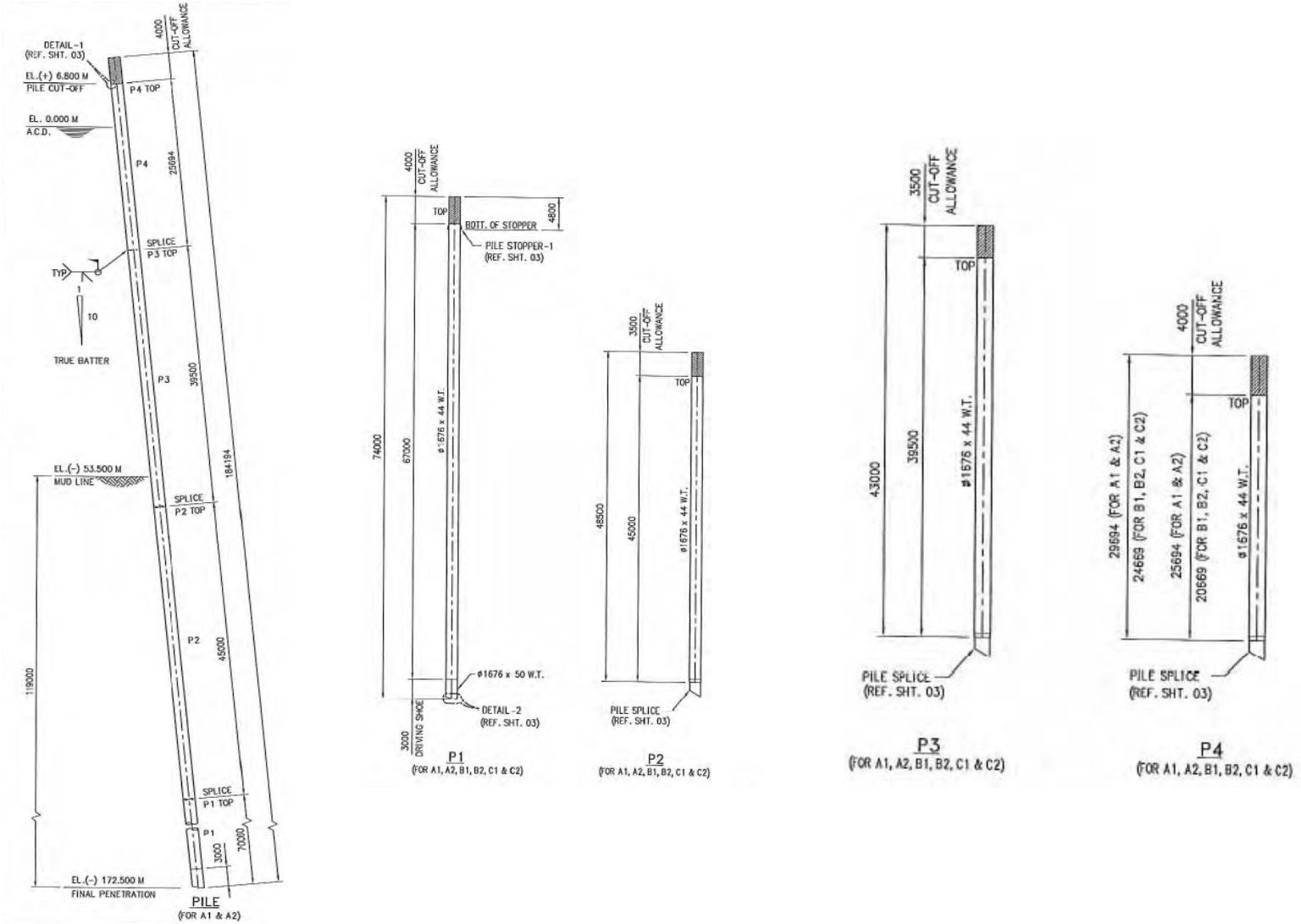
The foundation pile presented herein, consisted of 1676 mm (66-in) O.D. steel pipe piles with wall thickness varying from 44-mm (1.75-in) to 50-mm (2-in) along the pile length. The piles were planned to be driven on a 1:10 batter and in four sections with the first section (P1) being 74.0-m (243-ft) in length which included a 4-m (13-ft) cutoff allowance. The second section (P2) had a length of 48.5-m (159-ft), and the third section (P3) had a length of 43.0-m (141-ft). Both P2 and P3 sections had a cutoff allowance of 3.5-m (11.5-ft). Finally, the fourth section (P4) had a length of 29.7-m (98-ft) and a cutoff allowance of 4.0-m (13-ft), Figure 5.

Soil Properties

Boring logs associated with this project indicated that the predominant subsurface conditions consisted of interbedded layers of siliceous carbonate medium to coarse sands, and soft to stiff carbonate clays. Between the depths of 13.0-m (43-ft) and 27.5-m (90-ft) two silt layers with 1.0-m and 10.0-m thickness were encountered. Sand layers varied in thickness ranging from 1.0-m (3.3-ft) to 7.1-m (23.3-ft) with an average thickness of 3.2-m (10.5-ft). The thickness corresponding to the clay layers varied between 0.7-m (2.3-ft) and 12.0-m (39.4-ft) with an average thickness of 5.0-m (16.5-ft). In addition to the borings, one CPT was completed at the project site to a maximum depth of 120-m (394-ft) below the seabed, Figure 6. The CPT profile showed an average tip resistance of 10.4 MPa (217-ksf) and 7.2 MPa (150-ksf) for the sand and clay layers, respectively. Similarly, the average sleeve friction determined from the CPT profile was 0.30-MPa (6.3-ksf).

Hammer and Driving System Details

The proposed driving systems to install the main foundation steel pipe piles to the desired pile penetration depth consisted of a Menck MHU 500T which is a double acting hydraulic hammer with a ram weight of approximately 294-kN (66-kips). The maximum equivalent stroke is approximately 1.87-m (6.15-ft) which results in a maximum manufacturer's rated energy of 550-kJ (405-ft-lbs). However, the hammer energy may be controlled by the hammer operator for multiple energy settings. This Menck hammer does not use a hammer cushion, resulting in steel-on-steel impact, and the helmet weight was assumed to be 104.8-kN (24-kips). According to the manufacturer, the total weight of the hammer is approximately 828-kN (186-kips).



a) Schematics of the Pile A1 b) Sections P1 and P2 c) Sections P3 and P4

Figure 5. Open-ended pipe pile schematics

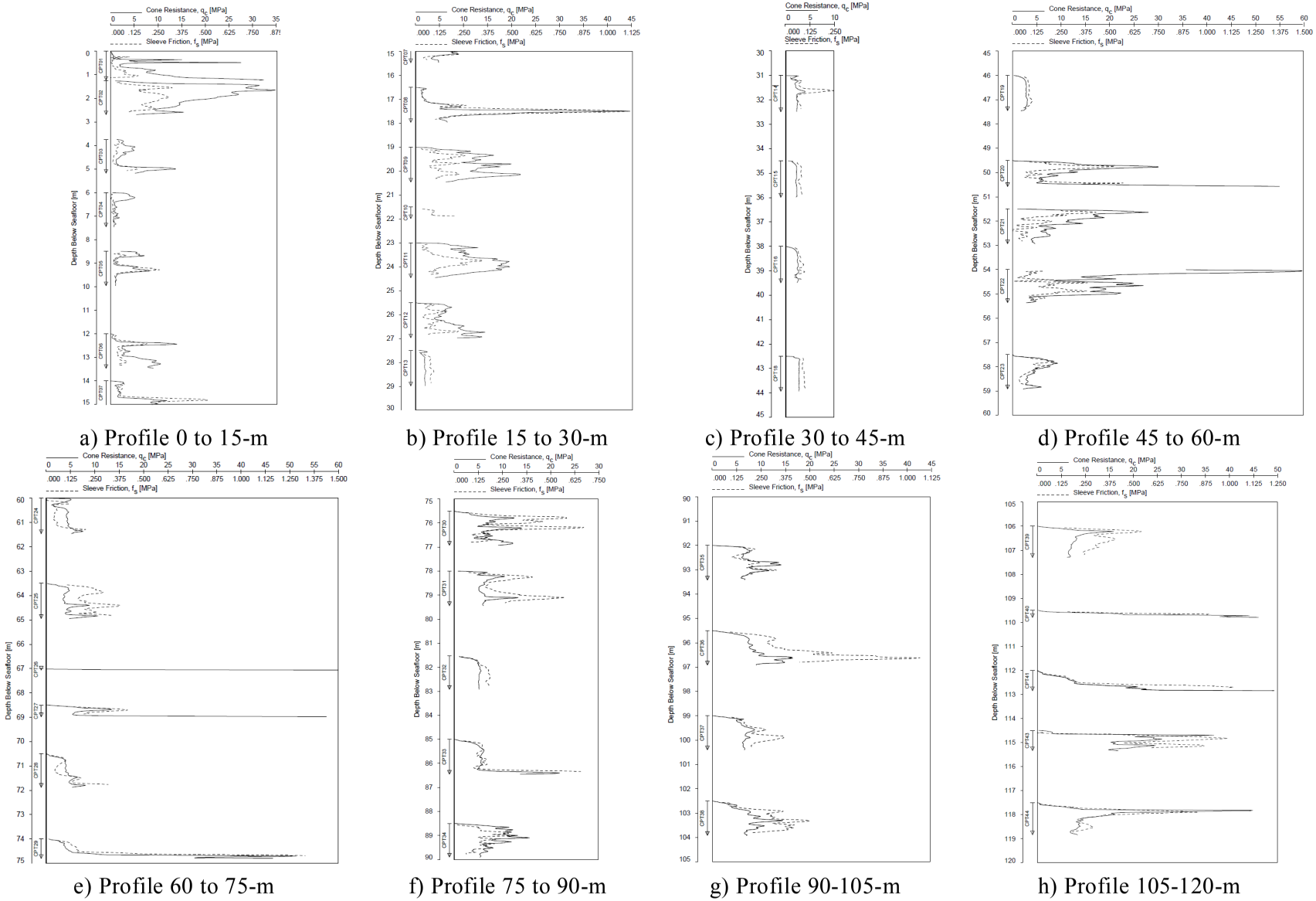


Figure 6. CPT profiles corresponding to the project site

Wave Equation Analysis

For comparison purposes, two separate series of analyses have been completed for the project presented in this paper to observe driveability predictions performed with and without considering the friction fatigue concept. For both sets of analyses a detail review of available geotechnical engineering information corresponding to the pile installation process yielded relevant data to prepare appropriate input parameters for the driveability analysis.

For the first analysis where the friction fatigue was not considered, the SRD values were determined using standard shaft setup factors of 2 for clay and 1 for sand. The base resistance was analyzed with its Long-Term Static Resistance (LTSR) value and considering the base area as the steel annulus. It is important to mention that these setup factors are based on results obtained from a large variety of land construction sites and are not based on specific offshore experience values. The unit skin friction and unit end bearing resistance values were determined based on API (2000) shown in Figure 7.

For shaft quake, the GRLWEAP recommended value of 2.5-mm (0.1-in) was selected, whereas, toe quakes selected for the analyses were based on the pile diameter and the expected soil conditions. A toe quake of 28.0-mm (1.1-in) was selected for the clay deposits, while a reduced toe quake of 14.0-mm (0.55-in) and 21.0-mm (0.83-in) were selected for the sand and silt layers, respectively. The driveability analyses were performed using Smith damping factors of 0.16, 0.41 and 0.65 s/m (0.05, 0.125 and 0.2 s/ft) for the pile shaft in the sand, silt and clay deposits, respectively. Furthermore, a Smith toe damping of 0.50 s/m (0.15 s/ft) was selected for all layers as per the software recommendations for the given soil profiles and to maintain a slightly conservative approach. These input parameters, as well as the LTSR were the same for both analysis completed for the open-ended pipe pile presented herein.

The second analysis utilized the A&H friction fatigue option of the GRLWEAP program. It is important to clarify that the $f_{s\text{-}i}$ and f_s in the Alm and Hamer (2001) model are equivalent to the LTSR and SRD in the GRLWEAP model, respectively. As previously mentioned, for the A&H model the SRD was determined using Equations (1a) and (1b), and those presented in Table 1. Also, no internal friction and no plug resistance were considered. From the CPT profile, and corresponding laboratory testing, the residual values of tip resistance, sleeve friction, and effective vertical stress were determined. Depending on the type of soil material, the appropriate equation was selected from Table 1, and the values of unit skin friction during driving ($f_{s\text{-}res}$), and the initial long-term unit skin friction resistance ($f_{s\text{-}i}$) were calculated. The friction fatigue setup factors, required as input in GRLWEAP, were determined from the ratio of $f_{s\text{-}i}$ to $f_{s\text{-}res}$., typically were near 5 while the land experience based setup factors of the comparison analysis were only between 1and 2.

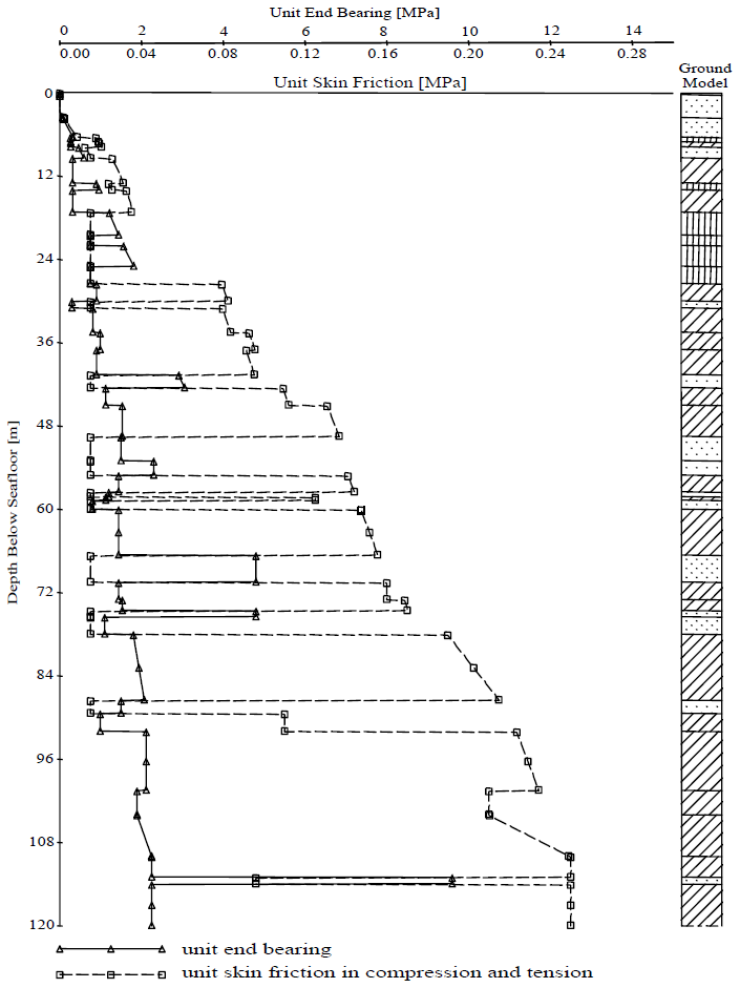


Figure 7. Unit skin friction and base resistance

Results of Wave Equation Analysis

For comparison purposes, the calculated blowcount results from both driveability analyses were plotted in Figure 8 together with the measured blowcounts. It is observed that despite the increasing trend of unit skin resistance shown in Figure 7, the measured blowcounts do not behave in the same fashion. Normally it would have been assumed that as the resistance increases with depth the measured blowcounts would do likewise. However, results from the analysis showed that predicted values based on a traditional approach with relatively low setup factors overpredict the blowcounts near the end of driving. In fact, it appears to increase like an exponential function with depth, and it is more noticeable within the last 30-m (98.4-ft) of the pile driving. In contrast, when the effect of friction fatigue is considered using the A&H model, the predicted blowcounts are in much better agreement with the measured values. One important trend to note is that as the pile is driven to greater depths, the effect of friction fatigue is more noticeable. In fact, for depths between 0.0 and 30.0-m (98-ft) both models calculate somewhat lower blow counts than those observed. Between depths of 30.0-m (98-ft) and 95-m (312-ft) the models follow the measured blow counts closely with an overprediction observed at approximately 95-m (312-ft). Below 95-m (312-ft) the friction fatigue model compares well with the measured values whereas the traditional model begins to deviate more and more severely. In this particular case, a higher setup factor for the lower layers should have provided a better agreement.

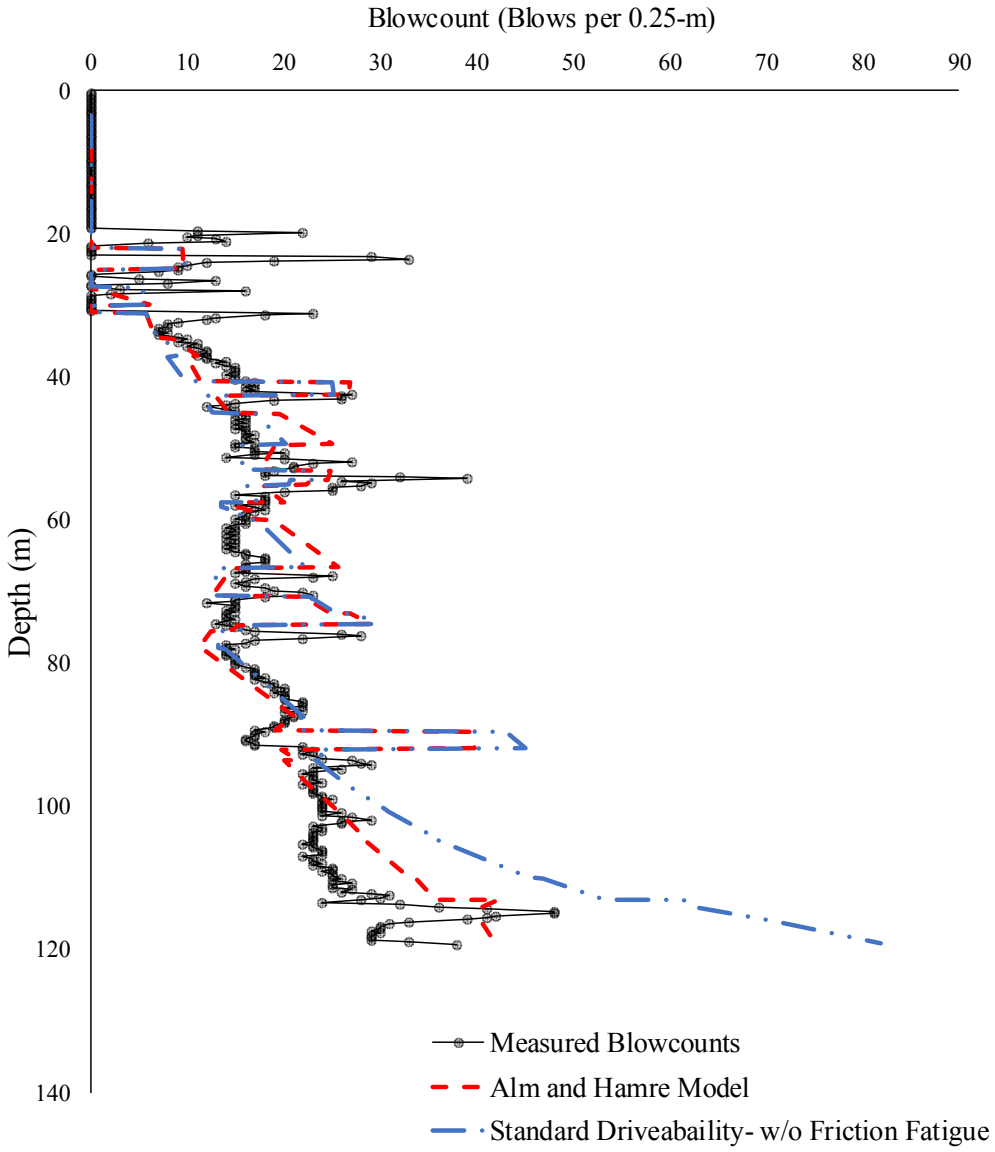


Figure 8. Driveability Analysis Results

Summary and Conclusions

This paper presented a brief history and background of the friction fatigue concept including a fitted model presented by Alm and Hamre (2001) which accounts for the friction fatigue concept in open-ended pipe piles. As a case study, details associated with a project where a large diameter open-ended pipe pile was driven through multilayered soils were presented. For this pile two different analyses were completed using the GRLWEAP program, one employed the traditional setup factor approach; the other one followed the A&H recommendations. In both cases the LTSR was based on the API recommendations, no internal friction and no plugging plus standard damping and quake values. The outcome of both analyses was compared to measured values determined from the pile driving monitoring.

Results of the analyses show good agreement for both approaches as long as blow counts are below 30 blows/0.25m at a depth of roughly 90 m. For higher blow counts at greater depths, the traditional model calculated increasing overpredictions while the A&H approach followed the observed blow count trend to a much greater degree.

Considering the wide use of driveability analyses for equipment selection, and the cost of offshore pile driving equipment and operations it is recommended to consider friction fatigue models such as A&H when performing wave equation analyses for piles with deep penetrations. In all cases, as also recommended by A&H, both lower bound and upper bound analyses should be performed for conservatism.

References

Alm, T., & Hamre, L. (2001). Soil model for pile driveability predictions based on CPT interpretations. In *Proceedings of The International Conference on Soil Mechanics and Geotechnical Engineering* (Vol. 2, pp. 1297-1302). AA BALKEMA PUBLISHERS

Heerema, E. P. (1979) Relationships between wall friction, displacement velocity and horizontal stress in clay and in sand, for pile driveability analysis. *Ground engineering*, *12*(1)

Heerema, E. P. (1980) Predicting pile driveability: Heather as an illustration of the" friction fatigue" theory. In *SPE European Petroleum Conference*. Society of Petroleum Engineers

Randolph, M. F., Leong, E. C., & Houlsby, G. T. (1991). One-dimensional analysis of soil plugs in pipe piles. *Geotechnique*, *41*(4), 587-598

Schneider, J. A., & Harmon, I. A. (2010). Analyzing Drivability of Open Ended Piles in Very Dense Sands. *DFI Journal-The Journal of the Deep Foundations Institute*, *4*(1), 32-44

White, D. J. (2005, September). A general framework for shaft resistance on displacement piles in sand. In *Proceedings of the 1st International Symposium on Frontiers in Offshore Geotechnics, ISFOG 2005* (pp. 697-704). Taylor and Francis

White, D. J., & Lehane, B. M. (2004). Friction fatigue on displacement piles in sand. *Géotechnique*, *54*(10), 645-658

CASE HISTORY: LARGE DIAMETER *MICRO*PILES FOR THE HIGHWAY 53 RELOCATION PROJECT

David S. Graham, P.E., Dan Brown and Associates, 205-427-0682, dgraham@dba.world

Paul J. Axtell, P.E., D.GE, Dan Brown and Associates, 913-744-4988, paxtell@dba.world

Nathan W. Iverson, P.E., Veit & Company, Inc., 763-428-2242, niverson@veitusa.com

ABSTRACT

The Highway 53 relocation project in Virginia, Minnesota, involves construction of a very tall bridge across a currently inactive iron ore mine pit. The inactive pit is partially flooded and serves as the community's drinking water source. The 1,132-ft long new bridge is a three-span, plate girder structure. Two intermediate, approximately 200-ft tall piers are located within the pit.

The foundations for the two piers consist of groups of 30-in diameter piles which, despite the contradiction in terms, are essentially very large micropiles. Extremely challenging and highly variable subsurface conditions exist at the site, ranging from uncontrolled iron ore mine waste fill to some of the hardest rock on earth that can also be highly fractured and abrasive. Despite the conditions, large diameter (30-in) micropile foundations up to 175 ft deep were successfully installed using down-the-hole hammer methods and full-length permanent casing under an extremely aggressive construction schedule.

Full-scale foundation load testing using the Statnamic rapid loading method was also conducted in support of the design and construction but under a separate pre-design phase contract. This paper describes the unique aspects of this foundation project, including design, construction, and load testing of the large micropiles.

Keywords: micropile, foundation, bridge, pier, statnamic, load test, construction

INTRODUCTION AND BACKGROUND

In 1960, a segment of Trunk Highway 53 (TH-53) in Virginia, Minnesota, was built on land owned by iron ore mining interests. As part of the roadway easement agreement, Minnesota Department of Transportation (MnDOT) was to be given notice three years prior to termination of the easement. In 2010, MnDOT received notice that the mining interests wished to access the ore. Through negotiations in 2010, MnDOT and the mining interests agreed to a 2017 date for abandoning the existing section of roadway. During this period, MnDOT needed to procure project funding, satisfy environmental permitting requirements, and acquire new right-of-way to permanently reroute TH-53 and keep it open to traffic. This was no easy task due to the existing mine pits surrounding the area.

The E-2 alignment option shown in Fig. 1 was ultimately selected for the rerouted highway in 2014. The new highway segment includes a three-span bridge across the currently inactive Rouchleau Mine Pit. The inactive pit is partially flooded and serves as Virginia's drinking water source. The 1,132-ft long new bridge is a three-span, plate girder bridge. Two intermediate approximately 200-ft tall piers are located within the pit. Fig. 2 is a conceptual rendering of the bridge.

The foundations for the two intermediate piers consist of groups of 30-in diameter piles which, despite the contradiction in terms, are essentially very large micropiles. The piles include full-length permanent steel casings installed using down-the-hole hammer (DHH) equipment with a pilot and ring bit system. Micropile foundations are up to 175-ft deep including as much as 45 ft of bedrock drilling.

 © 2017 DFI Annual Conference, New Orleans, LA, USA

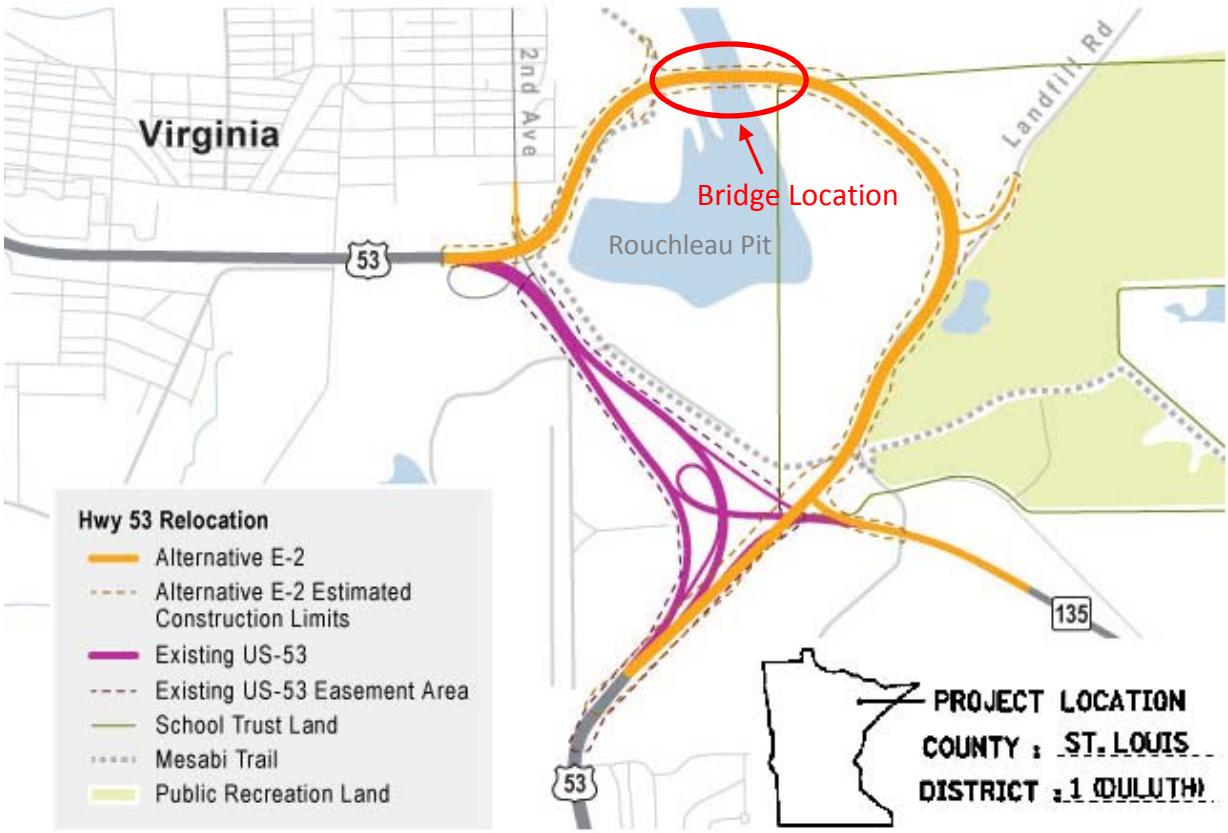


Fig. 1. Project Location and TH-53 Realignment (MnDOT 2017)

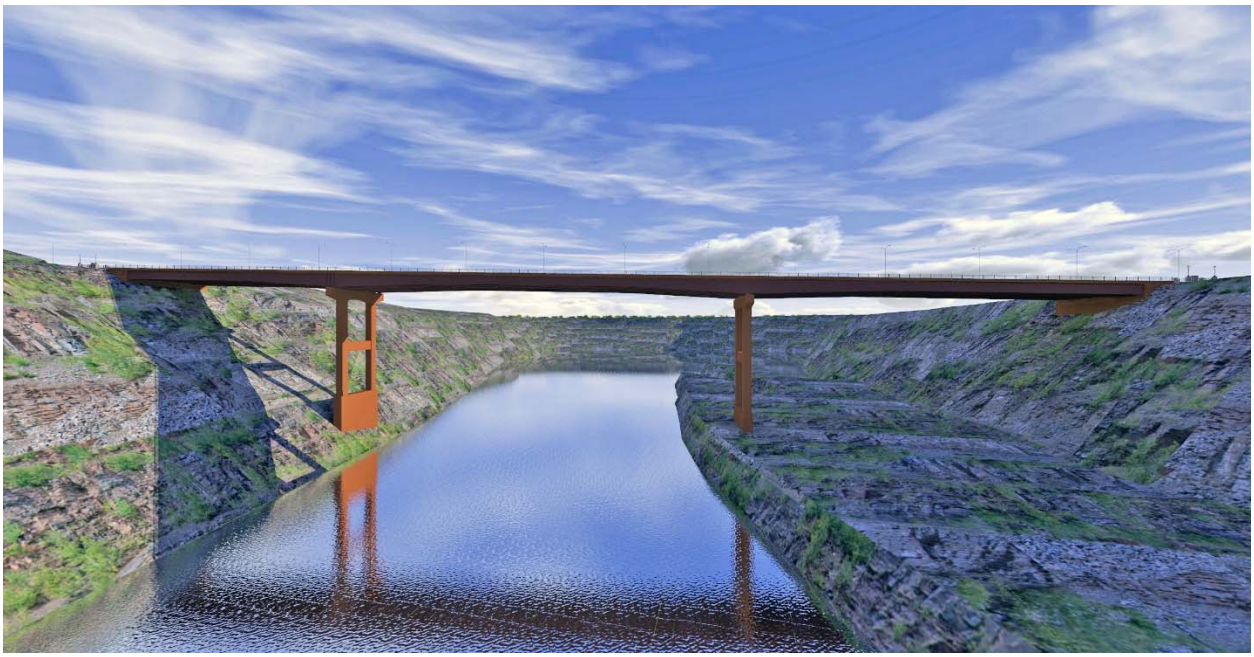


Fig. 2. Rendering of the TH-53 Bridge (MnDOT 2017)

GEOLOGIC SETTING

The project site is located within the Mesabi Iron Range. The Mesabi Iron Range is a narrow belt of iron ore deposits in the Superior Upland physiographic province of northeastern Minnesota. The bedrock unit of interest at the site is the Biwabik Iron Formation. The Biwabik was formed between 1.85 and 1.93 billion years ago as sediments deposited in a shallow marine environment. Since the early 20th century, the Biwabik Iron Formation has been subdivided into four members referred to as either cherty or slaty (Wolff 1917). The cherty members are typically characterized by a granular texture and thick-bedding; whereas, the slaty members are typically fine-grained and thin-bedded (Severson et al. 2010).

Intact pieces of the Biwabik rock are very hard and dense. The uniaxial compressive strength of specimens tested for this project averaged 20,600 psi with a maximum of 55,000 psi. Unit weight averaged 193 pcf.

The fractured rock mass of the Biwabik Iron Formation at the project site is defined by bedding plane joints, typically dipping within 20 degrees of horizontal and sub-vertical joints, typically dipping between 70 and 90 degrees. Two or three sub-vertical joint sets exist across the site. The sub-horizontal bedding plane joints and sub-vertical joints form blocks. The blocks vary in size depending on the spacing of the bedding planes and the nature of the bedding plane contacts. Rock blocks or chips range in size from an inch or less up to several feet in maximum dimension.

SUBSURFACE CONDITIONS

The bridge crosses the Rouchleau Pit at a location where the pit is long and narrow, resembling a rock canyon. At this location, the pit is approximately 1,100 ft wide and 300 ft deep. The pit is flooded with water to a depth of approximately 120 ft at the bridge crossing. The western side of the pit has an embankment of mine waste fill (MWF) originally placed to create a mining haul road. The MWF embankment is approximately 130 ft thick. The schematic in Fig. 3 shows the approximate extent of the MWF. Borings in the MWF provided visual evidence of its general characteristics. PQ sized coring yields recovery of rock of the nature illustrated by the photo in Fig. 4a. Rotosonic drilling recovers predominately soil-like materials with rock fragments as shown in Fig. 4b. Each of the two sampling methods effectively recovers a biased sampling of material of different sizes; it is probable that the fill consists of a wide range of particle sizes, from fine granular soil to boulder sized rocks. A reasonable conclusion is that the MWF is highly variable but consists mostly of Biwabik Iron Formation rock fragments that may have been crushed, blasted, and/or weathered resulting in rock fill with interstitial granular soil. Determining the MWF composition was not critical for pile design, as axial resistance was to be fully developed in the bedrock. However, the MWF composition was of interest for determining the best foundation type from a constructability standpoint and pile lateral response.

Pier 1, on the eastern side of the pit, sits on a notch carved into the highwall with no overburden. Pier 2, on the western side of the pit, sits on the existing embankment of MWF. Piers 1 and 2 are both supported on large diameter micropiles bearing in Biwabik bedrock and are the subject of this paper. The abutments are each supported on spread footings bearing on Biwabik bedrock. The East Abutment includes tie-back anchors which reduce the lateral demands on the very tall piers.

The surficial bedrock at the Pier 1 notch is a bed known as the Intermediate Slate (IS). The IS is thin bedded and relatively fractured. Recovery and RQD in the IS average 88 and 46 percent, respectively, on the basis of three exploratory NQ2 sized core holes. Uniaxial compressive strengths of intact IS core specimens average 12,600 psi. The IS interfaces a cherty bed known as the Lower Cherty 7 (LC7) approximately 30 ft below the bottom of the Pier 1 footing. Recovery and RQD in the LC7 average 94 and 82 percent, respectively. Uniaxial compressive strengths on intact LC7 core specimens average 38,800 psi. The Pier 1 piles are tipped in the LC7 bed.

Bedrock underlying the MWF at Pier 2 is the Lower Cherty member of the Biwabik. The upper approximately 40 to 50 ft of bedrock is highly weathered on the basis of three exploratory NQ2 sized core

holes. Below the weathered bedrock is an intact bed known as the Lower Cherty 5 (LC5). Recovery and RQD in the LC5 average 100 and 83 percent, respectively. Uniaxial compressive strengths of intact LC5 core specimens average 16,500 psi. The Pier 2 piles are tipped in the LC5 bed.

Groundwater at the site is consistent with the surface elevation of the flooded pit, which was around elevation 1,310 ft through the duration of the project.

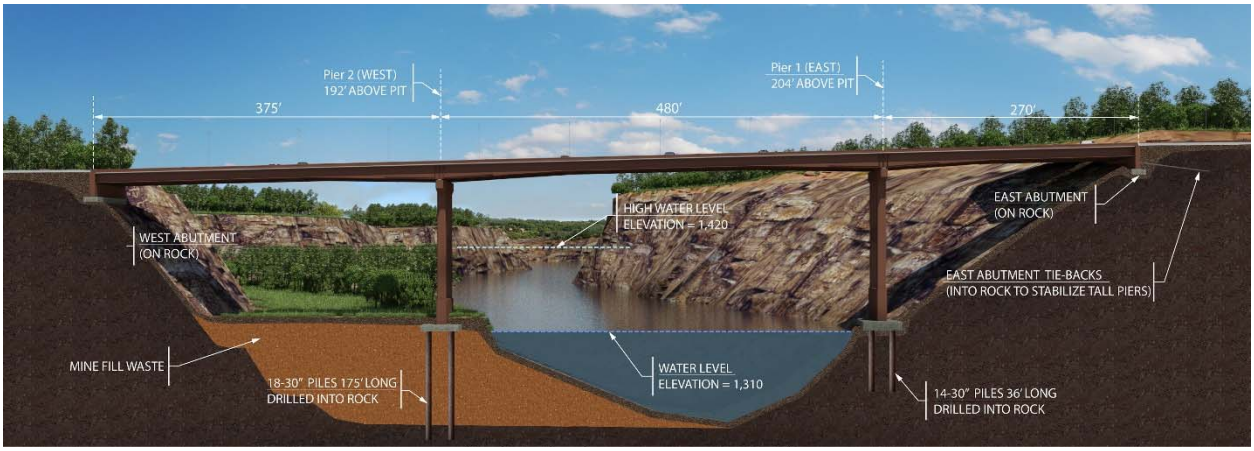


Fig. 3. Bridge schematic profile with generalize subsurface conditions (MnDOT 2017)



Fig. 4a. MWF material recovered by PQ sized coring



Fig. 4b. MWF material recovered by Rotosonic drilling

PRE-DESIGN LOAD TEST PROGRAM

A full scale, pre-construction load test program was conducted near Pier 2, on the west side of the pit where the mine waste overburden exists. Two 24-in diameter micropiles and one 16-in diameter micropile were installed. One of the 24-in piles included a 5-ft rock socket extending beyond the casing. The other two piles were fully cased.

Although load test performance of the piles was of interest, the primary goal of the test pile program was to evaluate constructability given the difficult and uncertain subsurface conditions. Veit Specialty Contracting (Veit) installed the test piles. A Bermingham BHD40 drill head and lead system attached to a Manitowoc 888 crawler crane was used in conjunction with Atlas Copco down-the-hole hammers (DHH) and tooling to simultaneously drill and advance casing. The reverse circulation method was used to transport the cuttings to the surface. Atlas Copco QL120 and QL200 DHH were used for the 16- and 24-in piles, respectively. An Atlas Copco Elemex pilot and ring bit system was used for the 24-in test piles and during the initial attempts to install the 16-in test pile. The 24-in equipment and tooling easily penetrated the MWF. However, there were issues with the 16-in ring bit detaching from the bit shoe in the overburden, allowing the drill to advance ahead of the casing. After two attempts in which the Elemex ring bit became detached from the casing, a Symmetrix pilot and ring system, also manufactured by Atlas Copco, was tried. The more robust Symmetrix system had no issues penetrating the MWF.

Bedrock drilling rate during the test pile program varied from less than a minute per foot to up to 33 minutes per foot. The deepest test pile, a 24-in pile, was tipped 187 ft below grade, penetrating approximately 65 ft into bedrock, although the upper 40 to 50 ft of bedrock was highly weathered. There were no issues drilling the cased holes. Initially, all three test piles were to include an uncased rock socket. The first rock socket attempted at one of the 24-in test piles collapsed shortly after drilling. The casing for that test pile was taken deeper and a seconded rock socket was not attempted. A 5-ft long rock socket was successfully drilled without stability issues at the other 24-in test pile. A rock socket was not attempted for the 16-in test pile. The reverse circulation drilling process left the bases of the holes clean without additional cleanout procedures employed, as verified by sounding with a weighted tape and subsequent observations during load testing.

The test piles were tested by means of an axial rapid load test (ASTM D7383-10) using a Statnamic device. All three test piles were loaded to a point where they began to demonstrate signs of structural failure without fully mobilizing the nominal geotechnical resistance. Review of the strain gage data indicated the piles were structurally overstressed during testing as manifested in prevalent cracking of the grout. However, because the grout was confined within a steel casing, full plastic yielding of the composite pile section did not occur. It can be concluded that under this substantial loading magnitude, the pile did not behave as a perfectly composite steel/concrete body.

While the strain gages did perform before, during, and after testing, the data were deemed unusable for the purposes of computing side resistance under maximum loading because of the cracking of the grout and the non-composite behavior. Test Pile 2 was loaded in two cycles, once with a smaller, 1,284-kip load that allowed measurement of partially mobilized side resistance. The partially mobilized unit side resistance in the rock socket under Load Cycle 1 was 18.3 ksf. Very little load was transferred in side resistance along the cased portion of the pile. The load test results are summarized in Table 1. The estimated mobilized unit base resistances in Table 1 assume all load applied load is carried in base resistance for Test Piles 1 and 3, and 75 percent is carried in base resistance for Test Pile 2.

Table 1: Load test results (Bailey and Muchard 2015).

Test Pile	Max Applied Load, kips	Estimated Mobilized Unit Base Resistance, ksf [psi]
TP-1 (24-in, fully cased)	4,088	1,301 [9,035]
TP-2 (24-in, with socket)	4,149	991 [6,879]
TP-3 (16-in, fully cased)	3,017	2,292 [15,917]

Upon unloading, the two end-bearing test piles (Test Piles 1 and 3) had no permanent set but rather rebounded and the final location of the pile top was above the location prior to testing. In fact, Test Pile 1 rebounded so dramatically that its pile top was approximately 2.0 in above the location prior to testing, as shown in Fig. 5. This highly unusual behavior was a result of a combination of the following:

1. enormous base resistance;
2. minimal side resistance; and
3. large elastic pile deformations.

The enormous base resistance results from a very hard, competent bedrock at the tip along with a clean hole prior to grout placement. The minimal side resistance was discussed above and anticipated as a result of the construction method which includes a slightly oversized hole relative to the diameter of the pile casing. The observed elastic pile deformations result from a relatively large magnitude of load applied to a long, relatively small diameter pile which, in cross-section, contained 20 percent steel and 80 percent grout. Upon dissipation of the rapid compression load, the elastic shortening of the pile was not restrained by sufficient side resistance causing large pile rebound accelerations.

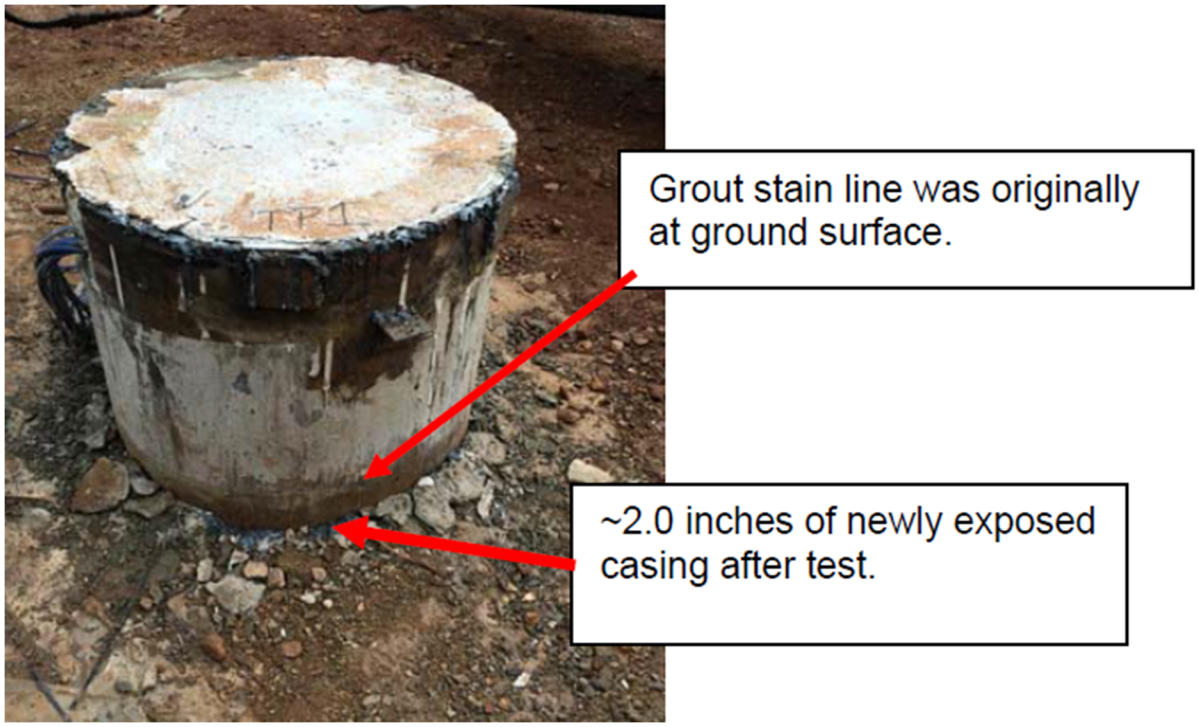


Fig. 5. Test Pile 1 following Statnamic test (Bailey and Muchard 2015)

PILE DESIGN

Considering the construction experiences during the test program and the load test results, 24-in and 30-in diameter, fully-cased piles were selected as design alternatives for the Contractor to select. The larger pile size was allowed since the 24-in test piles had been installed without issue, and the larger 30-in diameter piles were not expected to be more difficult to install while allowing for fewer individual pile installations. Since the 24-in test piles had been installed with relative ease, the design team, including the

Contractor as part of an early involvement procurement process, felt utilizing slightly larger 30-in piles was feasible with little additional construction risk. The 30-in piles were designed as fully-cased, end-bearing piles where the axial capacity of the piles is limited by the structural capacity of the section as was demonstrated by the load tests. Uncased rock sockets were not included since there was no uplift demand and rock socket instability had been an issue during the load test program. Tie-down anchors at the Pier 1 footing were included to handle uplift loads during construction.

The piles casings are ½-in thick wall steel pipe with a minimum yield strength of 45 ksi. The piles are cast with a 7,000 psi self-consolidating concrete mix. The piles are unreinforced except for the steel casings and a small reinforcing cage at the top that facilitates a connection to the reinforced concrete pile cap. The maximum factored axial demand on a single pile is 2,776 kips. Piers 1 and 2 utilize groups of 14 and 19 piles, respectively.

PRODUCTION PILE INSTALLATION

Veit, the same foundation contractor that installed the test piles, was selected to install the production piles. Veit utilized similar equipment as was used for the test program although some components were larger due to the increase in pile diameter. A Bermingham BHD80 drill head and lead system attached to a Terex HC275 crawler crane was used in conjunction with an Atlas Copco QL200S DHH and Robit ROX+ pilot and ring bit system to simultaneously drill and advance casing.

The production piles were installed without significant issue. Although, at times drill rates did slow to as much as approximately 1 ft/hr. Production rates recorded during test and production pile installation are plotted versus depth in Fig. 6. There is a strong negative correlation between production rate and pile depth that become asymptotic with zero in the rock. Production rate is also influenced by pile diameter despite differences in DHH size and other compensating differences in equipment. Worn

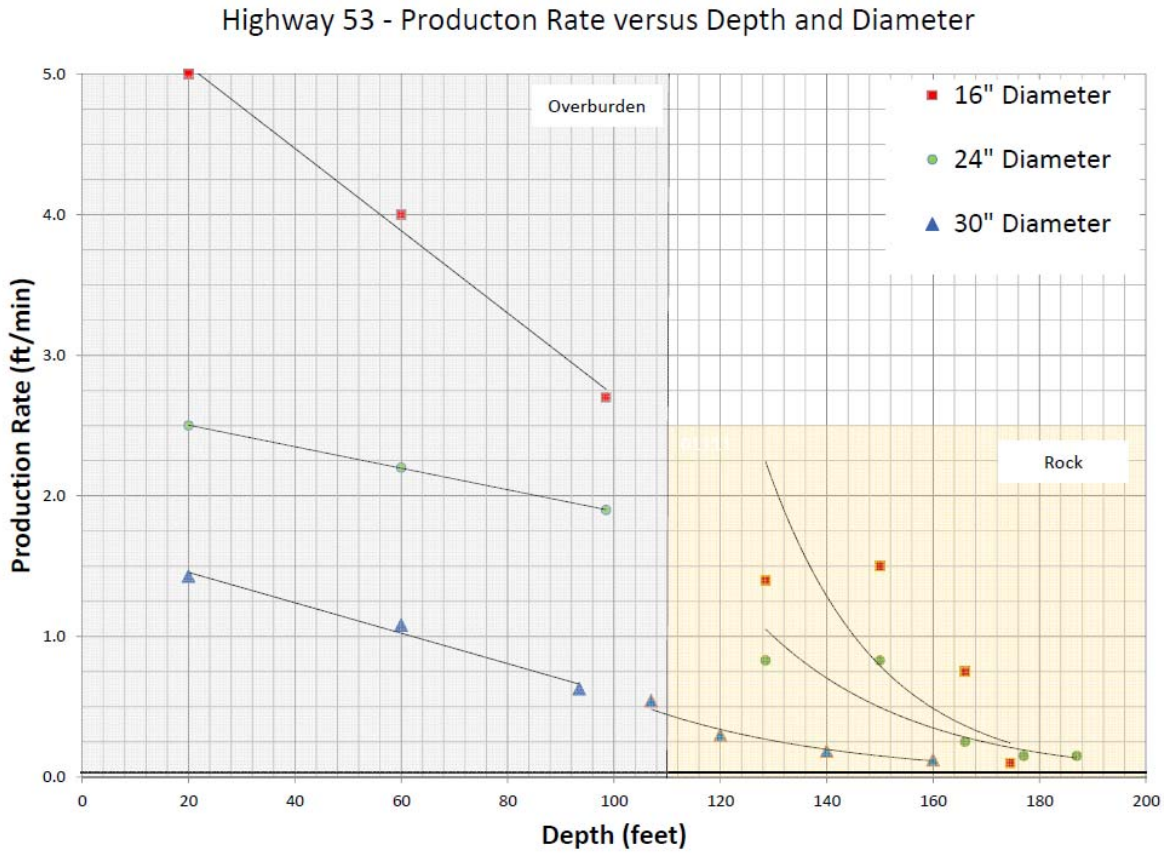


Fig. 6. Drilling Production versus depth for various diameter

bits, worn hammer internals, and insufficient supply of compressed air are also believed to have contributed to slow drilling at various times; however, depth appears to be the largest influencing factor.

As was observed during the test pile program, the cased holes drilled with the reverse circulato DHH equipment resulted in clean excavation bases without requiring additional cleanout effort, as determined by sounding with a weighted tape.

PRODUCTION PILE PERFORMANCE

As part of a comprehensive instrumentation and monitoring program for the project, two of the piles at Pier 2 are instrumented with strain gages, one in the northwest quadrant of the footing and one in the southeast quadrant of the footing. Each of the instrumented piles has 13 levels of gages with 4 gages at each level. Average force at each gage level is presented in Fig. 7 for measurements take in March of 2017, after the piers were completed and girders placed but before the start of deck construction. The average top of pile force is approximately 1,035 kips bassed on the top gage level in each pile. This per pile force is consistent with the factored per pile dead load of 1,380 kips considering it does not included weight of the deck and nonstructural attachments.

The data indicate little to no load is shed in side resistance, which is consistent with observations during the design-phase load test program. In fact, the data indicate there is a net increase in load due to the accumulation of negative skin friction. The development of drag load due to negative skin friction is consistent with the conclusion of Fellenius (2006) that negative skin friction will always develop when installed through a softer stratum into a stiffer bearing stratum. Drag load was anticipated and considered for design utilizing the procedures of the MnDOT *Geotechnical Engineering Manual* (2013). The MnDOT procedures utilize the neutral plane method within the LRFD framework as described by (Siegel et al. 2013). The neutral plane analysis predicted 245 kips of drag load at neutral plane depth of 134 ft. The trends of the data suggest a drag load of 140 kips at a neutral plane depth of 80 ft.

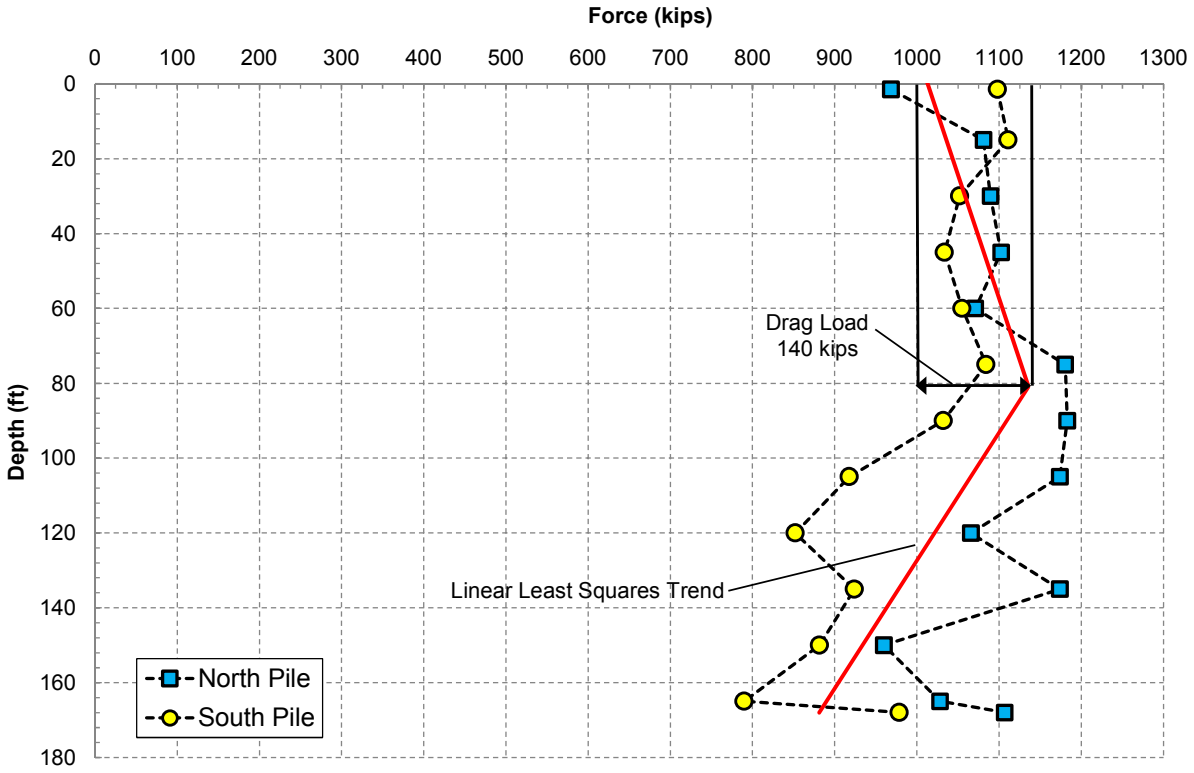


Fig. 7. Pier 2 Instrumented Piles, Load versus Depth

OBSERVATIONS AND CONCLUSIONS

Large diameter (>12 in) micropile style equipment is capable of installing steel casings through cobble and boulder overburden and penetrating hard bedrock. The pilot and ring bit systems from two separate manufacturers performed well with the exception of the Elemex ring bit becoming detached during the first two attempts to install the 16-in test pile. Based on recorded production rates for all three diameter piles, installing cased piles much deeper into such hard rock would likely require more aggressive means of advancement. Supplying an adequate volume of compressed air to efficiently operate the DHH and evacuate the cuttings, particularly cuttings with a relatively high specific gravity, is necessary to drill effectively. The drilling method leaves a clean excavation base.

As hypothesized and demonstrated during the load test program, high geotechnical resistance in excess of the structural strength is achievable in hard and competent bedrock. The bit systems cuts a slightly oversized hole necessary to advance the casing. The oversized hole substantially reduces the magnitude of side resistance even after the small annular void collapses around the exterior circumference of the casing following installation. Strain gage measurements from instrumented production piles also indicate very low side resistance.

Negative skin friction developed in the production piles despite the drilled installation. The neutral plane method produced a conservative prediction of drag load based on preliminary strain gage measurements during construction.

ACKNOWLEDGMENTS

The authors would like to acknowledge and thank the many people who collaborated to make this challenging project a success. Specifically the authors would like to thank foundation superintendent, Rill Oveson of Veit; MnDOT geotechnical engineers Derrick Dasenbrock, P.E. and Gary Person, P.E.; lead bridge engineer Vince Gastoni, P.E., of Parsons; load test specialists Joe Bailey, P.E. and Mike Muchard, P.E. of AFT; and engineer and geologist John Turner, Ph.D., P.E., P.G. of Dan Brown and Associates. Finally, the authors acknowledge the wisdom of MnDOT, particularly Kevin Western, P.E., and Pat Huston, P.E., for recognizing the benefits of full-scale foundation load testing and for leading the charge on this exciting bridge project.

REFERENCES

ASTM D7383, 2010. *Standard Test Methods for Axial Compressive Force Pulse (Rapid) Testing of Deep Foundation*, Annual Book of ASTM Standards, ASTM International, West Conshohocken, Pennsylvania. 9 p.

Baily, J.D. and Muchard, M.K, 2015. *Final Report of Statnamic Load Testing: T.H. 53 at Rouchleou Mine Water Crossing*. Applied Foundation Testing, report dated 26 May 2015, pp. 10-11.

Iverson, N.W. and Pedrson, E., 2017. *Highway 53 – Down the Hole Hammer Pile Case Study: Comparing Diameter to Production Rate*. Proceedings: 65th Annual Geotechnical Engineering Conference, Minnesota Geotechnical Society, February 24, 2017, 7 p.

Fellenius, B. H. 2006. "Results from long-term measurement in piles of drag load and downdrag." *Can. Geotech. J.*, 43(4), pp. 409-430.

MnDOT, 2013. *Geotechnical Engineering Manual*. MnDOT Geotechnical Engineering Section, Maplewood, Minnesota, pp. 97-98.

MnDOT, 2017. *Hwy 53 Relocation: Visualizations*. project website, http://www.dot.state.mn.us/d1/projects/hwy53relocation. Accessed 17-02-10.

Siegel, T.C., Lamb, R., Dasenbrock, D., and Axtell, P.J. 2013. ‘‘Alternative Design Approch for Drag Load and Downdrag of Deep Foundations within the LRFD Framework.’’ Proceedings of the 38th Annual Conference on Deep Foundations, 2013, Phoenix, AZ, USA, pp 23-39.

Severson, M.J., R.W. Ojakangas, P. Larson, and P.K. Jongewaard. 2010. “Geology and Stratigraphy of the Central Mesabi Iron Range.” *Field Guide to the Geology of Precambrian Iron Formations in the Western Lake Superior Region, Minnesota and Wisconsin*. Duluth: University of Minnesota Duluth, 38 p.

Wolff, J.F. 1917. ‘‘Recent geologic developments on the Mesabi Iron Range.’’ Minnesota: American Institute of Mining and Metallurgical Engineers, Transactions, v. 56, pp. 229-257.

CASE STUDY: LARGE DIAMETER HELICAL PILE FOUNDATION FOR HIGH VOLTAGE TRANSMISSION TOWERS IN SOFT GLACIAL DEPOSITS

Kashif Butt, Almita Piling, Edmonton, Alberta, Canada

John Dunn, Almita Piling, Edmonton, Alberta, Canada

Nicholas Gura, Kiewit Engineering Group, Omaha, Nebraska

Matt Hawley, Kiewit Engineering Group, Omaha, Nebraska

ABSTRACT

This paper presents the results of a static load testing program completed on helical pile foundations for the replacement of high voltage transmission line tower structures. The foundations were part of the Northeast Grid Reliability Project (NGRP) for the Public Service Electric & Gas Company (PSE&G) near Newark, New Jersey. Structure foundations "anchor bolts down" was a design build contract model with the superstructure as bid-build.

The soil stratigraphy along the alignment generally consisted of fill over about 10 ft of organic deposits underlain by up to 260 ft of normally consolidated glacial lake clays and silts. Additional project challenges included working under/adjacent the existing live high voltage lines, narrow site access due to environmental permits, foundations in a tidally influenced area, and pile projections in the order of 10 feet to meet the 10 year flood level requirements.

The helical piles were constructed of 12.75 inch diameter open ended pipe piles with 36 to 40 inch diameter helices. A total of seven static load tests (compression and tension) were completed on 60 ft and 90 ft long piles, using both welded and mechanical pile splices. To evaluate pile-soil setup in the sensitive fine grained soil and determine representative longer term installation torque factors (Kt) for the production piles, the static load tests were performed 7 to 49 days after pile installation.

Helical piles were found to be the most cost effective foundation alternative for this project. The required length of helical piles was less than other alternatives for similar allowable axial capacity. Helical piles with mechanical splices were installed for the varying structure foundations including tangent and heavy deadend, to a deadend monopole. Installation of 448 production piles (34,320 linear ft) was completed in three months. The installation timeline was critical to meeting the semi-annual PSEG outage for switching the old and new structures. Helical piles employing a mechanical splice resulted in an efficient and effective foundation solution for the conditions encountered on the project.

Keywords: helical piles, static load test, normally consolidated fine grain soil, transmission tower foundations

INTRODUCTION

NGRP consisted of three project sections beginning in North Arlington, NJ and terminating in Kearny, NJ. The project alignment spanned low lying inundated wetlands and industrial areas. Figure 1a illustrates the project alignment which is about six miles long. Helical pile foundations were selected for a total of 17 structures, primarily located in the northern most three miles of the project alignment. Most of the three miles was located in tidally influenced wetlands. As such, access for installation of the foundations including the test locations consisted of two to as many as eight layers of 12 inch thick timber crane mats. The superstructures were placed via helicopter. Figures 1b and 1c are photos of Test Site 3 and one of the typical production pile locations, respectively. Three types of helical piles were designed to meet the variety of foundation loadings, sub-surface soil conditions, and the allowable horizontal and vertical movement of

 © 2017 DFI Annual Conference, New Orleans, LA, USA

1.0 inch. The subjects of this paper are the transmission towers supported by helical piles and the static load testing program.

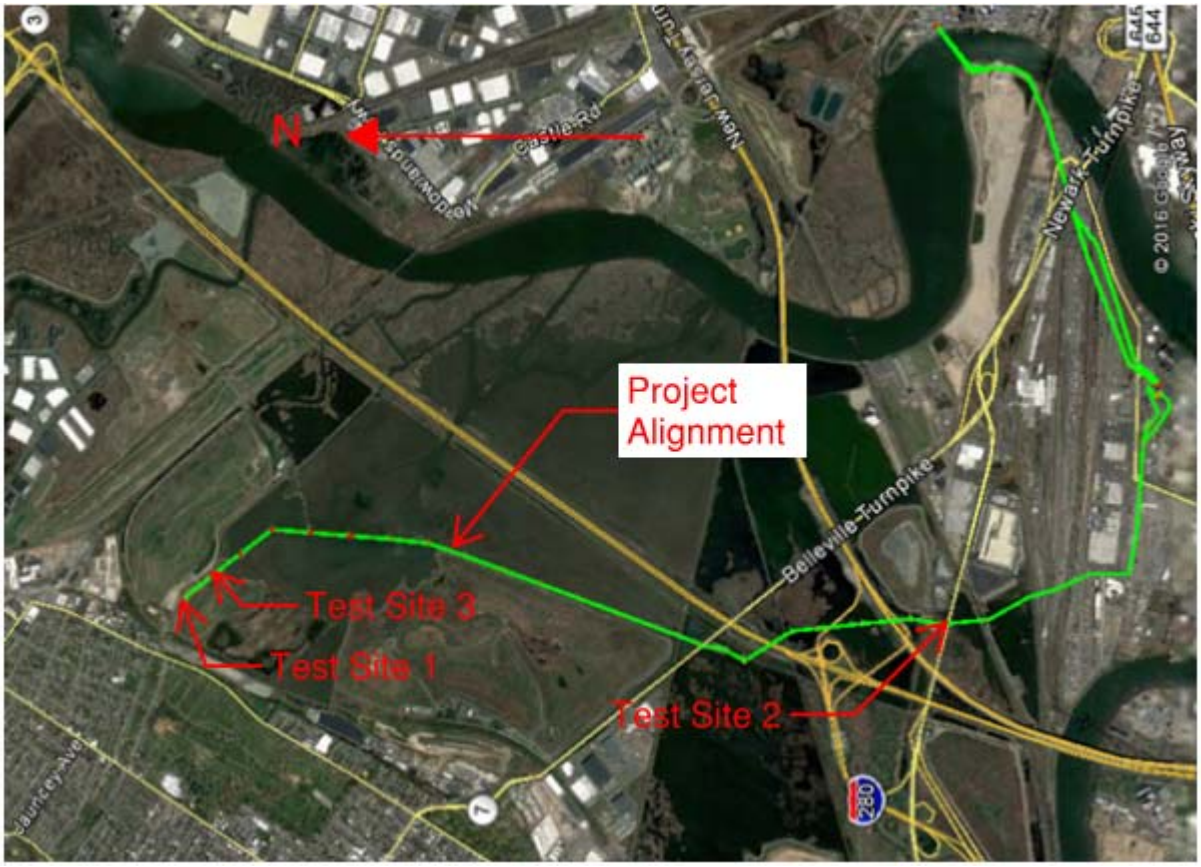


Figure 1a. NGRP Project Alignment

The initial test program consisted of two test sites, herein referred to as TP1 and TP2, did not consider a pile-soil setup time between the end of installation and static load testing similar to a driven pile in sensitive fine grained soil. The results of the initial static load testing and installation presented two challenges to the project team. First, the axial compression and tension capacities from the static load tests were about one-third less than the predicted capacity from the static analysis, indicating more piles would be required than had been budgeted. Second, the production rate of the pile installation was substantially slower due to the welding requirements and field conditions, indicating the team would have to mobilize more equipment and personnel than had been budgeted to meet the scheduled shutdown.

To address these issues a third test site (TP3) was selected for static load testing. TP3 was located at the adjacent structure to TP1 about 700 to 800 ft southeast. TP3 utilized a mechanical connection, developed by Almita, to minimize the splice time of the pile segments and included a waiting period of approximately two weeks between installation and testing to evaluate potential pile-soil setup. All of the test piles were installed in sacrificial locations adjacent to the permanent structures.



Figure 1b. Test Site # 2



Figure 1c. Typical Production Pile Location

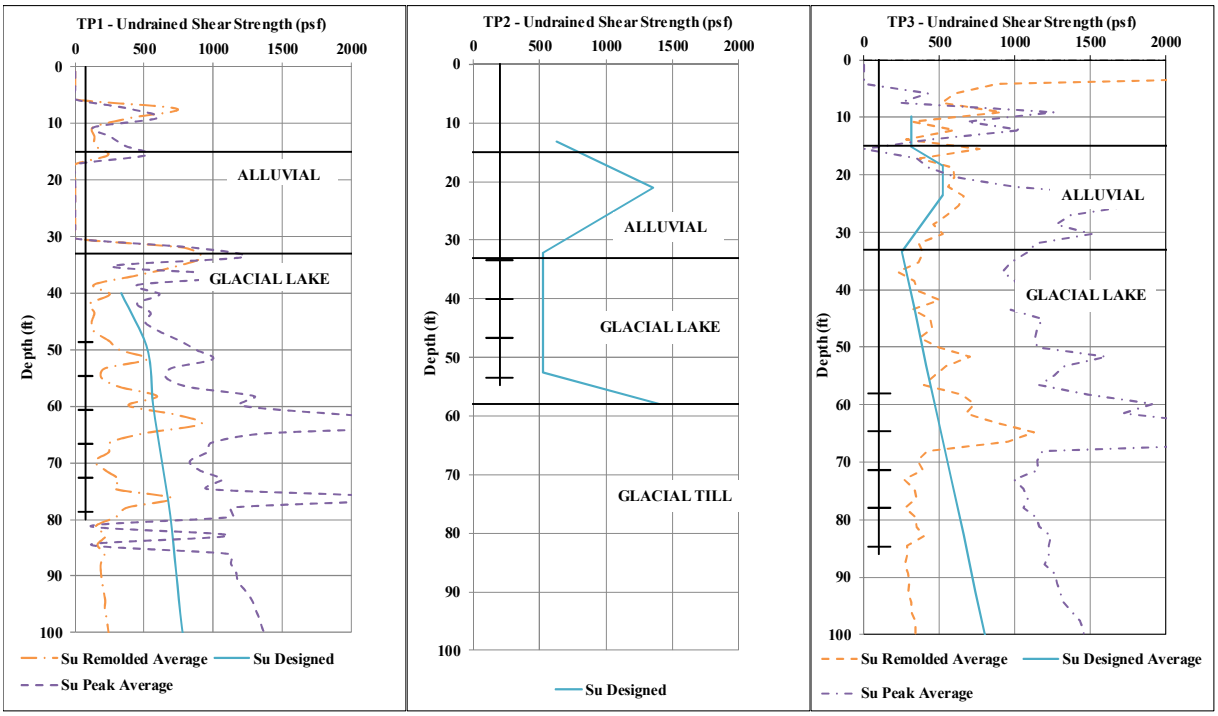
GEOTECHNCIAL INVESTIGATION AND SUBSURFACE SOIL CONDITION

Paulus, Sokolowski and Sartor, LLC carried out site specific geotechnical investigation including boring and CPT soundings close to the proposed new structure locations. Portions of the alignment were inaccessible and therefore no borings or CPTs were performed near approximately half of the structures. All of the borings and CPTs were completed on land, so additional consideration was necessary for structures located in the water 20 to 50 ft from the boring location. Standard penetration testing (SPT) was completed in boreholes from ground surface into the glacial lake deposits. Below that depth, drilling was continued without sampling to determine the depth of glacial till deposits. CPT soundings were also completed at selected locations adjacent to the borings to refusal depths. Laboratory testing on the collected samples consisted of Atterberg limits, moisture contents, unconfined compression testing, consolidation testing, soil corrosivity tests and chemical analysis.

Soil stratigraphy along the alignment was generally consistent with fine grained glacial lake deposits overlying glacial till or bedrock. The uppermost stratum (at the static load test locations) consisted of undocumented fine to coarse sand fill with construction and/or household debris underlain by layers of organic material, alluvial sand, glacial lake deposits and glacial till. Many of the locations were in inundated areas of the meadowlands and therefore the fill was not always present. The combined depth of the fill, organics and alluvial sand was generally 30 ft or less. According to the borings and CPTs, the depth of the glacial lake deposits was typically greater than 100 ft but ranged from 60 ft to more than 200 ft. The glacial lake deposits generally consisted of normally consolidated clayey silt to silty clay with thin layers or lenses of silt and fine sand.

Soil stratigraphy at test locations TP1 and TP3 were similar with the glacial till at depths of about 200 ft. The borings near TP 2 presented glacial till at a depth of 75 ft. Undrained shear strength estimated from N-values and CPTs are presented in Figure 2 along with the design profile. The undrained shear strength for locations 1 and 3, where SPT was not conducted or zero blow count soils were encountered, was calculated using the Stress History and Normalized Soil Engineering Parameter (SHANSEP) concept. Shear strength was calculated using $S_u = 0.21 \times \sigma_v'$; where S_u is the undrained shear strength and σ_v' is the effective vertical stress. Design undrained shear strength parameters for location 2 were estimated from SPT completed in the glacial lake deposits. A CPT was not performed in the area of TP2.

Groundwater was approximately 2 ft below the ground surface based on the dissipation tests completed during CPT testing at TP1 and TP2. Groundwater depth at TP3 was not established accurately due to use of mud rotary drilling. The groundwater was assumed at ground surface for helical pile design for all test locations.



(a) (b) (c)

Figure 2: Peak, remolded, and design undrained shear strength: a) TP1, b) TP2, and c) TP3

HELICAL PILE DESIGN

Aside from one monopole structure, the typical structure was a four legged lattice tower. Each leg was designed with a separate pile cap consisting 4 to 9 helical piles. The center pile was vertical and the peripheral piles were battered at angles of 3 to 15 degrees. All piles were manufactured in 30 ft lengths, so total pile lengths were either 60 or 90 ft long and utilized 36 inch or 40 inch diameter helices as the bearing elements. Varying helix diameters were not used on individual piles or structures. The helices began approximately one foot above the pile tip and were spaced at two times the helix diameter. The static analysis used traditional helical pile capacity analysis evaluating both individual bearing and cylindrical shear failure modes. The lower of the two calculated values was used for the static calculations.

Since a static load test was planned a factor of safety of 2 was used in the design and static analysis. The factor of safety was applied to the extreme loading conditions. In addition to the factor of safety of 2, the owner required an additional factor of 1.1 and 1.25 be applied to the factor of safety for lattice and monopole structures, respectively. Meaning the required factor of safety increased to 2.2 and 2.5 for the lattice and monopole foundations, respectively. The concept of the additional load factors or higher safety factors is to help ensure that the superstructure fails before the foundation, since it is typically more economical to replace the super structure as opposed to the foundation.

Based on the pile group configurations, design loads ranged from 48 to 108 kips in compression and 5 to 88 kips in tension. The corresponding required ultimate capacities were 96 to 216 kips in compression and 10 to 176 kips in tension.

STATIC LOAD TEST PROGRAM

One of the main purposes of the static load test program was to establish an installation torque to capacity ratio, which is typical of helical pile projects. The relationship between ultimate pile capacity (Qt), torque (T) and an empirical torque factor (Kt) can be expressed as:

$Qt = Kt \times T$

The Kt factor established by the load test program is then used for the production pile installation as a quality control /quality assurance measure.

The initial test program at TP1 and TP2 was based on the different helical pile designs, structures and load conditions. Each site had a dedicated pile installed for static axial compression and tension load tests. TP1 consisted of a 90 ft long helical piles with six – 36 inch-diameter helices. TP2 consisted of 60 ft long helical piles with four -40 inch diameter helices. TP3 consisted of a 90 ft long helical pile with five-40 inch-diameter helices. Table 1 summarizes the test pile configuration. Test sites TP1 and TP2 did not have specified wait times between installation and testing. The set-up time of seven days or less for these two sites were purely the product of pile installation time, relocation of equipment and work not being performed on weekends.

Table 1: Summary of test pile configuration

Test Pile	Pile Length, ft	Pile Dia, in	Pile Wall Thk, in	Helix Dia, in	Helix Thk, in	No. of Helices
TP1	90	12.75	0.5	36	1	6
TP2	60	12.75	0.5	40	1	4
TP3	90	12.75	0.5	40	1	5

TP3 utilized a mechanical connection, developed by Almita, to minimize the splice time of the piles and included a wait period of approximately two weeks between installation and testing to evaluate potential pile-soil setup. At the completion of the load testing at TP3, the test piles and reaction piles were extracted for inspection of the mechanical connection. The mechanical connection and its components were inspected for any deformation or damage due to the torque applied during installation, removal or loading applied during the static load testing. The performance of the connection was found to be satisfactory, and was employed for all production piling.

INSTALLATION MONITORING

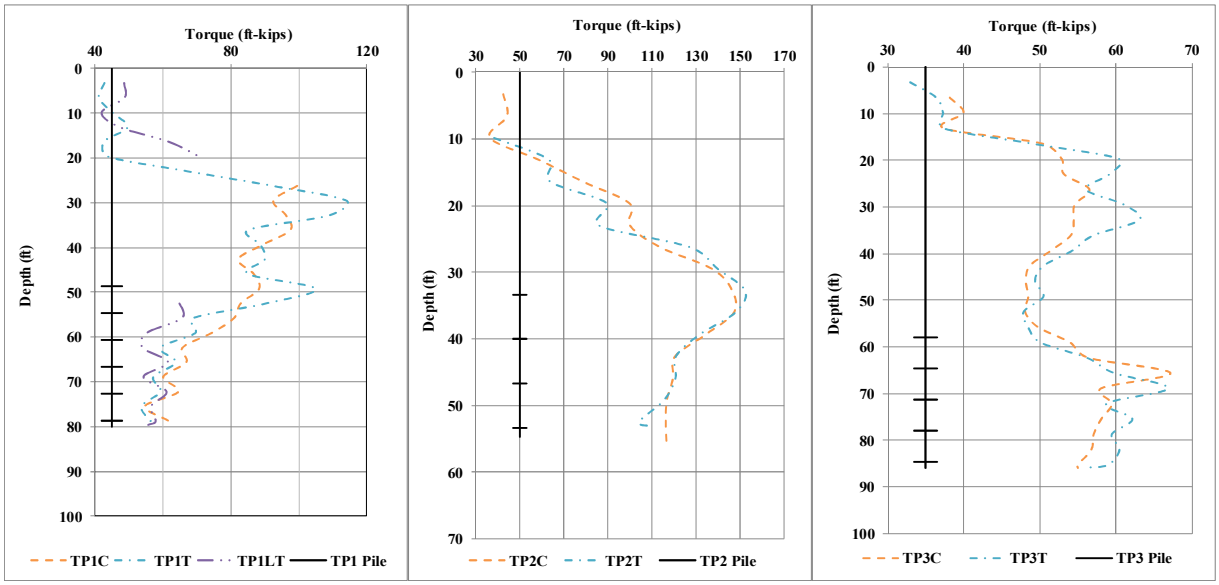
The test piles and reaction piles were installed using a drive unit mounted to a tracked excavator. The drive unit contains a hydraulic motor that provides a maximum torque of 250 ft-kip to rotate the helical pile into the ground. Installation torque profiles are provided in Figure 3. Torque was recorded continuously by a data logging system on the install machine. The final torque was determined by taking an average of the recorded installation torque over the final 6 feet of embedment.

The near-surface conditions varied between the test sites, but all sites required several layers of timber crane mats for equipment access. Due to construction debris, municipal waste and near surface organic deposits voids several feet deep developed around each helical pile location. At TP1 dry, un-compacted sand was

placed around the pile shaft during installation of the final section. At TP2 no backfill of any type was placed around the pile shaft and at TP3 loose woodchips were placed around the pile shaft after installation. The fill was used to fill holes and provide personnel a safe working surface for setup and execution of the load tests. Groundwater was within a foot of the ground surface at TP2 and TP3. Groundwater at TP1 was approximately 3 feet below the ground surface.

TEST SETUP

The static load tests were performed in general accordance with ASTM D1143-07, D3689-07, and D3966. The quick method was used for the compression and tension tests with 10 minute load durations. At the request of the owner, a one-hour hold at the maximum test load was performed. Displacement monitoring was accomplished with Linear Variable Displacement Transducers (LVDT), as well as mechanical dial gauges for backup. A custom data logger system was used to automatically record the hydraulic jack pressure, the load cell, and the LVDTs at thirty second intervals. The data was also manually recorded at 1, 5 and 10 minute intervals as backup.



(a) (b) (c)

Figure 3: Test pile installation torque profiles; a) TP1; b) TP2; c) TP3

AXIAL TEST RESULTS

Load-displacement curves were prepared for each compression and tension test completed. Analysis was completed using the Brinch-Hansen 90% pile ultimate failure criteria. Load displacement curves for axial tests are shown in Figures 4 and 5. Compression and uplift capacities of the test piles and corresponding load at 1.0 inch displacement are summarized in Table 2. The “C” or “T” indicates compression or tension test. Test pile TP1-LT was originally the lateral test pile at site TP1 and was later tested in tension 49 days after it had been installed.

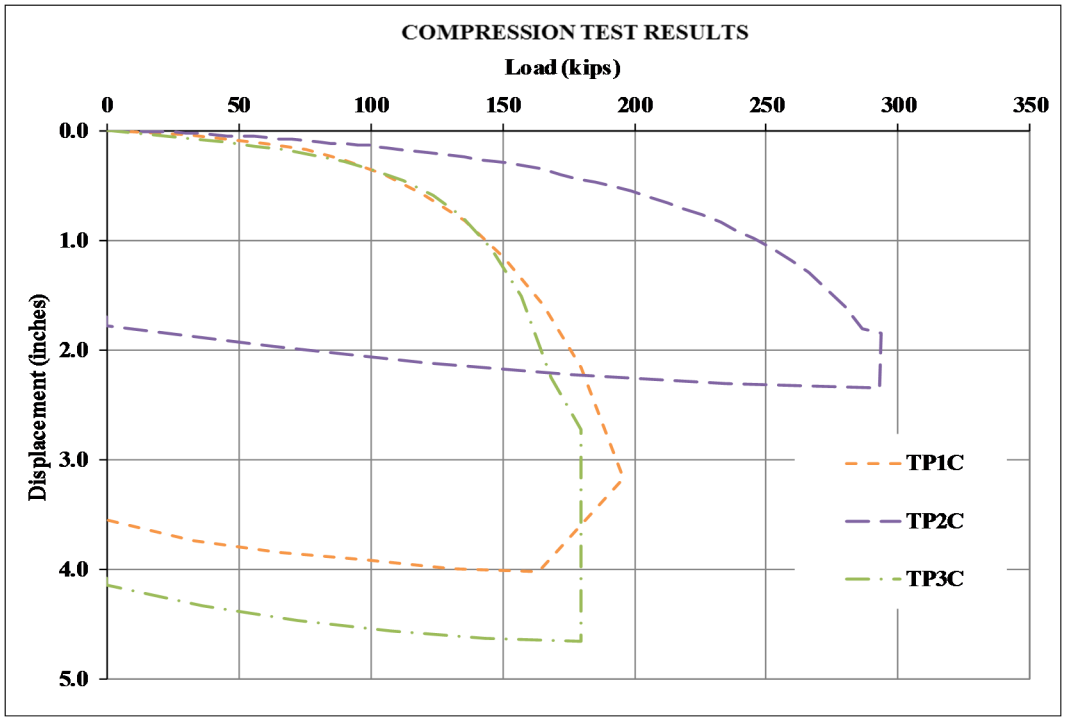


Figure 4: Compression test results

Table 2: Summary of compression and tension load tests

Test Pile	Set-up Time (days)	Ultimate Capacity (kips)	Capacity at 1.0" Displacement (kips)	Displacement at Ultimate Capacity (in)	Displacement at Ultimate Capacity as %age of Helix Dia.
TP1-C	6	193	149	4.0	11.1
TP1-T	7	168	156	2.0	5.5
TP1-LT	49	172	153	2.0	5
TP2-C	6	293	246	2.0	5
TP2-T	2	188	177	1.5	3.75
TP3-C	15	180	144	2.7	6.75
TP3-T	13	151	123	2.3	5.75

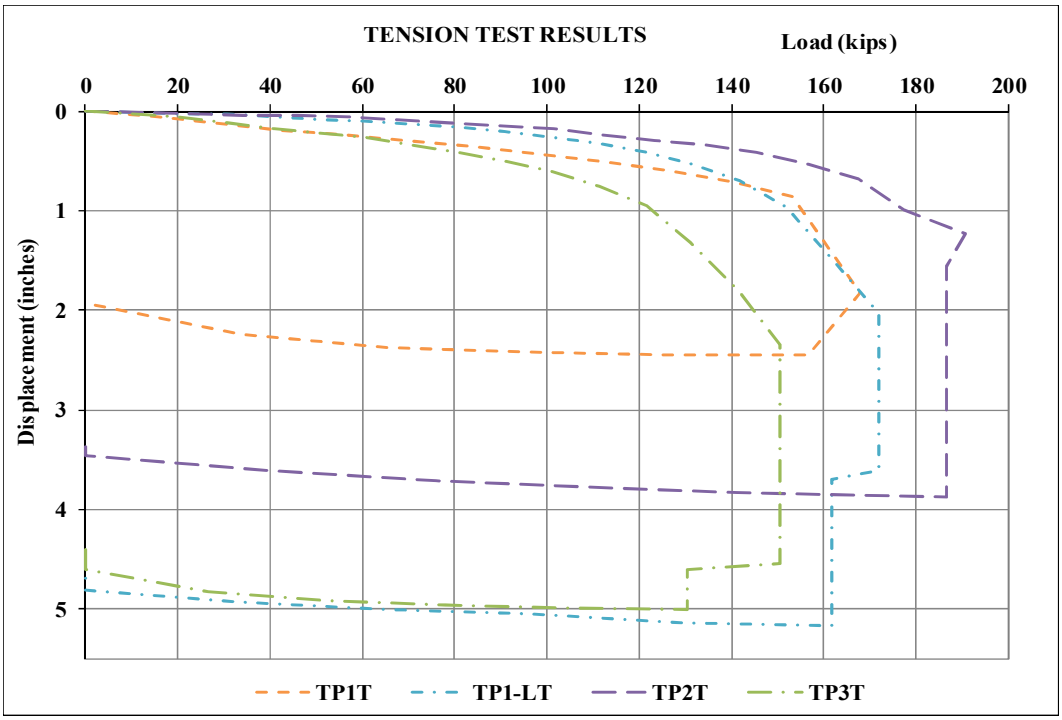


Figure 5: Tension test results

Compression load tests were carried out on piles TP1-C, TP2-C, and TP3-C at 6 to 15 days after installation. The performance of test piles TP1-C and TP3-C was similar up to a compressive load of 150 kips. Settlement of both piles started increasing at a faster rate associated with plunging failure beyond 2 inches of displacement. Compression capacity of TP1-C was slightly more than TP3-C. The compression test at TP2-C was terminated prior to achieving failure load.

Tension load tests were carried out on piles TP1-T, TP1-LT, TP2-T, and TP3-T at 2 to 49 days after installation. Two tension tests were completed at TP1 (TP1-T and TP1-LT) at 7 and 49 days after installation.

The initial response of all piles to loading was relatively linear in compression and tension testing. As a result, the measured displacement at around 150 kips was close to 1.0 inch for all piles. The vertical movement includes settlement of helical plates, elastic shortening/elongation of shaft, and movement of mechanical coupler. The displacement of test piles TP1-C and TP3-C was greater than TP2-C when approaching the failure load.

Although the ultimate capacity of TP3-C was slightly less than TP1-C, the resulting Kt factor was about 6% greater, indicating an increase in capacity versus time when relating capacity to installation torque. Higher axial capacities for TP2-C are due to encountering more competent soils, as indicated by the torque readings.

The tension test data indicated an increase in Kt factor from 1.7 at 2 days to 2.7 at seven days of setup. There was not a significant increase in the Kt factor from seven to 13 days. The 49 day tension test at TP1-LT at 49 resulted in a Kt factor 3 indicating increasing trend of Kt. The increased Kt factor was about 8% between the 13 day and 49 day test time. The Kt factor for compression and tension of the test piles are summarized in Table 3.

Table 3: Capacity to Installation Torque Ratio - Kt

Test Pile	Set-up time (days)	Capacity (kips)	Final Torque (ft-kips)	Kt (1/ft)
TP1-C	6	193	62.4	3.1
TP1-T	7	168	61.4	2.7
TP1-LT	49	172	58.1	3.0
TP2-C	6	293	123.7	2.4 (1)
TP2-T	2	188	111.1	1.7
TP3-C	15	180	55.0	3.3
TP3-T	13	151	55.0	2.8

(1): The compression test on TP2-C was terminated prior to reaching pile failure; the resulting Kt factor is therefore artificially low.

Figure 6 illustrates the change in Kt with increasing soil setup time. Based on the observed trend, the correlation between installation torque and long term capacity (Kt) was selected as 3.0 and 3.5 for tension and compression, respectively.

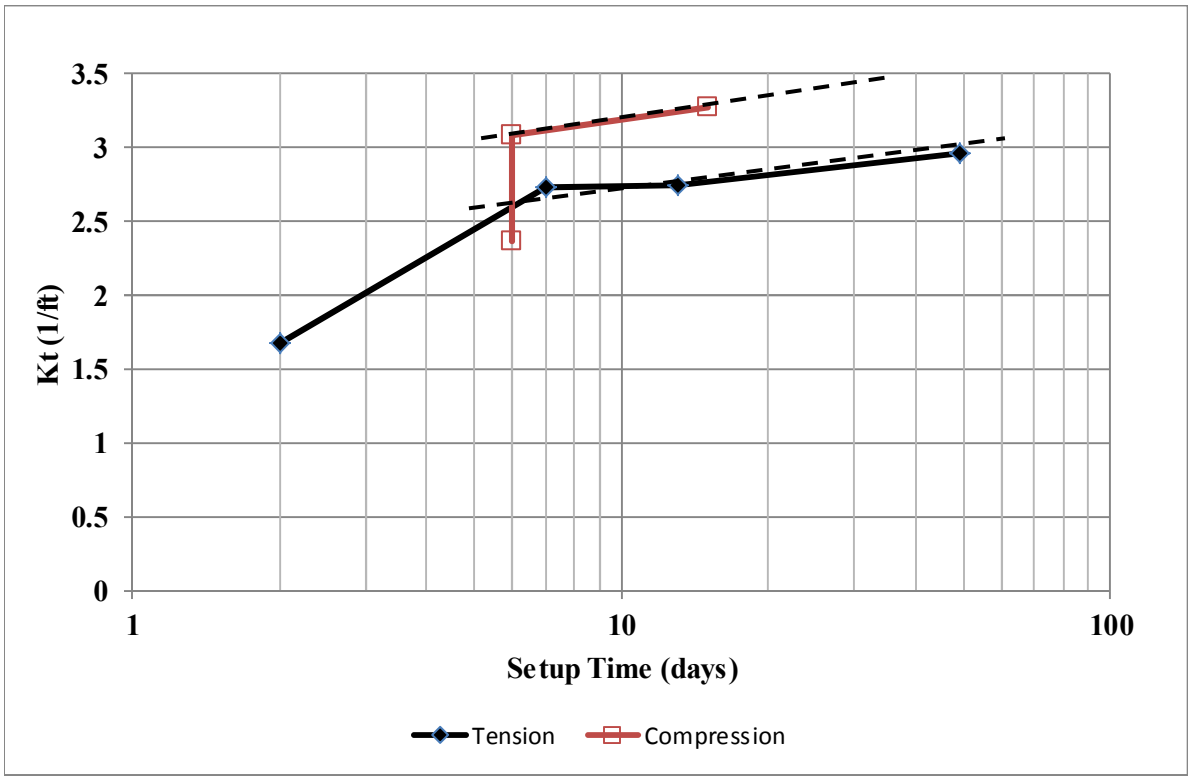


Figure 6: Torque Factor, Kt vs set-up time

SUMMARY AND CONCLUSIONS

The results of the static load test program allowed the project team to develop site specific Kt factors for the production pile quality assurance / quality control program. The evaluation of pile-soil setup over longer periods permitted the team to optimize the design and limit the amount of re-design and additional required piles. Ten of the 17 structures did not require additional pile to be added; however, the other seven structures resulted in 44 additional piles. A total of 448 helical piles were installed within a timeline of approximately 3 months to meet the schedule.

The mechanical connections used on 12 connections did not show any adverse effects from install, load testing and removal. This helped the project team meet the production rates required to get the foundations installed according to the project schedule shutdowns.

REFERENCES

Brinch Hansen, J., 1963. Hyperbolic Stress-Strain Response, Cohesive Soils, Journal of Soil Mechanics Foundation Division, ASCE, Vol. 89, No. SM4, pp. 241 – 242.

Butler, H. D. and Hoy, H. E., 1977. User's Manual for the Texas Quick-Load Method for Foundation Load Testing, Federal Highway Administration, Office of Development, Washington, DC., 59 pp.

Davisson, M. T., 1972. High Capacity Piles, Proceedings, Lecture Series Innovations in Foundation Construction, ASCE, Illinois Section, Chicago, 1972, 52 pp.

International Code Council, Inc., 2009. 2009 International Building Code (IBC).

ASTM D1143/D 1143M-07 – Test Methods for Deep Foundations Under Static Axial Compressive Load (ASTM International, 2007a).

ASTM D3689-07 – Test Methods for Deep Foundations Under Static Axial Tensile Load (ASTM International, 2007b).

ASTM D3966/D3966M-07 – Test Methods for Deep Foundations Under Lateral Load (ASTM International, 2007).

RESIDUAL LOADS MEASUREMENTS IN DRIVEN STEEL H-PILES

Reda M. Bakeer, Intertek PSI, Jefferson, LA, USA, (504) 733-9411, reda.bakeer@psiusa.com

ABSTRACT

Measurements obtained during load testing of two steel H-piles driven at a site in Northeastern Mississippi are discussed. The general site conditions, equipment used, testing procedures and results of the pile load tests are presented. Both piles were tested in compression and one of the piles was subsequently tested in tension. The piles were instrumented with strain gauges and extensometers to measure the mobilized soil resistance and pile movement. Three different "zero strain" conditions were used to determine the mobilized soil resistance and residual loads due to driving or a load cycle. It was concluded that the effect of residual loads on driven piles could be significant. Driving residual loads influenced the magnitude and distribution of the load transfer curves more than those due to a load cycle. Results of the tension test were impacted by the residual loads from the previous compression test performed on the same pile.

Keywords: Steel piles, static load test, pile driving, residual load, instrumentation, extensometers, strain gauges

INTRODUCTION

Several factors affect the performance of a deep foundation system including the subsoil conditions, loading settings, pile type and installation method. Residual stresses develop in piles particularly due to pile driving, but they are typically not accounted for in the analysis (Fellenius 2002). Siegel and McGillivray (2009) presented an assessment of residual loads measured during load testing of instrumented auger-cast-in-place (ACIP) piles. The magnitude and distribution of residual stresses along the pile shaft and toe depend on the pile installation method, previous load cycles and time effects. Poulos (1987) reported that residual load due to driving at the pile toe is independent of pile driving equipment and may significantly affect the results of a pile load test. Hunter and Davisson (1969) reported results of pile load tests performed in compression on fully instrumented piles driven in cohesionless soils along with a discussion of the effects of residual loads. Tension loads of about 445 kN (100 kips) were measured at the pile toe after driving. Unloading residual compression load at the toe was detected as "apparent" tension since the instrumentation was zeroed prior to the test. The researchers suggested a graphical approach to obtain the "corrected" load distribution curves considering that residual load will dissipate following the tension test. Holloway et al. (1975) conducted a study on the effect of residual stresses due to pile driving and developed a computer software that accounts for residual loads. Briaud and Tucker (1984) suggested a method to account for residual loads based on the results of 33 pile load tests performed in mostly cohesionless soils.

CASE STUDY

Pile load tests in compression and tension were performed by the U.S. Army Corps of Engineers (USACE), Vicksburg District (VXD) on two fully instrumented steel H-piles at the site of the Ascalmore-Creek Tippo-Bayou control structure in the Yazoo River basin near Greenwood in Northeastern Mississippi. Results of the pile load tests were compiled by the USACE in two reports (VXD 1992 and Bakeer et al. 1993) and incorporated in the design and installation of the project production piles. Field exploration for the project consisted of six general (G) and fourteen undisturbed (U) sample type soil borings. Figure 1 shows the general locations of the soil borings (1 through 20) and test piles P1 and P2. The original ground surface at the site varied between Elev. +41.2 m (+135 ft) and +42. 7 m (+140 ft) NGVD (National Geodetic Vertical Datum). The design invert of the inlet channel was at about Elev. +31.7 m (+104 ft) NGVD. The subsoil profile (Fig. 2) consisted of high plasticity clay (CH) to a depth of 15.3 to 22.9 m (50 to 75 ft) underlain by alluvial sand to a depth of 29.9 to 39.3 m (98 to 129 ft) and then by Tertiary Claiborne sand to the 36.6 to

 © 2017 DFI Annual Conference, New Orleans, LA, USA

45.7 m (120 to 150 ft) depth. This was followed by Tertiary clay that extended to the maximum explored depth of 51.9 m. (170 ft). Groundwater was detected in the borings at Elev. +38.1 m (+125.5 ft) NGVD.

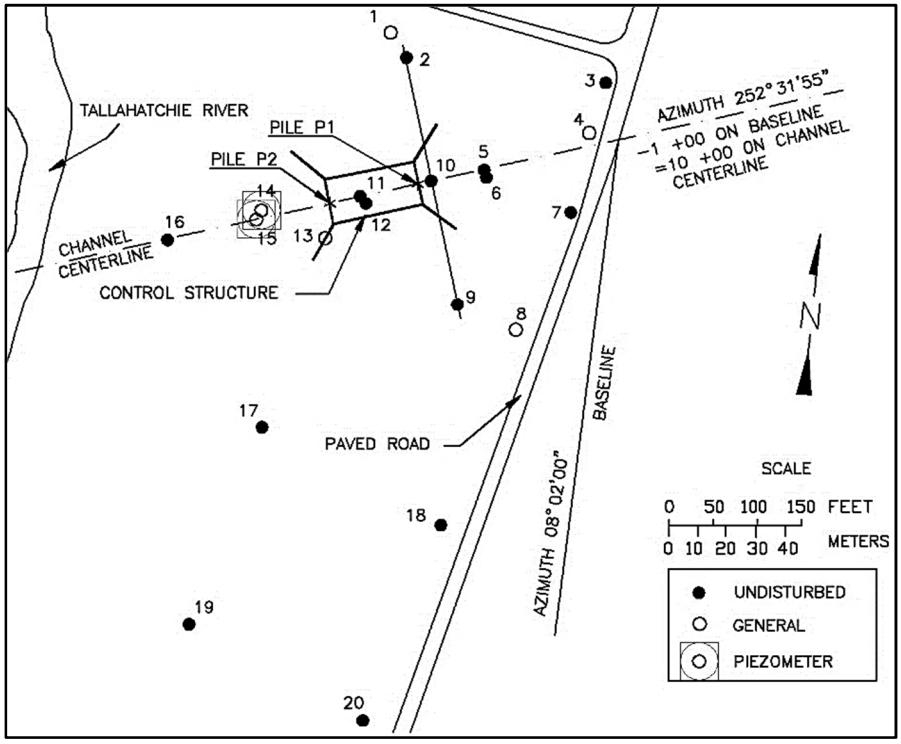


Fig. 1. Locations of the soil borings and test piles

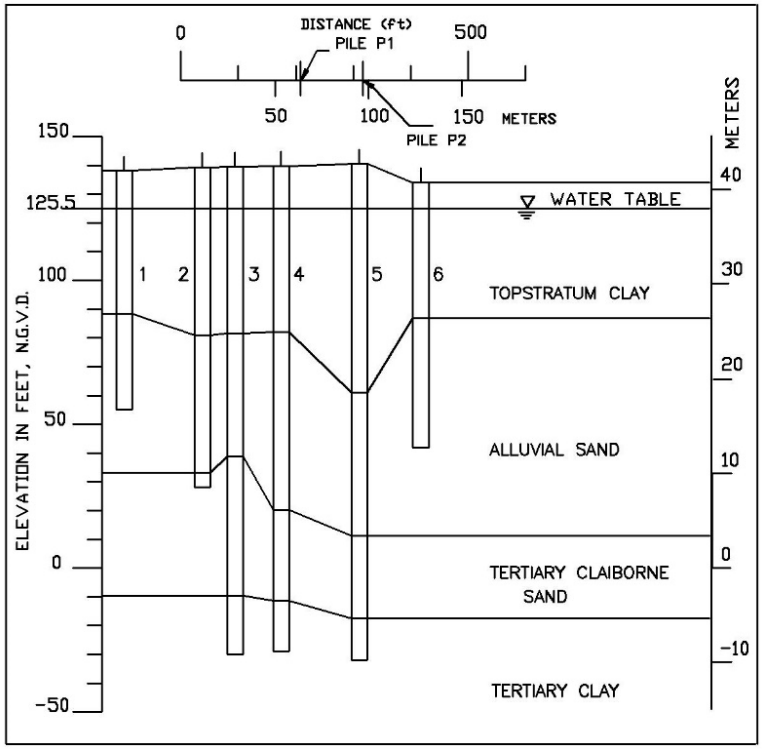


Fig. 2. Generalized subsoil stratification at the project site

Figure 3 shows the specific subsoil conditions in the immediate areas of the test pile inferred from the closest soil borings. Excavation for the control structure was made to depths of 7.8 m (25.5 ft) and 15 m (49 ft) prior to driving of piles P1 and P2, respectively. Therefore, forced dewatering was required due to the presence of sand strata near the excavation bottom. The clay stratum was generally normally consolidated to slightly overconsolidated. The undrained shear strength of the clay (S_u) was primarily obtained from unconsolidated-undrained (UU) triaxial tests. The undrained shear strength at the two pile locations was of medium stiff to stiff consistency and it increased with depth below the 10 m (33 ft) depth. Samples retrieved between the 3 m (10 ft) and 10 m (33 ft) depths contained organic and wood and exhibited high moisture content and liquid limit and lower wet density and undrained shear strength values. At the location of P1, a marked increase in the undrained shear strength with depth at the rate of about 3.2 kN/m^2 per m (20 psf/ft) was detected and a relatively weak zone was present at the 63.5 m (194 ft) depth near the interface with the underlying sand. The wet density profiles in the clay stratum indicated a small increase in the unit weight with depth from about 16 kN/m^3 (100 pcf) to about 17.6 kN/m^3 (110 pcf). Standard Penetration Test (SPT) N-values increased with depth in the dense to very dense alluvial and Tertiary sand strata with an average relative density (D_r) of about 70 percent. N-values averaged about 40 in the alluvial sand and 90 in the Tertiary sand with a measurable increase with depth recorded in the Tertiary sand. A significant decrease in the SPT N-value was noted at the P2 location at about 3.1 m. (10 ft) near the interface of the two sand strata and at the 37 m (121.5 ft) depth.

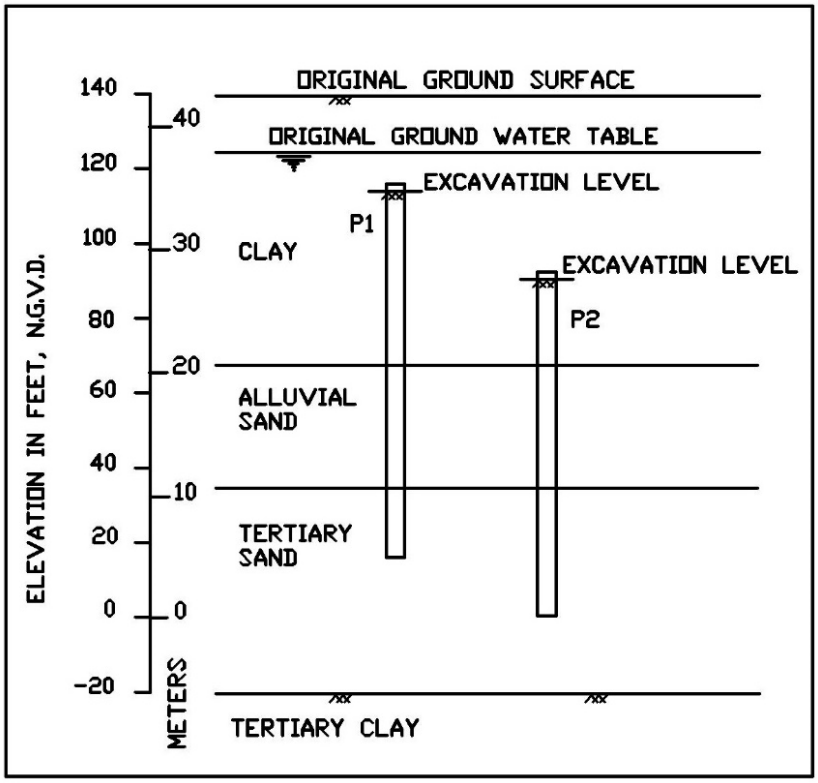


Fig. 3. Soil profiles at the specific locations of test piles P1 and P2

PILE INSTALLATION AND INSTRUMENTATION

Test piles P1 and P2 were 14 HP89 steel sections spliced to the required lengths of 30.5 m (100 ft) and 28 m (92 ft), respectively. The piles were instrumented at 3.1 m (10 ft) intervals with two electric strain gauges (A and B) placed on the opposite sides of the H-pile web. Each strain gauge was covered with a high strength epoxy resin and enclosed within a protective steel channel for waterproofing and protection. A

single acting diesel hammer (MKT DE-50B) with a rated energy of 40.7 to 57.6 kN-m (30,000 to 42,500 ft-lbs) was used to drive the test and reaction piles. The upper 3.1 to 4.6 m (10 to 15 ft) of clay were predrilled. Penetration resistance of test piles P1 and P2 are shown in Fig. 4 which correlated well with the subsoil profiles and SPT values. Driving blow counts remained relatively constant in the clay for P1 and a rapid increase was observed in the alluvial sand up to a depth of 24.5 m (75.5 ft). The blow counts then decreased within the next 1.5 m (5 ft) in the Tertiary sand and increased back gradually to the final penetration. The driving record of test pile P2 indicated similar resistance in the clay stratum and a steady increase within the alluvial sand to the 11.1 m (36.5 ft) depth where a decrease occurred until the Tertiary sands was penetrated where the resistance remained constant.

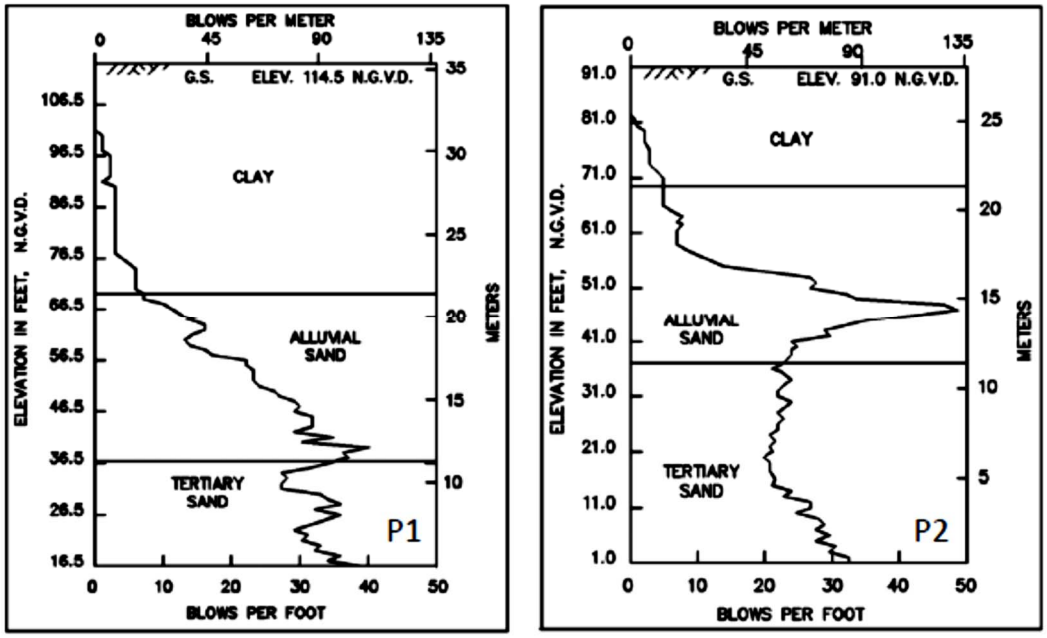


Fig. 4. P1 and P2 driving penetration resistance records

PILE LOAD TESTS

Load testing commenced 17 days after completion of pile driving. Cyclic compression load tests were conducted on both test piles and a cyclic tension test was subsequently performed on P1. Load was applied on the pile head by a Dudgeon 2,670 kN (300 ton) hydraulic cylinder jack acting against reaction frames attached to four 14 HP89 reaction piles with their toes driven 3.1 m (10 ft) deeper than the test piles. The reaction piles were driven first followed by P2 then P1. The four reaction piles were equally spaced diagonally at 2.6 m (104 inches) away from the test pile. Spherical bearing plates were placed on the pile head to assure concentric loading. Compression and tension loads were applied in equal increments of 222.5 kN (25 tons) up to a maximum compression load of 2,670 kN (300 tons). Load was applied at a constant rate of 0.3 kN/s (33.3 lbs/s) and was removed when it reached 445 kN (50 tons) above the previous cycle. The pile was then reloaded in increments to the next load interval. Scales were attached with epoxy to the reaction piles and both ends of the reference beam so that movement could be monitored by an engineer's level. A wire scale-mirror system was employed on both flanges of the test pile. Pile head movement was recorded at 150 s intervals during the loading or unloading phases which corresponded to a 44.5 kN (5 tons) load increment. For each load increment, the pile head movement was recorded at elapsed times of 120, 240, 480, 960, 1,920 and 3,600 s and thereafter at 1h intervals until the pile head movement was less than 0.25 mm/h (0.01 in/h). Strain gauge readings, wire-mirror readings and level readings for the test pile head, anchor piles and reference beams were also recorded at the completion of each load increment. The applied

load on the pile head was determined from the reading of the pressure gauge of the loading jack, which could result in an error of overestimation in the range of 10 to 20 percent of the applied load (Fellenius 1984). The average readings of the two extensometers was used to determine the gross movement. Net pile settlement in compression was calculated as the difference between gross settlement and total elastic rebound of the pile under zero load. The axial load along the pile shaft was calculated from the readings of the two strain gauges at the same level considering the following three different "zero strain" conditions:

1. Total pile load including residual loads due to driving and load cycles (**LRDC**) which is the difference in strain gauge readings before pile driving and during each load cycle.

2. Pile load including residual load due to load cycles, but excluding residual load due to driving (**LRC**) which is the difference in strain gauge readings after driving and during each load cycle.

3. Pile load excluding all residual loads due to driving and load cycles (**LRN**) which is the difference in the strain gauge readings within two consecutive load cycles.

The average of the two strain gauges on both sides of the pile web was used in the analyses. For test pile P1, readings of the strain gauges immediately above the toe (No. 2) were used to compute the toe load instead of the strain gauges No. 1 which were located too close to the pile toe and were affected by pile driving. For test pile P2, the third strain gauge location from the pile toe (No. 3) was used since one of the strain gauges at locations No.1 and No.2 was damaged during driving.

PILE LOAD TEST RESULTS

The measured load versus settlement curves for the test piles are given in Figs. 5 through 7. The net settlement curves were used to assess the failure loads. Settlement of P2 was generally higher than P1 at the same compressive load. This could be attributed to the differences in pile lengths and soil conditions at their locations. Figure 7 shows the response of test pile P1 in tension, during which it experienced an upward movement of about 50.8 mm (2 in) under a maximum load of 890 kN (100 tons).

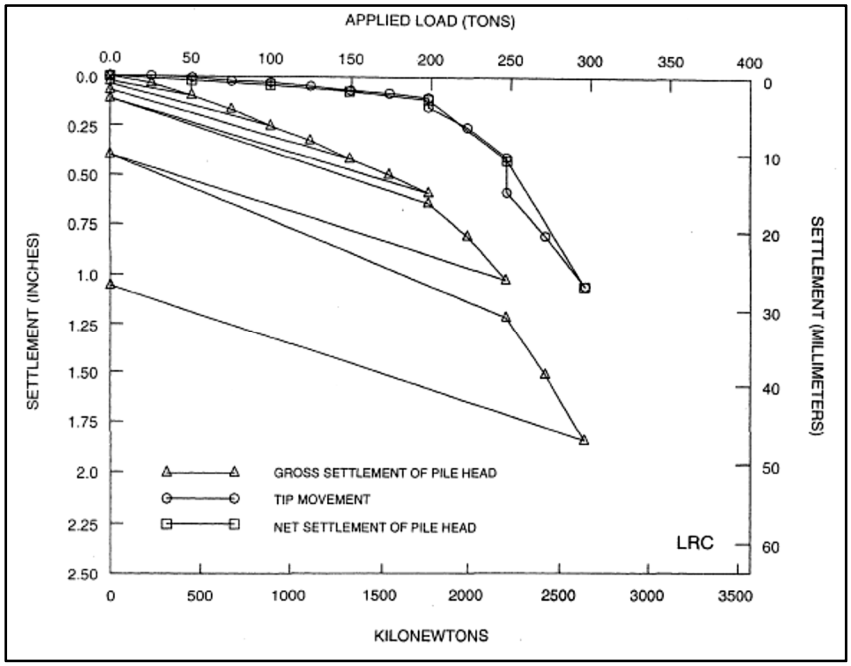


Fig 5. Load vs. pile head movement, P1 – Compression

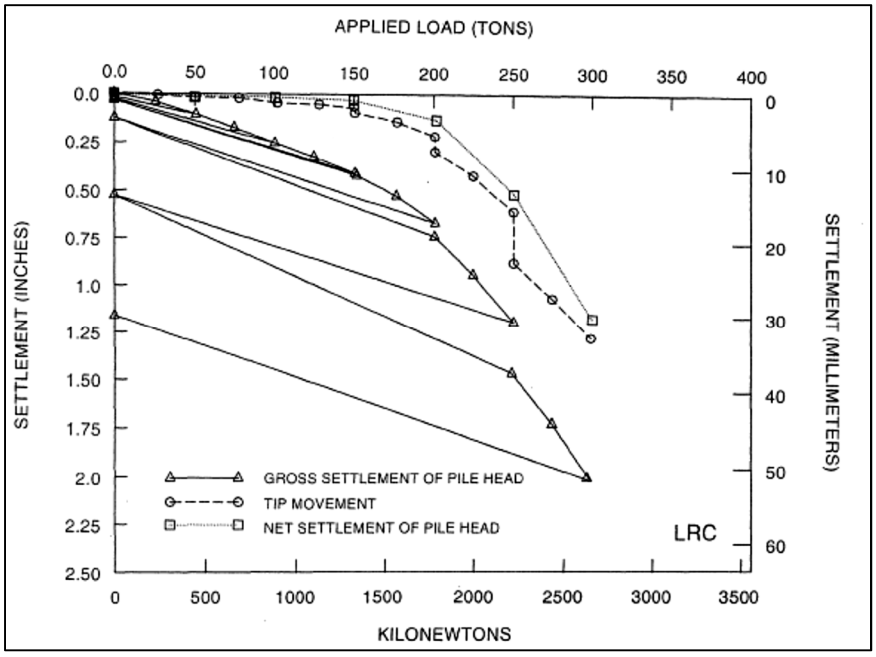


Fig 6. Load vs. pile head movement, P2 – Compression

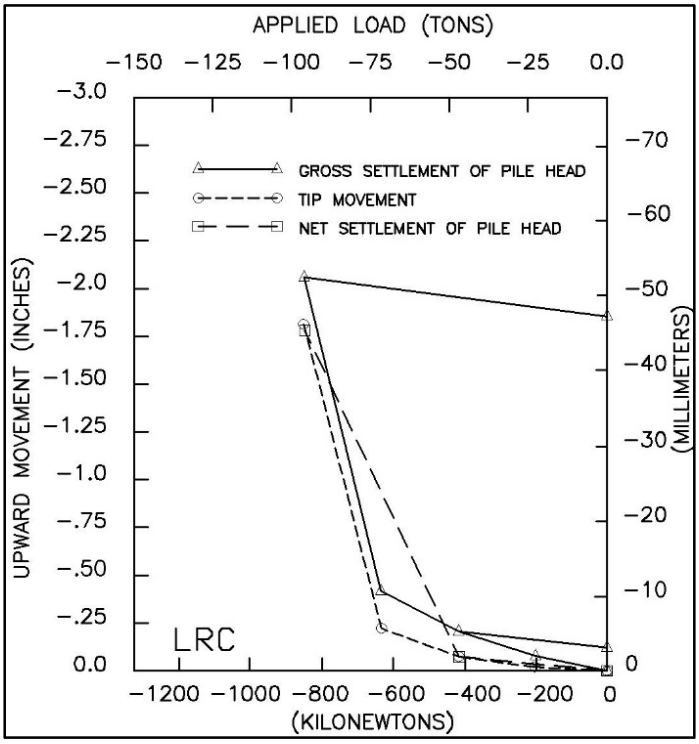


Fig 7. Load vs. pile head movement, P1 – Tension

Load transfer curves along the pile shaft and toe were constructed from the instrument readings considering the three "zero strain" conditions discussed above. The LRDC load transfer curves for P1 and P2 during the compression tests are shown on Figs. 8 and 9. Each curve in the figure represents the load transferred along the pile shaft at a specific load increment, including residual loads due to driving and load cycles. The first curve representing zero applied load, shows the "triangular" distribution of the residual driving

loads along the piles shaft. It should be noted that readings of the strain gauges near the toe of pile P2 which were damaged during driving were excluded from Fig. 9. The total residual loads due to driving of P1 and P2 were 320 and 258 kN (36 and 29 tons), respectively.

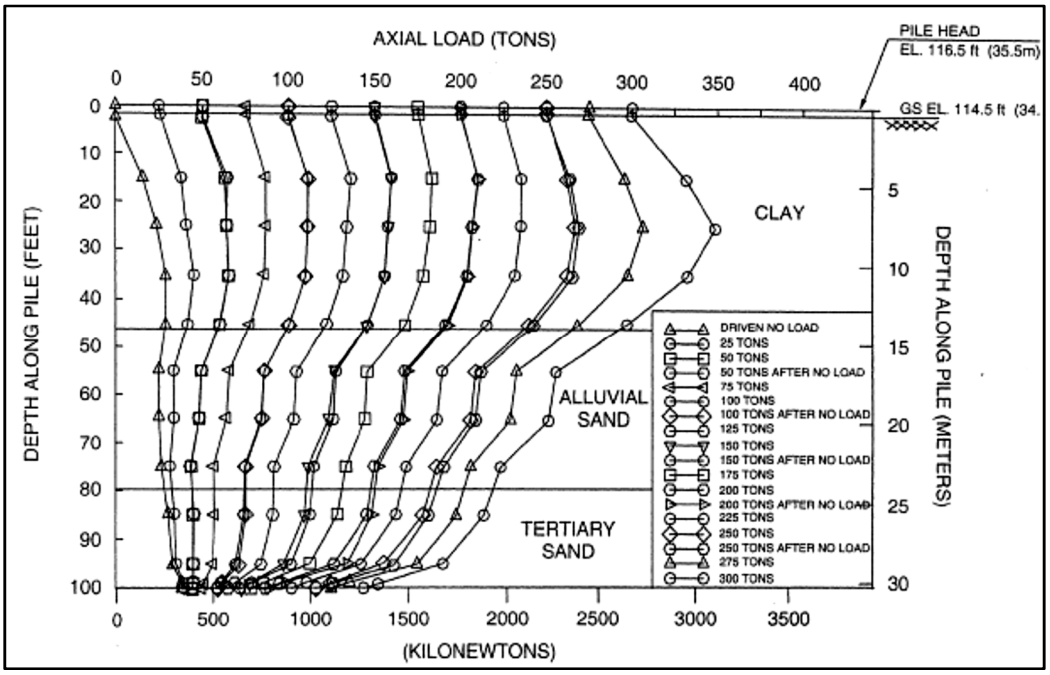


Fig 8. Pile load transfer curves, LRDC - P1 Compression

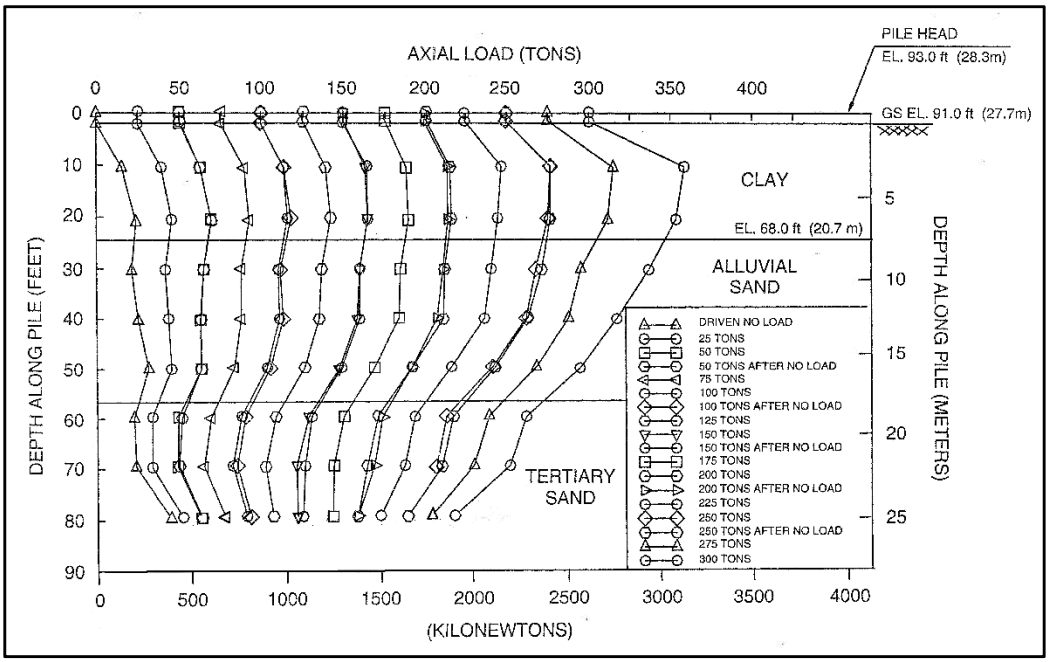


Fig 9. Pile load transfer curves, LRDC – P2 Compression

By excluding residual loads due to driving and load cycles, the shape of the compression load transfer curves became almost smooth "trapezoidal", as shown in Figs. 10 and 11. This condition, previously defined as a the LRN condition, represents the actual load capacity of the pile. At load increments higher

than 2,224 kN (250 tons), the load transfer distribution became almost parabolic in shape especially in the pile segment in the clay stratum. The effect of residual loads due to load cycles (LRN) was insignificant, especially at low load increments and could be ignored for all practical purposes.

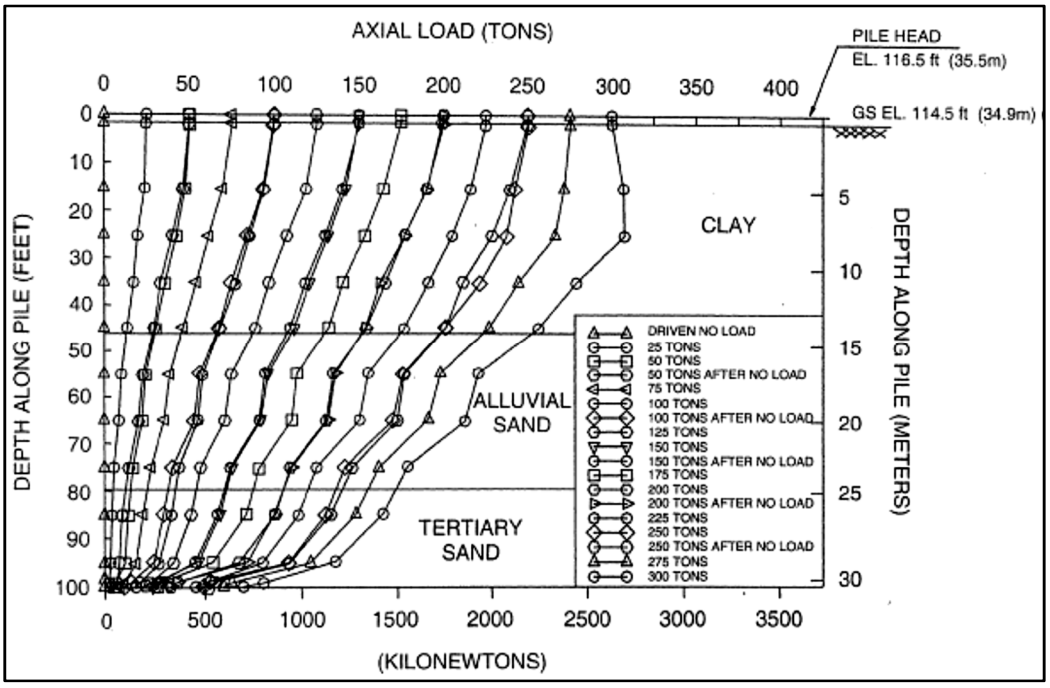


Fig 10. Pile load transfer curves, LRN – P1 Compression

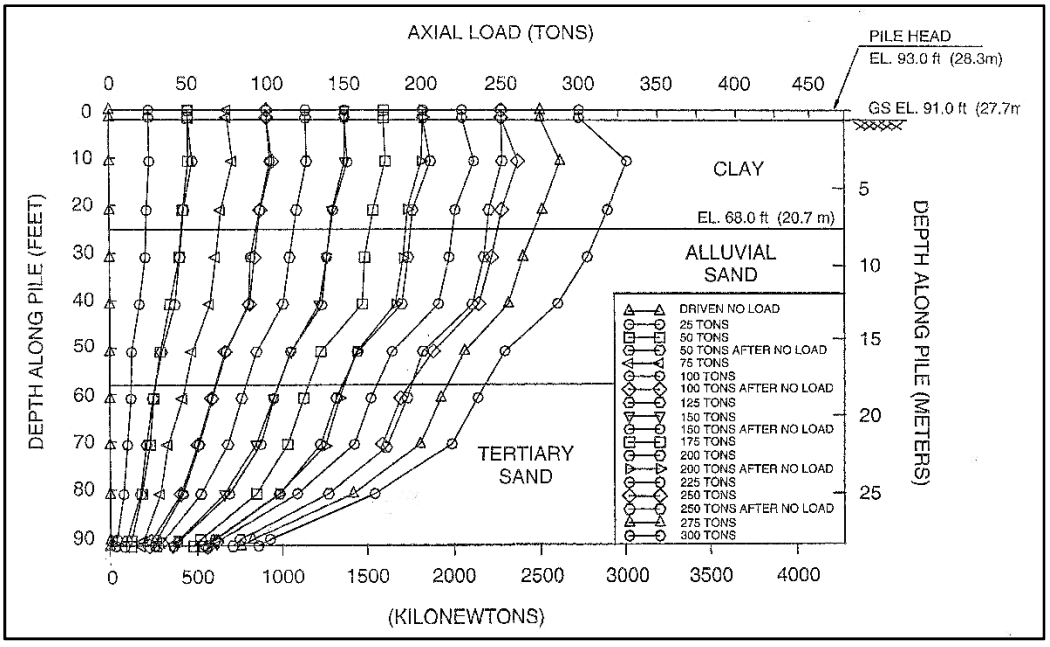


Fig 11. Pile load transfer curves, LRN – P2 Compression

The tension test was performed on pile P1 following the completion of the compression test. The LRDC distribution of the tension load mobilized along the pile shaft, shown in Fig. 12, is highly irregular and it implies that the pile toe is offering some "positive" contribution. This unusual distribution resulted from

residual loads due to driving and load cycles from the earlier compression test. Loading the pile almost to failure during the compression test have also disturbed the subsoils along the pile shaft. Elimination of all residual loads (LRN condition) yielded more trapezoidal shaped distributions with the maximum values at the pile head, as shown in Fig. 13. However, elimination of all residual loads due to driving and load cycles produced "apparent" tension contribution at the toe. This contribution is negligible and it is likely due to some deformation at the pile toe which damaged the bottom strain gauges, as previously discussed.

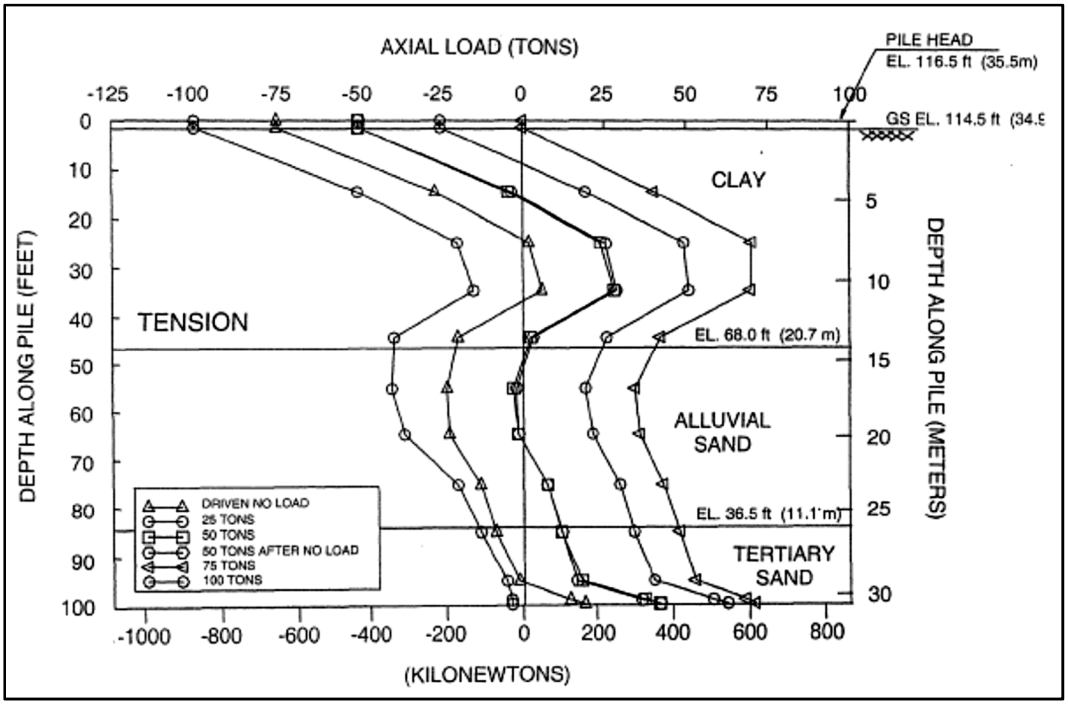


Fig 12. Pile load transfer curves, LRDC – P1 Tension

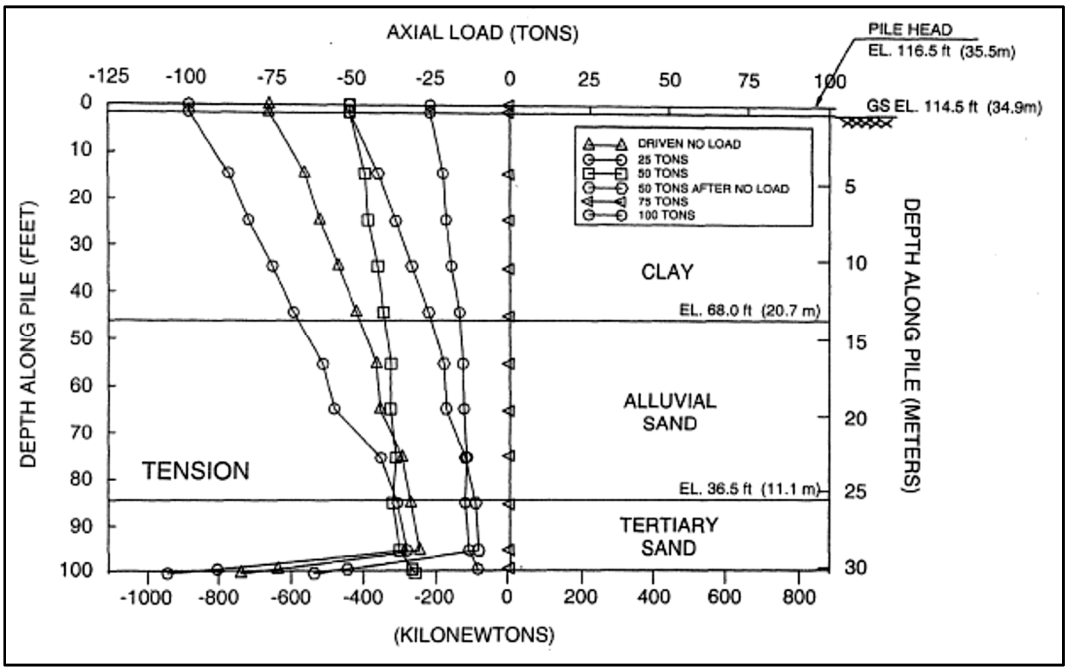


Fig 13. Pile load transfer curves, LRN – P1 Tension

CONCLUSIONS

Residual stresses develop in piles due to pile driving and load cycles. Therefore, three zero strain conditions were examined during driving and compression and tension load testing of two instrumented steel H-piles. The extreme conditions of all residual loads (LRDC) included and all residual loads excluded (LRN) were examined. Residual loads due to load cycles were found to be insignificant and could be neglected. Residual loads due to driving affected the magnitude and distribution of the load transfer curves. Distribution of the residual loads due to driving along the pile shaft was found to be near triangular with its base at the pile toe. Shape of the load transfer curve along the pile shaft under the LRN condition was near trapezoidal with its maximum value at the pile head. Results of the study indicated that the pullout (tension) capacity should not be determined from a pile previously tested in compression. Close monitoring (instrumented probe piles, dynamic monitoring, etc.) should be performed when steel H-piles are driven into dense sand or rock where toe damage could develop. The uncertainties associated with the measured load by the jack and the damaged strain gauges illustrate the importance of selecting instrumentation used in high cost full-scale studies in terms of their type, number, redundancy, precision, accuracy, etc.

ACKNOWLEDGMENTS

The investigation was sponsored by the U.S. Army Corps of Engineers (USACE), Lower Mississippi Valley Division LMVD under the supervision of Mr. Britt Mitchell and Mr. Milton Myers. The author acknowledges with deep gratitude the guidance and advice provided by the late Walter C. Sherman. Intertek PSI provided the author with the time and support needed to prepare the manuscript and presentation.

REFERENCES

Bakeer, R. M., Hadji-Hamou, T. and Rau, D. E., 1993. Analysis of pile load tests at the Ascalmore-Creek Tippo - Bayou Control Structure. Technical Report GT-90-1, Tulane University, New Orleans, LA, Prepared for the U.S. Army Engineer District, Vicksburg, MS, 201 p.

Briaud, J.L. and Tucker, L., 1984. Piles in sand: A method including residual stresses. American Society of Civil Engineers, ASCE, J. of Soil Mechanics and Foundation Engineering, 110(SM11) pp. 1666-1680

Fellenius, B. H., 1984. Ignorance is bliss and that is why we sleep so well. Geotechnical News, Canadian Geotechnical Society and the U. S. National Society of the ISSMFE, Vol. 2, No. 1, p. 14

Fellenius, B.H., 2002. Determining the true distributions of load in instrumented piles. Proceedings, ASCE International Deep Foundation Congress, Orlando, FL, February 14-16, Geotechnical Special Publication 116, Vol. 2, pp. 1455-1470

Holloway, D.M., Clough, G.W., and Vesic, A.S., 1975. The mechanics of pile soil interaction in cohesionless soils. Contract Report S-75-5, for the Office, Chief of Engineers, U.S. Army, U.S. Army Engineer Waterways Experiment Station (WES), Vicksburg, MS, December, 297 p.

Hunter, A.H., and Davisson, M.T., 1969. Measurement of pile load transfer. Performance of Deep Foundations, ASTM, STP 444, pp. 106-117

Polous, H. G., 1987. Analyses of residual stress effects in piles. American Society of Civil Engineers, ASCE, J. of Soil Mechanics and Foundation Engineering, 113(SM3), pp. 216-229

VXD, 1992. Ascalmore Creek - Tippo Bayou Item No. 3, Control Structure – Foundation Report. USACE, U.S. Army Engineer District, Vicksburg, MS, January, 87 p.

GROUND IMPROVEMENT FOR NEW JERSEY TURNPIKE INTERCHANGE 14A: A CASE STUDY

Shafiq I. Siddiqui, Gannett Fleming, Inc., 5 Eves Dr., Marlton, NJ, USA, 856-396-2226, ssiddiqui@gfnet.com
Daniel V. Cacciola, Gannett Fleming, Inc., Two Penn Plaza, Suite 552, New York, NY, USA, 212-967-9833, dcacciola@gfnet.com
Sarah Ramp, MENARD Group USA, 150 East Main Street, Carnegie, PA, USA, 412-620-6000, sramp@menardgroupusa.com
Faisal Ahmed, Gannett Fleming, Inc., 5 Eves Dr., Marlton, NJ, USA, 856-396-2226, fahmed@gfnet.com
Justin Labrozzi, MENARD Group USA, 150 East Main Street, Carnegie, PA, USA, 412-620-6000, jlabrozzi@menardgroupusa.com

ABSTRACT

Construction of embankments up to 34 ft in height for twelve ramps and roadways needed for the New Jersey Turnpike Interchange 14A project required ground improvement. The subsurface conditions, consisting of up to 30-ft thick layer of highly-compressible peat and organic soils, would induce up to 8 ft of primary and 4 in. of secondary consolidation settlements to the embankments over a long period of time. Innovative ground improvement solutions were needed to meet unique challenges posed by the poor subsurface conditions, space and existing utility constraints, aggressive construction schedule, and massive size of the project. A variety of ground improvement techniques were utilized in six different zones of the embankments to limit settlements and ensure stability of the embankments. These techniques included preloading with surcharge and prefabricated vertical drains (PVD), load balancing using light weight fill, and concrete column rigid inclusions (RI). Additionally, augercast piles with load transfer platform were used under an existing bridge with low vertical clearance. An innovative approach consisting of preloading with surcharge and PVDs followed by installation of RI was needed in one of the six embankment zones with the worst, i.e., very soft, soil conditions. The design of the RI was performed by a specialty ground improvement contractor (SGIC) using Plaxis 2D and 3D softwares. The performance of the ground improvement systems was verified and monitored by load tests and instrumentations. This paper presents details of the ground improvement design, construction, monitoring results, and lessons learned, with a focus on the RI.

Keywords: ground improvement, surcharge, PVD, light-weight fill, rigid inclusions, concrete columns, peat, organic soil, settlement

INTRODUCTION

New Jersey Turnpike Interchange 14A is located within the cities of Bayonne and Jersey City, in Hudson County, New Jersey. The New Jersey Turnpike Authority (NJTA) identified Interchange 14A as an area of mass congestion in need of redevelopment to improve the increasing demand of traffic and roadway safety. The New Jersey Turnpike Interchange 14A project included the construction of twelve (12) new roadways, in addition to the construction of four new bridges. The limits of construction are shown in Fig. 1.

The fill height required to construct the roadway embankments varied from 2 to 34 ft. The proposed embankment side slopes varied from 6H: 1V to 2H: 1V. Additionally, mechanically-stabilized-earth (MSE) walls were utilized to retain the embankment fill along some segments of the roadways. As shown in Table 1, the proposed roadways were divided into six zones, based on location, subsurface condition, and embankment height.

 © 2017 DFI Annual Conference, New Orleans, LA, USA

Numerous existing utilities are present at each zone within the project limits. New utilities were also installed within the project limits. Ground settlements due to new embankment fill needed to be limited in order to prevent damage to the utilities and the proposed structures and roadways. Ground Improvement was needed to reduce the embankment settlements to tolerable levels. This paper presents feasible ground improvement techniques for different zone, design and construction details, and field measurement results.

Table 1. Maximum Fill Height for Each Zone

Zone	Roadway	Proposed Max. Fill Height (ft)
1	Peninsula Road, Ramp TP-Peninsula and Ramp TP-440 NB	24
2	Connector Road ET/TE, Ramp TP-Peninsula, Ramp TP-440 NB/SB and Ramp Port-440 SB	34
3	Ramp 440 NB-TP, Ramp TP-440 SB, Ramp Port-440 SB and Route 440 NB	34
4	Jughandle Y and Ramp Port/TP-440 SB	19
5	Connector Road ET/TE	12
6	Ramp ET	3

SUBSURFACE CONDITIONS

Subsurface conditions for the roadways were explored by performing a total of 68 test borings to depths ranging from 7 to 115 ft and installing a total of 10 groundwater observation wells along or in the vicinity of the roadways. Based on the borings, the soil and rock encountered at the site were subdivided into five strata, i.e., Stratum F, Stratum C, Stratum S, Stratum G, and Stratum R, in order of increasing depths. Each strata is described in detail below. Additionally, a generalized subsurface profile for the site is shown in Fig. 2.

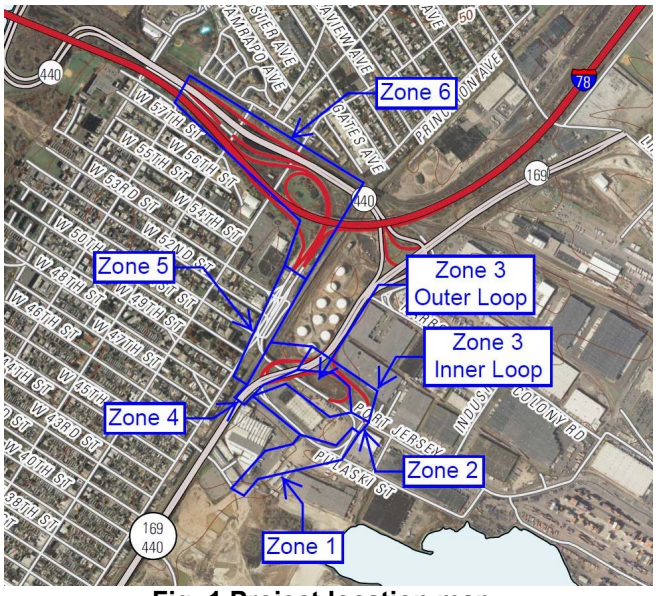


Fig. 1 Project location map

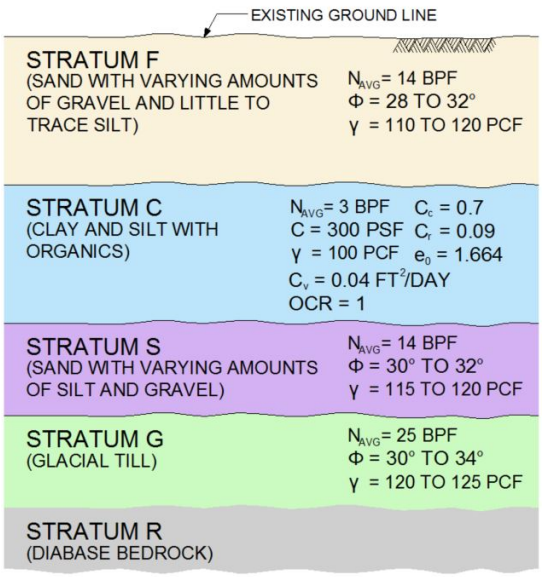


Fig. 2 Generalized subsurface profile

The fill (Stratum F) consists of sand and gravel with varying amounts of silt, brick, concrete and asphalt fragments, and other miscellaneous debris. The relative density of the fill material was very loose to dense.

The typical thickness of this layer was 5 to 15 ft. At some boring locations Stratum F was not encountered (i.e., Zone 3 Inner Loop).

Stratum C consists of silty clay, peat, and clay, and extends to depths of 13 to 38.5 ft. The typical thickness of Stratum C was 5 to 15 ft in Zones 1, 2, 4 and 5. At Zone 3 the typical thickness was 10 to 25 ft. Stratum C was not encountered in Zone 6. The consistency of the cohesive soils is very soft to stiff with pocket penetrometer readings ranging from 0.25 to 1.0 tons/sq. ft (tsf). SPT N-values of the Stratum C soils ranged from WOH to 23 bpf, averaging about 3 bpf. The consolidation parameters determined from eight consolidation tests range from 0.07 to 1.55 (compression index, C_c), 0.01 to 0.23 (recompression index, C_r), 1.0 to 3.4 ksf (preconsolidation stress, P_c), and an overconsolidation ratio (OCR) of about 1.0. These values indicate that the cohesive soils are highly compressible. The selected design parameters were as follows: unit weight (γ) = 100 pounds/cu. ft (pcf), cohesion (C) = 300 pounds/sq. ft (psf), C_c = 0.7, C_r = 0.09, void ratio (e_0) = 1.664, OCR = 1.0, and coefficient of consolidation (C_v) = 0.04 ft^2/day.

Stratum S consists of very loose to very dense sand with varying amounts of silt, silty clay, and gravel and extends to a depth of 13.5 to 58.5 ft. Stratum G (glacial till) consists of medium dense to very dense sand and gravel with varying amounts of silt and clay and extends to the maximum depths explored or the top of the bedrock. Stratum R consists of hard, fresh to slightly weathered, and slightly to moderately fractured diabase. The depth to bedrock was highly variable throughout the site, however, bedrock was typically encountered at or beyond a depth of 30 ft below ground surface.

ROADWAY SETTLEMENT ANALYSIS AND SIGNIFICANT ISSUES

The most significant issue affecting the stability of the roadway embankments is the presence of highly compressible cohesive soils (i.e., Stratum C). Settlement analyses without ground improvement were performed for the critical embankment sections with the maximum fill heights in each zone using FoSSA (2.0) software. A preloading period of 100 days was selected for evaluation as a reasonable time frame with respect to construction staging/scheduling. The settlements of the critical and representative embankment sections in each zone are summarized in Table 2. Total settlement includes elastic settlement and primary consolidation settlement.

Table 2. Estimated Settlements for Each Zone without Ground Improvement

Zone	Max. Fill Height (ft)	Total Settlement (in.)	Primary Consolidation Settlement (in.)	Post-construction (after 100 days) Settlement (in.)
1	24	31	22	14
2	34	58	47	36
3	34	94	84	67
4	3	4.2	3.5	1.9
5	33	37	27	18
6	5	0.8	0	0

The maximum calculated secondary settlement was 2.5 in. in 10 years and 4.0 in. in 50 years for the most critical zone, i.e., Zone 3. The maximum post construction settlement is 67 inches and corresponds to 84 inches and 94 inches of consolidation and total settlement, respectively. These settlements are excessive. To mitigate the excessive post construction and total settlements in Zones 1 through 5, ground improvement is needed.

GROUND IMPROVEMENT ALTERNATIVES

To minimize the settlements, ground improvement alternatives such as organic soil over-excavation and replacement, preload with surcharge and prefabricated vertical drains (PVDs), load balancing with lightweight fill, and concrete column-rigid inclusions (RI) were evaluated. Rigid inclusions are used to improve the composite modulus of the soil and transfer embankment fill loads to the dense bearing stratum. The rigid inclusions vary by installation method and contractor. A summary of the four ground improvement options considered technically feasible for this project with their advantages and disadvantages are provided in Table 3.

Considering all the factors shown in Table 3, RI is the most viable option for the embankments with fill heights of more than 5 ft. For the embankments with a maximum fill height of 5 ft, preload with surcharge is typically the most feasible option if no underground utilities are present. If utilities are present for embankments with a maximum fill height of 5 ft, lightweight aggregate is the most feasible option. Additionally, augercast piles can be utilized as rigid inclusions in place of the concrete columns in Zone 4 under the new Connector Road bridge where construction of concrete columns is not feasible due to limited vertical clearance. The augercast piles have similar characteristics to the concrete columns described in Table 3, however, the installation of the augercast piles does not improve the relative density of the surrounding soils as concrete columns would. Based on these criteria, ground improvement types were selected for different zones as shown Fig. 3.

Table 3. Evaluation of Ground Improvement Alternatives

Alternative	Preload with Surcharge and PVDs	Concrete Column-Rigid Inclusions	Preload with Surcharge	Lightweight Aggregate
Technical Feasibility	Advantages: -Accelerates consolidation -Reduces post-construction settlement -Reduces secondary consolidation Disadvantages: -Long quarantine periods -Significant surcharge height -Impacts utilities -Staged construction	Advantages: -Transfers load to dense stratum -Mitigates post-construction settlement -Minimal utility impacts Disadvantages: -Load Transfer Platform (LTP) needed -Requires performance specification	Advantages: -Cost-effective for embankments $\leq$ 5 ft where utilities not present -Accelerates consolidation -Reduces post-construction settlement Disadvantages: -Long quarantine periods -High surcharge required -Impacts utilities -Not feasible for fill height more than 5 ft	Advantages: -Cost-effective for embankments $\leq$ 5 ft where utilities are present -Mitigates post-construction settlement -Minimal utility impacts Disadvantages: -Durability, corrosion, and contamination issues
Constructability	Advantages: -Minimal spoil Disadvantages: -Difficult to install PVDs through dense fill -Quarantine periods result in longer construction duration -Staging issues -Hauling, stockpiling, and removal of surcharge material	Advantages: -Immediate construction -Minimal spoils Disadvantages: -Minimal to low vibration involved, depending on the installation method	Advantages: -Minimal spoil Disadvantages: -Quarantine periods, longer construction duration -Staging issues -Hauling, stockpiling, and removal of surcharge material	Advantages: -Immediate construction -Minimal spoils Disadvantages: -Some spoil could be produced if overexcavation is required
Preliminary Design	-10 ft soil surcharge -PVDs at 5 ft spacing, 40 ft deep	-Columns at 5 to 10 ft spacings, 40 ft deep	-6 ft soil surcharge for 3 ft embankment fill height	- 3 ft overexc. and repl. with lightweight aggregate for 3 ft embank fill
Cost	$11/SF -Additional cost of increased construction duration, hauling, stockpiling, and removal of surcharge	-$20 to $45/SF is typical range -$50/SF for thick WOH material (5 ft spacing, 35 ft length)	$3 to $6/SF -$3/SF for 5 ft surcharge -$6/SF for 10 ft surcharge	$7 to $9/SF
Installation Rate	6,000 to 10,000 linear ft/day/rig	700 to 1,000 linear ft/day/rig	200 to 400 cubic yard/day	200 to 400 cubic yard/day
Performance Verification	-Settlement criteria	-Settlement criteria -Load test	-Settlement criteria	-Settlement criteria

DESIGN-BUILD COLUMN SUPPORTED EMBANKMENTS SPECIFIED

As shown in Fig. 3, RI supported embankments were recommended in the Contract Plans to support the embankment within five zones. Typical sections of the RI supported embankments are shown in Fig. 4.

Performance Specifications

The Project Geotechnical Engineer opted for a design-build method for the RI supported embankments and prepared performance-based specifications for design and installation. Following are some notable performance criteria provided in the Specifications:

1. Minimum factor of safety of 2.0 for the axial compression capacity of concrete column and 1.4 for the global stability of embankments and MSE walls supported on concrete columns.
2. The total settlement at the base of the embankments or MSE walls shall not exceed 3.5 inches.
3. The post-construction settlement of the final pavement subgrade surface shall be less than 1.0 inch in 10 years.
4. The maximum differential settlement of the pavement subgrade surface must not exceed 1.0 inch per 100 feet at completion of the full load condition.
5. The embankments and MSE walls supported on concrete columns cannot cause any additional loading on existing or proposed foundations and new or existing utilities.

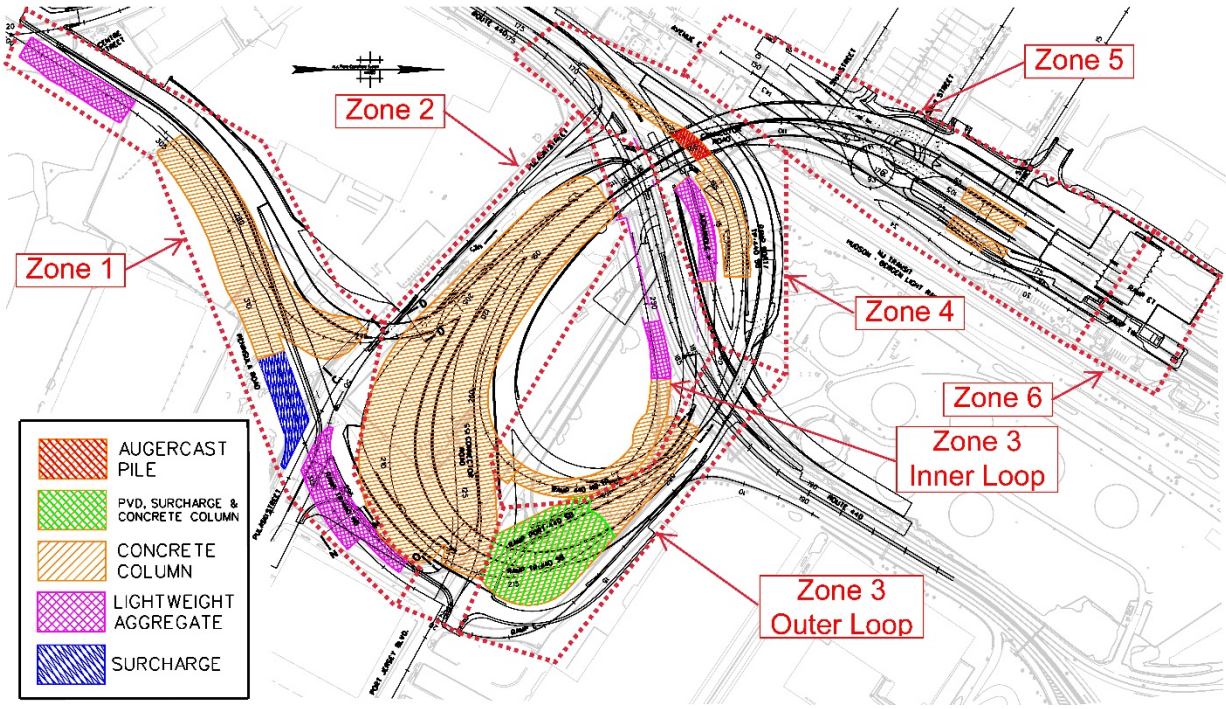


Fig. 3 Ground Improvement Zone Plan

With the exception of few areas, the plan above was implemented by the SGIC. During construction in Zone 1, about 60 ft long segment had numerous boulders at shallow depths. Boulder removal for RI installation was not economical; therefore lightweight cellular concrete was designed by GF and constructed, and the overall scope of the RI supported embankments was reduced.

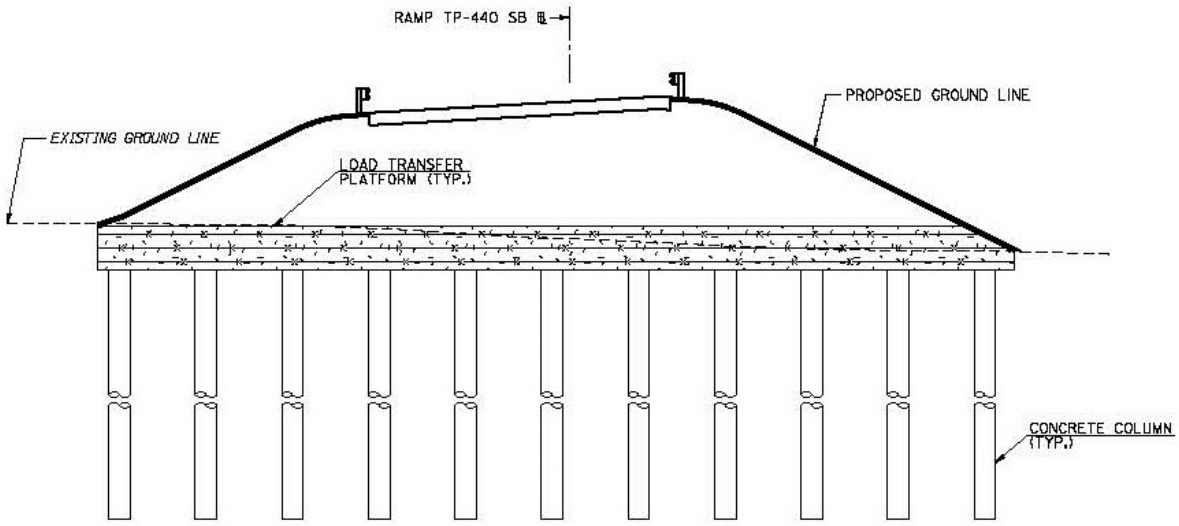


Fig. 4 Typical Section - Colum Supported Embankment

Design using Numerical Modeling

The RI design scope included total and differential settlement, global and sliding stability, and bearing capacity for the proposed MSE walls and general embankment regions. The RI design was performed to meet the performance specifications by the SGIC.

The finite element modeling software Plaxis was used to model the complex soil-structure interaction and estimate the distribution of the applied load within the improved ground. Recall that RI supported embankments are designed such that the RI share applied load with the surrounding soils, unlike piles, which are designed to transmit 100 percent of the load to the bearing stratum. Therefore, the design considers a controlled magnitude of settlement is occurring in the soft compressible soil layers along the length of the RI, which in turn, transfers additional load onto the RI in the form of negative skin friction. Fig. 5 depicts the difference in loading between conventional piling and RI.

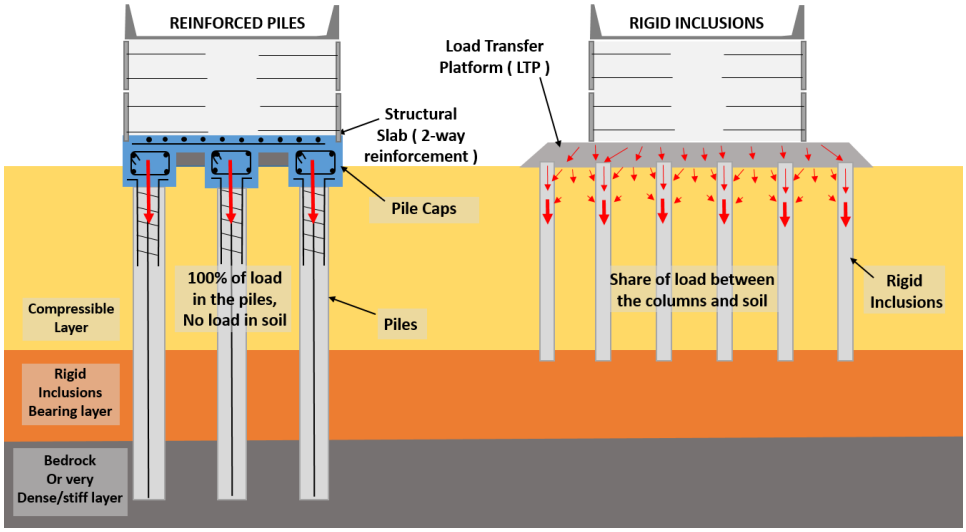


Fig. 5 Comparison of Rigid Inclusion Ground Improvement vs. Traditional Structural Pile Support

In total, 31 unit-cell (axisymmetric) 2-dimensional models were performed, each representing a different soil boring, LTP thickness and shear strength, RI diameter, net (embankment) fill height, and RI effective grid spacing. Based on the results of the axisymmetric modeling, key RI supported embankments components such as RI depth and spacing, and LTP thickness were chosen to meet the project settlement criteria. In addition to the axisymmetric models, one 3-dimensional strip model was performed to model the interaction between two adjacent RI supported ramps with different spacing densities of RI and to estimate the lateral movement of a proposed MSE wall.

2D Axisymmetric Modeling

In order to simplify a complex 3D problem into a more manageable 2D model, simplifying assumptions have to be made. Because of the symmetry of the loading conditions of RI, the problem is simplified from a 3D geometry to a more manageable 2D unit cell centered on a column, as depicted in Fig. 6.

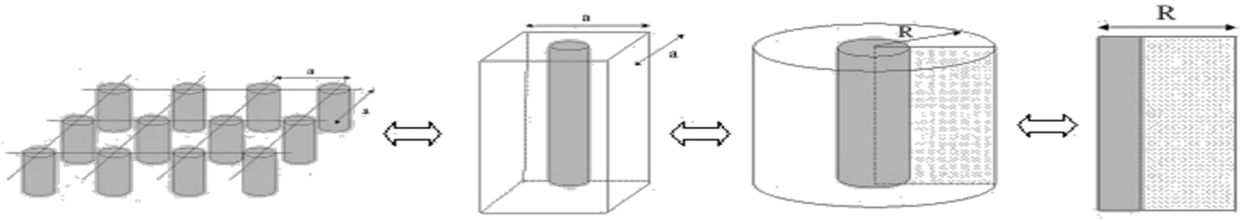


Fig. 6 Theory of 2D Axisymmetric Modeling

One particularly challenging area of the site for design was the previously marshy area in the southern portion of Zone 3, characterized by contract boring "RW14-1." Whereas the "F" (fill) stratum as present across the majority of the site, RW14-1 encountered WOH organic clay at the existing ground surface to a depth of 24.5-ft below grade. The proposed embankments in the vicinity of RW14-1 were up to 34-ft tall, the highest across the project; the initial design approach with RI improvement alone at the densest practical RI installation ratio was estimated to not meet the project performance criteria.

Numerous technical risks were associated with using a RI system for this marshy area, including excessive settlements beyond the allowable limits prior to engaging the full load transfer mechanism, undrained global and sliding stability of the embankments, and even stability and safety of the working platform during RI installation. To mitigate each of these risks, a PVD and surcharge program was implemented at the beginning of the project, designed to accelerate the consolidation of the thick organic clay stratum. The program was optimized to take advantage of available time in the project schedule and some of the surcharge materials were designed to remain-in-place as a working platform for the RI installation. Surcharges between 4 and 7 ft were used. Economization of the PVD and RI layout was achieved by installing the PVD on a square grid spacing equal to (or ½ of) the RI spacing. RI installation was then planned to disturb the least amount of PVD as possible, so a proportion of the PVD were assumed to remain-in-place and accelerate the controlled magnitude of settlement within the clay. As shown in Fig. 7, an axisymmetric finite element model was used for estimating settlement in the southern portion of Zone 3, based on soil boring RW14-1.

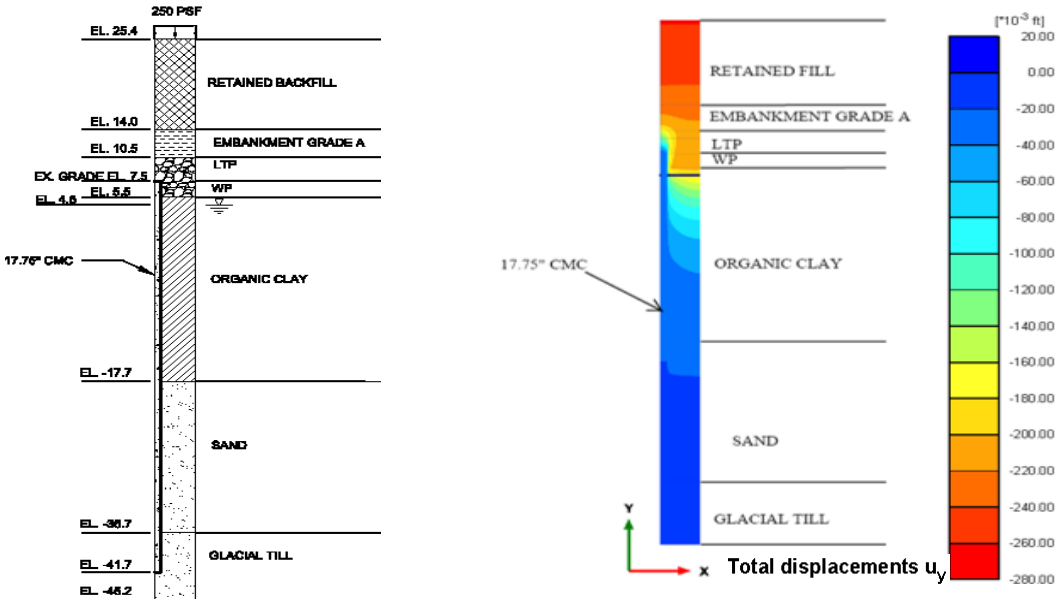


Fig. 7 Zone 3 2D Axisymmetric Model-5 Result

The PVDs were not literally modeled; instead, their effect was accounted for with a composite permeability of the clay. Using time rate of settlement hand calculations coupled with consolidation calculations in Plaxis, the following performance was estimated from 2D Axisymmetric Model 5:

- Total settlement measured at the top of the LTP of 2.6 inch. (excluding settlement during the initial PVD + surcharge period)
- 10 year post-construction settlement of 0.9 inch

Numerous configurations of the RI were designed for support of varied embankment fill heights. RI effective grid spacings ranging between 5.75-ft square and 9-ft square were used. In general, where the applied bearing pressures due to embankment loading were highest, so were the design densities of RI per area of ground. Within each RI supported embankment "Zone", similar post-construction settlements were targeted with the RI configurations, thereby reducing differential settlement potential and meeting the design criteria of less than 1-inch differential over 100-ft. For example, in Zone 3, the RI configuration was optimized until post-construction settlements were estimated between 0.7 and 1.0 inches. This design for relatively uniform settlement minimizes the potential for eccentric loading or unexpected downdrag on individual columns located near the transition zone between two different grid spacings.

3D (Strip) Modeling

One 3D finite element analysis was performed for the support of a 34-ft. high MSE wall and embankment side slope upon the former swamp in Zone 3. Unlike 2D axisymmetric analysis, a 3D model can replicate non-uniform loading while estimating lateral displacements of embankments and resultant shear and flexural forces within the RI. Figs. 8 and 9 show the 3D model input and output, respectively, at the end of primary consolidation. The 3D strip model estimated 1.9 inches of total settlement and 1.7 inches of horizontal wall displacement, including settlement during construction.

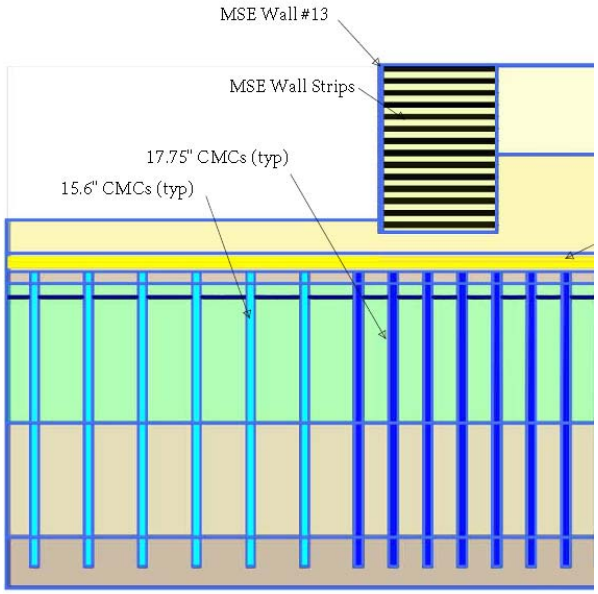


Fig. 8 Zone 3 3D Model Input

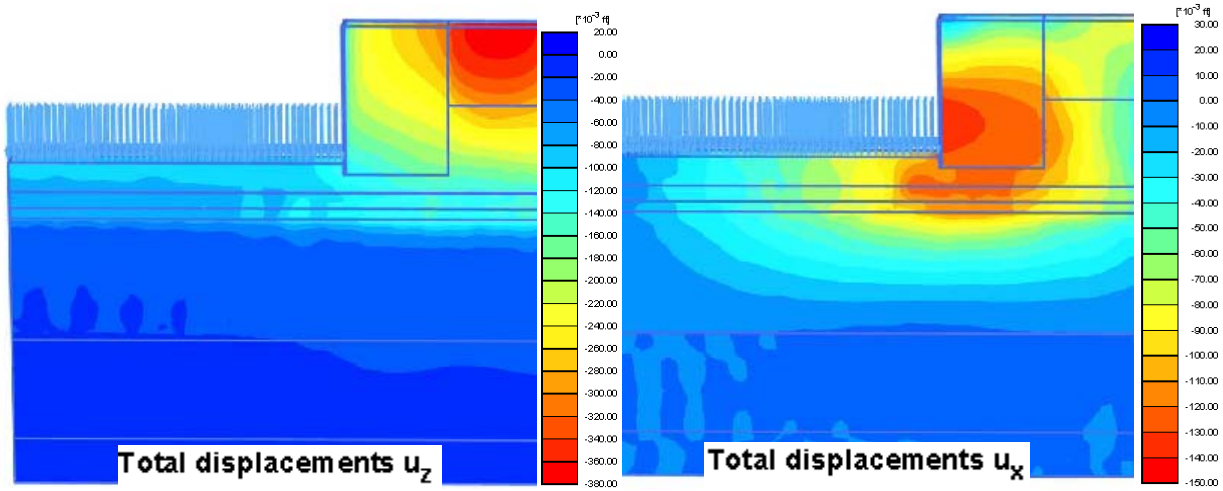


Fig. 9 Zone 3 3D Model Output

QUALITY CONTROL DURING CONSTRUCTION OF RI

Over 95% of the massive, design-build RI ground improvement system for support of this complex turnpike interchange was constructed within 1 year. For quality assurance during the rapid pace of construction, the actual installation of the RI was monitored using an on-board automated monitoring system which measured real-time installation parameters. A computer-generated log for each RI was reviewed daily by the SGIC. RI with issues such as low-grout volume and drill depth were remediated or replaced.

To verify the geotechnical bearing capacity of the RI, four single element static load tests were performed in general accordance with ASTM 1143 "Quick Test" on various diameter RI, each of which represented minimal embedment into the Stratum "S" (glacial till) bearing layer compared to the rest of the production columns. The results of the static load tests are shown in Table 4.

Table 4. Load Test Results

Test/Zone	Diameter	Length	Design Load	Test Deflection at Design Load (Top of RI)	Max. Load Applied
LT1/Z1	15.6-in	31-ft	134 kips	0.1-in	408 kips
LT2b/Z2	17.8-in	40-ft	159 kips	0.2-in	432 kips
LT3/Z2	15.6-in	32-ft	97 kips	0.1-in	285 kips
LT4/Z3	17.8-in	42-ft	125 kips	0.1-in	418 kips

To monitor uniformity of construction and quality of the completed RI, Column Integrity Tests (CIT) were performed on about 2 percent of the production columns, as well as the sacrificial load test elements described above. Integrity testing showed inconclusive results for a portion of the columns tested. Based on anomalies detected through early CIT, the team discovered that some RI were cracked/damaged during early stage of construction possibly due to the construction traffic. From that point on, greater precautions were taken to protect the green RI from disturbance, and RI expected to have been damaged by heavy traffic were supplemented. Later anomalies detected included variable cross-section, likely due to changes in soil profile over depth. The SGIC Designer of Record analyzed each anomaly individually, and no remediation was required when the presumed nature of the anomalies were variable cross-sections or horizontal cracks. The SGIC means and methods for monitoring RI installation in real time (including drill advancement speed, crowd and rotary head pressure, and grouting pressure and pump rate) and computer-generated as-built logs for each RI were the primary quality control mechanism. When severe anomalies on the logs were detected, the RIs were replaced.

SETTLEMENT MONITORING

PVD and RI – Zone 3

As shown in Fig. 10, an extensive settlement monitoring program consisting of sleeved metallic settlement plates was specified. The settlement plates were first used by the SGIC to estimate the degree of consolidation reached due to the initial surcharge period in Zone 3. Figure 11 shows the progress of settlements during the surcharge period in Zone 3, including the first couple weeks of rapid surcharge placement. The observed settlements match with the estimated high consolidation settlements (i.e., up to 2 inches of settlement per foot of fill). Once the design degree of consolidation was reached, the surcharges and settlement plates were removed and RI installation began.

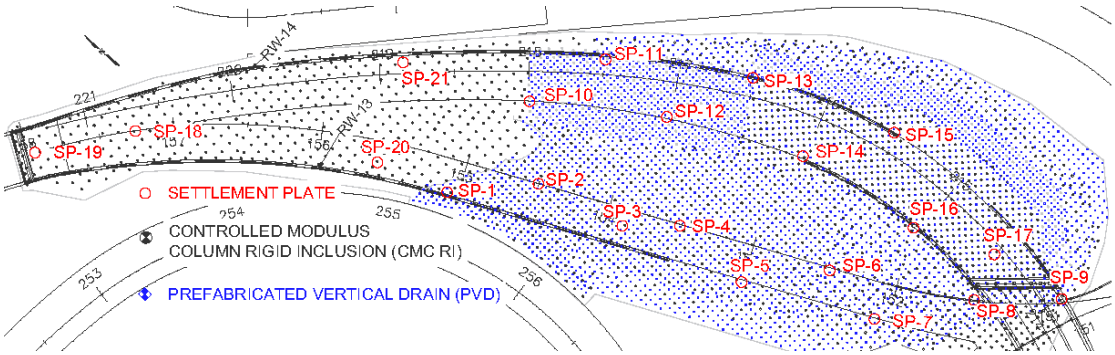


Figure 10. Zone 3 RI and PVD Ground Improvement and Instrumentation Layout

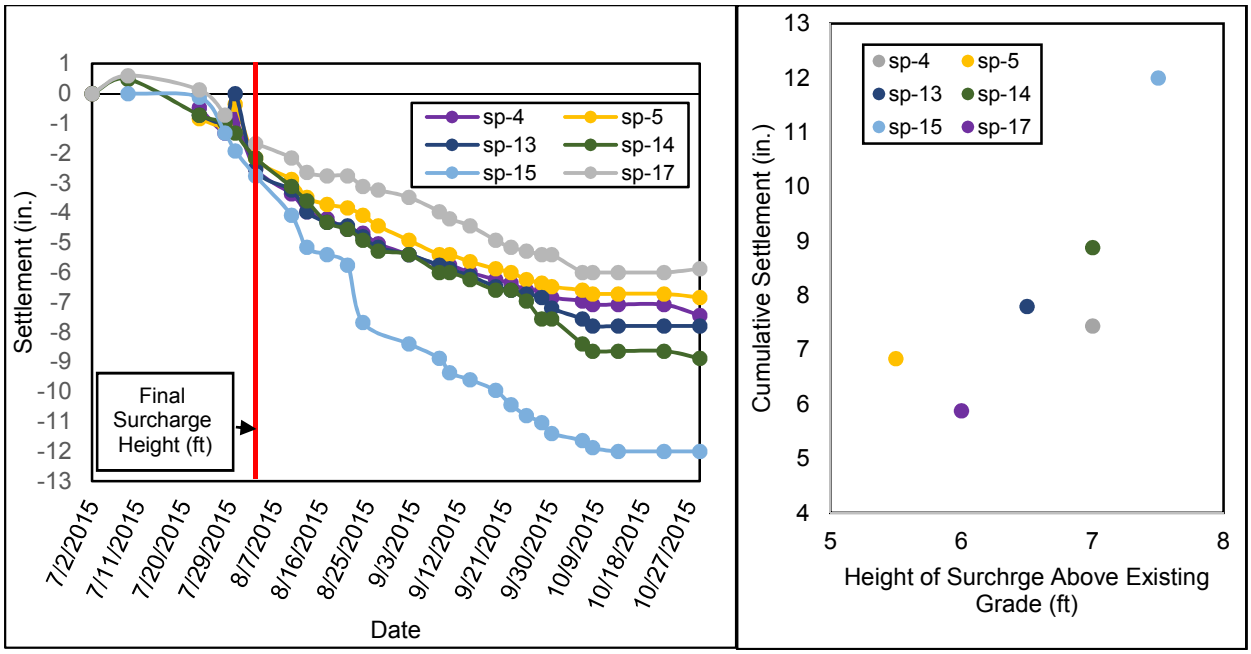


Fig. 11 Zone 3 Surcharge Settlement Readings

After RI installation, the settlement plates were replaced directly atop the finished granular load transfer platform. Thereby, the performance of the RI system was monitored independently from the total embankment settlement. During embankment construction, additional pipe segments were coupled to the inner pipe and to the outer sleeve. Elevations of each plate were estimated at regular intervals by survey of the inner pipe. A subset of the settlement plate data from Zone 3 is shown in Fig. 12.

The proposed grade in Zone 3 was reached by 10/22/16. During the approximate 3-month embankment construction period, the observed settlement at the top of the LTP was 2 inches or less. Notably, there was a lot of noise in the incremental settlement plate data that suggested upward vertical heave of the plates. That the ground at the settlement plate elevation was actually heaving during construction is highly unlikely; instead, the pipe sleeves were probably disturbed by construction traffic. Data starting from the beginning of embankment filling through 8/22/16 (the first month) for all of the above plates except SP-19 was highly disturbed and was omitted from the plot.

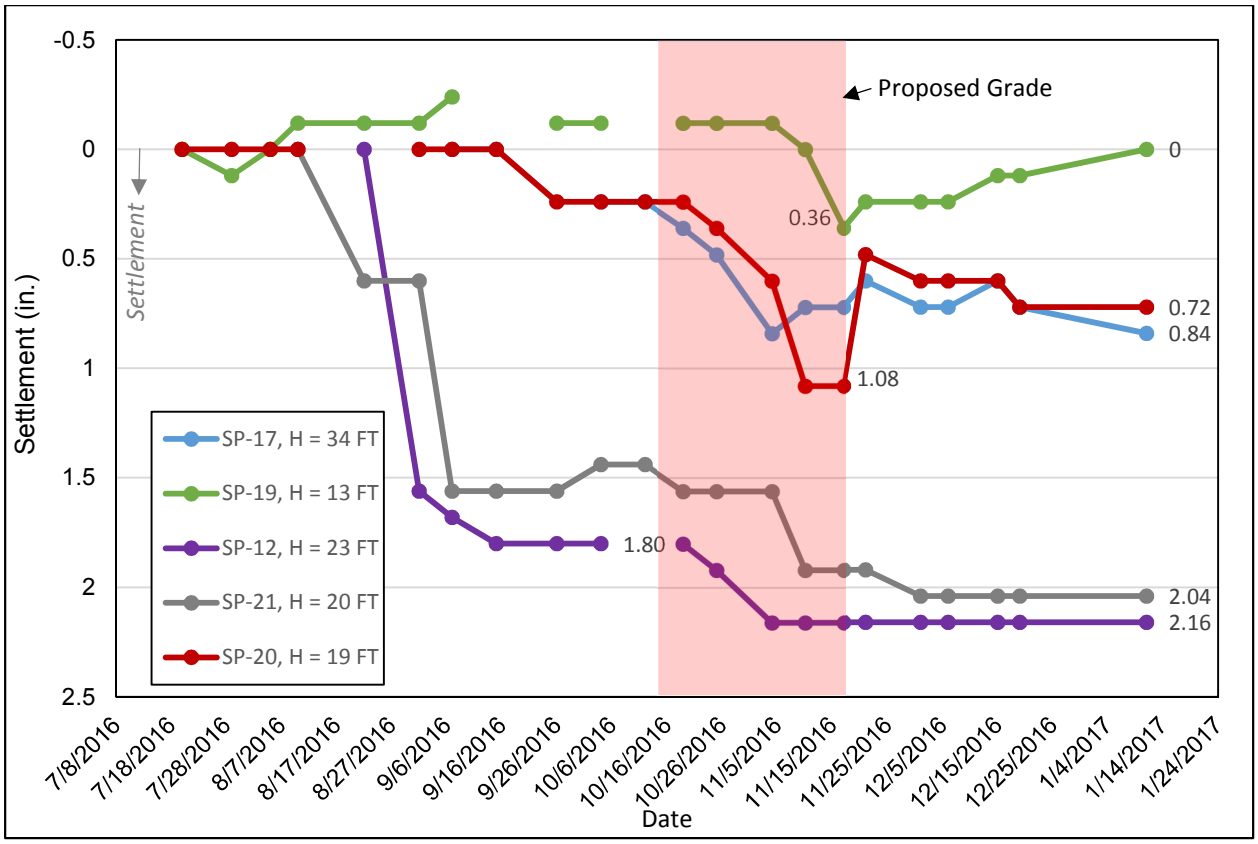


Figure 12. Zone 3 Settlement Monitoring Results

Table 5. Estimated versus Observed Settlements – Zone 3

Settlement Plate Location / Nearest FEM Model	PVD and Surcharge Program Used?	Estimated Settlement During Construction (in.)	Measured Settlement During Embankment Construction (in.)	Settlement Plate
STA 214+50 / 2D Model 1 ; 3D	Yes	1.2	0.8	SP-17
STA 216+70 / 2D Model 2	Yes	2.3	2.2	SP-12
STA 218+00 / 2D Model 3	No	0.8	2.0	SP-21
STA 157+00 / 2D Model 4	Yes	0.5	0	SP-19
STA 155+50 / 2D Model 7	No	0.9	0.7	SP-20

The measured settlement during embankment construction was overall less than the estimated settlement during embankment construction, with the exception of Model 3/SP-21. The settlement shots from SP-21 do suggest that the RI supported embankment has reached an equilibrium with flat survey elevations over the last month of data (characterized by no additional settlement since 12/5/16).

Surcharge and Lightweight Fill

Settlement monitoring was performed at two locations in Zone 1 where surcharge was used for ground improvement. Construction of embankment with 6 ft surcharge was completed on 6/17/15. Settlement platform data for those two locations are shown in Table 6 after completion of placement of surcharge.

Table 6. Settlement Monitoring Results for Ground Improvement with Surcharge – Zone 1

Settlement Platform #	Settlement Platform Elevations (ft) after Completion of Surcharge Placement											
	6/17/15	6/25/15	7/2/15	7/9/15	7/16/15	7/23/15	7/30/15	8/13/15	8/21/15	8/27/15	9/19/15	9/25/15
SP-1	16.35	16.29	16.30	16.27	16.28	16.22	16.23	16.20	16.22	16.21	16.20	16.20
SP-2	15.82	15.82	15.80	15.84	15.82	15.78	15.80	15.76	15.62	15.77	15.77	15.77

The measured maximum settlement (i.e., 1.8 in.) and duration of settlement (i.e., 3 months) were less than the estimated settlement and duration. Settlement monitoring was not performed at the lightweight aggregate fill locations (in Zones 1 thru 4 as shown in Fig. 3), since those were designed as zero net load increase. Embankments in both the surcharge and lightweight aggregate fill zones have been paved and to this date (July, 2017), no settlement or distress of pavement has been observed.

LESSONS LEARNED

This RI supported embankment project was successful due to the clear performance criteria that were established by the Project Geotechnical Engineer and enforced throughout the project with thorough review of the SGIC submittals. The extensive quality control program was implemented with positive results, with the exception of inconclusive column integrity testing and some damaged settlement plates. Proactive coordination between the Project Geotechnical Engineer, General Contractor and SGIC is important to protect the RI and settlement monitoring structures from damage or disturbance by construction traffic. Future RI supported embankment specifications should consider automated settlement monitoring systems and clearly define measures to be taken if unforeseen conditions arise during construction. The development of new technologies for verifying integrity of installed RI would also be beneficial, because CIT alone does not conclusively determine whether or not a RI will carry the axial compressive loads required by design. Finally, due to the nature of RI system, a significant portion of the applied load transfers to the soils. As a result, the RI system could experience long-term secondary settlements. The impact of secondary settlements on the RI system can be evaluated through long-term settlement monitoring of the embankments.

CONCLUSIONS

Utilization of a variety of ground improvement techniques (i.e., lightweight fill, preload with surcharge, concrete column rigid inclusion, rigid inclusion with surcharge and PVD), predominantly rigid inclusion, provided a cost-effective and time saving ground improvement solution for supporting the roadway embankments of the massive Interchange 14A project. Concrete column rigid inclusion for the 575,000 sq-ft area were successfully designed and constructed in less than one year. Rigid inclusion in combination with surcharge and PVD provided an efficient and innovative ground improvement solution for the historically marshy area with very soft soils. Settlement monitoring results show that the ground improvement systems met the performance criteria for the project, allowing construction to proceed on-schedule. The collaboration between the Project Geotechnical Engineer and the SGIC, during both the design and construction phases of work, resulted in successful implementation of a design-build concrete column rigid inclusion ground improvement system.

ACKNOWLEDGEMENTS

The Project Geotechnical Engineer (Gannett Fleming) and the SGIC (Menard and its Designer of Record GEI Consultants, Inc.) would like to thank the New Jersey Turnpike Authority (Client) and Union Paving Construction Company (General Contractor) for the use of the data presented in this paper.

SLOPING RUBBLE MARINE SEAWALLS FOUNDED ON SOFT SOIL IMPROVED BY STONE COLUMNS

Wilhelm S. Degen, Betterground (HK) Ltd., Hong Kong, +852 3628 3818, wdegen@mac.com
Chengbin Miao, Betterground (HK) Ltd., Hong Kong, +852 3628 3818, c.miao@betterground.hk
Eleonora Di Mario, Tony Gee & Partners LLP, formerly Benaim Ltd. (an AECOM company), Hong Kong, +852 3628 3818, eleonora.di-mario@tonygee.com
Matthew G. Mills, Benaim Ltd. (an AECOM company), Hong Kong, +852 2410 3825, matt.mills@aecom.com
Colin B. Turnbull, Benaim Ltd. (an AECOM company), Hong Kong, +852 2410 3828, colin.turnbull@aecom.com

ABSTRACT: In the past decade, the 'zero-dredge' philosophy has become the preferred option for the formation of marine seawalls and reclamations, compared to the partially or fully dredged options, as this solution presents several environmental advantages. Recent relevant project experience is presented herein in order to highlight key design principles and construction issues central to the successful construction and performance of a sloping rubble seawall founded on soft soil improved by stone columns. If designed and installed with proper quality control, correct treatment intensity and sensible construction staging, stone columns are a safe and cost effective method for seawall foundations. This paper provides guidelines with regards to the design, construction and quality control for the correct implementation of stone columns as a foundation element for sloping rubble marine seawalls.

INTRODUCTION

Benefits of sloping marine seawalls founded on stone columns

To suit the current environmental requirements in Hong Kong, recent projects are tending to favour zero-dredge solutions, such as the Hong Kong Boundary Crossing Facility and the forthcoming Three-Runway System. The installation of stone columns allows the underlying deposits, generally consisting of very soft to soft clay and silt (soft soil), to improve in strength to the extent that the seawall can be directly placed on the seabed. This negates the need to dredge the soft soil and, therefore, this ground improvement technique represents an ideal solution for zero-dredge projects.

Stone columns can also provide several other beneficial effects, including: accelerated drainage, reduced settlement, increased slope stability and soil reinforcement in the event of an earthquake. Stone columns, in contrast to competing cementitious methods, are a very ductile foundation method. This ductile behaviour is part of the design concept of stone columns in soft soil. Past projects located in Hong Kong and elsewhere, with an improved soft soil layer thickness of over 15m, have shown that stone columns can remain fully functional in terms of both drainage and horizontal reinforcement, even after settlements of over 3m and lateral displacements of up to 1m have occurred.

SEAWALL DESIGN PRINCIPLES

General design considerations

A critical design aspect for any seawall is the evaluation of its deformation behaviour (combined vertical and lateral displacements) and stability under horizontal loads induced by reclamation fill placement, including, in some cases, subsequent surcharge placement. This is particularly relevant when using a non-dredged approach where *in-situ* soft soil remains in place.

 © 2017 DFI Annual Conference, New Orleans, LA, USA

With regards to seawall construction, it is important to ensure that the *in-situ* soft soil provides sufficient horizontal confinement to the stone columns in order to ensure the stability in each stage. Such confinement is achieved through the consolidation of the soft soil under the overburden vertical load induced by the seawall, during and post seawall construction. This can be achieved by incorporating suitable 'pause periods'. These pause periods should be specified at, both, the end of each filling stage during seawall construction and prior to proceeding with the fill placement for the reclamation. Further consideration about the evaluation of the required overburden pressure is provided in the following section "*Mechanism of interaction between soft soil and stone columns*".

In the evaluation of the required pause periods, the designer should consider that a zone of reduced column permeability may develop at its perimeter due to mixing of the disturbed soft soil with the column material, when adopting the dry bottom feed method for stone column construction. A recent study (Weber et al., 2009) states that this 'smear zone' should be taken into account in the consolidation analysis, as smearing has a dominating effect on the consolidation behaviour of the improved soft soil. When an uncoupled consolidation analysis is performed, in terms of stability and consolidation, the smear zone may be accounted for in the consolidation assessment by reducing the diameter of the stone columns by 5% (Kirsch and Kirsch, 2010).

Within the main reclamation area behind the seawall, experience on various projects shows that the construction sequence and the methodology of fill placement have a significant influence on the horizontal displacement of the seawall. The designer is therefore recommended to plan a staged fill placement sequence, similar to that specified for the seawall construction, to ensure that the soft soil beneath the reclamation area is allowed to progressively consolidate and gain sufficient shear strength during construction. With regards to fill placement, it is not recommended to progressively fill perpendicular to the seawall as this practice will cause excessive lateral displacements of the seawall, i.e. filling should be progressed at as an oblique angle as practical to the seawall.

Recommended replacement factor for stone columns in soft soil

The first author has been involved in numerous stone column projects over the last 30 years. According to his experience, the most common application for stone columns has been in silty sands and sandy silts, with a design focus on liquefaction prevention, rather than slope stability. These projects have generally employed replacement factors (RF) (also known as 'area' or 'replacement' ratio) ranging between 8% and 20%, with the majority between 10% and 15%.

It should be noted that RFs in soft soil are generally higher when slope stabilisation is the primary objective. Although the range is similar, generally between 8% and 30%, the majority of such projects employ a RF between 15% and 25%. This correlates well with guidance given by Barksdale (1983).

Although projects implementing RFs below 15% may be successfully designed and constructed, they may also carry higher risks due to unforeseen challenges. It is therefore recommended that a RF>15% is employed for stone columns installed in soft soil. An example of installation grid pattern and relevant equations for the calculation of RF is given in Fig. 1 in Addendum 1.

Mechanism of interaction between soft soil and stone columns

To describe the distribution of the overburden vertical load induced by the seawall onto the *in-situ* soft soil and stone columns below, a stress concentration factor (n) is introduced (e.g. Priebe, 1995). The n factor is defined as the ratio between the stress in the stone columns over the stress into the soft soil. The combined shear resistance of the soft soil and stone columns can be analysed by considering a 'stone

column unit cell' (Barksdale and Bachus, 1983) beneath the footprint of the seawall, as shown below in Fig. 2 in Addendum 1.
The combined shear resistance of the unit cell along a potential failure surface can be expressed as shown in equation 1:

$$\tau_{uc} = (\tau_s \,.\, A_s + \tau_c \,.\, A_c)/A_{uc} = (c_u \,.\, A_s + \sigma'_c \,.\, \cos^2\delta \,.\, \tan\varphi'_c \,.\, A_c)/A_{uc} \qquad [1]$$

where, τ_{uc} = shear resistance of composite system, τ_s = shear resistance of soil, A_s = area of soil, τ_c = shear resistance of stone column, A_c = area of stone column, A_{uc} = area of composite system, c_u = undrained shear strength of soil, σ'_c = effective vertical stress in stone column, φ'_c = friction angle of stone column material, and δ = angle of assumed failure cone in stone column.

Although the vertical effective stress in the soft soil (σ'_s) is not taken into account in the above equation, there is generally a linear correlation between the undrained shear strength and the effective vertical stress. Therefore, the contribution from the soft soil ($c_u \,.\, A_s$) to the unit cell resistance can be directly correlated to the proportion of overburden stress transmitted to the soft soil. This contribution tends to decrease as *n* increases. Conversely, the contribution to the unit cell resistance from the stone columns ($\sigma'_c \,.\, \cos^2\delta \,.\, \tan\varphi'_c \,.\, A_c$) will tend to increase as *n* increases. The combined shear resistance of the unit cell generally increases less than linearly as *n* increases. A typical trend of unit cell combined shear resistance for a replacement factor of 17% is shown below in Graph 2.1 (see Fig. 3 in Addendum 1).

The response of the seawall in terms of horizontal displacements has been studied by implementing a 3-dimensional finite element model with commercially available software (PLAXIS 3D). In this model, the overburden from the seawall, reclamation fill and its surcharge has been represented by surface loads. The variability of *n* has therefore been modelled by varying the ratio between the surface load applied on the stone columns and soft soil.

The behaviour under lateral load is predominantly governed by the mechanical properties of the clay and these mechanical properties are directly affected by *n,* as shown in Equation 1. The results of the sensitivity analysis (see Graph 2.2 in Fig. 3 in Addendum 1), correlate well with this understanding and show that the horizontal displacements of the seawall and underlying improved soft soil increase more than linearly as *n* increases.

An example of both the model geometry and resultant horizontal displacement contour plan are shown in Fig. 4 in Addendum 1. The contour plan shows that the largest horizontal displacements occur approximately within the top 10 to 15m below the seawall footprint.

These results highlight the significant influence that *n* can have on the behaviour of the seawall. In practice, *n* may vary depending on various factors including, but not limited to: 1) the stone column replacement ratio, 2) the ratio between stone column length and diameter (L/D), 3) the ratio between the stiffness of the stone column and soft soil, 4) the properties of geotextiles used i.e. at the base of the seawall, and 5) the degree of consolidation of the soft soil (Castro and Sagaseta, 2009).

Unduly large horizontal displacements of the seawall during the initial filling stages may lead to integrity loss of the stone columns and/or excessive shear strain within the soft soil. This, in turn, may cause the undrained shear strength of the soft soil to reduce to its residual minimum value and adversely affect the overall stability performance. Therefore, it is recommended that the designer carefully consider the consequences of implementing techniques where high *n* values may be expected, which could lead to a significant adverse impact on the horizontal displacements of a laterally loaded seawall.

Design recommendations for enhancing stone column performance

Generally, the top 5 to 10m of the soft soil show very low undrained shear strength values (c_u = 0 to 10kPa), limiting the lateral confinement provided to the stone columns during installation and during early stages of construction. To increase the confinement of the stone columns in the early stages of construction, the designer should consider pre-consolidation of the top 5 to 10m of soft soil by means of Pre-fabricated Vertical Drains (PVDs) combined with a preload of approximately 2 to 3m of aggregate fill. The pre-consolidation phase should aim to increase the undrained shear strength of the soft soil by approximately 5kPa, providing an improved layer with an undrained shear strength ranging from 5 to 15kPa prior to the stone columns installation.

The designer should also consider recommending the installation of stone columns in two phases, as shown above in Fig. 1 in Addendum 1. Phase one should have double spaced columns and then phase two would 'fill in the gaps'. The stone columns installed during the first stage will provide additional lateral confinement during the second stage of stone column installation, beneficially improving the quality of the secondary stone columns.

Based on the results shown in section *"Mechanism of interaction between soft soil and stone columns"*, the largest horizontal displacements below the seawall footprint are expected to occur approximately within the top 10 to 15m below the top surface of the soft soil. Further to pre-consolidation, it is recommended that the designer consider the installation of stone columns with a variable diameter, i.e. a larger diameter in the upper part of the soft soil layer to increase the combined stiffness of the soil where these larger displacements can be expected. Within the same stone column, experience shows that the variation can be as large as 50% i.e. 1.5m diameter in very soft layers to 75cm in the competent layers.

STONE COLUMNS BEST PRACTICE

Determination of treatment depth and refusal depth

The design depth of a stone column installation must be sufficient to:

a) Carry vertical loads to a lower bearing layer such as to minimize the static settlement of the stone column to acceptable levels;
b) Reinforce all layers through which a critical slope failure might otherwise occur; and
c) Avoid negative surface effects from soil liquefaction of any layer below the treatment depth.

The CPT is a very efficient tool to assist in the evaluation of the depth of treatment required in order to meet design targets. However, CPTs can only be undertaken at a limited number of locations and therefore the base of the soft soil must be inferred via Kriging interpolation or similar. The soil boundary between CPT locations will, almost, never follow this inferred line, which can result in areas of competent soil above and, worse, areas of soft soil below the target refusal level (see Fig. 5 in Addendum 1). Therefore, a too strict adherence to a CPT evaluated treatment depth limit can cause challenges on site. To compensate, feedback on soil stiffness given by the vibroprobe during penetration must be considered. It is recommended that the Engineer provides provision within the project specification to allow for the termination criteria to be modified given the actual subsurface ground conditions encountered on site during construction, i.e. a performance based specification.

In a recent project, a suitable termination criterion in a clayey alluvial soil was assessed by comparing the cone resistance data from a large sample of CPT locations with the actual depth of refusal for their adjacent stone columns. A typical comparison report is given in Fig. 6 in Addendum 1, which shows that all of the uncorrected cone resistance (q_c) values at refusal depth were much higher (over 2MPa) than the required 1.5MPa, detailed in the project specification.

The resistance of the soil can be indirectly measured by the amount of effort (measured by ampere) required for the vibroprobe equipment to progress over a certain depth. For this project, the Contractor utilised this correlation to propose and successfully implement the following guideline for refusal depth:

"Penetration beyond the CPT based contract toe level will be carried out as far as practical. However, due to the capacity of the equipment, the stone column will be, in any case, terminated at a level determined from three trials of penetration that yield less than 20cm advancement while observing an increase in the amperes measured up to a maximum of 1.75 times the amperes measured under free hanging conditions."

The implementation of this guideline is shown in a typical quality control report below (see Fig. 7 in Addendum 1).

Quality control of stone column

By their nature, offshore stone columns are difficult to inspect visually or evaluate with load testing and, therefore, digital data recording of key installation parameters is crucial. It is recommended that the quality control system should contain, as a minimum, the following features:

1. Log of the stone column installation taken at one second intervals;
2. Log of ampere and depth over time;
3. Log of air pressure in the stone placement tube; and
4. Shape of the stone column plotted over depth.

A comparison between the quality control reports for a stone column with an installation defect (bottleneck) at 9m depth is shown below, where readings are taken at one second intervals (Fig. 8 in Addendum 1) and 20 second intervals (Fig. 9 in Addendum 1). The shapes of the stone columns are given over depth on the right side of the figures.

These figures highlight the importance of specifying an appropriate frequency of logging steps. The defect can be easily seen in both the graph and shape plot when the readings are taken at one second intervals. However, it can be seen that this defect is lost in the 'noise' created by the infrequency of the 20 second interval logging. More details on offshore quality control equipment and procedures are given in Degen (2014).

The pressure in the gravel tube is an important aspect to consider when installing stone columns. As the lower sections of the stone columns are likely to be subject to significant pressures, the pressure in the gravel tube must be maintained at a high enough level to ensure adequate flow of stones. Any defect in the telescoped rig which results in pressure release will lead to an imperfection in the lower end of the columns. As such, measurement of the pressure in the gravel tube (common practice in deep offshore works) is essential, as it acts as the sole quality check for any such issue.

IN-SITU TESTING, INTRUMENTATION AND MONITORING

Observational approach

The behaviour of a seawall founded on improved soft soil is complex and can be difficult to predict. It is therefore recommended that an observational approach is adopted for the design and construction (as suggested in BS EN 1997-1:2004). The designer may consider introducing appropriate 'check points' in-between construction stages, where the behaviour of the seawall, the stone columns and the soft soil should be reviewed. To support these reviews, appropriate instrumentation should be installed to help assess whether the performance of the seawall is consistent with the theoretical models adopted in the design.

When adopting the observational approach, the designer should be contracted to compare instrumentation readings to pre-set design trigger levels (Alert, Action, Alarm levels) for each construction design stage. This process enables the designer to assess the performance of the seawall and allows appropriate remedial measures to be recommended and implemented in a timely manner.

Instrumentation and monitoring

When an observational approach is adopted, validation of the design assumptions relating to the stability and displacement of the seawall is considered critical when assessing whether to proceed with subsequent construction design stages. An instrumentation and monitoring plan comprising a range of geotechnical instrumentation, together with *in-situ* testing, is therefore required to adequately monitor the behaviour of the seawall during reclamation fill and surcharge placement. The gain in undrained shear strength is a significant indicator of the degree of consolidation that has occurred and whether or not the foundation soil has improved sufficiently to maintain seawall stability. It is recommended that verification of the undrained shear strength of the soft soil should be undertaken by direct measurement utilising in-situ Vane Shear Tests (VSTs), or similar. Experience on previous projects shows that VSTs can be successfully carried out between the stone columns, without significant issues to the contractor. In the reclamation area treated with PVDs, CPTs can also be adopted for the evaluation of the shear strength gain. Suitable calibration field tests should first be undertaken, particularly in order to select an appropriate cone factor (N_k) for the interpretation of the CPTs.

A typical layout for monitoring instrumentation is shown in Fig. 10 in Addendum 1. Sub-surface settlement marker plates and extensometers may be installed to monitor the settlement of the seawall and the reclamation. Within the seawall footprint, the interpretation of the settlement data may be used as an indirect method to evaluate both the degree of consolidation in the soft soil and the stress concentration factor.

Vibrating wire piezometers may be installed at different depths to monitor the pore water dissipation during the construction sequence. It should be noted, however, that the pore water pressure measured at the piezometric cell location is highly influenced by the radial distance of the cell from the adjacent drainage elements (i.e. stone columns and/or PVDs). In practice, verticality errors in both the instrumentation and drainage elements, along with the accumulated horizontal displacement of the soil mass, will likely result in this distance differing from the theoretical assumption. As these errors are difficult to quantify, and could significantly affect the evaluation of the consolidation process, it is not recommended to solely rely on piezometric data to control the rate of filling, the length of the pause periods or assess stability. Rather, this evaluation may be used as a supplemental check for the *in-situ* testing to demonstrate that the dissipation of pore pressures is in accordance with that predicted from the design models and to compare their response to the other instrumentation and testing.

Based on project experience, inclinometers are generally preferred over surface movement markers for the monitoring of horizontal displacements of the seawall as the maximum horizontal displacement of the seawall was generally recorded at the seabed level, i.e. below the installation depth of surface movement markers. It is also recommended to combine the inclinometers with extensometers as these provide a reliable method to define settlements per stratum. It should also be noted that surface movement markers are often so significantly disturbed by site construction activities that readings become unreliable. A summary of typical instrumentation, testing and monitoring schedule is provided below in Table 1.

Table 1. Typical instrumentation, testing and monitoring schedule

Type of Testing/ Instrument	Typical Testing/ Installation Level	Purpose of Testing/Monitoring	Typical Monitoring Frequency
In-situ Vane Shear Test	1m below seabed level and every 3m to the base of the soft soil layer	Verify strengths within the soft soil at the end of prescribed pause periods, prior to further placement of fill	Check points prescribed by the designer
Inclinometer/ Extensometer	From top of fill level to 5m (min.)within the competent soil stratum	Compare the performance of the seawall in terms of displacements with design prediction	Twice per week
Sub-surface Movement Marker Plates	Top of stone blanket and at intermediate fill levels	Validate the assumptions for the consolidation process prediction	Twice per week
Double Tip Vibrating Wire Piezometer	Piezometric cells equally spaced within soft soil layer	Evaluate the overall performance of the drainage system	Twice per week

RISK MANAGEMENT – MITIGATION AND REMEDIAL MEASURES

As with any engineering project, it is important to capture as many of the potential risks as early as possible in order to manage them effectively. This is particularly pertinent when undertaking work in soft soil, where the behaviour of the seawall can be difficult to predict and large deformations may be expected.

The degree of risk associated with the geotechnical hazards should be assessed by the designer and included in a project risk register. In order to reduce risks to acceptable levels, this risk register should highlight possible mitigation measures to be implemented before and/or during construction. The designer may also consider providing information on possible remedial measures that may be adopted if the monitoring results or overall performance of the work deviate from design predictions. Some of the key hazards that should be considered in the risk assessment, together with typical mitigation and remedial measures, are summarised below in Table 2.

Table 2. Hazards and Mitigation and Remedial Measures

Hazard	Mitigation and Remedial Measures
Unforeseen ground conditions	i. Ensure adequate ground investigation is undertaken prior to construction and recommend additional site investigation, as necessary.
Monitoring and/or *in-situ* testing deviates from the specification	i. Ensure instrumentation and *in-situ* testing is fully detailed in drawings. ii. Advise contractor of the potential impact and risks of not installing the instrumentation and undertaking the monitoring and *in-situ* testing as per the design drawings and schedules. iii. Promptly recommend replacement of instruments when their serviceability limit is approached i.e. by deformations induced by the surrounding soil.
Inconsistent *in-situ* testing and/or monitoring results	i. Compare results from different instruments/tests in nearby locations in order to establish which instruments/tests should be considered unreliable. ii. Undertake additional *in-situ* testing to validate anomalous results.
Construction not in accordance with the prescribed construction sequence	i. Ensure the construction sequence is adequately detailed in the drawings. ii. Advise contractor of the potential impact of not following the proposed construction sequence, notably liability and associated costs of failure or not satisfying limiting design criteria. iii. If discrepancies are identified, a detailed review of the impact on the work performance should be undertaken to decide whether it is considered appropriate to proceed to the next construction design stage and, if necessary, modify the construction sequence accordingly.
In-situ testing indicates that the improvement in the foundation soil is not in accordance with the design models	i. Detailed review of monitoring results and reanalysis to decide whether it is considered appropriate to proceed to the next construction design stage. ii. Increasing the duration of the surcharge/pause period(s) to allow the underlying soft soil to improve in strength before proceeding with the next construction design stage. iii. Increasing the surcharge fill heights to increase the effect of consolidation and improvement in shear strength.
Monitoring results are not in accordance with the design models, or results reach/exceed, the relevant pre-set instrumentation trigger (AAA) levels earlier than predicted	i. Installation of additional PVDs to enhance the consolidation process. ii. Provision of a remedial toe berm to provide an increased stabilising force. iii. Installation of additional ground improvement beyond the seawall to increase the stability of the edge of the reclamation.

CONCLUSION AND RECOMMENDATIONS

Recent projects show that sloping rubble marine seawalls can be reliably founded on soft soil improved by stone columns. To successfully design and construct this type of seawall, the following key elements should be considered:

Design

- Confinement of the stone columns – sufficient confinement of the stone columns must be achieved through pre-consolidation and a staged construction design sequence of the seawall.
- Pause periods – in order to achieve required strength gains in the soft soil, thorough assessment of the required pause periods should be incorporated into the design along with proper staging of the works.
- Filling placement – filling direction should be progressed at as an oblique angle as practical to the seawall to reduce the lateral deformation of the seawall.
- Soil smearing – smearing of the soil immediately surrounding the stone column must be accounted for in the design.
- Stress concentration factor – it is not recommended to use techniques which increase the stress concentration factor as the potential for large horizontal displacements also increases.
- Variable column diameter – the stone column diameter should increase in softer layers and reduce in more competent layers.

Stone Column Construction

- Logging of key parameters – during installation amperes (i.e. effort of vibroprobe equipment), depth, gravel tube pressure and gravel consumption should be logged as a minimum. The maximum interval in logging steps should be one second; otherwise defects in the columns may remain undetected.
- Refusal depth of stone columns – the refusal depth should not rely solely on pre-construction data, such as CPTs. It has been shown that refusal depths can be reliably determined with vibroprobe ampere readings, which correlate well with soil shear strength.

Observational Approach

- Observational approach – this method should be adopted for seawalls installed in soft soils.
- Instrumentation and Monitoring – an appropriate suite of instrumentation and monitoring should be specified, which must complement the original design assumptions such that they may be compared with the observed behaviour of the seawall and reclamation.
- *In-situ* testing – adequate testing to verify strengths should be undertaken within the soft soil at the end of prescribed pause periods.
- Pre-set displacement trigger (AAA) levels – the vertical and lateral displacement trigger levels should be evaluated prior to the works for the seawall and regularly checked against the monitored displacements during construction.

Risk Management

- Risk register – a risk register should be adopted as part of the design, with clearly identified mitigation and remedial measures that could be implemented in a timely manner, as required.

REFERENCES

Barksdale R.D. and Bachus R.C., 1983. Design and construction of stone columns. Federal Highway Administration, RD-83/026.

Castro J. and Sagaseta C., 2009. Influence of stone column deformation on surrounding soil consolidation. Geotechnics of Soft Soils – Focus on Ground Improvement. Taylor & Francis Group, London, pp. 333-338.

Kirsch K. and Kirsch F., 2010. Ground improvement by deep vibratory methods. Spon Press, London and New York, pp.131.

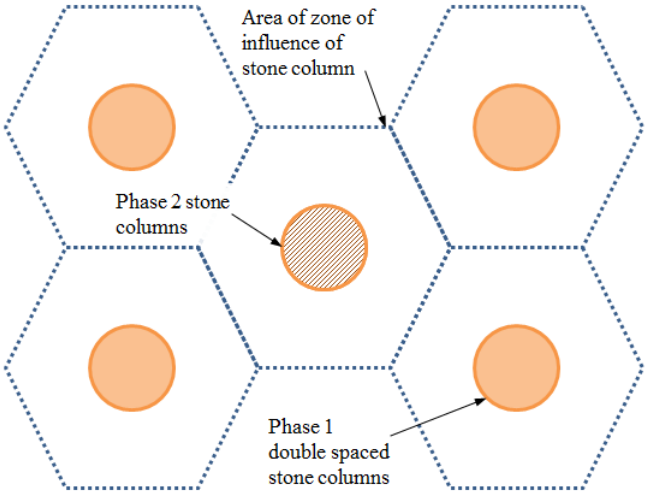
Weber T.M., Springman S.M., Gäb M., Racansky V. and Schweiger H.F., 2009. Numerical modelling of stone columns in soft clay under an embankment. In Karstunen & Leoni (eds), Geotechnics of soft soils – focus on ground improvement. Taylor & Francis Group, London, pp. 305-312.

Priebe, H.J., 1995. The design of vibro replacement. Ground Engineering, London, pp. 31-37.

Degen, W. 2014. Advances in equipment and quality control for offshore and onshore stone columns and vibro compaction. 18th Annual National Conf. on Geotech. Engineering, Jakarta, pp. 251- 255.

BS EN 1997-1:2004, 2004. Eurocode 7: Geotechnical design - Part 1: General rules. European Committee for Standardization, pp. 36.

ADDENDUM 1 – FIGURES



For a Triangular Grid:

$$RF = \frac{Ac}{As} = \left(\frac{\pi d^2}{2\sqrt{3}s^2}\right) \sim 0.91\left(\frac{d^2}{s^2}\right)$$

For a Square Grid:

$$RF = \frac{Ac}{As} = \pi\left(\frac{r}{s}\right)^2$$

Where:

Ac = Area of stone column
As = Area of zone of influence
d = Column diameter
s = Grid spacing

Fig. 1 Example installation phasing and triangular grid pattern with relevant equations for calculation of RF

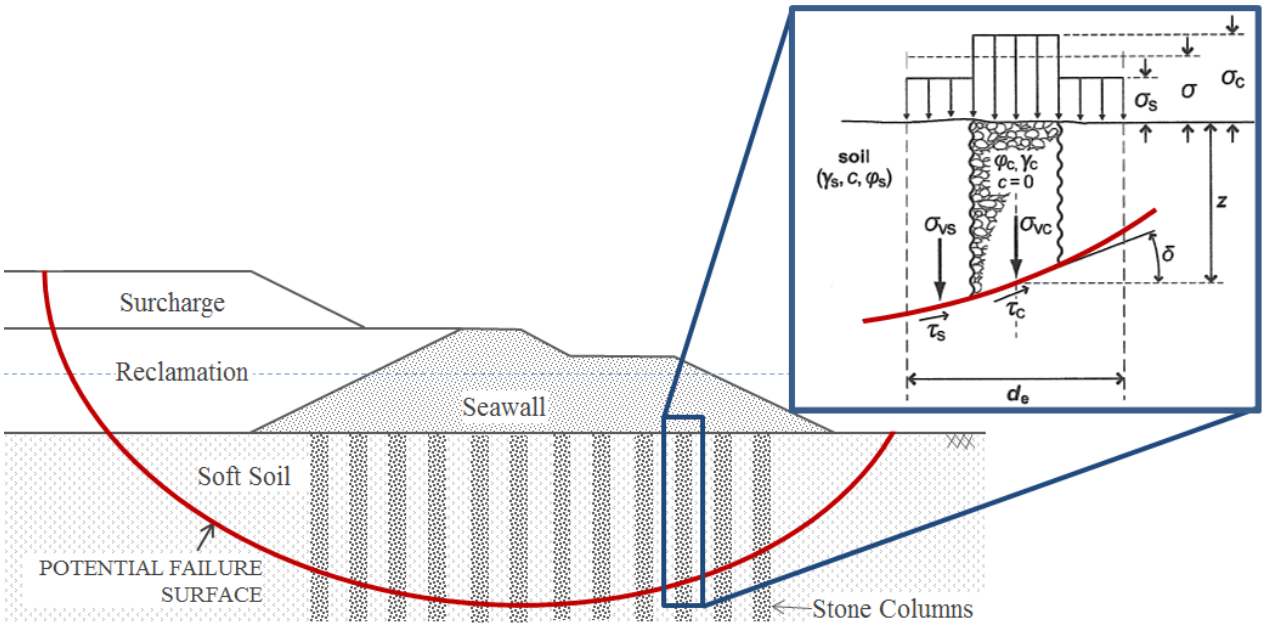


Fig. 2 Stone column unit cell concept (Barksdale and Bachus, 1983)

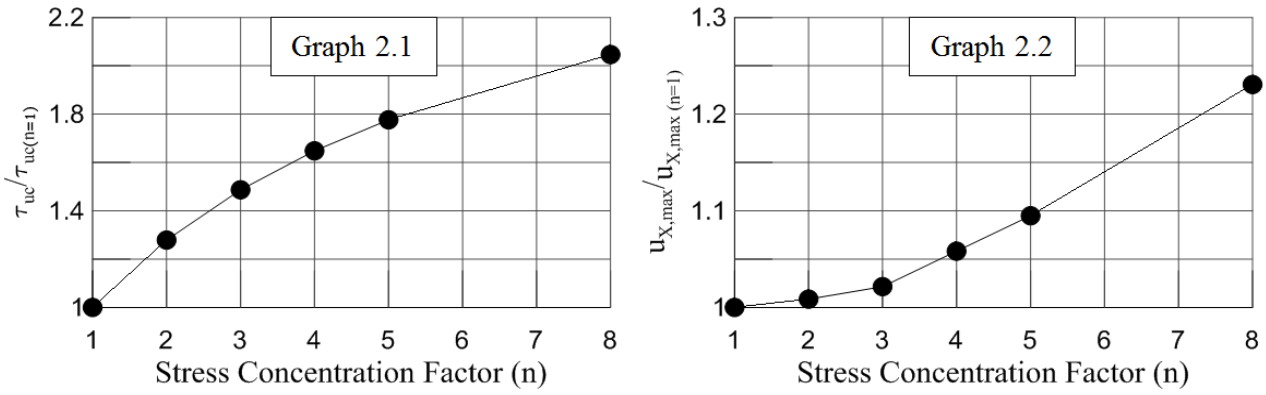


Fig. 3 Normalised unit cell strength (τ_{uc}) and maximum horizontal displacement ($U_{x,max}$) versus *n*

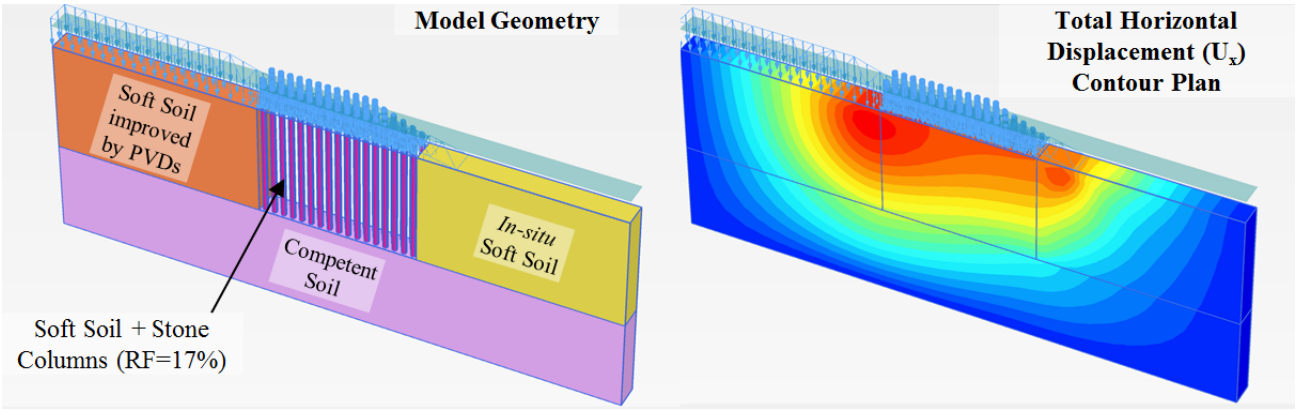


Fig. 4 Geometry of the PLAXIS 3D model and typical horizontal displacement (U_x) contour

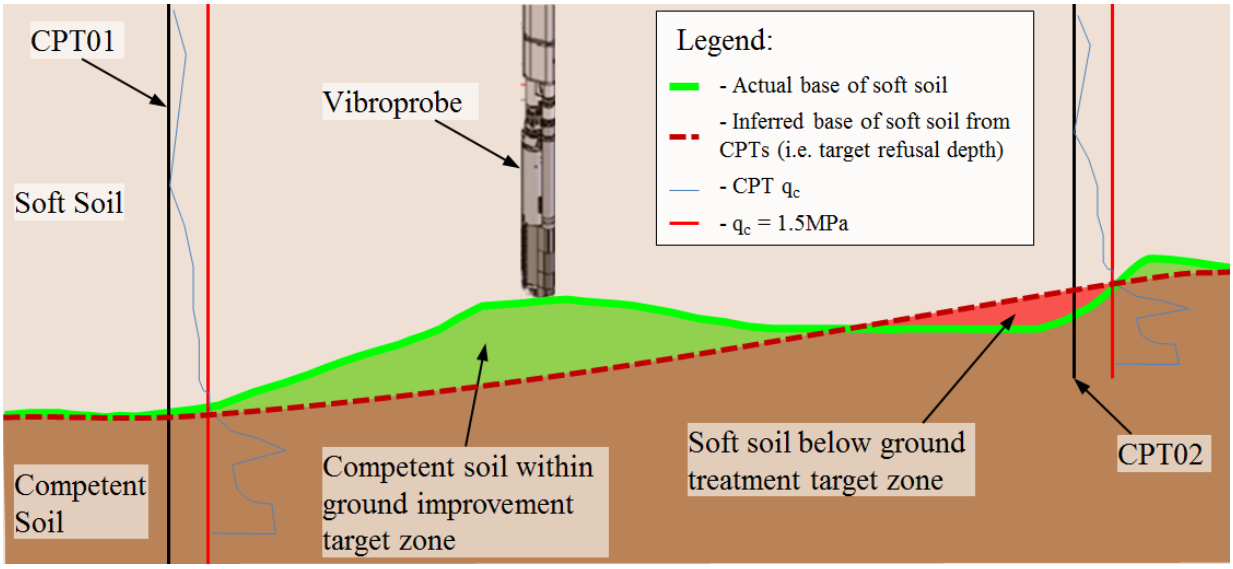


Fig. 5 Comparison of refusal depth in design and in practice

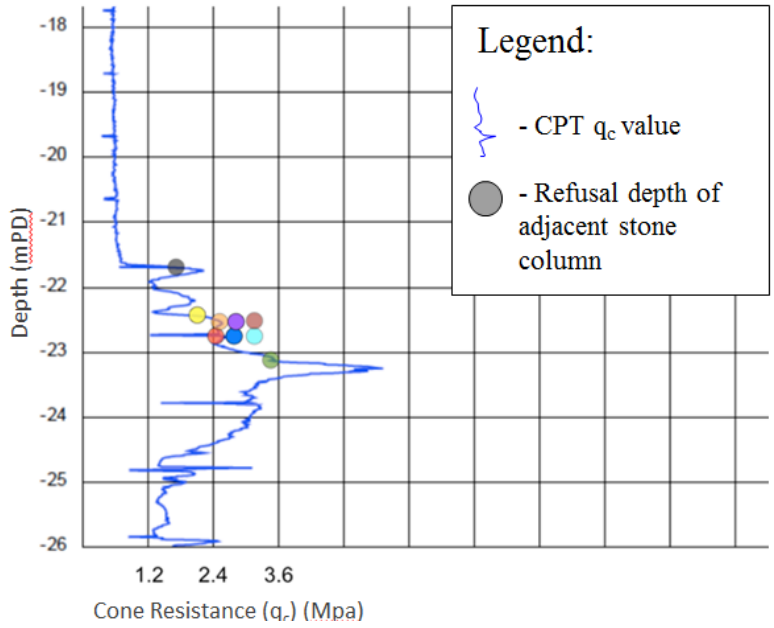


Fig. 6 CPT q_c plot against depth with actual refusal depths achieved in adjacent stone columns

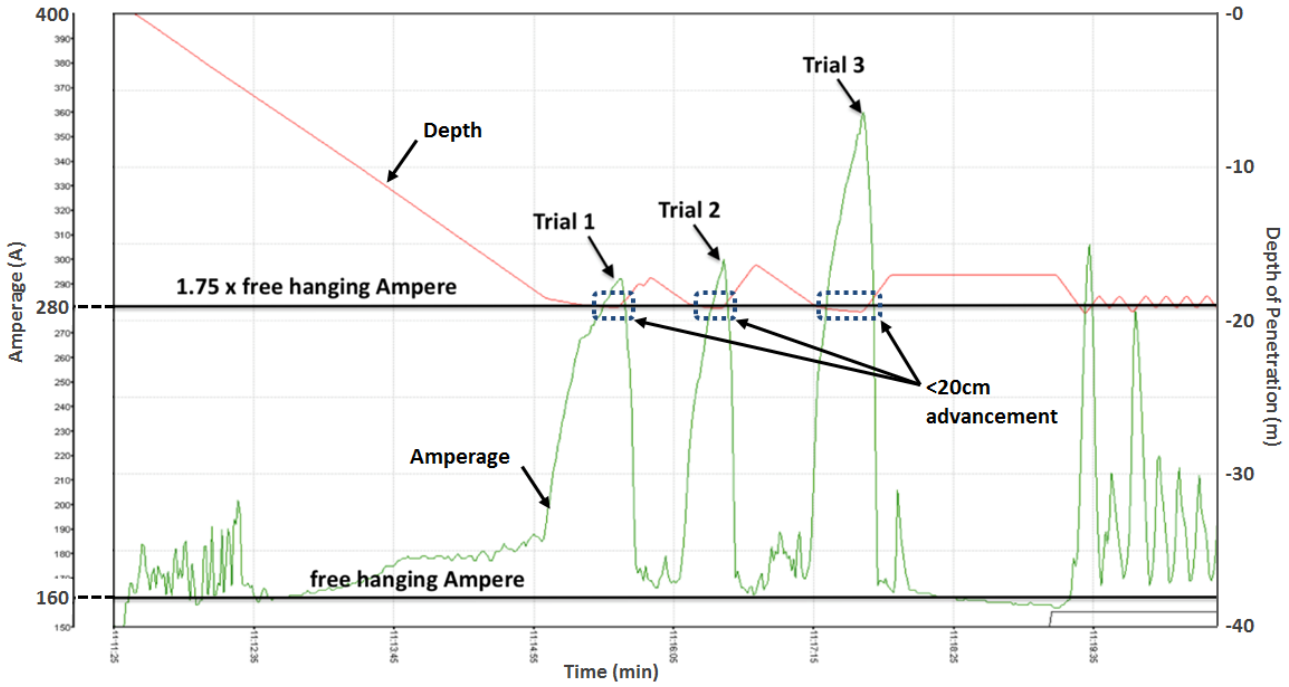


Fig. 7 Penetration stage in a typical quality control report for stone column installation

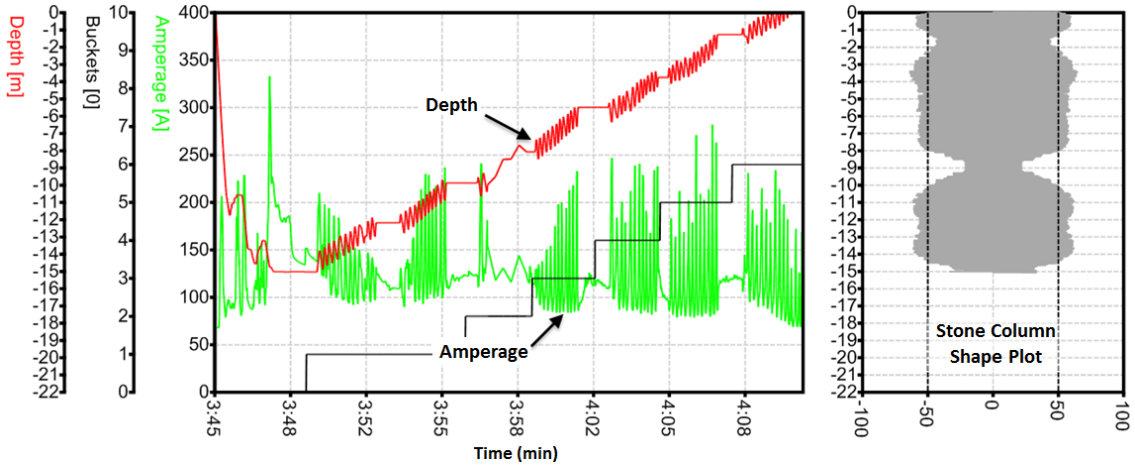


Fig. 8 Quality control report "record per second"

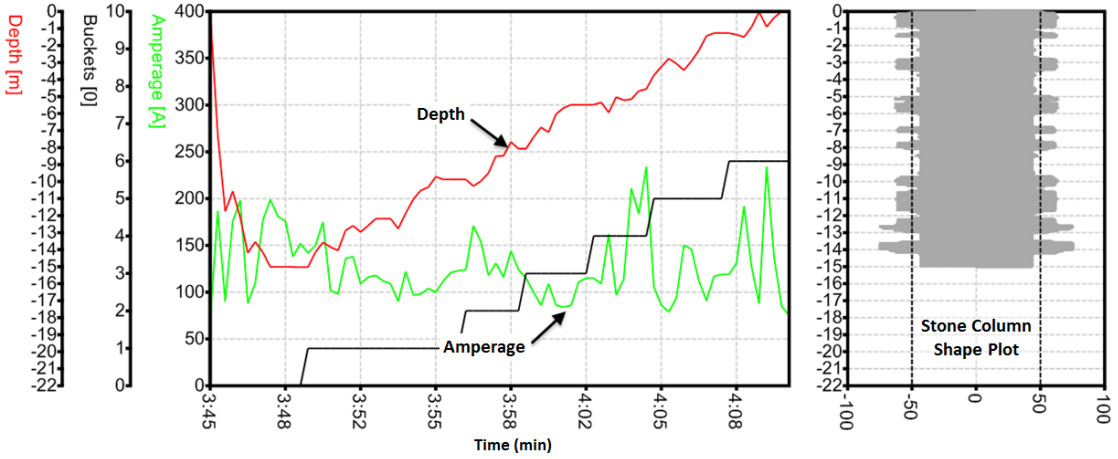


Fig. 9 Quality control reports "record per 20 seconds"

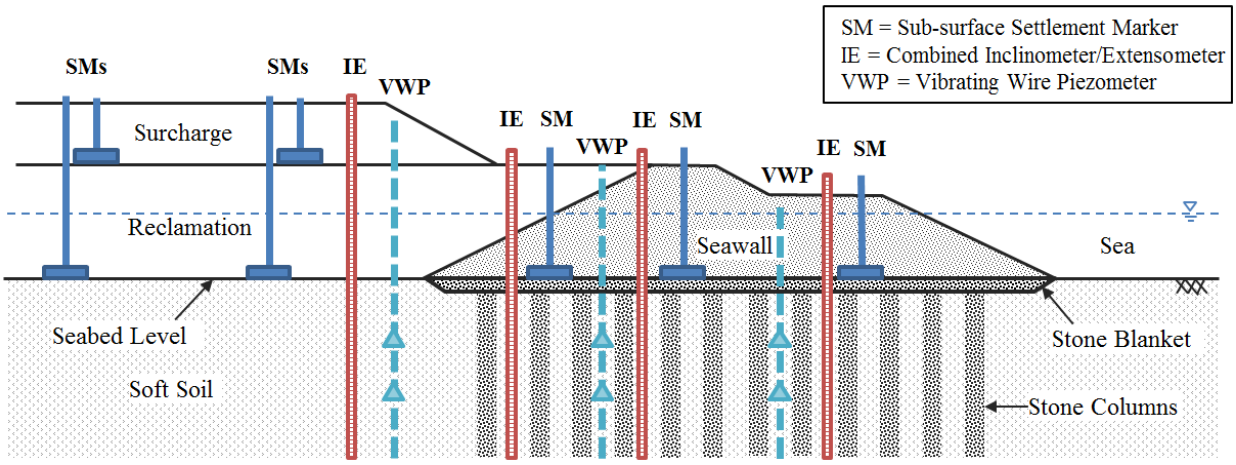


Fig. 10 Typical layout of monitoring instrumentation

STAGED CONSTRUCTION OF AN INTERSTATE I69 EMBANKMENT: COUPLED HYDRO-MECHANICAL NUMERICAL SIMULATION

Yazen A. Khasawneh, NTH Consultants, Northville, Michigan, khasawneh10@gmail.com
Malek Smadi, Geotill, Inc., Fishers, Indiana, msmadi@geotill.com

ABSTRACT

New embankments were constructed mostly on soft clays as part of interstate I69 extension in southern Indiana. The embankments serve as bridge abutments and as part of the fill sections along the interstate extension alignment. The height of the embankments range from 50-ft to 125-ft with a maximum foundation thickness of about 75-ft. The foundation soils comprise relatively high compressible fine grained soils. A fully coupled Hydro-Mechanical numerical simulations were conducted for optimizing the construction stages of the embankments. The objective of the staged construction is to allow for sufficient effective stress and undrained shear strength gain to ensure foundation stability under the stage load. Wick drains were utilized to shorten the drainage path and thus accelerate achieving the required undrained shear strength. The extensive field investigation and laboratory testing programs provided a good understanding of the subsurface conditions and allowed the use of a relatively advanced soil constitutive model in the numerical simulations of the staged construction. The effectively designed instrumentation program allowed for monitoring the settlement and pore water dissipation during construction. The pore water pressure, and surface and subsurface settlements from the numerical model predictions reasonably agreed with the instrumentation data over the construction period.

Keywords: staged construction, soft clay, ground improvement, wick drains, coupled analysis finite element

INTRODUCTION

The stability of soft fine grained foundation soils due to embankment construction is dependent on the undrained shear strength of such soils. The permeability, compressibility, and drainage boundaries control the foundation soils response (settlement magnitude and rate) to loading. The settlement magnitude is a function of minerology and soil structure. The settlement rate which is equivalent to the rate of excess pore water pressure dissipation is a function of the soil permeability and drainage boundary. The dissipation rate control the evolution of effective stress and thus the gain of undrained shear strength. As such, if the increase in total applied load is controlled such that enough time is granted for the evolution of the total stresses into effective stresses, then the stability of the foundation soils is enhanced by the gain of the undrained shear strength. The controlled application of the total stress is the definition of the staged construction. From the definition of the staged construction, it is obvious that the process is a coupling of the hydraulic and mechanical responses of the foundation soils.

The twenty-second Terzaghi lecture by Ladd (1986) provides a comprehensive insight on the evaluation of a staged construction problem. The lecture explains in depth the selection of the undrained shear strength and the SHANSEP parameters for the analyses. Ladd recommended the use of the undrained strength analysis (USA) to check the stability of the construction stages. The lecture explained that the use of Effective Stress Analysis (ESA) will overestimate the safety factor for clays with high plasticity and tends to underestimate the depth of the critical failure surface. In addition, the Peck's observational approach was recommended through the use of effective instrumentation program during construction to evaluate the design performance.

The use of wick drains to accelerate the evolution of total stress into effective stress (consolidation) during staged construction was extensively evaluated by Mesri and co-workers using the computer program ILLICON, which implements two important concepts the uniqueness of e-log $\sigma'v$ relationship and the law

 © 2017 DFI Annual Conference, New Orleans, LA, USA

of compressibility (C_α/C_c) (eg, Mesri and Choi (1985), Mesri and Khan (2012), and Mesri and Funk (2014), the results of Mesri's work showed excellent agreement between the predicted and observed settlement as a function of construction time.

In this paper, the project background, the development of the numerical model, comparison with the data from the instrumentation program, and conclusions and lessons learned will be presented and discussed.

PROJECT BACKGROUND

The plans called for the extension of interstate I69 in Indiana as shown in Fig. 1. The extension alignment was divided into nine reaches, four cut reaches and five fill reaches. The fill reaches vary in height between 50-ft and 125-ft. The Section analyzed in this paper is the east approach embankment of the I69 overpass over county road CR600E.

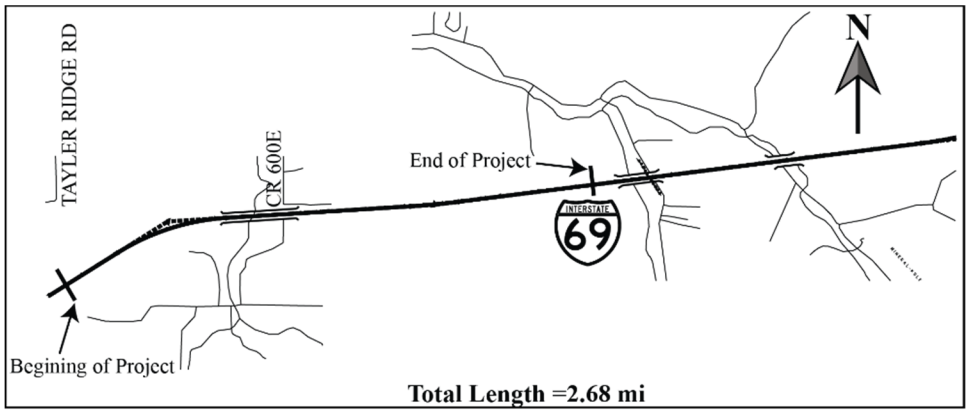


Fig. 1. Project location plan (after INDOT, 2012).

The original design called for the embankment at to be 60-ft in height and a crest width of about 150-ft, with slopes of 3H:1V. The contract was awarded as design-build contract, as such the design-build team proposed a modified embankment geometry with about 50-ft in height and 100-ft of crest width, while maintaining the slope of the embankment per the original design, the original design embankment section and the as-built section are both presented in Fig. 2. The first analyses were conducted for the original design and subsequently modified to capture the modified design (as-built).

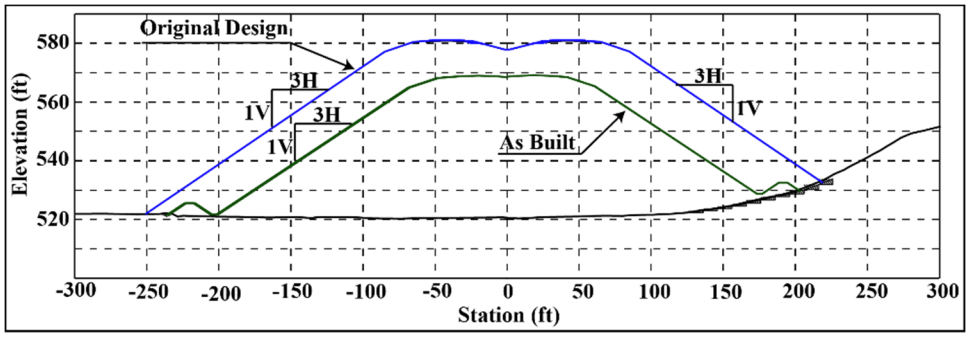


Fig. 2. Proposed and as-built embankment section.

The subsurface conditions at the site were established based on ATC geotechnical investigation (2013), which comprised borings and CPTs along the alignment. A schematic of the generalized soil profile is shown in Fig. 3.

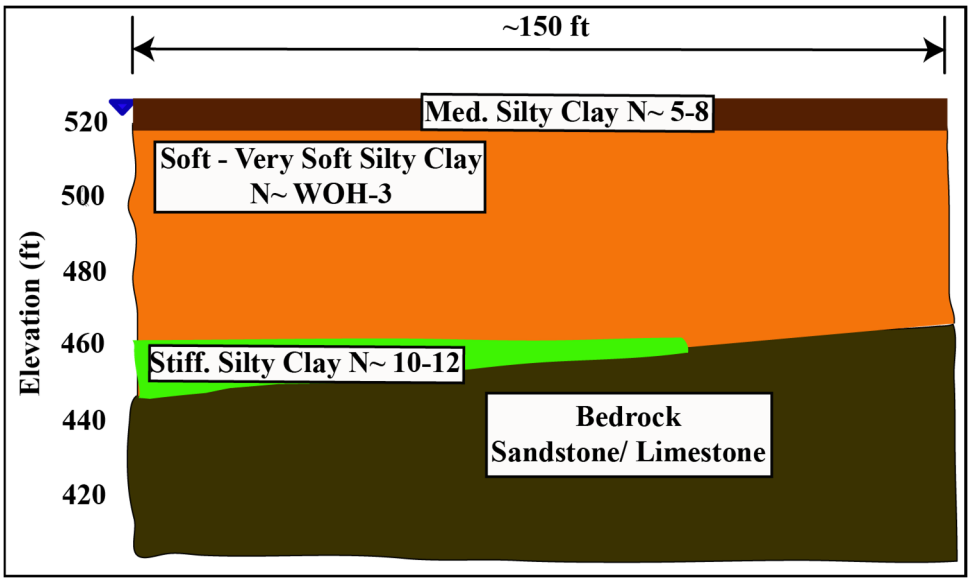


Fig. 3. Generalized soil profile.

As it can be seen from Fig. 3, the subsurface conditions comprise of about 75-ft of overburden soils. The overburden soils are predominantly cohesive in nature with medium stiff to stiff consistency in the upper 10 feet, underlain by soft clay to approximate depth of 50-ft, and then increasing in consistency to stiff clay to the top of bedrock. It should be noted that the lower 25-ft of the clay layer has traces of organic material and marl. There were no pore pressure dissipation tests conducted at the location of the CPT probes. As such, the ground water was estimated based on observation from borehole locations several days after drilling and sampling completion, to be at about 2-ft below the existing ground surface.

For the analyses and design purposes the clay deposit was divided into six sublayers, designated as C1 through C6, based on index properties and undrained shear strength profile. It should be noted that the undrained shear strength profile was obtained based on SHANSEP technique (eq. 1, Ladd, 1986) and from CPT (eq. 2, Mayne et al, 2009). The SHANSEP parameters and the N_{KT} were obtained after calibration with direct simple shear tests and consolidated undrained triaxial tests conducted on relatively undisturbed samples. The pre-consolidation stress profile (maximum past pressure σ'_p) was obtained from correlation with CPT (eq. 3, Mayne et al, 2009) and incremental loading consolidation tests. The different clay units' index properties profile along with the initial effective stress, preconsolidation pressure, and undrained shear strength are presented in Fig. 4.

$$s_u = 0.22(OCR)^{0.8} \quad [1]$$

$$s_u = (q_t - \sigma_{vo})N_{KT} \quad [2]$$

$$\sigma'_p = 0.33(q_t - \sigma_{vo})^{m'} \quad [3]$$

Where OCR = overconsolidation ratio, q_t = net cone resistance, σ_{vo} = total vertical stress, N_{KT} = undrained shear strength cone factor, and m' = constant dependent on grain size (for intact clay, m'=1.0).

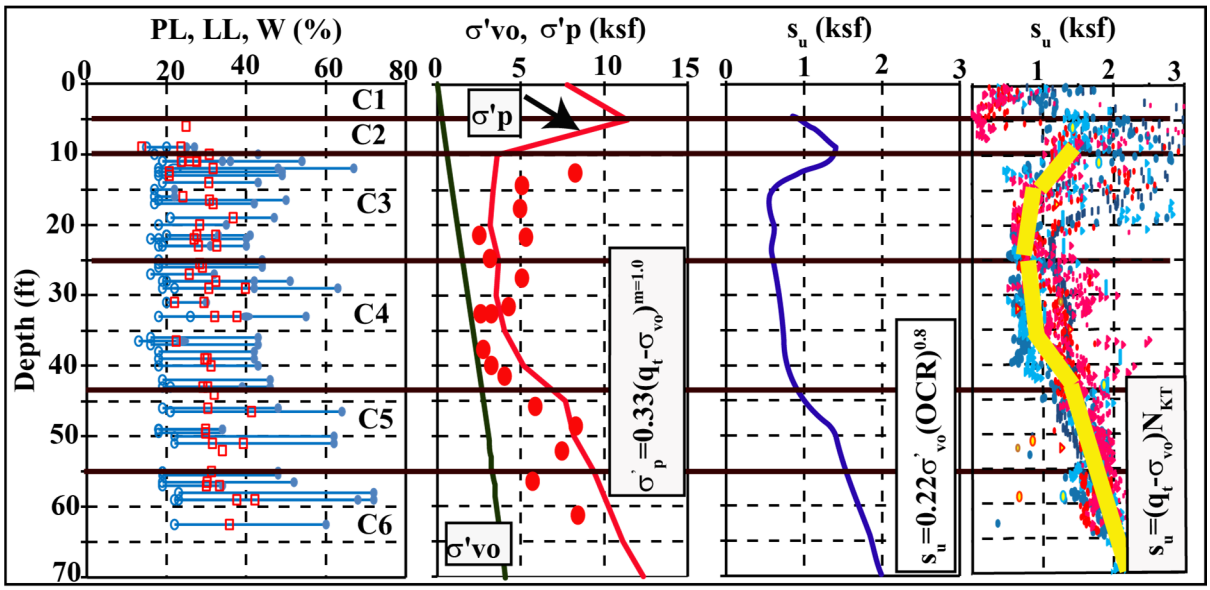


Fig. 4. Design soil profile.

As it can be seen in Fig. 4, units C1 and C2 have a relatively high overconsolidation ratio due probably to desiccation. Unit C3 and C4 are close to normally consolidated, unit C3 has slightly higher plasticity index than unit C4. Units C5 and C6 have a higher plasticity index than the upper layers.

The wick drains were used to accelerate the excess pore pressure dissipation; the selected pattern was triangular with 5-ft spacing. The wick drains were installed through all the six-clay formations and extended about 25-ft outside the embankment foot print, when it was possible. A coarse gravel layer was installed at the top of the drains to facilitate the drainage and to allow for the geotextile installation.

The instrumentation program consisted of inclinometers, settlement plates to monitor the embankment settlement at about 10-ft above the original ground surface, nested vibrating weir piezometers to record the pore pressure response in the clayey foundation soils under the centerline and both sides of the embankment, and magnetic extensometer to monitor the subsurface settlement under the embankment. The location of the geotechnical instrumentation sensors in plan view and the pattern of wick drains are shown in Figs. 5a and 5b, respectively.

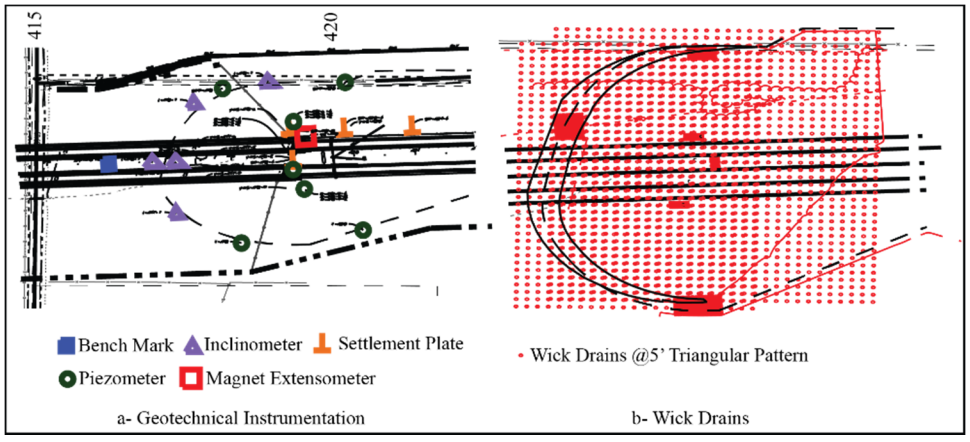


Fig. 5. Plan view of a- geotechnical instrumentation plan, and b- Wick Drains pattern.

NUMERICAL MODELING

The numerical simulation of the staged construction was conducted using the commercially available two-dimensional finite element package PLAXIS®. PLAXIS® software allows for a coupled hydro-mechanical analyses and can simulate the wick drains by applying a zero-excess pore pressure at time equal zero at the wick drain locations.

Model Dimensions and Configuration

The two-dimensional model was about 800-ft in width and about 140-ft in height, as shown in Fig. 6. The bedrock outcrops at about 70-ft from the left toe of the embankment. The embankment was modeled as solid elements with dimensions identical to the as-built section as shown in Fig. 2. A temporary surcharge loading was applied at top of the embankment (modeled as distributed load) to reduce secondary compression. The wick drains were modeled after adjusting the spacing for the plane strain analysis to maintain the design intended "contributory area". The model was discretized using the build in 15-node plane strain elements in PLAXIS®. The build in elements provides additional degrees of freedom to capture the pore pressure generation and dissipation.

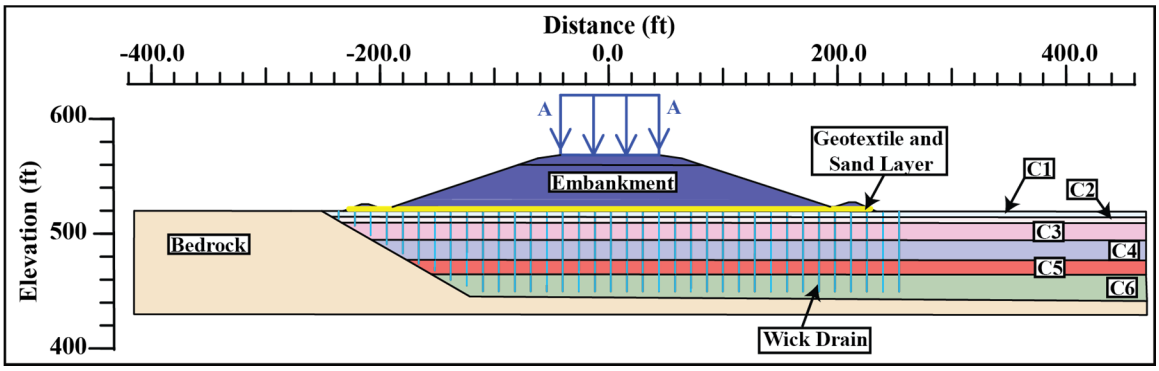


Fig. 6. Numerical model dimensions.

Analysis

The analysis was originally conducted for the design cross section and was later updated to reflect the as-built section. The updated analysis was conducted in stages, after the generation of the initial stress state in the model, using consolidation analyses with staged construction to reflect the actual progress of the embankment construction and the waiting periods between different stages. The various stages and corresponding time and analyses are presented in Table 1.

Soil Constitutive Model

The PLAXIS® build in Hardening Soil Model was used to model the response of the foundation soils. The stress-strain relationship is hyperbolic with stress dependent stiffness, which is important to capture the stiffer response of the soil with the increase in the effective stress. The model assumes that the soil obeys the Mohr-Coulomb yield criteria, with expansion yield surface, which provides the capability to capture the increase in the undrained shear strength resulting from the increase in the effective stress. The model captures the evolution of the plastic strains from both the compression component and from the deviatoric stress component. One disadvantage of the model, which is not of great effect in the case of staged construction is the elastic response for the unloading/ reloading. In the case of soft clay the unloading/

reloading stiffness to the loading stiffness ratio could be taken as the ratio of the compression index to the recompression index.

Table 1. Simulated Construction Stages

Stage	Stage Name	Analyses Type	Stage Description
I	Wick Drains	Plastic/ Staged	Activating the Wick Drains
II	Stage I	Consolidation/ Staged	Construction to El. 530 including the granular layer and Geotextile/ 60 days
III	Waiting I	Consolidation/ Staged	Waiting Period/ 120 days
IV	Stage II	Consolidation/ Staged	Construction to El. 560/ 51 days
V	Waiting II	Consolidation/ Staged	Waiting Period/ 33 days
VI	Stage III	Consolidation/ Staged	Construction to El. 569/ 15 days
VII	Surcharge I	Consolidation/ Staged	Surcharge to El. 578/ 6 days
VIII	Waiting Sur. I	Consolidation/ Staged	Waiting Period/ 32 days
IX	Surcharge II	Consolidation/ Staged	Surcharge to El. 583/ 10 days
X	Waiting Sur. II	Consolidation/ Staged	Waiting Period/ 87 days
XI	Sur. Removal	Consolidation/ Staged	Back to El. 569/ 35 day

The hardening soil model formulated within a plasticity framework with a hyperbolic stress strain relation and associative flow rule and it requires three moduli values at a reference pressure to identify loading (E_{50}^{ref}), unloading/ reloading (E_{ur}^{ref}), and hydrostatic loading (E_{oed}^{ref}). The hardening soil model is strain hardening (requiring the definition of the hardening exponent "m") and it obeys the Mohr-Coulomb yield criteria (i.e., c and ϕ are required).

It should be noted that the analysis was conducted as undrained analysis, as recommended by Ladd (1986), however, the parameters used were the effective stress parameters, because PLAXIS® considers the bulk density of water once the material behavior is selected to be undrained without the need to estimate the undrained parameters.

For the bedrock, granular layer, and embankment, where the evolution of the stiffness with the effective stress is not as important as the foundation soils, the elastic model with Mohr-Coulomb yield criteria was selected. The behavior of the bedrock was selected as non-porous, while undrained and drained responses were assigned to the embankment and granular layer, respectively.

Pore Pressure Generation and Dissipation

The excess pore pressure generation is controlled by Skempton's Parameter "B" and it correlates to the incremental rate of the volumetric strain (controlled by E_{oed}). The consolidation process in PLAXIS® is modeled based on Biot's theory with the flow from the consolidation process follows Darcy's law. As such, the change in permeability as a function of the volumetric strain should be evaluated. The Skempton's B parameter is calculated in PLAXIS® based on the bulk modulus of the soil to the bulk modulus of the pore fluid. The volumetric strains evolution is controlled by the oedometer stiffness. For appropriate capturing of the rate of consolidation the initial and change in both the horizontal and vertical permeability should be evaluated.

Mechanical and Hydraulic Parameters

To evaluate soil stiffness and hydraulic parameters, it is important to understand the structure of the soil (open structure that reached equilibrium under high void ratio), which is reflected by initial void ratio and compression index as plotted in Fig. 7a, which shows that the clay deposit possessed more open structure

with depth. The void ratio increased from about 0.65 near the ground surface to about 1.1 at depths closer to bedrock, this increase in the initial void ratio is associated with increase in the compression index from about 0.22 to 0.4. In addition, this increase in the void ratio will result in an increase of the rate of change in the permeability (C_k). It should be noted that the compressibility indices were obtained from the laboratory e-logσ'_v, without any correction, in accordance with the uniqueness of the e-logσ'_v (Mesri et al., 2014). In addition, the high compression indices indicate significant secondary compression in accordance to Mesri's law of compressibility, as such the use of surcharge was vital to assure that the foundation soils are over consolidated and thus reducing the C_α.

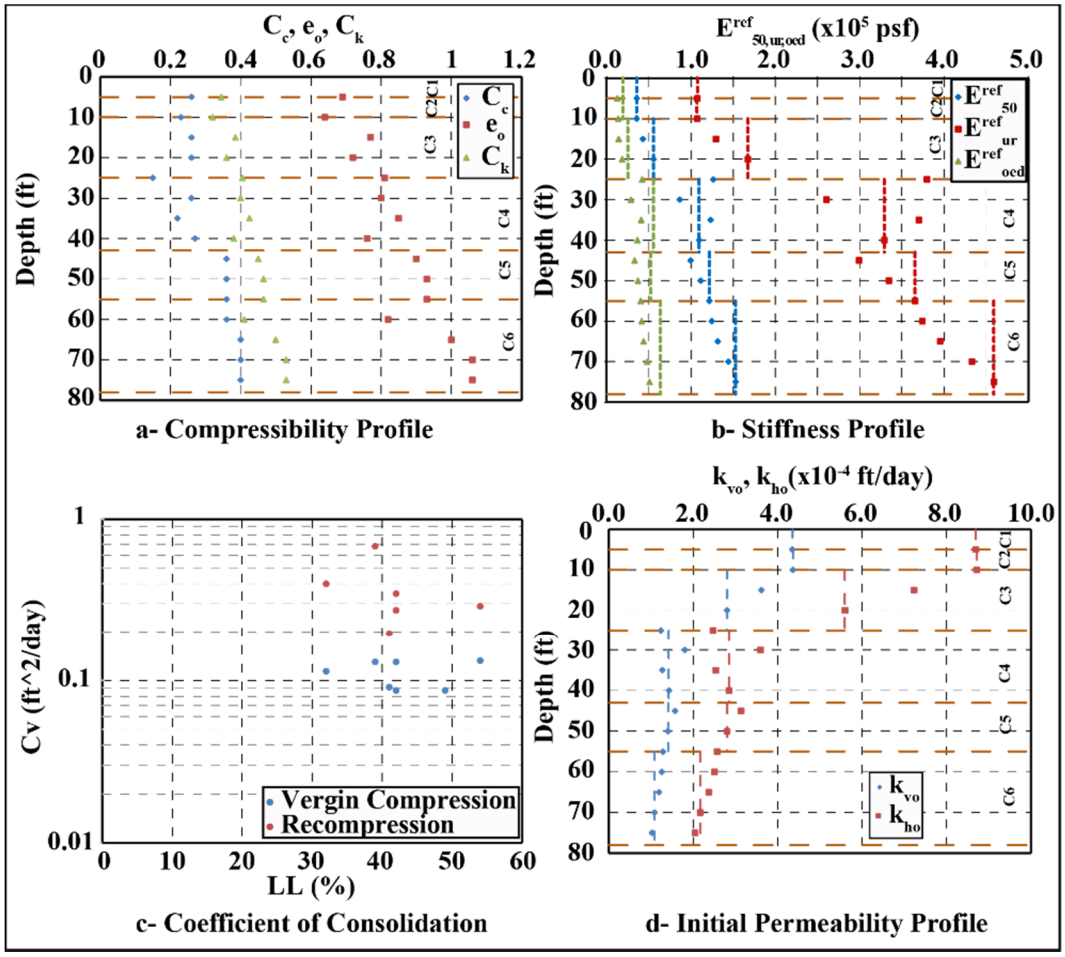


Fig. 7. Model mechanical and hydraulic parameters.

The stiffness parameters (E_{50}^{ref}, E_{ur}^{ref}, and E_{oed}^{ref}) were estimated based on laboratory tests. The E_{50}^{ref} profile was estimated from CIU and Ck_oU tests with pore pressure measurements, and were compared to published correlations (Kulhawy and Mayne, 1990), there was a general agreement between the parameters obtained from the laboratory results and published correlations. The E_{oed}^{ref} were estimated based on the compression index (which is valid for very soft clays with m~1), the ratio of the E_{50}^{ref} to E_{oed}^{ref} ranged from 2.5 at the top layers to 3.0 at layers below 10-ft. The obtained ratio is considered high and thus the E_{oed}^{ref} was adjusted to limit the ratio at the upper layers to 1.8 and lower layer to 2.4, in accordance with PLAXIS® manual recommendations. The E_{ur}^{ref} was selected as 3 E_{50}^{ref} as recommended by PLAXIS® manual. It should be noted however, for very soft clays the ratio of E_{ur}^{ref} to E_{50}^{ref} should reflect the ratio of the compression ratio to the recompression ratio, but as it was stated earlier for this study the E_{ur}^{ref} is not significant as the

unloading only occurs at the end (Stage XI in table 1). The computed and selected moduli for each sublayer are presented in Fig. 7b.

The coefficients of consolidation from all the incremental consolidation tests were plotted as a function of liquid limit (Fig. 7c) and were used to estimate the initial vertical permeability for various layers. The calculated permeability from the coefficient of consolidation were increased by a factor of 2 as recommended by Mesri et al (1994). The permeability profile was supplemented by initial vertical permeability computed using the relationship presented by Mesri et al. (1994) utilizing initial void ratio, clay size fraction, and activity. The initial horizontal permeability was assumed to be twice the initial vertical permeability. The C_k values were computed as $C_k=0.5e_o$ as recommended by Tavenase et al (1983) and Mesri et al (1994). The design permeabilities profile are plotted in Fig. 7d.

ANALYSES RESULTS AND DISCUSSION

The analyses were performed using the above discussed geometry, soil profile, and parameters for the original design and subsequently modified to reflect the as-built conditions. The computed total settlement at the original ground surface for the original design was about 40-in., while for the as-built was less than 30-in. The surface and subsurface settlements from the numerical model, for the as-built section, were compared to the recorded settlements from the settlement plates and the extensometer. The comparison along with the construction progress (the green line in Fig. 8a with the elevation axis) are presented in Fig. 8.

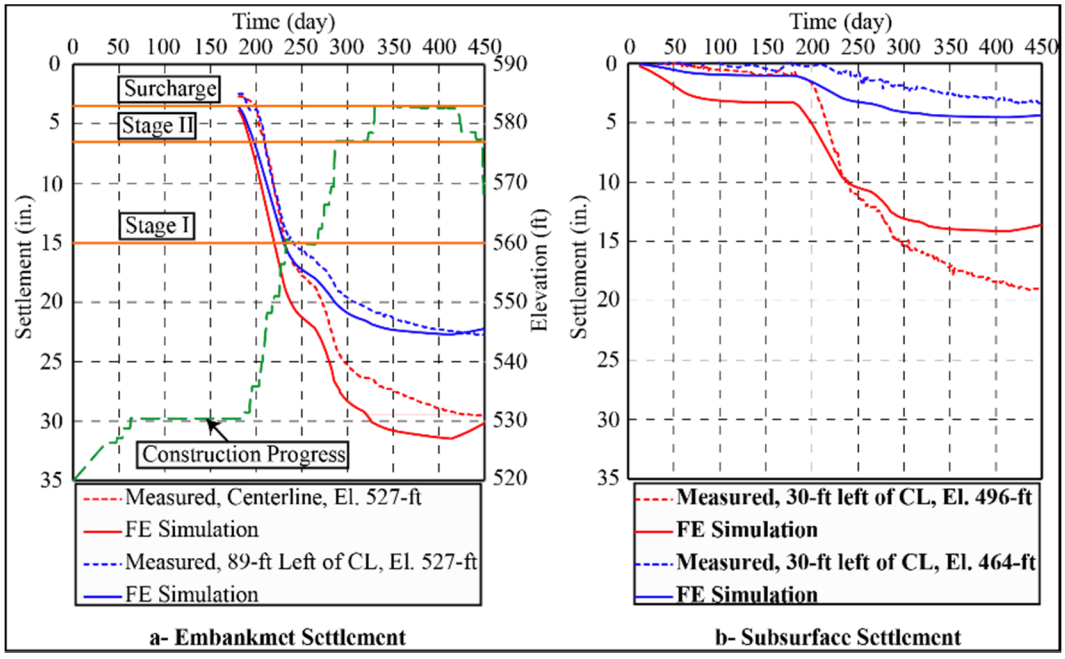


Fig. 8. Measured and computed settlements.

As it can be seen from Fig. 8, the model predictions were within few inches of the recorded settlement by settlement plates. The model captured well the rate of settlement during the load application and waiting periods. However, the model tends to under predict the settlement in unit C3 as shown in Fig. 8b. The good agreement between the predicted and measured settlements is a good indication on the validity of the selected stiffness parameters.

The comparison between the predicted and recorded development and subsequent dissipation of excess pore pressures is presented in Fig. 9. As it can be seen in Fig. 9, the model predictions were very reasonable

in terms of peak developed excess pore pressure at different locations within the subsoils. It should be noted that the existence of shallow rock at the left side of the embankment resulted in a higher predictions of excess pore pressure, as shown in Figs. 9c and 9d. This overprediction is attributed to the assumed non-porous behavior for the bedrock, which prevented any dissipation of excess pore water pressure at the rock boundary. The rock at the boundary has a low RQD which will provide some relief to the excess pore water pressure.

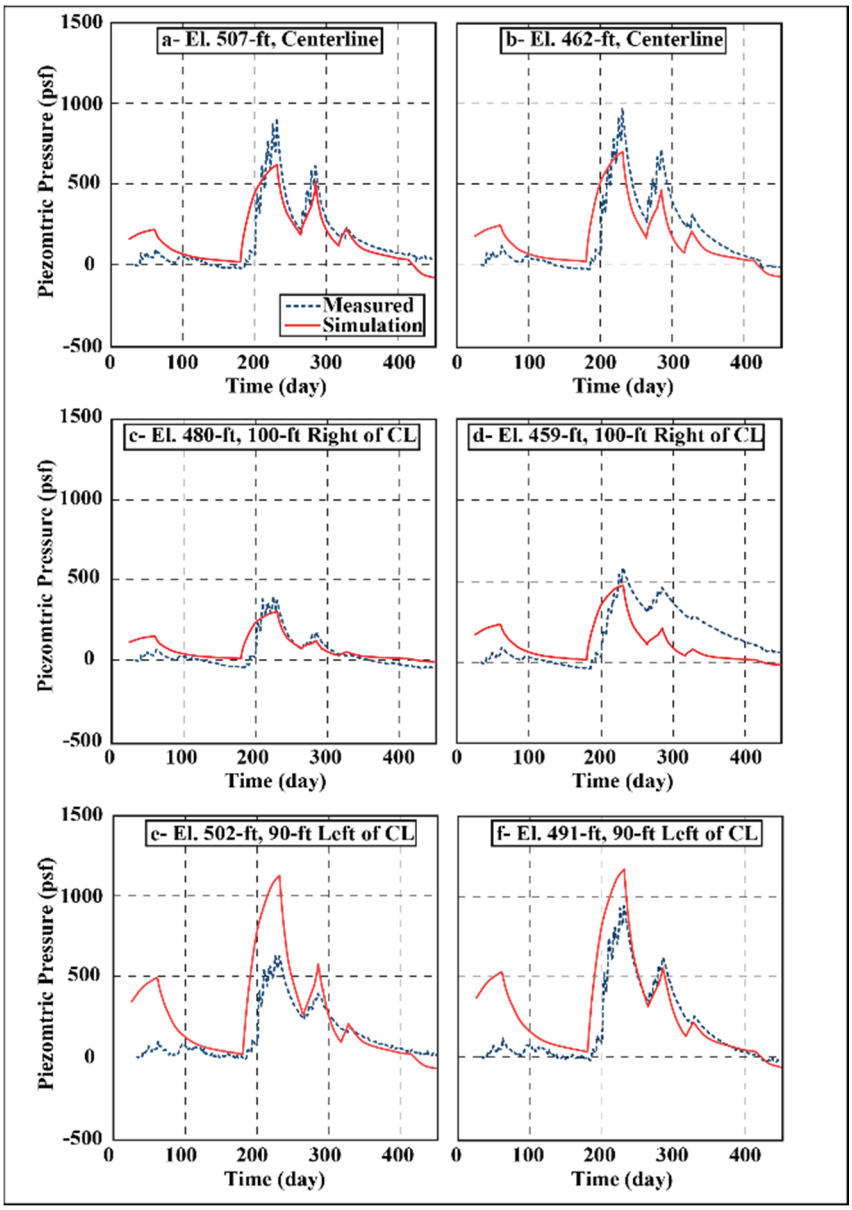


Fig. 9. Measured and computed excess pore water pressure evolution and dissipation.

CONCLUSION

A staged construction of embankment on soft clay was simulated using Finite Element with coupled Hydro-Mechanical analyses. The parameters selection was performed carefully based on extensive laboratory results. The careful selection of the parameters resulted in good agreement between the computed and measured settlements and pore pressure development and dissipation. The following could be concluded:

1- The staged construction is important in allowing the gain of the undrained shear strength with the effective stress evolution.
2- A well designed comprehensive site investigation and laboratory testing program of the subsurface soils are key elements in deriving reliable parameters for numerical modeling.
3- Carefully conducting numerical simulations with the proper selection of the appropriate constitutive model and the modeling parameters are essential to achieve "Class A" predictions.
4- It is recommended that pore pressure dissipation tests to be conducted during CPT probing to assist in determining the ground water levels and allow for the computation of in-situ permeability.

ACKNOWLEDGEMENT

The authors of this paper wish to acknowledge the contribution of Indian Department of Transportation (INDOT), ATC Associates, and Parsons, Inc.

REFERENCES

ATC Associates (2012) *Geotechnical Report for interstate I69 extension,* Indianapolis, IN.

INDOT (2012). *Issued for bid contract drawings for Interstate I69 extension,* Indianapolis, IN.

Ladd, C. C. (1986). "Stability evaluation during staged construction." *J. Geotec. Eng.,* 117(4), 540-615.

Kulhawy, F. H. and Mayne, P. W. (1990). *Estimating Soil Properties for Foundation Design.* EPRI Report EL-6800, Electric Power Research Institute, Palo Alto: 306P. www.epri.com.

Mayne, P.W. 2009. Geoengineering Design Using the Cone Penetration Test. 155 pages. Published by ConeTec Inc., 12140 Vulcan Way, Richmond, BC, V6V 1J8: Website: www.conetec.com.

Mesri, G., and Choi, Y. K. (1985). "Settlement analysis of embankment on soft clays." *J. Geotech. Eng.,* 111(4), 441-464.

Mesri, G., and Hayat, T. M. (1993). "The coefficient of earth pressure at rest." *Canadian Geotechnical J.,* 30(4), 647-666.

Mesri, G., Feng, T., Ali, S., and Hayat, T. M. (1994). "Permeability characteristics of soft clays." *Proc., 13th Int. Conf. on Soil Mechanics and Foundation Engineering,* Vol. 2, Japanese Society of Soil Mechanics Foundation Engineering, Tokyo, 187-192.

Mesri G., and Khan, A. Q. (2012). "Ground improvement using vacuum loading together with vertical drains." *J. Geotech. Geoenviron. Eng.,* 139(2), 680-689.

Mesri, G., and Funk, J. R. (2014). "Settlement of the Kansai International Airport." *J. Geotech. Geoenviron. Eng.,* 141(2), 1-16.

Parsons, Inc. (2012): Personal Communication.

PLAXIS (2008). *Plaxis 2D User Manual.* PLAXIS BV, Delft, Netherlands.

Tavenas, F., Jean, P., Leblond, P., and Leroueil, S (1983). "The permeability of natural soft clay. Part III: Permeability characteristics." *Canadian Geotechnical J.,* 20(4), 645-660.

SMART SOIL IMPROVEMENT: THE USE OF RIGID INCLUSIONS FOR SOIL CONSOLIDATION

Claudio Asioli, TREVI SpA, Cesena, Italy, +39 0547 319372, casioli@trevispa.com
Federico Pagliacci, SOILMEC SpA, Cesena, Italy, +39 0547 319386, f.pagliacci@soilmec.it
Marco Chiarabelli, SOILMEC North America, Fort Worth, TX, USA, +1 401 965-2575, m.chiarabelli@soilmec.it

ABSTRACT

"Rigid inclusions" are a consolidation method that provides improvement of soft soils thanks to the installation of cylindrical columns made up of a material with significant and permanent cohesive properties, whose stiffness is 500÷5000 times greater than the surrounding natural soil's. "Rigid inclusions" find their application in marginal areas (reclamations, polluted sites) to ensure stability of adjacent structures during construction of new buildings and to reduce the impact of natural disasters (liquefaction in the event of earthquakes, embankment collapse in the event of floods). This paper analyses the "rigid inclusion" construction method, related materials and equipment. Moreover, two performed projects will be illustrated. The first is the restoration of Lungarno Torrigiani Embankment in Florence, Italy. In May 2016, the Torrigiani embankment underwent a structural collapse causing a 3 m. displacement of the riverbank towards the Arno River. "Rigid inclusions" (with 300 mm diameter) have been used to re-compact the loose soil and create a stable working platform for the equipment. The second project illustrates the use of "rigid inclusions" (800 mm diameter and maximum depth of 36.6 m) to control the settlement of a new automatic cold store (30 m high with a 65 x 120 m foot print) for fresh frozen vegetables.

Keywords: rigid inclusions, soil consolidation, settlement control

RIGID INCLUSIONS

In general, the word "inclusions" means a type of consolidation that improves the strength of a soil mass through the inclusion of elements constituted by a material having better characteristics than those of the surrounding natural ground, to improve the overall mechanical characteristics of the treated soil. Inclusions are "rigid" when the material introduced into the ground has significant and permanent cohesive properties (concrete or cement mortar) and a significantly higher stiffness (500 ÷ 5000 times) than that of the surrounding natural ground.
Typically, medium-small diameters (from 300 to 800mm) with low percentages of treatment (from 2% to 10% of the volume of soil) are employed, ensuring a high quality and consistency of the obtained product, both in terms of diameters and elastic modulus.
According to the scope of the project and in urban areas, "rigid inclusion" columns can also be performed by means of small diameter drilling rigs (micropiles), weighing less than 20-25 tonnes.

THE RIGID INCLUSIONS TECHNOLOGY

Rigid Inclusions can be carried out via the continuous flight auger (CFA) or the displacement pile (DP) technologies.
Continuous Flight Auger piles (CFA) are produced by drilling into the ground with a continuous flight auger assembled on a central hollow pipe.
The tip of the auger excavates the soil and the material rises along the flights.
A plug is located at the bottom of the auger to prevent the soil from penetrating into the hollow pipe.
Once boring operations are completed, the auger is extracted while concrete is injected through the internal hollow pipe; the bottom plug is pushed out when concrete is pumped.
An auger cleaner at the base of the drilling rig mast keeps the auger in the right and vertical position and performs flight cleaning during the extraction phase.

 © 2017 DFI Annual Conference, New Orleans, LA, USA

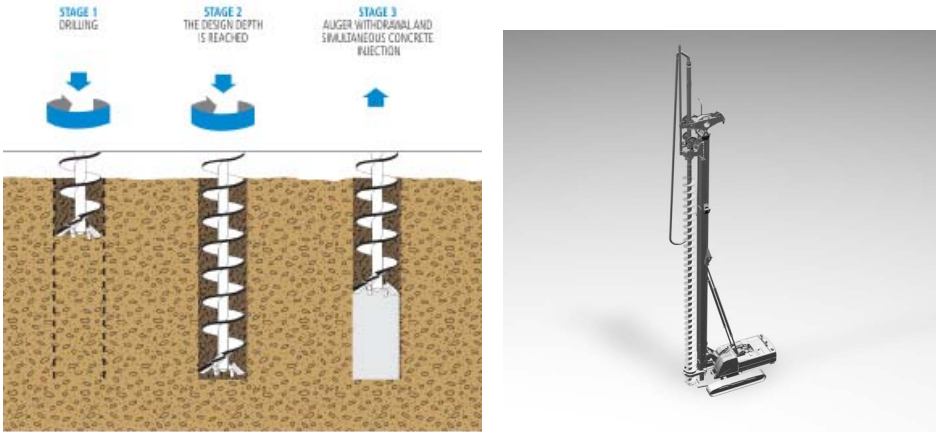


Fig. 1. CFA technology phases for the execution of Rigid Inclusions and typical drilling rig in CFA configuration



Fig. 2. Bottom plug and auger cleaner

Displacement piles (DP) excavate the soil by means of a hollow drilling string equipped with a displacement tool . at its bottom

Standard DP tools have four sections:

- The drilling tip to be fitted with teeth suitable for soil consistency.
- A bottom helix section with right-hand flight that brings the soil upward and starts the compaction process.
- A central cylindrical stabilizer, that laterally presses and compacts the soil, thus obtaining the actual pile diameter.
- An upper helix section with left-hand flight that displaces the possible falling soil, coming from the upper excavation, toward the stabilizer portion of the tool, which pushes it against the lateral soil.

Once boring operations are completed, the drilling string and the tool are extracted while concrete is injected through the internal hollow pipe.

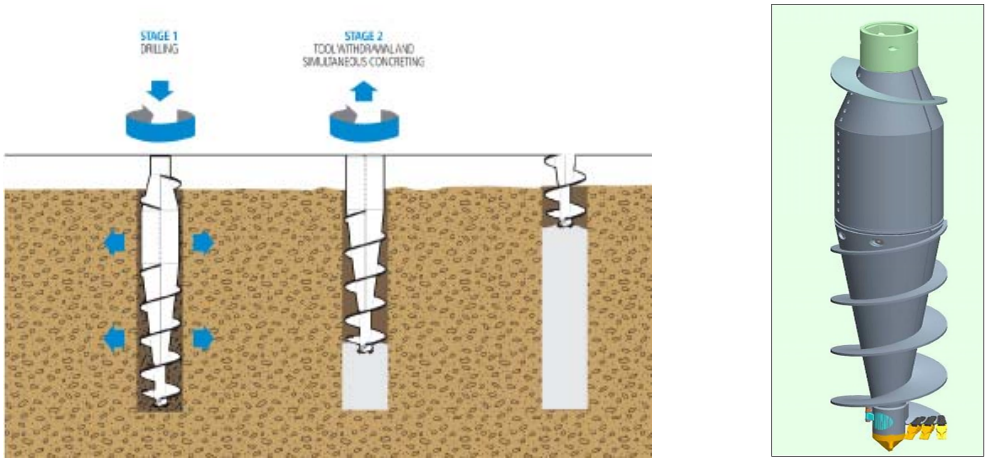


Fig. 3. DP technology phases for the execution of Rigid Inclusions and standard DP tool

Standard DP tools require high pull-down force and high torque, with consequent limitation of the possible pile diameter and the need to use a powerful piling machine.
The TCT tool has been developed to reduce the crowd force required to perform DP piles.
With the TCT tool, the displacement process takes place during the tool's extraction phase. All piling rigs in CFA or DP configuration are characterised by an extraction force that is greater than the pull-down force.
By adopting the TCT tool (see Figure 4) drilling is performed, as for CFA, by clockwise rotation.
Once penetration is completed, the drilling string is rotated anticlockwise. The central portion of the tool cannot rotate, causing friction against the hole's lateral surface. The upper and lower portions turn together, and the peculiar shape of the lower tip closes the flight's path in the central part of the tool. This mechanical gate separates the tip section, where concrete flows out, from the upper portion. By extracting the tool with an anticlockwise rotation, the soil in the upper part is forced downward and laterally displaced by the central tool's portion.

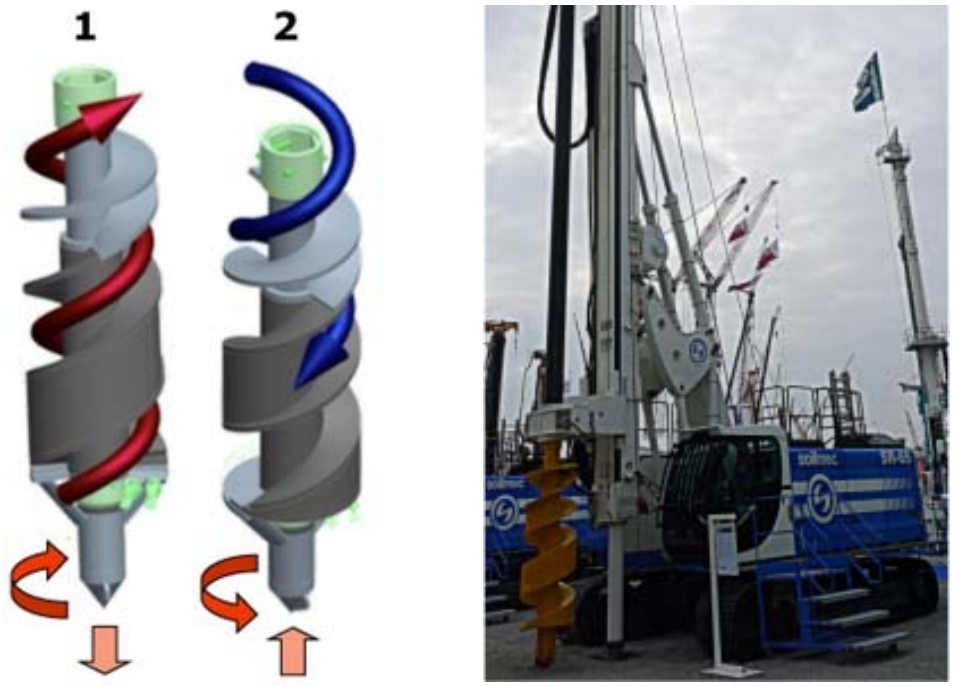


Fig. 4. TCT penetration (1) and extraction (2) and equipment in TCT configuration

RESTORATION OF LUNGARNO TORRIGIANI EMBANKMENT

In May 2016 the Torrigiani river wall experienced a structural collapse. The displacement of the wall towards the river was about 3 metres, with an extension of approximately 80 metres and a vertical displacement of about 3.5 metres.



Fig. 5. The river wall's collapse

With reference to the subsoil description and layers' mechanical characteristics (see Table 1), the hypotheses on the failure mechanism are illustrated in Figure 6.

Tab. 1. Subsoil description and layers' mechanical characteristics

Unit	from (m)	to (m)	Description	γ (kN/m3)	Cu (kPa)	ϕ (°)	E' (MPa)
U.1	0.0	-8,0	Backfill, consisting of silty-sandy materials with gravels, pebbles and clasts of bricks. This layer was artificially put in place in the XIX century to built the old Lungarno Torrigiani levee	20		28	15
U.2	-8,0	-15,0	Alluvial deposit consisting of gravel-pebbly (rounded elements with diameters from 3 to 8 cm) with sandy loam. The foundation of the embankment Lungarno Torrigiani wall is founded on top of this deposit.	20		32	30
U.3	-15,0	-30,5	Sillano Formation formed by lithofacies argillitic (SILB) and argillitic-marl (SILA) with centimetric levels of calcarenite and sandstone. It is the classic "structuraly complex formations" of the Appenini mountain, the young mountain chian crossing longitudinaly the whole Italian peninsula.	20,6 - 22,2	70 - 294		10-50
U.4	-30,5	End	Pietroforte formation formed by sandstone and calcarenite.	22	200	32	200

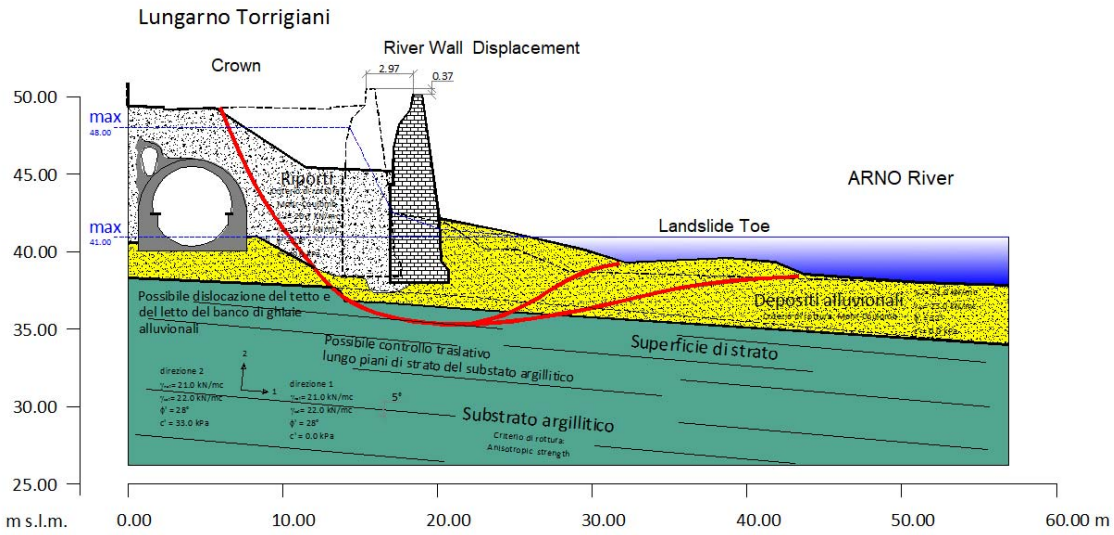


Fig. 6. Hypotheses on the failure mechanism

Restoration works demanded great care because of the jobsite location in the city centre, and due to tight schedule: the river wall had to be restored by early November, which marked the 50 Anniversary of Florence Great Flood of 1967 .
The envisaged solution entailed construction of a statically and hydraulically functional structure at the rear of the existing wall. This structure completely replaced the damaged river brick wall that was consolidated and kept in the current displaced position.
The wall's structural consolidation was aimed at:

- ensuring the safety of Galleria Poggi and of the adjacent existing buildings;
- minimising pressures and stresses on the existing brick wall, thus improving its stability and ensuring hydraulic protection against the Arno river floods;
- restoring the water sewer and road traffic along the Lungarno.

Consolidation works, structural restoration and hydraulic protection had to be completed before Winter, to avoid any risk of river floods. Trevi was awarded the contract under "top urgent procedure".
The operating sequence was based on the principle of "progressively increasing structural stability and safety" of both existing and ongoing structures to constantly operate under acceptable safety conditions.
The design solution (see Figure 7) is based on the new structures serving as support and protection of the historical wall against static and dynamic loads.

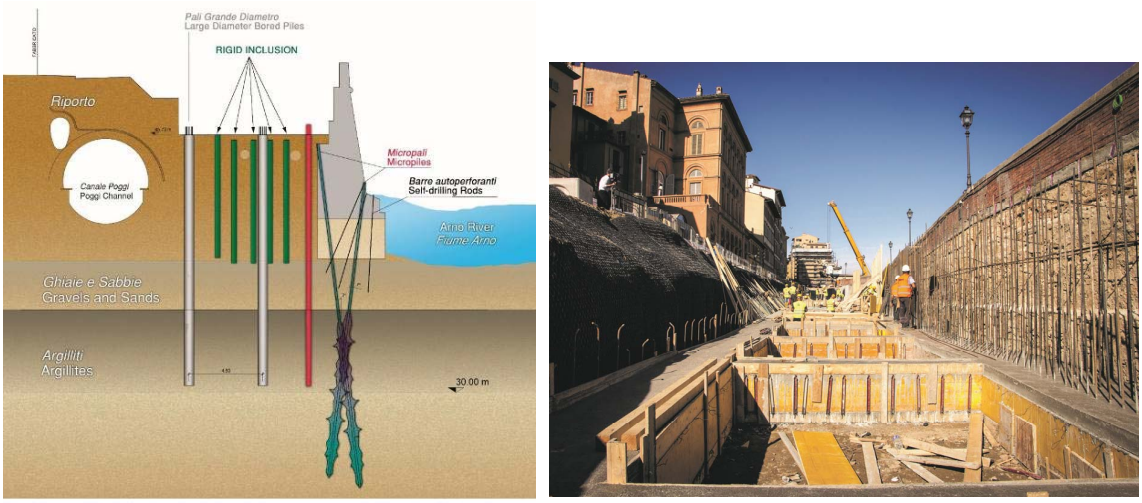


Fig. 7. New structures to support and protect the existing wall

The design solution included the following activities:

- "rigid inclusions" for the consolidation of the soil volume dislodged and displaced by the collapse, in order to consolidate the soil and create a stable work surface for the following activities with heavier equipment;
- raked micropiles (ø 170 mm, 1.2 m spacing, L = 12÷23 m, reinforced with a O.D. 110 mm steel pipe) embedded into the wall from both sides, to underpin the wall, thus improving its stability;
- hollow steel bars (O.D 40 mm, 1 m spacing, L = 6 m) injected with cement grout to strengthen and compact loose soil below the base of the wall;
- a double row of CFA piles (ø 600 mm, 1.05 m spacing, L = 15 m) as foundation elements of the frame structure.
- a micropiles' retaining wall (ø 300 mm, 0.9 m spacing, L = 15 m, reinforced with a O.D. 244 mm steel pipe) to support the frame in the cusp area, near the displaced river wall;
- civil works entailed earth movements, realisation of concrete beams and slab and of a vertical wall for soil support, installation of a new water sewer and road restoration;
- surface (asphalting, side walk and historical brick guard-rail).

Works were performed according to the sequence illustrated in Figure 8.
During all jobsite activities a real-time monitoring system controlled the dislodged wall and the nearby structures and buildings.

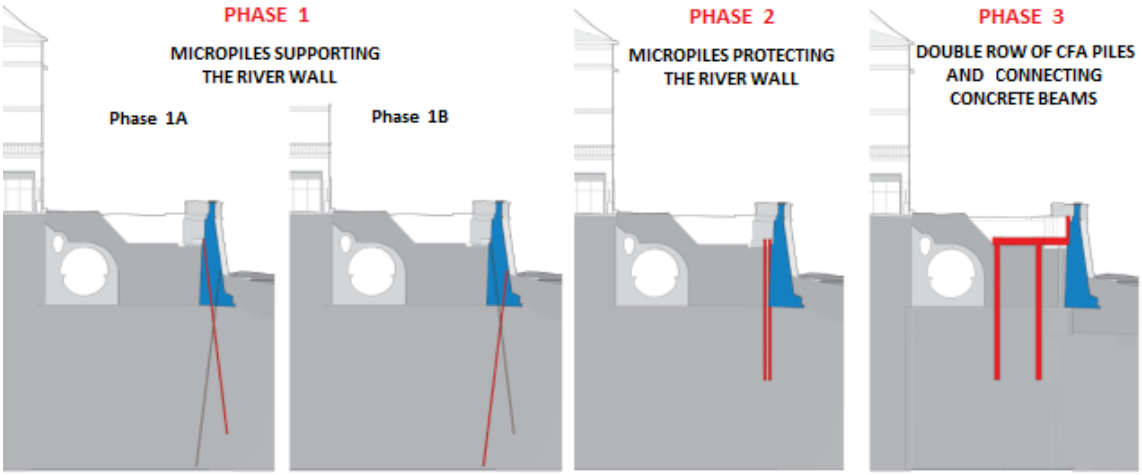


Fig. 8. Construction sequence

A three dimensional view of the design solution is shown in Figure 9



Fig. 9. The design solution 3-D overall view of the new structures

The first activity involved the realization of "rigid inclusions" for the consolidation of the volume of soil dislodged and displaced by the instability event to "strengthen" the soil and create a stable working platform on the surface where the equipment required for the following phases could be used.
Rigid Inclusions were performed in the backfill portion displaced by the instability event, starting from the working platform to a depth of about 7-8 m.
The instability of this soil mass and its poor mechanical properties forced engineers to adopt small drilling rigs, performing the columns by means of the micropile technology.
The columns, drilled with a continuous hollow flight auger, had a diameter of 300 mm and a length of 7.5 m. During auger extraction, a premixed mortar with a C30 strength class and an elastic modulus of 28000 MPa was pumped through the hollow auger to fill the column.
Columns were executed on a rectangular grid with a center to center distance of 1,0 x 0,9 m, with a percentage of treatment of about 8% of the affected volume. A total of 764 columns were executed for a total drilling length of about 5730 linear metres. Figure 10 shows the Soilmec SM-20 performing rigid inclusions.



Fig. 10. SM-20 performing rigid inclusions

NEW DIVISION AT THE OROGEL PLANT IN CESENA

Orogel is Italy's top producer of fresh frozen vegetables. The Group has 1590 associate producers who grow their products exclusively in Italy, as well as 2594 employees.
Orogel is headquartered in Cesena, just a couple of miles from Trevi Group's head office.
The business of these two companies, both leaders in their field in Italy and abroad, could not be further apart, yet they have come together thanks to the construction of the new "OROGEL 3" division. The project involves construction of three new production departments, one refrigerated warehouse with a product selection department and a 30 m high cold store with a footprint of 65m x 120m. All this on a site of approximately 45,000 m^2, more than 6000 m² of which will be used as a public green area. The project meets the most cutting-edge criteria of environmental sustainability and technological innovation: "OROGEL 3" will be powered by a natural gas power plant which will recover heat and transform it into cooling energy; the water used in the processes will be reused, once wastewater has been removed; the cold stores will be completely automated.



Fig. 11. The New Orogel 3 division

Trevi was awarded the contract to execute the foundation works of the cold store with the 120m x 65m footprint.
The foundation project consists of a mat foundation with a uniform thickness of 0.90m, on top of which the heating layer, the thermal insulation layer and the base slab for the superstructure will be installed. The soil below the mat will be consolidated by 486 rigid inclusion elements with a diameter of 800mm and working lengths of 20m, 26m, 32m and 36m, carried out via the continuous flight auger (CFA) technology and filled with a C30 strength class concrete (fig. 12). The piles, whose depth

increases from the edge of the mat to the centre, are arranged on a rectangular 3.3m÷4m x 4.4m pattern; the drilling depth from ground level is 0.6m greater than the working length of the piles.

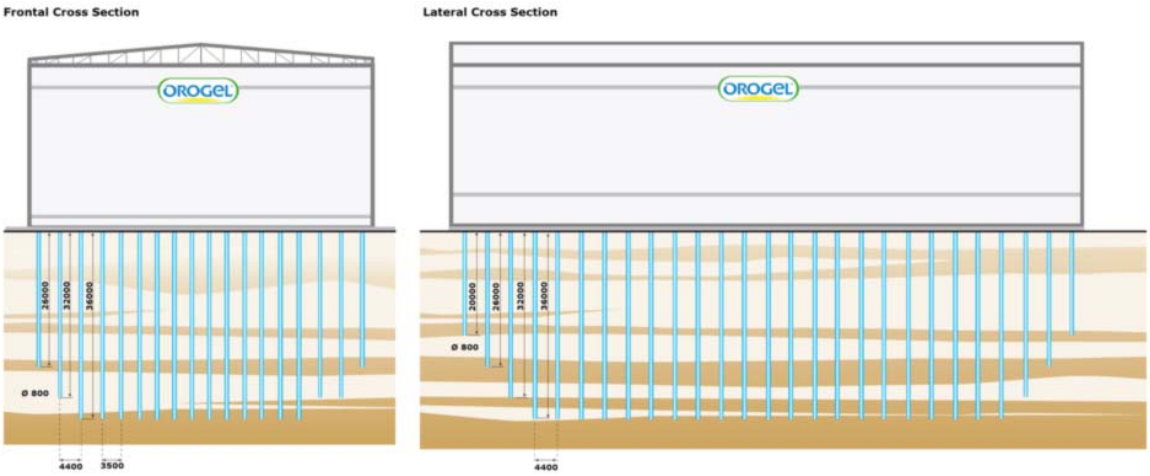


Fig. 12. Rigid inclusions under the cold store

Rigid inclusions have no structural function, but they are used to consolidate the soil in order to reduce and control total and differential soil settlements to the comply with the very strict requirements of the allowable settlements of the store's structure.

The work site lies on the alluvial fan of the Savio River, where the first subsoil layer consists of a casual lenticular sequence of clayey silty and gravelly sandy sediment; the gravel with varying degrees of sand is mainly encountered towards the hill, while clay clearly dominates towards the valley.

The surface soil in the area consists of clayey-silty alluviums with intercalations of sandy silt and sandy-gravelly alluviums which correspond to buried paleochannels. At a depth of approximately 9÷10 metres from ground level, a 2 m. deep clayey layer, heavily overconsolidated due to a drying process, can be found almost everywhere. At a depth of 25 metres, there is a first continuous layer of gravelly alluviums whose thickness ranges from approximately 5 to 7 metres; at a depth of around 50 metres, there is a second, more consistent layer of gravelly alluviums (about 10 m.thick).

A suspended ground water table lies in the upper layer, whose level can almost rise to ground level in the wet season, while in the dry season it lies some metres below ground level.

The soil stratigraphy are illustrated in figure 13, while the layers' mechanical characteristics are summarized in Table 2.

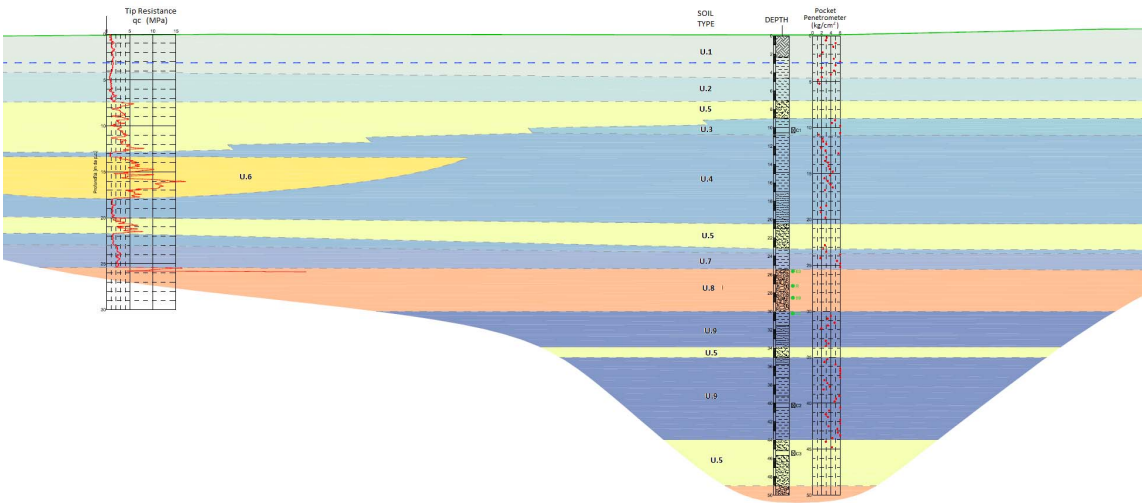


Fig.13. Soil stratigraphy

Tab. 2 Subsoil description and layers' mechanical characteristics

Unit	from (m)	to (m)	Description	γ (kN/m3)	Cu (kPa)	ϕ (°)	E (MPa)
U.1	0	4-5	from weak silty to silty clay, from average consistent to consistent	18.5	60		5
U.2	4-5	9-10	silty clay from low to average consistent	19	45		4
U.3	9-10	11-12	from weak silty to silty clay, from consistent to very consistent. The unit is heavily overconsolidated due to drying (paleosol)	19.5	80		8
U.4	11-12	max 23	from weak silty to silty clay, from average consistent to consistent	19.5	50		5
U.5	variously intercalated with units 1, 2, 3, 4 and 9		alternating 10 cm layers of sandy silt and fine sand with silt, with layers of silty clay, remains of organic substance are found locally	19		30	25
U.6	variously intercalated with the cohesive units		sand and medium-fine silty sand	19		30	25
U.7	23	25.5	weak silty to silty clay, from consistent to very consistent	19.5	60 - 90		10-15
U.8	25.5	30-33 and over 49	medium coarse gravel (average Ø = 2-3cm) in sandy-silty matrix, polygenic, from sub-rounded to rounded	19.5		35	60
U.9	variously interclated with units 1, 2, 3, 4 and 5		silty clay and clayey silt with silty-sandy laminations, from consistent to very consistent	20	100		20-30

Trevi used the new Soilmec SR-125 HIT (HIGH TECHNOLOGY) drilling rig, in CFA configuration, to execute the 486 rigid inclusion columns below the mat foundation (table 3)
The results recorded on the worksite confirm the rig's working profitability: production varied from 40 to 50 m/h per column, with peaks of 56.8 m/h. The overall time required to drill and cast a 36.6 m. column was only 37 minutes. Drilling alone took only 11 minutes (including pull-up back time).

Tab. 3. Rigid inclusions detail

800 mm diameter Rigid Inclusions		
Drilling depth	N° piles	Tot. Metres
20,6	36	741,6
26,6	82	2.181,2
32,6	116	3.781,6
36,6	252	9.223,2
Total	486	15.927,6

CONCLUSIONS

"Rigid inclusions" are a consolidation method that provides improvement of soft soils thanks to the installation of cylindrical columns made up of a material with significant and permanent cohesive properties, whose stiffness is 500÷5000 times greater than the surrounding natural soil's.
Typically, medium-small diameters (from 300 to 800mm) with low percentages of treatment (from 2% to 10% of the volume of soil) are employed.
Rigid Inclusions can be carried out via the continuous flight auger (CFA) or the displacement pile (DP) technologies.
The possibility to use large or small drilling rigs and to successfully operate in urban areas as well as in large-scale projects, allows to find suitable technical solutions concerning soil improvement both for new constructions and for remedial works.
The reduced job site installation, the absence of drilling fluids, the excavation of natural soil that is not contaminated by supporting fluids are all key elements of this environmentally-friendly technology.
In conclusion "Rigid inclusions" are a simple and fast method in the soil consolidation field.

REMEDIAL METHOD FOR COLLAPSE SOIL FOUNDATION OF MOSUL DAM

Ali N. Ibrahim, Al-Iraqia University, Baghdad, Iraq, Email: usace.tro@gmail.com
Arash Khosravifar, Portland State University, Portland, OR, USA, Email: karash@pdx.edu

ABSTRACT

Large areas of Iraq are covered with collapsible soils namely gypsiferous soil which is often used as the foundation soil for structures. In particular, the Mosul Dam foundation is comprised of high contents of gypsiferous soils. Intrusion of water through the foundation soil dissolves gypsum which acts as the binding material between soil particles. This phenomenon results in the formation of collapsible soils which can cause serious damages to the dam structure. The failure of Mosul Dam, with a reservoir as large as 11 billion cubic meter of water, can be catastrophic. In the past, Mosul Dam Authorities have been remediating the soil foundation by injecting cement mortar. This method has been proved not economic; therefore, new, more efficient, methods are desperately needed.

This research study focuses on finding practical methods to remediate collapsibility of gypsiferous soils by improving their geotechnical properties. This study presents remediation of collapsible gypsum-rich soil by grouting. Three types of stabilizer materials were used to make the grout; (1) sodium silicate (Na_2O_3Si) which is a well-known chemical soil stabilizer, (2) bentonite slurry, and (3) silicone oil. The purpose for using these stabilizer materials is to provide an impermeable layer (waterproofing coat) around the gypsiferous soil particles and to fill the voids that may occur in the soil as a result of gypsum dissolution when subjected to water.

A series of double oedometer (collapse) tests and direct shear tests were carried out on gypsiferous soils before and after remediation by grouting. The results show that the soil compressibility decreases in the grout-treated gypsiferous soil by reducing volumetric strain. Consequently, the potential for collapsibility decreases too. It was also shown that grouting, increases the shear strength of the soil at confining stresses smaller than 250 kPa by increasing the cohesion combined with a slight reduction in the internal friction angle.

KEYWORDS: grouting, compressibility, collapsibility, stabilizer.

INTRODUCTION

Grouting is one of the ground improvement techniques which is often used to improve the loose foundation soils. Bruce (2003) provides step-by-step procedures on using grouting techniques for sealing dams and other water reservoirs. Grouting can be classified as permeation grouting, compaction grouting or hydraulic fracturing. Permeation grouting is an effective way to send the grout into the ground without disturbing the soil structure, i.e. free flow of grout into the soil voids where grouting is accomplished by injection of a fluid-like material that is capable of forming a gel and binding the soil particles together. Grout materials may be solution grouts or suspension grouts. The permeation grouting technique is generally used to minimize ground permeability and to control ground water flow, but it can also be used to strengthen and harden the ground (Raman et al., 2012).

Gypsiferous soils are founded in vast urban areas and distinctive regions of Iraq and other countries. Many foundation failure problems that occur in these soils are associated with intrusion of water and dissolution of gypsum. Razouki et al. (1994) reported that the gypsiferous soils are classified as collapsing soils. This is due to the fact that gypsum provides an apparent cementation when the soil is dry

 © 2017 DFI Annual Conference, New Orleans, LA, USA

but the intrusion of the water causes dissolution and softening leading generally to a serious structural collapse.

Several researchers have attempted to treat and improve the gypsiferous soil properties to decrease the dissolution of gypsum and collapse potential (Fattah et al., 2012).

The aim of this study is to find practical methods to remediate collapsibility of gypsiferous soils by improving their geotechnical properties in order to sustain the applied structure loads. This study presents remediation of collapsible gypsum-rich soil by grouting. Three types of stabilizer materials were used to make the grout; (1) sodium silicate (Na_2 O_3 Si) which is a well-known chemical soil stabilizer, (2) bentonite slurry, and (3) silicone oil. The treated soil is to be spread to form an impermeable blanket of finite thickness below the foundation of Mosul dam and to control harmful effects of water leakage or percolation.

EXPERIMENTAL SOIL TESTS AND GROUTING MATERIALS

Gypsiferous soil samples from the lower-Jazera area in Iraq were used in this research. The soil includes 20.55% gypsum content, which is consider moderately gypsiferous soil according to Barazanji (1973). An auger drill was used to extract the soil samples from depths ranging from 1 to 4 m, as shown in Fig. 1.

Specific gravity tests were conducted according to ASTM D854 (2010). Kerosene was used instead of water for the same reason mentioned above.

Chemical tests were performed on the soil to find total soluble salts (TSS), gypsum content (GC), organic materials (OM) and sulphate content (SO_3). The results of the physical and chemical tests are summarized in Table 1.

Three stabilizer materials were used to be injecting in soil, which were:

1. *Sodium Silicate* (Na_2O_3Si) is a colorless solution which consists of 13.7% Na_2O and 33% SiO2. The specific gravity of this material is 1.55 and the viscosity (CPS) at 20 ^oC is 600. Chemical grouting has the advantages of allowing economical spacing of boreholes, greater penetration of the grout, and more flexibility in terms of duration of grouting.
2. *Silicone Oil,* which is an oil product from polymerized siloxane with a viscosity (CPS) 300.
3. *Bentointe,* which is produced from clay and has thixotropic properties. This mean that it forms a highly water resistance gel which, when mixed with additives, can create a permanent barrier to water flow. This is used where the size of the soil particle is too small for cement grouting. This method is widely used to combat seepage in alluvial soils beneath dam foundations or other water-bound structures. A bentonite to water dilution ratio of 1:2 was used in this study.

Ibrahim and Schanz (2017) successfully improved the gypsiferous soil strength by mixing the soil with three content ratios of silicone oil; namely, 4%, 10% and 16%. They attributed the increase in strength to the ability of the silicone oil to bond gypsiferous soil particles together and increased soil tenacity.

Several physical tests were conducted on this soil including grain size analyses (dry, soil samples washed on sieve No #200 by water, and soil samples washed on sieve No #200 by kerosene) according to ASTM D422. The reason for using kerosene to wash the soil was to overcome the dissolution of gypsum by water. These results show that using the standard grain size analysis can be misleading because the gypsum becomes semi-soluble and dissolved in water when the soil is washed on sieve during the preparation for sieve. So the soil samples washed on sieve No #200 by kerosene was used in this study for sieve size analysis. Fig. 2 shows the grain size distribution curves for gypsiferous soil.



Fig. 1 Gypsiferous soil sample extracted using Auger drill equipment

Table 1. Physical properties and chemical tests results of the gypsiferous soil

Property	Value
water content	2.4 %
Specific gravity	2.56
Field dry density (kN/m^3)	15.15
Atterberg limits	Non Plastic
Particle size distribution (ASTM D422- with kerosen)	
d10 (mm)	0.10
d30 (mm)	0.28
d60 (mm)	0.48
Gypsum Content %	20.55
Passing sieve (0.075 mm) (dry, kerosene, water) (%)	1.25 , 4.53, 39.25
Classification (USCS)	SP (poorly graded sand)
TSS	22.92 %
GC	20.55 %
SO_3	1.43 %
OM	3.46%

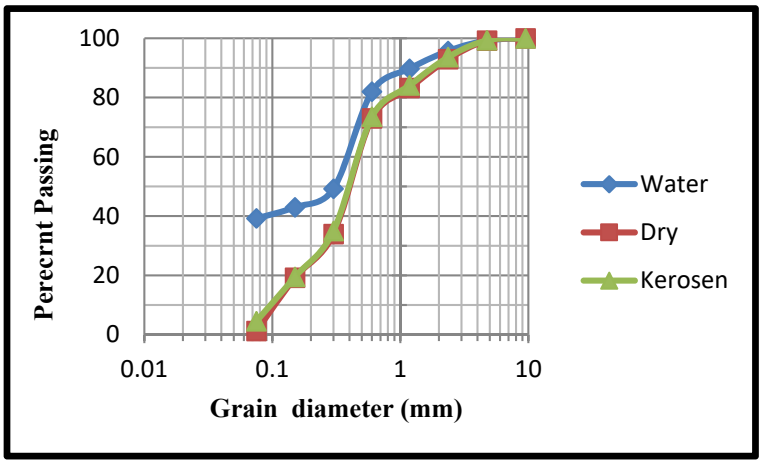


Fig. 2 Grain size distribution curves

ELEMENTARY CHARACTIRSITICS (XR-F AND ESM) ANALYSIS

X-Ray Fluorescence non- destructive tests were carried out on the natural soil to detect the soil elements, specifically the calcium (Ca) content which is one of the components in gypsum ($CaSO4.2H_2O$). The tests were performed using the Oxford instrument model type Twin-X manufactured in the UK.

The test results showed that the soil has the following elements: Ca, Na, Mg, Al, O, Si, S, K, Ti and Fe. The element percentage weights for three spectrums are shown in Table 2 and the spectrum analysis is shown in Fig. 3. The variations of the soil microstructure and crystal characteristics of the gypsum in the soil were examined by using Scanning Electronic Microscope (ESM) to obtain images of the tested gypsiferous soil for the quantitative analysis. The figure clearly shows that most crystals are gypsum with different size and varieties. Three varieties of gypsum crystal habits can be identified as: prismatic, fibrous, and tabular. These results agree with results from Ibrahim and Schanz (2014). The results of scanning electronic microscope are shown in Fig.4

Table 2. X-RF elements percentage weight

Spectrum Label	O	Na	Mg	Al	Si	S	K	Ca	Ti	Fe	Total
Spectrum 1	42.92	1.07	3.70	12.70	24.80	0.50	1.84	8.28	0.08	4.12	100.00
Spectrum 2	45.91	0.07	3.40	6.22	37.20	0.40	1.37	0.92	0.00	4.51	100.00
Spectrum 3	53.44	0.04	1.31	2.80	38.40	0.33	0.58	0.38	0.29	2.40	100.00

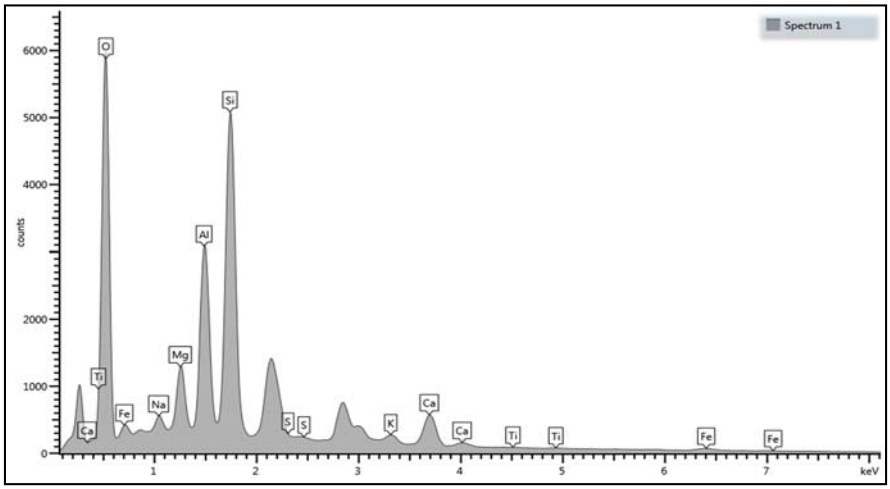


Fig. 3 X-FR spectrum for gypsiferous soil

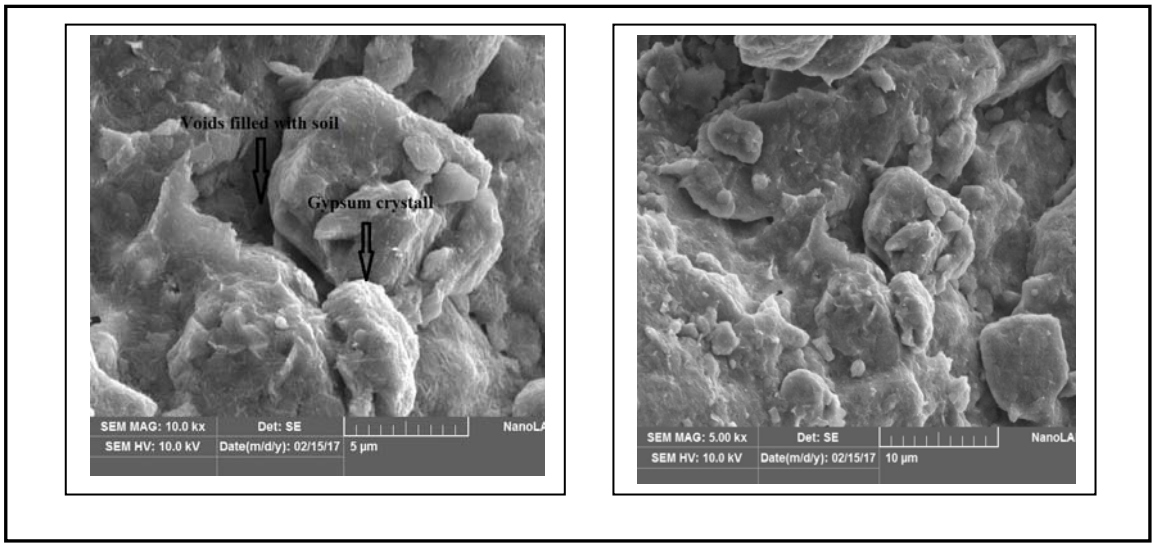


Fig. 4 Scanning Electronic Microscope (SEM) for gypsiferous soil

GROUTING LABORATORY APPARATUS

The grouting apparatus were designed and assembled in Al-Iraqia University for this study to simulate field soil grouting under Mosul dam as shown in Fig. 5. The apparatus consists of three main parts:

1- Electric air compressor machine with outlet pressure gage and the maximum pressure capacity of 12.5 kPa.
2- The grout liquid stabilizer mould, which is a cylindrical transparent mould of 15 cm diameter and 30 cm height. It has three valves at the top: an inlet valve which is connected to air compressor machine, an outlet valve which is connected to the soil sample mould, and a ventilation valve.
3- Soil sample mould, which has the same shape and size as the liquid mould, but it is open-ended at the top. Half of the mould is filled with the soil sample, i.e 15 cm high. A closed-end perforated Pyrex glass pipe is inserted in the soil sample and is fixed at the mould by a holder, which is used to grout the stabilizer materials in the soil samples. The pipe diameter is 12 mm and 35 cm. The pipe has 4 holes of 0.5mm diameter each starting at 2 cm from the bottom up to 12 cm length of the pipe. A total of 24 holes are used around the pipe surface to inject the stabilizer materials in all directions into the soil sample.

MATERIALS PREPARATION AND GROUTING PROCESS

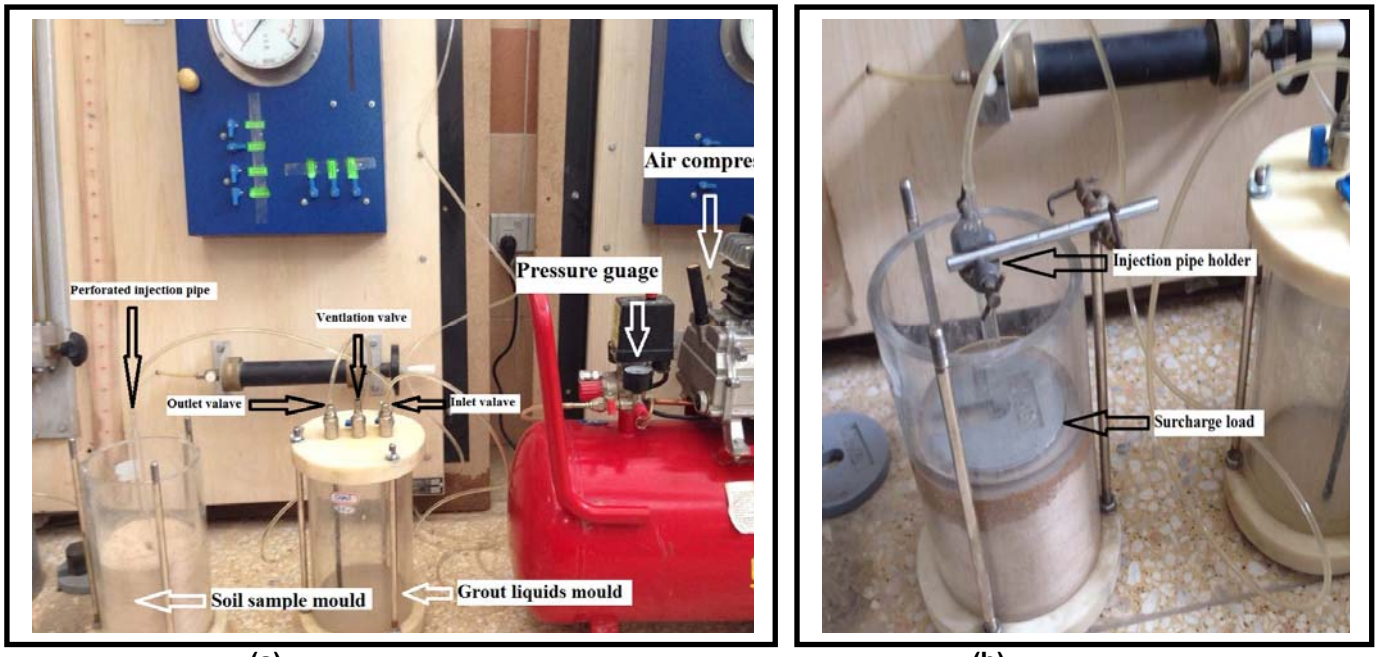
The materials preparation and grouting process can be summarized in the following sequences:

1- The gypsiferous soil sample was compacted at the field unit weight and water content in the soil mould to 15 cm height, i.e. soil sample dimensions were 15 cm diameter and 15 cm height. Three soil samples were prepared for three types of stabilizer materials (sodium silicate, silicone oil, and bentonite slurry). Two filter papers were placed at the top and bottom of the gypsiferous soil samples. A surcharge load of 2.22 kPa was applied at the top of gypsiferous soil sample to confine the soil.
2- The stabilizer materials were prepared and placed in the liquid mould.
3- The inlet valve in the grout mould is opened to fill the mould with compressed air at 10 kPa. Subsequently, the outlet valve in the liquid mould is opened to grout the stabilizer material to the gypsiferous soil sample. The process is continued until the gypsiferous soil becomes fully

saturated with the stabilizer material. This can be visually checked since the soil mould is transparence. It is worth mentioning that the amount of stabilizer materials injected into the gypsiferous soil varied from 620 to 810 ml. This process was repeated three times for three types of stabilizer materials utilized in this study.

4- After the grouting process was completed, the inlet and outlet valves were closed. Then, the treated soil sample was left for 24 hours to let the grout permeate in the gypsiferous soil, fill the voids and make a homogeneous treated soil.

5- Treated soil samples were extracted from the soil mould for odometer and simple shear tests. The oedometer rings were inserted gradually in the treated gypsiferous soil and the ring was removed with the treated soil to perform two types of oedometer tests (unsaturated and saturated oedometer tests) for three types of treated gypsiferous soils.



(a) (b)

Fig. 5 Grouting apparatus (a) full setup (b) soil sample and stabilizer grout moulds

FLOW RATE OF GROUT LIQUIDS

In the first stage of the grouting process, the stabilizer materials start to fill in the air voids. Following this tage, the quantity of the stabilizer materials increases over time until all voids are filled with the stabilizer materials. In the second stage, the stabilizer materials start infiltrating form the top surface of the soil sample and rise up from the central whole of the surcharge load. It is worth mentioning that the time required to grout a certain amount of bentonite slurry is greater than that required for sodium silicate and silicone oil for the same grout pressure (10 kPa). This may be attributed to the liquid consistency and its viscosity. Fig. 6 shows the quantity-time relationship for three types of stabilizer materials grout.

Karol (2003) reported that the comparative ability to penetrate a formation in the soil is primarily a function of their relative viscosities, and it should be used as a guide to relative penetrability of chemical grouts.

Fattah et al. (2014) used acrylate liquids grout by using two injection pressures (kPa and 14 kPa) to improve the collapsibility and the shear strength of gypsiferous soils. The observation of the grout injection process revealed that the time required for the injection of a certain quantity of acrylate liquid

was shorter under the injection pressure of 14 kPa compared to the injection pressure of 7 kPa. They attributed this observation to the difference in the rate of flow for two injection pressures.

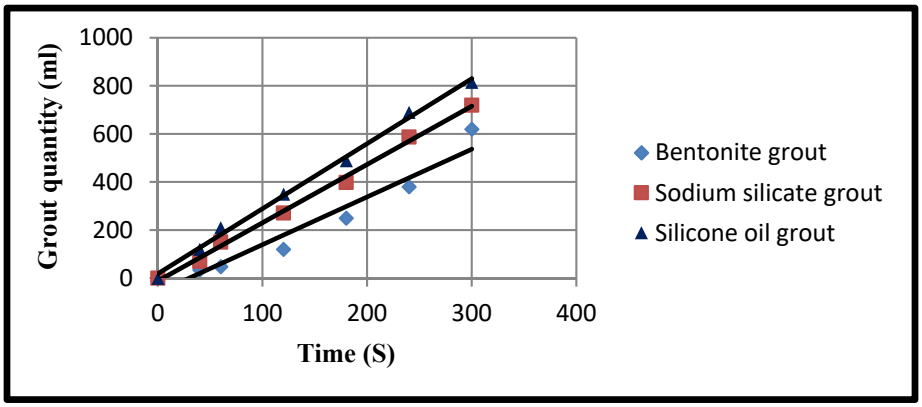


Fig. 6 Quantity-time relationships for three types of grout stabilizer liquids

GYPSIFEROUS SOIL COMPRESSIBILITY

The standard oedometer tests were conducted for remolded untreated gypsiferous soil samples and treated gypsiferous soil samples taken from soil mould in grout apparatus for three types of soils treated with sodium silicate, silicone oil and bentonite slurry.

Fig. 7 shows the relationship between the volumetric strain (ε_v) and the vertical pressure (log p) for treated and untreated gypsiferous soil. The results show that the use of stabilizer materials reduced the volumetric strain due to the applied pressure for gypsiferous soil treated by sodium silicate, bentonite, and silicone oil. This may be attributed to the fact that the stabilizer liquids cover the gypsum particle in the soil and avoid direct contact between water and gypsum particles, which acts as an impermeable layer to reduce the effects of water.

During the unloading stage, the rebound strain decreased for the treated samples. This is due to the reaction of the stabilizer materials that forms colloids, which in turn, polymerizes further and form a gel that binds soil particles together.

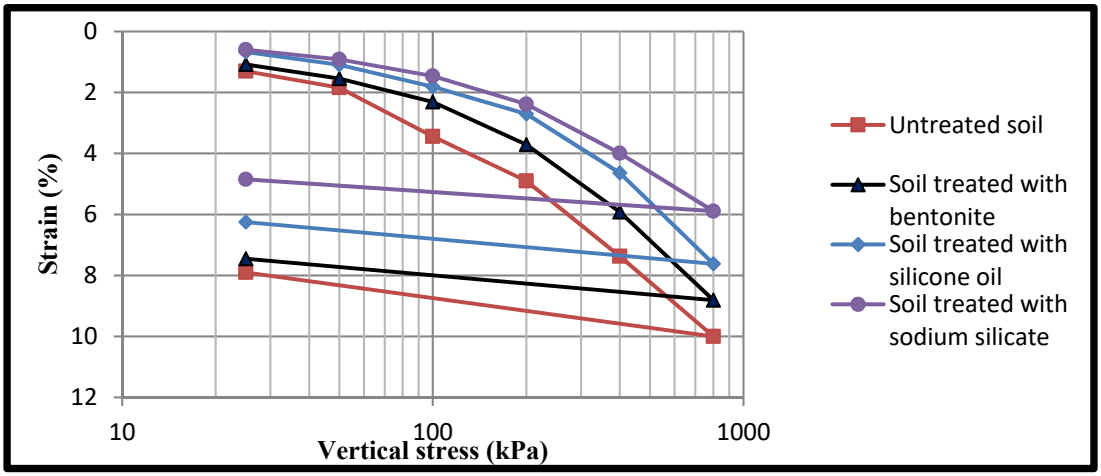


Fig. 7 Consolidation test for treated and untreated gypsiferous soil

COLLAPSE TEST OF GYPSIFEROUS SOIL

Ibrahim and Schanz (2014) reported that gypsum crystal dissolute due to soaking which results in formation of large voids that are responsible for the high collapsibility of gypsiferous soils under loading. This happens when the gypsum crystal acts as a binding material which could be easily destroyed when the soil is subjected to slight loading.

In order to study the collapsibility of treated and untreated gypsiferous soil, a set of double oedometer–collapse tests (unsaturated and saturated oedometer) were conducted. Fig. 8 shows the e-log(p) curves for the untreated gypsiferous soil, and Fig. 9 shows the e-log(p) curves for the gypsiferous soil treated with sodium silicate. Fig. 10 shows the e-log(p) curves for gypsiferous soil treated with bentonite.

The results show that the void ratios for all treated soil were less than that for untreated soils. This is attributed to the fact that the stabilizer materials fill the voids and reduce the void ratio. Also the treated gypsiferous became less effective in water in the saturation test, where the difference in e-log(p) curves between unsaturated and saturated tests were less than that in the untreated test. This behavior may be attributed to the presence of the stabilizer material, which makes an impermeable layer and prevents gypsum particles from direct contact with water; hence, it reduces the gypsum dissolution.

Fig. 11 shows the relationship between the collapse potential and the vertical stress for treated and untreated gypsiferous soils. The figure clearly shows that the collapse potential for treated gypsiferous soil is less than that in untreated soil for all types of stabilizers used in this study. This can be attributes to the fact that the stabilizer liquids form a gel that acts as a cementing agent between the soil particles and reduces the collapse potential.

It is worth mentioning that the sodium silicate and the silicone oil show high efficiency in reducing the collapse potential in comparison with bentonite.

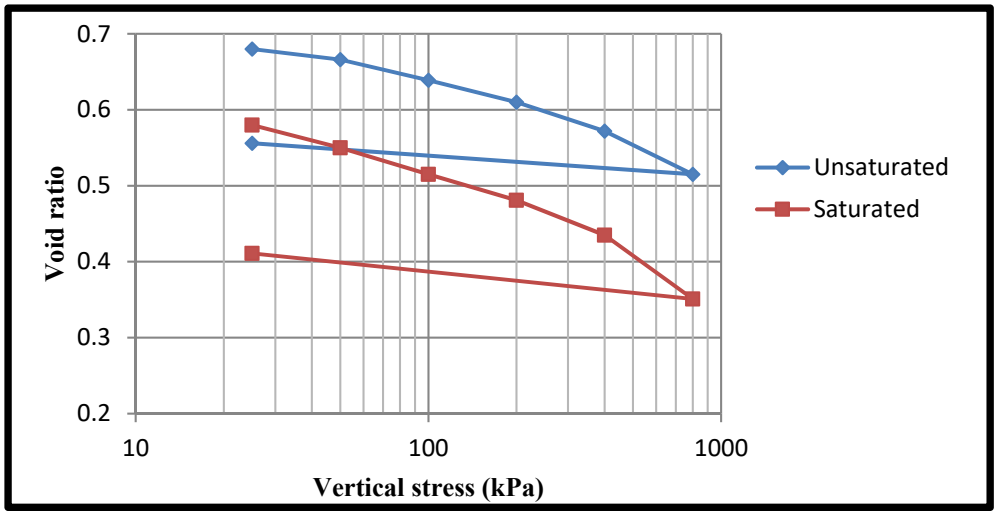


Fig. 8 Collapse test for untreated gypsiferous soil

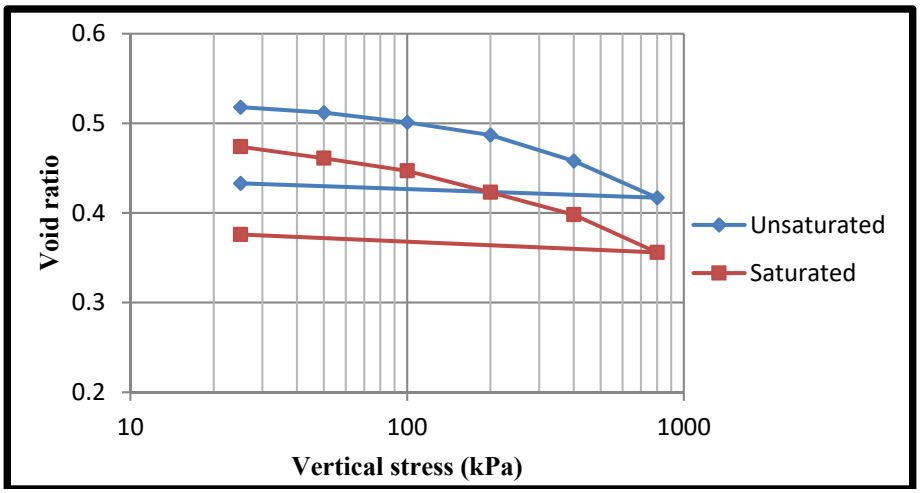


Fig. 9 Collapse test for treated gypsiferous soil with sodium silicate

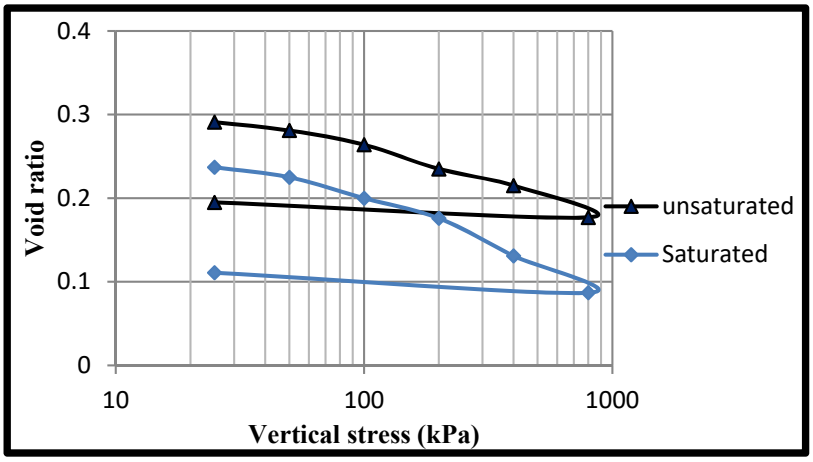


Fig. 10 Collapse test for treated gypsiferous soil with bentonite

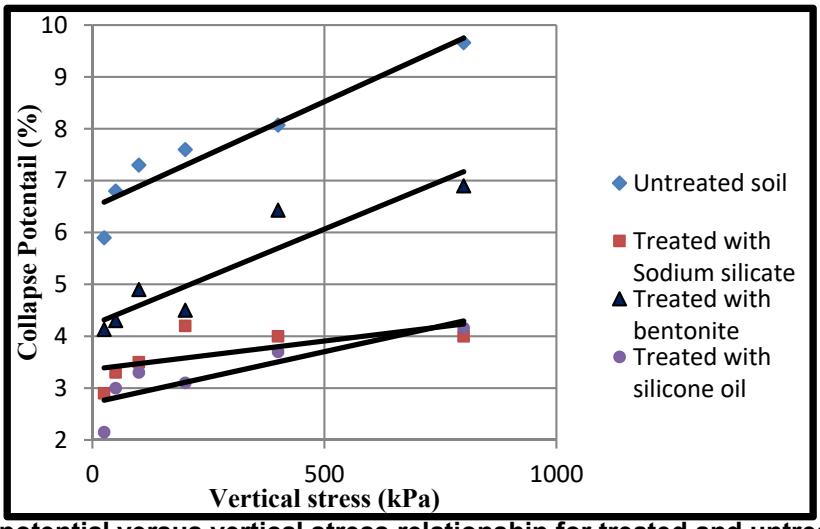


Fig. 11 Collapse potential versus vertical stress relationship for treated and untreated soil

DIRECT SHEAR TEST

To study the effects of different soil stabilizer grouts on the shear strength of treated gypsiferous soils, direct shear tests were conducted according to ASTM D3080-03 for untreated and treated gypsiferous soils improved by bentonite, sodium silicate, and silicone oil.

After the grouting process was completed and the treated soil was kept for 24 hours, the treated soil samples were extracted from the soil mould to conduct direct shear tests. Fig. 12 shows the relation between the maximum shear stress and the normal stress. Comparing the results of untreated and treated gypsiferous soils, it can be observed that the cohesion increases while the angle of internal friction slightly decreases with treatment. The presence of soil stabilizer is likely responsible for the increase in soil cohesion. In addition, the contact between soil particles is reduced in treated samples, which, in turn, reduced the internal friction angle. Also it can be clearly shown from Fig. 12 that all grout materials improved shear strength of the treated gypisferous soil compared to the untreated soils over the range of confining pressures studied here.

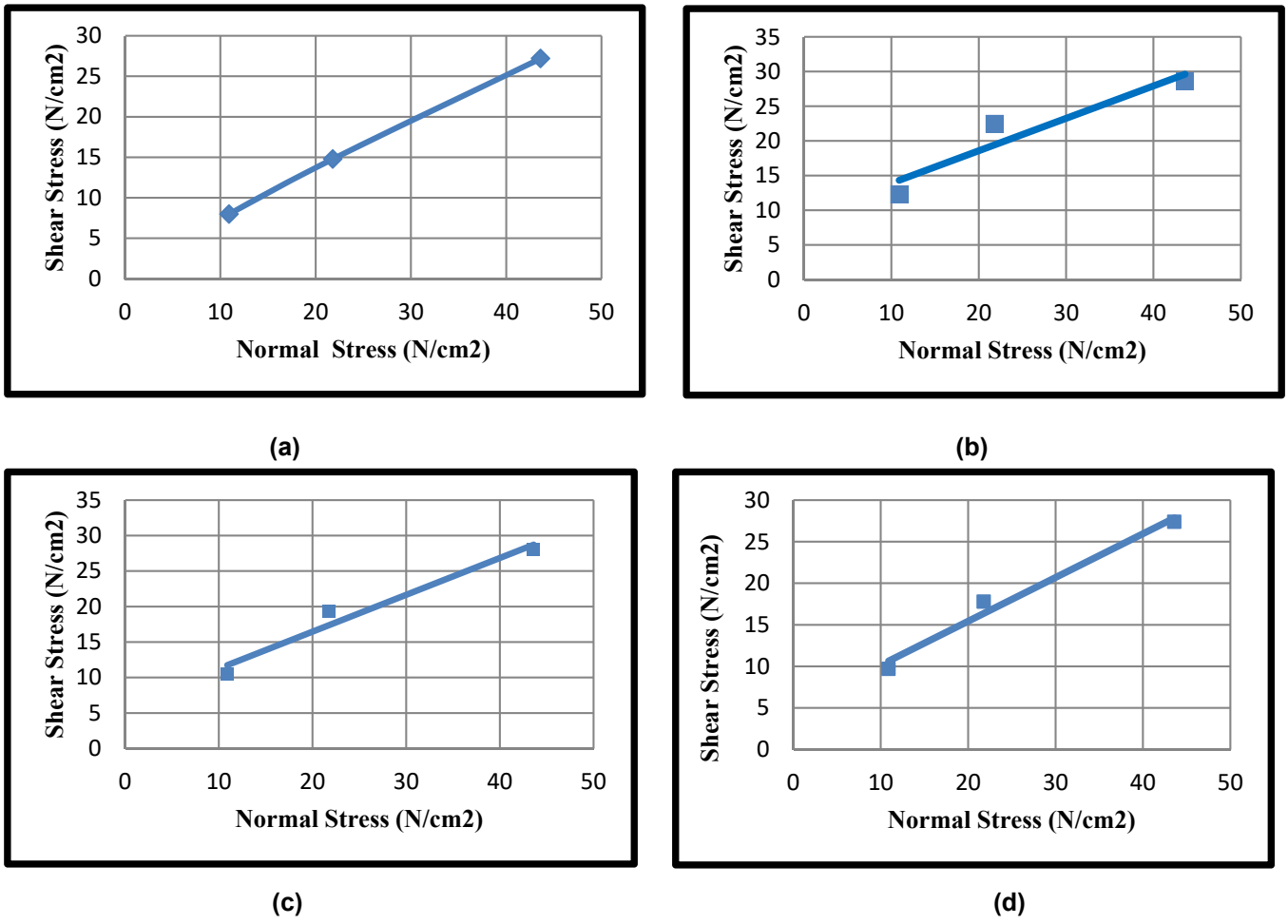


Fig.12 Direct shear test results (a) untreared soil , (b) soil treated with bentonite, (c) soil treated with sodium silicate , (d) soil treated with silicone oil.

SUMMARY AND CONCLUSIONS

A series of double oedometer tests and direct shear tests were carried out on gypsiferous soils before and after treatment by grouting. Three different grout treatments were studied here: bentonite, sodium silicate, and silicone oil. The following conclusions are drawn from this study:

1- Nonstandard sieve analysis provides more accurate results for gypsiferous soils and avoids misleading results due to gypsum dissolution.
2- Gypsum particles dissolved due to soaking which leads to the formation of cavities and holes in the soil structure. That, in turn, increases the compressibility and collapsibility of gypsiferous soil when subjected to slight levels of loading.
3- The ability of the stabilizer grouting materials to permeate in the gypsiferous soil depends on the consistency and viscosity of the stabilizer. The time required for injecting a certain amount of bentonite slurry is greater than those required for sodium silicate and silicone oil at the same injection pressure.
4- The compressibility test results show that all treatment stabilizers used in this study resulted in the reduction of volumetric strains under applied pressure. This may be attributed to the fact that the stabilizer liquids cover the gypsum particle in the soil and avoid the direct contact of water and gypsum particles, which acts as an impermeable layer to reduce the effects of water.
5- In collapse tests, the treated gypsiferous became less effective to water. This was manifested in the smaller difference in void ratios (in e-log(p) curves) between unsaturated and saturated tests for the treated samples. This behavior may be attributed to the presence of stabilizer materials, which made an impermeable layer and prevents gypsum particles from direct contact with water; hence, reducing the gypsum dissolution.
6- The collapse potential for the treated gypsiferous soil was observed to be less than that for untreated soil in all types of stabilizers used in this study. This can be attributed to the fact that the stabilizer materials form a gel and act as a cementing agent between the soil particles; thus, reducing the collapse potential. Sodium silicate and silicone oil show high efficiency in reducing the collapse potential in comparison with bentonite. Sodium silicate is believed to have lower costs in comparison with other stabilizers used in this research.
7- Direct shear test results show that the presence of stabilizer materials increases the soil cohesion and reduces the internal friction angle. The reduction in the friction angle is likely due to the reduction in the contact area between the soil particles.

REFFERENCES

ASTM D854, (2010). Standard test methods for specific gravity of soil solids by water pycnometer. Annual Book of ASTM Standards, Vol.04.08, West Conshohocken, PA.

ASTM D3080-03, (2003). Standard test method for direct shear test of soils under consolidated drained conditions. Annual Book of ASTM Standards, Vol.04.08, West Conshohocken, PA.

ASTM D533, (2003). Standard test methods for measurement of collapse potential of soils. Annual Book of ASTM Standards, Vol.04.08, West Conshohocken, PA.

ASTM D422, (1963). Standard test methods for particle size analysis of soils. Annual Book of ASTM Standards, Vol.04.08, West Conshohocken, PA.

Barzanji, A.F., (1973) . Gypseous soil of Iraq. State University of Ghent, Belgium, Ph.D. Thesis.

Bruce, D.A. (2003). " Sealing of Massive Water Inflows through Karst by Grouting: Principles and Practice." 9th Multidisciplinary Conference on Sinkholes and the Engineering and Environmental Impacts of Karst™, American Society of Civil Engineers, Huntsville, AL, September 6-10, 12 pp.

Fattah, M.Y., Al-Ani, M.M. and Al-Lamy, M.T., (2014). Studying collapse potential of gypseous soil treated by grouting. The Japanese Geotechnical Society, Soils and Foundation, 54 (3)396-404.

Fattah, M.Y., Al-Musawi,H.M. and Salman, F.A. , (2012). Treatment of collapsibility of gypseous soil by dynamic compaction. Geotechnical and Geological Journal, 30, pp. 1369-1387.

Ibrahim, A.N. and Schanz, T. (2017). Improvement of gypsiferous soil by silicone oil. Soil Mechanics and Foundation Engineering, Vol. 54, No. (2).

Ibrahim, A.N. and Schanz, T. (2014). Shear strength and collapsibility of Gypsiferous Soils. Proceedings. IAEG XII Congress, Engineering Geology for Society and Territory, Torino , Vol. 2, pp. 1109-1115.

Karol,H.R. (2003). Chemical grouting and soil stabilization. Marcel Dkker, Inc., New York, 142p.

Raman, K.V., Dayakar, P. and Raju, K.V.B., (2012). Effect of permeation grouting using cement bentonite grout in sandy soil. International Journal of Engineering Trends and Technology (IJETT), 3(5) 40-49.

Razouki,S.S., Al-Omari, R.R. , Nashat, I.H., Razouki , H.F. and Khalid, S. (1994). The problems of gypsiferous soils in Iraq. Symposium on Gypsiferous Soils and their Effect on Structures, National Center for Construction Laboratories, Baghdad.

BEARING CAPACITY OF SEMI-DEEP SKIRTED FOUNDATIONS

Samieh Rezazadeh, Amirkabir University of Technology, Tehran, Iran, +98-9113446085, Samieh.Rezazadeh@aut.ac.ir
Abolfazl Eslami, Amirkabir University of Technology, Tehran, Iran, +98-2164543057, afeslami@aut.ac.ir

ABSTRACT

Semi-Deep skirted foundations are considered to be a viable option for a variety of onshore and offshore applications. It is necessary to determine appropriate foundation configurations that allow loads to be transferred safely to the surrounding soil. For this purpose the bearing capacity and stability analyses subjected to combined vertical, horizontal and moment loadings must be found. In this paper the vertical undrained bearing capacity is estimated via finite element analyses. The circular skirted foundations with different geometries considering embedment depth (embedment ratio between 0-2) and size effects (diameter equals to 5, 10, and 20) have been studied. Stress field, kinematic mechanism accompanying failure and bearing capacity factors for total, end and shaft resistance in semi-deep foundations with various embedment ratios are investigated. Furthermore, two probable mechanisms i.e. internal flow and soil plug for estimating foundation capacity for design purpose in practice have been assessed. Comparisons with different research works including conventional methods, upper and lower bound approaches, and finite element analyses have indicated that the conventional methods underestimate the bearing capacity due to ignoring the significant role of shaft resistance.

Keywords: Semi-deep skirted foundation, Bearing capacity, Finite element method (FEM), Embedment depth effects

INTRODUCTION

Determining appropriate economic foundation configurations to transfer loads safely to the surrounding soil is a major issue in geotechnical engineering. Shape and dimension of foundations, embedment depth, soil characteristics and applied loading, all affect the foundation performance. Recent studies have shown that for foundations with large breadth and of D/B between 1 to 4, kinematic mechanisms and failure modes are different from the two main types of foundation (i.e. shallow and deep). Therefore, D/B factor must not be considered as the only factor for defining foundation type.

"Semi-Deep foundations" are another foundation category distinguished based on their performance. This relatively new concept is becoming increasingly an optimum alternative for shallow and deep foundations to support structures especially in accessible depth. As illustrated in "Fig. 1", different types of semi-deep foundations consist of:

- Bucket foundation or Suction caisson,
- Spudcan,
- Hybrid foundation,
- Floating and Box foundation,
- Well foundation,
- Skirted foundation.

 © 2017 DFI Annual Conference, New Orleans, LA, USA

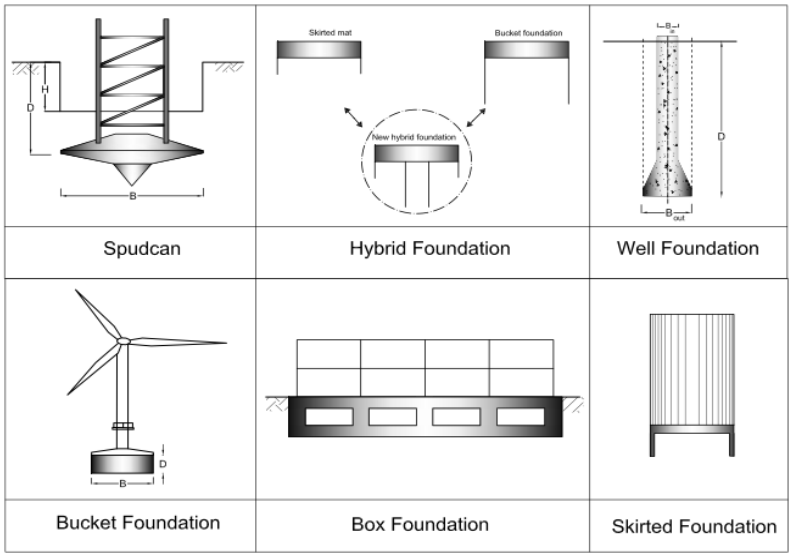


Fig. 1. Different types of semi-deep foundations

A skirted foundation is a circular semi-deep foundation with thin skirts around the circumference. The basic functions of the skirts are mainly confining soft surface soils and transfer the loads down to harder underlying layers to resist lateral loads and moments effectively against sliding and overturning. Also they are utilized to improve protection against piping and scour. Furthermore, using of peripheral skirts, the soil beneath the foundation can be prevented from squeezing out and any probable damage due to excavations for adjacent construction works.

Skirts can be made out of the steel or concrete. Having used in offshore facilities, skirt is first penetrated into the seabed by a self-weight. Further penetration is achieved by pumping water out of the skirted foundation, creating a suction pressure inside it. Penetration stops when the top-plate (footing) comes in contact with the seabed and the suction pressure confines a plugged soil within the skirt. In other situations, installation process including either concrete skirted foundations that are cast in place during construction or the steel skirts which are inserted into the soil until the footing rest on the soil. Any remaining void between the soil and footing is grouted. The relative ease of installation provides a significant economic incentive particularly in areas with difficulties related to pile construction. Moreover, they can transfer loads though end resistance at the tip level and shaft friction alongside the skirt.

Structural skirts improve the footing bearing capacity and reduce total and relative settlement as well as the stability advantages. Their performance depends upon the geometry and structural specifications of the skirts and footings, soil characteristics and conditions of both soil-skirt and soil-footing interfaces. The study of the relationship between the vertical load and the vertical displacement in soil-foundation interaction problems is essential not only from the vertical capacity point of view but also to solve combined loading capacity problems involving moment and horizontal loads (Yun and Bransby, 2007a). Despite the wide discussion in the bearing capacity of shallow foundation in geotechnical engineering literature, limited knowledge is available on the performance of skirted foundations, when it comes to their usage as conventional foundations and in land projects, such as storage tanks, towers and high rise buildings. Also, some numerical studies on skirted and bucket foundations in clay have been conducted which assumed that the foundation was either a skirted strip foundation (Bransby and Randolph, 1999; Yun and Bransby, 2007a; Bransby and Yun, 2009) or an equivalent surface circular foundation with surcharge without modeling the embedment of the foundation (Tani and Craig, 1995; Bransby and Randolph, 1998). Therefore, more investigation must be carried out on the geotechnical aspects of these foundations to highlight their advantages for practicing engineers. This paper presents numerical study to

evaluate the performance of a circular skirted foundation in terms of bearing capacity under vertical loading in uniform soft clay.

NUMERICAL ANALYSES

The basic bearing capacity equation or "the triple N formula" has been used for estimating both drained and undrained capacity of foundations and stability against static bearing failure for many years. In General, for determining bearing capacity of semi-deep foundations analogous to deep foundation, various parameters such as type of soil, construction method, foundation material and scale effect should be considered. (Rezazadeh et al., 2013; Eslami et al., 2013). For a rigid circular skirted foundation under vertical loading on purely cohesive soil in undrained condition, the net capacity can be written as Eq. [1]

$$V_0=S_uN_cd_cs_cA \quad [1]$$

Estimating foundations bearing capacity on frictionless soil depends upon the establishment of strength parameters and use of appropriate bearing capacity factors which can be predicted by different numerical approaches as discussed in followings. Finite element analysis accounts for kinematics and equilibrium and has been used to determine bearing capacities in close agreement with simpler solution but with more computing effort. The undrained condition of clay during loading can be reasonably analyzed using total stress analyses (TSA) (Tani and Craig, 1995). Therefore, the soil in the present study was modeled as a linear elastic-perfectly plastic model based on the Tresca failure criterion (φ=0 condition).The undrained shear strength of the clay (S_u) was assumed to be 5 kPa, with a Young's modulus (E_u) at 400 × S_u, for uniform clay. The poisson's ratio and the effective unit weight of soil at μ=0.495 and γ=6kN/m^3 were applied. The interface between the foundation and the soil was assumed to be rough, and the detachment between the skirted foundation and the soil was prevented (Gourvenec, 2008; Bransby and Yun, 2009; Ibsen et al., 2015).

The finite element analyses of this study were carried out using the ABAQUS software (Simulia, 2010). The four-node bilinear axisymmetric quadrilateral element, CAX4, was used to model the soil and a two-node linear axisymmetric rigid link, RAX2, to model foundation. Because of the large deformations related to ultimate bearing capacity estimation, adaptive meshing in ABAQUS using the Arbitrary Lagrangian-Eulerian (ALE) method was considered. Foundation was brought to failure by a displacement-controlled load path which increases vertical displacements (v) at a reference point (RP). B_V and B_H are the vertical and horizontal boundary extents from the corner and tip of the skirt equal to 3B and 6B respectively.

The bearing behavior of the skirted foundation was investigated in terms of total and normalized bearing capacities (V_0/AS_u), where V_0 is the vertical bearing capacity and A is the cross-sectional area of the skirted foundation. The vertical bearing capacity is determined using the tangent intersection method (Mansur and Kaufman, 1956) and Brinch Hansen method (1963). Tangent intersection method, plots two tangential lines along the initial and later portions of the load-displacement curve, and the load corresponding to the intersection point of these two lines is taken as the bearing capacity. Hansen defined bearing capacity as achieved stress q_{cap} that produces a displacement twice than produced at 90% of q_{cap}. These two criteria yield in the most reasonable results for defining bearing capacities of skirted foundations. The embedment ratio (D/B) and the diameter (B) of the skirted foundation varied at 0 (as a surface foundation), 0.1, 0.2, 0.5, 1, 1.5, 2 and 5, 10, 20 m, respectively.

Effect of Embedment Ratio

In order to investigating the effect of skirt embedment depth on the bearing capacity, several modeling with different embedment ratios of 0.1 to 2 were analyzed. "Figs. 2 a, b" present the total and normalized

vertical load-displacement curves and the variations of the vertical bearing capacity for the rigid plugs and skirted foundations versus the D/B. The initial slope increases with increasing D/B and indicates stiffer response for deeper foundations, but the general trend and failure points are almost the same.

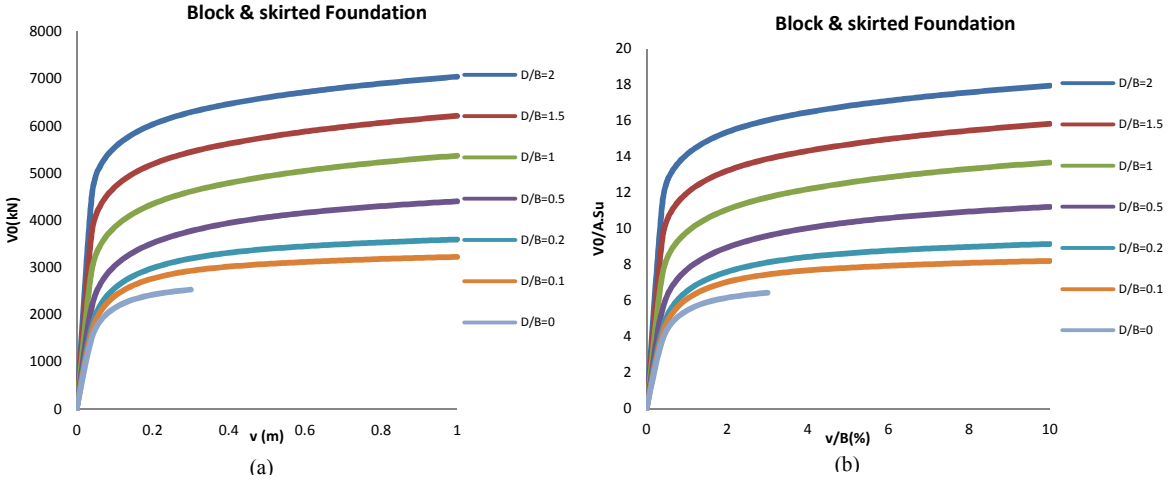


Fig.2. Load-displacement curves for block and skirted foundation (a) Ultimate load (b) Normalized capacity

The bearing capacity factors increase with increasing embedment ratio, as would be expected and the bearing capacity factors for skirted foundations are identical to those for a rigid solid plug or block foundation of equivalent embedment.

Failure Mechanism

The non-linear increase in the vertical bearing capacity can be explained by the transition of the failure mechanism, from a traditional Prandtl surface failure to vertical punch mechanism where the angle of exit at the soil surface tends to 90^0 and then became almost constant ("Fig. 3"). As illustrated in "Fig. 4" a general shear mechanism governed failure mode for shallow foundation. The mechanism will change to local shear and punch for both the rigid plug and the skirted foundation depending on the increased length of slip line due to foundation width or embedment depth. Failure contours and displacement vectors in "Figs. 3,4" indicate the soil plug displaced as a rigid body, consistent with the coincidence of the bearing capacity factors presented in "Fig. 2". Block foundation is depicted in the left side and skirted foundation in the right side of each picture in "Figs. 3,4".

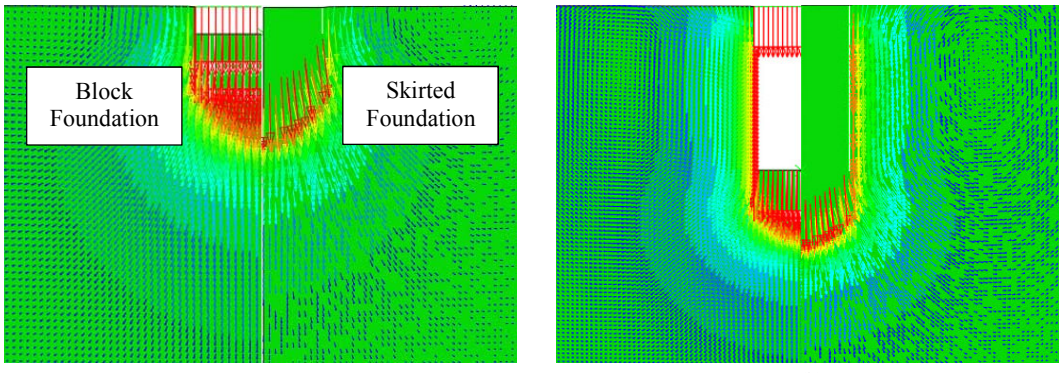


Fig. 3. Displacement vectors at failure for block (left side) and skirted (right side) foundation (a) D/B=0.2 (b) D/B=2

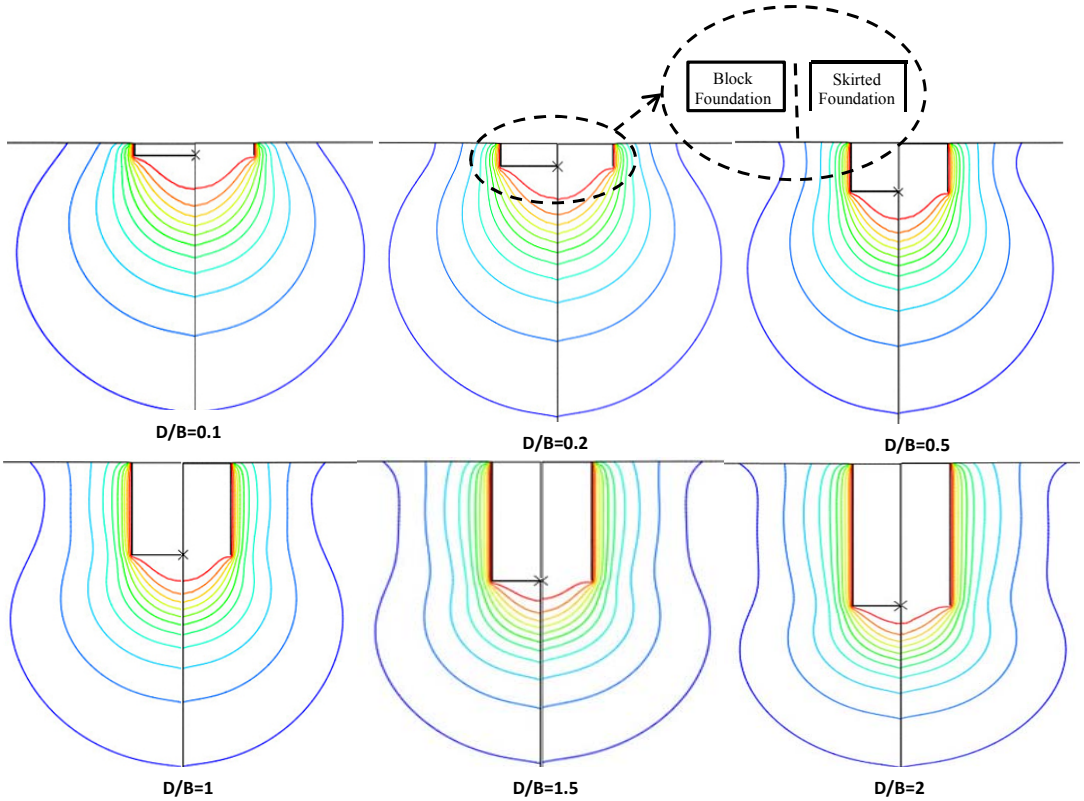


Fig. 4. Failure mechanism comparison for block (left side) and skirted foundation (right side) of different embedment ratios

Effect of Foundation Diameter

To investigate the effect of foundation diameter on the bearing capacity of the skirted foundations, three different diameters as 5, 10 and 20 m were selected. The embedment depth for these cases was selected as 1B which corresponds to embedment ratio of D/B=1. As it is evident from load-displacement relationship in "Fig. 5a" all curves almost have the same trend that results in decreasing total bearing capacity with diameter. "Fig. 5b" shows decreased bearing capacity factors for foundation with larger diameter and is in contrast with that reported by Hung and Kim (2012) as they confirmed the foundation diameter has no effect on the normalized bearing capacities.

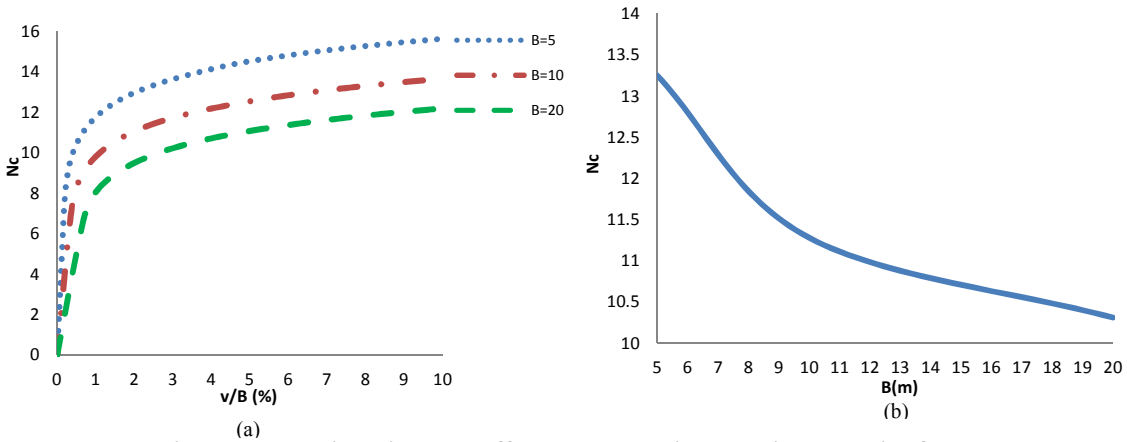


Fig. 5. Foundation diameter effect on the vertical bearing capacity factor

COMPARISONS AND DISCUSSIONS

The results of the present study have proved that skirted foundation can be considered as an embedded hybrid foundation. The total bearing capacity of a skirted foundation is made up of two components analogous to the axial capacity of a deep foundation :(i) the end (tip) bearing resistance, V_b (ii) the shaft friction resistance, V_s. This approach was also used by House and Randolph (2001), Byrne and Cassidy (2002), Yun and Bransby (2009). This is only valid if the end bearing and friction terms are independent and capable of being decoupled. This assumption has been investigated by Yun and Bransby (2009) and was proved to be accurate.

There are two different mechanisms for determining vertical bearing capacity of skirted foundations. As shown in "Fig. 6a" for internal soil flow, end resistance at the skirt tip and raft at the ground level add to the internal and external friction resistance. For skirted foundation in which trapped soil form within the skirt, the capacity can be obtained by summing up two components of tip and shaft friction terms according to "Fig. 6b".

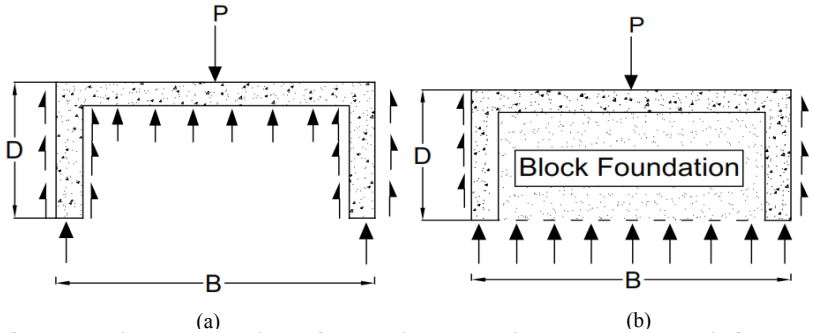


Fig. 6. Definition of two possible mechanisms for vertical capacity (a) Internal soil flow, (b) Block foundation

Calculations of two approaches indicate the results are almost the same. Therefore, for the skirted foundation in undrained clay, vertical bearing capacity can be expressed by Eq. [2].

$$V_0=V_b+V_s \qquad [2]$$

For the vertical loading, V_b follows the standard end bearing capacity formula according to Eq. [3.a]

$$V_b=N_c d_c s_c A S_u \qquad [3.a]$$

Where, s_c equals to 1.2 for a circular surface rough foundation and dc=1+n(D/B), where $0.2\leq n\leq 0.4$ (Skemton, 1951;Meyerhof, 1963; Brinch Hansen, 1970).V_b can be rewritten as the Eq. [3.b]

$$V_b=N_{cb} A S_u \qquad [3.b]$$

Where, N_{cb} is the end bearing capacity factor for rough-based and rough-sided circular skirted foundation, which is expected to depend only on the embedment ratio in uniform clay.

For skirted foundation, the skin friction term in soil with uniform strength, depends upon soil strength (S_u), interface roughness term (α), and embedment ratio (D/B).

$$Vs=\alpha S_u.\pi BD \qquad [4.a]$$

$$Vs=4\alpha\ (D/B) A S_u \qquad [4.b]$$

For the present study, the interface roughness term considered as rough (α=1) and Eq. [4.b] can be expressed as following:

$$V_S=N_{cs}AS_u \qquad [4.c]$$

Where, N_{cs} is the friction bearing capacity factor (4D/B) and becomes an increasing portion of the total bearing capacity of foundation as the embedment ratio increases.

The ultimate bearing capacity values obtained from finite element method, and several researchers have been presented in Table 1.

Table 1. Databank of calculated and analyzed ultimate vertical loads

D/B / Method	0	0.1	0.2	0.5	1	1.5	2
		Ultimate	Vertical	Load	(kN)		
(Meyerhof, 1963)	2422	2470	2519	2664	2906	3148	3391
(Skempton, 1951)	2422	2470	2519	2664	2906	3148	3391
(Vesic, 1975) (Hansen, 1970)	2422	2519	2615	2906	3391	3439	3494
(Gourvenec, 2008)	2422	2626	2823	3366	4117	-	-
(Hung&Kim, 2012)	2018	2215	2396	2835	3229	-	-
(Hung&Kim,2014)	3063	3267	3471	4084	5105	-	-
(Edwards et al., 2005) (Smooth side)	2391	2651	2913	3200	3616	3934	4201
(Edwards et al., 2005) (Rough side)	2391	2657	2925	3345	3820	4150	4410
(Salgado, 2004) UB	2464	2803	2954	3279	3702	4010	4322
(Salgado, 2004) LB	2299	2549	2708	2976	3444	3677	3916
FEM-V_0 (Present study)	2400	2680	2900	3500	4400	5400	6250
FEM-V_b (Present study)	2400	2500	2600	2700	2800	3000	3150
FEM-V_s (Present study)	0	180	300	800	1600	2400	3100

It is clear that the previous methods do not predict the effect of increasing D/B on the ultimate load, properly. Therefore, the bearing capacity factors N_{c0}, N_{cb}, N_{cs} are back-calculated by adoptingV_0,V_b,V_s, from finite element analyses. $V_{b(FEM)}$,$V_{s(FEM)}$ have been averaged from the vertical stresses in soil elements below the skirt tip level and shear stress alongside the skirt circumference, respectively, considering the

mechanism (a) in "Fig. 6" as explained before. "Fig. 7" indicates the back-calculated total, end and shaft bearing capacity factors.

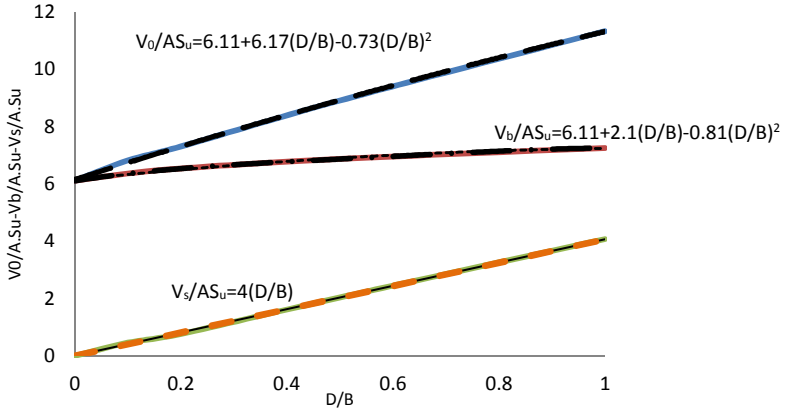


Fig. 7. Total, end, shaft bearing capacity factors versus D/B

Equations [5] through [7] are suggested to evaluate V_0,V_b,V_s using bearing capacity factors for calculating shaft, end and total loads.

$$N_{c0}=6.11+6.17(D/B)-0.73(D/B)^2 \quad [5]$$

$$N_{cb}=6.11+2.1(D/B)-0.81(D/B)^2 \quad [6]$$

$$N_{cs}=4(D/B) \quad [7]$$

The results of the FE analyses are obtained for total, end and shaft bearing capacity individually and compared with those of previous methods. The capacities predicted by conventional methods are illustrated in "Fig. 8" as "Skempton (1951)", "Meyerhof (1963)", "Brinch Hansen (1970)", "Vesic (1975)", "Salgado et al. (2004)", "Edwards et al. (2005)", " Gourvenec (2008)" and "Hung and Kim (2012, 2014)".

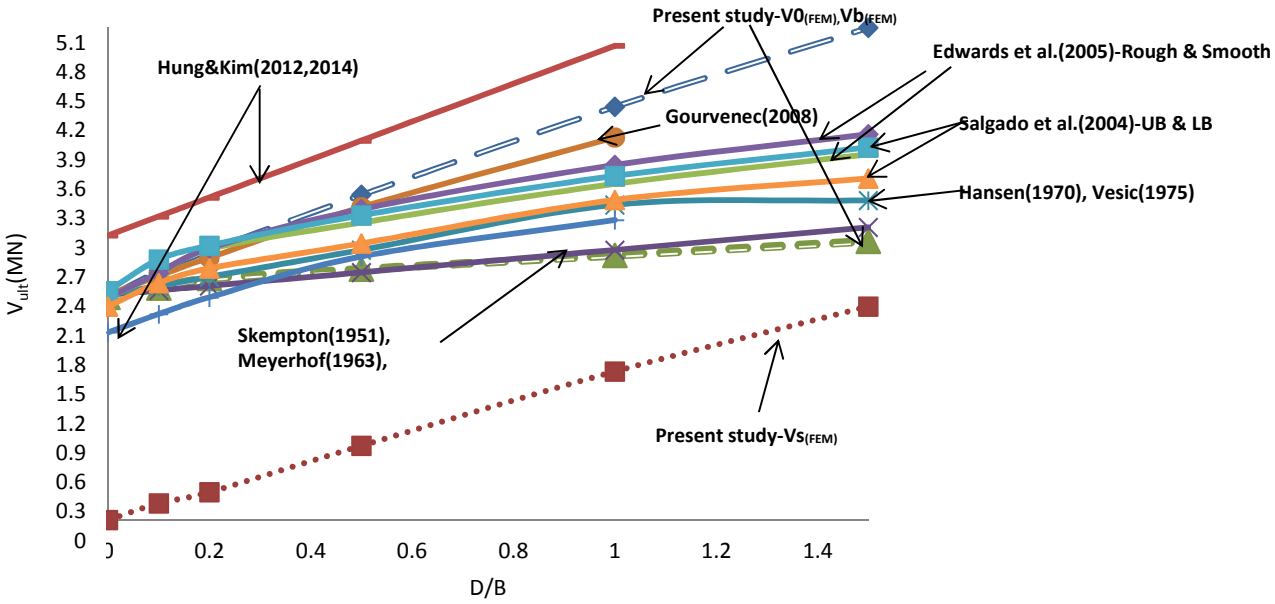


Fig. 8. Comparisons of ultimate vertical load

Comparisons with the finite element analyses results indicated that the conventional methods underestimate the bearing capacity and the difference between predictions and finite element results increases when D/B ratio increased. For $0.5 \leq D/B \leq 2$, the increase in total bearing capacity is provided mostly by skin friction (shaft resistance) as the peripheral area increased with embedment ratios. As it can be considered from "Fig. 8", there is a non-linear relationship leads to increasing the bearing capacity at higher embedment ratios. The rate of increase in the bearing capacity due to the increasing of depth ratio from 1 to 2 is higher than that caused by increasing the depth ratio from 0.5 to 1.

CONCLUSIONS

Finite element analyses have been used to investigate the vertical bearing capacity of circular semi-deep foundations. Moreover it has been assessed the effect of simulating skirted foundation geometry to a rigid soil plug or a block foundation in uniform clay. A method for determining ultimate bearing capacity of skirted foundation is proposed from finite element analyses via ABAQUS, suggesting modification factors (bearing capacity) as a function of D/B ratio, over a practical range between 0 to 2. The following results from this study are drawn:

- Adding peripheral skirt to conventional footing will improve foundation performance in terms of lowering installation time and cost by reducing excavation volume, increasing bearing capacity by increasing slip lines, confining the soil within skirts and transferring loads to deeper and stronger soil.
- The way of embedding foundation, i.e. solid embedded or skirted has almost no effect on the undrained vertical bearing capacity factors. Hence, for the design purpose it can be estimated as if the soil within the skirt is trapped (i.e. as an equivalent solid embedded foundation). In practice, internal mechanisms are supposed to be more significant under horizontal and moment loading than vertical loads.
- The vertical undrained bearing capacity of the skirted foundation evaluated through FEM analyses, increased with embedment ratios. Nevertheless, the increase fits a polynomial curve with order of two and is not linear because of the transition of the failure mechanism altering from a traditional general failure to a punch shear failure with almost vertical mechanism with the exit angle of 90^0 at the soil surface.
- The results of two probable mechanisms i.e. internal flow and soil plug for estimating foundation capacity are almost the same and the bearing capacity of skirted foundation can be determined from the end resistance at the skirt tip adding to external skin friction resistance. The second term becomes more significant in longer skirts because of the larger circumference.
- Comparisons between the results of finite element analyses with commonly used approaches including traditional methods, upper and lower bands, indicated that conventional methods underestimate foundation total bearing capacity, mostly because of ignoring the friction alongside skirt. Amongst the researchers, the trend and results of end bearing load from Skempton (1951), Meyerhof (1963) and ultimate load from Gourvenec (2008) for strip foundation using $s_c=1.2$ are similar to the present study, while the study of Hung and Kim (2014) on a circular bucket overestimates the ultimate load. Therefore, the proposed approach suitably predicts the undrained vertical bearing capacity of skirted semi-deep foundations considering the effect of embedment depth.

NOTATION

V_0	total (ultimate) vertical load
V_s	shaft capacity
V_b	end capacity
S_u	soil undrained shear strength

A	base area of the skirted foundation
D	embedment depth
D/B	embedment ratio
d_c	non-dimensional depth factor
s_c	non-dimensional shape factor
N_c	non-dimensional bearing capacity factor
N_{c0}	total bearing capacity factor
N_{cs}	shaft bearing capacity factor
N_{cb}	end bearing capacity factor
α	interface roughness term
E_u	Young's modulus
μ	poisson's ratio
ɣ́	effective unit weight of soil
v	vertical displacement
RP	reference point
φ	angel of friction
B_V,B_H	vertical and horizontal boundary limits

REFERENCES

Bransby, M. F., and Yun, G. J., 2009. Capacity of Skirted Strip Foundations under Combined Loading. Geotechnique.59(2) 115-125.

Bransby, M. F., and Randolph, M. F.,1999. The Effect of Embedment Depth on the Undrained Response of Skirted Foundations to Combined Loading. Japanese Geotechnical Society. 39(4) 19-33.

Cassidy, M. J., Byrne, B. W., and Houlsby, G. T., 2002. Modeling the Behavior of Circular Footings under Combined Loading on Loose Carbonate Sand. Geotechnique 52(10) 705-712.

Edwards, D. H., Zdravkovic, L., and Potts, D. M., 2005. Depth Factors for Undrained Bearing Capacity. Geotechnique. 55(10) 755-758.

Eslami, A., Lotfi, S., and Eslami, M., 2013. Pile Shaft Capacity from Cone Penetration test (CPT) Records: Considering Scale Effects. 38th Annual Conference on Deep Foundations, American Samoa.

Gourvenec, S., 2008. Effect of Embedment on the Undrained Capacity of Shallow Foundations under General Loading. Geotechnique. 58(3) 177-185.

House, A.R., Randolph, M.F., 2001. Installation and Pull out Capacity of Stiffened Suction Caissons in Cohesive Sediments. Proceedings of the 11th IOSPE, Stavanger, Norway. 574–580.

Hung, L. C., and Kim, S. R., 2014. Evaluation of Undrained Bearing Capacities of Bucket Foundations Under Combined Loads. Marine Georesources and Geotechnology. 32.76-92.

Hung, L. C., and Kim, S. R., 2012. Evaluation of Vertical and Horizontal Bearing Capacities of Bucket Foundations in Clay. Ocean Engineering. 52. 75-82.

Ibsen, L. B., Barari,A., Larsen, K. A., 2015. Effect of Embedment on the Plastic Behavior ofBucket Foundations", J. Waterway, Port, Coastal, Ocean Eng., Technical note, ASCE. 141(6) 06015005-1-06015005-9.

Martin, C. M., 2001.Vertical Bearing Capacity of Skirted Circular Foundations on Tresca Soil. Proc. 15th ICSMGE. 1. 743-746.

Rezazadeh, S., Eslami, A., Jafary Shalkoohy, A., 2013. Scale Effect Aspects for Correlation CPTu Data in Deep Foundation Analysis and Design. Life Science Journal. 10(6s) 387-396.

Salgado, R., Lyamin, A. V., Sloan, S. W., and Yu, H. S., 2004. Two- and Three-Dimensional Bearing Capacity of Foundations in Clay. Geotechnique. 54(5) 297-306.

Simulia, 2010. ABAQUS User's Manual. Dassault Systems Simulia Corp.

Skempton, A. W., 1951. The Bearing Capacity of Clays. Proc., Building Research Congress. 1.180–189.

Tani, K., and Craig, W. H., 1995. Bearing Capacity of Circular Foundations on Soft Clay of Strength Increasing with Depth. Japanese Geotechnical Society. 35(4) 21-35.

Yun, G., and Bransby, M. F., 2007a. The Undrained Vertical Bearing Capacity of Skirted Foundations. Soil and Foundations Japanese Geotechnical Society. 47(3) 493-505.

BAUM STATION – A NEW PILE DRIVING AND DRILLING NAVIGATION SYSTEM

Koji Mitani, KUMONOS Corporation, Osaka Japan, +81-72-749-1188, k.mitani@kankou.co.jp
Dzianis Proshchanka, KUMONOS Corporation, Osaka Japan, +81-70-2298-0002, dennis@kankou.co.jp
Yoshi Izumi, KUMONOS Corporation, Osaka Japan, +81-72-749-1188, y.izumi@kankou.co.jp
Ayuna Kitaura, KUMONOS Corporation, Osaka Japan, +81-72-749-1188, a.kitaura@kankou.co.jp

ABSTRACT

A new pile driving and drilling navigation system has been developed. It utilizes the commonly used surveying total station, combined with an innovative reticle. Conventional crosshairs have been replaced by a concentrically circular reticle called Baum. It allows for easily performed measurements of central axes of cylindrical objects such as piles, chimneys, electricity poles, etc. This provides several significant advantages compared to other existing systems. It is cost-effective as only one operator is required to control deviations in positioning and inclination. Furthermore, repetitive reinstallation of the instrument is not required for every pile driven or hole drilled. It is also a safer method, as workers have no need to be near a pile driver or drilling machine to perform the measurements. With Baum Station, necessary measurements can be performed away from the actual work area. Moreover, it is highly accurate with real-time solutions, as three-dimensional orientation information for the pile/drill is obtained simultaneously with the pile being driven or the hole being drilled. This allows for the highest levels of precision-control and correction to minimize eccentricity of the intended center positioning.

Keywords: total station, reticle, pile driving, cylindrical structure

INTRODUCTION

Background

In foundation construction for structures, pile foundations are widely used for deep bearing strata. There are two patterns to driving piles: vertically or obliquely to the ground. The shapes of the piles are normally cylindrical. Vertical pile foundations are employed as the foundations of many structures due to their high workability. There is a problem however, which is that this method does not bear measurement data as construction accuracy is visually checked. On the other hand, tilted pile foundations are rarely employed because it is too difficult to ensure construction accuracy. In addition, commonly used percussion methods create noise and vibrations when the piles are hit, while there are advantages that thinner piles are available, ensuring earthquake-resistance, as tilted piles curb horizontal displacements of structures, which may be caused by earthquake ground motion. However, current requirements of cost reduction bring professional attention to tilted pile foundations, which can be driven reasonably and economically with much research of tilted piles having been carried out to improve their capacity. Also, a method of screwing piling has been developed, which produces small amounts of noise and vibrations. This method has solved tasks of workability and environmental burdens, and is becoming more and more common. However, there is a necessity to develop a method to accurately measure angles of piles' axes in order to drive piles into the ground with appropriate angles. It is also expected to find out a way to control construction information, such as correction amount and driving record.

On the other hand, total stations (TSs) are commonly used for structure measurement. Crosshairs of the reticle are placed in the focus of the eyepiece of the optical instrument. TSs also have built-in computers to obtain and record the positional coordinates of measured points. However, if there is no mark showing the points to be measured, it can be difficult to align crosshairs with the points required. For example, surveyors cannot accurately measure the center of cylindrical structures with crosshairs. That is why TSs are rarely used to control accuracy for the construction of foundation piles.

 © 2017 DFI Annual Conference, New Orleans, LA, USA

To solve these problems, we developed a system with total station in which the reticle with concentric circles is placed. These concentric circles enable TS to be lined up with points on the center lines on the surfaces of cylindrical structures. This research shows that operators can accurately measure the position and the tilt of the axes of the structures by measuring two points on the center line. Applying this technology, we also developed a system which aids constructions by passing the information about the pile angles, which are obtained from measurements, to the operator of the piling machine and by recording shift amounts in real time.

Conventional method

In the common method of measuring verticality of piles for accuracy control of vertical pile foundations, workers position the pile tip at a predesignated position, set up two transits in two directions, as shown in Fig. 1, and align the vertical line of the crosshairs of the transits with the pile. The use of two transits requires more man-hours as the transits need an operator for each. It is also necessary to move the transits more frequently depending on the number of the piles to be driven, which requires more labor as well. Another problem is that measurement data is not logged because workers perform verticality checks visually.

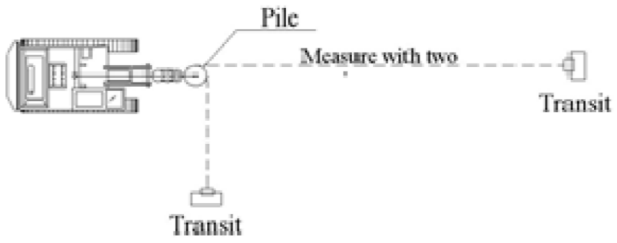


Fig. 1. Conventional method to drive foundation piles using two transits

Angles of tilted pile foundations are commonly measured using angle meters. A worker directly puts an angle meter on the pile to measure its verticality, which decreases the workability as it is necessary to halt the construction. The method causes safety concerns because a worker needs to approach the pile. There is also a problem regarding accuracy. The position and the way to place an angle meter causes differences in the measurement results.

MEASURING CYLINDRICAL STRUCTURES
Overview

A Total Station with Baum has concentric circles on the reticle as shown in Fig. 2. The ratio in terms of space between each circle and the distance between the instrument and the object is 1:1000. The width of the target object can be calculated from the relation between the read concentric scale marks and the distance. By vertically or horizontally lining up a circle of the Baum to both of the edges of a cylindrical structure, it is possible to obtain central coordinates of the center line of objects. For example, by lining up one circle on both edges of a cylindrical structure, points on the center line can be measured. Its radius can be calculated as well. For example, when a cylindrical structure stands vertical, and is 10m away from a TS with the Baum, its radius is calculated from 10(m)*10/1000.

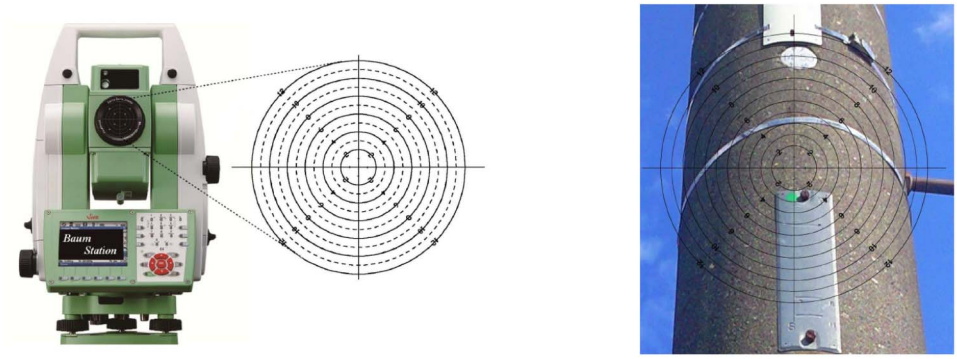


Fig. 2. A TS with the concentric reticle

EXPERIMENT IN ALIGNMENT

Overview

When conducting measurements using TSs with the Baum, the widths between both of edges of the structure sometimes do not exactly fit on any circle of the Baum. In this case, operators need to presumptively read the space between two circles. For example, in Fig. 3 the edges of the structure are between the circles numbered 5 and 6 (Presumptively read value: 5.45). As Fig. 4 also shows, the appearance of the pile in the viewing field of the lens varies depending on the diameter of cylindrical structures and the distance between the target object and the TS. However, experiments have not been carried out to estimate their effect on accuracy. Therefore, we conducted an experiment to estimate how much accuracy would vary, depending on the concentric circles' gauge number.

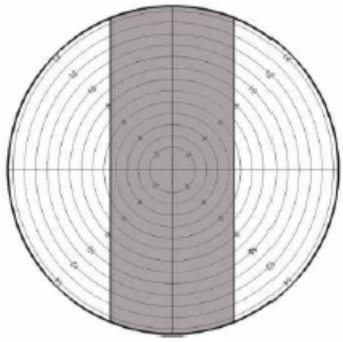


Fig. 3. Presumptive reading of the center (Read value: 5.45)

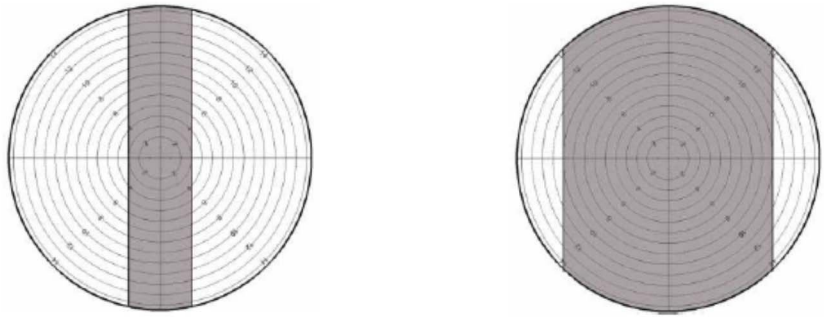


Fig. 4. Difference of piles' appearance in the viewing field (Used scale: 3 in left figure and 10 in right figure)

We used a Leica's TS11 with Baum reticle mounted and a vinyl-chloride cylindrical pipe with 60mm diameter. We set pipes up at the distances of 3m, 5m, 5.2m, 5.8m, 6m and 10m from the TS. Each of the 3 operators (Denoted by Operator A to C) aligned the Baum with the points on the center of the pile 10 times, and we recorded the variation of horizontal angles. We conducted trials under the condition that the TS was mounted on a leveling plate at around 1.4m in height, the instrument was 1.5m in height, and the vertical angle was 90 degrees.

Result

Table 1 shows averages of the values that each of the 3 operators obtained from 10 trials, as well as the average and mean square error of all trials according to distances, denoted by an L between the TS and the surface of the cylindrical structure. The table also shows values of distances, which have been translated from measured angles. We calculated the error values, translated from angles into distances, denoted by e from $e=L\tan\theta$, in which θ means the angle calculated from mean square errors. From the fact that the greatest error value in each trial was 5 seconds, we concluded that the variation of error is very small. Additionally, there was a lot of variation when the distance was 5.47m. We assume that this variation was caused by the presumptive readings skills of individuals, because the edges of the structure were almost in the middle of circles numbered 5 and 6, which was read as 5.45. We also found that operators can accurately measure centers of cylindrical structures by presumptive reading, as there was not a lot of variation when the distance was 5.175m and 5.770m. The errors which are translated from angles to distances increase in proportion to the distance to the target object, while the accuracy in horizontal angles does not nearly vary. From these facts we've concluded that the shorter the distance is to the object, the more accurately we can conduct measurements. From this result, we can calculate that the error is 1.25(mm) when we measure a pile with the diameter of 600mm from a distance of 100m (L=100m).

Table 1. Trial for accuracy

L(m)	2.971	4.969	5.175	5.47	5.77	5.974	10
Baum's Scale (Theoretical value)	10.00	6.00	5.77	5.45	5.17	5.00	3.00
Operator A	172°30:21	171°53:50	172°00:34	171°54:25	171°57:08	171°54:24	171°59:05
Operator B	172°30:20	171°53:50	172°00:33	171°54:24	171°57:06	171°54:23	171°59:06
Operator C	172°30:22	171°53:51	172°00:29	171°54:15	171°57:06	171°54:18	171°59:03
Average Value	172°30:21	171°53:50	172°00:32	171°54:21	171°57:07	171°54:21	171°59:05
Mean Square Error	0°00:03	0°00:02	0°00:03	0°00:05	0°00:03	0°00:04	0°00:03
Translated Error (mm)	0.039	0.049	0.079	0.143	0.074	0.108	0.125

MEASURING THE COORDINATES OF THE AXIS

The distance which total stations can measure is only to the surface of targeted objects. Meaning, it is impossible to directly measure the axes of structures using total stations. Therefore, we need to calculate positional coordinates of the axes from those on the surface of the object. As shown in Fig. 5, we measure two points, denoted by A and B on the center line of the surface and then perform calculation. Finally, we can calculate coordinates of the central axis by shifting one radius toward the center.

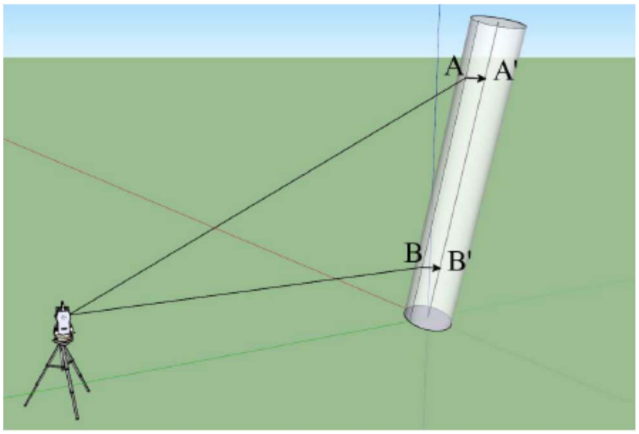


Fig. 5. How to measure the axis

APPLICATION TO PILE DRIVING SYSTEM

Applying center measurements of cylindrical structures using TS with Baum, we've developed a system for accuracy control of driving foundation piles. TS with Baum – we call the system Baum Station - performs highly effectively, as we can measure axes of piles from any direction using just one TS. We also do not need to move two instruments to measure other piles, which is usually done in the common method. The measurement results are recorded as numerical values. Moreover, workers' safety is ensured as it is not necessary to move two transits to measure other piles. There is another advantage in that measurement data is recorded as numerical values and the history of driven piles is also recorded. However, there are also some issues that need to be improved: collected information does not contain information about the direction the piling machine faces, and there are few ways to transfer the information from the operator of the Baum Station to the operator of the piling machine. Therefore, we developed a system to promptly and accurately transfer the information of the piling process to the operator of the piling machine. Fig. 7 illustrates the outline of the pile navigation system. As it shows, the information of the pile (the positional coordinates of the pile surface) go through the following steps: the information is collected using Baum Station via transmission from the transmitter mounted on the TS to the repeater device and is sent to the PDA which is in the operation room or the piling machine.

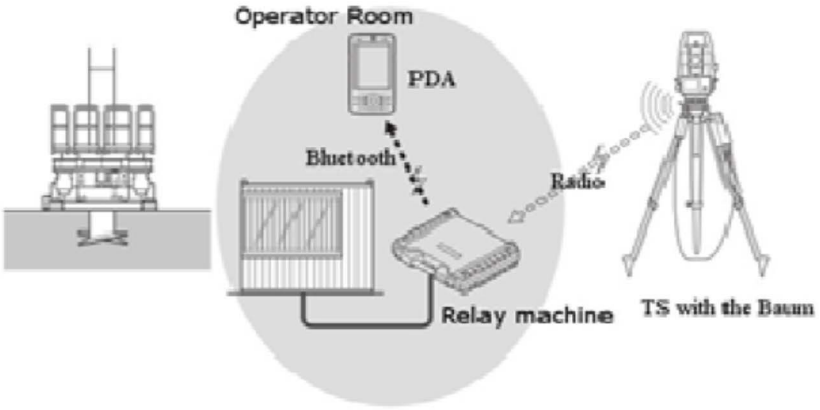


Fig. 6. Outline of the pile navigation system

The program in the PDA immediately calculates deviations and tilts of the pile at the planned height of the pile top, and displays correction values to the planned position. When operator knows how much the point is apart from the pile bottom by measuring the point as the first measurement point, it is possible to calculate

the present depth of the pile bottom and the gap between the present and planned height of the pile top, which are based on the height which should be achieved when driving is completed. The information is displayed from the view of the operator of the piling machine on the screen of the PDA, as in Fig. 7. Correction amounts are shown as numerical values, which help operators to accurately correct deviations and record the process history by accumulating measurement results.

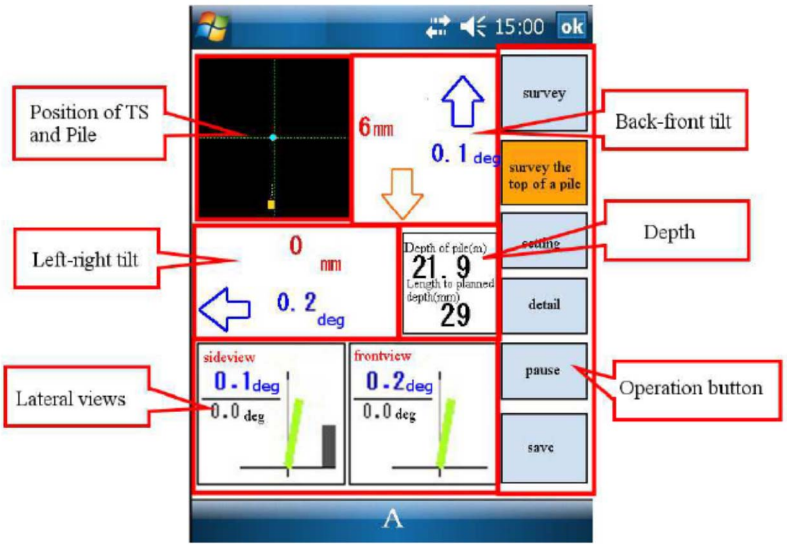


Fig. 7. Pile driving navigation screen displaying measurement result

MEASURMENT EXPERIMENT

Overview of the experiment

We conducted experiments with the Baum Station to figure out measurement efficacy during actual pile driving. We employed vertical pile foundation and screwing piling methods in this experiment and three steel pipes of 11.5 meters long and 800mm diameter welded into a pile foundation. We welded the piles at the site. In piling, when the length between the ground and the tip of the first pile was 3.74m, the second pile was jointed to the first one. Then, when the length between the ground and the tip of the jointed pile was 4.14m, the third pile was jointed. When the depth of the driven pile was 26m, we stopped driving the piles. The verticality was measured and corrected in the conventional method and compared with the results from the measurement using a TS with the Baum. We did not make a correction for the pile based on the measurement results from a Baum Station.

With the conventional method, we took measurements of the verticality using two transits from two right-angle directions. We took measurements before the first pile was driven, when the second and third piles were jointed, and when piling was stopped. The verticality correction was also made before the first pile was driven, and when the second and third piles were jointed.

The distance from Baum Station to the pile was approximately 40m. We employed an arbitrary coordinate system, in which errors of front-back direction from the pile are shown on the X-axis, and errors of left-right direction are shown on the Y-axis. We started the measurements when the pile depth was about 1m and took a measurement every 1m that followed. We collected 27 measurements of the pile during driving process and 4 when the pile was still.

Experimental results

Table 2 shows mean square error of deviation amount and angles in the method using Baum Station, and Figure 8 shows plotted deviation of the pile in 31 trials. In Figure 9, the horizontal axis shows deviations in the x direction, and the vertical axis shows deviations in the y direction. The results are under the condition that the planned height of pile top is z=0. The plots were made on a map with the origin (0,0), and circles with radii at 10mm, 20mm, 30mm, 40mm, 50mm, which were guide lines to plot.

We found that we can take measurements within this accuracy; deviations of piles are up to about 30mm, and mean square errors of measurement irregularities are up to about 10mm on both x and y axes. We also found that mean square errors of angles were 0.1° when the pile was still and 0.2° when the pile was driven. The deviation and tilt of piles when the piles were still were smaller than those when the piles in the process of driving. These differences are brought when the pile wobbled by the length of as much as 2 scales of the Baum, which is about 0.008m in left-right direction, calculated from 2x40(m)x1/1000. The pile bottom wobbled less than its top. Also, we compared screwing piles, seeing that the errors of still pile deviation in the y axis were smaller than that of the x axis. The Y direction is left-right direction from the TS. We attribute this result to the pile's wobbling while it was measured.

Table 2. Errors in measuring a foundation pile

	Trials (Time)	Deviation (mm)				Angle (°)	
		x		y		Average	Means Square Error
		Average	Means Square Error	Average	Means Square Error		
Total	21	3.4	8.7	2.4	9.5	0.19	0.22
Screwing	27	4.3	9.0	3.0	10.1	0.21	0.23
Still	4	-2.5	6.6	-1.5	2.2	0.10	0.10

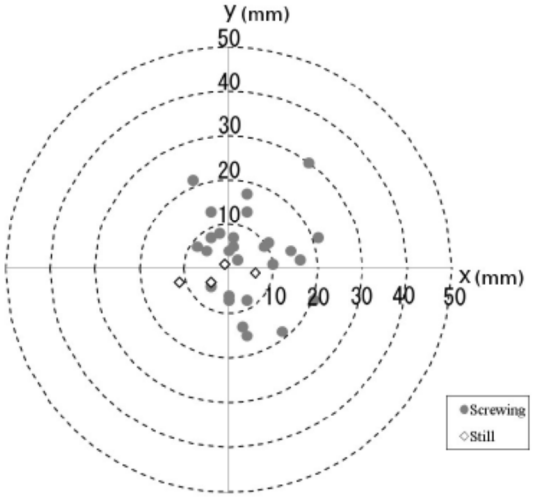


Fig. 8. Plot map of error on a horizontal plane

SUMMARY

The following are the findings of this research.

- We developed a TS equipped with Baum reticle instead of the conventional crosshairs.
- We performed experiments of measuring cylindrical structures and found that the closer the distance between the TS with the Baum and the target cylindrical structure, the more accurately we can conduct

measurements.

- By measuring two points on the center line of the cylindrical structures, the coordinates of central axes can be calculated.
- Applying the Baum technology to pile construction or shaft drilling, we developed a navigation system which assists driving piles, showing the horizontal position and tilt of the pile and correction amount from the view of the operator of the pile driving machine.
- This system requires just one person to measure the piles' verticality, deviation, and depth. Then, the system transfers measurement results to the operator in an easy-to-understand way in real time. As this system saves measurement data in chronological order, it will be a big help for pile foundation managements.
- The results of the measurement experiment in driving vertical foundations show that the error on a vertical plane when the pile was screwing was greater by 2mm in the back and front direction, by 8mm in the left and right direction, and by 0.1° more than the error when the pile was still.
- We can measure vertical and tilted piles in the same way using this system, we can use this system to control tilted pile foundations which had until now been too difficult.
- The newly developed system has already been effectively used in Japan and we expect it to contribute to the popularization of tilted pile foundations elsewhere.

References

Abe, Y. (2008). Geowing pilesII. The foundation Engineering and equipment, 36(12), 90-92.

Construction Research Institute kuikisonogaiyou, Retrieved from http://www.kensetu-navi.com/kuisin/outline.pdf on October 18, 2012.

Japan Institute of Construction Engineering. (2004). NS "Construction Technology Review and Certification"

Japan Road Association. (2007). kuikisosekoubinran, 65-66, 80, 117-118.

Nakaniwa, K., Yabuki, N., Kitayama, T., & Makizumi, T. (2012). Development of the concentric reticle "Baum" for optical surveying instrument. 14th International Conference on Computing in Civil and Building Engineering, 486-487.

Kiyota, S., Yonezawa, T., Aoki, H., Koda, M., Nishioka, H & Dewa, T. (2009). Study on lateral resistance and application to railway structures of batter pile foundation. The Japanese Geotechnical Society, 5(1), 299-306.

Ministry of Land, Infrastructure, Transport and Tourism. Sagoukitei no junsoku Retrieved from http://psgsv.gsi.go.jp/koukyou/jyunsoku/pdf/beppyou-1.pdf on October 18, 2012.

Okawa, K., Kamei, H., Kimura, M., & Zhang, F. (2003). Experimental Study on Dynamic behavior of a group-pile foundation with inclined piles. The Journal of Japan Society of Civil Engineers, B1,No.729 (III-62), 31-41.

Sato, M., Taji, Y., Jang, J., & Tazoh, T. (2011). Seismic Performance by Comparison of Batter-pile and Vertical-pile Foundation using Centrifuge Modeling. Report of the National Research Institute for Earth Science and Disaster Prevention, vol. 79, 1-8.

Yamashita, H., Hirata, H., & Kinoshita, M. (2010). Challenges in the past and for the future of design and installation technologies on steel pipe piles in Japan, The Journal of Japan Society of Civil Engineers, vol. 66, 319-336.

CAPACITY OF HYDRAULICALLY JACKED PILES

Melinda J. Hummel, Magnum Geo-Solutions, LLC, Loveland, Colorado, USA, 970-635-1851, mhummel@magnumgeo.com

Howard A. Perko, Magnum Piering, Inc, Loveland, Colorado, USA, 970-635-1851, hperko@magnumpiering.com

ABSTRACT

Hydraulically jacked piles, herein referred to as jacked piles, are commonly used for underpinning existing structures to arrest settlement or augment an existing foundation for higher loads. They consist of steel pipe segments coupled together and jacked into the ground using a hydraulic ram. Pipe sections can vary in size from 3" diameter to 18" diameter or larger. Jacking resistance is typically provided by dead loads of existing structures. This type of piling system has been utilized for foundation underpinning, repair, and augmentation for more than 120 years, yet little has been published on the capacity, installation standards, and reliability of these systems. Pile load tests from a number of projects are presented and analysed. The data show that previous methods of jacked pile capacity and depth prediction are crude at best. Empirical relationships between capacity, depth, soil type, and standard penetration resistance blow count contain a high degree of scatter. Scatter in the data indicate capacity prediction for jacked piles needs further research and refinement.

Keywords: pile, foundation, capacity, underpinning, load tests

INTRODUCTION

Push pier, resistance pile, steel pier, and jacked pile are some of the names often applied to hydraulically jacked piles used for underpinning. The term ‘jacked pile’ is more common in building codes and will be used herein. Although jacked piles can be installed for new construction, this paper is focused on piles used for support of existing structures.

Jacked piles consist of short segments of pipe or structural steel tube that are coupled together and forced into the ground using a hydraulic ram fastened to or beneath a footing, stem wall, or grade beam of an existing structure. In this way, the weight of the structure provides the resistance necessary to force the pile into the ground. A factor of safety can be achieved in design by redundancy, which is consecutively installing more than one jacked pile to support the same portion of foundation. Installing jacked piles consecutively using the same dead load and then releasing the load after each pile installation allows one to continue adding piles to the same general area until a total aggregate capacity is achieved to account for anticipated dead plus live loads and a desired factor of safety for that area.

An engineering schematic of an example jacked pile connected to a footing foundation is shown in Figure 1. Modern jacked piles typically incorporate a steel bracket. There are many sizes and styles of brackets available. Some categories include plate brackets that bolt to the outside of an existing foundation wall, wide and narrow angle brackets that extend under existing footings, pin brackets for attachment to structural steel, and reverse angle brackets for attachment to footing and wall. Table 1 lists example brackets and their benefits.

Jacked piles are driven using a hydraulic ram that temporarily mounts to the bracket. As the pressure builds, pile advancement slows. Eventually, the pile will achieve negligible rate of advancement at the

 © 2017 DFI Annual Conference, New Orleans, LA, USA

test load. The test load is often set by the available dead load, limitations of the hydraulic ram, or structural capacity of the bracket, its connection, or the structure. Since increasing the hydraulic ram pressure beyond the test load generally would result in a re-initiation of pile movement, the maximum test load corresponds to the ultimate geotechnical capacity of a jacked pile at its current depth. After jacked piles are driven individually and proof load tested, the rams often can be connected hydraulically and used to simultaneously lift and re-level structures as shown in Figure 2. The fact that each jacked pile is proof load tested during installation provides good quality assurance and reduces pile head deflections upon reloading.

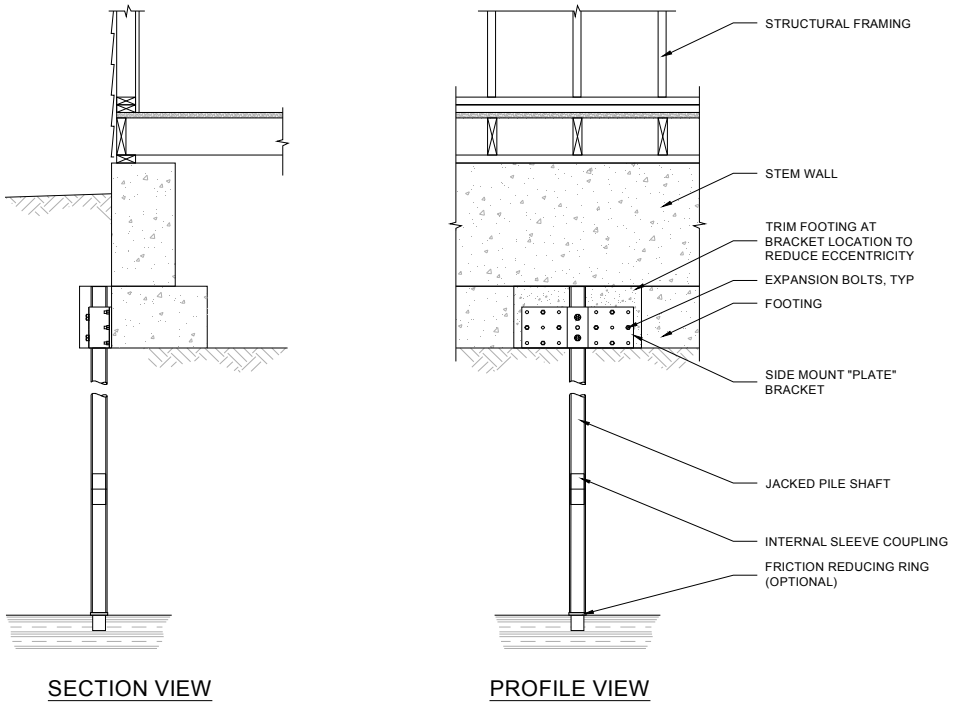


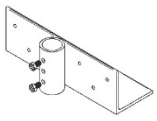
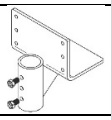
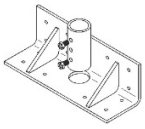
Figure 1. Modern Jacked Pile Engineering Schematic (Courtesy of Magnum Geo-Solutions, LLC)



Figure 2. Examples of Modern Jacked Pile Installation (Courtesy of The Dwyer Company, Inc)

Jacked pile technology has been used for at least 120 years. Yet, jacked piles remain absent from mainstream foundation engineering texts, academic papers, and many building codes. The goals of this paper are to review current design methodology, use results of numerous installation load tests to explain crudeness of depth and capacity correlations for these systems, and to discuss the reliability afforded by individual load testing during installation. This paper contains recommended standard procedures for installation and testing developed through years of practical experience engineering and applying these systems.

Table 1. Example Jacked Pile Brackets

Image	Type	Benefit	Common Use
	Plate	Low cost, avoid bottom of footing which is rough and pitted, no footing prep or seating grout required	Formed Concrete
	Wide Angle	Distribute load over a wide area, helps bridge cracks and reinforce existing foundation	Old Stone and Brick Foundations
	Narrow Gusseted Angle	Less footing prep than wide angle, preferred by contractors	Newer Reinforced Concrete
	Reverse Angle	Supports slabs and walls, less disturbance because it replaces chipping by coring thru footings	Structural Slabs, Tanks, Tilt-up Construction
	Pin	Welds directly to structural steel such as sister beams, needle beams, and embedded plates	Structural Steel

BUILDING CODE

Although jacked pile technology has been widely used and accepted, it is not specifically addressed in many building codes. Jacked piles are considered “specialty piles” in the International Building Code. Some codes that specifically recognize jacked piles include the New York City Building Code, which since 1938, provides a short section on, “Piles installed by jacking or other static forces.” This section of the New York City Building code defines allowable pile capacity for permanent applications as 2/3 the installation load if the load is held for 7 hours without measurable settlement, or 1/2 the installation load if the load is held for 1 hour without measurable settlement. For temporary applications, older versions of the New York City Building Code stated that the working load need only be less than or equal to the total jacking force at final penetration. Since 2008, temporary underpinning piles are no longer addressed under this section.

The City of Chicago Department of Buildings released a code memorandum on August 30, 2016 for Pile Deep Foundations that addresses Jacked Piles. This memorandum limits the compressive stress in the steel to 35 percent of the minimum specified yield strength, not to exceed 19,000 psi. It also requires the piles to be grouted. The installation of all production jacked piles are required to be loaded to at least 150 percent of the design load. All pile types must be load tested, and the allowable load shall be the total test load divided by a minimum factor of safety of 2.0.

CAPACITY REQUIREMENTS

The required capacity of a jacked pile used for underpinning is computed by the same techniques as those used for other deep foundations, with a few special precautions. Jacked piles must have sufficient capacity to support both the dead and live loads of the structure. If a structure is to be lifted and re-levelled, it is essential to add the soil weight above the footing (if any) to the total dead loads computed by conventional means. The adhesion of the soil on the bottom of the footing and/or slab and the friction of the soil along the foundation wall or grade beam also should be considered.

Some contractors only install a sufficient number of jacked piles to lift a structure. While the ability to lift and re-level a structure fixes aesthetic issues, it alone is an insufficient criterion for establishing pile spacing and a jacked pile's required capacity. If foundation underpinning only accounted for loads present at the time of pile installation, most would need further adjustments as loadings change. Therefore, the piling system must be capable of supporting live loads such as snow, wind, earthquake, people, and furnishings that may be added to the structure at a later time. As live loads drive the serviceability limit states, the spacing of jacked piles must be closer than that required to simply lift the structure.

After determining the total dead and live loads, an appropriate factor of safety must then be applied to establish pile spacing and required proof test load. The engineer of record should select a factor of safety suitable for each project and site conditions. Factors of safety used in foundation engineering vary depending on the reliability of soil and subsurface information, the heritage of a particular foundation, and the sensitivity of the structure to movement. The American Society of Civil Engineers Publication 20 96, "Standard Guidelines for Design and Installation of Pile Foundations", explains that a factor of safety of 1.5 is permissible for driven pile foundations since the method of installation provides a means of capacity determination in the field. Installation of a steel jacked pile provides an even more direct means of capacity determination as compared to conventional pile driving. A factor of safety of 1.5 is commonly used in practice for steel jacked pile design. As discussed in a previous section, some building codes may require a minimum factor of safety of 2.0 for jacked piles. The authors believe this requirement is excessively conservative because each pile is proof tested.

INSTALLATION

The installation of jacked piles generally involves the following procedures as outlined by Perko (2002):

(1) An engineer or contractor's technical representative observes the condition of the structure, computes building loads including available dead loads for jacking, and plans jacked pile locations
(2) All underground structures and utilities in the vicinity of the piles are located and moved or avoided
(3) Foundation access holes are excavated at each pile location
(4) Existing foundation is modified to allow connection of brackets as close to the foundation wall neutral axis as possible
(5) Piling brackets are mounted to the existing foundation
(6) Elevation of the structure at each pile location is measured and a building monitoring program is established
(7) Hydraulic rams are temporarily attached to the brackets on the existing structure
(8) Piles are jacked into the ground individually until the load used for driving the pile equals or exceeds the required proof test capacity and pile movement halts
(9) Ram pressure is measured and recorded at 3 foot intervals of jacked pile depth
(10) Local building official or special inspector observes pile proof testing for quality assurance
(11) After all piles are installed and inspected, the building often can be lifted (if necessary) and re-levelled to the extent practicable
(12) *The jacked piles are secured to the brackets and the hydraulic rams are removed (*Figure 4*)*
(13) Final building elevations are recorded
(14) Access holes are backfilled and landscaping materials are restored



Figure 3. Typical Jacked Pile Installation Procedure (Courtesy of The Dwyer Company, Inc)



Figure 4. Jacked piles secured to lifting brackets prior to pile cut-off (Courtesy of Hayward Baker)

PROOF TESTING

To date, no standard method has been developed for completion of installation step 8, which involves field verification of jacked pile capacity. The American Society for Testing and Materials specification D1143 - 81, "Standard Test Method for Piles Under Static Axial Compressive Load" explains routine methods for field performance testing. It is appropriate and sometimes required by local building codes to perform field performance testing on a select number of representative piles to establish the full spectrum of the load deflection characteristic. However, these procedures are time consuming and impractical for proof testing of every production pile. Based in part on this ASTM standard and the standard of care practiced by most engineers and contractors at the present time, the following procedure for proof testing jacked piles is suggested as modified from Perko (2002).

(1) The hydraulic ram used to load the pile shall be fitted with a pressure gauge, shall be capable of delivering the prescribed loads with a sensitivity of at least 5% of the required ultimate capacity of the pile, and shall be calibrated at least annually

(2) Continue pile installation until proof test pressure is achieved, the proof test load shall be at least 150% of the design allowable capacity.

(3) Jacked pile movement relative to a fixed frame of reference shall be measured optically or through the use of a dial gauge

(4) The proof test load shall be maintained until the rate of settlement is less than 1/16 in/hr, not less than 1/2 hr

(5) A field report shall be prepared that at a minimum shall contain pile location, applied proof test load, load duration, and final pile depth

DESIGN CONSIDERATIONS

The following design considerations should be considered as summarized by Perko (2002):

(1) Proof test load shall not exceed available dead load at jacked pile location. Dead load shall be calculated over maximum unsupported spans on both sides of the planned pile locations using LRFD/ASD factors for temporary construction loads
(2) The bracket and ram assembly shall be such that loads are applied vertically and directly to the central longitudinal axis of the jacked pile with eccentricity minimized to the extent practicable
(3) The structure to which the bracket and ram assembly is attached shall have sufficient integrity and weight to allow for application of loads to the jacked pile without excessive lifting and without causing damage to the structure
(4) If the structure is of insufficient weight to permit the required jacked pile loading, then an earth anchor, ballast weight, or battered pile must be used to provide the necessary reaction or the test load should be downgraded and additional piles added
(5) Jacked piles with minimum spacing less than 2 feet or less than 10% of their average depth should be evaluated for group efficiency

THEORETICAL CAPACITY

In practice, it is seldom necessary to compute the theoretical capacity of a jacked pile, since each pile is proof tested and verified in the field. However, on certain occasions it may be desirable to determine theoretical capacity in order to evaluate the suitability of a particular bearing stratum or to approximate jacked pile depth.

According to Meyerhof (1956, 1976), ultimate static pile point capacity can be related directly to Standard Penetration Resistance test blow count by

$$P_{ptu} = 840\ A\ N_{55}\ \frac{L}{D} \qquad [1]$$

where P_{ptu} = ultimate static pile point capacity (lbs); A = pile tip area (ft²); N_{55} = SPT blow count at 55% efficiency (blows/ft), L = penetration length (ft), and D = pile diameter (ft). Meyerhof also specified the criterion that

$$\frac{L}{D} \leq 10 \qquad [2]$$

As presented by Perko (2002) the pile tip area should be taken as that of a closed ended pile with the additional diameter provided by the friction reducing ring (if used). Perko (2002) also recommends the standard penetration resistance blow count used in the above equation should be taken as the average value from 3 D below the pile tip to about 8 D above the pile tip based on field data. Finally, Perko (2002) assumed that the penetration length, L, is equal to 25% of the depth of the pile minus 1.5 ft to account for the disturbed soil at the ground surface. In terms of mathematical symbols, L is given by

$$L = 25\% \times (L_T - 1.5) \qquad [3]$$

where L_T = total length of the pile (ft). Perko (2002) determined that Meyerhof's equation and the definition of penetration length given above matched field measurements very well for a single project involving approximately 30 piles.

Since 2002, the authors have gathered and analysed over 1,500 hydraulically jacked steel pipe pile installation field proof tests. A comparison of the proof test load and the bearing stratum SPT N-value as well as penetration length are shown in Figure 5 and 6. A linear best fit regression is shown in each Figure, which implies a general upward trend in proof test load with increasing SPT N-Value and penetration length. However, both charts contain considerable scatter.

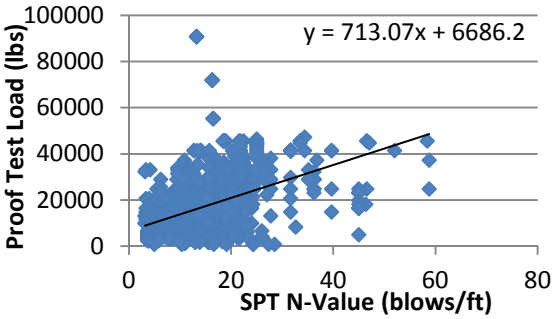


Figure 5. Effect of SPT N-Value on Proof Test Load

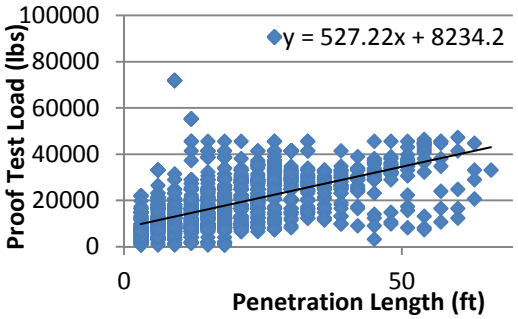


Figure 6. Effect of Penetration Length on Proof Test Load

Fitting the modified Meyerhof based equation from Perko (2002) to these data shows very poor to no correlation. These new data from Figure 5 and Figure **6** suggest refinement of capacity and length predictions is appropriate. Taking the pile tip area as that of a closed ended pile, Equation 1 can be rewritten as

$$P = 840 \left(\frac{\pi D^2}{4}\right) N \frac{L}{D} \qquad [4]$$

or

$$P = 210\, \pi\, D\, N\, L \qquad [5]$$

where P = proof test load (lbs) (ultimate capacity at length, L). To search for a new, more accurate constant, the value 210 in Equation 5 can be substituted for a variable, B_1, and the relationship re-written as

$$P = B_1\, \pi\, D\, N\, L \qquad [6]$$

This relationship can be further rearranged as

$$\frac{P}{\pi\, D\, N} = B_1\, L \qquad [7]$$

The expression in Equation 7 is plotted versus penetration length in Figure 7. The fitting parameter, B_1, is the slope obtained from linear regression analysis. This figure is a plot of all 1,500 proof test data, which includes several soil types. Since a linear regression of the data does not intercept zero, the data suggest that an additional y-intercept term needs to be included in the penetration length term, thus

$$P = \pi\, D\, N\, (B_1\, L + B_2) \qquad [8]$$

The parameters, B_1 and B_2, represent the intercept and slope of the linear best fit line. The R^2 regression is

an indication of quality of fit. The low value of 0.1189 reflects a high degree of scatter in the real data. There is clearly more involved in determining jacked pile capacity than a simple linear combination of pile diameter, SPT blow count, and penetration length. Some of the scatter may be from different rates of installation, varying installation crews, effect of different soil types, and non-standardized proof test methods.

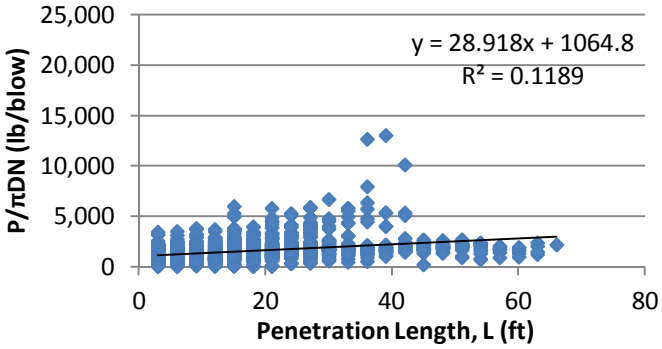


Figure 7. Empirical Fitting Function to Evaluate B_1 & B_2 Constants

Predicted proof test load from Equation 8 using the fitting parameters B_1 and B_2 obtained from Figure 7 are plotted versus the field measured proof test load in Figure 8. If Equation 8 exactly matched the data, the slope of a linear best-fit line would be equal to one. The comparison in Figure 8 has an R^2 value of 0.196. While still far from accurately predicting the pile penetration length, this correlation fits the bulk data better than the relationship provided by Perko (2002). Due to the amount of scatter, use of Equation 8 to predict jacked pile capacity and penetration length should be approached with caution. It is advisable to conduct pile test installations to better verify required length of piles and budget materials. In addition, a proof load test should be performed on every pile.

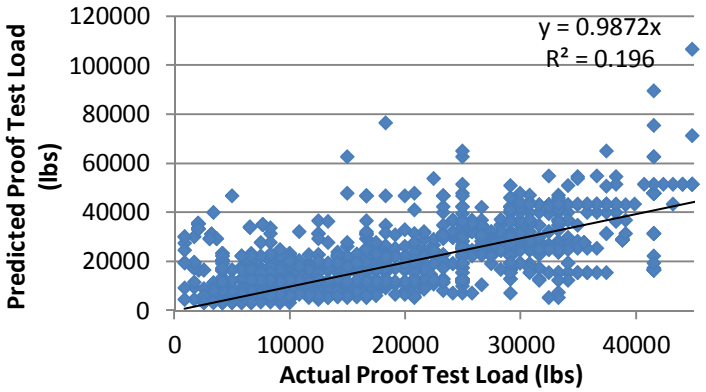


Figure 8. Model Comparison of Predicted Proof Test Load to Actual Proof Test Load

Thus far, the data have not been separated by soil type. To analyse the effect of type of soil on the penetration length, the data were filtered by soil type and fitted by linear regression similar to that shown in Figure 7. The constants, B_1 and B_2, that provide the best fit for various soil types are shown in Table 2. Differences in B_1 and B_2 contained in the table suggest a strong correlation between soil type and the effect of penetration length and SPT blow count on pile capacity. Each soil type continued to exhibit considerable scatter indicating there are likely other factors yet unknown that need to be taken into consideration in developing an accurate method of prediction for jacked pile length and capacity. The

reader is discouraged from using the parameters in Table 2 in practice; these parameters are only given for crude comparison and mainly to show the apparent significance of soil type on the calculations. Continued research and more data is needed.

Table 2. Capacity Equation Constants

	B_1	B_2	R^2
All Soils	29	1065	0.12
SP	27	1321	0.1
SM	35	465	0.45
ML	51	376	0.25
CL	25	1338	0.08
Bedrock	23	871	0.14

DISCUSSION

Plots in Figures 9 and 10 show the penetration length with respect to SPT N-values for 3" and 4.5" pile diameters, respectively. These plots were constructed using Equation 8 and the fitting parameters for "all soils", and they establish a crude "first approximation" of jacked pile installation lengths. However, the charts should be used with extreme caution, and checked for accuracy using a test pile for each site since the data used to construct these charts has considerable scatter.

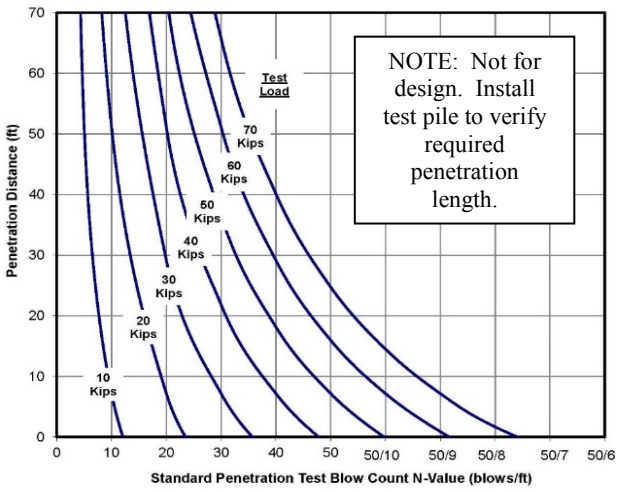


Figure 9. Average 3" Diameter Jacked Pile Penetration into Soil and Rock

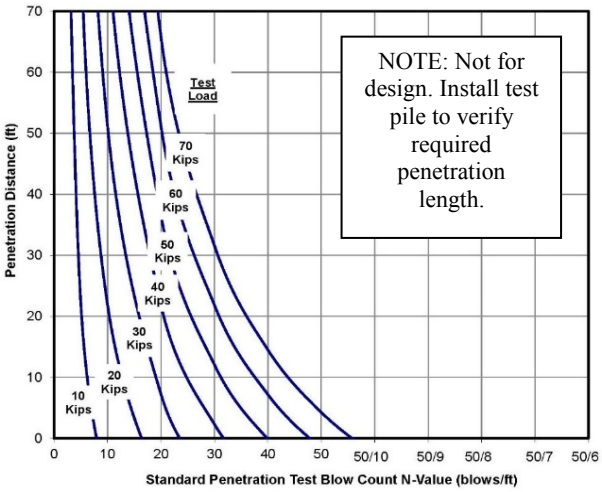


Figure 10. Average 4.5" Diameter Jacked Pile Penetration into Soil and Rock

In saturated low permeable soils, the installation of jacked piles causes high pore water pressures which substantially reduces soil effective stress. It is standard practice to proof test jacked piles immediately after installation. This procedure is conservative since the capacity of the pile should increase after pore pressures dissipate and effective stresses return to steady state. In most cases, jacked pile capacity should increase with time. Groundwater fluctuations and corrosion are exceptions that may adversely affect capacity.

CONCLUSIONS

1. Hydraulically jacked steel pipe piles have been used to underpin and stabilize foundations for at least 120 years yet information regarding these systems, standardized methods of installation and proof testing, as well as reliable methods of predicting penetration length and capacity are absent from mainstream literature.
2. Data from 1,500 jacked pile proof tests provided herein suggest penetration length and jacked pile capacity are affected by soil type, SPT blow count, pile diameter, and additional yet unknown factors. More data and research into the design elements of jacked pile systems is required.
3. Graphs are presented that show empirical penetration length as a function of pile diameter and SPT N-value. The graphs are based on data with considerable scatter and represent crude averages.
4. The capacity of jacked piles should be verified at each location by proof testing. Standardized procedures for jacked pile installation and proof testing would help to remove randomness in test data and could help develop better methods of prediction. Some suggested standardized procedures are provided herein.

ACKNOWLEDGMENTS

The authors would like to acknowledge Magnum Piering, Inc. for their support of this research.

REFERENCES

American Society for Testing and Materials (1994) "Standard Test Method for Piles Under Static Axial Compressive Load" Test Designation D1143, ASTM International

American Society of Civil Engineers (1996) "Standard Guidelines for Design and Installation of Pile Foundations" Publication 20-96, ASCE Press

Meyerhof, G.G. (1976) "Bearing Capacity and Settlement of Pile Foundations", J. Of the Geotechnical Eng., ASCE, Vol. 102, GT 3, pp. 195-228

Meyerhof, G.G. (1956) "Penetration Tests and Bearing Capacity of Cohesionless Soils", J. Of Soil Mechanics and Foundation Design, ASCE, Vol. 82, SM 1, pp.1-19

Miller, G.A. and Lutenegger, A.J. (1997) "Influence of Pile Plugging on Skin Friction in Overconsolidated Clay", J. Of Geotechnical and Geoenvironmental Eng., ASCE, Vl. 123, No. 6, p. 525

Paikowsky, S.G. and Whitman, R.V. (1990) "The Effects of Plugging on Pile Performance and Design" Can. Geotech. J., Ottawa, Canada, No. 27, pp.429-440

Perko, H.A. (2002) "Axial Capacity of Hydraulically-Jacked, Steel-Pipe Micropiles Used for Underpinning," Push Pier Engineering Manual, Magnum Piering, Inc.

Quality Assessment of Seismic Data Sets and the Impact on Interval Velocity Estimates in DST

Erick Baziw
Baziw Consulting Engineers Ltd., Vancouver, Canada
Gerald Verbeek
Baziw Consulting Engineers Ltd., Vancouver, Canada

ABSTRACT: Downhole Seismic Testing (DST) is an important geotechnical testing technique for site characterization as it provides low strain ($<10^{-5}$) *in-situ* interval compression (*Vp*) and shear (*V*s) wave velocity estimates. These velocities are determined by obtaining relative arrival times of source waves as they travel through the stratigraphy and are recorded by one or more vertically offset seismic sensors. A challenging aspect of this process is to characterize the seismic data sets to determine the analysis method that will result in the most accurate interval velocity values. This paper introduces an assessment technique which utilizes linearity estimates (i.e., hodograms fitting straight lines) from the polarization analysis in conjunction with cross-correlation coefficient calculations of the full waveforms as well as the deviation of the source wave frequency spectrum from a desirable bell-shaped curve. The paper will provide an overview of the technique and include some examples of actual data sets where the technique was applied to analyze those data sets.

1. INTRODUCTION

In general terms, Downhole Seismic Testing (DST) such as Seismic Cone Penetration Testing (SCPT) is a geotechnical technique for measuring in-situ shear and compression wave velocities (V_S and V_P respectively). The main goal in DST is to obtain arrival times as the source wave travels through the soil profile of interest, and from these arrival times the velocities are then calculated. Figure 1 shows a schematic of the typical DST configuration: a seismic source is used to generate a seismic wave train at the ground surface. One or more downhole seismic receivers are used to record the seismic wave train at predefined depth increments. The downhole receiver(s) may be positioned at selected test depths in a borehole or advanced as part of an instrumentation package as in the case of SCPT. When triggered by the seismic source a data recording system records the response of the downhole receiver(s).

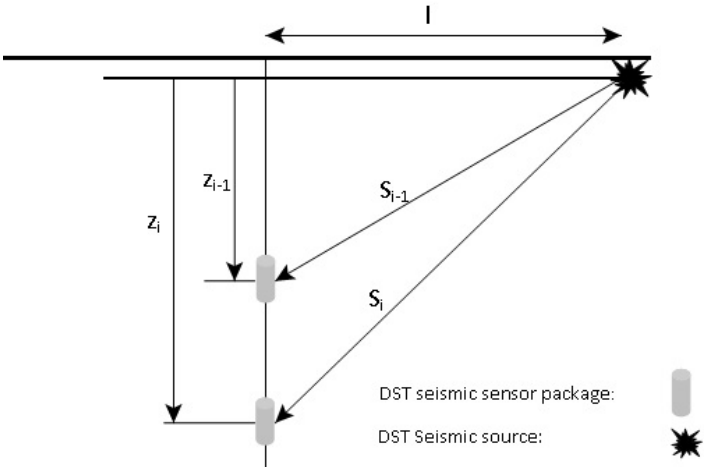


Figure 1. Schematic of the typical DST configuration (Baziw and Verbeek, 2014a)

The most common form of DST is the analysis of horizontally polarized shear waves (SH waves). These waves are

 © 2017 DFI Annual Conference, New Orleans, LA, USA

commonly generated by applying a hammer blow laterally to the sides of special designed plate that is pushed into the soil at the surface. Typically shear waves are generated on both the right side (RS) and left (LS) of the seismic probe, which provides two independent sets of seismic traces at each depth increment and thus two independent interval velocity estimates. The field data examples outlined in this paper are obtained in this manner. Details of the seismic cone and comparisons with the crosshole results at several sites have been described by Campanella et al., and the test method is also described in ASTM D7400.

Once the test has been performed three important issues arise during the analysis of the test data. First and foremost there is the issue of the quality of the acquired seismic data sets (Seismic Trace Characterization (STC)). Secondly the analyst needs to determine the most appropriate signal processing techniques to obtain accurate interval velocity estimates, and finally what is the appropriate confidence level in the calculated interval velocities estimates (Interval Velocity Characterization (IVC))?

In recent years the authors have focused on the development of techniques and algorithms to address these three issues, with the ultimate goal to develop signal processing algorithms that can be applied in batch mode. A major component of this effort was to define independent STC parameters by analyzing in both the time and the frequency domain a large number of DST data sets (incl. those with poor signal-to-noise ratios, which are typically due to near field responses, source wave reflections, or "dirty" signals due to poor source-ground coupling). These parameters can then be fused together into a single classification, and also provide guidance concerning the most appropriate signal processing technique. Initial work in this area (Baziw and Verbeek, 2016a and 2016b) resulted in the development of three seismic trace parameters:

- the Cross Correlation Coefficient (CCC) of the full waveforms at the particular depth and the preceding depth.
- the linearity estimates (LIN) from polarization analysis.
- the Signal Shape Parameter (SSP).

In this paper these parameters are succinctly outlined, after which it is described how each parameter can provide guidance during the data analysis process to obtain more accurate values for the calculated interval velocities. This is illustrated through actual field data that were obtained with high precision and high bandwidth (1 Hz to 10 KHz) piezoelectric accelerometers with integrated operational amplifiers. These accelerometers have highly desirable rise and decay times of approximately 5 μs, which ensures that the acoustic waves and ambient noise are recorded with minimal or no sensor distortion.

2. THE STC PARAMETERS

2.1 Seismic Trace Characterization Parameters

STC Parameter 1: Cross- Correlation Coefficient

The cross-correlation between two time or distance offset seismograms is given as (Gelb 1974)

$$\varphi_{xy}(\tau) = \sum_k X_k \, Y_{k+\tau} \tag{1}$$

where $\varphi_{xy}(\tau)$ is the cross-correlation function, Y_k the sampled data at distance 1 and at sample time k, X_k the sampled data at distance 2 at sample time k, and τ the time shift between the two

sets of recorded waves (note: distance 2 > distance 1). The value of the time shift at the maximum cross-correlation value is assumed to be the relative travel time difference, Δt, for the source wave to travel the distance increment. This technique has several advantages over selecting time markers within the seismogram (Baziw 1993, 2002), among others the human bias associated with visually selecting a reference point or time marker is minimized.

Normalizing the cross-correlation of the zero mean seismic signals by their standard deviations gives the cross-correlation coefficient:

$$\rho_{xy}(\tau) = \sum_k X_k \, Y_{k+\tau} \Big/ \sqrt{\sum_k X_k^2} \, \sqrt{\sum_k Y_K^2} \tag{2}$$

The CCC between the two DST waves is typically used to assess the quality of the interval velocity estimate as this parameter gives an indication of the similarity between the two waves being correlated. While on its own the CCC has proven to be an unreliable indicator of the overall quality of a seismic trace (since it is highly dependent on the digital filter applied to the raw seismic signals), it is still a useful component of seismic trace characterization. As an STC parameter the CCC value is calculated on the full waveforms after applying polarization analysis.

STC Parameter 2: Linearity Estimates from the Polarization Analysis

Polarization Analysis (PA) is applied when rotating the acquired X(t), Y(t) and Z(t) seismic recordings onto the full waveform axis. In PA the full seismic waveform's angle of incident is determined using hodograms, and rectilinearity estimates are obtained by calculating the covariance matrix of the orthogonal X(t), Y(t) and Z(t) seismic trace recordings (Kanasewich, 1981; Baziw *et. al.*, 2004b).

The PA begins with applying a time window to the seismic event of interest, after which a hodogram is created by plotting the X(t), Y(t), and Z(t) component seismic time series amplitudes against one another within this time window. Least squares straight line best fits are then applied to the hodograms and the slopes of these straight lines provide angle of incidence information, which allow the the X(t), Y(t) and Z(t) seismic responses to be rotated onto the full waveform. If SH(t) wave analysis is being carried out then only one Y(t) vs X(t) hodogram is required to obtain an angle of incidence estimate and subsequently the X(t) and Y(t) responses are rotated onto the SH(t) axis.

Next a covariance matrix is calculated for the X(t), Y(t) and Z(t) recordings over the hodogram time window specified (obviously in case of a SH wave analysis only one two dimensional covariance needs to be calculated for the X(t) and Y(t) axis recordings). This covariance matrix is defined as follows (using the notation of Kanasewich (1981):

$$\boldsymbol{V}_{xyz} = \begin{bmatrix} Var[X(t)] & Cov[X(t),Y(t)] & Cov[X(t),Z(t)] \\ Cov[Y(t),X(t)] & Var[Y(t)] & Cov[Y(t),Z(t)] \\ Cov[Z(t),X(t)] & Cov[Z(t),Y(t)] & Var[Z(t)] \end{bmatrix} \tag{3}$$

In (3) Var and Cov are abbreviations for variance and covariance, respectively. The Var of a variable (e.g., X(t)) is given as

$$Var[X(t)] = \frac{1}{N}\sum_{i=1}^{N}(X_i - \mu_x)^2 \tag{4}$$

where μ_x denotes the mean of the variable X(t). The Cov of two variables (e.g., X(t) and Y(t)) in discrete form is given as

$$Cov[X(t), Y(t)] = \frac{1}{N}\sum_{i=1}^{N}(X_i - \mu_x)(Y_i - \mu_y) \tag{5}$$

An estimate of the rectilinearity of the particle motion over the specified hodogram time window is obtained by diagonalizing the covariance matrix ((3)) and subsequently calculating the ratio of the principal axis of the diagonalized matrix. A measure of the rectilinearity is referred to as linearity and it is calculated as follows:

$$F(\lambda_1, \lambda_2) = 1 - \left(\lambda_2/\lambda_1\right) \tag{6}$$

where λ_1 and λ_2 denote the largest eigenvalue and next largest eigenvalue of the diagonalized covariance matrix, respectively. The linearity approaches unity when the rectilinearity is high ($\lambda_1 \gg \lambda_2$) and approaches zero when the rectilinearity is low ($\lambda_1 \approx \lambda_2$).

In DST interval velocity estimation it is desired to have data sets with linearity values near unity. This will be the case for seismic traces recorded in a transverse isotropic medium with minimal measurement noise, clean source waves, and no signal distortions (e.g., reflections).

STC Parameter 3: Signal Shape Parameter from Frequency Spectrum "Bell Curve" Fitting

Based upon frequency spectrum analysis of large sets of DST data it was determined that the shapes of high SNR DST data sets had frequency spectrums closely resembling Gaussian bell-shape pdf curves (Baziw and Verbeek, 2016b), which can be described as follows:

$$p(f|\mu, \sigma^2) = \frac{1}{\sigma\sqrt{2\pi}} e^{-\frac{(f-\mu)^2}{2\sigma^2}} \tag{7}$$

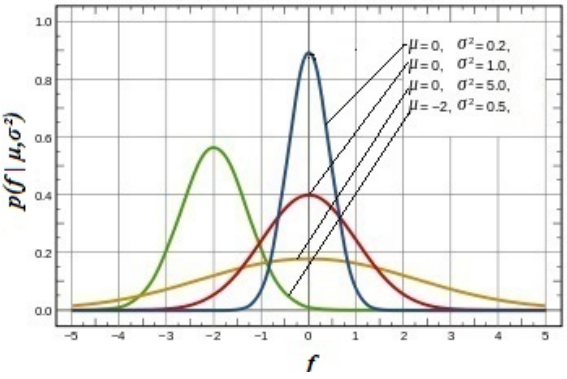


Figure 2: Example of normal pdfs for varying μ and σ² values. (Baziw and Verbeek (2016a)

where μ denotes the mean or expectation of the distribution and σ denotes the standard deviation with variance σ^2. Based on this observation a STC parameter was developed which quantified the deviation of the shape of the frequency spectrum of the seismic trace under analysis from a bell-shaped pdf curve.

2.2 Seismic Trace Classification Methodology

For the classification of microseismic source location estimation a methodology was developed by Ge (Ge and Mottahed 1993 and 1994; Ge 2003). As part of this method various parameters of the acquired microseismic data set are established, and then these parameters are fused together based upon analytic, derived and evolving empirical relationships to generate a microseismic source location estimate "Rank" varying from A (very good), B (good), C (acceptable), and D (not acceptable). In similar fashion the three STC parameters are fused together to provide for a quality assessment of the seismic traces using the following equation:

$$STC = 0.4 \times CCC + 0.18 \times (LIN_1 + LIN_2) + 0.12 \times (SSP_1 + SSP_2) \quad (8)$$

with CCC the cross correlation coefficient between the full waveforms obtained at depth1 and depth2 (where depth2 > depth1).
LIN_1 - the linearity value for seismic traces acquired at depth 1
LIN_2 - the linearity value for seismic traces acquired at depth 2
SSP_1 - the signal shape parameter for seismic traces acquired at depth 1
SSP_2 - the signal shape parameter for seismic traces acquired at depth 2

This value is then converted into a grade ranging from A to F as shown in Table 1, where A is highly desirable and F is unusable. However, the STC rank is automatically set to D (if not already set to D or F) when LIN < 0.78, SSP < 0.6 or CCC < 0.7. It should be noted that the proposed classification is based on a re-evaluation of many data sets previously processed (from over 40 different sites around the world, covering over 4000 seismic traces), but as additional data sets are analyzed the classification may well be refined either through adjustments of the constants in equation (8) and/or by adding additional parameters.

Table 1. Seismic Trace Classification and Description

STC Numeric Value [0-1]	STC Rank [A-F]	STC Description
0.9 to 1.0	A	very good to good
0.8 to 0.9	B	good to acceptable
0.7 to 0.8	C	acceptable to questionable
0.65 to 0.7	D	questionable to unacceptable
< 0.65	F	Unacceptable

Originally it was assumed that the rank of the seismic traces also indicated the accuracy of the calculated interval velocities. However, as the classifications were applied on more data sets it became apparent that instead it points towards the most appropriate signal processing technique for the data sets under review, resulting in a more accurate assessment of the interval velocities. Based on that finding the recommended analysis method for seismic traces now begins with the application of a minimal digital frequency filter to acquired time series (to eliminate obvious measurement noise components from the seismic trace), after which the STC parameters and the associated STC rank is established. For those traces with a low STC rank the values of the individual STC parameter are used to define the appropriate signal processing technique. Using

these techniques the interval velocities are then estimated for the RS and the LS for each depth interval. In addition the spread is calculated using the following calculation:

$$\text{Spread} = \tfrac{1}{2} \times (\text{LS Interval Velocity} - \text{RS Interval Velocity})/\text{Average Interval Velocity} \quad (9)$$

The spread can then be used as the basis for the IVC. If it is less than 10 % then there is good correlation between the left and the right side and therefore the calculated average interval velocity results can be used for engineering. In case the spread is more than 10 % greater weight should be given to the results from the side with the higher STC rank and the calculated interval velocity results should be considered indicative.

In case only one set of seismic traces is available (i.e. only LS or RS) the STC rank can give some indication of the reliability of the derived interval velocities (e.g. those from a set with an A rank at each depth interval are more than likely more reliable than those for a set with only D ranks), but this assessment should be used with extreme care.

3. GUIDANCE FOR SIGNAL PROCESSING BASED ON STC PARAMETERS

3.1 Low cross-correlation coefficients

The CCC values are derived from the calculated full waveforms and they quantify the similarity in shape and form between the traces at each depth increment. The CCC value can be very important for relative large depth increments where significant absorption is taking place and higher frequency components of the source wave are attenuated. For standard DST investigations, where the depth increment is relatively small, the CCC value generally reflects issues that also affect the LIN and/or SSP values, but in certain cases the CCC offer another "look" at the data independent of those two parameters. This can be especially true for near surface investigations where relatively small source-sensor radial offsets can result in significant near-field recordings, in which case the LIN and SSP values are still relatively high, while the CCC is relatively low.

Figure 3(A) illustrates low SNR X and Y axis seismic recordings at depths 1m and 2m with the LIN, SSP and CCC values as shown in Table 2:

Table 2. STC parameter values

Depth [m]	LIN [0-1]	SSP [0-1]	CCC [0-1]
1.000	0.8011	0.744	N/A
2.000	0.8818	0.916	0.75

The relatively low CCC value is more than likely due to source wave skewing as illustrated in Fig. 3(B). A signal decay was applied on the 1m full waveform recording to address the trough skewing and the corresponding low CCC value as illustrated in Fig. 3(C)

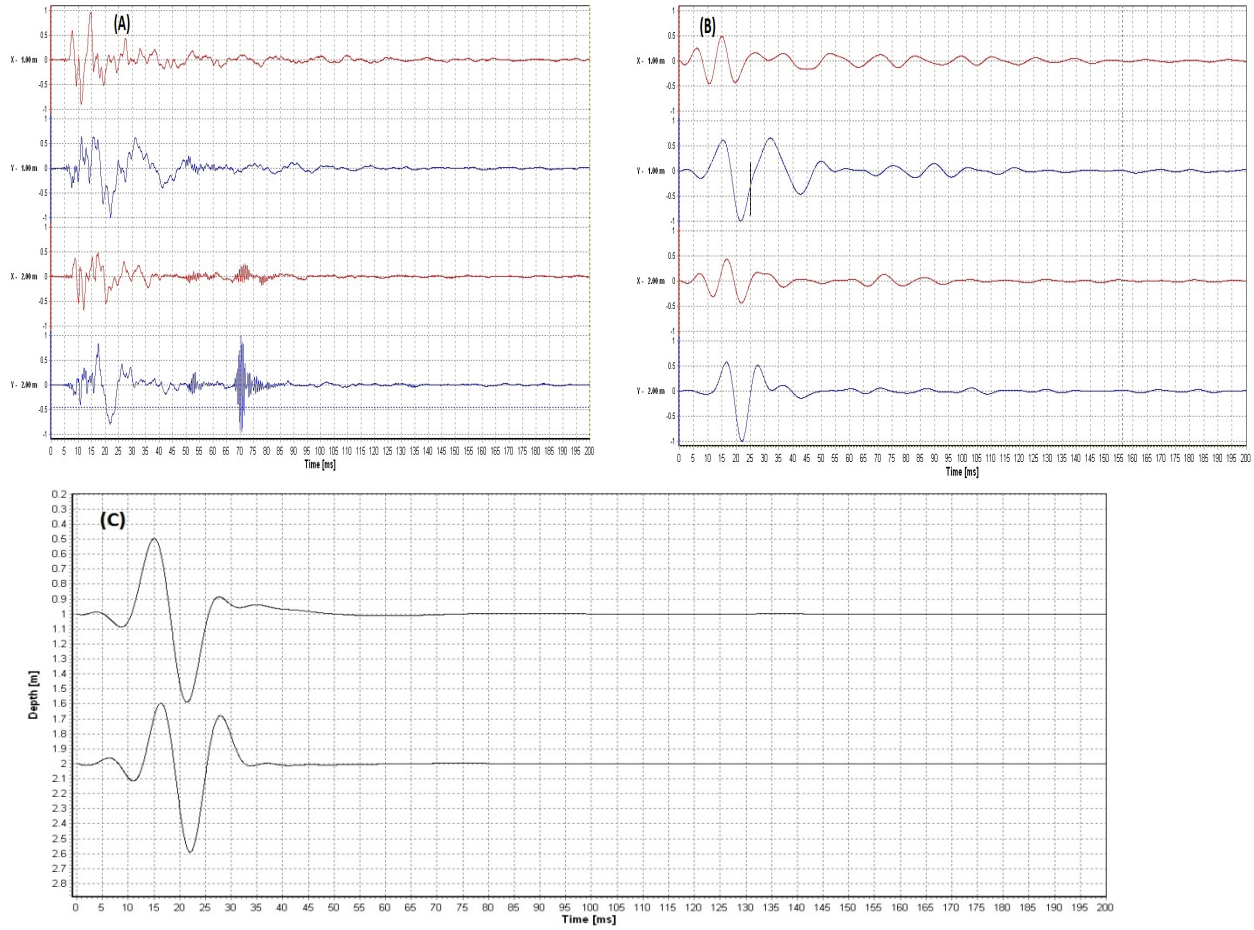


Figure 3: (A) Low SNR near field unfiltered recordings. (B) Filtered traces of (20Hz to 130Hz) outlining source trough skewing on the 1m Y axis recording. (C) Full waveforms with trough skewing on 1m recording minimized by applying signal decay.

3.1 Low linearity values

If the LIN parameter is low there are two possible ways to address it. First, by applying a narrower time window the dominant source wave response (either peak or trough) is more clearly defined and as a result the incorporation of measurement noise is minimized. The outcome is then most likely an improved rotation of the individual response onto the full waveform axis.

However, there are also cases when the low linearity is the result of very low SNR recordings on a specific seismic sensor axis, in which case time windowing will not resolve the issue. In those situations the appropriate action is to drop the trace with the low SNR recording and only using the higher SNR recording. This phenomenon is outlined in Fig. 4 where the X axis response has significant interference on the source wave peak compared to the corresponding source wave trough recording on the Y axis, resulting in a linearity value of 0.49. This interference results in both a broadening and skewing of the peak, and this adverse effect can result in significant errors in arrival time estimation. Since the Y-axis response has clearly a higher SNR the appropriate action is to use only the Y axis response for the analysis.

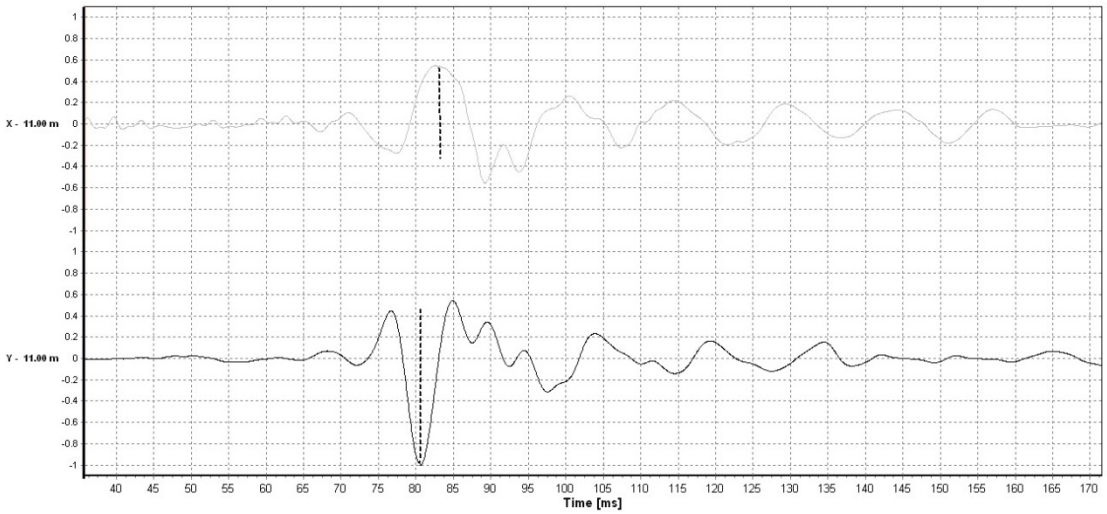


Figure 4: Significant source wave interference on the X axis resulting in peak skewing and broadening.

3.2 Low signal shape parameter values

"Ringing" due to measurement noise can be pronounced within a DST seismic trace in the presence of a very strong source wave maximum peak or trough. This "ringing" will decrease the SSP value and can lead to errors in the automated arrival time calculation from a batch analysis utilizing the cross-correlation function. Figure 5 illustrates this phenomenon. It shows a very strong source wave peak on the X axis (light grey trace) and a corresponding strong trough on the Y axis (black trace). Superimposed on the high SNR source responses is measurement noise which has "ringing" characteristics. The frequency spectrum for the Y axis response illustrated in Fig. 5(a) is illustrated in Fig. 5(b) (light grey trace). The best fit "bell-curve" is the black bold trace in Fig. 5(b), which corresponds with a SSP value of 0.41. Figure 5(c) illustrates the isolation of the dominant peak and trough by applying a time windowing algorithm

Another cause of low SSP values is excessive measurement noise, which can be addressed by applying more aggressive digital filtering to increase the SNR of the recorded traces. For example, traces recorded in high electrical magnetic noise environments (e.g, near power lines) may produce significant electronic noise at 60 Hz (or harmonics of 60 Hz) decreasing the SNR of the recorded DST traces. In this case the investigator can apply notch filters to remove the electronic noise. In other cases simply narrowing the bandpass filter may results in higher SNR traces. For example, the near surface (2m depth) trace illustrated in Fig. 6(A) has a minimally applied low pass filter of 300Hz and corresponding SSP value of 0.52. Figure 6(B) shows the trace illustrated in Fig. 6(A) with a bandpass filter of 20Hz to 130Hz. In this case the SSP value has been increased to 0.7.

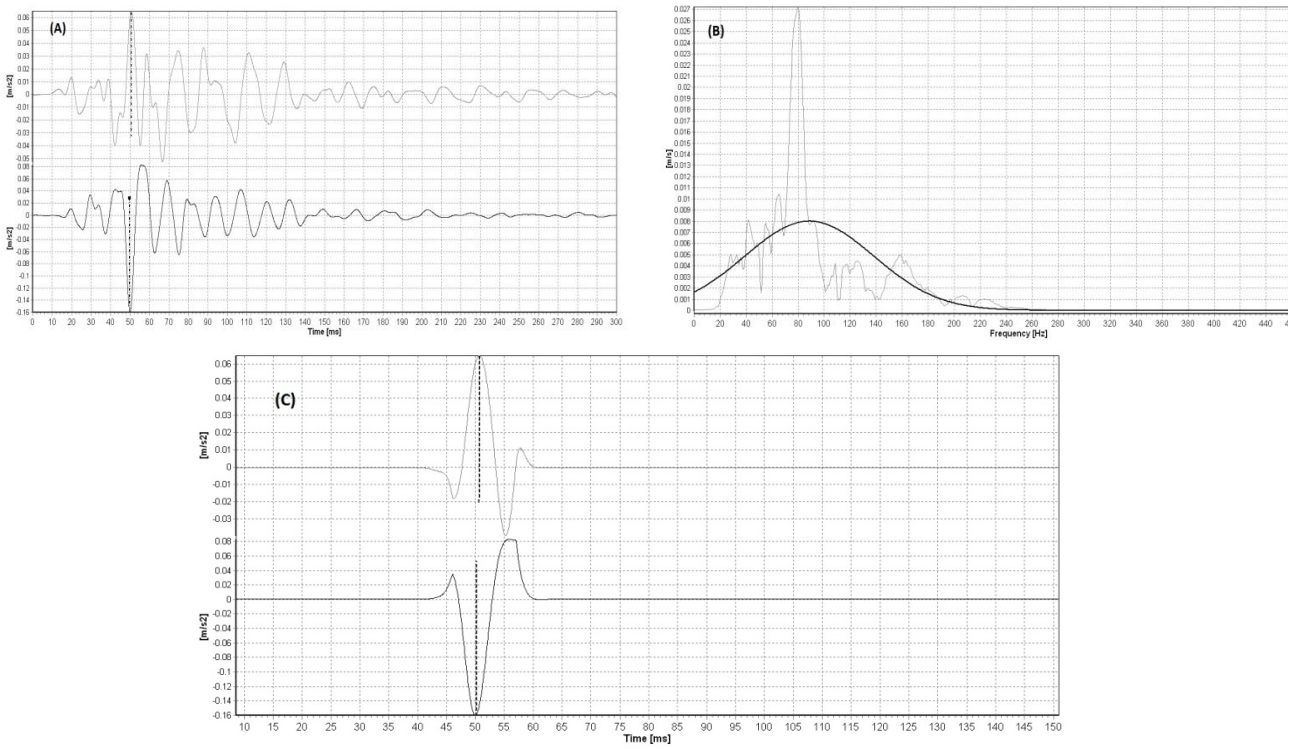


Figure 5: (A) DST seismic trace recorded with evidence of strong measurement noise "ringing". (B) After application of signal decay where first peak and trough are isolated. (B) Frequency spectrum for the Y axis response illustrated in (A) (light grey trace) and the best fit "bell-curve" (black bold trace). (C) Isolation of the dominant peak and trough by applying time windowing.

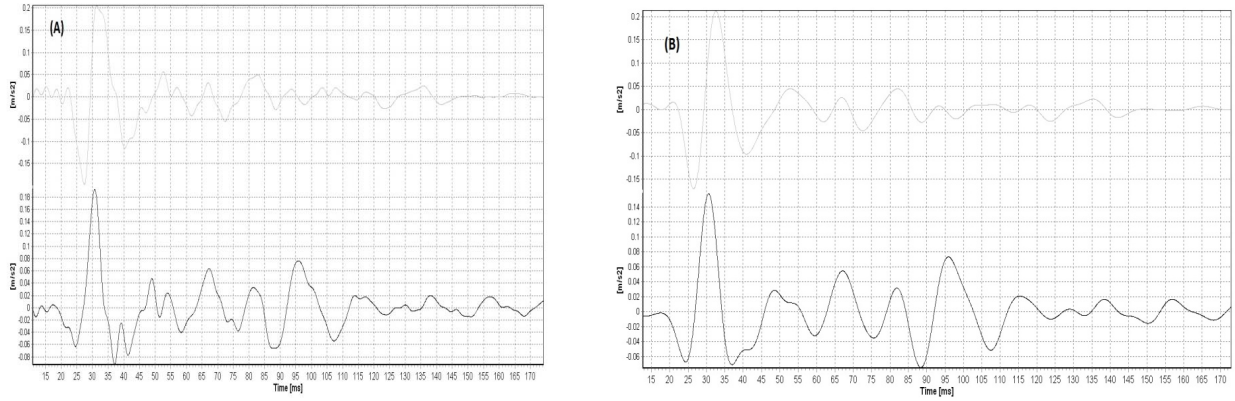


Figure 6: (A) Near surface DST trace with a 300 Hz low pass filter applied. (B) Trace illustrated in (A) with a bandpass filter 20Hz to 130Hz applied

3.3 Low linearity and low signal shape parameter values

There are DST testing conditions which can result in strong source wave reflections (Baziw and Verbeek, 2014c), which can lead to source wave speak skewing and subsequently lowering of the both the linearity and the SSP values. To address this case, time windowing can be applied to the effected traces so that unaffected first peaks and troughs can be isolated. This process is outlined in Fig. 7.

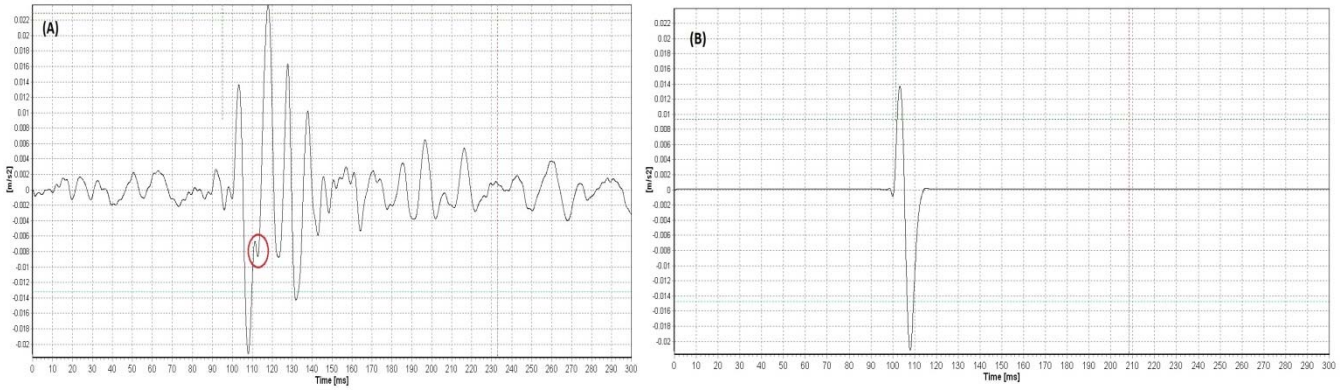


Figure 7: (A) DST seismic trace recorded with evidence of strong source wave reflections at 112ms. (B) After application of signal decay where first peak and trough are isolated.

CONCLUSIONS

Downhole Seismic Testing (DST) is an important geotechnical testing technique for site characterization and therefore it is essential that the quality of the acquired seismic traces can be assessed. The Seismic Trace Characterization (STC) provides the user with a good indication, but the individual parameters used to derive the STC (the cross-correlation coefficient of the full waveforms between successive depths of data acquisition, the linearity estimates from the polarization analysis, and the Signal Shape Parameter that quantifies the deviation of the source wave frequency spectrum from a desirable bell-shaped curve overview) also provide guidance on the most appropriate data analysis technique to ensure that the analysis results are as accurate as possible. More extensive use of the STC will provide further validation of the equation used to derive the STC and also an indication whether additional parameters need to be taken into account.

REFERENCES

ASTM (American Standards and Testing Methods). (2014). "D7400: Standard Test Methods for Downhole Seismic Testing." ASTM Vol. 4.09 Soil and Rock (II): D5877-latest.

Baziw, E. and Verbeek, G., (2016a), "Interval Velocity Classification Technique in Downhole Seismic Testing", http://www.bcengineers.com/images/BCE_IVC_2016.pdf

Baziw, E., and Verbeek, G. (2016b), "Frequency spectrum "bell-curve" fitting as a component of SCPT interval velocity accuracy assessment." In Proceedings of the 5th International Conference on Geotechnical Site Characterization (ISC-5), Queensland – Australia, 5-9 Sept. Australian Geomechanics Society, 1431-1436.

Baziw, E., and Verbeek, G. (2012). "Deriving Interval Velocities from Downhole Seismic Data." Geotechnical and Geophysical Site Characterization 4 – Mayne (eds), CRC Press, 1019–1024.

Baziw, E. (1993). "Digital Filtering Techniques for Interpreting Seismic Cone Data." Journal of Geotechnical Engineering, ASCE, Vol. 119, No. 6, pp. 98-1018.

Baziw, E., and Verbeek, G. (2014a). "Signal Processing Challenges when Processing DST and CST Seismic Data containing TIRs." ASTM International - Geotechnical Testing Journal (GTJ), vol. 37, no. 3, 1-21.

Baziw, E. and Verbeek, G. (2014b). "Identifying Critical Layers using SCPT and Seismic Source Moveout." In the Proceedings of the 3rd International Symposium on Cone Penetration Testing, CPT'14, May 12-14, 2014 - Las Vegas, Nevada, 357-364.

Baziw, E. and Verbeek, G (2014c), "Methodology for Processing Seismograms Containing Total Internal Reflections", IEEE Transactions on Geosci. Remote Sensing (TGRS), vol. 52, Issue 11, 7073-7085.

Baziw, E. (2011). “Incorporation of Iterative Forward Modeling into the Principle Phase Decomposition Algorithm for Accurate Source Wave and Reflection Series Estimation”. IEEE Transactions on Geosci. Remote Sensing (TGRS), vol. 49, No. 2, 650-660.

Baziw, E., Nedilko, B., and Weir Jones, I. (2004). “Microseismic Event Detection Kalman Filter: Derivation of the Noise Covariance Matrix and Automated First Break Determination for Accurate Source Location Estimation.”, Pure appl. geophys. vol. 161, no. 2, 303-329.

Baziw, E. (2002). “Derivation of Seismic Cone Interval Velocities Utilizing Forward Modeling and the Downhill Simplex Method.” Can. Geotech. J., Vol. 39, 1181-1192.

Baziw, E., Tichy, J, and de Caprona, G (2000),"Data Acquisition in Seismic Cone Penetration Testing". In Proceedings of the 3rd International Symposium on Integrated Technical Approaches to Site Characterization (ITASCE), Argonne, IL, 11 14 Sept. 2000. Argonne National Laboratory. 69-72.

Campanella, R.G., Robertson, F.T.C., & Gillespie, D. (1986). “Seismic Cone Penetration Test.” In Proceedings of INSITU86. American Society of Civil Engineers (ASCE) Geotechnical Special Publication. No. 6, 116–130.

Gelb, A. (1974). Applied Optimal Estimation (4th ed.). MIT Press, Cambridge, Mass, USA.

Gibowicz, S.J. and Kijko, A. (1994). An Introduction to Mining Seismology. Academic Press,
San Diego, USA.

Ishihara, K. (1982). “Evaluation of Soil Properties for use in Earthquake Response Analysis.” International Symposium on Numerical Models in Geomechanics, Zurich, 237-259.

Kanasewich, E.R. 1981. Time Sequence Analysis in Geophysics (3rd ed.). The University of Alberta Press, Edmonton, AB. Canada.

Shearer, P.M. (1999). Introduction to Seismology. Cambridge University Press, Cambridge, U.K.

PROBABILISTIC SUBSURFACE CHARACTERIZATION FOR TRANSMISSION LINE FOUNDATION DESIGN

Peter M. Kandaris, DiGioia Gray, Inc., Tempe, AZ, USA, 480.273.9445, pkandaris@digioiagray.com
Jogi S. Gadok, EC Source Services, Inc. Mesa, AZ, USA, 480.245.7200, jgadok@ecsourceservices.com
Neil T. Russo, Planet Forward Energy Sol'ns, Western Springs, IL, USA, 203.231.7580, nrusso@pfes.com

ABSTRACT

Assessment of subsurface data for foundation design in support of long high voltage electric transmission lines is best accomplished using a probabilistic strategy since only a small portion of structure locations are typically sampled. Probabilistic approaches provide a tool to evaluate site uncertainty in a systematic and rational manner. This paper provides a case history of a risk-based design approach for a recently completed 191-mile long 69/161/345kV steel monopole transmission line traversing Central Iowa. The project owner made available limited subsurface information at project initiation, requiring the design team to obtain additional data within a constrained budget for 1067 large diameter, laterally-loaded deep drilled shaft reinforced concrete piers. The team commissioned a geologic desktop study to reduce uncertainty in subsurface evaluations and aid in selecting additional sample sites. In total, investigation programs tested approximately 15 percent of structure sites. The paper details the probabilistic approach used to estimate foundation geotechnical design parameters, with information from the various studies categorizing strata both laterally and with depth. Low-bound parameters were estimated via a statistical approach at a pre-determined reliability level. Significant savings resulted from this approach when compared to conservative deterministic processes. Project QA/QC logged subsurface soil conditions during foundation excavation, then compared as-found conditions to the conditions assumed for design. The team redesigned foundations if either a non-conservative variance in soil conditions was observed or if bedrock elevation differed significantly from design assumptions. As a result, only 22 out of 1067 foundations required modification during construction (2% variance from initial design) with negligible impact on the construction budget and schedule.

Keywords: transmission line foundations, probabilistic analysis, load, foundation design, soils, geologic reconnaissance

INTRODUCTION

Foundation design for long high voltage transmission lines presents a unique challenge in that the assessment of subsurface conditions typically requires substantial data that may or may not be obtainable. Investigations are usually performed well in advance of construction, often with limited access to structure sites and typically in remote areas. Probability and risk-based investigation and design strategies offer an opportunity to systematically estimate subsurface profiles and geotechnical design properties with limited data. Risk can be further reduced with dedicated field inspection of foundation construction along with good field and design team communication during construction. This paper presents a case history of probabilistic methods used for the investigation and design of electric transmission line foundations.

The project consists of designing and constructing two transmission line segments in northern Iowa as part of the MidAmerican Energy Company (MEC) MVP Projects: upgrading 120 miles of an existing wood H-frame 161kV transmission line to 345kV and 161kV double circuit transmission lines from a new O'Brien Substation to an existing substation in Webster County, Iowa; and upgrading of 71 miles of similar transmission lines, linking interconnects with another utility near Hampton, Iowa and Dunkerton, Iowa (See Fig. 1). Transmission structures are primarily monopoles (with some H-frames) which impart large moment and shear reactions at ground line with relatively small axial compressive loads. In total 1066 drilled shaft

 © 2017 DFI Annual Conference, New Orleans, LA, USA

reinforced concrete foundations are required with design diameters ranging from 5.5 feet to 13 feet and embedded depths ranging from 17 to 82 feet below grade. Total neat-line concrete quantity is about 60,000 cubic yards.



Fig. 1. Site Location Map

GEOTECHNICAL INVESTIGATIONS

Preliminary investigation work was performed by MEC for contract bid preparation (Terracon 2012a; 2012b). The work included 62 auger borings to a maximum depth of 41 feet and 11 cone penetrometer tests to a maximum depth of 50 feet. Laboratory testing was performed on selected samples. Additional information was obtained from 9 borings at adjacent electric substation sites (Terracon 2013c; 2013d; 2013e; 2013f). During bid preparation by the contractor, EC Source Services, preliminary foundation estimating assumed only four soil and one rock zone along both routes. DiGioia Gray & Associates was tasked to evaluate subsurface conditions and provide foundation design. From a review of the existing data, it was apparent that actual conditions would require design evaluate a more complex subsurface model.

Based on Electric Power Research Institute (EPRI) best practices recommendations (EPRI 2012), further geologic mapping should be done prior to sampling to establishing foundation design zones, better understand the scope of planned supplement investigation work and reduced uncertainty in selecting sample sites for foundation design. Geologic desktop studies were performed by Terracon Consultants through a series of reports along the transmission line route (Terracon 2013a; 2013b). The study work reviewed readily available and published data for information regarding geologic, geohydrologic and geotechnical conditions along the proposed alignments, and compiled information for GIS presentation of known geologic, groundwater and geotechnical information. In addition to the Terracon work, the design team gathered online groundwater well log data GIS format from an extensive data base of the Iowa Department of Natural Resources. The logs from 40 water wells in close proximity to the transmission line alignments were included in the subsurface assessment.

Supplemental field investigation work was required to better understand subsurface strata as foundation depths were anticipated to extend below previous investigation limits. Additional borings were also required to gain subsurface knowledge in areas where the geologic mapping indicated more data was required and to obtain samples for laboratory testing (better define geotechnical design parameters).

The supplemental investigation program scope included 47 auger borings with standard penetration testing (SPT) to a maximum depth of 70 feet and 27 cone penetrometer tests (CPT) to a maximum depth of 79 feet. Pressuremeter tests were performed at various depths at sites where 14 auger boring or CPTs had been previously performed. Shear vane tests were taken at various depths in 6 auger borings. Six near surface auger samples to a 5-ft depth were obtained to aid in scour analyses. Laboratory testing focused on moisture/density information, unconfined compression strengths and gradation analyses of near-surface soils (for hydrologic scour evaluations).

In total, 147 sites were samples along the 191-mile alignment, encompassing data for design at 1059 structures, or just under 15% of the structure sites. This rate averages to about one boring/CPT for every 1.3 miles, or a boring/CPT for every 7 structures. A recent EPRI state-of-practice survey identified borehole sample frequency for large lines on the order of one boring per mile (+70% of respondents, EPRI, 2012). Others have reported performing one boring for every 1 to 10 structures as typical for transmission line investigations (Grigoriu et al. 1987).

GEOLOGY & SOILS

The transmission line alignments are located within the Central Lowlands Province – a region that extends from New York to western North Dakota, as far north as Canada and as far south as Texas. The Central Lowlands are distinguished by relatively low relief and elevations. Nearly horizontal or gently sloping bedrock (primarily limestone, shale, sandstone and conglomerate) is mantled with relatively thin soil deposits. Glaciation dominates the project area, where high features have been removed by glaciation and glacial till is deposited in remaining low lying areas. Glacial drift can be several hundred feet thick in valleys. Between glaciations, loess has been deposited across much of the province and during subsequent glaciations removed and/or buried below additional glacial deposits (Terracon 2012a). Geologic desktop studies characterized the subsurface as follows (Terracon 2013a; 2013b):

- Approximately nine mapped bedrock formations and significantly more soil series are found along the proposed transmission line alignment. These formations and soil series are in three general physiographic regions with similar engineering and construction characteristics (Northwest Iowa Plains on the western side, Des Moines Lobe central portion, Iowan Surface on the eastern side).
- Limestone, dolomite, and sandstone bedrock is present below overburden soil.
- Overburden soil include alluvial, lacustrine, aeolian (e.g. loess) and glacial deposits (e.g. glacial drift, till, and end moraine material, etc.) ranging in thickness from less than 25 to more than 250 feet are present along the proposed alignment. The composition of the glacial soils can be erratic due to the random nature of its deposition. Overburden soil is clayey in nature (typical plasticity indices vary from 5 to 30). Glacial deposits frequently contain isolated pockets of water bearing sand and gravel, as well as cobbles and boulders. In addition, alluvial, lacustrine, and aeolian soils, and materials deposited within end moraines are typically normally consolidated to slightly overconsolidated.
- Groundwater varies from at surface to tens of feet below surface and is commonly observed near interfaces of deposits. Perched groundwater is common and occurs when surface water percolates downward through more permeable, alluvial, loess and drift deposits to the less permeable glacial clays. This commonly creates zones of saturated soils that have lower strength. Artesian conditions are possible along the alignment.

Foundations will primarily bear within near-surface soils. Their deposition is controlled by the following processes:

- Major rivers, waterbodies, and associated floodplains: These soils are normally consolidated to slightly overconsolidated alluvial soils consist of clays, silts, sands, and gravels. Due to the complex process of erosion and deposition by the river, these soils generally have little continuity in their layering within the floodplain. Near surface soils are normally comprised of a combination of materials deposited by slack water during flooding and tend to be finer grained cohesive and moderately cohesive soils.
- Glacial deposits: These soils are prone to the formation of shallow depressions where soft, normally consolidated soils can be present. Low lateral capacity is expected in these materials.
- Aeolian deposits (i.e., loess): These nearly normally consolidated, wind-blow silt and fine-grained sand tend to be sandier near the material source (e.g., Missouri River floodplain) and grade to a higher clay content further from the source (e.g., eastern Iowa). The upper portion of loess deposits tend to be weathered, with a higher clay content, and may be slightly overconsolidated.

Lacustrine, alluvial and aeolian clays and silts dominate the near surface soil profile (upper 20 to 40 feet), varying from soft to stiff. More cohesionless soils in active channels and floodplains vary from loose to medium dense. These soils generally overlay either glacial tills or bedrock, but do extend locally to depths of 60 feet. Alluvial soils are typically coarser grained, having been deposited in faster flowing water. Locally, clay filled abandoned channels (oxbows) and other features are often present that may contain isolated zones of normally consolidated clay and other cohesive soils that extend to greater depths than in the areas of the floodplain.

Glacial deposits (e.g. glacial till, moraine material, etc.) are present across the majority of the alignment and underlie softer surface soils. The composition of the glacial soils is often erratic due to the random nature of deposition. Glacial till and materials deposited in end (terminal) moraines generally consist of clays with sand, gravel, cobbles, and boulders. Glacial till deposited below the ice mass is overconsolidated, whereas end moraines formed at the edge of the glacial ice mass are generally nearly normally consolidated to slightly over-consolidated. These soils are mostly in a cohesive matrix and vary in consistency from stiff to very hard.

Bedrock along the transmission line alignment consists of variable sedimentary units of marine shale with interbedded sandstone, limestone and coal (Pennsylvanian); marine limestone and dolomite with chert and shale (Mississippian); marine limestone and dolomite with shale (Devonian); and marine dolomite with chert (Silurian). Bedrock formations are generally good for foundation support. However, highly weathered and fractured bedrock likely overlays more competent sedimentary units.

GEOTECHNICAL DESIGN PARAMETERS

A probabilistic approach for selection of geotechnical design parameters assumes these properties as homogeneous within the same geologic unit or strata and normally distributed. Prior information gained from the geologic desktop studies and all subsurface data can be used to categorize strata by material type (both laterally along transmission line alignments and with depth).

Due to the wide spacing of soils test locations, the design team used detailed geologic and surface soils mapping from desktop studies and reconnaissance to categorize soils for the development of foundation design properties. Once categorized, similar soils were grouped and statistical analysis was performed. Data, in the form of field tests (blow counts, pressuremeter moduli) and laboratory tests (unconfined compression for both soil and rock) were analyzed to define the nominal (mean) and the spread range about the mean (variance) for use in further development of geotechnical design properties.

A confidence level, or level of acceptable variation, was set at a 5% lower exclusion limit (LEL) in accordance with ERPI guide document recommendations (EPRI 2012). Additionally, if the coefficient of variance for any data subset exceeded 35 percent, samples, geologic data and soil logs were re-examined to either exclude outlier data or split the data set and re-assign to additional or different soil zones or substrata. This type of probabilistic characterization methods provides a tool to evaluate the different types of uncertainty of site conditions in a systematic and rational manner. The function of site exploration and testing programs became an exercise in reducing these uncertainties to yield an acceptable level of geotechnical performance. In all circumstances, thought, engineering judgment was applied to the process to modify results as needed where statistics were inconsistent with the team's understanding of soils and rock.

Both lower bound (5% LEL) and average N_{60} blow counts were determined for each strata zone. From review of the geologic mapping and soils logs, categorization of soil zones was done based on the following depositional groups:

- (1) Surface deposits (loess, glacial drift, slough and lacustrine deposits)
- (2) Glacial till (glacial, moraines, intermixed)
- (3) Alluvial deposits (riverine and lacustrine origin)
- (BR) Bedrock

Table 1 summarizes the results of the geotechnical design property analysis as generalized across both alignments. Within each depositional group, sub-groups were delineated primarily by statistical evaluation of blow count values. Geotechnical design properties were estimated primarily by correlating N_{60} blow count values with standard industry correlation charts. Due to budget and time constraints, minimal laboratory testing was performed. Additionally, standard regional sampling practices did not accommodate more advanced strength testing (direct shear or triaxial methods). Since laboratory data relating to strength parameters was sparse, engineering judgment was used to selectively modify blow count correlation values of internal friction angle and undrained shear strength.

Table 1. Idealized Geotechnical Design Parameters

Strata No.	Strata Description	$N60_{avg}$ (bl/ft)	COV (%)	Soil Properties (5% LEL)				
				$N60_{5\%}$ (bl/ft)	$\gamma_{t\ or\ SAT}$ (pcf)	ϕ' (°)	c' (ksf)	E_p (ksi)
1 – Surface Deposits:								
1A	Soft	3	35	1	98	--	0.6	0.20
1B	Medium soft	6	33	4	120	--	0.9	0.35
1C	Stiff	10	35	8	125	--	1.2	0.50
2 – Glacial Till:								
2A	Upper deposits	11	33	9	129	--	1.4	0.65
2B	Middle deposits	19	34	17	131	--	2.3	1.10
2C	Lower deposits	38	26	34	135	--	2.8	2.50
3 – Alluvial Deposits:								
3A1	Loose sand & silt	7	35	5	116	32	--	0.50
3A2	Stiff clay/silt	9	31	6	126	--	0.8	0.50
3B	Loose to medium dense	14	35	11	116	33	--	1.10
3C	Medium dense to dense	27	35	22	125	34	--	1.80
BR – Bedrock:								
BR1	Weathered/fractured	--	--	--	140	45	1.0	30
BR2	Competent	--	--	--	145	50	3.0	100

$N60_{avg}$ = mean of the data set; COV = coefficient of variation

Project pressuremeter data was also correlated to associated blow count values to develop a project-specific design property relationship. Soil unit weight values were readily available from laboratory testing. Nominal values were used as this parameter has generally low variability (3% to 7% found in the data sets).

Bedrock was encountered intermittently along isolated sections of the alignments and was generally classified as either weak/weathered/fractured or competent. Insufficient bedrock data was available from the field investigation program to perform valid statistical analyses. Therefore, engineering judgment was used to select reasonable low-bound values from the data available and from known regional values. Strength and density properties shown in Table 1 were developed from discussions with local geotechnical consultants based on previous experience with other projects.

FOUNDATION DESIGN APPROACH

A strength limit design approach (shown in Equation 1) was used to determine the load and resistance relationship. The approach is an adaptation of reliability-based design, but instead of applying a resistance factor to nominal soils resistance, statistical low bound soils properties were developed and used to determine reduced soil resistance. In addition, MEC required factored loads be increased by a value of 1.1 so the foundations would be designed to fail at higher loads than the structures.

$$\Phi_{5\%}R_n \geq 1.1 \times Q_F \qquad [1]$$

where $\Phi_{5\%}R_n$ = Soil resisting strength resulting from use of 5% lower exclusion limit boundary values for soil properties, and where Q_F = Factored loads on soil from structure forces resulting from NESC code load cases or Owner-required load cases (these values are typically base plate maximum loads supplied by steel pole vendors).

Drilled shaft reinforced concrete foundations for supporting structures were designed as rigid piers, with deflection and rotation limits as noted in Table 2. These performance parameters were evaluated using factored loads at or near the elastic range of the load-deformation relationship. Deflection and rotation at failure were not evaluated for the design. In addition to the load cases, foundations in floodplains and waterways were to be embedded at sufficient depth to prevent loss due to scour. Hydrologic studies detailing scour and bank erosion (with ground loss up to 26 feet) were performed along the alignments. Additional load cases are included to evaluate combined structure loads with scour from a 100-year event. Wind loads on structures are reduced to every day event forces when evaluating the maximum scour event.

Laterally loaded reinforced concrete drilled shaft foundations were designed using EPRI MFAD 5.1.17 computer software. The MFAD model is a semi-empirical non-linear load deflection and ultimate capacity model, and is used for rigid shaft design.

Table 2. Top of Pier Deflection and Rotation Design Limits

Total Deflection:	0.04B $\geq$ 3.0 inches
Total Rotation:	1.0 degree
Non-recoverable Deflection	0.02B $\geq$ 1.5 inches
Non-recoverable Rotation	0.5 degree

1. The allowable Total and Non-Recoverable Deflection shall not be less than 3.0 inches and 1.5 inches, respectively.
2. B = Pier Diameter (inches)

Idealized soil profiles were developed at all structure locations using the strata and substrata shown in Table 1. Depth to, types of and thickness of strata at each site were primarily based on subsurface test logs (borings and CPTs). If no subsurface sample was obtained at the structure location, conditions were assumed to be

similar to that observed at the nearest boring or set of borings unless geologic or surface observations dictated otherwise. Ground topography, the need to accommodate scour ground loss, and the highly irregular nature of strata bedding observed during field investigation work was assessed in the development of idealized profiles. This often resulted in complex subsurface soil variations, where design estimated 178 different combinations of soil strata, thicknesses and depth (see typical example in Fig. 2).

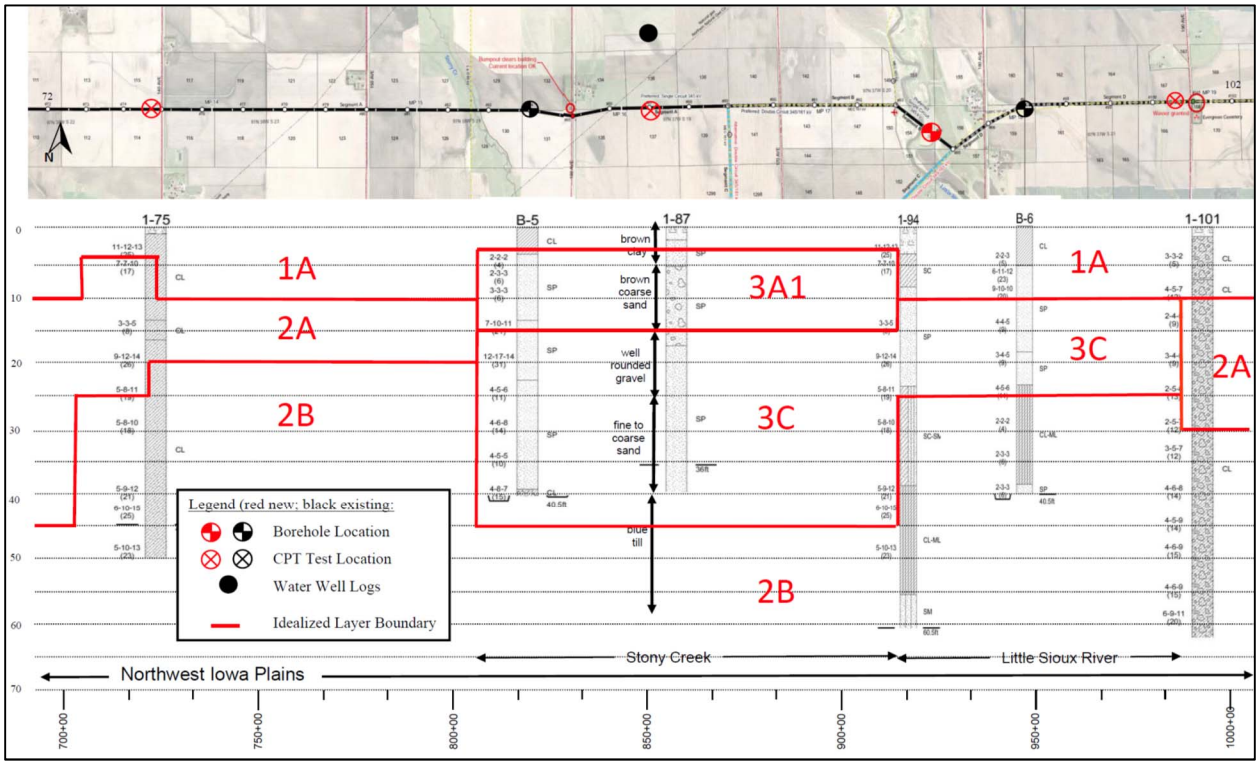


Fig. 2. Typical Idealized Subsurface Strata Cross Section

CONSTRUCTION QUALITY CONTROL

The complexity of the project and the widespread nature of subsurface data available at structure sites mandated a high-quality field inspection program during construction to verify conditions were as assumed in design at each site. EC Source dedicated a field inspection and quality control team to observe foundation excavation, monitor foundation installation and communication between construction and engineering. It was imperative that foundation excavations be inspected by highly competent personnel who could properly identify any potential differences in geotechnical conditions used in design and the encountered during construction.

Subsurface conditions resulting from design are a calculated interpretation of the probable site conditions based on desktop geologic reconnaissance and selected subsurface testing via borings, CPTs and adjacent water well logs. Testing could not be performed at every foundation; therefore, it was likely some differences in expected versus actual subsurface conditions would be found during construction. Geotechnical parameters recommended for foundation design include sufficient flexibility for expected statistical variances in condition. However, it was probable that atypical subsurface conditions would be encountered outside the probability range due to the limitations of standard industry transmission line investigation methodology. The contractor took on the responsibility of assigning qualified personnel to inspect each structure foundation during construction and verify the subsurface conditions assumed by the design team.

A good understanding of assumed subsurface conditions by the inspection teams is essential in properly assessing differences in site conditions. The following documents were prepared either by the design team or the construction inspection team, and reviewed by both entities:

- Foundation construction specification – prepared by the design team to include important design elements using guidance given in the owner's technical specification requirements,
- Foundation inspection documents – this effort included preparation of a project-specific foundation inspection manual along with detailed report forms for use by field inspectors (logs for drilling. concrete inspection, formwork, anchor bolt cages (Fig. 3), etc.),
- Foundation construction plans included tabular data on expected subsurface conditions – effectively a summary at each site of Table 1 data with anticipated depths and thicknesses of strata.



Fig. 3. Typical Foundation Anchor Bolt/Reinforcement Cage

The inspection team documented foundation inspection at the time of installation. This became a challenge due to the expedited nature of the work, as the contractor used multiple drilling crews simultaneously along one or more segments of the alignment. Shaft excavation was performed in advance of concrete placement using cased methods. Both thick-walled permanent casing driven into the ground and corrugated metal pipe (CMP) installed by drill and grout methods were utilized. Installation methods and practices were established in advance of the work with the review and approval of the design team. Because so much drilling was going on over sometimes larger reaches, the inspector and drilling foreman worked together so that all foundation excavations were accurately logged.

The geotechnical experience of inspectors and drillers differed, so subsurface descriptions would likely vary by individuals. To help standardize, general visual soils and bedrock descriptions were developed. The four depositional groups could be identified by the following descriptions:

- Group 1: Surface soils were generally softer fine-grained (clays & silts) and saturated;
- Group 2: Glacial till was more firm, with sand/gravel/cobble in a cohesive (clay) matrix and typically unsaturated;
- Group 3: Alluvium was generally granular (sands and gravels) or a cohesive-granular mix (clayey sand), again typically saturated and near waterways or in flood plains;
- Bedrock was identified as either fractured/weathered/broken or competent.

Those performing field logging were requested to also identify soils by consistency to help in understanding substrata groupings:

  - Group 1: Soft, medium soft or stiff
  - Group 2: Stiff, very stiff or hard
  - Group 3: Loose, loose to medium dense, medium dense to dense
  - Stiff alluvial cohesive soils (clays in waterways, rivers, etc.) were categorized as part of Group 3 and were generally recognized though their depositional environment.

As shafts were excavated, the drilling crew would log cuttings and provide an initial log of the subsurface condition. The foundation inspector would be visiting the site during this process, review the driller's log and create a separate inspector's log if differences were observed. The inspector would then review both subsurface logs to determine if the conditions found were at or better than those shown on the foundation plans. An example at Structure BW-253 is shown in Fig. 4, along with the nearest geotechnical borings performed during the initial investigations.

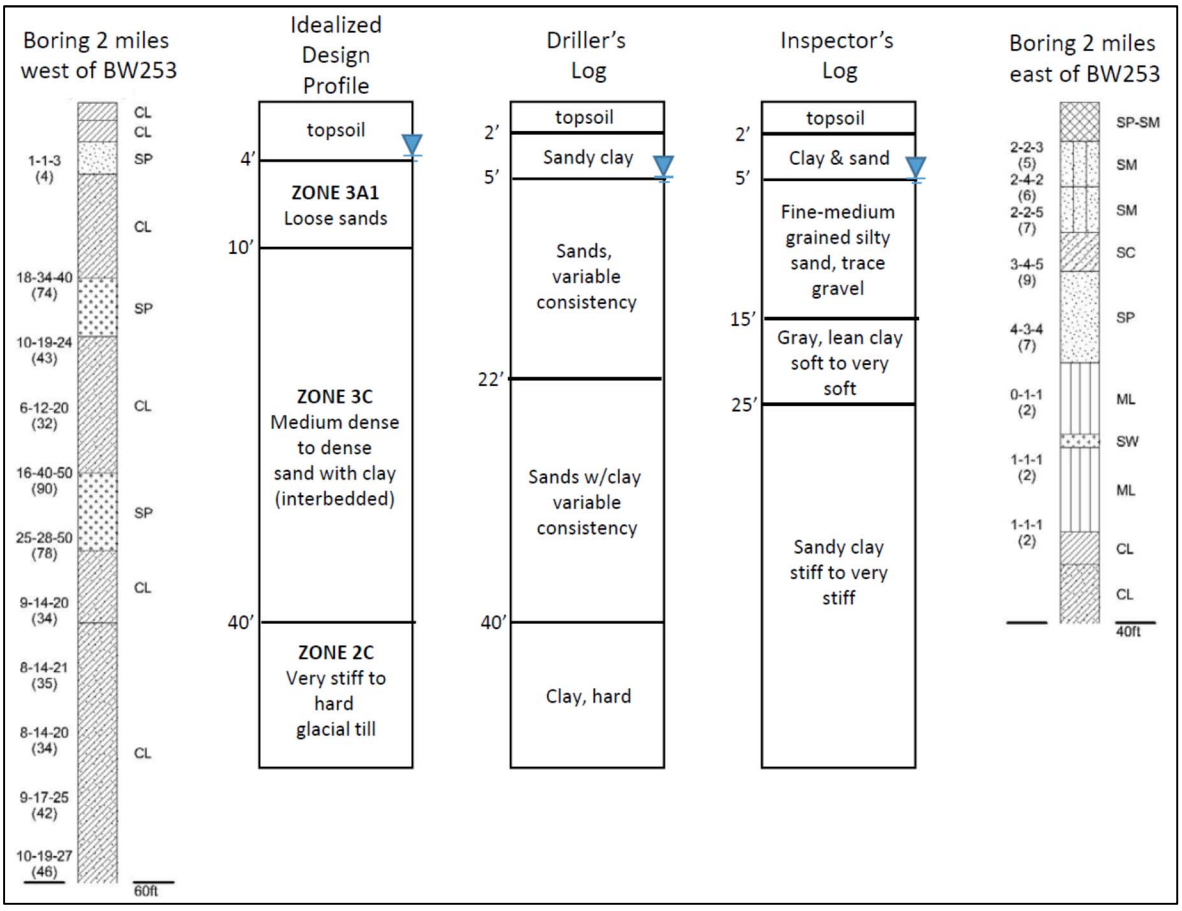


Fig. 4. Various Shaft Logs for BW-253

The foundation for BW-253 was planned at a 10-foot diameter, with 1 foot projecting out of ground and 50 feet embedded into the subgrade. At this site, the driller's log and the idealized profile from the foundation drawing were fairly similar. The inspector, though, observed a softer zone from 15 to 25 feet and the hard, fine-grained soil layer beginning at 25 feet below grade. From a design standpoint, the inspector's as-found profile would provide greater lateral load resistance, so the idealized profile was considered conservative.

Sloping ground conditions encountered at BW-253 required the foundation projection to be raised to 2 feet out of ground, so the engineer was requested to re-evaluate the foundation design. It should be understood that full length anchor bolt cages for monopoles were fabricated in advance of drilling. Since altering the cage would be costly, the design team was requested to evaluate the unchanged foundation length with a 49-foot embedment. The shaft was cased at a 10.5-foot diameter, 0.5 foot larger than the design diameter. Revised calculations using the inspector's as-found subsurface profile with the larger pier diameter accommodated anticipated loads with a 49-foot embedment. Construction proceeded with no change required for the anchor bolt cage.

Nearest adjacent borings also show the complexity of design based on the data available. A test boring two miles to the west showed stiff to hard clay glacial till below 15 feet, with a 5-foot sand lense from 27 to 32 feet. The test boring two miles to the east indicated loose and soft alluvium to about 35 feet below grade. Neither boring properly characterized the as-found site conditions. During design, surface soils and geology were included in the analysis to better estimate the likely conditions, along with site reconnaissance notes. It was predicted that soft/loose alluvium depth would be limited as the site as it was at some distance from the riverine source. Interbedded clays and sands would be more similar to the western boring. Weaker interbedded sand and clay layers were presumed to extend from 10 to 40 feet below grade. Both borings indicated stiff till below 40 feet, with the idealized profile indicating the same condition. This geology-focused approach provided flexibility to include observations in addition to subsurface data instead of simply selecting the nearest worst-case boring.

The described process was utilized through the project to evaluate conditions at each site. Upon completion of all work, 22 of the 1066 foundations (2%) required redesign to accommodate weaker (unconservative) soils, bedrock at elevations different than assumed in design, or differing site surface conditions. A 5% modification rate was assumed as part of the lower exclusion limit statistical approach, where upwards of 50 foundation designs were anticipated to require alteration during construction due to lower resistance capacity.

SUMMARY AND CONCLUSIONS

Probability or risk-based assessment of subsurface soils and rock for transmission line foundation design can be used to reasonably estimate geotechnical design properties, even with limited data. The investigation for this case study in Iowa directly sampled the subsurface at about 15% of the structure sites, supplemented with a detailed geologic reconnaissance study. Supplemental investigation site were selected based on a review of the alignment geology and surface soil conditions to find representative sites for additional testing. Data from testing was evaluated by probabilistic methods to establish a pre-defined level of reliability in terms of statistical low bound geotechnical design properties. A high-quality field inspection program verified subsurface conditions for all drilled shaft excavations, resulting in redesign and modification for about 2% of the foundations. Overall, the final product provides a reliable installation that was verified via inspection and analysis.

A relative cost assessment was performed to determine the value of this risk-based approach. The following estimates show significant savings:

- The geotechnical test firm was requested prior to the start of design to provide a proposal based on the available data for use in standard foundation design. It was recommended that 20% of the sites be investigated at cost 45% above the final geologic and geotechnical program performed for use with the discussed probabilistic approach.
- Design engineering costs involving geologic reconnaissance and probabilistic assessment of geotechnical design properties are on the order of 10% of the final geologic and geotechnical program costs.
- Full time transmission line construction inspection was required by owner for the project, so the additional cost related to enhanced foundation inspection and documentation is considered negligible.
- Modifications of the 22 foundations resulted in added construction and design costs estimated at less than 20% of the final geologic and geotechnical program costs.

Reliability-based designs typically result in smaller foundations since probabilistic parameters are used in lieu of deterministic (and often conservative) global safety factors. Though no specific evaluation was performed for this case history, previous case studies have shown upwards of 10% reduction in foundation costs result from similar approaches (Rojas-Gonzalez, et al, 1994).

ACKNOWLEDGEMENTS

Transmission line foundation engineers rarely have opportunities to work so closely with the owner and the contractor in all facets of design and construction. The authors would like to thank the engineers at MidAmerican Energy, and in particular Steve Ambrose and Karl Donaubauer for their help, counsel and valuable recommendations. The design team wishes to also thank the management of EC Source Services for their support during this project.

REFERENCES

Electric Power Research Institute (EPRI), 2012. Transmission structure foundation design guide, EPRI Technical Report 1024138, Palo Alto, CA.

Grigoriu, M.D., F.H. Kulhawy, M.J. Spry & O.B. Filippas, 1987. Probabilistic site strategy for transmission lines. *Foundations for transmission line towers*, GSP8:1-14, New York: ASCE.

Rojas-Gonzalez, L.F, Kondziolka, R.E., and Kandaris, P.M., 1994. Value of geotechnical efforts toward economizing foundation costs of transmission line projects. IEEE/PES 1994 Summer Meetings, Presentation for the Working Group on the Construction of Overhead Lines, San Francisco, California, July 26.

Terracon Consultants, 2012a. Geotechnical engineering report: O'Brien county 345kV sub to Webster 345kV sub, northern Iowa. Terracon No. AB125634-06. (includes addendum issued 10/1/12).

Terracon Consultants, 2012b. Geotechnical engineering report: Hampton interconnection to ITC midwest interconnection, northeastern Iowa. Terracon No. 13125067-04. (includes addendum issued 10/1/12).

Terracon Consultants, 2013a. Desktop study: O'Brien county 345kV sub to Webster 345kV sub, northern Iowa. Terracon No. AB135642-01.

Terracon Consultants, 2013b. Desktop Study: Hampton interconnection to ITC midwest interconnection, northeastern Iowa. Terracon No. 13135070-01.

Terracon Consultants, 2013c. Geotechnical engineering report: Black Hawk county substation north of Waterloo, Iowa. Terracon No. 13135065-02.

Terracon Consultants, 2013e. Geotechnical engineering report: Kossuth county substation northeast of Algona, Iowa. Terracon No. 135639-01.

Terracon Consultants, 2013d. Geotechnical engineering report: O'Brien county substation northeast of Sanborn, Iowa. Terracon No. 135638-01.

Terracon Consultants, 2013f. Geotechnical engineering report: Webster county substation northeast of Fort Dodge, Iowa. Terracon No. 135640-01.



Deep Foundations Institute
326 Lafayette Avenue
Hawthorne, NJ 07506
USA
Tel: 973-423-4030 | Fax: 973-423-4031
staff@dfi.org | www.dfi.org